



# Microbial Ecotoxicology Advances to Improve Environmental and Human Health Under Global Change

Aurélie Cébron, Dimitrios Georgios Karpouzas, Fabrice Martin-Laurent,  
Soizic Morin, Carmen Palacios, Mechthild Schmitt-Jansen

## ► To cite this version:

Dimitrios Georgios Karpouzas, Fabrice Martin-Laurent, Soizic Morin, Carmen Palacios, Mechthild Schmitt-Jansen (Dir.). Microbial Ecotoxicology Advances to Improve Environmental and Human Health Under Global Change. Frontiers Media SA, 2022, Frontiers Research Topics, 978-2-88974-921-8. 10.3389/978-2-88974-921-8 . hal-03683456

**HAL Id: hal-03683456**

**<https://hal.inrae.fr/hal-03683456>**


Submitted on 14 Jun 2022

**HAL** is a multi-disciplinary open access archive for the deposit and dissemination of scientific research documents, whether they are published or not. The documents may come from teaching and research institutions in France or abroad, or from public or private research centers.

L'archive ouverte pluridisciplinaire **HAL**, est destinée au dépôt et à la diffusion de documents scientifiques de niveau recherche, publiés ou non, émanant des établissements d'enseignement et de recherche français ou étrangers, des laboratoires publics ou privés.



Distributed under a Creative Commons Attribution 4.0 International License



# **MICROBIAL ECOTOXICOLOGY ADVANCES TO IMPROVE ENVIRONMENTAL AND HUMAN HEALTH UNDER GLOBAL CHANGE**

EDITED BY: Fabrice Martin-Laurent, Aurélie Cebron,  
Mechthild Schmitt-Jansen, Dimitrios Georgios Karpouzas,  
Soizic Morin and Carmen Palacios

PUBLISHED IN: Frontiers in Microbiology





# frontiers

## Frontiers eBook Copyright Statement

The copyright in the text of individual articles in this eBook is the property of their respective authors or their respective institutions or funders. The copyright in graphics and images within each article may be subject to copyright of other parties. In both cases this is subject to a license granted to Frontiers.

The compilation of articles constituting this eBook is the property of Frontiers.

Each article within this eBook, and the eBook itself, are published under the most recent version of the Creative Commons CC-BY licence.

The version current at the date of publication of this eBook is CC-BY 4.0. If the CC-BY licence is updated, the licence granted by Frontiers is automatically updated to the new version.

When exercising any right under the CC-BY licence, Frontiers must be attributed as the original publisher of the article or eBook, as applicable.

Authors have the responsibility of ensuring that any graphics or other materials which are the property of others may be included in the CC-BY licence, but this should be checked before relying on the CC-BY licence to reproduce those materials. Any copyright notices relating to those materials must be complied with.

Copyright and source acknowledgement notices may not be removed and must be displayed in any copy, derivative work or partial copy which includes the elements in question.

All copyright, and all rights therein, are protected by national and international copyright laws. The above represents a summary only. For further information please read Frontiers' Conditions for Website Use and Copyright Statement, and the applicable CC-BY licence.

ISSN 1664-8714

ISBN 978-2-88974-921-8

DOI 10.3389/978-2-88974-921-8

## About Frontiers

Frontiers is more than just an open-access publisher of scholarly articles: it is a pioneering approach to the world of academia, radically improving the way scholarly research is managed. The grand vision of Frontiers is a world where all people have an equal opportunity to seek, share and generate knowledge. Frontiers provides immediate and permanent online open access to all its publications, but this alone is not enough to realize our grand goals.

## Frontiers Journal Series

The Frontiers Journal Series is a multi-tier and interdisciplinary set of open-access, online journals, promising a paradigm shift from the current review, selection and dissemination processes in academic publishing. All Frontiers journals are driven by researchers for researchers; therefore, they constitute a service to the scholarly community. At the same time, the Frontiers Journal Series operates on a revolutionary invention, the tiered publishing system, initially addressing specific communities of scholars, and gradually climbing up to broader public understanding, thus serving the interests of the lay society, too.

## Dedication to Quality

Each Frontiers article is a landmark of the highest quality, thanks to genuinely collaborative interactions between authors and review editors, who include some of the world's best academicians. Research must be certified by peers before entering a stream of knowledge that may eventually reach the public - and shape society; therefore, Frontiers only applies the most rigorous and unbiased reviews.

Frontiers revolutionizes research publishing by freely delivering the most outstanding research, evaluated with no bias from both the academic and social point of view. By applying the most advanced information technologies, Frontiers is catapulting scholarly publishing into a new generation.

## What are Frontiers Research Topics?

Frontiers Research Topics are very popular trademarks of the Frontiers Journals Series: they are collections of at least ten articles, all centered on a particular subject. With their unique mix of varied contributions from Original Research to Review Articles, Frontiers Research Topics unify the most influential researchers, the latest key findings and historical advances in a hot research area! Find out more on how to host your own Frontiers Research Topic or contribute to one as an author by contacting the Frontiers Editorial Office: [frontiersin.org/about/contact](https://frontiersin.org/about/contact)

# MICROBIAL ECOTOXICOLOGY ADVANCES TO IMPROVE ENVIRONMENTAL AND HUMAN HEALTH UNDER GLOBAL CHANGE

Topic Editors:

**Fabrice Martin-Laurent**, Institut National de la Recherche Agronomique (INRA), France

**Aurélie Cebron**, UMR7360 Laboratoire Interdisciplinaire des Environnements Continentaux (LIEC), France

**Mechthild Schmitt-Jansen**, Helmholtz Centre for Environmental Research, Helmholtz Association of German Research Centres (HZ), Germany

**Dimitrios Georgios Karpouzas**, University of Thessaly, Greece

**Soizic Morin**, INRAE Nouvelle-Aquitaine Bordeaux, France

**Carmen Palacios**, Université de Perpignan Via Domitia, France

**Citation:** Martin-Laurent, F., Cebron, A., Schmitt-Jansen, M., Karpouzas, D. G., Morin, S., Palacios, C., eds. (2022). Microbial Ecotoxicology Advances to Improve Environmental and Human Health Under Global Change.

Lausanne: Frontiers Media SA. doi: 10.3389/978-2-88974-921-8

# Table of Contents

- 06 Editorial: Microbial Ecotoxicology Advances to Improve Environmental and Human Health Under Global Change**  
Aurélie Cébron, Dimitrios Georgios Karpouzas, Fabrice Martin-Laurent, Soizic Morin, Carmen Palacios and Mechthild Schmitt-Jansen
- 09 Comparison of Novel and Established Nitrification Inhibitors Relevant to Agriculture on Soil Ammonia- and Nitrite-Oxidizing Isolates**  
Evangelia S. Papadopoulou, Eleftheria Bachtsevani, Eleni Lampronikou, Eleni Adamou, Afroditi Katsaouni, Sotirios Vasileiadis, Cécile Thion, Urania Menkissoglu-Spirooudi, Graeme W. Nicol and Dimitrios G. Karpouzas
- 24 Assessing the Effects of  $\beta$ -Triketone Herbicides on the Soil Bacterial and hppd Communities: A Lab-to-Field Experiment**  
Clémence Thiour-Mauprivez, Marion Devers-Lamrani, David Bru, Jérémie Béguet, Aymé Spor, Arnaud Mounier, Lionel Alletto, Christophe Calvayrac, Lise Barthelmebs and Fabrice Martin-Laurent
- 34 Relative Influence of Plastic Debris Size and Shape, Chemical Composition and Phytoplankton-Bacteria Interactions in Driving Seawater Plastisphere Abundance, Diversity and Activity**  
Jingguang Cheng, Justine Jacquin, Pascal Conan, Mireille Pujo-Pay, Valérie Barbe, Matthieu George, Pascale Fabre, Stéphane Bruzard, Alexandra Ter Halle, Anne-Leila Meistertzheim and Jean-François Ghiglione
- 51 Variability of the Atmospheric PM<sub>10</sub> Microbiome in Three Climatic Regions of France**  
Abdoulaye Samaké, Jean M. F. Martins, Aurélie Bonin, Gaëlle Uzu, Pierre Taberlet, Sébastien Conil, Olivier Favez, Alexandre Thomasson, Benjamin Chazeau, Nicolas Marchand and Jean-Luc Jaffrezou
- 66 Graphene-Based Nanomaterials Modulate Internal Biofilm Interactions and Microbial Diversity**  
Lauris Evariste, Paul Braylé, Florence Mouchet, Jérôme Silvestre, Laury Gauthier, Emmanuel Flahaut, Eric Pinelli and Maialen Barret
- 81 Antibiotrophy: Key Function for Antibiotic-Resistant Bacteria to Colonize Soils—Case of Sulfamethazine-Degrading Microbacterium sp. C448**  
Loren Billet, Stéphane Pesce, Nadine Rouard, Aymé Spor, Laurianne Paris, Martin Leremboure, Arnaud Mounier, Pascale Besse-Hoggan, Fabrice Martin-Laurent and Marion Devers-Lamrani
- 94 Environmental Concentrations of Sulfonamides Can Alter Bacterial Structure and Induce Diatom Deformities in Freshwater Biofilm Communities**  
Laura Kergoat, Pascale Besse-Hoggan, Martin Leremboure, Jérémie Béguet, Marion Devers, Fabrice Martin-Laurent, Matthieu Masson, Soizic Morin, Amélie Roinat, Stéphane Pesce and Chloé Bonnineau
- 106 Side Effects of Pesticides and Metabolites in Groundwater: Impact on Denitrification**  
Caroline Michel, Nicole Baran, Laurent André, Mickael Charron and Catherine Joulian



- 123** *Relative Weight of Organic Waste Origin on Compost and Digestate 16S rRNA Gene Bacterial Profilings and Related Functional Inferences*  
Axel Aigle, Emilie Bourgeois, Laurence Marjolet, Sabine Houot, Dominique Patureau, Emmanuel Doelsch, Benoit Cournoyer and Wessam Galia
- 141** *Biofilm Formation, Production of Matrix Compounds and Biosorption of Copper, Nickel and Lead by Different Bacterial Strains*  
Md. Manjurul Haque, Md Khaled Mosharaf, Md. Amdadul Haque, Md. Zahid Hasan Tanvir and Md. Khairul Alam
- 160** *Description of Microbial Communities of Phosphate Mine Wastes in Morocco, a Semi-Arid Climate, Using High-Throughput Sequencing and Functional Prediction*  
Najoua Mghazli, Laila Sbabou, Rachid Hakkou, Ahmed Ouhammou, Mariam El Adnani and Odile Bruneel
- 177** *Microbial Diversity and Activity During the Biodegradation in Seawater of Various Substitutes to Conventional Plastic Cotton Swab Sticks*  
Justine Jacquin, Nolwenn Callac, Jingguang Cheng, Carolane Giraud, Yonko Gorand, Clement Denoual, Mireille Pujo-Pay, Pascal Conan, Anne-Leila Meistertzheim, Valerie Barbe, Stéphane Bruzard and Jean-François Ghiglione
- 192** *Bioleaching of E-Waste: Influence of Printed Circuit Boards on the Activity of Acidophilic Iron-Oxidizing Bacteria*  
Juan Anaya-Garzon, Agathe Hubau, Catherine Joulain and Anne-Gwénaëlle Guezennec
- 204** *Bioaugmentation With a Consortium of Bacterial Sodium Lauryl Ether Sulfate-Degraders for Remediation of Contaminated Soils*  
Ludovica Rolando, Anna Barra Caracciolo, Paola Grenni, Livia Mariani, Jasmin Rauseo, Francesca Spataro, Gian Luigi Garbini, Andrea Visca and Luisa Patrolecco
- 214** *The Response of Extracellular Polymeric Substances Production by Phototrophic Biofilms to a Sequential Disturbance Strongly Depends on Environmental Conditions*  
Emilie Loustau, Joséphine Leflaive, Claire Boscus, Quentin Amalric, Jessica Ferriol, Olga Oleinikova, Oleg S. Pokrovsky, Elisabeth Girbal-Neuhauser and Jean-Luc Rols
- 228** *Diversity, Functions and Antibiotic Resistance of Sediment Microbial Communities From Lake Geneva Are Driven by the Spatial Distribution of Anthropogenic Contamination*  
Emilie Lyautey, Chloé Bonnineau, Patrick Billard, Jean-Luc Loizeau, Emmanuel Naffrechoux, Ahmed Tlili, Edward Topp, Benoît J.D. Ferrari and Stéphane Pesce
- 243** *Driving Factors of Geosmin Appearance in a Mediterranean River Basin: The Ter River Case*  
Carmen Espinosa, Meritxell Abril, Èlia Bretxa, Marta Jutglar, Sergio Ponsá, Núria Sellarès, Lúdia Vendrell-Puigmitjà, Laia Llenas, Marc Ordeix and Lorenzo Proia

**257 *Microbial Transformation of Chlordecone and Two Transformation Products Formed During in situ Chemical Reduction***

Jennifer Hellal, Pierre-Loïc Saaidi, Sébastien Bristeau, Marc Crampon, Delphine Muselet, Oriane Della-Negra, Aourel Mauffret, Christophe Mouvet and Catherine Jouliau

**270 *Bacterial Abundance, Diversity and Activity During Long-Term Colonization of Non-biodegradable and Biodegradable Plastics in Seawater***

Charlene Odobel, Claire Dussud, Lena Philip, Gabrielle Derippe, Marion Lauters, Boris Eyheraguibel, Gaëtan Burgaud, Alexandra Ter Halle, Anne-Leila Meistertzheim, Stéphane Bruzard, Valerie Barbe and Jean-François Ghiglione

**286 *Dynamics of Soil Microbial Communities During Diazepam and Oxazepam Biodegradation in Soil Flooded by Water From a WWTP***

Marc Crampon, Coralie Soulier, Pauline Sidoli, Jennifer Hellal, Catherine Jouliau, Mickaël Charron, Quentin Guillemoto, Géraldine Picot-Colbeaux and Marie Pettenati

**305 *Resistance and Resilience of Soil Nitrogen Cycling to Drought and Heat Stress in Rehabilitated Urban Soils***

Mehdi Fikri, Catherine Jouliau, Mikael Motelica-Heino, Marie-Paule Norini and Jennifer Hellal



# Editorial: Microbial Ecotoxicology Advances to Improve Environmental and Human Health Under Global Change

Aurélie Cébron<sup>1\*</sup>, Dimitrios Georgios Karpouzas<sup>2</sup>, Fabrice Martin-Laurent<sup>3</sup>, Soizic Morin<sup>4</sup>, Carmen Palacios<sup>5,6</sup> and Mechthild Schmitt-Jansen<sup>7</sup>

<sup>1</sup> Université de Lorraine, CNRS, LIEC, F-54000 Nancy, France, <sup>2</sup> Laboratory of Plant and Environmental Biotechnology, Department of Biochemistry and Biotechnology, University of Thessaly, Larissa, Greece, <sup>3</sup> Agroécologie, INRAE, Institut Agro, Université de Bourgogne, Université de Bourgogne Franche-Comté, F-21000 Dijon, France, <sup>4</sup> UR EABX, INRAE, F-33612 Cestas, France, <sup>5</sup> Univ. Perpignan Via Domitia, CEFREM, UMR5110, F-66860, Perpignan, France, <sup>6</sup> CNRS, CEFREM, UMR5110, F-66860, Perpignan, France, <sup>7</sup> Helmholtz-Centre for Environmental Research—UFZ, Department of Bioanalytical Ecotoxicology, Leipzig, Germany

**Keywords:** microbial communities, impact of pollutants, environmental risk assessment, multiple stressors, biodegradation, bio-processes, ecosystem rehabilitation

## Editorial on the Research Topic

### Microbial Ecotoxicology Advances to Improve Environmental and Human Health Under Global Change

## OPEN ACCESS

### Edited and reviewed by:

Eric Altermann,  
AgResearch Ltd, New Zealand

### \*Correspondence:

Aurélie Cébron  
aurelie.cebron@univ-lorraine.fr

### Specialty section:

This article was submitted to  
Microbiotechnology,  
a section of the journal  
Frontiers in Microbiology

**Received:** 06 February 2022

**Accepted:** 23 February 2022

**Published:** 23 March 2022

### Citation:

Cébron A, Karpouzas DG,  
Martin-Laurent F, Morin S, Palacios C  
and Schmitt-Jansen M (2022)  
Editorial: Microbial Ecotoxicology  
Advances to Improve Environmental  
and Human Health Under Global  
Change. *Front. Microbiol.* 13:870404.  
doi: 10.3389/fmicb.2022.870404

Microbial Ecotoxicology is an interdisciplinary science at the intersection of microbial ecology, toxicology, ecotoxicology, and analytical chemistry (Ghiglione et al., 2016; Shahsavari et al., 2017; Pesce et al., 2020). This Research Topic was proposed aiming to present the full range of research currently in place in an emerging topic like microbial ecotoxicology. The research focus of microbial ecotoxicology spans from the assessment of the impact of various contaminants on microbial communities to the development of new bio-processes and includes studies on the microbial biodegradation of contaminants and rehabilitation of contaminated environments. In this Research Topic “*Microbial Ecotoxicology Advances to Improve Environmental and Human Health Under Global Change*,” we have collected 21 original articles presenting research on a range of contaminants (heavy metals, nanomaterials, biogenic and synthetic contaminants such as pesticides, herbicides, medicines, plastics and other agrochemicals). Presented research assesses their impacts on microbial diversity and activity, and their biodegradation. Contributions included the usage of microbial technologies to remove contaminants from contaminated environments and evaluation of essential microbial functions in contaminated and rehabilitated environments.

1. Microbial communities support several ecosystem functions and thus play a key role not only in biogeochemical cycles but also in a wide range of ecosystem services (Falkowski et al., 2008). Exposure of microbial communities to a range of contaminants can modify their abundance, composition and activity (Tang et al., 2019; Fei et al., 2020; Noyer et al., 2020) with consequences on the ecosystem functions they deliver as well as on higher levels of biological organization. In this Research Topic, changes in microbial community structure and functions under contamination stress were demonstrated in soils (Thiour-Mauprivez et al.), groundwater (Michel et al.), freshwater (Lyautey et al.; Kergoat et al.; Evariste et al.) and seawater (Cheng et al.). In Lake Geneva, the local anthropogenic contamination (organic matter, trace metals, PAH and PCB) induced lower bacterial and archaeal diversity but higher levels of many microbial



activities (respiration, denitrification, methanogenesis, phosphatase and beta-glucosidase) and high abundance of antibiotic resistance genes (Lyautey et al.). Further, microbial activity (nitrification, Papadopoulou et al.; or denitrification, Michel et al.) was affected while functional population abundance was not impacted by synthetic pesticides. In other cases, the effect of antibiotics and graphene-based nanomaterials on the bacterial and diatom community composition, viability, physiology and interactions in biofilms were observed (Kergoat et al.; Evariste et al.). Unexpectedly, teratogenic effects of sulfonamide antibiotics on diatoms within periphyton were reported for the first time (Kergoat et al.). However, other studies reported no marked impact of other synthetic pesticide groups like  $\beta$ -triketone herbicides toward bacterial communities (Thiour-Mauprivez et al.) or limited effects of plastic size and shape on the abundance, diversity and activity of bacterial communities on the plastic surfaces (Cheng et al.).

Only few studies have addressed how cumulative stressors can alter ecosystem services. In this Research Topic, combined stressors studies have shown that ecosystems already stressed by the presence of contaminants may become more sensitive to additional environmental stresses and functional consequences amplified (Loustau et al.; Fikri et al.). The effect of droughts following a previous exposure to copper in biofilms, highlighted the importance of considering not only direct but also indirect effects of global changes (Loustau et al.). Moreover, low resistance but high resilience of an ecosystem after exposure to multiple stressors on already degraded soils was shown (Fikri et al.).

2. Due to their often-demonstrated capacities to transform and degrade a large range of substances including organic pollutants, microbial communities play a key role in the environmental fate of pollutants by regulating their persistence and mitigating related ecotoxicological impacts in the environment (Holliger et al., 1997; Haritash and Kaushik, 2009; Singh and Singh, 2016; Mohanan et al., 2020). Biodegradation of pesticides, medicines, plastics, antibiotics and foaming agents were studied in different environments to evaluate bioremediation and auto-depuration of impacted sites (Odobel et al.; Jacquin et al.; Hellal et al.; Crampon et al., Rolando et al.; Billet et al.). *In situ*, the microbial degradation of benzodiazepines was evaluated in soils (Crampon et al.) and the degradation of bio-based and fossil-based plastics in seawater was explored, where potential degraders were additionally identified (Odobel et al.). Transformation of the pesticide chlordane and of two of its transformation products by microbial enrichment culture was assessed to identify degradation pathways, degradation key players and transformation products formed by microbial activities (Hellal et al.). The use of bacterial isolates or consortia capable of efficiently degrading organic contaminants such as antibiotics (Billet et al.) or foaming agents (Rolando et al.) in environmental matrices was explored. Finally, recommendations to improve future remediation strategies of polluted environments were proposed.

3. The cutting-edge research produced by microbial ecotoxicologists meets the demands of policy makers and the society in large. Specifically, it contributes to the tremendous challenges caused by intensive anthropogenic activities that threaten both environmental and human health worldwide. To bridge research to end-users, ecological engineering technologies are developed based on microbial technologies to support a more sustainable world. They aim to improve the management of contaminated environments and to bring up new treatment processes (Peng et al., 2018; Quintella et al., 2019; Bhatt et al., 2021). Here, new methods were developed to qualify and improve waste treatment and the quality of natural resources (Espinosa et al.; Anaya-Garzon et al.; Aigle et al.; Haque et al.). First, a better management of water quality (such as cyanobacterial metabolites affecting the taste of drinking water) through the monitoring of microbial development was proposed (Espinosa et al.). Bacterial activities can help to treat and recover wastes, such as agricultural and urban organic wastes *via* anaerobic digestion (Aigle et al.), e-waste treatment through metal bioleaching (Anaya-Garzon et al.) or metal biosorption by bacterial biofilms (Haque et al.).

Furthermore, after remediation or rehabilitation of contaminated sites, the recovery of the functioning of the rehabilitated ecosystem has to be assessed (Fikri et al.; Mghazli et al.). For example, the covering of acidic tailing with alkaline phosphate mine wastes was tested as a rehabilitation scenario of abandoned mines, and the status of microbial community diversity and functions were evaluated (Mghazli et al.). Nowadays, degraded urban soils can be ecologically rehabilitated by adding various materials to soils in order to restore the microbial functions involved in the C, P and N cycles (Fikri et al.).

Finally, emerging contaminants are constantly being introduced into the environment because of the implementation of new technologies in various industrial sectors and of the lack of prevention of possible contaminations issued from these new technologies. The fate and the impact of these emerging contaminants are often not well described and there is a need for monitoring. In particular, some environmental compartments are less monitored than others. For instance, the atmosphere is rarely considered in monitoring studies. In response to this, Samaké et al. demonstrated the importance of monitoring biogenic organic aerosol.

In summary, microbial ecotoxicology addresses several research challenges such as (i) providing an in-depth analysis of the changes imposed in the structure and functions of microbial communities under contamination, (ii) disentangling the complexity of environmental systems characterized of various interactors (toxicants, targets, multiple stressors), (iii) assessing the potential of contaminant biodegradation and utilization of the catabolic capacities of microbial communities for bioremediation of contaminated sites. Fundamental discoveries feed current applied developments including risk assessment using microbes in a changing world, development and validation of new methods to qualify environmental quality, guidelines for environmental policies and ecological

engineering technologies based on microbial technologies. This Research Topic brings together original results concerning these challenging questions as well as articles addressing the latest advances in microbial ecotoxicology.

We are delighted to present this Research Topic in *Frontiers in Microbiology*. We hope that this e-book will be interesting and useful to the readers of *Frontiers in Microbiology* while highlighting the value of focusing on microbial ecotoxicology to broaden our knowledge on contaminants effect, biodegradation and treatment.

## AUTHOR CONTRIBUTIONS

AC wrote the first version of the editorial manuscript. All authors contributed to manuscript write, revision, read,

and approved the submitted version. All authors were co-editors of the Research Topic: *Microbial Ecotoxicology Advances to Improve Environmental and Human Health Under Global Change*.

## ACKNOWLEDGMENTS

This Research Topic was promoted by the International Network on Microbial Ecotoxicology—EcotoxicoMic (<https://ecotoxicomic.org/>), following the second International Conference on Microbial Ecotoxicology held online in October, 2020. We thank all participating authors and reviewers for having made this Research Topic a success.

## REFERENCES

- Bhatt, P., Bhatt, K., Sharma, A., Zhang, W., Mishra, S., and Chen, S. (2021). Biotechnological basis of microbial consortia for the removal of pesticides from the environment. *Critic. Rev. Biotechnol.* 41, 317–338. doi: 10.1080/07388551.2020.1853032
- Falkowski, P. G., Fenchel, T., and Delong, E. F. (2008). The microbial engines that drive Earth's biogeochemical cycles. *Science* 320, 1034–1039. doi: 10.1126/science.1153213
- Fei, Y., Huang, S., Zhang, H., Tong, Y., Wen, D., Xia, X., et al. (2020). Response of soil enzyme activities and bacterial communities to the accumulation of microplastics in an acid cropped soil. *Sci. Total Environ.* 707, 135634. doi: 10.1016/j.scitotenv.2019.135634
- Ghiglione, J. F., Martin-Laurent, F., and Pesce, S. (2016). Microbial ecotoxicology: an emerging discipline facing contemporary environmental threats. *Environ. Sci. Pollut. Res.* 23, 3981–3983. doi: 10.1007/s11356-015-5763-1
- Haritash, A. K., and Kaushik, C. P. (2009). Biodegradation aspects of polycyclic aromatic hydrocarbons (PAHs): a review. *J. Hazard. Mater.* 169, 1–15. doi: 10.1016/j.jhazmat.2009.03.137
- Holliger, C., Gaspard, S., Glod, G., Heijman, C., Schumacher, W., Schwarzenbach, R. P., et al. (1997). Contaminated environments in the subsurface and bioremediation: organic contaminants. *FEMS Microbiol. Rev.* 20, 517–523. doi: 10.1111/j.1574-6976.1997.tb00334.x
- Mohan, N., Montazer, Z., Sharma, P. K., and Levin, D. B. (2020). Microbial and enzymatic degradation of synthetic plastics. *Front. Microbiol.* 11, 2837. doi: 10.3389/fmicb.2020.580709
- Noyer, M., Reoyo-Prats, B., Aubert, D., Bernard, M., Verneau, O., and Palacios, C. (2020). Particle-attached riverine bacteriome shifts in a pollutant-resistant and pathogenic community during a Mediterranean extreme storm event. *Sci. Total Environ.* 732, 139047. doi: 10.1016/j.scitotenv.2020.139047
- Peng, W., Li, X., Xiao, S., and Fan, W. (2018). Review of remediation technologies for sediments contaminated by heavy metals. *J. Soils Sediments* 18, 1701–1719. doi: 10.1007/s11368-018-1921-7
- Pesce, S., Ghiglione, J. F., Topp, E., and Martin-Laurent, F. (2020). Editorial: Microbial Ecotoxicology. *Front. Microbiol.* 20, 9. doi: 10.3389/fmicb.2020.288963
- Quintella, C. M., Mata, A. M., and Lima, L. C. (2019). Overview of bioremediation with technology assessment and emphasis on fungal bioremediation of oil contaminated soils. *Journal of environmental management* 241, 156–166. doi: 10.1016/j.jenvman.2019.04.019
- Shahsavari, E., Aburto-Medina, A., Khudr, L. S., Taha, M., and Ball, A. S. (2017). "From microbial ecology to microbial ecotoxicology," in *Microbial Ecotoxicology* (Cham: Springer), pp. 17–38
- Singh, B., and Singh, K. (2016). Microbial degradation of herbicides. *Critic. Rev. Microbiol.* 42, 245–261. doi: 10.3109/1040841X.2014.929564
- Tang, J., Zhang, J., Ren, L., Zhou, Y., Gao, J., Luo, L., et al. (2019). Diagnosis of soil contamination using microbiological indices: a review on heavy metal pollution. *J. Environ. Manage.* 242, 121–130. doi: 10.1016/j.jenvman.2019.04.061

**Conflict of Interest:** The authors declare that the research was conducted in the absence of any commercial or financial relationships that could be construed as a potential conflict of interest.

**Publisher's Note:** All claims expressed in this article are solely those of the authors and do not necessarily represent those of their affiliated organizations, or those of the publisher, the editors and the reviewers. Any product that may be evaluated in this article, or claim that may be made by its manufacturer, is not guaranteed or endorsed by the publisher.

Copyright © 2022 Cébron, Karpouzias, Martin-Laurent, Morin, Palacios and Schmitt-Jansen. This is an open-access article distributed under the terms of the Creative Commons Attribution License (CC BY). The use, distribution or reproduction in other forums is permitted, provided the original author(s) and the copyright owner(s) are credited and that the original publication in this journal is cited, in accordance with accepted academic practice. No use, distribution or reproduction is permitted which does not comply with these terms.



# Comparison of Novel and Established Nitrification Inhibitors Relevant to Agriculture on Soil Ammonia- and Nitrite-Oxidizing Isolates

Evangelia S. Papadopoulou<sup>1\*</sup>, Eleftheria Bachtsevani<sup>1</sup>, Eleni Lampronikou<sup>1</sup>, Eleni Adamou<sup>1</sup>, Afroditi Katsaouni<sup>1</sup>, Sotirios Vasileiadis<sup>1</sup>, Cécile Thion<sup>2</sup>, Urania Menkissoglu-Spiroudi<sup>3</sup>, Graeme W. Nicol<sup>2</sup> and Dimitrios G. Karpouzas<sup>1</sup>

## OPEN ACCESS

### Edited by:

Akihiko Terada,  
Tokyo University of Agriculture  
and Technology, Japan

### Reviewed by:

Haoran Duan,  
The University of Queensland,  
Australia  
Sanin Musovic,  
Danish Technological Institute (DTI),  
Denmark

### \*Correspondence:

Evangelia S. Papadopoulou  
evapapadopoulou@bio.uth.gr

### Specialty section:

This article was submitted to  
Microbiotechnology,  
a section of the journal  
Frontiers in Microbiology

**Received:** 08 July 2020

**Accepted:** 16 October 2020

**Published:** 04 November 2020

### Citation:

Papadopoulou ES, Bachtsevani E,  
Lampronikou E, Adamou E,  
Katsaouni A, Vasileiadis S, Thion C,  
Menkissoglu-Spiroudi U, Nicol GW  
and Karpouzas DG (2020)  
Comparison of Novel and Established  
Nitrification Inhibitors Relevant  
to Agriculture on Soil Ammonia-  
and Nitrite-Oxidizing Isolates.  
Front. Microbiol. 11:581283.  
doi: 10.3389/fmicb.2020.581283

<sup>1</sup> Laboratory of Plant and Environmental Biotechnology, Department of Biochemistry and Biotechnology, University of Thessaly, Larissa, Greece, <sup>2</sup> Laboratoire Ampère, École Centrale de Lyon, University of Lyon, Ecully, France, <sup>3</sup> Pesticide Science Laboratory, School of Agriculture, Forestry and Environment, Faculty of Agriculture, Aristotle University of Thessaloniki, Thessaloniki, Greece

Nitrification inhibitors (NIs) applied to soil reduce nitrogen fertilizer losses from agro-ecosystems. NIs that are currently registered for use in agriculture appear to selectively inhibit ammonia-oxidizing bacteria (AOB), while their impact on other nitrifiers is limited or unknown. Ethoxyquin (EQ), a fruit preservative shown to inhibit ammonia-oxidizers (AO) in soil, is rapidly transformed to 2,6-dihydro-2,2,4-trimethyl-6-quinone imine (QI), and 2,4-dimethyl-6-ethoxy-quinoline (EQNL). We compared the inhibitory potential of EQ and its derivatives with that of dicyandiamide (DCD), nitrapyrin (NP), and 3,4-dimethylpyrazole-phosphate (DMPP), NIs that have been used in agricultural settings. The effect of each compound on the growth of AOB (*Nitrosomonas europaea*, *Nitrosospira multiformis*), ammonia-oxidizing archaea (AOA; “*Candidatus Nitrosocosmicus franklandus*,” “*Candidatus Nitrosotalea sinensis*”), and a nitrite-oxidizing bacterium (NOB; *Nitrobacter* sp. NHB1), all being soil isolates, were determined in liquid culture over a range of concentrations by measuring nitrite production or consumption and qPCR of *amoA* and *nxB* genes, respectively. The degradation of NIs in the liquid cultures was also determined. In all cultures, EQ was transformed to the short-lived QI (major derivative) and the persistent EQNL (minor derivative). They all showed significantly higher inhibition activity of AOA compared to AOB and NOB isolates. QI was the most potent AOA inhibitor ( $EC_{50} = 0.3\text{--}0.7 \mu\text{M}$ ) compared to EQ ( $EC_{50} = 1\text{--}1.4 \mu\text{M}$ ) and EQNL ( $EC_{50} = 26.6\text{--}129.5 \mu\text{M}$ ). The formation and concentration of QI in EQ-amended cultures correlated with the inhibition patterns for all isolates suggesting that it was primarily responsible for inhibition after application of EQ. DCD and DMPP showed greater inhibition of AOB compared to AOA or NOB,



with DMPP being more potent ( $EC_{50} = 221.9\text{--}248.7 \mu\text{M}$  vs  $EC_{50} = 0.6\text{--}2.1 \mu\text{M}$ ). NP was the only NI to which both AOA and AOB were equally sensitive with  $EC_{50}$ s of 0.8–2.1 and 1.0–6.7  $\mu\text{M}$ , respectively. Overall, EQ, QI, and NP were the most potent NIs against AOA, NP, and DMPP were the most effective against AOB, while NP, EQ and its derivatives showed the highest activity against the NOB isolate. Our findings benchmark the activity range of known and novel NIs with practical implications for their use in agriculture and the development of NIs with broad or complementary activity against all AO.

**Keywords:** nitrification inhibitors, ammonia-oxidizing bacteria, ammonia-oxidizing archaea, nitrite-oxidizing bacteria, ethoxyquin, quinone imine

## INTRODUCTION

Modern agricultural systems depend heavily on large inputs of synthetic N fertilizers to maintain crop productivity and meet the increasing global food demand (Fowler et al., 2018). However, ca. 70% of the annual global input of 100 Tg N fertilizer is lost from agricultural ecosystems due to nitrification and subsequent denitrification processes leading to groundwater and atmospheric pollution (Raun and Johnson, 1999). To minimize N losses and improve N use efficiency in soil, nitrification inhibitors (NIs), compounds known to reduce the activity of nitrifying prokaryotes, are routinely incorporated into N-stabilized fertilizers (Abbasi and Adams, 1998; Moir et al., 2007).

Hundreds of compounds have been identified that inhibit nitrifying prokaryotes (Bédard and Knowles, 1989; McCarty, 1999) including plant-derived molecules (Coskun et al., 2017), aliphatic and aromatic n-alkynes (Taylor et al., 2015; Wright et al., 2020), statins (Zhao et al., 2020), and PTIO (2-phenyl-4,4,5,5-tetramethylimidazoline-1-oxyl 3-oxide; Martens-Habbena et al., 2015). Many of these are used as selective inhibitors of ammonia-oxidizing bacteria (AOB; e.g., octyne) or archaea (AOA; e.g., PTIO) in laboratory cultures, soil microcosms or slurries, but are not suitable for use in an agricultural setting due to rapid degradation in soil or application in a gaseous state. Only three compounds have gained importance for practical use as NIs in agriculture: 2-chloro-6-(trichloromethyl) pyridine (nitrapyrin; NP; Goring, 1962), dicyandiamide (DCD; Solansky, 1982), and 3,4-dimethylpyrazole phosphate (DMPP; Zerulla et al., 2001). All three are presumed to act as Cu chelators interfering with ammonia monooxygenase (AMO), a key enzyme in the first and rate-limiting step of nitrification (Ruser and Schulz, 2015). In addition, NP was also proposed to serve as a weak mechanism-based or “suicide” inhibitor (Vannelli and Hooper, 1992). However, the precise mode of action of these NIs has yet to be fully elucidated.

When NIs were first introduced in agriculture, soil nitrification was considered a two-step process carried out

by AOB and nitrite-oxidizing bacteria (NOB). AOB oxidize ammonia to hydroxylamine ( $\text{NH}_2\text{OH}$ ) using AMO, which is further oxidized to nitric oxide (NO) and finally nitrite ( $\text{NO}_2^-$ ). NOB subsequently transform  $\text{NO}_2^-$  to nitrate ( $\text{NO}_3^-$ ) using nitrite oxidoreductase (NXR; Coskun et al., 2017; Beeckman et al., 2018). However, over the last 15 years, other groups were demonstrated to contribute to soil nitrification including AOA (Leininger et al., 2006; Zhang et al., 2012), and recently “comammox” *Nitrospira*, (Wang et al., 2019; Li et al., 2019a) that perform complete oxidation of ammonia to nitrate within an individual cell (Daims et al., 2015; van Kessel et al., 2015). Isolation of soil AOA strains confirmed their role in soil ammonia oxidation (Tournia et al., 2011; Lehtovirta-Morley et al., 2014), while all *Nitrospira* strains isolated from soil are non-comammox strains.

Despite these breakthroughs in our understanding of the microbiology and biochemistry of nitrification, current knowledge regarding the spectrum of activity and the inhibition thresholds of NIs used in agriculture on soil ammonia-oxidizers (AO) is limited. The use of inhibition assays with pure cultures of a diverse range of soil-derived strains is a necessary benchmarking step to define the exact spectrum of activity of NIs destined for use in agriculture. Most culture inhibition assays have focused on AOB (e.g., Bélser and Schmidt, 1981; Vannelli and Hooper, 1992) or tested NIs not broadly applied in agricultural settings on soil AOA strains (i.e., allylthiourea, n-alkyl alkyne, and simvastatin; Wright et al., 2020; Zhao et al., 2020). Others have explored the activity of NIs of agricultural relevance on AOA (Jung et al., 2011; Kim et al., 2012), but only three provided a systematic assessment and inhibition thresholds for AOA soil strains like “*Candidatus Nitrosocosmicus agrestis*” (Liu et al., 2019), “*Candidatus Nitrosotalea devanaterre*” (Lehtovirta-Morley et al., 2013), and *Nitrososphaera viennensis* (Shen et al., 2013). In addition, most NIs are known to act on the ammonia oxidation step of nitrification (Bédard and Knowles, 1989), hence their activity on NOB remains unknown. The variation in sensitivity of AOA and AOB to different types of NIs, combined with their contribution to nitrification in distinct ecological niches (Prosser and Nicol, 2012; Kits et al., 2017), implies a potential suboptimal efficiency of the NIs currently used in agriculture, and stresses the need for the discovery of novel NIs with a broader range of activity against all microorganisms contributing to nitrification.

**Abbreviations:** NIs, nitrification inhibitors; EQ, ethoxyquin; QI, 2,6-dihydro-2,2,4-trimethyl-6-quinone imine; EQNL, 2,4-dimethyl-6-ethoxyquinoline; DCD, dicyandiamide; NP, nitrapyrin; DMPP, 3,4-dimethylpyrazole phosphate; AOB, ammonia-oxidizing bacteria; AOA, ammonia-oxidizing archaea; AO, ammonia-oxidizers; NOB, nitrite-oxidizing bacteria; comammox, complete ammonia-oxidizing bacteria; AMO, ammonia monooxygenase; EPS, extracellular polymeric substances.

In previous soil microcosm studies we showed that ethoxyquin (EQ; 1,2-dihydro-6-ethoxy-2,2,4-trimethylquinoline), an antioxidant used as preservative in fruit-packaging plants, and its derivative 2,6-dihydro-2,2,4-trimethyl-6-quinone imine (QI), strongly inhibited the activity of AOB and AOA (Papadopoulou et al., 2016). EQ in soil is rapidly transformed to QI and 2,4-dimethyl-6-ethoxyquinoline (EQNL; Karas et al., 2015). The potential capacity of EQ to be rapidly transformed in soil to potent NIs is of particular interest, considering that the spectrum and the duration of inhibition are desirable attributes of NIs used in agricultural practice.

We aimed to determine the inhibitory potency of EQ and its derivatives on representative isolates of diverse and globally distributed lineages of soil AOB and AOA in liquid culture, in comparison to NIs widely used in agricultural settings (NP, DCD, and DMPP). We expanded our liquid inhibition assays to NOB to gain insights on the impact of NIs on a microbial group functionally associated with ammonia oxidation, and directly linked to nitrogen loss from disturbed agricultural ecosystems in the form of nitrate production. Specifically, we used (i) AOB strains *Nitrosomonas europaea* and *Nitrospira multiformis*, belonging to AOB clusters 7 and 3, respectively, (Purkhold et al., 2000), with cluster 3 often being the dominant AOB lineage in soil ecosystems (Kowalchuk and Stephen, 2001); (ii) AOA strains “*Candidatus Nitrosocosmicus franklandus*” (Lehtovirta-Morley et al., 2016) and “*Candidatus Nitrosotalea sinensis*” (Lehtovirta-Morley et al., 2014), occupying contrasting ecological niches and representing widely distributed neutrophilic and acidophilic AOA lineages, respectively, (Herbold et al., 2017), and (iii) one NOB, *Nitrobacter* sp. NHB1 (de Boer et al., 1991) as a representative of one of the two dominant NOB lineages found in soil (Daims et al., 2016), with *Nitrobacter* strains typically having greater nitrite oxidation activity compared to *Nitrospira*, and dominating activity under excess nitrogen supply (e.g., fertilized soils; Xia et al., 2011; Nowka et al., 2015). While previous studies have examined the effective concentration of different NIs on ammonia oxidizer isolates, this study also examined the degradation of NIs during laboratory incubation.

## MATERIALS AND METHODS

### Microbial Strains, Growth Conditions and Chemicals

All strains were grown aerobically in the dark without shaking. AOB *N. europaea* ATCC25978 and *N. multiformis* ATCC25196 were grown at 28°C in Skinner and Walker's medium (Skinner and Walker, 1961) containing 1 mM  $\text{NH}_4^+$  [ $(\text{NH}_4)_2\text{SO}_4$ ] and phenol red ( $0.5 \text{ mg L}^{-1}$ ) as a pH indicator. AOA “*Ca. N. franklandus*” C13 and “*Ca. N. sinensis*” ND2, were incubated at 35°C in a medium supplemented with 1 mM  $\text{NH}_4^+$  ( $\text{NH}_4\text{Cl}$ ). The former was cultured in HEPES-buffered modified freshwater medium (pH 7.5; Lehtovirta-Morley et al., 2014), while the latter was grown in freshwater medium (pH 5.2; Lehtovirta-Morley et al., 2011). *Nitrobacter* sp. strain NHB1 was grown at 28°C in freshwater medium (pH 5.2; Lehtovirta-Morley et al., 2011) supplemented with  $0.5 \text{ mM NO}_2^-$  ( $\text{NaNO}_2$ ).

Analytical standards of DCD (99% purity), NP ( $\geq 98\%$ ), and EQ (95%) were purchased from Sigma-Aldrich (Germany), while DMPP (99.1%) analytical standard was provided by BASF Hellas. The oxidation derivatives of EQ, QI, and EQNL were synthesized as described by Thorisson et al. (1992). The chemical structures of all studied compounds are shown in **Supplementary Figure 1**.

### Liquid Culture Assays

The activity of all NIs was determined in liquid batch cultures over a range of concentrations to establish relevant inhibition thresholds per strain and compound. Preliminary assays with a broad range of concentrations for each NI and isolate ( $\text{NO}_2^-$  production) dictated the range of NI concentrations that will allow calculation of inhibition thresholds. Cultures were established in triplicate for each strain  $\times$  NI  $\times$  concentration combination in 100-mL Duran bottles containing 50 mL of growth medium and inoculated with a 1 or 2% (v/v) transfer of exponentially growing cultures of AOB or AOA/NOB, respectively. EQ, QI, EQNL, and NP were added to the cultures as filter sterilized dimethyl sulfoxide (DMSO) solutions due to their low water solubility ( $\leq 60 \text{ mg L}^{-1}$  at 20°C). The final concentration of DMSO in all cultures was 0.1% (v/v), which did not exert a significant inhibitory effect to any of the isolates tested (data not shown), in line with previous studies with the same isolates (Wright et al., 2020; Zhao et al., 2020). DCD and DMPP were dissolved in sterile  $\text{dH}_2\text{O}$  before addition of  $25 \mu\text{L}$  (0.5% v/v). All NIs were added to batch cultures at the beginning of the exponential growth phase. For all assays, triplicate cultures with the same inoculum not amended with NIs were included. Upon inoculation all liquid batch cultures were sampled at regular time intervals to determine the effect of NIs on the activity and growth of nitrifying microorganisms by measuring changes in nitrite concentrations and the abundance of *amoA* (AO) or *nxrB* (NOB) genes, respectively.

### Nitrite Measurements and Gene Abundance Quantification

Nitrite concentrations were determined colorimetrically at 540 nm in a 96-well plate format assay by diazotizing and coupling with Griess reagent (Shinn, 1941). *amoA* and *nxrB* gene abundance was determined in a Biorad CFX Real-Time PCR system. DNA was extracted from a cell pellet obtained from 2-ml aliquots of the microbial cultures using the tissue DNA extraction kit (Macherey-Nagel, Germany). The *amoA* genes of AOB and AOA was amplified with primers *amoA*-1F/*amoA*-2R (Rotthauwe et al., 1997) and Arch-*amoA*F/Arch-*amoA*R (Francis et al., 2005), respectively, as described by Rousidou et al. (2013), and the *nxrB* gene of *Nitrobacter* was quantified with primers *nxrB*-1F and *nxrB*-1R (Vanparys et al., 2007). All qPCR assays used the following thermal cycling conditions: 95°C for 3 min, followed by 40 cycles of 95°C for 30 s, 57°C for 20 s, 72°C for 30 s, with a final dissociation curve analysis. The abundance of *amoA* and *nxrB* genes were determined via external standard curves as described by Rousidou et al. (2013). qPCR amplification efficiencies ranged from 80.3% to 109.4%, with  $r^2$  values  $\geq 0.98$ .

## Nitrification Inhibitors Extraction

Ethoxyquin, QI, EQNL, and NP residues were extracted from liquid media by mixing 0.3 mL liquid culture with 0.7 mL of acetonitrile. Residues of DCD and DMPP were extracted by mixing 0.1 mL liquid culture with 0.9 mL of ddH<sub>2</sub>O water and methanol, respectively. The derived mixtures were vortexed for 30 s and stored at  $-20^{\circ}\text{C}$  until analysis. Recovery tests at three concentration levels (in the range of the tested concentrations) showed recoveries of  $>80\%$  for all compounds studied.

## Chromatographic Analyses

High performance liquid chromatography (HPLC) analyses were performed in a Shimadzu LC-20ADHPLC system equipped with an UV/VIS PDA detector. A Shimadzu GVP-ODs (4.6 mm by 150 mm, 5  $\mu\text{m}$ ) pre-column, connected to a RP Shimadzu VP-ODs (4.6 mm  $\times$  150 mm, 5  $\mu\text{m}$ ) column, was used for NI separation. The injection volume was 20  $\mu\text{l}$ . The flow rate of the mobile phase was set at 0.8 mL  $\text{min}^{-1}$  for DCD and at 1 mL  $\text{min}^{-1}$  for all other NIs. Column temperature was set at  $40^{\circ}\text{C}$  for DCD and DMPP, and at  $25^{\circ}\text{C}$  for all the other NIs. Mixtures of acetonitrile and ammonia [0.25% (vol/vol)] or *ortho*-phosphoric acid [0.1% (vol/vol)] were used at a ratio of 70:30 (vol/vol) for mobile phases in the analyses of EQ, QI, EQNL, and NP, respectively, and detection was achieved at 225, 245, 230, and 269 nm, respectively. Similarly, chromatographic separation of DCD and DMPP was achieved using ddH<sub>2</sub>O (100%) and a mixture of methanol and *ortho*-phosphoric acid [0.1% (vol/vol)] solution 50:50 by volume, respectively. DCD and DMPP residues were detected at 218 nm and 225 nm, respectively.

## Calculation of Inhibition Threshold Levels ( $\text{EC}_{50}$ )

In this study,  $\text{EC}_{50}$  describes the concentration of the inhibitor that reduces half of the activity (nitrite accumulation or consumption) of AO or NOB. Dose-response modeling was performed using normalized data whereby nitrite concentration values were divided by the mean value of the matching control. Analyses were carried out using the dose response curves (drc) v3.0-1 package (Ritz and Streibig, 2005) of the R software (R Core Team, 2020). A brief description of the tested models can be found in Ritz et al. (2016). An empirical modeling approach was initially used for selecting the best fitting model according to tested goodness of fit indices (see **Supplementary Material**), followed by the choice of the four-parameter log logistic model as the best compromise among tested models for comparing endpoint values.

## Data Analysis

Nitrite and qPCR data were subjected to one-way ANOVA, followed by Tukey's *post hoc* test ( $P < 0.05$ ). Variance between the  $\text{EC}_{50}$  values of the different NIs for one strain and between different strains for a given NI was analyzed by one-way ANOVA, and Duncan *post hoc* test ( $P < 0.05$ ). The four kinetic models proposed by the FOCUS working group on pesticide degradation kinetics (FOCUS, 2006) [single first order kinetic (SFO), biphasic models hockey stick (HS), first order

multi-compartment (FOMC), and double first order in parallel (DFOP) models] were used to calculate NI degradation kinetic parameters ( $\text{DT}_{50}$ ,  $k_{\text{deg}}$ ). Curve fitting was performed with the mkin v0.9.47.1 package (Ranke, 2018) of the R Studio v4.0.2 software (R Core Team, 2020).

## RESULTS

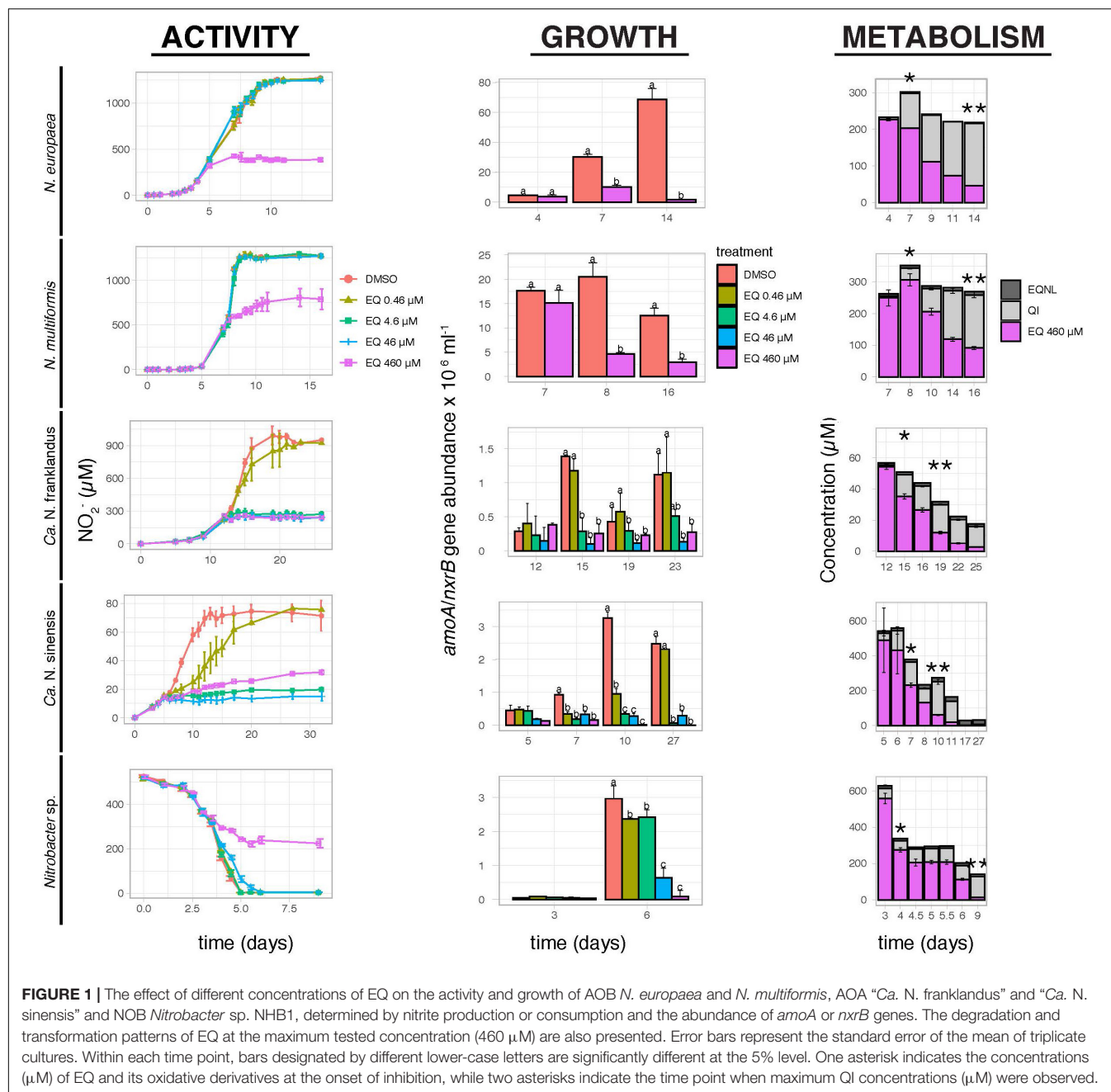
### The Impact and Degradation of EQ, QI, and EQNL in AO and NOB Cultures Effects on the Activity and Growth of AO and NOB Isolates

Ethoxyquin fully inhibited the activity of *N. europaea*, *N. multiformis*, and *Nitrobacter* sp. NHB1 only at the highest tested concentration of 460  $\mu\text{M}$  (**Figure 1**). In contrast, the activity of "*Ca. N. franklandus*" and "*Ca. N. sinensis*" was significantly reduced by EQ at concentrations  $\geq 4.6$   $\mu\text{M}$  and  $\geq 0.46$   $\mu\text{M}$  ( $p \leq 0.05$ ), respectively, while complete inhibition of "*Ca. N. sinensis*" was evident at levels  $\geq 4.6$   $\mu\text{M}$ . Growth inhibition profiles of AO isolates corresponded with  $\text{NO}_2^-$  production (**Figure 1**). In contrast to activity measurements, a significant reduction ( $p \leq 0.05$ ) in the growth of *Nitrobacter* sp. NHB1 was observed at the end of the incubation period for all EQ concentration levels.

2,6-dihydro-2,2,4-trimethyl-6-quinone imine fully inhibited ammonia oxidation by *N. europaea* and *N. multiformis* at concentrations  $\geq 270$   $\mu\text{M}$  and  $\geq 135$   $\mu\text{M}$ , respectively, (**Figure 2**). The activity of AOA was significantly reduced ( $p \leq 0.05$ ) at all QI concentrations, with little or no activity at concentrations  $\geq 2.7$   $\mu\text{M}$ , and a gradual recovery observed only for "*Ca. N. franklandus*" at the lowest concentration level (0.27  $\mu\text{M}$ ). Nitrite consumption by *Nitrobacter* sp. NHB1 was significantly suppressed at concentrations  $\geq 135$   $\mu\text{M}$  ( $p \leq 0.05$ ), though a persistent inhibitory effect was evident only at 540  $\mu\text{M}$ . The inhibition of QI on AO growth concurred with the  $\text{NO}_2^-$  production patterns, unlike NOB where QI persistently inhibited the growth of *Nitrobacter* sp. NHB1 at concentrations  $\geq 135$   $\mu\text{M}$  (**Figure 2**).

2,4-dimethyl-6-ethoxyquinoline only temporarily inhibited *N. europaea* activity at the highest concentration tested, 500  $\mu\text{M}$ , while at the same concentration level *N. multiformis* activity was fully inhibited (**Supplementary Figure 2**). Ammonia oxidation by "*Ca. N. franklandus*" and "*Ca. N. sinensis*" was significantly reduced at concentrations  $\geq 125$   $\mu\text{M}$  and  $\geq 25$   $\mu\text{M}$  ( $p \leq 0.05$ ), respectively, and complete inhibition occurred at 500  $\mu\text{M}$  and  $\geq 125$   $\mu\text{M}$ , respectively. Nitrite oxidation by *Nitrobacter* sp. NHB1 was completely inhibited by EQNL only at the highest tested concentrations of 500  $\mu\text{M}$  (**Supplementary Figure 2**). While the inhibition of AOB growth was congruent with  $\text{NO}_2^-$  production, the impact of EQNL on the growth of "*Ca. N. franklandus*" was not fully consistent with the activity measurements, and no significant differences among the different concentrations were observed at the end of the incubation period (day 22), probably due to the decreased number of living cells at EQNL concentrations  $\leq 25$   $\mu\text{M}$ . Variations in the growth





inhibition pattern of EQNL was observed also for *Nitrobacter* sp. NHB1 which was not significantly ( $p = 0.063$ ) affected by EQNL even at the highest tested concentration (500 μM; **Supplementary Figure 2**).

### Degradation Patterns of EQ, QI, and EQNL in Liquid Culture

In the liquid cultures of all tested isolates, EQ was rapidly transformed to QI and EQNL (**Figure 1** and **Supplementary Figure 3**). QI and EQNL constituted 10.4–34.9% and 1.1–4.5%, respectively, of the total amount of EQ recovered at the onset of inhibition in the liquid cultures amended with

the highest concentration of EQ (460 μM; **Figure 1**). The degradation half-life ( $DT_{50}$ ) for the sum of EQ + QI + EQNL in cultures supplemented with 460 μM of EQ ranged from 2.1 days for *Nitrobacter* sp. NHB1 to 60.1 days for *N. multiformis* (**Supplementary Table 1**).

The degradation of QI, when added directly into liquid culture, was best described by the SFO kinetic model ( $\chi^2 \leq 15$ ,  $r^2 \geq 0.75$ ). QI showed limited persistence and a weak dose-dependent degradation pattern with  $DT_{50} = 0.05$ –1.52 days at the lowest concentration level (2.7 μM), and 2.23–5.65 days at the highest concentration level (540 μM; **Figure 2** and **Supplementary Table 1**). In contrast, EQNL

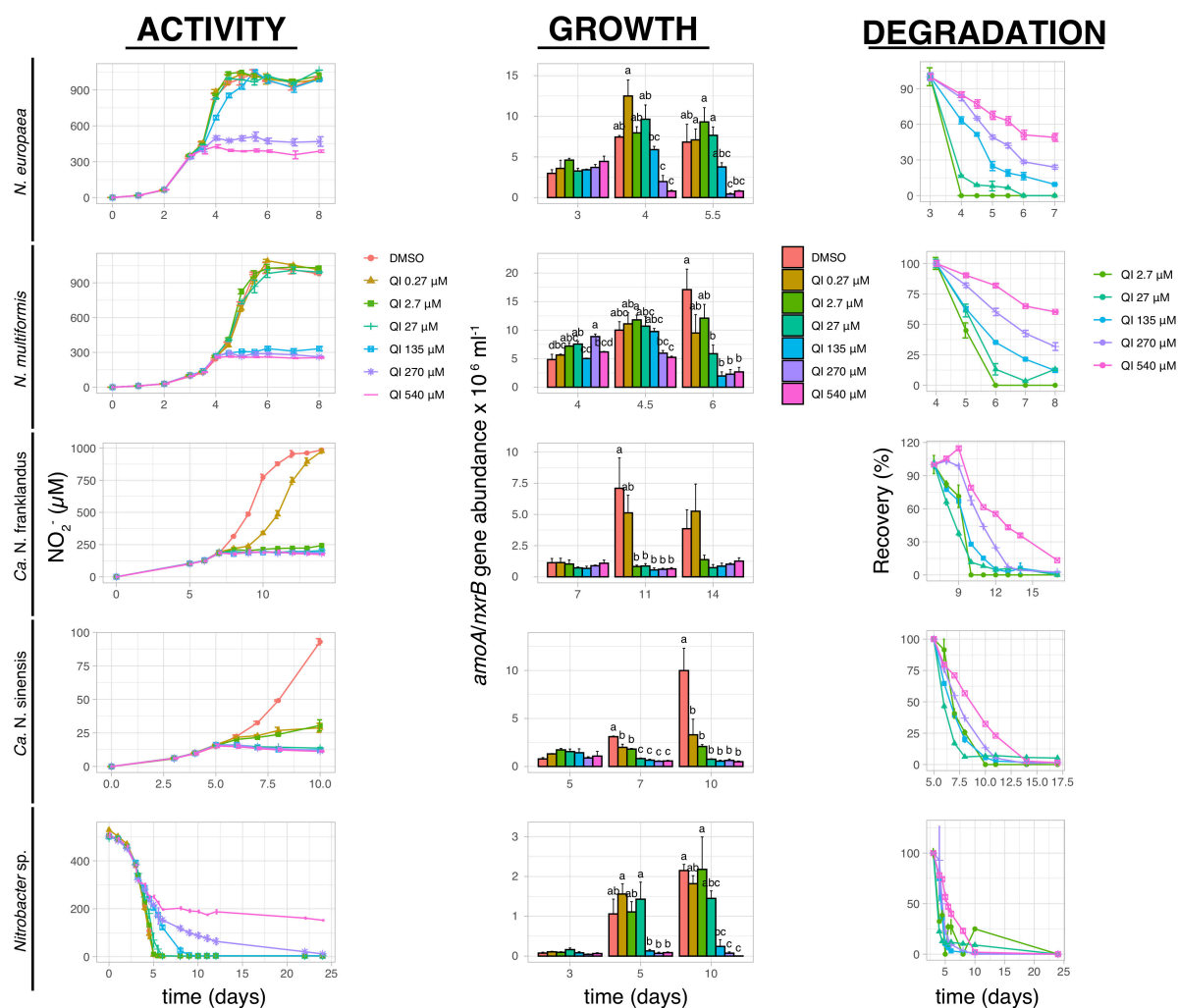


**FIGURE 2 |** The effect of different concentrations of QI on the activity and growth of AOB *N. europaea* and *N. multiformis*, AOA “*Ca. N. franklandus*” and “*Ca. N. sinensis*” and NOB *Nitrobacter* sp. NHB1, determined by nitrite production, or consumption and the abundance of *amoA* or *nxB* genes. The degradation pattern of QI applied over a range of concentrations is also presented. Error bars represent the standard error of the mean of triplicate cultures. At each time point, bars designated by different lower-case letters are significantly different at the 5% level.

persisted in the liquid cultures throughout the experiment (extrapolated  $DT_{50} > 1000$  days; **Supplementary Figure 2** and **Supplementary Table 1**).

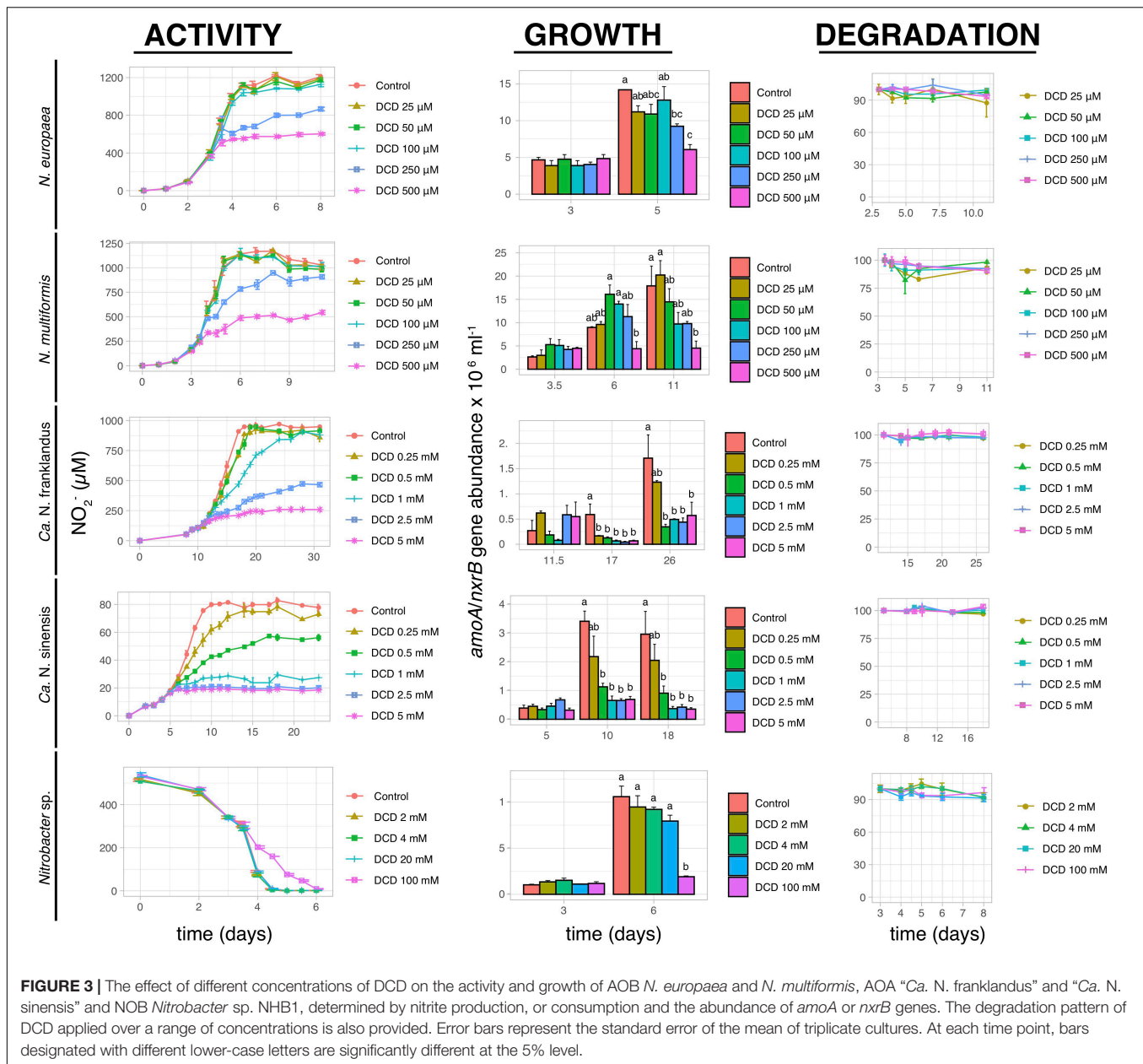
### The Impact and Degradation of DCD on AO and NOB Cultures

Dicyandiamide significantly inhibited ( $p < 0.05$ ) the activity of both AOB strains at concentrations of 250  $\mu$ M and 500  $\mu$ M, with complete inhibition observed only at 500  $\mu$ M (**Figure 3**). These concentrations had a reduced or no effect on the two AOA strains, with the activity of “*Ca. N. franklandus*” and “*Ca. N. sinensis*” being significantly inhibited ( $p < 0.05$ ) at concentrations  $\geq 1$  mM and  $\geq 0.5$  mM, respectively. However, persistent inhibition was evident only at concentrations  $\geq 2.5$  mM and  $\geq 1$  mM, respectively, (**Figure 3**). Nitrite oxidation by *Nitrobacter* sp. was significantly inhibited ( $p < 0.05$ ) by DCD

only at the highest concentration tested (100 mM). The growth inhibition patterns of AOB and NOB were congruent with the  $NO_2^-$  production patterns. This was not the case for AOA where “*Ca. N. franklandus*” growth was significantly reduced at 0.5 mM ( $p \leq 0.05$ ; **Figure 3**). DCD did not show a dose-dependent degradation pattern and was rather persistent with  $DT_{50}$  values ranging from 45.9 to  $>1000$  days (**Figure 3** and **Supplementary Table 1**).

### The Impact and Degradation of NP on AO and NOB Cultures

Nitrapyrin completely inhibited the activity of both *N. europaea* and *N. multiformis* at concentrations  $\geq 5$   $\mu$ M (**Figure 4**). The activity of “*Ca. N. franklandus*” and “*Ca. N. sinensis*” was significantly reduced at concentrations  $\geq 1$   $\mu$ M and  $\geq 5$   $\mu$ M ( $p \leq 0.05$ ), with complete inhibition observed at  $\geq 5$   $\mu$ M



and  $\geq 25 \mu\text{M}$ , respectively, (Figure 4). The activity of *Nitrobacter* sp. NHB1 was fully suppressed at concentrations  $\geq 100 \mu\text{M}$  (Figure 4). The growth inhibition patterns of all tested isolates concurred with the  $\text{NO}_2^-$  production patterns. NP rapidly degraded in all liquid cultures with  $\text{DT}_{50}$  values ranging from 0.12 to 12.5 days (Figure 4 and Supplementary Table 1).

## The Impact and Degradation of DMPP on AO and NOB Cultures

3,4-dimethylpyrazole phosphate induced complete inhibition of nitrite production by *N. europaea* and *N. multiformis* at concentrations  $\geq 10 \mu\text{M}$  and  $\geq 1 \mu\text{M}$ , respectively, (Figure 5). The pattern of AOB growth inhibition was congruent with

$\text{NO}_2^-$  production, except for a weak ( $22.9 \pm 3.9\%$ ) but significant ( $p < 0.05$ ) inhibition of *N. multiformis* growth at  $0.1 \mu\text{M}$  compared to the control. Conversely, DMPP significantly inhibited the activity of both AOA isolates at higher concentrations of  $\geq 0.5 \text{ mM}$  ( $p \leq 0.05$ ), with complete inhibition of “*Ca. N. franklandus*” and *Ca. N. sinensis*” occurring only at  $5 \text{ mM}$  and  $\geq 1 \text{ mM}$ , respectively, (Figure 5). In certain cases, the impact of DMPP on nitrite production was not concomitant with growth patterns, with DMPP concentrations  $\geq 0.5 \text{ mM}$  inducing a persistent reduction in *amoA* gene abundance of “*Ca. N. franklandus*” (Figure 5). DMPP completely inhibited nitrite oxidation by *Nitrobacter* sp. NHB1 only at the highest tested concentrations of  $25 \text{ mM}$ , while its growth was significantly suppressed at concentrations  $\geq 5 \text{ mM}$  ( $p < 0.05$ ; Figure 5). DMPP

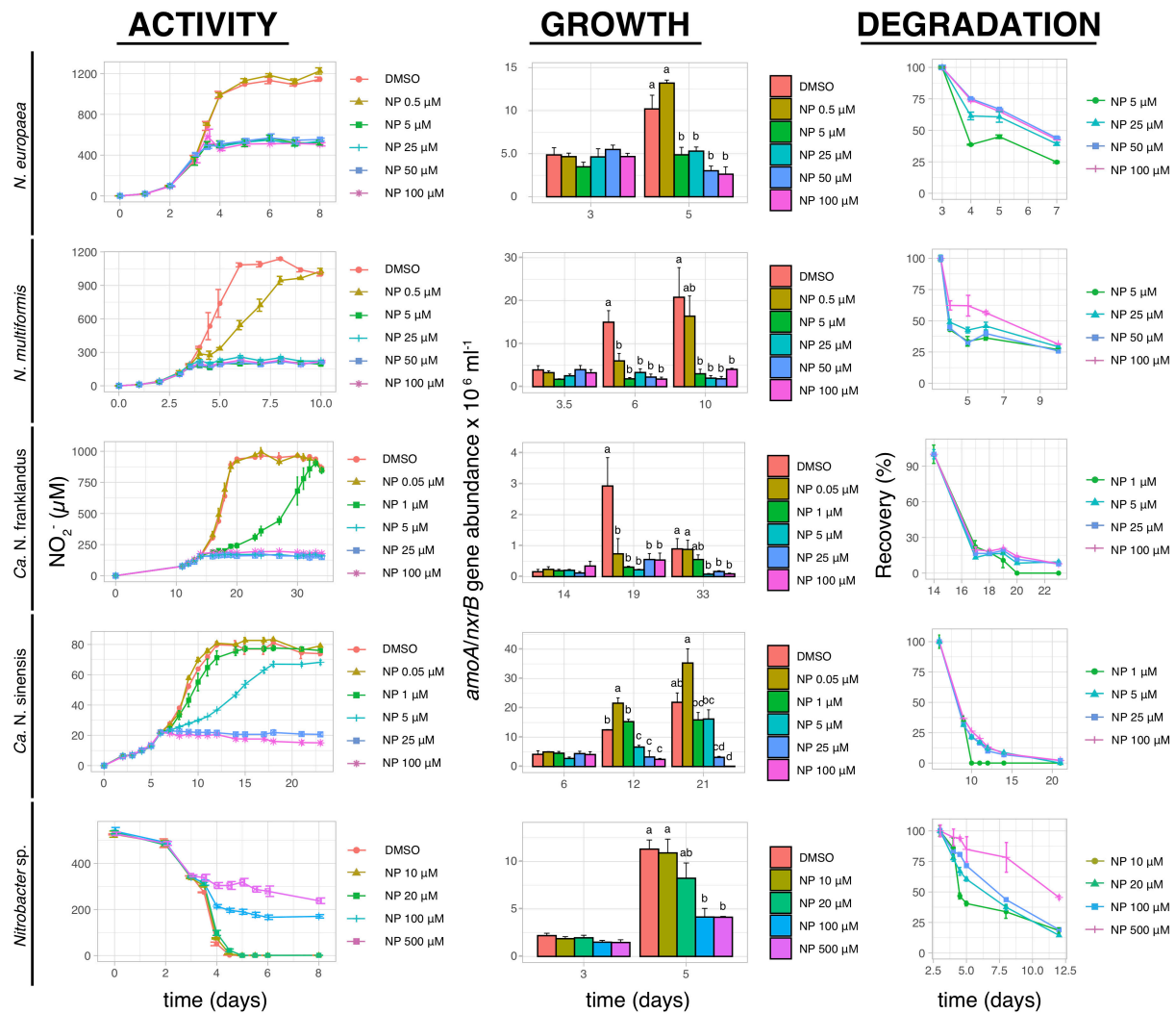


**FIGURE 4 |** The effect of different concentrations of NP on the activity and growth of AOB *N. europaea* and *N. multiformis*, AOA “*Ca. N. franklandus*” and “*Ca. N. sinensis*” and NOB *Nitrobacter sp.* NHB1, determined by nitrite production, or consumption and the abundance of *amoA* or *nxrB* genes. The degradation pattern of NP applied over a range of concentrations is also presented. Error bars represent the standard error of the mean of triplicate cultures. At each time point, bars designated with different lower-case letters are significantly different at the 5% level.

was rather persistent in liquid cultures with its DT<sub>50</sub> values ranging from 14.34 to >1000 days without a dose-dependent degradation pattern (Figure 5 and Supplementary Table 1).

## Comparison of NIs Activity Based on Calculated EC<sub>50</sub> Values

The two AOB isolates showed equivalent EC<sub>50</sub> values for the NIs tested (Figure 6) with the exception of EQ derivatives, where significantly higher EC<sub>50</sub> values were observed for *N. europaea* compared to *N. multiformis* for both QI and EQNL ( $p < 0.001$ ). DMPP and NP were the most potent inhibitors of *N. europaea*, followed by EQ, QI, and DCD which were not significantly different, with EQNL being the weakest inhibitor (EC<sub>50</sub> = 181.4 ± 23.3 μM). For *N. multiformis*, DMPP, NP, and QI were equally effective inhibitors, followed by EQ, DCD, and

EQNL. The two AOA strains exhibited contrasting responses, with “*Ca. N. franklandus*” having decreased sensitivity to DCD and DMPP compared to “*Ca. N. sinensis*.” EQ, its derivatives and NP were equally effective inhibitors of both AOA isolates, with QI having the lowest EC<sub>50</sub> values (0.3 ± 0.0–0.7 ± 0.4 μM), while DCD and DMPP were the weakest AOA inhibitors (Figure 6). EQ, its derivatives and NP were equally suppressive toward *Nitrobacter sp.* NHB1, while DMPP and DCD showed no appreciable inhibition.

## DISCUSSION

This study is the first to investigate the inhibitory effect of EQ, a novel NI of potential agricultural relevance, and its oxidation derivatives, QI and EQNL, on soil nitrifiers grown



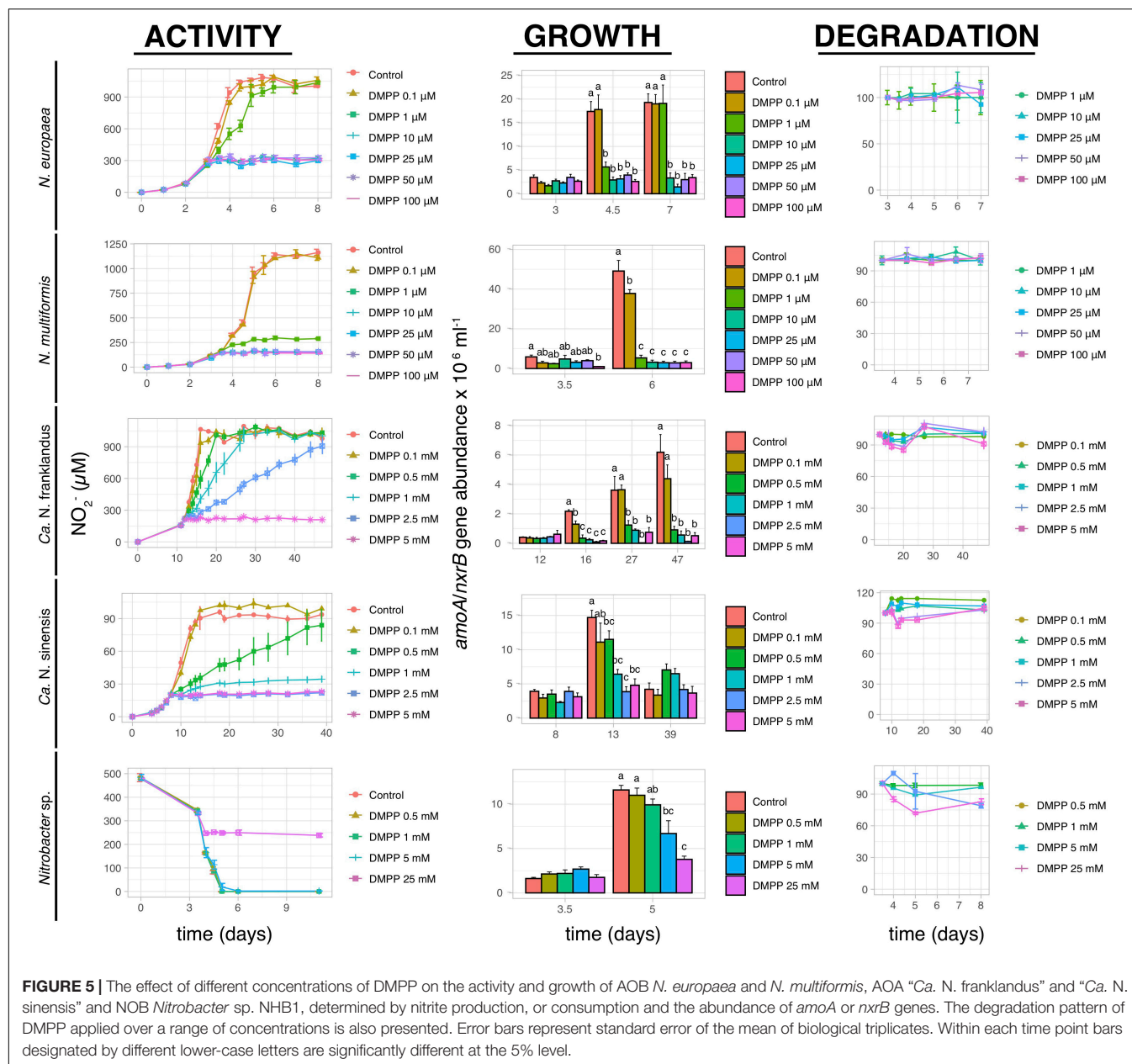


**FIGURE 5 |** The effect of different concentrations of DMPP on the activity and growth of AOB *N. europaea* and *N. multiformis*, AOA “*Ca. N. franklandus*” and “*Ca. N. sinensis*” and NOB *Nitrobacter* sp. NHB1, determined by nitrite production, or consumption and the abundance of *amoA* or *nxrB* genes. The degradation pattern of DMPP applied over a range of concentrations is also presented. Error bars represent standard error of the mean of biological triplicates. Within each time point bars designated by different lower-case letters are significantly different at the 5% level.

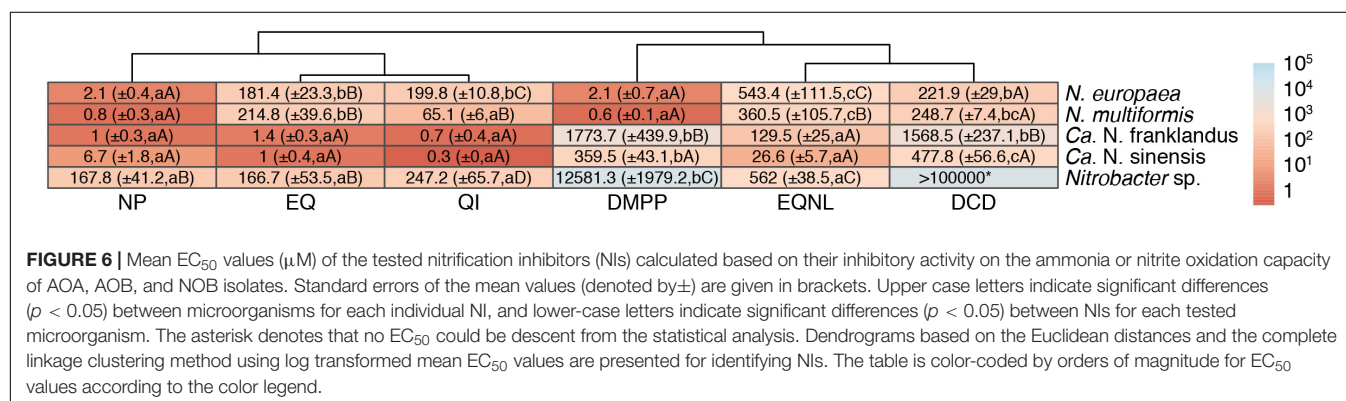


**FIGURE 6 |** Mean  $\text{EC}_{50}$  values ( $\mu\text{M}$ ) of the tested nitrification inhibitors (NIs) calculated based on their inhibitory activity on the ammonia or nitrite oxidation capacity of AOA, AOB, and NOB isolates. Standard errors of the mean values (denoted by  $\pm$ ) are given in brackets. Upper case letters indicate significant differences ( $p < 0.05$ ) between microorganisms for each individual NI, and lower-case letters indicate significant differences ( $p < 0.05$ ) between NIs for each tested microorganism. The asterisk denotes that no  $\text{EC}_{50}$  could be descendent from the statistical analysis. Dendrograms based on the Euclidean distances and the complete linkage clustering method using log transformed mean  $\text{EC}_{50}$  values are presented for identifying NIs. The table is color-coded by orders of magnitude for  $\text{EC}_{50}$  values according to the color legend.



in pure cultures and demonstrate greater inhibition of all three compounds on AOA compared to AOB isolates. In all cultures, EQ was rapidly transformed to QI and EQNL, with the former being the major but least persistent derivative, while the latter being the minor but more persistent derivative, and was consistent with previous studies in soil (Karas et al., 2015; Papadopoulou et al., 2016). Considering that (i) in all cultures, QI showed equivalent or higher inhibitory activity compared to its parent compound, and (ii) in EQ-amended cultures, QI was formed at concentrations equal or higher than those expected to induce an inhibitory effect on the AO tested, and EQNL was formed at levels substantially lower than those expected to result in an inhibitory effect on the AO tested (Figure 1 and Supplementary Table 2), we suggest that QI is the main determinant for the persistent inhibitory effect of EQ on AO and NOB, in line with our previous soil studies (Papadopoulou et al., 2016). The higher inhibition potential of QI for AOA compared to AOB isolates, contradicts our previous soil studies, where equivalent inhibitory effects against both groups were observed. Although direct comparisons between soil and culture studies cannot be made, we suggest that the concentrations of QI formed in soil samples (up to  $86.1 \mu\text{mol Kg}^{-1}$  dwt soil) probably reached or exceeded its inhibition threshold levels for both AO groups.

In contrast to EQ and its derivatives, DCD and DMPP exhibited higher inhibitory activity toward AOB isolates as observed by Shen et al. (2013) who reported greater inhibition by DCD on *N. multiformis* compared to the AOA *N. viennensis*. Of these two NIs, DMPP showed greater inhibitory activity toward both AOB isolates. Data on the inhibitory activity of DMPP toward soil-derived cultures of AOB and AOA strains are scarce. Liu et al. (2019) recently reported greater inhibition by DMPP ( $\text{EC}_{50} = 448 \mu\text{M}$ ) compared to DCD ( $\text{EC}_{50} = 947.1 \mu\text{M}$ ) to “*Ca. Nitrosocosmicus agrestis*,” a soil strain closely related to “*Ca. N. franklandus*.” Unlike DMPP, there are several reports on the inhibitory activity of DCD on soil AOA and AOB cultures with DCD strongly inhibiting *Nitrososphaera* sp. JG1 (Kim et al., 2012) and *Ca. Nitrosarchaeum koreensis* MY1 (Jung et al., 2011) at 0.5 mM which was in the same range to the two AOA strains examined here. Lehtovirta-Morley et al. (2013) showed that DCD induced a significant inhibition of “*Ca. Nitrosotalea devanattera*” at 1 mM, compared to 0.5 mM needed for the inhibition of “*Ca. N. sinensis*” in our study. Others reported  $\text{EC}_{50}$  values of  $950 \mu\text{M}$  for “*Ca. N. agrestis*” (Liu et al., 2019), and  $940.6 \mu\text{M}$  for *N. viennensis* (Shen et al., 2013) compared to  $1568.5 \mu\text{M}$  observed here for “*Ca. N. franklandus*.” For AOB, Shen et al. (2013) reported an  $\text{EC}_{50}$  of  $80.3 \mu\text{M}$  for DCD on *N. multiformis* compared to  $248.7 \mu\text{M}$  observed in our study for the same strain. Although there are no obvious differences between the two studies explaining this variation, the salt and concentration of ammonium was different which may have affected the growth characteristics of *N. multiformis*.

Nitrapyrin was the only tested NI that showed an equivalent and strong inhibitory effect toward both AOB and AOA isolates, suppressing their activity at concentrations  $\geq 0.5$ – $5 \mu\text{M}$  and  $\geq 1$ – $5 \mu\text{M}$ , respectively. This in line with previous studies which showed inhibition of AOB (*Nitrosomonas* sp., *Nitrospira* sp., *Nitrosolobus* sp., *N. europaea*, *N. multiformis*) and AOA strains

(*Nitrososphaera* sp. JG1, *Nitrosarchaeum koreensis* MY1) at levels varying from  $0.86 \mu\text{M}$  for AOB (Bélser and Schmidt, 1981) to  $10 \mu\text{M}$  for both AOB and AOA (Jung et al., 2011; Kim et al., 2012; Martens-Habbena et al., 2015). Comparison with other AOA isolates indicates that inhibition characteristics are similar between strains belonging to the same phylogenetic group. For example, Lehtovirta-Morley et al. (2013) demonstrated that NP halted the activity of “*Ca. N. devanattera* ND1” at concentrations  $\geq 10 \mu\text{M}$  compared to  $\geq 5 \mu\text{M}$  for “*Ca. N. sinensis* (ND2)” in our study, while Liu et al. (2019) reported an  $\text{EC}_{50}$  of  $0.6 \mu\text{M}$  for “*Ca. N. agrestis*” compared to  $1 \mu\text{M}$  for “*Ca. N. franklandus*” in our study. However, in contrast to our findings for NP inhibition of *N. multiformis* ( $\text{EC}_{50} 0.8 \pm 0.3 \mu\text{M}$ ), Shen et al. (2013) reported a much weaker inhibitory effect for the same strain ( $\text{EC}_{50} > 173 \mu\text{M}$ ). In addition to the minor differences in cultivation conditions between the two studies, Shen et al. added solid NP directly into the cultures to achieve concentrations in the range of  $40$ – $173 \mu\text{M}$ , with the highest level corresponding to the upper limit of NP water solubility at  $20^\circ\text{C}$  ( $40 \text{ mg L}^{-1}$ ), entailing a risk for precipitation of the active compound.

The considerable range in the inhibitory concentrations of the tested NIs may indicate differences in their mode of action not considered previously. For example, DCD, DMPP, and NP, all considered as Cu-chelators, varied in their ability to inhibit AOA (Lehtovirta-Morley et al., 2013; Shen et al., 2013; Liu et al., 2019). In addition, NP has also been proposed to function as an alternative AMO substrate, generating 6-chloropicolinic acid which irreversibly deactivates ammonia oxidation (Vannelli and Hooper, 1992). This inhibitory mechanism proposed for NP may offer an explanation for its rather universal inhibitory activity toward AOA and AOB. Both EQ and its derivatives possess high-antioxidative capacity acting as free radical scavengers (Błaszczuk et al., 2013). As EQ and its degradation product QI showed similar inhibitory effects to NO-scavengers (e.g., PTIO; Martens-Habbena et al., 2015), their efficiency against AOA may be due to a similar mode of action. Alternatively, as QI is a strong antioxidant, it could be involved in oxidative stress-related cell disruption particularly in AOA, with AOB being capable of coping with oxidative stress using catalases, enzymes which are largely absent in AOA (Kim et al., 2016).

In addition to the contrasting differences in sensitivity between AOA and AOB to all NIs tested (except for NP), we also observed differences in the sensitivity between the two AOA or two AOB strains examined. For QI and EQNL, *N. multiformis* was consistently more sensitive than *N. europaea*, and for DCD and DMPP, “*Ca. N. sinensis*” was consistently more sensitive than “*Ca. N. franklandus*.” Studies on the comparative sensitivity of AOB isolates to chemicals, including NIs, are scant. Brandt et al. (2001) reported a higher sensitivity of *N. multiformis* over *N. europaea* to linear alkylbenzene sulfonate surfactants. The different sensitivity of the two AOB isolates to EQ derivatives is probably related to differences in the physiology of these isolates. Comparative genomic and proteomic analysis of *N. europaea* and *N. multiformis* showed that the two strains possess a largely different set of stress response proteins, alkyl hydroperoxide reductase vs superoxide dismutase and rubrerythrin, respectively, that might exhibit different efficiencies to stress imposed by QI

and EQNL (Zorz et al., 2018). Alternatively, *N. europaea* has a greater array of membrane protein transporters, potentially enabling a greater efflux of toxic chemicals (Zorz et al., 2018).

The different sensitivities of the two tested AOA isolates to DCD and DMPP are also associated with the contrasting ecophysiologicals (Lehtovirta-Morley et al., 2014, 2016). In line with our findings, previous studies comparing the two strains reported a higher sensitivity of “*Ca. N. sinensis*” to both simvastatin (Zhao et al., 2020) and 3,5-dichloraniline (Vasileiadis et al., 2018). The higher tolerance of “*Ca. N. franklandus*” to DCD and DMPP might be associated with its capacity to produce extracellular polymeric substances (EPS) leading to aggregate formation that block the hydrophilic NIs DCD and DMPP of accessing the surface of cells engulfed into hydrophobic EPS (Gao et al., 2007). This production of EPS is a feature shared by all *Ca. Nitrosocosmicus* isolates (Jung et al., 2016; Lehtovirta-Morley et al., 2016; Sauder et al., 2017; Alves et al., 2019; Liu et al., 2019) and has been reported as a protection mechanism of AOB against NIs (Powell and Prosser, 1991).

The comparative analysis of the inhibitory range of the tested NIs highlights the practical implications of our findings. The two most widely used NIs, DCD, and DMPP, showed high inhibitory activity only to AOB, the latter being the most potent AOB inhibitor together with NP. While NP is the only NI currently used in agriculture that demonstrates equal inhibition of both AOB and AOA, it is not currently registered for use in Europe. These findings have serious practical implications for nitrification inhibition in agricultural soils with acidic to neutral pH, which constitute 30% of the World's soils (pH < 5.5) and a large fraction of European agricultural soils (mean soil pH = 5.8; Fabian et al., 2014), and where ammonia oxidation is often dominated by AOA (Zhao et al., 2020). Differences in the inhibition thresholds between AOA and AOB could affect agricultural practice, as AOA may contribute to nitrogen fertilizer loss under conditions when AOB are inhibited (Hink et al., 2018). Conversely, universal inhibitory effects on both AOB and AOA, and perhaps comammox bacteria recently reported to be inhibited by NP (primarily), DCD and DMPP in soil microcosm studies (Li et al., 2019b), suggest that nitrification inhibition would not be compromised by functional redundancy. Alternatively, the use of mixtures of NIs exhibiting complementary activity against different AO groups or targeting different parts of the ammonia oxidation pathway could be as efficient as using broad range NIs. In this regard, the potential agricultural use of EQ as a novel NI, applied alone or in combination with NIs selective to AOB (i.e., DMPP) could be promising, considering its low cost (equivalent or lower than that of DCD and NP; Błaszczuk et al., 2013), and its unique feature to be transformed in soil to QI, a highly potent inhibitor of AOA and whose activity to AOB is comparable with that of NIs currently used in agricultural settings such as DCD. Although extrapolating from pure culture tests to predicted effects in soil should be performed with caution, based on our liquid culture assays, a soil concentration of 10 mg Kg<sup>-1</sup> of EQ (corresponding to 14.4 Kg ha<sup>-1</sup>, assuming incorporation of the NI to the top 5 cm of the soil profile of a field site of 1 ha, and soil bulk density 1.3 g cm<sup>3</sup>) could have a universal inhibitory effect on both AOA and AOB, while 0.06 mg Kg<sup>-1</sup> (<0.1 Kg ha<sup>-1</sup>)

would be required to achieve effective inhibition AOA only. This is consistent with earlier studies that showed that EQ, when applied in soil at concentration levels (50 mg Kg<sup>-1</sup>) simulating a wastewater disposal scenario, resulted in inhibition of both AOA and AOB (Papadopoulou et al., 2016). Such application rates are in the same range as those of established NIs, providing the first evidence for the feasibility of EQ use in an agricultural setting. On-going studies will determine the effective dose rates of EQ under full-scale agricultural conditions.

There is less known about the direct effects of NIs on NOB, despite their important regulatory function in the overall nitrification process (Daims et al., 2016). NOB are closely associated with AOs and their activity results in the rapid conversion of potentially toxic nitrite to nitrate (Matsumoto et al., 2009), an important nitrogen source for plants and aerobic soil microorganisms (Koch et al., 2015). In disturbed agricultural ecosystems such as fertilized soils, NOB-derived nitrate production contributes to N losses and environmental pollution through nitrate leaching and subsequent denitrification processes (Raun and Johnson, 1999). We demonstrated that DMPP and DCD were not active against *Nitrobacter* sp. NHB1, in contrast to NP, EQ, and its derivatives which were suppressive to the tested isolate in μM concentration levels. Our study was the first to provide data regarding the impact of DCD, DMPP, EQ, and its derivatives on a pure NOB culture, while NP previously applied at rates up to 50 μM did not inhibit the nitrite-oxidizing activity of the widely distributed *Nitrobacter agilis* (Matsuba et al., 2003), in line with our results.

The impact of NP, EQ, and its derivatives on the activity of both AOs and NOB could affect the total nitrogen balance, and the direction and degree of nitrogen transformation during the nitrification process. This could have serious practical and ecological implications in cases where NIs inhibit NOB to a greater extent than AOs. This would lead to possible NO<sub>2</sub><sup>-</sup> accumulation in soil and increased NO<sub>2</sub><sup>-</sup> driven N<sub>2</sub>O production (Venterea et al., 2015) with reciprocal effects for the environment and plant productivity. However, our findings suggest a lower (DCD, NP, DMPP, and QI) or equivalent (EQ) inhibition potential of NIs against *Nitrobacter* sp. compared to AOs (Figure 6). Further studies extended to other NOB, including the widely distributed and diverse *Nitrospira*-like bacteria, would determine the full inhibitory potential of NIs on soil NOB.

In parallel, we determined the degradation and transformation of the tested NIs to identify potential links between the duration of exposure (persistence) and the effects observed. The total residues of EQ showed limited persistence in the AOA and NOB cultures (DT<sub>50</sub> = 2.4–8.7 days), and low to moderate persistence in the AOB cultures (DT<sub>50</sub> = 8.7–60.1 days), a difference most likely attributed to abiotic factors such as medium pH (acidic for *Ca. N. sinensis* and *Nitrobacter* sp. vs. alkaline for *N. europaea* and *N. multiformis*) rather than an enzymatic transformation, considering the autotrophic lifestyle of the tested isolates (Kim et al., 2016), the lack of genetic repertoire for the catabolism of organic pollutants (Chain et al., 2003; Norton et al., 2008), and the recalcitrance of EQ to biotic degradation under aerobic and anaerobic conditions (Shah et al., 2005). However, a direct

interaction of these compounds with the tested organisms cannot be fully excluded. The three commercial NIs showed remarkably different stability in the liquid cultures. DCD showed moderate to high persistence ( $DT_{50s} = 44.5$  to  $>1000$  days) with the lowest  $DT_{50}$  values observed in the liquid cultures of *Nitrobacter* sp. NHB1, suggesting a potential interaction with this strain. Microbial mineralization of DCD by pure cultures of soil isolated bacteria has been previously reported (Hallinger et al., 1990; Hawser and Haselwandter, 1990). Later studies suggested an enzymatic hydrolysis of the NI catalyzed by microbial ureases (Estermaier et al., 1992). This was not confirmed in our study since no significant differences in the stability of DCD between urease-positive (*N. multiformis*, *Ca. N. franklandus*) and urease-negative (*N. europaea*, *Ca. N. sinensis*, and *Nitrobacter* sp. NHB1) AOs were observed. Abiotic parameters such as temperature or pH could potentially influence the stability of DCD in soil (Amberger, 1986; Hallinger et al., 1990; Kelliher et al., 2008). However, in our studies we did not observe any clear effects of temperature (28°C for AOB and NOB, and 35°C for AOA) and pH (7.5–8.0 for AOB and *Ca. N. franklandus*, and 5.2 for *Ca. N. sinensis* and *Nitrobacter* sp. NHB1) on DCD stability in our liquid culture conditions. NP degraded rapidly ( $DT_{50} = 0.12$ –12.5 days) in all liquid cultures. In contrast, DMPP showed a high persistence in all liquid cultures, except of *Nitrobacter* where a great variation in its persistence was evident. Considering that *Nitrobacter* sp. NHB1 and AOA were cultured in media of similar content and pH, the above variation was most probably driven by interaction between DMPP and the bacterium. Genomic analysis suggested limited catabolic capacity of aromatic compounds by *Nitrobacter* strains (Starkenbourg et al., 2008), although some studies have shown an appreciable degradation of crude oil by *Nitrobacter* (Jong and Okpokwasili, 2012). Overall, we did not observe any clear correlations between NIs persistence and inhibition potency, except for the lower persistence of DCD and DMPP in the liquid cultures of *Nitrobacter* sp. NHB1 which coincided with the limited activity of these NIs to the bacterium.

## CONCLUSION

We compared the inhibition potential of EQ, a novel NI, and those currently used in agricultural practice, on the activity and growth of soil-derived AOA, AOB, and NOB isolates grown in liquid culture. EQ, and primarily its major derivative QI, showed high potency against AOA, in contrast to DCD and DMPP (the only NIs currently registered for use in Europe) which were inhibitory to AOB only. Conversely, NP showed an equally high inhibitory activity against both AOA and AOB isolates. EQ, QI, and NP were the most potent AOA and NOB inhibitors, unlike DCD and DMPP, which demonstrated no activity. DMPP and NP were the most potent AOB inhibitors, with EQ, QI, and DCD showing lower but still appreciable inhibitory activity. Our study (i) offers benchmarking knowledge of the activity range of currently used in agriculture and potentially new NIs to soil AO and *Nitrobacter* NOB, whose response to NIs were unknown, (ii) introduces a novel potential NI, EQ, which

possesses desirable characteristics, including transformation into a highly potent NI (QI) characterized by high inhibitory activity against AOA compared to currently registered NIs in Europe, and (iii) demonstrates the different sensitivity of AOA and AOB to NIs, which indicates that novel strategies for effective nitrification inhibition should rely on new broad-range NIs, or more likely, mixtures of NIs with complementary activity against different nitrifier groups. Future work will focus on the elucidation of EQ and QI inhibitory mechanisms, and on the evaluation of their environmental and agronomic performance under diverse edaphic and climatic conditions and on soils with different microbial communities.

## DATA AVAILABILITY STATEMENT

The raw data supporting the conclusions of this article will be made available by the authors, without undue reservation.

## AUTHOR CONTRIBUTIONS

EP planned, performed, and supervised the experiments, carried out data analysis, drafted and revised the final manuscript. EB, EL, EA, and AK participated in parts of the culture inhibition assays. SV performed the modeling for the calculation of  $EC_{50}$  and  $DT_{50}$  values, constructed and edited data figures, and reviewed the manuscript. CT planned and participated in part of the culture inhibition assays. UM-S supervised the chemical synthesis of EQ derivatives and reviewed the manuscript. GN provided nitrifying cultures, supervised part of the culture inhibition assays, and reviewed the manuscript. DK conceived the experimental rationale, co-supervised the experiments, and reviewed the manuscript. All authors contributed to the article and approved the submitted version.

## FUNDING

This work is part of the project “NITRIC – Looking up for Novel nITRification Inhibitors: New stories with old Compounds” which has received funding from the Hellenic Foundation for Research and Innovation (HFRI) and the General Secretariat for Research and Technology (GSRT), under grant agreement No. 1229. CT and GN were funded by the AXA Research Fund.

## ACKNOWLEDGMENTS

This manuscript has been released as a pre-print at [bioRxiv], (Papadopoulou et al., 2020 at doi: <https://doi.org/10.1101/2020.04.07.023168>).

## SUPPLEMENTARY MATERIAL

The Supplementary Material for this article can be found online at: <https://www.frontiersin.org/articles/10.3389/fmicb.2020.581283/full#supplementary-material>



**Supplementary Figure 1 |** The chemical structures of the tested nitrification inhibitors (NIs).

**Supplementary Figure 2 |** The effect of different concentrations of EQNL on the activity and growth of AOB *N. europaea* and *N. multiformis*, AOA “*Ca. N. franklandus*” and “*Ca. N. sinensis*” and NOB *Nitrobacter* sp. NHB1, determined by nitrite production or consumption and the abundance of *amoA* or *nrxB* genes. The degradation pattern of EQNL applied at a range of concentrations in the liquid cultures of the nitrifying isolates, is also presented. Error bars represent the standard error of the mean of triplicate cultures. Within each time point bars designated by different lower-case letters are significantly different at the 5% level.

**Supplementary Figure 3 |** The degradation and transformation patterns of EQ in the liquid cultures of “*Ca. N. franklandus*” (a, b) and “*Ca. N. sinensis*” (c, d)

amended with 4.6  $\mu\text{M}$  (a, c) and 46  $\mu\text{M}$  of EQ (b, d). Each value is the mean of triplicates  $\pm$  standard error. Bars designated by one asterisk show the concentration of EQ and its oxidative derivatives at the onset of inhibition, while bars designated by two asterisks indicate the time point when maximum QI concentrations were observed.

**Supplementary Table 1 |** DT<sub>50</sub> values (days) of the different nitrification inhibitors (NIs) tested per nitrifying isolate and NI concentrations used. DT<sub>50</sub> values were calculated by fitting the best fitting kinetic model to the degradation data.

**Supplementary Table 2 |** Mean concentrations  $\pm$  standard errors ( $\mu\text{M}$ ) of QI and EQNL formed in liquid cultures of nitrifying isolates amended with EQ at the (i) onset of inhibition, and (ii) time of detection of their maximum concentration levels. The timepoint (days) at which each measurement was taken is given in brackets.

## REFERENCES

- Abbasi, M. K., and Adams, W. A. (1998). Loss of nitrogen in compacted grassland soil by simultaneous nitrification and denitrification. *Plant Soil* 200, 265–277.
- Alves, R. J. E., Kerou, M., Zappe, A., Bittner, R., Abby, S. S., Schmidt, H. A., et al. (2019). Ammonia oxidation by the arctic terrestrial Thaumarchaeote *Candidatus Nitrosocosmicus arcticus* is stimulated by increasing temperatures. *Front. Microbiol.* 10:1571. doi: 10.3389/fmicb.2019.01571
- Amberger, A. (1986). Potentials of nitrification inhibitors in modern N-fertilizer management. *Z. Pflanzenernaehr. Bodenk.* 149, 469–484. doi: 10.1002/jpln.19861490410
- Bédard, C., and Knowles, R. (1989). Physiology, biochemistry, and specific inhibitors of CH<sub>4</sub>, NH<sub>4</sub><sup>+</sup>, and CO oxidation by methanotrophs and nitrifiers. *Microbiol. Rev.* 53, 6–84.
- Beekman, F., Motte, H., and Beekman, T. (2018). Nitrification in agricultural soils: impact, actors and mitigation. *Curr. Opin. Biotechnol.* 50, 166–173. doi: 10.1016/j.copbio.2018.01.014
- Bélser, L. W., and Schmidt, E. L. (1981). Inhibitory effect of nitrapyrin and the three genera of ammonia-oxidizing nitrifiers. *Appl. Environ. Microbiol.* 41, 819–821. doi: 10.1128/aem.41.3.819-821.1981
- Błaszczak, A. B., Augustyniak, A., and Skolimowski, J. (2013). Ethoxyquin: an antioxidant used in animal feed. *Int. J. Food Sci.* 2013:585931.
- Brandt, K., Hesselsoe, M., Roslev, P., Henriksen, K., and Sorensen, J. (2001). Toxic effects of linear alkylbenzene sulfonate on metabolic activity, growth rate, and microcolony formation of *Nitrosomonas* and *Nitrospira* strains. *Appl. Environ. Microbiol.* 67, 2489–2498. doi: 10.1128/aem.67.6.2489-2498.2001
- Chain, P., Lamerdin, J., Larimer, F., Regala, W., Lao, V., Land, M., et al. (2003). Complete genome sequence of the ammonia-oxidizing bacterium and obligate chemolithoautotroph *Nitrosomonas europaea*. *J. Bacteriol.* 185, 2759–2773. doi: 10.1128/jb.185.9.2759-2773.2003
- Coskun, D., Britto, D. T., Shi, W., and Kronzucker, H. J. (2017). Nitrogen transformations in modern agriculture and the role of biological nitrification inhibition. *Nat. Plants* 3:17074.
- Daims, H., Lebedeva, E. V., Pjevac, P., Han, P., Herbold, C., Albertsen, M., et al. (2015). Complete nitrification by *Nitrospira* bacteria. *Nature* 528, 504–509. doi: 10.1038/nature16461
- Daims, H., Lucker, S., and Wagner, M. (2016). A new perspective on microbes formerly known as nitrite-oxidizing bacteria. *Trends Microbiol.* 24, 699–712. doi: 10.1016/j.tim.2016.05.004
- de Boer, W., Klein Gunnewiek, P. G. A., Veenhuis, L. M., Bock, E., and Laanbroek, H. J. (1991). Nitrification at low pH by aggregated chemolithotrophic bacteria. *Appl. Environ. Microbiol.* 57, 3600–3604. doi: 10.1128/aem.57.12.3600-3604.1991
- Estermaier, L. M., Heidemarie Sieber, A., Lottspeich, F., Matern, D. H. M., and Hartmann, G. R. (1992). Biochemical degradation of cyanamide and dicyandiamide. *Angew. Chem. Int. Ed. Engl.* 31, 620–622. doi: 10.1002/anie.199206201
- Fabian, C., Reimann, C., Fabian, K., Birke, M., Baritz, R., and Haslinger, E. (2014). GEMAS: spatial distribution of the pH of European agricultural and grazing land soil. *Appl. Geochem.* 48, 207–216. doi: 10.1016/j.apgeochem.2014.07.017
- FOCUS (2006). *Guidance Document on Estimating Persistence and Degradation Kinetics From Environmental Fate Studies on Pesticides in EU Registration*. Report of the FOCUS Work Group on Degradation Kinetics, EC Document Reference Sanco/10058/2005 Version, 2.0, 434. Available online at: [https://esdac.jrc.ec.europa.eu/public\\_path/projects\\_data/focus/dk/docs/finalreportFOCDegKinetics.pdf](https://esdac.jrc.ec.europa.eu/public_path/projects_data/focus/dk/docs/finalreportFOCDegKinetics.pdf)
- Fowler, D., Coyle, M., Skiba, U., Sutton, M. A., Cape, J. N., Reis, S., et al. (2018). The global nitrogen cycle in the twenty first century. *Philos. Trans. R. Soc. B Biol. Sci.* 368:20130164.
- Francis, C. A., Roberts, K. J., Beman, J. M., Santoro, A. E., and Oakley, B. B. (2005). Ubiquity and diversity of ammonia-oxidizing archaea in water column sand sediments of the ocean. *Proc. Natl. Acad. Sci. U.S.A.* 102, 14683–14688. doi: 10.1073/pnas.0506625102
- Gao, B., Zhu, X., Xu, Q., Yue, Q., Li, W., and Wei, J. (2007). Influence of extracellular polymeric substances on microbial activity and cell hydrophobicity in biofilms. *J. Chem. Technol. Biotechnol.* 83, 227–232. doi: 10.1002/jctb.1792
- Goring, C. A. I. (1962). Control of nitrification of ammonium fertilizers and urea by 2-chloro-6-(trichloromethyl)-pyridine. *Soil Sci.* 93, 211–218. doi: 10.1097/00010694-196203000-00010
- Hallinger, S., Wallnöfer, P. R., Goldbach, H., and Amberger, A. (1990). Several aspects of bacterial dicyandiamide degradation. *Naturwissenschaften* 77, 332–334. doi: 10.1007/bf01138389
- Hawser, M., and Haselwandter, K. (1990). Degradation of dicyandiamide by soil bacteria. *Soil Biol. Biochem.* 22, 113–114.
- Herbold, C. W., Lehtovirta-Morley, L. E., Jung, M. Y., Jehmlich, N., Hausmann, B., Han, P., et al. (2017). Ammonia-oxidising archaea living at low pH: insights from comparative genomics. *Environ. Microbiol.* 19, 4939–4952. doi: 10.1111/1462-2920.13971
- Hink, L., Gubry-Rangin, C., Nicol, G. W., and Prosser, J. I. (2018). The consequences of niche and physiological differentiation of archaeal and bacterial ammonia oxidisers for nitrous oxide emissions. *ISME J.* 12, 1084–1093. doi: 10.1038/s41396-017-0025-5
- Jong, R. C., and Okpokwasili, G. C. (2012). Crude oil-degradation and plasmid profile of nitrifying bacteria isolated from oil-impacted mangrove sediment in the Niger Delta of Nigeria. *Bull. Environ. Contam. Toxicol.* 88, 1020–1026. doi: 10.1007/s00128-012-0609-8
- Jung, M. Y., Kim, J. G., Damsté, J. S. S., Rijpstra, W. I. C., Madsen, E. L., Kim, S. J., et al. (2016). A hydrophobic ammonia-oxidizing archaeon of the *Nitrosocosmicus* clade isolated from coal tar-contaminated sediment. *Environ. Microbiol. Rep.* 8, 983–992. doi: 10.1111/1758-2229.12477
- Jung, M.-Y., Park, S.-J., Min, D., Kim, J.-S., Rijpstra, W. I. C., Damsté, J. S. S., et al. (2011). Enrichment and characterization of an autotrophic ammonia-oxidizing Archaeon of mesophilic Crenarchaeal Group I.1a from an agricultural soil. *Appl. Environ. Microbiol.* 77, 8635–8647. doi: 10.1128/aem.05787-11
- Karas, P., Metsoviti, A., Zisis, V., Ehalotis, C., Omirou, M., Papadopolou, E., et al. (2015). Dissipation, metabolism and sorption of pesticides used in fruit-packaging plants: towards an optimized depuration of their pesticide-contaminated agro-industrial effluents. *Sci. Total Environ.* 530–531, 129–139. doi: 10.1016/j.scitotenv.2015.05.086
- Kelliher, F. M., Clough, T. J., Clark, H., Rys, G., and Sedcole, J. R. (2008). The temperature dependence of dicyandiamide (DCD) degradation in soils: a data synthesis. *Soil Biol. Biochem.* 40, 1878–1882. doi: 10.1016/j.soilbio.2008.03.013
- Kim, J.-G., Jung, M.-Y., Damsté, J. S. S., Schouten, S., Rijpstra, W. I. C., Jung, M.-Y., et al. (2016). *Nitrosopumilus maritimus* genome reveals unique mechanisms for nitrification and autotrophy in globally distributed marine crenarchaea. *Proc. Natl. Acad. Sci. U.S.A.* 113, 7888–7893.

- Kim, J.-G., Jung, M.-Y., Park, S.-J., Rijpstra, W. I. C., Damsté, J. S. S., Madsen, E. L., et al. (2012). Cultivation of a highly enriched ammonia-oxidizing archaeon of thaumarchaeotal group I.1b from an agricultural soil. *Environ. Microbiol.* 14, 1528–1543. doi: 10.1111/j.1462-2920.2012.02740.x
- Kits, K. D., Sedlacek, C. J., Lebedeva, E. V., Han, P., Bulaev, A., Pjevac, P., et al. (2017). Kinetic analysis of a complete nitrifier reveals an oligotrophic lifestyle. *Nature* 549, 269–272. doi: 10.1038/nature23679
- Koch, H., Lückner, S., Albertsen, M., Kitzinger, K., Herbold, C., Spieck, E., et al. (2015). Expanded metabolic versatility of ubiquitous nitrite-oxidizing bacteria from the genus *Nitrospira*. *Proc. Natl. Acad. Sci. U.S.A.* 112, 11371–11376. doi: 10.1073/pnas.1506533112
- Kowalchuk, G. A., and Stephen, J. R. (2001). Ammonia-oxidizing bacteria: a model for molecular microbial ecology. *Annu. Rev. Microbiol.* 55, 485–529. doi: 10.1146/annurev.micro.55.1.485
- Lehtovirta-Morley, L. E., Ge, C., Ross, J., Yao, H., Nicol, G. W., and Prosser, J. I. (2014). Characterisation of terrestrial acidophilic archaeal ammonia oxidisers and their inhibition and stimulation by organic compounds. *FEMS Microbiol. Ecol.* 89, 542–552. doi: 10.1111/1574-6941.12353
- Lehtovirta-Morley, L. E., Ross, J., Hink, L., Weber, E. B., Gubry-Rangin, C., Thion, C., et al. (2016). Isolation of “*Candidatus Nitrosocosmicus franklandus*,” a novel ureolytic soil archaeal ammonia oxidiser with tolerance to high ammonia concentration. *FEMS Microbiol. Ecol.* 92:fw057. doi: 10.1093/femsec/fiw057
- Lehtovirta-Morley, L. E., Stoecker, K., Vilcinskas, A., Prosser, J. I., and Nicol, G. W. (2011). Cultivation of an obligate acidophilic ammonia oxidizer from a nitrifying acid soil. *Proc. Natl. Acad. Sci. U.S.A.* 108, 15892–15897. doi: 10.1073/pnas.1107196108
- Lehtovirta-Morley, L. E., Verhamme, D. T., Nicol, G. W., and Prosser, J. I. (2013). Effect of nitrification inhibitors on the growth and activity of *Nitrosotalea devanattera* in culture and soil. *Soil Biol. Biochem.* 62, 129–133. doi: 10.1016/j.soilbio.2013.01.020
- Leininger, S., Urich, T., Schloter, M., Schwark, L., Qi, J., Nicol, G. W., et al. (2006). Archaea predominate among ammonia-oxidizing prokaryotes in soils. *Nature* 442, 806–809. doi: 10.1038/nature04983
- Li, C., Hu, H.-W., Chen, Q.-L., Chen, D., and He, J.-Z. (2019a). Comammox *Nitrospira* play an active role in nitrification of agricultural soils amended with nitrogen fertilizers. *Soil Biol. Biochem.* 138:107609. doi: 10.1016/j.soilbio.2019.107609
- Li, C., Hu, H.-W., Chen, Q.-L., Chen, D., and He, J.-Z. (2019b). Growth of comammox *Nitrospira* is inhibited by nitrification inhibitors in agricultural soils. *J. Soils Sediments* 20, 621–628. doi: 10.1007/s11368-019-02442-z
- Liu, L., Liu, M., Jiang, Y., Lin, W., and Luo, J. (2019). Physiological and genomic analysis of “*Candidatus Nitrosocosmicus agrestis*,” an ammonia tolerant ammonia-oxidizing archaeon from vegetable soil. *BioRxiv [Preprint]* doi: 10.1101/2019.12.11.872556
- Martens-Habbena, W., Qin, W., Horak, R. E., Urakawa, H., Schauer, A. J., Moffett, J. W., et al. (2015). The production of nitric oxide by marine ammonia-oxidizing archaea and inhibition of archaeal ammonia oxidation by a nitric oxide scavenger. *Environ. Microbiol.* 17, 2261–2274. doi: 10.1111/1462-2920.12677
- Matsuba, D., Takazaki, H., Sato, Y., Takahashi, R., Tokuyama, T., and Wakabayashi, K. (2003). Susceptibility of ammonia-oxidizing bacteria to nitrification inhibitors. *Z. Naturforsch.* 58c, 282–287. doi: 10.1515/znc-2003-3-424
- Matsumoto, S., Katoku, M., Saeki, G., Terada, A., Aoi, Y., Tsuneda, S., et al. (2009). Microbial community structure in autotrophic nitrifying granules characterized by experimental and simulation analyses. *Environ. Microbiol.* 1, 192–206. doi: 10.1111/j.1462-2920.2009.02060.x
- McCarty, G. W. (1999). Modes of action of nitrification inhibitors. *Biol. Fertil. Soils* 29, 1–9. doi: 10.1007/s003740050518
- Moir, J. L., Cameron, K. C., and Di, H. J. (2007). Effects of the nitrification inhibitor dicyandiamide on soil mineral N, pasture yield, nutrient uptake and pasture quality in a grazed pasture system. *Soil Use Manag.* 23, 111–120. doi: 10.1111/j.1475-2743.2006.00078.x
- Norton, J. M., Klotz, M. G., Stein, L. Y., Arp, D. J., Bottomley, P. J., Chain, P. S. G., et al. (2008). Complete genome sequence of *Nitrosospora multififormis*, an ammonia-oxidizing bacterium from the soil environment. *Appl. Environ. Microbiol.* 74, 3559–3572. doi: 10.1128/aem.02722-07
- Nowka, B., Daims, H., and Spieck, E. (2015). Comparison of Oxidation kinetics of nitrite-oxidizing bacteria: nitrite availability as a key factor in niche differentiation. *Appl. Environ. Microbiol.* 81, 745–753. doi: 10.1128/aem.02734-14
- Papadopoulou, E. S., Bachtsevani, E., Lampronikou, E., Adamou, E., Katsaouni, A., Vasileiadis, S., et al. (2020). Comparison of the in vitro activity of novel and established nitrification inhibitors applied in agriculture: challenging the effectiveness of the currently available compounds. *BioRxiv [Preprint]* doi: 10.1101/2020.04.07.023168
- Papadopoulou, E. S., Tsachidou, B., Sulowicz, S., Menkissoglu-Spiroudi, U., and Karpouzias, D. G. (2016). Land spreading of wastewaters from the fruit packaging industry and potential effects on soil microbes: effects of the antioxidant ethoxyquin and its metabolites on ammonia oxidizers. *Appl. Environ. Microbiol.* 82, 747–755. doi: 10.1128/aem.03437-15
- Powell, S. J., and Prosser, J. I. (1991). Protection of *Nitrosomonas europaea* colonizing clay minerals from inhibition by nitrapyrin. *J. Gen. Microbiol.* 137, 1923–1929. doi: 10.1099/00221287-137-8-1923
- Prosser, J. I., and Nicol, G. W. (2012). Archaeal and bacterial ammonia-oxidisers in soil: the quest for niche specialisation and differentiation. *Trends Microbiol.* 20, 523–531. doi: 10.1016/j.tim.2012.08.001
- Purkhold, U., Pommerening-Röser, A., Juretschko, S., Schmid, M. C., Koops, H. P., and Wagner, M. (2000). Phylogeny of all recognized species of ammonia oxidizers based on comparative 16S rRNA and amoA sequence analysis: implications for molecular diversity surveys. *Appl. Environ. Microbiol.* 66, 5368–5382. doi: 10.1128/aem.66.12.5368-5382.2000
- R Core Team (2020). *R: A Language and Environment for Statistical Computing*. Vienna, Austria: R Foundation for Statistical Computing. Available online at: <https://www.R-project.org/>
- Ranke, J. (2018). *mkim: Kinetic Evaluation of Chemical Degradation Data. R package version 0.9.47.1*.
- Raun, W. R., and Johnson, G. V. (1999). Improving nitrogen use efficiency for cereal production. *Agron. J.* 9, 357–363. doi: 10.2134/agronj1999.00021962009100030001x
- Ritz, C., Baty, F., Streibig, J. C., and Gerhard, D. (2016). Dose-response analysis using R. *PLoS One* 11:e0146021. doi: 10.1371/journal.pone.0146021
- Ritz, C., and Streibig, J. C. (2005). Bioassay analysis using R. *J. Stat. Softw.* 12:32875.
- Rotthauwe, J. H., Witzel, K. P., and Liesack, W. (1997). The ammonia monooxygenase structural gene amoA as a functional marker: molecular fine-scale analysis of natural ammonia-oxidizing populations. *Appl. Environ. Microbiol.* 63, 4704–4712. doi: 10.1128/aem.63.12.4704-4712.1997
- Rousidou, C., Papadopoulou, E., Kortsinidou, M., Giannakou, I. O., Singh, B. K., Menkissoglu-Spiroudi, U., et al. (2013). Bio-pesticides: harmful or harmless to ammonia oxidizing microorganisms? The case of a *Paecilomyces lilacinus*-based nematicide. *Soil Biol. Biochem.* 67, 98–105. doi: 10.1016/j.soilbio.2013.08.014
- Ruser, R., and Schulz, R. (2015). The effect of nitrification inhibitors on the nitrous oxide (N<sub>2</sub>O) release from agricultural soils — a review. *J. Plant Nutr. Soil Sci.* 178, 171–188. doi: 10.1002/jpln.201400251
- Sauder, L. A., Albertsen, M., Engel, K., Schwarz, J., Nielsen, P. H., Wagner, M., et al. (2017). Cultivation and characterization of *Candidatus Nitrosocosmicus exaquare*, an ammonia-oxidizing archaeon from a municipal wastewater treatment system. *ISME J.* 11, 1142–1157. doi: 10.1038/ismej.2016.192
- Shah, A. G., Pierson, J. A., and Pavlostathis, S. G. (2005). Fate and effect of the antioxidant ethoxyquin on a mixed methanogenic culture. *Water Res.* 39, 4251–4263. doi: 10.1016/j.watres.2005.08.014
- Shen, T., Stieglmeier, M., Dai, J., Urich, T., and Schleper, C. (2013). Responses of the terrestrial ammonia-oxidizing archaeon *Ca. Nitrososphaera viennensis* and the ammonia-oxidizing bacterium *Nitrosospora multififormis* to nitrification inhibitors. *FEMS Microbiol. Lett.* 344, 121–129. doi: 10.1111/1574-6968.12164
- Shinn, M. B. (1941). Colorimetric method for determination of nitrite. *Ind. Eng. Chem.* 13, 33–35.
- Skinner, F. A., and Walker, N. (1961). Growth of *Nitrosomonas europaea* in batch and continuous culture. *Arch. Mikrobiol.* 38, 339–349. doi: 10.1007/bf00408008
- Solansky, S. (1982). N-stabilisator SKW-DIDIN verbessert die stickstoffwirkung der Gülle. *Blickfeld* 61, 1–4. doi: 10.1159/000404405
- Starkenburger, S. R., Larimer, F. W., Stein, L. Y., Klotz, M. G., Chain, P. S. G., Sayavedra-Soto, L. A., et al. (2008). Complete genome sequence of *Nitrobacter hamburgensis* X14 and comparative genomic analysis of species within the



- genus *Nitrobacter*. *Appl. Environ. Microbiol.* 74, 2852–2863. doi: 10.1128/aem.02311-07
- Taylor, A. E., Taylor, K., Tennigkeit, B., Palatinszky, M., Stieglmeier, M., Myrold, D. D., et al. (2015). Inhibitory effects of C2 to C10 1-alkynes on ammonia oxidation in two *Nitrososphaera* species. *Appl. Environ. Microbiol.* 81, 1942–1948. doi: 10.1128/aem.03688-14
- Thorisson, S., Gunstone, F. D., and Hardy, R. (1992). Some oxidation products of ethoxyquin including those found in autoxidising systems. *Chem. Phys. Lipids* 60, 263–271. doi: 10.1016/0009-3084(92)90078-4
- Tourna, M., Stieglmeier, M., Spang, A., Könneke, M., Schintlmeister, A., Urich, T., et al. (2011). *Nitrososphaera viennensis*, an ammonia oxidizing archaeon from soil. *Proc. Natl. Acad. Sci. U.S.A.* 108, 8420–8425. doi: 10.1073/pnas.1013488108
- van Kessel, M. A. H. J., Speth, D. R., Albertsen, M., Nielsen, P. H., Op den Camp, H. J. M., Kartal, B., et al. (2015). Complete nitrification by a single microorganism. *Nature* 528, 555–559. doi: 10.1038/nature16459
- Vannelli, T., and Hooper, A. B. (1992). Oxidation of nitrapyrin to 6-chloropicolinic acid by the ammonia-oxidizing bacterium *Nitrosomonas europaea*. *Appl. Environ. Microbiol.* 58, 2321–2325. doi: 10.1128/aem.58.7.2321-2325.1992
- Vanparys, B., Spieck, E., Heylena, K., Wittebollec, L., Geets, J., Boon, N., et al. (2007). The phylogeny of the genus *Nitrobacter* based on comparative rep-PCR, 16S rRNA and nitrite oxidoreductase gene sequence analysis. *Syst. Appl. Microbiol.* 30, 297–308. doi: 10.1016/j.syapm.2006.11.006
- Vasileiadis, S., Puglisi, E., Papadopoulou, E. S., Pertile, G., Suciu, N., Pappolla, R. A., et al. (2018). Blame it on the metabolite: 3,5-dichloroaniline rather than the parent compound is responsible for the decreasing diversity and function of soil microorganisms. *Appl. Environ. Microbiol.* 84:e01536-18.
- Venterea, R. T., Clough, T. J., Coulter, J. A., Breuillin-Sessoms, F., Wang, P., and Sadowsky, M. J. (2015). Ammonium sorption and ammonia inhibition of nitrite-oxidizing bacteria explain contrasting soil N<sub>2</sub>O production. *Sci. Rep.* 5:12153.
- Wang, Z., Cao, Y., Zhu-Barker, X., Nicol, G. W., Wright, A. L., Jia, Z., et al. (2019). Comammox *Nitrospira* clade B contributes to nitrification in soil. *Soil Biol. Biochem.* 135, 392–395. doi: 10.1016/j.soilbio.2019.06.004
- Wright, C. L., Schatteman, A., Crombie, A. T., Murrell, J. C., and Lehtovirta-Morley, L. E. (2020). Inhibition of ammonia monooxygenase from ammonia-oxidizing archaea by linear and aromatic alkynes. *Appl. Environ. Microbiol.* 86:e02388-19.
- Xia, W., Zhang, C., Zeng, X., Feng, Y., Weng, J., Lin, X., et al. (2011). Autotrophic growth of nitrifying community in an agricultural soil. *ISME J.* 5, 1226–1236. doi: 10.1038/ismej.2011.5
- Zerulla, W., Barth, T., Dressel, J., Erhardt, K., von Locquenghien, K. H., Pasda, G., et al. (2001). 3,4-Dimethylpyrazole phosphate (DMPP) – a new nitrification inhibitor for agriculture and horticulture – an introduction. *Biol. Fertil. Soils* 34, 79–84. doi: 10.1007/s003740100380
- Zhang, L. M., Hu, H. W., Shen, J. P., and He, J. Z. (2012). Ammonia-oxidizing archaea have more important role than ammonia-oxidizing bacteria in ammonia oxidation of strongly acidic soils. *ISME J.* 6, 1032–1045. doi: 10.1038/ismej.2011.168
- Zhao, J., Bello, M. O., Meng, Y., Prosser, J. I., and Gubry-Rangin, C. (2020). Selective inhibition of ammonia oxidising archaea by simvastatin stimulates growth of ammonia oxidising bacteria. *Soil Biol. Biochem.* 141:107673. doi: 10.1016/j.soilbio.2019.107673
- Zorz, J. K., Kozłowski, J. A., Stein, L. Y., Strous, M., and Kleiner, M. (2018). Comparative proteomics of three species of ammonia-oxidizing bacteria. *Front. Microbiol.* 9:938. doi: 10.3389/fmicb.2018.00938

**Conflict of Interest:** The authors declare that the research was conducted in the absence of any commercial or financial relationships that could be construed as a potential conflict of interest.

Copyright © 2020 Papadopoulou, Bachtsevani, Lampronikou, Adamou, Katsaouni, Vasileiadis, Thion, Menkissoglu-Spiroudi, Nicol and Karpouzas. This is an open-access article distributed under the terms of the Creative Commons Attribution License (CC BY). The use, distribution or reproduction in other forums is permitted, provided the original author(s) and the copyright owner(s) are credited and that the original publication in this journal is cited, in accordance with accepted academic practice. No use, distribution or reproduction is permitted which does not comply with these terms.



# Assessing the Effects of $\beta$ -Triketone Herbicides on the Soil Bacterial and *hppd* Communities: A Lab-to-Field Experiment

Clémence Thiour-Mauprivez<sup>1,2,3</sup>, Marion Devers-Lamrani<sup>3</sup>, David Bru<sup>3</sup>, Jérémie Béguet<sup>3</sup>, Aymé Spor<sup>3</sup>, Arnaud Mounier<sup>3</sup>, Lionel Alletto<sup>4</sup>, Christophe Calvayrac<sup>1,2</sup>, Lise Barthelmebs<sup>1,2</sup> and Fabrice Martin-Laurent<sup>3\*</sup>

<sup>1</sup> Biocapteurs-Analyses-Environnement, Université de Perpignan Via Domitia, Perpignan, France, <sup>2</sup> Laboratoire de Biodiversité et Biotechnologies Microbiennes, USR 3579 Sorbonne Universités (UPMC) Paris 6 et CNRS Observatoire Océanologique, Banyuls-sur-Mer, France, <sup>3</sup> Agroécologie, AgroSup Dijon, INRAE, Université Bourgogne Franche-Comté, Dijon, France, <sup>4</sup> Université de Toulouse, INRAE, UMR AGIR, Castanet-Tolosan, France

## OPEN ACCESS

### Edited by:

Christopher Bagwell,  
Pacific Northwest National Laboratory  
(DOE), United States

### Reviewed by:

Giorgia Pertile,  
Institute of Agrophysics (PAN), Poland  
Małgorzata Baćmaga,  
University of Warmia and Mazury  
in Olsztyn, Poland

### \*Correspondence:

Fabrice Martin-Laurent  
fabrice.martin@inrae.fr

### Specialty section:

This article was submitted to  
Microbiotechnology,  
a section of the journal  
Frontiers in Microbiology

**Received:** 25 September 2020

**Accepted:** 07 December 2020

**Published:** 11 January 2021

### Citation:

Thiour-Mauprivez C,  
Devers-Lamrani M, Bru D, Béguet J,  
Spor A, Mounier A, Alletto L,  
Calvayrac C, Barthelmebs L and  
Martin-Laurent F (2021) Assessing  
the Effects of  $\beta$ -Triketone Herbicides  
on the Soil Bacterial and *hppd*  
Communities: A Lab-to-Field  
Experiment.  
Front. Microbiol. 11:610298.  
doi: 10.3389/fmicb.2020.610298

Maize cultivators often use  $\beta$ -triketone herbicides to prevent the growth of weeds in their fields. These herbicides target the 4-HPPD enzyme of dicotyledons. This enzyme, encoded by the *hppd* gene, is widespread among all living organisms including soil bacteria, which are considered as “non-target organisms” by the legislation. Within the framework of the pesticide registration process, the ecotoxicological impact of herbicides on soil microorganisms is solely based on carbon and nitrogen mineralization tests. In this study, we used more extensive approaches to assess with a lab-to-field experiment the risk of  $\beta$ -triketone on the abundance and the diversity of both total and *hppd* soil bacterial communities. Soil microcosms were exposed, under lab conditions, to 1× or 10× the recommended dose of sulcotrione or its commercial product, Decano<sup>®</sup>. Whatever the treatment applied, sulcotrione was fully dissipated from soil after 42 days post-treatment. The abundance and the diversity of both the total and the *hppd* bacterial communities were not affected by the herbicide treatments all along the experiment. Same measurements were led in real agronomical conditions, on three different fields located in the same area cropped with maize: one not exposed to any plant protection products, another one exposed to a series of plant protection products (PPPs) comprising mesotrione, and a last one exposed to different PPPs including mesotrione and tembotrione, two  $\beta$ -triketones. In this latter, the abundance of the *hppd* community varied over time. The diversity of the total and the *hppd* communities evolved over time independently from the treatment received. Only slight but significant transient effects on the abundance of the *hppd* community in one of the tested soil were observed. Our results showed that tested  $\beta$ -triketones have no visible impact toward both total and *hppd* soil bacteria communities.

**Keywords:** soil, microorganisms,  $\beta$ -triketone, herbicide, *hppd* gene, lab-to-field, non-target organisms

## INTRODUCTION

Soils are known as complex and dynamic habitats where a wide diversity of species lives. Soils could potentially shelter about a quarter of the world biodiversity (Decaëns et al., 2006). Among their inhabitants, microorganisms constitute a huge part of this biodiversity with several billions of bacterial species and more than a hundred thousand fungi species living in one gram of soil (Schloss and Handelsman, 2006). These microorganisms contribute to a series of complex processes and support key soil ecosystem functions associated to food supply, climate regulation or biochemical cycles among others (Wall et al., 2013; Graham et al., 2016). It then appears important to preserve and protect soil microorganisms and their habitats. In 2010, the European Commission officially recognized the need to protect soils and raised them as a non-renewable resource, as this was already the case for water (European Commission, 2010). The European soil biodiversity expert group identified the main pressures on soil organisms and human intensive exploitation appeared as a major threat (Gardi et al., 2013). This intensive exploitation is irretrievably linked to the use of plant protection products (PPPs), applied in conventional agriculture to protect crops from various pests. Among them, herbicides are still widely used to control weeds which enter in competition with crops. Some of them, developed during these last two decades are inspired by the biomimeticism. They mimicked active natural products and are consequently considered as “eco-friendly” (Cantrell et al., 2012).

This is the case for  $\beta$ -triketone herbicides, for which the chemical structure derived from a natural phytotoxin obtained from the Californian bottlebrush plant, *Callistemon citrinus* (Mitchell et al., 2001). Three  $\beta$ -triketone active substances are mainly used as herbicides on maize cultures: sulcotrione, mesotrione, and tembotrione (Schulz et al., 1993; Mitchell et al., 2001; Lee et al., 2008). These molecules inhibit the 4-hydroxyphenylpyruvate dioxygenase (HPPD) and lead to bleaching and death of weeds (Dayan et al., 2007; Rocaboy-Faquet et al., 2014). This enzyme is not only found in plants but in almost all living organisms, including microorganisms where it takes part to the tyrosine degradation pathway (Moran, 2005). The *hppd* gene, coding the targeted enzyme, is described in about 2000 bacterial species (Thiour-Mauprivez et al., 2020). Thus, soil bacteria, classified as “non-target organisms” by current EU regulation for pesticide authorization, might be impacted by  $\beta$ -triketones, with a possible domino effect on microbial functions supporting soil ecosystem services (Thiour-Mauprivez et al., 2019). In this context, studies assessing the ecotoxicological impact of  $\beta$ -triketone herbicides on soil total bacteria have recently been led (Romdhane et al., 2016a, 2019). In order to get a closer look to the direct effect of  $\beta$ -triketone, we report here the assessment of its ecotoxicological effect on the abundance and the diversity of the total bacterial community and the bacterial community harboring the *hppd* gene. These parameters were measured in a lab-to-field experiment in which lab conditions were led with the active substance at higher doses than the recommended ones, to test the “worst-case scenario” and field experiments were led with recommended field doses (RfDs), in frame with a “realistic scenario of exposure,” as recommended

by the European Food Safety Authority (Ockleford et al., 2017). Our lab-to-field experiment complies the two-tiered approach to assess the possible toxicity of  $\beta$ -triketones on the *hppd* bacterial community which harbors the gene encoding the enzyme targeted by these herbicides.

Under lab conditions, soil microcosms were treated with  $1\times$  or  $10\times$  the RfD of sulcotrione using the active ingredient or the formulated product (Decano<sup>®</sup>) or not treated (control). Under these conditions, dissipation studies of the active substance or the formulated PPP in soil microcosms were carried out in order to estimate the scenario of exposure of soil microorganisms. Under field conditions, samples were collected in maize crops exposed to PPP treatments comprising several  $\beta$ -triketones or not treated at all (control). For both lab and field experiments, the abundance and the diversity of both the total and the *hppd* bacterial communities were estimated by quantitative PCR (qPCR) and high throughput sequencing, respectively.

## MATERIALS AND METHODS

### Laboratory Experiment Reagents

Standard of sulcotrione [(S) 98.8% purity], a weak acidic herbicide with pKa value of 2.87 and MW = 328.7 g.mol<sup>-1</sup> was purchased from Sigma-Aldrich, France. Formulated sulcotrione [Decano<sup>®</sup> (D)] was purchased from (SAPEC Agro, France). Methanol and acetonitrile (HPLC quality) were purchased from Carlo Erba, dichloromethane for pesticide analysis from Riedel-de-Haën GmbH, trifluoroacetic acid (99.0% purity) and hydrochloric acid (38.0%) from Aldrich and water was Milli-Q quality.

### Soil Sampling and Microcosm Set-up Under Lab Conditions

Soil samples were collected from the surface layer (0–20 cm) of an arable field located in Perpignan, France. According to the World Reference Base of Soil Resources, it is a sandy loam clay-rich soil composed of 16.2% clay, 29.1% silt, and 54.7% sand. Granulometry was measured according to the particle size 5 fractions with no decarbonization method (NF X 31-107). Soil contains 27.5 g/kg of organic matter, 15.99 g/kg of organic carbon, and 1.25 g/kg of nitrogen. These contents were measured by dry combustion according to the standard methods NF ISO 10694 and NF ISO 13878. Soil physicochemical characteristics are 99 meq/kg Cation Exchange Capacity (CEC), 260.3% Ca2/CEC and water pH 8.04. CEC was measured according to the Metson method (NF X 31-130) and water pH was determined using a glass electrode (NF ISO 10390). Soil samples were sieved to 2 mm and soil moisture was of 3%. Soil samples were divided in microcosm of 20 g of soil each and treated or not with active ingredient {2-[2-chloro-4-(methylsulfonyl)benzoyl]-1,3-cyclohexanedione} (S) or formulated compound [Decano<sup>®</sup> (D)]. For each treatment (sulcotrione or Decano<sup>®</sup>), twelve microcosms were treated at  $1\times$  RfD (1.5  $\mu$ g/g), twelve were treated at  $10\times$  RfD (15  $\mu$ g/g) and twelve remained untreated (control). These doses were chosen to fulfill the two-tier scenario

of exposure. Soil moisture was adjusted at 22% relative humidity. Soil microcosms were incubated at  $21 \pm 2^\circ\text{C}$  in the dark. Every 2 days, microcosms were ventilated and soil moisture was adjusted if needed under sterile conditions. Soil samples were collected after 30 min of treatment (day 0), 7, 14, and 42 days of incubation and immediately stored at  $-20^\circ\text{C}$  for further analyses. Three replicates were prepared for each treatment (S control, S  $1 \times \text{RfD}$ , S  $10 \times \text{RfD}$ , D control, D  $1 \times \text{RfD}$ , and D  $10 \times \text{RfD}$ ).

## Herbicide Quantification

### Extraction step

This analytical method was an adaptation of the procedure previously published by Chaabane et al., 2008. In order to follow active substance or formulated PPP dissipation in soil, 10 g of soil (triplicates) for each condition were extracted twice with 30 mL of acetonitrile/0.1 M hydrochloric acid (90/10; V/V) under agitation at 100 rpm orbital shaking for 50 min and then filtered on a Whatman filter GF/A 47 mm. The organic filtrate was evaporated at  $30^\circ\text{C}$  and the acidic aqueous solution was then extracted twice with 6.0 mL of dichloromethane. The organic phase was evaporated to dryness and then solubilized with 3.0 mL of methanol. The final extract was analyzed by High Performance Liquid Chromatography (HPLC).

### Chromatographic analysis

Soil extracts treated with sulcotrione were analyzed using a VWR Hitachi LaChrom apparatus consisted of auto-sampler L-2200 and HTA L-2130 pump modules equipped with a Kinetex C18 column (5  $\mu\text{m}$ , 150 mm  $\times$  3 mm) and a DAD L-2450 UV/Vis detector set at 285 nm. For sulcotrione, the mobile phase consisted of a mixture of water acidified with 0.1% acetic acid (AW) and acetonitrile (ACN) delivered at a flow-rate of 0.5 mL/min with an isocratic mode 70/30 (AW/ACN) for 15 min. For soil extracts treated with Decano<sup>®</sup>, the mobile phase was the same as the one used for sulcotrione but was delivered at a flow-rate of 1 mL/min with an isocratic mode 80/20 (AW/ACN) for 8 min.

### Analytical performance

Recovered analytically were evaluated by spiking soil samples replicates ( $n = 5$ ) with increasing doses (0.1–75  $\mu\text{g/g}$ ) of analytical standards of sulcotrione or formulated sulcotrione (Decano<sup>®</sup>) prior to extraction. The mean recovery rates were estimated as  $85 \pm 10$  and  $52 \pm 4\%$ , for sulcotrione and Decano<sup>®</sup>, respectively. The limit of quantification, defined as the sample concentration required to give a signal-to-noise ratio of 5:1 was evaluated to 0.1  $\mu\text{g/g}$  for both sulcotrione and Decano<sup>®</sup>.

## Field Experiment

Soil samples were collected from the surface layer (0–20 cm) of three arable fields located near Tarbes, France. These fields were not part of an experimental parcel, they were exploited by farmers and, thus, were treated at RfDs of PPPs with a crop protection program which we did not choose. Field 1 has not received any PPPs for 3 years and was historically cultivated with maize but is now cultivated with walnut tree and will constitute the control field. Field 2 was sown with maize on the 30th April 2019 and

was treated with Camix<sup>®</sup> (containing 40 g/L mesotrione, applied at 2.5 L/ha) on the 23th May 2019 and with Auxo<sup>®</sup> (containing 50 g/L tembotrione, applied at 0.6 L/ha), Nisshin (nicosulfuron-based, 0.6 L/ha), Banvel (dicamba-based, 0.2 L/ha), and Sakol (alkylpolyglucoside-based, 0.1 L/ha) on the 3rd June 2019. Three samplings were made over one crop cycle on these three fields with three replicates made of seven composite-samples each done using an auger. The first sampling time was before seedling and treatments on the 16th September 2018 (September 2018). The second was made after treatment for field 3 whereas in the field 2, it was made between the first and the second treatment on the 6th June 2019 (June 2019). For all the fields, the last sampling campaign was led on the 28th August 2019 (August 2019). Soil properties and chemical characteristics are described in the **Supplementary Table 1**. Soil samples were stored at  $-20^\circ\text{C}$  until use.

## Ecotoxicological Impact of $\beta$ -Triketone on Soil Bacterial Communities

### Soil DNA Extraction

At each sampling time of the experiment, nucleic acids were extracted with RNeasy PowerSoil DNA Elution Kit (Qiagen). DNA quality was checked and concentrations quantified by Quant-iT<sup>™</sup> PicoGreen<sup>™</sup> (Thermo Fischer Scientific, France). A mean of  $0.19 \pm 0.18$  and  $0.38 \pm 0.29 \mu\text{g/g}$  of soil were extracted from laboratory and field samples, respectively. DNA extracts were stored at  $-20^\circ\text{C}$  until use.

### Abundance of Total and *hppd* Bacterial Communities

Prior to quantification, inhibition tests were performed as previously described in Petric et al. (2011), in order to detect the presence of DNA co-extracts possibly inhibiting the qPCR assays. Samples were then diluted at 1 ng/ $\mu\text{L}$ . Amplification of both *hppd* and 16S rRNA genes were carried out using a ViiA<sup>™</sup> 7 (Thermo Fisher Scientific, France) in a final reaction mixture of 15  $\mu\text{L}$ . The mixture contained SYBR Green PCR Master Mix (Takyon<sup>™</sup> Low ROX SYBR<sup>®</sup> 2 $\times$  Mastermix Blue, Eurogentec, Belgium), 250 ng of T4 gp32 (Qbiogene, MP Biomedicals, France), 10  $\mu\text{M}$  of each *hppd* primer (HIAF and FFER, Thiour-Mauprivez et al., 2020), or 1  $\mu\text{M}$  of each 16S rRNA primer (341F and 534R, Muyzer et al., 1996) and 1 ng of soil DNA template. qPCR runs were as follow for the amplification of the *hppd* gene: *Taq* polymerase enzyme activation step for 3 min at  $95^\circ\text{C}$ , then 40 cycles of 10 s of denaturation at  $95^\circ\text{C}$ , 30 s of annealing at  $54^\circ\text{C}$ , elongation for 30 s at  $72^\circ\text{C}$ , and a melting curve stage with 15 s at  $95^\circ\text{C}$ , 1 min at  $68^\circ\text{C}$ , and 15 s at  $95^\circ\text{C}$  (data were collected at this step). Run parameters used for the amplification of 16S rRNA gene were previously described by Romdhane et al. (2016a). Standard curves were generated using serial dilutions of linearized plasmid pGEM-T easy vector system containing each standard gene sequence (ranging from  $10^2$  to  $10^7$  copies per qPCR reaction). For each condition tested, two qPCR assays were conducted. In each assay, qPCR calibration was performed in triplicate and three no-template controls (NTC) were also included.



## Diversity of Total and *hppd* Bacterial Communities

Total and *hppd* bacterial diversities were monitored using a high throughput sequencing of 16S rRNA and *hppd* amplicons, respectively (Illumina MiSeq, Microsynth). A two-step PCR procedure was used to amplify the *hppd* gene from obtained DNA extracts. In the first step, 27 cycles of amplification were performed in duplicate using the NGS\_FFER-NGS\_HIAF primer pair (Thiour-Mauprivez et al., 2020). Duplicates were then pooled and a second step of PCR was conducted, in duplicate, using 1  $\mu$ L of the previous PCR as template to carry out eight cycles of amplification with barcoded primers. To amplify the 16S rRNA gene from obtained DNA extracts, 20 cycles of amplification were performed in duplicate using the U341F-805R primer pair (Takahashi et al., 2014). Duplicates were then pooled and a second step of PCR was conducted, in duplicate, using 1  $\mu$ L of the previous PCR as template to carry out 15 cycles of amplification with barcoded primers. After pooling, amplicon size was checked by electrophoresis on a 2% agarose gel. 25  $\mu$ L of PCR products were normalized using SequalPrep™ Normalization Plate Kit (Invitrogen) and 10  $\mu$ L of each sample were sent to Microsynth for sequencing. 16S rRNA amplicon data analysis were conducted as described in Romdhane et al. (2016a). For the *hppd* amplicon data analysis, reads were quality-controlled and assembled using PEAR (Zhang et al., 2014). Unassembled reads and once-assembled reads outside the expected range were discarded. Sequences were corrected and converted into protein sequences using framebot (Wang et al., 2013), then clustered into OTUs using cd-hit (Li and Godzik, 2006). Representative *hppd* sequences for each OTU were aligned using Muscle (Edgar, 2004) and the maximum likelihood phylogeny was calculated using FastTree 2 algorithm (Price et al., 2009). Several  $\alpha$ -diversity indices (PD whole tree, Simpson reciprocal, and Shannon indices) were then calculated using rarefied OTU tables at the depth of 6000 sequences per sample in the microcosms treated with sulcotrione, 15,000 sequences per sample in those treated with Decano® and 20,000 sequences per sample in the soils sampled directly from fields considering the 16S rRNA amplicons. Same indices were calculated using rarefied OTU tables of 2300 sequences per sample in the microcosms treated with sulcotrione, 2000 sequences per sample in those treated with Decano® and 4200 sequences per sample in the soils sampled directly from fields considering the *hppd* amplicons. Principal Coordinate Analysis (PCoA) plots were generated in QIIME based on weighted UniFrac distance matrix and coordinates were used to draw 3D figures.

## Statistical Analysis

Statistical analysis were conducted using R software and a significance threshold was set at a *p*-value of 0.05 (R Development Core Team, 2005). For qPCR results, data were log-transformed. Data normality was verified by a Shapiro–Wilk test. The homogeneity of variances of the residues was verified by a Levene test. Data were subjected to an analysis of variance (ANOVA) and Tukey test was performed for each treatment and each time point. Not all data showed a normal distribution. Consequently, non-parametric test (Kruskal–Wallis test) was carried out on

non-normal distributed data. Weighted or unweighted UniFrac distance matrices were subjected to a PERMANOVA analysis using the ADONIS function from R package “vegan” (Oksanen et al., 2020). Sparse Partial Least Squares Discriminant Analysis (sPLS-DA) was performed to select discriminant OTUs between different treatments using the function “splsd” from R package mixOmics (Rohart et al., 2017). A homemade R script was used to identify the discriminant OTUs by performing an ANOVA on each of these OTUs.

## RESULTS

### Fate of Sulcotrione and Decano® in Soil Microcosms

In order to decipher the exposure scenario of bacteria in soil microcosms, kinetics of dissipation of sulcotrione and Decano® in soils were measured at each time point (Table 1). Sulcotrione and Decano® dissipation kinetics could be reasonably described by a first-order kinetics ( $C = C_0 e^{-kt}$ ) for the application at 1 $\times$  RfD. Half-life time of sulcotrione in Perpignan soil was estimated at *ca* 4 days for 1 $\times$  RfD. Regarding Decano®, half-life time in Perpignan soil was evaluated at *ca* 1.5 days for the 1 $\times$  RfD condition. For the application at 10 $\times$  RfD, we were only able to estimate graphically the half-life time of sulcotrione at *ca* 14 days and of Decano® at *ca* 18 days (Supplementary Figure 1). Anyhow, sulcotrione and Decano® both reached an unquantifiable concentration after 42 days of exposure in Perpignan soil, whatever the starting concentration of RfD applied.

### Impact of Sulcotrione and Decano® on the Abundance of the Total and the *hppd* Bacterial Community

The impact of sulcotrione and Decano® on the abundance of the total and the *hppd* bacterial community in the soil microcosms was monitored by qPCR. Sequence copy numbers ranged from  $8.99 \times 10^3$  to  $3.82 \times 10^5$  sequences of 16S rRNA per nanogram of DNA and from  $4.81 \times 10^3$  to  $2.75 \times 10^5$  sequences of *hppd* per nanogram of DNA. The abundances of both the total and the *hppd* bacterial communities were not affected by the  $\beta$ -triketone treatments applied. Similarly, the relative abundance of *hppd* sequences per 1000 sequences of 16S rRNA (Figure 1) was not affected by any of the  $\beta$ -triketone treatments applied. In both cases, only a time effect was observable with relative abundance measured at day 0 different from the other sampling days

**TABLE 1** | Main environmental parameters of sulcotrione and Decano® estimated by modeling their kinetics of dissipation in Perpignan soil.

Treatment	Sulcotrione		Decano®	
RfD	1	10	1	10
k (day)	0.36 $\pm$ 0.02	n.d.	0.43 $\pm$ 0.03	n.d.
DT <sub>50</sub> (day)	1.94 $\pm$ 0.08	n.d.	1.63 $\pm$ 0.11	n.d.
R <sup>2</sup>	0.81 $\pm$ 0.10	n.d.	0.99 $\pm$ 0.01	n.d.



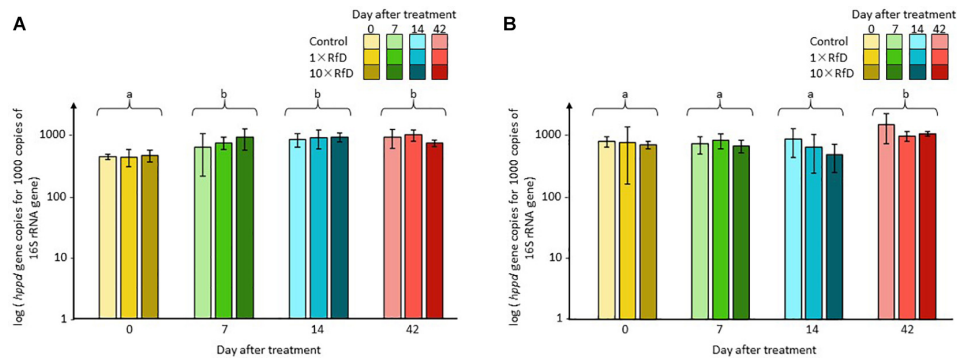


**FIGURE 1** | *hppd* sequence copy number per 1000 sequences of 16S rRNA. Soil microcosms (A) treated with sulcotrione; (B) with Decano<sup>®</sup>. Values shown are averages of  $n = 3$  biological replicates for each series. Error bars are calculated from the standard deviation for each series. ANOVA and Kruskal–Wallis test  $p < 0.05$  were considered as significant and, if needed, indicated by a small letter.

(ANOVA,  $p = 0.001$ ) for microcosms treated with sulcotrione and relative abundance measured at day 42 different from those measured at 0, 7, or 14 days (Kruskal–Wallis test,  $p = 0.002$ ) for microcosms treated with Decano<sup>®</sup>.

## Impact of Sulcotrione and Decano<sup>®</sup> on the Diversity of the *hppd* Bacterial Community

To further investigate the possible ecotoxicological impact of sulcotrione and Decano<sup>®</sup> on the diversity of total and *hppd* bacterial communities, the 16S rRNA and the *hppd* amplicons were amplified from soil DNA extracts and sequenced. These sequences were grouped into 2849 OTUs and 1688 OTUs at 80% amino-acid sequence identity threshold for sulcotrione and Decano<sup>®</sup> treatment respectively.  $\alpha$ -Diversity was estimated for each treatment by a range of indices depicted in Table 2. No significant differences neither overtime nor in response to the RfD applied was shown for all tested treatments. Same measurements were made on the total bacterial  $\alpha$ -diversity by sequencing the 16S rRNA gene. Sequences were grouped in 4099 OTUs in the soil treated with sulcotrione and in 4767 OTUs in the soil treated with Decano<sup>®</sup> at 94% nucleotide sequence identity threshold. A time effect was highlighted but no significant differences due to the treatment applied were shown (Supplementary Table 2). Together, these results indicate that the  $\alpha$ -diversity of both the total and the *hppd* communities are not affected by sulcotrione or Decano<sup>®</sup> in our experimental conditions.

The ecotoxicological impact of sulcotrione and Decano<sup>®</sup> on the *hppd* bacterial  $\beta$ -diversity of soil microcosms was evaluated. For each treatment, the analysis of the PCoA, representing the weighted UniFrac distances, showed no significant difference in the *hppd* bacterial community composition between RfD applied (Control, 1 $\times$  RfD, or 10 $\times$  RfD) and sampling time (0, 7, 14, 42 days after treatment) (Figure 2).

Altogether, the results obtained for  $\alpha$ - and  $\beta$ -diversity measurements indicate that the diversity of the *hppd* bacterial

community was not modified over time or according to the RfD applied. Same conclusions were made on the measurements of the total bacterial diversity, monitored by 16S rRNA Illumina sequencing (Supplementary Figure 2).

**TABLE 2** | Richness and diversity indices of the *hppd* bacterial community calculated for soil microcosms exposed for 0, 7, 14, and 42 days to sulcotrione (S, in brown) or Decano<sup>®</sup> (D, in blue) applied at different concentrations (control, 1 $\times$  RfD, and 10 $\times$  RfD).

Day after treatment	Treatment	Observed species	PD whole tree	Simpson reciprocal
0	S control	211 $\pm$ 24	62 $\pm$ 5	18 $\pm$ 6
	S 1 $\times$ RfD	188 $\pm$ 26	55 $\pm$ 7	16 $\pm$ 2
	S 10 $\times$ RfD	184 $\pm$ 49	54 $\pm$ 13	15 $\pm$ 8
	D control	196 $\pm$ 17	52 $\pm$ 4	16 $\pm$ 2
	D 1 $\times$ RfD	216 $\pm$ 38	59 $\pm$ 8	26 $\pm$ 17
	D 10 $\times$ RfD	200 $\pm$ 15	54 $\pm$ 2	17 $\pm$ 1
7	S control	165 $\pm$ 21	49 $\pm$ 6	9 $\pm$ 2
	S 1 $\times$ RfD	192 $\pm$ 28	56 $\pm$ 6	16 $\pm$ 6
	S 10 $\times$ RfD	167 $\pm$ 11	49 $\pm$ 3	11 $\pm$ 1
	D control	206 $\pm$ 24	55 $\pm$ 6	21 $\pm$ 7
	D 1 $\times$ RfD	208 $\pm$ 17	57 $\pm$ 4	26 $\pm$ 14
	D 10 $\times$ RfD	233 $\pm$ 12	63 $\pm$ 1	26 $\pm$ 1
14	S control	177 $\pm$ 28	50 $\pm$ 7	11 $\pm$ 1
	S 1 $\times$ RfD	168 $\pm$ 18	48 $\pm$ 5	9 $\pm$ 1
	S 10 $\times$ RfD	180 $\pm$ 35	52 $\pm$ 7	10 $\pm$ 2
	D control	204 $\pm$ 3	55 $\pm$ 2	18 $\pm$ 1
	D 1 $\times$ RfD	230 $\pm$ 24	61 $\pm$ 5	26 $\pm$ 11
	D 10 $\times$ RfD	225 $\pm$ 17	59 $\pm$ 5	25 $\pm$ 5
42	S control	176 $\pm$ 21.2	51 $\pm$ 5	11 $\pm$ 2
	S 1 $\times$ RfD	167 $\pm$ 25	50 $\pm$ 6	12 $\pm$ 2
	S 10 $\times$ RfD	199 $\pm$ 31	57 $\pm$ 8	14 $\pm$ 4
	D control	211 $\pm$ 1	57 $\pm$ 0	19 $\pm$ 1
	D 1 $\times$ RfD	213 $\pm$ 7	57 $\pm$ 1	19 $\pm$ 2
	D 10 $\times$ RfD	204 $\pm$ 11	57 $\pm$ 3	16 $\pm$ 2

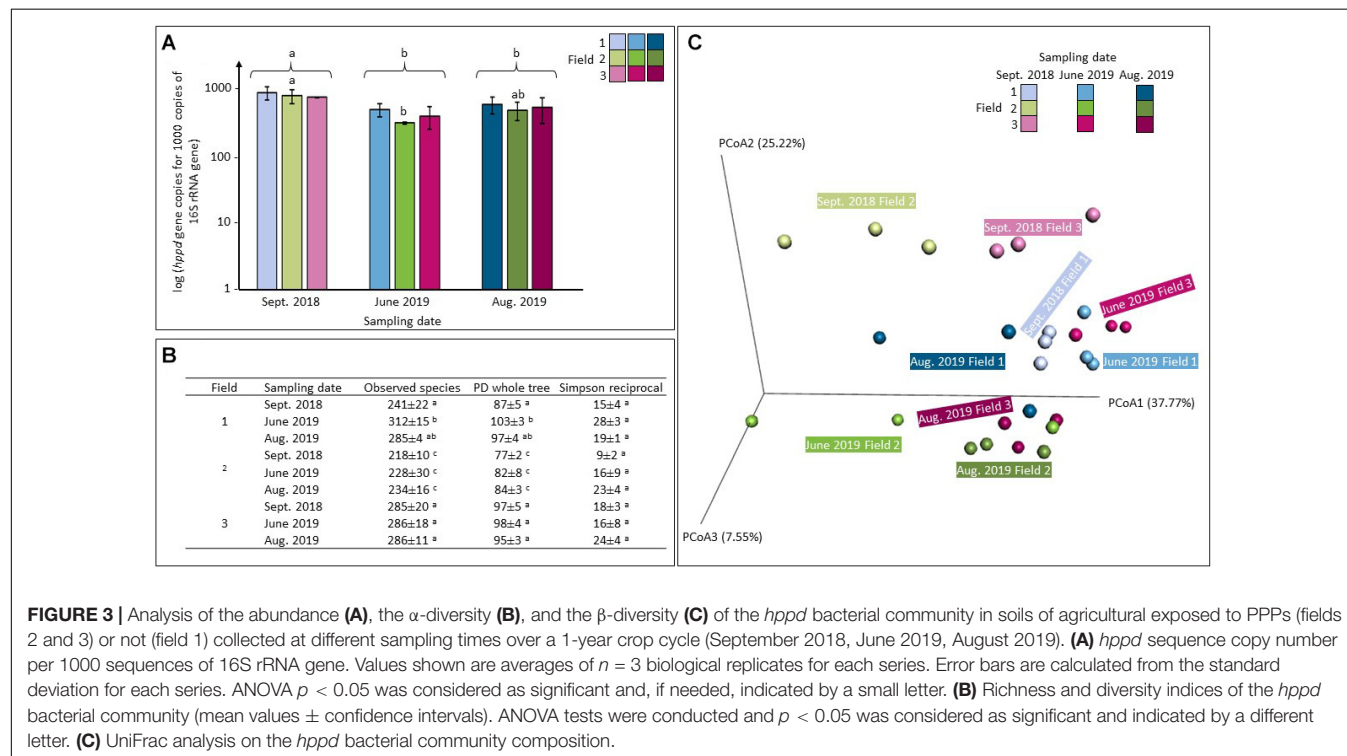
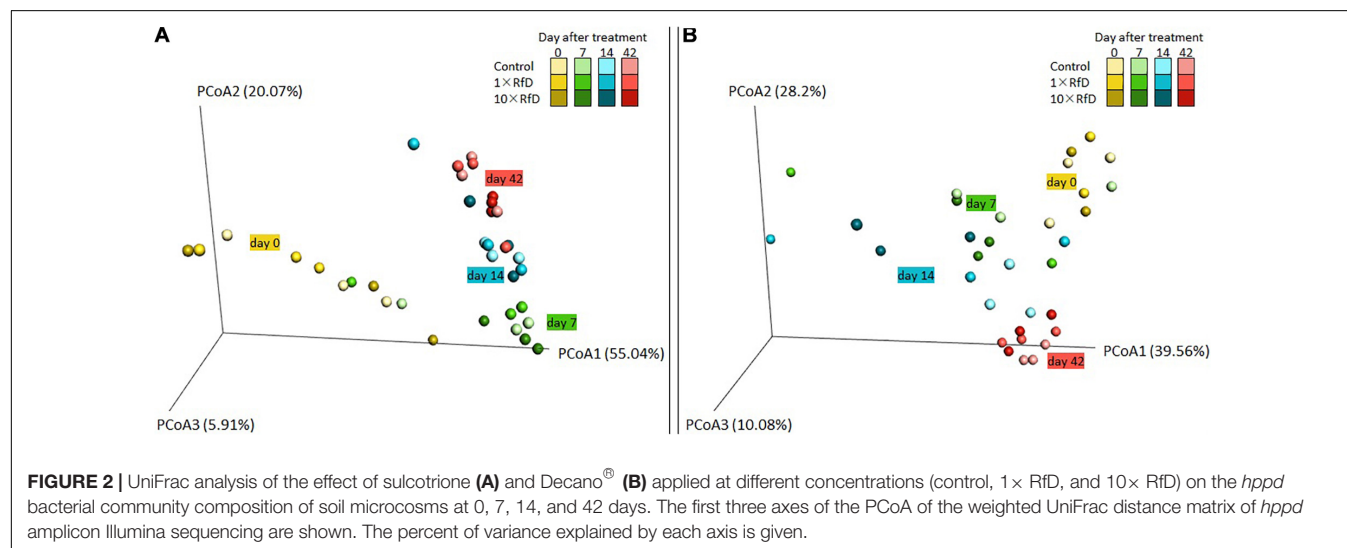
Mean values  $\pm$  confidence intervals are shown. No significant difference for each treatment and each time point was shown (Kruskal–Wallis test  $p < 0.05$  were considered as significant and, if needed, indicated by a small letter).

## Abundance and Diversity of the Total and the *hppd* Bacterial Community in Agricultural Soils Exposed to $\beta$ -Triketone Herbicides

The ecotoxicological impact of PPP treatments on the abundance, the diversity and the composition of the total and the *hppd* bacterial communities was also assessed under real agronomical conditions.

Sequence copy numbers ranged from  $1.21 \times 10^5$  to  $4.63 \times 10^5$  sequences of 16S rRNA per nanograms of DNA and from

$7.90 \times 10^4$  to  $2.62 \times 10^5$  sequences of *hppd* per ng of DNA. The relative abundance of *hppd* gene copies per 1000 sequences of 16S rRNA is shown in **Figure 3A**. An ANOVA test suggest that whatever the treatment applied, values recorded in the samples collected in September 2018 were significantly higher than that of the two others (June 2019 and August 2019) ( $p < 0.01$ ). Considering the relative abundance of *hppd* found in each treated soil, only values observed in field 2 were statistically different from those measured in the others: values recorded in June 2019 (ANOVA,  $p < 0.01$ ) were significantly lower than those of September 2018. This was no longer observed on samples of



August 2019, which were not statistically different from those obtained in September 2018 (ANOVA,  $p = 0.09$ ) or in June 2019 (ANOVA,  $p = 0.17$ ).

The *hppd* sequences were grouped into 1562 OTUs at 80% amino-acid sequence identity threshold.  $\alpha$ -Diversity was estimated for each condition by a range of indices depicted in **Figure 3B**. The observed species and the Phylogenetic Diversity (PD) indices calculated in field 2 were significantly lower than those of field 1 and field 3, no matter what the sampling date (ANOVA,  $p < 0.01$ ). Same measurements were made on the total bacterial  $\alpha$ -diversity and they led to the similar conclusions: the three indices calculated in the case of for field 2 were significantly lower from those calculated for fields 1 and 3, respectively (ANOVA,  $p < 0.05$ , **Supplementary Figure 3**). The total and the *hppd* bacterial  $\alpha$ -diversities are different in field 2 than in the other two fields. On June 2019, the observed species and the PD whole tree indices calculated on the *hppd* bacterial  $\alpha$ -diversities within field 1 were significantly different from those calculated on September 2018 (ANOVA,  $p < 0.01$ ) but not from those measured in August 2019 (ANOVA,  $p_{\text{observed\_species}} = 0.66$  and  $p_{\text{PD\_whole\_tree}} = 0.88$ ). It has to be noticed that the  $\alpha$ -diversity of the total bacterial community was also modified over time (ANOVA,  $p < 0.05$ , **Supplementary Figure 3**).

The *hppd* bacterial  $\beta$ -diversity is illustrated on **Figure 3C** by a PCoA representing the weighted UniFrac distances. In addition, an sPLS-DA was performed in parallel to an ANOVA test performed on each *hppd* OTU taken separately. All of these tests showed no statistical differences between soils: the  $\beta$ -diversity of *hppd* bacterial community remained unchanged among time and between the different studied soils. Same tests were performed on the total bacterial  $\beta$ -diversity obtained by sequencing the 16S rRNA gene with sequences grouped in 5739 OTUs at 94% nucleotide sequence identity threshold. Whatever the soil considered, no significant differences were found (data not shown).

## DISCUSSION

The aim of this study was to evaluate, in a lab-to-field experimental design, the ecotoxicological impact of  $\beta$ -triketone herbicides on the abundance, the composition and the diversity of total and *hppd* bacterial communities. Under lab conditions, the worst-case scenario (up to 10 times the agronomical dose) as well as the effect of the formulation (sulcotrione vs Decano<sup>®</sup>) were tested. Under field conditions, agronomical scenario exposure including the application of several PPP treatments over a 1-year cropping cycle was tested.

### Estimation of the Fate and Ecotoxicological Impact of Sulcotrione and Decano<sup>®</sup> on the Total and *hppd* Bacterial Communities Under Lab Conditions

Under lab conditions, soil microcosms were exposed for 42 days to 1 $\times$  or 10 $\times$  RfD of sulcotrione or Decano<sup>®</sup>. Kinetics of

dissipation of the active substance were established. Although the dissipation of sulcotrione in the Perpignan soil has already been monitored in several studies (Chaabane et al., 2008; Romdhane et al., 2019), this is the first time that the kinetic of dissipation of the active substance of Decano<sup>®</sup> was measured in this soil. Even if the recovery rate of sulcotrione from microcosms treated with Decano<sup>®</sup> was not optimal (52%), one could observe that, 42 days after application, sulcotrione was fully dissipated from both batches of microcosms. Our results are consistent with previous studies where similar concentrations were applied, showing a complete dissipation of sulcotrione within 45 days in Perpignan soil (Calvayrac et al., 2012; Romdhane et al., 2016b, 2019). Observed DT<sub>50</sub> at 1 $\times$  RfD were in the range of those measured in other studies (4–7 days in dark) confirming that sulcotrione is rapidly dissipated from soils (Barchanska et al., 2016). Concomitantly to sulcotrione dissipation and, as previously observed by Romdhane et al. (2016b), CMBA, the principal transformation product of sulcotrione, is accumulated in Perpignan soil in both microcosm batches. As expected, for both Decano<sup>®</sup> and sulcotrione, at a higher dose rate of application, dissipation lasted longer than at lower rate of application.

The effect of sulcotrione and of Decano<sup>®</sup> on the abundance and the diversity of both the total and *hppd* soil bacterial communities was measured by qPCR and amplicon Illumina sequencing, respectively. Both treatments had no effect on the abundance of the total soil bacterial community. This observation is in accordance with that of Romdhane et al. (2016a) showing that natural triketone (i.e., leptospermone) has either no effect or very short-lasting effect on the abundance of the total bacterial community. It has to be noticed that mesotrione, another  $\beta$ -triketone, was shown to transiently modify the abundance and the diversity of both soil bacterial and fungal communities (Du et al., 2018). It suggests that  $\beta$ -triketone ecotoxicological effect on microorganisms depends on the active compound, on the soil type and on their interactions. Similarly, the two treatments, at both doses, had no effect on the composition and structure of the total bacterial community. This is in agreement with Romdhane et al. (2019) who reported no change of  $\alpha$ - and  $\beta$ -diversities of the total bacterial community in the soil of Perpignan exposed to either 1 $\times$  or 10 $\times$  RfD of sulcotrione. Interestingly, one can observe that different studies carried out on the same soil at different times with different sequencing technologies (454 pyrosequencing vs Illumina sequencing) under similar conditions led to similar conclusions showing the reliability of such approaches, as already suggested (Luo et al., 2012) and consolidating our observations.

Soil bacterial *hppd* abundance and diversity have already been monitored in Perpignan soil (Thiour-Mauprivez et al., 2020) but, to our best knowledge, this was the first time they were monitored in response to a sulcotrione and Decano<sup>®</sup> exposure. As observed for the total bacterial community, both treatments applied at both doses have no effect on the abundance and diversity of the *hppd* bacterial community. Therefore, one can conclude that, under our experimental conditions, the *hppd* bacterial community harboring the gene target of  $\beta$ -triketone herbicides is insensitive to formulated sulcotrione or to the active substance. The low

persistence of sulcotrione in Perpignan soil indicates that soil bacterial community is only shortly exposed to  $\beta$ -triketone and such a short exposure is not enough to modify the abundance or the diversity of the soil bacterial community. In addition, detoxification mechanisms such as efflux transporters, known as unspecific drivers of resistance of bacteria to antibiotics, could work as a detoxification mechanism against  $\beta$ -triketones and even could stop them entering the cell. Such mechanisms have already been observed in an *Escherichia coli* strain exposed to glyphosate (Staub et al., 2012). However, another  $\beta$ -triketone formulated product called Callisto® (mesotrione) is shown to transiently inhibit the nitrification process in bacteria when applied at  $10\times$  RfD, probably because of a direct effect (Crouzet et al., 2016). This further reinforces the assumption that like for other herbicidal active substances, the  $\beta$ -triketone ecotoxicological effect on microorganisms depends on the properties of active compound, of soil type and of their interactions.

### Estimation of the Ecotoxicological Effect of $\beta$ -Triketone on the Abundance, Composition, and Diversity of Both Total- and *hppd*-Bacterial Communities Under Field Conditions

The lab-to-field assessment of the ecotoxicological impact of active substances on soil microorganisms has been proposed as a gold standard to conduct environmental risk assessment of pesticides (Karpouzias et al., 2016). Consequently, in parallel to lab-experiments, the impact of  $\beta$ -triketone PPPs, including mesotrione- and/or tembotrione-based PPPs was measured on the abundance, the composition and the diversity of both the total and the *hppd* bacterial communities in field samples collected over 1 year cropping cycle.

The main result of this field study concerns one of the tested fields (field 2), in which the *hppd* bacterial community abundance decreased after the first treatment with mesotrione-based herbicide (Camix®) to finally increase after the second treatment with tembotrione-, dicamba-, nicosulfuron-, and alkylpolyglucoside-based herbicides but without reaching the level of abundance measured initially. This suggests a partial resilience of the *hppd* community in this field. This observed time effect might be due to different factors such as climatic conditions or the phenology of the crop. It could also be explained by the PPP treatments applied to this field. However, we are not able to conclude whether the abundance decrease is due to mesotrione because: (i) Camix® is composed, in addition to mesotrione, of S-metolachlor (400 g/L) and benoxacor (20 g/L); (ii) the  $\alpha$ -diversity of this field is significantly lower than those measured in fields 1 and 3, making a comparison uneasy. Regarding the  $\beta$ -diversity measured in this field, it remained unchanged and identical to the other fields all along the cropping cycle.

This field experiment reveals the difficulty to define reliable references when working on formulated product composed of several active compounds with different action modes and of several other compounds entering in their formulation that are usually bound by confidentiality by the agrochemical firms.

Considering this, it becomes evident that the conclusions of *a priori* risk assessment carried out under control conditions for a single active compound cannot be expanded for a formulated PPP applied in combination with others in the field all along the cropping cycle. This study also highlights the difficulty to define reliable controls when working on real agronomical situations encountered on farms. Indeed, in our experimental design, we chose a control field not exposed to  $\beta$ -triketones located closely to the other two sampled fields cropped with maize and exposed to herbicides. Even if the soils of chosen fields are subjected to the same pedoclimatic conditions and harbor similar physicochemical properties, differences in the bacterial composition were readily observed at the first sampling date. This raises the question of the reference to interpret the changes in response to the PPP treatments applied. Consequently, there is a need to define a normal operating range (NOR) for each studied indicator as it has been evaluated on diverse indicators (soil microbial biomass and bacterial diversity) in a 13 km<sup>2</sup> parcel on 278 soils all spaced from 215 meters (Constancias et al., 2015). The fully randomized block design that is usually applied in agronomical assay has been shown in the past to be of interest to estimate the impact of several active substances applied one by one on soil microorganisms (Papadopoulou et al., 2016; Storck et al., 2018), but it seems not appropriate to evaluate the risk encountered in-farm at a systemic level which is far more complex with a combination of PPPs applied simultaneously or one after the other all along the cropping cycle.

## CONCLUSION

Our study provides a comprehensive lab-to-field assessment of the ecotoxicity of  $\beta$ -triketone herbicides (active compound and formulated one) on both the total and *hppd* bacterial communities. Our lab-experiment confirmed the low persistence of the active substance in both sulcotrione and Decano® treated soil microcosms. Under our experimental conditions, both treatments at agronomical doses have no effect on the abundance, the composition and the diversity of both total and *hppd* bacterial communities. Our field-experiment led to similar conclusions thereby comforting the eco-friendly reputation of  $\beta$ -triketone herbicides.

## DATA AVAILABILITY STATEMENT

The datasets presented in this study can be found in online repositories. The names of the repository/repositories and accession number(s) can be found below: NCBI, accession number: PRJNA666084 (<https://www.ncbi.nlm.nih.gov/sra/?term=PRJNA666084>).

## AUTHOR CONTRIBUTIONS

CT-M, LB, FM-L, MD-L, and CC conceived and designed the research. CT-M and CC conducted the chemical analysis. CT-M, MD-L, AS, and AM conducted the bioinformatics analysis.



JB and DB conducted the PCR experiments. LA conducted the field sampling. CT-M, FM-L, and LB wrote the manuscript. All authors read and approved the manuscript.

## FUNDING

This work was supported by the Région Occitanie and European Funds for Regional Development (FEDER). Authors also

thank Perpignan University Via Domitia for their financial support (BQR, 2018).

## SUPPLEMENTARY MATERIAL

The Supplementary Material for this article can be found online at: <https://www.frontiersin.org/articles/10.3389/fmicb.2020.610298/full#supplementary-material>

## REFERENCES

- Barchanska, H., Kluza, A., Krajczewska, K., and Maj, J. (2016). Degradation study of mesotrione and other triketone herbicides on soils and sediments. *J. Soils Sediments* 16, 125–133. doi: 10.1007/s11368-015-1188-1
- Calvayrac, C., Martin-Laurent, F., Faveaux, A., Picault, N., Panaud, O., Coste, C.-M., et al. (2012). Isolation and characterisation of a bacterial strain degrading the herbicide sulcotrione from an agricultural soil. *Pest. Manag. Sci.* 68, 340–347. doi: 10.1002/ps.2263
- Cantrell, C. L., Dayan, F. E., and Duke, S. O. (2012). Natural products as sources for new pesticides. *J. Nat. Prod.* 75, 1231–1242. doi: 10.1021/np300024u
- Chaabane, H., Vulliet, E., Calvayrac, C., Coste, C.-M., and Cooper, J.-F. (2008). Behaviour of sulcotrione and mesotrione in two soils. *Pest. Manag. Sci.* 64, 86–93. doi: 10.1002/ps.1456
- Constancias, F., Terrat, S., Saby, N. P. A., Horrigue, W., Villerd, J., Guillemin, J.-P., et al. (2015). Mapping and determinism of soil microbial community distribution across an agricultural landscape. *Microbiologyopen* 4, 505–517. doi: 10.1002/mbo3.255
- Crouzet, O., Poly, F., Bonnemoy, F., Bru, D., Batisson, I., Bohatier, J., et al. (2016). Functional and structural responses of soil N-cycling microbial communities to the herbicide mesotrione: a dose-effect microcosm approach. *Environ. Sci. Pollut. Res. Int.* 23, 4207–4217. doi: 10.1007/s11356-015-4797-8
- Dayan, F. E., Duke, S. O., Sauldubois, A., Singh, N., McCurdy, C., and Cantrell, C. (2007). p-Hydroxyphenylpyruvate dioxygenase is a herbicidal target site for beta-triketones from *Leptospermum scoparium*. *Phytochemistry* 68, 2004–2014. doi: 10.1016/j.phytochem.2007.01.026
- Decaens, T., Jiménez, J. J., Gioia, C., Measey, G. J., and Lavelle, P. (2006). The values of soil animals for conservation biology. *Eur. J. Soil Biol.* 42, S23–S38. doi: 10.1016/j.ejsobi.2006.07.001
- Du, Z., Zhu, Y., Zhu, L., Zhang, J., Li, B., Wang, J., et al. (2018). Effects of the herbicide mesotrione on soil enzyme activity and microbial communities. *Ecotoxicol. Environ. Saf.* 164, 571–578. doi: 10.1016/j.ecoenv.2018.08.075
- Edgar, R. C. (2004). MUSCLE: multiple sequence alignment with high accuracy and high throughput. *Nucleic Acids Res.* 32, 1792–1797. doi: 10.1093/nar/gkh340
- European Commission (2010). *Soil Biodiversity: Functions, Threats and Tools for Policy Makers*. Brussels: European Commission.
- Gardi, C., Jeffery, S., and Saltelli, A. (2013). An estimate of potential threats levels to soil biodiversity in EU. *Glob. Chang. Biol.* 19, 1538–1548. doi: 10.1111/gcb.12159
- Graham, E. B., Knelman, J. E., Schindlbacher, A., Siciliano, S., Breulmann, M., Yannarell, A., et al. (2016). Microbes as engines of ecosystem function: when does community structure enhance predictions of ecosystem processes? *Front. Microbiol.* 7:214. doi: 10.3389/fmicb.2016.00214
- Karpouzias, D. G., Tsiamis, G., Trevisan, M., Ferrari, F., Malandain, C., Sibourg, O., et al. (2016). “LOVE TO HATE” pesticides: felicity or curse for the soil microbial community? An FP7 IAPP Marie Curie project aiming to establish tools for the assessment of the mechanisms controlling the interactions of pesticides with soil microorganisms. *Environ. Sci. Pollut. Res. Int.* 23, 18947–18951. doi: 10.1007/s11356-016-7319-4
- Lee, C.-M., Yeo, Y.-S., Lee, J.-H., Kim, S.-J., Kim, J.-B., Han, N. S., et al. (2008). Identification of a novel 4-hydroxyphenylpyruvate dioxygenase from the soil metagenome. *Biochem. Biophys. Res. Commun.* 370, 322–326. doi: 10.1016/j.bbrc.2008.03.102
- Li, W., and Godzik, A. (2006). Cd-hit: a fast program for clustering and comparing large sets of protein or nucleotide sequences. *Bioinformatics* 22, 1658–1659. doi: 10.1093/bioinformatics/btl158
- Luo, C., Tsementzi, D., Kyrpides, N., Read, T., and Konstantinidis, K. T. (2012). Direct comparisons of Illumina vs. Roche 454 sequencing technologies on the same microbial community DNA sample. *PLoS One* 7:e30087. doi: 10.1371/journal.pone.0030087
- Mitchell, G., Bartlett, D. W., Fraser, T. E., Hawkes, T. R., Holt, D. C., Townson, J. K., et al. (2001). Mesotrione: a new selective herbicide for use in maize. *Pest. Manag. Sci.* 57, 120–128. doi: 10.1002/1526-4998(200102)57:2<120::AID-PS254<3.0.CO;2-E
- Moran, G. R. (2005). 4-Hydroxyphenylpyruvate dioxygenase. *Arch. Biochem. Biophys.* 433, 117–128. doi: 10.1016/j.abb.2004.08.015
- Muyzer, G., Hottentrager, S., Teske, A., and Waver, C. (1996). “Denaturing gradient gel electrophoresis of PCR-amplified 16S rDNA. A new molecular approach to analyze the genetic diversity of mixed microbial communities,” in *Molecular Microbial Ecology Manual*, eds A. D. L. Akkermans, J. D. van Elsas, and F. J. de Bruijn (Dordrecht: Kluwer Academic Publishing), 3.4.4.1–3.4.4.22.
- Ockleford, C., Adriaanse, P., Berny, P., Brock, T., Duquesne, S., Grilli, S., et al. (2017). Scientific Opinion addressing the state of the science on risk assessment of plant protection products for in-soil organisms. *EFSA J.* 15:e04690. doi: 10.2903/j.efsa.2017.4690
- Oksanen, J., Blanchet, G., Friendly, M., Kindt, R., Legendre, P., McGlinn, D., et al. (2020). *Vegan: Community Ecology Package. Version 2.5–7*. Available online at: <http://vegan.r-forge.r-project.org/>
- Papadopolou, E. S., Karas, P. A., Nikolaki, S., Storck, V., Ferrari, F., Trevisan, M., et al. (2016). Dissipation and adsorption of Isoproturon, Tebuconazole, Chlorpyrifos and their main transformation products under laboratory and field conditions. *Sci. Total Environ.* 569–570, 86–96. doi: 10.1016/j.scitotenv.2016.06.133
- Petric, I., Philippot, L., Abbate, C., Bispo, A., Chesnot, T., Hallin, S., et al. (2011). Inter-laboratory evaluation of the ISO standard 11063 Soil quality — method to directly extract DNA from soil samples. *J. Microbiol. Methods* 84, 454–460. doi: 10.1016/j.mimet.2011.01.016
- Price, M. N., Dehal, P. S., and Arkin, A. P. (2009). FastTree: computing large minimum evolution trees with profiles instead of a distance matrix. *Mol. Biol. Evol.* 26, 1641–1650. doi: 10.1093/molbev/msp077
- R Development Core Team (2005). *R: A Language and Environment for Statistical Computing*. Vienna: R Foundation for Statistical Computing.
- Rocaboy-Faquet, E., Noguer, T., Romdhane, S., Bertrand, C., Dayan, F. E., and Barthelmebs, L. (2014). Novel bacterial bioassay for a high-throughput screening of 4-hydroxyphenylpyruvate dioxygenase inhibitors. *Appl. Microbiol. Biotechnol.* 98, 7243–7252. doi: 10.1007/s00253-014-5793-5
- Rohart, F., Gautier, B., Singh, A., and Cao, K.-A. L. (2017). mixOmics: an R package for ‘omics feature selection and multiple data integration. *PLoS Comput. Biol.* 13:e1005752. doi: 10.1371/journal.pcbi.1005752
- Romdhane, S., Devers-Lamrani, M., Barthelmebs, L., Calvayrac, C., Bertrand, C., Cooper, J.-F., et al. (2016a). Ecotoxicological impact of the bioherbicide leptosperone on the microbial community of two arable soils. *Front. Microbiol.* 7:775. doi: 10.3389/fmicb.2016.00775
- Romdhane, S., Devers-Lamrani, M., Martin-Laurent, F., Calvayrac, C., Rocaboy-Faquet, E., Riboul, D., et al. (2016b). Isolation and characterization of *Bradyrhizobium* sp. SR1 degrading two  $\beta$ -triketone herbicides. *Environ. Sci. Pollut. Res. Int.* 23, 4138–4148. doi: 10.1007/s11356-015-4544-1

- Romdhane, S., Devers-Lamrani, M., Beguet, J., Bertrand, C., Calvayrac, C., Salvia, M.-V., et al. (2019). Assessment of the ecotoxicological impact of natural and synthetic  $\beta$ -triketone herbicides on the diversity and activity of the soil bacterial community using omic approaches. *Sci. Total Environ.* 651, 241–249. doi: 10.1016/j.scitotenv.2018.09.159
- Schloss, P. D., and Handelsman, J. (2006). Toward a census of bacteria in soil. *PLoS Comput. Biol.* 2:e020092. doi: 10.1371/journal.pcbi.0020092
- Schulz, A., Ort, O., Beyer, P., and Kleinig, H. (1993). SC-0051, a 2-benzoyl-cyclohexane-1,3-dione bleaching herbicide, is a potent inhibitor of the enzyme p-hydroxyphenylpyruvate dioxygenase. *FEBS Lett.* 318, 162–166. doi: 10.1016/0014-5793(93)80013-k
- Staub, J. M., Brand, L., Tran, M., Kong, Y., and Rogers, S. G. (2012). Bacterial glyphosate resistance conferred by overexpression of an *E. coli* membrane efflux transporter. *J. Ind. Microbiol. Biotechnol.* 39, 641–647. doi: 10.1007/s10295-011-1057-x
- Storck, V., Nikolaki, S., Perruchon, C., Chabanis, C., Sacchi, A., Pertile, G., et al. (2018). Lab to field assessment of the ecotoxicological impact of Chlorpyrifos, Isoproturon, or Tebuconazole on the diversity and composition of the soil bacterial community. *Front. Microbiol.* 9:1412. doi: 10.3389/fmicb.2018.01412
- Takahashi, S., Tomita, J., Nishioka, K., Hisada, T., and Nishijima, M. (2014). Development of a prokaryotic universal primer for simultaneous analysis of bacteria and archaea using Next-generation sequencing. *PLoS One* 9:e105592. doi: 10.1371/journal.pone.0105592
- Thiour-Mauprivez, C., Devers-Lamrani, M., Mounier, A., Beguet, J., Spor, A., Calvayrac, C., et al. (2020). Design of a degenerate primer pair to target a bacterial functional community: the *hpd* bacterial gene coding for the enzyme targeted by herbicides, a study case. *J. Microbiol. Methods* 170:105839. doi: 10.1016/j.mimet.2020.105839
- Thiour-Mauprivez, C., Martin-Laurent, F., Calvayrac, C., and Barthelmebs, L. (2019). Effects of herbicide on non-target microorganisms: towards a new class of biomarkers? *Sci. Total Environ.* 684, 314–325. doi: 10.1016/j.scitotenv.2019.05.230
- Wall, D. H., Bardgett, R. D., Behan-Pelletier, V., Herrick, J. E., Jones, T. H., and Strong, D. R. (2013). *Soil Ecology and Ecosystem Services*. Oxford: Oxford University Press.
- Wang, Q., Quensen, J. F., Fish, J. A., Lee, T. K., Sun, Y., Tiedje, J. M., et al. (2013). Ecological Patterns of *nifH* genes in four terrestrial climatic zones explored with targeted metagenomics using FrameBot, a new informatics tool. *mBio* 4:e00592-13. doi: 10.1128/mBio.00592-13
- Zhang, J., Kobert, K., Flouri, T., and Stamatakis, A. (2014). PEAR: a fast and accurate Illumina Paired-End reAd mergeR. *Bioinformatics* 30, 614–620. doi: 10.1093/bioinformatics/btt593

**Conflict of Interest:** The authors declare that the research was conducted in the absence of any commercial or financial relationships that could be construed as a potential conflict of interest.

Copyright © 2021 Thiour-Mauprivez, Devers-Lamrani, Bru, Béguet, Spor, Mounier, Alletto, Calvayrac, Barthelmebs and Martin-Laurent. This is an open-access article distributed under the terms of the Creative Commons Attribution License (CC BY). The use, distribution or reproduction in other forums is permitted, provided the original author(s) and the copyright owner(s) are credited and that the original publication in this journal is cited, in accordance with accepted academic practice. No use, distribution or reproduction is permitted which does not comply with these terms.



# Relative Influence of Plastic Debris Size and Shape, Chemical Composition and Phytoplankton-Bacteria Interactions in Driving Seawater Plastisphere Abundance, Diversity and Activity

## OPEN ACCESS

### Edited by:

Aurélië Cebron,  
UMR7360 Laboratoire  
Interdisciplinaire des Environnements  
Continents (LIEC), France

### Reviewed by:

Inga Vanessa Kirstein,  
Aalborg University, Denmark  
Luciano Procópio,  
Federal University of Rio de Janeiro,  
Brazil  
Daniela Batista,  
University of Minho, Portugal

### \*Correspondence:

Jean-François Ghiglione  
ghiglione@obs-banyuls.fr

### Specialty section:

This article was submitted to  
Microbiotechnology,  
a section of the journal  
Frontiers in Microbiology

**Received:** 25 September 2020

**Accepted:** 11 December 2020

**Published:** 13 January 2021

### Citation:

Cheng J, Jacquin J, Conan P,  
Pujo-Pay M, Barbe V, George M,  
Fabre P, Bruzard S, Ter Halle A,  
Meistertzheim A-L and Ghiglione J-F  
(2021) Relative Influence of Plastic  
Debris Size and Shape, Chemical  
Composition  
and Phytoplankton-Bacteria  
Interactions in Driving Seawater  
Plastisphere Abundance, Diversity  
and Activity.  
Front. Microbiol. 11:610231.  
doi: 10.3389/fmicb.2020.610231

Jingguang Cheng<sup>1</sup>, Justine Jacquin<sup>1</sup>, Pascal Conan<sup>1</sup>, Mireille Pujo-Pay<sup>1</sup>, Valérie Barbe<sup>2</sup>,  
Matthieu George<sup>3</sup>, Pascale Fabre<sup>3</sup>, Stéphane Bruzard<sup>4</sup>, Alexandra Ter Halle<sup>5</sup>,  
Anne-Leila Meistertzheim<sup>6</sup> and Jean-François Ghiglione<sup>1\*</sup>

<sup>1</sup> UMR 7621, CNRS, Laboratoire d'Océanographie Microbienne, Observatoire Océanologique de Banyuls-sur-Mer, Sorbonne Université, Banyuls-sur-Mer, France, <sup>2</sup> Génétique Métabolique, Genoscope, Institut François Jacob, CEA, CNRS, Univ Evry, Université Paris-Saclay, Evry, France, <sup>3</sup> Laboratoire Charles Coulomb (L2C), UMR 5221 CNRS-UM, Place Eugène Bataillon, Montpellier, France, <sup>4</sup> Institut de Recherche Dupuy de Lôme (IRD), Université Bretagne Sud, UMR CNRS 6027, Lorient, France, <sup>5</sup> IMRCP, Université de Toulouse, CNRS, Toulouse, France, <sup>6</sup> SAS Plastic@Sea, Observatoire Océanologique de Banyuls-sur-Mer, Banyuls-sur-Mer, France

The thin film of life that inhabits all plastics in the oceans, so-called “plastisphere,” has multiple effects on the fate and impacts of plastic in the marine environment. Here, we aimed to evaluate the relative influence of the plastic size, shape, chemical composition, and environmental changes such as a phytoplankton bloom in shaping the plastisphere abundance, diversity and activity. Polyethylene (PE) and polylactide acid (PLA) together with glass controls in the forms of meso-debris (18 mm diameter) and large-microplastics (LMP; 3 mm diameter), as well as small-microplastics (SMP) of 100  $\mu$ m diameter with spherical or irregular shapes were immersed in seawater during 2 months. Results of bacterial abundance (confocal microscopy) and diversity (16S rRNA Illumina sequencing) indicated that the three classical biofilm colonization phases (primo-colonization after 3 days; growing phase after 10 days; maturation phase after 30 days) were not influenced by the size and the shape of the materials, even when a diatom bloom (*Pseudo-nitzschia* sp.) occurred after the first month of incubation. However, plastic size and shape had an effect on bacterial activity (<sup>3</sup>H leucine incorporation). Bacterial communities associated with the material of 100  $\mu$ m size fraction showed the highest activity compared to all other material sizes. A mature biofilm developed within 30 days on all material types, with higher bacterial abundance on the plastics compared to glass, and distinct bacterial assemblages were detected on each material type. The diatom bloom event had a great impact on the plastisphere of all

materials, resulting in a drastic change in diversity and activity. Our results showed that the plastic size and shape had relatively low influence on the plastisphere abundance, diversity, and activity, as compared to the plastic composition or the presence of a phytoplankton bloom.

**Keywords:** plastic litter, plastisphere, biofilm, biofouling, colonization, microbial ecotoxicology

## INTRODUCTION

Plastic pollution has become a global environmental problem affecting all parts of oceans worldwide, including the most remote areas such as deep seafloor or polar regions. In this area, the longevity of the plastics is estimated to be hundreds to thousands of years (Barnes et al., 2009; Lusher et al., 2015; Kane et al., 2020). Vast accumulation zones have been identified in the five subtropical oceanic gyres (Van Sebille et al., 2015), but also in the Mediterranean Sea that has been proposed as the sixth great accumulation zone for marine litter (Cózar et al., 2015). Variation in quantity and composition was observed throughout the different environmental compartments: polyethylene (PE) and polypropylene (PP) were mostly observed in epipelagic waters, whereas polyamide and polyester dominated in sediments. These variations have been explained through the differences in density, surface area, and the size of plastic litter (Chubarenko et al., 2016; Kowalski et al., 2016; Schwarz et al., 2019).

Once entering the environment, plastic litter is subjected to degradation caused by a combination of mechanical abrasion, photo- or thermal-oxidation, hydrolysis and biodegradation (Andrady, 2003). Plastic degradation results in the formation of tiny plastic fragments of <5 mm size, so-called “secondary microplastics” that differ from the “primary microplastics” that are designed and produced as purpose, for example in industrial cleaners and personal care products. Larger plastics are classically categorized into meso-debris (5 mm–2 cm) and macro-debris (>2 cm) for large-scale and long-term monitoring of plastic litter across countries and environments (Thompson et al., 2009). Over the estimated 5.25 trillion particles are afloat in the global ocean, 34.8% of which are small microplastics (SMP; 330 µm–1 mm), 57.5% of large microplastics (LMP; 1–5 mm), 7% of meso-plastics, and 0.2% of macro-plastics (Eriksen et al., 2014). Large debris have been shown to have adverse effects on fish, seabirds, and other top consumers, whereas microplastics are suitable for ingestion by smaller organisms at lower trophic levels (Wang et al., 2019).

When directly released at sea, plastics are primarily colonized by microorganisms that form dense biofilms on their surfaces, the so-called “plastisphere” (Zettler et al., 2013). The plastisphere has multiple effects on the fate and impacts of plastic in the marine environment. First, the biofilm growing on the surface and inside plastic cracks can contribute to a loss of physical integrity, a phenomenon called “biodeterioration” that play a significant role on the breakdown of large plastic debris into microplastics when coupled with abiotic degradation (Sabev et al., 2006; Dussud and Ghiglione, 2014). Second, the biofouling may increase or decrease the buoyancy of the plastic particles, rendering them susceptible to vertical transport (Kooi et al., 2017; Kane et al.,

2020). Third, extracellular polymeric substances produced by the biofilm contribute to co-aggregation of microorganisms and detritus together with microplastics, thus resulting in an increase or decrease of sedimentation rates of algal bloom (such as diatoms or cryptophytes) with important impact on ecosystem functioning (Long et al., 2015; Severin et al., 2017). Fourth, biofilms alter the physico-chemical properties of plastics and increase further colonization by metazoan larvae (Hadfield, 2011; Ghiglione and Laudet, 2020). Fifth, biofilms can host pathogens species that can be transported across the marine environment by plastic dispersion and thus participate to the diffusion of infectious diseases (Zettler et al., 2013; Kirstein et al., 2016). And finally, plastic biodegradation is promoted by the biofilm by secreting extracellular enzymes able to transform polymers into oligomers and monomers (“biofragmentation”), which can serve as carbon source for microbial growth (“bio-assimilation”) that may result in the complete mineralization of polymers into CO<sub>2</sub> and H<sub>2</sub>O (“biomineralization”) (Jacquin et al., 2019).

A growing literature is reporting the large diversity of microorganisms that composed the plastisphere, which differed from the surrounding communities living in a free-living state (Zettler et al., 2013; Bryant et al., 2016; Pinto et al., 2019), or attached to organic particles (Dussud et al., 2018b), sediment particles (Basili et al., 2020) or other substrates such as wood, cellulose or glass (Kirstein et al., 2018; Oberbeckmann et al., 2018; Ogonowski et al., 2018). The reasons for the preferential attachment of specific communities to plastic particles is still enigmatic. Within the plastisphere communities directly sampled at sea, several factors such as plastic type (polyethylene, polypropylene, polystyrene), geographical location or seasons appeared to differentiate the biofilm communities (Amaral-Zettler et al., 2015; Oberbeckmann et al., 2018). Other factors such as hydrophobicity, topography, roughness, crystallinity, and surface charge may play a role in the selection of bacterial community in the early stages of colonization, which is a crucial step for the following colonizing communities by modifying the material-specific surface properties (Rummel et al., 2017). Most of the above studies focused on microbial diversity and abundance, but only one evaluated the corresponding activity of the microorganisms that form the biofilm (Dussud et al., 2018a). Moreover, only one observation based on field study tested the influence of plastic size and shape (Frère et al., 2018) that is often mentioned as having a crucial role in shaping the biofilm (Oberbeckmann et al., 2015; Harrison et al., 2018), but no specifically designed experiment was dedicated to this question so far.

The aim of this study was to test how much plastisphere was influenced by different polymer composition (PE and PLA), sizes (SMP, LMP, and meso-plastics of 100 µm, 3 mm, and 1.8 cm



in diameter, respectively) and shape (spherical vs. irregular in the case of SMP). During the 2-months incubation in natural seawater from the NW Mediterranean Sea, we also evaluated the impact of environmental change such as a phytoplankton bloom. We hypothesized that the plastisphere may be more influenced by phytoplankton-bacteria interactions rather than the plastic composition, size or shape. Temporal variations of bacterial abundance (confocal microscopy), diversity (16S rRNA sequencing) and heterotrophic activity (radiolabeled leucine incorporation) were measured on all plastic types, but also compared to glass of similar size and shape, as well as to the surrounding seawater.

## MATERIALS AND METHODS

### Preparation of Polymers of Different Composition, Size and Shape

High density-polyethylene (HDPE) and Poly L lactic acid (PLA) were supplied by the Good Fellow company (Avilés, Spain) in a form of film of 10 and 50  $\mu\text{m}$  thickness ( $\pm 20\%$ ), respectively. Circular pieces of respectively 3 mm and 1.8 cm in diameter were cut using a hole puncher. Glass coverslip (soda lime composition) were supplied by the Verres Vagner company (Toulouse, France) in circular form with 1.8 cm and 3 mm diameter of 170  $\mu\text{m}$  thickness.

Irregular PLA and glass microbeads were obtained by cryo-grinding the polymer and glass films described above (SPEX sample Prep), which were further sieved with ethanol in order to recover the microparticles for which the size was ranging from 90 to 125  $\mu\text{m}$ . Material for HDPE irregular microbeads were obtained from Good Fellow films with 1 mm thickness to ensure the 3-dimensional structure, and then reduced in size by cryo-grinding as described above.

Spherical HDPE microbeads of size distribution between 96–125  $\mu\text{m}$  were commercially available (CPMS-0.96, Cospheric<sup>TM</sup>). Spherical PLA microbeads were obtained as pellets and transformed in spherical microbeads by solvent emulsion-evaporation technique (O'Donnell and McGinity, 1997). It consisted in dissolving the polymer in a volatile organic solvent immiscible with water (dichloromethane), then introducing this solution into an aqueous solution containing an emulsifier as poly(vinyl alcohol) (PVA, 2%). The emulsion was finally placed under moderate magnetic stirring for 24 h at atmospheric pressure and ambient temperature, in order to allow the microbeads to harden, until complete evaporation of the organic solvent. The spherical PLA microbeads were collected by wet sieving between 90 and 125  $\mu\text{m}$ , rinsed with permuted water and lyophilized until further use. Spherical glass microbeads were mainly made up with soda lime and commercially available (Good Fellow company, Avilés, Spain).

Granulometry analysis using a laser diffraction particle size analyzer (Mastersizer 2000 model with a Scirocco 2000 module, Malvern, United Kingdom) showed a gaussian distribution of the microbeads that always peaked at 100  $\mu\text{m}$  for all polymers for spherical or non-spherical beads. Before the experiment, all the materials (including irregular microbeads (IR), spherical regular

microbeads (RE) of average 100  $\mu\text{m}$  diameter as well as films of 3 mm and 1.8 cm in diameter) were washed for 1 h with ethanol followed by 3 rounds of vortex (1 min) and sonic bath (3 min) and then dried under the sterile hood.

### Experiment Setup

Each material type (spherical or irregular 100  $\mu\text{m}$  microbeads, 3 mm and 1.8 cm films of PE, PLA and glass, respectively) was placed separately in 12 identical glass tanks of 2 L capacity (Plastic@Sea, Banyuls-sur-mer, France), in which seawater was continually renewed (flow rate was set on 20  $\text{mL min}^{-1}$ ) by direct pumping at 14 m depth in Banyuls bay closed to the SOLA observatory station (NW Mediterranean Sea, France). Three additional tanks containing circulating seawater served as controls. Seawater was pre-filtered with 20  $\mu\text{m}$  porosity filters (Dutscher<sup>TM</sup>, France) to remove inorganic matter and potential predator in front of each tank. The tanks were placed in a dark room and illuminated from above in a 12/12 h light/dark rhythm by Lumivie LED RAL G2-SBM lamps (Zoomalia, France) with a nominal luminous flux of 1860 lm each. The experiment started from 13 August 2019, and samples were taken after 3, 10, 30, and 66 days (designated as D3, D10, D30, and D66, hereafter).

### Seawater Environmental Variables

Temperature, salinity, inorganic nutrients, chlorophyll *a*, and particulate organic carbon were weekly recorded *in situ* at the SOLA station (0.5 miles off the coast) in the framework of the French national coastal monitoring program “Service d’Observation en Milieu Littoral” (SOMLIT) according to protocols previously described (Ghiglione et al., 2005; Blanchet et al., 2017) and available on the SOMLIT website<sup>1</sup>. All samples were processed after sampling within 30 min.

### Confocal Microscopy and Flow Cytometry

For each sampling date, triplicate samples were fixed with 1% (v/v) glutaraldehyde for 30 min before freezing until analysis. Samples were stained with a 4,6-diamidino-2-phenylindole (DAPI) solution (final concentration 10% [v/v], Sigma Aldrich, France) for at least 5 min in the dark at ambient temperature before confocal microscopy observations (TCS SP8 confocal laser scanning microscope, Leica, Germany). Photomultiplier tubes (PMT3) detector was used for detecting the fluorescence signal and transmitted light detector (TLD) was used to capture the white light signal. The light intensity was compensated for the microbeads, and the Z-Step size were set on 1  $\mu\text{m}$  to get regularly spaced cross sections. For each sample, 3 beads or 3 pieces of films were used for counting the bacterial abundance using the image J software (Abramoff et al., 2004). For the regular spherical microbeads, the surface area was calculated using a simple geometrical formula. For irregular microbeads, the surface area was estimated using two different methods. First, a simple geometrical calculation based on the overall shape of the particle, i.e., ellipsoidal, cylindrical or conic. The main dimensions used

<sup>1</sup><http://somalit.epoc.u-bordeaux1.fr/>

for the surface area calculation were measured from optical images. In addition, for a series of samples, the surface was calculated via a full reconstruction of the particle surface using 1  $\mu\text{m}$  separated confocal microscopy cross-sections, using the image-J software. A 10% agreement was found between the two methods (geometrical estimation and 3D volume reconstruction) for the samples studied, thus validating the use of a simple geometrical method for irregular beads and giving us the surface measurement uncertainty. Cell counts were verified using the Gwyddion software (Nečas and Klapetek, 2012) threshold filter and grains numbering. Manual counting was performed on a series of samples to double check the cell counts accuracy, which was found to be of 10%. Cell counts were then expressed as the number of cells over surface area (in cells  $\text{mm}^{-2}$ ) with an accuracy of 20%.

In parallel, 1 mL of seawater from the control tank was also fixed using the same procedure. A volume of 500  $\mu\text{L}$  control seawater was mixed with the nucleic acid dye SYBR Green I (final concentration 0.05% [v/v], Sigma Aldrich) for 15 min at room temperature in the dark. Cell counts were performed with a FACSCanto II flow cytometer (BD Bioscience, San Jose, CA, United States) equipped with a blue laser (488-nm, air-cooled, 20-mW solid state), as previously described (Mével et al., 2008).

## Heterotrophic Bacterial Production

Bacterial production was measured in triplicate for each material at each sampling time by  $^3\text{H}$ -leucine incorporation (Dussud et al., 2018a). In brief, the films with the size of 3 and 18 mm were rinsed with sterile filtered seawater using a wash bottle before transferring to the microtubes containing 1.5 mL sterile filtered seawater (0.2  $\mu\text{m}$  pore size, polycarbonate filter, Nucleopore). Microbeads were collected on a membrane filter with 10  $\mu\text{m}$  pore size membrane filter (LCWG02500, Mitex<sup>TM</sup>) and then rinsed with sterile filtered seawater, and the seawater was removed by air pumping for 30 s to get accurate sample weight. Different mass of materials (15 mg for PE, 18 mg for PLA, and 33 mg for glass microbeads) were collected in order to homogenize the total surface areas, and then transferred into microtubes before adding 1.5 mL of sterile filtered seawater. A cell detachment pre-treatment was applied for all the materials using 3 cycles of 3 min sonication bath (Delta Sonic, France) followed by 3 min vortex at maximum speed (Skyline, Elmi Ltd., Russia). Immediately after cell-detachment,  $^3\text{H}$ -leucine (125.6 Ci  $\text{mmol}^{-1}$ , Perkin Elmer<sup>TM</sup>) were added at 1 nmol  $\text{L}^{-1}$  final concentration (completed with cold leucine to 150 nmol  $\text{L}^{-1}$ ), which consisted of 1.5 ml sterile seawater containing the film or microbeads and detached bacteria. For seawater samples from the control tanks,  $^3\text{H}$ -leucine was added at a final concentration of 4.3 nmol  $\text{L}^{-1}$  to 1.5 mL of control seawater. All the samples were incubated in the dark at 18°C for 3 h. The empirical conversion factor of 1.55 ngC  $\text{pmol}^{-1}$  of incorporated leucine was used to calculate the bacterial heterotrophic production (Kirchman, 2001; C  a et al., 2015). For each microbeads on each sampling date, the percentage of hydration of the beads were assessed by weighting 3 additional aliquots (wet weight), that were frozen, lyophilized and weighted a second time to measure dry weight. Knowing the wet weight and the percentage

of hydration of each material during the kinetic, the bacterial activity was expressed per dry weight.

Knowing the number of cells (N) per unit area for each sample and the average specific surface  $R_{SV}$  (i.e., surface to volume ratio) for each type of microbeads, we expressed the heterotrophic bacterial production as the carbon produced per unit area per unit time (ngC  $\text{mm}^{-2} \text{h}^{-1}$ ) or the specific bacterial activity as the carbon produced per cell per unit time (fgC  $\text{cell}^{-1} \text{h}^{-1}$ ). This data representation allows to meaningfully compare materials having different shapes, i.e., different surface to volume ratios.

Additionally, we used bacterial production data derived from leucine incorporation to estimate the bacterial growth rate on plastsphere, using a conversion factor of 12 fgC per cell as previously described (Fukuda et al., 1998).

## DNA Extraction, PCR, Sequencing and Data Analysis

On each sampling date, triplicates of plastic or glass were harvested from each sample by using the same method described above for the bacterial production and immediately stored at  $-80^\circ\text{C}$ . Triplicates of 2 L seawater from control tanks were also obtained using 0.2  $\mu\text{m}$  pore size polycarbonate filters (47 mm diameter, Nucleopore). The microbial genomic DNA extraction were followed with classic phenol-chloroform protocol (Ghiglione et al., 1999; Marty et al., 2012) and DNA was quantified by DeNovix (DS-11 series, United States). Polymerase chain reaction (PCR) amplification was done using universal small subunit ribosomal RNA (SSU rRNA) primers (515Y, 5'-GTGYCAGCMGCCGCGGTAA-3'; 926R, 5'-CCGYCAATTYMTTTRAGTTT-3') which has been shown to be well-suited for quantitative profiling of marine natural communities by simultaneously amplifying templates from Bacteria, Archaea and Eukaryota in a single PCR reaction (Parada et al., 2016; Yeh et al., 2019). Illumina MiSeq sequencing were performed at Genoscope (Evry, France) for the 156 samples, corresponding to the 144 samples of PE, PLA and glass (3 substrate \* 4 sampling date \* 4 size fraction \* 3 replicates) and the 12 seawater samples (4 sampling date \* 3 replicates). All the SSU rRNA data are available in the NCBI SRA repository (accession number PRJNA663787).

Processing of SSU rRNA sequences was performed using the DADA2 R package (Callahan et al., 2016). Forward and reverse 16S reads were trimmed off before error correction and denoising step. Paired reads were merged (average length from 367 to 377 bp) and all the singletons and chimeras were removed. 18S reads are 575–595 bp, which is too long for forward and reverse reads to overlap. As recommended by Parada et al. (2016) and Yeh et al. (2019), we trimmed the 18S forward reads to fixed length (220 bp) and the reverse reads was discarded before error correction and denoising step. Denoised reads were concatenated and chimeric reads were discarded. The 16S and 18S amplicon sequence variants (ASVs) were assigned with SILVA 128 database (Quast et al., 2013). The taxonomic affiliation of ASVs of interest were further verified against sequences from the NCBI database using the BLASTnt. The ASVs corresponding to eukaryotes, archaea, chloroplast and mitochondria were removed and all the

samples were rarified to the same number ( $\text{rngseed} = 1$ ) before the analyses on bacteria using the phyloseq R package (McMurdie and Holmes, 2013). The  $\alpha$ -diversity was performed using the *alpha()* function from the microbiome R package. Square root transformation was performed for the  $\beta$ -diversity analyses and hypotheses test. The taxonomy compositions were visualized using the histogram and bubble plot with the ggplot2 R package (Wickham, 2016).

To investigate the unique and shared bacterial community between biofilm and seawater, the reads from plastic or glass with different size fractions were pooled and rarefied into the same number to that of seawater. Two levels of comparison were conducted: in ASV level (presence or absence) and in tags levels.

## Statistical Analyses

An unweighted-pair group method with arithmetic (UPGMA) dendrogram based on Bray-Curtis similarities was used for visualization of beta-diversity. A similarity profile test (SIMPROF, PRIMER 6) was performed on the null hypothesis that a specific sub-cluster can be recreated by permuting the entry species and samples. The significant branch was used as a prerequisite for defining bacterial cluster.

The significance of the factor size (including irregular and regular microbeads), the substrate and the date were analyzed using the global or pairwise permutational multivariate analysis of variance (PERMANOVA) (Anderson and Walsh, 2013) using the *adonis()* function with the vegan R package (Oksanen et al., 2007), the homogeneity of variances was tested using the *betadisper()* function. The *p* value was adjusted with the Benjamin-Hochberg method. To test the bacterial community relationship between seawater and plastic, a Mantel test was performed in Vegan using the *mantel()* based on Pearson correlation method.

Three-way analyses of variance (ANOVA) were performed for statistical analyses with the type I sum of square applied for the results on bacterial abundance, bacterial production, bacterial activity and bacterial growth rate. Tukey's *post hoc* test was used when necessary. Relative importance of each predictor (in R square) for ANOVA results was further determined with function of *calc.relimp()* from relaimpo R package (Grömping, 2006). When the data did not meet homogeneity, the Welch's ANOVA was chosen for the analyses of  $\alpha$ -diversity and the ASVs comparison on results of the bubble plot. Games-Howell test was used as *post hoc* test.

## RESULTS

### Environmental Conditions

During the studied period (13th August – 20th October), the environmental conditions in the Bay of Banyuls were characteristic of an autumn situation in a temperate Mediterranean area. The surface water temperature remained stable (from 20 to 23°C) as well as the salinity that stayed around 38 (Supplementary Figure 1A).

As expected in late summer, concentrations of silicate were low ( $\sim 0.5 \mu\text{M}$ ) or often close to the detection limit for nitrate and

phosphate ( $<0.05 \mu\text{M}$  and  $<0.02$ , respectively) (Supplementary Figure 1B). Two events were clearly identified during the period and marked by a nutrient enrichment in the water column. The first had a limited magnitude on 24th September and the second was more important at the very end of the experiment on 25th October with concentrations of 2.4, 0.93, and  $0.18 \mu\text{M}$  in  $\text{Si(OH)}_4$ ,  $\text{NO}_3$  and  $\text{PO}_4$ , respectively.

These nutrient inputs due to the first mixing inducing the disruption of the water column stratification were responsible for an increase in particulate matter in the water column as shown in Supplementary Figure 1C in terms of Total Suspended Matter (TSM), and especially in terms of chlorophyll. After a low and homogeneous concentration during August and the beginning of September (range between 0.1 and  $0.2 \text{ mg m}^{-3}$  of chlorophyll a), we observed 2 peaks ( $0.5$  and  $0.6 \text{ mg m}^{-3}$  of chlorophyll a) characteristic of a coastal autumn bloom situation.

### Microbial Cell Counts and Shape

Confocal microscopy revealed a large diversity of morphological forms including spherical, rod-shaped or spiral-shaped bacterial like structure at the surface of PE, PLA and glass, for which rod-shaped and spiral-shaped structure was more observed on D3 and D10 compared to D30 and D66 (Figure 1). Typical morphotypes of diatoms appeared at D66 and were not visible before. Confocal microscopy was also useful to confirm the size distribution of microbeads between 90 and  $125 \mu\text{m}$ , as well as their shape (regular versus irregular).

Triplicate samples analyzed by confocal microscopy allowed us to follow the changes in bacterial counts for each material type and size. The data highlighted three distinct phases of biofilm formation: primo-colonization, growth, and maturation (Figure 2). Interestingly, the three distinct phases were found whatever the material type or size. Three-way ANOVA revealed significant difference in bacterial counts according to the sampling date and material type, but not within material sizes (material sizes containing the two shapes of IR and RE) ( $R^2 = 0.29, 0.29$ , and  $0.01$ , respectively). PE presented the largest bacterial abundance on average together with PLA, whereas it appeared to be ten-fold smaller on glass. A rapid primo-colonization was observed after D3, with average abundance of  $3.0 \times 10^3$ ,  $1.6 \times 10^3$ , and  $0.3 \times 10^3 \text{ cells mm}^{-2}$  for PE, PLA and glass, respectively. Slight growth was observed between D3 and D10 for PE, PLA and glass, where the bacterial abundance for glass samples remained relatively low ( $8.6 \times 10^3$ ,  $2.8 \times 10^3$ , and  $0.9 \times 10^3 \text{ cells mm}^{-2}$ , respectively). We observed a significant increase in bacterial abundance between D10 and D30. Since we did not find significant increase in bacterial counts at a later time point (between D30 and D66,  $p > 0.05$ ), it indicates that the maturation phase corresponding to the stabilization of bacterial abundance was reached for all material types from D30 and until the end of the experiment (D66). On average the mature biofilm was of  $2.5 \times 10^4$ ,  $1.5 \times 10^4$ , and  $0.2 \times 10^4 \text{ cells mm}^{-2}$  for PE, PLA and glass, respectively, with non-significant differences between size and shapes within each material type. It should be noted that PLA regular microbeads was excluded from the statistical analysis for bacterial abundance and activity, because we noted a significantly lower abundance



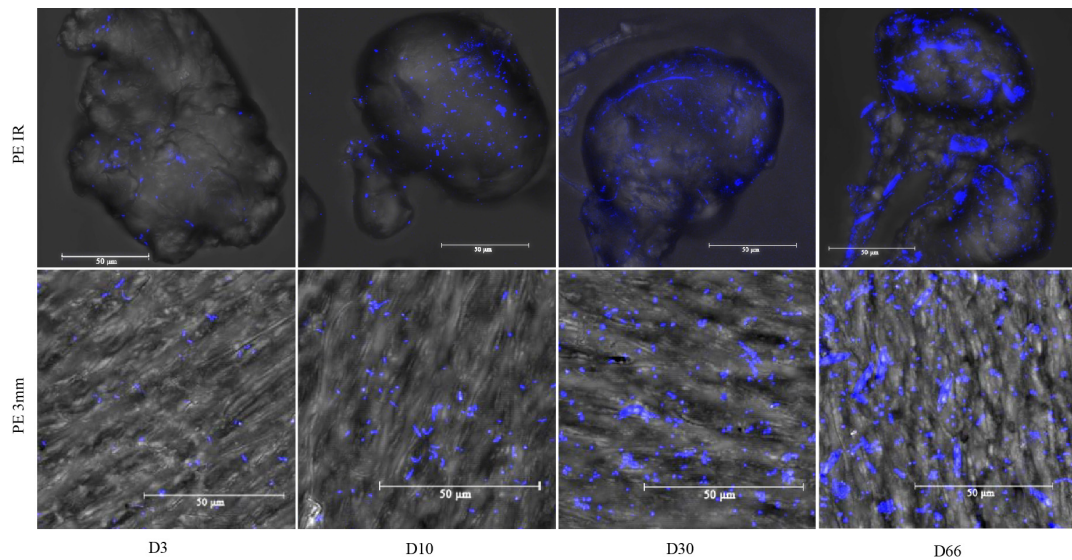


**FIGURE 1** | Confocal microscopy for polyethylene irregular microbeads of around 100  $\mu\text{m}$  diameter (PE IR) and 3 mm film (PE 3 mm) at days 3 (D3), 10 (D10), 30 (D30), and 66 (D66). Scale bar: 50  $\mu\text{m}$ . Arrows are pointing typical shape of diatoms that appeared at D66 only.

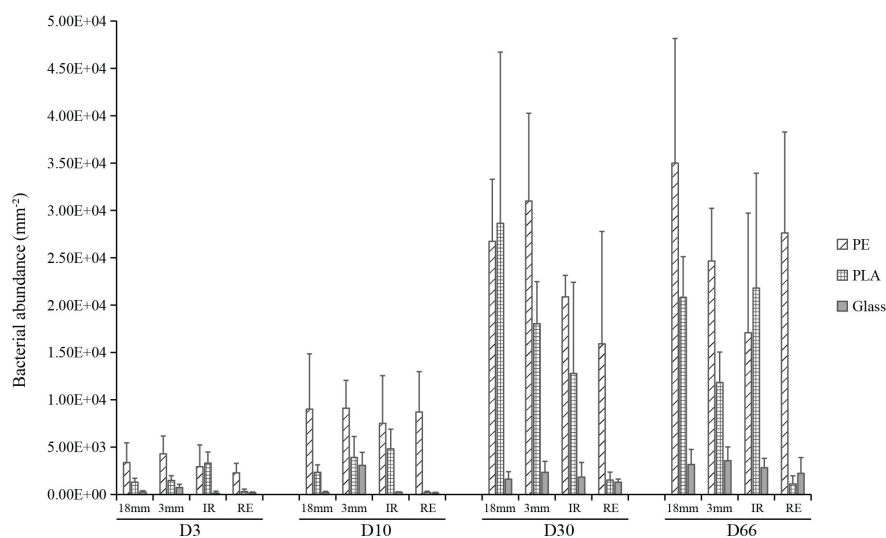


**FIGURE 2** | Bacterial cell counts per surface area ( $\text{mm}^{-2}$ ) for PE, PLA and glass on mesoplastics (18 mm diameter), large microplastics (3 mm diameter) and small microplastics microbeads (100  $\mu\text{m}$  diameter) with irregular (IR) or regular spherical shapes (RE) during the course of the experiment at days 3 (D3), 10 (D10), 30 (D30), and 66 (D66).

compared to other PLA samples, which was much closer to those of the glass samples. Indeed, we realized that the use of surfactants in the home-made synthesis of PLA regular beads could be responsible for this behavior, as surfactant could be able to remain at the beads surfaces and considerably modify their hydrophobicity.

Diatoms with the average length around 11  $\mu\text{m}$  were observed only on D66 on all materials, with higher abundance for 3 mm and 1.8 cm sizes on PE ( $3.5 \times 10^3$  cells  $\text{mm}^{-2}$ ) and PLA ( $2.4 \times 10^3$  cells  $\text{mm}^{-2}$ ) compared to glass ( $0.8 \times 10^3$  cells  $\text{mm}^{-2}$ ). They were rarely visible on spherical or regular microplastics.

The bacterial counts from seawater controls remained stable from  $4.5 \times 10^4$  to  $1.0 \times 10^5$  cells per mL all along the experiment.

## Heterotrophic Bacterial Production

Heterotrophic bacterial production (BP) was measured alongside the time course of the experiment and it was expressed in units of incorporated carbon per square millimeter per hour ( $\text{pgC mm}^{-2} \text{h}^{-1}$ ) (Figure 3A). Three-way ANOVA showed that all the factors (sampling date, material type, and size) could significantly impact the BP, being the sampling date and material type factors explaining more variation than the material size (material sizes



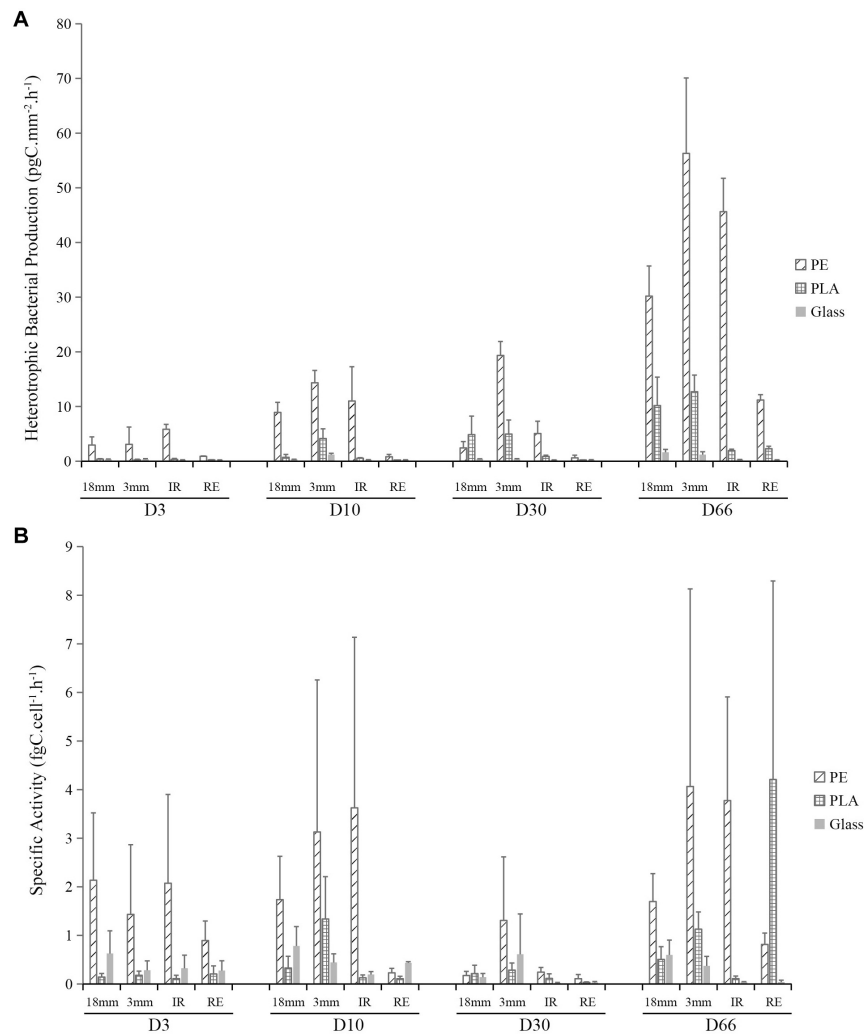


**FIGURE 3 |** Bacterial heterotrophic production (BP, pgC mm<sup>-2</sup> h<sup>-1</sup>) **(A)** and bacterial activity (fgC cell<sup>-1</sup> h<sup>-1</sup>) **(B)** for PE, PLA and glass on larger pieces (18 mm diameter), microplastics (3 mm diameter) and irregular (IR) or regular spherical (RE) microbeads (100 μm diameter) during the course of the experiment at days 3 (D3), 10 (D10), 30 (D30), and 66 (D66).

containing the two shapes of IR and RE) ( $R^2 = 0.20, 0.25$  and  $0.07$ , respectively). Significant increase has been observed from the primo-colonization phase (on D3) to the growing phase (on D10). Interestingly, the BP did not show significant differences between D10 and D30, even though there was a significant increase in bacterial abundance (Figure 2). The maturation phase showed a significant increase of BP from D30 to D66. Differences in BP were also observed on the three sample types, with PE being significantly higher than PLA and glass. In average, BP of PE is 16 and 110 times higher than that of PLA and glass by comparing within each material size. The BP of PE, PLA and glass have increased from 3.2, 0.2, and 0.1 pgC mm<sup>-2</sup> h<sup>-1</sup> at the primo-colonization phase (D3) to 35.8, 6.8, and 0.7 pgC mm<sup>-2</sup> h<sup>-1</sup> at the maturation phase (D66), with intermediate maturation phase showing 6.8, 2.7, and 0.1 pgC mm<sup>-2</sup> h<sup>-1</sup>, respectively (D30). Besides, BP difference from material type was also observed, with LMP of 3 mm size being higher than

the rest of the samples, and the regular SMP microplastics of 100 μm size presenting the lowest values. Generally, PE and glass in regular SMP were 11 and 6 times lower than other material sizes (also containing form). PLA regular SMP were 150 times lower than other sizes or shape. The BP for seawater ranged from 88 to 150 pgC mL h<sup>-1</sup> without significant difference between sampling dates.

Bacterial specific activity was further calculated by dividing the BP by the bacterial abundance in the unit of incorporated carbon per cell per hour (fgC cell<sup>-1</sup> h<sup>-1</sup>). Three-way ANOVA also showed that all the factors (sampling date, material type, and size) could significantly impact the specific activity, the material type explaining more variation than the sampling date and material size (material sizes containing the two shapes of IR and RE) ( $R^2 = 0.08, 0.27$ , and  $0.07$ , respectively). Interestingly, BP on the primo-colonization phase of D3 and growing phase of D10 and maturation phase of D66 were significantly higher

than during the maturation phase at D30 ( $p < 0.05$ ) (**Figure 3B**). When it came to the material type, specific activity of PE showed significantly higher levels than PLA and glass, which confirmed that the material type could influence the bacterial specific activity on plastics. The BP of PE, PLA and glass in the average of the first two sampling dates (D3 and D10) were 1.9, 0.3, and 0.4  $\text{fgC cell}^{-1} \text{h}^{-1}$ , respectively, decreased to D30 (0.45, 0.15, and 0.20  $\text{fgC cell}^{-1} \text{h}^{-1}$ , respectively), and increased until D66 (2.5, 1.5, and 0.2  $\text{fgC cell}^{-1} \text{h}^{-1}$ , respectively). The material size and shape could also impact the specific activity, no difference was found between the size of 18 mm and irregular microplastic of 100  $\mu\text{m}$ , while BP of the samples in 3 mm showed higher activity, and regular microbeads of 100  $\mu\text{m}$  showing the lowest.

Accordingly, the bacterial growth rate on PE was higher than on PLA and glass. The bacterial growth rate of PE, PLA and glass had the average of the first two sampling dates (D3 and D10) with 3.8, 0.6, and 0.8  $\text{day}^{-1}$ , respectively, decreased to D30 (0.9, 0.3, and 0.4  $\text{day}^{-1}$ ), and drastically increased until D66 (5.2, 3.0, and 0.5  $\text{day}^{-1}$ , respectively). The growth rate measured in seawater was 2.8, 6.4, 2.0, and 5.2  $\text{day}^{-1}$  for D3, D10, D30, and D66, respectively.

## Diversity Indexes

Illumina MiSeq DNA sequencing generated 3 823 342 sequences tags, falling into 5293 ASVs after randomly resampling to 5177 sequences per sample to provide statistical robustness when comparing diversity measures among samples. DNA quantity were not sufficient to allow the sequencing of several samples at the early colonization stage (D3) that failed for glass samples including regular microbeads of 100  $\mu\text{m}$ , 3 and 1.8 mm size, and also 3 mm for PE and PLA. A total of 123 samples were used for the following analyses, excluding also two samples (irregular PE microbeads and seawater) with low number of reads at D30. Rarefaction analysis suggested that all samples reached a stationary phase (data not shown).

Chao 1 estimator showed that the richness increased drastically in seawater during the course of the experiment, ranging on average from 570 to 1110 ASVs at D3 and D66, respectively. A slighter Chao 1 estimator increased was also found from D3 (average of 363, 265, and 267, respectively) to D66 (468, 395, and 288, respectively) for PE, PLA and glass, indicating that on the primo-colonization phase, a handful of bacterial species already colonizing the plastic surface (**Figure 4A**). Seawater sample showed significant higher Chao1 richness than PE, PLA, and glass. No difference was found on the Pielou index between seawater and PE, PLA or glass (Welch's  $p > 0.05$ ), where evenness increased for all materials and seawater samples at the end of the experiment (**Figure 4B**). Shannon diversity index of PE and glass was significantly higher than PLA (average of 4.6, 4.5, and 4.3, respectively) and no significant difference could be found in relation to the size of the different materials (Welch's ANOVA test) (**Figure 4C**). High correlation of the temporal dynamic of Shannon index and Pielou evenness was found between 3 material types and seawater diversity (Pearson correlation,  $p = 0.018$ ,  $r = 0.75$ ; and  $p = 0.03$ ,  $r = 0.71$ , respectively).

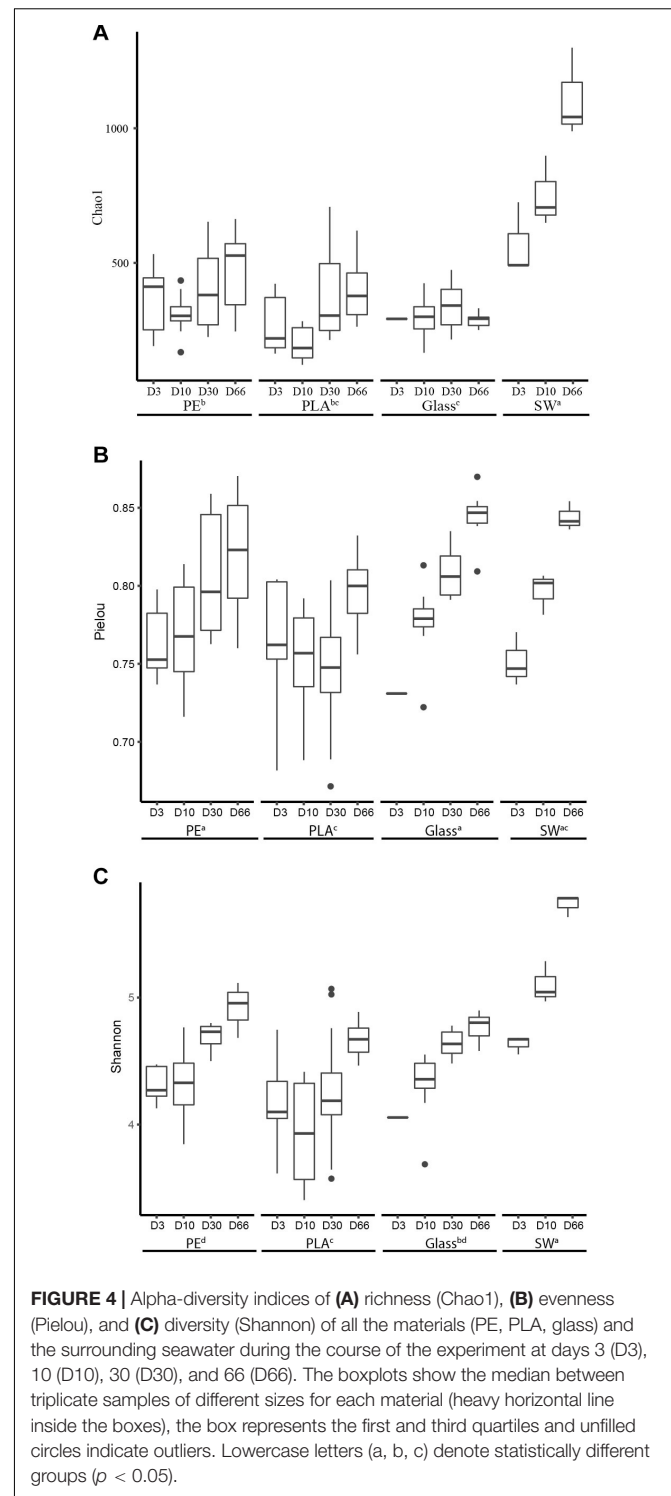
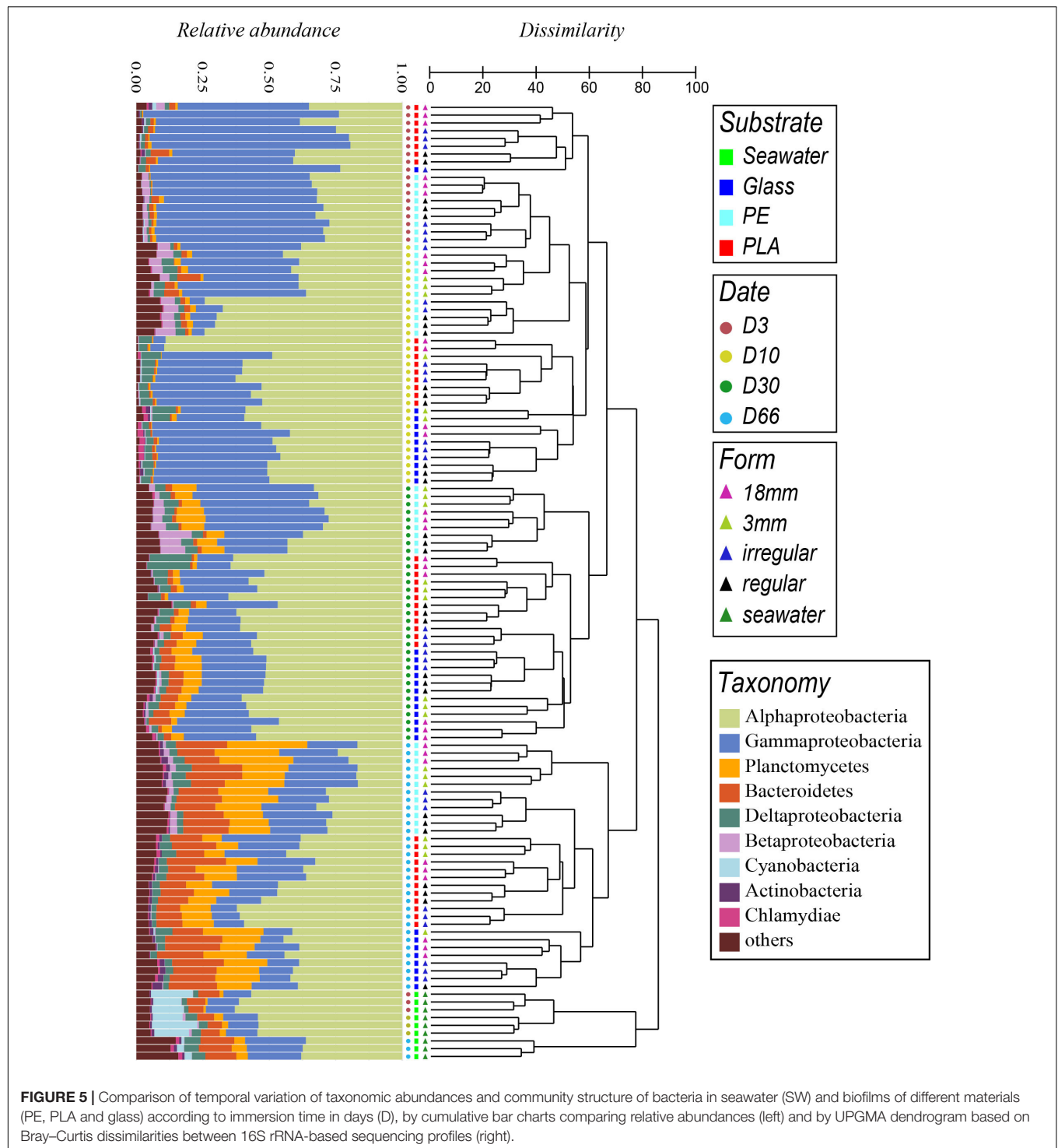


**FIGURE 4** | Alpha-diversity indices of (A) richness (Chao1), (B) evenness (Pielou), and (C) diversity (Shannon) of all the materials (PE, PLA, glass) and the surrounding seawater during the course of the experiment at days 3 (D3), 10 (D10), 30 (D30), and 66 (D66). The boxplots show the median between triplicate samples of different sizes for each material (heavy horizontal line inside the boxes), the box represents the first and third quartiles and unfilled circles indicate outliers. Lowercase letters (a, b, c) denote statistically different groups ( $p < 0.05$ ).

## Bacterial Community Structure

Unweighted-pair group method with arithmetic dendrogram based on Bray-Curtis dissimilarities showed that each of the triplicate samples in each sampling time and condition clustered together (except for one sample D10-PE-IR), confirming the homogeneity within the triplicates and also the proper



sampling strategy, rigorous DNA extraction, sequencing and data processing (Figure 5).

Clear dissimilarities were found between bacterial communities in seawater and material types (PA, PLA, glass) (dissimilarity > 85%) and between samples corresponding to before (D3 to D30) and after the diatom bloom (D66) within each cluster (dissimilarity > 75%). Similarity profile

testing (SIMPROF) showed these groups to be highly significant ( $p < 0.001$ ).

Global PERMANOVA analyses with all samples confirmed the variance were highly explained by sampling date, to a less extent by chemical composition and material size ( $R^2 = 0.39$ , 0.14, and 0.05 for PE, PLA, and glass, respectively,  $p < 0.01$ ) (Supplementary Table 1). Pairwise PERMANOVA analyses

confirmed that the factors of sampling date or material chemical composition can significantly explain the changes of bacterial community structure within each group, with higher values found between the primo-colonization or the growing phase compared to the mature biofilm influenced by the diatom bloom ( $R^2 > 0.37$ ,  $p < 0.01$ ). Smaller but significant differences were found between substrate types ( $R^2 = 0.07$  between PLA and glass and  $R^2 = 0.11$  and  $0.14$  between PE and PLA or glass, respectively;  $p < 0.01$ ), indicating that the bacterial community is more similar between PLA and glass than with PE. However, no significant difference between material size or shape could be found ( $p > 0.05$ ), which was also supported by dispersion analyses ( $p > 0.05$ ) (Supplementary Table 2).

Samples from the primo-colonization (D3) and the growing phases of the biofilms (D10) grouped in separated clusters for PLA and glass (dissimilarity 59%), and also for PE but with less dissimilarity among samples (48%). A clear shift in bacterial community was observed when the biofilms became mature (within D30 – dissimilarity 66%) followed by a drastic change after the diatom bloom (within D66 – dissimilarity 77%), whatever the material type (PE, PLA, glass) and size. All the above cited clusters were significantly different when using the SIMPROF tests ( $p < 0.05$ ).

The time was the main factor driving the bacterial communities, the material type showed also different patterns. At each sampling date, PE formed always a specific cluster with all the size fractions. This was also the case for PLA and glass, except for the primo-colonization (D3) where they grouped in a same cluster.

Interestingly, the Mantel tests showed a significant relation between temporal changes in the seawater communities and in the biofilms growing on the different material types (Supplementary Table 3). Permutating correspondence between seawater and biofilms communities showed high correlation (Spearman rank = 0.84;  $p < 0.05$ ) within dates (D3, D10, D66 seawater samples compared to biofilms at the same dates) that decreased drastically when permutating dates and for D66 in particular (Spearman rank < 0.5;  $p < 0.05$ ). Shared ASVs between seawater and biofilms were <25% for PE, <17% for PLA and glass, but these ASVs were abundant in the samples since they represented >48% of the tags in all cases, and maximum reached at 62% for PE on D3 (Supplementary Figure 2). SIMPER analyses based on presence and absence data showed high dissimilarity among each substrate alongside the temporal evolution (61, 65, 63, and 60% for PE, PLA, glass, and seawater, respectively), while the shared ASVs and shared tags remained constant, suggesting that the bacterial community from the biofilm and seawater shift in the same direction.

## Taxonomic Composition

Taxonomic analyses confirmed the specificity of the community structures formed on the different materials compared to seawater, the latter being dominated by Alphaproteobacteria and composed mainly of Gammaproteobacteria, Cyanobacteria, Bacteroidetes, and Actinobacteria throughout the experimentation (Figure 5).

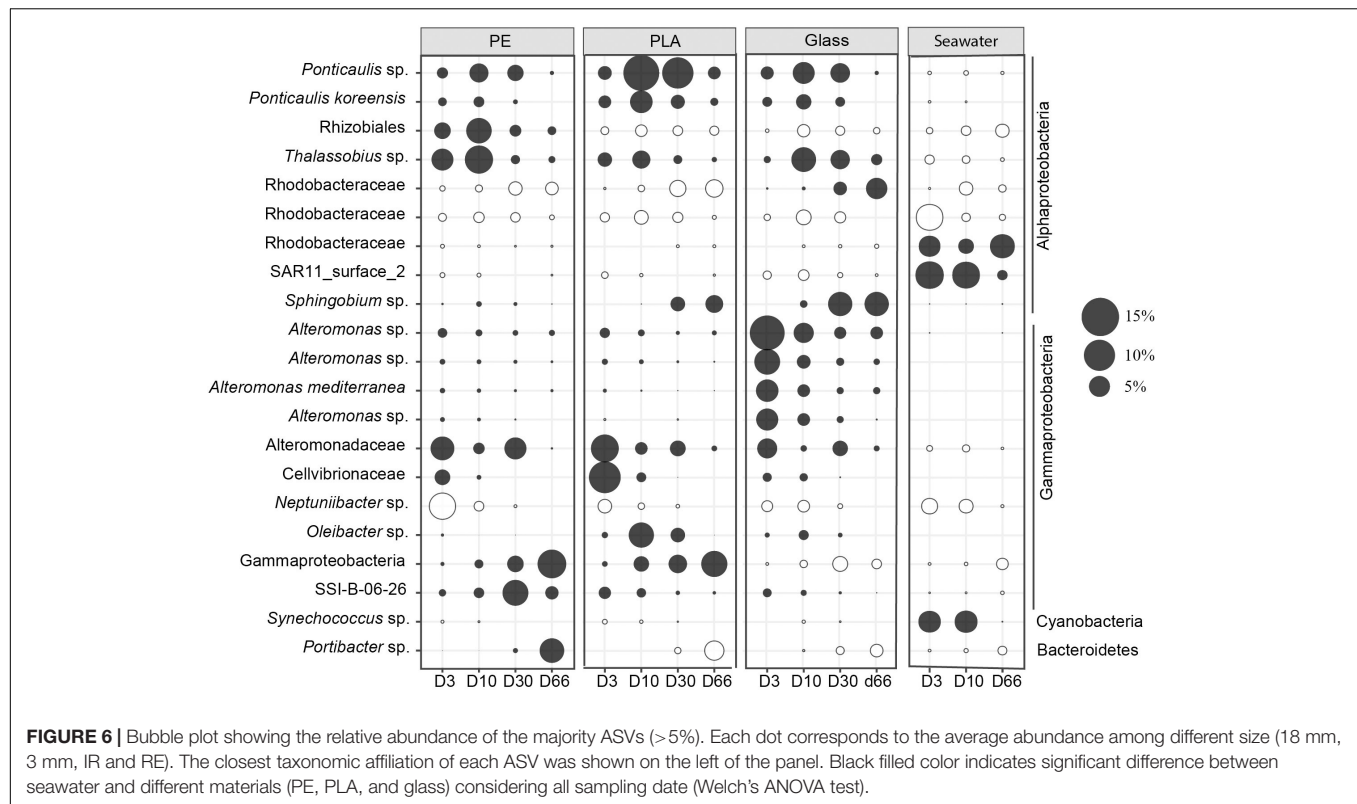
The distinct phases of biofilm formation were also clearly visible. The primo-colonization phase (D3) was dominated by Gammaproteobacteria ( $61 \pm 0\%$ ,  $61 \pm 12\%$ , and  $71\%$  for PE, PLA, and glass, respectively) and Alphaproteobacteria ( $31 \pm 2\%$ ,  $31 \pm 9\%$ , and  $23\%$  for PE, PLA and glass, respectively), dominant family were Alteromonadaceae from Gammaproteobacteria and Rhodobacteraceae from Alphaproteobacteria. The growing phase resulted in a decrease of Gammaproteobacteria ( $27 \pm 18\%$ ,  $29 \pm 15\%$ , and  $40 \pm 8\%$  for PE, PLA, and glass, respectively) and a concomitant increase of Alphaproteobacteria ( $53 \pm 17\%$ ,  $64 \pm 15\%$ , and  $51 \pm 5\%$  for PE, PLA, and glass, respectively). The main change for the maturation phase (D30) was the increase of Planctomycetes ( $8 \pm 1\%$ ,  $4 \pm 2\%$ , and  $6 \pm 2\%$  for PE, PLA and glass, respectively) and of Bacteroidetes mainly for glass but not for PE and PLA ( $5 \pm 2\%$  for glass). At this stage, Gammaproteobacteria ( $39 \pm 9\%$ ,  $22 \pm 5\%$ , and  $25 \pm 5\%$ ) became as abundant or even less abundant as Alphaproteobacteria ( $34 \pm 6\%$ ,  $58 \pm 5\%$ , and  $54 \pm 4\%$  for PE, PLA, and glass, respectively).

The mature biofilm changed drastically in the presence of diatoms (D66) with a continuous increase of Planctomycetes ( $20 \pm 5\%$ ,  $10 \pm 5\%$ , and  $16 \pm 3\%$  for PE, PLA, and glass, respectively) and Bacteroidetes ( $16 \pm 2\%$ ,  $12 \pm 3\%$ , and  $18 \pm 3\%$  for PE, PLA, and glass, respectively). The presence of diatoms at this stage was confirmed when looking at the eukaryote sequences that were initially removed for the bacterial diversity analysis. Note that the number of eukaryotic sequences increased at the end of the experiment (D66), especially for glass where eukaryotic sequences could reach until 19% of the total reads per sample, but also for PE and PLA where they can reach until 12 and 9%, respectively (data not shown). Interestingly, eukaryotic sequences were always <4% before the D66 on these materials and represented <0.7% all along the experiment in seawater. More than 50% and until 86% of the eukaryotic sequences belonged to the diatom *Pseudo-nitzschia* sp. on D66 for PE, PLA, and glass, whereas the sequences of *Pseudo-nitzschia* sp. in seawater remained relative very low (<10%).

We followed in particular 21 dominant bacterial ASVs that accounted for >5% of the sequences in each substrate for individual sampling date (Figure 6). Among those top 21 ASVs, 5 were unique for PE, PLA or glass that were not visible in seawater (Figure 6). We found the SAR11\_surface\_2 and ASV of Rhodobacteraceae more abundant in seawater compared to biofilms on the different material types.

During the primary colonization phase (D3), one ASV belonging to Alteromonadaceae was abundant in all material types, and distinction could be made between *Neptuniibacter* sp. and *Thalassobius* sp. that were more abundant on PE, whereas ASV of Cellvibrionaceae were more abundant in PLA, and *Alteromonas* sp. in glass samples. During the growing phase (D10), *Thalassobius* sp. were more represented on both PE and glass, while *Ponticaulis* sp. and *Oleibacter* sp. were more found for PLA. Changes between the maturation phase (D30) and the diatom bloom event (D66) varied according to the material types. The ASV of SSI-B-06-26 was more abundant on PE at D30 and ASV of Gammaproteobacteria and *Portibacter* sp. increased drastically at D66. *Ponticaulis* sp. dominated PLA at D30, while it





switched to ASV of Gammaproteobacteria at D66. Less changes were found for glass where *Sphingobium* sp. remain abundant for glass both at D30 and D66.

## DISCUSSION

Our results are providing the first complete description of bacterial abundance, diversity and activity during the three classical colonization phases (primo-colonization, growing and maturation phases) of biofilm formation on plastics. We also showed that the mature biofilm can be drastically modified by a phytoplankton bloom, thus indicating that environmental conditions may have a crucial role on shaping the plastisphere. Our experimental design enable us to evaluate the relative influence of plastic composition, size or shape as well as the importance of phytoplankton-bacteria interactions in shaping the plastisphere.

### Effect of Size and Shape of the Substrate and Its Chemical Composition on the Plastisphere

Raw measured values of abundance were found to differ between diverse size (meso-plastics of 18 mm diameter, LMP of 3 mm diameter and SMP of 100  $\mu$ m diameter) and shapes (irregular IR and regular RE) for a given material. However, once the abundance was expressed per unit surface as in **Figure 2**, the differences disappeared between mesoplastics, LMP and SMP of RE or IR shapes. These results show, for the first time, that the

apparent size effect on raw data is only due to the difference in specific surface (i.e., surface to volume ratio) for different particle shapes. For a same mass of material, an irregular surface has a larger available surface than a regular one, which therefore leads to a higher abundance hence a higher activity. In the present experiments, the excess surface is typically around 1.5 fold higher for IR shape compared to RE shape.

Besides, there was also no effect on the bacterial diversity from the different material size or shape. This result is in accordance with the only one study focusing on the effect of plastic size on bacterial diversity from coastal seawater (Brest, France), where no size effect was found between SMP (0.3 to 1 mm) and LMP (1 to 5 mm) (Frère et al., 2018). By contrast, our data showed dissimilarity in bacterial heterotrophic activities between different plastic size and shape. For instance, bacterial activity from PE in 3 mm (slight curly) was higher than other that of 18 mm, and bacterial activity from IR shape was higher than that of RE shape. This could be explained by very large roughness at the typical scale of a bacteria, one could expect in addition, a different packing of bacteria or a different biofilm structure – due for example to adhesion differences – which could induce differences in density of bacteria and/or in their heterotrophic production. In this study though, the roughness of all samples (including IR beads) was of the order of 100 nm over 100  $\times$  100 squared microns areas, so that such effects -if any- would not be visible for the bacterial abundance or diversity. Other studies on roughness at a very small scale would need to be undertaken if one wants to conclude on this aspect. The present experiments also seem to show that in the present

case, the temporal dynamic of biofilm formation together with the material type were always more important factors than the material size and shape for shaping the bacterial abundance, diversity and activity. However, it has been previously shown that the bacterial spatial position of natural plastisphere on particles is not totally even distributed and hence could depend on the size of the particles (Schludt et al., 2019). Further studies with particle size less than the minimum size used in this study (100  $\mu\text{m}$ ) would probably be necessary to clarify this point.

During the three phases of its development, the biofilm evolved in a fairly different way on the two polymers studied (PE and PLA) and glass. PLA and glass were more similar in terms of bacterial activity and diversity compared to PE, while PE and PLA had similar and higher bacterial abundance compared to glass. In general, PE showed drastic differences compared to glass, while PLA showed intermediate values between them. The result is also pointing out that the bacterial activity could be not correlated to its abundance on plastisphere, which is similar to that found in seawater (Campbell et al., 2011). Our results are in accordance with another demonstration of significant influence of material type (PE, PLA, and Glass) on bacterial diversity (Kirstein et al., 2018). Our results tends to confirm the role of wetting properties: polymer surfaces being far more hydrophobic than glass. Attachment to surface are indeed supposed to be mediated via specific and non-specific interactions, both depending on surface hydrophobicity/hydrophilicity, roughness, charge and functional groups (Caruso, 2020). The role of hardness cannot, however, be excluded since it was recently shown to also be a key factor compared with other physicochemical properties (Cai et al., 2019).

Other factors may impact the plastisphere, such as the buoyancy: HDPE (0.95  $\text{g cm}^{-3}$ ) was floating, whereas PLA (1.25  $\text{g cm}^{-3}$ ) settled on tank bottom in our experimental conditions, which could lead to a different oxygenation of water or a different exposure to bacteria (composition, light intensity, contact frequency, exposition to air versus water). The buoyancy may explain the small but significantly higher average activity on PE compared to PLA, which differed also in term of community structure. Even though PLA is a compostable polymer and degradable in human body (Pillai and Sharma, 2010), it is known that PLA, like PE, is not biodegradable in marine environment (Karamanlioglu et al., 2017), and certainly not in the relatively short time frame of this experiment. Colonization, heterotrophic activity as well as the specificity of the species observed are therefore certainly not related to any biodegradation of the polymers. It seems more relevant to attribute the colonization, activity and specialization of bacteria to the formation of a conditioning film and subsequently the chemical composition of extracellular polymeric substance which could also be surface properties dependent.

## Presence of Three Following Phases of the Biofilm Development in All Substrates

Confocal microscopy was a powerful tool to follow the biofilm formation on the various samples tested in our

study. For all studied material, the triplicate samples out of all the sampling dates highlighted three classical successive phases (primo-colonization, growth, and maturation) of biofilm formation. Such succession has already been observed on natural (rocks and algae) or artificial surfaces (glass, acryl, steel, and plastics) immersed in seawater (Caruso, 2020), such as PE sheets and dolly ropes during long-term exposure experiment in the North Sea (De Tender et al., 2017) or non-biodegradable and biodegradable plastics in the Mediterranean sea (Dussud et al., 2018a).

First, the primo-colonization designates the pioneer bacteria that shape the first layer of initial biofilm (Lorite et al., 2011). After 3 days of immersion in natural seawater, we observed that the primo-colonizers presented a higher abundance and heterotrophic activity ( $^3\text{H}$  leucine incorporation) on PE compared to PLA and glass. MiSeq 16S rRNA sequencing revealed that bacterial richness was already high after 3 days with a minimum average Chao1 estimation of 265 ASVs whatever the material types. We observed distinct but closed bacterial communities in PE, PLA, and glass, dominated by Gammaproteobacteria (61, 61, and 71% for PE, PLA, and glass, respectively) and Alphaproteobacteria (31, 31, and 23% for PE, PLA, and glass, respectively). Previous studies showed that the *Roseobacter* clade and *Alteromonas* were the main bacterial primary colonizers (Dang and Lovell, 2000; Salta et al., 2013; Dang and Lovell, 2016). From our results, we reported that *Thalassobius* sp. of the *Roseobacter* clade could be also the primary colonizer on plastisphere. *Thalassobius* sp. was also found on 3-day-old polymethyl methacrylate (PMMA) panel immersed the Arabian Gulf with relatively low abundance compared to our study (Abed et al., 2019) as well as on PE plastisphere from North Atlantic (Zettler et al., 2013). *Alteromonas* sp. was extremely abundant on glass samples compared to PE and PLA, where the three materials occupied different ASVs from Alteromonadaceae (Figure 5). *Neptuniibacter* sp. was also one of the main taxa revealed in our study, but also on 7-day-old colonized poly(3-hydroxybutyrate-co-3-hydroxyvalerate) (PHBV) from the Banyuls Bay, France (Dussud et al., 2018a). Even though it is considered that the *Neptuniibacter* sp. is an hydrocarbonoclastic bacteria (Dombrowski et al., 2016), we showed here that it might be just a primary colonizer, while not participating to the plastic degradation.

Second, the growing phase of the biofilm is described growth by secondary species, which induce modifications in the properties of the substratum (Lorite et al., 2011). After 10 days immersion in seawater, we have seen an increase in bacterial abundance and heterotrophic activity, together with significant changes in bacterial community structure for all material types. In particular, Alphaproteobacteria became more abundant (53, 64, and 51% for PE, PLA and glass, respectively) compared to Gammaproteobacteria (27, 29, and 40% for PE, PLA, and glass, respectively). *Thalassobius* sp. was still abundant in the growing phase after the primo-colonization phase. In addition, we firstly reported the *Ponticaulis* sp. as an important group of primary colonizers on plastisphere, strikingly on PLA. Besides, previous study also showed that *Ponticaulis* sp. was one of the main

colonizers for the metallic alloys (Procópio, 2020). It suggested that the *Oleibacter* sp. could be one of the pioneer bacteria for plastic colonization within hours (Pollet et al., 2018), while we showed that it was more obvious on PLA in the growing phase after 10 days.

Third, the “maturation phase” occurs through diverse, competitive or synergistic interactions between cells, with either further recruitment or loss of species (Lorite et al., 2011). This has led to a stabilization of bacterial abundance and heterotrophic bacterial production, together with a drastic shift in bacterial community structure in all material types. PE still presented significantly higher abundance and activity compared to glass, whereas PLA showed similar bacterial abundance compared to PE and similar bacterial activity compared to glass. At this stage, Gammaproteobacteria (39, 22, and 25%) were as abundant or even less abundant as Alphaproteobacteria (34, 58, and 54% for PE, PLA, and glass, respectively). Bacteroidetes and Planctomycetes were also found as secondary colonizers in other studies (Dang and Lovell, 2016; Pinto et al., 2019). We observed noticeable increases of Planctomycetes (8, 4, and 6% for PE, PLA, and glass, respectively) and also Bacteroidetes (mainly for glass (5%) but not for PE and PLA). Interestingly, we observed a similar evenness associated to an increase of richness during the growing and maturation phases, which is characteristic abundant and heterogeneous resources and nutrients offered by plastic particles compared to the nutrient-depleted oceanic deserts (Zhou et al., 2002).

During this study, we found that the *Roseobacter* and *Alteromonas* were important clades for whatever the three-colonization phases, while the two clades were also found as bacterial “phycosphere” (bacterial taxa colonizing on phytoplankton) (Seymour et al., 2017). Thus, we suspect that the plastic surface and phytoplankton surface could have some similar trait to be the environmental cue for these two clades. Another long term study identified the consistent presence of *Polaribacter* sp., *Kangiella* sp., *Lacinutrix* sp. during a 44 weeks experiment using plastic sheet and dolly rope immersed at an offshore station in the North Sea (De Tender et al., 2017). These taxonomic groups were dissimilar from the persistent taxa observed in our study, probably because of difference between the plastic substrates and the environmental conditions.

## Influence of Phytoplankton Bloom on the Mature Biofilm

In our study, the diatoms were presented in seawater during the entire course of the experiment course, while a diatom bloom was observed at D66 on plastisphere. It suggested that a bacterial biofilm would be a prerequisite for the diatom bloom on plastisphere. Most of the microalgae sequences on plastisphere belonged to *Pseudo-Nitzschia* sp., which was in accordance to the observation of their typical morphotype on D66 with confocal microscopy technique on all material surfaces. The diatoms were more observed on the film other than small microplastics, suggesting that the rigidity morphology of diatoms require more flatter surface area for the colonization comparing to bacteria. *Pseudo-nitzschia* is a global distributed diatom genus in the

marine environment (Lelong et al., 2012). It has not only been reported in the Mediterranean Sea of marine observatory stations in the Banyuls Bay (France), but also in the 150 km-south Blanes Bay (Spain) where the phytoplanktonic bloom in seawater were consistently attributable to chromophytes, the most abundant taxa being *Pseudo-nitzschia calliantha* (Mura and Agustí, 1996; Charles et al., 2005).

Diatoms have been found as omnipresent and sometimes dominant colonizers on plastic debris (Oberbeckmann et al., 2014; Maso et al., 2016; Michels et al., 2018; Kettner et al., 2019). Morphological identification by microscopy together with new chloroplast databases from bacterial amplicon surveys (Decelle et al., 2015) included *Mastogloia*, *Cyclotella*, *Pleurosigma*, *Amphora*, and *Pseudo-Nitzschia* genera in the Arabian Gulf, Grenada Island, Atlantic, and Pacific gyres (Amaral-Zettler et al., 2020). *Pseudo-nitzschia* spp. has been identified as the dominant diatoms on 10-day-old biofilm developed on polystyrene Petri dishes immersed at the low intertidal zone, Hong Kong (China) (Chiu et al., 2008). To our knowledge, it is the first time that *Pseudo-nitzschia* spp. were identified as dominant phototrophs on plastic debris on Mediterranean plastisphere. The diatoms event happened on plastisphere could be also related to the diatom bloom events happened on Banyuls Bay (Supplementary Figure 1C).

Interaction between phytoplankton and bacteria are known to play key roles in mediating biogeochemical cycling and the food web structure in the ocean, including the microbial loop (Mayali, 2018). Diatom blooms are also known to be one of the main drivers of the temporal dynamics of bacterial abundance, diversity and activity in the Mediterranean Sea and elsewhere (Ghiglione et al., 2005; Lambert et al., 2019), with consistent taxonomic association between specific bacteria and diatom taxa (Behringer et al., 2018). Our results confirm that such association exist also within the biofilms associated with plastic, as it has been observed in other studies (Amaral-Zettler et al., 2020). We found co-associated bacterial epibionts on the mature biofilms at D66 that were related to the specific biofilm of each polymer type. For example, we found common colonizers of diatom detritus, such as *Portibacter* sp. (Crenn et al., 2018), and *Sphingobium* sp. (Ramanan et al., 2015) and Rhodobacteraceae (previously mostly assigned as *Roseobacter* clade) (Simon et al., 2017). The interaction between diatoms and bacteria within the mature biofilms was accompanied with a drastic increase of bacterial heterotrophic activities in PE and PLA. This is a typical response of nutrient recycling heterotrophs to primary producing photoautotrophs, where bacterial activity per cell increases drastically together with changes in community structure (Mayali, 2018). Our results showed that the diversity and activity of the mature biofilms on plastic can be rapidly and drastically changed due to phytoplanktonic growth on plastics, whatever the polymer type, size or shape. To our knowledge, only one study so far measuring chlorophyll *a* and net primary production in the North Pacific gyre showed that microplastic particles were creating net autotrophic hot-spots in the oligotrophic ocean (Bryant et al., 2016). In parallel, another unique study in the Mediterranean Sea revealed higher

bacterial heterotrophic activity on plastic compared to the surrounding seawater (Dussud et al., 2018a).

During this study, we cannot really compare the bacterial activity or growth rate between plastisphere vs. our seawater samples, because of the potentially lower bacterial abundance numeration on seawater samples. Instead, we propose the following scenario: the bacterial growth rate on the primo-colonization and growing phase should be higher than that of seawater, at least on PE samples, as previous study showed that the *Roseobacter* and *Alteromonadaceae* have relative high growth rate compared to the bulk bacterial community (Ferrera et al., 2011). The bacterial activity or growth rate on the maturation phase in the marine environment could be higher than seawater considering that autotroph microbes such as diatoms were omnipresent on plastics. Further works coupling both primary and heterotrophic production measurements are needed to determine the bacterial activity difference between plastisphere and seawater, but also test if the microscale algal-bacterial interactions on the large amount of plastic floating in sea surface have consequences on ecosystem functioning and/or biogeochemical cycling.

## Concluding Remarks

Here we prove that phytoplankton-bacteria interactions may greatly modify the plastisphere, which can no longer be considered as a vector of a durable and stable community, but rather a vector of communities interacting with their environment and subjected to changes. We showed that phytoplankton-bacteria interactions do not influence the abundance of the mature biofilm formed on plastics, but may drastically impact the diversity and the heterotrophic activities of the plastisphere. These results may have consequences in the further evaluation of the functional role of the plastisphere, such as its contribution to the biogeochemical cycles of elements. Another major finding of our study was that the size and the shape of the plastics showed little influence on the plastisphere abundance, diversity and activity, which is in accordance with the few studies dealing with this aspect but focusing on the diversity only. Hydrophobicity, topography, roughness, crystallinity, and surface charge have been previously found to influence the early stage of plastic colonization, whereas the plastisphere directly sampled at sea was found to be rather driven by geographical location or seasons, which are typically related to environmental conditions. Our results, together with the growing literature in this field, are opening the description of the complex and fascinating interactions between the plastisphere and its plastic support, but also with the surrounding environment that may greatly influence its spatial and temporal dynamics.

## REFERENCES

Abed, R. M. M., Al Fahdi, D., and Muthukrishnan, T. (2019). Short-term succession of marine microbial fouling communities and the identification of primary and secondary colonizers. *Biofouling* 35, 526–540. doi: 10.1080/08927014.2019.1622004

## DATA AVAILABILITY STATEMENT

The datasets presented in this study can be found in online repositories. The names of the repository/repositories and accession number(s) can be found below: <https://www.ncbi.nlm.nih.gov/genbank/>, PRJNA663787.

## AUTHOR CONTRIBUTIONS

JC, A-LM, and J-FG: conception and design of study. JC, JJ, and VB: acquisition of data. JC, MG, PF, A-LM, and J-FG: analysis and interpretation of data. SB, AT, A-LM, and J-FG: provision of equipment. JC and J-FG: drafting the manuscript. PF, MG, SB, AT, and A-LM: revising the manuscript critically for important intellectual content. JC, JJ, PC, MP-P, VB, MG, PF, SB, AT, A-LM, and J-FG: approval version of the manuscript to be published. All authors contributed to the article and approved the submitted version.

## FUNDING

This work was supported by the European project JRA-ASSEMBLE +, the French National Research Agency (project ANR-OXOMAR), the Tara Ocean Foundation (project Microplastic 2019), and by the CNRS (project PEPSTI-PHABIO). This work was part of the Ph.D. thesis of JC supported by the China Scholarship Council (CSC; NO, 201706330086).

## ACKNOWLEDGMENTS

We are grateful to Valerie Bayo, Charlene Odobel, and Caroline Pandin for their kind laboratory supports, David Pecqueur for the support on Confocal microscopy, Philippe Catala for the advice on flow cytometry data and to Guigui PA and VF for insightful comments on the manuscript. We also thank A. Kirkman for her careful reading and corrections of the manuscript.

## SUPPLEMENTARY MATERIAL

The Supplementary Material for this article can be found online at: <https://www.frontiersin.org/articles/10.3389/fmicb.2020.610231/full#supplementary-material>

Abramoff, M. D., Magalhães, P. J., and Ram, S. J. (2004). Image processing with imageJ. *Biophotonics Int.* 11, 36–41.

Amaral-Zettler, L. A., Zettler, E. R., and Mincer, T. J. (2020). Ecology of the plastisphere. *Nat. Rev. Microbiol.* 18, 139–151. doi: 10.1038/s41579-019-0308-0

Amaral-Zettler, L. A., Zettler, E. R., Slikas, B., Boyd, G. D., Melvin, D. W., Morrall, C. E., et al. (2015). The biogeography of the Plastisphere:



- implications for policy. *Front. Ecol. Environ.* 13, 541–546. doi: 10.1890/150017
- Anderson, M. J., and Walsh, D. C. I. (2013). PERMANOVA, ANOSIM, and the Mantel test in the face of heterogeneous dispersions: What null hypothesis are you testing? *Ecol. Monogr.* 83, 557–574. doi: 10.1890/12-2010.1
- Andrady, A. (2003). *Plastics and the Environment*. Hoboken, NJ: John Wiley & Sons.
- Barnes, D. K. A., Galgani, F., Thompson, R. C., and Barlaz, M. (2009). Accumulation and fragmentation of plastic debris in global environments. *Philos. Trans. R. Soc. B Biol. Sci.* 364, 1985–1998. doi: 10.1098/rstb.2008.0205
- Basili, M., Quero, G. M., Giovannelli, D., Manini, E., Vignaroli, C., Avio, C. G., et al. (2020). Major role of surrounding environment in shaping biofilm community composition on marine plastic debris. *Front. Mar. Sci.* 7:2622. doi: 10.3389/fmars.2020.00262
- Behringer, G., Ochsenkühn, M. A., Fei, C., Fanning, J., Koester, J. A., and Amin, S. A. (2018). Bacterial communities of diatoms display strong conservation across strains and time. *Front. Microbiol.* 9:659. doi: 10.3389/fmicb.2018.00659
- Blanchet, M., Pringault, O., Panagiotopoulos, C., Lefèvre, D., Charrière, B., Ghiglione, J. F., et al. (2017). When riverine dissolved organic matter (DOM) meets labile DOM in coastal waters: changes in bacterial community activity and composition. *Aquat. Sci.* 79, 27–43. doi: 10.1007/s00027-016-0477-0
- Bryant, J. A., Clemente, T. M., Viviani, D. A., Fong, A. A., Thomas, K. A., Kemp, P., et al. (2016). Diversity and activity of communities inhabiting plastic debris in the north pacific gyre. *mSystems* 1:e00024-16.
- Cai, L., Wu, D., Xia, J., Shi, H., and Kim, H. (2019). Influence of physicochemical surface properties on the adhesion of bacteria onto four types of plastics. *Sci. Total Environ.* 671, 1101–1107. doi: 10.1016/j.scitotenv.2019.03.434
- Callahan, B. J., McMurdie, P. J., Rosen, M. J., Han, A. W., Johnson, A. J. A., and Holmes, S. P. (2016). DADA2: high resolution sample inference from Illumina amplicon data. *Nat. Methods* 13, 581–583. doi: 10.1038/nmeth.3869
- Campbell, B. J., Yu, L., Heidelberg, J. F., and Kirchman, D. L. (2011). Activity of abundant and rare bacteria in a coastal ocean. *Proc. Natl. Acad. Sci. U.S.A.* 108, 12776–12781. doi: 10.1073/pnas.1101405108
- Caruso, G. (2020). Microbial colonization in marine environments: overview of current knowledge and emerging research topics. *J. Mar. Sci. Eng.* 8, 1–22.
- Céa, B., Lefèvre, D., Chirurgical, L., Raimbault, P., Garcia, N., Charrière, B., et al. (2015). An annual survey of bacterial production, respiration and ectoenzyme activity in coastal NW Mediterranean waters: temperature and resource controls. *Environ. Sci. Pollut. Res. Int.* 22, 13654–13668. doi: 10.1007/s11356-014-3500-9
- Charles, F., Lantoin, F., Brugel, S., Chrétiennot-Dinet, M. J., Quiroga, I., and Rivière, B. (2005). Seasonal survey of the phytoplankton biomass, composition and production in a littoral NW Mediterranean site, with special emphasis on the picoplanktonic contribution. *Estuar. Coast. Shelf Sci.* 65, 199–212. doi: 10.1016/j.ecss.2005.06.006
- Chiu, J. M. Y., Zhang, R., Wang, H., Thiyagarajan, V., and Qian, P. Y. (2008). Nutrient effects on intertidal community: from bacteria to invertebrates. *Mar. Ecol. Prog. Ser.* 358, 41–50. doi: 10.3354/meps07310
- Chubarenko, I., Bagaev, A., Zobkov, M., and Esiukova, E. (2016). On some physical and dynamical properties of microplastic particles in marine environment. *Mar. Pollut. Bull.* 108, 105–112. doi: 10.1016/j.marpolbul.2016.04.048
- Cózar, A., Sanz-Martín, M., Martí, E., González-Gordillo, J. I., Ubeda, B., Gálvez, J. Á., et al. (2015). Plastic accumulation in the Mediterranean Sea. *PLoS One* 10:e0121762. doi: 10.1371/journal.pone.0121762
- Crenn, K., Duffieux, D., and Jeanthon, C. (2018). Bacterial epibiotic communities of ubiquitous and abundant marine diatoms are distinct in short- and long-term associations. *Front. Microbiol.* 9:2879. doi: 10.3389/fmicb.2018.02879
- Dang, H., and Lovell, C. R. (2000). Bacterial primary colonization and early succession on surfaces in marine waters as determined by amplified rRNA gene restriction analysis and sequence analysis of 16S rRNA genes. *Appl. Environ. Microbiol.* 66, 467–475. doi: 10.1128/aem.66.2.467-475.2000
- Dang, H., and Lovell, C. R. (2016). Microbial surface colonization and biofilm development in marine environments. *Am. Soc. Microbiol.* 80, 91–138. doi: 10.1128/mmbr.00037-15
- De Tender, C., Devriese, L. I., Haegeman, A., Maes, S., Vangheyte, J., Cattrijse, A., et al. (2017). Temporal dynamics of bacterial and fungal colonization on plastic debris in the North Sea. *Environ. Sci. Technol.* 51, 7350–7360. doi: 10.1021/acs.est.7b00697
- Decelle, J., Romac, S., Stern, R. F., Bendif, E. M., Zingone, A., Audic, S., et al. (2015). PhytoREF: a reference database of the plastidial 16S rRNA gene of photosynthetic eukaryotes with curated taxonomy. *Mol. Ecol. Resour.* 15, 1435–1445. doi: 10.1111/1755-0998.12401
- Dombrowski, N., Donaho, J. A., Gutierrez, T., Seitz, K. W., Teske, A. P., and Baker, B. J. (2016). Reconstructing metabolic pathways of hydrocarbon-degrading bacteria from the Deepwater Horizon oil spill. *Nat. Microbiol.* 1:16057.
- Dussud, C., and Ghiglione, J. (2014). *Bacterial Degradation of Synthetic Plastics*. (Monaco: CIESM), 43–48.
- Dussud, C., Hudec, C., George, M., Fabre, P., Higgs, P., Bruzard, S., et al. (2018a). Colonization of non-biodegradable and biodegradable plastics by marine microorganisms. *Front. Microbiol.* 9:1571. doi: 10.3389/fmicb.2018.01571
- Dussud, C., Meistertzheim, A. L., Conan, P., Pujo-Pay, M., George, M., Fabre, P., et al. (2018b). Evidence of niche partitioning among bacteria living on plastics, organic particles and surrounding seawaters. *Environ. Pollut.* 236, 807–816. doi: 10.1016/j.envpol.2017.12.027
- Eriksen, M., Lebreton, L. C. M., Carson, H. S., Thiel, M., Moore, C. J., Borerro, J. C., et al. (2014). Plastic Pollution in the World's Oceans: more than 5 Trillion Plastic Pieces Weighing over 250,000 Tons Afloat at Sea. *PLoS One* 9:e111913. doi: 10.1371/journal.pone.0111913
- Ferrera, I., Gasol, J. M., Sebastián, M., Hojerová, E., and Kobíček, M. (2011). Comparison of growth rates of aerobic anoxygenic phototrophic bacteria and other bacterioplankton groups in coastal mediterranean waters. *Appl. Environ. Microbiol.* 77, 7451–7458. doi: 10.1128/aem.00208-11
- Frère, L., Maignien, L., Chalopin, M., Huvet, A., Rinnert, E., Morrison, H., et al. (2018). Microplastic bacterial communities in the Bay of Brest: influence of polymer type and size. *Environ. Pollut.* 242, 614–625. doi: 10.1016/j.envpol.2018.07.023
- Fukuda, R., Ogawa, H., Nagata, T., and Koike, I. (1998). Direct determination of carbon and nitrogen contents of natural bacterial assemblages in marine environments. *Appl. Environ. Microbiol.* 64, 3352–3358. doi: 10.1128/aem.64.9.3352-3358.1998
- Ghiglione, J. F., Larcher, M., and Lebaron, P. (2005). Spatial and temporal scales of variation in bacterioplankton community structure in the NW Mediterranean Sea. *Aquat. Microb. Ecol.* 40, 229–240. doi: 10.3354/ame040229
- Ghiglione, J. F., and Laudet, V. (2020). Marine life cycle: a polluted terra incognita is unveiled. *Curr. Biol.* 30, R130–R133.
- Ghiglione, J. F., Philippot, L., Normand, P., Lensi, R., and Potier, P. (1999). Disruption of narG, the gene encoding the catalytic subunit of respiratory nitrate reductase, also affects nitrite respiration in *Pseudomonas fluorescens* YT101. *J. Bacteriol.* 181, 5099–5102. doi: 10.1128/jb.181.16.5099-5102.1999
- Grömping, U. (2006). Relative importance for linear regression in R: the package relaimpo. *J. Stat. Softw.* 17, 1–27. doi: 10.3758/s13428-010-0043-y
- Hadfield, M. G. (2011). Biofilms and marine invertebrate larvae: what bacteria produce that larvae use to choose settlement sites. *Ann. Rev. Mar. Sci.* 3, 453–470. doi: 10.1146/annurev-marine-120709-142753
- Harrison, J. P., Boardman, C., O'Callaghan, K., Delort, A. M., and Song, J. (2018). Biodegradability standards for carrier bags and plastic films in aquatic environments: a critical review. *R. Soc. Open Sci.* 5:171792. doi: 10.1098/rsos.171792
- Jacquin, J., Cheng, J., Odobel, C., Pandin, C., Conan, P., Pujo-Pay, M., et al. (2019). Microbial ecotoxicology of marine plastic debris: a review on colonization and biodegradation by the “plastisphere”. *Front. Microbiol.* 10:865. doi: 10.3389/fmicb.2019.00865
- Kane, I. A., Clare, M. A., Miramontes, E., Wogelius, R., Rothwell, J. J., Garreau, P., et al. (2020). Seafloor microplastic hotspots controlled by deep-sea circulation. *Science* 5899:eaba5899.
- Karamanlioglu, M., Preziosi, R., and Robson, G. D. (2017). Abiotic and biotic environmental degradation of the bioplastic polymer poly(lactic acid): a review. *Polym. Degrad. Stab.* 137, 122–130. doi: 10.1016/j.polymdegradstab.2017.01.009
- Kettner, M. T., Oberbeckmann, S., Labrenz, M., and Grossart, H. P. (2019). The eukaryotic life on microplastics in brackish ecosystems. *Front. Microbiol.* 10:538. doi: 10.3389/fmicb.2019.00538

- Kirchman, D. (2001). Measuring bacterial biomass production and growth rates from leucine incorporation in natural aquatic environments. *Methods Microbiol.* 30, 227–237. doi: 10.1016/s0580-9517(01)30047-8
- Kirstein, I. V., Kirmizi, S., Wichels, A., Garin-Fernandez, A., Erler, R., Löder, M., et al. (2016). Dangerous hitchhikers? Evidence for potentially pathogenic *Vibrio* spp. on microplastic particles. *Mar. Environ. Res.* 120, 1–8. doi: 10.1016/j.marenvres.2016.07.004
- Kirstein, I. V., Wichels, A., Krohne, G., and Gerdts, G. (2018). Mature biofilm communities on synthetic polymers in seawater - Specific or general? *Mar. Environ. Res.* 142, 147–154. doi: 10.1016/j.marenvres.2018.09.028
- Kooi, M., Van Nes, E. H., Scheffer, M., and Koelmans, A. A. (2017). Ups and downs in the ocean: effects of biofouling on vertical transport of microplastics. *Environ. Sci. Technol.* 51, 7963–7971. doi: 10.1021/acs.est.6b04702
- Kowalski, N., Reichardt, A. M., and Waniek, J. J. (2016). Sinking rates of microplastics and potential implications of their alteration by physical, biological, and chemical factors. *Mar. Pollut. Bull.* 109, 310–319. doi: 10.1016/j.marpolbul.2016.05.064
- Lambert, S., Tragin, M., Lozano, J. C., Ghiglione, J. F., Vaulot, D., Bouget, F. Y., et al. (2019). Rhythmicity of coastal marine picoeukaryotes, bacteria and archaea despite irregular environmental perturbations. *ISME J.* 13, 388–401. doi: 10.1038/s41396-018-0281-z
- Lelong, A., Hégaret, H., Soudant, P., and Bates, S. S. (2012). Pseudo-nitzschia (Bacillariophyceae) species, domoic acid and amnesic shellfish poisoning: revisiting previous paradigms. *Phycologia* 51, 168–216. doi: 10.2216/11-37.1
- Long, M., Moriceau, B., Gallinari, M., Lambert, C., Huvet, A., Raffray, J., et al. (2015). Interactions between microplastics and phytoplankton aggregates: impact on their respective fates. *Mar. Chem.* 175, 39–46. doi: 10.1016/j.marchem.2015.04.003
- Lorite, G. S., Rodrigues, C. M., de Souza, A. A., Kranz, C., Mizaikoff, B., and Cotta, M. A. (2011). The role of conditioning film formation and surface chemical changes on *Xylella fastidiosa* adhesion and biofilm evolution. *J. Colloid Interface Sci.* 359, 289–295. doi: 10.1016/j.jcis.2011.03.066
- Lusher, A. L., Tirelli, V., O'Connor, I., and Officer, R. (2015). Microplastics in Arctic polar waters: the first reported values of particles in surface and sub-surface samples. *Sci. Rep.* 5:14947.
- Marty, F., Ghiglione, J. F., Paise, S., Gueuné, H., Quillet, L., van Loosdrecht, M. C. M., et al. (2012). Evaluation and optimization of nucleic acid extraction methods for the molecular analysis of bacterial communities associated with corroded carbon steel. *Biofouling* 28, 363–380. doi: 10.1080/08927014.2012.672644
- Maso, M., Fortuño, J. M., De Juan, S., and Demestre, M. (2016). Microfouling communities from pelagic and benthic marine plastic debris sampled across Mediterranean coastal waters. *Sci. Mar.* 80, 117–127. doi: 10.3989/scimar.04281.10a
- Mayali, X. (2018). Editorial: metabolic interactions between bacteria and phytoplankton. *Front. Microbiol.* 9:e00727. doi: 10.3389/fmicb.2018.00727
- McMurdie, P. J., and Holmes, S. (2013). Phyloseq: an R package for reproducible interactive analysis and graphics of microbiome census data. *PLoS One* 8:e00612-17. doi: 10.1371/journal.pone.0061217
- Mével, G., Vernet, M., Goutx, M., and Ghiglione, J. F. (2008). Seasonal to hour variation scales in abundance and production of total and particle-attached bacteria in the open NW Mediterranean Sea (0–1000 m). *Biogeosciences* 5, 1573–1586. doi: 10.5194/bg-5-1573-2008
- Michels, J., Stippkugel, A., Lenz, M., Wirtz, K., and Engel, A. (2018). Rapid aggregation of biofilm-covered microplastics with marine biogenic particles. *Proc. R. Soc. B Biol. Sci.* 285:20181203. doi: 10.1098/rspb.2018.1203
- Mura, M. P., and Agustí, S. (1996). Growth rates of diatoms from coastal Antarctic waters estimated by in situ dialysis incubation. *Mar. Ecol. Prog. Ser.* 144, 237–245. doi: 10.3354/meps144237
- Neëas, D., and Klapetek, P. (2012). Gwyddion: an open-source software for SPM data analysis. *Cent. Eur. J. Phys.* 10, 181–188.
- Oberbeckmann, S., Kreikemeyer, B., and Labrenz, M. (2018). Environmental factors support the formation of specific bacterial assemblages on microplastics. *Front. Microbiol.* 8:2709. doi: 10.3389/fmicb.2017.02709
- Oberbeckmann, S., Loeder, M. G. J., Gerdts, G., and Mark Osborn, A. (2014). Spatial and seasonal variation in diversity and structure of microbial biofilms on marine plastics in Northern European waters. *FEMS Microbiol. Ecol.* 49, 478–492. doi: 10.1111/1574-6941.12409
- Oberbeckmann, S., Loeder, M. G. J., and Labrenz, M. (2015). Marine microplastic-associated biofilms - a review. *Environ. Chem.* 12, 551–562. doi: 10.1071/en15069
- O'Donnell, P. B., and McGinity, J. W. (1997). Preparation of microspheres by the solvent evaporation technique. *Adv. Drug Deliv. Rev.* 28, 25–42. doi: 10.1016/s0169-409x(97)00049-5
- Ogonowski, M., Motiei, A., Ininbergs, K., Hell, E., Gerdts, Z., Udekwu, K. I., et al. (2018). Evidence for selective bacterial community structuring on microplastics. *Environ. Microbiol.* 20, 2796–2808. doi: 10.1111/1462-2920.14120
- Oksanen, J., Kindt, R., Legendre, P., O'Hara, B., Stevens, M. H. H., Oksanen, M. J., et al. (2007). The vegan package. *Comm. Ecol. Packag.* 10:719.
- Parada, A. E., Needham, D. M., and Fuhrman, J. A. (2016). Every base matters: assessing small subunit rRNA primers for marine microbiomes with mock communities, time series and global field samples. *Environ. Microbiol.* 18, 1403–1414. doi: 10.1111/1462-2920.13023
- Pillai, C. K. S., and Sharma, C. P. (2010). Review paper: absorbable polymeric surgical sutures: chemistry, production, properties, biodegradability, and performance. *J. Biomater. Appl.* 25, 291–366. doi: 10.1177/0885328210384890
- Pinto, M., Langer, T. M., Hüffer, T., Hofmann, T., and Herndl, G. J. (2019). The composition of bacterial communities associated with plastic biofilms differs between different polymers and stages of biofilm succession. *PLoS One* 14:e0217165. doi: 10.1371/journal.pone.0217165
- Pollet, T., Berdjeb, L., Garnier, C., Durrieu, G., Le Poupon, C., Misson, B., et al. (2018). Prokaryotic community successions and interactions in marine biofilms: the key role of *Flavobacteriia*. *FEMS Microbiol. Ecol.* 94:fiy083.
- Procópio, L. (2020). Microbial community profiles grown on 1020 carbon steel surfaces in seawater-isolated microcosm. *Ann. Microbiol.* 70:13.
- Quast, C., Pruesse, E., Yilmaz, P., Gerken, J., Schweer, T., Yarza, P., et al. (2013). The SILVA ribosomal RNA gene database project: improved data processing and web-based tools. *Nucleic Acids Res.* 41, 590–596.
- Ramanan, R., Kang, Z., Kim, B. H., Cho, D. H., Jin, L., Oh, H. M., et al. (2015). Phycosphere bacterial diversity in green algae reveals an apparent similarity across habitats. *Algal Res.* 8, 140–144. doi: 10.1016/j.algal.2015.02.003
- Rummel, C. D., Jahnke, A., Gorokhova, E., Kühnel, D., and Schmitt-Jansen, M. (2017). Impacts of biofilm formation on the fate and potential effects of microplastic in the aquatic environment. *Environ. Sci. Technol. Lett.* 4, 258–267. doi: 10.1021/acs.estlett.7b00164
- Sabe, H. A., Barratt, S. R., Greenhalgh, M., Handley, P. S., and Robson, G. D. (eds) (2006). "Biodegradation and biodeterioration of man-made polymeric materials," in *Fungi in Biogeochemical Cycles*, (Cambridge: Cambridge University Press), 212–235. doi: 10.1017/cbo9780511550522.010
- Salta, M., Wharton, J. A., Blache, Y., Stokes, K. R., and Briand, J. F. (2013). Marine biofilms on artificial surfaces: structure and dynamics. *Environ. Microbiol.* 15, 2879–2893.
- Schlundt, C., Mark Welch, J. L., Knochel, A. M., Zettler, E. R., and Amaral-Zettler, L. A. (2019). Spatial structure in the "Plastisphere": molecular resources for imaging microscopic communities on plastic marine debris. *Mol. Ecol. Resour.* 620–634. doi: 10.1111/1755-0998.13119
- Schwarz, A. E., Lighthart, T. N., Boukris, E., and van Harmelen, T. (2019). Sources, transport, and accumulation of different types of plastic litter in aquatic environments: a review study. *Mar. Pollut. Bull.* 143, 92–100. doi: 10.1016/j.marpolbul.2019.04.029
- Severin, T., Kessouri, F., Rembauville, M., Sánchez-Pérez, E., Oriol, L., Caparros, J., et al. (2017). Open-ocean convection process: a driver of the winter nutrient supply and the spring phytoplankton distribution in the Northwestern Mediterranean Sea. *J. Geophys. Res. Ocean* 122, 4587–4601. doi: 10.1002/2016jc012664

- Seymour, J. R., Amin, S. A., Raina, J. B., and Stocker, R. (2017). Zooming in on the phycosphere: the ecological interface for phytoplankton-bacteria relationships. *Nat. Microbiol.* 2:17065.
- Simon, M., Scheuner, C., Meier-Kolthoff, J. P., Brinkhoff, T., Wagner-Döbler, I., Ulbrich, M., et al. (2017). Phylogenomics of Rhodobacteraceae reveals evolutionary adaptation to marine and non-marine habitats. *ISME J.* 11, 1483–1499. doi: 10.1038/ismej.2016.198
- Thompson, R. C., Moore, C. J., Saal, F. S. V., and Swan, S. H. (2009). Plastics, the environment and human health: current consensus and future trends. *Philos. Trans. R. Soc. B Biol. Sci.* 364, 2153–2166. doi: 10.1098/rstb.2009.0053
- Van Sebille, E., Wilcox, C., Lebreton, L., Maximenko, N., Hardesty, B. D., Van Franeker, J. A., et al. (2015). A global inventory of small floating plastic debris. *Environ. Res. Lett.* 10:124006. doi: 10.1088/1748-9326/10/12/124006
- Wang, W., Gao, H., Jin, S., Li, R., and Na, G. (2019). The ecotoxicological effects of microplastics on aquatic food web, from primary producer to human: a review. *Ecotoxicol. Environ. Saf.* 173, 110–117. doi: 10.1016/j.ecoenv.2019.01.113
- Wickham, H. (2016). *ggplot2 - Elegant Graphics for Data Analysis*, 2nd Edn. New York, NY: Springer-Verlag.
- Yeh, Y. C., McNichol, J. C., Needham, D. M., Fichot, E. B., and Fuhrman, J. A. (2019). Comprehensive single-PCR 16S and 18S rRNA community analysis validated with mock communities and denoising algorithms. *bioRxiv* 1, 1. doi: 10.1101/866731
- Zettler, E. R., Mincer, T. J., and Amaral-Zettler, L. A. (2013). Life in the “plastisphere”: microbial communities on plastic marine debris. *Environ. Sci. Technol.* 47, 7137–7146. doi: 10.1021/es401288x
- Zhou, J., Xia, B., Treves, D. S., Wu, L., Marsh, T. L., Neill, R. V. O., et al. (2002). Spatial and resource factors influencing high microbial diversity in soil. *Appl. Environ. Microbiol.* 68, 326–334. doi: 10.1128/aem.68.1.326-334.2002

**Conflict of Interest:** The authors declare that the research was conducted in the absence of any commercial or financial relationships that could be construed as a potential conflict of interest.

Copyright © 2021 Cheng, Jacquin, Conan, Pujo-Pay, Barbe, George, Fabre, Bruzaud, Ter Halle, Meistertzheim and Ghiglione. This is an open-access article distributed under the terms of the Creative Commons Attribution License (CC BY). The use, distribution or reproduction in other forums is permitted, provided the original author(s) and the copyright owner(s) are credited and that the original publication in this journal is cited, in accordance with accepted academic practice. No use, distribution or reproduction is permitted which does not comply with these terms.



# Variability of the Atmospheric PM<sub>10</sub> Microbiome in Three Climatic Regions of France

Abdoulaye Samaké<sup>1</sup>, Jean M. F. Martins<sup>1\*</sup>, Aurélie Bonin<sup>2</sup>, Gaëlle Uzu<sup>1</sup>, Pierre Taberlet<sup>2</sup>, Sébastien Conil<sup>3</sup>, Olivier Favez<sup>4</sup>, Alexandre Thomasson<sup>5</sup>, Benjamin Chazeau<sup>6</sup>, Nicolas Marchand<sup>6</sup> and Jean-Luc Jaffrezo<sup>1</sup>

<sup>1</sup> University Grenoble Alpes, CNRS, IRD, INP-G, IGE (UMR 5001), Grenoble, France, <sup>2</sup> University Grenoble Alpes, CNRS, LECA (UMR 5553), BP 53, Grenoble, France, <sup>3</sup> ANDRA DRD/OPE Observatoire Pérenne de l'Environnement, Bure, France, <sup>4</sup> INERIS, Parc Technologique Alata, BP 2, Verneuil-en-Halatte, France, <sup>5</sup> AtmoAuvergne-Rhône Alpes, Grenoble, France, <sup>6</sup> Aix Marseille Univ, CNRS, LCE, Marseille, France

## OPEN ACCESS

### Edited by:

Dimitrios Georgios Karpouzas,  
University of Thessaly, Greece

### Reviewed by:

Naresh Singhal,  
The University of Auckland,  
New Zealand  
Savvas Genitsaris,  
International Hellenic University,  
Greece

### \*Correspondence:

Jean M. F. Martins  
jean.martins@univ-grenoble-alpes.fr

### Specialty section:

This article was submitted to  
Microbiotechnology,  
a section of the journal  
Frontiers in Microbiology

**Received:** 26 June 2020

**Accepted:** 10 December 2020

**Published:** 13 January 2021

### Citation:

Samaké A, Martins JMF, Bonin A, Uzu G, Taberlet P, Conil S, Favez O, Thomasson A, Chazeau B, Marchand N and Jaffrezo J-L (2021) Variability of the Atmospheric PM<sub>10</sub> Microbiome in Three Climatic Regions of France. *Front. Microbiol.* 11:576750. doi: 10.3389/fmicb.2020.576750

Primary Biogenic Organic Aerosols (PBOA) were recently shown to be produced by only a few types of microorganisms, emitted by the surrounding vegetation in the case of a regionally homogeneous field site. This study presents the first comprehensive description of the structure and main sources of airborne microbial communities associated with temporal trends in Sugar Compounds (SC) concentrations of PM<sub>10</sub> in 3 sites under a climatic gradient in France. By combining sugar chemistry and DNA Metabarcoding approaches, we intended to identify PM<sub>10</sub>-associated microbial communities and their main sources at three sampling-sites in France, under different climates, during the summer of 2018. This study accounted also for the interannual variability in summer airborne microbial community structure (bacteria and fungi only) associated with PM<sub>10</sub>-SC concentrations during a 2 consecutive years' survey at one site. Our results showed that temporal changes in PM<sub>10</sub>-SC in the three sites are associated with the abundance of only a few specific taxa of airborne fungi and bacterial. These taxa differ significantly between the 3 climatic regions studied. The microbial communities structure associated with SC concentrations of PM<sub>10</sub> during a consecutive 2-year study remained stable in the rural area. Atmospheric concentration levels of PM<sub>10</sub>-SC species varied significantly between the 3 study sites, but with no clear difference according to site typology (rural vs. urban), suggesting that SC emissions are related to regional rather than local climatic characteristics. The overall microbial beta diversity in PM<sub>10</sub> samples is significantly different from that of the main vegetation around the urban sites studied. This indicates that the airborne microorganisms at these urban sites are not solely from the immediate surrounding vegetation, which contrasts with observations at the scale of a regionally homogeneous rural site in 2017. These



results improve our understanding of the spatial behavior of tracers of PBOA emission sources, which need to be better characterized to further implement this important mass fraction of Organic Matter (OM) in Chemical Transport models (CTM).

**Keywords:** airborne microorganisms, bioaerosol, regional sources, bacteria, fungi, sugar compounds, DNA metabarcoding, climatic gradient

## INTRODUCTION

Primary biogenic organic aerosols (PBOAs) are basically a subgroup of atmospheric organic particles that are directly introduced from the biosphere to the atmosphere (Després et al., 2012). PBOAs include many types of biological particles, notably including living and non-living organisms (e.g., bacteria, viruses, green algae, microbial fragments, etc.), dispersal units (e.g., plant pollen, fungal and bacterial spores, etc.) and other types of biological materials (e.g., plant and pollen debris, etc.) (Forde et al., 2019; Huffman et al., 2020). They constitute a major fraction of the total concentration of organic matter (OM) in the atmosphere (Coz et al., 2010; Bozzetti et al., 2016). For instance, it has recently been shown that the contribution of PBOA to the mass load of organic aerosols in PM<sub>10</sub> is comparable to that of secondary aerosol collected at a rural background site in Switzerland in both winter and summer (Bozzetti et al., 2016). PBOAs are subject of increasing research interest, not least because of the growing evidence of their adverse effects on human health and agricultural issues (e.g., allergic asthma, aspergillosis, rhinitis, damage to food crops, etc.) and their influence on the hydrological cycle and climate by acting as condensation or ice nuclei in mixed-phase clouds (Després et al., 2012; Forde et al., 2019). These various impacts are likely to be effective on a regional scale due to the transport of PBOA-containing air masses (Després et al., 2012; Yu et al., 2016).

Although recent studies have revealed useful information on the size, segregation, and abundance of specific PBOA components, quantitative studies on the overall contribution to OM and their predominant atmospheric emission processes are still relatively scarce (Bozzetti et al., 2016; Yu et al., 2016). As a result, the estimation of global emissions of terrestrial PBOAs into the atmosphere is still relatively poorly constrained, ranging from 50 to 1,000 Tg y<sup>-1</sup> (Boucher et al., 2005; Jaenicke, 2005; Yu et al., 2016), indicating that considerable uncertainties in the modeling of their physico-chemical influences in a climate system still remain (Bozzetti et al., 2016; Yu et al., 2016). Consequently, the need for more studies to better quantify the atmospheric loading of PBOAs on regional and global scales has been highlighted in recent studies (Yu et al., 2016; Helin et al., 2017). Such information would certainly allow better parameterization of source-resolved chemical transport models (CTM), which are still generally unable to accurately simulate the relevant fractions of OM (Heald et al., 2011; Ciarelli et al., 2016).

Primary sugar compounds (SC, defined here as sugar alcohols and primary saccharides), emitted continuously from biological sources, are one of the main water-soluble organic compounds present in atmospheric aerosols (Medeiros and Simoneit, 2007; Li et al., 2018; Yan et al., 2019). Due to their ubiquity and

abundance, specific SCs have been used as relevant markers to describe sources and estimate the contributions of PBOAs to the OM mass in the atmosphere (Zhu et al., 2015; Kang et al., 2018; Samaké et al., 2019a). For example, glucose and trehalose (also called mycose) are the most common primary saccharides in vascular plants and are an important source of carbon for soil microorganisms (e.g., bacteria, fungi, etc.) (Medeiros and Simoneit, 2007; Pietrogrande et al., 2014). Although other sources of glucose in atmospheric aerosols have been suggested in a few previous studies, such as biomass combustion and marine emissions (Yang et al., 2012; Zhu et al., 2015), these two chemical compounds have been used mainly as generic markers for soil biota emitted to the atmosphere from natural soil suspension and agricultural soils (Medeiros and Simoneit, 2007; Pietrogrande et al., 2014). Similarly, sugar alcohols, particularly mannitol and arabitol, have long been proposed as markers for airborne fungi, and have been used to estimate their contribution to the mass of PBOAs in various studies around the world (Bauer et al., 2008; Golly et al., 2018; Li et al., 2018). Sugar alcohols, especially arabitol and mannitol are together an important fraction of the dry weight of fungi as they are both intracellular osmoprotectant and common storage carbohydrates (Medeiros and Simoneit, 2007; Pietrogrande et al., 2014).

Our recent study on daily (24 h) filter samples of particulate matter with aerodynamic diameter below 10 µm (PM<sub>10</sub>) collected simultaneously at 16 sites, grouped by sets of increasing spatial scales in France, revealed very synchronous temporal trends in SC concentrations and species ratio at city scale and scales up to 200 km (Samaké et al., 2019b). Such a pattern indicates that the processes responsible for the evolution of SC concentrations in PM<sub>10</sub> show spatial homogeneity over typical areas of at least tens of kilometers, which could most probably be attributed to a very dynamic assemblage in the airborne microbiome that is strongly influenced by the local environment (e.g., meteorological conditions, land use, etc.) (Forde et al., 2019). Nevertheless, little is known about the identity of airborne microbial communities (i.e., community composition and diversity) associated with the temporal dynamics of atmospheric SC concentrations. In this context, our recent taxonomic analyses conducted in summer 2017 at a rural agricultural site in France showed that the daily dynamics in PM<sub>10</sub> SC concentrations are clearly determined by the abundance of only a few specific taxa of airborne fungi and bacteria measured at that study site (Samaké et al., 2020). As a follow-up, the present study aimed to use the DNA metabarcoding approach (Taberlet et al., 2012) to identify PM<sub>10</sub>-associated microbial communities and their main sources at three climatically very different sampling sites in France

during the summer of 2018. Our main objectives were 2-fold: (i) to examine the interannual variability of the structure of summer airborne microbial community (bacteria and fungi only) associated with PM<sub>10</sub> SC concentrations during a consecutive 2-year survey, (ii) to determine whether the airborne microbial community structure associated with PM<sub>10</sub> SC concentrations differs between 3 different French climatic conditions in order to test the hypothesis of local rather than regional emissions of PBOA and associate SC. The results of this study can provide insight into the structure of airborne microbiomes reflecting the spatiotemporal dynamics of PM<sub>10</sub> SC concentrations, which is essential to improve the modeling accuracy of PBOA emission processes in CTM models.

## MATERIALS AND METHODS

### Site Description and Sampling Strategy

Samples of PM<sub>10</sub> aerosols were collected at three representative sites in different geographic regions of France. The sampling sites were selected to cover several main types of environmental conditions in terms of site topography, climate, land use and cover (**Figure 1**). Two urban background sites (Grenoble and Marseille) and one rural background site (OPE) were selected for this study. These sites are respectively located in alpine (Grenoble, 45°09'41" N, 5°44'07" E, 220 m a.s.l.), mediterranean (Marseille, 43°18'20" N, 5°23'40" E, 64 m a.s.l.) and continental (OPE, 48°56'2" N; 5°5' E, 392 m a.s.l.) areas of France. The detailed geographical characteristics of the sampling sites have been described previously (Favez et al., 2010; Salameh et al., 2015; Samaké et al., 2020) and will only be briefly described here. In short, the city of Grenoble is by far the most densely populated urban area in the French Alps and is located at the junction of three mountain ranges (Favez et al., 2010). Marseille is the second most populated city in France and displays a large port area that extends over almost 70 km of the Mediterranean coastline (Salameh et al., 2015). The two sampling sites are part of French regional air quality monitoring networks. Finally, the OPE is a specific long-term multi-disciplinary observatory, with no major sources of pollution nearby (Samaké et al., 2020). The sampling site itself is located in the middle of an intensive agricultural area and is surrounded by field crops (several tens of kilometers in all directions) (Samaké et al., 2020).

Two seasonal aerosol sampling campaigns were conducted during the summers of 2017 and 2018 at the study sites. PM<sub>10</sub> aerosol samples were collected according to the methodology described previously (Samaké et al., 2019b) using a high-volume sampler (DA80, Digitel; 24 h at 30 m<sup>3</sup> h<sup>-1</sup>). In brief, PM<sub>10</sub> samples were collected onto quartz fiber filters (Tissue-quartz PALL QAT-UP 2500 150 mm diameter) pre-heated 6 h at 500°C to remove potential trace of organic contaminants. One 150 mm filter is obtained over a 24 h cycle (starting at 9 am UTC to 9 am UTC the next day) and no replicate is done according to a national procedure validated for atmospheric aerosols sampling: a filtration at 30 m<sup>3</sup>/h for 24 h produces a homogenous deposition on the surface area within 5%. Then the filter is kept to freezer prior analysis. More details can be found

in the recommendations: (EN 16450:2017<sup>1</sup>; EN 12341:2014<sup>2</sup>). All the analyses are done on the same filter after punching some parts directed toward different analysis or extraction before their analysis. The summer 2018 monitoring campaign was achieved simultaneously at the three sites and samples were taken at different frequencies: 1 day out of 6 for the OPE site from 14/05 to 30/08 (16 samples), every 3 days for Grenoble from 23/06 to 31/08 (24 samples) and on a daily basis for the Marseille sites from 05/07 to 25/07 (20 samples).

At the OPE site, a daily collection of filters has already been carried out during the summer 2017 (June to August) (Samaké et al., 2020), allowing to assess the inter-annual variation in the microbial composition of PM<sub>10</sub>. Field blank filters (about 10% of the samples) were obtained by setting the filters in the sampler without air flow during the sampling period. They were handled as real samples for quality assurance purposes. DNA extraction and PCR controls were also included. The dataset presented here has been corrected from negative controls.

A previous source-tracking analysis indicated that airborne microbial communities are most likely the result of high intakes from nearby sources, whereas intakes from distant sources are low and diluted (Tignat-Perrier et al., 2019). Since our previous study showed that the local vegetation was the main sources of airborne microbial communities in relation to SC concentrations at the OPE site (Samaké et al., 2020), leaf samples of the main vegetation type within 100 meters of each aerosol sampler were collected at the same time as the PM<sub>10</sub> sampling. After collection, the samples were stored in airtight containers (sterile bottles, Schott, GL45, 100 ml) containing 15 g of silica gel. More details on sampling procedures and storage conditions are reported elsewhere (Samaké et al., 2020). Approximately 10 to 15 vegetation samples were analyzed per site, which is probably sufficient to conclude about local influence but is clearly insufficient to have an exhaustive image of the microbial communities from regions beyond the immediate surroundings of the urban sites. Due to unfortunate circumstances, leaf samples collected at the OPE site were lost during transport to the laboratory. This is not, however, a prohibitive factor for this study as we had already been able to observe stable SC concentrations trends over 7 consecutive years at this site.

### Chemical Analyses

Details on the chemical analysis of aerosol are presented elsewhere (Golly et al., 2018; Samaké et al., 2019a,b). Briefly, each aerosol sample was analyzed for various chemical species using subsampled fractions of the collection filters and a wide range of analytical methods. In particular, SCs (i.e., arabinol, mannitol, trehalose, and glucose) were systematically analyzed in PM<sub>10</sub> samples by high-performance liquid chromatography with pulsed amperometric detection (Waked et al., 2014; Golly et al., 2018). Elemental and organic carbon (EC, OC) were analyzed

<sup>1</sup>Ambient Air—Automated Measuring Systems for the Measurement of The Concentration of Particulate Matter (PM<sub>10</sub>; PM<sub>2.5</sub>); Technical Report EN 16450:2017; CEN: Paris, France, 2017.

<sup>2</sup>Ambient Air—Standard Gravimetric Measurement Method for the Determination of the PM<sub>10</sub> or PM<sub>2.5</sub> Mass Concentration of Suspended Particulate Matter; Technical Report EN 12341:2014; CEN: Paris, France, 2014.

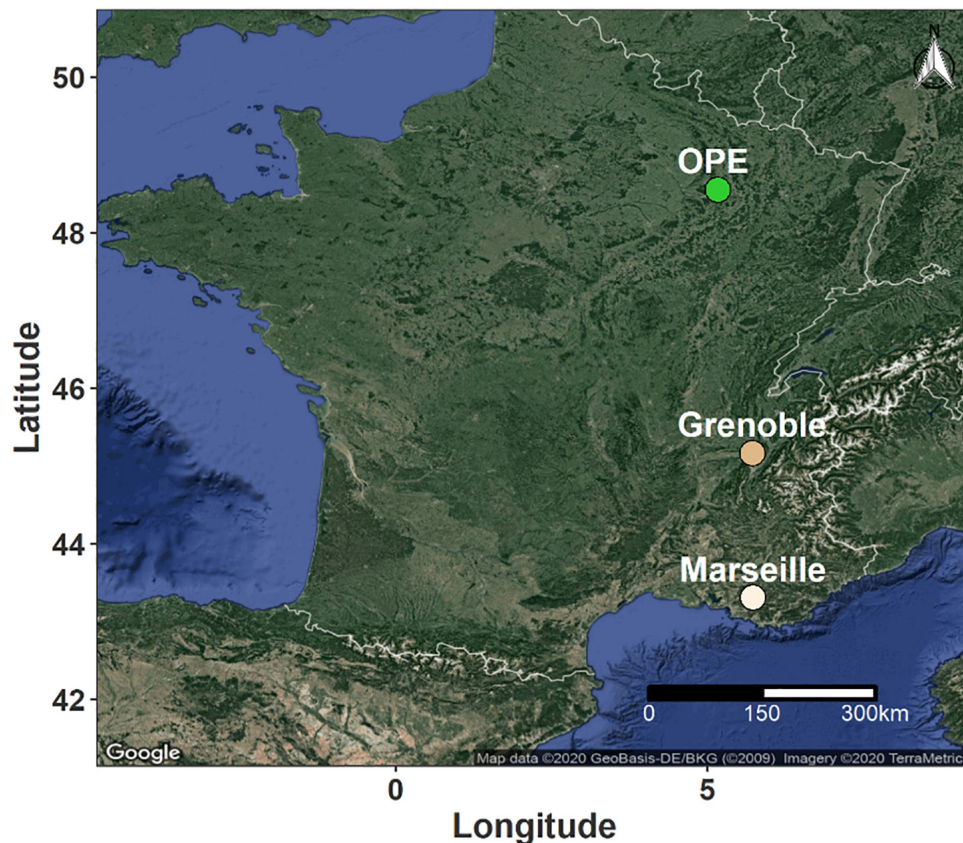


**FIGURE 1 |** Geographical location of the sampling sites in France. The green dot indicates a rural background site in an area of intensive agriculture, while the light and dark beige dots correspond to urban background sites in Mediterranean and Alpine environments, respectively.

using a Sunset Lab. instrument and following the EUSSAR2 thermo-optical protocol (Cavalli et al., 2010).

## Biological Analyses

### DNA Extraction

Aerosol samples pre-treatment and DNA extraction experiments were performed according to an optimized protocol, as presented elsewhere (Samaké et al., 2020). Briefly, 2 filter punches of a diameter of 38 mm each were extracted with the DNeasy PowerWater kit (QIAGEN, Germantown, MD) according to the supplier's instructions, with the following modifications (Samaké et al., 2020): Elution of biological materials on the polyethersulphone membrane disc filter (PES, Supor® 47 mm 200, 0.2 µm, PALL), 30 min sonication at 65°C in a thermal water bath (EMAG, Emmi-60 HC, Germany; 50% of efficiency), 5 min bead-beating before and after sonication, and the DNA was finally eluted with 50 µL EB buffer.

Leaf samples were dried in contact of about 30 g of silica gel. To extract DNA from epiphytic or endophytic microorganisms, aliquots of leaf samples (approx. 25–30 mg) were crushed using a Tissue-Lyser (QIAGEN, Germany). DNA was extracted with the DNeasy Plant Mini Kit (QIAGEN, Germany) according to the original manufacturer's protocol, with some minor modifications as already detailed elsewhere (Samaké et al., 2020).

### PCR Amplification and Sequencing

The PCR amplification procedures and materials used in this study were similar to those described in our recent work (Samaké et al., 2020). Briefly, the hypervariable V4 region of the bacterial 16S rRNA gene was amplified using the Bact02 primer (Forward 5'-KGCCAGCMGCCGCGGTAA-3' and Reverse 3'-GGACTACCMGGGTATCTAA-5'). The nuclear ribosomal internal transcribed spacer region 1 (ITS1) of the fungal gene was amplified with the Fung02 primer (Forward 5'-GGAAGTAAAAGTCGTAACAAGG-3' and Reverse 3'-CAAGAGATCCGTTGTTGAAAGTK-5'). The expected length of the produced reads was of 250 base pairs (bp) for each set of primers. Eight-nucleotide tags were added to both primer ends to uniquely identify each sample, ensuring that each PCR replicate is labeled with a unique combination of forward and reverse tags. The tag sequences were created with the oligotag command in the OBITools software (Boyer et al., 2016), so that all pairwise tag combinations were differentiated by at least five different base pairs (Taberlet et al., 2018).

Four independent PCR replicates were performed for each DNA extract. Amplification of the bacterial 16S rDNA gene and fungal ITS1 region was performed in a 20 µL PCR reaction mixture containing 10 µL of AmpliTaq Gold 360 Master Mix (Applied Biosystems, Foster City, CA, United States),



0.16  $\mu$ L of 20 mg ml<sup>-1</sup> bovine serum albumin (BSA; Roche Diagnostics, Basel, Switzerland), 0.2  $\mu$ M of each primer, and 2  $\mu$ L of diluted DNA extract. The DNA extracts from the air samples were diluted eight times, while DNA extracts from the leaves were diluted four times. The thermal cycling program was as follows: an initial activation of DNA polymerase for 10 min at 95°C; 40 denaturation cycles of 30 s at 95°C, 30 s annealing at 53°C and 56°C for Bacteria and Fungi, respectively, 90 s elongation at 72°C; and a final elongation at 72°C for 7 min. Approximately 10% of the PCR products were randomly selected and controlled using a QIAxel Advance device (QIAGEN, Hilden, Germany) equipped with a high-resolution separation cartridge.

After amplification, PCR products from the same marker were pooled in equal volumes and purified with the MinElute kit (Qiagen, Hilden, Germany) following the manufacturer's instructions. Both pools were sent to Fasteris SA (Geneva, Switzerland) for library preparation and MiSeq Illumina 2 × 250 bp paired-end sequencing. The two sequencing libraries (one per marker) were prepared and libraries as are presented elsewhere (Samaké et al., 2020), which aims to limit the formation of chimeras. Negatives of DNA extraction and of PCR, as well as unused tag combinations were included in the sequencing experiment to monitor for potential false positives due to tag jumps and contamination (Schnell et al., 2015).

### Bioinformatics Analyses of Raw Sequences

The raw read sequences were processed separately for each library using the OBITools software suite (Boyer et al., 2016) and the detailed workflow has recently been presented elsewhere (Samaké et al., 2020). Note that all raw reads (i.e., 2017 and 2018) have been processed simultaneously. In short, the raw paired-ends were assembled and the low-quality sequences (Fastq average quality score < 40) were rejected. The aligned sequences were then assigned to the corresponding PCR replicates allowing zero and two mismatches on the tags and primers, respectively. Strictly identical sequences were de-replicated and a base filtration step was performed to select sequences within the expected range length (i.e., longer than 65 or 39 bp for fungi and bacteria, respectively, excluding tags and primers), without ambiguous nucleotides, and observed at least 10 times in at least one PCR replicate.

The remaining unique sequences were then clustered into Molecular Taxonomic Units (MOTUs) at a 97% threshold using Sumatra and Sumacust algorithms (Mercier et al., 2013). Taxonomy assignments of each MOTU were made to a reference set of full-length metabarcodes using the open reference *ecotag* program (Boyer et al., 2016). The reference database was built with the *ecoPCR* program (Ficetola et al., 2010) for each library based on the version 113 of the EMBL database. The resulting datasets were then processed with the open source software R (R studio interface, version 3.4.1) to filter out chimeric sequences, potential contaminants and failed PCR replicates. Finally, the remaining PCR replicates were summed per sample. The final datasets, as well as the OBITools commands applied, have been uploaded to the DRYAD repository (doi: 10.5061/dryad.dv41ns1wf).

### Statistical Analyses

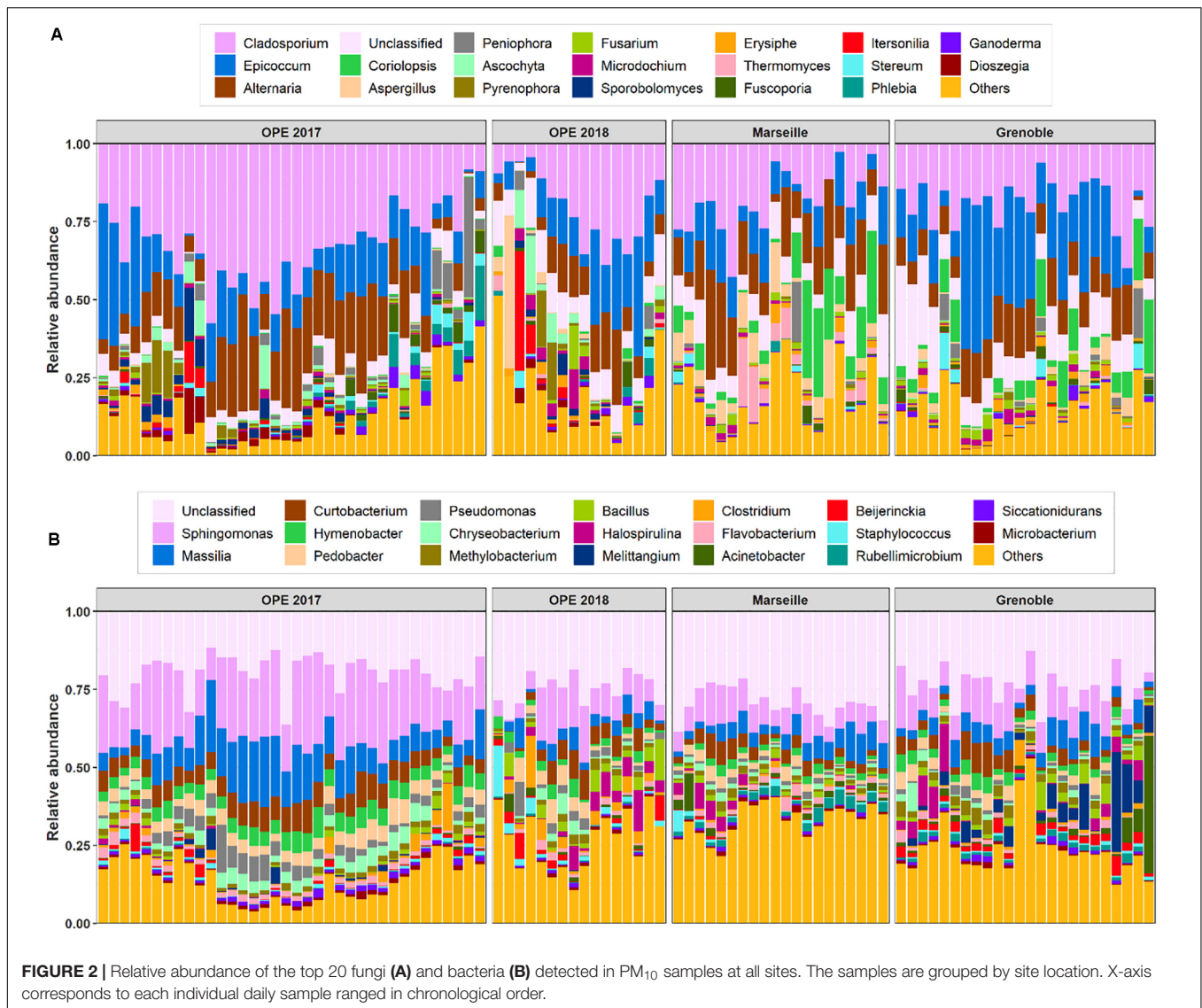
All statistical analyses were carried out with R (R Core Team, 2017). First of all, raw MOTU abundances were rarefied at the same sequencing depth as before any statistical analyses to cope with the heterogeneity of the number of sequences per sample. The rarefaction and extrapolation curves were obtained with the *iNext 2.0-12* package (Hsieh et al., 2016), to study the gain in species richness as we increased the sequencing depth for each sample. The alpha diversity estimator was calculated using the *phyloseq* package 1.22-3 (McMurdie and Holmes, 2013) to estimate the Chao1 index and Shannon diversity. The similarity of microbial communities was represented by non-metric multidimensional scale (NMDS) using the Morisita-Horn similarity distance metric. The NMDS ordination analyses were performed with the *metaMDS* function within the *vegan* package (Oksanen et al., 2020) with the number of random starts set to 999. The samples were also visualized using hierarchical cluster analysis based on the same dissimilarity index. An analysis of similarities (ANOSIM) was performed to assess whether sample categories contained significantly different microbial communities. An analysis of homogeneity of variance was performed with the *betadisper* function in the *vegan* package to test whether airborne microbial compositions differed in their dispersion over time. The null hypothesis was that the mean dispersion within a group was the same across all groups. The relationship between airborne microbial communities and PM<sub>10</sub> SC species was assessed using Kendall's rank correlation.

## RESULTS AND DISCUSSION

### Richness and Diversity Indexes of Microbial Communities

The structures of airborne bacterial and fungal communities (the fraction of micro-eucaryotes was not considered here) were obtained for the 121 samples collected, consisting of 96 aerosols and 25 leaf samples. After paired-end assembly of reads, sample assignment, and stringent quality filtering (including chimera and contaminant filtering), 4,678,172 and 8,721,309 sequences were obtained in total for the bacterial and fungal dataset, respectively. These sequences represented 3,460 bacterial and 1,490 fungal MOTUs in all collected samples. The rarefaction curves of MOTU richness revealed common logarithmic shapes approaching a plateau for each sample (Supplementary Figure S1), indicating that most bacterial and fungal species were detected in our samples. Alpha-diversity estimators, including Chao1 and Shannon indices, were calculated to estimate the mean richness and biodiversity of microbial communities in PM<sub>10</sub> samples analyzed at each study site. MOTU tables were refined to 2,468 and 8,072 bacterial and fungal sequence reads respectively, prior to diversity analyses. As shown in Supplementary Figure S2, the microbial diversity and richness of PM<sub>10</sub> differed significantly at each sampling site ( $p < 0.05$ ), confirming that the diversity and composition of atmospheric bacteria and fungi in aerosol samples are most likely determined by the surrounding landscape and their





corresponding local climatic conditions. On average, the Chao1 richness estimators and Shannon diversity indices of the bacterial MOTU in Marseille were the highest ( $p < 0.05$ ), while that of the OPE site was the lowest ( $p < 0.05$ ). Chao1 values of airborne fungi were highest in Grenoble and lowest at the OPE site ( $p < 0.05$ ), while the Shannon index values remained similar at the different study sites.

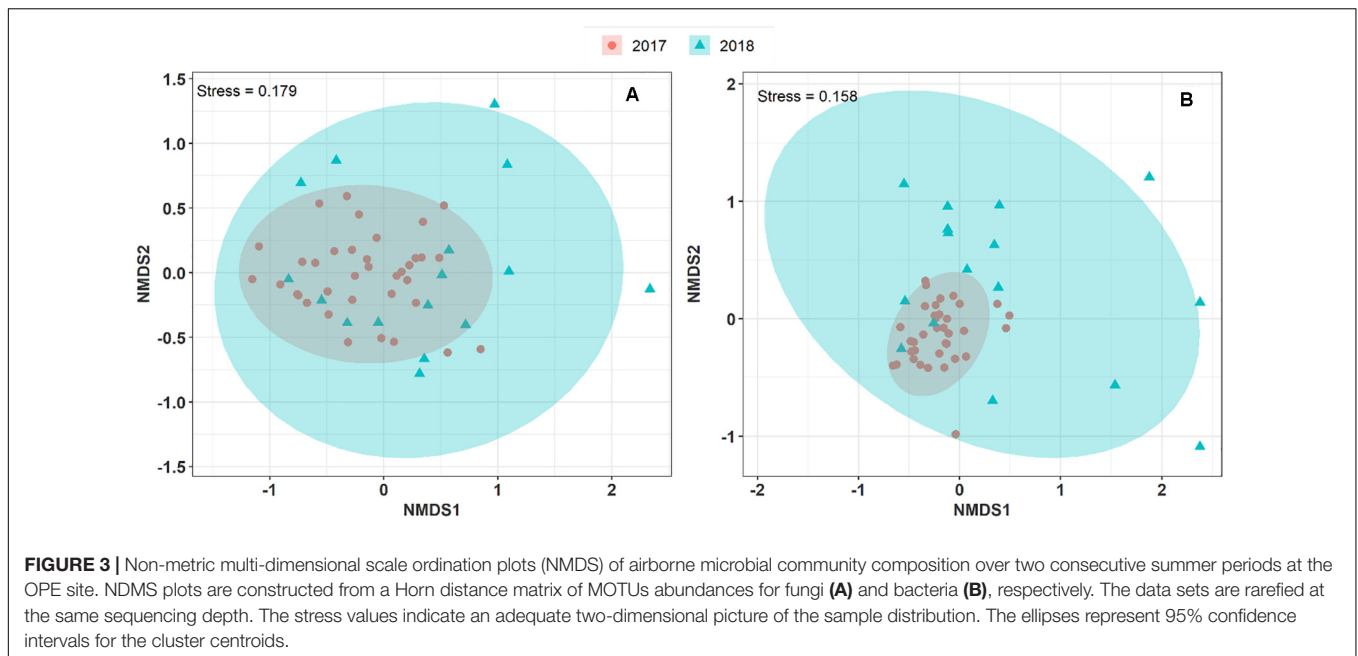
We also compared the microbial diversity of PM<sub>10</sub> during two consecutive summer periods at the rural OPE site. Samples from summer 2017 had the highest richness (number of MOTUs) in bacterial and fungal MOTUs ( $p < 0.05$ ), while, the summer 2018 samples presented approximately the highest bacterial and fungal MOTU diversity (Richness and Evenness).

## Microbial Community in Airborne PM<sub>10</sub>

### Airborne Bacterial Community Composition

In total, the airborne bacterial microbiome was divided into 24 microbial phyla, 54 classes, 124 orders, and 275 families for all

PM<sub>10</sub> samples. Despite very different geographical conditions, the average bacterial sequence reads (mean  $\pm$  SD) were dominated in the three sites by Proteobacteria ( $48.7 \pm 10.7\%$ ), followed by Bacteroidetes ( $18.9 \pm 6.1\%$ ), Actinobacteria ( $16.5 \pm 5.1\%$ ), Firmicutes ( $9.2 \pm 7.4\%$ ), Cyanobacteria ( $1.9 \pm 3.2\%$ ), with less than 3% of the total bacterial sequence reads unclassified. These phyla have been commonly observed in the atmosphere (Maron et al., 2005; Liu et al., 2019; Wei et al., 2020). Proteobacteria constitute a major taxonomic group among prokaryotes, and have previously been reported as the most abundant bacterial phylum in air samples from central northern France (Maron et al., 2005). At the class level, the predominant Bacteria are Alphaproteobacteria ( $25.5 \pm 6.4\%$ ), Actinobacteria ( $15.8 \pm 4.9\%$ ), Gammaproteobacteria ( $10.6 \pm 7.3\%$ ), Betaproteobacteria ( $8.0 \pm 4.9\%$ ), Cytophagia ( $6.4 \pm 2.5\%$ ), Bacilli ( $6.2 \pm 4.6\%$ ), Sphingobacteriia ( $6.0 \pm 3.0\%$ ), Flavobacteriia ( $4.0 \pm 2.3\%$ ), Clostridia ( $2.5 \pm 3.6\%$ ), and Deltaproteobacteria ( $2.3 \pm 4.7\%$ ). Up to 650 genera were detected in all aerosol



samples, although many sequences ( $24.5 \pm 6.7\%$ ) could not be taxonomically attributed at the genus level. The most abundant genera ( $>2\%$ , see **Figure 2B**) are *Sphingomonas* ( $13.9 \pm 7.3\%$ ), followed by *Massilia* ( $7.4 \pm 5.0\%$ ), *Curtobacterium* ( $5.0 \pm 2.6\%$ ), *Hymenobacter* ( $3.3 \pm 1.9\%$ ), *Pedobacter* ( $3.1 \pm 2.0\%$ ), *Pseudomonas* ( $2.3 \pm 2.4\%$ ), *Chryseobacterium* ( $2.1 \pm 1.8\%$ ), and *Methylobacterium* ( $1.9 \pm 1.0\%$ ).

### Airborne Fungal Community Composition

In all aerosol samples, fungal communities were characterized by 3 phyla, 24 classes, 73 orders, and 212 families. The fungal sequence reads in air samples of the three sites are consistently dominated by the Ascomycota phylum ( $76.5 \pm 19.1\%$ ), followed by the Basidiomycota ( $23.4 \pm 19.0\%$ ), which are known to actively eject spores into the atmosphere along with aqueous jets or droplets containing a mixture of inorganic solutes and carbohydrates into the atmosphere (Després et al., 2007). The remaining sequences are affiliated to Mucoromycota ( $<0.03\%$ ) and to unclassified sequences (approximately  $0.03\%$ ). This is consistent with the results of previous studies also indicating that the subkingdom of Dikarya (Ascomycota and Basidiomycota) accounts for 98% of known species in the biological kingdom of Eumycota (i.e., fungi) in the atmosphere (James et al., 2006; Fröhlich-Nowoisky et al., 2009). Among these observed phylotypes, the predominant classes ( $>1\%$ ) are Dothideomycetes ( $69.4 \pm 19.9\%$ ), followed by Agaricomycetes ( $18.1 \pm 18.9\%$ ), Eurotiomycetes ( $5.7 \pm 8.1\%$ ), Sordariomycetes ( $5.5 \pm 6.3\%$ ), Leotiomyces ( $3.7 \pm 3.9\%$ ), Tremellomycetes ( $3.2 \pm 5.8\%$ ), and Microbotryomycetes ( $1.1 \pm 2.3\%$ ). The predominant orders are Pleosporales ( $3.2 \pm 5.8\%$ ) and Capnodiales ( $3.2 \pm 5.8\%$ ), which belong to Ascomycota. Similarly, the dominant orders in Basidiomycota are Polyporales ( $10.2 \pm 10.5\%$ ), followed by Russulales ( $3.2 \pm 6.8\%$ ) and Tremellales ( $2.0 \pm 2.6\%$ ). At the genus level, about 528 taxa

are characterized in all air samples (**Figure 2A**), of which *Cladosporium* ( $24.0 \pm 12.2\%$ ), *Epicoccum* ( $15.7 \pm 11.2\%$ ), *Alternaria* ( $13.7 \pm 8.0\%$ ), *Corioloopsis* ( $4.1 \pm 7.1\%$ ), *Aspergillus* ( $2.5 \pm 5.8\%$ ), and *Peniophora* ( $1.9 \pm 5.0\%$ ) are the most abundant communities.

### Interannual Variation in the Airborne Microbe Composition at the OPE Site

To explore and visualize the variation of airborne microbial communities in PM<sub>10</sub> collected during two consecutive summer periods at the OPE site, we performed an NMDS ordination analysis based on Morishita-Horn dissimilarity distance matrices. As shown in **Figure 3**, the airborne bacterial and fungal communities in the aerosol samples collected in summer 2017 and 2018 are closely grouped. An unsupervised hierarchical cluster analysis shows a pattern similar to that observed on the NMDS ordination, where the airborne bacterial and fungal MOTUs in PM<sub>10</sub> are clustered together regardless of the sampling year. It indicates that the structure of the predominant airborne bacterial and fungal community has remained stable over the years at the OPE site (**Supplementary Figure S3**). This result is logical since agricultural practices (types of crops, harvests, etc.) have been shown to drive airborne microbial communities (Mhuireach et al., 2016; Wei et al., 2019). Although crops around the OPE observatory are subject to a 3-year rotation system, overall crops in the vicinity do not vary significantly from 1 year to the next (Samaké et al., 2019b). However, the microbial communities observed in summer 2018 are dispersively distributed with longer distances between samples (Betadisper,  $p < 0.05$ ) than in summer 2017, for both fungi and bacteria. This result could be, at least partially, attributed to the lower aerosol sampling frequency applied in 2018.

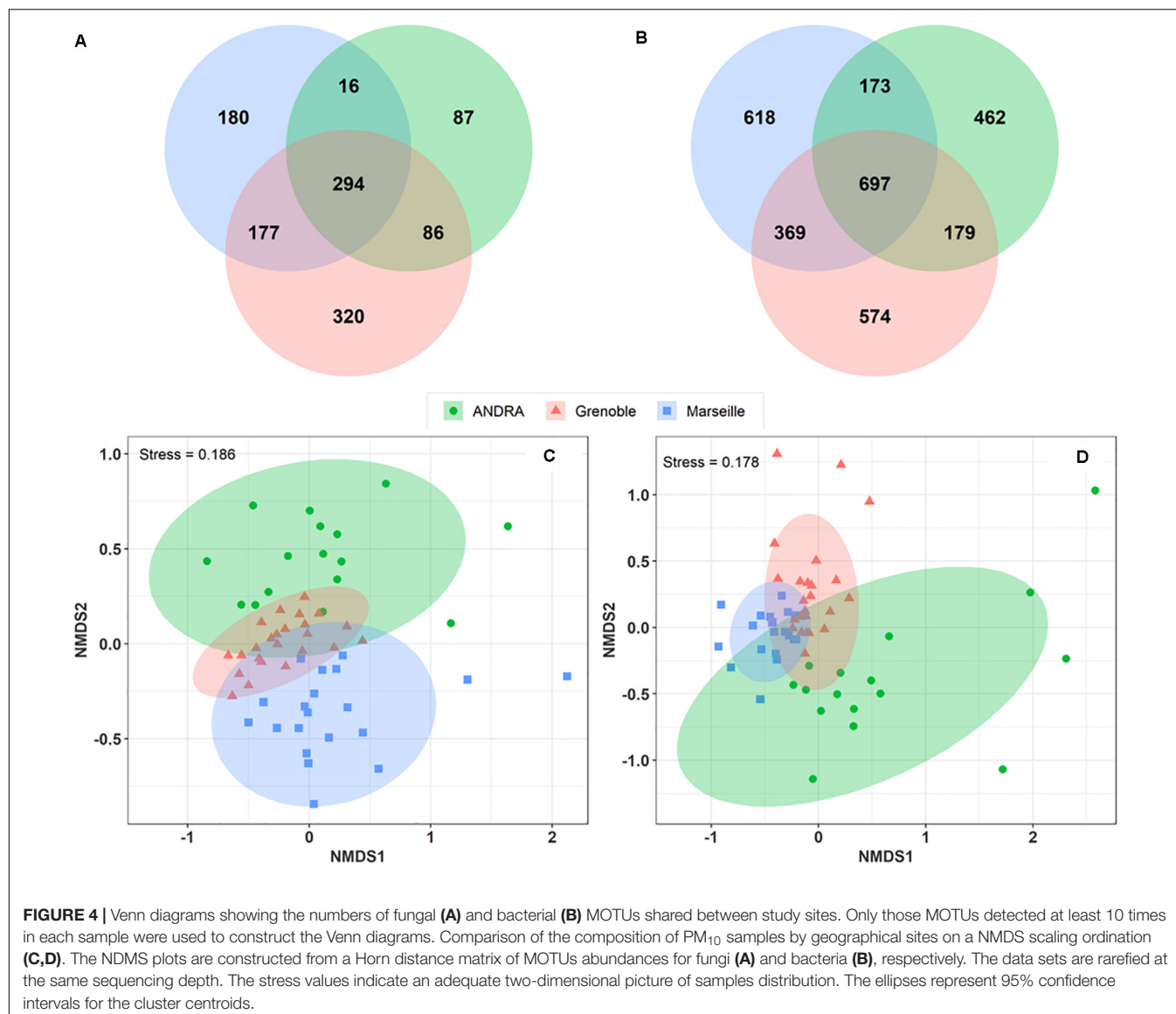


**FIGURE 4 |** Venn diagrams showing the numbers of fungal (A) and bacterial (B) MOTUs shared between study sites. Only those MOTUs detected at least 10 times in each sample were used to construct the Venn diagrams. Comparison of the composition of PM<sub>10</sub> samples by geographical sites on a NMDS scaling ordination (C,D). The NDMS plots are constructed from a Horn distance matrix of MOTUs abundances for fungi (A) and bacteria (B), respectively. The data sets are rarefied at the same sequencing depth. The stress values indicate an adequate two-dimensional picture of samples distribution. The ellipses represent 95% confidence intervals for the cluster centroids.

**TABLE 1 |** Abundances (mean ± standard deviation) of four major primary sugar compounds measured at each study site over two campaigns (2017 and 2018).

Compounds	OPE		Grenoble		Marseille	
	Annual	Summer	Annual	Summer	Annual	Summer
<b>2017</b>	<b>(n = 107)</b>	<b>(n = 64)</b>	<b>(n = 123)</b>	<b>(n = 31)</b>	<b>(n = 66)</b>	<b>(n = 15)</b>
Arabitrol	46.2 ± 71.8	69.4 ± 85.0	19.6 ± 21.2	39.1 ± 27.3	8.0 ± 7.8	12.0 ± 6.8
Mannitol	46.0 ± 65.9	69.2 ± 76.4	21.5 ± 22.7	43.9 ± 22.1	6.9 ± 6.1	11.6 ± 6.7
Glucose	36.1 ± 33.8	48.3 ± 37.5	26.8 ± 22.0	44.5 ± 25.6	11.7 ± 7.4	15.8 ± 8.1
Trehalose	34.6 ± 47.5	53.7 ± 53.1	10.9 ± 15.4	24.0 ± 19.8	NA	NA
<b>2018</b>	<b>(n = 57)</b>	<b>(n = 16)</b>	<b>(n = 186)</b>	<b>(n = 71)</b>		<b>(n = 21)</b>
Arabitrol	16.4 ± 19.4	37.9 ± 25.3	24.8 ± 23.4	38.5 ± 25.1	NA	151.2 ± 81.5
Mannitol	20.8 ± 20.8	37.3 ± 24.0	25.8 ± 22.0	40.5 ± 19.2	NA	164.6 ± 67.4
Glucose	25.6 ± 30.3	36.3 ± 37.8	33.1 ± 27.9	37.7 ± 19.7	NA	155.8 ± 128.7
Trehalose	4.5 ± 10.3	8.4 ± 15.5	9.2 ± 14.6	12.9 ± 15.7	NA	85.9 ± 43.7

In 2018, data for the Marseille site were only available in July. NA denotes not measured. Summer period corresponds to June–July–August.

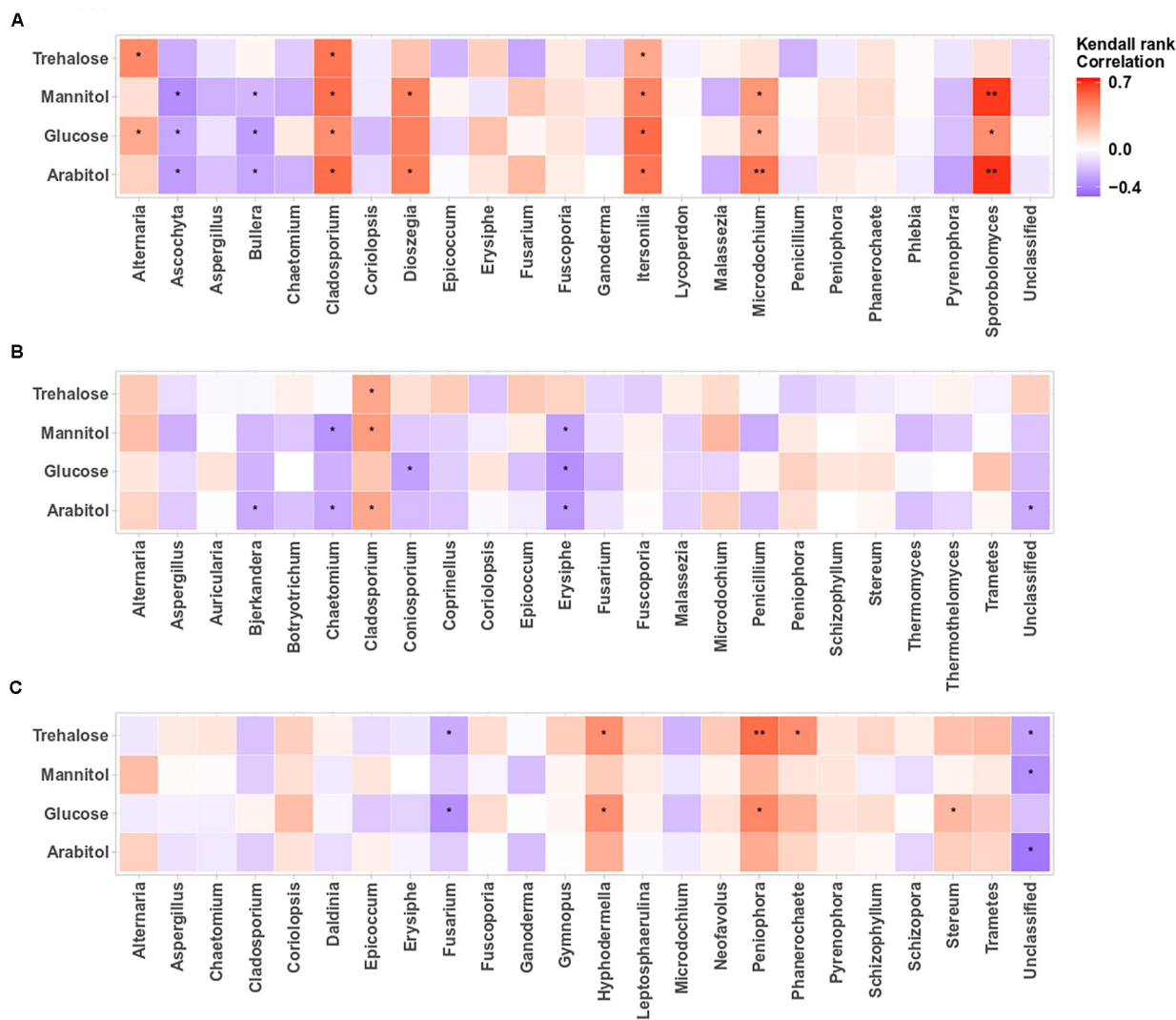


**FIGURE 5 |** Heatmaps of Kendall's rank correlation between SCs and abundance of airborne fungal communities at the study sites: **(A–C)** correspond to the OPE, Marseille and Grenoble sites, respectively. Only the 24 most abundant fungal genera (relative abundance  $\geq 1$ ) are indicated. Asterisks indicate significant correlations ( $**0.001 < p < 0.01$ ,  $*0.01 < p < 0.05$ ).

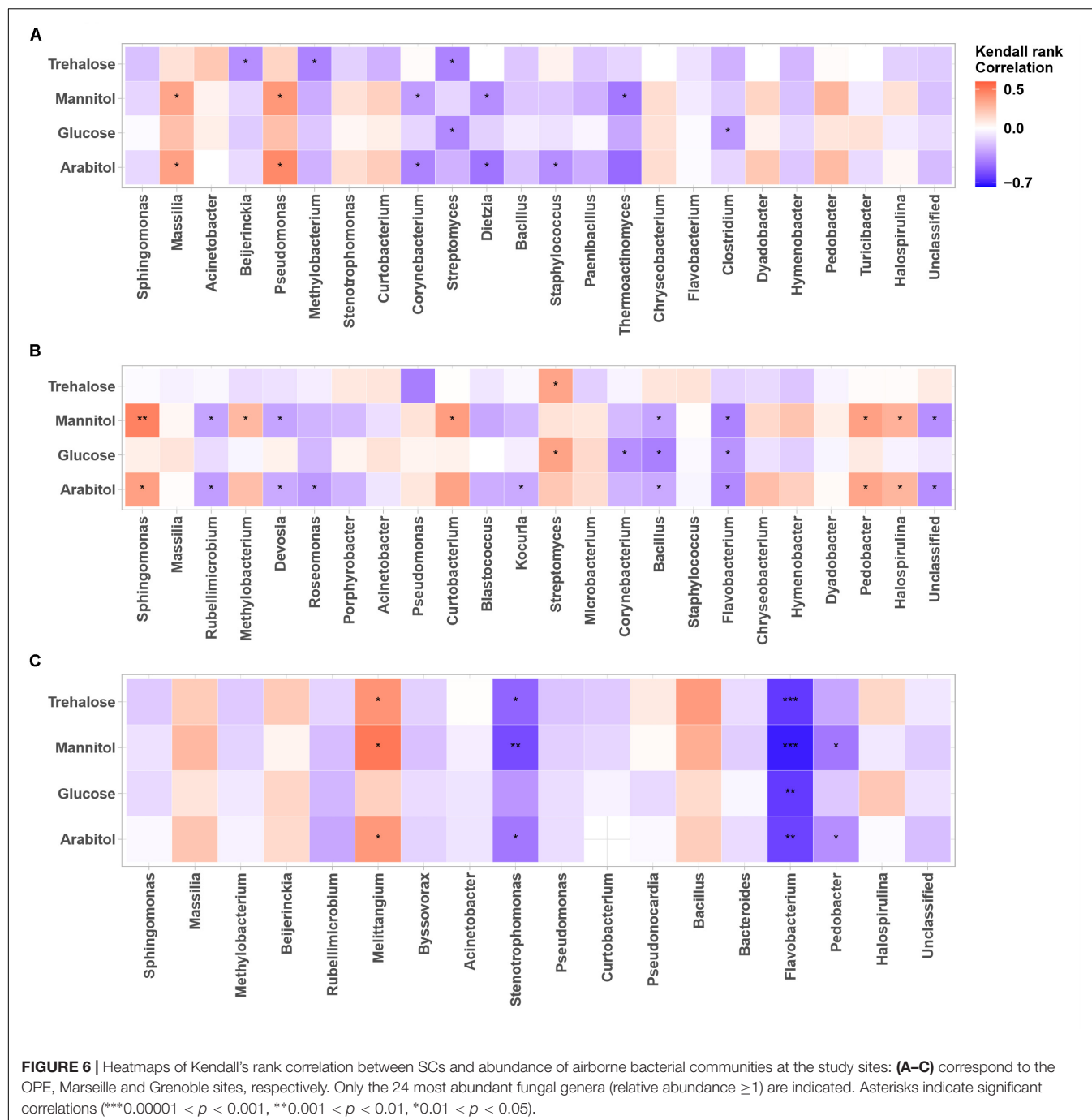
## Spatial Variation in the Composition of Airborne Microbes

A Venn diagram was constructed to analyze the overlap of MOTUs on the pairs of sites (**Figures 4A,B**). A total of 177 fungal MOTUs are shared between the urban background sites of Marseille and Grenoble, whereas the rural OPE site shared only 16 and 86 MOTUs respectively with the Marseille and Grenoble sites. Similarly, 369 bacterial MOTUs are shared between the Marseille and Grenoble sites, whereas the bacterial community of OPE shared only 173 and 179 MOTUs with the Marseille and Grenoble site, respectively. Summer PM<sub>10</sub> samples from the urban sites shared the highest proportion of microbial MOTUs, suggesting that the Marseille and Grenoble sites tend to have more similar airborne bacterial and fungal community compositions. This

suggests that agricultural practices have a different influence on the composition of the local microbiome in the air than urbanization activities.

To study the overall similarity and disparity of microbial community between sites, a NMDS ordination analysis based on the Horn distance matrix was performed (**Figures 4C,D**). **Figures 4C,D** show that, in general, PM<sub>10</sub> samples from the same location are closely grouped together. Further similarity analysis (ANOSIM, overall  $R = 0.28$  and  $R = 0.34$  with  $p < 0.01$  for fungal and bacterial communities, respectively) confirmed the significant difference between the 3 distinct clusters by geographic locations. These results indicate that the bacterial and fungal communities in PM<sub>10</sub> samples are grouped by geographical region, although some taxa are common to all three sites.

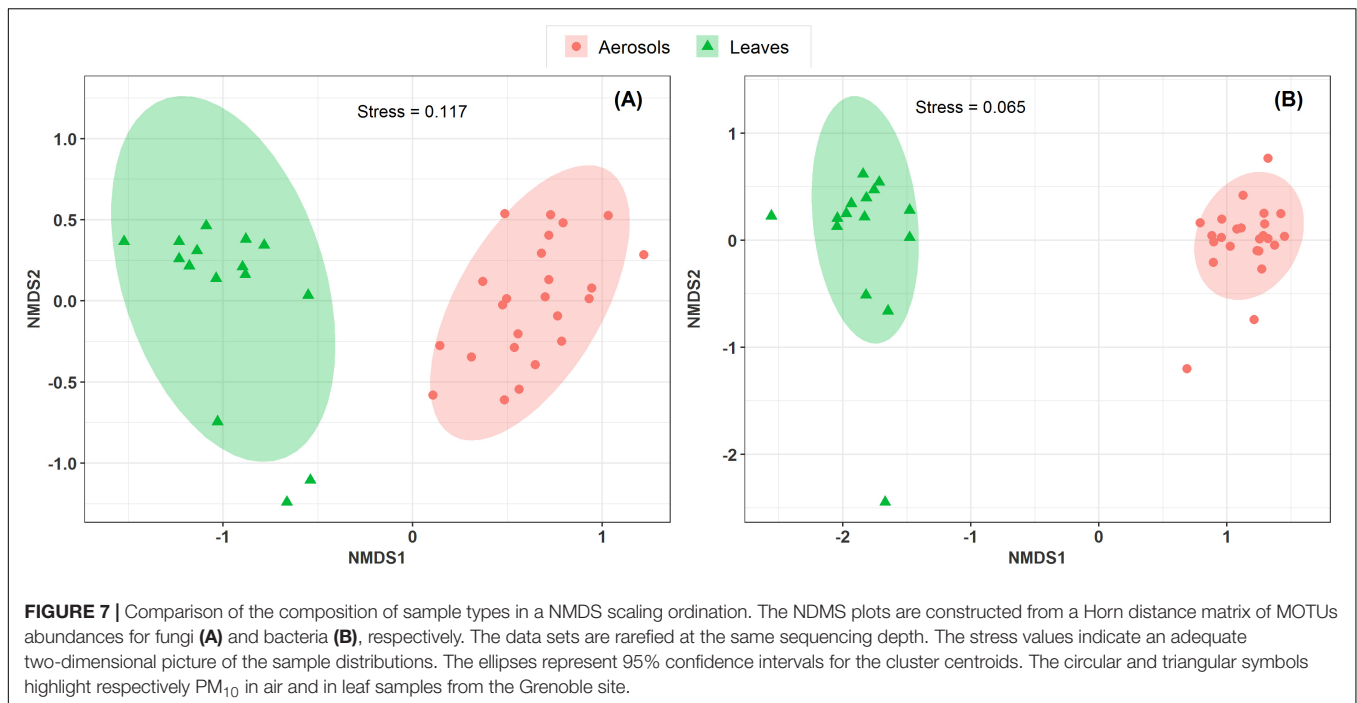




### Spatial and Temporal Variability in Concentrations of Primary Sugar Compounds

A large database on concentrations of PM<sub>10</sub> SC at study sites has been acquired previously at many sites all over France (Samaké et al., 2019a,b), including the three sites of this study. It has already been shown that arabinol, mannitol, glucose, and trehalose are generally the main SC species in all urban and rural areas investigated in France (Samaké et al., 2019a). Their mean annual and summer concentrations at the 3 sites of the present study for the years 2017 and 2018 are shown in

**Table 1.** This table shows that the concentration of individual SC species at the Grenoble site remained almost constant throughout the 2 years of sampling, indicating a reproducibility in the concentration trends of SC species. At the OPE site, mean concentrations of individual SC species in 2018 are generally lower than in 2017. However, it should be noted that this result may have been biased by the difference in sampling frequency used in summer 2018 (1 every 6 days) compared to 2017 (daily). This is important because the source contribution is episodic in nature (e.g., harvesting)



(Samaké et al., 2020), therefore the most intense episodes were not necessarily collected.

As also shown in **Table 1**, the ambient concentration of the main SC species varies significantly between the sites, but with no clear difference according to the site typology (rural vs. urban). This suggests that SC emissions are less site specific but more related with regional climatic characteristics.

### Relationship Between Primary Sugar Compounds and Dominant Airborne Microbial MOTUs

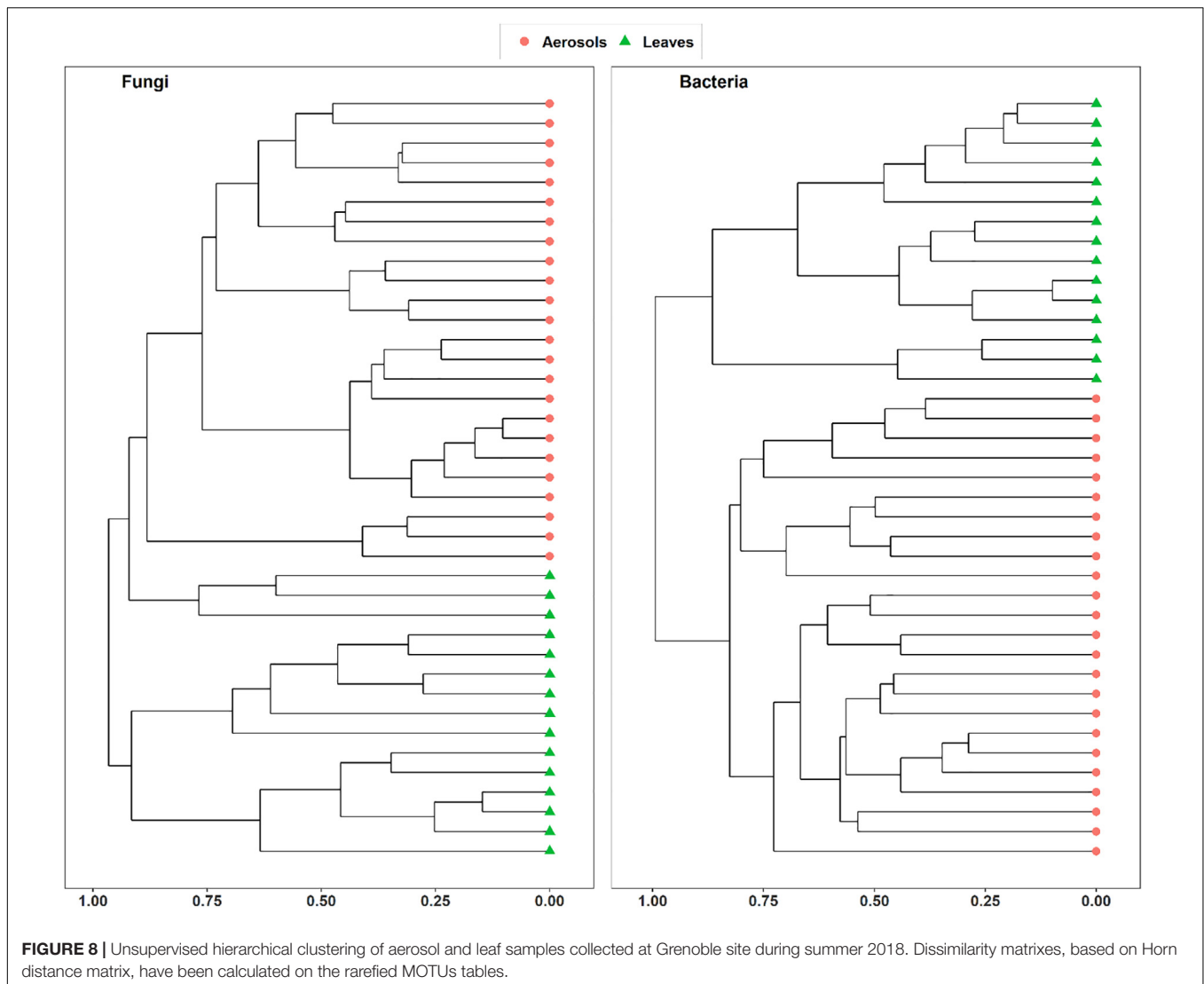
The structure of airborne PM<sub>10</sub> microbial taxa associated with the temporal trends in atmospheric SC concentration levels may vary in different geographical areas. Therefore, we calculated the Kendall's rank correlation between the dominant SC species (i.e., arabinol, mannitol, glucose, trehalose) and the abundance of airborne microbial community at genus level. This analysis reveals variable relationships among sampling sites (**Figures 5A–C, 6A–C**). At the OPE site, the temporal dynamics of SC species is mainly better correlated ( $p < 0.05$ ) with the fungal genera *Alternaria*, *Cladosporium*, *Dioszegia*, *Itersonilia*, *Microdochium*, and *Sporobolomyces* (**Figure 5A**). This observation is consistent with that made in summer 2017 at the same site (Samaké et al., 2020). Similarly, at the Marseille site (**Figure 5B**), time series of SC species are positively correlated ( $p < 0.05$ ) only with *Cladosporium*, and to a lesser degree (not significant) with the fungal genus *Alternaria*, whereas they are best correlated ( $p < 0.05$ ) with the abundances of fungal genera *Hyphodermella*, *Phanerochaete*, *Peniophora*, and *Stereum* at the Grenoble site (**Figure 5C**).

As for airborne fungi, we also found that the temporal dynamics of concentration levels of SC species are positively correlated with the abundances of the bacterial genera *Massilia*

( $p < 0.05$ ) and *Pseudomonas* ( $p < 0.05$ ) at the OPE site (**Figure 6A**), whereas it is better correlated ( $p < 0.05$ ) with the abundances of the bacterial genera *Sphingomonas*, *Curtobacterium*, *Streptomyces*, *Pedobacter*, and *Halospirulina* at the Marseille site (**Figure 6A**). Some bacterial genera, notably *Melittangium*, also showed a strong positive correlation ( $p < 0.05$ ) with PM<sub>10</sub> SC species at the Grenoble site (**Figure 6C**). These results clearly show site-specific microbiome signatures measured in the PM<sub>10</sub> of the 3 sites, with overlaps of only few fungal and bacterial genera. Overall, these observed regional trends probably result from ecosystems heterogeneity, such as site topography, microclimate, vegetation structure, around our study sites. A recent study has shown that the atmospheric microbiome composition is indeed primarily structured by the surrounding landscape types (Tignat-Perrier et al., 2019).

### Potential Sources of Airborne Microbial Communities at Study Sites

Vegetation structure has been proposed as one of the main sources of airborne microorganisms in urban background areas (Genitsaris et al., 2017). A recent study has shown that the episodic daily fluctuations in PM<sub>10</sub> SC concentrations at the Grenoble site are very often well synchronized with those of cellulose (Samaké et al., 2019b), a suitable molecular tracer of atmospheric plant biomass (Puxbaum and Tenze-Kunit, 2003). The latter study in Grenoble (Samaké et al., 2019b) also reported maximum atmospheric concentrations of SCs when the vegetation density indicator (leaf area index) was at its maximum in late summer. Therefore, to determine whether the atmospheric microbial genera most positively correlated with SC species were derived from surrounding vegetation, the overall microbial beta diversity in leaf samples of the main



vegetation around the two urban stations was analyzed. For the Grenoble site, the NMDS ordination analysis (**Figure 7**) shows that the overall beta diversities are very similar within the same habitat (PM<sub>10</sub> or plant) and are very different from a habitat to another (ANOSIM,  $R = 0.89$  and  $0.97$ ,  $p < 0.01$  for fungal and bacterial communities, respectively). These results are also confirmed by an unsupervised hierarchical cluster analysis, which reveals a pattern similar to that observed in the NMDS ordinate (**Figure 8**), where airborne PM<sub>10</sub> taxa are grouped separately from those in leaf samples. Similar results were also obtained for the Marseille site (**Supplementary Figure S4**). These results suggest that the airborne microorganisms at the urban sites studied here do not originate only from the immediate surrounding vegetation. To validate this suggestion, specific samplings of PM<sub>10</sub> and vegetation should be conducted beyond all immediate surroundings of the urban sites, although this appears a complicate, if not impossible, task, being the large number of potential and heterogeneous sources. In this study, the collection of vegetation samples was clearly not

exhaustive and microorganisms typical of each site may have been missed, and do not appear in our analysis. Although not fully supported by direct evidence, these results clearly invalidate, however, our initial hypothesis of specific local emissions of PBOA and SC at urban sites. In other words, airborne microbes in urban areas are probably of allochthonous origin, as already suggested in other contexts (Genitsaris et al., 2017; Tignat-Perrier et al., 2019), with influence on emissions within a radius of several tens of kilometers (Tignat-Perrier et al., 2019).

## CONCLUSION

This study presents the first comprehensive description of the structure and main sources of airborne microbial communities associated with temporal trends in PM<sub>10</sub> SC concentration levels at 3 French sites with different climatic conditions. The following main conclusions could be drawn from the results obtained:

- Temporal trends of SC in PM<sub>10</sub> in the three sites are associated with the abundance of only a few specific taxa of airborne fungal and bacterial. These microbial taxa differ significantly between the 3 different climatic zones studied.
- The structure of summer airborne microbial community associated with PM<sub>10</sub> SC concentrations during a consecutive 2 year survey remains stable at one site in an agricultural area.
- Atmospheric concentration levels of PM<sub>10</sub> SC species vary significantly between the 3 study sites, but without clear differences according to site typology (rural vs urban), suggesting that SC emissions are not only local, around the site, but also related to regional climatic characteristics.
- The overall microbial beta diversity in PM<sub>10</sub> samples are significantly different from that of the main vegetation around the urban sites studied. This indicates that the airborne microorganisms at the urban sites studied here do not originate only from the immediate surrounding vegetation, and are likely to be of allochthonous origin, although no direct evidence could be provided, given the great difficulty in comprehensively sampling the wide variety of potential sources at long distances. The hypothesis of only specific local emissions in urban areas is however ruled out as already suggested in recent studies. This is a different conclusion to that obtained for our rural site in 2017 with homogeneous agricultural practices on a large scale.

Overall, these results improve our understanding of the spatial behavior of tracers of PBOA emission sources in general, which is imperative for further implementation of this large OM mass fraction into CTM models. However, contributions from remote sources in urban areas still need to be validated through specific sampling. Similarly, direct validation of the important SC contents of some species among the dominant microbial taxa identified in each site of this study still needs to be performed, after growth under controlled laboratory conditions. This will allow to decipher the environmental conditions controlling the profile and concentration levels of the SC species produced by the dominant microorganisms, relevant in PBOA emissions.

## DATA AVAILABILITY STATEMENT

The datasets presented in this study can be found in online repositories. The names of the repository/repositories and accession number(s) can be found below: doi.org/10.5061/dryad.dv41ns1wf.

## REFERENCES

- Bauer, H., Claeys, M., Vermeylen, R., Schueller, E., Weinke, G., Berger, A., et al. (2008). Arabitol and mannitol as tracers for the quantification of airborne fungal spores. *Atmos. Environ.* 42, 588–593. doi: 10.1016/j.atmosenv.2007.10.013
- Boucher, O., Randall, D., Artaxo, P., Bretherton, C., Feingold, G., Forster, P., et al. (2005). “Clouds and Aerosols,” in *Climate Change 2013: The Physical Science Basis. Contribution of Working Group I to the Fifth Assessment Report of the Intergovernmental Panel on Climate Change*, eds D. Qin, G.-K. Plattner, M.

## AUTHOR CONTRIBUTIONS

GU, J-LJ, and JM supervised the thesis of AS. GU and J-LJ designed the atmospheric chemistry part of the Mobil’Air program. AT and SC supervised the sampling at Grenoble and ANDRA sites, respectively. BC and NM supervised the sampling at Marseille site. AS, AB, and JM designed the microbiological aspects of the study. AS and AB performed the experiments. AB performed the bioinformatic analyses. AS performed statistical analyses and wrote the original manuscript. All authors revised the manuscript.

## FUNDING

This work was supported by the French National Research Agency in the framework of the “Investissements d’avenir” program (ANR-15-IDEX-02), for the Mobil’Air program. It also received support from the program CAREMBIOS funded by LEFE and EC2CO-Microbien national CNRS programs, from the program QAMECS funded by ADEME (convention 1662C0029), and from the French reference laboratory for air quality monitoring (LCSQA) for the chemical analyses of the filter collected in Grenoble as part of the CARA program. Chemical and microbiological analysis on the Air-O-Sol facility at IGE was made possible with the funding of some of the equipment by the Labex OSUG@2020 (ANR10 LABX56). The Ph.D. of AS was funded by the government of Mali.

## ACKNOWLEDGMENTS

We acknowledge the work of many engineers in the lab at the Institut des Géosciences de l’Environnement for the analyses (A. Crouzet, A. Vella, C. Vérin, and E. Vince). We would like to kindly thank the dedicated efforts of many other people at the sampling sites.

## SUPPLEMENTARY MATERIAL

The Supplementary Material for this article can be found online at: <https://www.frontiersin.org/articles/10.3389/fmicb.2020.576750/full#supplementary-material>

- Tignor, S. K. Allen, J. Boschung, A. Nauels, et al. (Cambridge: Cambridge University Press), 571–892.
- Boyer, F., Mercier, C., Bonin, A., Le Bras, Y., Taberlet, P., and Coissac, E. (2016). OBITOOLS: a UNIX -inspired software package for DNA metabarcoding. *Mol. Ecol. Resour.* 16, 176–182. doi: 10.1111/1755-0998.12428
- Bozzetti, C., Daellenbach, K. R., Hueglin, C., Fermo, P., Sciare, J., Kasper-Giebl, A., et al. (2016). Size-resolved identification, characterization, and quantification of primary biological organic aerosol at a european rural site. *Environ. Sci. Technol.* 50, 3425–3434. doi: 10.1021/acs.est.5b05960



- Cavalli, F., Viana, M., Yttri, K. E., Genberg, J., and Putaud, J.-P. (2010). Toward a standardised thermal-optical protocol for measuring atmospheric organic and elemental carbon: the EUSAAR protocol. *Atmos. Meas. Tech.* 3, 79–89. doi: 10.5194/amt-3-79-2010
- Ciarelli, G., Aksoyoglu, S., Crippa, M., Jimenez, J.-L., Nemitz, E., Sellegri, K., et al. (2016). Evaluation of European air quality modelled by CAMx including the volatility basis set scheme. *Atmos. Chem. Phys.* 16, 10313–10332. doi: 10.5194/acp-16-10313-2016
- Coz, E., Artiñano, B., Clark, L. M., Hernandez, M., Robinson, A. L., Casuccio, G. S., et al. (2010). Characterization of fine primary biogenic organic aerosol in an urban area in the northeastern United States. *Atmos. Environ.* 44, 3952–3962. doi: 10.1016/j.atmosenv.2010.07.007
- Després, V. R., Alex Huffman, J., Burrows, S. M., Hoose, C., Safatov, A. S., Buryak, G., et al. (2012). Primary biological aerosol particles in the atmosphere: a review. *Tellus B* 64:15598.
- Després, V. R., Nowoisky, J. F., Klose, M., Conrad, R., Andreae, M. O., and Pöschl, U. (2007). Characterization of primary biogenic aerosol particles in urban, rural, and high-alpine air by DNA sequence and restriction fragment analysis of ribosomal RNA genes. *Biogeosciences* 4, 1127–1141. doi: 10.5194/bg-4-1127-2007
- Favez, O., Haddad, I. E., Piot, C., Boreave, A., Abidi, E., and Marchand, N. (2010). Inter-comparison of source apportionment models for the estimation of wood burning aerosols during wintertime in an Alpine city (Grenoble, France). *Atmos. Chem. Phys.* 10, 5295–5314. doi: 10.5194/acp-10-5295-2010
- Ficetola, G., Coissac, E., Zundel, S., Riaz, T., Shehzad, W., Bessière, J., et al. (2010). An In silico approach for the evaluation of DNA barcodes. *BMC Genom.* 11:434. doi: 10.1186/1471-2164-11-434
- Forde, E., Gallagher, M., Foot, V., Sarda-Esteve, R., Crawford, I., Kaye, P., et al. (2019). Characterisation and source identification of biofluorescent aerosol emissions over winter and summer periods in the United Kingdom. *Atmos. Chem. Phys.* 19, 1665–1684. doi: 10.5194/acp-19-1665-2019
- Fröhlich-Nowoisky, J., Pickersgill, D. A., Després, V. R., and Pöschl, U. (2009). High diversity of fungi in air particulate matter. *Proc. Natl. Acad. Sci. U.S.A.* 106, 12814–12819. doi: 10.1073/pnas.0811003106
- Genitsaris, S., Stefanidou, N., Katsiapi, M., Kormas, K. A., Sommer, U., and Moustaka-Gouni, M. (2017). Variability of airborne bacteria in an urban Mediterranean area (Thessaloniki, Greece). *Atmos. Environ.* 157, 101–110. doi: 10.1016/j.atmosenv.2017.03.018
- Golly, B., Waked, A., Weber, S., Samake, A., Jacob, V., Conil, S., et al. (2018). Organic markers and OC source apportionment for seasonal variations of PM<sub>2.5</sub> at 5 rural sites in France. *Atmos. Environ.* 198, 142–157. doi: 10.1016/j.atmosenv.2018.10.027
- Heald, C. L., Coe, H., Jimenez, J. L., Weber, R. J., Bahreini, R., Middlebrook, A. M., et al. (2011). Exploring the vertical profile of atmospheric organic aerosol: comparing 17 aircraft field campaigns with a global model. *Atmos. Chem. Phys.* 11, 12673–12696. doi: 10.5194/acp-11-12673-2011
- Helin, A., Sietiö, O.-M., Heinonsalo, J., Bäck, J., Riekkola, M.-L., and Parshintsev, J. (2017). Characterization of free amino acids, bacteria and fungi in size-segregated atmospheric aerosols in boreal forest: seasonal patterns, abundances and size distributions. *Atmos. Chem. Phys.* 17, 13089–13101. doi: 10.5194/acp-17-13089-2017
- Hsieh, T. C., Ma, K. H., and Chao, A. (2016). iNEXT: an R package for rarefaction and extrapolation of species diversity (Hill numbers). *Methods Ecol. Evol.* 7, 1451–1456. doi: 10.1111/2041-210X.12613
- Huffman, J. A., Perring, A. E., Savage, N. J., Clot, B., Crouzy, B., Tummon, F., et al. (2020). Real-time sensing of bioaerosols: review and current perspectives. *Aerosol Sci. Technol.* 54, 465–495. doi: 10.1080/02786826.2019.1664724
- Jaenicke, R. (2005). Abundance of cellular material and proteins in the atmosphere. *Science* 308, 73–73. doi: 10.1126/science.1106335
- James, T. Y., Kauff, F., Schoch, C. L., Matheny, P. B., Hofstetter, V., Cox, C. J., et al. (2006). Reconstructing the early evolution of fungi using a six-gene phylogeny. *Nature* 443, 818–822. doi: 10.1038/nature05110
- Kang, M., Ren, L., Ren, H., Zhao, Y., Kawamura, K., Zhang, H., et al. (2018). Primary biogenic and anthropogenic sources of organic aerosols in Beijing, China: insights from saccharides and n-alkanes. *Environ. Pollut.* 243, 1579–1587. doi: 10.1016/j.envpol.2018.09.118
- Li, L., Ren, L., Ren, H., Yue, S., Xie, Q., Zhao, W., et al. (2018). Molecular characterization and seasonal variation in primary and secondary organic aerosols in Beijing, China. *J. Geophys. Res. Atmos.* 123, 12394–12412. doi: 10.1029/2018JD028527
- Liu, H., Hu, Z., Zhou, M., Hu, J., Yao, X., Zhang, H., et al. (2019). The distribution variance of airborne microorganisms in urban and rural environments. *Environ. Pollut.* 247, 898–906. doi: 10.1016/j.envpol.2019.01.090
- Maron, P.-A., Lejon, D. P. H., Carvalho, E., Bizet, K., Lemanceau, P., Ranjard, L., et al. (2005). Assessing genetic structure and diversity of airborne bacterial communities by DNA fingerprinting and 16S rDNA clone library. *Atmos. Environ.* 39, 3687–3695. doi: 10.1016/j.atmosenv.2005.03.002
- McMurdie, P. J., and Holmes, S. (2013). PhyloSeq: an R package for reproducible interactive analysis and graphics of microbiome census data. *PLoS One* 8:e61217. doi: 10.1371/journal.pone.0061217
- Medeiros, P. M., and Simoneit, B. R. T. (2007). Analysis of sugars in environmental samples by gas chromatography–mass spectrometry. *J. Chromatogr. A* 1141, 271–278. doi: 10.1016/j.chroma.2006.12.017
- Mercier, C., Boyer, F., Kopylova, E., Taberlet, P., Bonin, A., and Coissac, E. (2013). SUMATRA and SUMACLUSt: fast and exact comparison and clustering of sequences. *Programs Abstr. SeqBio Workshop* 14, 27–28.
- Mhuireach, G., Johnson, B. R., Altrichter, A. E., Ladau, J., Meadow, J. F., Pollard, K. S., et al. (2016). Urban greenness influences airborne bacterial community composition. *Sci. Total Environ.* 571, 680–687. doi: 10.1016/j.scitotenv.2016.07.037
- Oksanen, J., Blanchet, F. G., Friendly, M., Kindt, R., Legendre, P., McGlinn, D., et al. (2020). *Vegan: Community Ecology Package*. Available online at: <https://cran.r-project.org/web/packages/vegan/index.html> (accessed February 10, 2020).
- Pietrogrande, M. C., Bacco, D., Visentin, M., Ferrari, S., and Casali, P. (2014). Polar organic marker compounds in atmospheric aerosol in the Po Valley during the Supersito campaigns — Part 2: seasonal variations of sugars. *Atmos. Environ.* 97, 215–225. doi: 10.1016/j.atmosenv.2014.07.056
- Puxbaum, H., and Tenze-Kunit, M. (2003). Size distribution and seasonal variation of atmospheric cellulose. *Atmos. Environ.* 37, 3693–3699. doi: 10.1016/s1352-2310(03)00451-5
- R Core Team (2017). *R: A Language and Environment for Statistical Computing*. Available online at: <https://www.R-project.org/>
- Salameh, D., Detournay, A., Pey, J., Pérez, N., Liguori, F., Saraga, D., et al. (2015). PM<sub>2.5</sub> chemical composition in five European Mediterranean cities: a 1-year study. *Atmos. Res.* 155, 102–117. doi: 10.1016/j.atmosres.2014.12.001
- Samaké, A., Bonin, A., Jaffrez, J.-L., Taberlet, P., Weber, S., Uzu, G., et al. (2020). High levels of primary biogenic organic aerosols are driven by only a few plant-associated microbial taxa. *Atmos. Chem. Phys.* 20, 5609–5628. doi: 10.5194/acp-20-5609-2020
- Samaké, A., Jaffrez, J.-L., Favez, O., Weber, S., Jacob, V., Albinet, A., et al. (2019a). Polyols and glucose particulate species as tracers of primary biogenic organic aerosols at 28 French sites. *Atmos. Chem. Phys.* 19, 3357–3374. doi: 10.5194/acp-19-3357-2019
- Samaké, A., Jaffrez, J.-L., Favez, O., Weber, S., Jacob, V., Canete, T., et al. (2019b). Arabitol, mannitol, and glucose as tracers of primary biogenic organic aerosol: the influence of environmental factors on ambient air concentrations and spatial distribution over France. *Atmos. Chem. Phys.* 19, 11013–11030. doi: 10.5194/acp-19-11013-2019
- Schnell, I. B., Bohmann, K., and Gilbert, M. T. P. (2015). Tag jumps illuminated - reducing sequence-to-sample misidentifications in metabarcoding studies. *Mol. Ecol. Resour.* 15, 1289–1303. doi: 10.1111/1755-0998.12402
- Taberlet, P., Bonin, A., Zinger, L., and Coissac, E. (2018). *Environmental DNA: For Biodiversity Research and Monitoring*. Oxford: Oxford University Press.
- Taberlet, P., Coissac, E., Pompanon, F., Brochmann, C., and Willerslev, E. (2012). Towards next-generation biodiversity assessment using DNA metabarcoding: next-generation dna metabarcoding. *Mol. Ecol.* 21, 2045–2050. doi: 10.1111/j.1365-294X.2012.05470.x
- Tignat-Perrier, R., Dommergue, A., Thollot, A., Keuschnig, C., Magand, O., Vogel, T. M., et al. (2019). Global airborne microbial communities controlled by surrounding landscapes and wind conditions. *Sci. Rep.* 9:14441. doi: 10.1038/s41598-019-51073-4
- Waked, A., Favez, O., Alleman, L. Y., Piot, C., Petit, J.-E., Delaunay, T., et al. (2014). Source apportionment of PM<sub>10</sub> in a north-western Europe regional

- urban background site (Lens, France) using positive matrix factorization and including primary biogenic emissions. *Atmos. Chem. Phys.* 14, 3325–3346. doi: 10.5194/acp-14-3325-2014
- Wei, M., Liu, H., Chen, J., Xu, C., Li, J., Xu, P., et al. (2020). Effects of aerosol pollution on PM<sub>2.5</sub>-associated bacteria in typical inland and coastal cities of northern China during the winter heating season. *Environ. Pollut.* 262:114188. doi: 10.1016/j.envpol.2020.114188
- Wei, M., Xu, C., Xu, X., Zhu, C., Li, J., and Lv, G. (2019). Characteristics of atmospheric bacterial and fungal communities in PM<sub>2.5</sub> following biomass burning disturbance in a rural area of North China Plain. *Sci. Total Environ.* 651, 2727–2739. doi: 10.1016/j.scitotenv.2018.09.399
- Yan, C., Sullivan, A. P., Cheng, Y., Zheng, M., Zhang, Y., Zhu, T., et al. (2019). Characterization of saccharides and associated usage in determining biogenic and biomass burning aerosols in atmospheric fine particulate matter in the North China Plain. *Sci. Total Environ.* 650, 2939–2950. doi: 10.1016/j.scitotenv.2018.09.325
- Yang, Y., Chan, C., Tao, J., Lin, M., Engling, G., Zhang, Z., et al. (2012). Observation of elevated fungal tracers due to biomass burning in the Sichuan Basin at Chengdu City, China. *Sci. Total Environ.* 431, 68–77. doi: 10.1016/j.scitotenv.2012.05.033
- Yu, X., Wang, Z., Zhang, M., Kuhn, U., Xie, Z., Cheng, Y., et al. (2016). Ambient measurement of fluorescent aerosol particles with a WIBS in the Yangtze River Delta of China: potential impacts of combustion-related aerosol particles. *Atmos. Chem. Phys.* 16, 11337–11348. doi: 10.5194/acp-16-11337-2016
- Zhu, C., Kawamura, K., and Kunwar, B. (2015). Organic tracers of primary biological aerosol particles at subtropical Okinawa Island in the western North Pacific Rim: organic biomarkers in the north pacific. *J. Geophys. Res. Atmos.* 120, 5504–5523. doi: 10.1002/2015jd023611

**Conflict of Interest:** The authors declare that the research was conducted in the absence of any commercial or financial relationships that could be construed as a potential conflict of interest.

Copyright © 2021 Samaké, Martins, Bonin, Uzu, Taberlet, Conil, Favez, Thomasson, Chazeau, Marchand and Jaffrezo. This is an open-access article distributed under the terms of the Creative Commons Attribution License (CC BY). The use, distribution or reproduction in other forums is permitted, provided the original author(s) and the copyright owner(s) are credited and that the original publication in this journal is cited, in accordance with accepted academic practice. No use, distribution or reproduction is permitted which does not comply with these terms.



# Graphene-Based Nanomaterials Modulate Internal Biofilm Interactions and Microbial Diversity

Lauris Evariste<sup>1\*</sup>, Paul Braylé<sup>1</sup>, Florence Mouchet<sup>1</sup>, Jérôme Silvestre<sup>1</sup>, Laury Gauthier<sup>1</sup>, Emmanuel Flahaut<sup>2</sup>, Eric Pinelli<sup>1</sup> and Maialen Barret<sup>1</sup>

<sup>1</sup>Laboratoire d'écologie fonctionnelle et environnement, Université de Toulouse, CNRS, INPT, UPS, Toulouse, France,

<sup>2</sup>CIRIMAT, Université de Toulouse, CNRS, INPT, UPS, UMR CNRS-UPS-INP N°5085, Université Toulouse 3 Paul Sabatier, Bât. CIRIMAT, Toulouse, France

## OPEN ACCESS

### Edited by:

Soizic Morin,  
INRAE Nouvelle-Aquitaine  
Bordeaux, France

### Reviewed by:

Mariana Carmen Chifiriuc,  
University of Bucharest, Romania  
Lingzhan Miao,  
Hohai University, China

### \*Correspondence:

Lauris Evariste  
lauris.evariste@gmail.com

### Specialty section:

This article was submitted to  
Microbiotechnology,  
a section of the journal  
Frontiers in Microbiology

**Received:** 30 October 2020

**Accepted:** 28 February 2021

**Published:** 26 March 2021

### Citation:

Evariste L, Braylé P, Mouchet F,  
Silvestre J, Gauthier L, Flahaut E,  
Pinelli E and Barret M (2021)  
Graphene-Based Nanomaterials  
Modulate Internal Biofilm Interactions  
and Microbial Diversity.  
Front. Microbiol. 12:623853.  
doi: 10.3389/fmicb.2021.623853

Graphene-based nanomaterials (GBMs), such as graphene oxide (GO) and reduced graphene oxide (rGO), possess unique properties triggering high expectations for the development of new technological applications and are forecasted to be produced at industrial-scale. This raises the question of potential adverse outcomes on living organisms and especially toward microorganisms constituting the basis of the trophic chain in ecosystems. However, investigations on GBMs toxicity were performed on various microorganisms using single species that are helpful to determine toxicity mechanisms but fail to predict the consequences of the observed effects at a larger organization scale. Thus, this study focuses on the ecotoxicological assessment of GO and rGO toward a biofilm composed of the diatom *Nitzschia palea* associated to a bacterial consortium. After 48 and 144 h of exposure to these GBMs at 0, 0.1, 1, and 10 mg.L<sup>-1</sup>, their effects on the diatom physiology, the structure, and the metabolism of bacterial communities were measured through the use of flow cytometry, 16S amplicon sequencing, and Biolog ecoplates, respectively. The exposure to both of these GBMs stimulated the diatom growth. Besides, GO exerted strong bacterial growth inhibition as from 1 mg.L<sup>-1</sup>, influenced the taxonomic composition of diatom-associated bacterial consortium, and increased transiently the bacterial activity related to carbon cycling, with weak toxicity toward the diatom. On the contrary, rGO was shown to exert a weaker toxicity toward the bacterial consortium, whereas it influenced more strongly the diatom physiology. When compared to the results from the literature using single species tests, our study suggests that diatoms benefited from diatom-bacteria interactions and that the biofilm was able to maintain or recover its carbon-related metabolic activities when exposed to GBMs.

**Keywords:** microbial ecotoxicology, graphene, freshwater, biofilm, diatom, metabarcoding

## INTRODUCTION

Two-dimensional nanomaterials derived from graphene possess unique properties such as high surface area, electrical and thermal conductivity, mechanical strength, and optical transmittance that are currently being explored for the development of new applications in multiple area including composite improvement, energy storage, electronics, medicine, or water

purification (Perreault et al., 2015; Dasari Shareena et al., 2018; Mohan et al., 2018; Nag et al., 2018). Among these graphene-based nanomaterials (GBMs), graphene oxide (GO), and reduced graphene oxide (rGO) appear as very attractive due to their ease of synthesis, their high stability after dispersion in various solvents and the possibility for surface functionalization (Smith et al., 2019). rGO, which carries a lower amount of oxygen-containing functions compared to GO (Lavin-Lopez et al., 2017), constitutes a good compromise between GO and graphene, especially for electrical conductivity properties, leading to its use for the development of electrochemical sensors (Rowley-Neale et al., 2018; Tarcan et al., 2020). As the production of high quality graphene suffers from high energy consumption and cost, GO and rGO constitute major products in the graphene market (Lin et al., 2019). For these reasons, these GBMs are forecasted to be mass-produced and are thus likely to be released in the environment during their whole life cycle, from the production to the recycling (Mottier et al., 2017). However, the monitoring of environmental pollutions by GBMs is not possible yet due to technical limitations for their detection at current low concentrations in complex matrices (Goodwin et al., 2018). Nevertheless, despite the lack of modeling data about their expected environmental concentrations, it is estimated that with increasing needs, GBMs could reach concentrations between 1 and 1,000 µg/L in aqueous environment (Zhang et al., 2017), with an accumulation trend in sediment (Sun et al., 2016; Avant et al., 2019). This requires to carefully evaluate the potential impact of these materials on environmental health, in order to contribute to the development of this nanotechnology in a safety and sustainable way (Fadeel et al., 2018).

Previous studies investigated the toxicity of GBMs toward various aquatic organisms including vertebrates (Clemente et al., 2019; Evariste et al., 2019; Paítal et al., 2019) or invertebrates (Castro et al., 2018; Lv et al., 2018), while the most abundant literature concerns the effects on bacteria and microalgae (Han et al., 2019; Kumar et al., 2019; Tashan et al., 2019; Saxena et al., 2020). Studying the effects of GBMs on these microorganisms is essential since they play crucial roles in aquatic ecosystems. Indeed, microalgae ensure primary production through photosynthesis while bacterial heterotrophic activities contribute to organic matter and nutrient cycling (Paerl and Pinckney, 1996; Scala and Bowler, 2001). Moreover, these microorganisms are at the basis of the trophic chain in the environment and act as a resource supplier for many primary consumers. Thus, impairment of these communities by GBMs exposure could indirectly affect organisms from higher trophic levels (Evariste et al., 2020). The vast majority of the studies available on bacteria and algae were performed on isolated single strains (e.g., *Escherichia coli*, *Staphylococcus aureus*, and *Chlorella* sp.) and highlighted antibacterial activities, and algal growth inhibitory effects of GBMs that were both associated to oxidative stress and membrane injuries (Ouyang et al., 2015; Ji et al., 2016; Zhao et al., 2017). Although these effects are well-documented in free-living cells, data concerning GBMs toxicity toward microorganisms living in complex biofilms remain scarce and inconsistent despite the fact that environmental

biofilms are recognized to bind and accumulate nanoparticles (Ikuma et al., 2015). Biofilm lifestyle confers ecological advantages over free-living cells as it includes social cooperation as well as enhanced resource capture and resistance to antimicrobials for the organisms embedded in a matrix of extracellular polymeric substances (EPS; Flemming et al., 2016).

The main literature available focus on the effects of metallic nanoparticles toward biofilms, while studies focusing on carbon-based nanomaterials remains scarce (González et al., 2015; Lawrence et al., 2016; Hou et al., 2017; Miao et al., 2019). Specifically, the effects of GBMs toward biofilms were monitored on single bacterial strains in order for the development of antimicrobial treatments to avoid the formation of pathogenic biofilms for biomedical purposes (Han et al., 2019; Liu et al., 2019; Cacaci et al., 2020; Cao et al., 2021). In this context, studies indicated that GO-coated surfaces could either promote or inhibit biofilm formation by *E. coli* and *S. aureus* (Ruiz et al., 2011; Guo et al., 2017; Yadav et al., 2017). However, these studies were performed under conditions that are not fully relevant within environmental-based contexts that are not sufficiently investigated (Jastrzębska and Olszyna, 2015; Montagner et al., 2016). Thus, understanding the toxicological effects of GBMs toward more complex communities is crucial to better characterize the ecotoxic potential of these nanomaterials and to further determine the possible consequences of their presence in freshwater environments on the ecosystem functioning. The aim of this study was to investigate the toxicity of a commercial GO and its reduced form toward a complex assembly composed by the diatom *Nitzschia palea* associated to a bacterial consortium. This biofilm was exposed under controlled conditions to GBMs at concentrations ranging from 0.1 to 10 mg.L<sup>-1</sup> to determine the effects on diatom physiology using flow cytometry, as well as on bacterial community structure and activity using high throughput 16S sequencing and community-level physiological profiles, respectively.

## MATERIALS AND METHODS

### Graphene-Based Nanomaterials

Graphene oxide was provided by Antolin Group and prepared by oxidizing Grupo Antolin Carbon Nanofibers (GANF®; Grupo Antolin, Burgos, Spain) using the Hummer's method (Hummers and Offeman, 1958; Lobato et al., 2016). We thermally reduced it at 200°C in H<sub>2</sub> atmosphere into rGO, as previously described (Evariste et al., 2019). GBMs were stored as dry powder in the dark and dispersions were prepared extemporaneously in order to avoid any possible change of material characteristics. Full characterization of the tested materials was detailed in previous work (Evariste et al., 2019) and characterization data are summarized in **Table 1**.

### Complex Biofilm Model and Exposure Procedure

The experimental model for complex biofilms was composed of an association between an axenic strain of *N. palea* CPC-160



**TABLE 1 |** Physico-chemical characteristics of graphene oxide (GO) and reduced graphene oxide (rGO) used in the study.

	Graphene Oxide	Reduced Graphene Oxide
Carbon content (at. %)	69.0 ± 0.4	83.8 ± 0.5
Oxygen content (at. %)	31.0 ± 0.4	16.2 ± 0.3
Csp <sup>2</sup> graphene (at. %)	35.5	64.5
C—OH/C—O—C (at. %)	24.7	7.8
C=O (at. %)	2.5	5.8
O=C—O (at. %)	5.3	1.3
Sat. (at. %)	1.4	4.5
Number of layers (HRTEM)	1–5	1–5
Lateral size (TEM; μm)	0.2–8	0.2–8
Specific surface area (BET; m <sup>2</sup> ·g <sup>-1</sup> )	228 ± 7	16 ± 0.5

TEM, transmission electron microscope; HRTEM, high resolution TEM; BET, Brunauer-Emmett-Teller; at. %, atomic %.

provided by the Canadian Phycological Culture Center (University of Waterloo, Waterloo, ON, Canada) and a bacterial consortium isolated from water filters of the freshwater Museum-Aquarium of Nancy (France). After sampling, the consortium was suspended in 50% glycerol and stored at −80°C until use.

Before the beginning of the exposure to GBMs, microorganisms were sequentially introduced in culture Flasks (Falcon 355,001, 600 ml – 150 cm<sup>2</sup>) as follows. *Nitzschia palea* was cultured as previously described in a modified CHU no. 10 basic medium, called SPE medium (SPE; 6.4 < pH < 6.6; Garacci et al., 2017). Standard growth conditions consisted in an incubation at 22 ± 1°C on a rotary shaker (50 rpm) in a culture room. An illumination of 50 μmol m<sup>-2</sup> s<sup>-1</sup> with a day/night period of 14/10 h, respectively, was applied. Two days prior to exposure (T<sub>-48h</sub>), diatoms were transferred at a density of 5 × 10<sup>4</sup> cells/ml in a flask containing 50 ml of SPE medium. After 24 h of growth in standard conditions (T<sub>-24h</sub>), diatoms reached a concentration of 9 × 10<sup>4</sup> cells/ml. Glycerol was removed from the bacterial consortium after centrifugation and the consortium was suspended in 100 ml of SPE medium. Thus, at T<sub>-24h</sub>, flasks containing diatoms were inoculated with the bacterial consortium to reach the concentration of 3 × 10<sup>4</sup> bacterial cells/ml, leading to the ratio of 3 diatoms per bacterial cells in each flask. After 24 h, flasks were contaminated with GBMs (T<sub>0</sub>). For this purpose, nanomaterials were dispersed in SPE medium through the use of an ultrasonic bath for 10 min and autoclaved. Dilutions of the GBMs stock dispersions were carried out under axenic conditions in order to avoid contamination. Intermediary dispersions were prepared at 0.2, 2 and 20 mg.L<sup>-1</sup>. A volume of 50 ml of GBMs-contaminated SPE media was added in the flasks to reach a final concentration of 0.1, 1, or 10 mg.L<sup>-1</sup> of GBMs while uncontaminated medium was added in the control groups (T<sub>0</sub>). Exposures were performed over 144 h under standard conditions as previously indicated.

Biofilm was sampled after 48 and 144 h of exposure with the different concentrations of GBMs (*n* = 3 per time and GBM concentration). For each sampling, the biofilm was gently scrapped and flask content was homogenized and divided into two fractions of 50 ml. The first fraction was used for diatom

and bacteria counts as well as analysis of the diatom physiological parameters using flow cytometry. In addition, this fraction was also used to perform community level physiological profiles (CLPP) analysis. The second 50 ml fraction was filtrated at 0.45 μm (Whatman® Nuclepore™) to collect the whole microorganism community and investigate the microbial community structure. Filters were stored individually in sterile tubes at −80°C prior to further processing.

## Flow Cytometry Analysis

Flow cytometric (FCM) analysis of the diatom *N. palea* and bacterial counts were performed using a Beckman-Coulter Cytoflex flow cytometer equipped with a 488 nm laser and data were collected and analyzed using Cytexpert v. 2.2.0.97 software.

## Microorganisms Counts and Growth Rate Calculation

For *N. palea* counts, unstained algae were gated based on their forward scatter parameters (FSC-A) and chlorophyll fluorescence (690/50 nm). Bacteria were accounted using SYTO9 dye (Invitrogen). Samples were incubated with 5 μM of the probe for 15 min in the dark at room temperature. Bacteria were detected and enumerated based on the fluorescence emitted by SYTO9-positive events (525/40 nm) and side scatter parameters (SSC-H). Normalized growth rates of the diatoms and bacteria were calculated as follows:

$$\text{Growth rate} = \left( \frac{Cs - Mic}{Mic} \right)$$

$$\text{Normalized growth rate (\%)} = \left( \frac{\text{Growth rate}}{MCtGr} \right) \times 100$$

Cs corresponds to the organism concentration at sampling time, Mic is the mean initial concentration of organisms (at T<sub>-48h</sub> for diatoms and at T<sub>-24h</sub> for bacteria) and MCtGr is the mean growth rate in the control group at sampling time.

## Diatom Physiological Parameters

The relative chlorophyll a content of *N. palea* was determined through the measurement of natural chlorophyll a fluorescence emitted at 690/50 nm. The mean fluorescence intensity (MFI in arbitrary unit) collected is expressed as a percentage of the negative control.

Diatom viability was evaluated using SYTOX® Green. After incubation with the probe for 10 min at a final concentration of 0.5 μM, cell suspensions were analyzed by flow cytometry to measure the fluorescence emitted at 525/40 nm. Diatoms with injured or permeable membrane are positive to the green fluorescence-emitting probe bound to DNA. Results are expressed as viability percentage (100% – percentage of SYTOX-positive cells).

Neutral lipid relative content of the diatoms was evaluated using BODIPY (4,4-difluoro-1,3,5,7-tetramethyl-4-bora-3a,4a-diaza-s-indacene; 505/515). Algae were incubated for 1.5 min with the lipophilic dye at a final concentration of 1 μg.ml<sup>-1</sup>

before FCM. The BODIPY fluorescence emitted by the stained diatoms was collected using a 530/30 nm band-pass filter. The MFI measured is presented as a percentage of the negative control.

The intracellular reactive oxygen species (ROS) produced by the diatoms was measured using 2',7'-dichlorofluoresceindiacetate (DCFH-DA), a marker of oxidative stress. Samples were stained for 30 min with the probe at a final concentration of 10  $\mu$ M prior running flow cytometry measurements. Diatoms with elevated intracellular ROS are positively stained by the probe (Thamatrakoln et al., 2012). The results are presented as a percentage of the diatom population emitting probe-related fluorescence.

## Analysis of Community Level Physiological Profiles

BIOLOG® EcoPlates, consisting of 96-well plates containing a triplicate of 31 different carbon sources and a control with no carbon source, were used to analyze the CLPP of the microorganism communities. Samples were diluted 100 times with fresh SPE medium and 120  $\mu$ l of the diluted suspension was transferred into each well of the plate. After inoculation, EcoPlates were incubated in aerobic conditions at  $22 \pm 1^\circ\text{C}$  in darkness for 144 h. Optical density (OD) at 590 nm was measured immediately after microorganism plating ( $T_{\text{in}}$ ) and was monitored daily over the 144 h with a CLARIOStar plate reader (BMG Labtech). Over these 144 h, OD increased linearly ( $r^2 = 0.94$ ) and did not reach a plateau phase. For each substrate, absorbance was corrected by subtracting the absorbance of the control well containing media only. Negative values of the corrected readings were set to zero. The average well color development (AWCD) of substrate utilization was calculated across all wells per plate as follows:

$$AWCD = (\sum OD_i) / 31,$$

where  $OD_i$  represent the corrected optical density of the  $i$ th well. AWCD was also calculated for each guild of carbon sources, grouped into (1) carbohydrates, (2) carboxylic acids, (3) amino acids, (4) amines and amides, and (5) polymers as defined by Weber and Legge (2009). To compensate the influence of the microorganism density on the AWCD measurement, corrected OD values were calculated per bacteria by dividing the OD value per the number of bacteria introduced in each well at  $T_{\text{in}}$ . The normalized carbon source utilization data were also subjected to principal components analysis (PCA). All the results reported refer to the 144 h time point.

## Analysis of Bacterial Community Structure: DNA Extraction, PCR, Sequencing, and Data Processing

After cutting filters into pieces, total DNA was extracted using the QIAGEN DNeasy PowerSoil kit following manufacturer's instructions. Extraction controls were performed using unused filters to ensure the absence of DNA contamination. The DNA extracts quantity and quality were analyzed using a NanoDrop 2000 UV spectrophotometer (Thermo Scientific). The V4-V5 region of 16S rRNA gene was targeted for *Archaea*

and *Bacteria* using 515F (5'-GTGYAGCMGCCGCGGTA-3') and 928R (5'-CCCGYCAATTCMTTTRAGT-3') primers set (Wang and Qian, 2009). PCR reactions were run in a final volume of 50  $\mu$ l containing: 37.5  $\mu$ l of PCR water, 5  $\mu$ l of 10X PCR buffer, 2  $\mu$ l of DNA extract, 2  $\mu$ l of both primer, 1  $\mu$ l of dNTP (2.5 mM) and 0.5  $\mu$ l of Taq DNA polymerase (5 U/ $\mu$ l – Sigma Aldrich). The following PCR protocol was applied:  $94^\circ\text{C}$  for 120 s, 30 cycles of  $94^\circ\text{C}$  for 60 s,  $65^\circ\text{C}$  for 40 s,  $72^\circ\text{C}$  30 s, and  $72^\circ\text{C}$  for 10 min. Sequencing of the resulting amplicons was performed using Illumina MiSeq technology ( $2 \times 250$  pb) by the Get\_PlaGe platform (Genotoul, Toulouse, France). Bioinformatic analysis was performed using Find Rapidly Operational Taxonomic Units Galaxy Solution (FROGS) pipeline on Galaxy (Escudié et al., 2018). Briefly, sequences with mismatch in the primers were excluded and PCR primers were trimmed. Reads were clustered into operational taxonomic units (OTUs) using the Swarm clustering method (Mahé et al., 2014). Chimera was removed and filters were applied to remove singletons and keep OTUs present in at least two samples. OTUs were assigned at different taxonomic levels (from Kingdom to species) using RDP classifier and NCBI Blast+ against Silva 138 database (pintail 80; Quast et al., 2012). Amplicons affiliated to the diatom chloroplast and mitochondria were removed from the dataset prior to data analysis.

## Statistical Analysis

As interactive effects were observed between the exposure duration and the contaminant concentrations using two-ways ANOVA, one-way ANOVA was performed at each sampling time to compare the effects induced by the different concentrations of contaminant. Thus, data related to microorganism growth rates, diatom physiological parameters, and community physiological profiles were analyzed using one-way ANOVA when assumptions of normality and homogeneity of variance were met. Otherwise, data were transformed to meet these assumptions and data were analyzed using Minitab 16 Statistical software. Concentrations leading to 50% of bacterial growth inhibition ( $IC_{50}$ ) were determined using non-linear Hill regression in Graphpad Prism software.

Sequencing data analyses for OTUs counts, alpha diversity indexes, and Weighted Unifrac Distances calculations as well as multidimensional scaling (MDS) plot were carried out using the R package “Phyloseq” (McMurdie and Holmes, 2013). Differential abundance of bacterial genera between exposed conditions compared to the control group was examined using “Deseq2” R package (Love et al., 2014). PERMANOVA was performed using Adonis function from the “vegan” R package (Oksanen et al., 2015).

## RESULTS

### Effects on Microorganism Growth Rates

Exposure to the GBMs led to a transitory growth stimulation of the diatom. At  $T_{48h}$ , the growth rate calculated in the control

group reached a value of  $5.4 \pm 0.95$  (Supplementary Figure S1). Except after exposure to GO at  $0.1 \text{ mg.L}^{-1}$ , a significant growth stimulation was observed in all GBMs-containing conditions (ANOVA  $p < 0.001$ ), reaching  $268 \pm 31\%$  of the control group value after exposure to  $10 \text{ mg.L}^{-1}$  of rGO (Figure 1A). After 144 h of exposure, none of the growth rates calculated in the exposure conditions were significantly different from the control group (Figure 1B). In addition, growth rates of the diatom calculated after 48 h of exposure to GBMs reached values similar to the control group at  $T_{144\text{h}}$  ( $12.7 \pm 2.6$ ;  $t$ -test;  $p = 0.604$ ; Supplementary Figure S1).

For the bacterial compartment, exposure to GO led to a dose dependant growth inhibition from  $1 \text{ mg.L}^{-1}$ , while only a slight inhibition was noticed after exposure to rGO at  $10 \text{ mg.L}^{-1}$  (Figure 1C). The calculated concentrations leading to a growth inhibition of 50% ( $IC_{50}$ ) were  $2.18 \text{ mg.L}^{-1}$  and  $13.25 \text{ mg.L}^{-1}$  after 48 and 144 h of exposure to GO, respectively. Contrary to the recovery observed for diatoms at 144 h, bacterial growth rates were still significantly different from the control at 1 and  $10 \text{ mg.L}^{-1}$  of GO to at  $10 \text{ mg.L}^{-1}$  of rGO (Figure 1D).

### Effects on *N. palea* Physiology

The relative chlorophyll content of the diatom remained unchanged after 48 h of exposure to the GBMs (Figure 2A)

while a higher relative chlorophyll content could be measured in the diatoms exposed to GO at  $10 \text{ mg.L}^{-1}$  during 144 h (Figure 2B). On the contrary, exposure to rGO led to a slight decrease of the chlorophyll content after 144 h of contact with rGO (Figure 2B).

Graphene oxide exposure did not lead to any significant change in the lipid content of the diatom while in rGO containing conditions, an accumulation of lipids was measured, with a more marked effect after 48 h of exposure (Figures 2C,D).

Measurement of oxidative stress in the diatom indicated a significant oxidative stress after 48 h of exposure to rGO at  $10 \text{ mg.L}^{-1}$  (Figure 2E) while no DCF-positive cells were observed at  $T_{144\text{h}}$  (data not shown). Monitoring of the diatom viability highlighted a significantly higher percentage of alive diatoms after 48 h of exposure to GO at 1 and  $10 \text{ mg.L}^{-1}$  (ANOVA,  $p = 0.027$ , Figure 2F). At  $T_{144\text{h}}$ , no differences were observed between the different GBMs-containing conditions and the control group in the diatom viability that reached that  $99 \pm 0.64\%$  (data not shown).

### Effects of GBMs Exposure on Community Level Physiological Profiles

The community level physiological profile of the biofilm was monitored using Biolog® Ecoplate after 48 and 144 h

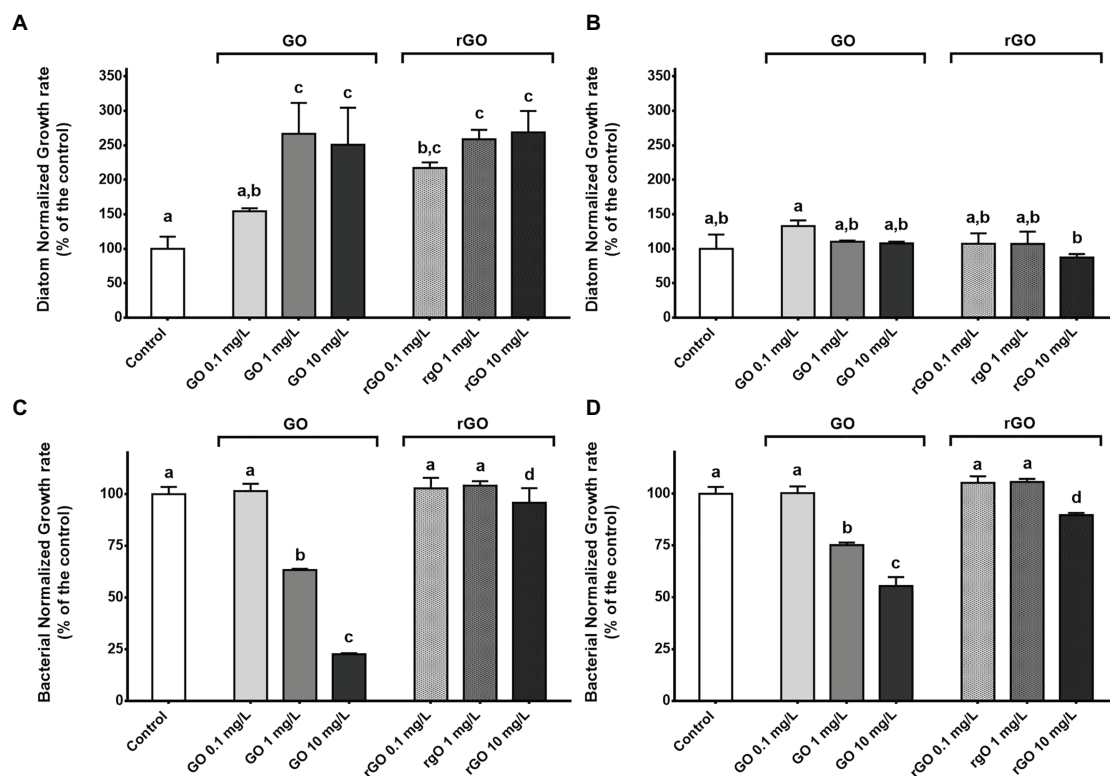


**FIGURE 1 |** Normalized growth rate of the diatom *Nitzschia palea* calculated after 48 h (A) and 144 h (B) of exposure to graphene-based nanomaterials (GBMs). Normalized growth rate of the bacterial consortium calculated after 48 h (C) and 144 h (D) of exposure to GBMs. ANOVA was followed by Tukey test. Letters indicate significant differences between the tested conditions.

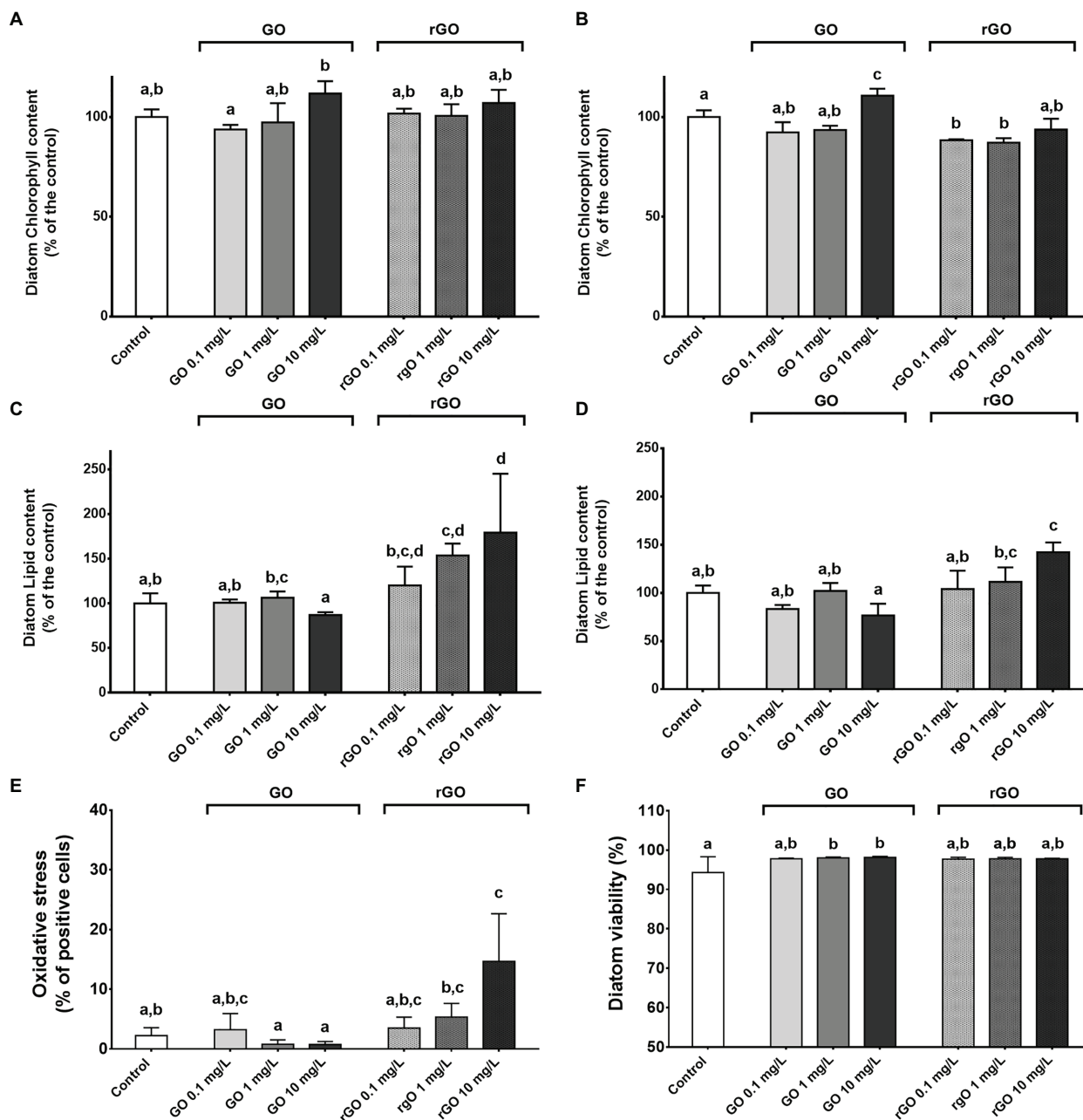


**FIGURE 2 |** Physiological parameters of the diatom *N. palea* following exposure to GBMs. Normalized chlorophyll content measured after 48 h (A) and 144 h of exposure (B), normalized lipid content measured after 48 h (C) and 144 h (D), oxidative stress (E) and viability (F) following 48 h of exposure to GBMs. Values are presented as mean  $\pm$  SD. ANOVA ( $p < 0.05$ ) was followed by Tukey test. Letters indicate significant differences between the tested conditions.

of exposure to the different concentrations of GBMs. As indicated by the normalized AWCD values as well as the PCA results, a dose-dependent increase of the overall utilization of carbon sources was noticed after 48 h of exposure to GO while the substrate utilization did not differ from the control group after exposure to rGO (Figure 3A; Supplementary Figures S2A,B). In the case of GO exposure, this increase of normalized AWCD values resulted from an

increase of the utilization of all the different guilds of carbon sources (Supplementary Figure S3A). At  $T_{144h}$ , the normalized AWCD values were significantly lower in the control group compared to  $T_{48h}$  ( $t$ -test,  $p = 0.016$ ) and values were not significantly different from the control group after exposure to GBMs (Figure 3B). However, according to PCA results, carbon sources utilization appears to be different from the control in every GO-containing condition



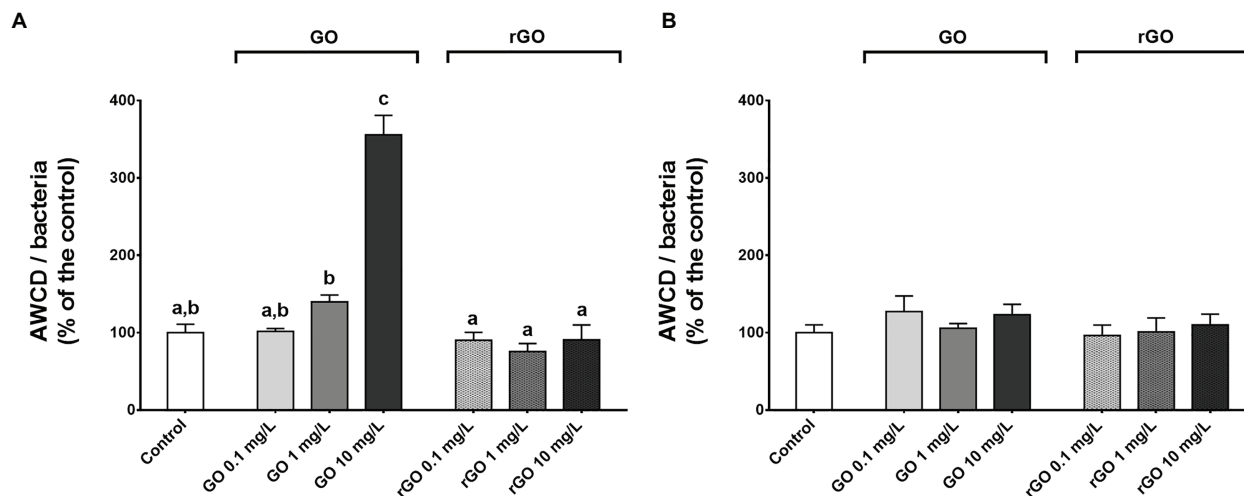


**FIGURE 3 |** Normalized average well color development (AWCD) values measured after 48 h (A) and 144 h (B) of exposure to GBMs. ANOVA followed by Tukey test. Letters indicate significant differences between the tested conditions.

(Supplementary Figure S2C). This is associated to an increased utilization of the polymers guild (Supplementary Figure S3B). Similarly, PCA results suggest changes in the CLPP after 144 h of exposure to rGO at 10 mg.L<sup>-1</sup> compared to unexposed biofilm (Supplementary Figure S2D). In this condition, carbon sources 4-hydroxy benzoic acid, itaconic acid, and D-xylose appeared to be utilized by the microbial consortium while it was not the case in other conditions. The highest average AWCD values measured in the control group at both 48 and 144 h was for the carbohydrate and amino acid guilds while after 144 h of exposure to GO at 1 and 10 mg.L<sup>-1</sup>, the utilization of the substrates from the polymers guild is favored.

## Effects on Bacterial Community Structure

After 48 h of exposure, the Shannon indexes calculated for the bacterial communities were similar in the GBMs containing conditions compared to the control group (ANOVA  $p = 0.305$ ; Figure 4A) and the bacterial community structure was not significantly affected as revealed by MDS and PERMANOVA analysis using weighted UniFrac distances (PERMANOVA,  $p = 0.221$ ; Figure 4B). Between 48 and 144 h, the trajectory of bacterial communities in control conditions resulted in a decrease of Shannon index (Figure 4B). However, after 144 h of exposure to GO at 10 mg.L<sup>-1</sup>, the Shannon index was significantly higher than in the control (ANOVA,  $p < 0.001$ ; Figure 4C) when compared to the control group. At T<sub>144h</sub>, the exposure to GBMs significantly affected the bacterial community structure (PERMANOVA:  $p = 0.001$ ) and MDS analysis revealed that the effects were more marked after exposure to GO at 10 mg.L<sup>-1</sup> (Figure 4D).

At T<sub>48h</sub> in the control group, over 98% of the bacteria constituting the biofilm belonged to the phyla Proteobacteria and Bacteroidota, accounting for  $60.7 \pm 2.0\%$  and  $38 \pm 1.5\%$

of the total bacteria, respectively (Figure 5). At T<sub>144h</sub>, these two phyla represented over 99% of the whole community but the relative abundance of the phylum Proteobacteria decreased to  $37.0 \pm 4.9\%$  while it increased to  $62.5 \pm 4.7\%$  for the phylum Bacteroidota (Figure 5). At T<sub>48h</sub>, the relative abundances of these two phyla were not affected by the GBMs exposure (Bacteroidota: ANOVA,  $p = 0.954$ ; Proteobacteria: ANOVA,  $p = 0.944$ ). After 144 h of exposure to the different concentrations of GBMs, only the exposure to GO at 10 mg.L<sup>-1</sup> led to significant changes in the phyla distribution. In this condition, the relative abundance of the phylum Bacteroidota was significantly lower ( $51.8 \pm 3.5\%$ ) compared to the one observed in the control group (ANOVA,  $p = 0.001$  followed by Tuckey test), while the relative abundance of the phylum Proteobacteria was significantly higher ( $47.8 \pm 3.4\%$ ; ANOVA,  $p = 0.002$  followed by Tuckey test).

At T<sub>48h</sub>, OTUs assigned to the phylum Bacteroidota were mainly members of the orders *Chitinophagales* and *Sphingobacteriales* (Supplementary Figure S4A). Members from the order *Burkholderiales* and *Rhodobacterales* predominated among OTUs affiliated to the phylum Proteobacteria (Supplementary Figure S4B). While *Burkholderiales* and *Rhodobacterales* members still predominated over other Proteobacteria after 144 h of incubation, the relative abundance of OTUs affiliated to the Order *Xanthomonadales* increased over time in all conditions (Supplementary Figure S4B). Statistical analysis of the OTUs relative abundances in the biofilm indicated that four OTUs from the phylum Proteobacteria were differentially abundant upon exposure to GBMs, with a significance threshold fixed at  $p = 0.01$ . All four OTUs were more abundant after exposure to 10 mg.L<sup>-1</sup> of GO during 144 h than in control condition. Two of these OTUs, with a log<sub>2</sub>-fold change of  $6.79 \pm 1.2$  and  $5.82 \pm 1.1$ , were affiliated to the genus *Acidovorax* while the two others with a log<sub>2</sub>-fold

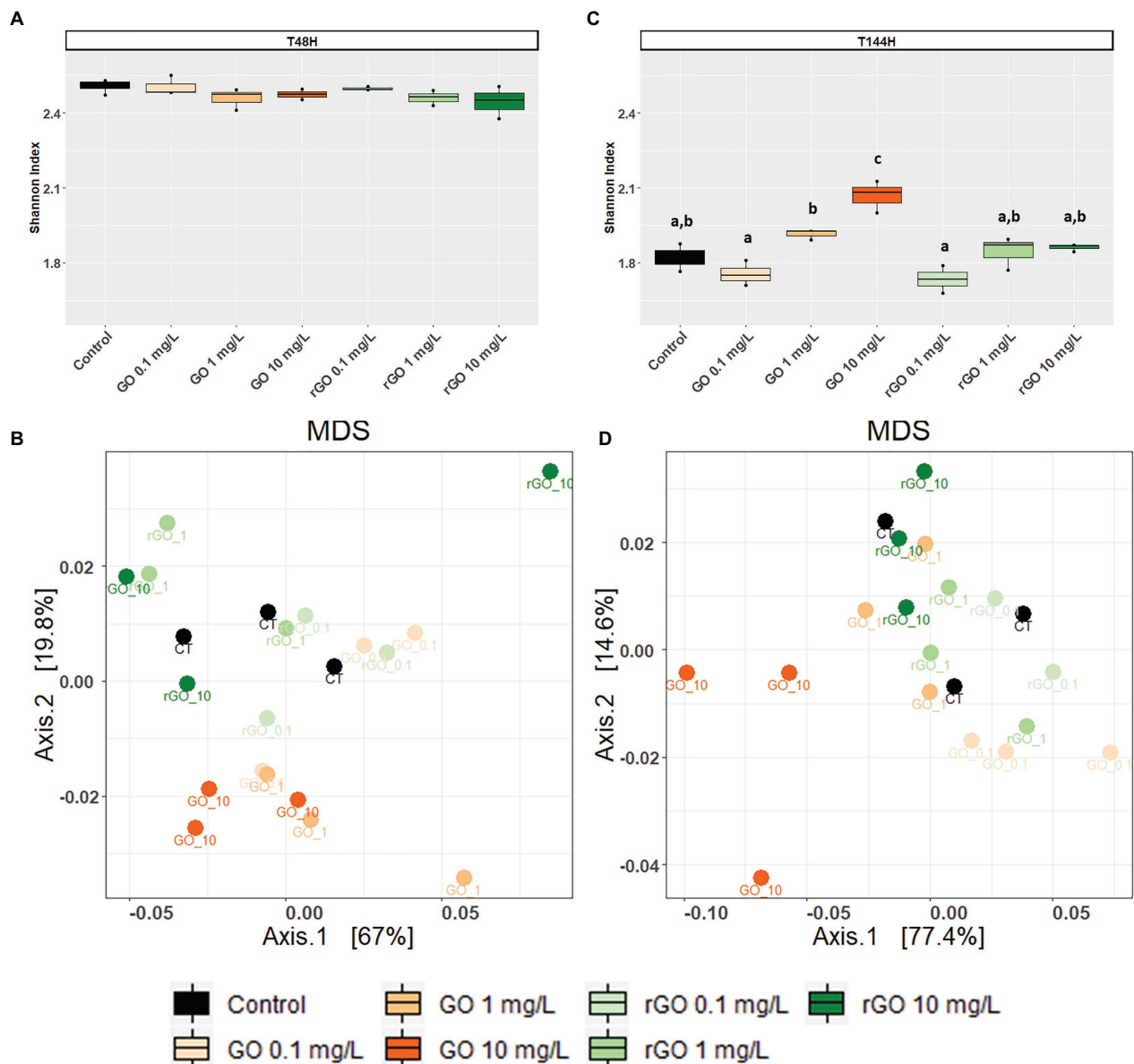


**FIGURE 4 |** Effects of exposure to GBMs on bacterial communities from the biofilm. Shannon evenness index following 48 h (A) or 144 h of exposure to GBMs (C) are compared between the exposure conditions. ANOVA followed by Tukey test. Letters indicate significant differences between the tested conditions. Multidimensional scaling (MDS) plot of bacterial communities based on unweighted Unifrac distances after 48 h (B) and 144 h (D) of exposure to the different conditions.

change of  $1.81 \pm 0.4$  and  $1.95 \pm 0.2$  belonged to the genus *Silanimonas* (Table 2). In the control group, the relative abundance of the two *Acidovorax* members (OTUs 29 and 18) decreased between  $T_{48h}$  and  $T_{144h}$  while it increased for the two *Silanimonas* sp. (OTUs 9 and 61; Figure 6). Upon exposure to GO at  $10 \text{ mg.L}^{-1}$ , these OTUs followed different trajectories compared to the control conditions. Thus, the increases of the former OTUs were enhanced while the decreases were less marked over time for the latter OTUs (Figure 6). For example, the OTU 9 increased from  $0.18 \pm 0.02\%$  at  $T_{48h}$  to  $1.7 \pm 0.2\%$  at

$T_{144h}$  in the control group whereas it reached  $6.2 \pm 1.2\%$  following exposure to GO at  $10 \text{ mg.L}^{-1}$ .

## DISCUSSION

Due to the multiple crucial roles played by microbial communities in the environment, studying the effects of GBMs toward these communities is essential to better assess the ecosystemic consequences of a contamination of the environment by these

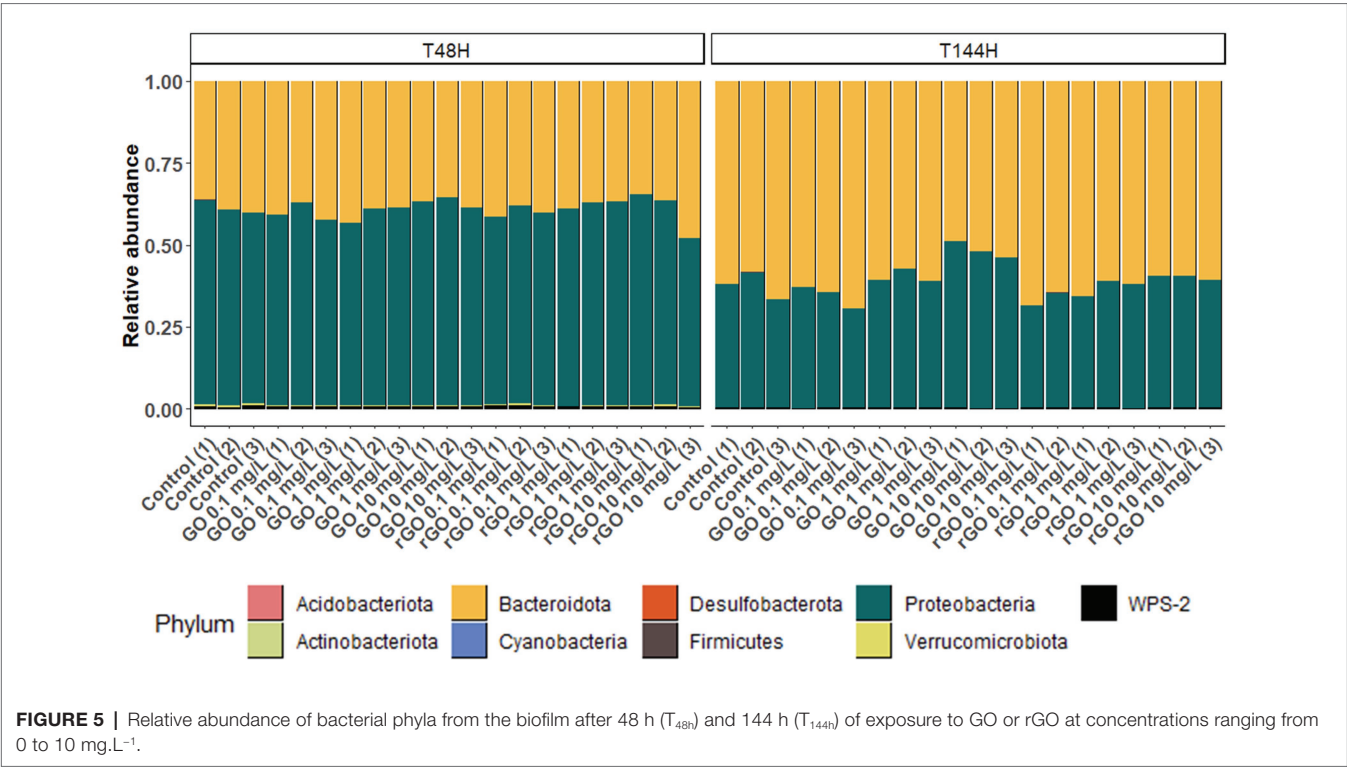
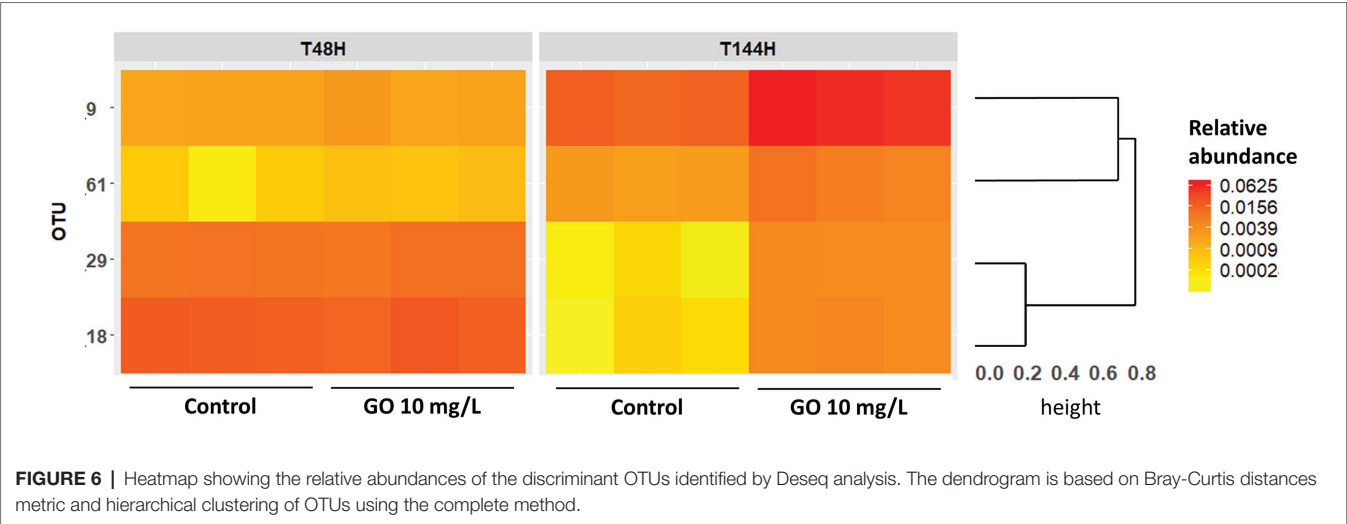


**TABLE 2 |** Operational taxonomic units (OTUs) differentially abundant ( $p < 0.01$ ) at 10 mg.L<sup>-1</sup> of GO compared to the control group after 144 h of exposure.

OTU	Log2-fold change	Phylum	Class	Order	Family	Genus
18	6.79	Proteobacteria	Gammaproteobacteria	Burkholderiales	Comamonadaceae	Acidovorax
29	5.82	Proteobacteria	Gammaproteobacteria	Burkholderiales	Comamonadaceae	Acidovorax
61	1.81	Proteobacteria	Gammaproteobacteria	Xanthomonadales	Xanthomonadaceae	Silanimonas
9	1.95	Proteobacteria	Gammaproteobacteria	Xanthomonadales	Xanthomonadaceae	Silanimonas

Positive log2-fold change values indicate enriched OTUs in the exposure condition.



nanomaterials. For this purpose, many studies evaluated their ecotoxic potential through the use of single-species-based assays. These tests are relevant to determine the toxicological effects and pathways associated to GBMs exposure but they are not realistic and fail to inform the consequences that could occur when interacting species are exposed. As literature about GBMs

impact on complex communities is scarce for the aquatic environment, this study aims to fill the gap on the subject.

## Consequences of the GBMs Exposure on the Algal Compartment

In our study, exposure to the different GBMs concentrations led to a growth stimulation of the diatom *N. palea*, reaching the maximum growth rate earlier compared to the control group, the growth rate of the latter being comparable to previous studies (Garacci et al., 2017). These results are contradictory with the vast majority of single-species-based studies which indicated that exposure to engineered nanoparticles led to algal growth inhibition associated to oxidative stress induced by cellular damages (Chen et al., 2019; Saxena et al., 2020). For example, this was observed for green pelagic algae such as *Raphidocelis subcapitata*, *Chlorella pyrenoidosa*, or *Scenedesmus obliquus* after exposure to GO or rGO (Du et al., 2016; Zhao et al., 2017, 2019; Malina et al., 2019). It was also indicated that the exposure of the freshwater diatom *N. palea* to few layer graphene (FLG) increased the production of EPS substances which mitigated its toxicity (Garacci et al., 2017, 2019). Despite the difference of sensitivity of the different algal species to GBMs, the concentrations leading to 50% of algal growth inhibitions all ranged from 20 to over 150 mg.L<sup>-1</sup>, which is approximately one order of magnitude higher than the concentrations tested in our study (Nogueira et al., 2015; Du et al., 2016; Zhao et al., 2017). In our work, the similar trends observed on the increase of the diatom growth following exposure to GO or rGO suggest that this response may not be influenced by specific physico-chemical characteristics such as oxidation level. In addition, the weak oxidative stress measured in the diatom is consistent with the absence of growth impairment and highlights the protective effect associated to the biofilm lifestyle. Growth inhibitory effects were also hypothesized to be associated to indirect ecotoxic effects through shading as well as to nutrient depletion by GBMs (Garacci et al., 2017; Zhao et al., 2017). As the algal growth increased, these two hypotheses are unlikely under the exposure conditions used in this study or they could have been counterbalanced by favorable interactions with bacteria.

According to the FCM analyses performed, we observed that exposure to GO led to an increase of chlorophyll content and to a decrease of lipid content in the diatom while opposite results were observed following rGO exposure. Although few studies monitored changes in algal physiological parameters, the results obtained in the latter case are in line with studies from the literature focusing on the effects associated to low-oxygen content GBMs exposure. Indeed, a significant reduction of chlorophyll level and an under-expression of genes associated to chlorophyll biosynthesis resulted from an exposure to rGO or few layer graphene in the algae *Scenedesmus obliquus* or *N. palea*, respectively (Du et al., 2016; Garacci et al., 2019). In addition, exposure to graphene nanosheets was shown to favor lipid accumulation in *Chlorella pyrenoidosa* (Khanra et al., 2018). However, in the case of GO exposure, our results are contradictory with the single-species-based literature that usually reports a decrease of chlorophyll pigments (Tang et al., 2015; Hu et al., 2016; Hazeem et al., 2017;

Malina et al., 2019). *Nitzschia palea* is a mixotrophic diatom able to grow using autotrophic metabolism (e.g., photosynthesis) using an inorganic carbon source (CO<sub>2</sub>) and/or through a heterotrophic metabolism using organic carbon sources (Villanova et al., 2017). It was reported that mixotrophic algae accumulated chlorophyll when cultured in autotrophy, while this content decreased and lipids were accumulated by the algae under heterotrophic conditions (Cheirsilp and Torpee, 2012; da Silva Ferreira and Sant'Anna, 2017). Thus, our observations suggest that in *N. palea*, when it is associated to a bacterial consortium, autotrophic and heterotrophic metabolism were differentially balanced under GO or rGO exposure. In any case, these changes of the energy acquisition pathways in the diatom did not alter growth performance following 144 h of exposure to GBMs.

## Consequences of the GBMs Exposure on the Bacterial Compartment

The effects of GBMs toward bacteria have been mainly investigated through the exposure of single bacterial strains. The effects toward bacterial communities were studied in soil (Du et al., 2015; Xiong et al., 2018; Forstner et al., 2019) or in activated sludge (Ahmed and Rodrigues, 2013; Guo et al., 2018; Yujie et al., 2020) but data remain scarce in aquatic ecosystems (Evariste et al., 2020). Given the important bacterial growth inhibition and the relatively weak consequences on microbial composition noticed after 48 h of exposure to GO, we can suggest that the effects of this nanomaterial could be associated to a mechanism that impacts in a similar manner most bacterial species found in this biofilm. Previous studies suggested that the membrane composition, especially in gram-negative bacteria, as well as bacterial shape could constitute a criteria of resistance to GBMs (Kang et al., 2009; Akhavan and Ghaderi, 2010; Pulingam et al., 2019; Sengupta et al., 2019). Despite that the four OTUs benefiting from exposure to high GO concentrations are Gram-negative bacteria, it is more likely that their metabolic capacities are involved in the greater tolerance to GO. Indeed, it was recently reported that bacteria from the genus *Acidovorax* sp. were tolerant to GO concentrations up to 95 mg.L<sup>-1</sup> in granulated sludge treating wastewater (Kedves et al., 2020). This genus is also well-known to be able to degrade organic matter in wastewater treatment plants (Schulze et al., 1999) as well as aromatic compounds like phenanthrene (Singleton et al., 2018) or biphenyl (Ohtsubo et al., 2012). Similarly, *Silanimonas* spp. are categorized as benzene-degrading species (Mosmeri et al., 2019). Thus, we can hypothesize that these graphene-tolerant bacteria benefited from the presence of GBMs in the media (i) by outcompeting other less tolerant species and (ii) because they could be able to degrade or modify the GO structure.

According to the literature, bactericidal activities of GO and rGO toward planktonic bacteria indicated generally stronger bactericidal effects of GO compared to rGO as observed in our study (Han et al., 2019). However, results concerning antibacterial effects toward bacterial biofilms are more contradictory. Indeed, strong bactericidal effects of GO were previously observed like in our study (Mejías Carpio et al., 2012; Yadav et al., 2017; Giulio et al., 2018; Pandit et al., 2018; Song et al., 2018) while others indicated that GO enhanced biofilm formation and that



rGO exerted strong inhibitory effects (Ruiz et al., 2011; Guo et al., 2017). The interstudy discrepancies may be associated to several causes influencing the biological responses. Among the previously cited studies, when available, the characterization data indicate a wide variability within the range of oxygen content of the tested GO (from 27.8 to over 36 atomic %), with different distribution of the types of oxygen-containing functions. In addition, depending on the method applied, the reduction of these materials lead to the production of a wide variety of rGO. This underline the need to provide detailed characterization data and the use of a classification framework to facilitate interstudy comparisons (Wick et al., 2014). Among other possible causes, it was indicated that the effects of GBMs may vary depending on the medium composition and/or on the biofilm maturity (Hui et al., 2014; Guo et al., 2017; Fallatah et al., 2019). The results obtained in our study are in line with the latter assumption as the  $IC_{50}$  values increased between  $T_{48h}$  and  $T_{144h}$ , indicating that the effects of GO on bacterial growth were mitigated over time with biofilm maturation. This suggests that bacterial growth was delayed by GO exposure and that bacterial communities were recovering. However, after 144 h of exposure, the presence of GBMs in the media resulted in bacterial communities with diverging community structure trajectories compared to the control group. Further research would be needed to determine if bacterial communities are able to fully recover and to assess the time duration necessary for full recovery.

In addition to the effects on bacterial growth and diversity, exposure to GBMs was shown to influence microbial activities and could potentially lead to disturbances of carbon or nitrogen cycles (Zhou et al., 2019; Yilihamu et al., 2020). For example, previous studies indicated that exposure to GO or rGO could enhance the anaerobic ammonium oxidation activity that is involved in nitrogen removal in ecosystems (Wang et al., 2013; Yin et al., 2015; Tomaszewski et al., 2019). Extracellular enzymatic activities involved in carbon cycling were also shown to be lowered by short term exposure to GO (Chung et al., 2015). The results obtained in our study using Biolog Ecoplates suggested that the effects of GBMs exposure on the community level physiological profiles were transitory. Indeed, the activity levels of the microbial communities were similar to the control group in the different tested conditions after 144 h of exposure. However, this method does not allow to determine if the increased activity is associated to an increase of intra- or extracellular metabolism. The recovery of carbon-related metabolic activities despite the changes occurring in microbial community composition could be explained by functional redundancy between the species composing the biofilm. Further experiment using other omics tools would be needed to examine the metabolic pathways that are influenced by GBMs exposure and to determine if the metabolism of compounds involved in algae-bacteria mutualistic interactions are modified (Cooper and Smith, 2015).

## Consequences of the Diatom-Bacteria Interactions on the Response to GBMs Exposure

In the case of mixed-species biofilms containing phototropic microorganisms like diatoms as in our study case, the EPS

produced can be used by heterotrophic bacteria as carbon and energy sources (Mühlenbruch et al., 2018). In return, bacteria may benefit diatoms by providing sources of nutrients such as vitamins or nitrogen but are also able to reduce algal oxidative stress through the production of enzymes such as catalase (Hünken et al., 2008; Amin et al., 2012; Natrah et al., 2014). Diatom-associated microbiota from environmental samples was described to mainly belong to the phylum Proteobacteria and Bacteroidota (ex phylum Bacteroidetes) that are involved in EPS degradations (Schäfer et al., 2002; Amin et al., 2012; Bohórquez et al., 2017). Thus, the composition of the bacterial compartment in the biofilm of our study is consistent with the data from the literature. The heterotrophic bacteria remineralize the organic matter produced by the diatom, ensuring an efficient nutrient cycling (Christie-Oleza et al., 2017). The functioning of biofilms relies on this mutual benefit between the algae and the bacterial consortium. In the present study, diatom and bacteria growth were not correlated across our experimental conditions, demonstrating an interplay between multiple/complex interactions and GBMs direct effects.

It has been previously shown that the exposure to carbon-based nanomaterials such as carbon nanotubes and FLG increased the EPS excretion by *N. palea* (Verneuil et al., 2015; Garacci et al., 2017). This mechanism was suggested to constitute a strategy allowing toxicity mitigation for the algae. However, this could have several consequences for the bacterial compartment. Indeed, the embedment of GBMs into the biofilm EPS could increase contacts with bacteria and favor membrane impairments (Dizaj et al., 2015), which could explain the strong bacterial growth inhibition that we observed in presence of GO. The differential effects observed between GO and rGO on bacterial growth might be associated to the oxidation level of the materials. Indeed, the GBMs were shown to be able to interact with natural organic matter including polysaccharides (Chowdhury et al., 2014). As these interactions depend on the nature of oxygen-containing functional groups (Saya et al., 2021), the interaction dynamics between EPS and GO or rGO could be different, influencing the contact with bacterial cells embed in EPS. In addition to the increase in EPS excretion, the composition and the quality of the EPS produced by the diatoms could be modified by the presence of GBMs. This was previously observed after exposure of bacteria or algae to metallic nanoparticles (Hou et al., 2015, 2017; You et al., 2015; Chen et al., 2019). Moreover, it was suggested that the energy balance between growth and EPS production could be modified following exposure to nanoparticles that is likely to occur in the case of the growth stimulation observed in our study (Taylor et al., 2016). As it was indicated that the EPS composition could affect the bacterial communities in biofilms (Haynes et al., 2007; Bohórquez et al., 2017), we can hypothesize that the changes observed in the bacterial communities could be associated to indirect effects associated to modifications of the EPS quantity and quality.

As discussed in paragraph “Consequences of the GBMs Exposure on the Algal Compartment,” the growth stimulation observed in the diatom is more likely to be due to indirect effects. We can hypothesize that the overproduction of EPS associated to the

presence of GBMs might benefit *in fine* to the diatoms through the increase of metabolite quantities produced by bacterial activity. In addition, the results obtained from the community level physiological profiles indicated an activation of heterotrophic metabolism of the biofilm following short term exposure to GO. This metabolic increase allowed to compensate the loss of activity that can be expected due to the bacterial growth inhibition measured in presence of GO. Indeed, considering the AWCD values for the whole biofilm (data not shown) instead of AWCD per bacterial cell as previously presented, the overall carbon-related metabolic activities are maintained at the level of the control group until 1 mg.L<sup>-1</sup> and a slight decrease is noticed at 10 mg.L<sup>-1</sup> of GO. This should allow to maintain a baseline carbon and nutrient cycling between the algae and the bacteria.

## CONCLUSION

In this study, we observed that the biological responses of mixed microbial communities facing exposure to GBMs were complex and contradictory to the results of single-species experiments found in the literature. Here and according to the obtained data, we suggest that the biofilm responses were mainly associated to indirect effects initiated by the overproduction of EPS by the diatom. This potentially increased the amount of carbon available for bacterial metabolism and further benefit to the diatom. However, the oxidized form of graphene was shown to strongly impact bacterial biomass. The activities of carbon sources utilization were maintained in most conditions except at 10 mg.L<sup>-1</sup> of GO that is unlikely to occur under a scenario of chronic release into the environment. However, changes associated to the diatom physiology and changes in bacterial community composition might lead to modifications of the biofilm biochemical properties and potentially affect higher trophic level organisms feeding on it. Thus, future research on the environmental risk associated to GBMs should increase environmental relevance of the bioassays.

## REFERENCES

- Ahmed, F., and Rodrigues, D. F. (2013). Investigation of acute effects of graphene oxide on wastewater microbial community: a case study. *J. Hazard. Mater.* 256–257, 33–39. doi: 10.1016/j.jhazmat.2013.03.064
- Akhavan, O., and Ghaderi, E. (2010). Toxicity of graphene and graphene oxide nanowalls against bacteria. *ACS Nano* 4, 5731–5736. doi: 10.1021/nn101390x
- Amin, S. A., Parker, M. S., and Armbrust, E. V. (2012). Interactions between diatoms and bacteria. *Microbiol. Mol. Biol. Rev.* 76, 667–684. doi: 10.1128/MMBR.00007-12
- Avant, B., Bouchard, D., Chang, X., Hsieh, H.-S., Acrey, B., Han, Y., et al. (2019). Environmental fate of multiwalled carbon nanotubes and graphene oxide across different aquatic ecosystems. *NanoImpact* 13, 1–12. doi: 10.1016/j.impact.2018.11.001
- Bohórquez, J., McGenity, T. J., Papaspyrou, S., García-Robledo, E., Corzo, A., and Underwood, G. J. C. (2017). Different types of diatom-derived extracellular polymeric substances drive changes in heterotrophic bacterial communities from intertidal sediments. *Front. Microbiol.* 8:245. doi: 10.3389/fmicb.2017.00245
- Cacaci, M., Martini, C., Guarino, C., Torelli, R., Bugli, F., and Sanguinetti, M. (2020). Graphene oxide coatings as tools to prevent microbial biofilm

## DATA AVAILABILITY STATEMENT

The original contributions presented in the study are publicly available. These data can be found in NCBI under accession number PRJNA674395.

## AUTHOR CONTRIBUTIONS

LE: writing original draft – investigation – formal analysis. PB: formal analysis – investigation. FM and LG: project administration – funding acquisition. JS: resources – methodology. EF: formal analysis – funding acquisition – review and editing. EP: supervision – review and editing. MB: writing, review and editing – methodology – supervision. All authors contributed to the article and approved the submitted version.

## FUNDING

The authors thank the European Union's Horizon 2020 research and innovation programme under grant agreement no 785219.

## ACKNOWLEDGMENTS

We thank the Genotoul bioinformatics platform Toulouse Midi-Pyrenees and Sigenae group for providing computing and storage resources through Galaxy.

## SUPPLEMENTARY MATERIAL

The Supplementary Material for this article can be found online at: <https://www.frontiersin.org/articles/10.3389/fmicb.2021.623853/full#supplementary-material>

formation on medical device. *Adv. Exp. Med. Biol.* 1282, 21–35. doi: 10.1007/5584\_2019\_434

- Cao, G., Yan, J., Ning, X., Zhang, Q., Wu, Q., Bi, L., et al. (2021). Antibacterial and antibiofilm properties of graphene and its derivatives. *Colloids Surf. B: Biointerfaces* 200:111588. doi: 10.1016/j.colsurfb.2021.111588
- Castro, V. L., Clemente, Z., Jonsson, C., Silva, M., Vallim, J. H., de Medeiros, A. M. Z., et al. (2018). Nanoecotoxicity assessment of graphene oxide and its relationship with humic acid: nanoecotoxicity of graphene oxide and humic acid. *Environ. Toxicol. Chem.* 37, 1998–2012. doi: 10.1002/etc.4145
- Cheirsilp, B., and Torpee, S. (2012). Enhanced growth and lipid production of microalgae under mixotrophic culture condition: effect of light intensity, glucose concentration and fed-batch cultivation. *Bioresour. Technol.* 110, 510–516. doi: 10.1016/j.biortech.2012.01.125
- Chen, F., Xiao, Z., Yue, L., Wang, J., Feng, Y., Zhu, X., et al. (2019). Algae response to engineered nanoparticles: current understanding, mechanisms and implications. *Environ. Sci. Nano* 6, 1026–1042. doi: 10.1039/C8EN01368C
- Chowdhury, I., Duch, M. C., Mansukhani, N. D., Hersam, M. C., and Bouchard, D. (2014). Interactions of graphene oxide nanomaterials with natural organic matter and metal oxide surfaces. *Environ. Sci. Technol.* 48, 9382–9390. doi: 10.1021/es5020828
- Christie-Olea, J. A., Sousoni, D., Lloyd, M., Armengaud, J., and Scanlan, D. J. (2017). Nutrient recycling facilitates long-term stability of marine microbial

- phototroph-heterotroph interactions. *Nat. Microbiol.* 2, 1–10. doi: 10.1038/nmicrobiol.2017.100
- Chung, H., Kim, M. J., Ko, K., Kim, J. H., Kwon, H., Hong, I., et al. (2015). Effects of graphene oxides on soil enzyme activity and microbial biomass. *Sci. Total Environ.* 514, 307–313. doi: 10.1016/j.scitotenv.2015.01.077
- Clemente, Z., Silva, G. H., de Souza Nunes, M. C., Martinez, D. S. T., Maurer-Morelli, C. V., Thomaz, A. A., et al. (2019). Exploring the mechanisms of graphene oxide behavioral and morphological changes in zebrafish. *Environ. Sci. Pollut. Res.* 26, 30508–30523. doi: 10.1007/s11356-019-05870-z
- Cooper, M. B., and Smith, A. G. (2015). Exploring mutualistic interactions between microalgae and bacteria in the omics age. *Curr. Opin. Plant Biol.* 26, 147–153. doi: 10.1016/j.pbi.2015.07.003
- Dasari Shareena, T. P., McShan, D., Dasmahapatra, A. K., and Tchounwou, P. B. (2018). A review on graphene-based nanomaterials in biomedical applications and risks in environment and health. *Nano-Micro Lett.* 10:53. doi: 10.1007/s40820-018-0206-4
- da Silva Ferreira, V., and Sant'Anna, C. (2017). Impact of culture conditions on the chlorophyll content of microalgae for biotechnological applications. *World J. Microbiol. Biotechnol.* 33:20. doi: 10.1007/s11274-016-2181-6
- Dizaj, S. M., Mennati, A., Jafari, S., Khezri, K., and Adibkia, K. (2015). Antimicrobial activity of carbon-based nanoparticles. *Adv. Pharm. Bull.* 5, 19–23. doi: 10.5681/apb.2015.003
- Du, J., Hu, X., and Zhou, Q. (2015). Graphene oxide regulates the bacterial community and exhibits property changes in soil. *RSC Adv.* 5, 27009–27017. doi: 10.1039/C5RA01045D
- Du, S., Zhang, P., Zhang, R., Lu, Q., Liu, L., Bao, X., et al. (2016). Reduced graphene oxide induces cytotoxicity and inhibits photosynthetic performance of the green alga *Scenedesmus obliquus*. *Chemosphere* 164, 499–507. doi: 10.1016/j.chemosphere.2016.08.138
- Escudé, F., Auer, L., Bernard, M., Mariadassou, M., Cauquil, L., Vidal, K., et al. (2018). FROGS: find, rapidly, OTUs with galaxy solution. *Bioinformatics* 34, 1287–1294. doi: 10.1093/bioinformatics/btx791
- Evariste, L., Lagier, L., Gonzalez, P., Mottier, A., Mouchet, F., Cadarsi, S., et al. (2019). Thermal reduction of graphene oxide mitigates its in vivo genotoxicity toward *Xenopus laevis* tadpoles. *Nano* 9:584. doi: 10.3390/nano9040584
- Evariste, L., Mottier, A., Lagier, L., Cadarsi, S., Barret, M., Sarrieu, C., et al. (2020). Assessment of graphene oxide ecotoxicity at several trophic levels using aquatic microcosms. *Carbon* 156, 261–271. doi: 10.1016/j.carbon.2019.09.051
- Fadeel, B., Bussy, C., Merino, S., Vázquez, E., Flahaut, E., Mouchet, F., et al. (2018). Safety assessment of graphene-based materials: focus on human health and the environment. *ACS Nano* 12, 10582–10620. doi: 10.1021/acsnano.8b04758
- Fallatah, H., Elhaneid, M., Ali-Boucetta, H., Overton, T. W., El Kadri, H., and Gkatzionis, K. (2019). Antibacterial effect of graphene oxide (GO) nanoparticles against *Pseudomonas putida* biofilm of variable age. *Environ. Sci. Pollut. Res.* 26, 25057–25070. doi: 10.1007/s11356-019-05688-9
- Flemming, H.-C., Wingender, J., Szewzyk, U., Steinberg, P., Rice, S. A., and Kjelleberg, S. (2016). Biofilms: an emergent form of bacterial life. *Nat. Rev. Microbiol.* 14, 563–575. doi: 10.1038/nrmicro.2016.94
- Forstner, C., Orton, T. G., Skarshewski, A., Wang, P., Kopittke, P. M., and Dennis, P. G. (2019). Effects of graphene oxide and graphite on soil bacterial and fungal diversity. *bioRxiv* 530485. doi: 10.1101/530485
- Garacci, M., Barret, M., Folgoas, C., Flahaut, E., Chimowa, G., Bertucci, A., et al. (2019). Transcriptomic response of the benthic freshwater diatom *Nitzschia palea* exposed to few layer graphene. *Environ. Sci. Nano* 6, 1363–1381. doi: 10.1039/C8EN00987B
- Garacci, M., Barret, M., Mouchet, F., Sarrieu, C., Lonchambon, P., Flahaut, E., et al. (2017). Few layer graphene sticking by biofilm of freshwater diatom *Nitzschia palea* as a mitigation to its ecotoxicity. *Carbon* 113, 139–150. doi: 10.1016/j.carbon.2016.11.033
- Giulio, M. D., Zappacosta, R., Lodovico, S. D., Campli, E. D., Siani, G., Fontana, A., et al. (2018). Antimicrobial and antibiofilm efficacy of graphene oxide against chronic wound microorganisms. *Antimicrob. Agents Chemother.* 62, e00547–e00518. doi: 10.1128/AAC.00547-18
- González, A. G., Mombo, S., Leflaive, J., Lamy, A., Pokrovsky, O. S., and Rols, J.-L. (2015). Silver nanoparticles impact phototrophic biofilm communities to a considerably higher degree than ionic silver. *Environ. Sci. Pollut. Res.* 22, 8412–8424. doi: 10.1007/s11356-014-3978-1
- Goodwin, D. G., Adeleye, A. S., Sung, L., Ho, K. T., Burgess, R. M., and Petersen, E. J. (2018). Detection and quantification of Graphene-family nanomaterials in the environment. *Environ. Sci. Technol.* 52, 4491–4513. doi: 10.1021/acs.est.7b04938
- Guo, C., Wang, Y., Luo, Y., Chen, X., Lin, Y., and Liu, X. (2018). Effect of graphene oxide on the bioactivities of nitrifying and denitrifying bacteria in aerobic granular sludge. *Ecotoxicol. Environ. Saf.* 156, 287–293. doi: 10.1016/j.ecoenv.2018.03.036
- Guo, Z., Xie, C., Zhang, P., Zhang, J., Wang, G., He, X., et al. (2017). Toxicity and transformation of graphene oxide and reduced graphene oxide in bacteria biofilm. *Sci. Total Environ.* 580, 1300–1308. doi: 10.1016/j.scitotenv.2016.12.093
- Han, W., Wu, Z., Li, Y., and Wang, Y. (2019). Graphene family nanomaterials (GFNs)—promising materials for antimicrobial coating and film: a review. *Chem. Eng. J.* 358, 1022–1037. doi: 10.1016/j.cej.2018.10.106
- Haynes, K., Hofmann, T. A., Smith, C. J., Ball, A. S., Underwood, G. J. C., and Osborn, A. M. (2007). Diatom-derived carbohydrates as factors affecting bacterial community composition in estuarine sediments. *Appl. Environ. Microbiol.* 73, 6112–6124. doi: 10.1128/AEM.00551-07
- Hazeem, L. J., Bououdina, M., Dewailly, E., Slomianny, C., Barras, A., Coffinier, Y., et al. (2017). Toxicity effect of graphene oxide on growth and photosynthetic pigment of the marine alga *Picochlorum* sp. during different growth stages. *Environ. Sci. Pollut. Res. Int.* 24, 4144–4152. doi: 10.1007/s11356-016-8174-z
- Hou, J., Miao, L., Wang, C., Wang, P., Ao, Y., and Lv, B. (2015). Effect of CuO nanoparticles on the production and composition of extracellular polymeric substances and physicochemical stability of activated sludge flocs. *Bioresour. Technol.* 176, 65–70. doi: 10.1016/j.biortech.2014.11.020
- Hou, J., Yang, Y., Wang, P., Wang, C., Miao, L., Wang, X., et al. (2017). Effects of CeO<sub>2</sub>, CuO, and ZnO nanoparticles on physiological features of *Microcystis aeruginosa* and the production and composition of extracellular polymeric substances. *Environ. Sci. Pollut. Res.* 24, 226–235. doi: 10.1007/s11356-016-7387-5
- Hu, X., Gao, Y., and Fang, Z. (2016). Integrating metabolic analysis with biological endpoints provides insight into nanotoxicological mechanisms of graphene oxide: from effect onset to cessation. *Carbon* 109, 65–73. doi: 10.1016/j.carbon.2016.07.068
- Hui, L., Piao, J.-G., Auletta, J., Hu, K., Zhu, Y., Meyer, T., et al. (2014). Availability of the basal planes of graphene oxide determines whether it is antibacterial. *ACS Appl. Mater. Interfaces* 6, 13183–13190. doi: 10.1021/am503070z
- Hummers, W. S. Jr., and Offeman, R. E. (1958). Preparation of graphitic oxide. *J. Am. Chem. Soc.* 80, 1339–1339. doi: 10.1021/ja01539a017
- Hünken, M., Harder, J., and Kirst, G. O. (2008). Epiphytic bacteria on the Antarctic ice diatom *Amphiprora kufferathii* Manguin cleave hydrogen peroxide produced during algal photosynthesis. *Plant Biol. (Stuttg.)* 10, 519–526. doi: 10.1111/j.1438-8677.2008.00040.x
- Ikuma, K., Decho, A. W., and Lau, B. L. T. (2015). When nanoparticles meet biofilms—interactions guiding the environmental fate and accumulation of nanoparticles. *Front. Microbiol.* 6:591. doi: 10.3389/fmicb.2015.00591
- Jastrzębska, A. M., and Olszyna, A. R. (2015). The ecotoxicity of graphene family materials: current status, knowledge gaps and future needs. *J. Nanopart. Res.* 17:40. doi: 10.1007/s11051-014-2817-0
- Ji, H., Sun, H., and Qu, X. (2016). Antibacterial applications of graphene-based nanomaterials: recent achievements and challenges. *Adv. Drug Deliv. Rev.* 105, 176–189. doi: 10.1016/j.addr.2016.04.009
- Kang, S., Mauter, M. S., and Elimelech, M. (2009). Microbial cytotoxicity of carbon-based nanomaterials: implications for river water and wastewater effluent. *Environ. Sci. Technol.* 43, 2648–2653. doi: 10.1021/es8031506
- Kedves, A., Santa, L., Balázs, M., Kesseri, P., Kiss, I., Rónavári, A., et al. (2020). Chronic responses of aerobic granules to the presence of graphene oxide in sequencing batch reactors. *J. Hazard. Mater.* 389:121905. doi: 10.1016/j.jhazmat.2019.121905
- Khanra, A., Sangam, S., Shakeel, A., Suhag, D., Mistry, S., Rai, M. P., et al. (2018). Sustainable growth and lipid production from *Chlorella pyrenoidosa* using N-doped carbon nanosheets: unravelling the role of graphitic nitrogen. *ACS Sustain. Chem. Eng.* 6, 774–780. doi: 10.1021/acssuschemeng.7b03103
- Kumar, P., Huo, P., Zhang, R., and Liu, B. (2019). Antibacterial properties of graphene-based nanomaterials. *Nano* 9:737. doi: 10.3390/nano9050737
- Lavin-Lopez, M. P., Paton-Carrero, A., Sanchez-Silva, L., Valverde, J. L., and Romero, A. (2017). Influence of the reduction strategy in the synthesis of reduced graphene oxide. *Adv. Powder Technol.* 28, 3195–3203. doi: 10.1016/j.appt.2017.09.032



- Lawrence, J. R., Waiser, M. J., Swerhone, G. D. W., Roy, J., Tumber, V., Paule, A., et al. (2016). Effects of fullerene (C60), multi-wall carbon nanotubes (MWCNT), single wall carbon nanotubes (SWCNT) and hydroxyl and carboxyl modified single wall carbon nanotubes on riverine microbial communities. *Environ. Sci. Pollut. Res.* 23, 10090–10102. doi: 10.1007/s11356-016-6244-x
- Lin, L., Peng, H., and Liu, Z. (2019). Synthesis challenges for graphene industry. *Nat. Mater.* 18, 520–524. doi: 10.1038/s41563-019-0341-4
- Liu, Y., Shi, L., Su, L., van der Mei, H. C., Jutte, P. C., Ren, Y., et al. (2019). Nanotechnology-based antimicrobials and delivery systems for biofilm-infection control. *Chem. Soc. Rev.* 48, 428–446. doi: 10.1039/C7CS00807D
- Lobato, B., Merino, C., Barranco, V., and Centeno, T. A. (2016). Large-scale conversion of helical-ribbon carbon nanofibers to a variety of graphene-related materials. *RSC Adv.* 6, 57514–57520. doi: 10.1039/C6RA08865A
- Love, M. I., Huber, W., and Anders, S. (2014). Moderated estimation of fold change and dispersion for RNA-seq data with DESeq2. *Genome Biol.* 15:550. doi: 10.1186/s13059-014-0550-8
- Lv, X., Yang, Y., Tao, Y., Jiang, Y., Chen, B., Zhu, X., et al. (2018). A mechanism study on toxicity of graphene oxide to *Daphnia magna*: direct link between bioaccumulation and oxidative stress. *Environ. Pollut.* 234, 953–959. doi: 10.1016/j.envpol.2017.12.034
- Mahé, F., Rognes, T., Quince, C., de Vargas, C., and Dunthorn, M. (2014). Swarm: robust and fast clustering method for amplicon-based studies. *PeerJ* 2:e593. doi: 10.7717/peerj.593
- Malina, T., Maršáková, E., Holá, K., Tuček, J., Scheibe, M., Zbořil, R., et al. (2019). Toxicity of graphene oxide against algae and cyanobacteria: nanoblade-morphology-induced mechanical injury and self-protection mechanism. *Carbon* 155, 386–396. doi: 10.1016/j.carbon.2019.08.086
- McMurdie, P. J., and Holmes, S. (2013). Phyloseq: an R package for reproducible interactive analysis and graphics of microbiome census data. *PLoS One* 8:e61217. doi: 10.1371/journal.pone.0061217
- Mejias Carpio, I. E., Santos, C. M., Wei, X., and Rodrigues, D. F. (2012). Toxicity of a polymer-graphene oxide composite against bacterial planktonic cells, biofilms, and mammalian cells. *Nanoscale* 4, 4746–4756. doi: 10.1039/c2nr30774j
- Miao, L., Wang, P., Hou, J., Yao, Y., Liu, Z., and Liu, S. (2019). Low concentrations of copper oxide nanoparticles alter microbial community structure and function of sediment biofilms. *Sci. Total Environ.* 653, 705–713. doi: 10.1016/j.scitotenv.2018.10.354
- Mohan, V. B., Lau, K., Hui, D., and Bhattacharyya, D. (2018). Graphene-based materials and their composites: a review on production, applications and product limitations. *Compos. Part B Eng.* 142, 200–220. doi: 10.1016/j.compositesb.2018.01.013
- Montagner, A., Bosi, S., Tenori, E., Bidussi, M., Alshatwi, A. A., Tretiach, M., et al. (2016). Ecotoxicological effects of graphene-based materials. *2D Mater.* 4:012001. doi: 10.1088/2053-1583/4/1/012001
- Mosmeri, H., Gholami, F., Shavandi, M., Dastgheib, S. M. M., and Alaie, E. (2019). Bioremediation of benzene-contaminated groundwater by calcium peroxide (CaO<sub>2</sub>) nanoparticles: continuous-flow and biodiversity studies. *J. Hazard. Mater.* 371, 183–190. doi: 10.1016/j.jhazmat.2019.02.071
- Mottier, A., Mouchet, F., Pinelli, É., Gauthier, L., and Flahaut, E. (2017). Environmental impact of engineered carbon nanoparticles: from releases to effects on the aquatic biota. *Curr. Opin. Biotechnol.* 46, 1–6. doi: 10.1016/j.copbio.2016.11.024
- Mühlenbruch, M., Grossart, H.-P., Eigemann, F., and Voss, M. (2018). Mini-review: phytoplankton-derived polysaccharides in the marine environment and their interactions with heterotrophic bacteria. *Environ. Microbiol.* 20, 2671–2685. doi: 10.1111/1462-2920.14302
- Nag, A., Mitra, A., and Mukhopadhyay, S. C. (2018). Graphene and its sensor-based applications: a review. *Sensors Actuators A Phys.* 270, 177–194. doi: 10.1016/j.sna.2017.12.028
- Natrah, F. M. I., Bossier, P., Sorgeloos, P., Yusoff, F. M., and Defoirdt, T. (2014). Significance of microalgal–bacterial interactions for aquaculture. *Rev. Aquac.* 6, 48–61. doi: 10.1111/raq.12024
- Nogueira, P. F. M., Nakabayashi, D., and Zucolotto, V. (2015). The effects of graphene oxide on green algae *Raphidocelis subcapitata*. *Aquat. Toxicol.* 166, 29–35. doi: 10.1016/j.aquatox.2015.07.001
- Ohtsubo, Y., Maruyama, E., Mitsui, H., Nagata, Y., and Tsuda, M. (2012). Complete genome sequence of *Acidovorax* sp. strain KKS102, a polychlorinated-biphenyl degrader. *J. Bacteriol.* 194, 6970–6971. doi: 10.1128/JB.01848-12
- Oksanen, J., Blanchet, F. G., Kindt, R., Legendre, P., Minchin, P. R., O'hara, R. B., et al. (2015). Package 'vegan'. Community Ecol. Package Version 2.
- Ouyang, S., Hu, X., and Zhou, Q. (2015). Envelopment–internalization synergistic effects and metabolic mechanisms of graphene oxide on single-cell *Chlorella vulgaris* are dependent on the nanomaterial particle size. *ACS Appl. Mater. Interfaces* 7, 18104–18112. doi: 10.1021/acsami.5b05328
- Paerl, H. W., and Pinckney, J. L. (1996). A mini-review of microbial consortia: their roles in aquatic production and biogeochemical cycling. *Microb. Ecol.* 31, 225–247. doi: 10.1007/BF00171569
- Paital, B., Guru, D., Mohapatra, P., Panda, B., Parida, N., Rath, S., et al. (2019). Ecotoxic impact assessment of graphene oxide on lipid peroxidation at mitochondrial level and redox modulation in fresh water fish *Anabas testudineus*. *Chemosphere* 224, 796–804. doi: 10.1016/j.chemosphere.2019.02.156
- Pandit, S., Cao, Z., Mokkapati, V. R. S. S., Celauro, E., Yurgens, A., Lovmar, M., et al. (2018). Vertically aligned graphene coating is bactericidal and prevents the formation of bacterial biofilms. *Adv. Mater. Interfaces* 5:1701331. doi: 10.1002/admi.201701331
- Perreault, F., Fonseca de Faria, A., and Elimelech, M. (2015). Environmental applications of graphene-based nanomaterials. *Chem. Soc. Rev.* 44, 5861–5896. doi: 10.1039/C5CS00021A
- Pulingam, T., Thong, K. L., Ali, M. E., Appaturi, J. N., Dinshaw, I. J., Ong, Z. Y., et al. (2019). Graphene oxide exhibits differential mechanistic action towards gram-positive and gram-negative bacteria. *Colloids Surf. B: Biointerfaces* 181, 6–15. doi: 10.1016/j.colsurfb.2019.05.023
- Quast, C., Pruesse, E., Yilmaz, P., Gerken, J., Schweer, T., Yarza, P., et al. (2012). The SILVA ribosomal RNA gene database project: improved data processing and web-based tools. *Nucleic Acids Res.* 41, D590–D596. doi: 10.1093/nar/gks1219
- Rowley-Neale, S. J., Randviir, E. P., Abo Dena, A. S., and Banks, C. E. (2018). An overview of recent applications of reduced graphene oxide as a basis of electroanalytical sensing platforms. *Appl. Mater. Today* 10, 218–226. doi: 10.1016/j.apmt.2017.11.010
- Ruiz, O. N., Fernando, K. A. S., Wang, B., Brown, N. A., Luo, P. G., McNamara, N. D., et al. (2011). Graphene oxide: a nonspecific enhancer of cellular growth. *ACS Nano* 5, 8100–8107. doi: 10.1021/nn202699t
- Saxena, P., Sangela, V., Ranjan, S., Dutta, V., Dasgupta, N., Phulwaria, M., et al. (2020). Aquatic nanotoxicology: impact of carbon nanomaterials on algal flora. *Energy Ecol. Environ.* 5, 240–252. doi: 10.1007/s40974-020-00151-9
- Saya, L., Gautam, D., Malik, V., Singh, W. R., and Hooda, S. (2021). Natural polysaccharide based graphene oxide nanocomposites for removal of dyes from wastewater: a review. *J. Chem. Eng. Data* 66, 11–37. doi: 10.1021/acs.jced.0c00743
- Scala, S., and Bowler, C. (2001). Molecular insights into the novel aspects of diatom biology. *Cell. Mol. Life Sci.* 58, 1666–1673. doi: 10.1007/PL00000804
- Schäfer, H., Abbas, B., Witte, H., and Muyzer, G. (2002). Genetic diversity of “satellite” bacteria present in cultures of marine diatoms. *FEMS Microbiol. Ecol.* 42, 25–35. doi: 10.1111/j.1574-6941.2002.tb00992.x
- Schulze, R., Spring, S., Amann, R., Huber, I., Ludwig, W., Schleifer, K.-H., et al. (1999). Genotypic diversity of *Acidovorax* strains isolated from activated sludge and description of *Acidovorax defluvii* sp. nov. *Syst. Appl. Microbiol.* 22, 205–214. doi: 10.1016/S0723-2020(99)80067-8
- Sengupta, I., Bhattacharya, P., Talukdar, M., Neogi, S., Pal, S. K., and Chakraborty, S. (2019). Bactericidal effect of graphene oxide and reduced graphene oxide: influence of shape of bacteria. *Colloid Interface Sci. Commun.* 28, 60–68. doi: 10.1016/j.colcom.2018.12.001
- Singleton, D. R., Lee, J., Dickey, A. N., Stroud, A., Scholl, E. H., Wright, F. A., et al. (2018). Polyphasic characterization of four soil-derived phenanthrene-degrading *Acidovorax* strains and proposal of *Acidovorax carolinensis* sp. nov. *Syst. Appl. Microbiol.* 41, 460–472. doi: 10.1016/j.syapm.2018.06.001
- Smith, A. T., LaChance, A. M., Zeng, S., Liu, B., and Sun, L. (2019). Synthesis, properties, and applications of graphene oxide/reduced graphene oxide and their nanocomposites. *Nano Mater. Sci.* 1, 31–47. doi: 10.1016/j.nanoms.2019.02.004
- Song, C., Yang, C.-M., Sun, X.-F., Xia, P.-F., Qin, J., Guo, B.-B., et al. (2018). Influences of graphene oxide on biofilm formation of gram-negative and gram-positive bacteria. *Environ. Sci. Pollut. Res. Int.* 25, 2853–2860. doi: 10.1007/s11356-017-0616-8
- Sun, T. Y., Bornhöft, N. A., Hungerbühler, K., and Nowack, B. (2016). Dynamic probabilistic modeling of environmental emissions of engineered nanomaterials. *Environ. Sci. Technol.* 50, 4701–4711. doi: 10.1021/acs.est.5b05828
- Tang, Y., Tian, J., Li, S., Xue, C., Xue, Z., Yin, D., et al. (2015). Combined effects of graphene oxide and cd on the photosynthetic capacity and survival



- of *Microcystis aeruginosa*. *Sci. Total Environ.* 532, 154–161. doi: 10.1016/j.scitotenv.2015.05.081
- Tarcan, R., Todor-Boer, O., Petrovai, I., Leordean, C., Astilean, S., and Botiz, I. (2020). Reduced graphene oxide today. *J. Mater. Chem. C* 8, 1198–1224. doi: 10.1039/C9TC04916A
- Tashan, H., Khosravi-Darani, K., Yazdian, F., Omid, M., Sheikhpour, M., Farahani, M., et al. (2019). Antibacterial properties of graphene based nanomaterials: an emphasis on molecular mechanisms, surface engineering and size of sheets. *Mini-Rev. Org. Chem.* 16, 159–172. doi: 10.2174/1570193X15666180712120309
- Taylor, C., Matzke, M., Kroll, A., Read, D. S., Svendsen, C., and Crossley, A. (2016). Toxic interactions of different silver forms with freshwater green algae and cyanobacteria and their effects on mechanistic endpoints and the production of extracellular polymeric substances. *Environ. Sci. Nano* 3, 396–408. doi: 10.1039/C5EN00183H
- Thamatrakoln, K., Korenovska, O., Niheu, A. K., and Bidle, K. D. (2012). Whole-genome expression analysis reveals a role for death-related genes in stress acclimation of the diatom *Thalassiosira pseudonana*. *Environ. Microbiol.* 14, 67–81. doi: 10.1111/j.1462-2920.2011.02468.x
- Tomaszewski, M., Cema, G., and Ziemińska-Buczyńska, A. (2019). Short-term effects of reduced graphene oxide on the anammox biomass activity at low temperatures. *Sci. Total Environ.* 646, 206–211. doi: 10.1016/j.scitotenv.2018.07.283
- Verneuil, L., Silvestre, J., Randrianjatovo, I., Marcato-Romain, C.-E., Girbal-Neuhausser, E., Mouchet, F., et al. (2015). Double walled carbon nanotubes promote the overproduction of extracellular protein-like polymers in *Nitzschia palea*: an adhesive response for an adaptive issue. *Carbon* 88, 113–125. doi: 10.1016/j.carbon.2015.02.053
- Villanova, V., Fortunato, A. E., Singh, D., Bo, D. D., Conte, M., Obata, T., et al. (2017). Investigating mixotrophic metabolism in the model diatom *Phaeodactylum tricornutum*. *Philos. Trans. R. Soc. B Biol. Sci.* 372:20160404. doi: 10.1098/rstb.2016.0404
- Wang, A., Pu, K., Dong, B., Liu, Y., Zhang, L., Zhang, Z., et al. (2013). Role of surface charge and oxidative stress in cytotoxicity and genotoxicity of graphene oxide towards human lung fibroblast cells: toxicity of graphene oxide to HLF cells. *J. Appl. Toxicol.* 33, 1156–1164. doi: 10.1002/jat.2877
- Wang, Y., and Qian, P.-Y. (2009). Conservative fragments in bacterial 16S rRNA genes and primer design for 16S ribosomal DNA amplicons in metagenomic studies. *PLoS One* 4:e7401. doi: 10.1371/journal.pone.0007401
- Weber, K. P., and Legge, R. L. (2009). One-dimensional metric for tracking bacterial community divergence using sole carbon source utilization patterns. *J. Microbiol. Methods* 79, 55–61. doi: 10.1016/j.mimet.2009.07.020
- Wick, P., Louw-Gaume, A. E., Kucki, M., Krug, H. F., Kostarelos, K., Fadeel, B., et al. (2014). Classification framework for graphene-based materials. *Angew. Chem. Int. Ed. Eng.* 53, 7714–7718. doi: 10.1002/anie.201403335
- Xiong, T., Yuan, X., Wang, H., Leng, L., Li, H., Wu, Z., et al. (2018). Implication of graphene oxide in Cd-contaminated soil: a case study of bacterial communities. *J. Environ. Manag.* 205, 99–106. doi: 10.1016/j.jenvman.2017.09.067
- Yadav, N., Dubey, A., Shukla, S., Saini, C. P., Gupta, G., Priyadarshini, R., et al. (2017). Graphene oxide-coated surface: inhibition of bacterial biofilm formation due to specific surface-interface interactions. *ACS Omega* 2, 3070–3082. doi: 10.1021/acsomega.7b00371
- Yilihamu, A., Ouyang, B., Ouyang, P., Bai, Y., Zhang, Q., Shi, M., et al. (2020). Interaction between graphene oxide and nitrogen-fixing bacterium *Azotobacter chroococcum*: transformation, toxicity and nitrogen fixation. *Carbon* 160, 5–13. doi: 10.1016/j.carbon.2020.01.014
- Yin, X., Qiao, S., Yu, C., Tian, T., and Zhou, J. (2015). Effects of reduced graphene oxide on the activities of anammox biomass and key enzymes. *Chem. Eng. J.* 276, 106–112. doi: 10.1016/j.cej.2015.04.073
- You, G., Hou, J., Xu, Y., Wang, C., Wang, P., Miao, L., et al. (2015). Effects of CeO<sub>2</sub> nanoparticles on production and physicochemical characteristics of extracellular polymeric substances in biofilms in sequencing batch biofilm reactor. *Bioresour. Technol.* 194, 91–98. doi: 10.1016/j.biortech.2015.07.006
- Yujie, S., Jian, L., Yu, J., Xu, S., Wenning, Y., Zhenghua, L., et al. (2020). Effect of graphene oxide on the ammonia removal and bacterial community in a simulated wastewater treatment process. *J. Environ. Eng.* 146:04020097. doi: 10.1061/(ASCE)EE.1943-7870.0001781
- Zhang, X., Zhou, Q., Zou, W., and Hu, X. (2017). Molecular mechanisms of developmental toxicity induced by graphene oxide at predicted environmental concentrations. *Environ. Sci. Technol.* 51, 7861–7871. doi: 10.1021/acs.est.7b01922
- Zhao, J., Cao, X., Wang, Z., Dai, Y., and Xing, B. (2017). Mechanistic understanding toward the toxicity of graphene-family materials to freshwater algae. *Water Res.* 111, 18–27. doi: 10.1016/j.watres.2016.12.037
- Zhao, J., Li, Y., Cao, X., Guo, C., Xu, L., Wang, Z., et al. (2019). Humic acid mitigated toxicity of graphene-family materials to algae through reducing oxidative stress and heteroaggregation. *Environ. Sci. Nano* 6, 1909–1920. doi: 10.1039/C9EN00067D
- Zhou, N., Zhao, Z., Wang, H., Chen, X., Wang, M., He, S., et al. (2019). The effects of graphene oxide on nitrification and N<sub>2</sub>O emission: dose and exposure time dependent. *Environ. Pollut.* 252, 960–966. doi: 10.1016/j.envpol.2019.06.009

**Conflict of Interest:** The authors declare that the research was conducted in the absence of any commercial or financial relationships that could be construed as a potential conflict of interest.

Copyright © 2021 Evariste, Braylé, Mouchet, Silvestre, Gauthier, Flahaut, Pinelli and Barret. This is an open-access article distributed under the terms of the Creative Commons Attribution License (CC BY). The use, distribution or reproduction in other forums is permitted, provided the original author(s) and the copyright owner(s) are credited and that the original publication in this journal is cited, in accordance with accepted academic practice. No use, distribution or reproduction is permitted which does not comply with these terms.



# Antibiotrophy: Key Function for Antibiotic-Resistant Bacteria to Colonize Soils—Case of Sulfamethazine-Degrading *Microbacterium* sp. C448

Loren Billet<sup>1,2\*</sup>, Stéphane Pesce<sup>2</sup>, Nadine Rouard<sup>1</sup>, Aymé Spor<sup>1</sup>, Laurianne Paris<sup>3</sup>, Martin Leremboure<sup>3</sup>, Arnaud Mounier<sup>1</sup>, Pascale Besse-Hoggan<sup>3</sup>, Fabrice Martin-Laurent<sup>1</sup> and Marion Devers-Lamrani<sup>1</sup>

## OPEN ACCESS

### Edited by:

Ales Lapanje,  
Institut Jožef Stefan (IJS), Slovenia

### Reviewed by:

Mariusz Cycoń,  
Medical University of Silesia, Poland  
Pratyosh Shukla,  
Banaras Hindu University, India

### \*Correspondence:

Loren Billet  
loren.billet@gmail.com

### Specialty section:

This article was submitted to  
Microbiotechnology,  
a section of the journal  
Frontiers in Microbiology

**Received:** 17 December 2020

**Accepted:** 22 February 2021

**Published:** 26 March 2021

### Citation:

Billet L, Pesce S, Rouard N,  
Spor A, Paris L, Leremboure M,  
Mounier A, Besse-Hoggan P,  
Martin-Laurent F and  
Devers-Lamrani M (2021)  
Antibiotrophy: Key Function  
for Antibiotic-Resistant Bacteria  
to Colonize Soils—Case  
of Sulfamethazine-Degrading  
*Microbacterium* sp. C448.  
Front. Microbiol. 12:643087.  
doi: 10.3389/fmicb.2021.643087

Chronic and repeated exposure of environmental bacterial communities to anthropogenic antibiotics have recently driven some antibiotic-resistant bacteria to acquire catabolic functions, enabling them to use antibiotics as nutritive sources (antibiotrophy). Antibiotrophy might confer a selective advantage facilitating the implantation and dispersion of antibiotrophs in contaminated environments. A microcosm experiment was conducted to test this hypothesis in an agroecosystem context. The sulfonamide-degrading and resistant bacterium *Microbacterium* sp. C448 was inoculated in four different soil types with and without added sulfamethazine and/or swine manure. After 1 month of incubation, *Microbacterium* sp. (and its antibiotrophic gene *sadA*) was detected only in the sulfamethazine-treated soils, suggesting a low competitiveness of the strain without antibiotic selection pressure. In the absence of manure and despite the presence of *Microbacterium* sp. C448, only one of the four sulfamethazine-treated soils exhibited mineralization capacities, which were low (inferior to  $5.5 \pm 0.3\%$ ). By contrast, manure addition significantly enhanced sulfamethazine mineralization in all the soil types (at least double, comprised between  $5.6 \pm 0.7\%$  and  $19.5 \pm 1.2\%$ ). These results, which confirm that the presence of functional genes does not necessarily ensure functionality, suggest that sulfamethazine does not necessarily confer a selective advantage on the degrading strain as a nutritional source. 16S rDNA sequencing analyses strongly suggest that sulfamethazine released trophic niches by biocidal action. Accordingly, manure-originating bacteria and/or *Microbacterium* sp. C448 could gain access to low-competition or competition-free ecological niches. However, simultaneous inputs of manure and of the strain could induce competition detrimental for *Microbacterium* sp. C448, forcing it to use sulfamethazine as a

nutritional source. Altogether, these results suggest that the antibiotrophic strain studied can modulate its sulfamethazine-degrading function depending on microbial competition and resource accessibility, to become established in an agricultural soil. Most importantly, this work highlights an increased dispersal potential of antibiotrophs in antibiotic-polluted environments, as antibiotics can not only release existing trophic niches but also form new ones.

**Keywords:** sulfonamide, microbial ecotoxicology, bacterial community invasion, soil, antibiotic biodegradation

## INTRODUCTION

Antibiotics and their residues deserve specific attention as pollutants of emerging concern. Most are slightly and partially metabolized in humans or animals prior to excretion (Lamshöft et al., 2007; Hawkshead, 2008), resulting in heavy contamination of wastewater and livestock manure (Kümmerer, 2001; Watkinson et al., 2007; Feng et al., 2017), where they can reach concentrations of up to micrograms per liter (Peng et al., 2006; Rodriguez-Mozaz et al., 2020) and milligrams per kilogram (Haller et al., 2002; Cid et al., 2018), respectively. The disposal processes applied to these matrices lack efficiency, and so the discharge of wastewater into aquatic ecosystems or manure spread on soils, a common agricultural practice for nutrient recycling and soil fertilization, contributes to the release of antibiotics into different environmental compartments (Watkinson et al., 2007; Heuer et al., 2011; Ghirardini et al., 2020).

By their mode of action and their targets, antibiotics have several ecotoxicological effects on environmental bacteria. First, the direct biocidal action of an antibiotic can alter microbial communities and disturb their function supporting ecosystem services (Costanzo et al., 2005; Ding and He, 2010; Hammesfahr et al., 2011; Pinna et al., 2012; Proia et al., 2013; Cycoń et al., 2019). For instance, tetracycline can alter the denitrification process of soil microbial communities (Shan et al., 2018), while sulfamethazine was shown to negatively impact the phosphatase activity and the respiration of soil microflora (Liu et al., 2009). Second, exposure to antibiotics can induce an adaptive response of microbial communities, notably through the development and spread of antibiotic-resistant bacteria and genes. Numerous studies have shown a positive correlation between antibiotic contamination and the occurrence of antibiotic-resistance genes in ecosystems receiving the above polluted matrices (Hawkshead, 2008; Zhang et al., 2009; Bengtsson-Palme and Larsson, 2016; Bengtsson-Palme et al., 2018). Contamination of ecosystems by antibiotics is thus a major health concern, as these environmental microbial communities constitute reservoirs of resistance that might potentially be transferred to pathogenic bacteria (Perry and Wright, 2013; Zrimec, 2020).

The adaptive capacities of environmental microorganisms toward organic pollutants are not only limited to the increased tolerance or resistance but also include the development of catabolic pathways (Pesce et al., 2020). In this way, the long-term exposure of microbial communities to these substances can lead to the emergence of bacteria able to use them as

nutrient sources (Copley, 2000; Janssen et al., 2005). Although the pesticide-degrading function has been extensively studied (Behki and Khan, 1986; Rani and Lalithakumari, 1994; Aislabie et al., 1997; Gisi et al., 1997), the existence of antibiotic-degrading bacteria was reported more recently (Barnhill et al., 2010; Xin et al., 2012; Topp et al., 2013; Leng et al., 2016; Crofts et al., 2018). The low environmental concentrations of antibiotics compared to pesticides, together with their biocidal effects on many microorganisms, have probably slowed down the development, emergence, and spread of antibiotic-degrading functions. However, the likelihood of such emerging abilities has risen with the increasing concentrations of antibiotics in the environmental compartments along with the decreasing sensitivity of microbial communities. The latest effect is due to the spread of a wide range of antibiotic resistances (Stoll et al., 2012; Bengtsson-Palme et al., 2018) and/or to phenotypic adaptation following chronic exposure to antibiotics (Schmitt et al., 2005; Corona and Martinez, 2013).

In the last decade, a handful of antibiotic-resistant bacteria able to use some antibiotics as nutritive sources were isolated from various environmental matrices repeatedly exposed to relatively high concentrations of antibiotics as agricultural soil (Topp et al., 2013), membrane bioreactor (Bouju et al., 2012), and activated sewage sludge (Lin et al., 2015). The degradative function, termed “antibiotrophy” (Woappi et al., 2016), is specific to an antibiotic or a class of antibiotics, such as  $\beta$ -lactams (Lin et al., 2015; Crofts et al., 2018) or erythromycin (Gao et al., 2015). The case of sulfonamide is currently the most documented (Bouju et al., 2012; Tappe et al., 2013; Topp et al., 2013; Ricken et al., 2017; Kim et al., 2019).

Among antibiotics, sulfonamides are synthetic bacteriostatic compounds largely used in veterinary and human medicine (Shah et al., 2013). They act as competitive inhibitors of the dihydropteroate synthase involved in the synthesis pathway of nucleic acids (Brown, 1962). The most documented resistance mechanism relies on four genes (*sul1*, *sul2*, *sul3*, and *sulA*), coding for dihydropteroate synthase isoproteins insensitive to sulfonamide (Wise and Abou-Donia, 1975; Yun et al., 2012). Both sulfonamides and *sul* genes are widely detected in different environmental matrices such as livestock manure, surface water, and river sediment (Pei et al., 2006; McKinney et al., 2010; Stoll et al., 2012). The dispersion potential of these plasmid-borne resistant genes is enhanced by their common association with integrons (Antunes et al., 2005; Wei et al., 2018), which also contain a variety of resistance genes toward many kinds of biocides (e.g., disinfectants, metals, and antibiotics). Exposure

to these biocides can therefore lead to a co-selection of sulfonamide resistances (Pei et al., 2006; Luo et al., 2010; McKinney et al., 2010; Hoa et al., 2011; Stoll et al., 2012). Sulfonamide antibiotrophy is a recent discovery. Reports on environmental sulfonamide-degrading bacteria are still few but increasing. Those already described originate from different geographically distant matrices, but are phylogenetically close, and their sulfonamide degradative pathway relies on the same cluster of genes (Ricken et al., 2017; Kim et al., 2019). It composed of two flavin-dependent monooxygenases (*sadA* and *sadB*) and one flavin mononucleotide reductase (*sadC*). Although genetic and metabolic studies have been conducted on isolated sulfonamide antibiotrophs, information is lacking on the ecological impact of this function for bacterial carriers in complex environmental bacterial communities. Manure amendment on soils, known not only to increase the fertility of soils but also to introduce biological contaminants and chemical pollutants, may also be involved in the environmental dispersion of antibiotrophy (Heuer et al., 2011; Tappe et al., 2013; Chen et al., 2019).

At first glance, the development of antibiotic degradation capacities might seem environmentally beneficial by increasing the self-purifying potential of ecosystems, contributing to the natural attenuation of their contamination by antibiotics. Likewise, it could be perceived as a bioremediation tool that could improve the removal of antibiotics from contaminated matrices before their discharge into the environment (Hirth et al., 2016; Sharma et al., 2018; Kumar et al., 2019; Silva et al., 2020). However, given that currently known antibiotrophs are also antibiotic-resistant, the question arises of whether antibiotrophy could lend them a selective advantage and so facilitate their implantation and dispersion in the environment.

We conducted a microcosm study to investigate the mechanisms driving the emergence and development of antibiotrophy in agricultural soils. Specifically, we investigated whether an allochthonous bacterium harboring both sulfonamide resistance and degradation genes could become established within natural microbial communities in soils subjected to both sulfonamide contamination and manure amendment. For this purpose, we considered four different soil types with and without added sulfamethazine (SMZ) and/or swine manure, and with and without inoculation with the sulfonamide-degrading and resistant bacterial strain, *Microbacterium* sp. C448. This model bacterium was isolated from experimental soils exposed for 10 years to an annual increasing dose of SMZ ranging from 1 to 10 mg kg<sup>-1</sup> (Topp et al., 2013). It presents the advantage of being well-characterized genetically and physiologically (Martin-Laurent et al., 2014). To assess the establishment of *Microbacterium* sp. C448 in soil communities, its abundance was measured, after 1 month of incubation, by qPCR assay targeting its *groL* gene sequence. The resulting effect of applied treatments on the soil community's genetic potential for sulfonamide degradation was assessed through the quantification of the *sadA* gene sequence. To determine whether the degradation potential was expressed, we measured the mineralization kinetics of <sup>14</sup>C-SMZ during the incubation period and quantified the remaining extractable fraction of SMZ at the end of the incubation period. Finally, we assessed the effects of the eight treatments on the soil

microbial community structure and diversity by Illumina 16S rDNA sequencing.

## MATERIALS AND METHODS

### Collection and Analyses of Soils and Manure

Soils and manure were collected in the Bourgogne-Franche-Comté region of France in November 2018. Four soils, A, B, C, and D, selected for their different textures, were sampled from the upper 20 cm of different agricultural fields, air-dried, sieved (mesh size 5 mm), and stored in airtight plastic bags at 4°C until use. Soil A originated from an agricultural field frequently flooded by the nearby Saône River. Soil B came from the same plot but was less often flooded owing to its higher altitude. Soil C originated from the experimental farm of Epoisses. Soil D was sampled near a hog nursery and had received manure 6 months before the sampling. The pedological variables of the soils (pH, ion retention, grain size, and water content at pF 2.7) are given in **Supplementary Table 1**. Manure was collected from the covered pit of a hog nursery and stored in plastic bottles at 4°C until use. SMZ quantification was performed on soil and manure samples (**Supplementary Table 1**). SMZ concentration reached 0.94 µg L<sup>-1</sup> in manure.

### Microcosm Experiment Setup

The experiment consisted in incubating soil treated or not with manure, contaminated or not with SMZ, and inoculated or not with *Microbacterium* sp. C448. Considering eight conditions and five replicates per condition, 40 microcosms for each soil were prepared as described below. Microcosms containing 50 g dry weight (DW) of soils were prepared in glass bottles closed with air-permeable lids made of gauze and cotton (**Supplementary Figure 1**). They were incubated for 1 week at 20°C (±1°C) to gently activate the native soil microorganisms. Soil microcosms were humidified up to 80% of their water content at pF 2.7. To inoculate microcosms with *Microbacterium* sp. C448, the strain was first grown in LB-Miller liquid medium at 28°C under 130 rpm agitation. The grown cells were collected in their exponential phase (OD<sub>600nm</sub> ~ 1 AU) and washed twice with NaCl 0.9%. SMZ sodium salt [SMZ, CAS number: 1981-58-4, 4-amino-*N*-(4,6-dimethyl-2-pyrimidinyl)benzenesulfonamide, Sigma-Aldrich, France] was diluted to 100 mg ml<sup>-1</sup> in water and filtered (0.2 µm). The manure was incubated overnight at room temperature (20 ± 1°C). Treatments were prepared a few minutes before their application on soils to reach nominal concentrations of 10<sup>4</sup> cells of *Microbacterium* sp. C448 g<sup>-1</sup> dry soil, 100 mg of SMZ kg<sup>-1</sup> dry soil, and 13 ml of manure kg<sup>-1</sup> dry soil [eight treatments, five replicates (**Supplementary Figure 1**)]. The microcosms were incubated at room temperature in the dark for 1 month and maintained at a stable humidity by regular watering (80% of their water content at pF 2.7). At the end of the incubation, we subsampled each microcosm for DNA extraction and further molecular analyses.



## SMZ Fate Monitoring

### SMZ Mineralization Monitoring

For the soil treated with SMZ, the mineralization SMZ was monitored over the time of incubation by radiorespirometry. To do so, the SMZ-treated microcosms were duplicated, with one series being exposed to  $^{12}\text{C}$ -SMZ and another one being exposed to a mixture of  $^{12}\text{C}$ - and  $^{14}\text{C}$ -SMZ (**Supplementary Figure 1**). These last ones were treated with 0.11  $\mu\text{Ci}$  of  $^{14}\text{C}$ -ring-labeled SMZ ( $^{14}\text{C}$ -SMZ, CAS number: 57-68-1, radiochemical purity: >98%, specific radioactivity: X MBq  $\text{mmol}^{-1}$ ) and placed in closed respirometer jars.  $^{14}\text{CO}_2$  released from the  $^{14}\text{C}$ -SMZ degradation was trapped in 5 ml of 0.2 M NaOH solution and regularly analyzed by liquid scintillation counting using ACS II scintillation fluid (Amersham).

### SMZ Quantification

The initial concentration of SMZ in the matrices used in this study (soil and manure) as well as the SMZ remaining in the soil microcosms at the end of the incubation was measured as described below. To Nalgene PPCO 50-ml centrifuge tubes (checked for lack of SMZ sorption capacity) were added  $6.0000 \pm 0.0005$  g of each previously dried and crushed SMZ-contaminated soil sample and 20 ml of MeOH/ $\text{H}_2\text{O}$  4/1 (v/v) mixture. The tubes were stirred for 18 h using an orbital shaker (Heidolph Reax) at 50 rpm and room temperature. After centrifuging ( $12,500 \times g$  for 15 min), the supernatant was filtered on a 0.45- $\mu\text{m}$  syringe PVDF filter (after checking for lack of sorption) before injecting on HPLC. The four soils were spiked with standard SMZ solutions at different concentrations and underwent the same protocol. The recovery percentages ranged between  $79 \pm 1\%$  and  $93 \pm 2\%$  according to the soil. The antibiotic concentrations of soil liquid extracts were determined by HPLC on an Agilent 1,100 apparatus (Courtaboeuf, France) equipped with a reverse-phase column (C18 Zorbax Eclipse Plus column, 75 mm  $\times$  4.6 mm, 3.5  $\mu\text{m}$ ) at 22°C and a diode array detector set at  $\lambda = 260$  and 298 nm. The mobile phase composed of aqueous  $\text{H}_3\text{PO}_4$  (0.01% v/v, pH = 2.9) (A) and acetonitrile (B) at a flow rate of 1 ml  $\text{min}^{-1}$ . Gradient (linear): 0–5 min: 2% B; 5–8 min: 2–30% B; 8–10 min: 30–90% B; 10–10.5 min: 90–100% B; 10.5–11.5 min: 100% B; 11.5–13 min: 100–2% B. Injection volume: 10  $\mu\text{l}$ . Each sample was analyzed twice (technical duplicate). Some samples were also treated with the LC/ESI-MS protocol (below) to check the SMZ concentrations. These were diluted 1/1000 before LC/MS analysis.

For the non-contaminated soil samples, the protocol was the same except that 50  $\mu\text{l}$  of a 5000  $\mu\text{g L}^{-1}$  SMZ- $\text{d}_4$  (LCG standards) solution was added to each centrifuge tube. After centrifuging, the supernatant was concentrated in a Speed-Vac vacuum concentrator heated at 35°C. The residue was dissolved in 10 ml of distilled water. After adjusting the pH to  $3.8 \pm 0.2$ , samples were concentrated 40-fold on Oasis HLB 500-mg cartridges (Waters<sup>TM</sup>) according to the manufacturer's recommendations (elution: 10 ml methanol). The antibiotic concentrations were determined by LC/ESI-MS on a Thermo Scientific UHPLC Ultimate 3000 RSLC coupled with an Orbitrap Q-Exactive analyzer. The analyses were carried out in positive

mode. The UHPLC was equipped with a Luna Omega Polar C18 column; 100  $\times$  2.1 mm; 1.6  $\mu\text{m}$  (Phenomenex) at 30°C with acetonitrile gradient +0.1% formic acid (Solvent A) and water +0.1% formic acid (Solvent B): 0–2.5 min: 30–64.5% A (linear); 2.5–2.6 min: 64.5–99% A (linear); 2.6–5 min: 99% A; 5–5.1 min: 99–30% A; 5.1–8 min: 30% A. Flow rate of 0.45 ml  $\text{min}^{-1}$ . For the mass spectrometer, gaseous  $\text{N}_2$  was used as nebulizer gas (50 A.U.). The spray voltage was 3.0 kV.

### Soil DNA Extraction and Real-Time PCR

DNA was extracted from 250 mg of soil from each sample using the DNeasy PowerSoil-htp 96-well DNA isolation kit (Qiagen, France) following the manufacturer's instructions and stored at  $-20^\circ\text{C}$ .

Real-time PCR reactions were carried out in a ViiA7 (Life Technologies, United States) in a 15- $\mu\text{l}$  reaction volume. For *sadA* and *rss* genes, the mixture contained 7.5  $\mu\text{l}$  of Takyon MasterMix (Eurogentec, France), 1  $\mu\text{M}$  of each primer (**Supplementary Table 2**), 250 ng of T4 gene 32 (QBiogene, France), and 3 ng of DNA. The quantification of *Microbacterium* sp. C448's *groL* required a specific probe. The reaction mixture contained 7.5  $\mu\text{l}$  of Takyon Low ROX Probe 2X MasterMix dTTP blue (Eurogentec, France), 400 nM of each primer, 200 nM of the probe (**Supplementary Table 2**), 250 ng of T4 gene 32, and 3 ng of soil DNA. Each real-time PCR assay was performed twice independently. Standard curves were obtained using serial dilutions of linearized plasmids containing the appropriate cloned target genes from bacterial strains. The qPCR efficiencies ranged between 80 and 100%. Inhibition was assessed for each sample in accordance with ISO17601 (2016). No inhibition was detected in any case. The thermal cycling was performed as follows: 95°C for 10 min, 40 cycles of 95°C for 30 s, annealing (**Supplementary Table 2**) for 30 s, and 30 s at 60°C. Relative abundances were obtained by normalizing the copy number of genes *sadA* and *groL* with bacterial 16S rRNA gene *rss* copies. The detection limit was 50 copies/ng of DNA for *sadA* and *groL* and 5,000 copies/ng of DNA for *rss*. The threshold expressed by 1,000 copies of *rss* was determined by dividing the detection limit of the gene by the lowest quantification value of *rss*.

### 16S rDNA Sequencing and Bioinformatic Analysis

The V3–V4 hypervariable region of the bacterial 16S rRNA gene was amplified using a two-step PCR and sequenced on MiSeq (Illumina, 2  $\times$  250 bp) as previously described (Spor et al., 2020).

A Jupyter Notebook developed in-house was used to analyze the sequence data. Briefly, sequences were assembled using PEAR (Zhang et al., 2014) with default settings. Further quality checks were conducted using the QIIME pipeline (Caporaso et al., 2010) and short sequences were removed (<400 bp). Reference-based and *de novo* chimera detection together with clustering in OTUs were performed using VSEARCH (Rognes et al., 2016) and Greengenes' representative set of 16S rRNA sequences as the reference database. The identity thresholds were set at 94%. Representative sequences for each OTU were aligned

using Infernal (Nawrocki and Eddy, 2013) and a 16S rRNA phylogenetic tree was constructed using FastTree (Price et al., 2010). Taxonomy was assigned using RDP Classifier (Wang et al., 2007) and the latest released Greengenes database (v.05/2013; McDonald et al., 2012).  $\alpha$ -Diversity metrics (PD whole tree, species richness, and equitability index) were determined from rarefied OTU tables of 25,700, 24,500, 28,300, and 23,100 sequences per sample for soils A, B, C, and D, respectively. Sequences were deposited in the SRA at NCBI under the accession number SUB8712901.

## Statistical Analyses

Statistical analyses were carried out using RStudio statistical software (version 1.2.5033). For each soil, we built an *ad hoc* analysis of variance (ANOVA) model to determine the effects of treatments on gene abundances and on the alpha diversity indices of bacterial communities. Normality and homogeneity of the residual distribution were inspected and log10-transformations were performed when necessary. Differences in response variable related to the treatment (antibiotic treatment, manure amendment, and strain inoculation) were detected using the following model:

$$Y_{ijkl} = \mu + A_i + T_j + I_k + A : T_{ij} + A : I_{ik} \\ + T : I_{jk} + A : T : I_{ijk} + \varepsilon_{ijkl},$$

where  $Y_{ijkl}$  is the response variable,  $A$  is the fixed effect of manure amendment ( $i = 1, 2$ ),  $T$  is the fixed effect of sulfamethazine treatment ( $j = 1, 2$ ),  $I$  is the fixed effect of inoculation by *Microbacterium* sp. C448 ( $k = 1, 2$ ), and  $\varepsilon_{ijkl}$  are the residuals.

Tukey's test was performed to detect significant pairwise differences for each treatment (significance threshold set at  $p < 0.05$ ).

The OTU table was also filtered to keep the dominant OTUs (relative abundance  $> 0.1\%$ ). For each soil, the OTUs that were significantly impacted by treatments were detected with the previous linear model. We opted for a custom model analysis to take into account the relative complexity of our experimental design that cannot be handled by classical analysis packages such as edgeR or DESeq2. A false discovery rate procedure was used to decrease substantially the probability of detecting false positives. The FDR significance threshold was set at 0.05.

## RESULTS AND DISCUSSION

### The Soils, Regardless of Manure Amendment, Did Not Have Innate Antibiotrophic Potential or Activity

After a 1-month incubation period, the antibiotrophic gene *sadA* was not detected in the four soils even when they were amended with manure (Figure 1B, detection limit of 0.1 *sadA* copies per 1,000 *rrs*). Despite the exposure to SMZ, its abundance remained below the detection limit. This strongly suggests that the microbial communities of the four soils and manure do not initially possess bacteria carrying *sadA*, although

some of them were previously exposed to low concentrations of SMZ (Supplementary Table 3). *sadA* has only appeared in recent literature on sulfonamide-degrading bacteria isolated from environmental compartments after high and long-term exposure to sulfonamide antibiotics, such as bioreactor membranes (Bouju et al., 2012), active sludges (Reis et al., 2014), or manure-amended soils (Tappe et al., 2013; Chen et al., 2019). However, the lack of detection of the key gene coding for the first enzyme of the only currently established SMZ antibiotrophy pathway cannot exclude the possibility of antibiotrophic activity catalyzed by other still unknown enzymes. We also measured the antibiotrophic potential activity. These analyses relied on a similar microcosm experiment differing only by the addition of  $^{14}\text{C}$ -labeled SMZ to monitor the mineralization of its phenyl ring. The mineralization rates obtained for soils, regardless of manure amendment and SMZ treatment modalities, did not exceed 3% of initially added  $^{14}\text{C}$ -SMZ (Figure 2). Although an alternative low-efficiency SMZ-antibiotrophic pathway can explain this slight observed mineralization, it can be reasonably assumed that it results from residual mineralization. Nonspecific biotic and abiotic mechanisms can partially break complex molecules (Gold et al., 2000; Mitchell et al., 2015), promoting fortuitous biological degradation. Moreover, the mineralization rates did not increase during the 1 month of exposure of native soil microbial communities to a high concentration of SMZ. We note that the experimental conditions were insufficient to guarantee enhancement and development of antibiotrophic abilities.

### *Microbacterium* sp. C448 Needs SMZ to Become Established in the Soil Community

After a 1-month incubation period, quantification of the *Microbacterium* sp. C448 through the estimation of the abundance of its *groL* gene sequence (Figure 1A) indicated that it could establish in the four tested soils but only under SMZ exposure. The relative abundance of the strain was relatively homogenous in the four treated soils (from  $1.3 \pm 0.1$  to  $4.6 \pm 1.6$  *groL* copies per 1,000 copies of the 16S rRNA gene *rrs*), despite their different biotic and abiotic properties. Adding manure had either no impact (soils A and C) or a relatively limited one (soils B and D,  $n = 5$ ,  $p < 0.05$ ) on the relative abundance of the *groL* gene sequence. Extrapolating *groL* quantification and assuming a soil DNA extraction yield of 1, at least  $10^6$  cells of *Microbacterium* sp. C448 per gram of dry soil were counted at the end of incubation in the SMZ-treated soils inoculated with  $10^4$  cells per gram of dry soil, indicating growth. Conversely, in the SMZ-untreated soils, *groL* gene sequences were below the detection limit of 0.1 *groL* per 1,000 *rrs*, suggesting that *Microbacterium* sp. C448, initially absent, did not become established in these conditions. This indicates a low competitiveness for this strain, which possesses a low invasion potential under SMZ-free conditions and highlights the mandatory presence of the antibiotic for its establishment. SMZ may therefore be the main environmental driver controlling the efficiency of the establishment of *Microbacterium* sp. C448, at least in our experimental conditions. Given that this strain is also known to resist and degrade other sulfonamides such

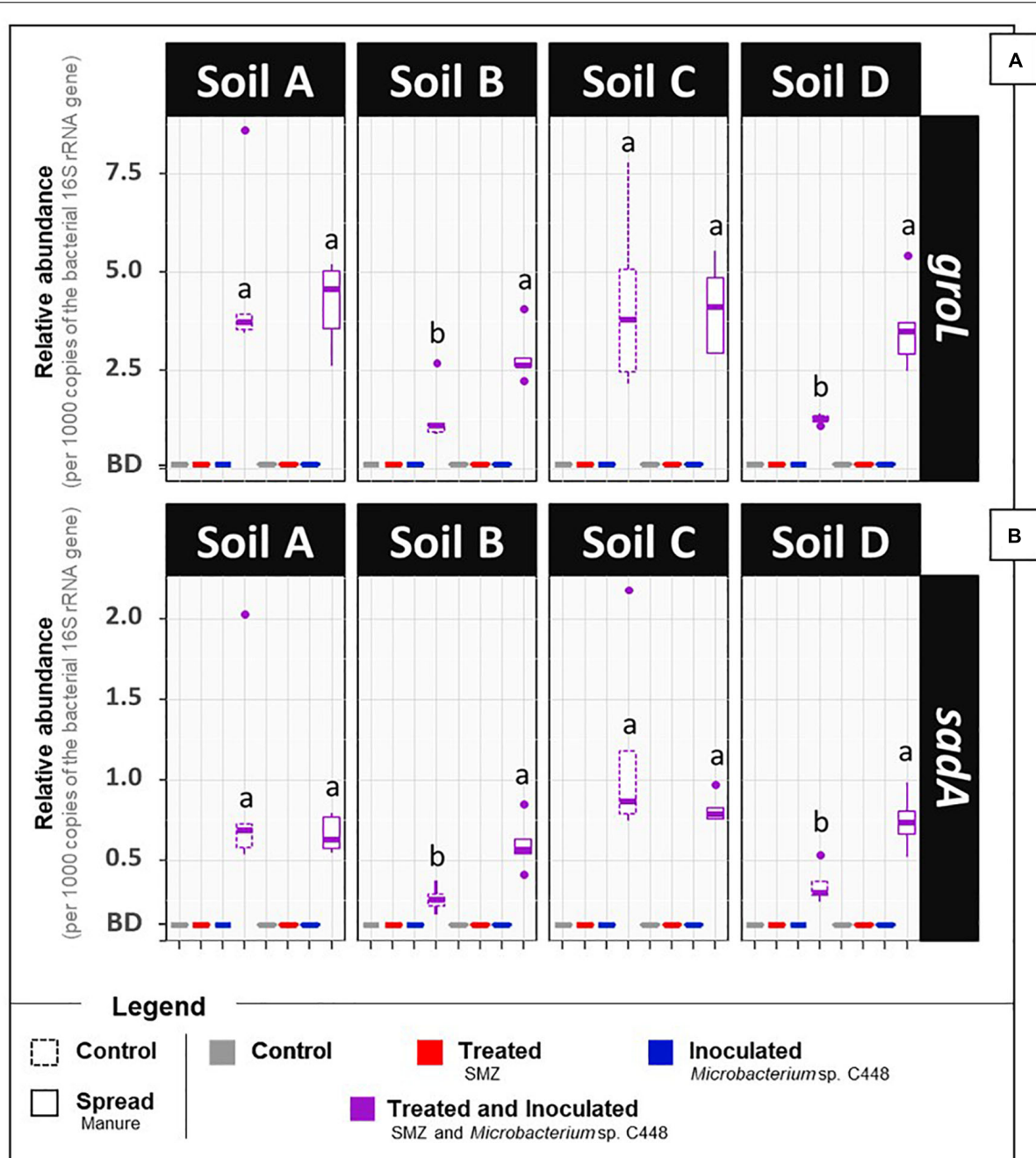


**FIGURE 1 |** Relative abundances of *groL* (A) and *sadA* (B) gene sequences in the soil microcosms (four types of soil, A, B, C, and D, amended or not with manure, treated or not with SMZ, and inoculated or not with *Microbacterium* sp. C448). After 1 month of incubation, gene sequence abundances were measured by quantitative PCR and expressed per 1000 copies of the bacterial 16S rRNA gene *rss* (Tukey's test,  $n = 5$ ,  $p < 0.05$ ). BD: below the detection limit (0.1 copy per 1,000 16S rRNA gene).

as sulfamethoxazole, sulfadiazine, or sulfadimethoxine (Martin-Laurent and Topp, unpublished data), this effect might hold for a wider range of antibiotics in this family.

Two main hypotheses could explain this selective advantage conferred by SMZ. The first is that the antibiotic may be used as a nutrient source exclusively dedicated to *Microbacterium* sp. C448, thus playing a major role in ecological selectivity

(Nishiyama et al., 1993; Karpouzias and Walker, 2000; Hong et al., 2007). Specialized microorganisms, when they are the only ones possessing the required catabolic enzymes to mineralize selected xenobiotics, are able to establish and perform mineralization even if they are initially scant in the microbial community (van Veen et al., 1997). The second hypothesis is that SMZ may release trophic niches by biocidal action

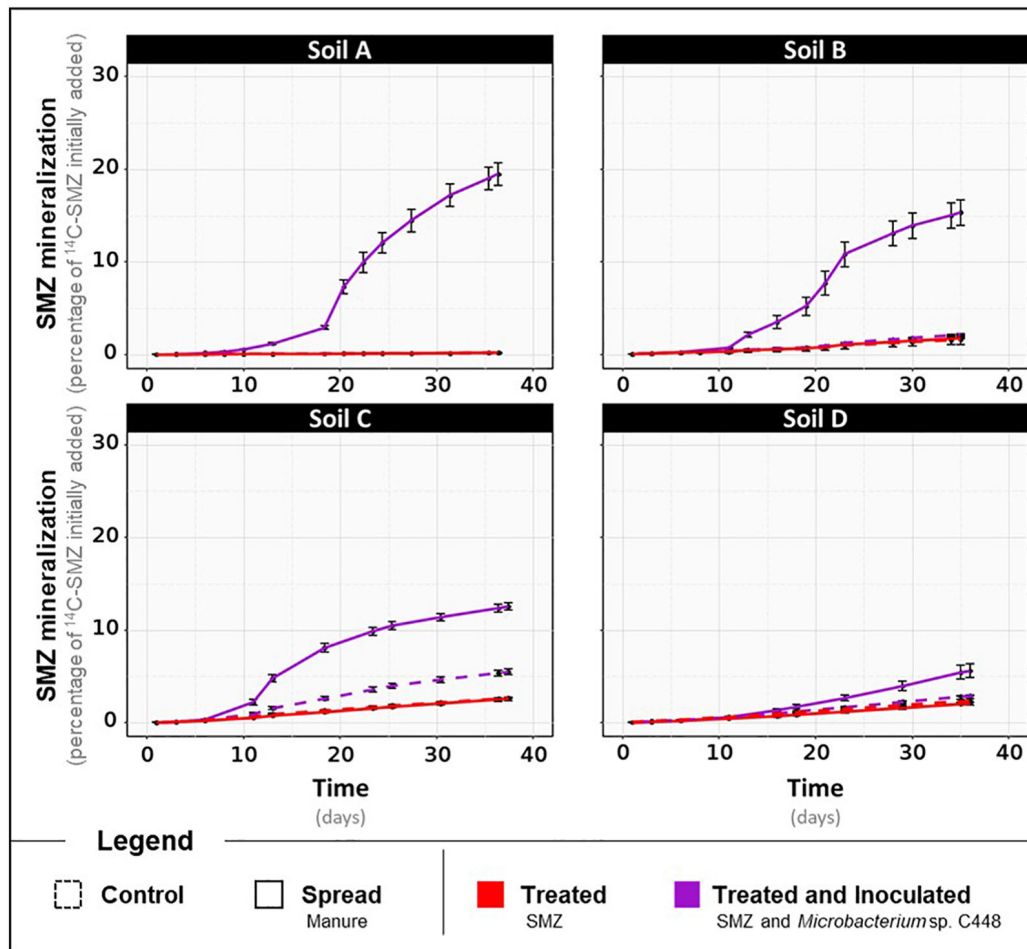


**FIGURE 2 |** Kinetics of  $^{14}\text{C}$ -SMZ mineralization throughout the incubation for the four different types of soils, A, B, C, and D, treated with SMZ, amended or not with manure, and inoculated or not with *Microbacterium* sp. C448. Results are expressed in percentage of initially added  $^{14}\text{C}$ -SMZ.

(Pinna et al., 2012; Reichel et al., 2015), thus reducing negative interactions such as trophic interactions or competition (van Elsas et al., 2012). These two non-exclusive hypotheses may explain why SMZ facilitates the establishment of the strain in the soil communities.

## The Presence of Genetic Potential for Antibiotrophy in Soil Does Not Guarantee Its Expression

The relative abundance of the antibiotrophic gene *sadA* (Figure 1B) followed trends similar to those of *groL*. *sadA* was detected only when *Microbacterium* sp. C448 was present (i.e., when *groL* was detected), with relative abundances fluctuating between  $0.3 \pm 0.1$  and  $1.1 \pm 0.4$  *sadA* copies per 1,000 copies of *rrs* gene. More than just indicating that *Microbacterium* sp. C448 was initially the only host of *sadA* gene, it suggests that it kept its antibiotrophic genetic potential after its establishment in the SMZ-treated soils, whether or not manure was added. This agrees with the idea that the antibiotrophic

function carried by *sadA* gene is probably useful in SMZ-polluted conditions.

Although previous studies have indicated that *sadA* is potentially mobile in other antibiotrophic strains (Ricken et al., 2017; Reis et al., 2019), our results did not show any increase in the *sadA/groL* ratio (data not shown), suggesting an absence of horizontal gene transfer. This is consistent with the chromosomal localization of *sadA*, which makes its mobility *via* a horizontal gene transfer event unlikely (whole genome sequencing of *Microbacterium* sp. C448, Martin-Laurent et al., 2014).

The main outcome of *groL* and *sadA* gene sequence quantification is that installation of *Microbacterium* sp. C448 and its antibiotrophic gene *sadA* both succeed as long as they are under SMZ selection pressure. However, and since the gene's presence does not guarantee its functional expression (Browning and Busby, 2004; Pietramellara et al., 2008), qPCR assessments were complemented with functional analyses to assess potential  $^{14}\text{C}$ -SMZ mineralization. As stated above, mineralization rates obtained for conditions without *Microbacterium* sp. C448 were low and did not exceed 3% in any of the soils (Figure 2).



When *Microbacterium* sp. C448 was inoculated, a mineralization activity was observed for each soil, but it occurred only (in soils A, B, and D) or preferentially (in soil C) under manure spreading conditions (Figure 2). When the strain was applied simultaneously with manure, soils A, B, and D reached, respectively,  $19.5 \pm 1.2\%$  (Figure 2),  $15.3 \pm 1.4\%$  (Figure 2), and  $5.6 \pm 0.7\%$  (Figure 2) of SMZ mineralization. Soil C was the only one where *Microbacterium* sp. C448 was able to express its mineralization potential without manure spreading (Figure 2). However, the mineralization rate was about half that with manure ( $5.5 \pm 0.3\%$  versus  $12.6 \pm 0.4\%$ ). Altogether, these results reveal that the presence of *Microbacterium* sp. C448 and its antibiotrophic gene *sadA* does not always result in effective antibiotrophy in SMZ-contaminated soils. In our experimental conditions, they reflect a modularity of the functional expression depending on the kind of soil and on manure addition what is commonly observed in particular for antibiotic degradation (Cycón et al., 2019). This lack of mineralization did not seem to result from the absence of SMZ bioavailability. The quantification of the SMZ extractable fraction performed at the end of the incubation period indicates that the amount of bioavailable SMZ was not or only slightly affected by manure amendment (Table 1). *Microbacterium* sp. C448 thus potentially had access to as much SMZ with manure amendment as without. Moreover, the variation of free SMZ amount between soils does not seem to be correlated with the variation of mineralization between soils, since the soil C with the lowest SMZ concentration was not the one with the lowest degradation rate. Altogether, these observations provide a nuanced response to the hypothesis for how SMZ can give *Microbacterium* sp. C448 a selective advantage. Without manure, the absence of mineralization (or the drastically diminished mineralization compared to manure treatment for soil C) indicates that SMZ is not always essential as an exclusive dedicated nutrient source. We therefore investigated whether SMZ could also give this strain a selective advantage by its biocidal action to release ecological niches.

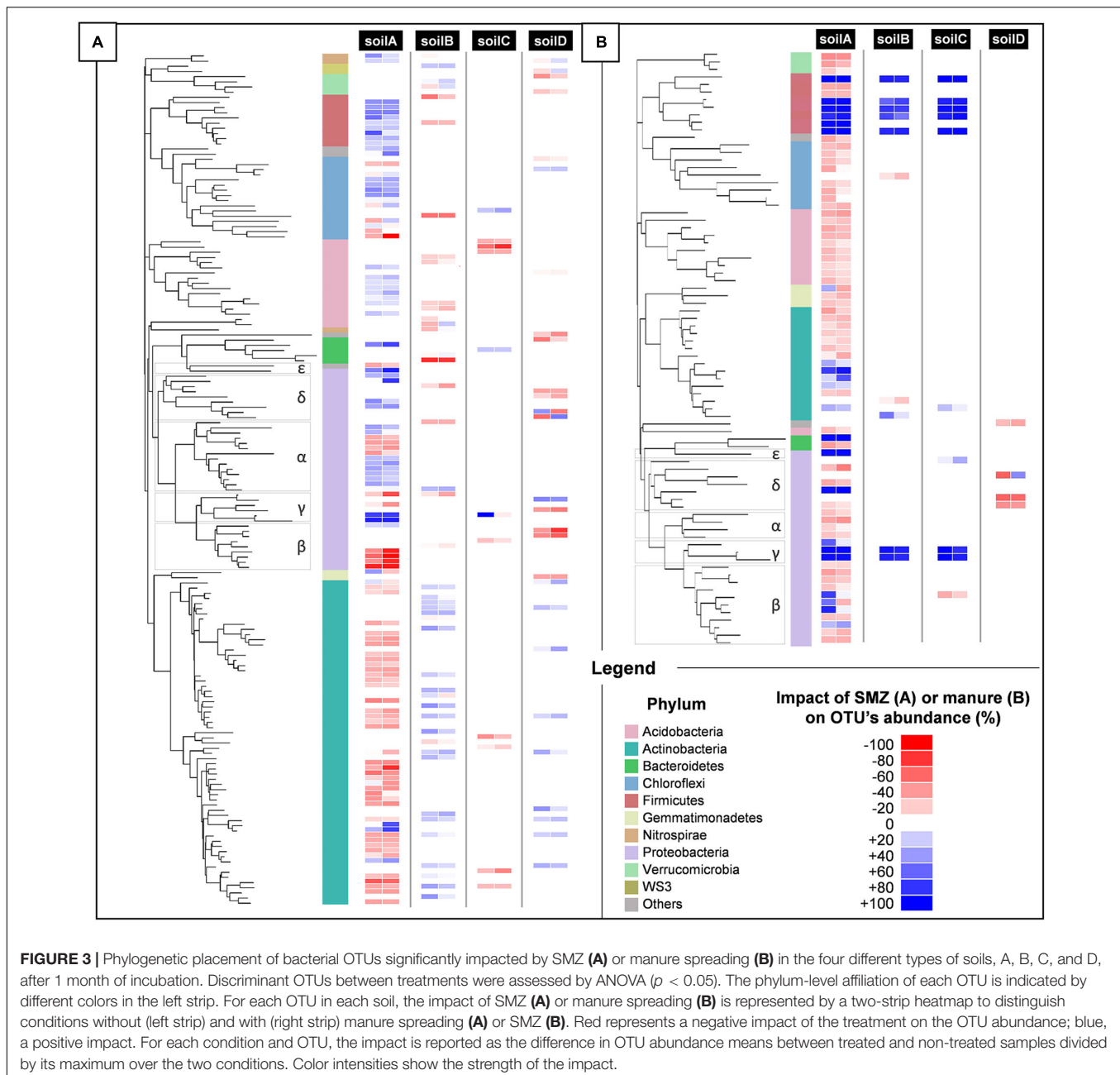
## Antibiotrophy Efficiency Depends on SMZ Biocidal Impact

The biocidal impact of SMZ on soil communities was evaluated by 16S rDNA sequencing to assess the resulting changes in the bacterial and archaeal community diversity and structure. From this sequencing, more than 23,100 partial 16S rDNA sequences were analyzed from each microcosm, accounting for 15,195 OTUs. The overall diversity indices (richness, equitability, and observed species) in the four tested soils were not significantly impacted by SMZ addition, whether or not manure and/or *Microbacterium* sp. C448 were added (Supplementary Table 4). This suggests no or only transient effects of SMZ on community diversity, but it does not exclude impacts on the members of the community. Further OTU-level ANOVAs revealed that about 165 of the studied OTUs were significantly affected by SMZ in at least one of the soils (Figure 3A). This limited impact is coherent with the previous study of Cleary et al. (2016) in which few OTUs were significantly affected by the input of SMZ into soils. The response of the bacterial community to SMZ varied between soils.

**TABLE 1 |** Concentrations of extractable SMZ measured after 1 month of incubation in the four different types of soils treated with SMZ, amended or not with manure, and inoculated or not with *Microbacterium* sp. C448 (C448).

		Concentration of extractable SMZ (mg kg <sup>-1</sup> dry soil)
Soil A	SMZ	54.1 ± 0.4
	SMZ × C448	54.4 ± 1.7
	SMZ × MANURE	45.4 ± 1.7
	SMZ × C448 × MANURE	34.6 ± 1.8
Soil B	SMZ	21.8 ± 2.7
	SMZ × C448	21.4 ± 0.8
	SMZ × MANURE	21.0 ± 2.6
	SMZ × C448 × MANURE	19.9 ± 1.5
Soil C	SMZ	0.9 ± 0.1
	SMZ × C448	0.6 ± 0.0
	SMZ × MANURE	1.1 ± 0.1
	SMZ × C448 × MANURE	0.5 ± 0.0
Soil D	SMZ	6.4 ± 0.2
	SMZ × C448	4.1 ± 0.1
	SMZ × MANURE	6.8 ± 0.1
	SMZ × C448 × MANURE	3.7 ± 0.1

The soil A community was clearly the most negatively impacted with 55 OTUs whose abundance was significantly reduced by the antibiotic, while the soil C community appeared to be the most robust one, with only eight OTUs negatively impacted (accounting for 14.1 and 2.3% of the bacterial community of untreated and non-amended soils, respectively). SMZ moderately affected soil B and D communities with, respectively, 15 and 20 OTUs with significantly reduced abundance (accounting for 5.3 and 2.7% of the bacterial community of untreated and non-amended soils, respectively). In parallel, the abundance of some OTUs was also increased, probably benefiting from the decrease in others. Pre-adaptation of bacterial communities to antibiotics could have been the main factor explaining the variations in the biocidal impact (Schmitt et al., 2004, 2005; Brandt et al., 2009). This was not the case here since the SMZ impact on the community of soil A was much stronger than on that of soil B, whereas they were exposed before the experiment to similar concentrations of SMZ (Supplementary Table 1). The second most probable factor explaining the variation of SMZ impact could be its bioavailability, since only the free fraction can be bioavailable for bacteria and exert its biocidal action. The SMZ quantification supports this hypothesis (Table 1). In the non-inoculated soils where no specific mineralization took place, the greatest SMZ available fraction was found in the most impacted soil (soil A,  $54.1 \pm 0.4\%$  of SMZ available) and the lowest in the least impacted one (soil C,  $0.9 \pm 0.1\%$ ). The bioavailability of SMZ (and more generally of organic contaminants) relies on its intrinsic properties and on soil characteristics and especially clay content, organic carbon fraction, and pH (Supplementary Table 1). It is expected that their increases will reduce the bioavailability of SMZ in soil and therefore its biocidal activity (Gao and Pedersen, 2005; Lertpaitoonpan et al., 2009; Pinna et al., 2012). Our results are in line with this hypothesis since soil A,



which hosted the most impacted community, and soil C, which hosted the least impacted one, exhibited, respectively, the lowest and highest values for clay content, organic carbon fraction, and pH (84, 5.2, and 5.6‰, and 360, 13, and 6.9‰, respectively).

Besides confirming that the biocidal activity of SMZ depends on the soil's physical and chemical properties, microbial diversity and structure analyses suggest that ecological niches may have been freed after the reduction in abundance of some OTUs following the SMZ exposure. *Microbacterium* sp. C448 could have potentially colonized and used these unoccupied niches, thus facilitating its establishment in the soil community. This outcome supports the hypothesis of released niches, which could

explain the crucial positive role of SMZ for *Microbacterium* sp. C448 establishment even when it does not use this antibiotic as a nutrient source. The lack (or limited level) of SMZ mineralization observed in the absence of manure spreading, although the antibiotic was available, may indicate a niche preference of the strain for readily available organic nutrients as already shown in other studies dealing with inoculation of xenobiotics degraders in soils (Benimeli et al., 2008). The degradation of antibiotics like many other synthetic organic contaminants can be arduous as the successive steps leading to their complete degradation can release intermediate transformation products that can be toxic for the degrading bacteria involved. For instance, sulfur

dioxide, one dead-end product of SMZ mineralization (Ricken et al., 2017), is known for its antibacterial properties (Malwal et al., 2012). However, SMZ can constitute a nutritive source of prime choice for *Microbacterium* sp. C448, especially if the strain lacks niches to support its growth. The measurements of SMZ mineralization potential for the soil C fits this hypothesis. The slight mineralization of SMZ ( $5.5 \pm 0.3\%$ ) and its reduced biocidal action on the bacterial community suggest that the release of trophic niches was insufficient to entirely support *Microbacterium* sp. C448 growth, which therefore used its antibiotic degradation in compensation.

## Antibiotrophy Efficiency Depends on Soil Permissiveness to Invasion of Manure-Originating OTUs and Resulting Trophic Competition

In soils spread with manure, antibiotic mineralization was enhanced although biocidal action of SMZ and therefore niche releases occurred in a similar way (Figure 2). This suggests that *Microbacterium* sp. C448 encountered difficulties in accessing trophic niches released by SMZ and had to rely on antibiotic degradation to become established.

We observed that adding manure significantly increased the alpha diversity of bacteria and archaea in each SMZ-treated soil, except for soil D (Supplementary Table 4). Phylogenetic diversity values increased by about 5.7, 5.2, and 7.2% in soils A, B, and C, respectively, with a respective gain of about 75, 68, and 116 observed OTUs. ANOVAs conducted on each OTU individually indicated that 79 of the 15,195 OTUs were significantly increased or decreased in response to manure application in at least one of these four soils (Figure 3B). In detail, soil A was the most affected, with a strong increase in abundance of 21 OTU (+80% of their abundance at least) and a slight decrease in abundance of 51 OTU (−60% at most). In the presence of manure, soils B and C presented increasing abundances only for eight and nine OTUs and decreasing abundances for one and two OTUs, respectively. Interestingly, a cluster of seven OTUs presented the same pattern in soils A, B, and C. They were below or near the detection limit without manure. Their abundance significantly increased in manure-spread soils. Some of these OTUs (two  $\gamma$ -Proteobacteria and five Firmicutes including four Clostridiales) are known as fecal markers (Hagey et al., 2019). Moreover, they were abundant in manure (Supplementary Table 5). According to Gravuer and Scow (2021), those observations are signs that these OTUs originate manure and are soil invaders. This supports the hypothesis that manure brought exogenous OTUs that compete with *Microbacterium* sp. C448 for establishment in soil. As stated above, *Microbacterium* sp. C448 seems to be a poor competitor in the studied soils. Simultaneous inputs of manure and the antibiotrophic strain could thus induce detrimental competition for *Microbacterium* sp. C448, in favor of using SMZ as a nutritional support of choice. This could thus explain why manure spreading led to a strong stimulation of SMZ mineralization, which reached 19.5, 15.3, and 12.6% in soils A, B, and C, respectively (Figure 2). On the contrary, the soil D community structure was only slightly affected by

manure. Its diversity indices were not changed (Supplementary Figure 4) and the OTU-level analyses indicated that only four OTUs were significantly decreased, with no detected increase in individual OTU abundances (Figure 3B). Whether or not manure was added, soil D exhibited most of the seven OTUs belonging to the above cluster that was abundant in soils A, B, and C spread with manure (Supplementary Table 5). This initial presence in soil D might be due to its agronomical history, which involved regular application of manure as organic fertilizer (the latest occasion being 6 months before the experiment). Based on these results, we can hypothesize that the previous in-field manure exposure led to a pre-colonization of soil communities by manure OTUs (Gravuer and Scow, 2021), thus limiting further microbial disturbance in response to the experimental amendment of manure. It therefore suggests that most of the ecological niches made available by the biocidal effect of SMZ in this soil remained free for *Microbacterium* sp. C448, thus explaining, at least partially, the low SMZ mineralization rate ( $5.6 \pm 0.7\%$ ) measured in soil D spread with manure (Figure 2).

## CONCLUSION

The sulfonamide-resistant function confers a selective advantage in competitive environments impacted by the biocidal action of SMZ. Our study strongly suggests that sulfonamide-degrading capacities could provide an additional selective advantage to sulfonamide-resistant bacteria by enhancing their dispersion potential. Besides eliminating sensitive trophic competitors, and so releasing niches, SMZ can constitute an exclusive trophic niche for sulfonamide-degraders. Our study shows that antibiotrophy is mainly beneficial when the SMZ biocidal activity on competitors is insufficient. Indeed, antibiotrophy promoted *Microbacterium* sp. C448 establishment when the impact of SMZ on soil microbial diversity and structure was low and when outsider competitors were added by manure amendment. The emergence of antibiotrophy among antibiotic-resistant bacteria might promote their dispersion and survival in the environment and thus might constitute a health concern. Antibiotrophy would be expected to provide an environmental benefit by contributing to the self-purifying of antibiotic-contaminated ecosystems. Yet, in our experiment, SMZ degradation was neither high nor automatic in soils with antibiotrophs. Further research is needed to better assess the role of the antibiotroph function in the dispersion of antibiotic-resistant bacteria in the environment. One of the possible ways to achieve this goal will be to compare the dispersion potential of the wild-type strain to that of a mutant unable to degrade and grow on SMZ.

## DATA AVAILABILITY STATEMENT

The datasets presented in this study can be found in online repositories. The names of the repository/repositories and accession number(s) can be found below:

<https://www.ncbi.nlm.nih.gov/>, SUB8712901. The latest accession in the SRA at NCBI number is: PRJNA684125.

## AUTHOR CONTRIBUTIONS

LB, SP, MD-L, and FM-L contributed to the conception and design of the study. LB, NR, and MD-L performed the laboratory experiments. LB, MD-L, AS, and AM analyzed the results. LB, SP, and MD-L wrote the first draft of the manuscript. LP, ML, and PB-H developed the analytical methods for the SMZ quantification in soil and manure and analyzed the results. LP and PB-H prepared the soil and manure samples, and ML carried out the LC-MS analyses. All authors contributed to manuscript revision and read and approved the submitted version.

## FUNDING

This research was funded by the French National Research Agency (ANTIBIOTOX project, ref: ANR-17-CE34-0003).

## ACKNOWLEDGMENTS

The authors thank Dr. Ed Topp and his team for previous characterization studies of *Microbacterium* sp. C448 and

for helpful discussions within the framework of the ANTIBIOTOX project.

## SUPPLEMENTARY MATERIAL

The Supplementary Material for this article can be found online at: <https://www.frontiersin.org/articles/10.3389/fmicb.2021.643087/full#supplementary-material>

**Supplementary Figure 1** | Experimental design of soil microcosm experiment with  $^{12}\text{C}$ -SMZ or  $^{14}\text{C}$ -SMZ, consisting of amendment or not with manure, treatment.

**Supplementary Table 1** | GPS coordinates and physical-chemical properties of the four different soils used in the study.

**Supplementary Table 2** | Primers and probe used in this study.

**Supplementary Table 3** | Mass balances of  $^{14}\text{C}$ -radioactivity in the four different soils treated with SMZ, amended or not with manure, and inoculated or not with *Microbacterium* sp. C448 (C448) obtained at the end of the month of incubation. Between 75% and 100% of the initially added radioactivity was retrieved. Results are expressed in percent of  $^{14}\text{C}$ -SMZ initially retrieved.

**Supplementary Table 4** | Alpha diversity indices of the four different soils amended or not with manure, treated or not with SMZ and inoculated or not with *Microbacterium* sp. C448 (C448).

**Supplementary Table 5** | Initial abundance and phylogeny (phylum, class, order) of the seven OTUs highly likely to come from manure in the four soils and in the manure.

## REFERENCES

- Aislabie, J., Richards, N., and Boul, H. (1997). Microbial degradation of DDT and its residues—A review. *N. Z. J. Agric. Res.* 40, 269–282. doi: 10.1080/00288233.1997.9513247
- Antunes, P., Machado, J., Sousa, J. C., and Peixe, L. (2005). Dissemination of sulfonamide resistance genes (sul1, sul2, and sul3) in Portuguese *Salmonella enterica* strains and relation with integrons. *Antimicrob. Agents Chemother.* 49, 836–839. doi: 10.1128/AAC.49.2.836-839.2005
- Barnhill, A. E., Weeks, K. E., Xiong, N., Day, T. A., and Carlson, S. A. (2010). Identification of multiresistant *Salmonella* isolates capable of subsisting on antibiotics. *Appl. Environ. Microbiol.* 76, 2678–2680. doi: 10.1128/AEM.02516-09
- Behki, R. M., and Khan, S. U. (1986). Degradation of atrazine by *Pseudomonas*: N-dealkylation and dehalogenation of atrazine and its metabolites. *J. Agric. Food Chem.* 34, 746–749. doi: 10.1021/jf00070a039
- Bengtsson-Palme, J., Kristiansson, E., and Larsson, D. G. J. (2018). Environmental factors influencing the development and spread of antibiotic resistance. *FEMS Microbiol. Rev.* 42:fux053. doi: 10.1093/femsre/fux053
- Bengtsson-Palme, J., and Larsson, D. G. J. (2016). Concentrations of antibiotics predicted to select for resistant bacteria: proposed limits for environmental regulation. *Environ. Int.* 86, 140–149. doi: 10.1016/j.envint.2015.10.015
- Benimeli, C. S., Fuentes, M. S., Abate, C. M., and Amoroso, M. J. (2008). Bioremediation of lindane-contaminated soil by *Streptomyces* sp. M7 and its effects on *Zea mays* growth. *Int. Biodeter. Biodegr.* 61, 233–239. doi: 10.1016/j.ibiod.2007.09.001
- Bouju, H., Ricken, B., Beffa, T., Corvini, P. F.-X., and Kolvenbach, B. A. (2012). Isolation of bacterial strains capable of sulfamethoxazole mineralization from an acclimated membrane bioreactor. *Appl. Environ. Microbiol.* 78, 277–279. doi: 10.1128/AEM.05888-11
- Brandt, K. K., Sjöholm, O. R., Krogh, K. A., Halling-Sørensen, B., and Nybroe, O. (2009). Increased pollution-induced bacterial community tolerance to sulfadiazine in soil hotspots amended with artificial root exudates. *Environ. Sci. Technol.* 43, 2963–2968. doi: 10.1021/es803546y
- Brown, G. M. (1962). The biosynthesis of folic acid. II. Inhibition by sulfonamides. *J. Biol. Chem.* 237, 536–540.
- Browning, D. F., and Busby, S. J. (2004). The regulation of bacterial transcription initiation. *Nat. Rev. Microbiol.* 2, 57–65. doi: 10.1038/nrmicro787
- Caporaso, J. G., Kuczynski, J., Stombaugh, J., Bittinger, K., Bushman, F. D., Costello, E. K., et al. (2010). QIIME allows analysis of high-throughput community sequencing data. *Nat. Methods* 7, 335–336. doi: 10.1038/nmeth.f.303
- Chen, J., Jiang, X., Tong, T., Miao, S., Huang, J., and Xie, S. (2019). Sulfadiazine degradation in soils: dynamics, functional gene, antibiotic resistance genes and microbial community. *Sci. Total Environ.* 691, 1072–1081. doi: 10.1016/j.scitotenv.2019.07.230
- Cid, C., Álvarez-Esmoris, C., Paradelo Núñez, R., Nóvoa-Muñoz, J. C., Arias-Estévez, M., Álvarez-Rodríguez, E., et al. (2018). Occurrence of tetracyclines and sulfonamides in manures, agricultural soils and crops from different areas in Galicia (NW Spain). *J. Clean. Prod.* 197, 491–500. doi: 10.1016/j.jclepro.2018.06.217
- Cleary, D. W., Bishop, A. H., Zhang, L., Topp, E., Wellington, E. M. H., and Gaze, W. H. (2016). Long-term antibiotic exposure in soil is associated with changes in microbial community structure and prevalence of class 1 integrons. *FEMS Microbiol. Ecol.* 92:fiw159. doi: 10.1093/femsec/fiw159
- Copley, S. D. (2000). Evolution of a metabolic pathway for degradation of a toxic xenobiotic: the patchwork approach. *Trends Biochem. Sci.* 25, 261–265. doi: 10.1016/S0968-0004(00)01562-0
- Corona, F., and Martínez, J. L. (2013). Phenotypic resistance to antibiotics. *Antibiotics* 2, 237–255. doi: 10.3390/antibiotics2020237
- Costanzo, S. D., Murby, J., and Bates, J. (2005). Ecosystem response to antibiotics entering the aquatic environment. *Mar. Pollut. Bull.* 51, 218–223. doi: 10.1016/j.marpolbul.2004.10.038
- Crofts, T. S., Wang, B., Spivak, A., Gianoulis, T. A., Forsberg, K. J., Gibson, M. K., et al. (2018). Shared strategies for  $\beta$ -lactam catabolism in the soil microbiome. *Nat. Chem. Biol.* 14, 556–564. doi: 10.1038/s41589-018-0052-1



- Cycon, M., Mrozik, A., and Piotrowska-Seget, Z. (2019). Antibiotics in the soil environment—degradation and their impact on microbial activity and diversity. *Front. Microbiol.* 10:338. doi: 10.3389/fmicb.2019.00338
- Ding, C., and He, J. (2010). Effect of antibiotics in the environment on microbial populations. *Appl. Microbiol. Biotechnol.* 87, 925–941. doi: 10.1007/s00253-010-2649-5
- Feng, L., Casas, M. E., Ottosen, L. D. M., Möller, H. B., and Bester, K. (2017). Removal of antibiotics during the anaerobic digestion of pig manure. *Sci. Total Environ.* 603–604, 219–225. doi: 10.1016/j.scitotenv.2017.05.280
- Gao, J., and Pedersen, J. A. (2005). Adsorption of sulfonamide antimicrobial agents to clay minerals. *Environ. Sci. Technol.* 39, 9509–9516. doi: 10.1021/es050644c
- Gao, P., Wei, X., Gu, C., Wu, X., Xue, G., Shi, W., et al. (2015). Isolation and characterization of an erythromycin-degrading strain and application for bioaugmentation in a biological aerated filter. *Water. Air. Soil Pollut.* 226:190. doi: 10.1007/s11270-015-2449-8
- Ghirardini, A., Grillini, V., and Verlicchi, P. (2020). A review of the occurrence of selected micropollutants and microorganisms in different raw and treated manure – environmental risk due to antibiotics after application to soil. *Sci. Total Environ.* 707:136118. doi: 10.1016/j.scitotenv.2019.136118
- Gisi, D., Stucki, G., and Hanselmann, K. W. (1997). Biodegradation of the pesticide 4,6-dinitro-ortho-cresol by microorganisms in batch cultures and in fixed-bed column reactors. *Appl. Microbiol. Biotechnol.* 48, 441–448. doi: 10.1007/s002530051077
- Gold, R. S., Wales, M. E., Grimsley, J. K., and Wild, J. R. (2000). “Ancillary function of housekeeping enzymes: fortuitous degradation of environmental contaminants,” in *Enzymes in Action: Green Solutions for Chemical Problems*, eds B. Zwanenburg, M. Mikolajczyk, and P. Kielbasiński (Dordrecht: Springer Netherlands), 263–286. doi: 10.1007/978-94-010-0924-9\_13
- Gravuer, K., and Scow, K. M. (2021). Invader-resident relatedness and soil management history shape patterns of invasion of compost microbial populations into agricultural soils. *Appl. Soil Ecol.* 158:103795. doi: 10.1016/j.apsoil.2020.103795
- Hagey, J., Bhatnagar, S., Heguy, J. M., Karle, B. M., Price, P. L., Meyer, D., et al. (2019). Fecal microbial communities in a large representative cohort of California dairy cows. *Front. Microbiol.* 10:1093. doi: 10.3389/fmicb.2019.01093
- Haller, M. Y., Müller, S. R., McArdell, C. S., Alder, A. C., and Suter, M. J. F. (2002). Quantification of veterinary antibiotics (sulfonamides and trimethoprim) in animal manure by liquid chromatography-mass spectrometry. *J. Chromatogr. A* 952, 111–120. doi: 10.1016/S0021-9673(02)00083-3
- Hammesfahr, U., Bierl, R., and Thiele-Bruhn, S. (2011). Combined effects of the antibiotic sulfadiazine and liquid manure on the soil microbial-community structure and functions. *J. Plant Nutr. Soil Sci.* 174, 614–623. doi: 10.1002/jpln.201000322
- Hawkshead, J. (2008). Hospital wastewater containing pharmaceutically active compounds and drug-resistant organisms: a source of environmental toxicity and increased antibiotic resistance. *J. Residuals Sci. Technol.* 5, 51.
- Heuer, H., Schmitt, H., and Smalla, K. (2011). Antibiotic resistance gene spread due to manure application on agricultural fields. *Curr. Opin. Microbiol.* 14, 236–243. doi: 10.1016/j.mib.2011.04.009
- Hirth, N., Topp, E., Dörfler, U., Stupperich, E., Munch, J. C., and Schroll, R. (2016). An effective bioremediation approach for enhanced microbial degradation of the veterinary antibiotic sulfamethazine in an agricultural soil. *Chem. Biol. Technol. Agr.* 3:29. doi: 10.1186/s40538-016-0080-6
- Hoa, P. T. P., Managaki, S., Nakada, N., Takada, H., Shimizu, A., Anh, D. H., et al. (2011). Antibiotic contamination and occurrence of antibiotic-resistant bacteria in aquatic environments of northern Vietnam. *Sci. Total Environ.* 409, 2894–2901. doi: 10.1016/j.scitotenv.2011.04.030
- Hong, Q., Zhang, Z., Hong, Y., and Li, S. (2007). A microcosm study on bioremediation of fenitrothion-contaminated soil using *Burkholderia* sp. FDS-1. *Int. Biodeter. Biodegr.* 59, 55–61. doi: 10.1016/j.ibiod.2006.07.013
- Janssen, D. B., Dinkla, I. J. T., Poelarends, G. J., and Terpstra, P. (2005). Bacterial degradation of xenobiotic compounds: evolution and distribution of novel enzyme activities. *Environ. Microbiol.* 7, 1868–1882. doi: 10.1111/j.1462-2920.2005.00966.x
- Karpouzias, D. G., and Walker, A. (2000). Factors influencing the ability of *Pseudomonas putida* ePI to degrade ethoprophos in soil. *Soil Biol. Biochem.* 32, 1753–1762. doi: 10.1016/S0038-0717(00)00093-6
- Kim, D.-W., Thawng, C. N., Lee, K., Wellington, E. M. H., and Cha, C.-J. (2019). A novel sulfonamide resistance mechanism by two-component flavin-dependent monooxygenase system in sulfonamide-degrading actinobacteria. *Environ. Int.* 127, 206–215. doi: 10.1016/j.envint.2019.03.046
- Kumar, M., Jaiswal, S., Sodhi, K. K., Shree, P., Singh, D. K., Agrawal, P. K., et al. (2019). Antibiotics bioremediation: perspectives on its ecotoxicity and resistance. *Environ. Int.* 124, 448–461. doi: 10.1016/j.envint.2018.12.065
- Kümmerer, K. (2001). Drugs in the environment: emission of drugs, diagnostic aids and disinfectants into wastewater by hospitals in relation to other sources—a review. *Chemosphere* 45, 957–969. doi: 10.1016/S0045-6535(01)00144-8
- Lamshöft, M., Sukul, P., Zühlke, S., and Spittler, M. (2007). Metabolism of <sup>14</sup>C-labelled and non-labelled sulfadiazine after administration to pigs. *Anal. Bioanal. Chem.* 388, 1733–1745. doi: 10.1007/s00216-007-1368-y
- Leng, Y., Bao, J., Chang, G., Zheng, H., Li, X., Du, J., et al. (2016). Biotransformation of tetracycline by a novel bacterial strain *Stenotrophomonas maltophilia* DT1. *J. Hazard. Mater.* 318, 125–133. doi: 10.1016/j.jhazmat.2016.06.053
- Lertpaitoonpan, W., Ong, S. K., and Moorman, T. B. (2009). Effect of organic carbon and pH on soil sorption of sulfamethazine. *Chemosphere* 76, 558–564. doi: 10.1016/j.chemosphere.2009.02.066
- Lin, B., Lyu, J., Lyu, X., Yu, H., Hu, Z., Lam, J. C. W., et al. (2015). Characterization of cefalexin degradation capabilities of two *Pseudomonas* strains isolated from activated sludge. *J. Hazard. Mater.* 282, 158–164. doi: 10.1016/j.jhazmat.2014.06.080
- Liu, F., Ying, G.-G., Tao, R., Zhao, J.-L., Yang, J.-F., and Zhao, L.-F. (2009). Effects of six selected antibiotics on plant growth and soil microbial and enzymatic activities. *Environ. Poll.* 157, 1636–1642. doi: 10.1016/j.envpol.2008.12.021
- Luo, Y., Mao, D., Rysz, M., Zhou, Q., Zhang, H., Xu, L., et al. (2010). Trends in antibiotic resistance genes occurrence in the Haihe River, China. *Environ. Sci. Technol.* 44, 7220–7225. doi: 10.1021/es100233w
- Malwal, S. R., Sriram, D., Yogeeswari, P., and Chakrapani, H. (2012). Synthesis and antimicrobial activity of prodrugs of sulfur dioxide (SO<sub>2</sub>). *Bioorg. Med. Chem. Lett.* 22, 3603–3606. doi: 10.1016/j.bmcl.2012.04.048
- Martin-Laurent, F., Marti, R., Waglechner, N., Wright, G. D., and Topp, E. (2014). Draft genome sequence of the sulfonamide antibiotic-degrading *Microbacterium* sp. strain C448. *Genome Announc.* 2, e1113–e1113. doi: 10.1128/genomeA.01113-13
- McDonald, D., Price, M. N., Goodrich, J., Nawrocki, E. P., DeSantis, T. Z., Probst, A., et al. (2012). An improved Greengenes taxonomy with explicit ranks for ecological and evolutionary analyses of bacteria and archaea. *ISME J.* 6, 610–618. doi: 10.1038/ismej.2011.139
- McKinney, C. W., Loftin, K. A., Meyer, M. T., Davis, J. G., and Pruden, A. (2010). tet and sul antibiotic resistance genes in livestock lagoons of various operation type, configuration, and antibiotic occurrence. *Environ. Sci. Technol.* 44, 6102–6109. doi: 10.1021/es9038165
- Mitchell, S. M., Ullman, J. L., Teel, A. L., and Watts, R. J. (2015). Hydrolysis of amphenicol and macrolide antibiotics: chloramphenicol, florfenicol, spiramycin, and tylosin. *Chemosphere* 134, 504–511. doi: 10.1016/j.chemosphere.2014.08.050
- Nawrocki, E. P., and Eddy, S. R. (2013). Infernal 1.1: 100-fold faster RNA homology searches. *Bioinformatics* 29, 2933–2935. doi: 10.1093/bioinformatics/btt509
- Nishiyama, M., Senoo, K., and Matsumoto, S. (1993). gamma-1,2,3,4,5,6-Hexachlorocyclohexane-assimilating bacterium, *Sphingomonas paucimobilis* strain SS86, in soil. *Soil Biol. Biochem.* 25, 769–774.
- Pei, R., Kim, S.-C., Carlson, K. H., and Pruden, A. (2006). Effect of river landscape on the sediment concentrations of antibiotics and corresponding antibiotic resistance genes (ARG). *Water Res.* 40, 2427–2435. doi: 10.1016/j.watres.2006.04.017
- Peng, X., Wang, Z., Kuang, W., Tan, J., and Li, K. (2006). A preliminary study on the occurrence and behavior of sulfonamides, ofloxacin and chloramphenicol antimicrobials in wastewaters of two sewage treatment plants in Guangzhou, China. *Sci. Total Environ.* 371, 314–322. doi: 10.1016/j.scitotenv.2006.07.001
- Perry, J., and Wright, G. (2013). The antibiotic resistance “mobilome”: searching for the link between environment and clinic. *Front. Microbiol.* 4:138. doi: 10.3389/fmicb.2013.00138
- Pesce, S., Ghiglione, J.-F., Topp, E., and Martin-Laurent, F. (2020). Editorial: microbial ecotoxicology. *Front. Microbiol.* 11:1342. doi: 10.3389/fmicb.2020.01342

- Pietramellara, G., Ascher-Jenull, J., Borgogni, F., Ceccherini, M. T., Guerri, G., and Nannipieri, P. (2008). Extracellular DNA in soil and sediment: fate and ecological relevance. *Biol. Fertil. Soils* 45, 219–235. doi: 10.1007/s00374-008-0345-8
- Pinna, M. V., Castaldi, P., Deiana, P., Pusino, A., and Garau, G. (2012). Sorption behavior of sulfamethazine on unamended and manure-amended soils and short-term impact on soil microbial community. *Ecotoxicol. Environ. Saf.* 84, 234–242. doi: 10.1016/j.ecoenv.2012.07.006
- Price, M. N., Dehal, P. S., and Arkin, A. P. (2010). FastTree 2-approximately maximum-likelihood trees for large alignments. *PLoS One* 5:e9490. doi: 10.1371/journal.pone.0009490
- Proia, L., Lupini, G., Osorio, V., Pérez, S., Barceló, D., Schwartz, T., et al. (2013). Response of biofilm bacterial communities to antibiotic pollutants in a Mediterranean river. *Chemosphere* 92, 1126–1135. doi: 10.1016/j.chemosphere.2013.01.063
- Rani, N. L., and Lalithakumari, D. (1994). Degradation of methyl parathion by *Pseudomonas putida*. *Can. J. Microbiol.* 40, 1000–1006. doi: 10.1139/m94-160
- Reichel, R., Michelini, L., Ghisi, R., and Sören, T.-B. (2015). Soil bacterial community response to sulfadiazine in the soil-root zone. *J. Plant Nutr. Soil Sci.* 178, 499–506. doi: 10.1002/jpln.201400352
- Reis, A. C., Kolvenbach, B. A., Chami, M., Gales, L., Egas, C., Corvini, P. F.-X., et al. (2019). Comparative genomics reveals a novel genetic organization of the sad cluster in the sulfonamide-degrader 'Candidatus *Leucobacter sulfamidivorax*' strain GP. *BMC Genom.* 20:885. doi: 10.1186/s12864-019-6206-z
- Reis, P., Reis, A., Ricken, B., Kolvenbach, B., Manaia, C., Corvini, P., et al. (2014). Biodegradation of sulfamethoxazole and other sulfonamides by *Achromobacter denitrificans* PR1. *J. Hazard. Mater.* 280, 741–749. doi: 10.1016/j.jhazmat.2014.08.039
- Ricken, B., Kolvenbach, B. A., Bergesch, C., Benndorf, D., Kroll, K., Strnad, H., et al. (2017). FMNH2-dependent monooxygenases initiate catabolism of sulfonamides in *Microbacterium* sp. strain BR1 subsisting on sulfonamide antibiotics. *Sci. Rep.* 7:15783. doi: 10.1038/s41598-017-16132-8
- Rodriguez-Mozaz, S., Vaz-Moreira, I., Varela Della Giustina, S., Llorca, M., Barceló, D., Schubert, S., et al. (2020). Antibiotic residues in final effluents of European wastewater treatment plants and their impact on the aquatic environment. *Environ. Int.* 140:105733. doi: 10.1016/j.envint.2020.105733
- Rognes, T., Flouri, T., Nichols, B., Quince, C., and Mahé, F. (2016). VSEARCH: a versatile open source tool for metagenomics. *PeerJ* 4:e2584. doi: 10.7717/peerj.2584
- Schmitt, H., Haapakangas, H., and van Beelen, P. (2005). Effects of antibiotics on soil microorganisms: time and nutrients influence pollution-induced community tolerance. *Soil Biol. Biochem.* 37, 1882–1892. doi: 10.1016/j.soilbio.2005.02.022
- Schmitt, H., van Beelen, P., Tolls, J., and van Leeuwen, C. L. (2004). Pollution-induced community tolerance of soil microbial communities caused by the antibiotic sulfachloropyridazine. *Environ. Sci. Technol.* 38, 1148–1153. doi: 10.1021/es034685p
- Shah, S. S. A., Rivera, G., and Ashfaq, M. (2013). Recent advances in medicinal chemistry of sulfonamides. Rational design as anti-tumoral, anti-bacterial and anti-inflammatory agents. *Mini Rev. Med. Chem.* 13, 70–86.
- Shan, J., Yang, P., Rahman, M. M., Shang, X., and Yan, X. (2018). Tetracycline and sulfamethazine alter dissimilatory nitrate reduction processes and increase N<sub>2</sub>O release in rice fields. *Environ. Poll.* 242, 788–796. doi: 10.1016/j.envpol.2018.07.061
- Sharma, B., Dangi, A. K., and Shukla, P. (2018). Contemporary enzyme based technologies for bioremediation: a review. *J. Environ. Manag.* 210, 10–22. doi: 10.1016/j.jenvman.2017.12.075
- Silva, V., Correia, S., Pereira, J. E., Igrejas, G., and Poeta, P. (2020). "Surveillance and environmental risk assessment of antibiotics and amr/args related with mrsa: one health perspective," in *Antibiotics and Antimicrobial Resistance Genes: Environmental Occurrence and Treatment Technologies*, ed. M. Z. Hashmi (Cham: Springer International Publishing), 271–295. doi: 10.1007/978-3-030-40422-2\_13
- Spor, A., Camargo, A. R. O., Bru, D., Gaba, S., Garmyn, D., Gal, L., et al. (2020). Habitat disturbances modulate the barrier effect of resident soil microbiota on *Listeria monocytogenes* invasion success. *Front. Microbiol.* 11:927. doi: 10.3389/fmicb.2020.00927
- Stoll, C., Sidhu, J. P. S., Tiehm, A., and Toze, S. (2012). Prevalence of clinically relevant antibiotic resistance genes in surface water samples collected from Germany and Australia. *Environ. Sci. Technol.* 46, 9716–9726. doi: 10.1021/es302020s
- Tappe, W., Herbst, M., Hofmann, D., Koeppchen, S., Kummer, S., Thiele, B., et al. (2013). Degradation of sulfadiazine by *Microbacterium lacus* strain SDZm4, isolated from lysimeters previously manured with slurry from sulfadiazine-medicated pigs. *Appl. Environ. Microbiol.* 79, 2572–2577. doi: 10.1128/AEM.03636-12
- Topp, E., Chapman, R., Devers-Lamrani, M., Hartmann, A., Marti, R., Martin-Laurent, F., et al. (2013). Accelerated biodegradation of veterinary antibiotics in agricultural soil following long-term exposure, and isolation of a sulfamethazine-degrading sp. *J. Environ. Qual.* 42, 173–178. doi: 10.2134/jeq2012.0162
- van Elsas, J. D., Chiurazzi, M., Mallon, C. A., Elhottová, D., Křišťůf, V., and Salles, J. F. (2012). Microbial diversity determines the invasion of soil by a bacterial pathogen. *Proc. Natl. Acad. Sci. U.S.A.* 109, 1159–1164. doi: 10.1073/pnas.1109326109
- van Veen, J. A., van Overbeek, L. S., and van Elsas, J. D. (1997). Fate and activity of microorganisms introduced into soil. *Microbiol. Mol. Biol. Rev.* 61, 121–135.
- Wang, Q., Garrity, G. M., Tiedje, J. M., and Cole, J. R. (2007). Naïve bayesian classifier for rapid assignment of rRNA sequences into the new bacterial taxonomy. *Appl. Environ. Microbiol.* 73, 5261–5267. doi: 10.1128/AEM.00062-07
- Watkinson, A., Murby, E. J., and Costanzo, S. (2007). Removal of antibiotics in conventional and advanced wastewater treatment: implications for environmental discharge and wastewater recycling. *Water Res.* 41, 4164–4176. doi: 10.1016/j.watres.2007.04.005
- Wei, Z., Feng, K., Li, S., Zhang, Y., Chen, H., Yin, H., et al. (2018). Exploring abundance, diversity and variation of a widespread antibiotic resistance gene in wastewater treatment plants. *Environ. Int.* 117, 186–195. doi: 10.1016/j.envint.2018.05.009
- Wise, E. M., and Abou-Donia, M. M. (1975). Sulfonamide resistance mechanism in *Escherichia coli*: R plasmids can determine sulfonamide-resistant dihydropteroate synthases. *Proc. Natl. Acad. Sci. U. S. A.* 72, 2621–2625. doi: 10.1073/pnas.72.7.2621
- Woappi, Y., Gabani, P., Singh, A., and Singh, O. V. (2016). Antibiotrophs: the complexity of antibiotic-subsisting and antibiotic-resistant microorganisms. *Crit. Rev. Microbiol.* 42, 17–30. doi: 10.3109/1040841X.2013.875982
- Xin, Z., Fengwei, T., Gang, W., Xiaoming, L., Qiuxiang, Z., Hao, Z., et al. (2012). Isolation, identification and characterization of human intestinal bacteria with the ability to utilize chloramphenicol as the sole source of carbon and energy. *FEMS Microbiol. Ecol.* 82, 703–712. doi: 10.1111/j.1574-6941.2012.01440.x
- Yun, M.-K., Wu, Y., Li, Z., Zhao, Y., Waddell, M. B., Ferreira, A. M., et al. (2012). Catalysis and sulfa drug resistance in dihydropteroate synthase. *Science* 335, 1110–1114. doi: 10.1126/science.1214641
- Zhang, J., Kobert, K., Flouri, T., and Stamatakis, A. (2014). PEAR: a fast and accurate illumina paired-end reAd mergeR. *Bioinforma. Oxf. Engl.* 30, 614–620. doi: 10.1093/bioinformatics/btt593
- Zhang, Y., Marrs, C. F., Simon, C., and Xi, C. (2009). Wastewater treatment contributes to selective increase of antibiotic resistance among *Acinetobacter* spp. *Sci. Total Environ.* 407, 3702–3706. doi: 10.1016/j.scitotenv.2009.02.013
- Zrimec, J. (2020). Multiple plasmid origin-of-transfer regions might aid the spread of antimicrobial resistance to human pathogens. *Microbiologyopen* 9:e1129. doi: 10.1002/mbo3.1129

**Conflict of Interest:** The authors declare that the research was conducted in the absence of any commercial or financial relationships that could be construed as a potential conflict of interest.

Copyright © 2021 Billet, Pesce, Rouard, Spor, Paris, Leremboure, Mounier, Besse-Hoggan, Martin-Laurent and Devers-Lamrani. This is an open-access article distributed under the terms of the Creative Commons Attribution License (CC BY). The use, distribution or reproduction in other forums is permitted, provided the original author(s) and the copyright owner(s) are credited and that the original publication in this journal is cited, in accordance with accepted academic practice. No use, distribution or reproduction is permitted which does not comply with these terms.



# Environmental Concentrations of Sulfonamides Can Alter Bacterial Structure and Induce Diatom Deformities in Freshwater Biofilm Communities

Laura Kergoat<sup>1</sup>, Pascale Besse-Hoggan<sup>2</sup>, Martin Leremboure<sup>2</sup>, Jérémie Beguet<sup>3</sup>, Marion Devers<sup>3</sup>, Fabrice Martin-Laurent<sup>3</sup>, Matthieu Masson<sup>1</sup>, Soizic Morin<sup>4</sup>, Amélie Roinat<sup>1</sup>, Stéphane Pesce<sup>1</sup> and Chloé Bonnineau<sup>1\*</sup>

<sup>1</sup> INRAE, UR RiverLy, Villeurbanne, France, <sup>2</sup> Université Clermont Auvergne, CNRS, Sigma Clermont, Institut de Chimie de Clermont-Ferrand, Clermont-Ferrand, France, <sup>3</sup> AgroSup Dijon, INRAE, Univ. Bourgogne Franche-Comté, Agroécologie, Dijon, France, <sup>4</sup> INRAE, UR EABX, Cestas, France

## OPEN ACCESS

### Edited by:

Obulisamy Parthiba Karthikeyan,  
University of Houston, United States

### Reviewed by:

Nikolina Udikovic-Kolic,  
Rudjer Boskovic Institute, Croatia  
Yuyi Yang,  
Chinese Academy of Sciences, China

### \*Correspondence:

Chloé Bonnineau  
chloe.bonnineau@inrae.fr

### Specialty section:

This article was submitted to  
Microbiotechnology,  
a section of the journal  
Frontiers in Microbiology

**Received:** 18 December 2020

**Accepted:** 22 February 2021

**Published:** 07 May 2021

### Citation:

Kergoat L, Besse-Hoggan P, Leremboure M, Beguet J, Devers M, Martin-Laurent F, Masson M, Morin S, Roinat A, Pesce S and Bonnineau C (2021) Environmental Concentrations of Sulfonamides Can Alter Bacterial Structure and Induce Diatom Deformities in Freshwater Biofilm Communities. *Front. Microbiol.* 12:643719. doi: 10.3389/fmicb.2021.643719

Since the early 1920s, the intensive use of antibiotics has led to the contamination of the aquatic environment through diffuse sources and wastewater effluents. The antibiotics commonly found in surface waters include sulfamethoxazole (SMX) and sulfamethazine (SMZ), which belong to the class of sulfonamides, the oldest antibiotic class still in use. These antibiotics have been detected in all European surface waters with median concentrations of around 50 ng L<sup>-1</sup> and peak concentrations of up to 4–6 µg L<sup>-1</sup>. Sulfonamides are known to inhibit bacterial growth by altering microbial production of folic acid, but sub-lethal doses may trigger antimicrobial resistance, with unknown consequences for exposed microbial communities. We investigated the effects of two environmentally relevant concentrations (500 and 5,000 ng L<sup>-1</sup>) of SMZ and SMX on microbial activity and structure of periphytic biofilms in stream mesocosms for 28 days. Measurement of sulfonamides in the mesocosms revealed contamination levels of about half the nominal concentrations. Exposure to sulfonamides led to slight, transitory effects on heterotrophic functions, but persistent effects were observed on the bacterial structure. After 4 weeks of exposure, sulfonamides also altered the autotrophs in periphyton and particularly the diversity, viability and cell integrity of the diatom community. The higher concentration of SMX tested decreased both diversity (Shannon index) and evenness of the diatom community. Exposure to SMZ reduced diatom species richness and diversity. The mortality of diatoms in biofilms exposed to sulfonamides was twice that in non-exposed biofilms. SMZ also induced an increase in diatom teratologies from 1.1% in non-exposed biofilms up to 3% in biofilms exposed to SMZ. To our knowledge, this is the first report on the teratological effects of sulfonamides on diatoms within periphyton. The increase of both diatom growth rate and mortality suggests a high renewal of diatoms under sulfonamide exposure. In conclusion, our

study shows that sulfonamides can alter microbial community structures and diversity at concentrations currently present in the environment, with unknown consequences for the ecosystem. The experimental set-up presented here emphasizes the interest of using natural communities to increase the ecological realism of ecotoxicological studies and to detect potential toxic effects on non-target species.

**Keywords:** periphyton, antibiotic, teratogenicity, microbial ecotoxicology, sulfamethazine, sulfamethoxazole

## INTRODUCTION

The number of scientific articles on the occurrence and impact of pharmaceutical residues in the environment has greatly increased since the early 2000s (Daughton, 2016), illustrating a growing concern with the wide dissemination of these biologically active substances in the environment and their potential impact on ecosystems. Pharmaceutical residues can reach freshwater ecosystems directly from aquaculture, run-off from agricultural soils amended with organic matter or from the effluents of wastewater treatment plants, pharmaceutical manufacturing plants and animal husbandry (Halling-Sørensen et al., 1998; Paíga et al., 2016; Mandaric et al., 2017). Numerous monitoring studies have shown the wide distribution of pharmaceutical products and their transformation products in European freshwaters at concentrations ranging from ng L<sup>-1</sup> up to µg L<sup>-1</sup>, with a high proportion of antibiotics (for more details, see the reviews of Carvalho and Santos, 2016; Szymańska et al., 2019).

The work reported here focuses on sulfonamides, one of the oldest antibiotic classes still in use for both animal and human health care. Sulfonamides are bacteriostatic compounds that inhibit the growth of microbial organisms (e.g., protozoa, fungi, certain bacteria; Straub, 2016) that rely on folate synthesis for the synthesis of purine and pyrimidine nucleotides (McDermott et al., 2003). The occurrence of sulfonamides in European surface waters is well documented (e.g., Kovalakova et al., 2020): in a review on environmental risk assessment of sulfamethoxazole, Straub (2016) found that in most studies, sulfamethoxazole concentrations in surface water were <286 ng L<sup>-1</sup> with a median of 52 ng L<sup>-1</sup> ( $n = 5,536$  surface water samples). A few measured environmental concentrations reached higher levels, up to 4 µg L<sup>-1</sup>, such concentrations being mainly found in streams where wastewater treatment plant effluents were released (Straub, 2016). Sulfamethazine concentrations in European freshwaters are in the range of those observed for sulfamethoxazole (see Figure 1 in Charuaud et al., 2019). However, this antibiotic has also been found at concentrations of up to 6 µg L<sup>-1</sup> in the Llobregat river (Spain) by Díaz-Cruz et al. (2008) and up to 12 µg L<sup>-1</sup> in a Croatian river receiving industrial waste water (Bielen et al., 2017).

A major concern regarding the general contamination of freshwaters (and other environmental compartments) by sulfonamides (and other antibiotics) is the increasing occurrence of microbial antibiotic resistance in the environment (Martin-Laurent et al., 2019). At sub-lethal doses, antibiotics exert a selection pressure that will promote the emergence and development of antibiotic resistance (for a complete review

on antibiotic resistance mechanisms, see McDermott et al., 2003). Resistance to sulfonamides is generally conferred by the acquisition of an enzyme insensitive to sulfonamides that restores the folic acid synthesis pathway (McDermott et al., 2003). This enzyme is encoded by *sul* genes (i.e., *sul1*, *sul2*, and *sul3*), generally found on a plasmid, which facilitates their dissemination by horizontal gene transfer across microbial communities (Sköld, 2000; Perreten and Boerlin, 2003). Antibiotic resistance genes are frequently detected in natural microbial communities (Martínez, 2008) in both periphytic biofilms (e.g., Di Cesare et al., 2017; Guo et al., 2018) and sediments (e.g., Marti et al., 2013; Czekalski et al., 2014; Calero-Cáceres et al., 2017) with higher levels being detected downstream from the discharge of effluents of wastewater treatment plants (Proia et al., 2016). The dissemination and occurrence of antibiotic resistance genes in aquatic ecosystems are likely to be a threat for environmental health and have led several authors to qualify antibiotic resistance genes as emerging contaminants (Sanderson et al., 2016; O'Flaherty and Cummins, 2017).

Besides their implication in the dissemination of antibiotic resistance genes, antibiotics could have a direct toxic impact on aquatic organisms. Ecotoxicity of sulfamethoxazole in a wide range of aquatic model species is well known, with 236 entries for NOEC (no observed effect concentration) in the ECOTOX database of US EPA (U.S. Environmental Protection Agency, 2019). Focusing on endpoints directly related to population dynamics (i.e., growth, reproduction, survival, etc.), sulfamethoxazole NOECs range from 5.9 µg L<sup>-1</sup> for the cyanobacterium *Synechococcus leopoliensis* to 253 mg L<sup>-1</sup> for the protist *Tetrahymena pyriformis* (reviewed by Straub, 2016). Information on sulfamethazine ecotoxicity is scarce, with only three entries available for NOEC in the ECOTOX database of US EPA. Yang et al. (2008) reported a NOEC of 1 mg L<sup>-1</sup> for the growth of the microalga *Pseudokirchneriella subcapitata*. De Liguoro et al. (2009) reported a NOEC of 50 mg L<sup>-1</sup> for the survival of the crustacean *Daphnia magna*. The distribution of species sensitivity toward sulfonamides underlines a high sensitivity of cyanobacteria and microbial communities to this antibiotic (Straub, 2016; Charuaud et al., 2019).

In aquatic environments, antibiotics are generally present at lower concentrations than those producing bactericidal or bacteriostatic effects. Even so, this does not rule out an ecotoxicological risk for chronically exposed communities. For example, sub-lethal concentrations of antibiotics may act as signaling molecules (e.g., “danger signal,” Moon et al., 2017) and trigger specific responses (e.g., biofilm formation, Linares et al., 2006) different from the effects of inhibitory



concentrations (Fajardo and Martínez, 2008). Environmental concentrations of antibiotics might therefore affect natural microbial communities, with possible consequences for microbial diversity and functions and thereby for ecosystem processes supported by those communities.

Among aquatic microbial communities, periphytic biofilms are complex communities composed of bacteria, microalgae, fungi and protozoa, among other organisms. In lotic ecosystems, they play an essential role in important ecological processes including primary production and nutrient recycling (Battin et al., 2016). Previous studies have shown that environmental concentrations of antimicrobial agents and/or antibiotics can modify aquatic biofilm structure (e.g., triclosan in Lawrence et al., 2015) and function (e.g., tetracycline on bacterial productivity, Quinlan et al., 2011; triclosan on phosphate uptake capacity, Proia et al., 2013b). Microbial exposure to sulfamethoxazole and/or sulfamethazine has been shown to reduce microbial activity and/or inhibit extracellular enzymatic activities in soil (e.g., Liu et al., 2009; Frková et al., 2020). However, only a few authors have investigated the specific effects of these antibiotics on aquatic microbial community structure and functions (Yergeau et al., 2010, 2012; Johansson et al., 2014; Paumelle et al., 2021). Johansson et al. (2014) showed that sulfamethoxazole concentrations higher than  $35 \mu\text{g L}^{-1}$  could trigger modifications in C source utilization in marine biofilm exposed for 4 days. Yergeau et al. (2010) showed that 8 weeks exposure to environmental concentrations of sulfonamides ( $0.5 \mu\text{g L}^{-1}$  of sulfamethoxazole or sulfamethazine) induced transcriptional changes in biofilm microbial communities. In a follow-up study, Yergeau et al. (2012) identified a negative impact of sulfamethoxazole on cyanobacteria abundance and on photosynthesis-related transcripts. Although sulfamethoxazole and sulfamethazine are structurally closely related and have the same modes of action, their effects on microbial communities are different in several ways (Yergeau et al., 2010, 2012).

Based on these findings, we made the following two hypotheses:

- (1) Environmentally relevant concentrations of sulfamethoxazole and sulfamethazine will directly affect the bacterial structure (by exerting selection pressure toward resistant species) and functions (by reducing microbial activities) of periphytic biofilm.
- (2) The ensuing changes to the bacterial community within the periphytic community will have indirect negative effects on the autotroph component.

To test these hypotheses, we investigated the effects of two levels of environmentally relevant concentrations of sulfamethazine (SMZ) and sulfamethoxazole (SMX), tested individually, on microbial activities and structure of natural periphytic biofilms cultivated in stream mesocosms for 28 days. The use of natural communities, such as periphytic biofilms, in controlled experiments is particularly useful for considering non-target species and biological interactions (Gessner and Tlili, 2016). This approach allowed us to increase the ecological realism of this ecotoxicological study. Microbial activities were assessed on a time scale by measuring functional parameters

of the heterotroph (extracellular enzymatic activities, microbial respiration) and autotroph (photosynthesis) components of the biofilm. Structural effects were studied at the end of the experiment by assessing the taxonomic structure of diatoms and the genetics of bacterial communities. After 28 days of exposure, the main effects of both sulfonamides were observed on bacterial structure and on the diversity, viability and cell integrity of the diatom community. In particular, exposure to SMZ induced an increase in diatom teratologies at both concentrations. Thus, our study shows that sulfonamides can alter microbial community structure and diversity at concentrations currently present in the environment.

## MATERIALS AND METHODS

### Biofilm Colonization

Natural biofilm was collected from the upstream Morcille river (Saint Joseph,  $46^{\circ}10'39.1''\text{N}$   $4^{\circ}38'10.1''\text{E}$ ) where the absence of any sulfonamide contamination in the sediment had previously been confirmed ( $[\text{SMX}] < 0.035 \text{ ng g}^{-1}$ ;  $[\text{SMZ}] < 0.005 \text{ ng g}^{-1}$ ). Biofilm was scraped from about 30 medium-sized stones and resuspended in river water before inoculation in aquaria to colonize glass slides ( $7.6 \text{ cm} \times 2.5 \text{ cm}$ ) for 22 days. Aquaria were filled with a mixture of demineralized water:groundwater (2:1 v/v, local groundwater used in previous experiments: Mahamoud Ahmed et al., 2018; Pesce et al., 2018) supplemented with  $\text{K}_2\text{HPO}_4$  solution ( $0.1 \text{ mg L}^{-1}$ ). A submersible pump (NEWA Jet 600) ensured water recirculation in each aquarium, which was exposed to a stable temperature ( $20^{\circ}\text{C}$ ) and natural light.

### Mesocosm Experiment

The experiment was performed in 15 glass indoor channels (length  $\times$  width  $\times$  height =  $83 \times 10.5 \times 10 \text{ cm}$ ) previously described (Supplementary Figure S1; Mahamoud Ahmed et al., 2018). The bottom of each channel was covered with 28 glass slides previously colonized by biofilm and filled with 10 L of recirculating water (2:1 v/v demineralized water:groundwater). Flow rate and temperature conditions were similar to those described above. Light-emitting diodes (Radiometrix modules, total luminous flux 25116 lm) provided stable light conditions (12/12 h light/dark photoperiod). Light intensity was recorded every hour by a data logger (HOBO® Pendant Temperature/light, Prosensor).

Three channels were exposed independently to one of the five different treatments tested:

1. Control: biofilm without antibiotic;
2. SMX: biofilm exposed to SMX at  $500 \text{ ng L}^{-1} = 126 \mu\text{M}$ ;
3. SMX+: biofilm exposed to SMX at  $5,000 \text{ ng L}^{-1} = 1,266 \mu\text{M}$ ;
4. SMZ: biofilm exposed to SMZ at  $500 \text{ ng L}^{-1} = 139 \mu\text{M}$ ;
5. SMZ+: biofilm exposed to  $5,000 \text{ ng L}^{-1} = 1,391 \mu\text{M}$ .

These sulfonamide concentrations of 500 and  $5,000 \text{ ng L}^{-1}$  were chosen to reflect environmental concentrations (Deng et al., 2018). Antibiotic stock solutions of SMX (Sigma Aldrich, No-CAS: 723-46-6) or SMZ (Sigma Aldrich, No-CAS: 57-68-1) were

prepared in water (2:1 v/v demineralized water:groundwater) and frozen at  $-20^{\circ}\text{C}$  (final concentration:  $16.5\text{ mg L}^{-1}$ ) before contamination.

To limit antibiotic loss by adsorption on the abiotic surfaces during the experiment, the experimental material was exposed to the corresponding concentrations of antibiotics for 4 days before the experiment started. Biofilm exposure to the five different treatments was then conducted for 4 weeks, and water was renewed every week using demineralized water:groundwater (2:1 v/v) phosphate-supplemented with  $\text{K}_2\text{HPO}_4$  (final concentration  $0.1\text{ mg L}^{-1}$ ) and contaminated or not by SMX or SMZ according to the treatment.

## Water Analyses

Physical and chemical parameters of water from each channel were measured each week before water renewal. Dissolved oxygen, conductivity, pH and temperature were quantified using portable meters (WTW, Germany). Water samples were collected to determine the concentrations of silicon dioxide ( $\text{SiO}_2$ ) according to NF T 90-007 and of chloride ( $\text{Cl}^-$ ), sulfate ( $\text{SO}_4^{2-}$ ), nitrite ( $\text{NO}_2^-$ ), nitrate ( $\text{NO}_3^-$ ) and orthophosphate ( $\text{PO}_4^{3-}$ ) ions according to EN ISO 10304-1.

Water samples (1 L) were also collected each week in each channel before water renewal and kept at  $-20^{\circ}\text{C}$  before analyses of SMX and SMZ dissolved concentrations. The pH of a 100 mL water sample was adjusted to  $4.0 \pm 0.2$  with HCl and 50  $\mu\text{L}$  of 500  $\mu\text{g L}^{-1}$  SMX- $\text{d}_4$  and SMZ- $\text{d}_4$  solutions (Toronto Research Chemicals and LGC standards, respectively) was added. The sample was then concentrated 200-fold on an Oasis HLB-200 mg cartridge (Waters<sup>TM</sup>) according to the manufacturer's recommendations (elution solvent methanol). The SMX and SMZ concentrations were determined by LC/ESI-MS on a Thermo Scientific UHPLC Ultimate 3000 RSLC coupled to an Orbitrap Q-Exactive Analyzer. The analyses were carried out in positive mode. The UHPLC was equipped with a Luna Omega Polar C18 column;  $100 \times 2.1\text{ mm}$ ;  $1.6\text{ }\mu\text{m}$  (Phenomenex) at  $30^{\circ}\text{C}$  with acetonitrile gradient + 0.1% formic acid (Solvent A) and water + 0.1% formic acid (Solvent B): 0–2.5 min: 30–64.5% A (linear); 2.5–2.6 min: 64.5–99% A (linear); 2.6–5 min: 99% A; 5–5.1 min: 99–30% A; 5.1–8 min: 30% A, flow rate  $0.45\text{ mL min}^{-1}$ . For the mass spectrometer, gaseous  $\text{N}_2$  was used as nebulizer gas (50 A.U.). The spray voltage was 3.0 kV.

## Biofilm Sampling

Biofilm was sampled before exposure (Day 0) and after 7, 14, 21, 28 days of exposure. For this purpose, glass slides were collected before weekly water renewal and then scraped with a razor blade. The detached biofilm was suspended in a known volume of demineralized water:groundwater (2:1 v/v). On the day of sampling, the measurements of exo-enzymatic activities, respiration, photosynthetic yield and chlorophyll *a* concentrations were directly made on fresh biofilms. Biofilm suspension was kept either frozen to determine bacterial community structure or with preservatives to determine algal composition and diatom taxonomy as described below.

## Analyses of Microbial Community Functions

### Respiration

Respiration was assessed under aerobic conditions on Days 0, 14, and 28 (Foulquier et al., 2013). When necessary, biofilm suspensions were diluted down to 2,000  $\mu\text{g}$  of chlorophyll *a*  $\text{L}^{-1}$ . 10 mL of biofilm suspension was then placed in a glass flask hermetically closed and incubated for 3 h, in the dark, under gentle agitation, at  $20^{\circ}\text{C}$ . Carbon dioxide production was measured by gas chromatography (490 MicroGC, Agilent Technologies) after 4 h and 24 h of incubation at ambient temperature ( $20^{\circ}\text{C}$ ). Respiration was expressed in  $\text{nmol CO}_2\text{ cm}^{-2}\text{ h}^{-1}$ .

### Exo-Enzymatic Activities

At Days 0, 7, 14, 21, and 28, potential activities of three extracellular enzymes ( $\beta$ -glucosidase EC 3.2.1.21, phosphatase EC 3.1.3.1, and leucine aminopeptidase EC 3.4.11.1) were measured by fluorimetry using substrate analogs coupled with a fluorochrome: MUF-Glu (4-methylumbelliferyl- $\beta$ -D-glucopyranoside M3633 Sigma-Aldrich, CAS No. 18997-57-4) for  $\beta$ -glucosidase, MUF-Pho (4-methylumbelliferyl-phosphate M8883 Sigma-Aldrich, CAS No. 3368-04-5) for phosphatase, and MCA-Leu (L-leucine-7 amido-4-methylcoumarin hydrochloride L2145 Sigma-Aldrich, CAS No. 62480-44-8.) for leucine aminopeptidase (Romani et al., 2004; Pesce et al., 2018). Enzyme activities were measured for a range of substrate concentrations (0–3,000  $\mu\text{M}$  for MUF-Glu and MUF-Pho, 0–2,000  $\mu\text{M}$  for MCA-Leu) to ensure activity measurement at optimal substrate concentration. When necessary, biofilm suspension was diluted down to 650  $\mu\text{g L}^{-1}$  of chlorophyll *a*. In a 96-well microplate, 70  $\mu\text{L}$  of substrate and 150  $\mu\text{L}$  of biofilm suspension were mixed and incubated at  $15^{\circ}\text{C}$  for 3 h 45 min. To stop the enzyme reaction, 20  $\mu\text{L}$  of glycine buffer (0.05 M glycine, 0.2 M  $\text{NH}_4\text{OH}$ , pH 10.4) was added. Fluorescence was then measured with a microplate reader (Synergy HT BioTek Instruments) with excitation wavelength 360 nm and emission wavelength 460 nm. To convert fluorescence values into enzymatic activities, standard curves of MUF (Sigma M1381 CAS No. 90-33-5) for  $\beta$ -glucosidase and phosphatase and MCA (Sigma A9891, CAS No. 26093-31-2) for leucine aminopeptidase were plotted at each time. Activities were expressed in nanomoles of hydrolyzed compound  $\text{h}^{-1}\text{ cm}^{-2}$ .

### Chlorophyll *a* Concentration and Photosystem II Activity

At Days 0, 7, 14, 21, and 28, 3 mL of fresh biofilm suspension was used to estimate chlorophyll *a* (chl *a*) concentration and photosynthetic efficiency by multi-wavelength pulse-amplitude-modulated (PAM) fluorimetry using a Phyto-PAM instrument (H. Walz, GmbH) (Schmitt-Jansen and Altenburger, 2008). Characterization of photosynthetic efficiency is based on the measurement of maximum photosynthetic yield of photosystem II ( $\Phi_{PSII}$ ). Biofilm samples were adapted for a few minutes to actinic light and two saturating pulses were done. Parameter  $\Phi_{PSII}$  was calculated according to Genty et al. (1989)

$\Phi PSII = \frac{F_m - F}{F_m}$  where  $F_m$  is the maximal fluorescence yield after the saturating pulse and  $F$  is the steady state of fluorescence.

## Analyses of Microbial Community Structure

### Algal Community Composition

The enumeration of cyanobacteria, green algae and diatom cells was performed at Days 0, 14, and 28. On the day of each sampling, 4 mL of biofilm suspension was mixed with 150  $\mu$ L of formol (37%) and stored at 4°C before analysis.

Samples were exposed to ultrasounds for 7 min for correct homogenization and 100  $\mu$ L was placed in a Nageotte counting cell. Counting was done for 10 microscopy fields (200 cells minimum). Density was expressed in cells  $\text{cm}^{-2}$  (Morin et al., 2010).

Diatom species were identified as described in Morin et al. (2017) in the samples collected at Days 0 and 28 ( $n = 3$  per treatment). Briefly, samples were exposed to boiling hydrogen peroxide (30%) and rinsed several times with distilled water. A few droplets were placed on slides and fixed with Naphtrax® (AFNOR NF EN 13946). Over 200 frustules per slide were counted (i.e., >600 individuals identified per treatment) and diversity indices (specific richness, Shannon, evenness) were calculated.

### Bacterial Community Structure

At Days 0, 7, 14, 21, and 28, 2 mL of biofilm suspension was centrifuged ( $6,500 \times g$ , 2 min, ambient temperature) and after removing the supernatant, the pellets were stored at  $-80^\circ\text{C}$ .

Total genomic DNA was extracted using FastDNA Spin kit for soil (MP Biomedicals, France) according to the manufacturer's instructions. Evolution of bacterial community structure was assessed using a molecular fingerprint technique based on the polymorphism length of the intergenic transcribed spacer (ITS) between rRNA 16S and 23S gene. Amplification by PCR adapted from Ranjard et al. (2001) coupled with an automated ribosomal intergenic spacer analysis (ARISA) was carried out. Amplification of the ITS 16S-23S region was performed using primers 5'-6-carboxyfluorescein (FAM)-labeled S-D-Bact-1552-b-S-20 (5'-TGCGGCTGGATCCCCCTCCTT-3') and L-D-Bact-132-a-A-18 (5'-CCGGGTTTCCCCATTCGG-3') (Normand et al., 1996). The reaction medium contained, in a total volume of 50  $\mu$ L: 5  $\mu$ L of  $10\times$  Taq reaction buffer (GE Healthcare), 200  $\mu$ M of each deoxynucleotide, 0.5  $\mu$ M of each primer, 5% dimethylsulfoxide, 0.5 U of rTaq DNA polymerase (illustra™ rTaq DNA Polymerase GE Healthcare), bovine serum albumin (Sigma, 0.3  $\text{mg}\cdot\text{mL}^{-1}$  final concentration) and 20 ng of DNA template. PCRs were obtained using a Thermal Cycler Tpersonal (Biometra, Göttingen, Germany) with the following program: initial denaturation at  $94^\circ\text{C}$  for 5 min, 35 cycles of denaturation (1 min at  $94^\circ\text{C}$ ), annealing (1 min at  $55^\circ\text{C}$ ), and extension (1 min at  $72^\circ\text{C}$ ) and a final extension at  $72^\circ\text{C}$  for 10 min. DNA fragments were separated with sequencer ABI 3730xl (BIOlidal, Vaulx-en-Velin). An internal size standard G1200LIZ (20–1,200 pb) was used to normalize the data.

### Quantification of Antibiotic Resistance Gene *sul1*

Before quantification of *sul1* and 16S rRNA sequence copy numbers, an inhibition test was carried out on each DNA sample as recommended by ISO 17601 (2016). qPCR reactions were carried out in a 15  $\mu$ L reaction volume in a ViiA7 (Life Technologies, United States). For each reaction, the qPCR mixture contained 7.5  $\mu$ L of Takyon MasterMix (Eurogentec, France), 1  $\mu$ M of each primer [*sul1* (51F: AAATGCTGCGAGTYGGMKCA and 280R: AACMACCAKCCCTRCAGTCCG, Wei et al. (2018); 16S rRNA primers according to Petrić et al. (2011)], 250 ng of T4 gene 32 (QBiogene, France), and 3 ng of DNA. The thermal cycling was performed as follows:  $95^\circ\text{C}$  for 10 min, 40 cycles of  $95^\circ\text{C}$  for 30 s, annealing at  $60^\circ\text{C}$  for 30 s and extension at  $72^\circ\text{C}$  for 30 s with data acquisition. A melting curve step was then run with 15 s at  $95^\circ\text{C}$ , 1 min at  $68^\circ\text{C}$  and then increase in temperature of  $0.5^\circ\text{C}\cdot\text{s}^{-1}$  to  $95^\circ\text{C}$  with data acquisition. Standard curves were obtained using serial dilutions of linearized plasmid containing *sul1* amplicon. For each treatment, three independent replicates were analyzed. qPCR assays were duplicated. For each assay, three non-template samples were included. qPCR results were expressed as log of relative abundance of *sul1* sequence copy number per 16S rRNA copy number.

### Data Analyses

Statistical analyses were performed with R software version 3.4.4 (R Core Team, 2020). Normality of the residuals and data homoscedasticity were checked using Shapiro-Wilk (Royston, 1982) and Fligner-Killeen (Conover et al., 1981) tests, respectively. For each sampling time, differences in microbial parameters between treatments were estimated by analysis of variance (ANOVA) followed by a Dunnett *post-hoc* test. Results were considered significant if  $p < 0.05$ .

ARISA electropherograms obtained after sequencing were analyzed using Peak Scanner Software (Applied Biosystems). To eliminate background noise, an “optimal divisor” (Osborne et al., 2006) of 1/1,000 was used. An abundance matrix of operational taxonomic units was obtained using the interactive biner script (Ramette, 2009).

For both diatoms and bacteria, abundance matrices were used to perform structure analyses. Distances between samples were represented by a non-multidimensional scaling (nMDS) based on a Bray Curtis dissimilarity index, using R package FactoMineR (Le et al., 2008). The stress value was calculated as an indicator of the agreement between the 2D projection and the predicted value from the regression following Clarke and Warwick (2001). To check whether the sample clustering observed on the nMDS plot was significant, an analysis of variance using distance matrices was performed (ADONIS test, 999 permutations, package Vegan: Oksanen et al., 2019).

## RESULTS

### Physico-Chemical Parameters

Throughout the experiment, physical and chemical parameters in the channels remained stable and similar between treatments



with mean values ( $n = 60$ ) of  $19.4 \pm 0.3^\circ\text{C}$  for water temperature,  $7.9 \pm 0.1$  for pH,  $180.5 \pm 5.9 \mu\text{S cm}^{-1}$  for conductivity and  $91.2 \pm 1.3\%$  for oxygen saturation. Most of these parameters were close to the characteristics of the sampling location in the Morcille river where pH was 7.3, oxygen saturation was 88.8%, and conductivity was  $136.8 \mu\text{S cm}^{-1}$  on the day of sampling. However, the water temperature was 4 times colder in the natural environment in January ( $5.1^\circ\text{C}$ ). Nutrient levels were also similar between treatments with mean values ( $n = 20$ ) of  $2.30 \pm 0.13 \text{ mg L}^{-1}$  for silica,  $2.78 \pm 0.16 \text{ mg L}^{-1}$  for nitrate and  $0.06 \pm 0.02 \text{ mg L}^{-1}$  for phosphate in water before addition to the channels (data not shown).

## SMZ and SMX Concentrations

Sulfonamide concentrations in channel water varied according to the active substance and the level of contamination (Table 1). At Day 7, SMX concentrations were higher than SMZ ones for both the low ( $\sim 220 \text{ ng SMX L}^{-1}$  vs.  $\sim 157 \text{ ng SMZ L}^{-1}$ ) and high ( $\sim 4,286 \text{ ng SMX L}^{-1}$  vs.  $\sim 2,780 \text{ ng SMZ L}^{-1}$ ) contamination levels. However, whatever the sulfonamide and the contamination level considered, measured concentrations were lower than the expected ones (i.e.,  $500 \text{ ng L}^{-1}$  and  $5,000 \text{ ng L}^{-1}$ , respectively). In the high concentration treatments (SMZ+ and SMX+), concentrations of both SMX and SMZ decreased continuously over time, with mean values of  $2,783 \text{ ng L}^{-1}$  and  $960 \text{ ng L}^{-1}$  at Day 28. SMZ and SMX concentrations were more stable in channels exposed to the nominal concentrations of  $500 \text{ ng L}^{-1}$  and were relatively similar for the two studied active substances at the end of the experiment ( $179.8 \pm 13.6 \text{ ng SMX L}^{-1}$  vs.  $186.1 \pm 104.0 \text{ ng SMZ L}^{-1}$ ).

**TABLE 1** | Sulfonamide concentrations measured in the water of the channels.

Treatments	Sulfonamide	Expected concentrations ( $\text{ng L}^{-1}$ )	Days	Measured concentrations ( $\text{ng L}^{-1}$ )
SMX	Sulfamethoxazole	500	7	$220.1 \pm 32.8$
SMX	Sulfamethoxazole	500	14	$204.1 \pm 21.6$
SMX	Sulfamethoxazole	500	21	$189.9 \pm 6.8$
SMX	Sulfamethoxazole	500	28	$179.8 \pm 13.6$
SMX+	Sulfamethoxazole	5000	7	$4285.8 \pm 266.9$
SMX+	Sulfamethoxazole	5000	14	$4135.8 \pm 310.7$
SMX+	Sulfamethoxazole	5000	21	$3189.4 \pm 74.7$
SMX+	Sulfamethoxazole	5000	28	$2783.0 \pm 129.4$
SMZ	Sulfamethazine	500	7	$157.2 \pm 13.1$
SMZ	Sulfamethazine	500	14	$105.8 \pm 48.8$
SMZ	Sulfamethazine	500	21	$156.2 \pm 61.7$
SMZ	Sulfamethazine	500	28	$186.1 \pm 104.0$
SMZ+	Sulfamethazine	5000	7	$2779.5 \pm 582.9$
SMZ+	Sulfamethazine	5000	14	$1011.5 \pm 192.7$
SMZ+	Sulfamethazine	5000	21	$1376.7 \pm 313.9$
SMZ+	Sulfamethazine	5000	28	$959.7 \pm 288.3$

Concentrations were measured every week of the 4-week experiment, before water renewal. Mean and standard deviations of measured SMX and SMZ concentrations (in  $\text{ng L}^{-1}$ ) are indicated ( $n = 3$ , per each treatment).

## Heterotrophic Microbial Community

Sulfonamide contamination had few effects on the measured bacterial parameters, and most of the observed functional changes in response to sulfonamide exposure were transient.

Microbial respiration was similar between treatments and increased over time from  $0.29 \pm 0.09 \text{ nmol cm}^{-2} \text{ h}^{-1}$  at Day 0 ( $n = 3$ ) to  $14.88 \pm 1.92$  at Day 14 and  $57.68 \pm 11.10 \text{ nmol cm}^{-2} \text{ h}^{-1}$  at Day 28 ( $n = 15$  channels, **Supplementary Table S2**).

Extra-cellular enzymatic activities exhibited various temporal trends independently of sulfonamide exposure (Table 2). The general trends observed were a decrease over time of microbial  $\beta$ -glucosidase activity (except at Day 14) and an increase over time of both phosphatase and leucine aminopeptidase activities. In unexposed biofilms (control),  $\beta$ -glucosidase activity was divided by almost 4 at the end of the experiment, while phosphatase activity was multiplied by 4 and leucine aminopeptidase by 6 (Table 2). In biofilms exposed to SMX or SMZ,  $\beta$ -glucosidase activity was mostly similar or lower than in unexposed biofilms. However, no significant difference ( $p > 0.05$ ) was found between treatments (Table 2). During the first 14 days of the experiment, phosphatase activity was significantly lower ( $p < 0.05$ ) in biofilms exposed to the sulfonamides tested than in unexposed biofilms (Table 2). In the last 14 days of exposure, phosphatase activity was slightly higher in biofilms exposed to the low and high concentrations of SMX than in unexposed biofilms ( $p < 0.05$  at Day 21, Table 2). After 14 days of exposure, leucine aminopeptidase activity was almost 2 times higher in biofilms exposed to low SMX and SMZ concentrations than in unexposed communities ( $p < 0.05$ ). However, this effect was transient, and no other significant difference was observed whatever the treatment or the sampling time (Table 2).

The antibiotic resistance gene *sul1* was detected in biofilms from all the treatments (including control). In all treatments, the relative abundance of *sul1* was similar, with an average of  $25.1 \pm 5.3$  *sul1* sequence copies per 1,000 16S rRNA sequence copy ( $n = 20$ , **Supplementary Figure S2**).

The ARISA performed after 28 days of exposure allowed retrieving 267 OTUs, bacterial community structure was slightly affected by the exposure to SMX and SMZ, at both the low and high concentrations (Figure 1). The permutational analysis of variance (ADONIS) shows that the exposure to sulfonamides explained 32% of the variance in the bacterial structure between samples ( $p < 0.01$ ) and indicated a significant difference in bacterial structure between control biofilms, biofilms exposed to SMX and biofilms exposed to SMZ.

## Phototrophic Microbial Community

Sulfonamide exposure did not affect the effective quantum yield of photosystem II, which was relatively stable over time and between treatments (e.g., average yield  $0.28 \pm 0.05$  at Day 28, **Supplementary Table S1**).

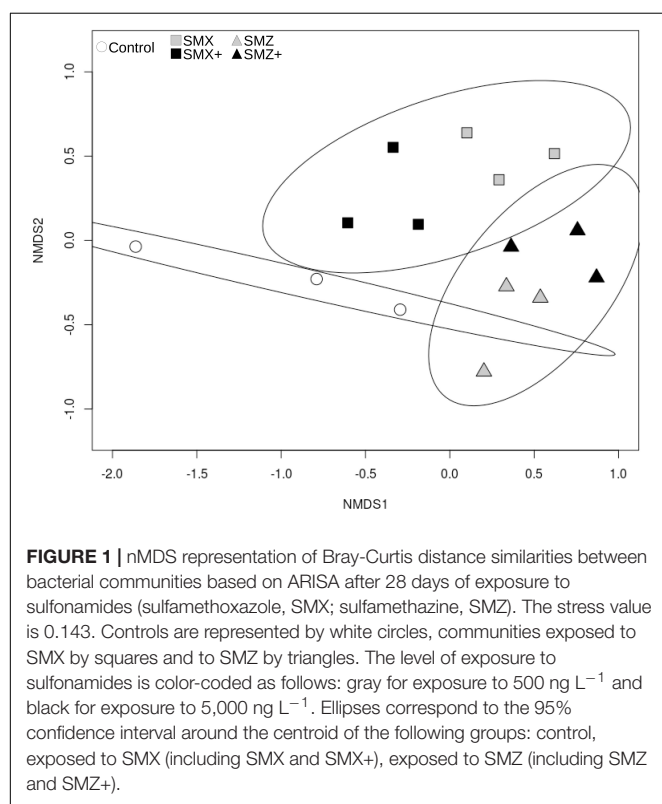
The relative proportions of the different algal groups (cyanobacteria, diatoms and green algae) were relatively constant over time and similar between treatments (Supplementary Figure S3). Nevertheless, cell densities of the different algal groups were different between treatments, with generally



**TABLE 2 |** Phosphatase and leucine aminopeptidase activities ( $\text{nmol MUF cm}^{-2} \text{ h}^{-1}$ ) of microbial communities non-exposed (control) and exposed to 500 or 5,000  $\text{ng L}^{-1}$  of sulfamethoxazole (SMX) or sulfamethazine (SMZ) over time.

Activity ( $\text{nmol MUF cm}^{-2} \text{ h}^{-1}$ )	Days	Control	SMX	SMX+	SMZ	SMZ+
$\beta$ -glucosidase	7	$10.08 \pm 3.63$	$7.95 \pm 3.22$	$5.01 \pm 2.72$	$4.26 \pm 2.31$	$10.39 \pm 1.95$
	14	$7.56 \pm 0.55$	$9.43 \pm 1.04$	$5.22 \pm 0.95$	$8.24 \pm 2.71$	$7.35 \pm 1.92$
	21	$7.60 \pm 3.34$	$4.16 \pm 2.19$	$2.43 \pm 0.55$	$6.00 \pm 3.13$	$4.27 \pm 1.34$
	28	$2.66 \pm 1.54$	$2.44 \pm 1.76$	$2.23 \pm 1.91$	$1.15 \pm 0.05$	$1.22 \pm 0.14$
Phosphatase	7	$12.57 \pm 0.73$	$7.21 \pm 0.40^*$	$11.02 \pm 0.84$	$6.18 \pm 1.45^*$	$9.34 \pm 1.17^*$
	14	$11.39 \pm 0.53$	$9.12 \pm 0.15^*$	$12.13 \pm 1.03$	$9.11 \pm 1.01^*$	$8.56 \pm 0.89^*$
	21	$14.01 \pm 0.88$	$17.99 \pm 1.35^*$	$17.42 \pm 0.93^*$	$13.45 \pm 2.22$	$13.34 \pm 0.84$
	28	$57.38 \pm 26.42$	$65.10 \pm 20.19$	$66.70 \pm 18.22$	$49.78 \pm 12.13$	$43.79 \pm 8.13$
Leucine aminopeptidase	7	$3.47 \pm 0.83$	$3.29 \pm 0.39$	$3.44 \pm 0.20$	$3.96 \pm 0.42$	$3.37 \pm 0.42$
	14	$4.35 \pm 0.07$	$7.43 \pm 0.31^*$	$4.17 \pm 0.37$	$9.08 \pm 1.97^*$	$3.14 \pm 0.27$
	21	$13.68 \pm 2.91$	$13.28 \pm 2.67$	$15.96 \pm 1.11$	$16.18 \pm 5.61$	$9.81 \pm 2.64$
	28	$20.52 \pm 4.49$	$19.64 \pm 5.52$	$16.58 \pm 1.78$	$17.85 \pm 3.86$	$21.30 \pm 4.41$

Mean  $\pm$  standard deviation of enzyme activities ( $\text{nmol MUF cm}^{-2} \text{ h}^{-1}$ ) measured in the different treatments are indicated ( $n = 3$  per treatment). Stars indicate significant differences between treatments and controls (Dunnett,  $p < 0.05$ ).



the highest cell densities observed in biofilms exposed to sulfonamides (**Figure 2**). Thus densities of cyanobacteria, diatoms and green algae were significantly higher ( $p < 0.05$ ) in biofilms exposed to the low and high concentrations of SMX at Day 14 than in control biofilms (**Figure 2**).

All the microbial communities in biofilm were dominated by diatoms, whatever the treatment (**Supplementary Figure S3** and **Figure 2**). Although sulfonamides did not have a clear effect on the structure of the diatom community (as

illustrated in the nMDS plot in **Supplementary Figure S4**), exposure to sulfonamides led to a decrease in diatom specific richness, diversity and evenness, depending on the treatment (**Table 3**). Exposure to low and high concentrations of SMZ significantly reduced the specific richness and the Shannon index ( $p < 0.05$ ) of the biofilm but no significant effect was observed on the evenness. Neither the low nor the high concentration of SMX had a significant effect on the specific richness, but exposure to the highest tested concentration of SMX significantly reduced both Shannon and evenness indices (**Table 3**).

The physiology and morphology of diatoms were also affected by sulfonamides (**Figure 3**). At Days 14 and 28, diatom mortality was significantly higher in biofilms exposed to SMX than in control biofilms ( $p < 0.05$ , **Figure 3A**) and a similar trend was observed at Day 28 for biofilms exposed to both concentrations of SMZ (significant result only for biofilm exposed to 5,000  $\text{ng L}^{-1}$ , **Figure 3B**). Diatom growth rates were also slightly higher in biofilms exposed to sulfonamides than in control biofilms despite the lack of significant difference (**Figure 3C**). In biofilms exposed to the highest sulfonamide concentrations tested, we observed an increase in the abundance of diatoms exhibiting deformities, in particular the abundance of teratological diatoms was more than 2 times higher in biofilms exposed to SMZ (reaching 3%) than in control biofilms (1.1%).

## DISCUSSION

Water contamination by environmentally realistic concentrations of SMZ and SMX affected both the heterotrophic and autotrophic communities of biofilms with various effects according to the sulfonamide and to the exposure level. Supporting our hypotheses, exposure to SMX, and to a lesser extent to SMZ, modified bacterial structure and impaired microbial enzyme functions. Moreover, sulfonamide exposure also had negative effects on the autotroph component of periphytic biofilm.

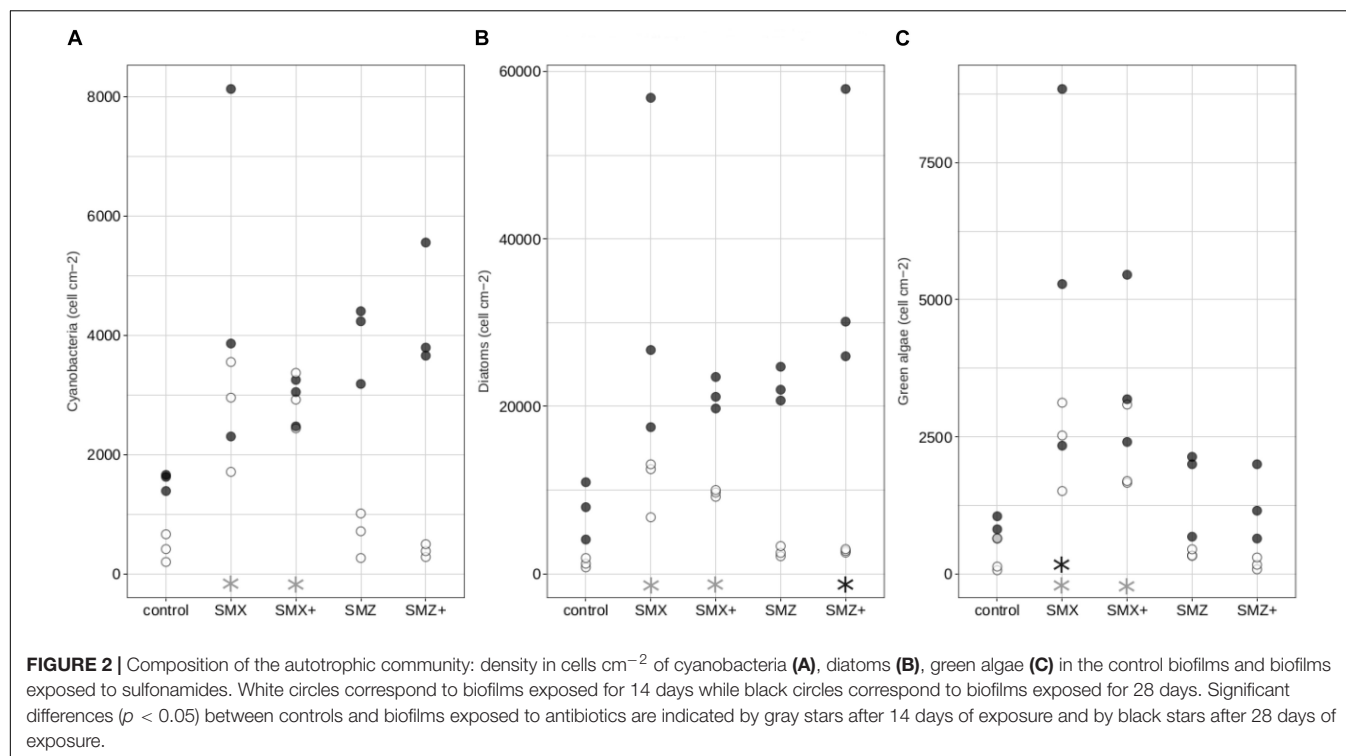


**TABLE 3 |** Structure and diversity of diatom community non-exposed (control) and exposed to 500 or 5,000  $\text{ng L}^{-1}$  of sulfamethoxazole (SMX) or sulfamethazine (SMZ) after 28 days or exposure, represented by diversity index (specific richness, Shannon, evenness).

Diversity index	Control	SMX	SMX+	SMZ	SMZ+
Specific richness	20.67 $\pm$ 1.08	16.67 $\pm$ 1.47	19.00 $\pm$ 2.55	15.00 $\pm$ 0.00*	13.67 $\pm$ 1.47*
Shannon	2.00 $\pm$ 0.10	1.77 $\pm$ 0.07	1.66 $\pm$ 0.16*	1.64 $\pm$ 0.07*	1.58 $\pm$ 0.04*
Evenness	0.65 $\pm$ 0.03	0.63 $\pm$ 0.03	0.56 $\pm$ 0.03*	0.61 $\pm$ 0.03	0.60 $\pm$ 0.01

Mean  $\pm$  standard deviation of diversity indices estimated in the different treatments are indicated ( $n = 3$  per treatment). Stars indicate significant differences between treatments and controls (Dunnnett,  $p < 0.05$ ).

Concerning the heterotrophic component of the biofilm, both sulfonamides modified phosphatase and leucine aminopeptidase extracellular enzyme activities in the first weeks of exposure, with no effect on  $\beta$ -glucosidase activity. Nevertheless, these effects were transient: after 4 weeks of exposure, all the measured extracellular enzymatic activities recovered and were similar between control communities and communities exposed to sulfonamides. Together with this functional recovery, small changes in the structure of the bacterial communities exposed to sulfonamides were also observed. These results suggest first a direct effect of the sulfonamides on the exposed communities, resulting in impairment of the bacterial functions as already observed in soil microbial communities exposed to SMX (Liu et al., 2016) or in biofilm exposed to river water strongly contaminated by pharmaceutical residues including antibiotics (Proia et al., 2013a). In addition, the functional recovery observed after 4 weeks of exposure, together with the changes in bacterial community structure, suggests that sulfonamide exposure acted as a selection pressure on the microbial communities, selecting the most tolerant species able to maintain the reference level of extracellular enzyme activities on exposure to sulfonamides.

Previous studies highlighted the impact of environmentally realistic levels of antibiotics, including sulfonamides, on the bacterial structure in soil (Liu et al., 2016), sediments (own unpublished results), or biofilm (Proia et al., 2013a).

In our study, bacterial structural changes following sulfonamide exposure were not associated with a higher relative abundance of the *sul1* resistance gene in microbial communities exposed to sulfonamides than in controls. The level of this antibiotic resistance gene remained stable throughout the experiment. This result is in agreement with the observation of Subirats et al. (2018) who found no significant difference in the relative abundance of *sul1* genes between control biofilms and biofilms exposed to a mixture of five contaminants, including sulfamethoxazole, at 0.1  $\text{mg L}^{-1}$  each (methylparaben, ciprofloxacin, diclofenac, erythromycin and sulfamethoxazole) for 28 days in mesocosms. To go beyond the community capacity to resist antibiotics (assessed here by the relative abundance of *sul1* gene in the total bacterial community) and to validate the above hypothesis of the selection of the most tolerant species, it would be of interest to assess the functional resistance of the community to the acute toxicity of antibiotics through

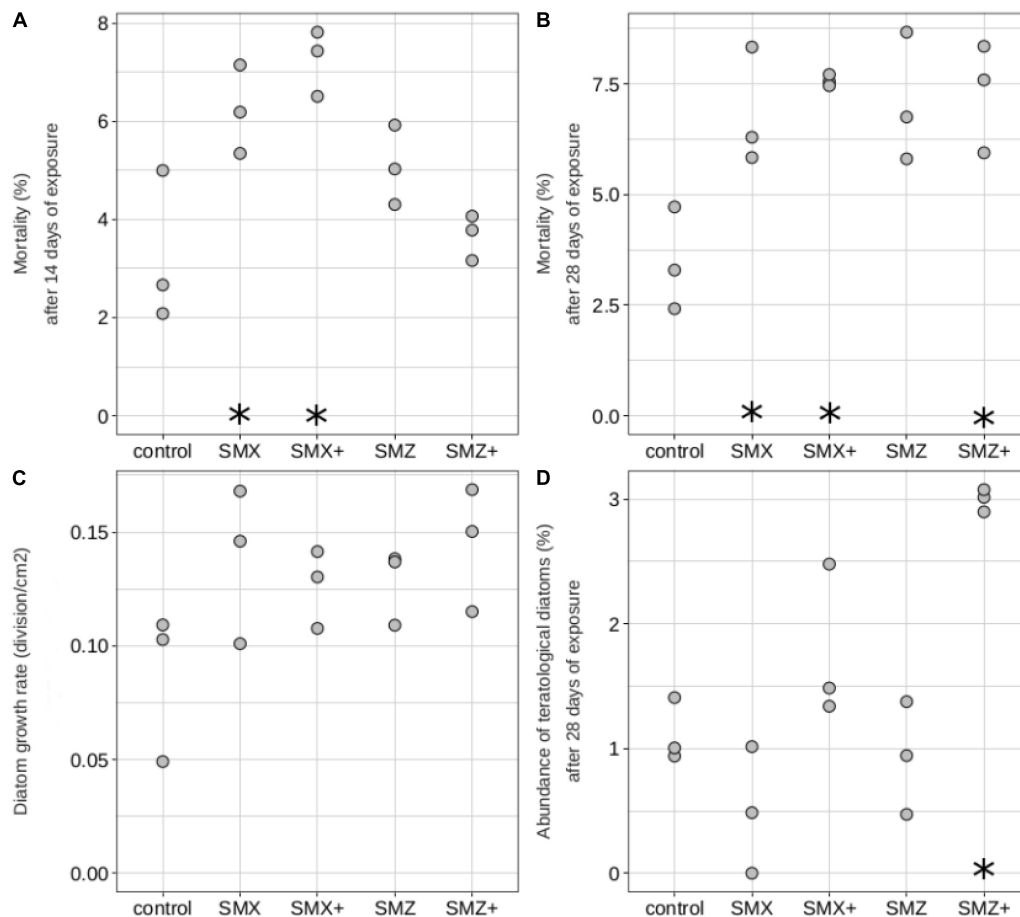


**FIGURE 3 |** Diatoms mortality (in%, on Day 14: **A**, and on Day 28: **B**), diatom growth rate (in division cm<sup>-2</sup>, **C**), abundance of teratological diatoms (in%, on Day 28: **D**) of biofilms non-exposed (control) and exposed to sulfamethoxazole (500 ng L<sup>-1</sup>: SMX, 5,000 ng L<sup>-1</sup>: SMX+) or sulfamethazine (500 ng L<sup>-1</sup>: SMZ, 5,000 ng L<sup>-1</sup>: SMZ+). Significant differences ( $p < 0.05$ ) between controls and biofilms exposed to antibiotics are indicated by stars.

pollution-induced community tolerance (PICT) measurements based on short-term toxicity tests (e.g., Corcoll et al., 2014).

Concerning the autotrophic component of the biofilm, the exposure to both sulfonamides led to an increase in cell density and diatom mortality with no impact on the autotrophic community structure based on the relative distribution of the main groups (i.e., diatoms, cyanobacteria and green algae). This stimulatory effect of low concentrations of SMX on algal growth has been previously observed in marine biofilms exposed to SMX (Johansson et al., 2014) and may be a consequence of temporarily decreased fitness of the heterotrophic compartment (e.g., Proia et al., 2011). The higher cell density observed in biofilm communities exposed to sulfonamides in our experiment is therefore likely to be due to the presence of tolerant species with high competitive abilities. The higher mortality values in these communities may reflect the presence and elimination of the sensitive species following SMX/SMZ exposure.

Sulfonamides did not affect only microalgal growth dynamics but also diatom morphology, since the percentage of teratologies was higher in communities exposed to the highest concentration

of sulfonamides tested than in non-exposed ones. Metals are known to induce deformities in diatoms (e.g., Lavoie et al., 2017; Tiam et al., 2019), but to our knowledge, this is the first report of a teratogenic effect of antibiotics on diatoms. There is no evidence in the literature that sulfonamides can directly cause diatom deformities, and the teratogenic effects of sulfamethoxazole exposure observed in our experiment could be due to indirect effects. The higher diatom mortality and cell density in exposed communities than in non-exposed ones suggest a higher renewal rate of diatom cells in those exposed communities. This higher renewal rate could be the result of greater growth rates of teratological individuals over normal ones (Coquillé and Morin, 2019).

The observed effects of sulfonamides on non-target species, such as diatoms, may also result from interactions between microalgae and bacteria within the periphytic biofilm. Indeed, previous studies have highlighted the tight link between these two complementary groups (e.g., in the carbon cycle: Battin et al., 2016), and the repercussion of direct toxic effects on one group to another (non-target) one (e.g., after exposure to the bactericide triclosan: Proia et al., 2011). The direct effect

of sulfonamides on bacteria may also change the heterotrophic community composition and the quality of bacterial exudates for microalgae and then lead to alterations in the morphology and survival of diatoms. Since Windler et al. (2014) showed that the absence of essential accompanying bacteria in laboratory cultures induced teratologies in diatoms, we can hypothesize that the structural changes in bacterial structure induced by sulfonamides led to the observed increase in diatom deformities. Further experiments are needed to better understand how sulfonamides might modulate microalgae-bacteria interactions within biofilms.

Altogether, our results highlight that even low concentrations of antibiotics can modify, at least transiently, microbial community structure and functions.

## CONCLUSION

Sulfamethazine and sulfamethoxazole had similar effects on biofilm communities after 4 weeks of chronic exposure to nominal concentrations of 500 and 5,000 ng L<sup>-1</sup>, with exposure to the higher concentration generally resulting in stronger effects. Exposure to sulfonamides mainly affected bacterial structure within the heterotrophic component of biofilm. In the autotrophic compartment, those two antibiotics particularly affected the dominant algal component (diatoms), by increasing their mortality and inducing teratologies at the higher of the two concentrations tested. Our study shows that sulfonamides are susceptible to alter microbial community structure and diversity at concentrations frequently found in the environment. In particular, non-target species such as diatoms are likely to be affected by contamination by sulfonamides, with unknown functional consequences for the ecosystem.

## DATA AVAILABILITY STATEMENT

The raw data supporting the conclusions of this article will be made available by the authors, without undue reservation.

## REFERENCES

- Battin, T. J., Besemer, K., Bengtsson, M. M., Romani, A. M., and Packmann, A. I. (2016). The ecology and biogeochemistry of stream biofilms. *Nat. Rev. Microbiol.* 14, 251–263. doi: 10.1038/nrmicro.2016.15
- Bielen, A., Šimatović, A., Kosić-Vukšić, J., Senta, I., Ahel, M., Babić, S., et al. (2017). Negative environmental impacts of antibiotic-contaminated effluents from pharmaceutical industries. *Water Res.* 126, 79–87. doi: 10.1016/j.watres.2017.09.019
- Calero-Cáceres, W., Méndez, J., Martín-Díaz, J., and Muniesa, M. (2017). The occurrence of antibiotic resistance genes in a Mediterranean river and their persistence in the riverbed sediment. *Environ. Pollut.* 223, 384–394. doi: 10.1016/j.envpol.2017.01.035
- Carvalho, I. T., and Santos, L. (2016). Antibiotics in the aquatic environments: a review of the European scenario. *Environ. Int.* 94, 736–757. doi: 10.1016/j.envint.2016.06.025
- Charuau, L., Jarde, E., Jaffrezic, A., Thomas, M.-F., and Le Bot, B. (2019). Veterinary pharmaceutical residues from natural water to tap water: sales, occurrence and fate. *J. Hazard. Mater.* 361, 169–186. doi: 10.1016/j.jhazmat.2018.08.075

## AUTHOR CONTRIBUTIONS

CB and SP designed the experiment with the help of LK and AR. LK and AR led the experimental work during mesocosm exposure. PB-H, LK, and ML did the chemical analyses of sulfonamides. MM did the analyses of major ions in water surface. LK, AR, and CB did the functional microbial analyses. LK did the DNA extraction. FM-L, MD, and JB did the quantification of *sul1* genes. SM did all the analyses of algal community composition. LK and CB did the data treatment, statistical analyses, and wrote the first version of the manuscript. SP, FM-L, PB-H, and SM reviewed, completed, and improved the first version of the manuscript. All authors contributed to the article and approved the submitted version.

## FUNDING

This study was supported by the ANTIBIOTOX project (contract no ANR-17-CE34-0003) funded by the ANR (Agence Nationale de la Recherche).

## ACKNOWLEDGMENTS

We thank Bernadette Volat, Bernard Motte, Anaïs Charton, and Christophe Rosy for their participation in experiment maintenance, sampling, and analysis.

## SUPPLEMENTARY MATERIAL

The Supplementary Material for this article can be found online at: <https://www.frontiersin.org/articles/10.3389/fmicb.2021.643719/full#supplementary-material>

- Clarke, K. R., and Warwick, R. M. (2001). A further biodiversity index applicable to species lists: variation in taxonomic distinctness. *Mar. Ecol. Prog. Ser.* 216, 265–278. doi: 10.3354/meps216265
- Conover, W. J., Johnson, M. E., and Johnson, M. M. (1981). A comparative study of tests for homogeneity of variances, with applications to the outer continental shelf bidding data. *Technometrics* 23, 351–361. doi: 10.1080/00401706.1981.10487680
- Coquillé, N., and Morin, S. (2019). Fitness of teratological morphotypes and heritability of deformities in the diatom *Gomphonema gracile*. *Ecol. Indic.* 106:105442. doi: 10.1016/j.ecolind.2019.105442
- Corcoll, N., Acuña, V., Barceló, D., Casellas, M., Guasch, H., Huerta, B., et al. (2014). Pollution-induced community tolerance to non-steroidal anti-inflammatory drugs (NSAIDs) in fluvial biofilm communities affected by WWTP effluents. *Chemosphere* 112, 185–193.
- Czekalski, N., Gascón, D., and Bürgmann, H. (2014). Wastewater as a point source of antibiotic-resistance genes in the sediment of a freshwater lake. *ISME J.* 8, 1381–1390. doi: 10.1038/ismej.2014.8
- Daughton, C. G. (2016). Pharmaceuticals and the environment (PiE): evolution and impact of the published literature revealed by bibliometric analysis. *Sci. Total Environ.* 562, 391–426. doi: 10.1016/j.scitotenv.2016.03.109



- De Liguoro, M., Fioretto, B., Poltronieri, C., and Gallina, G. (2009). The toxicity of sulfamethazine to *Daphnia magna* and its additivity to other veterinary sulfonamides and trimethoprim. *Chemosphere* 75, 1519–1524. doi: 10.1016/j.chemosphere.2009.02.002
- Deng, Y., Li, B., and Zhang, T. (2018). Bacteria that make a meal of sulfonamide antibiotics: blind spots and emerging opportunities. *Environ. Sci. Technol.* 52, 3854–3868. doi: 10.1021/acs.est.7b06026
- Di Cesare, A., Eckert, E. M., Rogora, M., and Corno, G. (2017). Rainfall increases the abundance of antibiotic resistance genes within a riverine microbial community. *Environ. Pollut.* 226, 473–478. doi: 10.1016/j.envpol.2017.04.036
- Díaz-Cruz, M. S., García-Galán, M. J., and Barceló, D. (2008). Highly sensitive simultaneous determination of sulfonamide antibiotics and one metabolite in environmental waters by liquid chromatography–quadrupole linear ion trap–mass spectrometry. *J. Chromatogr. A* 1193, 50–59. doi: 10.1016/j.chroma.2008.03.029
- Fajardo, A., and Martínez, J. L. (2008). Antibiotics as signals that trigger specific bacterial responses. *Curr. Opin. Microbiol.* 11, 161–167. doi: 10.1016/j.mib.2008.02.006
- Foulquier, A., Volat, B., Neyra, M., Bornette, G., and Montuelle, B. (2013). Long-term impact of hydrological regime on structure and functions of microbial communities in riverine wetland sediments. *FEMS Microbiol. Ecol.* 85, 211–226. doi: 10.1111/1574-6941.12112
- Frková, Z., Vystavna, Y., Koubová, A., Kotas, P., Grabicová, K., Grabic, R., et al. (2020). Microbial responses to selected pharmaceuticals in agricultural soils: microcosm study on the roles of soil, treatment and time. *Soil Biol. Biochem.* 149:107924. doi: 10.1016/j.soilbio.2020.107924
- Genty, B., Briantais, J. M., and Baker, N. R. (1989). The relationship between the quantum yield of photosynthetic electron transport and quenching of chlorophyll fluorescence. *Biochim. Biophys. Acta* 990, 87–92. doi: 10.1016/s0304-4165(89)80016-9
- Gessner, M. O., and Tilili, A. (2016). Fostering integration of freshwater ecology with ecotoxicology. *Freshwater Biol.* 61, 1991–2001. doi: 10.1111/fwb.12852
- Guo, X.-P., Yang, Y., Lu, D.-P., Niu, Z.-S., Feng, J.-N., Chen, Y.-R., et al. (2018). Biofilms as a sink for antibiotic resistance genes (ARGs) in the Yangtze estuary. *Water Res.* 129, 277–286. doi: 10.1016/j.watres.2017.11.029
- Halling-Sørensen, B., Nors Nielsen, S., Lanzky, P. F., Ingerslev, F., Holten Lützhøft, H. C., and Jørgensen, S. E. (1998). Occurrence, fate and effects of pharmaceutical substances in the environment – a review. *Chemosphere* 36, 357–393. doi: 10.1016/s0045-6535(97)00354-8
- Johansson, C. H., Janmar, L., and Backhaus, T. (2014). Toxicity of ciprofloxacin and sulfamethoxazole to marine periphytic algae and bacteria. *Aquat. Toxicol.* 156, 248–258. doi: 10.1016/j.aquatox.2014.08.015
- Kovalakova, P., Cizmas, L., McDonald, T. J., Marsalek, B., Feng, M., and Sharma, V. K. (2020). Occurrence and toxicity of antibiotics in the aquatic environment: a review. *Chemosphere* 251:126351. doi: 10.1016/j.chemosphere.2020.126351
- Lavoie, I., Hamilton, P. B., Morin, S., Kim Tiam, S., Kahlert, M., Gonçalves, S., et al. (2017). Diatom teratologies as biomarkers of contamination: are all deformities ecologically meaningful? *Ecol. Indic.* 82, 539–550. doi: 10.1016/j.ecolind.2017.06.048
- Lawrence, J. R., Topp, E., Waiser, M. J., Tumber, V., Roy, J., Swerhone, G. D. W., et al. (2015). Resilience and recovery: the effect of triclosan exposure timing during development, on the structure and function of river biofilm communities. *Aquat. Toxicol.* 161, 253–266. doi: 10.1016/j.aquatox.2015.02.012
- Le, S., Josse, J., and Husson, F. (2008). FactoMineR: an R package for multivariate analysis. *J. Stat. Soft.* 25, 1–18.
- Linares, J. F., Gustafsson, I., Baquero, F., and Martinez, J. L. (2006). Antibiotics as intermicrobial signaling agents instead of weapons. *Proc. Natl. Acad. Sci. U.S.A.* 103, 19484–19489. doi: 10.1073/pnas.0608949103
- Liu, A., Cao, H., Yang, Y., Ma, X., and Liu, X. (2016). Combinational effects of sulfomethoxazole and copper on soil microbial community and function. *Environ. Sci. Pollut. Res.* 23, 4235–4241. doi: 10.1007/s11356-015-4892-x
- Liu, F., Ying, G.-G., Tao, R., Zhao, J.-L., Yang, J.-F., and Zhao, L.-F. (2009). Effects of six selected antibiotics on plant growth and soil microbial and enzymatic activities. *Environ. Poll.* 157, 1636–1642. doi: 10.1016/j.envpol.2008.12.021
- Mahamoud Ahmed, A., Lyautey, E., Bonnineau, C., Dabrin, A., and Pesce, S. (2018). Environmental concentrations of copper, alone or in mixture with arsenic, can impact river sediment microbial community structure and functions. *Front. Microbiol.* 9:1852. doi: 10.3389/fmicb.2018.01852
- Mandarić, L., Diamantini, E., Stella, E., Cano-Paoli, K., Valle-Sistac, J., Molins-Delgado, D., et al. (2017). Contamination sources and distribution patterns of pharmaceuticals and personal care products in Alpine rivers strongly affected by tourism. *Sci. Total Environ.* 590–591, 484–494. doi: 10.1016/j.scitotenv.2017.02.185
- Marti, E., Jofre, J., and Balcazar, J. L. (2013). Prevalence of antibiotic resistance genes and bacterial community composition in a river influenced by a wastewater treatment plant. *PLoS One* 8:e78906. doi: 10.1371/journal.pone.0078906
- Martínez, J. L. (2008). Antibiotics and antibiotic resistance genes in natural environments. *Science* 321, 365–367. doi: 10.1126/science.1159483
- Martin-Laurent, F., Topp, E., Billet, L., Batisson, I., Malandain, C., Besse-Hoggan, P., et al. (2019). Environmental risk assessment of antibiotics in agroecosystems: ecotoxicological effects on aquatic microbial communities and dissemination of antimicrobial resistances and antibiotic biodegradation potential along the soil-water continuum. *Environ. Sci. Pollut. Res.* 26, 18930–18937. doi: 10.1007/s11356-019-05122-0
- McDermott, P. F., Walker, R. D., and White, D. G. (2003). Antimicrobials: modes of action and mechanisms of resistance. *Int. J. Toxicol.* 22, 135–143. doi: 10.1080/10915810305089
- Moon, K. H., Weber, B. S., and Feldmana, M. F. (2017). Subinhibitory concentrations of trimethoprim and sulfamethoxazole prevent biofilm formation by *Acinetobacter baumannii* through inhibition of csu pilus expression. *Antimicrob. Agents Chemother.* 61:e778-17.
- Morin, S., Lambert, A. S., Rodriguez, E. P., Dabrin, A., Coquery, M., and Pesce, S. (2017). Changes in copper toxicity towards diatom communities with experimental warming. *J. Hazard. Mater.* 334, 223–232. doi: 10.1016/j.jhazmat.2017.04.016
- Morin, S., Proia, L., Ricart, M., Bonnineau, C., Geislinger, A., Ricciardi, F., et al. (2010). Effects of a bactericide on the structure and survival of benthic diatom communities. *Vie Milieu* 60, 109–116.
- Normand, P., Ponsonnet, C., Nesme, X., Neyra, M., and Simonet, P. (1996). “ITS analysis of prokaryotes,” in *Molecular Microbial Ecology Manual*, eds D. L. Akkermans, J. D. van Elsas, and F. J. de Bruijn (Dordrecht: Kluwer Academic Publishers), 1–12. doi: 10.1016/b978-0-12-509001-8.50008-1
- O’Flaherty, E., and Cummins, E. (2017). Antibiotic resistance in surface water ecosystems: presence in the aquatic environment, prevention strategies, and risk assessment. *Hum. Ecol. Risk Assess. Int. J.* 23, 299–322. doi: 10.1080/10807039.2016.1247254
- Oksanen, J., Guillaume Blanchet, F., Friendly, M., Kindt, R., Legendre, L., McGlinn, D., et al. (2019). *vegan: Community Ecology Package. R Package Version 2.5-6*.
- Osborne, C. A., Rees, G. N., Bernstein, Y., and Janssen, P. H. (2006). New threshold and confidence estimates for terminal restriction fragment length polymorphism analysis of complex bacterial communities. *Appl. Environ. Microbiol.* 72, 1270–1278. doi: 10.1128/aem.72.2.1270-1278.2006
- Paíga, P., Santos, L. H. M. L. M., Ramos, S., Jorge, S., Silva, J. G., and Delerue-Matos, C. (2016). Presence of pharmaceuticals in the Lis river (Portugal): sources, fate and seasonal variation. *Sci. Total Environ.* 573, 164–177. doi: 10.1016/j.scitotenv.2016.08.089
- Paumelle, M., Donnadieu, F., Joly, M., Besse-Hoggan, P., and Artigas, J. (2021). Effects of sulfonamide antibiotics on aquatic microbial community composition and functions. *Environ. Int.* 146:106198. doi: 10.1016/j.envint.2020.106198
- Perreten, V., and Boerlin, P. (2003). A new sulfonamide resistance gene (sul3) in *Escherichia coli* is widespread in the pig population of Switzerland. *Antimicrob. Agents Chemother.* 47, 1169–1172. doi: 10.1128/aac.47.3.1169-1172.2003
- Pesce, S., Lambert, A.-S., Morin, S., Foulquier, A., Coquery, M., and Dabrin, A. (2018). Experimental warming differentially influences the vulnerability of phototrophic and heterotrophic periphytic communities to copper toxicity. *Front. Microbiol.* 9:1424. doi: 10.3389/fmicb.2018.01424
- Petrić, I., Bru, D., Udiković-Kolić, N., Hršak, D., Philippot, L., Martin-Laurent, F., et al. (2011). Evidence for shifts in the structure and abundance of the microbial community in a long-term PCB-contaminated soil under bioremediation. *J. Hazard. Mater.* 195, 254–260. doi: 10.1016/j.jhazmat.2011.08.036
- Proia, L., Morin, S., Peipoch, M., Romani, A. M., and Sabater, S. (2011). Resistance and recovery of river biofilms receiving short pulses of Triclosan and Diuron. *Sci. Total Environ.* 409, 3129–3137. doi: 10.1016/j.scitotenv.2011.05.013
- Proia, L., Lupini, G., Osorio, V., Pérez, S., Barceló, D., Schwartz, T., et al. (2013a). Response of biofilm bacterial communities to antibiotic pollutants in a

- Mediterranean river. *Chemosphere* 92, 1126–1135. doi: 10.1016/j.chemosphere.2013.01.063
- Proia, L., Vilches, C., Boninneau, C., Kantiani, L., Farré, M., Romani, A. M., et al. (2013b). Drought episode modulates the response of river biofilms to triclosan. *Aquat. Toxicol.* 127, 36–45. doi: 10.1016/j.aquatox.2012.01.006
- Proia, L., von Schiller, D., Sánchez-Melsió, A., Sabater, S., Borrego, C. M., Rodríguez-Mozaz, S., et al. (2016). Occurrence and persistence of antibiotic resistance genes in river biofilms after wastewater inputs in small rivers. *Environ. Pollut.* 210, 121–128. doi: 10.1016/j.envpol.2015.11.035
- Quinlan, E. L., Nietch, C. T., Blocksom, K., Lazorchak, J. M., Batt, A. L., Griffiths, R., et al. (2011). Temporal dynamics of periphyton exposed to tetracycline in stream mesocosms. *Environ. Sci. Technol.* 45, 10684–10690. doi: 10.1021/es202004k
- R Core Team (2020). *R: A Language and Environment for Statistical Computing*. Vienna: R Foundation for Statistical Computing.
- Ramette, A. (2009). Quantitative community fingerprinting methods for estimating the abundance of operational taxonomic units in natural microbial communities. *Appl. Environ. Microbiol.* 75, 2495–2505. doi: 10.1128/aem.02409-08
- Ranjard, L., Poly, F., Lata, J.-C., Mougél, C., Thioulouse, J., and Nazaret, S. (2001). Characterization of bacterial and fungal soil communities by automated ribosomal intergenic spacer analysis fingerprints: biological and methodological variability. *Appl. Environ. Microbiol.* 67, 4479–4487. doi: 10.1128/aem.67.10.4479-4487.2001
- Romani, A. M., Guasch, H., Munoz, I., Ruana, J., Vilalta, E., Schwartz, T., et al. (2004). Biofilm structure and function and possible implications for riverine DOC dynamics. *Microb. Ecol.* 47, 316–328.
- Royston, J. P. (1982). An extension of shapiro and Wilk's W test for normality to large samples. *J. R. Stat. Soc. Ser. C Appl. Stat.* 31, 115–124. doi: 10.2307/2347973
- Sanderson, H., Fricker, C., Brown, R. S., Majury, A., and Liss, S. N. (2016). Antibiotic resistance genes as an emerging environmental contaminant. *Environ. Rev.* 24, 205–218. doi: 10.1139/er-2015-0069
- Schmitt-Jansen, M., and Altenburger, R. (2008). Community-level microalgal toxicity assessment by multiwavelength-excitation PAM fluorometry. *Aquat. Toxicol.* 86, 49–58. doi: 10.1016/j.aquatox.2007.10.001
- Sköld, O. (2000). Sulfonamide resistance: mechanisms and trends. *Drug Resist. Updat.* 3, 155–160. doi: 10.1054/drup.2000.0146
- Straub, J. O. (2016). Aquatic environmental risk assessment for human use of the old antibiotic sulfamethoxazole in Europe. *Environ. Toxicol. Chem.* 35, 767–779. doi: 10.1002/etc.2945
- Subirats, J., Timoner, X., Sánchez-Melsió, A., Balcázar, J. L., Acuña, V., Sabater, S., et al. (2018). Emerging contaminants and nutrients synergistically affect the spread of class 1 integron-integrase (intI1) and sulI genes within stable streambed bacterial communities. *Water Res.* 138, 77–85. doi: 10.1016/j.watres.2018.03.025
- Szymańska, U., Wierowski, M., Sołtyszewski, I., Kuzemko, J., Wierowska, G., and Woźniak, M. K. (2019). Presence of antibiotics in the aquatic environment in Europe and their analytical monitoring: recent trends and perspectives. *Microchem. J.* 147, 729–740. doi: 10.1016/j.microc.2019.04.003
- Tiam, S. K., Lavoie, I., Liu, F., Hamilton, P. B., and Fortin, C. (2019). Diatom deformities and tolerance to cadmium contamination in four species. *Environment* 6:102. doi: 10.3390/environments6090102
- U.S. Environmental Protection Agency (2019). *ECOTOX User Guide: ECOTOXicology Knowledgebase System. Version 5.0*.
- Wei, Z., Feng, K., Li, S., Zhang, Y., Chen, H., Yin, H., et al. (2018). Exploring abundance, diversity and variation of a widespread antibiotic resistance gene in wastewater treatment plants. *Environ. Int.* 117, 186–195. doi: 10.1016/j.envint.2018.05.009
- Windler, M., Bova, D., Kryvenda, A., Straile, D., Gruber, A., Kroth, P. G., et al. (2014). Influence of bacteria on cell size development and morphology of cultivated diatoms. *Phycol. Res.* 62, 269–281. doi: 10.1111/pre.12059
- Yang, L.-H., Ying, G.-G., Su, H.-C., Stauber, J. L., Adams, M. S., and Binet, M. T. (2008). Growth-inhibiting effects of 12 antibacterial agents and their mixtures on the freshwater microalga *Pseudokirchneriella subcapitata*. *Environ. Toxicol. Chem.* 27, 1201–1208. doi: 10.1897/07-471.1
- Yergeau, E., Lawrence, J. R., Waiser, M. J., Korber, D. R., and Greer, C. W. (2010). Metatranscriptomic analysis of the response of river biofilms to pharmaceutical products, using anonymous DNA microarrays. *Appl. Environ. Microbiol.* 76, 5432–5439. doi: 10.1128/aem.00873-10
- Yergeau, E., Sanschagrin, S., Waiser, M. J., Lawrence, J. R., and Greer, C. W. (2012). Sub-inhibitory concentrations of different pharmaceutical products affect the meta-transcriptome of river biofilm communities cultivated in rotating annular reactors. *Environ. Microbiol. Rep.* 4, 350–359. doi: 10.1111/j.1758-2229.2012.00341.x

**Conflict of Interest:** The authors declare that the research was conducted in the absence of any commercial or financial relationships that could be construed as a potential conflict of interest.

Copyright © 2021 Kergoat, Besse-Hoggan, Leremboure, Beguet, Devers, Martin-Laurent, Masson, Morin, Roinat, Pesce and Bonnineau. This is an open-access article distributed under the terms of the Creative Commons Attribution License (CC BY). The use, distribution or reproduction in other forums is permitted, provided the original author(s) and the copyright owner(s) are credited and that the original publication in this journal is cited, in accordance with accepted academic practice. No use, distribution or reproduction is permitted which does not comply with these terms.



# Side Effects of Pesticides and Metabolites in Groundwater: Impact on Denitrification

Caroline Michel<sup>1\*</sup>, Nicole Baran<sup>1</sup>, Laurent André<sup>1,2</sup>, Mickael Charron<sup>1</sup> and Catherine Jouliau<sup>1</sup>

<sup>1</sup> BRGM, DEPA (Direction de l'Eau, de l'Environnement, des Procédés et Analyses), Orléans, France, <sup>2</sup> Université d'Orléans, CNRS, BRGM, UMR 7327 Institut des Sciences de la Terre d'Orléans, Orléans, France

## OPEN ACCESS

### Edited by:

Dimitrios Georgios Karpouzias,  
University of Thessaly, Greece

### Reviewed by:

Evangelia Papadopoulou,  
University of Thessaly, Greece

Aqiang Ding,  
Chongqing University, China

### \*Correspondence:

Caroline Michel  
c.michel@brgm.fr

### Specialty section:

This article was submitted to  
Microbiotechnology,  
a section of the journal  
Frontiers in Microbiology

Received: 01 February 2021

Accepted: 30 March 2021

Published: 13 May 2021

### Citation:

Michel C, Baran N, André L,  
Charron M and Jouliau C (2021) Side  
Effects of Pesticides and Metabolites  
in Groundwater: Impact on  
Denitrification.  
Front. Microbiol. 12:662727.  
doi: 10.3389/fmicb.2021.662727

The impact of two pesticides (S-metolachlor and propiconazole) and their respective main metabolites (ESA-metolachlor and 1,2,4-triazole) on bacterial denitrification in groundwater was studied. For this, the denitrification activity and the bacterial diversity of a microbial community sampled from a nitrate-contaminated groundwater were monitored during 20 days in lab experiments in the presence or absence of pesticides or metabolites at 2 or 10  $\mu\text{g/L}$ . The kinetics of nitrate reduction along with nitrite and  $\text{N}_2\text{O}$  production all suggested that S-metolachlor had no or only little impact, whereas its metabolite ESA-metolachlor inhibited denitrification by 65% at 10  $\mu\text{g/L}$ . Propiconazole and 1,2,4-triazole also inhibited denitrification at both concentrations, but to a lesser extent (29–38%) than ESA-metolachlor. When inhibition occurred, pesticides affected the reduction of nitrate into nitrite step. However, no significant differences were detected on the abundance of nitrate reductase *narG* and *napA* genes, suggesting an impact of pesticides/metabolites at the protein level rather than on denitrifying bacteria abundance. 16S rRNA gene Illumina sequencing indicated no major modification of bacterial diversity in the presence or absence of pesticides/metabolites, except for ESA-metolachlor and propiconazole at 10  $\mu\text{g/L}$  that tended to increase or decrease Shannon and InvSimpson indices, respectively. General growth parameters suggested no impact of pesticides, except for propiconazole at 10  $\mu\text{g/L}$  that partially inhibited acetate uptake and induced a decrease in microbial biomass. In conclusion, pesticides and metabolites can have side effects at environmental concentrations on microbial denitrification in groundwater and may thus affect ecosystem services based on microbial activities.

**Keywords:** denitrification, groundwater, chloroacetanilide, conazole, pesticides, metabolites, non-target effects

## INTRODUCTION

One consequence of the increasing use of pesticides is the presence of both parent molecules and transformation products (metabolites) in various environmental matrices and notably groundwater, with metabolites being even referred to as emerging groundwater contaminants (Jurado et al., 2012; Lapworth et al., 2012; Baran and Gourcy, 2013; Lopez et al., 2015). One drawback is that pesticides used in agriculture to target insects, fungi, or plants are now known to have side effects on non-target surface and subsurface living (micro)organisms (Iker et al., 2010;

Staley et al., 2015). The environmental consequence of such side effects of pesticides and metabolites on microbial ecosystems is that they can threaten the ecosystem services based on microbial activities in soil (e.g., litter degradation, plant growth, nutrient cycling, and degradation of pollutants) and groundwater (e.g., production of drinking water, nutrient cycling, degradation of contaminant) (Tuinstra and van Wensem, 2014; Griebler and Avramov, 2015).

Most studies on the side effects of pesticides have been conducted in soils, and the main impacts were noticed on microbial abundance, presence or absence of microbial species, increase or decrease in gene expression (mainly linked to the N cycle), and increase or decrease of functional diversity [activities measured using the Biolog EcoPlates (C cycle) or soil activities linked to P, N, S, and C cycles] (Hussain et al., 2009; Lo, 2010; Kalia and Gosal, 2011; Yang et al., 2011; Jacobsen and Hjelmsø, 2014). Moreover, the presence of pesticides was shown to usually lead to the selection of microorganisms having the ability to degrade them (Bælum et al., 2008; Lancaster et al., 2010). The modes of actions of pesticides are multiple, which could explain the diversity of side effects observed on microbial communities and activities (Saez et al., 2003, 2006). In addition, the effects of pesticides on soil microbial ecosystems mainly depend on the type of pesticides and their concentration, as well as time after application. They also depend on the microbial community structure and on the diversity of the microbial processes that are taking place in the studied soil. Physical and chemical factors such as the type of soil, pesticide concentration, presence of organic matter, and adsorption and desorption processes also influence the impact of pesticides on microbial communities (Hussain et al., 2009). It was also demonstrated that some metabolites obtained after the biological and physicochemical transformations of pesticides can be more persistent and/or more toxic than the parent molecules (Bollag and Kurek, 1980). Taking all together, these factors increase the difficulty to evaluate the risks associated with pesticides use and to predict the net effects of pesticides on soil ecosystem health (Yang et al., 2011; Staley et al., 2015). In addition, contradictory conclusions on the impacts of pesticides can be found among studies due to the difficulty to compare results from different works done with great differences in experimental setups, pesticide concentrations, and methods (Jacobsen and Hjelmsø, 2014). The bioavailability/sorption/biodegradation of pesticides can also vary a lot for the same pesticides according to the studied system (Jacobsen and Hjelmsø, 2014).

The very few studies conducted in groundwater have also underlined the potential side effects of pesticides on groundwater microbial communities. Results first suggested that the presence of pesticides could increase microbial biodiversity. For instance, Imfeld et al. (2018) obtained higher Shannon and Simpson diversity indices (from T-RFLP fingerprints) for groundwater communities in batch experiments amended with pesticides (metolachlor) compared with experiments without the addition of pesticides. de Liphay et al. (2004) also demonstrated that the diversity of colony morphotypes (culturable) in sediments from a subsurface aquifer exposed to herbicides (as mixture)

was higher compared with the non-exposed samples. These authors also observed an increase of the relative abundance of bacterial heterotrophs in aquifer sediment exposed to pesticides, but no specific bacterial species were found for herbicide-exposed samples. Janniche et al. (2012) also noticed high diversity indices from microbial community-level physiological profiles (CLPP) using EcoPlates™ in herbicide (isoproturon, atrazine, and acetochlor)-exposed groundwater. Studies, however, underlined the difficulties to determine *in situ* the impact of pesticides on groundwater biodiversity due to natural spatial and temporal variations of groundwater bacterial communities (de Liphay et al., 2004; Imfeld et al., 2018). Moreover, they suggested that biodiversity modifications induced by pesticides were not associated to changes in general catabolic properties. The role of the contamination history of pesticides on its impact on groundwater microbial communities has also been underlined. As an example, Iker et al. (2010) showed that in an aquifer impacted with atrazine over a long time, a new contamination with this pesticide leads to the decrease of the relative abundance of *amoA* gene and nitrite-oxidizing bacteria, even if ammonia is the primary degradation product of atrazine. On the opposite, in an aquifer never impacted with atrazine before, atrazine spiking led to an increase in the relative abundance of nitrite-oxidizing bacteria. In another study, Mauffret et al. (2017) showed that a triazine concentration of 1 µg/L was enough to induce modification of the bacterial community structure in non-contaminated groundwater batch experiments, but a 10 times higher (10 µg/L) triazine concentration was needed to obtain the same impact in historically contaminated groundwater.

The possibility to extrapolate all the knowledge obtained for soil communities to groundwater ecosystems is still difficult to establish. The first reason is that the concentrations of pesticides in groundwater are low (in hundreds of nanograms to micrograms per liter order) compared with those found in soil, with metabolite contents usually higher than parent molecules (Amalric et al., 2013; Lopez et al., 2015). The second reason is that aquifers are physically, chemically, and biologically different from soil. Groundwater is indeed characterized by a quite constant temperature (around 12–14°C in temperate climates), no sunlight, and a low easily available nutrient content (low organic carbon and oxygen availability) (Griebler and Lueders, 2009; Gregory et al., 2014; Taubert et al., 2019; Retter et al., 2021). Aquifers can be connected to the surface but this connection greatly varies from an aquifer to another, and transfer rates can be so slow that some aquifers can be considered as isolated environments (Hubalek et al., 2016). All of this represents the most important differences with soils and can greatly influence microbial diversity and activities. In particular, lithoautotrophs that fix CO<sub>2</sub> and oxidize inorganic electron donors as energy sources are an important part of groundwater microbial communities. Previous studies also support the idea that groundwater microbial diversity is different from that found in the overlying surface soil (Griebler and Lueders, 2009; Taubert et al., 2019) even if soil microorganisms can be transported into groundwater (Dibbern et al., 2014; Lazar et al., 2017). Moreover, groundwater is usually characterized by lower biodiversity and biomass than soil, and the presence of several novel microbial



phyla has also been demonstrated (Griebler and Lueders, 2009; Anantharaman et al., 2016). Finally, the composition of microbial communities varies across aquifers, which is mainly due to species sorting imposed by local environmental conditions (mineralogy, water chemistry, etc.) as well as other factors such as dispersal limitation and drift across areas, type of aquifer and its connection to the surface, anthropogenic activities, etc. (Gregory et al., 2014; Fillinger et al., 2019; Sonthiphand et al., 2019). When considering all of this, and due to the low nutrient content of aquifers, it can be expected that the addition of exogenous organic compounds such as pesticides and/or their metabolites even at low concentration has impacts on the microbial community in terms of biodiversity and/or activity. This is particularly true as pesticides and metabolites are quite persistent (due to low or no biodegradation) and tend to persist in groundwater. Indeed, even if the potential biodegradation of pesticides in aquifers was already demonstrated (Janniche et al., 2012) with the isolation of pesticide-degrading bacteria, the biodegradation rates of pesticides in aquifers are significantly lower than those observed in topsoil (Hoyle and Arthur, 2000; Albrechtsen et al., 2001; Grenni et al., 2009; Barra Caracciolo et al., 2010).

Among the most used pesticides in Europe that are found in groundwater, chloroacetanilide pesticides, used for the control of annual weeds, mainly on corn, sugar beet, and sunflower, are frequently detected together with their transformation products, notably ethane sulfonic, and oxanilic acids (Kalkhoff et al., 2012; Amalric et al., 2013; Baran and Gourcy, 2013; Sidoli et al., 2016). Among the chloroacetanilide family, S-metolachlor, an herbicide used worldwide, is one of the top five pesticides detected in France [with a maximal concentration of 20.9  $\mu\text{g/L}$  in Amalric et al. (2013) and 0.95  $\mu\text{g/L}$  in Lopez et al. (2015)] and in the EU (Loos et al., 2010). Its metabolite ESA-metolachlor is also widely detected in French groundwater [at a maximum of 4.8  $\mu\text{g/L}$  in Amalric et al. (2013) and with an average concentration of 0.21  $\mu\text{g/L}$  in Baran and Gourcy (2013)]. Triazole fungicides, widely used on fruits, vegetables, and cereals, are also frequently detected in groundwater. During the French national campaign of 2012, propiconazole was one of the most quantified fungicides (Lopez et al., 2015). One of the main metabolites of all triazole fungicides is 1,2,4-triazole, also used in Europe as a nitrification and urease inhibitor. Few data exist on its surveillance in France: its presence was reported in surface waters (Scheurer et al., 2016), and no quantification was done in groundwater during the French national campaigns, which might be due to a high limit of quantification (0.1  $\mu\text{g/L}$ ). Recent publications of compiled groundwater monitoring in the United States demonstrate once again the occurrence of these molecules in groundwater and the significant levels that can be observed there. As examples, Bexfield et al. (2021), on a panel of 1,204 sites, measured maximum concentrations of 0.0237, 1.419, and 2.509  $\mu\text{g/L}$  for propiconazole, metolachlor, and ESA-metolachlor, respectively, and Fisher et al. (2021) (54 sites) obtained concentrations of 0.0254, 0.075, and 4.04  $\mu\text{g/L}$  for propiconazole, metolachlor, and ESA-metolachlor, respectively. Both studies also provided new data on 1,2,4-triazole with a maximum concentration of 0.296  $\mu\text{g/L}$  for Bexfield et al.

(2021) (with a detection frequency of 1.4%) and 0.436  $\mu\text{g/L}$  for Fisher et al. (2021).

There is thus a need to study the impact of pesticides and metabolites on the microbial communities and the linked ecosystem services in groundwater. As mentioned above, pesticides/metabolites can affect the N cycle and thus microbial denitrification activity involved in ecosystem services such as the production of drinking water. The objective of this study was thus to evaluate in controlled conditions the impact of pesticides or metabolites on the potential denitrification activity and biodiversity of a groundwater microbial community. One herbicide (S-metolachlor) and one fungicide (propiconazole) belonging to two different chemical classes (respectively, chloroacetanilide and conazole) and their major metabolite ESA-metolachlor and 1,2,4-triazole, respectively, were selected. These two active substances were chosen due to their wide use in France and Europe and their occurrence in groundwater, as mentioned above. These four compounds were tested at two concentrations, 2 and 10  $\mu\text{g/L}$ , similar to those measured in groundwater, in a batch experimental approach to investigate their impacts on groundwater microbial denitrification activity and biodiversity. Groundwater from an agricultural site historically submitted to nitrate use was chosen for this study. The denitrification activity was determined by following the evolution of nitrate, nitrite, and nitrous oxide concentrations, whereas variations of bacterial biodiversity between the start and the end of the experiment were determined thanks to genomic characterizations.

## MATERIALS AND METHODS

### Chemicals

Molecules were provided as pure chemicals by Dr. Ehrenstorfer (S-metolachlor), Sigma Aldrich (ESA-metolachlor), and HPC Standards (propiconazole and 1,2,4-triazole). Individual concentrated solutions (500 mg/L) were prepared in methanol and then diluted in sterile water to obtain a 10-mg/L solution used to spike groundwater samples. Two final concentrations of pesticides and metabolites were used in this study: 2 and 10  $\mu\text{g/L}$ .

### Field Site and Groundwater Sampling and Chemical Analyses

Sampling was done on a catchment located in the NW of France (Plourhan, French Brittany) (Petelet-Giraud et al., 2021; Surdyk et al., 2021). Several piezometers have been drilled in 2006 in the sector. The geological setting corresponds to an amphibolite (metamorphic rock, basement rock).

In the frame of a monitoring campaign in October 2017, a groundwater sample (8 L) was collected from piezometer Pz3 after discarding three purge volumes and stabilization of parameters measured *in situ* (temperature, pH, redox potential, electrical conductivity, and dissolved oxygen). This piezometer has a depth of 19 m and a water table level fluctuating between 2 and 4 m below soil level (bsl) in average and is equipped with a screen between 7 and 19 m bsl. For the analyses of anions and major cations, a sample was collected in 100 ml PE bottles after filtration through a 0.45- $\mu\text{m}$  filter. The sample for major

cation analyses was acidified to pH 2 with ultrapure nitric acid. All samples were cooled for transportation to the laboratory and stored at 4°C until chemical analysis. Pesticides and major ions were then analyzed at the laboratory (Table 1). Chemical analyses were performed by using ICP-AES for  $\text{Ca}^{2+}$ ,  $\text{Na}^+$ ,  $\text{K}^+$ ,  $\text{Si}^{2+}$ , and  $\text{Mg}^{2+}$  (with 5% uncertainty); ion chromatography for  $\text{Cl}^-$ ,  $\text{SO}_4^{2-}$ , and  $\text{NO}_3^-$  (with 10% uncertainty); colorimetric method based on NF ISO 15923-1 for  $\text{NH}_4^+$ ,  $\text{PO}_4^{3-}$ , and  $\text{NO}_2^-$ ; and potentiometric methods according to NF EN ISO 9963-1 (1996) for  $\text{HCO}_3^-$  and  $\text{CO}_3^{2-}$  (with 5% uncertainty). Dissolved organic carbon (DOC) was quantified according to NF EN 1484 (1997) procedures. For pesticides, a 55-pesticides monitoring (occurrence and concentration), including mother molecules and metabolites from pesticides degradation, was performed by liquid chromatography-mass spectrometry (LC-MS/MS) following an online solid-phase extraction (Amalric et al., 2013). The chemical analysis done on Pz3 groundwater validated previous results and showed that this piezometer is impacted by nitrate (78 mg/L) but not by pesticides or metabolites (Table 1).

## Groundwater Incubation (Batch Experiments)

To study the impact of pesticides and metabolites at two concentrations on denitrification in groundwater, pesticide/metabolite-spiked batch experiments were undergone in triplicate. Flasks (300 ml) were filled in with 150 ml groundwater (to obtain a gas/liquid ratio of 50/50) in anoxic conditions (nitrogen atmosphere). Taking into account nitrate concentration in the piezometer (Table 1), flasks were also supplemented with nitrate to reach a final  $\text{NO}_3^-$  concentration

of 100 mg/L. Pesticides and metabolites were added at a final concentration of 2 or 10  $\mu\text{g/L}$  with the exception of positive control flasks (denitrification in the absence of pesticides/metabolites) and abiotic test flasks (addition of sodium azide) (Cabrol et al., 2017). Acetylene was added in the gas phase (10% acetylene/90% nitrogen) to inhibit the last step of the denitrification pathway, i.e., nitrous oxide ( $\text{N}_2\text{O}$ ) reduction into nitrogen gas, leading to  $\text{N}_2\text{O}$  accumulation instead of  $\text{N}_2$  production (Milenkovski et al., 2010; Crouzet et al., 2016). Acetate ( $\text{C}_2\text{H}_3\text{NaO}_2$ ) was added as a carbon source in each flask at a final concentration of 100 mg/L. This initial acetate concentration was defined in order to cover the carbon needs of heterotrophic bacteria (catabolism and anabolism) during the denitrification process and to avoid any substrate limitation in relation with initial nitrate concentration (André et al., 2011). Flasks were incubated during 20 days in the dark at 25°C under stirring (100 rpm) to favor water contact with acetylene. At regular times (every 2–3 days), gas sampling (5 ml, using a Vacuette tube system) for  $\text{N}_2\text{O}$  quantification and water sampling (8 ml) for nitrate, nitrite, and acetate quantification were done. To circumvent the depression linked to gas and water sampling, an equal volume of nitrogen (90%)/acetylene (10%) gas was added after each sampling. Nitrate and acetate were quantified by ionic chromatography (Dionex IC3000-SP-EG-DC system equipped with an AS50 autosampler and a conductimetric detector) according to the NF EN ISO 10304-1 (2009) method. Nitrite was analyzed by colorimetry according to the NF ISO 15923-1 (2014) method.  $\text{N}_2\text{O}$  was analyzed by gas chromatography using a Varian CP-3800 GC equipped with a gas injection valve and an electron capture detector. Finally, after 20 days of incubation, 20 ml of water was sampled, filtered (0.22  $\mu\text{m}$ ), and stored at  $-20^\circ\text{C}$  for molecular analyses.

**TABLE 1 |** Water chemistry and physical properties of groundwater collected from well Pz3 in October 2017.

Water level (from topsoil) (m)	4
Temperature ( $^\circ\text{C}$ )	12
pH ( <i>in situ</i> measurement)	6.1
Conductivity (mS/cm)	455
Redox potential (Eh, mV)	223
Dissolved oxygen (mg/L)	1.8
Ca (calcium) (mg/L)	29
Cl (chloride) (mg/L)	50
$\text{HCO}_3$ (bicarbonates) (mg/L)	61
$\text{CO}_3$ (carbonates) (mg/L)	<LQ
K (potassium) (mg/L)	1.4
Mg (magnesium) (mg/L)	9.2
Ammonium (as $\text{NH}_4$ ) (mg/L)	<LQ
Nitrite (as $\text{NO}_2$ ) (mg/L)	<LQ
Nitrate (as $\text{NO}_3$ ) (mg/L)	79
Na (sodium) (mg/L)	43
P (phosphate as $\text{PO}_4$ ) (mg/L)	0.1
S (sulfur as $\text{SO}_4$ ) (mg/L)	18
Si (silica as $\text{SiO}_2$ ) (mg/L)	34
Dissolved organic carbon (DOC) (mg/L)	<LQ
Pesticides and metabolites (mg/L)	<LQ

LQ, limit of quantification.

## Molecular Analyses

Microbial DNA was extracted from frozen filters using the FastDNA<sup>TM</sup> Spin Kit for Soil (MP Biomedicals, United States) according to the manufacturer's recommendations with a FastPrep<sup>®</sup>-24 instrument at a speed of 5  $\text{ms}^{-1}$  for 30 s and quantified using the Quantifluor dsDNA sample kit and the Quantus fluorimeter, according to the manufacturer's instructions (Promega, United States). The abundance of the bacterial universal marker (16S rRNA gene) and of nitrate-reducing bacterial markers *narG* and *napA* genes was assessed by duplicated real-time quantitative PCR (qPCR). The reaction mixture contained 1 $\times$  SSO Advanced Supermix (Bio-Rad), 0.4  $\mu\text{M}$  of each primer, 100 ng of T4gp32 (MP Biomedicals), 2  $\mu\text{l}$  of 0.03–0.5 ng/ $\mu\text{l}$  of template DNA, and qs 20  $\mu\text{l}$  of nuclease-free water. For 16S rRNA gene, primers 341F (5'-CCTACGGGAGGCAGCAG-3') and 515R (5'-ATTACCGCGGCTGCTGGCA-3') (López-Gutiérrez et al., 2004; Crouzet et al., 2016) and the following thermocycling conditions were used: 95°C for 3 min, 35 cycles of 95°C for 30 s, 60°C for 30 s, 72°C for 30 s, and a data acquisition step at 80°C for 30 s at each cycle. For *narG* and *napA* genes, the respective primer sets narG-F (5'-TCGCCSATYCCGGCSATGTC-3') and narG-R (5'-GAGTTGTACCAGTCRGC SGAYTCSG-3') and V17m (5'-TGGACVATGGGYTTYAAYC-3') and napA4r

(5'-ACYTCRCGHGCVGTRCCCA-3') described in Bru et al. (2007) and the following thermocycling conditions were used: 3 min at 95°C; 6 cycles of 30 s at 95°C, 30 s at 63°C (*narG*) or 61°C (*napA*) with a touchdown of  $-1^{\circ}\text{C}$  by cycle, 30 s at 72°C; 34 (*narG*) or 40 (*napA*) cycles of 30 s at 95°C, 30 s at 58°C (*narG*) or 56°C (*napA*), 30 s at 72°C, 30 s at 80°C. Standard curves were obtained from serial 10-fold dilutions of linearized plasmids containing known copy numbers of the target gene. No-template controls were run for each qPCR assay. qPCR was run in a CFX Connect Real-Time PCR Detection and data were analyzed with the CFX Manager 3.1 software (Bio-Rad).

Diversity of the bacterial community was determined by 16S rRNA gene Illumina sequencing. Amplicon libraries and sequences were generated by the MetaHealth CIRAD platform (Montpellier, France) using a modified version of the Illumina 16S "Metagenomic" Sequencing Library Preparation Protocol. Briefly, the 16S rRNA V3-V4 gene region was targeted for PCR amplification, in a nested PCR strategy using primers 341F (5'-CCTACGGGNGGCWGCAG-3') and 785R (5'-GACTACHVGGGTATCTAATCC-3') modified with Illumina-specific overhang sequences for barcoding. The first PCRs were run in duplicate using the Phusion Flash High-Fidelity PCR Master Mix (Thermo Fisher), and 10-fold diluted PCR products were then subjected to the second PCR to implement dual barcodes. DNA library was obtained after two successive purifications (Wizard® DNA Clean-Up System kit, Promega) of the second PCR products. Library quantitation was performed by running the library on a D5000 ScreenTape bioanalyzer (Agilent). Sequencing was performed on an Illumina MiSeq platform with MCS v2.6.2.1. For Fastq generation, base calling and associated quality scores were done with Illumina RTA 1.18.54, and demultiplexing was done with MiSeq Reporter 2.6.2.3. Fastq quality control was evaluated with FastQC v0.11.7 (Andrews, 2010) and summarized with multiqc v1.5 (Ewels et al., 2016).

Fastq sequences were processed using the FROGS bioinformatics pipeline (Escudié et al., 2017) implemented into the GenoToul Galaxy platform (Afgan et al., 2018). In brief, after denoising and primer and adapter removal, paired reads were merged with VSEARCH and clustered into OTU with SWARM and an aggregation distance of 3. After chimera removal and filtering for OTU abundance (threshold of 0.00005%), taxonomic affiliation was performed using BLASTn and the 132 Silva database. Filtration on taxonomic affiliation was done at minimum identity of 98.2% and minimum coverage of 99%. Random resampling of the sequences obtained from the 24 samples was applied to have an equal number of 11,200 good-quality sequences per sample. The FROGS implemented Phyloseq R package was used for OTU structure visualization, rarefaction curve, and diversity index calculations. Shannon's index ( $H'$ ) (heterogeneity of microbial community:  $H'$  is minimal if all the individuals of a community belong to the same species, or if in a community, all the present species are represented by one individual except for one species which is represented by the remaining individuals of the community) and Simpson's index ( $1/D$  in this paper: probability that two individuals picked at random do not belong to the same species; diversity is low if  $1/D$  is low and vice versa) were calculated.

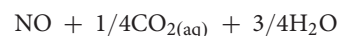
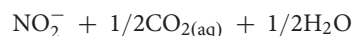
## Statistics

For statistical analyses, boxplots were calculated from triplicate flasks with data obtained during the 0–7-day period and corresponding to the maximal rates and using R4.0.1 and RStudio (R Development Core Team, 2009)<sup>1</sup>. Data ( $n = 3$ ) were analyzed using the non-parametric Kruskal–Wallis test. Difference was considered significant at  $p$  value  $< 0.05$ . Principal component analysis (PCA) was calculated using XLSTAT (Pearson correlation matrix).

## RESULTS

### Impact of Pesticides and Metabolites on Potential Denitrification Activity

The impact of pesticides on denitrification was tested in batch conditions in the presence of fungicide (propiconazole) and herbicide (S-metolachlor) or their major metabolites (1,2,4-triazole and ESA-metolachlor, respectively) at two concentrations (2 and 10  $\mu\text{g/L}$ ). In presence of acetate and since the last denitrification step was inhibited with the use of acetylene leading to  $\text{N}_2\text{O}$  accumulation, the denitrification pathway studied is as follows:



The following parameters were quantified: nitrate reduction, nitrite production (step 1), and  $\text{N}_2\text{O}$  production (step 3) rates (Figures 1, 2); these parameters are specific to the denitrification pathway. NO produced during step 2 is a short-lived compound difficult to analyze. Indeed, NO is immediately reduced to nitrous oxide ( $\text{N}_2\text{O}$ ) by cytochrome c (cNOR) or quinone (qNOR) membrane-bound reductases (Santana et al., 2017). For this reason, NO was not quantified and we focused on the other nitrogen-bearing compounds. The nitrogen balance was verified and validated for all the batch experiments with a constant nitrogen concentration all along the experiment (Table 2). No nitrate reduction and no nitrite and  $\text{N}_2\text{O}$  production were observed in abiotic test flasks.

The nitrate reduction rate measured in the absence of pesticides or metabolites (control) was about  $5.6 \times 10^{-5}$  g N/L/h (Figure 1A). With S-metolachlor (at both concentrations) and ESA-metolachlor at 2  $\mu\text{g/L}$ , the kinetic rates were similar. However, ESA-metolachlor at 10  $\mu\text{g/L}$  had the most significant impact on nitrate reduction rate among all the tested conditions, as on average a decrease of 65% was observed. For triazoles,

<sup>1</sup><http://www.R-project.org>

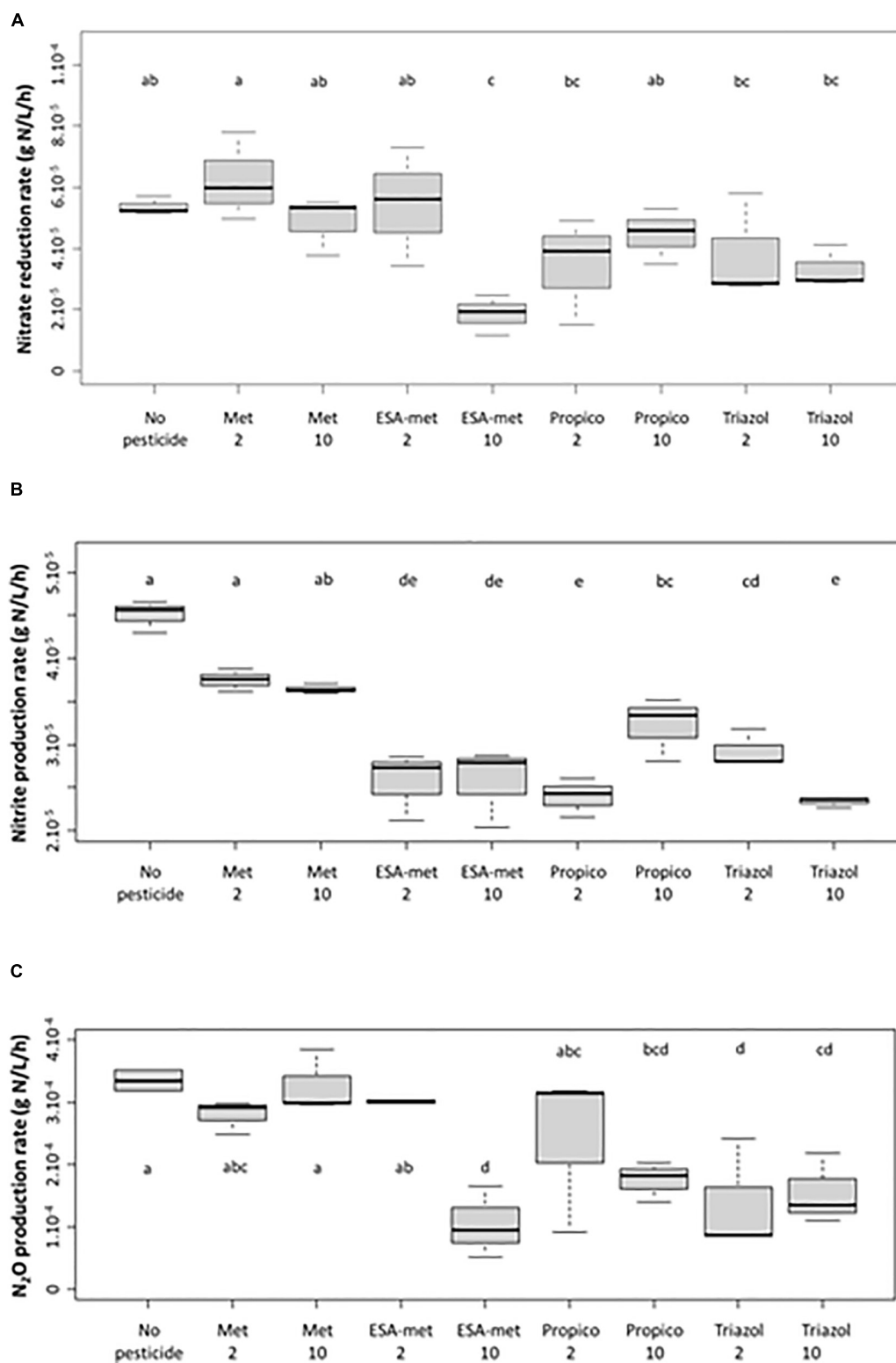


**FIGURE 1 |** Impact of pesticides and metabolites on the potential denitrification activity (batch experiments) measured as the impact on nitrate (as  $\text{NO}_3^-$ ) reduction (A), nitrite (as  $\text{NO}_2^-$ ) production (B), and  $\text{N}_2\text{O}$  production (C) rates. Significant differences between conditions were searched applying the Kruskal-Wallis non-parametric test and are mentioned as a, b, c, d, and e letters. No pesticide: control (absence of pesticides or metabolites); Met: metolachlor; ESA-met: ESA-metolachlor; Propico: propiconazole; Triazol: 1,2,4 triazole. 2 and 10 are pesticide or metabolite concentrations in  $\mu\text{g/L}$ . No nitrate reduction nor nitrite and  $\text{N}_2\text{O}$  production took place in abiotic test batch (data not shown).



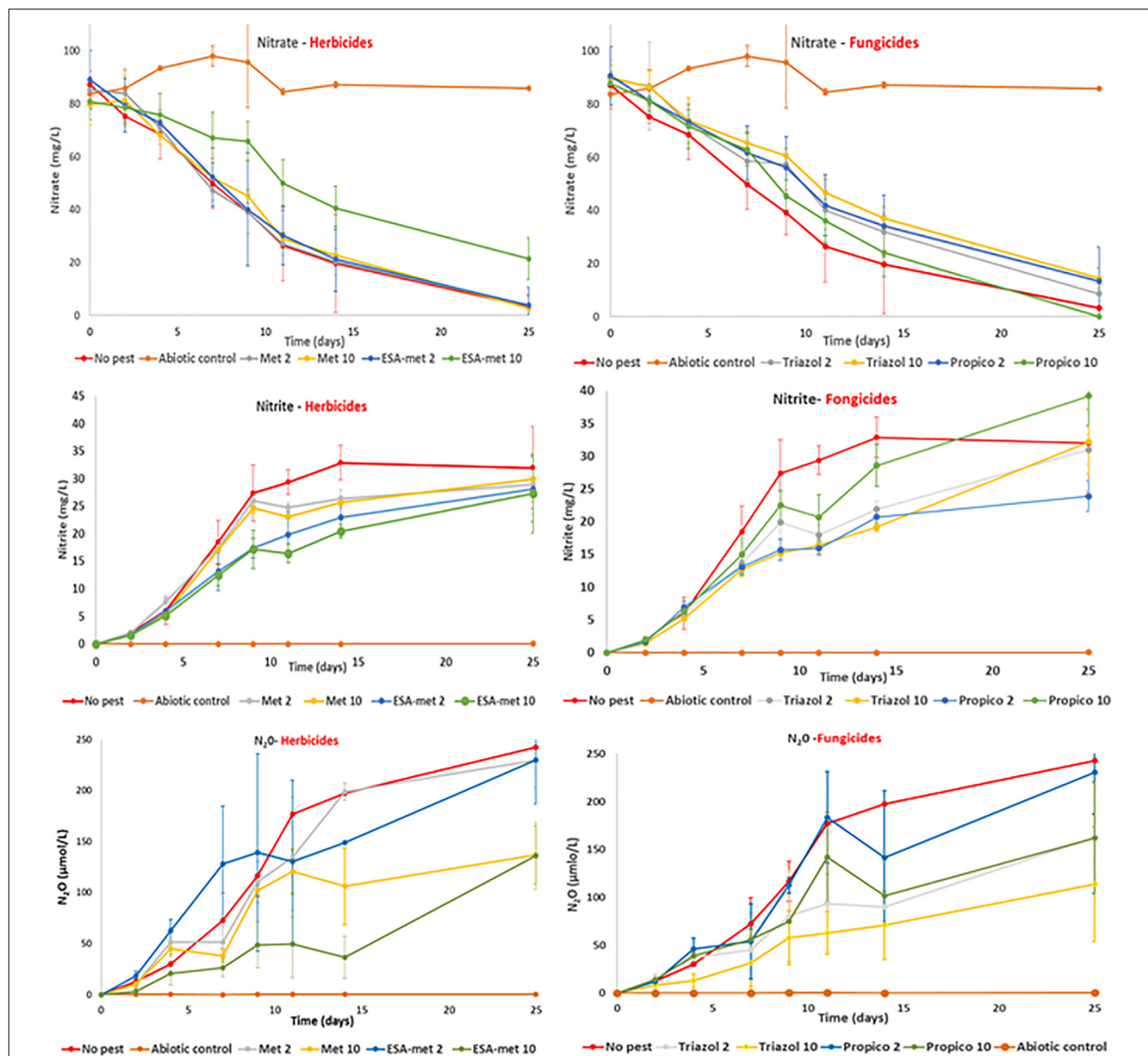


**FIGURE 2 |** Kinetics of nitrate consumption (**top**), nitrite production (**middle**), and  $N_2O$  production (**bottom**) measured in batch experiments in the absence (no pest) or presence of herbicides [Left: Metolachlor (Met) or its metabolite ESA-metolachlor (ESA-met)] or fungicides [Right: Propiconazole (Propico) or its metabolite 1,2,4-triazole (Triazol)] at 2 or 10  $\mu\text{g/L}$ . Abiotic control were performed in the presence of azide (cf. “Materials and Methods” section).

both propiconazole and 1,2,4-triazole decreased the nitrate reduction rate by 29–38% at both concentrations so that high concentrations (10  $\mu\text{g/L}$ ) did not result in higher impacts.

In the presence of pesticides or metabolites, a decrease in nitrite production compared with the control (estimated at  $4.5 \times 10^{-5}$  g N/L/h) was observed (**Figure 1B**). With S-metolachlor, at both concentrations, the nitrite production rates decreased by about 10% with respect to the control, but this weak decrease was statistically not significant. With the other compounds, the decrease was significant and could reach almost 50%. As a reminder, the nitrite concentrations

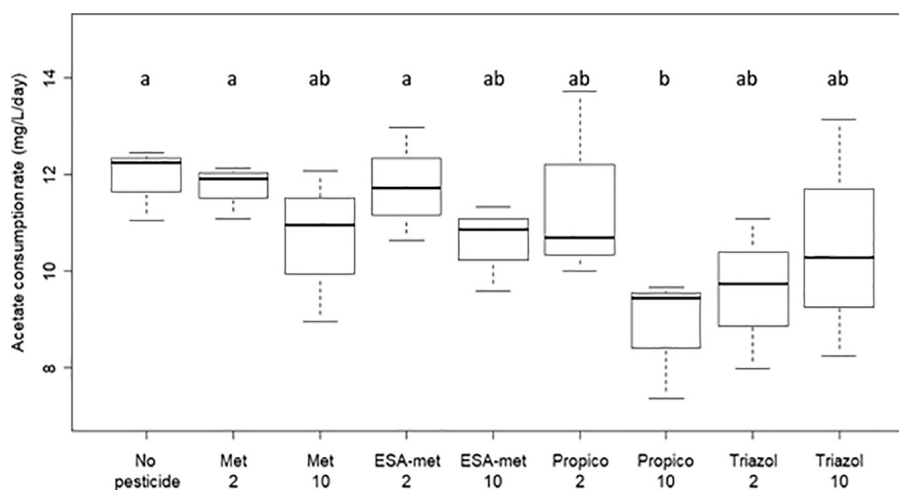
measured in flasks correspond to a mean value taking into account nitrite production due to nitrate reduction and nitrite consumption due to nitrite reduction into NO and then  $N_2O$ .

The production rate of  $N_2O$  (**Figure 1C**) was statistically not affected by the presence of metolachlor and ESA-metolachlor at 2  $\mu\text{g/L}$  since the values were similar to the ones of the control (production close to  $3.4 \times 10^{-4}$  g N/L/h). In contrast,  $N_2O$  production rate was negatively affected by the presence of ESA-metolachlor at 10  $\mu\text{g/L}$  (by 70%) and triazole at both concentrations (by 40–70%).

**TABLE 2 |** Nitrogen balance and transformation and acetate concentration during denitrification experiments (batch,  $n = 3$ ) in the presence or absence of pesticides or metabolites (at 2 or 10  $\mu\text{g/L}$ ) (here after 7 days of incubation).

Treatment	Nitrogen (after 7 days batch experiments)			Acetate concentration (mg/L) (after 7 days batch experiments)
	As N- $\text{NO}_3^-$ (%)	As N- $\text{NO}_2^-$ (%)	As N- $\text{N}_2\text{O}$ (%)	
Abiotic control	100	0	0	130.1 $\pm$ 4.8
No pesticide	54.8 $\pm$ 3.4	34.2 $\pm$ 0.2	10.9 $\pm$ 3.1	48.2 $\pm$ 5.5
Metolachlor, 2 $\mu\text{g/L}$	62.3 $\pm$ 4.6	31.1 $\pm$ 1.3	6.6 $\pm$ 3.4	50.4 $\pm$ 4.2
Metolachlor, 10 $\mu\text{g/L}$	66.2 $\pm$ 2.9	29.3 $\pm$ 1.9	4.5 $\pm$ 2.7	53.3 $\pm$ 8.6
ESA-Metolachlor, 2 $\mu\text{g/L}$	63.2 $\pm$ 8.6	21.3 $\pm$ 4.2	15.5 $\pm$ 11.6	55.7 $\pm$ 8.1
ESA-Metolachlor, 10 $\mu\text{g/L}$	77.4 $\pm$ 5.7	19.6 $\pm$ 3.8	3 $\pm$ 2	53.2 $\pm$ 3.1
Propiconazole, 2 $\mu\text{g/L}$	72.6 $\pm$ 5.3	21 $\pm$ 2.3	6.4 $\pm$ 5.3	54.4 $\pm$ 5.6
Propiconazole, 10 $\mu\text{g/L}$	69.8 $\pm$ 5.3	22.5 $\pm$ 4.3	7.5 $\pm$ 1.1	66 $\pm$ 7.3
1,2,4-triazole, 2 $\mu\text{g/L}$	72.2 $\pm$ 5.5	22.8 $\pm$ 1.2	5.1 $\pm$ 5.3	55.3 $\pm$ 4.9
1,2,4-triazole, 10 $\mu\text{g/L}$	76.6 $\pm$ 3.3	20 $\pm$ 1.6	3.4 $\pm$ 3.7	56.4 $\pm$ 1.2

For denitrification activity characterization, rates for nitrate consumption, nitrate production, and  $\text{N}_2\text{O}$  production were calculated with the data obtained during the 0–7-day period, corresponding to the maximal rates. At T0, nitrogen was present as N- $\text{NO}_3^-$  (100%) in all flasks. The nitrogen balance was also verified at all sampling times.

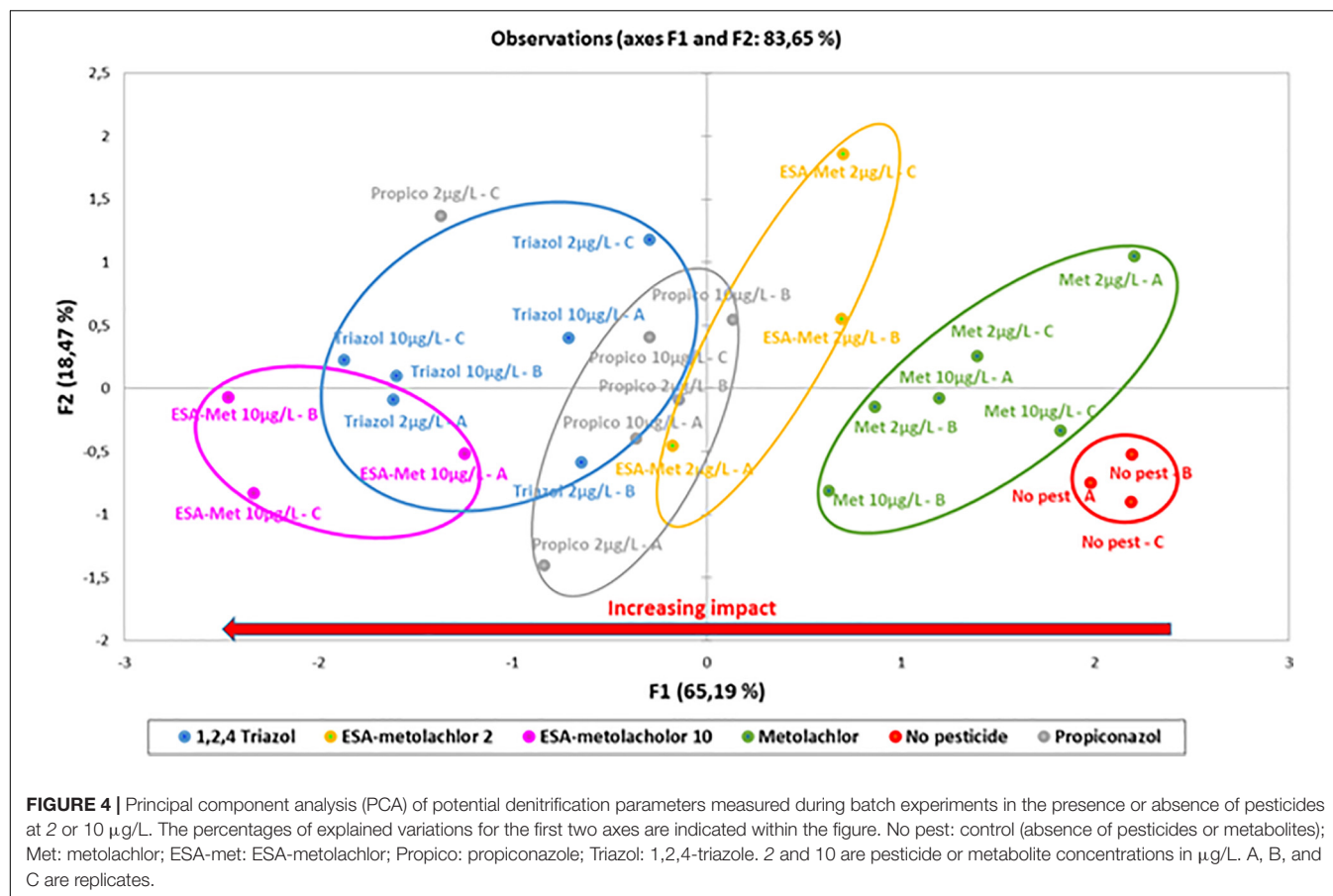
**FIGURE 3 |** Acetate consumption rate during denitrification in batch experiments with or without pesticides or metabolites. No acetate consumption took place in abiotic test batch (data not shown). No pesticide: control (absence of pesticides or metabolites); Met: metolachlor; ESA-met: ESA-metolachlor; Propico: propiconazole; Triazol: 1,2,4-triazole. 2 and 10 are pesticide or metabolite concentrations in  $\mu\text{g/L}$ . Significant differences between conditions were searched applying the Kruskal-Wallis non-parametric test and are mentioned as a and b letters.

All the results suggest that according to the compound and, in some cases, its concentration, denitrification activity was either not affected or negatively impacted (decrease of nitrate reduction rate and nitrite and  $\text{N}_2\text{O}$  production rates). As mentioned above, the denitrification process in the batch experiments was based on acetate consumption. Acetate was in excess in the solution (Table 2) and its consumption rates in the presence of the tested pesticides and metabolites did not vary significantly from the control (no pesticide), except in the presence of propiconazole at 10  $\mu\text{g/L}$  for which a lower acetate consumption rate was measured (Figure 3). This strongly suggests that there is no direct link between denitrification activity and acetate consumption (in such case, acetate consumption rate would be lowered in conditions such as ESA-metolachlor 10  $\mu\text{g/L}$ ).

The PCA analysis of the parameters used to characterize the potential denitrification activity during batch experiments

indicated, according to F1 explaining 65% of the variability (nitrate consumption, nitrite production, and  $\text{N}_2\text{O}$  production rates all contribute to this axis), the following order for the impact of pesticides and metabolites on denitrification (Figure 4): control (without pesticides or metabolites) < S-metolachlor (2 and 10  $\mu\text{g/L}$ ) < ESA-metolachlor (2  $\mu\text{g/L}$ ) < propiconazole (2 and 10  $\mu\text{g/L}$ ) < 1,2,4-triazole (2 and 10  $\mu\text{g/L}$ ) < ESA-metolachlor (10  $\mu\text{g/L}$ ). ESA-metolachlor at 10  $\mu\text{g/L}$  is thus the condition for which all the denitrification rates (nitrate reduction, nitrite production, and  $\text{N}_2\text{O}$  production) were the most significantly decreased.

Results from batch experiments also suggested that when denitrification inhibition was observed, at least the first step of denitrification was impacted as nitrate reduction rate significantly decreased (Figure 1A). To determine if pesticides also impacted the other steps of the denitrification pathway, the nitrate



reduction rate vs.  $\text{N}_2\text{O}$  production rate ratio was calculated. Whatever the compound and its concentration, its presence did not modify significantly this ratio (data not shown). This suggested that the lower  $\text{N}_2\text{O}$  production rates measured in some conditions were directly linked to lower nitrate reduction rates. The impact of the tested pesticides and metabolites thus mainly concerned the first step of denitrification, i.e., nitrate reduction into nitrite.

### Impact of Pesticides and Metabolites on the Bacterial Denitrifying Community

As the first step (nitrate reduction into nitrite) of the denitrification pathway was shown to be mainly impacted, and in order to determine if the proportion of the denitrifying community changed among the microbial community, the relative abundance of *narG* and *napA* genes, both encoding nitrate reductase, was measured using qPCR approaches (Figure 5). Data were normalized by taking into account molecular biomass (total DNA) (Bru et al., 2007; Wakelin et al., 2011; Hernández-del Amo et al., 2018). The presence of pesticides or metabolites did not significantly modify the relative abundance of both genes even in conditions for which nitrate reduction rate was decreased (in particular ESA-metolachlor at 10 µg/L), suggesting an impact (inhibition) of pesticides and metabolites at the protein level rather

than on the nitrate-reducing bacteria abundance within the bacterial community.

### Impact on Microbial Biomass

The impact of pesticides and metabolites on groundwater microbial biomass was evaluated at the end of the batch experiments *via* the measure of molecular biomass (total DNA) and bacterial biomass. Both parameters were the same in the presence or absence of pesticides or metabolites whatever the molecule and its concentration with the exception of propiconazole at 10 µg/L. In this condition, a significant decrease in molecular biomass was observed, and the lowest bacterial biomass was measured (Figure 6). This first strongly suggests that there is no direct correlation between denitrification activity and molecular biomass or bacterial biomass (in this case, a decrease of these parameters should have been observed in the ESA-metolachlor 10 µg/L condition particularly). This also suggests that propiconazole at 10 µg/L can inhibit groundwater microbial growth.

### Impact on Bacterial Diversity

The bacterial community diversity was determined by Illumina 16S rRNA sequencing on batch experiment samples after pesticide or metabolite exposure during 20 days. Results first showed that among all the samples, the two main phyla were

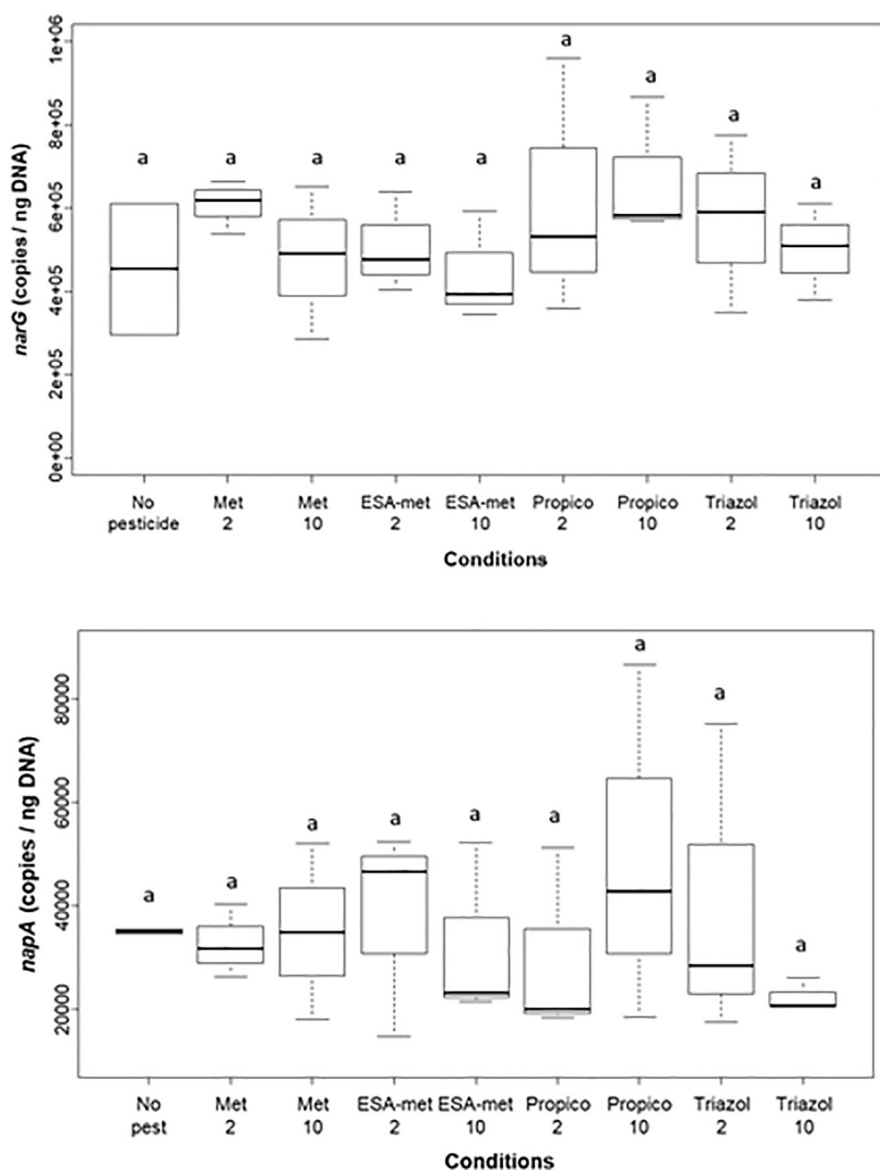


**FIGURE 5 |** Abundance of *narG* (top) and *napA* (bottom) genes (involved in nitrate reduction) at the end of batch experiments. Results are given as relative abundance, i.e., data were normalized by taking into account molecular biomass. No pest: no pesticide or metabolite (control); Met: metolachlor; ESA-met: ESA-metolachlor; Propico: propiconazole; Triazol: 1,2,4 triazole. 2 and 10 are pesticide or metabolite concentrations in  $\mu\text{g/L}$ . Significant differences between conditions were searched applying the Kruskal-Wallis non-parametric test and are mentioned as a letter.

Proteobacteria (as the most dominant phylum) and to a lesser extent Bacteroidetes. As expected, when looking at the genus level, the conditions applied in batch experiments in favor of denitrification led to the selection of bacteria involved in the N cycle. Indeed, the *Aquabacterium* genus, known to reduce nitrate into nitrite (Kalmbach et al., 1999), was the most dominant genus at the end of all batch experiments (Figure 7). In addition, other genera such as *Azospirillum* (Kloos et al., 2001) and *Rhodferax* (Hougardy and Klemme, 1995), also known to reduce nitrate into nitrite, were detected. No genus was specific to a given batch condition except *Ideonella* that was found only in the condition with ESA-metolachlor at 10  $\mu\text{g/L}$

and *Rhodferax* found in the condition with 1,2,4-triazole at 10  $\mu\text{g/L}$ . There was no significant difference between values of Shannon and InvSimpson ( $1/D$ ) biodiversity indices among most samples (Figure 8), suggesting that pesticides and metabolites at low (environmental) concentrations did not significantly impact groundwater bacterial community diversity. However, results suggested that ESA-metolachlor at 10  $\mu\text{g/L}$  tended to increase Shannon and InvSimpson indices and that propiconazole at 10  $\mu\text{g/L}$  tended to decrease both biodiversity indices. When comparing diversity depending on the pesticide or metabolite type and concentration, bacterial communities were comparable in terms of genus presence and relative abundance tendencies,



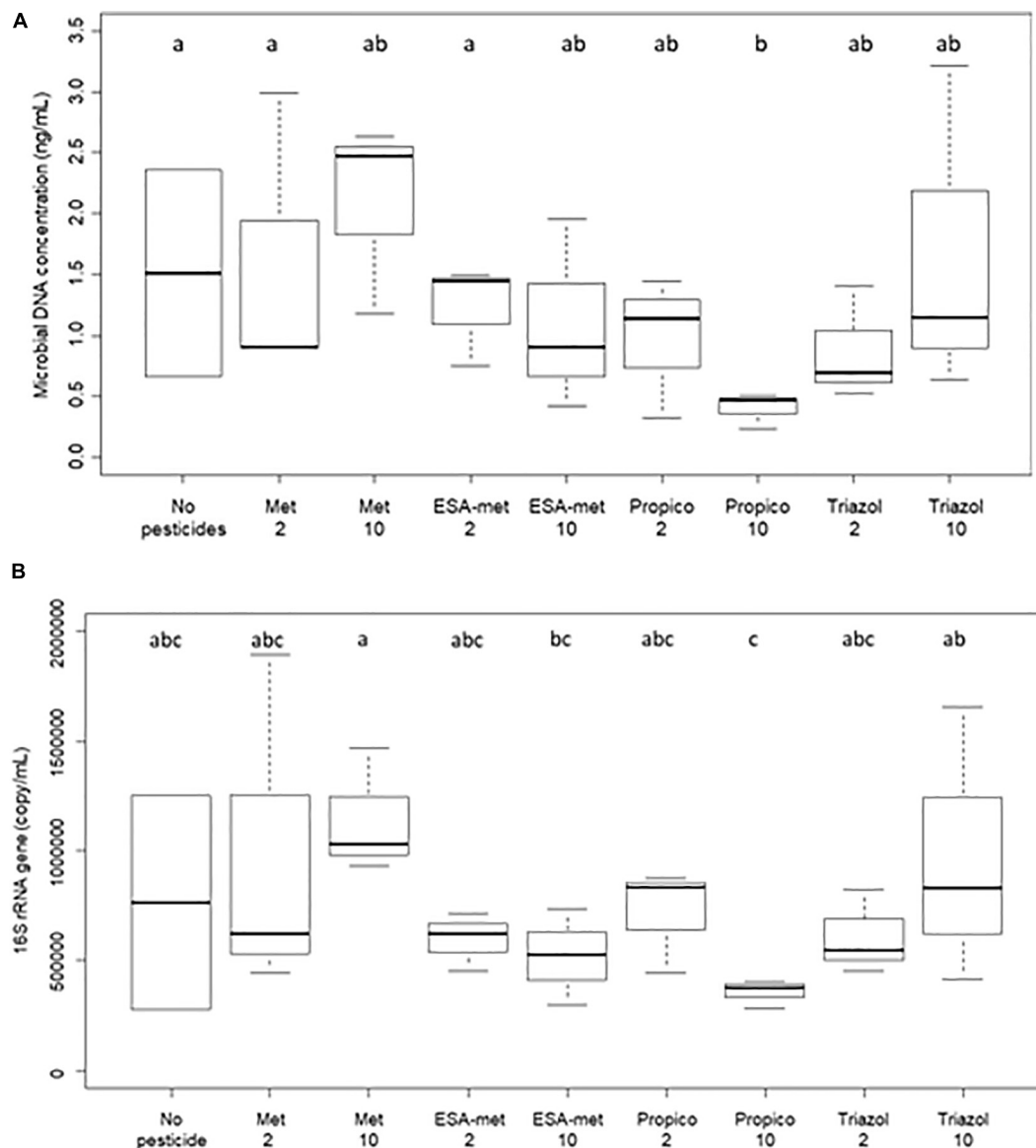


**FIGURE 6 |** Biomass quantification in flasks at the end of batch experiments. **(A)** Molecular biomass (measured as total DNA concentration) and **(B)** bacterial biomass (measured as bacterial 16S rRNA gene copies). No pesticide: control (absence of pesticides or metabolites); Met: metolachlor; ESA-met: ESA- metolachlor; Propico: propiconazole; Triazol: 1,2,4-triazole. 2 and 10 are pesticide or metabolite concentrations in  $\mu\text{g/L}$ . Significant differences between conditions were searched applying the Kruskal–Wallis non- parametric test and are mentioned as a, b, and c letters.

except for the conditions with ESA-metolachlor at  $10 \mu\text{g/L}$  and 1,2,4-triazole at  $10 \mu\text{g/L}$ , in which *Ideonella* and *Rhodoferrax* were specifically found, respectively, as mentioned above.

## DISCUSSION

In this paper, the potential side effects of some pesticides and their metabolites frequently detected in groundwater on groundwater microbial ecosystems were investigated. In particular, a focus was done on the potential impact of these compounds on the denitrification activity supported by the groundwater bacterial

community. The strategy used in the study was to perform all the tests (batch experiments at the lab scale) with the same groundwater sample, which allowed comparing the results. Indeed, such a strategy enables to circumvent the potential effects due to hydrogeochemical and seasonal variations in groundwater and to strong spatial and temporal variations in groundwater bacterial communities (de Liphay et al., 2004; Imfeld et al., 2018). In our study, nitrate reduction rate measured in the absence of pesticides/metabolites (control) was about  $5.6 \times 10^{-5} \text{ g N/L/h}$ . Even if it is difficult to compare acquired data with already published denitrification rates because of the numerous factors affecting this process (pH, temperature, nitrate and electron

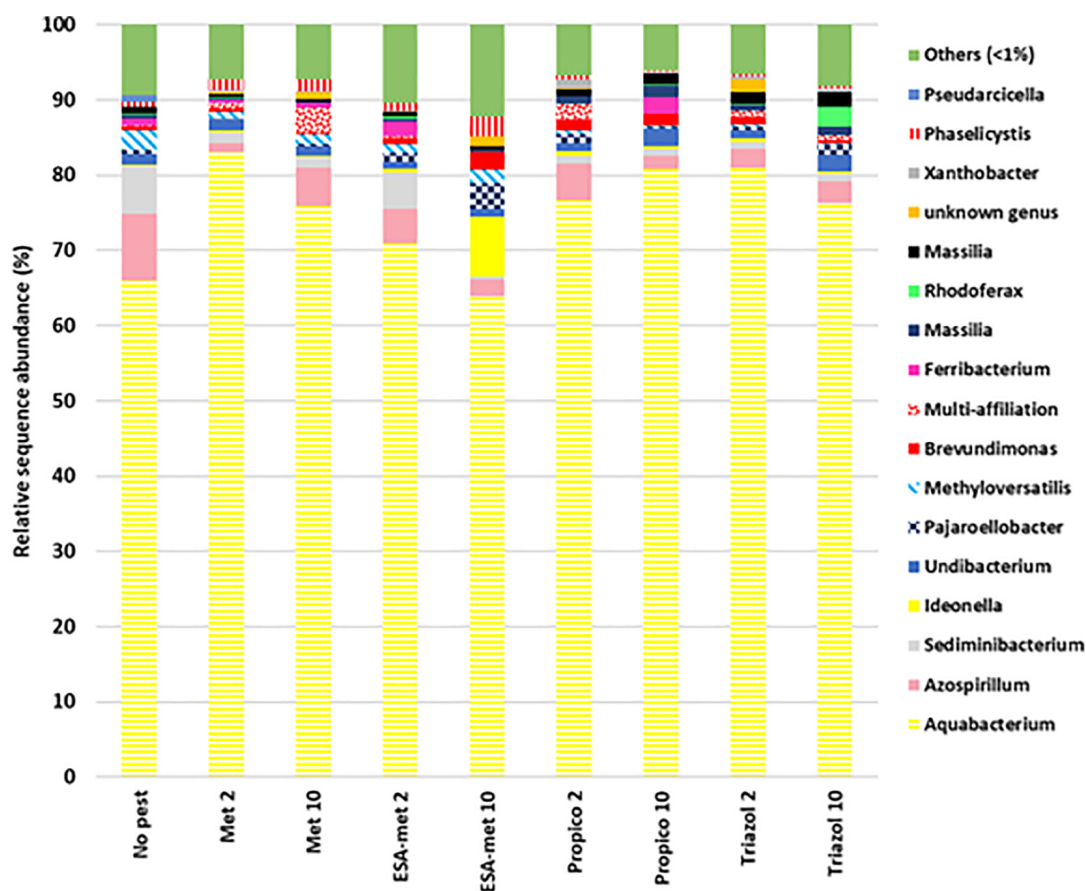


**FIGURE 7 |** Relative abundance of bacterial genera at the end of batch experiments, representing at least 1% of obtained sequences in at least one sample. Data represent average values of experimental replicates. No pest: control (absence of pesticides or metabolites); Met: metolachlor; ESA-met: ESA-metolachlor; Propico: propiconazole; Triazol: 1,2,4-triazole. 2 and 10 are pesticide or metabolite concentrations in  $\mu\text{g/L}$ .

donor concentrations, etc.), denitrification rates measured in laboratory experiments generally vary between  $7.0 \times 10^{-6}$  and  $1.0 \times 10^{-4}$  g N/L/h (Trudell et al., 1986; Starr and Gillham, 1993; Schipper and Vojvodic Vukovic, 1998, 2000; Devlin et al., 2000; André et al., 2011). The values determined in this study for the control (without pesticide) and for the conditions with pesticide/metabolite are thus in the same order of magnitude than other studies.

### Side Effects of Pesticides and Their Metabolites on the Metabolism of Groundwater Microbial Community

Among the compounds tested, S-metolachlor at environmental concentrations was shown to have no or minor impact on denitrification as well as on general microbial parameters (biomass, acetate consumption) of the tested groundwater microbial community. This is in agreement with previous studies such as that of de Lipthay et al. (2004) who suggested no major effect of S-metolachlor on *in situ* groundwater bacterial community (using Ecolog and DGGE fingerprinting approaches). Mauffret et al. (2017) showed that

the chloroacetanilide family had no impact on the bacterial community structure but increased the abundance of nitrate reductase *napA* gene. This last point is not in agreement with our results that showed no impact of the tested pesticides on the relative abundance of the nitrate reductase *narG* and *napA* genes involved in the first step of denitrification. One explanation is probably that the data of Mauffret et al. (2017) were obtained from *in situ* groundwater, whereas our results concern batch experiments, and it has been demonstrated that for *in situ* studies particularly, there are difficulties to tease apart the effect of pesticides from the effects of variations of hydrogeological conditions (Imfeld et al., 2018). Moreover, as mentioned above, microbial community diversity as well as the history of pesticide contamination (i.e., communities previously in contact or not with pesticides) can influence the impact of pesticides. Finally, the work of Imfeld et al. (2018) also suggested a little effect of metolachlor on *in situ* bacterial groundwater community (Microtox test and T-RFLP fingerprints). In this same work, the transformation products of S-metolachlor (as ESA and OXA-metolachlor) were shown to have no effect on microbial metabolism. We obtained a similar result in denitrifying condition when considering general growth

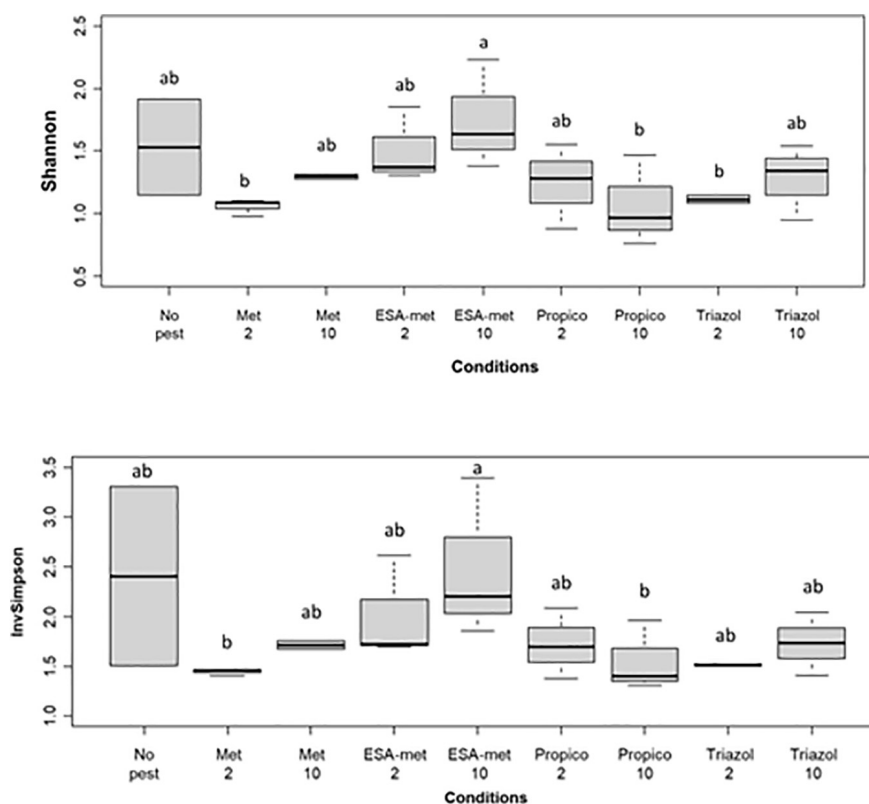


**FIGURE 8 |** Biodiversity index of the bacterial communities at the end of batch experiments (20 days): **(Top)** Shannon index and **(Bottom)** InvSimpson index. No pest: control (absence of pesticides or metabolites); Met: metolachlor; ESA-met: ESA-metolachlor; Propico: propiconazole; Triazol: 1,2,4-triazole. 2 and 10 are pesticide or metabolite concentrations in  $\mu\text{g/L}$ . Significant differences between conditions were searched applying the Kruskal-Wallis non-parametric test and are mentioned as a, b, and c letters.

parameters. Indeed, ESA-metolachlor had no impact on biomass and acetate consumption. However, in such anoxic conditions, ESA-metolachlor (at  $10 \mu\text{g/L}$ ) had the highest negative impact on denitrification. Taking into account our study and that of Imfeld et al. (2018), it can be suggested that pesticides or metabolites (like ESA-metolachlor) could mainly have side effects on specific communities and/or targeted metabolisms (like denitrification), and not on the whole microbial community.

Concerning the potential side effects of the members of the conazole family, our results suggested that propiconazole and 1,2,4-triazole had a higher adverse effect on the microbial denitrifying community of the studied groundwater than chloroacetanilide [as S-metolachlor and ESA-metolachlor (at  $2 \mu\text{g/L}$ )]. Moreover, propiconazole (at  $10 \mu\text{g/L}$ ) was shown to inhibit microbial growth as less microbial biomass was produced in its presence. This is in agreement with Milenkovski et al. (2010) who found (via leucine incorporation experiments) that propiconazole and other fungicides belonging to different chemical classes had an inhibitory effect on microbial metabolism. In their study, these authors did not notice any impact of propiconazole on denitrification but measured an inhibition of the denitrification pathway with other fungicides. Saez et al. (2003), by comparing the impact of various insecticides, herbicides, and fungicides (at  $10 \mu\text{g/L}$ ) on the pure denitrifying

strain *Paracoccus denitrificans*, observed the more severe effects on bacterial growth and activity with fungicides. Staley et al. (2015) also concluded, by comparing a large number of studies, that fungicides seemed to be most deadly to microorganisms than herbicides.

At last, this study showed that among the tested compound, metabolites (here, ESA-metolachlor and 1,2,4-triazole) have a more significant impact on denitrification than mother molecules (Figure 4). Bollag and Kurek (1980) already demonstrated that chlordimeform (organochloride insecticide) metabolites (at  $25 \text{ mg/L}$  and more) negatively impacted soil microbial denitrification (accumulation of nitrite and nitrous oxide), whereas chlordimeform itself had no impact at the same concentrations (and even at  $100 \text{ mg/L}$ ). As mentioned in the *Introduction*, metabolites exhibit high occurrence in groundwater and sometimes with concentrations of the order of micrograms per liter. This was demonstrated by several studies such as Fisher et al. (2021) for ESA-metolachlor and 1,2,4-triazole as well as for other metabolites such as 4-hydroxychlorothalonil (ranging from  $0.13$  to  $368 \mu\text{g/L}$ ). Another recent study in which 116 metabolites on 1,204 sites were analyzed also showed that six metabolites exhibit concentrations higher than  $0.1 \mu\text{g/L}$  [notably 4-hydroxychlorothalonil in 1.6% of the samples with a maximum concentration of  $17.540 \mu\text{g/L}$ , and 22 metabolites with a detection

frequency higher than 1% (Bexfield et al., 2021)]. Our results together with other studies thus suggest that metabolites can greatly impact the microbial ecosystem in groundwater.

## Side Effects of the Tested Pesticides and Metabolites on the Denitrification Pathway

Our study showed that the first step of denitrification (reduction of nitrate into nitrite) supported by nitrate reductase enzymes was the main step impacted/inhibited by the studied pesticides or metabolites. Nitrate reductase is encoded by *narG* or *napA* genes, depending on the bacterial strain. In our study, the abundance of *narG* and *napA* genes was not impacted by the presence of the tested pesticides and metabolites. This suggests that the impact of the tested compounds probably occurs rather on gene expression and/or enzymatic activity itself. Pankaj and Gore (2015) already showed that the activity of enzyme nitrate reductase of plants was inhibited by some phytopharmaceutical products (confidor, omite, and karathane) and their active substances (imidacloprid, propargite, and meptyldinocap). The work of Saez et al. (2003) also suggested that some pesticides (methylparathion, atrazine, and simazine) affected the expression of the nitrate reductase activity of the bacterial strain *P. denitrificans* at a concentration of 10 mg/L. The activity of other enzymes of the denitrification pathway was shown, in some cases, to be also affected by pesticides. As an example, the presence of aldrin, lindane, dimethoate, and methidathion led to the inhibition of nitrite reductase activity in the study conducted by Saez et al. (2003). Su et al. (2019) also observed (in riparian sediments) an inhibition of the activity of nitrate reductase, nitrite reductase, and  $N_2O$  reductase (but not  $NO$  reductase) enzymes involved in the denitrification pathway by the pesticide chlorothalonil (at 2 mg/kg and more). These authors also demonstrated an impact of this pesticide on *narG* gene relative abundance, but not on the relative abundance of *nirK*, *norB*, and *nosZ* genes involved in the next steps of denitrification. This indicates that there was no direct matching between responses to the presence of pesticides at the protein and genetic levels. In our study, only nitrate reductase activity was impacted and this impact was detected for concentrations as low as 2 or 10  $\mu\text{g/L}$  according to the pesticides or metabolites (Figure 1). However, it has to be mentioned that as we used acetylene in our experiment, the impact of pesticides or metabolites on the last step of denitrification (reduction of  $N_2O$  into  $N_2$  by the enzyme nitrous oxide reductase encoded by *nosZ* gene) cannot be evaluated here.

## Diversity of the Groundwater Bacterial Community in the Presence of Pesticides and Metabolites

In our study, the presence and relative abundance of bacterial genera were similar for most of the conditions, suggesting that the composition of the bacterial community was generally weakly affected by the presence of pesticides or metabolites at environmental concentrations. Only two genera were found specific (*Ideonella* for ESA-metolachlor at 10  $\mu\text{g/L}$  and *Rhodospirillum* for 1,2,4-triazole at 10  $\mu\text{g/L}$ ). This is in agreement

with previous studies that reported minor effects of pesticides on the overall composition of the groundwater microbial community. Indeed, Imfeld et al. (2018) found that OTUs specific to pesticide presence and correlating with metolachlor (even at 5 mg/L) addition in batch experiments ranged only between 0.4 and 3.6% of the total. In the same way, de Liphay et al. (2004) found no DGGE DNA bands that were unique for the herbicide (a mixture of six herbicides at 40  $\mu\text{g/L}$  each)-exposed subsurface sediments (shallow aquifer). Shannon and InvSimpson diversity indices obtained at the end of our batch experiments suggested a potential increase or decrease of bacterial diversity in the presence of ESA-metolachlor or propiconazole at 10  $\mu\text{g/L}$ , respectively. On the opposite, ESA-metolachlor and propiconazole at 2  $\mu\text{g/L}$ , as well as the other tested pesticides and metabolites, did not impact diversity indices suggesting that the diversity may be impacted differently according to the molecule and its concentration. Results obtained with ESA-metolachlor at 10  $\mu\text{g/L}$  are in agreement with several other studies on groundwater impacted by pesticides that, as mentioned above, displayed higher diversity indices [based on carbon source utilization (EcoPlate), colony morphology, DGGE analyses, or Illumina sequencing] in the presence of some pesticides (de Liphay et al., 2004; Janniche et al., 2012; Imfeld et al., 2018). The higher diversity observed in some pesticide-polluted aquifers compared with unpolluted aquifers can be explained by various hypotheses. First, as some microorganisms can metabolize pesticides and use them as a source of C (Munoz et al., 2011; Satapute and Kaliwal, 2016) and even N (Sanchez-Sanchez et al., 2013; Wang et al., 2016) or P (Shushkova et al., 2012) according to pesticide composition, the presence of pesticides can result in an increase in microbial abundance and diversity. This is particularly true in the case of groundwater that is naturally weakly charged in organic matter [as the groundwater we used in this study, whose DOC content was under the limit of detection (Table 1)] and where pesticides can represent a new source of nutrients. Secondly, as pesticides have a lethal effect on some microorganisms but not on all microorganisms, their presence can lead to the cell lysis of non-resistant microorganisms and thus increase nutrient sources for resistant microorganisms and thus impact biodiversity. Thirdly, the presence of a toxic compound, by killing sensitive strains and/or inhibiting (even partially) their activity, limits the number of competitors for available nutrients. Resistant microorganisms can thus thrive in an easier manner, and strains initially in minority, if resistant, can become dominant strains. This could be the case in batch experiments with ESA-metolachlor (10  $\mu\text{g/L}$ ) in our study. Indeed, this metabolite partially inhibits and slows down the activity of denitrifying bacteria, and its presence allows the development of microorganisms such as *Ideonella*, *Brevundimonas*, and *Pajaroellobacter* that are in higher abundance or even specific to this condition and that are not known to be linked to denitrification, which leads to a higher diversity. This is in agreement with Staley et al. (2015) who concluded that in a microbial community, even if the direct effects of a pesticide family on some microorganisms are negative, some indirect positive effects can occur for other microorganisms. The direct negative effects can thus tend to be



offsetted when considering the impact at the community level. These authors also insist on the fact that it is difficult to conclude on the direct impacts of pesticides on bacterial communities as the impact can be contrasting according to bacterial species, pesticide concentration, time of exposure, etc., probably due to the broad diversity of strategies used by bacteria. Finally, as underlined by Jacobsen and Hjelmsø (2014), conclusions on the direct and/or indirect effects induced by the presence of pesticides on microbial diversity are not easy to determine. Indeed, in most cases, the links between phylogeny and functions are not directly established for bacteria, and because in all ecosystems, many groups (such as – according to the ecosystem – bacteria, archaea, fungi, plants, and nematodes) interact within or between each other.

## CONCLUSION

The current study demonstrates that some pesticides and metabolites can have a negative impact on the activity of the denitrifying community in groundwater (decrease of the activity) at environmental concentrations. The impact of metabolites can be higher than that of pesticides (parent molecules) and mainly concerns the first step of the denitrification pathway, very probably because of an inhibitory impact on the nitrate reductase enzyme itself. Finally, the presence of some pesticides and metabolites in groundwater can also impact the global growth of the groundwater microbial community as well as its biodiversity. The study thus emphasizes that pesticides and metabolites affect groundwater communities even at environmental low concentrations (2 µg/L and potentially less), strongly insisting on the need to carry out studies at low pesticide/metabolite concentrations to get a realistic picture on how these molecules can affect subsurface microbial communities and activities.

This study, with a few others, is of particular interest as the side effects of pesticides and metabolites on soil microorganisms already have to be taken into account during European pesticide registration (regulation EC no. 1107/2009). Indeed, approved pesticides shall have no unacceptable effects on the environment, e.g., impact on soil biodiversity and the ecosystem. To date, scientific methods accepted by the authority are available for studying the impact on N cycle in soils (test guideline OCDE 216 “Soil Microorganisms: Nitrogen Transformation Test”), thus

allowing a systematic evaluation for each new approved (or re-approved) active substance. Our results illustrate the importance to also consider more systematically the impacts on subterranean ecosystems in the frame of the European pesticide registration procedure. Finally, the impacts of pesticides and/or metabolites as cocktail will have also to be taken into account in future evaluations of pesticides for their registration.

## DATA AVAILABILITY STATEMENT

The datasets presented in this study can be found in online repositories. The names of the repository/repositories and accession number(s) can be found below: <https://www.ebi.ac.uk/ena>, PRJEB42682.

## AUTHOR CONTRIBUTIONS

CM, NB, LA, and CJ conceived and designed the research. CM and CJ conducted the experiments, with the technical support of MC, and were actively involved in microbial analyses. NB was involved in sampling site chemical characterization and groundwater sampling as well as chemical analysis. LA was involved in chemical and nitrogen balance analysis. CM wrote and revised the manuscript. NB, LA, and CJ were actively involved in its editing and revision. All authors read, corrected, and approved the manuscript.

## FUNDING

This work was funded by Agence de l'Eau Loire Bretagne (France) and BRGM in the frame of the IPAD project (Decision 2016C.007 du 22/12/2016).

## ACKNOWLEDGMENTS

The authors would like to thank Thibault Conte for chemical analysis management, Chems Mohamad for DNA extraction, and Benoit Henry for gas analysis. The authors also thank the MetaHealth metagenomic-based services (CIRAD, PHIM, Eco&Sols, Montpellier, France) for MiSeq Illumina sequencing.

## REFERENCES

- Afgan, E., Baker, D., Batut, B., van den Beek, M., Bouvier, D., Čech, M., et al. (2018). The Galaxy platform for accessible, reproducible and collaborative biomedical analyses: 2018 update. *Nucl. Acids Res.* 46, W537–W544.
- Albrechtsen, H. J., Mills, M. S., Aamand, J., and Bjerg, P. (2001). Degradation of herbicides in shallow Danish aquifers: an integrated laboratory and field study. *Pest Manag. Sci.* 57, 341–350.
- Amalric, L., Baran, N., Coureau, C., Maingot, L., Buron, F., and Routier, S. (2013). Analytical developments for 47 pesticides: first identification of neutral chloroacetanilide derivatives in French groundwater. *Int. Environ. Anal. Chem.* 93, 1660–1675. doi: 10.1080/03067319.2013.853758
- Anantharaman, K., Brown, C., Hug, L., Sharon, I., Castelle, C., Probst, A., et al. (2016). Thousands of microbial genomes shed light on interconnected biogeochemical processes in an aquifer system. *Nat. Commun.* 7:13219.
- André, L., Pauwels, H., Dictor, M.-C., Parmentier, M., and Azaroual, M. (2011). Experiments and numerical modelling of microbially-catalysed denitrification reactions. *Chem. Geol.* 287, 171–181. doi: 10.1016/j.chemgeo.2011.06.008
- Andrews, S. (2010). *FastQC: A Quality Control Tool for High Throughput Sequence Data*. Available online at: <http://www.bioinformatics.babraham.ac.uk/projects/fastqc/> (accessed October 30, 2020).
- Bælum, J., Nicolaisen, M. H., Holben, W. E., Strobel, B. W., Sørensen, J., and Jacobsen, C. S. (2008). Direct analysis of tfdA gene expression by indigenous bacteria in phenoxy acid amended agricultural soil. *ISME J.* 2, 677–687. doi: 10.1038/ismej.2008.21

- Baran, N., and Gourcy, L. (2013). Sorption and mineralization of S-metolachlor and its ionic metabolites in soils and vadose zone solids: consequences on groundwater quality in an alluvial aquifer (Plaine de l'Ain, France). *J. Contam. Hydrol.* 154, 20–28. doi: 10.1016/j.jconhyd.2013.07.009
- Barra Caracciolo, A., Grenni, P., Sacca, M. L., Amalfitano, S., Ciccoli, R., Martin, M., et al. (2010). The role of a groundwater bacterial community in the degradation of the herbicide terbuthylazine. *FEMS Microbiol. Ecol.* 71, 127–136. doi: 10.1111/j.1574-6941.2009.00787.x
- Bexfield, L. M., Belitz, K., Lindsey, B. D., Toccalino, P. L., and Nowell, L. H. (2021). Pesticides and pesticide degradates in groundwater used for public supply across the United States: occurrence and human-health context. *Environ. Sci. Technol.* 55, 362–372. doi: 10.1021/acs.est.0c05793
- Bollag, J. M., and Kurek, E. (1980). Nitrite and nitrous oxide accumulation during denitrification in the presence of pesticides derivatives. *Appl. Environ. Microbiol.* 39, 845–849. doi: 10.1128/aem.39.4.845-849.1980
- Bru, D., Sarr, A., and Philippoy, L. (2007). Relative abundances of proteobacterial membrane-bound and periplasmic nitrate reductases in selected environments. *Appl. Environ. Microbiol.* 73, 5971–5974. doi: 10.1128/aem.00643-07
- Cabrol, L., Quéméneur, M., and Misson, B. (2017). Inhibitory effects of sodium azide on microbial growth in experimental resuspension of marine sediment. *J. Microbiol. Methods* 133, 62–65. doi: 10.1016/j.mimet.2016.12.021
- Crouzet, O., Poly, F., Bonnemoy, F., Bru, D., Batisson, I., Bohatier, J., et al. (2016). Functional and structural responses of soil N-cycling microbial communities to the herbicide mesotrione: a dose-effect microcosm approach. *Environ. Sci. Pollut. Res.* 23, 4207–4217. doi: 10.1007/s11356-015-4797-8
- de Liphay, J. R., Johnsen, K., Albrechtsen, H.-J., Rosenberg, P., and Aamand, J. (2004). Bacterial diversity and community structure of a sub-surface aquifer exposed to realistic low herbicide concentrations. *FEMS Microbiol. Ecol.* 49, 59–69. doi: 10.1016/j.femsec.2004.02.007
- Devlin, J. F., Eedy, R., and Butler, B. J. (2000). The effects of electron donor and granular iron on nitrate transformation rates in sediments from a municipal water supply aquifer. *J. Contam. Hydrol.* 46, 81–97. doi: 10.1016/s0169-7722(00)00126-1
- Dibbern, D., Schmalwasser, A., Lueders, T., and Totsche, K. (2014). Selective transport of plant root-associated bacterial populations in agricultural soils upon snowmelt. *Soil Biol. Biochem.* 69, 187–196. doi: 10.1016/j.soilbio.2013.10.040
- Escudié, F., Auer, L., Bernard, M., Mariadassou, M., Cauquil, L., Vidal, K., et al. (2017). FROGS: find, rapidly, OTUs with Galaxy solution. *Bioinformatics* 34, 1287–1294. doi: 10.1093/bioinformatics/btx791
- Ewels, P., Magnusson, M., Lundin, S., and Käller, M. (2016). MultiQC: summarize analysis results for multiple tools and samples in a single report. *Bioinformatics* 32, 3047–3048. doi: 10.1093/bioinformatics/btw354
- Fillinger, L., Hug, K., and Griebler, C. (2019). Selection imposed by local environmental conditions drives differences in microbial community composition across geographically distinct groundwater aquifers. *FEMS Microbiol. Ecol.* 95:fiz160. doi: 10.1093/femsec/fiz160
- Fisher, I. J., Philipps, P. J., Bayraktar, B. N., Chan, S., McCarthy, B. A., and Sandstrom, M. W. (2021). Pesticides and their degradates in groundwater reflect past use and current management strategies, Long Island, New York, USA. *Sci. Total Environ.* 752:141895. doi: 10.1016/j.scitotenv.2020.141895
- Gregory, S., Maurice, L., West, J., and Gooddy, D. (2014). Microbial communities in UK aquifers: current understanding and future research needs. *Q. J. Eng. Geol. Hydrogeol.* 47, 145–157. doi: 10.1144/qjegh2013-059
- Grenni, P., Gibello, A., Barra Caracciolo, A., Fajardo, C., Nande, M., Vargas, R., et al. (2009). A new fluorescent oligonucleotide probe for in situ detection of s-triazine-degrading *Rhodococcus wratislaviensis* in contaminated groundwater and soil samples. *Water Res.* 43, 2999–3008. doi: 10.1016/j.watres.2009.04.022
- Griebler, C., and Avramov, M. (2015). Groundwater ecosystem services: a review. *Freshw. Sci.* 34, 355–367. doi: 10.1086/679903
- Griebler, C., and Lueders, T. (2009). Microbial biodiversity in groundwater ecosystems. *Freshw. Biol.* 54, 649–677. doi: 10.1111/j.1365-2427.2008.02013.x
- Hernández-del Amo, E., Menció, A., Gich, F., Mas-Pla, J., and Baneras, L. (2018). Isotope and microbiome data provide complementary information to identify natural nitrate attenuation processes in groundwater. *Sci. Total Environ.* 613–614, 579–591. doi: 10.1016/j.scitotenv.2017.09.018
- Hougardey, A., and Klemme, J.-H. (1995). Nitrate reduction in a new strain of *Rhodoferrax fermentans*. *Arch. Microbiol.* 164, 358–362. doi: 10.1007/s002030050275
- Hoyle, B. L., and Arthur, E. L. (2000). Biotransformation of pesticides in saturated-zone materials. *Hydrogeol. J.* 8, 89–103. doi: 10.1007/s100400050010
- Hubalek, V., Wu, X., Eiler, A., Buck, M., Heim, C., Dopson, M., et al. (2016). Connectivity to the surface determines diversity patterns in subsurface aquifers of the Fennoscandian shield. *ISME J.* 10, 2447–2458. doi: 10.1038/ismej.2016.36
- Hussain, S., Siddique, T., Saleem, M., Arshad, M., and Khalid, A. (2009). Impact of pesticides on soil microbial diversity, enzymes, and biochemical reactions. *Adv. Agron.* 102, 159–200. doi: 10.1016/s0065-2113(09)01005-0
- Iker, B. C., Kambesis, P., Oehrlé, S. A., Groves, C., and Barton, H. A. (2010). Microbial atrazine breakdown in a karst groundwater system and its effect on ecosystem energetics. *J. Environ. Qual.* 39, 509–518. doi: 10.2134/jeq2009.0048
- Imfeld, G., Besaury, L., Maucourt, B., Donadello, S., Baran, N., and Vuilleumier, S. (2018). Toward integrative bacterial monitoring of metolachlor toxicity in groundwater. *Front. Microbiol.* 9:2053. doi: 10.3389/fmicb.2018.02053
- Jacobsen, C. S., and Hjelmso, M. H. (2014). Agricultural soils, pesticides and microbial diversity. *Curr. Opin. Biotechnol.* 27, 15–20. doi: 10.1016/j.copbio.2013.09.003
- Janniche, G. S., Spliid, H., and Albrechtsen, H.-J. (2012). Microbial community-level physiological profiles (CLPP) and herbicide mineralization potential in groundwater affected by agricultural land use. *J. Contam. Hydrol.* 140–141, 45–55. doi: 10.1016/j.jconhyd.2012.08.008
- Jurado, A., Vázquez-Suñé, E., Carrera, J., López de Alda, M., Pujades, E., and Barceló, D. (2012). Emerging organic contaminants in groundwater in Spain: a review of sources, recent occurrence and fate in a European context. *Sci. Total Environ.* 440, 82–94. doi: 10.1016/j.scitotenv.2012.08.029
- Kalia, A., and Gosal, S. (2011). Effect of pesticide application on soil microorganisms. *Arch. Agron. Soil Sci.* 57, 569–596. doi: 10.1080/03650341003787582
- Kalkhoff, S., Vecchia, A., Capel, P., and Meyer, M. (2012). Eleven-year trend in acetanilide pesticide degradates in the Iowa River, Iowa. *J. Environ. Qual.* 41, 1566–1579. doi: 10.2134/jeq2011.0426
- Kalmbach, S., Manz, W., Wecke, J., and Szewzyk, U. (1999). *Aquabacterium* gen. nov., with description of *Aquabacterium citratiphilum* sp. nov., *Aquabacterium parvum* sp. nov. and *Aquabacterium commune* sp. nov., three in situ dominant bacterial species from the Berlin drinking water system. *Int. J. Syst. Bacteriol.* 49, 769–777. doi: 10.1099/00207713-49-2-769
- Kloos, K., Mergel, A., Rösch, C., and Bothe, H. (2001). Denitrification within the genus *Azospirillum* and other associative bacteria. *Aust. J. Plant Physiol.* 28, 991–998. doi: 10.1071/PP01071
- Lancaster, S. H., Hollister, E. B., Senseman, S. A., and Gentry, T. J. (2010). Effects of repeated glyphosate applications on soil microbial community composition and the mineralization of glyphosate. *Pest Manag. Sci.* 66, 59–64. doi: 10.1002/ps.1831
- Lapworth, D., Baran, N., Stuart, M., and Ward, R. (2012). Emerging organic contaminants in groundwater: a review of sources, fate and occurrence. *Environ. Pollut.* 163, 287–303. doi: 10.1016/j.envpol.2011.12.034
- Lazar, C., Stoll, W., Lehmann, R., Herrmann, M., Schwab, V., Akob, D., et al. (2017). Archaeal diversity and CO<sub>2</sub> fixers in carbonate-/siliciclastic-rock groundwater ecosystems. *Archaea* 2017:2136287. doi: 10.1155/2017/2136287
- Lo, C. C. (2010). Effect of pesticides on soil microbial community. *J. Environ. Sci. Health. B* 45, 348–359. doi: 10.1080/03601231003799804
- Loos, R., Locoro, G., Comero, S., Contini, S., Schwesig, D., Werres, F., et al. (2010). Pan-European survey on the occurrence of selected polar organic persistent pollutants in ground water. *Water Res.* 44, 4115–4126. doi: 10.1016/j.watres.2010.05.032
- Lopez, B., Ollivier, P., Togola, A., Baran, N., and Ghestem, J. P. (2015). Screening of French groundwater for regulated and emerging contaminants. *Sci. Total Environ.* 518–519, 562–573. doi: 10.1016/j.scitotenv.2015.01.110
- López-Gutiérrez, J. C., Henry, S., Hallet, S., Martin-Laurent, F., Catroux, G., and Philippot, L. (2004). Quantification of a novel group of nitrate-reducing bacteria in the environment by real-time PCR. *J. Microbiol. Methods* 57, 399–407. doi: 10.1016/j.mimet.2004.02.009
- Mauffret, A., Baran, N., and Joulain, C. (2017). Effect of pesticides and metabolites on groundwater bacterial community. *Sci. Total Environ.* 576, 879–887. doi: 10.1016/j.scitotenv.2016.10.108

- Milenkovski, S., Bååth, E., Lindgren, P.-E., and Berglund, O. (2010). Toxicity of fungicides to natural bacterial communities in wetland water and sediment measured using leucine incorporation and potential denitrification. *Ecotoxicology* 19, 285–294. doi: 10.1007/s10646-009-0411-5
- Munoz, A., Koskinen, W., Cox, L., and Sadowsky, M. (2011). Biodegradation and mineralization of metolachlor and alachlor by *Candida xestobii*. *J. Agric. Food Chem.* 59, 619–627. doi: 10.1021/jf103508w
- Pankaj, S., and Gore, R. (2015). Effect of pesticide on nitrate reductase activity in *Trigonella foenum* i.e., Fenugreek. *J. Hort.* 2:166. doi: 10.4172/2376-0354.1000166
- Petelet-Giraud, E., Baran, N., Vergnaud-Ayraud, V., Portal, A., Michel, C., Joulain, C., et al. (2021). How to reveal nitrate fate and processes in a basement aquifer? A multidisciplinary approach based on N and O isotopes of NO<sub>3</sub>, CFCs and SF<sub>6</sub>, microbiological activity, geophysics and hydrogeology. *J. Contam. Hydrol.* (in press).
- R Development Core Team (2009). *R: A Language and Environment for Statistical Computing*. Vienna: R Foundation for Statistical Computing. Available online at: <http://www.R-project.org>
- Retter, A., Karwautz, C., and Griebler, C. (2021). Groundwater microbial communities in times of climate change. *Curr. Issues Mol. Biol.* 41, 509–538. doi: 10.21775/cimb.041.509
- Saez, F., Pozo, C., Gomez, M. A., Martinez-Toledo, M. V., Rodelas, B., and Gonzalez-Lopez, J. (2006). Growth and denitrifying activity of *Xanthobacter autotrophicus* CECT 7064 in the presence of selected pesticides. *Appl. Microbiol. Biotechnol.* 71, 563–567. doi: 10.1007/s00253-005-0182-8
- Saez, F., Pozo, C., Gomez, M. A., Rodelas, B., and Gonzalez-Lopez, J. (2003). Growth and nitrite and nitrous oxide accumulation of *Paracoccus denitrificans* ATCC 19367 in the presence of selected pesticides. *Environ. Toxicol. Chem.* 22, 1993–1997. doi: 10.1897/02-351
- Sanchez-Sanchez, R., Ahuatz-Chacon, D., Galindez-Mayer, J., Ruiz-Ordaz, N., and Salmeron-Alcocer, A. (2013). Removal of triazine herbicides from aqueous systems by a biofilm reactor continuously or intermittently operated. *J. Environ. Manag.* 128, 421–426. doi: 10.1016/j.jenvman.2013.05.050
- Santana, M. M., Gonzalez, J. M., and Cruz, C. (2017). Nitric oxide accumulation: the evolutionary trigger for phytopathogenesis. *Front. Microbiol.* 8:1947. doi: 10.3389/fmicb.2017.01947
- Satapute, P., and Kaliwal, B. (2016). Biodegradation of the fungicide propiconazole by *Pseudomonas aeruginosa* PS-4 strain isolated from a paddy soil. *Ann. Microbiol.* 66, 1355–1365. doi: 10.1007/s13213-016-1222-6
- Scheurer, M., Brauch, H.-J., Schmidt, C. K., and Sacher, F. (2016). Occurrence and fate of nitrification and urease inhibitors in the aquatic environment. *Environ. Sci.* 18, 999–1010. doi: 10.1039/c6em00014b
- Schipper, L., and Vojvodic Vukovic, M. (1998). Nitrate removal from groundwater using a denitrification wall amended with sawdust: field trial. *J. Environ. Qual.* 27, 664–668. doi: 10.2134/jeq1998.00472425002700030025x
- Schipper, L., and Vojvodic Vukovic, M. (2000). Nitrate removal from groundwater and denitrification rates in a porous treatment wall amended with sawdust. *Ecol. Eng.* 14, 269–278. doi: 10.1016/s0925-8574(99)00002-6
- Shushkova, T., Ermakova, I., Sviridov, A., and Leontievsky, A. (2012). Biodegradation of glyphosate by soil bacteria: optimization of cultivation and the method for active biomass storage. *Microbiology* 81, 44–50. doi: 10.1134/s0026261712010134
- Sidoli, P., Lassabatere, L., Angulo-Jaramillo, R., and Baran, N. (2016). Experimental and modelling of the unsaturated transports of S-metolachlor and its metabolites in glaciofluvial vadose zone materials. *J. Contam. Hydrol.* 190, 1–14. doi: 10.1016/j.jconhyd.2016.04.001
- Sonthiphand, P., Ruangroengkulrith, S., Mhuantong, W., Charoensawan, V., Chotpanarat, S., and Boonkaewwan, S. (2019). Metagenomic insights into microbial diversity in a groundwaterbasin impacted by a variety of anthropogenic activities. *Environ. Sci. Pollut. Res.* 26, 26765–26781. doi: 10.1007/s11356-019-05905-5
- Staley, Z., Harwood, V., and Tohr, J. (2015). A synthesis of the effects of pesticides on microbial persistence in aquatic ecosystems. *Crit. Rev. Toxicol.* 45, 813–836. doi: 10.3109/10408444.2015.1065471
- Starr, R. C., and Gillham, R. W. (1993). Denitrification and organic carbon availability in two aquifers. *Ground Water* 31, 934–947. doi: 10.1111/j.1745-6584.1993.tb00867.x
- Su, X., Chen, Y., Wang, Y., Yang, X., and He, Q. (2019). Impacts of chlorothalonil on denitrification and N<sub>2</sub>O emission in riparian sediments: microbial metabolism mechanism. *Water Res.* 148, 188–197. doi: 10.1016/j.watres.2018.10.052
- Surdyk, N., Gutierrez, A., Baran, N., and Thiéry, D. (2021). A lumped model to simulate nitrate concentration evolution in groundwater at catchment scale. *J. Hydrol.* 596:125696. doi: 10.1016/j.jhydrol.2020.125696
- Taubert, M., Stähly, J., Kolb, S., and Küsel, K. (2019). Divergent microbial communities in groundwater and overlying soils exhibit functional redundancy for plant-polysaccharide degradation. *PLoS One* 14:e0212937. doi: 10.1371/journal.pone.0212937
- Trudell, M. R., Gillham, R. W., and Cherry, J. A. (1986). An in-situ study of the occurrence and rate of denitrification in a shallow unconfined sand aquifer. *J. Hydrol.* 83, 251–268. doi: 10.1016/0022-1694(86)90155-1
- Tuinstra, J., and van Wensem, J. (2014). Ecosystem services in sustainable groundwater management. *Sci. Total Environ.* 485–486, 798–803.
- Wakelin, S., Nelson, P., Armour, J., Rasiah, V., and Colloff, M. (2011). Bacterial community structure and denitrifier (nir-gene) abundance in soil water and groundwater beneath agricultural land in tropical North Queensland, Australia. *Soil Res.* 49, 65–76. doi: 10.1071/sr10055
- Wang, G., Xu, D., Xiong, M., Zhang, H., Li, F., and Liu, Y. (2016). Novel degradation pathway and kinetic analysis for bupropion removal by newly isolated *Bacillus* sp. *J. Environ. Manag.* 180, 59–67. doi: 10.1016/j.jenvman.2016.04.061
- Yang, C., Hamel, C., Vujanovic, V., and Gan, Y. (2011). Fungicide: modes of action and possible impact on non-target microorganisms. *Int. Scholar. Res. Net. Ecol.* 2011:130289. doi: 10.5402/2011/130289

**Conflict of Interest:** The authors declare that the research was conducted in the absence of any commercial or financial relationships that could be construed as a potential conflict of interest.

Copyright © 2021 Michel, Baran, André, Charron and Joulain. This is an open-access article distributed under the terms of the Creative Commons Attribution License (CC BY). The use, distribution or reproduction in other forums is permitted, provided the original author(s) and the copyright owner(s) are credited and that the original publication in this journal is cited, in accordance with accepted academic practice. No use, distribution or reproduction is permitted which does not comply with these terms.



# Relative Weight of Organic Waste Origin on Compost and Digestate 16S rRNA Gene Bacterial Profilings and Related Functional Inferences

Axel Aigle<sup>1†</sup>, Emilie Bourgeois<sup>1</sup>, Laurence Marjolet<sup>1</sup>, Sabine Houot<sup>2</sup>,  
Dominique Patureau<sup>3</sup>, Emmanuel Doelsch<sup>4,5</sup>, Benoit Cournoyer<sup>1‡</sup> and Wessam Galia<sup>1\*‡</sup>

## OPEN ACCESS

### Edited by:

Dimitrios Georgios Karpouzas,  
University of Thessaly, Greece

### Reviewed by:

Heribert Insam,  
University of Innsbruck, Austria  
Panagiotis A. Karas,  
University of Thessaly, Greece

### \*Correspondence:

Wessam Galia  
wessam.galia@vetagro-sup.fr

### †Present address:

Axel Aigle,  
ILM, Villeurbanne, France

‡These authors have contributed  
equally to this work

### Specialty section:

This article was submitted to  
Microbiotechnology,  
a section of the journal  
Frontiers in Microbiology

Received: 11 February 2021

Accepted: 06 April 2021

Published: 14 May 2021

### Citation:

Aigle A, Bourgeois E, Marjolet L,  
Houot S, Patureau D, Doelsch E,  
Cournoyer B and Galia W (2021)  
Relative Weight of Organic Waste  
Origin on Compost and Digestate  
16S rRNA Gene Bacterial Profilings  
and Related Functional Inferences.  
Front. Microbiol. 12:667043.  
doi: 10.3389/fmicb.2021.667043

Even though organic waste (OW) recycling via anaerobic digestion (AD) and composting are increasingly used, little is known about the impact of OW origin (fecal matters and food and vegetable wastes) on the end products' bacterial contents. The hypothesis of a predictable bacterial community structure in the end products according to the OW origin was tested. Nine OW treatment plants were selected to assess the genetic structure of bacterial communities found in raw OW according to their content in agricultural and urban wastes and to estimate their modifications through AD and composting. Two main bacterial community structures among raw OWs were observed and matched a differentiation according to the occurrences of urban chemical pollutants. Composting led to similar 16S rRNA gene OTU profiles whatever the OW origin. With a significant shift of about 140 genera (representing 50% of the bacteria), composting was confirmed to largely shape bacterial communities toward similar structures. The enriched taxa were found to be involved in detoxification and bioremediation activities. This process was found to be highly selective and favorable for bacterial specialists. Digestates showed that OTU profiles differentiated into two groups according to their relative content in agricultural (manure) and urban wastes (mainly activated sludge). About one third of the bacterial taxa was significantly affected by AD. In digestates of urban OW, this sorting led to an enrichment of 32 out of the 50 impacted genera, while for those produced from agricultural or mixed urban/agricultural OW (called central OW), a decay of 54 genera over 60 was observed. Bacteria from activated sludge appeared more fit for AD than those of other origins. Functional inferences showed AD enriched genera from all origins to share similar functional traits, e.g., chemoheterotrophy and fermentation, while being often taxonomically distinct. The main functional traits among the dominant genera in activated sludge supported a role in



AD. Raw OW content in activated sludge was found to be a critical factor for predicting digestate bacterial contents. Composting generated highly predictable and specialized community patterns whatever the OW origin. AD and composting bacterial changes were driven by functional traits selected by physicochemical factors such as temperature and chemical pollutants.

**Keywords:** organic waste, anaerobic digestion, composting, 16S rRNA gene meta-barcoding, functional traits

## INTRODUCTION

Organic wastes (OWs) have increased 10-fold since the last century and are likely to double by 2025 as a result of the growth of the world population (Hoornweg et al., 2013). There is thus a strong need for sustainable OW management. From a waste management standpoint, aerobic (composting) and anaerobic digestions (AD) are the most obvious operational processes prior to soil applications. These recycling treatments can also be combined by performing a composting of digestates. A major constraint in these OW recycling scenarios is the capacity to assess the related OW health hazards, which are, in fact, dependent on their origin and contents in terms of chemical and microbiological contaminants, and the efficacy of the treatments at reducing these hazards.

AD implies a breakdown of organic materials naturally found in raw OW into biogas (50–75% CH<sub>4</sub>, 25–50% CO<sub>2</sub>, and 1–2% H<sub>2</sub>S, H<sub>2</sub>, and NH<sub>3</sub>) and organic residues (called digestate) by a microbial consortium (Atelge et al., 2020). The success of this process relies on the synergies between microorganisms acting in a coordinated succession driven by the environmental changes occurring during the process (Rivière et al., 2009; Yu et al., 2010). To avoid deviation of microbial communities during the AD process, parameters such as volatile fatty acids (VFAs), ammonia and hydrogen sulfide concentrations, acetate:propionate ratios, and pH are regularly monitored (Kayhanian, 1994; Chen et al., 2008; González-Fernández and García-Encina, 2009; Wang et al., 2009; Franke-Whittle et al., 2014; Wagner et al., 2014). The microbial reactions of these processes can be performed by psychrophiles, mesophiles, and thermophiles (Moset et al., 2015; Saady and Massé, 2015; Hupfauf et al., 2018). Mesophilic digestion is considered the most stable AD process (Gou et al., 2014) because diversity of bacterial and archaeal assemblages are greater at mesophilic (35–37°C) temperatures (Levén et al., 2007; Pycke et al., 2011). The initial hydrolysis step of OW is performed by many facultative anaerobes or strictly anaerobic bacteria. This hydrolysis can degrade complex molecules into simple sugar monomers, amino acids, and alcohols. Fermentative bacteria will then convert these monomers into short-chain fatty acids, primary alcohols, as well as H<sub>2</sub> and CO<sub>2</sub>. The production of acetate from the fatty acids will be performed by homoacetogenic bacteria like *Butyribacterium* and *Acetobacterium*, that of H<sub>2</sub> will be performed by the acetogenic microbiota such as *Syntrophomonas*, and that of CO<sub>2</sub> and H<sub>2</sub>S will be performed by sulfate-reducing bacteria such as *Desulfovibrio* and *Desulfobacter*. Some of these compounds will then be used by methanogens to generate CH<sub>4</sub>. Hydrogenotrophic methanogens such as *Methanobacterium* and *Methanogenium* sp. convert H<sub>2</sub> and CO<sub>2</sub>

into CH<sub>4</sub>, and acetotrophic ones such as *Methanosarcina* will convert acetate into CH<sub>4</sub> (Demirel and Scherer, 2008; Lykidis et al., 2011).

In the same way, composting is a natural process characterized by the conversion of OW into by-products that can be used as soil conditioners and/or organic fertilizers (Reinikainen and Herranen, 2001; Ahmad et al., 2007). This process is performed by an aerobic microbial consortium composed of *Proteobacteria*, *Actinobacteria*, and fungi. During the process of composting, microbial community successions are driven by environmental parameters such as moisture, temperature, and the aeration conditions (Blanc et al., 1999; Tian et al., 2013; Zhang et al., 2016). Composting in its initial phase can be carried out by several mesophiles including bacteria, which represent environmental health hazards such as *E. coli*, *Salmonella*, *Klebsiella*, and *Nocardia* (Insam and de Bertoldi, 2007). These organisms can break down soluble organic compounds by exothermic reactions. As the temperature rises above 40°C, these mesophiles will be outcompeted by more thermophilic bacteria such as *Bacillus stearothermophilus* and species from the *Deinococcus/Thermus* group (Insam and de Bertoldi, 2007). These will continue the breakdown processes and generate higher temperatures that will partly sanitize the end products by killing heat-sensitive hazardous microbial agents. A compost pile can reach 65–70°C. As the supply of high-energy compounds will get low, thermo-tolerant mesophiles will be favored and will perform the last transformation or “stabilization” reactions (Day and Shaw, 2001). The cool zones in the composting systems, particularly with those having no or little mixing, can favor a survival and (re)growth of some bacterial pathogens (Noble and Roberts, 2004).

Beyond the general microbial structures described previously for AD and composting, several questions remain, including how the high inputs of microorganisms and cells from the feeding substrates (OW) under conditions of continuous flow impact the microbial community structure in the end products. On one hand, some studies suggested that the microbial communities of digested OW are unique to a digester because of high differences in substrate and operating conditions (Werner et al., 2011; Sundberg et al., 2013; Zhang et al., 2014; De Vrieze et al., 2016). However, some of these analyses on full-scale AD plants fed with a mixture of substrates (De Vrieze et al., 2016) or with activated sludge (Wang et al., 2018) also indicated that the microbial communities could be stable over time. Nevertheless, in other studies, the microbial communities in AD were found variable over time (among a same digester), even when substrate and operational conditions remained constant (Supaphol et al., 2011; De Vrieze et al., 2013; Williams et al., 2013; Vanwonterghem et al., 2014). On the other hand, during composting, microbial

communities of the raw OW were found to trigger a rise and decrease in temperature (Palaniveloo et al., 2020). These changes are highly selective but their incidence on microbial community patterns of mature compost remain to be evaluated according to the origin of OW. A knowledge gap thus remains about the relative contribution of the raw OW microbiome on the digestate and compost structural and functional microbial community patterns.

Here, we made the hypothesis that the microbiomes found among digesters and composts will be (i) significantly structured by the communities of the raw OW inputs, but that (ii) functional redundancy among these communities would generate distinct community profiles between treatment plants. Similar biodegradation activities between distinct treatment plants would thus be achieved by different microbial organizations because of this functional redundancy. To test these hypotheses, nine full-scale treatment plants located in various rural and urban backgrounds were investigated. These treatment plants were fed with agricultural or urban wastes or a mixture of both. Bacterial genetic structures were inferred from 16S rRNA gene meta-barcoding approaches, and patterns were compared between process types and according to the origin and nature of the raw OW. Functional traits were inferred from the 16S rRNA gene taxonomic allocations and databases recording the metabolic processes of well-defined bacterial taxa (FAPROTAX). The theoretical metabolic pathways of the genera impacted by treatment were further inferred from sequenced genomes using the MACADAM software (Le Boulch et al., 2019).

## MATERIALS AND METHODS

### OW Recycling Sites and Samplings

Nine full-scale OW treatment plants (numbered as Urban-1-2-3, Agri-1-2-3 and Central-1-2-3) were considered in this study (Table 1). The sampling strategy implied the use of at least three independent treatment plants per sample categories. OWs were treated by AD (Urban-1-2, Agri-1-2, and Central-1-2-3) or composting (Urban-1-3 and Agri-1-3). Five of the AD plants applied a post-treatment to the digestate: solid/liquid separation (Central-1-2), solid/liquid separation followed by composting (Urban-1 and Agri-1), or solid/liquid separation followed by solid phase drying (Urban-2). Raw OWs were chosen to represent the most common origins of OW: urban [sewage sludge produced by wastewater treatment plants (WWTP): Urban-1-2-3], agricultural (exclusively or mainly composed of animal manure and/or slurry: Agri-1-2-3), and central (a mix of food industry waste, harvest residues, livestock effluents, and/or sewage sludge: Central-1-2-3) (see Table 1 for details of the OWs compositions). For all sites, samples were taken at each treatment step to capture treatment effects on the microbial community's composition and abundance. Thus, a raw OW sample was taken from each site, resulting in nine samples, respectively, defined as urban (Urban-1-2-3-OW), agricultural (Agri-1-2-3-OW), and central (Central-1-2-3-OW) (Table 1). Digestates were available and sampled for six sites (Urban-1-D, Agri-1-2-D, and Central-1-2-3-D), as well as solid and dried

digestates, respectively, from liquid/solid phase separation, and from solid phase drying (Urban-1-2-SD, Agri-1-SD, Central-1-2-SD, and Urban-2-DD) (Table 1). Liquid digestates were available for four sites (Urban-2-LD, Agri-1-LD, and Central-1-2-LD), and finally, compost was produced and sampled also at four sites (Urban-1-3-C and Agri-1-3-C) (Table 1). At least 1 kg of OW, composts, or digestates was collected per treatment. Samples were coded as indicated in Le Bars et al. (2018). For each sample, certain pollutants and physicochemical parameters were measured (Supplementary Tables 1, 2). These datasets have been presented in Le Bars et al. (2018) and Sertillanges et al. (2020) and further analyzed in order to verify the chemical differentiation of samples according to their origin (urban, agricultural, and central). Total nitrogen (ISO 13878) and total carbon (ISO 10694) were determined by dry combustion with an elemental NC 2100 Soil Analyzer (Thermo Electron Corp.). Inorganic carbon (ISO 10693) was determined with a Bernard Calcimeter by adding HCl and measuring released CO<sub>2</sub>. Organic carbon (C<sub>org</sub>) was deduced from the difference between total and inorganic carbon. Concentrations of trace elements (TE) were measured using an inductively coupled plasma mass spectrometer (ICP-MS iCAP Q Thermo Fisher Scientific). pH was directly measured on liquid samples, or according to the ISO 10390. More details for those procedures are described in Le Bars et al. (2018). The concentrations of all the elements are expressed on a dry matter (DM) basis. Nonylphenols (NPs) and polycyclic aromatic hydrocarbons (PAHs) were measured in 1 g subsample according to Trably et al. (2004) and Mailler et al. (2017). More details for these monitorings are given in Sertillanges et al. (2020).

### DNA Extractions and MST

DNA was extracted from 0.5 g of solid samples or 500 µl of liquid samples using the FastDNA Spin kit for soil and the FastPrep-24 (MP Biomedicals) following the manufacturer's instructions. All the DNA extractions were triplicated for each sample. DNA was eluted in 50 µl of ultrapure water, and quantity and quality were measured using a nanodrop-One UV-Vis Spectrophotometer (Thermo Fisher Scientific). DNA extracts were visualized after electrophoresis at 6 V/cm using a TBE buffer [89 mM Tris-borate, 89 mM boric acid, and 2 mM EDTA (pH 8.0)] through a 0.8% (w/v) agarose gel, and DNA staining with 0.4 mg ml<sup>-1</sup> ethidium bromide. A Gel Doc XR+ System (Bio-Rad, France) was used to observe the stained DNA and confirm their relative quantities and qualities. DNA was kept at -80°C and shipped on ice within 24 h to the DNA sequencing services when appropriate.

MST methods were used to monitor host fecal contaminations by human, bovine, and pig (Supplementary Table 3). These tests were performed on all DNA extracts including all replicates from the same sample. MST qPCR amplifications of general and host-specific *Bacteroides* markers, as well as general 16S rRNA gene qPCR assays, were performed as described in Marti et al. (2017) and Voisin et al. (2020). The human-specific marker (HF183) and the 16S rRNA genes were quantified by the SYBR Green chemistry while the bovine-specific, pig-specific, and the total *Bacteroidetes* markers were quantified using the Taqman chemistry. Six qPCR assays were performed per sample using DNA obtained from three independent extractions

**TABLE 1** | Organic waste treatment plants and sample features.

Sampling sites	Reactor size (m <sup>3</sup> )/temperature for AD	Samples	Duration <sup>a</sup> /treatment <sup>b</sup>	Sample code	Organic waste composition and co-substrate used for composting
Urban-1 French wastewater treatment plant and composting platform	6,200 32–42°C	Organic waste Digestate Solid digestate Compost <sup>c</sup>	38d/AD 4w/C	Urban-1-OW Urban-1-D Urban-1-SD Urban-1-C	Drained activated sludge Co-substrate: green waste
Urban-2 French wastewater treatment plant	6,000 32–42°C	Organic waste Liquid digestate Solid digestate Dried digestate	34d/AD	Urban-2-OW Urban-2-LD Urban-2-SD Urban-2-DD	Drained sludge
Urban-3 French wastewater treatment plant and composting platform		Organic waste Compost <sup>d</sup>	6w/C	Urban-3-OW Urban-3-C	Dehydrated activated sludge Co-substrate: green waste
Agri-1 Anaerobic digestion plant and composting platform (France)	950 32–42°C	Organic waste Digestate Liquid digestate Solid digestate Compost <sup>c</sup>	38d/AD 12w/C	Agri-1-OW Agri-1-D Agri-1-LD Agri-1-SD Agri-1-C	Porcine slurry (for 6–7 T/day) and grass clippings, food and vegetable wastes, corn silage and straws Co-substrate: none
Agri-2 Anaerobic digestion plant (France)	740 45°C	Organic waste Digestate	42d/AD	Agri-2-OW Agri-2-D	80% of bovine manure and 20% of stercoral material, poultry litter, corn cob, cooking oils, lawn mowing and bran
Agri-3 Composting platform (France)		Manure Compost <sup>d</sup>	12w/C	Agri-3-OW Agri-3-C	Raw cattle, sheep and equine manures Co-substrate: none
Central-1 Anaerobic digestion plant (France)	1,600 32–42°C	Organic waste Digestate Liquid digestate Solid digestate	70d/AD	Central-1-OW Central-1-D Central-1-LD Central-1-SD	50% livestock manures (N <sub>2</sub> manure + animal slurry), 28% wastewater treatment plant sludge, 22% food industry by-products
Central-2 Anaerobic digestion plant (France)	6000 32–42°C	Organic waste Digestate Liquid digestate Solid digestate	30d/AD	Central-2-OW Central-2-D Central-2-LD Central-2-SD	45% pig slurry, 45% wastes from food industries, 10% cereal mixture
Central-3 Anaerobic digestion plant (France)	8,000 32–42°C	Organic waste Digestate	90d/AD	Central-3-OW Central-3-D	50% biowastes (community, catering, mass distribution), 20% dairy cow slurry, 30% wastes from food industries and agricultural by-products

<sup>a</sup>Process duration (d = days/w = weeks). <sup>b</sup>Treatments (AD = anaerobic digestion/C = composting). <sup>c</sup>The substrates used for composting were solid digestates from the matching site (Urban-1 or Agri-1). <sup>d</sup>Raw organic wastes were used for the composting at the Urban-3 and Agri-3 sites.

(**Supplementary Table 4**). Standard curves were generated using 10-fold serial dilutions (ranging from 10<sup>5</sup> to 10<sup>0</sup> gene copies) of cloned targeted sequences (Marti et al., 2017). MST qPCR datasets were expressed per copy number of DNA targets per gram of dry sample and normalized by dividing their numbers by the 16S rRNA gene copy numbers per gram of dry sample.

## V5–V6 16S rRNA Gene Sequencing and Reads Processing

The V5–V6 region of the 16S rRNA genes were amplified using the 799F forward (barcode + ACCMGGATTAGATACCKG) and 1193R reverse (CRTCCMCACCTTCCTC) primers (Chelius and Triplett, 2001; Bodenhausen et al., 2013; **Supplementary Table 3**) by the Molecular Research DNA lab (MrDNA, Shallowater, United States) and were sequenced by the Illumina MiSeq V3 technology. PCR amplifications were performed on pooled DNA extracts obtained per sample (equimolar mixes

of the triplicates) in order to handle variability between DNA extracts. The HotStarTaq Plus Master Mix Kit (Qiagen, United States) using the following temperature cycles was used to generate the PCR products: 94°C for 3 min, followed by 28 cycles of 94°C for 30 s, 53°C for 40 s, and 72°C for 1 min, with a final elongation step at 72°C for 5 min. PCR products and blank control samples were verified using a 2% agarose gel and following the electrophoretic procedure described above. PCR products obtained from field samples showed sizes around 430 bp but blanks did not show detectable and quantifiable PCR products. Dual-index adapters were ligated to the PCR fragments using the TruSeq® DNA Library Prep Kit, which also involved quality controls of the ligation step (Illumina, Paris, France). Illumina MiSeq DNA sequencings of the PCR products were paired-end and set up to obtain around 40K reads per sample.

The generated sequences were processed with the Mothur package (Schloss et al., 2009) according to a standard operation

protocol (SOP) for MiSeq-based microbial community analysis (Schloss et al., 2009; Kozich et al., 2013), so-called MiSeq SOP, and available at [http://www.mothur.org/wiki/MiSeq\\_SOP](http://www.mothur.org/wiki/MiSeq_SOP). Briefly, primers and barcodes were trimmed according to quality and size filtration, followed by sequence alignment. Size filtration was refined, and unique sequences were extracted. The `pre.cluster` command was applied in order to mask the remaining sequencing errors as well as the `split.abund` command where the cutoff was set to 1. Chimera removal was performed using the `chimera.uchime` command and chimeric sequences were removed. At this stage, sequences were processed following two normalization strategies: (i) subsampling according to the sample containing the lowest number of sequences, and (ii) no subsampling (see statistical analysis for normalization strategy). Finally, for both datasets, the SILVA 16S rRNA Bacterial reference library was used for taxonomic allocation of the OTUs (cutoff 80)<sup>1</sup> and OTU clustering was performed with a similarity threshold of 97% for subsampled reads (**Supplementary Table 5**) or using the `phylotype` command at the genus level, for non-subsampled reads (**Supplementary Table 6**). The Mothur package was also used to calculate diversity indices (Shannon, Simpson, evenness, and richness) on the 16S rRNA subsampled OTU table (**Supplementary Table 7**).

## Statistical Analyses

Relations between sample groupings and chemical datasets were tested by principal component analysis using the `rda` function and plotted using the `biplot` function; confidence ellipses were drawn to show the variance observed per group. Kruskal–Wallis tests were performed using the `kruskal.test` function on 16S rRNA diversity indices, MST markers ratio, and physical–chemical data. When significant differences were found ( $p < 0.05$ ), a Dunn test was applied using the `kwAllPairsDunnTest` function from the `PMCMRplus` package (Pohlert, 2020) for *post hoc* analysis.

Hellinger transformation was applied on the 16S rRNA subsampled OTU table using the `decostand` function (method = “total”), and Bray–Curtis dissimilarities were computed between pairs of samples using the `vegdist` function (“bray”). NMDS was generated using the `metaNMDS` function. `ordiellipse` option was used to display the variance observed per group, and PERMANOVA tests were performed using the `pairwise.adonis` and `vegdist` functions (Bray–Curtis dissimilarities) to confirm the significance of differences between groups.

The non-subsampled 16S rRNA gene reads genus table (**Supplementary Table 6**) was processed with the DESEQ2 package (Love et al., 2014) in order to reveal genera with significant change in abundance before and after treatment. Counts normalized by the median of ratios method (Anders and Huber, 2010) were recovered and relative abundances were calculated in order to present the percentage of significant differences in abundances at the genus level before and after treatment. Change in abundance has been considered significant if a genus shows a log<sub>2</sub> fold change  $\leq -2$  or  $\geq +2$  with a minimum Base Mean value of 10 and adjusted  $p$  value of  $< 0.05$ . To facilitate

global comparison with other studies, computations were also performed at the phylum level. All the functions used without package indication were from the `vegan` package (Oksanen et al., 2019) and all analyses were performed on RStudio (R v3.3.3). The statistical experimental design (Kruskal–Wallis tests on 16S rRNA diversity indices and MST markers, as well as NMDS and DESEQ2 analyses) implied first testing relations according to treatment (AD against composting), regardless of the OW origin and regardless of the post-treatments. Thus, all OW samples were compared to composted samples and digestates. Second, the OW origins were considered in the comparisons to infer their impact on the V5–V6 16S rRNA gene datasets.

The 16S rRNA gene sequences produced in this study are available from webin under the accession number PRJEB40193.

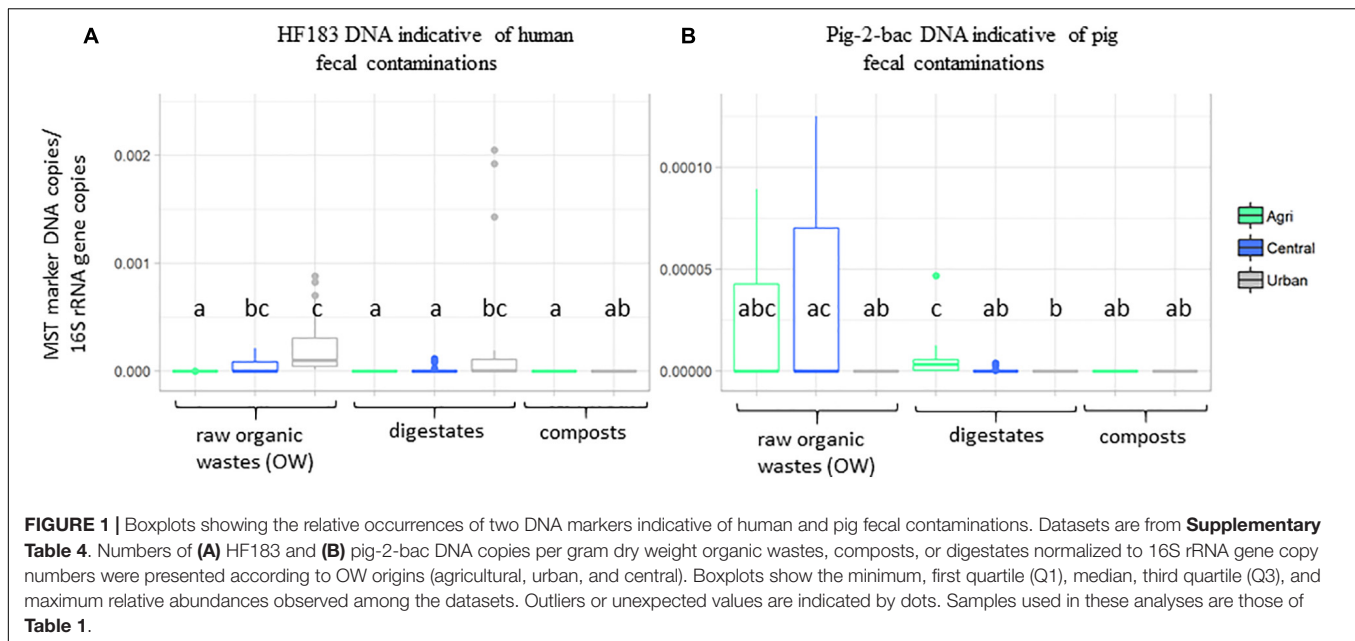
## RESULTS

### General Chemical and Microbiological Features of the Raw OWs, Digestates, and Composts

Principal component analyses were performed on the physicochemical datasets (organic carbon, total nitrogen, C:N ratio, pH, and phosphorus) and pollutants (iron and zinc concentrations, PAHs, NPs, and TE) measured on all samples (**Supplementary Tables 1, 2** and **Supplementary Figure 1**). The first two axes of these PCAs explained a significant part of the variability observed among these datasets ( $> 60\%$ ) (**Supplementary Figure 1**). The origin of the sample was found to explain the chemical dataset (**Supplementary Figure 1**). The urban samples (treated or not) were significantly differentiated from the agricultural and central (mixed) samples by a set of pollutants including several TE (Ag, Al, As, Cd, Ce, Co, Cr, Cu, Ga, K, Mo, Ni, P, Pb, and Ti), 4-nonylphenol (A2), phenanthrene (H5), anthracene (H6), and total nitrogen concentrations (KW–Dunn’s *post hoc* tests;  $p < 0.05$ ) (**Supplementary Figure 2**). Similarly, global indicators of the microbiological content of the samples were analyzed by qPCR using microbial source tracking DNA targets (**Supplementary Table 4** and **Figure 1**). These qPCR analyses showed that 16S rRNA gene numbers varied from  $4.26 \times 10^5$  copies/g sample up to  $6.41 \times 10^{11}$  copies/g (**Supplementary Table 4**). Lowest 16S rRNA gene copy numbers/g sample were obtained for digestates. Monitorings of total *Bacteroides* cell numbers were correlated with the 16S rRNA gene dataset (Kendall’s rank correlation tau;  $p < 0.01$ ) but the range of values was lower ( $2.44 \times 10^2$  copies/g sample up to  $1.12 \times 10^9$  copies/g). The DNA indicators for pig and bovine fecal contaminations were most significant among central and agricultural raw OW (**Figure 1** and **Supplementary Table 4**). These distributions were in agreement with the information given by the operators of the OW treatment sites. The human DNA fecal marker was most often detected among the raw OW but in significantly higher numbers (KW and Dunn’s *post hoc*;  $p < 0.05$ ) among the urban and central groups of samples (**Supplementary Table 4** and **Figure 1**). Digestates and composts showed lower occurrences of these markers but

<sup>1</sup><https://www.arb-silva.de/documentation/>





a significant number of HF183 DNA was detected among the urban digestates (**Figure 1**).

### Bacterial Diversity of Raw OWs, Digestates, and Composts Inferred From V5 to V6 16S rRNA Gene Sequences

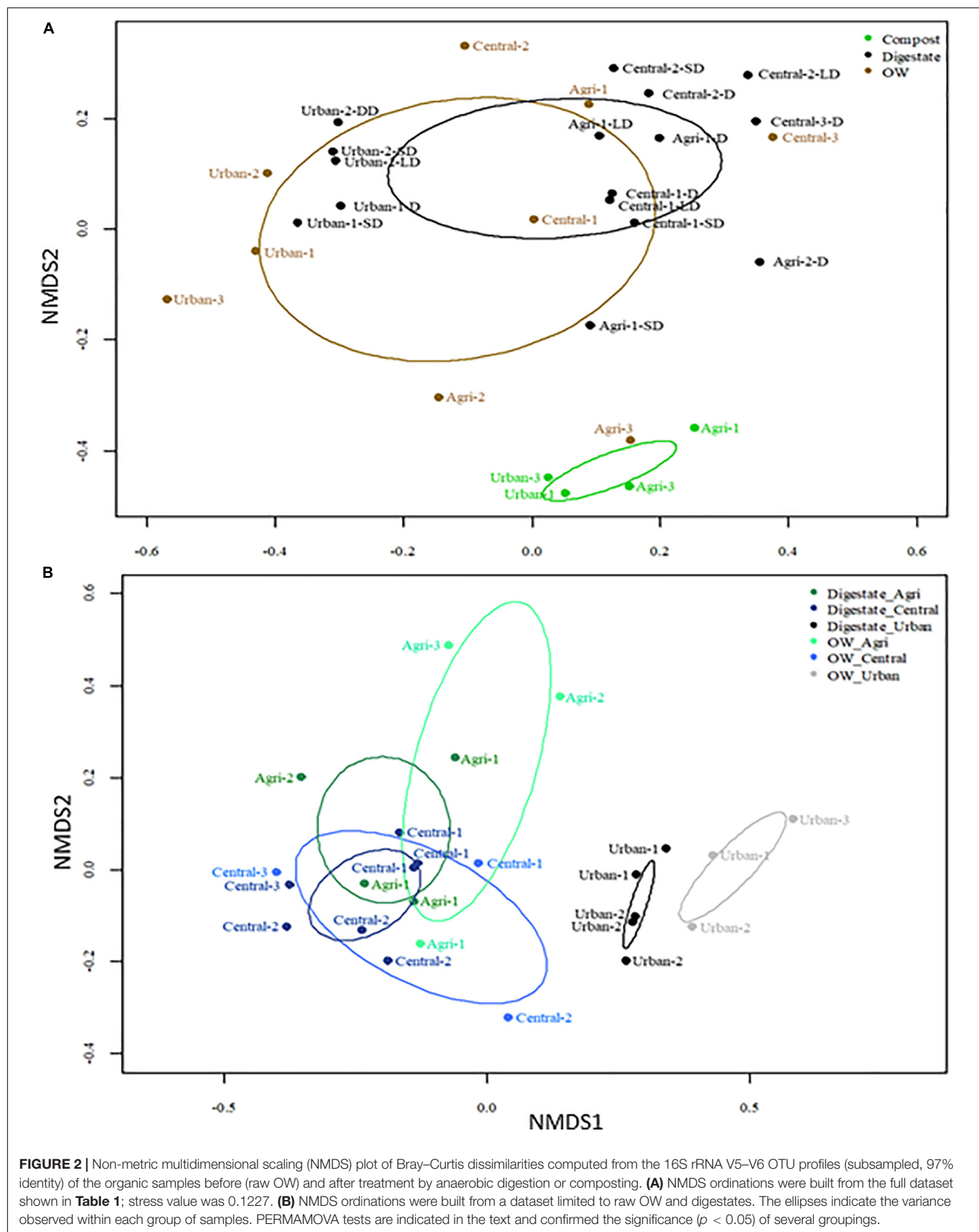
About 5 million DNA sequences were obtained for the samples investigated in this work, and 45% were validated as high-quality 16S rRNA gene sequences. The number of high-quality V5–V6 16S rRNA gene sequences per sample ranged from 26,465 to 119,793 (**Supplementary Table 7**). The number of reads per sample were negatively correlated to the 16S rRNA gene qPCR dataset (Spearman Rank Correlation;  $\rho = -0.45$ ,  $p < 0.05$ ). This highlighted a variability in the dataset that required a normalization of the 16S rRNA gene dataset prior to performing statistical analyses. The global representation of the dataset and the computing of diversity indices were thus performed after a subsampling of the gene reads at the lowest value for the number of reads on a sample, i.e., 26,465 reads. This subsampled dataset led to a grouping of reads into 7755 OTUs, which varied in their distribution from 318 to 1404 per sample (**Supplementary Table 5**). Accordingly, Shannon diversity, Shannon-evenness, and the Simpson diversity indices were computed (**Supplementary Table 7** and **Supplementary Figure 3**). Significant differences in these indices were observed between those computed for the urban digestates and those of the agricultural or central samples (KW test;  $p < 0.05$ ). More diverse OTU contents and even distributions of the reads between OTUs were observed among the urban digestates than the other ones. However, the initial OTU contents of raw OW were found similar between sites, and diversity indices remained similar between raw OW and digestates of a same site (**Supplementary Figure 3**).

To better resolve differences in the genetic diversity among samples, Bray–Curtis dissimilarities between OTU profiles of

each pair of samples were computed. NMDS plots were then performed to visualize the differences (**Figure 2A**). All OTU profiles could be differentiated according to their site category (urban, central, or agricultural) (PERMANOVA  $p < 0.05$ ). A significant effect on the profiles of the OW treatment by composting or AD could also be resolved (PERMANOVA  $p < 0.05$ ). Digestates' OTU profiles could not be differentiated into three categories (PERMANOVA  $p > 0.05$ ) but into two entities with (i) grouping the agricultural/mixed central samples and (ii) the urban ones (PERMANOVA  $p < 0.01$ ) (**Figure 2B**). A further differentiation of OTU profiles according to post-treatments of the digestates was tested. The OTU patterns of liquid and solid digestates could not be differentiated (**Supplementary Figure 4**). Composting was found to drive bacterial community changes toward similar structures even though the nature of the OWs was variable (WWTP activated sludge, manure, green wastes, etc.) (PERMANOVA  $p < 0.05$ ) (**Figure 2A**).

### Incidence of AD or Composting on Bacterial Taxa as Inferred From 16S rRNA Gene Taxonomic Allocations

The chemical and V5–V6 16S rRNA gene OTU pattern analyses indicated in the previous sections showed (i) a significant proximity between the agricultural and central samples (raw OW and digestates), (ii) a significant differentiation of the urban samples (raw OW and digestates) from the agricultural/central samples, and (iii) a significant differentiation of the compost samples from all the other samples. Accordingly, in the following analyses, the datasets were grouped into these latter three entities. Informative groupings of V5–V6 DNA reads matching significant changes (higher or lower) in relative abundances between these entities were analyzed.



### Variations at the Scale of Phyla

Raw OWs showed a high variability in their OTU contents (**Figure 2A**). However, these OTUs can be grouped into larger taxonomic entities, which can be conserved between raw OWs, and contribute reproducibly to the buildup of the microbial communities among composts or digestates. These core taxa were found to be distributed among 6 major phyla: *Firmicutes* (31.2%), *Proteobacteria* (26.4%), *Bacteroidetes* (26.2%), *Actinobacteria* (6.1%), *Tenericutes* (4.4%), and *Spirochaetae* (0.7%) but discrepancies were observed in terms of proportion of reads per phylum according to the site category (urban, central, and agricultural) (**Supplementary Table 8**). Raw urban OW showed lower relative numbers (7.1%) of *Firmicutes* [converted into  $2.05 \times 10^9$  equivalent 16S rRNA gene copy numbers (16S) per gram of OW] than the raw OWs from the central and agricultural sites (29.9%; equivalent to  $1.01 \times 10^{10}$  16S per gram) (**Supplementary Table 9** and **Figure 3**). These urban OWs were found to have higher relative counts of *Proteobacteria* (46.6%;

equivalent to  $3.97 \times 10^{10}$  16S per gram) and *Actinobacteria* (11.7%; equivalent to  $6.51 \times 10^9$  16S per gram) than the central and agricultural samples (respectively, 29.3%; equivalent to  $8.74 \times 10^9$  16S per gram and 2.9%; equivalent to  $1.2 \times 10^9$  16S per gram) (**Supplementary Table 9** and **Figure 3**). It is to be noted that 16S rRNA gene reads allocated to the *Nitrospirae*, *Chloroflexi*, and *Acidobacteria* represented more than 1% (equivalent to  $7.41 \times 10^9$  16S rRNA gene copies per gram) of the urban OW dataset, but these phyla occurred at a much lower score (equivalent to  $4.32 \times 10^6$  16S rRNA gene copies per gram) among the OW of the other sites (**Supplementary Table 9** and **Figure 3**).

As observed among raw OW, *Firmicutes* and *Proteobacteria* were among the most abundant phyla in digestates and composts (**Supplementary Table 9** and **Figure 3**). However, a decrease in the relative abundance of the *Proteobacteria* was observed in all treated samples (**Supplementary Table 9** and **Figure 3**) and was supported by a significant statistical test for the urban

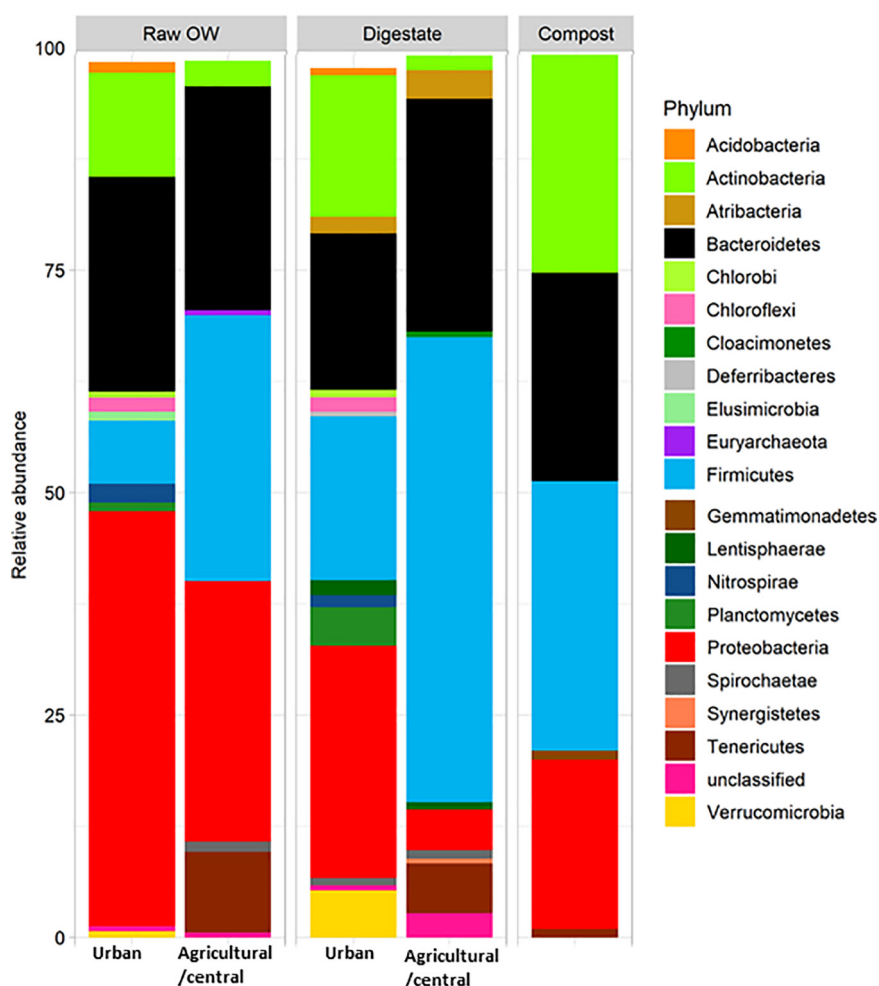


**FIGURE 3 |** Relative averaged abundances of V5–V6 16S rRNA gene reads allocated to phyla before and after treatment of raw organic wastes (OWs) by anaerobic digestion or composting performed by treatment plants located in rural areas (agricultural/central sites) or urban ones. Only phyla with a relative abundance above 0.5% are displayed (see **Supplementary Table 9** for the complete dataset).

samples (KW  $p \leq 0.05$ ). These changes in proportion were not correlated to a significant reduction in bacterial cell numbers (between  $1.77 \times 10^9$  and  $3.19 \times 10^{10}$  16S rRNA gene copies per gram of digestates or composts). The observed change in relative abundance thus implies a significant re-shuffling of bacterial phyla with some of these taking advantage of the treatment conditions or becoming negligible. For example, increases in the relative proportion of *Firmicutes* from the raw OW to the digestates were observed among both categories of samples (agricultural/central, and urban). *Firmicutes* showed the highest occurrence among the central/agricultural digestates (52.2% of the bacterial taxa). These relative changes matched an averaged one log increase in *Firmicutes* 16S rRNA gene copies between the raw OW and the digestates of the urban sites or composts (Supplementary Table 9 and Figure 3). Similarly, relative increases in *Actinobacteria*, *Deferribacteres*, and *Thermotogae* among composts matched significant increases in 16S rRNA gene copies estimated from the qPCR datasets (Supplementary Table 9 and Figure 3; KW  $p \leq 0.05$ ). Similar trends were also observed between raw OW and urban digestates for the *Cloacimonetes*, which showed up to a five-log increase in 16S rRNA gene copies per gram. Significant decreases in the relative abundance of some phyla were also recorded such as the raw OW *Fusobacteria*, which became negligible among the digestates and composts (Supplementary Table 9 and Figure 3; KW  $p \leq 0.05$ ).

### Variations at the Scale of Genera Among Digestates

To go deeper into the understanding of community changes, variations of V5–V6 16S rRNA gene reads allocated at the genus level were investigated. A DESEQ2 analysis was performed to highlight these changes (Figures 4, 5 and Supplementary Tables 10, 11). These analyses were performed with the non-resampled sequenced gene reads dataset (Supplementary Table 6) because a normalization scheme is directly run by DESEQ2. This approach revealed that the digestates of the central/agricultural category of samples led to a significant increase in the relative proportion of six genera: *Gelria* (*Firmicutes*), *Sporosarcina* (*Firmicutes*), *Dethiobacter* (*Firmicutes*), and three unclassified groups belonging to the *Spirochaetales*, *Cloacimonetes*, and *Firmicutes*. Four (*Gelria*, *Sporosarcina* and two others unclassified at genus level) of these genera were part of the core bacterial taxa found among digestates (Figure 4 and Supplementary Table 10). Four of these were also found to be part of the *Firmicutes* and confirmed the trends observed at the scale of phyla, which indicated an increase in *Firmicutes*. These six genera were two to five times (Log2 fold change) more abundant in the digestates than the non-treated samples (raw OWs). They represented from 0.1 to 6.1% (according to the mean normalized counts) of the total digestate bacterial community (Supplementary Table 10). Conversion of relative read numbers into 16S rRNA gene copies from the subsampled contingency table supported these trends and indicated an abundance of about  $3.0 \times 10^7$  *Gelria* 16S rRNA gene copies per gram of dry weight in the raw OW while  $5.0 \times 10^8$  *Gelria* 16S rRNA gene copies were estimated in average in the digestates (Supplementary Table 9). Similarly, *Sporosarcina* and *Dethiobacter* 16S rRNA

gene copies per gram of dry weight indicated a gain of one log between the raw OW and digestates. Regarding genera that showed a relative decrease, 54 (of which 15 are parts of the core bacterial taxa found among digestates) (Supplementary Table 8) were subjected to a significant decrease after AD of OW of the agricultural/central sites (Figure 4 and Supplementary Table 10). This relative reduction varied from 2.6- to 9.9-fold when compared to raw OW (Figure 4 and Supplementary Table 10). *Lactobacillus* (4.8–0.1%), *Bacteroides* (4.1–0.4%), *Prevotella* 9 (1.8–0.0%), and *Methanobrevibacter* (0.5–0.1%) were found to have undergone the most significant reductions (Figure 4 and Supplementary Table 10). The decrease in bacterial numbers was confirmed through a conversion of the dataset into 16S rRNA gene copies. *Lactobacillus* 16S rRNA gene copies went down by about two logs, and those of *Bacteroides* went down by about one log (supported by Wilcoxon rank sum tests;  $p < 0.05$ ). Similar trends were observed for the other genera (Supplementary Table 9).

Several bacterial genera of the urban OWs were shown to be significantly enriched in the digestates. A total of 32 genera (of which 25 were part of the core microbiome) showed a significant increase (Figure 5 and Supplementary Table 11). These genera were enriched by three to sevenfold while comparing with the concentrations observed among OW. These genera represented from 0.03 to 3.6% of the total digestate microbial community. The most significant increases in the digestates were observed for V5–V6 16S rRNA gene reads allocated to the *Smithella* (0.03–3.0%), part of the *vadinBC27\_wastewater-sludge\_group* (0.1–2.1%), *Candidatus\_Caldatibacterium* (0.1–1.9%), *Gracilibacter* (0.0–1.8%), *Proteiniphilum* (0.02–1.6%), *Sedimentibacter* (0.01–1.5%), *Syntrophorhabdus* (0.01–1.0%), and *Petrimonas* genus (0.01–0.5%). Conversion of these values into 16S rRNA gene copies showed the *Smithella* to have undergone an increase from  $6.15 \times 10^6$  copies per gram of OW to  $2.64 \times 10^9$  copies per gram of digestates, and the *Gracilibacter* 16S rRNA gene copies went up from about  $3.0 \times 10^6$  to  $1.61 \times 10^9$  (Supplementary Table 9). Similar trends were observed for the other above-cited genera (Supplementary Table 9) but a significant number ( $n = 18$ ) of genera also underwent a relative reduction in V5–V6 gene reads from the OW to the digestates (Figure 5 and Supplementary Table 11). These decreases were about four- to ninefold in comparison to their relative numbers among the raw OW samples. Hence, the *Uliginosibacterium* (1.3–0.1%), *Simiduia* (0.3–0.0%), *Cellvibrio* (0.1–0.01%), *Fonticella* (0.1–0.0%) *Polyangium* (0.04–0.0%), and *Clostridium\_sensu\_stricto\_12* (0.03–0.0%) genera showed such a decrease (Figure 5 and Supplementary Table 11). These shifts were confirmed while converting these datasets into 16S rRNA gene copy numbers (Supplementary Table 9).

Global changes in the relative abundance of digestates' bacterial genera significantly affected by ADs over the dataset were investigated. DESEQ2 analyses revealed that 30.8 and 35.5% of the total relative abundance of the digestate genera were significantly affected by the AD treatment, respectively, at the urban and agricultural/central sites (Supplementary Tables 10, 11). The relative abundances of 50 and 60



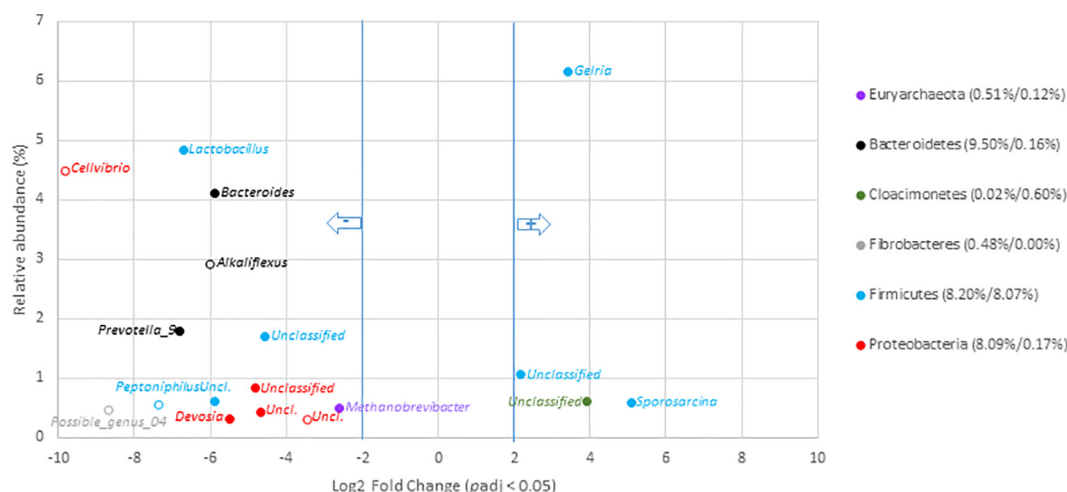


**FIGURE 4 |** Genera with significant changes in relative abundance after anaerobic digestion of raw organic waste samples from agricultural and central mixed origin. Genera with significant ( $p_{adj} < 0.05$ ) decrease in digestates compared to raw OW samples (left part of the plot) are presented according to their initial relative abundance in raw OW. Genera with significant increase in digestates compared to raw OW samples (right part of the plot) are presented according to their relative abundance in digestate. Genera are colored according to the phylum to which they belong. Full mark represents genus present in the core microbiome; empty mark represents genus not present in the core microbiome (raw OW and digestate core microbiomes were, respectively, considered at the left and right part of the plot). Numbers in brackets represent the sum at the phylum level of relative abundances of all genera with significant change after AD calculated before and after AD (raw OW%/digestate%). Only genera with relative abundance  $\geq 0.3\%$  and significant change ( $-2 \geq \text{Log}_2 \text{FC} \geq +2$ ,  $p_{adj} < 0.05$ , minimum normalized read count = 10) are shown (see **Supplementary Table 10** for the other groups).

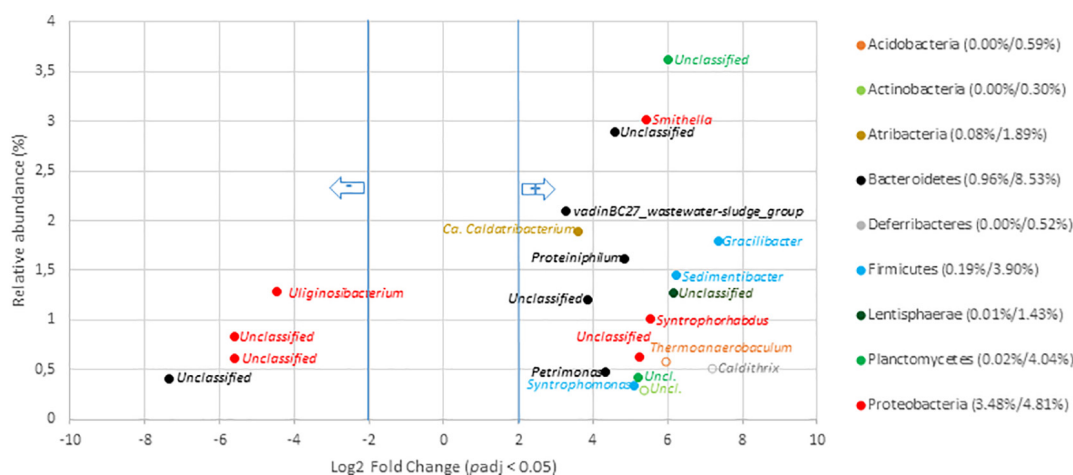


**FIGURE 5 |** Genera with significant change in relative abundance after anaerobic digestion of raw organic waste samples from urban origin. Genera with significant ( $p_{adj} < 0.05$ ) decrease in digestates compared to raw OW samples (left part of the plot) are presented according to their initial relative abundance in raw OW. While genera with significant increase in digestates compared to raw OW samples (right part of the plot) are presented according to their relative abundance in digestate. Genera are colored according to the phylum to which they belong. Full mark represents genus present in the core microbiome while empty mark represents genus not present in the core microbiome (raw OW and digestate core microbiomes were, respectively, considered at the left and right part of the plot). Numbers in brackets represent the sum at the phylum level of relative abundances of all genera with significant change after AD calculated before and after AD (raw OW%/digestate%). Only genera with relative abundance  $\geq 0.3\%$  and significant change ( $-2 \geq \text{Log}_2 \text{FC} \geq +2$ ,  $p_{adj} < 0.05$ , minimum normalized read count = 10) are shown (see **Supplementary Table 11** for the other groups).

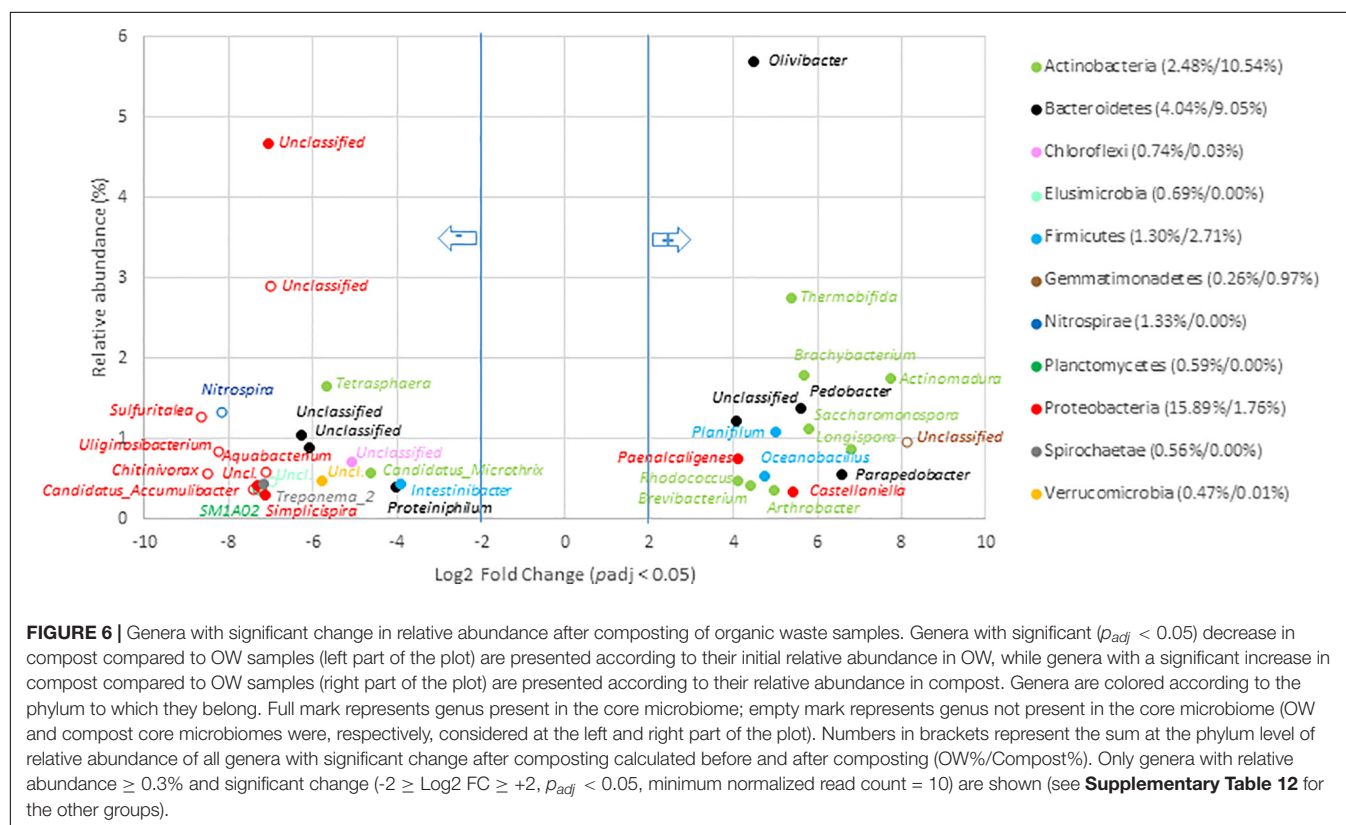
genera were significantly impacted by AD in, respectively, the urban and central/agricultural digestates. Despite this similar effect, a remarkable difference depending on OW origins was highlighted. In digestates of urban origin, this sorting mainly involved an enrichment of genera (32 out of the 50 impacted genera) while those produced from agricultural/central OW

led essentially to a reduction of several taxa (54 out of 60 impacted genera) (**Supplementary Tables 10, 11**). These comparisons suggested a full re-shuffling of agricultural/central OW bacterial taxa while those of the urban OW appeared to be well adapted for the living conditions prevailing in the anaerobic digester.

## Variations at the Scale of Genera Among Composts

Composting was found to drive microbial communities toward similar V5–V6 genetic structures whatever the origin of the OW including those that had undergone AD (Figure 2A). These conserved compost microbiomes appeared to have been selected by strong environmental constraints that led to an increase in the relative abundance of, among others, *Actinobacteria*, *Deferribacteres*, *Firmicutes*, and *Thermotogae*. These trends were confirmed while considering the numbers of 16S rRNA gene copies between OW and composts for these phyla. In fact, a significant one log increase was observed for the *Actinobacteria* and *Firmicutes* per gram of composts (Supplementary Table 9). Furthermore, the 16S rRNA gene copies allocated to the *Thermotogae* and *Deferribacteres* went from a negligible score up to several millions. Simultaneously, V5–V6 reads of six phyla (*Nitrospirae*, *Elusimicrobia*, *Acidobacteria*, *Saccharibacteria*, TM6, and GOUTA4) became negligible and were associated to a two-log reduction in 16S rRNA gene copies (Supplementary Table 9). These shifts among these phyla were confirmed at the scale of genera (Figure 6 and Supplementary Table 12). The compost microbiome was enriched in 36 genera of which only 6 were versatile and not found among all composts (Figure 6 and Supplementary Table 12). Relative distribution patterns of these genera changed by 4.1- to 8.1-Log2 fold when compared to the non-treated OW samples (going from 0.04 to 5.7% of the total compost microbial community). The most significant relative distribution increases were observed for reads allocated to the *Actinomadura*, *Longispora*, *Parapedobacter*, *Saccharomonospora*,

*Brachybacterium*, *Pedobacter*, *Thermobifida*, *Planifilum*, *Oceanobacillus*, *Olivibacter*, and *Paenaltcaligenes*. These genera are part of the *Actinobacteria* (50%), *Bacteroidetes*, or *Firmicutes*. In most cases, about two log increases in 16S rRNA gene copy numbers were associated with these changes (all statistical tests were significant; Wilcoxon  $p < 0.05$ ) (Supplementary Table 9). For example, the number of 16S rRNA copies for the *Olivibacter* went up from  $2.0 \times 10^8$  to  $1.0 \times 10^{10}$ . Most impressive was the shift from negligible numbers of *Longispora* among the OW going up to about  $2.0 \times 10^9$  16S rRNA gene copies (Supplementary Table 9). These changes were associated with the relative decreases of V5–V6 16S rRNA gene reads allocated to 105 genera including 29 found in the raw OWs core microbiome (Figure 6 and Supplementary Table 12). This reduction went from 3.8- to 8.1-Log2 fold change compared to OW where these genera originally represented 0.02–4.7% of the total raw OW microbial community (Figure 6 and Supplementary Table 12). Reads from *Tetrasphaera* (1.7–0.04%), *Microthrux* (0.6–0.03%), *Intestinibacter\_9* (0.4–0.04%), *Treponema\_2* (0.4% to 0.0%), *Proteiniphilum* (0.4–0.04%), *Simplicispira* (0.3–0.0%), *Christensenellaceae\_R7\_group* (0.3–0.03%), *Lautropia* (0.2–0.0%), *Macellibacteroides* (0.2–0.01%), BD17\_clade (0.1–0.0%), *Propionivibrio* (0.1–0.0%), *Proteocatella* (0.1–0.0%), and *Streptococcus* (0.1–0.0%) in the OW were the most significantly impacted (Figure 6 and Supplementary Table 12). These decreases among the community were confirmed by an analysis of the equivalent 16S rRNA gene copies for these genera in the OW and composts (Supplementary Table 9). DESEQ2 analyses



indicated that a re-shuffling of 52.6% of the read distribution patterns occurred during composting of OW. Composting was thus highly selective with a decline of 28.3% of the total relative abundance of the compost's bacterial taxa and an enrichment of 24.4% of the other taxa in the composts (**Supplementary Table 12**).

## Incidence of OW Digestion Processes on Bacterial Functional Groups

Functional traits selected by AD and composting were inferred from the taxonomic allocations performed at the genus level. At first, the sum of relative abundances of enriched genera potentially covering a functional trait extracted from the FAPROTAX database using MACADAM was calculated (**Supplementary Table 13**). The contribution of each genus to differences in hypothetical functional profiles is based on relative abundances before and after treatment (**Supplementary Table 13**). Based on the most abundant taxa in digestates from urban origin, the five main hierarchical functional traits were chemoheterotrophy (6.3%), fermentation (6.2%), human and mammal gut colonizers (each feature at 2.1%), and animal parasites or symbionts (2.1%) (**Supplementary Table 13D**). Similarly, these functional traits were also associated with the most abundant taxa in digestates from agricultural and central origin (**Supplementary Table 13F**). In composts, the functional traits of the enriched genera (as suggested from the number of equivalent 16S rRNA gene copies) were related to aliphatic non-methane hydrocarbon degradation, arsenate detoxification, dissimilatory arsenate reduction, hydrocarbon degradation, nitrate and nitrite ammonification, nitrate and nitrite respiration, and oil bioremediation. These taxa had increased by at least 8.5 log after composting of raw OWs (**Supplementary Table 13B**).

Functional traits related to health hazards were also investigated based on changes in relative abundances of bacterial genera before and after OW treatment (**Supplementary Table 13**). AD and composting processes contributed significantly at reducing genera potentially harboring infectious agents. The number of 16S rRNA gene copies of genera potentially causing diseases in human, plants, or fishes decreased by 9.3, 7.4, and 7.9 log, respectively, after composting of OW (**Supplementary Table 13A**). Similar trends could be observed during AD for genera harboring potential human pathogens. The number of 16S rRNA gene copies of genera potentially associated with human pathogens went down by about 7.4 and 1.7 log, respectively, in digestates from urban and agricultural/central categories (**Supplementary Tables 13C,E**). Interestingly, the number of 16S rRNA gene copies of genera possibly including lung pathogens or plant pathogens went down by about 7.5 log in digestates from the agricultural/central category (**Supplementary Table 13E**).

The theoretical metabolic pathways of the genera identified in this study were further inferred from sequenced genomes using the MACADAM software. Metabolic pathways (with a  $PS \geq 0.5$ ) potentially present in genera significantly impacted by the investigated digestion processes were counted, and

their relative distribution patterns were compared (**Table 2** and **Supplementary Table 14**). Distribution patterns between these functional categories observed among OWs from urban sites and from central/agricultural ones were found positively correlated (Spearman Rank Correlation;  $\rho = 0.69$ ,  $p < 0.05$ ). Such correlations were not observed between the anaerobic and aerobic digestion processes (digestates and composts).

After AD treatments, biosynthesis pathways for cofactors, nucleotides, amino acids, lipids, and aminoacyl-tRNAs charging were more abundant in the enriched genera than in the decaying ones whatever the raw OW origin (**Table 2** and **Supplementary Table 14**). Whereas biosynthesis pathways for secondary metabolites, cell structure, metabolic regulators, and alcohol and hormone biosynthesis were less abundant in the enriched genera than in the decaying ones (**Table 2** and **Supplementary Table 14**). Similarly, degradation pathways for fatty acids and lipids, carbohydrates, secondary metabolites, aromatic compounds, and sulfur-containing compounds metabolism degradation were less abundant in the enriched genera than the decaying ones (**Table 2** and **Supplementary Table 14**). Interestingly, in digestates from agricultural and central origin, nitrogen cycle-related processes (nitrate-reduction, ammonia-assimilation, ammonia-oxidation, denitrification, taurine-degradation, and nitrogen-fixation pathways) were more abundant in the enriched genera than the decaying ones, but the opposite situation occurred among digestates of urban origin (**Table 2** and **Supplementary Table 14**). After composting treatment, excepting the biosynthesis pathways involved in cell structure and the aromatic compounds degradation pathways, the inferred pathways ( $n = 29$ ) had a similar distribution among the impacted genera (**Table 2** and **Supplementary Table 14**). Cell structure biosynthesis pathways were less abundant in the enriched genera after both types of treatment (AD and composting) than in the decaying ones. Aromatic compounds degradation pathways were more abundant in the enriched genera found among composts but not among those of digestates (**Table 2** and **Supplementary Table 14**).

## DISCUSSION

OW recycling of sewage sludge and livestock effluents represent a major challenge because not only the bioenergy production but also environmental and sanitary issues must be considered. A key criterion in the assessment of the microbiological risks of OW recycling that remain poorly defined is the nature and structure of the various microbiomes getting into these processes and their potential health and ecological hazards. Here, the core and flexible components of the end product microbiomes were inferred, and the likelihood of these at being reproducibly found among highly diverse OW treatment plants was evaluated. Nine full-scale treatment plants distributed over France were selected to obtain a global view of microbiome bacterial taxa in the French OW treatment sector. These inferred bacterial taxa (from metabarcoding 16S rRNA gene datasets) are discussed below according to process type (AD, composting) and OW origins (fecal wastes from WWTP or agricultural sites, and food

products). Key functional traits of the bacterial genera impacted by the digestion processes were investigated to go further with the identification of key structuring bacterial processes.

According to NMDS ordinations of 16S rRNA gene metabarcoding datasets, two main bacterial community structures could be identified and found to match a segregation

**TABLE 2 |** Metabolic pathways recorded among the bacterial genera significantly impacted by the anaerobic digestion or composting processes as observed by the MACADAM approach.

Main hierarchical groups of pathways		Percentage of theoretical metabolic pathways <sup>a</sup> based on available sequenced genomes of isolates correlated to significantly impacted genera <sup>b</sup> in								
		Digestates from urban origin			Digestates from agricultural/central origin			Compost		
		TMP-EG (n = 252)	TMP-DG (n = 645)	R	TMP-EG (n = 321)	TMP-DG (n = 746)	R	TMP-EG (n = 753)	TMP-DG (n = 800)	R
Biosynthesis pathways	Cofactor <sup>c</sup>	23.0	15.0	1.5	21.8	11.7	1.9	13.8	13.5	1.0
	Amino acid	13.9	8.7	1.6	12.8	6.4	2.0	8.6	8.6	1.0
	Nucleotide	9.9	6.1	1.6	8.4	3.6	2.3	5.1	5.3	1.0
	Lipid	7.5	4.3	1.7	4.7	4.0	1.2	4.3	4.5	1.0
	Carbohydrates	4.8	5.1	0.9	2.2	4.8	0.5	4.5	5.4	0.8
	Aminoacyl-tRNAs-charging	1.2	0.5	2.4	0.9	0.1	9.0	0.4	0.4	1.0
	Secondary metabolite	1.2	2.2	0.5	0.9	3.0	0.3	2.7	2.4	1.1
	Cell structure	0.8	1.6	0.5	0.6	1.3	0.5	1.1	1.8	0.6
	Metabolic regulators	0.8	1.4	0.6	0.3	1.6	0.2	1.7	1.6	1.1
	Aromatic compounds	0.8	1.1	0.7	1.3	1.1	1.2	1.3	1.1	1.2
Degradation pathways	Alcohol	0.4	1.7	0.2	0.6	1.3	0.5	1.2	1.3	0.9
	Hormone	0.0	0.6	0	0.0	0.4	0	0.5	0.5	1.0
	Amino acid	6.4	7.4	0.9	8.1	8.3	0.9	7.6	7.8	1.0
	Nucleotide	4.8	3.6	1.3	4.4	2.7	1.6	2.8	3.0	0.9
	Fatty acid and lipid	0.0	1.4	0	0.6	1.2	0.5	1.2	1.4	0.9
	Carbohydrates	4.8	7.1	0.7	2.5	7.6	0.3	5.4	6.4	0.8
	Secondary metabolite	2.0	3.3	0.6	1.6	4.2	0.4	4.1	3.3	1.2
	Aromatic compounds	0.0	2.0	0	0.9	7.4	0.1	7.7	5.3	1.5
	Alcohol	1.2	1.7	0.7	1.3	1.3	1.0	1.3	1.5	0.9
	Carboxylates	3.2	5.0	0.6	4.1	5.6	0.7	5.1	5.1	1.0
Energy-metabolism	C1 compounds <sup>d</sup>	2.0	2.3	0.9	2.8	2.7	1.0	2.1	2.4	0.9
	Non-carbon nutrients	1.2	2.3	0.5	2.2	4.0	0.6	2.4	2.9	0.8
	Sulfur metabolism	0.4	0.8	0.5	1.3	1.2	1.1	1.2	1.0	1.2
Others	Phosphorus compounds	0.4	0.8	0.5	1.3	1.2	1.1	1.2	1.0	1.2
	Anaerobic respiration	1.6	1.9	0.8	1.9	3.2	0.6	2.8	2.9	1.0
	Aerobic respiration	1.2	1.6	0.8	2.8	1.6	1.8	1.6	1.6	1.0
	Fermentation	1.2	4.7	0.3	3.1	3.5	0.9	3.3	3.3	1.0
	Hydrogen-production	1.2	0.8	1.5	0.6	0.7	0.9	0.7	0.6	1.2
Others	Hydrogen-oxidation	0.4	0.5	0.8	0.3	0.4	0.8	0.4	0.4	1.0
	Nitrogen cycling processes <sup>e</sup>	1.6	3.1	0.5	4.1	2.7	1.5	2.8	2.8	1.0
	Detoxification <sup>f</sup>	1.2	1.9	0.6	2.2	2.0	1.1	1.9	1.9	1.0
Others	Nucleic acid processing	1.6	0.6	2.7	0.9	0.3	3.0	0.5	0.5	1.0

<sup>a</sup>A minimum pathway score (PS) and pathway frequency score (PSF) of 0.5 was used for hypothetical metabolic pathways filtering.

<sup>b</sup>To see the list of organisms with the targeted metabolic pathway, see **Supplementary Tables 14A–F**. <sup>c</sup>Cofactor biosynthesis are coenzyme A biosynthesis, vitamin biosynthesis, CoA biosynthesis, reductants, NAD metabolism, porphyrin compounds biosynthesis, quinone biosynthesis, polyprenyl biosynthesis, molybdenum cofactor, lipoate biosynthesis, and tetrapyrrole biosynthesis. <sup>d</sup>C1 compounds are CO<sub>2</sub> fixation, formaldehyde oxidation, methanol oxidation, formaldehyde assimilation, and methane oxidation. <sup>e</sup>Nitrogen cycling processes consist of nitrate reduction, ammonia assimilation, ammonia oxidation, denitrification, taurine degradation, and nitrogen fixation. <sup>f</sup>Detoxification involves acid resistance, arsenate detoxification, methylglyoxal detoxification, antibiotic resistance, and reactive oxygen species degradation. Abbreviations: TMP-EG, theoretical metabolic pathways in the enriched genera after treatments; TMP-DG, theoretical metabolic pathways in the decaying genera; R, relative proportion of pathways per category between the enriched genera and the decaying ones.



between bacterial taxa from OW containing agricultural wastes or not (restricted to urban WWTP activated sludge). This segregation was also in line with a differentiation between their contents in micropollutants particularly the TEs. The urban samples (treated or not) had significantly more micropollutants including 14 TEs (Ag, Al, As, Cd, Ce, Co, Cr, Cu, Ga, Mo, Ni, P, Pb, and Ti), 4-nonylphenol, and 2 PAHs (phenanthrene and anthracene) than the agricultural and mixed (agricultural/urban; termed “central” in the text) samples. The 16S rRNA gene microbial community structures of the investigated OW urban samples were in agreement with previous studies (Juretschko et al., 2002; Wong et al., 2005; Hu et al., 2012; Díaz et al., 2018). Inferred 16S rRNA gene taxonomic allocations were predominantly among the *Proteobacteria*, *Bacteroidetes*, *Actinobacteria*, *Firmicutes*, and *Nitrospirae* phyla. *Proteobacteria* were reported to be recurrent among WWTP activated sludge and have been shown to represent almost 50% of the bacterial taxa (Juretschko et al., 2002; Wong et al., 2005; Hu et al., 2012). *Actinobacteria* were also previously mentioned as highly abundant organisms in such wastes and being favored by the high phosphorus content of activated sludge (Wagner et al., 1994). *Nitrospirae* known to be nitrite-oxidizing bacteria were previously considered as common in activated sludge but were not mentioned as being abundant core organisms (Saunders et al., 2016).

After AD of both categories of raw OWs (urban and central/agricultural categories), 16S rRNA gene inferred phyla with similar relative changes were observed. These shifts occurred whatever the raw OW origin. Both categories of digestates (urban and central/agricultural categories) were impacted by selective environmental changes, which led to a decrease in the relative abundance of *Proteobacteria* but an enrichment in *Firmicutes* (which nearly doubled in relative abundance). *Firmicutes* had been reported by several authors as one of the most abundant phyla in AD processes of activated sludge (Hu et al., 2012; Zhang et al., 2012; Abendroth et al., 2015; Díaz et al., 2018). Sundberg et al. (2013) also found that *Firmicutes* were the most prevalent in samples taken from reactors fed with various combinations of wastes (from slaughterhouses, restaurants, households, etc.). In this work, with 52.2% of V5–V6 rRNA gene reads, *Firmicutes* were dominant in the digestates from central (mixed)/agricultural sites. Furthermore, they were enriched by 2.6-fold in digestates from urban sites to reach an 18.4% relative abundance. These results seem to indicate that the AD conditions favored their growth whatever the OW origins. To go deeper into the understanding of these community changes, the impact of AD on the structuration of end product microbiomes was assessed by grouping 16S rRNA gene reads according to their allocations at the genus level, and making comparisons by DESEQ2. These analyses revealed that about one third of the total relative abundance (according to the mean normalized counts) of the digestate bacterial taxa were significantly affected by the AD treatment whatever the raw OW origin. The relative abundances of 50 and 60 genera were significantly impacted by AD as observed from, respectively, urban and central/agricultural digestates. However, differences in the shifts of the 16S rRNA gene reads of these taxa were found

related to the origin of the OW. In digestates of urban origin, this sorting mainly implied an increase in the relative abundance of OW urban taxa while those generated from agricultural/central OW led essentially to a reduction in the relative abundance of most of the initial OW taxa. This indicates that the coalescence of bacterial taxa of raw OW with the microbial community of the digesters will be largely dependent on their origin (and nature). In fact, urban OWs (mainly composed of activated sludge) were found to contain better fit communities for the AD process that could interact with the digesters' microbial communities. Bacterial taxa present in agricultural raw OW were outcompeted by the digesters' communities. This could be explained by the pre-treatment conditions performed in municipal wastewater facilities, leading to an increase of specialized bacterial taxa in the activated sludge. These taxa can perform multiple biodegradation processes (Shchegolkova et al., 2016) and can form heterogeneous structures termed flocs (Ju and Zhang, 2015). Functional inferences through FAPROTAX (Louca et al., 2016) were undertaken to highlight their potential contributions to the AD process.

The functional traits of the dominant microbial taxa inferred from the 16S rRNA gene datasets in the AD end products were investigated. Based on FAPROTAX analyses, functional traits such as chemoheterotrophy and fermentation were highly common among the taxa found in digestates of the urban and agricultural/central categories. Chemoheterotrophic bacteria are usually acting as primary decomposers (hydrolysis step), which are responsible for OW recycling in diverse ecosystems (Kämpfer et al., 1993). Fermentation, a widespread anaerobic pathway, is an essential step in AD process where fermentative bacteria convert simple monomers such as simple sugar, amino acids, and alcohols into short-chain fatty acids, primary alcohols, as well as H<sub>2</sub> and CO<sub>2</sub> (Cardinali-Rezende et al., 2009; Bajpai, 2017; Anukam et al., 2019). Interestingly, these functions (chemoheterotrophy and fermentation) were also previously reported by Wei et al. (2018) as the most dominant functions in activated sludge. This elucidates why bacterial genera from activated sludge could directly contribute to the observed diversity in the digestates. This observation is in line with the hypothesis of a selection of the most fit K-strategists (specialists) with ecologically relevant functions during the AD process. Also, these results confirmed that the changes in the AD community composition were driven by functional traits and less constrained by taxonomic relatedness.

To corroborate the above conclusion, closer analyses of the metabolic potential of bacterial communities were performed. Pathways inferred to be present in the enriched genera after treatment against those of the decreased ones were compared according to the origin/natures of the OWs. Interestingly, AD treatment was confirmed to impact similarly numerous metabolic pathways in both categories of OWs (urban and central/agricultural categories). Ten biosynthesis pathways (10/12) involved in the production of secondary metabolites, cell structure, metabolic regulators, biosynthesis, etc., and nine degradation pathways (9/11) (e.g., aromatic compounds and sulfur-containing compounds degradation) were affected similarly in both digestates from urban and agricultural/central categories. Nevertheless, some categories of pathways were

not impacted in the same way according to the OW origin. For example, in digestates from agricultural and central origin, nitrogen cycling processes (e.g., nitrate-reduction, ammonia-assimilation, denitrification, and nitrogen-fixation pathways) were more abundant in the enriched genera than in the decaying ones, but the opposite situation was observed for digestates of urban origin. These pathways (related to nitrogen cycle) have been reported by Wei et al. (2018) as central key functions in activated sludge. Thus, these pathways could be critical in the ecology of activated sludge but less important during AD.

The impact of composting per OW type on the bacterial communities was also investigated. After composting, a NMDS plot grouped together the 16S rRNA community profiles whatever the OW origin. Composting was found to drive bacterial communities toward similar genetic structures in all samples without differentiating OW inputs that had previously undergone AD. This conserved microbiome appeared to have been selected by highly selective constraints leading to a significant decrease in the relative abundance of *Bacteroidetes*, *Chlorobi*, *Chloroflexi*, *Lentisphaerae*, *Planctomycetes*, *Proteobacteria*, *Verrucomicrobia*, and *Spirochaetae* and the loss of six phyla (*Nitrospirae*, *Elusimicrobia*, *Acidobacteria*, *Saccharibacteria*, *TM6*, and *GOUTA4*) from the inputs OW. Other studies reported similar findings (Steger et al., 2007a; Song et al., 2014). In a compost pile, changes in physicochemical factors such as pH, temperature, moisture, and organic carbon were found to be correlated with bacterial growth. Microbial community structures were found to be affected by these evolving parameters (Cahyani et al., 2003; Liang et al., 2003; Tang et al., 2007; Zhang et al., 2011). Among these, temperature was shown to be highly selective (Palmisano and Barlaz, 1996; Steger et al., 2007a). Interestingly, with their large shift in relative abundance (4.3-fold) observed between OW and composts, *Actinobacteria* showed a major re-shuffling with an up to 20% increase. These are clearly key players in the composting process.

To go deeper into the understanding of these effects, changes in the composition of the compost bacterial taxa were investigated at genus level. A total of 141 genera were found to be affected by composting, with 105 genera showing a significant decrease (equivalent to 53.7% of the total relative abundance of the compost's bacterial taxa). Only three of these decaying genera were allocated to the *Actinobacteria*. However, 16 of the 36 enriched genera were part of this phylum. Previous studies have reported the persistence of *Actinobacteria* over the composting process from the thermophilic to the curing stage, regardless of the nature of treated OW (Danon et al., 2008). This bacterial group also constituted a significant part of the microbial community in the late composting stages (Herrmann and Shann, 1997; Tiquia et al., 2002; Hiraishi et al., 2003; Steger et al., 2007b). *Actinobacteria* are Gram-positive bacteria with high G + C contents in DNA, widely distributed in a diversity of ecological environments, including extreme ecosystem (Qin et al., 2011, 2019; Dhakal et al., 2017; Goodfellow et al., 2018). They can perform several important functions. Some *Actinobacteria* can synthesize a wide diversity of secondary

metabolites, which may promote survival in highly selective environments (Fang et al., 2017; Puttaswamygowda et al., 2019; Qin et al., 2019). Several studies have highlighted the importance of temperature as a selective factor of thermo-tolerant *Actinobacteria*. In fact, *Saccharomonospora viridis*, *Thermobifida fusca*, and *Thermobispora bispora* have been reported in the later composting stages. In our study, many genera of thermo-tolerant *Actinobacteria*, e.g., *Thermobifida*, *Actinomadura*, *Saccharomonospora*, *Arthrobacter*, *Thermomonospora*, and *Thermocrispum* were enriched in compost irrespective of the origin of the treated OW. *Actinobacteria* are capable of breaking down a wide range of animal wastes and plant debris particularly complex compounds (e.g., lignocelluloses), playing an important role in the later stages of composting (Herrmann and Shann, 1997; Wang et al., 2016). It is to be noted that thanks to the occurrences of bacterial genera degrading xenobiotics, composting offers the advantage of decreasing the concentration of chemical contaminants (Semple et al., 2001; Ghaly, 2011; Cascant et al., 2016; Ren et al., 2018). In line with these reports, genera of xenobiotic degrading *Actinobacteria*, e.g., *Arthrobacter*, were found to be enriched in the 16S rRNA gene datasets generated from composts DNA. To go deeper, closer analyses of functional potentials *per taxa* enriched after composting were performed. The functional profiles of the enriched genera suggested that the number of 16S rRNA copies of genera, e.g., *Arthrobacter*, *Alcanivorax*, *Rhodococcus*, *Brevibacterium*, etc., known to consist of many strains having functional traits involved in arsenate detoxification, dissimilatory arsenate reduction, plastic degradation, and oil bioremediation have significantly increased through composting. This further supports the idea that composting is an efficient bioremediation process.

## CONCLUSION

In conclusion, AD and composting induced bacterial changes that were found driven by pH, temperature, but also the C- and energy sources which require specialized metabolic properties. These factors were more selective in composting than AD. Consequently, composting generated highly predictable community patterns whatever the OW origin. In AD, the relative contribution of the raw OW microbiomes on the digestate structural and functional bacterial community patterns was dependent on its origin. Bacterial genera from activated sludge were found to be well-suited for the AD process and contributed directly to the observed diversity observed in the digestates. Content in activated sludge among the OW was thus considered to be a critical factor for predicting the digestate bacterial contents. Our findings provided new insights into our understanding of bacterial coalescence phenomena in aerobic and anaerobic digesters. However, knowledge gap remains regarding potential health hazards associated with the emerging communities observed in the end products. These organic matter biodegradation processes being built from a large panel of exogenous communities, they might offer conditions

favorable for horizontal gene transfer (HGT) events such as the HGT of antibiotic resistance genes (ARG). The next step in these analyses will be to evaluate the frequency of these HGT.

## DATA AVAILABILITY STATEMENT

The datasets presented in this study can be found in online repositories. The names of the repository/repositories and accession number(s) can be found below: European Nucleotide Archive (<https://www.ebi.ac.uk/research>) under the accession number PRJEB40193.

## AUTHOR CONTRIBUTIONS

AA, EB, LM, BC, and WG conceived and designed experiments. AA, EB, LM, SH, DP, ED, BC, and WG performed the experiments. AA, EB, BC, and WG performed the data curation and statistical analyses. AA, BC, and WG wrote the manuscript. All authors read and approved the final manuscript.

## REFERENCES

- Abendroth, C., Vilanova, C., Günther, T., Luschign, O., and Porcar, M. (2015). Eubacteria and archaea communities in seven mesophile anaerobic digester plants in Germany. *Biotechnol. Biofuels* 8:87. doi: 10.1186/s13068-015-0271-6
- Ahmad, R., Jilani, G., Arshad, M., Zahir, Z. A., and Khalid, A. (2007). Bio-conversion of organic wastes for their recycling in agriculture: an overview of perspectives and prospects. *Ann. Microbiol.* 57, 471–479. doi: 10.1007/BF03175343
- Anders, S., and Huber, W. (2010). Differential expression analysis for sequence count data. *Genome Biol.* 11:R106.
- Anukam, A., Mohammadi, A., Naqvi, M., and Granström, K. (2019). A review of the chemistry of anaerobic digestion: methods of accelerating and optimizing process efficiency. *Processes* 7:504. doi: 10.3390/pr7080504
- Atelge, M. R., Krisa, D., Kumar, G., Eskicioglu, C., Nguyen, D. D., Chang, S. W., et al. (2020). Biogas production from organic waste: recent progress and perspectives. *Waste Biomass Valorization* 11, 1019–1040. doi: 10.1007/s12649-018-00546-0
- Bajpai, P. (2017). “Basics of anaerobic digestion process,” in *Anaerobic Technology in Pulp and Paper Industry SpringerBriefs in Applied Sciences and Technology*, ed. P. Bajpai, (Singapore: Springer), 7–12. doi: 10.1007/978-981-10-4130-3\_2
- Blanc, M., Marilley, L., Beffa, T., and Aragno, M. (1999). Thermophilic bacterial communities in hot composts as revealed by most probable number counts and molecular (16S rDNA) methods. *FEMS Microbiol. Ecol.* 28, 141–149. doi: 10.1111/j.1574-6941.1999.tb00569.x
- Bodenhause, N., Horton, M. W., and Bergelson, J. (2013). Bacterial communities associated with the leaves and the roots of *Arabidopsis thaliana*. *PLoS One* 8:e56329. doi: 10.1371/journal.pone.0056329
- Cahyani, V. R., Matsuya, K., Asakawa, S., and Kimura, M. (2003). Succession and phylogenetic composition of bacterial communities responsible for the composting process of rice straw estimated by PCR-DGGE analysis. *Soil Sci. Plant Nutr.* 49, 619–630. doi: 10.1080/00380768.2003.10410052
- Cardinali-Rezende, J., Debarry, R. B., Colturato, L. F. D. B., Carneiro, E. V., Chartone-Souza, E., and Nascimento, A. M. A. (2009). Molecular identification and dynamics of microbial communities in reactor treating organic household waste. *Appl. Microbiol. Biotechnol.* 84, 777–789. doi: 10.1007/s00253-009-2071-z
- Cascant, M. M., Sisouane, M., Tahiri, S., Krati, M. E., Cervera, M. L., Garrigues, S., et al. (2016). Determination of total phenolic compounds in compost by infrared spectroscopy. *Talanta* 153, 360–365. doi: 10.1016/j.talanta.2016.03.020

## FUNDING

This study was partly funded by the ANR (Agence Nationale de la Recherche, France) DIGESTATE project ANR-15-CE340003-01, Bacteri'eau project ANR-16-CE04-0014-01, and the “Auvergne-Rhône-Alpes” Region (France) “pack ambition recherche” project ITAS-MZ2M.

## ACKNOWLEDGMENTS

We wish to thank J. P. Delgenes, N. Sertillanges, D. Montenach, A. Savoie (INRAe), M. Montels, and C. Chevassut-Rosset (CIRAD) who provided us the samples analyzed in this project.

## SUPPLEMENTARY MATERIAL

The Supplementary Material for this article can be found online at: <https://www.frontiersin.org/articles/10.3389/fmicb.2021.667043/full#supplementary-material>

- Chelius, M. K., and Triplett, E. W. (2001). The diversity of archaea and bacteria in association with the roots of *Zea mays* L. *Microb. Ecol.* 41, 252–263. doi: 10.1007/s002480000087
- Chen, Y., Cheng, J. J., and Creamer, K. S. (2008). Inhibition of anaerobic digestion process: a review. *Bioresour. Technol.* 99, 4044–4064. doi: 10.1016/j.biortech.2007.01.057
- Danon, M., Franke-Whittle, I. H., Insam, H., Chen, Y., and Hadar, Y. (2008). Molecular analysis of bacterial community succession during prolonged compost curing. *FEMS Microbiol. Ecol.* 65, 133–144. doi: 10.1111/j.1574-6941.2008.00506.x
- Day, M., and Shaw, K. (2001). “Biological, chemical and physical processes of composting,” in *Compost Utilization In Horticultural Cropping Systems*, eds P. J. Stoffella, and B. A. Kahn, (Boca Raton FL: Lewis Publication), 17–50.
- De Vrieze, J., Raport, L., Roume, H., Vilchez-Vargas, R., Jäuregui, R., Pieper, D. H., et al. (2016). The full-scale anaerobic digestion microbiome is represented by specific marker populations. *Water Res.* 104, 101–110. doi: 10.1016/j.watres.2016.08.008
- De Vrieze, J., Verstraete, W., and Boon, N. (2013). Repeated pulse feeding induces functional stability in anaerobic digestion. *Microb. Biotechnol.* 6, 414–424. doi: 10.1111/1751-7915.12025
- Demirel, B., and Scherer, P. (2008). The roles of acetotrophic and hydrogenotrophic methanogens during anaerobic conversion of biomass to methane: a review. *Rev. Environ. Sci. Biotechnol.* 7, 173–190. doi: 10.1007/s11157-008-9131-1
- Dhakal, D., Pokhrel, A. R., Shrestha, B., and Sohng, J. K. (2017). Marine rare actinobacteria: isolation, characterization, and strategies for harnessing bioactive compounds. *Front. Microbiol.* 8:1106. doi: 10.3389/fmicb.2017.01106
- Díaz, A. I., Oulego, P., Collado, S., Laca, A., González, J. M., and Díaz, M. (2018). Impact of anaerobic digestion and centrifugation/decanting processes in bacterial communities fractions. *J. Biosci. Bioeng.* 126, 742–749. doi: 10.1016/j.jbiosc.2018.05.024
- Fang, B.-Z., Salam, N., Han, M.-X., Jiao, J.-Y., Cheng, J., Wei, D.-Q., et al. (2017). Insights on the effects of heat pretreatment, pH, and calcium salts on isolation of rare actinobacteria from Karstic caves. *Front. Microbiol.* 8:1535. doi: 10.3389/fmicb.2017.01535
- Franke-Whittle, I. H., Walter, A., Ebner, C., and Insam, H. (2014). Investigation into the effect of high concentrations of volatile fatty acids in anaerobic digestion on methanogenic communities. *Waste Manag.* 34, 2080–2089. doi: 10.1016/j.wasman.2014.07.020
- Ghaly, (2011). Biodegradation of phenolic compounds in creosote treated wood waste by a composting microbial culture augmented with the fungus



- Thermoascus aurantiacus*. *Am. J. Biochem. Biotechnol.* 7, 90–103. doi: 10.3844/ajbbsp.2011.90.103
- González-Fernández, C., and García-Encina, P. A. (2009). Impact of substrate to inoculum ratio in anaerobic digestion of swine slurry. *Biomass Bioenergy* 33, 1065–1069. doi: 10.1016/j.biombioe.2009.03.008
- Goodfellow, M., Nouioui, I., Sanderson, R., Xie, F., and Bull, A. T. (2018). Rare taxa and dark microbial matter: novel bioactive actinobacteria abundant in Atacama Desert soils. *Antonie Van Leeuwenhoek* 111, 1315–1332. doi: 10.1007/s10482-018-1088-7
- Gou, C., Yang, Z., Huang, J., Wang, H., Xu, H., and Wang, L. (2014). Effects of temperature and organic loading rate on the performance and microbial community of anaerobic co-digestion of waste activated sludge and food waste. *Chemosphere* 105, 146–151. doi: 10.1016/j.chemosphere.2014.01.018
- Herrmann, R. F., and Shann, J. F. (1997). Microbial community changes during the composting of municipal solid waste. *Microb. Ecol.* 33, 78–85. doi: 10.1007/s002489900010
- Hiraishi, A., Narihiro, T., and Yamanaka, Y. (2003). Microbial community dynamics during start-up operation of flowerpot-using fed-batch reactors for composting of household biowaste. *Environ. Microbiol.* 5, 765–776. doi: 10.1046/j.1462-2920.2003.00473.x
- Hoornweg, D., Bhada-Tata, P., and Kennedy, C. (2013). Environment: waste production must peak this century. *Nature* 502, 615–617. doi: 10.1038/502615a
- Hu, M., Wang, X., Wen, X., and Xia, Y. (2012). Microbial community structures in different wastewater treatment plants as revealed by 454-pyrosequencing analysis. *Bioresour. Technol.* 117, 72–79. doi: 10.1016/j.biortech.2012.04.061
- Hupfaut, S., Plattner, P., Wagner, A. O., Kaufmann, R., Insam, H., and Podmirseg, S. M. (2018). Temperature shapes the microbiota in anaerobic digestion and drives efficiency to a maximum at 45°C. *Bioresour. Technol.* 269, 309–318. doi: 10.1016/j.biortech.2018.08.106
- Insam, H., and de Bertoldi, M. (2007). “Chapter 3 microbiology of the composting process,” in *Waste Management Series Compost Science and Technology*, eds L. F. Diaz, M. de Bertoldi, W. Bidlingmaier, and E. Stentiford, (Amsterdam: Elsevier), 25–48. doi: 10.1016/S1478-7482(07)80006-6
- Ju, F., and Zhang, T. (2015). Bacterial assembly and temporal dynamics in activated sludge of a full-scale municipal wastewater treatment plant. *ISME J.* 9, 683–695. doi: 10.1038/ismej.2014.162
- Juretschko, S., Loy, A., Lehner, A., and Wagner, M. (2002). The microbial community composition of a nitrifying-denitrifying activated sludge from an industrial sewage treatment plant analyzed by the full-cycle rRNA approach. *Syst. Appl. Microbiol.* 25, 84–99. doi: 10.1078/0723-2020-00093
- Kämpfer, P., Steiof, M., Becker, P. M., and Dott, W. (1993). Characterization of chemoheterotrophic bacteria associated with the in situ bioremediation of a waste-oil contaminated site. *Microb. Ecol.* 26, 161–188.
- Kayhanian, M. (1994). Performance of a high-solids anaerobic digestion process under various ammonia concentrations. *J. Chem. Technol. Biotechnol.* 59, 349–352. doi: 10.1002/jctb.280590406
- Kozich, J. J., Westcott, S. L., Baxter, N. T., Highlander, S. K., and Schloss, P. D. (2013). Development of a dual-index sequencing strategy and curation pipeline for analyzing amplicon sequence data on the MiSeq Illumina sequencing platform. *Appl. Environ. Microbiol.* 79, 5112–5120. doi: 10.1128/AEM.01043-13
- Le Bars, M., Legros, S., Levard, C., Chaurand, P., Tella, M., Rovezzi, M., et al. (2018). Drastic change in zinc speciation during anaerobic digestion and composting: instability of nanosized Zinc Sulfide. *Environ. Sci. Technol.* 52, 12987–12996. doi: 10.1021/acs.est.8b02697
- Le Boulch, M., Déhais, P., Combes, S., and Pascal, G. (2019). The MACADAM database: a metabolic pathways database for microbial taxonomic groups for mining potential metabolic capacities of archaeal and bacterial taxonomic groups. *Database* 2019:baz049. doi: 10.1093/database/baz049
- Levin, L., Eriksson, A. R. B., and Schnürer, A. (2007). Effect of process temperature on bacterial and archaeal communities in two methanogenic bioreactors treating organic household waste. *FEMS Microbiol. Ecol.* 59, 683–693. doi: 10.1111/j.1574-6941.2006.00263.x
- Liang, C., Das, K. C., and McClendon, R. W. (2003). The influence of temperature and moisture contents regimes on the aerobic microbial activity of a biosolids composting blend. *Bioresour. Technol.* 86, 131–137. doi: 10.1016/S0960-8524(02)00153-0
- Louca, S., Parfrey, L. W., and Doebeli, M. (2016). Decoupling function and taxonomy in the global ocean microbiome. *Science* 353, 1272–1277. doi: 10.1126/science.aaf4507
- Love, M. I., Huber, W., and Anders, S. (2014). Moderated estimation of fold change and dispersion for RNA-seq data with DESeq2. *bioRxiv* [Preprint] doi: 10.1101/002832
- Lykidis, A., Chen, C.-L., Tringe, S. G., McHardy, A. C., Copeland, A., Kyrpides, N. C., et al. (2011). Multiple syntrophic interactions in a terephthalate-degrading methanogenic consortium. *ISME J.* 5, 122–130. doi: 10.1038/ismej.2010.125
- Mailler, R., Gasperi, J., Patureau, D., Vulliet, E., Delgenes, N., Danel, A., et al. (2017). Fate of emerging and priority micropollutants during the sewage sludge treatment: Case study of Paris conurbation. Part 1: contamination of the different types of sewage sludge. *Waste Manag.* 59, 379–393. doi: 10.1016/j.wasman.2016.11.010
- Marti, R., Bécouze-Lareure, C., Ribun, S., Marjolet, L., Souibgui, C. B., Aubin, J.-B., et al. (2017). Bacteriome genetic structures of urban deposits are indicative of their origin and impacted by chemical pollutants. *Sci. Rep.* 7:13219. doi: 10.1038/s41598-017-13594-8
- Moset, V., Poulsen, M., Wahid, R., Højberg, O., and Møller, H. B. (2015). Mesophilic versus thermophilic anaerobic digestion of cattle manure: methane productivity and microbial ecology. *Microb. Biotechnol.* 8, 787–800. doi: 10.1111/1751-7915.12271
- Noble, R., and Roberts, S. J. (2004). Eradication of plant pathogens and nematodes during composting: a review. *Plant Pathol.* 53, 548–568. doi: 10.1111/j.0032-0862.2004.01059.x
- Oksanen, J., Blanchet, F. G., Friendly, M., Kindt, R., Legendre, P., McGlinn, D., et al. (2019). *vegan: Community Ecology Package*. Available online at: <https://CRAN.R-project.org/package=vegan> (accessed November 3, 2020).
- Palaniveloo, K., Amran, M. A., Norhashim, N. A., Mohamad-Fauzi, N., Peng-Hui, F., Hui-Wen, L., et al. (2020). Food waste composting and microbial community structure profiling. *Processes* 8:723. doi: 10.3390/pr8060723
- Palmisano, A. C., and Barlaz, M. A. (1996). *Microbiology of Solid Waste*. Boca Raton, FL: CRC Press.
- Pohlert, T. (2020). *PMCMRplus: Calculate Pairwise Multiple Comparisons of Mean Rank Sums Extended*. Available online at: <https://CRAN.R-project.org/package=PMCMRplus> (accessed November 3, 2020).
- Puttaswamygowda, G. H., Olakkaran, S., Antony, A., and Kizhakke Purayil, A. (2019). “Chapter 22 – present status and future perspectives of marine actinobacterial metabolites,” in *Recent Developments in Applied Microbiology and Biochemistry*, ed V. Buddolla, (Cambridge, MA: Academic Press), 307–319. doi: 10.1016/B978-0-12-816328-3.00022-2
- Pycke, B., Etchebehere, C., Van de Cavey, P., Negroni, A., Verstraete, W., and Boon, N. (2011). A time-course analysis of four full-scale anaerobic digesters in relation to the dynamics of change of their microbial communities. *Water Sci. Technol.* 63, 769–775. doi: 10.2166/wst.2011.307
- Qin, S., Li, W.-J., Klenk, H.-P., Hozzein, W. N., and Ahmed, I. (2019). Editorial: actinobacteria in special and extreme habitats: diversity, function roles and environmental adaptations, second edition. *Front. Microbiol.* 10:944. doi: 10.3389/fmicb.2019.00944
- Qin, S., Xing, K., Jiang, J.-H., Xu, L.-H., and Li, W.-J. (2011). Biodiversity, bioactive natural products and biotechnological potential of plant-associated endophytic actinobacteria. *Appl. Microbiol. Biotechnol.* 89, 457–473. doi: 10.1007/s00253-010-2923-6
- Reinikainen, O., and Herranen, M. (2001). Different methods for measuring compost stability and maturity. *Acta Hort.* 549, 99–104. doi: 10.17660/ActaHortic.2001.549.10
- Ren, X., Zeng, G., Tang, L., Wang, J., Wan, J., Wang, J., et al. (2018). The potential impact on the biodegradation of organic pollutants from composting technology for soil remediation. *Waste Manag.* 72, 138–149. doi: 10.1016/j.wasman.2017.11.032
- Rivière, D., Desvignes, V., Pelletier, E., Chaussonnerie, S., Guermazi, S., Weissenbach, J., et al. (2009). Towards the definition of a core of microorganisms involved in anaerobic digestion of sludge. *ISME J.* 3, 700–714. doi: 10.1038/ismej.2009.2
- Saad, N. M. C., and Massé, D. I. (2015). A start-up of psychrophilic anaerobic sequence batch reactor digesting a 35 % total solids feed of



- dairy manure and wheat straw. *AMB Express* 5:144. doi: 10.1186/s13568-015-0144-1
- Saunders, A. M., Albertsen, M., Vollertsen, J., and Nielsen, P. H. (2016). The activated sludge ecosystem contains a core community of abundant organisms. *ISME J.* 10, 11–20. doi: 10.1038/ismej.2015.117
- Schloss, P. D., Westcott, S. L., Ryabin, T., Hall, J. R., Hartmann, M., Hollister, E. B., et al. (2009). Introducing mothur: open-source, platform-independent, community-supported software for describing and comparing microbial communities. *Appl. Environ. Microbiol.* 75, 7537–7541. doi: 10.1128/AEM.01541-09
- Semple, K. T., Reid, B. J., and Fermor, T. R. (2001). Impact of composting strategies on the treatment of soils contaminated with organic pollutants. *Environ. Pollut.* 112, 269–283. doi: 10.1016/s0269-7491(00)00099-3
- Sertillanges, N., Haudin, C.-S., Bourdat-Deschamps, M., Bernet, N., Serre, V., Danel, A., et al. (2020). Process type is the key driver of the fate of organic micropollutants during industrial scale treatment of organic wastes. *Sci. Total Environ.* 734:139108. doi: 10.1016/j.scitotenv.2020.139108
- Shchegolkova, N. M., Krasnov, G. S., Belova, A. A., Dmitriev, A. A., Kharitonov, S. L., Klimina, K. M., et al. (2016). Microbial community structure of activated sludge in treatment plants with different wastewater compositions. *Front. Microbiol.* 7:90. doi: 10.3389/fmicb.2016.00090
- Song, C., Li, M., Jia, X., Wei, Z., Zhao, Y., Xi, B., et al. (2014). Comparison of bacterial community structure and dynamics during the thermophilic composting of different types of solid wastes: anaerobic digestion residue, pig manure and chicken manure. *Microb. Biotechnol.* 7, 424–433. doi: 10.1111/1751-7915.12131
- Steger, K., Jarvis, Å., Vasara, T., Romantschuk, M., and Sundh, I. (2007a). Effects of differing temperature management on development of Actinobacteria populations during composting. *Res. Microbiol.* 158, 617–624. doi: 10.1016/j.resmic.2007.05.006
- Steger, K., Sjögren, Å.M., Jarvis, Å., Jansson, J. K., and Sundh, I. (2007b). Development of compost maturity and Actinobacteria populations during full-scale composting of organic household waste. *J. Appl. Microbiol.* 103, 487–498. doi: 10.1111/j.1365-2672.2006.03271.x
- Sundberg, C., Al-Soud, W. A., Larsson, M., Alm, E., Yekta, S. S., Svensson, B. H., et al. (2013). 454 pyrosequencing analyses of bacterial and archaeal richness in 21 full-scale biogas digesters. *FEMS Microbiol. Ecol.* 85, 612–626. doi: 10.1111/1574-6941.12148
- Supaphol, S., Jenkins, S. N., Intomo, P., Waite, I. S., and O'Donnell, A. G. (2011). Microbial community dynamics in mesophilic anaerobic co-digestion of mixed waste. *Bioresour. Technol.* 102, 4021–4027. doi: 10.1016/j.biortech.2010.11.124
- Tang, J.-C., Shibata, A., Zhou, Q., and Katayama, A. (2007). Effect of temperature on reaction rate and microbial community in composting of cattle manure with rice straw. *J. Biosci. Bioeng.* 104, 321–328. doi: 10.1263/jbb.104.321
- Tian, W., Sun, Q., Xu, D., Zhang, Z., Chen, D., Li, C., et al. (2013). Succession of bacterial communities during composting process as detected by 16S rRNA clone libraries analysis. *Int. Biodeterior. Biodegrad.* 78, 58–66. doi: 10.1016/j.ibiod.2012.12.008
- Tiquia, S. M., Wan, H. C., and Tam, N. F. Y. (2002). Microbial population dynamics and enzyme activities during composting. *Compost Sci. Util.* 10, 150–161. doi: 10.1080/1065657X.2002.10702075
- Trably, E., Delgènes, N., Patureau, D., and Delgènes, J. P. (2004). Statistical tools for the optimization of a highly reproducible method for the analysis of polycyclic aromatic hydrocarbons in sludge samples. *Int. J. Environ. Anal. Chem.* 84, 995–1008. doi: 10.1080/03067310412331298412
- Vanwonterghem, I., Jensen, P. D., Dennis, P. G., Hugenholtz, P., Rabaey, K., and Tyson, G. W. (2014). Deterministic processes guide long-term synchronised population dynamics in replicate anaerobic digesters. *ISME J.* 8, 2015–2028. doi: 10.1038/ismej.2014.50
- Voisin, J., Cournoyer, B., Marjolet, L., Vienney, A., and Mermillod-Blondin, F. (2020). Ecological assessment of groundwater ecosystems disturbed by recharge systems using organic matter quality, biofilm characteristics, and bacterial diversity. *Environ. Sci. Pollut. Res.* 27, 3295–3308. doi: 10.1007/s11356-019-06971-5
- Wagner, A. O., Reitschuler, C., and Illmer, P. (2014). Effect of different acetate:propionate ratios on the methanogenic community during thermophilic anaerobic digestion in batch experiments. *Biochem. Eng. J.* 90, 154–161. doi: 10.1016/j.bej.2014.05.014
- Wagner, M., Erhart, R., Manz, W., Amann, R., Lemmer, H., Wedi, D., et al. (1994). Development of an rRNA-targeted oligonucleotide probe specific for the genus *Acinetobacter* and its application for in situ monitoring in activated sludge. *Appl. Environ. Microbiol.* 60, 792–800.
- Wang, C., Dong, D., Wang, H., Müller, K., Qin, Y., Wang, H., et al. (2016). Metagenomic analysis of microbial consortia enriched from compost: new insights into the role of Actinobacteria in lignocellulose decomposition. *Biotechnol. Biofuels* 9:22. doi: 10.1186/s13068-016-0440-2
- Wang, P., Yu, Z., Zhao, J., and Zhang, H. (2018). Do microbial communities in an anaerobic bioreactor change with continuous feeding sludge into a full-scale anaerobic digestion system? *Bioresour. Technol.* 249, 89–98. doi: 10.1016/j.biortech.2017.09.191
- Wang, Y., Zhang, Y., Wang, J., and Meng, L. (2009). Effects of volatile fatty acid concentrations on methane yield and methanogenic bacteria. *Biomass Bioenergy* 33, 848–853. doi: 10.1016/j.biombioe.2009.01.007
- Wei, Z., Liu, Y., Feng, K., Li, S., Wang, S., Jin, D., et al. (2018). The divergence between fungal and bacterial communities in seasonal and spatial variations of wastewater treatment plants. *Sci. Total Environ.* 628–629, 969–978. doi: 10.1016/j.scitotenv.2018.02.003
- Werner, J. J., Knights, D., Garcia, M. L., Scalfone, N. B., Smith, S., Yarasheski, K., et al. (2011). Bacterial community structures are unique and resilient in full-scale bioenergy systems. *Proc. Natl. Acad. Sci. U.S.A.* 108, 4158–4163. doi: 10.1073/pnas.1015676108
- Williams, J., Williams, H., Dinsdale, R., Guwy, A., and Esteves, S. (2013). Monitoring methanogenic population dynamics in a full-scale anaerobic digester to facilitate operational management. *Bioresour. Technol.* 140, 234–242. doi: 10.1016/j.biortech.2013.04.089
- Wong, M.-T., Mino, T., Seviour, R. J., Onuki, M., and Liu, W.-T. (2005). In situ identification and characterization of the microbial community structure of full-scale enhanced biological phosphorous removal plants in Japan. *Water Res.* 39, 2901–2914. doi: 10.1016/j.watres.2005.05.015
- Yu, Z., Morrison, M., and Schanbacher, F. L. (2010). “Production and utilization of methane biogas as renewable fuel,” in *Biomass to Biofuels*, eds A. A. Vertès, N. Qureshi, H. P. Blaschek, and H. Yukawa, (Hoboken, NJ: Blackwell Publishing Ltd), 403–433. doi: 10.1002/9780470750025.ch20
- Zhang, J., Zeng, G., Chen, Y., Yu, M., Yu, Z., Li, H., et al. (2011). Effects of physico-chemical parameters on the bacterial and fungal communities during agricultural waste composting. *Bioresour. Technol.* 102, 2950–2956. doi: 10.1016/j.biortech.2010.11.089
- Zhang, L., Zhang, H., Wang, Z., Chen, G., and Wang, L. (2016). Dynamic changes of the dominant functioning microbial community in the compost of a 90-m<sup>3</sup> aerobic solid state fermentor revealed by integrated meta-omics. *Bioresour. Technol.* 203, 1–10. doi: 10.1016/j.biortech.2015.12.040
- Zhang, T., Shao, M.-F., and Ye, L. (2012). 454 Pyrosequencing reveals bacterial diversity of activated sludge from 14 sewage treatment plants. *ISME J.* 6, 1137–1147. doi: 10.1038/ismej.2011.188
- Zhang, W., Werner, J. J., Agler, M. T., and Angenent, L. T. (2014). Substrate type drives variation in reactor microbiomes of anaerobic digesters. *Bioresour. Technol.* 151, 397–401. doi: 10.1016/j.biortech.2013.10.004

**Conflict of Interest:** The authors declare that the research was conducted in the absence of any commercial or financial relationships that could be construed as a potential conflict of interest.

Copyright © 2021 Aigle, Bourgeois, Marjolet, Houot, Patureau, Doelsch, Cournoyer and Gaila. This is an open-access article distributed under the terms of the Creative Commons Attribution License (CC BY). The use, distribution or reproduction in other forums is permitted, provided the original author(s) and the copyright owner(s) are credited and that the original publication in this journal is cited, in accordance with accepted academic practice. No use, distribution or reproduction is permitted which does not comply with these terms.



# Biofilm Formation, Production of Matrix Compounds and Biosorption of Copper, Nickel and Lead by Different Bacterial Strains

Md. Manjurul Haque<sup>1\*</sup>, Md Khaled Mosharaf<sup>1</sup>, Md. Amdadul Haque<sup>2</sup>,  
Md. Zahid Hasan Tanvir<sup>1</sup> and Md. Khairul Alam<sup>3</sup>

<sup>1</sup> Department of Environmental Science, Faculty of Agriculture, Bangabandhu Sheikh Mujibur Rahman Agricultural University, Gazipur, Bangladesh, <sup>2</sup> Department of Agro-Processing, Faculty of Agriculture, Bangabandhu Sheikh Mujibur Rahman Agricultural University, Gazipur, Bangladesh, <sup>3</sup> Soil Science Division, Bangladesh Agricultural Research Institute, Gazipur, Bangladesh

## OPEN ACCESS

### Edited by:

Mechthild Schmitt-Jansen,  
Helmholtz Centre for Environmental  
Research (UFZ), Germany

### Reviewed by:

Zhengbo Yue,  
Hefei University of Technology, China  
Eldon R. Rene,  
IHE Delft Institute for Water  
Education, Netherlands

### \*Correspondence:

Md. Manjurul Haque  
haque\_bes@bsmrau.edu.bd

### Specialty section:

This article was submitted to  
Microbiotechnology,  
a section of the journal  
Frontiers in Microbiology

**Received:** 08 October 2020

**Accepted:** 06 May 2021

**Published:** 10 June 2021

### Citation:

Haque MM, Mosharaf MK,  
Haque MA, Tanvir MZH and Alam MK  
(2021) Biofilm Formation, Production  
of Matrix Compounds and  
Biosorption of Copper, Nickel and  
Lead by Different Bacterial Strains.  
Front. Microbiol. 12:615113.  
doi: 10.3389/fmicb.2021.615113

Bacterial biofilms play a key role in metal biosorption from wastewater. Recently, *Enterobacter asburiae* ENSD102, *Enterobacter ludwigii* ENSH201, *Vitreoscilla* sp. ENSG301, *Acinetobacter lwoffii* ENSG302, and *Bacillus thuringiensis* ENSW401 were shown to form air-liquid (AL) and solid-air-liquid (SAL) biofilms in a static condition at 28 and 37°C, respectively. However, how environmental and nutritional conditions affect biofilm formation; production of curli and cellulose; and biosorption of copper (Cu), nickel (Ni), and lead (Pb) by these bacteria have not been studied yet. In this study, *E. asburiae* ENSD102, *E. ludwigii* ENSH201, and *B. thuringiensis* ENSW401 developed the SAL biofilms at pH 8, while *E. asburiae* ENSD102 and *Vitreoscilla* sp. ENSG301 constructed the SAL biofilms at pH 4. However, all these strains produced AL biofilms at pH 7. In high osmolarity and 1/2-strength media, all these bacteria built fragile AL biofilms, while none of these strains generated the biofilms in anaerobic conditions. Congo red binding results showed that both environmental cues and bacterial strains played a vital role in curli and cellulose production. Calcofluor binding and spectrophotometric results revealed that all these bacterial strains produced significantly lesser amounts of cellulose at 37°C, pH 8, and in high osmotic conditions as compared to the regular media, at 28°C, and pH 7. Metal biosorption was drastically reduced in these bacteria at 37°C than at 28°C. Only *Vitreoscilla* sp. ENSG301 and *B. thuringiensis* ENSW401 completely removed (100%) Cu and Ni at an initial concentration of 12.5 mg l<sup>-1</sup>, while all these bacteria totally removed (100%) Pb at concentrations of 12.5 and 25 mg l<sup>-1</sup> at pH 7 and 28°C. At an initial concentration of 100 mg l<sup>-1</sup>, the removal of Cu (92.5 to 97.8%) and Pb (89.3 to 98.3%) was the highest at pH 6, while it was higher (84.7 to 93.9%) for Ni at pH 7. Fourier transform infrared spectroscopy results showed metal-unloaded biomass biofilms contained amino, hydroxyl, carboxyl, carbonyl, and phosphate groups. The

peak positions of these groups were shifted responding to Cu, Ni, and Pb, suggesting biosorption of metals. Thus, these bacterial strains could be utilized to remove Cu, Ni, and Pb from aquatic environment.

**Keywords:** biofilm, curli, cellulose, heavy metal, removal, pH, temperature, metal concentration

## INTRODUCTION

Metals at molecular densities greater than 5 g/cm<sup>3</sup> are known as heavy metals (Weast, 1984). Heavy metal release from various industries [such as steel, leather, electroplating, mine tailings, paints, wastewater treatment plants, and agricultural operations (fertilizers, pesticides, and irrigations)] is one of the major causes of environmental pollution. Some heavy metals like copper (Cu), zinc (Zn), iron (Fe), cobalt (Co), chromium (Cr), and nickel (Ni) are required for growth and metabolism of organisms when they are present in trace amount, known as trace elements or micronutrients. However, they become toxic when the concentration increases. Conversely, non-essential heavy metals including lead (Pb), cadmium (Cd), mercury (Hg), and arsenic (As) are toxic even at very low concentrations. Accumulation of such heavy metals in soils and water bodies poses threat to human health (including potential carcinogenicity), other living organisms, and eventually overall biodiversity (Naser et al., 2014; Ahmed et al., 2016; Alam et al., 2017; Burakov et al., 2018). Various physicochemical technologies such as reverse osmosis, filtration, electro-dialysis, flocculation, ion exchange, activated carbon, and chemical precipitation are being practiced to remove the heavy metals from aqueous systems. However, all these methods have some disadvantages like being expensive, having high energy and reagent requirements, not being appropriate for the removal of low concentrations (1–50 mg l<sup>-1</sup>) of heavy metals, releasing of chemical sludge, and being less practical under natural environmental conditions (Ahluwalia and Goyal, 2007; Pan et al., 2009; Edwards and Kjellerup, 2013; Redha, 2020). Biosorption is one of the bioremediation technologies and uses fungi, bacteria, algae, and plants to sequester heavy metals (Nies, 1999). In the biosorption process, microbes adsorb metals on the cellular surface through attachment/linkage onto many anionic functional groups (Lo et al., 2014). Indeed, biosorption technique offers several benefits over the physicochemical methods in terms of economic aspects, high metal-binding capacity, eco-friendliness, and regeneration of biosorbents with the possibility of the recovery of metals (Kratochvil and Volesky, 1998; Sag and Kutsal, 2001; He and Chen, 2014; Santhosh et al., 2016). Compared to fungi, algae, and plants, bacterial strains were found effective to remove heavy metals from aquatic environment (Oves et al., 2013; Banerjee et al., 2015; Wei et al., 2016; Yang et al., 2017; El-Naggar et al., 2018). Though free-living bacterial cells have a greater capacity for metal removal from aquatic environment (Malik, 2004; Zeng et al., 2009), their survival is less likely due to decreased protection and the low metabolic activity (von Canstein et al., 2002). Hence, it is urgently needed to find out effective indigenous bacterial biosorbents that can survive

even under toxic environmental conditions along with diverse metabolic states.

Bacterial biofilms are highly structured, surface-associated cells, enclosed in a matrix of self-produced extracellular polymeric substances (EPS) (Costerton et al., 1999). Compared to free-living planktonic counterparts, bacterial biofilms provide numerous benefits, including protection of cells from adverse environmental stresses (e.g., toxic chemicals, pH change, dehydration, and predation), the ability to communicate by expression of quorum-sensing molecules, exchange of genetic material (e.g., horizontal gene transfer) and nutrient availability from waste products, and persistence in different metabolic functions with respect to electron acceptor reduction (Teitzel and Parsek, 2003; Boles et al., 2004; Vu et al., 2009; Haque et al., 2012, 2017; Edwards and Kjellerup, 2013). The bacterial EPS is composed of different high-molecular-weight biopolymers including proteins, cellulose-rich polysaccharides, nucleic acids, and lipids (Flemming and Wingender, 2010; Mosharaf et al., 2018). Bacterial surface appendages including the flagella, pili, and aggregative fimbriae/curli were also reported to stabilize the biofilm matrices (Flemming et al., 2007). Several researchers have shown that negatively charged functional groups/ligands of EPS serve as a trap for heavy metal ions (Sutherland, 1984; Deng et al., 2007; Wei et al., 2016). Enzymatic activities in EPS play a key role in detoxification of heavy metals by transformation and subsequent precipitation in the polymeric mass (Pal and Paul, 2008). Both living and dead biomass biofilms can be applied to remove heavy metals from the wastewater. Among them, living biofilms were found effective to remove heavy metals from both in the continuous treatment effluents (Gadd, 2009) and in the real industrial and municipal effluents (Kotrba et al., 2011). Both biosorption and bioaccumulation simultaneously take place in living bacterial biofilms. Nevertheless, several cellular mechanisms including synthesis of specific enzymes and action of cytoplasmic or membrane proteins were shown to express in the living bacterial biofilms (Kumar et al., 2007). Therefore, instead of free-living planktonic bacteria/dead bacterial biofilms, growing (living) bacterial biofilms have been appreciated for several bacterial-dominated processes and recommended for the removal of heavy metals from the environment (Singh et al., 2006; Pal and Paul, 2008; Edwards and Kjellerup, 2013; Meliani and Bensoltane, 2016; Balan et al., 2020).

*Enterobacter asburiae* ENSD102, *Enterobacter ludwigii* ENSH201, *Vitreoscilla* sp. ENSG301, and *Acinetobacter lwoffii* are Gram-negative bacteria that are positive to catalase and acetoin tests but are negative to gelatin liquefaction, methyl red, and indole tests. Some strains of *E. asburiae* degraded polyethylene plastic (Sato et al., 2016) and augmented crop growth (Dolkar et al., 2018; Mahdi et al., 2020). *Vitreoscilla* sp. was reported to synthesize hemoglobin used

in metabolic engineering (Wakabayashi et al., 1986). On the other hand, *Bacillus thuringiensis* is a Gram-positive spore-forming bacterium and well known for the production of insecticidal crystalline (Cry) proteins. Recently, all these bacterial strains were isolated from the wastewater of Bangladesh and reported to form biofilms by expression of curli (a proteinaceous component of the EPS) and nanocellulose fibers (Mosharaf et al., 2018). Important environmental applications of these bacterial strains are summarized in Table 1.

Several studies have shown that environmental conditions affect biofilm formation (Rinaudi et al., 2006; Liang et al., 2010; Haque et al., 2015; Ross et al., 2018) and the expression of curli and cellulose in different bacterial strains (Gerstel and Römmling, 2003; Barnhart and Chapman, 2006). Initial metal concentration, temperature, pH, and contact time were shown to affect the biosorption of heavy metals (Oves et al., 2013; Yang et al., 2017; El-Naggar et al., 2018; Redha, 2020). Among the factors, pH plays a key role in the metal speciation, metal solubility, and dissociation of functional groups present in the bacterial cell wall (Esposito et al., 2002). Metal ions in solution undergo hydrolysis as the pH increases. However, the extent of hydrolysis at different pH values differs with each metal, but the usual sequence of hydrolysis is the formation of hydroxylated monomeric species followed by the formation of polymeric species and then the formation of crystalline oxide precipitates after aging (Bacs and Mesmer, 1976). Therefore, adsorption of metals on interfaces is highly pH-dependent. For example, Cu can be present in solution as three different species:  $\text{Cu}^{2+}$ ,  $\text{CuOH}^+$ , and  $\text{Cu}(\text{OH})_2$ .  $\text{Cu}^{2+}$  and  $\text{CuOH}^+$  are more favorable Cu species under lower pH conditions (Yang et al., 2017). Cu, Ni, and Pb are frequently found in industrial wastewater, rivers, sediments, fish, and vegetables in Bangladesh (Naser et al., 2014; Ahmed et al., 2016; Mosharaf et al., 2018; Uddin and Jeong, 2021). Concentrations of these metals were also reported to increase day by day in the environment of Bangladesh (Uddin and Jeong, 2021). Thus, it is urgently needed to study the biosorption of Cu, Ni, and Pb from the environment. How environmental factors affect biofilm formation, the expression of biofilm matrix components (e.g., curli and cellulose), and the biosorption of Cu, Ni, and Pb has never been investigated in *E. asburiae* ENSD102, *E. ludwigii* ENSH201, *Vitreoscilla* sp. ENSG301, *A. lwoffii* ENSG302, and *B. thuringiensis* ENSW401. Therefore, it is aimed to quantify the effects of different environmental cues such as temperature, pH, osmolarity, oxygen tension, and nutritional strength on biofilm formation and production of curli and cellulose in these bacterial strains. It is also intended to evaluate these bacterial strains for their efficacies to remove Cu, Ni, and Pb from aqueous solutions in response to initial metal concentration, temperature, and pH. Furthermore, it is aimed to identify the chemical functional groups/ligands present in both metal-unloaded and metal-loaded biomass biofilms produced by these bacterial strains using Fourier transform infrared (FTIR) spectroscopy. The study will contribute toward understanding the mechanisms and potential of these bacterial strains in biosorption of heavy metals from aquatic environment.

## MATERIALS AND METHODS

### Chemicals

Heavy metals {copper sulfate ( $\text{CuSO}_4 \cdot 5\text{H}_2\text{O}$ ), nickel sulfate ( $\text{NiSO}_4 \cdot 6\text{H}_2\text{O}$ ), and lead nitrate [ $\text{Pb}(\text{NO}_3)_2$ ]}, Congo red, and Calcofluor were obtained from Sigma-Aldrich (St. Louis, MO, United States). All other chemicals used were of an analytical grade and were purchased from Wako Pure Chemical Industries, Ltd. (Osaka, Japan), Bio Basic Canada Inc. (Markham, ON, Canada), and HiMedia (Mumbai, India).

### Bacterial Strains and Growth Conditions

*Enterobacter asburiae* ENSD102, *E. ludwigii* ENSH201, *Vitreoscilla* sp. ENSG301, *A. lwoffii* ENSG302, and *B. thuringiensis* ENSW401 used in this study were recently isolated from wastewaters of Bangladesh and reported to form air-liquid (AL) and solid-air-liquid (SAL) biofilms on salt-optimized broth plus glycerol [(SOBG, pH 7.0) (per liter, 20 g tryptone, 5 g yeast extract, 0.5 g NaCl, 2.4 g  $\text{MgSO}_4$ , 0.186 g KCl, and 2% glycerol)] in a static condition at 28 and 37°C, respectively (Mosharaf et al., 2018). In this study, all these bacterial strains were found non-pathogenic to human and animals based on hemolytic test performed using 5% sheep blood (data not shown). These strains were routinely grown in yeast extract peptone (YP) medium (pH 7) at 28°C. An absorption spectrophotometer (Intertech, Inc., Tokyo, Japan) was used to measure the bacterial optical density (OD) at 660 nm.

### Preparation of Inoculum for Different Experiments

In order to prepare inoculum for different studies, a single colony of each bacterium was inoculated in YP broth and incubated at 28°C in a shaking (160 rpm) condition until  $\text{OD}_{660}$  reached at 0.6–0.8. Then, each bacterial culture was harvested and centrifuged at 10,000 rpm for 5 min. The supernatant was carefully discarded and the pellet was re-suspended in YP broth and used for the experiments.

### Role of Environmental Factors on Biofilm Formation and Expression of Curli and Cellulose

To quantify the effect of pH, pH of the SOBG was adjusted to pH 4, 7, and 8 by adding malic acid or NaOH and autoclaved. For biofilm formation, a 50- $\mu\text{l}$  culture [ca.  $10^5$  colony forming unit (CFU)  $\text{ml}^{-1}$ ] of each bacterium was suspended in the glass test tubes (Pyrex, flat bottom) containing 5 ml SOBG at pH 4, 7, or 8. For high osmolarity, SOBG (pH 7) was supplemented with 0.3 M NaCl or 0.3 M D-sorbitol. To examine the role of oxygen tension on biofilm formation, a 50- $\mu\text{l}$  culture of each strain was inoculated in the glass test tubes containing 5 ml SOBG broth and then sealed with paraffin oil (1.5 ml) or without sealing with paraffin oil. The inoculated test tubes were incubated in an incubator or in an anaerobic chamber (Thermo Fisher Scientific, Inc., Portsmouth, NH, United States) at 28°C in a static condition. To study the effect of nutritional strength on biofilm formation,  $1/2$ -strength SOBG (pH 7) was used instead of



**TABLE 1** | Environmental applications of bacterial strains used in this study.

Bacteria	Important environmental applications	References
<i>E. asburiae</i>	Degradation of polythene, detoxification of carcinogenic dyes, removal of heavy metals, solubilization of nutrients, fixation of nitrogen, crop growth promoter, utilization as biofertilizer, and reduction of metal toxicity in crop plants.	Jetiyanon, 2015; Kang et al., 2015; Paul and Mukherjee, 2016; Ren et al., 2019; Mahdi et al., 2020; Haque et al., 2021a
<i>E. ludwigii</i>	Degradation of dyes, biosorption of heavy metals, functions as nematicides, solubilization of nutrients, reduction of cadmium stress in plants, plant growth enhancer, and prevention of drought and salinity stress in crop plants.	Shoebitz et al., 2009; Gontia–Mishra et al., 2016; Radwan et al., 2017; Adhikari et al., 2020; Haque et al., 2021b
<i>Vitreoscilla</i> sp.	Decolorization, degradation, and detoxification of textile dyes; hemoglobin technology used in bio-product synthesis; bioremediation; and enhancement of tolerance of submergence, oxidative, and nitrosative stress in plants.	Stark et al., 2015; Zelasco et al., 2006; Haque et al., 2021a,b
<i>A. lwoffii</i>	Detoxification of dyes, biodegradation of diesel, bioremediation of heavy metals, and solubilization of phosphate.	Sadiq et al., 2013; Mindlin et al., 2016; Imron and Tttah, 2018; Haque et al., 2021a,b
<i>B. thuringiensis</i>	Decolorization of azo dyes; degradation of naproxen, ibuprofen, and chlorpyrifos; removal of heavy metals; used in insect control; plant growth activator; solubilization of nutrients; fixation of nitrogen; and mitigation of drought stress in plants.	Oves et al., 2013; Armada et al., 2014; Aceves-Diez et al., 2015; de Maagd, 2015; Marchlewicz et al., 2016; Martins et al., 2018; Haque et al., 2021a,b

full strength. In all the cases, AL or SAL biofilm was identified within 72-h incubation as described in Haque et al. (2012) and photographs were taken. All the biofilm formation assays were performed three times.

The role of environmental cues [temperature (28 and 37°C), pH (4, 7, and 8), high osmolarity, and nutritional strength] on the expression of curli and cellulose in different bacterial strains was also studied. Congo red binding assays were performed to detect both curli and cellulose production as described by Haque et al. (2017). Calcofluor binding assays were also done to detect specifically the cellulose production as described by Haque et al. (2017). Moreover, cellulose production by different bacterial strains in response to different environmental cues was quantified by using a spectrophotometer (Ultrospec-3000, Pharmacia Biotech, Cambridge, England) as described by Haque et al. (2017). All these assays were performed twice.

## Determination of Maximum Tolerance Concentration of Cu, Ni, and Pb

The maximum tolerance concentration (MTC) was determined as the method described in Schmidt and Schlegel (1994) with a few modifications. In brief, a single colony of each bacterial strain was inoculated in the glass test tube containing 5 ml YP broth and incubated at 28°C in a shaking condition until optical density (OD<sub>660</sub>) reached at 1.0. Then, 50 µl (ca. 10<sup>7</sup> CFU ml<sup>-1</sup>) culture of each strain was spread onto YP agar plates (three plates/concentration) containing 0 to 1,000 mg l<sup>-1</sup> Cu, Ni, or Pb and incubated at 28°C in a static condition. The MTC was designated as the highest concentration of Cu, Ni, and Pb that allows confluent growth after 72 h of incubation. This experiment was repeated three times.

## Initial Metal Concentration, Temperature, and pH on Biosorption of Cu, Ni, and Pb

To examine the effect of initial heavy metal ion concentration on biosorption, a 50-µl suspension (ca. 10<sup>6</sup> CFU ml<sup>-1</sup>) of each

bacterium was inoculated in 5 ml SOBG (pH 7) supplemented with 12.5, 25, 50, 100, 150, or 200 mg l<sup>-1</sup> Cu, Ni, or Pb. The inoculated test tubes were incubated at 28°C in a static condition. To evaluate the impacts of pH, the pH of the SOBG containing 100 mg l<sup>-1</sup> Cu, Ni, or Pb was adjusted to pH 5, 6, 7, 8, and 9 and then autoclaved. The inoculation was done as described above and then kept at 28°C in a static condition. To quantify the effect of temperature, a 50-µl suspension (ca. 10<sup>6</sup> CFU ml<sup>-1</sup>) of each strain was inoculated in SOBG (pH 7) with 100 mg l<sup>-1</sup> Cu, Ni, or Pb and then incubated at two different temperatures such as 28 and 37°C in a static condition. In all the cases, 1-ml culture was collected from beneath of the biofilms after 72-h incubation and centrifuged at 15,000 rpm for 15 min. Heavy metals such as Cu, Ni, or Pb from the supernatants were determined using an atomic absorption spectrophotometer (VARIAN model AA2407). All these experiments were repeated twice. The percentage of metal removal efficiency (% RE) was calculated using the following equation:

$$\% \text{ RE} = \frac{(C_o - C_f)}{C_o} \times 100$$

where C<sub>o</sub> and C<sub>f</sub> are initial and final concentrations (mg l<sup>-1</sup>) of Cu, Ni, or Pb in the solution, respectively.

## Identification of Functional Groups in Metal-Loaded and -Unloaded Biomass Biofilms Using FTIR Spectroscopy

Initially, a 50-µl suspension (ca. 10<sup>6</sup> CFU ml<sup>-1</sup>) of each bacterium was inoculated in glass test tubes containing 5 ml SOBG (pH 7) or 5 ml magnesium-deprived SOBG (pH 7) containing 100 mg l<sup>-1</sup> Cu, Ni, or Pb. Then, the tubes were incubated at 28°C in a static condition. After 72-h incubation, each bacterial biofilm was carefully collected and centrifuged at 14,000 rpm for 10 min. Each pellet was scanned (450 to 4,000 cm<sup>-1</sup>, 16 scans at 4 cm<sup>-1</sup> resolution) at 0.2 cm s<sup>-1</sup> scanning speed using a triglycine sulfate (TGS)

detector. The IR spectra of the metal-unloaded and metal-loaded biofilm matrices were acquired using the PerkinElmer FTIR spectroscopy (Spectrum-2) instrument operated by CPU32M software. PerkinElmer's proprietary software (version 10.05.03) was used to analyze the baseline-subtracted biofilm spectra.

## Experimental Design and Statistical Analysis

All the experiments were performed in a complete randomized design with at least three replications and repeated at least three times unless otherwise stated. Analysis of variance (ANOVA), distribution of data, homogeneity of variance, and mean comparison were analyzed using the R software version 3.3.6. The Fisher's least significant difference test was applied to compare the means.

## RESULTS

### Effect of pH on Biofilm Formation

Information regarding the role of pH on biofilm formation by *E. asburiae* ENSD102, *E. ludwigii* ENSH201, *Vitreoscilla* sp. ENSG301, *A. lwoffii* ENSG302, and *B. thuringiensis* ENSW401 were not available in the literature. Therefore, these bacterial strains were evaluated for their abilities to form biofilm in response to different pH levels. Initially, growth of these strains was examined in SOBG media at pH 4, 7, and 8 under a shaking condition (160 rpm) at 28°C. All these strains grew rapidly both at pH 7 (**Figure 1A**) and pH 8 (data not shown). However, the growth rate of these strains was not significantly differed at pH 7 and pH 8 (data not shown). At pH 4, *E. ludwigii* ENSH201, *A. lwoffii* ENSG302, and *B. thuringiensis* ENSW401 were unable to grow (**Figure 1B**), while *E. asburiae* ENSD102 ( $OD_{660} = 0.81$  at 24 h) and *Vitreoscilla* sp. ENSG301 ( $OD_{660} = 0.78$  at 24 h) cells grew moderately (**Figure 1B**). Like growth, biofilm formation was also affected by different pH levels. All these bacterial strains confirmed the development of thick and robust AL biofilms at pH 7 (**Figure 1D**). *E. asburiae* ENSD102 and *Vitreoscilla* sp. ENSG301 produced a prominent SAL biofilms at pH 4 (**Figure 1E**). *A. lwoffii* ENSG302 built a strong AL biofilm at pH 8, while *Vitreoscilla* sp. ENSG301 created a weak and fragile AL biofilm at pH 8 (**Figure 1F**). Conversely, *E. asburiae* ENSD102, *E. ludwigii* ENSH201, and *B. thuringiensis* ENSW401 developed the SAL biofilms at pH 8 (**Figure 1F**). Thus, these bacterial strains synthesized two types of biofilms, i.e., AL and SAL biofilm, depending on the pH levels.

### The Effect of Osmolarity and Availability of Oxygen on Biofilm Formation

When these bacterial strains were grown in SOBG (pH 7) supplemented with 0.3 M NaCl in a shaking condition at 28°C, the growth rate of *Vitreoscilla* sp. ENS301 and *A. lwoffii* ENSG302 was drastically reduced as compared to that of *E. asburiae* ENSD102, *E. ludwigii* ENSH201, and *B. thuringiensis* ENSW401 (**Figure 1C**). Similar results were also found when SOBG (pH 7) was supplemented with 0.3 M D-sorbitol (data

not shown). Like bacterial growth, biofilm formation in all these strains was dramatically reduced in high-osmolarity media (**Figure 1G**) as compared to that of regular SOBG media (**Figure 1D**). Taken together, these observations suggest that both NaCl and D-sorbitol negatively affect biofilm formation through an osmotic effect.

None of these strains formed the biofilm in the glass test tubes containing 5 ml SOBG broth sealed with paraffin oil after 72-h incubation at 28°C in a static condition (data not shown). Similar results were also found when inoculated tubes were placed in an anaerobic chamber at 28°C (data not shown).

## The Effect of the Nutritional Conditions on Biofilm Formation

Bacterial growth was indistinguishable in  $1/2$ -strength SOBG (data not shown) and full-strength SOBG. However, all these bacterial strains formed a lighter and fragile AL biofilms in  $1/2$ -strength SOBG after 72-h incubation at 28°C in a static condition (**Figure 1H**). These bacterial strains did not build AL or SAL biofilm in magnesium-deprived SOBG media (Mosharaf et al., 2018). When magnesium-deprived SOBG media was supplemented with 0.009 M  $Ca^{2+}$ ,  $Cu^{2+}$ , and  $Zn^{2+}$ , all these strains developed dense and stout AL biofilms (data not shown). Thus, media composition plays an important role in biofilm formation of these bacteria.

### Effect of Initial Cu, Ni, and Pb Concentrations on Biomass Biofilm Formation

Biofilm formation in terms of the production of biomass (wet) biofilms by *E. asburiae* ENSD102, *E. ludwigii* ENSH201, *Vitreoscilla* sp. ENSG301, *A. lwoffii* ENSG302, and *B. thuringiensis* ENSW401 was also examined in response to different concentrations (12.5, 25, 50, 100, 150, and 200 mg  $l^{-1}$ ) of Cu, Ni, and Pb. Biomass biofilm production (wet) was not significantly differed in these bacterial strains responding to 12.5 to 200 mg  $l^{-1}$  Cu, Ni, and Pb (**Supplementary Figure 1**). However, biomass biofilm production (mean) was higher in different concentrations of Cu (11.45 mg  $l^{-1}$ ) and Ni (11.53 mg  $l^{-1}$ ) as compared to the varying concentrations of Pb (9.52 mg  $l^{-1}$ ) in these bacterial strains. The amount of biofilm production by *E. asburiae* ENSD102, *E. ludwigii* ENSH201, *Vitreoscilla* sp. ENSG301, *A. lwoffii* ENSG302, and *B. thuringiensis* ENSW401 ranged from 11.2 to 11.5, 11.2 to 11.6, 11.3 to 11.6, 11.3 to 11.6, and 11.4 to 11.7 mg  $ml^{-1}$ , respectively, in response to 12.5 to 200 mg  $l^{-1}$  Cu (**Supplementary Figure 1A**). In case of Ni, it varied from 11.4 to 11.7, 11.1 to 11.5, 11.5 to 11.7, 11.4 to 11.6, and 11.5 to 11.8 mg  $ml^{-1}$  in *E. asburiae* ENSD102, *E. ludwigii* ENSH201, *Vitreoscilla* sp. ENSG301, *A. lwoffii* ENSG302, and *B. thuringiensis* ENSW401, respectively, responding to 12.5 to 200 mg  $l^{-1}$  (**Supplementary Figure 1B**). In 12.5 to 200 mg  $l^{-1}$  Pb, production of biomass biofilms by *E. asburiae* ENSD102, *E. ludwigii* ENSH201, *Vitreoscilla* sp. ENSG301, *A. lwoffii*

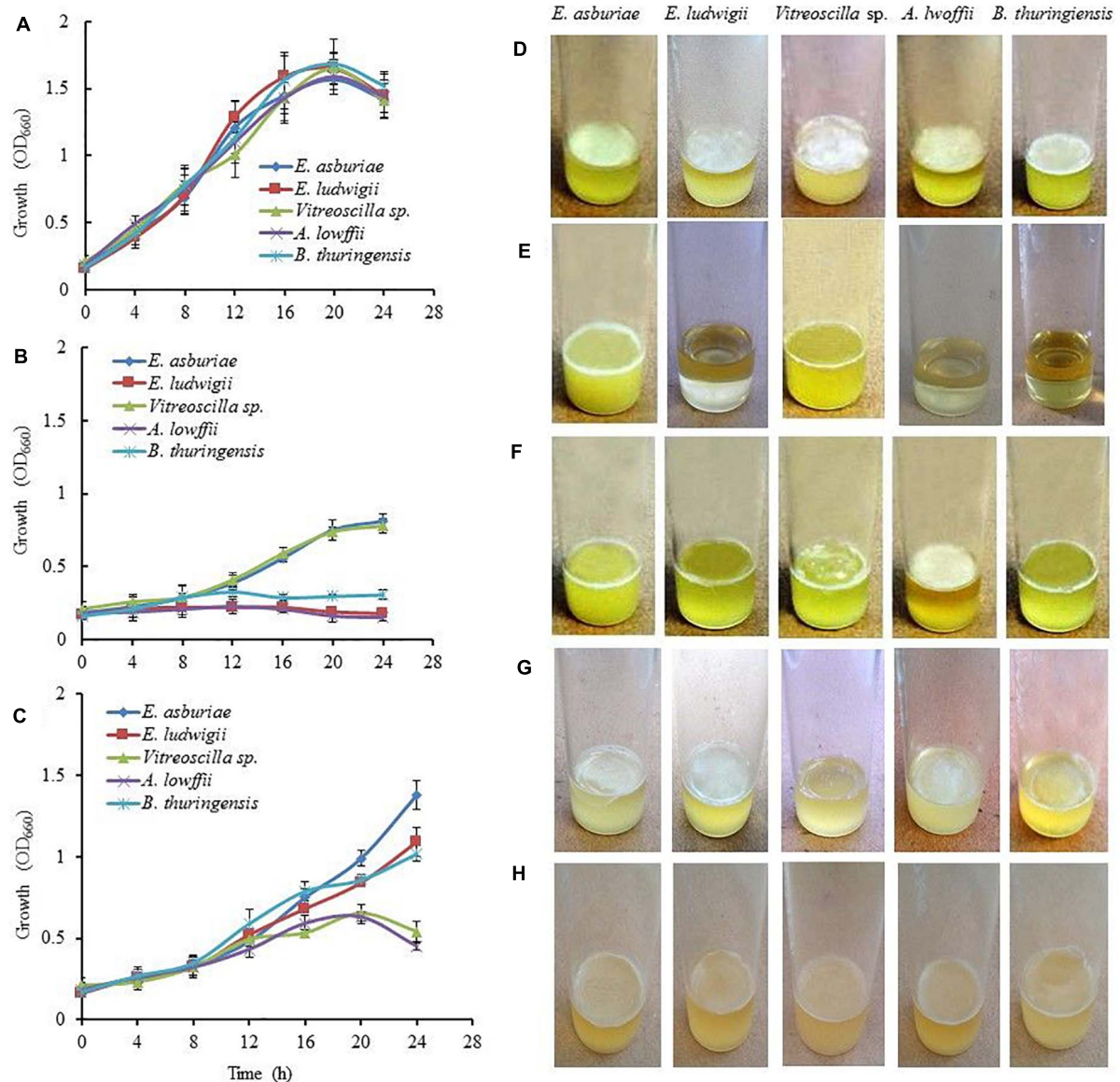


**FIGURE 1 |** The Effect of environmental cues on bacterial growth and biofilm formation. Growth of the bacterial strains in SOB at pH 7 (A), pH 4 (B), and high osmotic condition, i.e., SOB containing 0.3 M NaCl (C) in a shaking condition. Biofilm formation on SOB at pH 7 (D), pH 4 (E), pH 8 (F), SOB containing 0.3 M NaCl (G), and 1/2-strength SOB (H) by different bacterial strains after 72-h incubation in a static condition. The values are mean, and error bars indicate standard deviations ( $\pm$ ) of three independent experiments. SOB, salt-optimized broth plus glycerol.

ENSG302, and *B. thuringiensis* ENSW401 fluctuated from 9.3 to 9.7, 9.2 to 9.7, 9.5 to 9.9, 9.2 to 9.5, and 9.5 to 9.7  $\text{mg ml}^{-1}$ , respectively (Supplementary Figure 1C).

## Congo Red Binding Assays

Numerous studies have shown that biofilm-producing bacteria expressed curli and cellulose – two important components of the biofilm matrices (Römling, 2005; Haque et al., 2009, 2012, 2017; Milanov et al., 2015). Milanov et al. (2015) have demonstrated that bacterial strains producing the red, dry, and rough (rdar) phenotype on Congo red agar plates leads to both curli and cellulose, while only cellulose expresses the pink, dry,

and rough (pdar) phenotype and only curli induces the brown, dry, and rough (bdar) phenotype. When no components are expressed, the phenotype is smooth and white (saw). Bokranz et al. (2005), on the other hand, have reported that bacterial strains generating the red and smooth (ras) and pink and smooth (pas) lead to only cellulose, while brown and smooth (bas) triggers only curli in certain *E. coli* strains. However, the effect of temperature, pH, osmolarity, and nutritional strength on the expression of curli and cellulose has never been investigated in *E. asburiae* ENSD102, *E. ludwigii* ENSH201, *Vitreoscilla sp.* ENSG301, *A. lowffii* ENSG302, and *B. thuringiensis* ENSW401 by any other researches. Thus, the phenotypes were examined in



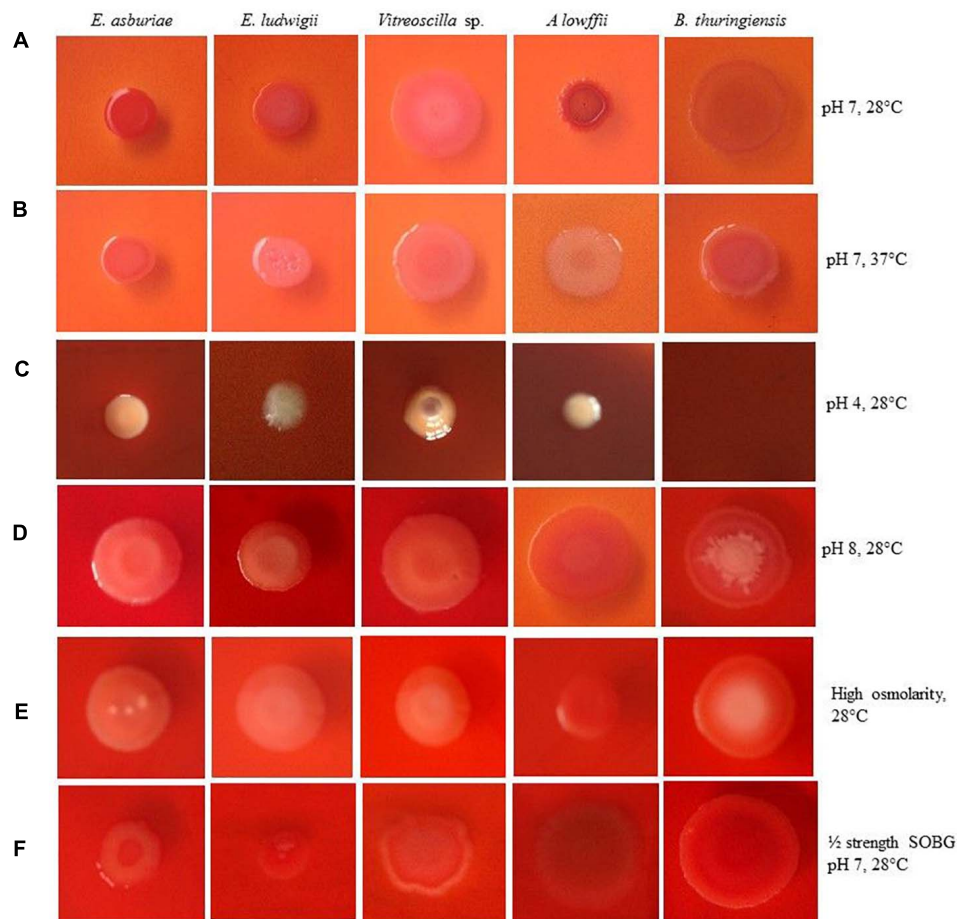


**FIGURE 2 |** Congo red binding abilities of different bacterial strains in response to pH 7 at 28°C (A), pH 7 at 37°C (B), pH 4 at 28°C (C), pH 8 at 28°C (D), high osmolarity at 28°C (E) and  $\frac{1}{2}$  strength SOB, pH 7 at 28°C (F) after 48-h incubation. Photographs represent one of two experiments, which gave similar results.

response to different environmental conditions, and the results are depicted in **Figure 2**.

*Enterobacter asburiae* ENSD102 and *B. thuringiensis* ENSW401 expressed the rdar phenotypes, linked with both curli and cellulose production at both temperatures, i.e., 28 and 37°C (**Figures 2A,B**), while *Vitreoscilla* sp. ENSG301 triggered the pdar phenotypes, associated with cellulose only at both temperatures (**Figures 2A,B**). *E. ludwigii* ENSH201 and *A. lwoffii* ENSG302 produced the rdar and pdar phenotypes at 28°C (**Figure 2A**) and 37°C (**Figure 2B**), respectively.

When pH of the SOB Congo red broth was adjusted to 4 with malic acid, the color of the SOB media was slightly changed after being autoclaved (**Figure 2C**). At pH 4, *E. asburiae* ENSD102 and *Vitreoscilla* sp. ENSG301 induced the bdar phenotype (**Figure 2C**), linked with curli production only, while *E. ludwigii* ENSH201 and *A. lwoffii* ENSG302 produced the saw (no expression of cellulose or curli) phenotypes (**Figure 2C**). At pH 8, *E. asburiae* ENSD102, *E. ludwigii* ENSH201, and *Vitreoscilla* sp. ENSG301 triggered the pas phenotypes (**Figure 2D**), while *A. lwoffii* ENSG302 produced the rdar phenotype (**Figure 2D**). Furthermore, the center of

the colonies of *B. thuringiensis* ENSW401 was decorated and pink in color, while the side of the colonies was red at pH 8 (**Figure 2D**).

Like pH 8, *E. asburiae* ENSD102, *E. ludwigii* ENSH201, and *Vitreoscilla* sp. ENSG301 also constructed the pas phenotypes in high osmotic condition (**Figure 2E**), while *A. lwoffii* ENSG302 developed the rdar phenotype at the same condition (**Figure 2E**). In *B. thuringiensis* ENSW401, the side of the colony was red and the center was pink in color but not decorated like pH 8 (**Figure 2E**). All these bacterial strains developed the rdar phenotypes in  $\frac{1}{2}$ -strength SOB. Thus, both environmental cues and bacterial strains might be involved in the production of curli and cellulose.

### Calcofluor Binding Assays

The rdar/pdar/pas-expressing bacteria were also shown to bind with Calcofluor, a cellulose-specific dye (Römling, 2005; Steenackers et al., 2012; Haque et al., 2017). The abilities of these bacteria to bind with Calcofluor were also found to be influenced by various environmental factors (**Figure 3**). All these bacterial strains fluoresced strongly at 28°C and at pH 7 (**Figure 3A**), while



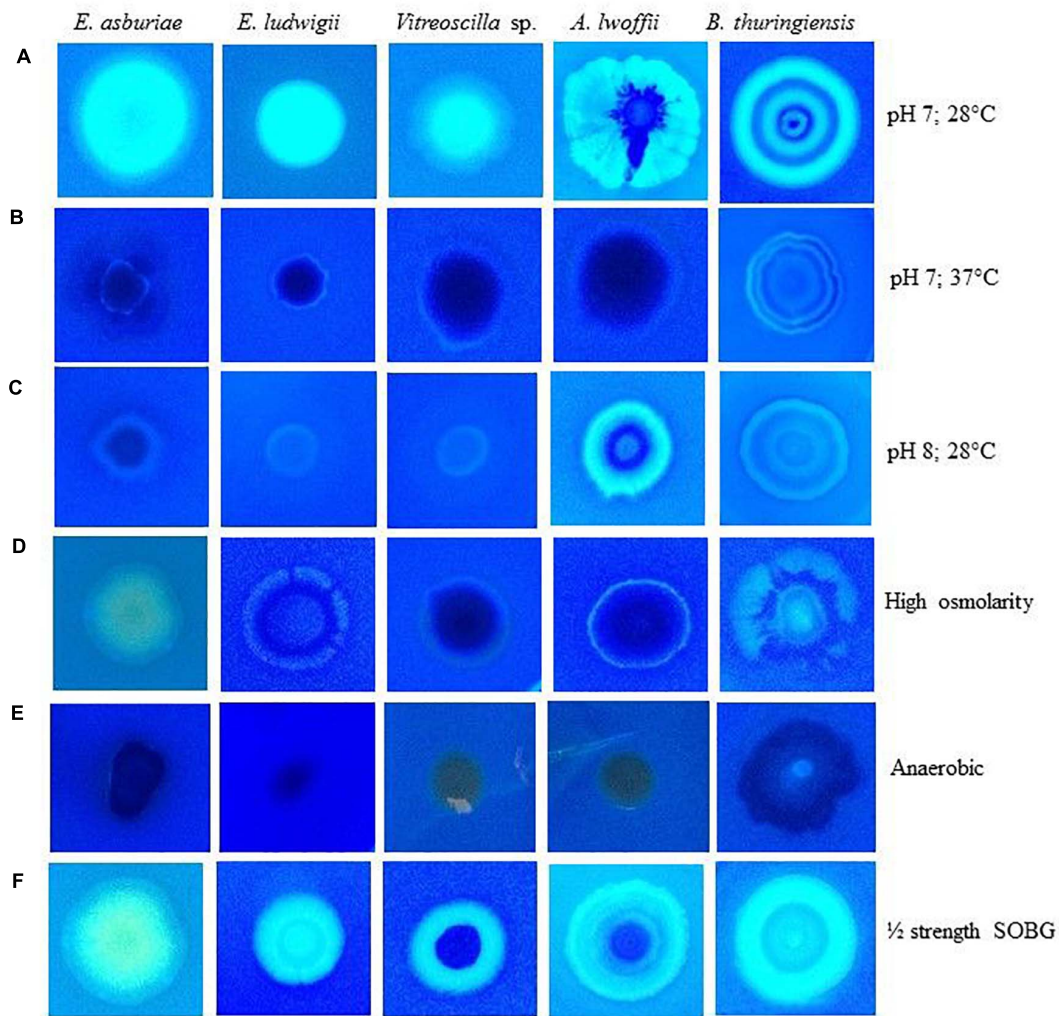


**FIGURE 3** | Calcofluor binding abilities of different bacterial strains in response to pH 7 at 28°C (**A**), pH 7 at 37°C (**B**), pH 8 at 28°C (**C**), high osmolarity at 28°C (**D**), anaerobic condition (**E**) and  $\frac{1}{2}$  strength SOB at 28°C (**F**) after 48-h incubation. Photographs represent one of two experiments, which gave similar results.

they fluoresced only slightly at 37°C (**Figure 3B**) and at pH 7. At pH 8, except *A. lwoffii* ENSG302, all the other strains fluoresced weakly (**Figure 3C**). All these bacterial strains also weakly fluoresced in high osmotic condition (**Figure 3D**). As expected, no fluorescence was observed when these strains were incubated in an anaerobic chamber (**Figure 3E**). Interestingly, all these strains fluoresced strongly in  $\frac{1}{2}$ -strength SOB (**Figure 3F**). Thus, inability/weak/fragile biofilm formation by these strains might be due to no/lesser amounts of cellulose production.

### Spectrophotometric Determination of Cellulose

Differences of Calcofluor binding were shown through the discrepancy of cellulose production in bacteria (Anriany et al., 2006; Haque et al., 2017). Therefore, cellulose production was quantified in different bacterial strains grown in various environmental conditions (**Figure 4**). In this study, cellulose

production was reduced by 12.0-, 20.9-, 17.7-, 17.6-, and 2.8-fold in *E. asburiae* ENSD102, *E. ludwigii* ENSH201, *Vitreoscilla* sp. ENSG301, *A. lwoffii* ENSG302, and *B. thuringiensis* ENSW401, respectively, at 37°C as compared at 28°C. Cellulose production was also reduced in these strains responding to pH 8 (than at pH 7) and high osmolarity (compared to regular SOB). Thus, increase of fluorescence in Calcofluor agar plates seemed to have been reflected in the increase of cellulose production in these bacteria.

### Maximum Tolerance Concentration of Cu, Ni, and Pb by Different Bacterial Strains

Before biosorption studies, the MTC of different heavy metals including Cu, Ni, and Pb by *E. asburiae* ENSD102, *E. ludwigii* ENSH201, *Vitreoscilla* sp. ENSG301, *A. lwoffii* ENSG302, and *B. thuringiensis* ENSW401 was determined. The MTC of Cu, Ni, and

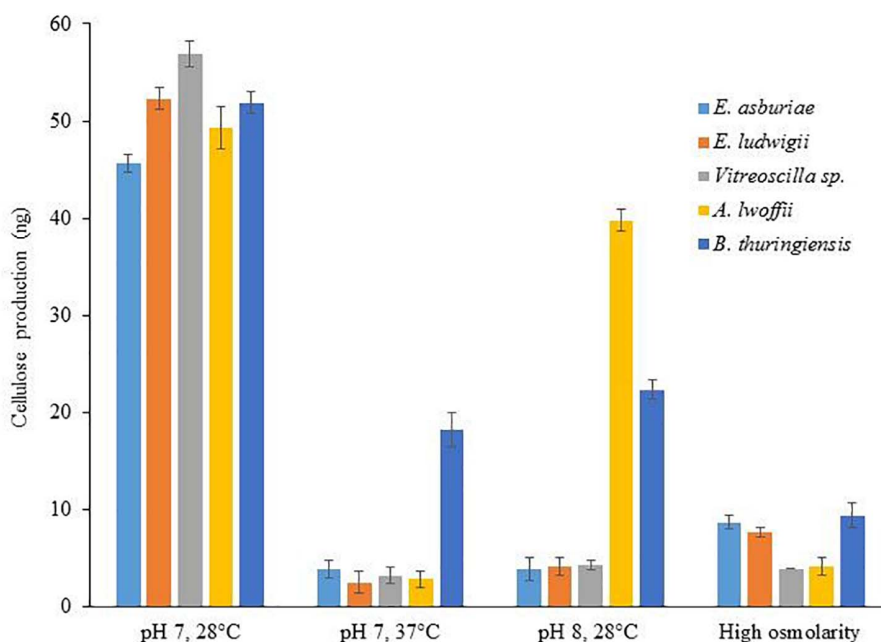


**FIGURE 4 |** Cellulose production by different biofilm-producing bacterial strains in different environmental conditions. Cellulose was isolated from 250 mg of lyophilized cell mass obtained from each bacterium grown on Calcofluor agar plates after 48-h incubation at 28°C. The amount of cellulose was determined (OD<sub>620</sub>) by addition of anthrone reagent, and Avicel cellulose was used as standard. The values are mean, and error bars indicate standard deviations ( $\pm$ ) of two independent experiments.

Pb was remarkably varied in these bacterial strains (Table 2). All these bacterial strains showed the highest (500 to 650 mg l<sup>-1</sup>) MTC in response to Pb. The MTC of Cu ranged from 250 to 600 mg l<sup>-1</sup>. Among the bacterial strains, *B. thuringiensis* ENSW401 exhibited the highest MTC (600 mg l<sup>-1</sup>) in response to Cu followed by *Vitreoscilla sp.* ENSG301 (550 mg l<sup>-1</sup>), *A. lwoffii* ENSG302 (400 mg l<sup>-1</sup>), *E. ludwigii* ENSH201 (300 mg l<sup>-1</sup>), and *E. asburiae* ENSD102 (250 mg l<sup>-1</sup>). However, the MTC of Ni by these bacterial strains was fluctuated from 200 to 300 mg l<sup>-1</sup>. Thus, the MTC might be dependent on both metals and bacterial strains used in the study.

## The Effect of Initial Metal Concentration on the Biosorption of Cu, Ni, and Pb

The physicochemical technologies are not suitable for the removal of low concentrations (1 to 50 mg l<sup>-1</sup>) of heavy metals

from wastewater. Therefore, the effect of initial concentrations of 12.5, 25, 50, 100, 150, and 200 mg l<sup>-1</sup> Cu, Ni, and Pb on metal uptake by *E. asburiae* ENSD102, *E. ludwigii* ENSH201, *Vitreoscilla sp.* ENSG301, *A. lwoffii* ENSG302, and *B. thuringiensis* ENSW401 was examined. The biosorption rate was not significantly differed in these bacterial strains at initial concentrations of 12.5, 25, and 50 mg l<sup>-1</sup> Cu, Ni, and Pb, respectively (Figure 5). Surprisingly, *Vitreoscilla sp.* ENSG301 and *B. thuringiensis* ENSW401 completely removed (100%) both Cu (Figure 5A) and Ni (Figure 5B) at an initial concentration of 12.5 mg l<sup>-1</sup>. On the other hand, all these bacterial strains completely removed (100%) Pb at initial concentrations of 12.5 and 25 mg l<sup>-1</sup> (Figure 5C). At an initial concentration of 50 mg l<sup>-1</sup>, the removal percentage of Cu ranged from 97.8 to 99.4% by these bacterial strains (Figure 5A). Ni and Pb ranged from 98.9 to 99.8% and 99.1 to 99.8%, respectively, by these bacterial strains (Figure 5C). *Vitreoscilla sp.* ENSG301 sorped the highest percentage (97.1%) of Cu at an initial concentration of 100 mg l<sup>-1</sup>, which was statistically akin with *B. thuringiensis* ENSW401 (96.8%). *E. asburiae* ENSD102, *E. ludwigii* ENSH201, and *A. lwoffii* ENSG302 removed 92.7, 90.2, and 92.5% Cu, respectively, which were incredibly differed from *Vitreoscilla sp.* ENSG301 and *B. thuringiensis* ENSW401 at an initial concentration of 100 mg l<sup>-1</sup> Cu (Figure 5A). The biosorption percentage of Ni by *Vitreoscilla sp.* ENSG301 was also significantly higher (94.2%) at an initial concentration of 100 mg l<sup>-1</sup>, which was statistically alike with *E. asburiae* ENSD102, *A. lwoffii* ENSG302, and *B. thuringiensis* ENSW401 (Figure 5B). On the other hand,

**TABLE 2 |** Maximum tolerance concentration (MTC) of heavy metals by different bacterial strains.

Bacterial strains	MTC of different heavy metals (mg l <sup>-1</sup> )		
	Cu	Ni	Pb
<i>E. asburiae</i> ENSD102	250	250	500
<i>E. ludwigii</i> ENSH201	300	200	500
<i>Vitreoscilla sp.</i> ENSG301	550	250	550
<i>A. lwoffii</i> ENSG302	400	200	550
<i>B. thuringiensis</i> ENSW401	600	300	650

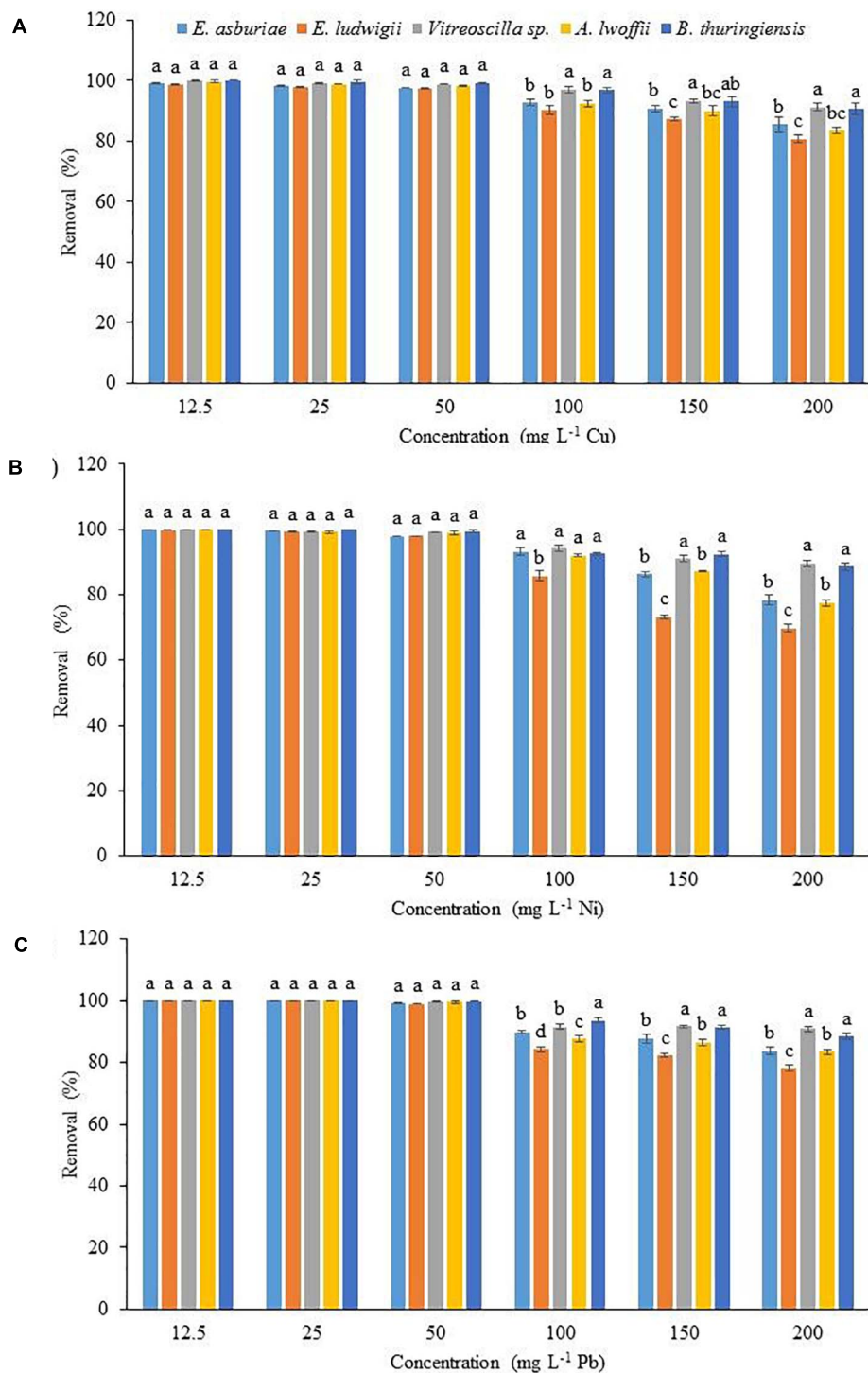


**FIGURE 5 |** The effect of initial metal concentration on the biosorption of Cu (A), Ni (B), and Pb (C) by different bacterial strains at pH 7 and 28°C after 72 h. The values are mean, and error bars indicate standard deviations ( $\pm$ ) of two independent experiments.

*B. thuringiensis* ENSW401 removed significantly the maximum Pb (93.5%) followed by *Vitreoscilla sp.* ENSG301 (91.5%), *E. asburiae* ENSD102 (89.8%), *A. lwoffii* ENSG302 (87.6%), and *E. ludwigii* ENSH201 (84.2%) at an initial concentration of

100 mg l<sup>-1</sup> (Figure 5C). A significant percentage of Cu (80.7 to 91.2%), Ni (69.8 to 89.6%), and Pb (78.1 to 88.5%) was also removed by these bacterial strains at an initial concentration of 200 mg l<sup>-1</sup> (Figure 5).

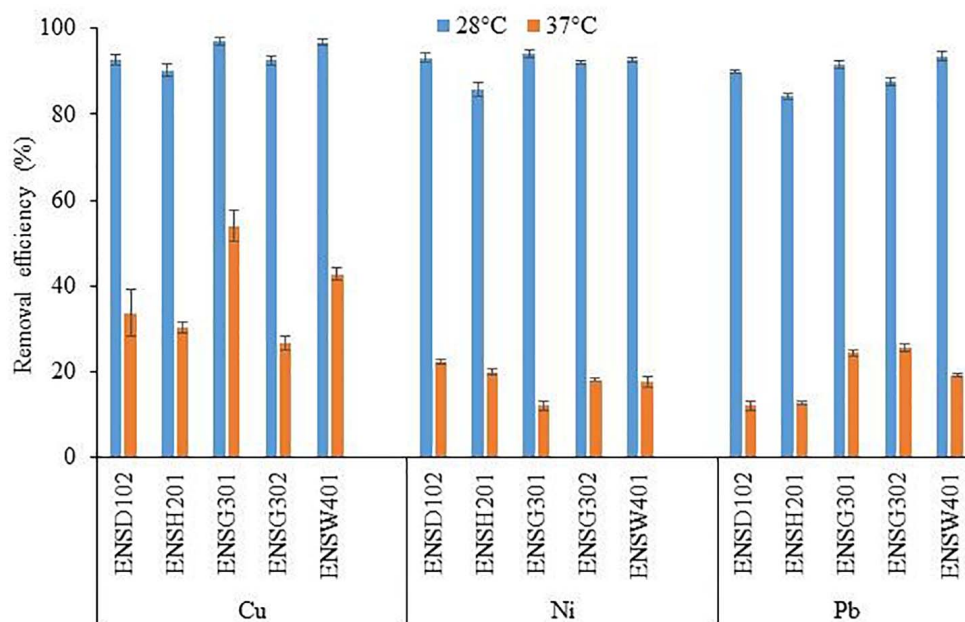


**FIGURE 6 |** The effect of different temperatures on the biosorption of Cu, Ni, and Pb by different bacterial strains at an initial concentration of 100 mg l<sup>-1</sup> and pH 7 after 72 h. The values are mean, and error bars indicate standard deviations ( $\pm$ ) of two independent experiments.

## The Effect of Temperature and pH on the Biosorption of Cu, Ni, and Pb

The biosorption of Cu, Ni, and Pb by different bacterial strains was significantly influenced by temperature as shown in **Figure 6**. Copper biosorption was reduced by 2.76-, 2.98-, 1.80-, 3.48-, and 2.26-fold in *E. asburiae* ENSD102, *E. ludwigii* ENSH201, *Vitreoscilla* sp. ENSG301, *A. lwoffii* ENSG302, and *B. thuringiensis* ENSW401, respectively, at 37°C as compared with 28°C, while Ni biosorption was diminished by 4.17-, 4.29-, 7.85-, 5.08-, and 5.32-fold in these bacterial strains. Lead biosorption by *E. asburiae* ENSD102, *E. ludwigii* ENSH201, *Vitreoscilla* sp. ENSG301, *A. lwoffii* ENSG302, and *B. thuringiensis* ENSW401 at 37°C was also decreased by 7.42-, 6.68-, 3.75-, 3.43-, and 4.9-fold than at 28°C. Thus, temperature plays a crucial role in the biosorption of Cu, Ni, and Pb.

To study the impact of pH on metal biosorption, an experiment was set up with varying pH (5, 6, 7, 8, and 9) with 100 mg l<sup>-1</sup> of Cu, Ni, or Pb (**Figure 7**). The abilities of biosorption for each metal ion by different bacterial strains increased with an increase in pH up to 8, while biosorption capacities of these metal ions decreased at pH 9. The Cu and Pb biosorption was the highest at pH 6, while it was higher for Ni at pH 7 than the sorption at other pH.

## FTIR Analysis

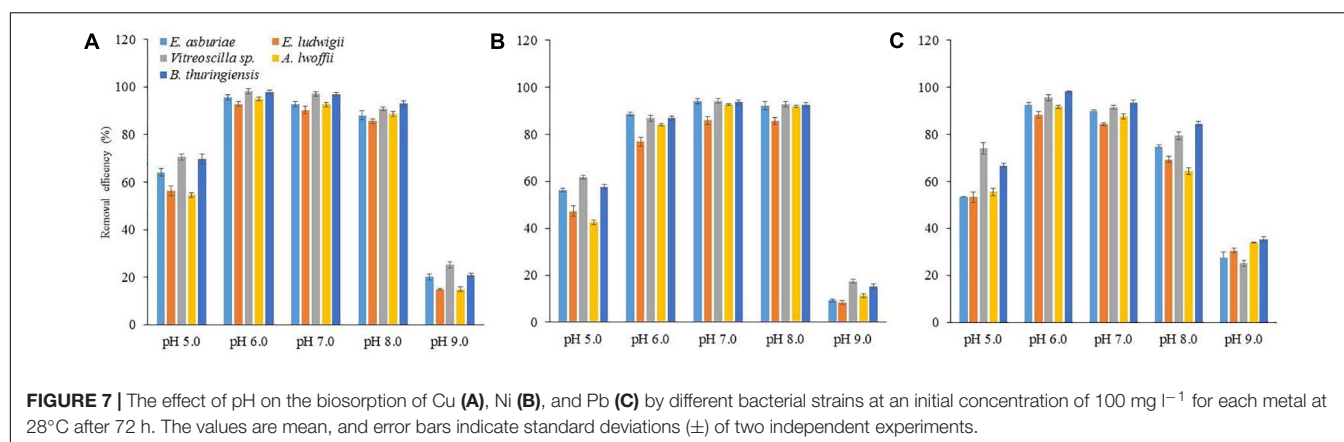
In order to determine the chemical functional groups/ligands responsible for biosorption processes, FTIR analysis was done using metal-loaded (Cu, Ni, and Pb) and metal-unloaded biomass biofilms of *E. asburiae* ENSD102 (**Supplementary Figure 2**), *E. ludwigii* ENSH201 (**Supplementary Figure 3**),

*Vitreoscilla* sp. ENSG301 (**Figure 8A**), *A. lwoffii* ENSG302 (**Supplementary Figure 4**), and *B. thuringiensis* ENSW401 (**Figure 8B**). In the present study, several functional groups/ligands including -OH, -NH, -CH, C = O, COO<sup>-</sup>, and P-O were found in different wave numbers (cm<sup>-1</sup>) in metal-unloaded biomass biofilms of different bacterial strains as shown in **Figures 8A,B** and **Supplementary Figures 2–4**. Overall, the peak position was shifted in metal-loaded biomass biofilms in response to 100 mg l<sup>-1</sup> Cu, Ni, and Pb as compared to that of metal-unloaded biomass biofilms.

The IR spectra of metal-unloaded biomass biofilm of *E. asburiae* ENSD102 exhibited C = O of amide groups at 1,641.90 cm<sup>-1</sup> and were shifted at 1,645.90, 1,636.51 and 1,635.85 cm<sup>-1</sup> in response to Cu, Ni, and Pb, respectively (**Supplementary Figure 2**), while COO<sup>-</sup> of the carboxylate groups appeared at 1,544.10 cm<sup>-1</sup> in metal-unloaded biomass biofilm of *E. asburiae* ENSD102 and was changed to 1,544.0, 1,545.21, and 1,545.78 cm<sup>-1</sup>. Moreover, phosphate groups and P-O of the (C-PO<sub>2</sub><sup>-3</sup>) moiety at 1,045 cm<sup>-1</sup> in metal-unloaded biomass biofilm of *E. asburiae* ENSD102 were shifted to 1,049, 1,083.27, and 1,045.84 cm<sup>-1</sup> in response to Cu, Ni, and Pb, respectively. Thus, Cu, Ni, and Pb could be sorbed by carbonyl, carboxyl, and phosphate groups of *E. asburiae* ENSD102.

The spectra of the metal-unloaded biomass of *E. ludwigii* ENSH201 exhibited 1,445.90 cm<sup>-1</sup> for C = O of amide group and were moved to 1,635.98, 1,635.72, and 1,635.99 cm<sup>-1</sup>, respectively, responding to Cu, Ni, and Pb, respectively (**Supplementary Figure 3**), while 1,544.77 cm<sup>-1</sup> for COO<sup>-</sup> of carboxylate group was displaced to 1,544.20, 1,544.36, and 1,546.70 cm<sup>-1</sup>, respectively (**Supplementary Figure 2**).





Furthermore, phosphate group and P-O of the (C-PO<sub>2</sub><sup>-3</sup>) moiety at 1,045 cm<sup>-1</sup> in metal-unloaded biomass biofilm were changed to 1,080.50 and 1,047.67 cm<sup>-1</sup>, respectively, challenging to Ni and Pb, respectively. However, phosphate group and P-O of the (C-PO<sub>2</sub><sup>-3</sup>) moiety at 1,045 cm<sup>-1</sup> in metal-unloaded and Cu-loaded biomass biofilm were not changed (Supplementary Figure 2). Thus, phosphate groups and P-O of the (C-PO<sub>2</sub><sup>-3</sup>) moiety of the biomass biofilm of *E. ludwigii* ENSH201 might not be involved in the removal of Cu.

Similarly, shifting of band of metal-unloaded biomass of *Vitreoscilla* sp. ENSG301 showed a stretched band appearing at 1,645.16 cm<sup>-1</sup> for C = O of amide groups and was moved to 1,635.28, 1,629.09, and 1,636.07 cm<sup>-1</sup>, respectively, in response to Cu, Ni, and Pb, respectively (Figure 7A), while COO<sup>-</sup> of the carboxylate groups displayed at 1,545.64 cm<sup>-1</sup> was changed to 1,545.71, 1,542.37, and 1,545.71 cm<sup>-1</sup>, respectively. Moreover, band positioning at 1,064.70 cm<sup>-1</sup> was shifted to 1,056.84, 1,053.50, and 1,053.24 cm<sup>-1</sup> in response to Cu, Ni, and Pb, respectively (Figure 8A). Thus, carbonyl, carboxyl, and phosphate groups of *Vitreoscilla* sp. ENSG301 could sorp Cu, Ni, and Pb.

Compared to the metal-unloaded biomass biofilm of *A. lwoffii* ENSG302, C = O group was remarkably shifted to 10.92, 10.90, and 9.40 cm<sup>-1</sup> in response to Cu, Ni, and Pb, respectively (Supplementary Figure 3). However, COO<sup>-</sup> group was moved to 0.66, 1.11, and 0.91 cm<sup>-1</sup>, respectively, responding to Cu, Ni, and Pb, respectively. Band positioning of phosphate groups and P-O of the (C-PO<sub>2</sub><sup>-3</sup>) moiety were incredibly changed to 30.38, 28.54, and 5.49 cm<sup>-1</sup>, respectively, in response to Cu, Ni, and Pb, respectively (Supplementary Figure 4).

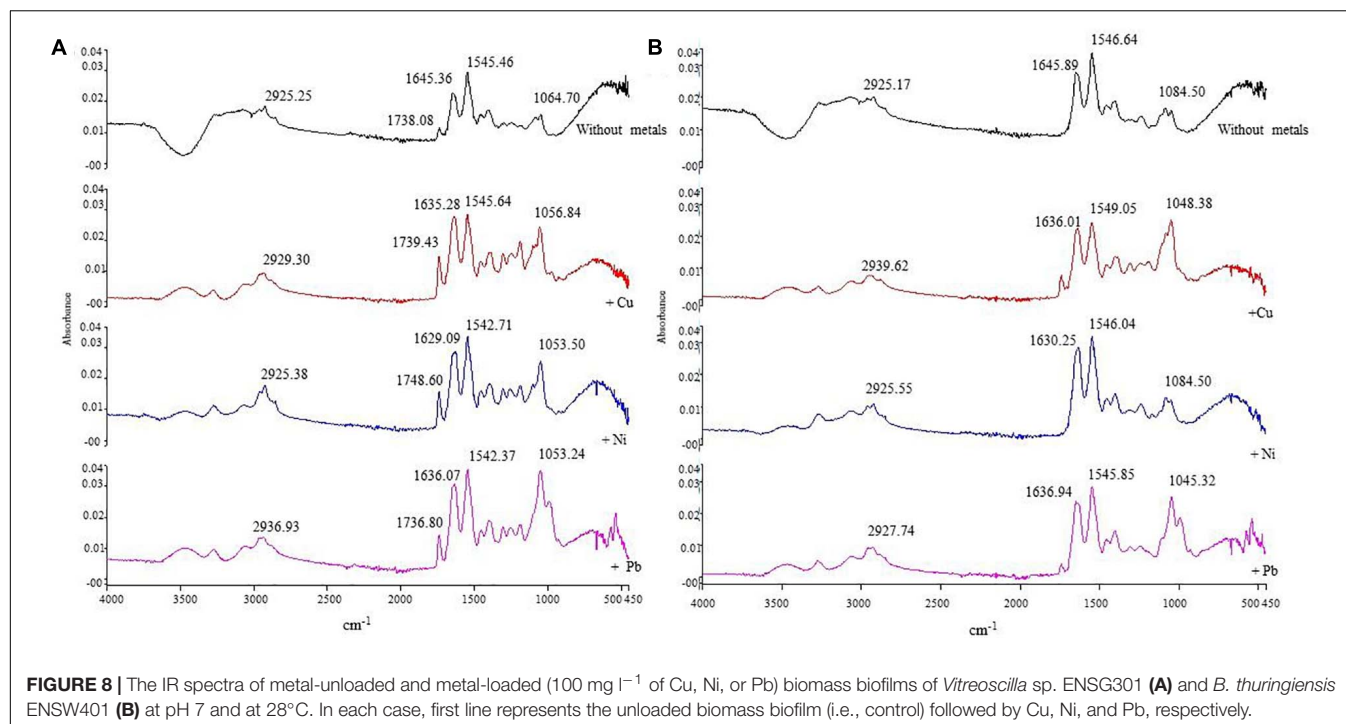
C = O group in metal-unloaded biomass biofilm of *B. thuringiensis* ENSW401 at the position of 1,645.89 cm<sup>-1</sup> was shifted to 1,636.01, 1,630.25, and 1,636.94 cm<sup>-1</sup> in responding to Cu, Ni, and Pb, respectively (Figure 8B). The COO<sup>-</sup> group that appeared at 1,546.68 cm<sup>-1</sup> in metal-unloaded biomass biofilm was moved to 1,549.05, 1,546.04, and 1,545.85 cm<sup>-1</sup>, challenging to Cu, Ni, and Pb, respectively. Nevertheless, phosphate groups and P-O of the (C-PO<sub>2</sub><sup>-3</sup>) moiety at 1,084.50 cm<sup>-1</sup> in metal-unloaded biomass biofilm were shifted to 1,084.38, 1,084.50, and

1,045.32 cm<sup>-1</sup> in response to Cu, Ni, and Pb, respectively. Thus, carbonyl, carboxyl, and phosphate groups might play a vital role in the biosorption of Cu, Ni, and Pb.

## DISCUSSION

### Environmental Conditions Affect Bacterial Biofilm Formation

In this study, it was observed that environmental cues play a vital role in biofilm formation (Figure 1), production of curli and cellulose (Figures 2–4), and biosorption of Cu, Ni, and Pb (Figures 5–7) by *E. asburiae* ENSD102, *E. ludwigii* ENSH201, *Vitreoscilla* sp. ENSG301, *A. lwoffii* ENSG302, and *B. thuringiensis* ENSW401. *E. asburiae* ENSD102 and *Vitreoscilla* sp. ENSG301 produced the SAL biofilms both at pH 4 (Figure 1E) and pH 8 (Figure 1F), while *E. ludwigii* ENSH201 and *B. thuringiensis* ENSW401 constructed the SAL biofilms only at pH 8 (Figure 1F). However, all these bacterial strains developed the AL biofilm at pH 7 (Figure 1D). Furthermore, only *Vitreoscilla* sp. ENSG301 and *B. thuringiensis* ENSW401, but not other bacterial strains, generated the SAL biofilms in high osmotic condition (Figure 1G). Thus, temperature, pH, and osmolarity and bacterial strains might play an important role in SAL and AL biofilm formation. Numerous researchers have differentiated AL and SAL biofilm genetically, enzymatically, and based on cultural conditions (Friedman and Kolter, 2004; Yap et al., 2005; Haque et al., 2012). Bacterial biofilm formation in different bacterial strains was shown to be influenced by the pH (Hostacká et al., 2010; Ramli et al., 2012; Nguyen et al., 2014; Zhou et al., 2014; Haque et al., 2017), high osmolarity (Lebeer et al., 2007; Hou et al., 2014; Kavamura and de Melo, 2014; Haque et al., 2017), and oxygen tension (Gerstel and Römling, 2001; Bjergbæk et al., 2006; Ahn and Burne, 2007; Liang et al., 2010; Wu et al., 2013). Except temperature (Mosharaf et al., 2018), effect of pH, osmolarity, and oxygen tension on biofilm formation by *E. asburiae* ENSD102, *E. ludwigii* ENSH201, *Vitreoscilla* sp. ENSG301, *A. lwoffii* ENSG302, and *B. thuringiensis* ENSW401 was not studied by any other contemporary researches.



## Bacterial Biofilm Formation as Affected by Nutritional Factors

In  $1/2$ -strength SOBG media, all these bacterial strains generated thin and fragile AL biofilms (Figure 1H) as compared to those of regular SOBG media (Figure 1D). Shen et al. (2018) reported that at higher nutrient concentrations, biofilms are thicker and denser than under nutrient-poor conditions. Bacterial biofilm formation was also shown to be activated by different divalent cations (such as  $\text{Mg}^{2+}$  and  $\text{Ca}^{2+}$ ) through their effect on electro-static interactions (Patrauchan et al., 2005). Among the divalent cations,  $\text{Ca}^{2+}$  impacts the mechanical properties of biofilms, as well as cross linkers (Patrauchan et al., 2005). On the other hand,  $\text{Mg}^{2+}$  increased initial attachment in *P. fluorescens* (Song and Leff, 2006) by reducing the repulsive force between the negatively charged bacterial and substratum surfaces and between negative functional groups of the polysaccharides (Koechler et al., 2015). Haque et al. (2012) have reported that a low concentration ( $10 \mu\text{M}$ ) of  $\text{Mg}^{2+}$  increases the AL biofilm formation of *Dickeya dadantii* 3937 in a PhoP-PhoQ-dependent manner. AL biofilm formation controlled by the CytR homolog in *Pectobacterium carotovorum* subsp. *carotovorum* PC1 was also shown to be increased by the different divalent cations, e.g.,  $\text{Mg}^{2+}$ ,  $\text{Ca}^{2+}$ ,  $\text{Cu}^{2+}$ ,  $\text{Zn}^{2+}$ , and  $\text{Mn}^{2+}$  (Haque et al., 2017). In this study, *E. asburiae* ENSD102, *E. ludwigii* ENSH201, *Vitreoscilla* sp. ENSG301, *A. lwoffii* ENSG302, and *B. thuringiensis* ENSW401 also produced the dense and stout AL biofilms by addition of different divalent cations ( $0.009 \text{ M}$ ) including  $\text{Mg}^{2+}$ ,  $\text{Ca}^{2+}$ ,  $\text{Cu}^{2+}$ , and  $\text{Zn}^{2+}$  (data not shown). Thus, not only environmental cues but also nutritional conditions might play a crucial role in the formation of a thick and robust AL biofilm.

## Environmental and Nutritional Cues Affect Curli and Cellulose Expression in Bacteria

Protein filaments, known as curli, and cellulose played a pivotal role in AL biofilm/pellicle formation in *E. coli* (Prigent-Combaret et al., 2000) and *Salmonella enterica* serovar Enteritidis (White et al., 2003). The production of curli in *Enterobacteriaceae* was shown to be regulated by temperature. For example, curli in *Salmonella* usually is visible under  $30^\circ\text{C}$  (Gerstel and Römling, 2003; Bokranz et al., 2005), but some strains such as *S. typhimurium* can express at  $37^\circ\text{C}$  (Olsen et al., 1998). Conversely, in clinical isolates of the *E. coli*, the expression of the curli at  $37^\circ\text{C}$  is a rarely visible phenomenon (Barnhart and Chapman, 2006). In the present study (in Congo red binding assays), *E. asburiae* ENSD102 and *B. thuringiensis* ENSW401 produced the curli both at  $28$  and  $37^\circ\text{C}$  (Figures 2A,B), while *E. ludwigii* ENSH201 expressed only curli at  $28^\circ\text{C}$  (Figure 2A). Curli was not synthesized by *Vitreoscilla* sp. ENSG301 both at  $28^\circ\text{C}$  (Figure 2A) and  $37^\circ\text{C}$  (Figure 2B), while this bacterial strain generated the curli at pH 4 at  $28^\circ\text{C}$  (Figure 2C). The production of cellulose was also found to be dramatically reduced by high temperature (i.e.,  $37^\circ\text{C}$ ), pH 8, high osmolarity, and anaerobic conditions in *E. asburiae* ENSD102, *E. ludwigii* ENSH201, *Vitreoscilla* sp. ENSG301, *A. lwoffii* ENSG302, and *B. thuringiensis* ENSW401 (Figures 3B–D, 4). The expression of the curli fimbriae and cellulose in *Salmonella* spp. is most intense at temperatures under  $30^\circ\text{C}$ , in low osmolarity, limited availability of nutrients, and aerobic conditions (Gerstel and Römling, 2003; Solomon et al., 2005; Steenackers et al., 2012). Thus, a variation of biofilm formation in *E. asburiae* ENSD102, *E. ludwigii* ENSH201, *Vitreoscilla* sp. ENSG301,

*A. lwoffii* ENSG302, and *B. thuringiensis* ENSW401 in response to environmental and nutritional conditions might be due to differential expression of curli and cellulose.

## Mechanisms of Heavy Metal Tolerance in Bacteria

The determination of MTC in different heavy metals is of particular interest, when bacterial strains are applied for biosorption. In this study, the MTC of Cu, Ni, and Pb was remarkably higher in *B. thuringiensis* ENSW401 as compared to other bacterial strains tested (Table 2). *E. asburiae* ENSD102, *E. ludwigii* ENSH201, *Vitreoscilla* sp. ENSG301, and *A. lwoffii* ENSG302 are Gram-negative bacteria, while *B. thuringiensis* ENSW401 is a Gram-positive bacterium. Generally, the cell wall of both types encompass a peptidoglycan layer that is rich in carboxylate groups and completely surrounds the cell. The peptidoglycan layer of Gram-positive bacterium is thicker (three layers) than the peptidoglycan layer of Gram-negative bacterium (two layers). Thus, cell wall structure might play a pivotal role in MTC of Cu, Ni, and Pb in these bacterial strains. Roane et al. (2009) have reported that (i) binding of metals to extracellular materials of the bacterial cells immobilizes the metals and prevents them from entering into the bacterial cells, (ii) several bacterial strains produced siderophore (iron-complexing, low-molecular-weight organic compounds) complexes that increase metal tolerance, (iii) bacterial strains also generated biosurfactant (excreted from the bacterial cells) complexes of metals that are non-toxic to the cells, and (iv) numerous plasmid-encoded genes [e.g., *cusCBA* (resistance to copper), *chrCBA* (cobalt-nickel resistance), and *pbrA* (encoding lead resistance)] conferred higher levels of metal tolerance in different bacteria. Thus, several mechanisms might be used in these bacterial strains for the tolerance to Cu, Ni, and Pb.

## Mechanisms of Heavy Metal Toxicity in Bacteria

The growth of *E. asburiae* ENSD102, *E. ludwigii* ENSH201, *Vitreoscilla* sp. ENSG301, *A. lwoffii* ENSG302, and *B. thuringiensis* ENSW401 was severely inhibited with the increase of the concentration of Cu, Ni, and Pb after MTC (data not shown). Bacterial growth, morphological characteristics, and biochemical processes were reported to be disrupted due to toxicity of heavy metals (Roane et al., 2009). Koechler et al. (2015) stated that high concentrations of heavy metals including Cu, Ni, and Pb directly or indirectly generate reactive oxygen species (ROS) upon reacting with DNA, resulting in damaged bases or strand breaks, lipid peroxidation, or protein modification. Roane et al. (2009) reported that metals bind to many cellular ligands and displace essential metals from their native binding sites due to ionic interactions. Moreover, they have shown that metals affect the oxidative phosphorylation and membrane permeability. Some metals can inhibit cellular activity because they present a structural homology with enzyme substrates leading to the metal toxicity. Heavy metal can also cause ion imbalance by adhering to the cell surface and entering through ion channels or transmembrane carriers (Chen et al., 2014).

Therefore, future studies should focus on the mechanism of the toxicity of *E. asburiae* ENSD102, *E. ludwigii* ENSH201, *Vitreoscilla* sp. ENSG301, and *B. thuringiensis* ENSW401 in response to higher concentrations of Cu, Ni, and Pb.

## Biofilm Formation in Relation to Heavy Metal Uptake in Bacteria

Biofilm production in *E. asburiae* ENSD102, *Vitreoscilla* sp. ENSG301, and *A. lwoffii* ENSG302 was reported to be affected by 500 to 2,000 mg l<sup>-1</sup> of CuSO<sub>4</sub>·5H<sub>2</sub>O, Pb(NO<sub>3</sub>)<sub>2</sub>, or NiCl<sub>2</sub> (Mosharaf et al., 2018). In this study, biofilm production was not remarkably varied in *E. asburiae* ENSD102, *E. ludwigii* ENSH201, *Vitreoscilla* sp. ENSG301, *A. lwoffii* ENSG302, and *B. thuringiensis* ENSW401 in response to 12.5 to 200 mg l<sup>-1</sup> Cu, Ni, or Pb (Supplementary Figure 1). Accordingly, biosorption capacity was not significantly varied in these bacterial strains in response to 12.5, 25, and 50 mg l<sup>-1</sup> Cu, Ni, and Pb (Figure 5). Interestingly, only *Vitreoscilla* sp. ENSG301 and *B. thuringiensis* ENSW401 completely removed (100%) Cu and Ni at an initial concentration of 12.5 mg l<sup>-1</sup>, while all these bacterial strains totally removed (100%) Pb at initial concentrations of 12.5 and 25 mg l<sup>-1</sup> at pH 7 and 28°C. However, *Vitreoscilla* sp. ENSG301 and *B. thuringiensis* ENSW401 removed much more Cu, Ni, or Pb as compared to *E. asburiae* ENSD102, *E. ludwigii* ENSH201, and *A. lwoffii* ENSG302 in response to 100, 150, and 200 mg l<sup>-1</sup> (Figure 5). Thus, biosorption might be dependent on both concentrations of the heavy metals (Cu, Ni, and Pb) and bacterial strains. At present, various ordinance, laws, rules, acts, and policies have been made to control environmental pollution in Bangladesh. The Department of Environment of Bangladesh also set safety limit of different heavy metals in industrial effluent [DoE (Department of Environment), 2008]. The World Health Organization [WHO (World Health Organization), 2017], European Union [European Union (EU), 2002], United States Environmental Protection Agency [USEPA (United States Environmental Protection Agency), 2012], and Bangladesh [DoE (Department of Environment), 2008] prescribed the maximum acceptable concentrations at (mg l<sup>-1</sup>) 2.0, 0.5, 0.2, and 0.5, respectively, for Cu; 0.02, 0.5, 0.2, and 1.0, respectively, for Ni; and 0.01, 0.5, 0.05, and 0.10, respectively, for Pb. Thus, treated wastewater by these bacterial strains at an initial concentration of 12.5 mg l<sup>-1</sup> for Cu and 12.5 and 25.0 mg l<sup>-1</sup> for both Ni and Pb are within the safety limit set by the abovementioned organizations, while concentrations of Cu, Ni, and Pb are higher than the maximum acceptable values in all other treated samples.

## Cellular Structure, EPS, and Enzymes on Metal Biosorption in Bacteria

Bacterial cellular structure, EPS, and extracellular enzyme play a vital role in metal biosorption. Both Gram-positive and Gram-negative bacterial cell wall contain peptidoglycan that determines the metal-binding capability. However, teichoic acids are present only in Gram-positive bacteria that provide an overall negative charge to the cell wall, due to the presence of phosphodiester bonds. On the other hand, lipopolysaccharides (LPS) are only present in Gram-negative bacteria that confer



an overall negative charge to the cell wall of Gram-negative bacteria. The anionic functional groups present in the cell wall of Gram-positive and Gram-negative bacteria are the key contents primarily responsible for the anionic character and metal-binding or biosorption capacity of the cell wall (Moat et al., 2002). Notably, bacterial biofilm EPS also play a key role in metal biosorption (Pal and Paul, 2008; Li and Yu, 2014). Among the contents of the EPS, proteins form complexes with heavy metal ions (Mej  re and B  low, 2001), while polysaccharides cross-link with metals (Li and Yu, 2014). Biofilm EPS matrix has abundant chemical functional groups such as amino, carboxyl, carboxylate, phosphate, and hydroxyl groups (Mosharaf et al., 2018). It was reported that negatively charged functional groups present in the EPS matrix formed organometallic complexes with multivalent metal cations via electrostatic interactions and subsequent metal removal (Gutnick and Bach, 2000). Numerous extracellular enzymes (e.g., protease, peptidase, endocellulase,  $\alpha$ -glucosidase,  $\beta$ -glucosidase, peroxidase, etc.) have been detected in bacterial biofilms (Flemming and Wingender, 2010). Many of them were reported to degrade the contents of EPS (Flemming and Wingender, 2010) and detoxify the heavy metals (Pal and Paul, 2008). However, extracellular enzymes synthesized by *E. asburiae* ENSD102, *E. ludwigii* ENSH201, *Vitreoscilla* sp. ENSG301, and *B. thuringiensis* ENSW401 and their involvement in detoxification of heavy metals are yet to be examined.

## Physicochemical Conditions Alter Metal Biosorption in Bacteria

Removal of heavy metals from aqueous solution by bacteria is a complex process due to the effect of different physicochemical factors such as initial metal concentration, temperature, pH, time, ionic strength, and metal chemistry (Gabr et al., 2008; Hassan et al., 2009). In this study, increasing the concentrations of Cu, Ni, and Pb decreased the metal biosorption (Figure 5). Higher metal biosorption at lower concentrations of heavy metals was reported to be due to the availability of free metal-binding sites, while lower metal biosorption at higher concentrations is due to lack of free metal-binding sites (Kadukov   and Vir   kov  , 2005; Oves et al., 2013; Kirova et al., 2015).

Cellulose-based materials including cellulose gels, cellulose composites, cellulose derivatives, functionalized cellulose, and nano-crystalline cellulose are widely used for the adsorption of heavy metals from wastewater (Jamshaid et al., 2017). *E. asburiae* ENSD102, *E. ludwigii* ENSH201, *Vitreoscilla* sp. ENSG301, *A. lwoffii* ENSG302, and *B. thuringiensis* ENSW401 were shown to produce nanocellulose that is amorphous in nature (Mosharaf et al., 2018). In this study, cellulose production (Figure 4) and biosorption of Cu, Ni, and Pb by these bacterial strains were dramatically reduced at 37  C as compared with 28  C (Figure 6). Bacterial cellulose production was shown to be linked with biosorption of metals (Teitzel and Parsek, 2003; Li and Yu, 2014). Thus, reduction of the removal of Cu, Ni, and Pb by these bacterial strains at 37  C might be due to a lower production of cellulose. Redha (2020) has shown that metal biosorption is not highly affected in temperatures ranging from 20 to 35  C.

On the other hand, Ta  sar et al. (2014) have reported that increasing temperature from 20 to 40  C decreases the surface activity of biosorbents such as peanut shells leading to decreased biosorption of Pb.

In this study, pH levels regulated the biosorption of Cu, Ni, and Pb (Figure 7). The difference in metal biosorption at different pH was associated with the effect of both the chemistry of the functional groups and the chemistry of metal ions (Wei et al., 2016). At low pH, functional groups present in the biofilm EPS tightly bound with hydronium ions leading to restricting the binding of metal cations due to repulsive force. Conversely, with increasing pH, various functional groups including carbonyl, carboxyl, phosphate, and amino start experiencing negative charges due to deprotonation leading to binding with metal cations and thus increasing the biosorption capacity (Oves et al., 2013; Abdi and Kazemi, 2015). In this study, the chemical functional groups present in the biofilm EPS of *E. asburiae* ENSD102, *E. ludwigii* ENSH201, *Vitreoscilla* sp. ENSG301, *A. lwoffii* ENSG302, and *B. thuringiensis* ENSW401 were determined using FTIR in both metal-loaded and -unloaded (control) samples at an initial Cu, Ni, and Pb concentration of 100 mg l<sup>-1</sup>, pH 7, and at 28  C. Several functional groups including -OH, -NH, -CH, C=O, COO-, and P-O were detected in the samples (Figures 8A,B and Supplementary Figures 2-4). FTIR results revealed that Cu, Ni, and Pb could be sorbed by carbonyl, carboxyl, and phosphate groups of *E. asburiae* ENSD102, *Vitreoscilla* sp. ENSG301, *A. lwoffii* ENSG302, and *B. thuringiensis* ENSW401, while phosphate groups and P-O of the (C-PO<sub>2</sub><sup>-3</sup>) moiety have no role in Cu removal by *E. ludwigii* ENSH201. The chemical functional groups in metal-loaded biofilm EPS in *E. asburiae* ENSD102, *E. ludwigii* ENSH201, *Vitreoscilla* sp. ENSG301, *A. lwoffii* ENSG302, and *B. thuringiensis* ENSW401 were not reported by any other contemporary researches.

## Future Perspective and Scale Up

Future studies should focus on the biosorption of heavy metal from real wastewater by these bacterial strains. The mechanisms involved in metal toxicity in these bacterial strains should be studied. Extracellular enzymes produced in the EPS matrix of these bacterial strains and their role in the detoxification of heavy metals should also be examined. Nevertheless, genetic engineering tools should be used to construct the engineered *E. asburiae* ENSD102, *E. ludwigii* ENSH201, *Vitreoscilla* sp. ENSG301, *A. lwoffii* ENSG302, and *B. thuringiensis* ENSW401 with higher metal sorption capacity. For scale up, large amounts of biomass biofilm can be produced in less expensive growth media by using these bacterial strains. Currently, bacterial biofilm biomass is being used in different types of bioreactors including fixed bed reactor, packed bed reactor, and fluidized bed reactor to remove heavy metals from wastewater. Thus, biomass biofilm produced by *E. asburiae* ENSD102, *Vitreoscilla* sp. ENSG301, *A. lwoffii* ENSG302, and *B. thuringiensis* ENSW401 can be utilized in the *ex situ* conditions for different engineered bioreactor systems. This will require an interdisciplinary approach with the integration of metallurgical, chemical, mathematical, and civil engineering skills along with



sorption and wastewater treatment plan to combat heavy metal pollution from the aquatic environment. The last but not the least, in order to get the best out of the results obtained and to get this technology used for heavy metal pollution mitigation, it needs to be integrated into the policy simultaneously by the concerned government and international donor agencies.

## CONCLUSION

Biofilm formation and biofilm matrix compounds such as curli and cellulose production in *E. asburiae* ENSD102, *E. ludwigii* ENSH201, *Vitreoscilla* sp. ENSG301, *A. lwoffii* ENSG302, and *B. thuringiensis* ENSW401 were remarkably affected by different environmental and nutritional conditions. Only *Vitreoscilla* sp. ENSG301 and *B. thuringiensis* ENSW401 completely removed (100%) Cu and Ni at an initial concentration of 12.5 mg l<sup>-1</sup>, while all these strains totally removed (100%) Pb at initial concentrations of 12.5 and 25 mg l<sup>-1</sup> at pH 7 and 28°C. FTIR study showed that Cu, Ni, and Pb could be sorbed by carbonyl, carboxyl, and phosphate groups of the biomass biofilms of *E. asburiae* ENSD102, *Vitreoscilla* sp. ENSG301, *A. lwoffii* ENSG302, and *B. thuringiensis* ENSW401, while phosphate groups and P–O of the (C–PO<sub>2</sub><sup>-3</sup>) moiety have no role in Cu removal by *E. ludwigii* ENSH201. Thus, all these bacterial strains can be utilized in biosorption of heavy metals from wastewater.

## DATA AVAILABILITY STATEMENT

The original contributions presented in the study are included in the article/**Supplementary Material**, further inquiries can be directed to the corresponding author.

## REFERENCES

- Abdi, O., and Kazemi, M. (2015). A review study of biosorption of heavy metals and comparison between different biosorbents. *J. Mat. Environ. Sci.* 6, 1386–1399.
- Aceves-Diez, A. E., Estrada-Castañeda, K. J., and Castañeda-Sandoval, L. M. (2015). Use of *Bacillus thuringiensis* supernatant from a fermentation process to improve bioremediation of chlorpyrifos in contaminated soils. *J. Environ. Manage.* 157, 213–219. doi: 10.1016/j.jenvman.2015.04.026
- Adhikari, A., Lee, K.-E., Khan, M. A., Kang, S.-M., Adhikari, B., Imran, M., et al. (2020). Effect of silicate and phosphate solubilizing rhizobacterium *Enterobacter ludwigii* GAK2 on *Oryza sativa* L. under cadmium stress. *J. Microbiol. Biotechnol.* 30, 118–126. doi: 10.4014/jmb.1906.06010
- Ahluwalia, S. S., and Goyal, D. (2007). Microbial and plant derived biomass for removal of heavy metals from wastewater. *Bioresour. Technol.* 98, 2243–2257. doi: 10.1016/j.biortech.2005.12.006
- Ahmed, M. K., Baki, M. A., Kundu, G. K., Islam, M. S., Islam, M. M., and Hossain, M. M. (2016). Human health risks from heavy metals in fish of Buriganga river, Bangladesh. *SpringerPlus* 5:1697. doi: 10.1186/s40064-016-3357-0
- Ahn, S.-J., and Burne, R. A. (2007). Effects of oxygen on biofilm formation and the Atla autolysin of *Streptococcus mutans*. *J. Bacteriol.* 189, 6293–6302. doi: 10.1128/JB.00546-07
- Alam, M. Z., Carpenter-Boggs, L., Rahman, A., Haque, M. M., Miah, M. R. U., Moniruzzaman, M., et al. (2017). Water quality and resident perceptions of declining ecosystem services at Shitalakka wetland in Narayanganj city. *Sustain. Water Qual. Ecol.* 9–10, 53–66. doi: 10.1016/j.swaqe.2017.03.002
- Anrany, Y., Sahu, S. N., Wessels, K. R., McCann, L. M., and Joseph, S. W. (2006). Alteration of the rugose phenotype in waaG and ddhC mutants of *Salmonella*

## AUTHOR CONTRIBUTIONS

MMH conceived the idea, developed the methodologies, conducted the experiments, wrote the manuscript, and collected the research fund. MKM and MZHT conducted the experiments. MAH and MKA performed FTIR and AAS, respectively. All authors read the manuscript and approved for publication.

## FUNDING

This project was supported by the Bangladesh Bureau of Educational Information and Statistics (Project ID: LS2018751) and Ministry of Education, Government of the People's Republic of Bangladesh to MMH.

## ACKNOWLEDGMENTS

We would like to thank Dr. Ziban Chandra Das, Department of Gynecology, Obstetrics and Reproductive Health for supplying sheep blood for hemolytic test.

## SUPPLEMENTARY MATERIAL

The Supplementary Material for this article can be found online at: <https://www.frontiersin.org/articles/10.3389/fmicb.2021.615113/full#supplementary-material>

*enterica* Serovar Typhimurium DT104 is associated with inverse production of curli and cellulose. *Appl. Environ. Microbiol.* 7, 5002–5012. doi: 10.1128/AEM.02868-05

Armada, E., Roldan, A., and Azcon, R. (2014). Differential activity of autochthonous bacteria in controlling drought stress in native *Lavandula* and *Salvia* plants species under drought conditions in natural arid soil. *Microb. Ecol.* 67, 410–420. doi: 10.1007/s00248-013-0326-9

Bacs, C. F., and Mesmer, R. E. (1976). *The Hydrolysis of Cations*. New York, NY: John Wiley and Sons, 241–310.

Balan, B., Dhaulaniya, A. S., Varma, D. A., Sodhi, K. K., Kumar, M., Tiwari, M., et al. (2020). Microbial biofilm ecology, in silico study of quorum sensing receptor-ligand interactions and biofilm mediated bioremediation. *Arch. Microbiol.* 203, 13–30. doi: 10.1007/s00203-020-02012-9

Banerjee, G., Paney, S., Ray, A. K., and Kumar, R. (2015). Bioremediation of heavy metals by a novel bacterial strain *Enterobacter cloacae* and its antioxidant activity, flocculent production, and protein expression in presence of lead, cadmium and nickel. *Water Air Soil Pollut.* 226:91. doi: 10.1007/s11270-015-2359-9

Barnhart, M. M., and Chapman, M. R. (2006). Curli biogenesis and function. *Annu. Rev. Microbiol.* 60, 131–147. doi: 10.1146/annurev.micro.60.080805.142106

Bjergbæk, L., Haagenen, J., Reisner, A., Molin, S., and Roslev, P. (2006). Effect of oxygen and growth medium on in vitro biofilm formation by *Escherichia coli*. *Biofilms* 3, 1–10. doi: 10.1017/S1479050507002074

Bokranz, W., Wang, X., Tschape, H., and Romling, U. (2005). Expression of cellulose and curli fimbriae by *Escherichia coli* isolated from the gastrointestinal tract. *J. Med. Microbiol.* 54, 1171–1182. doi: 10.1099/jmm.0.46064-0

- Boles, B. R., Theoendel, M., and Singh, P. K. (2004). Self-generated diversity produces “insurance effects” in biofilm communities. *FEMS Microb. Rev.* 20, 291–303. doi: 10.1073/pnas.0407460101
- Burakov, A. E., Galunin, E. V., Burakova, I. V., Kuchero, A. E., Agarwal, S., Tkachev, A. G., et al. (2018). Adsorption of heavy metals on conventional and nanostructured materials for wastewater treatment purposes: a review. *Ecotoxicol. Environ. Safe.* 148, 702–712. doi: 10.1016/j.ecoenv.2017.11.034
- Chen, S., Duan, J., Jaroniec, M., and Qiao, S. Z. (2014). Nitrogen and oxygen dual-doped carbon hydrogel film as a substrate-free electrode for higher efficient oxygen evolution reaction. *Adv. Mat.* 26, 2925–2930. doi: 10.1002/adma.201305608
- Costerton, J. W., Stewart, P. S., and Greenberg, E. P. (1999). Bacterial biofilms: a common cause of persistent infections. *Science* 284, 1318–1322. doi: 10.1126/science.284.5418.1318
- de Maagd, R. (2015). “*Bacillus thuringiensis*-based products for insect pest control,” in *Principles of Plant-Microbe Interactions*, ed. B. Lugtenberg (Cham: Springer), doi: 10.1007/978-3-319-08575-3\_20
- Deng, L., Su, Y., Su, H., Wang, X., and Zhu, X. (2007). Sorption and desorption of lead (II) from wastewater by green algae *Cladophora fascicularis*. *J. Hazard. Mater.* 143, 220–225. doi: 10.1016/j.jhazmat.2006.09.009
- DoE (Department of Environment) (2008). *Guide for Assessment of Effluent Treatment Plants*. Dhaka: Department of Environment.
- Dolkar, D., Dolkar, P., Chaurasia, S. A. O. P., and Stobdan, T. (2018). Stress tolerance and plant growth promotion potential of *Enterobacter ludwigii* PS1 isolated from *Seabuckthorn* rhizosphere. *Biocatal. Agril. Biotechnol.* 14, 438–443. doi: 10.1016/j.bcab.2018.04.012
- Edwards, S. J., and Kjellerup, B. V. (2013). Applications of biofilms in bioremediation and biotransformation of persistent organic pollutants, pharmaceutical/personal care products, and heavy metals. *Appl. Microbiol. Biotechnol.* 97, 9909–9921. doi: 10.1007/s00253-013-5216-z
- El-Naggar, N., Hamouda, R. A., Mousa, I. E., Abdel-Hamid, M. S., and Rabei, N. H. (2018). Biosorption optimization, characterization, immobilization and application of *Gelidium amansii* biomass for compete Pb<sup>2+</sup> removal from aqueous solutions. *Sci. Rep.* 8:13456. doi: 10.1038/s41598-018-31660-7
- Esposito, A., Pagnanelli, F., and Vegli, F. (2002). pH related equilibria models for biosorption in single metal system. *Chem. Eng. Sci.* 67, 307–313. doi: 10.1016/S0009-2509(01)00399-2
- European Union (EU) (2002). *Heavy Metals in Wastes, European Commission on Environment*. Brussels: European Union.
- Flemming, H. C., Neu, T. R., and Wozniak, D. (2007). The EPS matrix: the house of biofilm cells. *J. Bacteriol.* 189, 7945–7947. doi: 10.1128/JB.00858-07
- Flemming, H. C., and Wingender, J. (2010). The biofilm matrix. *Nat. Rev. Microbiol.* 8, 623–633. doi: 10.1038/nrmicro2415
- Friedman, L., and Kolter, R. (2004). Genes involved in matrix formation in *Pseudomonas aeruginosa* PA14 biofilms. *Mol. Microbiol.* 51, 675–690. doi: 10.1046/j.1365-2958.2003.03877.x
- Gabr, R. M., Hassan, S. H. A., and Shoreit, A. A. M. (2008). Biosorption of lead and nickel by living and nonliving cells of *Pseudomonas aeruginosa* ASU 6a. *Int. Biodeterior. Biodegrad.* 62, 195–203. doi: 10.1016/j.ibiod.2008.01.008
- Gadd, G. M. (2009). Biosorption: critical review of scientific rationale, environmental importance and significance for pollution treatment. *J. Chem. Technol. Biotechnol.* 84, 13–28. doi: 10.1002/jctb.1999
- Gerstel, U., and Römling, U. (2001). Oxygen tension and nutrient starvation are major signals that regulate *agfD* promoter activity and expression of the multicellular morphotype in *Salmonella typhimurium*. *Environ. Microbiol.* 3, 638–648. doi: 10.1046/j.1462-2920.2001.00235.x
- Gerstel, U., and Römling, U. (2003). The *csfD* promoter, a control unit for biofilm formation in *Salmonella typhimurium*. *Res. Microbiol.* 154, 659–667. doi: 10.1016/j.resmic.2003.08.005
- Gontia-Mishra, I., Sapre, S., Sharma, A., and Tiwari, S. (2016). Amelioration of drought tolerance in wheat by the interaction of plant growth—promoting rhizobacteria. *Plant Biol.* 18, 992–1000. doi: 10.1111/plb.12505
- Gutnick, D. L., and Bach, H. (2000). Engineering bacterial biopolymers for the biosorption of heavy metals; new products and novel formulations. *Appl. Microbiol. Biotechnol.* 54, 451–460. doi: 10.1007/s002530000438
- Haque, M. M., Haque, M. A., Mosharaf, M. K., and Marcus, P. K. (2021a). Decolorization, degradation and detoxification of carcinogenic sulfonated azo dye methyl orange by newly developed biofilm consortia. *Saudi J. Biol. Sci.* 28, 793–804. doi: 10.1016/j.sjbs.2020.11.012
- Haque, M. M., Haque, M. A., Mosharaf, M. K., and Marcus, P. K. (2021b). Novel bacterial biofilm consortia that degrade and detoxify the carcinogenic diazo dye Congo red. *Arch. Microbiol.* 203, 643–654. doi: 10.1007/s00203-020-02044-1
- Haque, M. M., Hirata, H., and Tsuyumu, S. (2012). Role of PhoP-PhoQ two-component system in pellicle formation, virulence and survival in harsh environments of *Dickeya dadantii* 3937. *J. Gen. Plant Pathol.* 78, 176–189. doi: 10.1007/s10327-012-0372-z
- Haque, M. M., Hirata, H., and Tsuyumu, S. (2015). SlyA regulates *motA* and *motB*, virulence and stress-related genes under conditions induced by the PhoP-PhoQ system in *Dickeya dadantii* 3937. *Res. Microbiol.* 166, 467–475. doi: 10.1016/j.resmic.2015.05.004
- Haque, M. M., Kabir, M. S., Aini, L. Q., Hirata, H., and Tsuyumu, S. (2009). SlyA, a MarR family transcriptional regulator, is essential for virulence in *Dickeya dadantii* 3937. *J. Bacteriol.* 191, 5409–5419. doi: 10.1128/JB.00240-09
- Haque, M. M., Oliver, M. M. H., Nahar, K., Alam, M. Z., Hirata, H., and Tsuyumu, S. (2017). CytR homolog of *Pectobacterium carotovorum* subsp. *carotovorum* controls air-liquid biofilm formation by regulating multiple genes involved in cellulose production, c-di-GMP signaling, motility, and type III secretion system in response to nutritional and environmental signals. *Front. Microbiol.* 8:972. doi: 10.3389/fmicb.2017.00972
- Hassan, S. H. A., Kim, S. J., Jung, A.-Y., Joo, J. H., Oh, S. E., and Yang, J. E. (2009). Biosorptive capacity of Cd(II) and Cu(II) by lyophilized cells of *Pseudomonas stutzeri*. *J. Gen. Appl. Microbiol.* 55, 27–34. doi: 10.2323/jgam.55.27
- He, J., and Chen, P. (2014). A comprehensive review on biosorption of heavy metals by algal biomass: materials, performances, chemistry, and modeling simulation tools. *Bioresour. Technol.* 160, 67–78. doi: 10.1016/j.biortech.2014.01.068
- Hostacká, A., Ciznář, I., and Stefkovicová, M. (2010). Temperature and pH affect the production of bacterial biofilm. *Folia Microbiol.* 55, 75–78. doi: 10.1007/s12223-010-0012-y
- Hou, B., Meng, X.-R., Zhang, L.-Y., Tan, C., Jin, H., Zhou, R., et al. (2014). ToIC promotes ExPEC biofilm formation and curli production in response to medium osmolarity. *BioMed. Res. Intl.* 10:574274. doi: 10.1155/2014/574274
- Imron, M. F., and Tttah, H. S. (2018). Biodegradation of diesel by *Acinetobacter lwoffii* and *Vibrio alginolyticus* isolated from ship dismantling facility in Tanjungjati Coast, Madura, Indonesia. *J. Appl. Biol. Sci.* 12, 01–08.
- Jamshaid, A., Hamid, A., Muhammad, N., Naseer, A., Ghauri, M., Iqbal, J., et al. (2017). Cellulose-based materials for the removal of heavy metals from wastewater – an overview. *ChemBioEng. Rev.* 4, 1–18. doi: 10.1002/cben.201700002
- Jettyanon, K. (2015). Multiple mechanisms of *Enterobacter asburiae* strain RS83 for plant growth enhancement. *Songklanakaraj J. Sci. Technol.* 37, 29–36.
- Kaduková, J., and Viréiková, E. (2005). Comparison of differences between copper accumulation and biosorption. *Environ. Intl.* 31, 227–232. doi: 10.1016/j.envint.2004.09.020
- Kang, S. -M., Radhakrishnan, R., You, Y. -H., Khan, A. -L., Lee, K. -E., Lee, J. -D., et al. (2015). *Enterobacter asburiae* KE17 association regulates physiological changes and mitigates the toxic effects of heavy metals in soybean. *Plant Physiol* 17, 1013–1022. doi: 10.1111/plb.12341
- Kavamura, V. N., and de Melo, I. S. (2014). Effects of different osmolarities on bacterial biofilm formation. *Braz. J. Microbiol.* 45, 627–631. doi: 10.1590/S1517-83822014000200034
- Kirova, G., Velkova, Z., Stoytcheva, M., Hristova, Y., Iliev, I., and Gochev, V. (2015). Biosorption of Pb (II) ions from aqueous solutions by waste biomass of *Streptomyces fradiae* pretreated with NaOH. *Biotechnol. Biotechnol. Equip.* 29, 689–695. doi: 10.1080/13102818.2015.1036775
- Koehler, S., Farasin, J., Cleiss-Arnold, J., and Arsène-Pløetze, F. (2015). Toxic metal resistance in biofilms: diversity of microbial responses and their evolution. *Res. Microbiol.* 166, 764–773. doi: 10.1016/j.resmic.2015.03.008
- Kotrba, P., Macek, T., Mavkova, M., Naja, G., Volesky, B., and Pagnanelli, F. (2011). “Biosorption and metal removal through living cells,” in *Microbial Biosorption of Metals*, eds P. Kotrba, M. Mackova, J. Fišer, and T. Macek (Dordrecht: Springer Science Business Media), 197–333. doi: 10.1007/978-94-007-0443-5\_9
- Kratochvil, D., and Volesky, B. (1998). Advances in the biosorption of heavy metals. *Trends Biotechnol.* 16, 291–300. doi: 10.1016/S0167-7799(98)01218-9

- Kumar, S. A., Abyaneh, M. K., Gosavi, S. W., Kulkarni, S. K., Pasricha, R., Ahmad, A., et al. (2007). Nitrate reductase-mediated synthesis of silver nanoparticles from AgNO<sub>3</sub>. *Biotechnol. Lett.* 29, 439–445. doi: 10.1007/s10529-006-9256-7
- Lebeer, S., Verhoeven, T. L. A., Véléz, M. P., Vanderleyden, J., and De Keersmaecker, S. C. J. (2007). Impact of environmental and genetic factors on biofilm formation by the probiotic strain *Lactobacillus rhamnosus* GG. *Appl. Environ. Microbiol.* 73, 6768–6775. doi: 10.1128/AEM.01393-07
- Li, W. W., and Yu, H. Q. (2014). Insight into the roles of microbial extracellular polymer substances in metal biosorption. *Bioresour. Technol.* 160, 15–23. doi: 10.1016/j.biortech.2013.11.074
- Liang, Y., Gao, H., Chen, J., Dong, Y., Wu, L., He, Z., et al. (2010). Pellicle formation in *Shewanella oneidensis*. *BMC Microbiol.* 10:291. doi: 10.1186/1471-2180-10-291
- Lo, Y. C., Chang, C. L., Han, Y. L., Chen, B. Y., and Chang, J. S. (2014). Recovery of high-value metals from geothermal sites by biosorption and bioaccumulation. *Bioresour. Technol.* 160, 182–190. doi: 10.1016/j.biortech.2014.02.008
- Mahdi, I., Fahsi, N., Hafidi, M., Allaoui, A., and Biskri, L. (2020). Plant growth enhancement using rhizospheric halotolerant phosphate solubilizing bacterium *Bacillus licheniformis* QA1 and *Enterobacter asburiae* QF11 isolated from *Chenopodium quinoa* wild. *Microorganisms* 8:948. doi: 10.3390/microorganisms8060948
- Malik, A. (2004). Metal bioremediation through growing cells. *Environ. Int.* 30, 261–278. doi: 10.1016/j.envint.2003.08.001
- Marchlewicz, A., Domaradzka, D., Guzik, U., and Wojcieszynska, D. (2016). *Bacillus thuringiensis* B1 (2015b) is a Gram-positive bacteria able to degrade Naproxen and Ibuprofen. *Water Air Soil Pollut.* 227, 197. doi: 10.1007/s11270-016-2893-0
- Martins, S. J., Rocha, G. A., de Melo, H. C., Georg, R. C., Ulhoa, C. J., Dianese, E. C., et al. (2018). Plant-associated bacteria mitigate drought stress in soybean. *Environ. Sci. Pollut. Res.* 25, 13676–13686. doi: 10.1007/s11356-018-1610-5
- Mejäre, M., and Bülow, L. (2001). Metal-binding proteins and peptides in bioremediation and phytoremediation of heavy metals. *Trends Biotechnol.* 19, 67–73. doi: 10.1016/S0167-7799(00)01534-1
- Meliani, A., and Bensoltane, A. (2016). Biofilm-mediated heavy metals bioremediation in PGPR *Pseudomonas*. *J. Bioremediat. Biodegrad.* 7:370. doi: 10.4172/2155-6199.1000370
- Milano, D. S., Prunich, B. Z., Velhner, M. J., Pajic, M. L., and Cabarkapa, I. S. (2015). Rdar morphotype—a resting stage of some *Enterobacteriaceae*. *Food Feed Res.* 42, 43–50. doi: 10.5937/ffr1501043m
- Mindlin, S., Petrenko, A., Kurakov, A., Beletsky, A., Mardanov, A., and Petrova, M. (2016). Resistance of permafrost and modern *Acinetobacter lwoffii* strains to heavy metals and arsenic revealed by genome analysis. *Mol. Phylogenet.* 2016:3970831. doi: 10.1155/2016/3970831
- Moat, A. G., Foster, J. W., and Spector, M. P. (2002). *Microbial Physiology*. New York, NY: Wiley-Liss.
- Mosharaf, M. K., Tanvir, M. Z. H., Haque, M. M., Haque, M. A., Khan, M. A. A., Molla, A. H., et al. (2018). Metal-adapted bacteria isolated from wastewaters produce biofilms by expressing *Proteinaceous curli* fimbriae and cellulose nanofibers. *Front. Microbiol.* 9:1334. doi: 10.3389/fmicb.2018.01334
- Naser, H. M., Sultana, S., Haque, M. M., Akhter, S., and Begum, R. A. (2014). Lead, cadmium and nickel accumulation in some common spice grown in industrial areas of Bangladesh. *Agriculturists* 12, 122–130. doi: 10.3329/agric.v12i1.19867
- Nguyen, H. D. N., Yang, Y. S., and Yuk, H. G. (2014). Biofilm formation of *Salmonella Typhimurium* on stainless steel and acrylic surfaces as affected by temperature and pH level. *LWT Food Sci. Technol.* 55, 383–388. doi: 10.1016/j.lwt.2013.09.022
- Nies, D. H. (1999). Microbial heavy metal resistance. *Appl. Microbial. Biotechnol.* 51, 730–750. doi: 10.1007/s002530051457
- Olsén, A., Wick, M. J., Mörgelin, M., and Björck, L. (1998). Curli, fibrous surface proteins of *Escherichia coli*, interact with major histocompatibility complex class I molecules. *Infect. Immun.* 66, 944–949. doi: 10.1128/IAI.66.3.944-949.1998
- Oves, M., Khan, M. S., and Zaidi, A. (2013). Biosorption of heavy metals by *Bacillus thuringiensis* strain OSM29 originating from industrial effluent contaminated north Indian soil. *Saudi J. Biol. Sci.* 20, 121–129. doi: 10.1016/j.sjbs.2012.11.006
- Pal, A., and Paul, A. K. (2008). Microbial extracellular polymeric substances: central elements in heavy metal bioremediation. *Indian J. Microbiol.* 48, 49–64. doi: 10.1007/s12088-008-0006-5
- Pan, R., Cao, L., and Zhang, R. (2009). Combined effects of Cu, Cd, Pb and Zn on the growth and uptake of consortium of Cu-resistant *Penicillium* sp. A1 and Cd-resistant *Fusarium* sp. A19. *J. Hazard. Mater.* 171, 761–766. doi: 10.1016/j.jhazmat.2009.06.080
- Patrauchan, M. A., Sarkisova, S., Sauer, K., and Franklin, M. J. (2005). Calcium influences cellular and extracellular product formation during biofilm-associated growth of a marine *Pseudomonas* sp. *Microbiology* 151, 2885–2897. doi: 10.1099/mic.0.28041-0
- Paul, A., and Mukherjee, S. K. (2016). *Enterobacter asburiae* KUNi5, a nickel resistant bacterium for possible bioremediation of nickel contaminated sites. *Pol. J. Microbiol.* 65, 115–118. doi: 10.5604/17331331.1197284
- Prigent-Combaret, C., Prensier, G., Le Thai, T. T., Vidal, O., Lejeune, P., and Dorel, C. (2000). Development pathway of biofilm formation in curli-producing *Escherichia coli* strains: role of flagella, curli and colonic acid. *Environ. Microbiol.* 2, 450–464. doi: 10.1046/j.1462-2920.2000.00128.x
- Radwan, T. E. E., Reyad, A. M. M., and Essa, A. M. M. (2017). Bioremediation of the nematocidal oxamyl by *Enterobacter ludwigii* isolated from agricultural wastewater. *Egypt. J. Exp. Biol. (Bot.)* 13, 19–30. doi: 10.5455/egyeb.20170131064321
- Ramli, N. S. K., Eng Guan, C., Nathan, S., and Vadivelu, J. (2012). The effect of environmental conditions on biofilm formation of *Burkholderia pseudomallei* clinical isolates. *PLoS One* 7:e44104. doi: 10.1371/journal.pone.0044104
- Redha, A. A. (2020). Removal of heavy metals from aqueous media by biosorption. *Arab. J. Basic Sci.* 27, 183–193. doi: 10.1080/25765299.2020.1756177
- Ren, L., Men, L., Zhang, Z., Guan, F., Tian, J., Wang, B., et al. (2019). Biodegradation of polyethylene by *Enterobacter* sp. D1 from the guts of wax moth *Galleria mellonella*. *Int. J. Environ. Res. Public Health* 16:1941. doi: 10.3390/ijerph16111941
- Rinaudi, L., Fujishige, N. A., Hirsch, A. M., Banchio, E., Zorreguieta, A., and Giordano, W. (2006). Effects of nutritional and environmental conditions on *Sinorhizobium meliloti* biofilm formation. *Res. Microbiol.* 15, 867–875. doi: 10.1016/j.resmic.2006.06.002
- Roane, T. M., Rensing, C., Pepper, I. L., and Maier, R. M. (2009). “Microorganisms and metal pollutants,” in *Environmental Microbiology*, eds R. M. Maier, I. L. Pepper, and C. P. Gerba (Cambridge, MA: Academic Press), 421–430. doi: 10.1016/b978-0-12-370519-8.00021-3
- Römling, U. (2005). Characterization of the rdar morphotype, a multicellular behavior in *Enterobacteriaceae*. *Cell Mol. Life Sci.* 62, 1234–1246. doi: 10.1007/s00018-005-4557-x
- Ross, E., Paroni, M., and Landini, P. (2018). Biofilm and motility in response to environmental and host-related signals in Gram negative opportunistic pathogens. *J. Appl. Microbiol.* 125, 1587–1602. doi: 10.1111/jam.14089
- Sadiq, H. M., Jahangir, G. Z., Nasir, I. A., Iqtidar, M., and Iqbal, M. (2013). Isolation and characterization of phosphate-solubilizing bacteria from rhizosphere Soil. *Biotechnol. Biotechnol. Equip.* 27, 4248–4255. doi: 10.5504/BBEQ.2013.0091
- Sag, Y., and Kutsal, T. (2001). Recent trends in the biosorption of heavy metals: a review. *Biotechnol. Bioprocess Eng.* 6:376. doi: 10.1007/BF02932318
- Santhosh, C., Velmurugan, V., Jacob, G., Jeong, S. K., Grace, A. N., and Bhatnagar, A. (2016). Role of nanomaterials in water treatment applications: a review. *Chem. Eng. J.* 306, 1116–1137. doi: 10.1016/j.cej.2016.08.053
- Sato, V. S., Júnior, R. F. G., Rodrigues, G. R., Lemos, E. G. M., and Junior, J. M. P. (2016). Kinetic characterization of a novel acid ectophosphatase from *Enterobacter asburiae*. *J. Microbiol.* 54, 106–113. doi: 10.1007/s12275-015-5354-3
- Schmidt, T., and Schlegel, H. G. (1994). Combined nickel-cobalt-cadmium resistance encoded by the ncc locus of *Alcaligenes xylosoxidans* 31A. *J. Bacteriol.* 176, 7054–7054.
- Shen, Y., Huang, P. C., Huang, C., Sun, P., Monroy, G. L., Wu, W., et al. (2018). Effect of divalent ions and a polyphosphate on composition, structure, and stiffness of simulated drinking water biofilms. *NPJ Biofilms Microb.* 4:15. doi: 10.1038/s41522-018-0058-1
- Shoebitz, M., Ribaud, C. M., Pardo, M. A., Cantore, M. L., Ciampi, L., and Curá, J. A. (2009). Plant growth promoting properties of a strain of *Enterobacter ludwigii* isolated from *Lolium perenne* rhizosphere. *Soil Biol. Biochem.* 41, 1768–1774. doi: 10.1016/j.soilbio.2007.12.031
- Singh, R., Paul, D., and Jain, R. K. (2006). Biofilms: implications in bioremediation. *Trends Microbiol.* 14, 389–397. doi: 10.1016/j.tim.2006.07.001

- Solomon, E. B., Niemira, B. A., Sapers, G. M., and Annous, B. A. (2005). Biofilm formation, cellulose production, and curli biosynthesis by *Salmonella* originating from produce, animal, and clinical sources. *J. Food Prot.* 68, 906–912. doi: 10.4315/0362-028X-68.5.906
- Song, B., and Leff, L. G. (2006). Influence of magnesium ions on biofilm formation by *Pseudomonas fluorescens*. *Microbiol. Res.* 161, 355–361. doi: 10.1016/j.micres.2006.01.004
- Stark, B. C., Pagilla, K. R., and Dikshit, K. L. (2015). Recent applications of *Vitreoscilla* hemoglobin technology in bioproduct synthesis and bioremediation. *Appl. Microbiol. Biotechnol.* 99, 1627–1636. doi: 10.1007/s00253-014-6350-y
- Steenackers, H., Hermans, K., Vanderleyden, J., and Keersmaecker, D. (2012). *Salmonella* biofilms: an overview on occurrence, structure, regulation and eradication. *Food Res. Int.* 45, 502–531. doi: 10.1016/j.foodres.2011.01.038
- Sutherland, I. W. (1984). Microbial exopolysaccharides—their role in microbial adhesion in aqueous systems. *CRC Crit. Rev. Microbiol.* 10, 173–201. doi: 10.3109/10408418209113562
- Taşar, Ş., Kaya, F., and Özer, A. (2014). Biosorption of lead (II) ions from aqueous solution by peanut shells: equilibrium, thermodynamic and kinetic studies. *J. Environ. Chem. Eng.* 2, 1018–1026. doi: 10.1016/j.jece.2014.03.015
- Teitzel, G. M., and Parsek, M. R. (2003). Heavy metal resistance of biofilm and planktonic *Pseudomonas aeruginosa*. *Appl. Environ. Microbiol.* 69, 2313–2320. doi: 10.1128/AEM.69.4.2313-2320.2003
- Uddin, M. J., and Jeong, Y.-K. (2021). Urban river pollution in Bangladesh during last 40 years: potential public health and ecological risk, present policy, and future prospects toward smart water management. *Heliyon* 7:e06107. doi: 10.1016/j.heliyon.2021.e06107
- USEPA (United States Environmental Protection Agency) (2012). *Edition of the Drinking Water Standards and Health Advisories; EPA 822-S-12-001*. Washington, DC: Office of Water U.S. Environmental Protection Agency.
- von Canstein, H., Kelly, S., Li, Y., and Wangner-Döbler, I. (2002). Species diversity improves the efficiency of mercury-reducing biofilms under changing environmental conditions. *Appl. Environ. Microbiol.* 68, 2829–2837. doi: 10.1128/AEM.68.6.2829-2837.2002
- Vu, B., Chen, M., Crawford, R. J., and Ivanova, E. P. (2009). Bacterial extracellular polysaccharide involved in biofilm formation. *Molecules* 14, 2535–2554. doi: 10.3390/molecules14072535
- Wakabayashi, S., Matsubara, H., and Webster, D. A. (1986). Primary sequence of a dimeric bacterial hemoglobin from *Vitreoscilla*. *Nature* 322, 481–483. doi: 10.1038/322481a0
- Weast, R. C. (1984). *CRC Handbook of Chemistry and Physics*, 64th Edn. Boca Raton, FL: CRC Press Inc.
- Wei, W., Wang, Q., Li, A., Yang, J., Ma, F., Pi, S., et al. (2016). Biosorption of Pb (II) from aqueous solution by extracellular polymeric substances extracted from *Klebsiella* sp. J1: adsorption behavior and mechanism assessment. *Sci. Rep.* 6:10. doi: 10.1038/srep31575
- White, A. P., Gibson, D. L., Collinson, S. K., Banser, P. A., and Kay, W. W. (2003). Extracellular polysaccharides associated with thin aggregative fimbriae of *Salmonella enterica* serovar Enteritidis. *J. Bacteriol.* 185, 5398–5407. doi: 10.1128/jb.185.18.5398-5407.2003
- WHO (World Health Organization) (2017). *Guidelines for Drinking-water Quality*. Fourth Edition Incorporating the First Addendum. Cham: WHO.
- Wu, C., Yuan-Yuan Cheng, Y.-Y., Yin, H., Song, X.-N., Li, W.-W., Zhou, X.-X., et al. (2013). Oxygen promotes biofilm formation of *Shewanella putrefaciens* CN32 through a diguanylate cyclase and an adhesion. *Sci. Rep.* 3:1945. doi: 10.1038/srep01945
- Yang, Y., Hu, M., Zhou, D., Fan, W., Wang, X., and Huo, M. (2017). Bioremoval of Cu<sup>2+</sup> from CMP wastewater by a novel copper-resistant bacterium *Cupriavidus gilardii* CR3: characteristics and mechanisms. *RCS Adv.* 7:18793. doi: 10.1039/C7RA01163F
- Yap, M.-N., Yang, C.-H., Barak, J. D., Jahn, C. E., and Charkowski, A. O. (2005). The *Erwinia chrysanthemi* type III secretion system is required for multicellular behavior. *J. Bacteriol.* 187, 639–648. doi: 10.1128/JB.187.2.639-648.2005
- Zelasco, S., Reggi, S., Calligari, P., Balestrazzi, A., Bongiorno, C., Quattrini, E., et al. (2006). Expression of the *Vitreoscilla* hemoglobin (VHb)-encoding gene in transgenic white poplar: plant growth and biomass production, biochemical characterization and cell survival under submergence, oxidative and nitrosative stress conditions. *Mol. Breed.* 17, 201–216. doi: 10.1007/s11032-005-5295-3
- Zeng, X., Tang, J., Xue-duan, L. I. U., and Pei, J. (2009). Isolation, identification of cadmium-resistant *Pseudomonas aeruginosa* strain E1. *J. Cent. South Univ. Technol.* 16, 416–421. doi: 10.1007/s11771-009-0070-y
- Zhou, L., Xia, S., Zhang, Z., Ye, B., Xu, X., Gu, Z., et al. (2014). Effects of pH, temperature and salinity on extracellular polymeric substances of *Pseudomonas aeruginosa* biofilm with N-(3-oxooxetanoyl)-L-homoserine lactone addition. *J. Water Sustain.* 4, 91–110.

**Conflict of Interest:** The authors declare that the research was conducted in the absence of any commercial or financial relationships that could be construed as a potential conflict of interest.

Copyright © 2021 Haque, Mosharaf, Haque, Tanvir and Alam. This is an open-access article distributed under the terms of the Creative Commons Attribution License (CC BY). The use, distribution or reproduction in other forums is permitted, provided the original author(s) and the copyright owner(s) are credited and that the original publication in this journal is cited, in accordance with accepted academic practice. No use, distribution or reproduction is permitted which does not comply with these terms.





# Description of Microbial Communities of Phosphate Mine Wastes in Morocco, a Semi-Arid Climate, Using High-Throughput Sequencing and Functional Prediction

Najoua Mghazli<sup>1,2</sup>, Laila Sbabou<sup>1</sup>, Rachid Hakkou<sup>3,4</sup>, Ahmed Ouhammou<sup>5</sup>,  
Mariam El Adnani<sup>6</sup> and Odile Bruneel<sup>2\*</sup>

## OPEN ACCESS

### Edited by:

Aurélien Cebron,  
UMR 7360 Laboratoire  
Interdisciplinaire des Environnements  
Continents (LIEC), France

### Reviewed by:

Pinaki Sar,  
Indian Institute of Technology  
Kharagpur, India  
Rajeev Kaushik,  
Indian Council of Agricultural  
Research, India

### \*Correspondence:

Odile Bruneel  
odile.bruneel@ird.fr

### Specialty section:

This article was submitted to  
Microbiotechnology,  
a section of the journal  
Frontiers in Microbiology

**Received:** 11 February 2021

**Accepted:** 07 June 2021

**Published:** 08 July 2021

### Citation:

Mghazli N, Sbabou L, Hakkou R,  
Ouhammou A, El Adnani M and  
Bruneel O (2021) Description of  
Microbial Communities of Phosphate  
Mine Wastes in Morocco, a Semi-Arid  
Climate, Using High-Throughput  
Sequencing and Functional  
Prediction.  
Front. Microbiol. 12:666936.  
doi: 10.3389/fmicb.2021.666936

<sup>1</sup> Center of Research Plants and Microbial Biotechnologies, Biodiversity and Environment, Team of Microbiology and Molecular Biology, Faculty of Sciences, Mohammed V University in Rabat, Rabat, Morocco, <sup>2</sup> HydroSciences Montpellier, University of Montpellier, CNRS, IRD, Montpellier, France, <sup>3</sup> IMED\_Laboratory, Faculty of Science and Technology, Cadi Ayyad University (UCA), Marrakech, Morocco, <sup>4</sup> Mining Environment and Circular Economy Program, Mohammed VI Polytechnic University (UM6P), Benguerir, Morocco, <sup>5</sup> Laboratory of Microbial Biotechnologies, Agrosciences and Environment (BioMAgE), Team of Agrosciences, PhytoBiodiversity and Environment, Regional Herbarium 'MARK', Faculty of Sciences Semlalia, Cadi Ayyad University, Marrakech, Morocco, <sup>6</sup> Resources Valorisation, Environment and Sustainable Development Laboratory, National School of Mines of Rabat, Mohammed V University in Rabat, Rabat, Morocco

Soil microbiota are vital for successful revegetation, as they play a critical role in nutrient cycles, soil functions, and plant growth and health. A rehabilitation scenario of the abandoned Kettara mine (Morocco) includes covering acidic tailings with alkaline phosphate mine wastes to limit water infiltration and hence acid mine drainage. Revegetation of phosphate wastes is the final step to this rehabilitation plan. However, revegetation is hard on this type of waste in semi-arid areas and only a few plants managed to grow naturally after 5 years on the store-and-release cover. As we know that belowground biodiversity is a key component for aboveground functioning, we sought to know if any structural problem in phosphate waste communities could explain the almost absence of plants. To test this hypothesis, bacterial and archaeal communities present in these wastes were assessed by 16S rRNA metabarcoding. Exploration of taxonomic composition revealed a quite diversified community assigned to 19 Bacterial and two Archaeal phyla, similar to other studies, that do not appear to raise any particular issues of structural problems. The dominant sequences belonged to *Proteobacteria*, *Bacteroidetes*, *Actinobacteria*, and *Gemmatimonadetes* and to the genera *Massilia*, *Sphingomonas*, and *Adhaeribacter*. LEfSe analysis identified 19 key genera, and metagenomic functional prediction revealed a broader phylogenetic range of taxa than expected, with all identified genera possessing at least one plant growth-promoting trait. Around 47% of the sequences were also related to genera possessing strains that facilitate plant development under biotic and environmental stress conditions, such as drought and heat.

**Keywords:** phosphate mine wastes, microbial communities, PICRUST prediction, metabarcoding, biodiversity

## INTRODUCTION

Mining is vital for the global economy, but the extraction of valuable elements also produces large quantities of solid wastes corresponding to uneconomic materials such as waste rock, refuse material, tailings, sediment, roasted ore, and processing chemicals (Hudson-Edwards, 2016).

The mining sector, and particularly phosphate exploitation, is one of the pillars of the Moroccan economy. Among many closed mines in the country, Kettara mine located in a semi-arid region that was exploited for pyrrhotite, is particularly problematic (Hakkou et al., 2008a,b). Mining produced more than 5.2 million metric tons of pyrrhotite concentrate, producing acid mine drainage following rainfall events leading to groundwater contamination (Lghoul et al., 2014). Dominant winds also transport toxic dust and sulfur emissions, from the mine wastes to the village of Kettara (2,000 inhabitants, located in the immediate vicinity of the mine), polluting homes, cattle, and farmland, putting the population under significant environmental and health risks (Khalil et al., 2013; Babi et al., 2016). Morocco holds around three-quarters of the world's phosphate reserves and is the leading exporter of phosphate and its derivatives (Edixhoven et al., 2013; Hakkou et al., 2016). According to a United States Geological Survey<sup>1</sup> in 2019, Morocco produced around 36 million tons of phosphate rocks representing an economical currency inflow. However, open-pit mining and beneficiation processes including crushing, screening, washing, flotation, or chemical attack generate million tons of tailings called phosphate sludge every year, which is stockpiled over a huge area (Hakkou et al., 2016; Jalali et al., 2019; Elfadil et al., 2020; Trifi et al., 2020). In semi-arid areas, the poor quality of these phosphate mine wastes, containing small quantities of nutrients and contaminated by metals and fluoride, prevents good plant growth (Cross and Lambers, 2017; Jalali et al., 2019; Elfadil et al., 2020). In Morocco, huge piles of phosphate waste rock and tailing ponds that cover thousands of hectares, with very limited vegetation and subjected to wind and water erosion, not only spoil the landscape but are also a serious source of pollution (Hakkou et al., 2016). Revegetation of phosphate mine wastes has therefore become a national priority for Morocco.

The rehabilitation scheme for Kettara mine consists of depositing a layer of alkaline phosphate waste on top of the acidic tailings to limit infiltration of water and to control acid mine drainage generation (Ouakibi et al., 2013; Bossé et al., 2015). In semi-arid climates characterized by low annual precipitation and high evaporation rates, store-and-release covers can prevent percolation of water during wet periods and allow evaporation (or evapotranspiration) during dry periods thus preventing water from penetrating acidic wastes (Bossé et al., 2013). Lab tests (using columns) and field tests (with experimental cells constructed on-site) showed very good results, proving that water infiltration can be controlled, even during extreme rainfall events (Ouakibi et al., 2014; Bossé et al., 2015). The final step in this scheme is the revegetation of the phosphate cover to limit the

dispersion of fine dust, but revegetation is highly challenging for naturally growing biota.

Microbial communities are essential for soil functioning and for the development and maintenance of plant diversity (Hassani et al., 2018; van Bruggen et al., 2019). Soil microorganisms perform essential roles in the development and maintenance of healthy soil structure, including the decomposition of biomass (cellulose degradation, etc.), the transformation or biomineralization of biogenic element, increasing the quantity and availability of nutrients, degrading or biotransforming pollutants, mobilizing/immobilizing metals, etc. (Schulz et al., 2013; Thavamani et al., 2017). Microorganisms can also influence the development of plants *via* nitrogen fixation, phosphorus solubilization, sequestration of iron by siderophores or phytohormones production, etc. (Goswami et al., 2016; Kong and Glick, 2017; Olanrewaju et al., 2017). They can also limit biotic (pathogenic) stresses and abiotic environmental stresses for plants, including drought, salinity, heat, or toxic metals, which are particularly common in alkaline mine tailings in semi-arid areas (Armada et al., 2014; Fahad et al., 2015; Kumar and Verma, 2018; Gupta and Pandey, 2019). Studies dedicated to plant-microorganism associations are currently a very active area of research, and the interest of using microbial communities to stimulate plant growth in damaged and polluted soils, in semi-arid areas has been demonstrated in many countries (Mendez and Maier, 2008; Nirola et al., 2016; Bruneel et al., 2019). Different methods are currently used to inoculate plants with microorganisms. Ju et al. (2020) demonstrated that plant root inoculation with plant growth-promoting (PGP) rhizobia increased the phytostabilization by improving alfalfa growth by decreasing Cu accumulation in shoots in a Cu-contaminated site. Seeds can also be soaked in a bacterial inoculum before germination, as shown by Ke et al. (2021) where PGP bacteria enhanced ryegrass growth and phytostabilization in Cu-Cd-polluted soil. Indeed, pot experiment revealed that PGP bacteria addition increased shoot and root biomasses and limited stress of ryegrass by decreasing metal uptake and translocation. Direct application of bacterial inocula in contaminated soils has also shown positive results for the phytoextraction of excess phosphorus in soils (Ye et al., 2020; Guo et al., 2021). Guo et al. (2021) showed, for example, in pot experiments that two native phosphate-solubilizing microorganisms increased phosphate availability by reducing soil pH. Inoculation of these strains in soil also significantly increased the total biomass of two native plants, like their root and shoot length, and chlorophyll content.

As only a few plants managed to grow naturally after 5 years on the store-and-release cover, we sought to know if any structural problem in phosphate waste communities could explain the almost absence of plants. The aims of the present work were thus to (i) investigate the structure of the microbial communities (using 16S rRNA metabarcoding approach) and (ii) identify their potential metabolic functions in phosphate mine wastes using PICRUST2 prediction, to test this hypothesis. To our knowledge, this is the first study to describe the microbial communities present in alkaline phosphate mine wastes in Morocco using high-throughput sequencing and the first study

<sup>1</sup>[http://minerals.usgs.gov/minerals/pubs/commodity/phosphate\\_rock/](http://minerals.usgs.gov/minerals/pubs/commodity/phosphate_rock/)

on overburden phosphate waste rocks and phosphate sludge issuing from processing. This phylogenetic classification of microbial communities of phosphate mine wastes and *in silico* identification of their potential plant growth-promoting diversity will provide useful information to prepare media dedicated to the isolation of the most interesting plant growth-promoting microorganisms identified in this study, helping revegetation in a semi-arid climate.

## MATERIALS AND METHODS

### Description of Study Site and Experimental Cells

To evaluate the feasibility and effectiveness of using alkaline phosphate mine wastes as a store-and-release layer to limit infiltration of water in acidogenic tailing mine, field investigations were conducted at Kettara mine (31°52'15"N–8°10'31"W). Instrumented experimental cells (10 m × 10 m), with different configurations of store-and-release layer, and comprising two types of mine wastes, phosphate waste rock (overburden waste, removed to reach the phosphate ore) and phosphate sludge (produced during the concentration processes) were constructed in 2011 (Bossé et al., 2015; **Table 1** and

**Supplementary Figure 1**). The final step in the scheme of rehabilitation is the revegetation of the phosphate cover to limit the dispersion of fine dust, but after 5 years, only a few plants naturally grew on the experimental cells. Like belowground biodiversity is a key component for aboveground functioning, we conducted an *in situ* investigation, to identify bacterial and archaeal communities present in these experimental cells. To see if the presence of some annual plants, naturally growing, modified the structure of microbial communities, the microbial communities in soils sampled close to plants and in bare soils were also compared for each cell. Due to lack of plants naturally growing on these cells, three different species were chosen, *Spergularia rubra* (L.) for cell 1, *Atriplex semibaccata* for cell 3, and *Echium vulgare* (L.) for cell 4. *Echium vulgare* (L.) is a metallicolous plant that grows naturally in mine wastes and highly tolerant to Cd soil contamination (Dresler et al., 2015; Kompala-Baba et al., 2019). *Atriplex semibaccata*, found in abandoned mine, hyperaccumulate Cu and Cd and accumulate Fe (Baycu et al., 2015). *Atriplex* is also highly salt tolerant and has already been used as a pioneer species for revegetation in semi-arid areas (Nirola et al., 2016). *Spergularia rubra* (L.) J.Presl and C.Presl has been found as a pioneer plant in mine tailings (Garcia-Carmona et al., 2019) and is known to accumulate Cu in shoots (Bech et al., 2017).

**TABLE 1** | Description of experiment cells (10 m × 10 m), constructed in 2011 to test their capacities to limit infiltration of water and comprising two types of phosphate wastes used as store and release cover (Bossé et al., 2015).

Type of material	Sample name	Thickness of cover	Fraction	Name of plants sampled	Sample code	Main composition*	Electrical conductivity**
Phosphate waste rock, overburden wastes, removed to reach the phosphate ore	Cell 1	100 cm	Raw material	<i>Spergularia rubra</i> (L.)	C1VS1	Calcite (40.7 wt%)	147 to 496 $\mu\text{S cm}^{-1}$
					C1VS2	Apatite (25.9 wt%)	
					C1VS3	Dolomite (25.2 wt%)	
				Bare soil	C1BS1	Quartz (8.2 wt%)	
					C1BS2	Chromium (Cr, 137 mg/kg)	
					C1BS3	Strontium (Sr, 769 mg/kg)	
	Cell 4	100 cm	< 1 mm	<i>Echium vulgare</i> (L.)	C4VS1	Fluor (F, 1.3 wt%)	
					C4VS2		
					C4VS3		
				Bare soil	C4BS1		
					C4BS2		
					C4BS3		
Phosphate sludge, produced during the concentration processes	Cell 3	100 cm	Raw material	<i>Atriplex semibaccata</i>	C3VS1	Fluorapatite (44 wt%)	178.6 to 691 $\mu\text{S cm}^{-1}$
					C3VS2	Quartz (17 wt%)	
					C3VS3	Calcite (15 wt%)	
				Bare soil		Dolomite (7 wt%)	
						Cadmium (Cd, 131 mg/kg)	
						Chromium (Cr, 275 mg/kg)	
						Strontium (Sr, 927 mg/kg)	
						Fluor (F, 2.6 wt%).	
					C3BS1		
					C3BS2		
					C3BS3		

\*According to Hakkou et al., 2009, 2016.

\*\*Personal communication from Rachid Hakkou.

## Sample Collection

In this study, three experimental cells already present were investigated (cells 1, 3, and 4, Bossé et al., 2015). For each cell, soil samples were collected in triplicate at the surface (0 to 5 cm) close to the roots of each plant (some centimeters from the roots) or in bulk soils located a few meters away from the plants to avoid the influence of plants. To obtain more homogenous representative samples, each of the three topsoil replicates was formed by mixing five soils, collected in 1 m<sup>2</sup> subsamples of bare soil and in close proximity of the roots of five annual plants. These five samples were thoroughly homogenized to form three composite samples. Samples were named as follows: C1BS and C1VS for cell 1 with “BS” for bare soils and “VS” for soils with plants and with 1, 2, and 3 as replicates; C3BS and C3VS for cell 3, and C4BS and C4VS for cell 4. All 18 samples were immediately placed in Falcon tubes and stored in the field in coolers containing blocks of ice and transported to laboratory where they were stored at −20°C until DNA extraction. One tube from each site was stored at 4°C for physicochemical analyses.

## Physicochemical Characterization

The chemical composition of the samples was determined using X-ray fluorescence (XRF, Epsilon 4 Model, Malvern Panalytical). The device contains a kV tube with a silver (Ag) anode that produces X-rays. Its detector energy resolution was 4,000–50,000 keV. The samples were ground to a powder to obtain a particle size close to that of standards. The quality of the data was assessed using duplicate sample analyses, and measurement accuracy was estimated at ± 5% for all the elements analyzed. The total organic carbon was determined by potassium bichromate digester (Behrotest Heiz block K-40). The total nitrogen was measured using sulfuric acid–salicylic acid digestion following Kjeldahl method adjusted (Bremner, 1960) and determined by Kjeldahl K-375 BUCHI Kjel Master analyzer. The pH was measured by WTW/INOLAB pH710 following the pH-meter instructions. Hundred milliliters of soil suspension was prepared in distilled water with a ratio of 1:5, then pH was measured using 1 mol/L of KCl.

## DNA Extraction and Amplification Using Illumina MiSeq Sequencing

Soil DNA was extracted in triplicates using the DNeasy® PowerMax® Soil kit Qiagen following the manufacturer's instructions. All extracted genomic DNA samples were stored at −20°C until further analysis. Amplicon libraries were constructed according to ADNid<sup>2</sup> dual indexing strategy. The universal primer set 519F (S-D-Arch-0519-a-S-15) (5'-CAGCMGCCGCGGTAA-3') and 805R (S-D-Bact-0785-a-A-21) (5'-GACTACHVGGGTATCTAATCC-3') designed to target bacterial and archaeal taxa (Klindworth et al., 2013) was used to amplify a 286-bp region targeting the V4 region of 16S rRNA genes. Amplicons were generated using Hot start DNA polymerase (QIAGEN). First, PCR (PCR1) was performed on 10 ng of template DNA in 15 µl total mix, submitted to an initial

denaturation of 5 min at 95°C, followed by 35 cycles of 30 s at 95°C, 1 min at 60°C, and 30 s at 72°C. A final extension of 30 min at 60°C completed the reaction. Amplicons were checked on 1.5% agarose gel and purified using AMPure beads. A second PCR step (PCR2) was performed using a specific Illumina adapter, the index and the Illumina overhang adapter primers in 2 × KAPA Hifi Hotstart Ready Mix (Roche, Switzerland). A previously prepared 5-µl volume of PCR products was used to obtain a final volume of PCR mix of 50 µl. A 3-min denaturation step at 95°C was performed followed by 12 cycles of 30 s at 95°C, 30 s at 55°C, 30 s at 72°C, and a final 5-min extension step at 72°C. PCR2 products were purified (AMPure Beads), quantified (Nanodrop, Spark), normalized at 15 ng/µl, and pooled in a final library. The library was then purified using AMPure Beads, and its quality was checked using a fragment analyzer. Final quantification was performed by qPCR (KAPA library quantification Kits, Roche, Switzerland). Sequencing runs, generating 2 bp × 250 bp, reads were performed on an Illumina MiSeq using V2 chemistry.

## Sequence Analysis of Metabarcoding Datasets

The sequencing data analysis was conducted using FROGS v3.1.0 (Find Rapidly OTUs with Galaxy Solution, Escudié et al., 2018). Briefly, paired reads were merged using FLASH (v1.2.11, Magoc and Salzberg, 2011) with a minimum length of 240 bp and an overlap length of 270 bp. After denoising and removal of primer/adapters with cutadapt (v1.18, Martin, 2011), *de novo* clustering was implemented with SWARM (v2.2.2), which uses a local clustering threshold (Mahé et al., 2015), with an aggregation distance of  $d = 3$ . Chimeric sequences were removed using VSEARCH (v2.91, Rognes et al., 2016). The dataset was filtered, and sequences present in less than two samples and sequences representing less than 0.005% of the total set of sequences were discarded, as recommended by Bokulich et al. (2013). The taxonomic affiliation of operational taxonomic units (OTUs) was performed using Blastn<sup>+</sup> against the Silva database (release 132, December 2017) for 16S rRNA gene amplicons using an innovative multi-affiliation output to identify conflicting sequences in the database and uncertainties (Escudié et al., 2018).

## Statistical Analysis and Predictive Metagenome Analysis

All statistical analyses were performed using R software<sup>3</sup> unless otherwise stated. The alpha diversity statistics were calculated for each sample, and the rarefaction curves and the diversity indexes (Chao1, Shannon, and Simpson) were generated. The variation of beta diversity was graphically illustrated using non-metric multidimensional scaling (nMDS) analysis. Environmental variables were vector fitted to the nMDS ordination plots using the function “envfit” in the R “vegan” package to assess possible explanatory variables. Analysis of variance (ANOVA) was used at 95% confidence level and was completed by Tukey's *post hoc* test to analyze significant distribution of the chemical parameters. Pearson

<sup>2</sup>www.qualtech-groupe.com, Montpellier, France

<sup>3</sup>v3.6.0, <http://www.r-project.org/>



correlations were used to assess the relationships between environmental factors, and the microbial community diversity. A linear discriminant analysis effect size (LEfSe) method (Segata et al., 2011) was also used to identify statistically significant microbial indicators associated with each cell and to identify the most discriminating clades. This analysis was done through the online interface at <https://huttenhower.sph.harvard.edu/galaxy>. Network analysis was used to reveal the relationship between genera present in bare soils and those present in soils sampled near plants. The preparation of data for network analysis was carried out using “psych” package as described by Batushansky et al. (2016). The “*r* coefficient” and “*p*-value” tables were generated, and only significant interactions were selected and visualized using Cytoscape V3.8.0 with the organic layout. The nodes represent the genera that differed significantly between bare soil and soil near the plant roots ( $p < 0.05$ ) based on the results of ANOVA, and the edges represent the correlation between these genera.

Finally, PICRUST2 (phylogenetic investigation of communities by reconstruction of unobserved states, Douglas et al., 2020) analysis was used to explore the possible functional profiles of the microbial communities. This was done following the pipeline command «`picrust2_pipeline.py`» using the “-stratified” flag as described in the PICRUST2 GitHub<sup>4</sup>. The weighted Nearest Sequences Taxon Index (NSTI) was calculated to assess the accuracy of the PICRUST2 analysis (Langille et al., 2013). The EC table resulting from PICRUST2 was filtered, and only enzymes that contribute to pathways of interest in the present study were retained, i.e., phosphate solubilization, nitrogen metabolism, thiosulfate oxidation, cellulase degradation, and indole 3-acetic acid (IAA) and siderophore production. Phosphate solubilization in soil can be catalyzed by bacteria that produce enzymes including phosphatases, phosphonates, phytases, and C-P lyase (Billah et al., 2019; Prabhu et al., 2019). For all other metabolisms, our study was based on the pathways published by the MetaCyc database<sup>5</sup>. To determine the presence of a function in one of the genera detected, all the enzymes involved in the given function's pathway must be present in the same genus. The number of enzymes/functions was converted to “1” if present and to “0” if absent, and a presence/absence heatmap was then constructed using the “ggplot2” package.

## RESULTS

### Physicochemical Characteristics of Phosphate Mine Wastes in Morocco

The environmental characteristics of soil samples in the three cells are presented in **Figure 1**. ANOVA was used to test differences in geochemical factors among the samples and was completed with Tukey's *post hoc* test at a confidence interval of 95%. Phosphate mining wastes were highly alkaline (pH 8–9) with low nutrient contents [total organic carbon (TOC) between 0.3 and 0.4%, and total nitrogen (N) < 0.034%] but very

high level of  $P_2O_5$  ( $> 75 \text{ g kg}^{-1}$ ). Significant differences were observed between five parameters, pH,  $SiO_2$ ,  $P_2O_5$ ,  $Fe_2O_3$ , and to a lesser extent in MgO between the two types of phosphate mine wastes, phosphate waste rocks (cells 1 and 4), and phosphate sludge (cell 3). pH,  $SiO_2$ ,  $P_2O_5$ , and MgO concentrations were statistically higher in phosphate sludge than in waste rocks. Inversely, concentrations of  $Fe_2O_3$  were higher in waste rocks. No clear differences were found in many elements, including TOC, N, or CaO, between the three cells thus between the two types of phosphate wastes. No significant differences were found inside cells, between soils sampled near plants, and bare soils, except for TOC and N in cell 3, where the highest percentage was found in C3VS. No differences in  $K_2O$ ,  $TiO_2$ , and  $Al_2O_3$  were observed between samples.

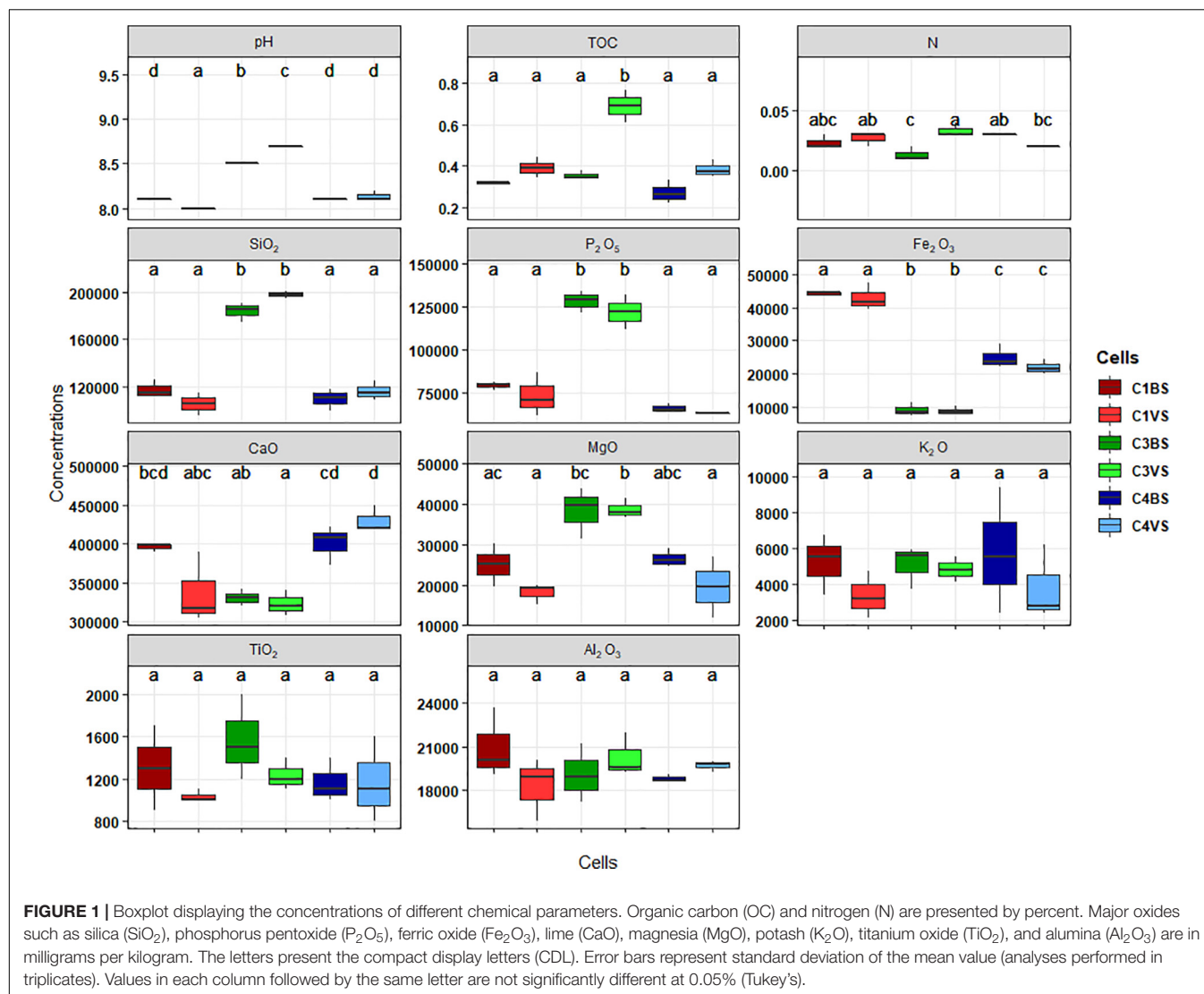
### Diversity and Taxonomic Assignment of Microbial Communities in Phosphate Wastes

A total of 8,507,878 sequences paired-end reads were obtained from the samples collected in 18 phosphate mine wastes. After cleaning and processing, 7,633,309 high-quality sequences were obtained with an average of 428,414 sequences per sample. The number of sequences per sample was then made equal by random resampling (191,792 sequences per sample, based on the smaller number of sequences) giving 3,452,256 good-quality reads. At 97% similarity, all effective normalized sequences were distributed among 869 microbial OTUs (**Supplementary Table 1**). Rarefaction curves achieved an asymptote for all samples, suggesting that almost all OTUs were detected (**Supplementary Figure 2**). The number of OTUs estimated by Chao1 was also very similar to the richness (observed number of OTUs), ranging, respectively, from 650 to 800 for Chao1 and from 640 to 800 for richness, confirming that virtually all the microbial diversity was explored (**Supplementary Figure 3**). No statistical differences were observed between different cells but statistical differences were found between bare soils (C1BS, C3BS, and C4BS) and soils located near plants (C1VS, C3VS, and C4VS), with systematically higher richness and Chao1 in soils near plants than in bare soils. No statistical differences in Shannon and Simpson indices were found in the three cells or between bare soils and soils near plants, except for C4BS, which had lower Shannon and Simpson values.

Exploration of taxonomic composition revealed that the 869 bacterial and archaeal OTUs were assigned to 19 phyla with only two Archaea (this kingdom represented only 0.11% of the total sequences, **Figure 2A**). Over 98% of the OTUs were assigned to a taxonomic phylum with 80% confidence. Across all 18 samples, *Proteobacteria* (51.3%), *Bacteroidetes* (22%), *Actinobacteria* (9.3%), and *Gemmatimonadetes* (7.9%) were the dominant phyla represented by more than 90% of all sequences. For Bacteria, at the genus level, 59.7% of sequences were attributed to known genera, 22.1% to unknown genera, and 18.2% were multi-affiliated (**Supplementary Table 2**). The majority of sequences were affiliated to the genera *Massilia* (9.4%), *Sphingomonas* (5.7%), *Adhaeribacter* (3.9%), and *Hymenobacter* (2.7%, **Figure 2B** and **Supplementary Table 2**). Only 18 genera

<sup>4</sup><https://github.com/picrust/picrust2/wiki/Full-pipeline-script>

<sup>5</sup><https://biocyc.org/>



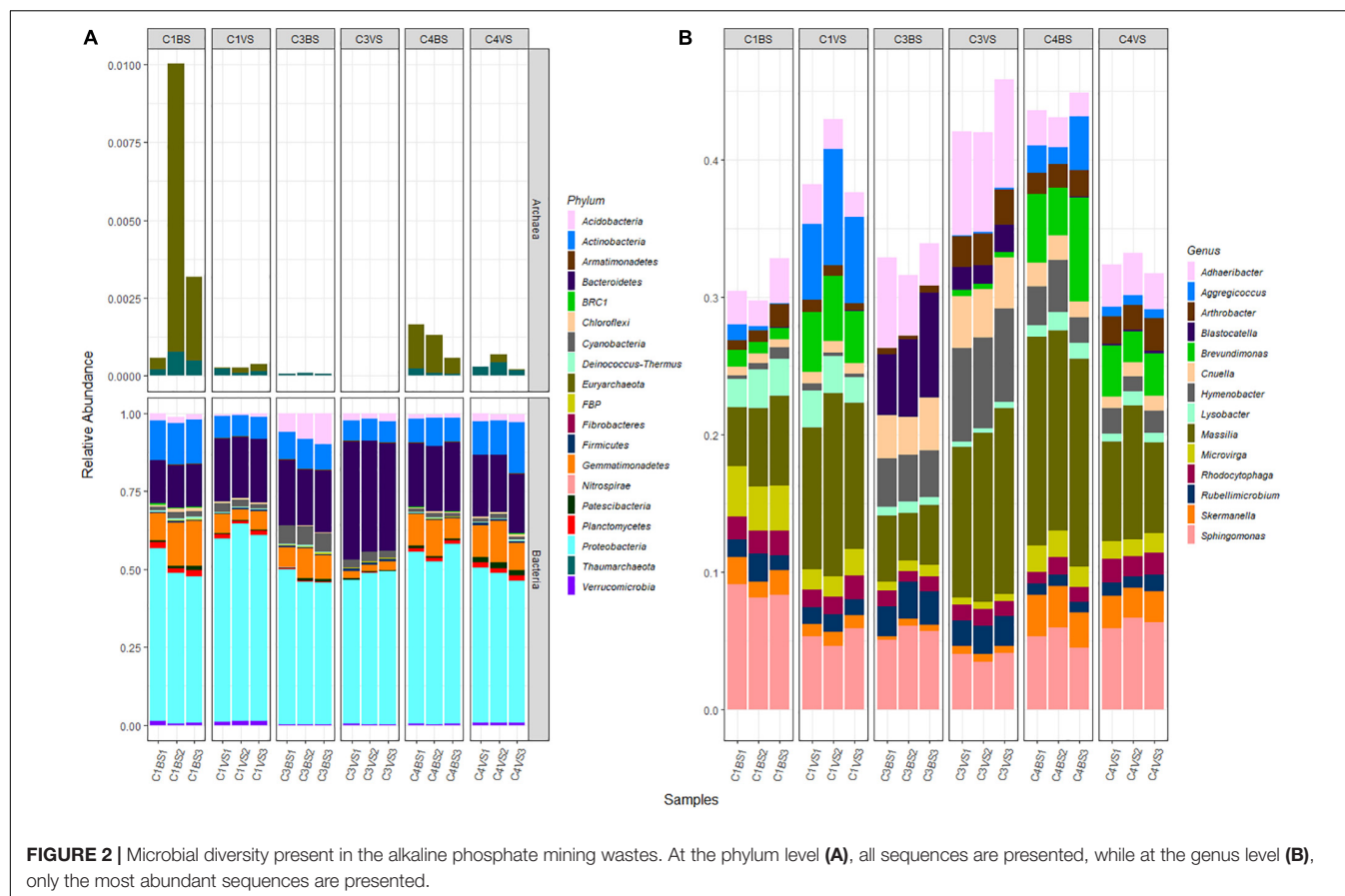
had more than 1% of total sequences. For Archaea, up to 82.7% of sequences were affiliated to *Euryarchaeota* phylum and to unknown genera, while the remaining 17.3% were affiliated to *Thaumarchaeota* phylum, among which 70.8% were multi-affiliated to different genera of the *Nitrososphaeraceae* family and 29.2% were affiliated to the genus *Nitrososphaera*.

## Structure of Microbial Communities in Phosphate Mining Wastes and the Effect of Plants

nMDS ordination and PERMANOVA was performed to explore the relationships between the structure of the microbial communities and the physicochemical characteristics of the phosphate mining wastes (Figure 3 and Supplementary Table 3). Phosphate sludge (six replicates of cell 3) and waste rocks (12 replicates of cell 1 and cell 4) were clearly separated along the first ordination axis. The second axis separated samples into two distinct groups, bare soils in all three

cells and those of soils sampled near plants. This result was confirmed by statistical analysis using Jaccard dissimilarities (PERMANOVA,  $p$ -value = 0.002), indicating that community composition differed significantly between the two types of mine wastes and between soils near plants and bare soils (Supplementary Table 3). Vector fitting of environmental parameters on nMDS revealed that  $\text{P}_2\text{O}_5$ , pH,  $\text{SiO}_2$ , and  $\text{MgO}$  were positively correlated with cell 3 and separated the two types of phosphate mining wastes (Figure 3 and Supplementary Table 4).  $\text{Fe}_2\text{O}_3$  and, to a lesser degree,  $\text{CaO}$ , were negatively correlated with the first four parameters and were more abundant in cell 1 and cell 4. Vector fitting also revealed that TOC and, at a lesser degree, N, were positively correlated with soils near plants.

Among the 130 identified genera, Pearson analysis indicated that 79 were significantly correlated with environmental variables (Figure 4). Many correlations were observed with  $\text{SiO}_2$  (35),  $\text{P}_2\text{O}_5$  (31), pH (31),  $\text{Fe}_2\text{O}_3$  (30),  $\text{MgO}$  (21), TOC (17),  $\text{CaO}$  (18), and N (9) but only one with  $\text{Al}_2\text{O}_3$  and  $\text{TiO}_2$ . For



SiO<sub>2</sub>, P<sub>2</sub>O<sub>5</sub>, pH, Fe<sub>2</sub>O<sub>3</sub>, MgO, and TOC, 20, 18, 14, 20, 11, and 14 genera were, respectively, positively correlated, whereas 15, 13, 17, 10, 10, and 3 were negatively correlated. All 18 correlations found for CaO were positive, and all nine correlations found for N were negative. Very similar correlation indices were also observed between P<sub>2</sub>O<sub>5</sub>, pH, SiO<sub>2</sub>, and, to a lesser extent, MgO, with relatively dominant genera such as *Adhaeribacter*, *Hymenobacter*, and *Cnuella* positively affected, while *Brevundimonas*, *Arctibacter*, and *Devosia* were strongly negatively affected. The LEfSe analysis identified 9, 20, and 11 bacterial taxa, containing 3, 10, and 6 genera that statistically distinguished, respectively, cell 1, cell 3, and cell 4 (with LDA score > 2, Figure 5). The family *Hymenobacteraceae* was the most differentially abundant taxon with a LDA score > 4, reflecting higher abundance in cell 3 than in cells 1 and 4. At the genus level, *Adhaeribacter*, *Cnuella*, *Blastocatella*, *Tychonema*, *Bdellovibrio*, *Segetibacter*, *Rubritepedia*, *Deinococcus*, *Pajaroellobacter*, and *Nostoc* were overrepresented in cell 3. In cell 1, only *Marmoricola*, *Bacillus*, and *Myxococcus* were prevalent, while in cell 4, *Skermanella*, *Sphingaurantiacus*, *Ohtaekwangia*, *Geodermatophilus*, *Solirubrobacter*, and *Pedomicrobium* were more abundant. These 19 genera were also highlighted by Pearson's correlation. A correlogram of these core genera separated them into two distinct groups (Figure 6). The first group contained all genera found in the phosphate sludge (cell 3) identified by LEfSe and presented quite strong positive

correlations among themselves and negative correlations among genera sampled in phosphate waste rocks (except for *Bdellovibrio*, which was positively correlated with *Ohtaekwangia*). The second group comprised genera retrieved in phosphate waste rocks (cells 1 and 4), and correlations between members of this group were generally positive, while correlations with phosphate sludge were negative.

Network analysis was also used to identify the relationships between genera found in bare soils and in soils sampled near annual plants (Supplementary Figure 4). Fifteen genera were found to be significantly associated with bare soils and 16 were shown to be more abundant in soils near plants.

## Potential Plant Growth Promotion Traits of Microbial Communities of Phosphate Wastes

PICRUSt2 analysis was used to explore the possible metabolic pathways associated with microbial communities in phosphate wastes (Figure 7). The NSTI values < 0.06, confirmed the prediction accuracy (Supplementary Table 5). All 130 OTUs affiliated to known genera were predicted to possess at least one of the interesting enzymes involved in important traits related to plant development. For the phosphate solubilization, 102 genera were predicted to possess the alkaline phosphatase enzyme while only 39 were predicted to possess phytase 1, 23 acid phosphatase,

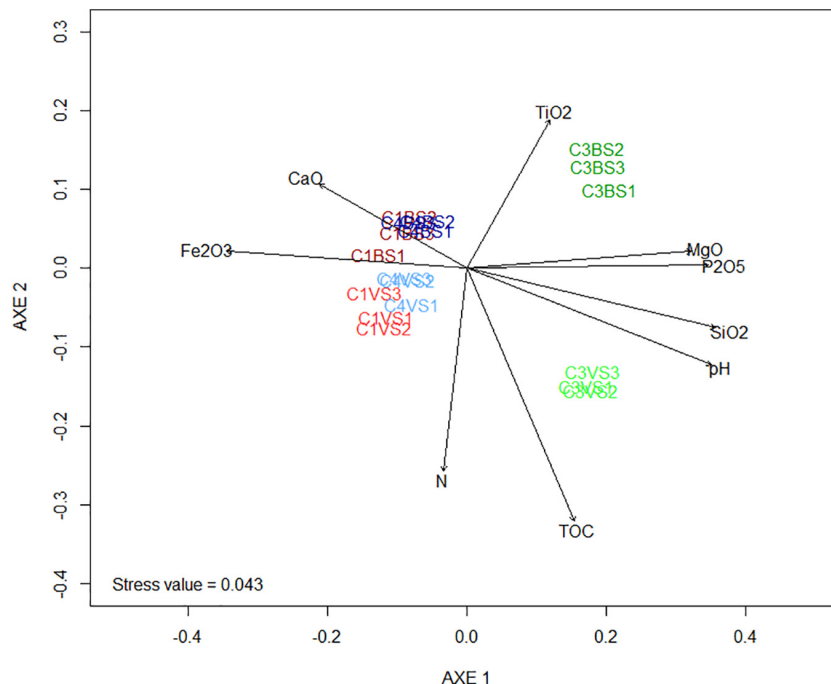


**FIGURE 3 |** Non-metric multidimensional scaling (NMDS) presenting the differences of the microbial communities between the different replicates of phosphate mining waste samples. The stress values were  $< 0.05$ , indicating that these data were very well represented by the two-dimensional representation. Arrows are the projections of possible explanation variables obtained by vector fitting. Only correlations with a false discovery rate (fdr) corrected  $p < 0.05$  were indicated. The angle and length of the vector indicate the direction and strength of the variable. The  $r^2$  correlation coefficient and the  $p$ -values are presented in **Supplementary Table 3**.

18 C-P lyase, 8 phosphonate, and only 4 phytase 2. The OTUs assigned to *Novosphingobium* appeared to have all the phosphate-solubilizing enzymes except C-P lyase. For nitrogen metabolism, all genera were predicted to possess at least one of the seven enzymes involved in N assimilation and referenced in PICRUSt2 and also to produce nitrate-reducing enzymes. Only 2 genera were predicted to be able to oxidize ammonia (*Nitrosomonas* and the archaea *Nitrososphaera*), 59 were predicted to reduce nitrite, and 10 to fix nitrogen. For phytohormones production, 96 genera were predicted to possess at least one enzyme involved in different auxin biosynthesis pathways. Twenty-six genera were predicted to possess the thiosulfate oxidation enzyme and only 14 to biosynthesize aerobactin, an enzyme involved in siderophore production.

## DISCUSSION

### Characteristics of Phosphate Mining Wastes and Development of Plants

Many mine tailings disposed in artificial dumps have not been subject to the long-term natural soil formation processes, representing challenging conditions for biota (Cross and Lambers, 2017). Mine wastes containing generally ultrafine particles, present also often dysfunctional and unstable physical and geochemical structures, altered or inadequate hydrological functioning, associated generally with extreme pH, limited

concentrations of organic material and nutrients, and often presenting an accumulation of toxic or radioactive substances (Cross and Lambers, 2017; Cross et al., 2017). The phosphate mine wastes in the present study share many of these characteristics with highly alkaline soils (pH 8–9), very low levels of nutrients (TOC and N), very high concentrations of  $P_2O_5$  (mass percent between 10% and 20%) and associated with high levels of hazardous contaminants (e.g., Sr, Cr, Cd, or F, Hakkou et al., 2016). Phosphate mine wastes mainly comprise ultrafine material with significant quantities of calcite and dolomite (Hakkou et al., 2009). In arid and semi-arid areas, soils present usually low moisture content and limited organic matter associated with extreme temperatures and irradiance (Padmavathiamma et al., 2014). They are also quite often saline, because of the high evaporation rate and the low water infiltration (Mendez and Maier, 2008). However, phosphate mine wastes in this study were not saline according to their electrical conductivity (Table 1). All these harsh properties could explain the almost absence of plants.

### Structure of Microbial Communities and Potential Physicochemical Drivers

Characterization of the microbial communities in phosphate wastes enabled most OTUs to be classified at the phylum level; whereas, only 55.3% of sequences were classified at the genus level. The high proportion of unclassified genera suggests the presence of possible novel microorganisms and is in



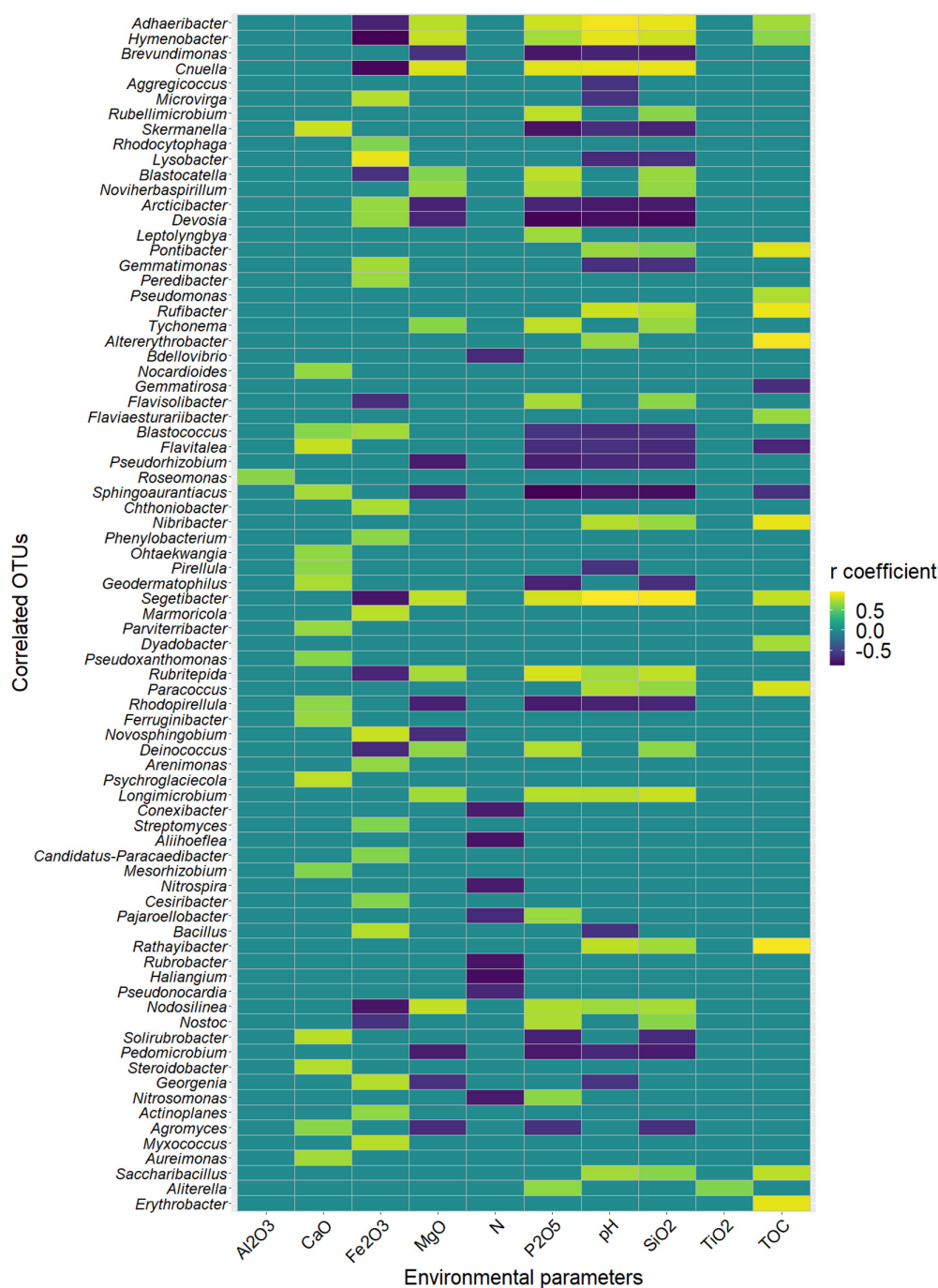
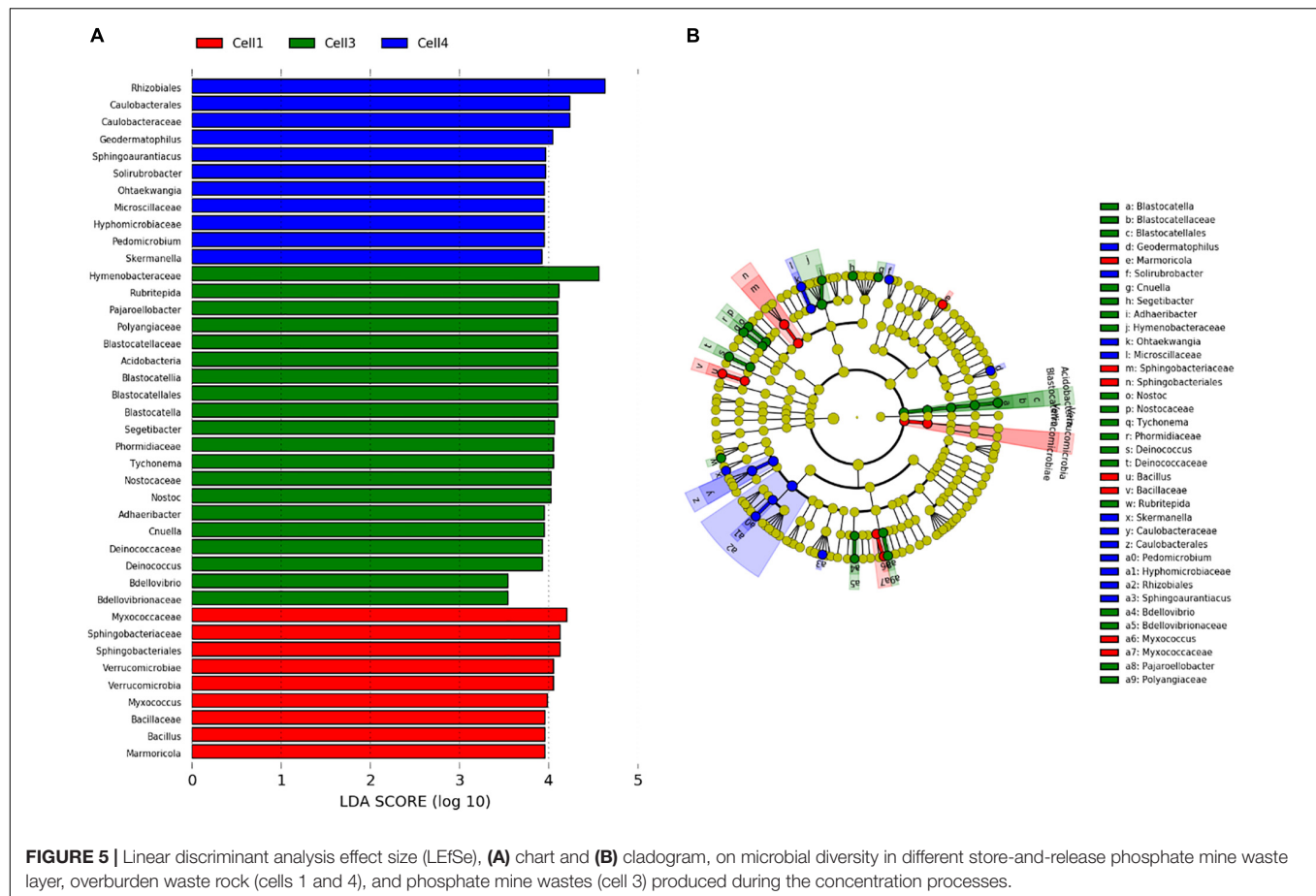


**FIGURE 4 |** Heatmap of the statistically significant coefficients of Pearson's correlations (false discovery rate (fdr) corrected;  $p < 0.05$ ) between the relative abundance of taxa and concentrations of environmental parameters across all sites. Only threshold higher than 0.7 was plotted.

agreement with the results of many studies conducted in mining environments (Bruneel et al., 2017; Liu et al., 2019). Around 90% of sequences belonged to only four phyla *Proteobacteria*, *Bacteroidetes*, *Actinobacteria*, and *Gemmatimonadetes*, and the dominant genera were identified as *Massilia*, *Sphingomonas*, *Adhaeribacter*, *Hymenobacter*, and *Brevundimonas*. Archaea formed a very small minority, and only one genus was identified,

*Nitrososphaera*. Zouch et al. (2017) obtained similar results for phosphogypsum in Tunisia, where Archaea accounted for only 1.5% of the microbial community and no more than 3% in pyrrhotite mine tailings of Kettara (Bruneel et al., 2017). Among the 130 identified genera, only 18 had more than 1% of the total number of sequences. This is in agreement with the results obtained by Trifi et al. (2020), indicating that in



Tunisia, phosphogypsum contained only five low abundance genera (between 1 and 5% of sequences) out of the 193 detected.

The composition of microbial communities differed significantly between the two types of mining wastes and was affected by soil chemical properties, particularly soil pH,  $P_2O_5$ ,  $Fe_2O_3$ ,  $MgO$ ,  $CaO$ , and  $SiO_2$ . Phosphorus and pH have been recognized as drivers of microbial communities, and pH is generally recognized to be the best predictor of microbial composition and diversity (Rousk et al., 2010; Wu et al., 2018; Ye et al., 2020).

Our investigation, combining Pearson correlations and LefSe, also identified 19 genera divided into two groups, those found in phosphate sludge and those found in phosphate waste rocks. These core genera probably have significant functions in phosphate mining wastes, but, apart from *Bacillus*, *Nostoc*, and, to a lesser extent, *Myxococcus*, many of them are not known as PGP microorganisms such as *Adhaeribacter*, *Cnuella*, *Blastocatella*, *Tychonema*, *Sphingaurantiacus*, *Segetibacter*, *Rubritepida*, *Deinococcus*, and *Pajaroellobacter* (Supplementary Table 6). Other genera possessed only few PGP traits: *Skermanella*, *Geodermatophilus*, and *Marmoricola* are involved in nitrogen cycling, *Ohtaekwangia* sp. displays antimicrobial activity, *Solirubrobacter* sp. is able to degrade cellulose, or *Bdellovibrio* and *Myxococcus*, which are known to be predators of other bacteria.

The composition of the microbial communities differed significantly between bare soils and soils sampled near plants. Richness and estimated OTUs were also higher in wastes associated with plants than in bare soils in all the three cells. Although our study did not analyze the rhizosphere, the proximity of plants appeared to have an impact on the structure of microbial communities, and organic carbon and N were identified as the main drivers. This is consistent with many studies reporting differences in the diversity and taxonomic composition of microbial communities in bulk soils and in the rhizosphere (Edwards et al., 2015; Luo et al., 2018; Orozco-Mosqueda et al., 2020; Ye et al., 2020). Plant species or even genotypes are also known to select divergent microbial communities (Bulgarelli et al., 2013; Edwards et al., 2015; Ye et al., 2020). This is usually explained by the presence of many elements exuded by roots including sugars, amino acids, and organic acids, which can account for one-third of the carbon fixed by plants (Bulgarelli et al., 2013; Edwards et al., 2015; Olanrewaju et al., 2017). Many significantly different genera were observed in soils near plants and in bare soils, but no clear differences were observed concerning their potential PGP traits as symbiotic  $N_2$  fixers, contrary with that reported by Luo et al. (2018). Although in agreement with Ye et al. (2020) in phosphogypsum, the relative abundance of three genera (*Blastocatella*, *Thermithiobacillus*, and *Sphingomonas*) was higher in soils associated with plants.

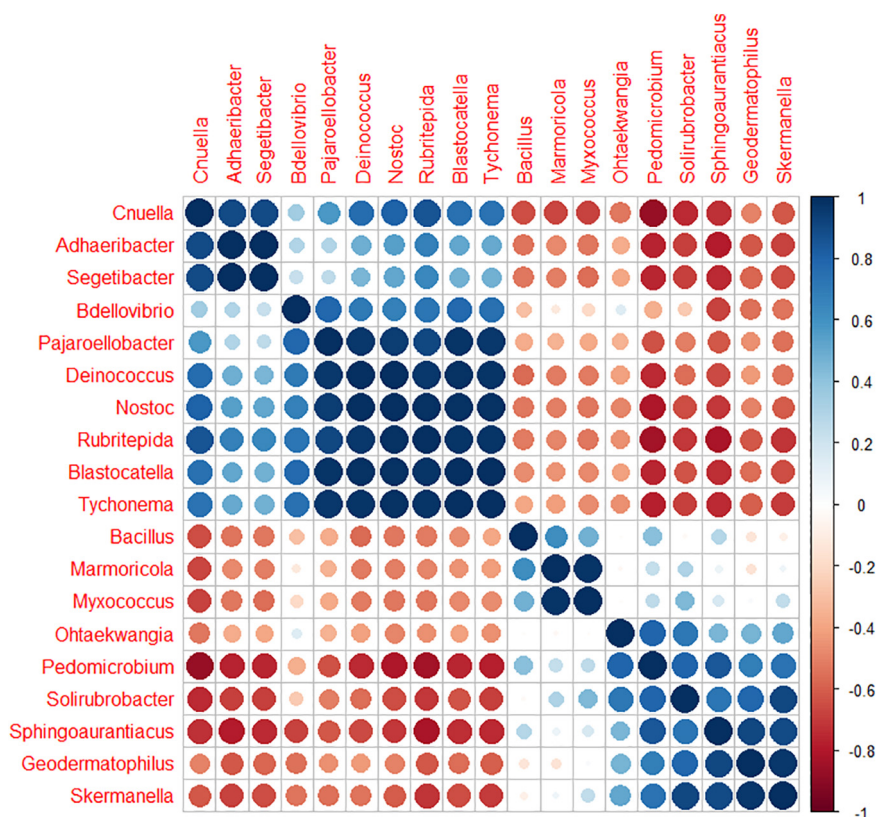


**FIGURE 6 |** Correlogram representing the Pearson's correlation coefficient  $r^2$  between the 19 key bacterial genera ordered by the "hclust" method.

Other factors affect the abundance, structure, and activity of microbial communities, including the type, properties, and texture of the soil, as well as climatic conditions (Edwards et al., 2015; Luo et al., 2018; Ye et al., 2020). The structure of the microbial communities analyzed in this study differed from that identified in other studies conducted in phosphate mine wastes, such as in Ragot et al. (2013) using T-RFLP and clone libraries to study apatite, the principal phosphate mineral. Next-generation sequencing are generally used to investigate microbial communities in phosphate mining area in China (Ye et al., 2020) and in phosphogypsum in Portugal (Martins et al., 2016), in China (Wang et al., 2018), or in Tunisia (Zouch et al., 2017; ben Mefteh et al., 2019; Trifi et al., 2020). However, phosphogypsum, the main byproduct of phosphoric acid, obtained after sulfuric acid digestion, present clearly different physicochemical characteristics, compared with phosphate wastes in this study. Nevertheless, our microbial communities were quite similar to those associated with turfgrass seeds of three turf species (*Festuca rubra*, *Lolium arundinacea*, and *Lolium perenne*) in low moisture climates (annual precipitation < 750 mm), containing a majority of *Proteobacteria* (89%) followed by *Actinobacteria* (6%, Chen et al., 2020). At the genus level, Chen et al. (2020) found a high proportion of *Massilia* (25%), and *Pseudomonas* (29%), followed by *Sphingomonas* (6%), *Paenibacillus* (3%), *Pedobacter* (1%), *Flavobacterium*, and *Chryseobacterium* (< 1%). This structure is also quite similar to the core of phyllosphere

communities composed of *Pseudomonas*, *Sphingomonas*, *Methylobacterium*, *Bacillus*, *Massilia*, *Arthrobacter*, and *Pantoea* (Bulgarelli et al., 2013).

## Potential Ecological Role in Plant Growth-Promoting Traits

Surprisingly, a huge number of microorganisms recognized as potential PGP genera, were found in alkaline phosphate mining wastes according to the PICRUSt2 predictions. Indeed, all 130 OTUs assigned to known genera were predicted to possess at least one enzyme involved in plant growth-promoting traits. These results are quite consistent with the literature and show that a very large proportion of our sequences (66.15%) resemble microorganisms that contain isolated strains known to present one plant growth-promoting trait (**Supplementary Table 6**). Many sequences were similar to very well-known PGP genera such as *Pseudomonas*, *Bacillus*, *Arthrobacter*, *Azospirillum*, *Herbaspirillum*, *Rhizobium*, *Flavobacterium*, *Variovorax*, *Streptomyces*, *Sphingomonas*, and *Paenibacillus* (Goswami et al., 2016, **Supplementary Table 6**). Some of these microorganisms are also currently sold in international markets as biofertilizers or biocontrol agents (Bio-Save®, Mycostop®, Galltrol-A, etc.) and are used by farmers in the field as inocula (Goswami et al., 2016; Pathak and Kumar, 2016; Kumari et al., 2019). Many of the most abundant sequences, representing



**FIGURE 7 |** Binary heatmap highlighting presence (■) absence (■) of the interested enzymes in identified genera. Enzymes implicated in: cellulose degradation by producing the cellulase enzyme (EC:3.2.1.4); sulfur metabolism by oxidizing thiosulfate (EC:1.8.2.2); siderophores production by catalyzing aerobactin biosynthesis pathway (EC:1.14.13.59, EC:2.3.1.102, EC:6.3.2.38 and EC:6.3.2.39); phosphate solubilization by producing either one or multiple of the enzymes C-P lyases (EC:4.7.1.1), phytase 1 (EC:3.1.3.8), phytase 2 (EC:3.1.3.26), alkaline phosphatase (EC:3.1.3.1), acid phosphatase (EC:3.1.3.2), and phosphonate (EC:3.11.1.1); nitrogen metabolism by catalyzing at least one of the following pathways: nitrogen fixation I (ferredoxin) (EC:1.18.6.1), ammonia assimilation cycle I (EC:6.3.1.2 and EC:1.4.1.14); ammonia assimilation cycle II (EC:6.3.1.2 and EC:1.4.7.1), ammonia assimilation cycle III (EC:6.3.1.2 and EC:1.4.1.13), ammonia oxidation I and IV nitrite producing (EC:1.14.99.39 and EC:1.7.2.6), nitrate reduction VI L-glutamine forming (EC:1.7.7.2, EC:1.7.7.1, and EC:1.4.1.4), and finally in auxin biosynthesis by producing enzymes implicated in indole-3-acetate biosynthesis III (EC:1.13.12.3 and EC:3.5.1.4, or in indole-3-acetate biosynthesis IV (EC:4.2.1.84 and EC:3.5.1.4) or in indole-3-acetate biosynthesis V (EC:3.5.5.1).



more than 1% of the total sequences, also possessed many plant growth-promoting traits including *Massilia*, *Brevundimonas*, *Lysobacter*, or *Noviherbaspirillum* or genera belonging to *Hymenobacteraceae* family (identified by LEfSe as very abundant in phosphate sludge) comprising *Adhaeribacter*, *Hymenobacter*, *Pontibacter*, or *Rufibacter*.

According to PICRUSt2 prediction, all the microorganisms possessed at least one of the five enzymes involved in nitrogen cycling and more than 43 genera possessed isolated strains implicated in nitrogen cycling (**Supplementary Table 6**). Among them, *Rhizobium* is the main contributor to symbiotic nitrogen fixation in legume crops (Pathak and Kumar, 2016), but many free-living nitrogen fixers were also present, including *Azospirillum*, *Herbaspirillum*, *Bacillus*, or *Paenibacillus* (Goswami et al., 2016). *Azospirillum* is thought to fix from 5 to 20 kg/ha/year of N<sub>2</sub>, corresponding between 20 and 25% of total nitrogen required by maize or rice (Pathak and Kumar, 2016). For Archaea, *Nitrososphaera* is known to be an ammonia-oxidizing archaeon (Stieglmeier et al., 2014) and could thus contribute to the global nitrogen cycle in soils via nitrification (Hatzenpichler, 2012). According to metagenome functional prediction, 95% of the genera identified possess enzymes involved in phosphate solubilization and 44 of our sequences resembled genera containing isolated strains with phosphate solubilization capacity and comprising very well-known phosphate solubilizers (**Supplementary Table 6**). These results are in agreement with those of Khan et al. (2007) and Goswami et al. (2016), who showed that phosphate-solubilizing microorganisms could account for, respectively, from 1 to 50% and 20 to 40% of culturable populations in the soil. Among dominant genera, *Massilia* could also play a key role and a novel species, *M. phosphatilytica*, has been described with a phosphate-solubilizing potential of 40.32 µg in 48 h (Zheng et al., 2017). Potassium, calcium, or zinc solubilizers such as *Pseudomonas*, *Paenibacillus*, *Pontibacter*, *Variovorax*, or *Bacillus* improve plant nutrition and were also retrieved in our sequences (**Supplementary Table 6**). For iron, 14 genera could possess enzymes involved in this pathway, as predicted by PICRUSt2 and 36 sequences resembled genera containing isolated strains that produce siderophores (**Supplementary Table 6**). Sulfate is another important nutrient for plant development (Smith et al., 2000). PICRUSt2 prediction also identified genera increasing the availability of sulfate for plants, 26 genera potentially able to oxidize thiosulfate whereas two genera were found to contain isolated strains involved in sulfur metabolism such as *Thiobacillus* or *Stenotrophomonas*. These bacteria are also able to solubilize phosphate and K/Ca- or Na-bearing minerals due to the large quantity of sulfuric acid they produce (Ullah et al., 2013; Thabet et al., 2017). Microorganisms that produce cellulase which breaks cellulose down, also facilitate plant growth (El-Sayed et al., 2014). PICRUSt2 predicted that 83 genera possess enzymes involved in this pathway, but only eight genera possessed strains able to degrade cellulose. PGP microorganisms also improve soil formation, texture, and structure, by helping to aggregate soil particles through the production of exopolysaccharides that promote the formation of strong biofilms and hence the formation of soil crust (Kaushal and Wani, 2016; Thavamani et al., 2017). Microorganisms

such as *Leptolyngbya*, *Pseudomonas*, or *Rhizobium* that are able to increase soil aggregation were retrieved in our phosphate mining wastes (**Supplementary Table 6**). For phytohormone, 96 genera should produce IAA according to PICRUSt2, while our literature survey indicated that 43 genera contain at least one isolated strain able to produce this hormone (**Supplementary Table 6**). PICRUSt2 prediction was in agreement with other studies showing that around 80% of microorganisms have been documented to produce IAA (Patten and Glick, 1996; Kochar et al., 2013). Strains producing other phytohormones were also retrieved including gibberellin (20 strains) and cytokinin (10 strains, **Supplementary Table 6**).

In alkaline phosphate mining wastes, more than 27 sequences resembled genera containing isolated strains that produce ACCD, able to inhibit the formation of ethylene, the stress hormone with *Sphingomonas*, *Brevundimonas*, *Arthrobacter*, *Devosia*, or *Pseudomonas* being the most abundant (**Supplementary Table 6**). Many microorganisms known to be capable of combat phytopathogens were also retrieved in the present study: *Pseudomonas*, *Bacillus*, *Streptomyces*, *Stenotrophomonas*, *Rhizobium*, or *Streptomyces*, as well as less well-known microorganisms, such as *Massilia* or *Sphingomonas* (**Supplementary Table 6**). *Pseudomonas* sp. is able to inhibit diseases caused by many pathogens and possesses antimicrobial, antifungal, and antiviral properties, in addition to providing protection against insects (Kumari et al., 2019; Pattnaik et al., 2019, **Supplementary Table 6**). These fast-growing genera induce systemic resistance and produce different compounds including antibiotics, polysaccharides, or siderophores (limiting iron for phytopathogens, Santoyo et al., 2012). *Bacillus* sp. is known to produce a wide range of antibacterial and antifungal antibiotics (Goswami et al., 2016). *Streptomyces* are also known to produce many antibiotics (Olanrewaju and Babalola, 2019). Different genera, able to decrease or even suppress development of nematodes, were also retrieved, including *Arthrobacter*, *Pseudomonas*, *Streptomyces*, *Bacillus*, *Rhizobium*, or *Variovorax* (Topalovic et al., 2020). *Sphingomonas* sp. can suppress disease symptoms and limit the growth of the foliar pathogen of tomato, *Pseudomonas syringae* (Bulgarelli et al., 2013). Strains such as *Paenibacillus*, *Streptomyces*, *Bacillus*, or *Pseudomonas* produce lytic enzymes.

Many microorganisms present in our phosphate mining wastes are also related to strains able to improve growth of plants under drought stress; *Pseudomonas*, *Azospirillum*, *Paenibacillus*, *Rhizobium*, *Bacillus*, or *Variovorax* are among these well-known microorganisms (**Supplementary Table 6**). Indeed, *Azospirillum* sp. is able to mediate drought tolerance in many plants, even in deserts, by modifying root development and increasing water contents, grain yield, and mineral quality (Mg, K, and Ca) by producing IAA, gibberellin, or abscisic acid (a stress phytohormone that controls stomatal closure and stress signal transduction, Vurukonda et al., 2016; Fukami et al., 2018). *Bacillus* sp. is also known to increase the growth of *Lavandula* under drought conditions by producing IAA, improving physiology, increasing metabolic activity, and enhancing plant nutrition (Armada et al., 2014). Saline stress is also currently considered to be one of the main constraints

affecting both plants and microorganisms (Kaushal and Wani, 2016; Etesami and Beattie, 2018; Numan et al., 2018; Gupta and Pandey, 2019). Even if electrical conductivity was not high in our study, the high evaporation rate in the area could lead to high salinity in soil surface. Many microorganisms can improve the growth of plants in saline conditions, including strains of *Stenotrophomonas*, *Azospirillum*, *Bacillus*, and *Pseudomonas* (Supplementary Table 6). *Pseudomonas* sp. has been shown to improve the tolerance of wheat seedlings and sorghum to high temperatures by increasing levels of cellular metabolites (Ali et al., 2009; Vurukonda et al., 2016).

Diverse sequences related to resistant genera to different types of metals were identified, reflecting the stressors present in phosphate mining wastes in Morocco (Supplementary Table 6). This was particularly true for three metals that are present in large quantities, Cd, Cr, and Sr. Twenty-six genera contained strains resistant to Cd, but only six were resistant to Cr and four to Sr. High concentrations of Cd can reduce photosynthesis, nutrient, and water uptake, leading to growth inhibition, chlorosis, etc., and finally to death (Yadav et al., 2010). Chromium excess inhibits plant growth, causes nutrient imbalance, chlorosis, and root injury, and affects germination (Yadav et al., 2010), while excess Sr usually inhibits plant growth and weight (Burger and Lichtscheidl, 2019). *Sphingomonas* sp. was shown to actively increase the growth and stress tolerance of many plants in the presence of metals such as cadmium (Asaf et al., 2020, Supplementary Table 6). Long et al. (2017) also highlighted the capacity of *Bacillus* to immobilize Sr from aqueous solution by sorption. Fluorine, also present in quite large quantities in this study, can have also detrimental effects on the environment and human health (Fordyce, 2011; Wang et al., 2018) and can affect the growth of microorganisms (Li et al., 2014). In our phosphate wastes, various microorganisms were related to strains known to be tolerant to fluorine including *Bacillus*, *Actinobacter*, or *Pseudomonas* (Wang et al., 2018, Supplementary Table 6).

In light of these results, the microbial community present in the phosphate store-and-release cover seems not to be responsible for the almost absence of plants, explaining that their supplement in sufficient quantities may help in the phytostabilization of the phosphate cover. Further studies need to be done in order to address this conundrum.

## CONCLUSION

This study examined the composition and structuration of bacterial and archaeal communities in alkaline phosphate mining wastes in a Moroccan mine. The dominant sequences belonged to *Proteobacteria*, *Bacteroidetes*, *Actinobacteria*, and *Gemmatimonadetes* and to the genera *Massilia*, *Sphingomonas*, *Adhaeribacter*, *Hymenobacter*, and *Brevundimonas*. Significant differences in the composition of microbial communities were found between the two types of mining wastes studied (phosphate waste rocks and phosphate sludge), and differences were also found due to the presence of some indigenous annual plants. Soil pH, P<sub>2</sub>O<sub>5</sub>, Fe<sub>2</sub>O<sub>3</sub>, MgO, CaO, SiO<sub>2</sub>, TOC, and N were, respectively, identified as the main drivers influencing microbial

community structure. This study improves our knowledge of the microbial communities present in alkaline phosphate mining wastes. This work also highlights the very high abundance of predicted plant growth-promoting microorganisms that can improve soil formation, nutrient uptake, and alleviating the biotic and abiotic stresses of this harsh environment in semi-arid areas. Furthermore, a great majority of our sequences resemble genera possessing more than one potential plant growth trait, which could be very useful in revegetation projects. In light of these results, the exploration of taxonomic composition of the phosphate store-and-release cover seems not to be able to explain the almost absence of plants, with a quite diversified communities, similar to other studies, without any particular structural issues and with a majority of microorganisms presenting plant growth-promoting factors. This is probably due to the harsh conditions of this damaged soil in semi-arid area that could prevent the plants from growing *in situ*. Future efforts should be oriented toward isolation of these interesting genera, using them as an inoculum to help the growth of local plants in such harsh environment. An in-depth understanding of the phosphate mine waste microbial communities and of their potential metabolic capabilities can provide useful information to prepare media dedicated to the isolation of the most interesting plant growth-promoting microorganisms identified in this study, a work currently in progress.

## DATA AVAILABILITY STATEMENT

The datasets presented in this study can be found in online repositories. The names of the repository/repositories and accession number(s) can be found below: <https://www.ebi.ac.uk/ena, PRJEB39890>.

## AUTHOR CONTRIBUTIONS

OB, LS, ME, and RH designed and contributed to the conception of the work. AO identified the plants and contributed to the sampling along with NM, OB, and RH. NM performed the experiments. NM and OB analyzed the data. RH, ME, AO, and LS contributed to the data interpretation. NM and OB wrote the first draft of the manuscript. All authors reviewed and approved the final version of this manuscript.

## FUNDING

This work was supported by the Moroccan Ministry of Higher Education (MESRSFC), the CNRST under Grant Number PPR1/2015/64, and the Ph.D. fellowship of NM by IRD (French National Research Institute, 2018–2020).

## SUPPLEMENTARY MATERIAL

The Supplementary Material for this article can be found online at: <https://www.frontiersin.org/articles/10.3389/fmicb.2021.666936/full#supplementary-material>

## REFERENCES

- Ali, S. Z., Sandhya, V., Grover, M., Kishore, N., Rao, L. V., and Venkateswarlu, B. (2009). *Pseudomonas* sp. strain AKM-P6 enhances tolerance of sorghum seedlings to elevated temperatures. *Biol. Fertil. Soils* 46, 45–55. doi: 10.1007/s00374-009-0404-9
- Armada, E., Portela, G., Roldán, A., and Azcón, R. (2014). Combined use of beneficial soil microorganism and agrowaste residue to cope with plant water limitation under semiarid conditions. *Geoderma* 232–234, 640–648. doi: 10.1016/j.geoderma.2014.06.025
- Asaf, S., Numan, M., Khan, A. L., and Al-Harrasi, A. (2020). *Sphingomonas*: from diversity and genomics to functional role in environmental remediation and plant growth. *Crit. Rev. Biotechnol.* 40, 138–152. doi: 10.1080/07388551.2019.1709793
- Babi, K., Asselin, H., and Benzaazoua, M. (2016). Stakeholders' perceptions of sustainable mining in Morocco: a case study of the abandoned Kettara mine. *Extr. Indust. Soc.* 3, 185–192. doi: 10.1016/j.exis.2015.11.007
- Batushansky, A., Toubiana, D., and Falt, A. (2016). Correlation-based network generation, visualization, and analysis as a powerful tool in biological studies: a case study in cancer cell metabolism. *BioMed. Res. Int.* 2016:8313272. doi: 10.1155/2016/8313272
- Baycu, G., Tolunay, D., Ozden, H., Csatari, I., Karadag, S., Agba, T., et al. (2015). An abandoned copper mining site in cyprus and assessment of metal concentrations in plants and soil. *Int. J. Phytoremed.* 17, 622–631. doi: 10.1080/15226514.2014.922929
- Bech, J., Roca, N., and Tume, P. (2017). "Hazardous element accumulation in soils and native plants in areas affected by mining activities in south america," in *Assessment, Restoration and Reclamation of Mining Influenced Soils*, eds C. Bini, J. Bech, and M. A. Pashkevich (Amsterdam: Elsevier Inc), 419–461. doi: 10.1016/B978-0-12-809588-1.00016-5
- ben Meftah, F., Bouket, A. C., Daoud, A., Luptakova, L., Alenezi, F. N., Gharsallah, N., et al. (2019). Metagenomic insights and genomic analysis of phosphogypsum and its associated plant endophytic microbiomes reveals valuable actors for waste bioremediation. *Microorganisms* 7:382. doi: 10.3390/microorganisms7100382
- Billah, M., Khan, M., Bano, A., Hassan, T. U., Munir, A., and Gurmani, A. R. (2019). Phosphorus and phosphate solubilizing bacteria: keys for sustainable agriculture. *Geomicrobiol. J.* 36, 904–916. doi: 10.1080/01490451.2019.1654043
- Bokulich, N. A., Subramanian, S., Faith, J. J., Gevers, D., Gordon, J. I., Knight, R., et al. (2013). Quality-filtering vastly improves diversity estimates from *Illumina* amplicon sequencing. *Nat. Methods* 10, 57–59. doi: 10.1038/nmeth.2276
- Bossé, B., Bussiére, B., Hakkou, R., Maqsoud, A., and Benzaazoua, M. (2013). Bewertung von phosphat-kalkstein-abraum als bestandteil einer speicher-verdunstungs-abdeckung unter semiariden bedingungen. *Mine Water Environ.* 32, 152–167. doi: 10.1007/s10230-013-0225-9
- Bossé, B., Bussiére, B., Hakkou, R., Maqsoud, A., and Benzaazoua, M. (2015). Field experimental cells to assess hydrogeological behaviour of store-and-release covers made with phosphate mine waste. *Can. Geotech. J.* 52, 1255–1269. doi: 10.1139/cgj-2014-0263
- Bremner, J. M. (1960). Determination of nitrogen in soil by the Kjeldahl method. *J. Agric. Sci.* 55, 11–33. doi: 10.1017/s0021859600021572
- Bruneel, O., Mghazli, N., Hakkou, R., Dahmani, I., Filali Maltouf, A., and Sbabou, L. (2017). In-depth characterization of bacterial and archaeal communities present in the abandoned Kettara pyrrhotite mine tailings (Morocco). *Extremophiles* 21, 671–685. doi: 10.1007/s00792-017-0933-3
- Bruneel, O., Mghazli, N., Sbabou, L., Héry, M., Casiot, C., and Filali-Maltouf, A. (2019). "Role of microorganisms in rehabilitation of mining sites, focus on Sub Saharan African countries," in *Journal of Geochemical Exploration*, Vol. 205, ed. S. Albanese (Amsterdam: Elsevier B.V.), doi: 10.1016/j.gexplo.2019.06.009
- Bulgarelli, D., Schlaeppli, K., Spaepen, S., van Themaat, E. V. L., and Schulze-Lefert, P. (2013). Structure and functions of the bacterial microbiota of plants. *Annu. Rev. Plant Biol.* 64, 807–838. doi: 10.1146/annurev-arplant-050312-120106
- Burger, A., and Lichtscheidl, I. (2019). Strontium in the environment: review about reactions of plants towards stable and radioactive strontium isotopes. *Sci. Total Environ.* 653, 1458–1512. doi: 10.1016/j.scitotenv.2018.10.312
- Chen, Q., Meyer, W. A., Zhang, Q., and White, J. F. (2020). 16S rRNA metagenomic analysis of the bacterial community associated with turf grass seeds from low moisture and high moisture climates. *PeerJ* 2020:e8417. doi: 10.7717/peerj.8417
- Cross, A. T., and Lambers, H. (2017). Young calcareous soil chronosequences as a model for ecological restoration on alkaline mine tailings. *Sci. Total Environ.* 607–608, 168–175. doi: 10.1016/j.scitotenv.2017.07.005
- Cross, A. T., Stevens, J. C., and Dixon, K. W. (2017). One giant leap for mankind: can ecopiepsis avert mine tailings disasters? *Plant Soil* 421, 1–5. doi: 10.1007/s11104-017-3410-y
- Douglas, G. M., Maffei, V. J., Zaneveld, J. R., Yurgel, S. N., Brown, J. R., Taylor, C. M., et al. (2020). PICRUSt2 for prediction of metagenome functions. *Nat. Biotechnol.* 38, 685–688. doi: 10.1038/s41587-020-0548-6
- Dresler, S., Tyrka, M., Szeliga, M., Ciura, J., Wielbo, J., Wójcik, M., et al. (2015). Increased genetic diversity in the populations of *Echium vulgare* L. colonising Zn-Pb waste heaps. *Biochem. Syst. Ecol.* 60, 28–36. doi: 10.1016/j.bse.2015.03.003
- Edixhoven, J. D., Gupta, J., and Savenije, H. H. G. (2013). Recent revisions of phosphate rock reserves and resources: reassuring or misleading? An in-depth literature review of global estimates of phosphate rock reserves and resources. *Earth Syst. Dyn. Discuss.* 4, 1005–1034. doi: 10.5194/esdd-4-1005-2013
- Edwards, J., Johnson, C., Santos-Medellin, C., Lurie, E., Podishetty, N. K., Bhatnagar, S., et al. (2015). Structure, variation, and assembly of the root-associated microbiomes of rice. *Proc. Natl. Acad. Sci. U.S.A.* 112, E911–E920. doi: 10.1073/pnas.1414592112
- Elfadil, S., Hamamouch, N., Jaouad, A., Mahrouz, M., and Bouchdoug, M. (2020). The effect of phosphate flotation wastes and phosphogypsum on cattle manure compost quality and plant growth. *J. Mater. Cycles Waste Manag.* 22, 996–1005. doi: 10.1007/s10163-020-00997-5
- El-Sayed, W. S., Akhkhia, A., El-Naggar, M. Y., and Elbadry, M. (2014). In vitro antagonistic activity, plant growth promoting traits and phylogenetic affiliation of rhizobacteria associated with wild plants grown in arid soil. *Front. Microbiol.* 5:651. doi: 10.3389/fmicb.2014.00651
- Escudé, F., Auer, L., Bernard, M., Mariadassou, M., Cauquil, L., Vidal, K., et al. (2018). FROGS: find, rapidly, OTUs with galaxy solution. *Bioinformatics* 34, 1287–1294. doi: 10.1093/bioinformatics/btx791
- Etesami, H., and Beattie, G. A. (2018). Mining halophytes for plant growth-promoting halotolerant bacteria to enhance the salinity tolerance of non-halophytic crops. *Front. Microbiol.* 9:148. doi: 10.3389/fmicb.2018.00148
- Fahad, S., Hussain, S., Matloob, A., Khan, F. A., Khaliq, A., Saud, S., et al. (2015). Phytohormones and plant responses to salinity stress: a review. *Plant Growth Regul.* 75, 391–404. doi: 10.1007/s10725-014-0013-y
- Fordey, F. M. (2011). "Fluorine: human health risks," in *Encyclopedia of Environmental Health*, Vol. 2, ed. J. O. Nriagu (Burlington: Elsevier), 776–785.
- Fukami, J., Cerezini, P., and Hungria, M. (2018). *Azospirillum*: benefits that go far beyond biological nitrogen fixation. *AMB Express* 8:73. doi: 10.1186/s13568-018-0608-1
- García-Carmona, M., García-Robles, H., Turpín Torrano, C., Fernández Ondoño, E., Lorite Moreno, J., Sierra Aragón, M., et al. (2019). Residual pollution and vegetation distribution in amended soils 20 years after a pyrite mine tailings spill (Aznalcóllar, Spain). *Sci. Total Environ.* 650, 933–940. doi: 10.1016/j.scitotenv.2018.09.092
- Goswami, D., Thakker, J. N., and Dhandhukia, P. C. (2016). Portraying mechanics of plant growth promoting rhizobacteria (PGPR): a review. *Cogent Food Agric.* 2:1127500. doi: 10.1080/23311932.2015.1127500
- Guo, S., Feng, B., Xiao, C., Wang, Q., and Chi, R. (2021). Phosphate-solubilizing microorganisms to enhance phytoremediation of excess phosphorus pollution in phosphate mining wasteland soil. *Bioremed. J.* 1–15. doi: 10.1080/10889868.2021.1884528
- Gupta, S., and Pandey, S. (2019). ACC deaminase producing bacteria with multifarious plant growth promoting traits alleviates salinity stress in French Bean (*Phaseolus vulgaris*) plants. *Front. Microbiol.* 10:1506. doi: 10.3389/fmicb.2019.01506
- Hakkou, R., Benzaazoua, M., and Bussiére, B. (2008a). Acid mine drainage at the abandoned Kettara mine (Morocco): 1. environmental characterization. *Mine Water Environ.* 27, 145–159. doi: 10.1007/s10230-008-0036-6
- Hakkou, R., Benzaazoua, M., and Bussiére, B. (2008b). Acid mine drainage at the abandoned Kettara mine (Morocco): 2. mine waste geochemical behavior. *Mine Water Environ.* 27, 160–170. doi: 10.1007/s10230-008-0035-7
- Hakkou, R., Benzaazoua, M., and Bussiére, B. (2009). Laboratory evaluation of the use of alkaline phosphate wastes for the control of acidic mine drainage. *Mine Water Environ.* 28, 206–218. doi: 10.1007/s10230-009-0081-9



- Hakkou, R., Benzaazoua, M., and Bussière, B. (2016). Valorization of phosphate waste rocks and sludge from the Moroccan phosphate mines: challenges and perspectives. *Proc. Eng.* 138, 110–118. doi: 10.1016/j.proeng.2016.02.068
- Hassani, M. A., Durán, P., and Hacquard, S. (2018). Microbial interactions within the plant holobiont. *Microbiome* 6:58. doi: 10.1186/s40168-018-0445-0
- Hatzenpichler, R. (2012). Diversity, physiology, and niche differentiation of ammonia-oxidizing archaea. *Appl. Environ. Microbiol.* 78, 7501–7510. doi: 10.1128/AEM.01960-12
- Hudson-Edwards, K. (2016). Tackling mine wastes. *Science* 352, 288–290. doi: 10.1126/science.aaf3354
- Jalali, J., Gaudin, P., Capiiaux, H., Ammar, E., and Lebeau, T. (2019). Fate and transport of metal trace elements from phosphogypsum piles in Tunisia and their impact on soil bacteria and wild plants. *Ecotoxicol. Environ. Safety* 174, 12–25. doi: 10.1016/j.ecoenv.2019.02.051
- Ju, W., Jin, X., Liu, L., Shen, G., Zhao, W., Duan, C., et al. (2020). Rhizobacteria inoculation benefits nutrient availability for phytostabilization in copper contaminated soil: drivers from bacterial community structures in rhizosphere. *Appl. Soil Ecol.* 150:103450. doi: 10.1016/j.apsoil.2019.103450
- Kaushal, M., and Wani, S. P. (2016). Rhizobacterial-plant interactions: strategies ensuring plant growth promotion under drought and salinity stress. *Agric. Ecosyst. Environ.* 231, 68–78. doi: 10.1016/j.agee.2016.06.031
- Ke, T., Guo, G., Liu, J., Zhang, C., Tao, Y., Wang, P., et al. (2021). Improvement of the Cu and Cd phytostabilization efficiency of perennial ryegrass through the inoculation of three metal-resistant PGPR strains. *Environ. Pollut.* 271:116314. doi: 10.1016/j.envpol.2020.116314
- Khalil, A., Hanich, L., Bannari, A., Zouhri, L., Pourret, O., and Hakkou, R. (2013). Assessment of soil contamination around an abandoned mine in a semi-arid environment using geochemistry and geostatistics: pre-work of geochemical process modeling with numerical models. *J. Geochem. Explor.* 125, 117–129. doi: 10.1016/j.gexplo.2012.11.018
- Khan, M. S., Zaidi, A., and Wani, P. A. (2007). Role of phosphate-solubilizing microorganisms in sustainable agriculture – a review. *Agron. Sustain. Dev.* 27, 29–43. doi: 10.1051/agro:2006011
- Klindworth, A., Pruesse, E., Schweer, T., Peplies, J., Quast, C., Horn, M., et al. (2013). Evaluation of general 16S ribosomal RNA gene PCR primers for classical and next-generation sequencing-based diversity studies. *Nucleic Acids Res.* 41:e1. doi: 10.1093/nar/gks808
- Kochar, M., Vaishnavi, A., Upadhyay, A., and Srivastava, S. (2013). “Bacterial biosynthesis of indole-3-acetic acid: signal messenger service,” in *Molecular Microbial Ecology of the Rhizosphere*, Vol. 1, ed. F. J. de Bruijn (Hoboken, NJ: John Wiley and Sons), 309–325. doi: 10.1002/9781118297674.ch29
- Kompala-Baba, A., Bierza, W., Błońska, A., Sierka, E., Magurno, F., Chmura, D., et al. (2019). Vegetation diversity on coal mine spoil heaps – how important is the texture of the soil substrate? *Biologia* 74, 419–436. doi: 10.2478/s11756-019-00218-x
- Kong, Z., and Glick, B. R. (2017). The role of plant growth-promoting bacteria in metal phytoremediation. *Adv. Microb. Physiol.* 71, 97–132. doi: 10.1016/bs.ampbs.2017.04.001
- Kumar, A., and Verma, J. P. (2018). Does plant—Microbe interaction confer stress tolerance in plants: a review? *Microbiol. Res.* 207, 41–52. doi: 10.1016/j.micres.2017.11.004
- Kumari, B., Mallick, M. A., Solanki, M. K., Solanki, A. C., Hora, A., and Guo, W. (2019). “Plant growth promoting rhizobacteria (pgpr): modern prospects for sustainable agriculture,” in *Plant Health Under Biotic Stress*, eds I. Mahmood and R. A. Ansari (Singapore: Springer), 109–127. doi: 10.1007/978-981-13-6040-4\_6
- Langille, M. G. I., Zaneveld, J., Caporaso, J. G., McDonald, D., Knights, D., Reyes, J. A., et al. (2013). Predictive functional profiling of microbial communities using 16S rRNA marker gene sequences. *Nat. Biotechnol.* 31, 814–821. doi: 10.1038/nbt.2676
- Lghoul, M., Maqoud, A., Hakkou, R., and Kchikach, A. (2014). Hydrogeochemical behavior around the abandoned Kettara mine site, Morocco. *J. Geochem. Explor.* 144, 456–467. doi: 10.1016/j.gexplo.2013.12.003
- Li, X., Huang, L., Bond, P. L., Lu, Y., and Vink, S. (2014). Bacterial diversity in response to direct revegetation in the Pb-Zn-Cu tailings under subtropical and semi-arid conditions. *Ecol. Eng.* 68, 233–240. doi: 10.1016/j.ecoleng.2014.03.044
- Liu, J. L., Yao, J., Wang, F., Min, N., Gu, J. H., Li, Z. F., et al. (2019). Bacterial diversity in typical abandoned multi-contaminated nonferrous metal(loid) tailings during natural attenuation. *Environ. Pollut.* 247, 98–107. doi: 10.1016/j.envpol.2018.12.045
- Long, J., Li, H., Jiang, D., Luo, D., Chen, Y., Xia, J., et al. (2017). Biosorption of strontium (II) from aqueous solutions by *Bacillus cereus* isolated from strontium hyperaccumulator *Andropogon gayanus*. *Process Safety Environ. Prot.* 111, 23–30. doi: 10.1016/j.psep.2017.06.010
- Luo, Y., Wu, Y., Wang, H., Xing, R., Zheng, Z., Qiu, J., et al. (2018). Bacterial community structure and diversity responses to the direct revegetation of an artisanal zinc smelting slag after 5 years. *Environ. Sci. Pollut. Res.* 25, 14773–14788. doi: 10.1007/s11356-018-1573-6
- Magoc, T., and Salzberg, S. L. (2011). FLASH: fast length adjustment of short reads to improve genome assemblies. *Bioinformatics* 27, 2957–2963. doi: 10.1093/bioinformatics/btr507
- Mahé, F., Rognes, T., Quince, C., de Vargas, C., and Dunthorn, M. (2015). Swarmv2: highly-scalable and high-resolution amplicon clustering. *PeerJ*. 3:e1420. doi: 10.7717/peerj.1420
- Martin, M. (2011). Cutadapt removes adapter sequences from high-throughput sequencing reads. *EMBnet J.* 17:10. doi: 10.14806/ej.17.1.200
- Martins, M., Assunção, A., Neto, A., Silva, G., Sghaier, H., and Costa, M. C. (2016). Performance and bacterial community shifts during phosphogypsum biotransformation. *Water Air Soil Pollut.* 227:437. doi: 10.1007/s11270-016-3129-z
- Mendez, M. O., and Maier, R. M. (2008). Phytoremediation of mine tailings in temperate and arid environments. *Rev. Environ. Sci. Biotechnol.* 7, 47–59. doi: 10.1007/s11157-007-9125-4
- Nirola, R., Megharaj, M., Beecham, S., Aryal, R., Thavamani, P., Vankateswarlu, K., et al. (2016). Remediation of metalliferous mines, revegetation challenges and emerging prospects in semi-arid and arid conditions. *Environ. Sci. Pollut. Res.* 23, 20131–20150. doi: 10.1007/s11356-016-7372-z
- Numan, M., Bashir, S., Khan, Y., Mumtaz, R., Shinwari, Z. K., Khan, A. L., et al. (2018). Plant growth promoting bacteria as an alternative strategy for salt tolerance in plants: a review. *Microbiol. Res.* 209, 21–32. doi: 10.1016/j.micres.2018.02.003
- Olanrewaju, O. S., and Babalola, O. O. (2019). Streptomyces: implications and interactions in plant growth promotion. *Appl. Microbiol. Biotechnol.* 103, 1179–1188. doi: 10.1007/s00253-018-09577-y
- Olanrewaju, O. S., Glick, B. R., and Babalola, O. O. (2017). “Mechanisms of action of plant growth promoting bacteria,” in *World Journal of Microbiology and Biotechnology*, Vol. 33, ed. P. J. Large (Dordrecht: Springer), doi: 10.1007/s11274-017-2364-9
- Orozco-Mosqueda, M., del, C., Glick, B. R., and Santoyo, G. (2020). ACC deaminase in plant growth-promoting bacteria (PGPB): an efficient mechanism to counter salt stress in crops. *Microbiol. Res.* 235:126439. doi: 10.1016/j.micres.2020.126439
- Ouakibi, O., Hakkou, R., and Benzaazoua, M. (2014). Phosphate carbonated wastes used as drains for acidic mine drainage passive treatment. *Proc. Eng.* 83, 407–414. doi: 10.1016/j.proeng.2014.09.049
- Ouakibi, O., Loqman, S., Hakkou, R., and Benzaazoua, M. (2013). The potential use of phosphatic limestone wastes in the passive treatment of AMD: a laboratory study. *Mine Water Environ.* 32, 266–277. doi: 10.1007/s10230-013-0226-8
- Padmavathiamma, P. K., Ahmed, M., and Rahman, H. A. (2014). Phytoremediation – A sustainable approach for contaminant remediation in arid and semi-arid regions – a review. *Emirates J. Food Agric.* 26, 757–772. doi: 10.9755/efja.v26i9.18202
- Pathak, D. V., and Kumar, M. (2016). “Microbial inoculants as biofertilizers and biopesticides,” in *Microbial Inoculants in Sustainable Agricultural Productivity: Vol. 1: Research Perspectives*, eds D. P. Singh, H. B. Singh, and R. Prabha (Delhi: Springer), 197–209. doi: 10.1007/978-81-322-2647-5\_11
- Patten, C. L., and Glick, B. R. (1996). Bacterial biosynthesis of indole-3-acetic acid. *Can. J. Microbiol.* 42, 207–220. doi: 10.1139/m96-032
- Pattanaik, S., Mohapatra, B., Kumar, U., Pattanaik, M., and Samantaray, D. (2019). “Microbe-mediated plant growth promotion: a mechanistic overview on cultivable plant growth-promoting members,” in *Biofertilizers for Sustainable Agriculture and Environment. Soil Biology*, Vol. 55, eds B. Giri, R. Prasad, Q. S. Wu, and A. Varma (Cham: Springer), 435–463.



- Prabhu, N., Borkar, S., and Garg, S. (2019). "Phosphate solubilization by microorganisms: overview, mechanisms, applications and advances," in *Advances in Biological Science Research: A Practical Approach*, eds M. Naik and S. N. Meena (Amsterdam: Elsevier), 161–176. doi: 10.1016/B978-0-12-817497-5.00011-2
- Ragot, S., Zeyer, J., Zehnder, L., Reusser, E., Brandl, H., and Lazzaro, A. (2013). Bacterial community structures of an alpine apatite deposit. *Geoderma* 202–203, 30–37. doi: 10.1016/j.geoderma.2013.03.006
- Rognes, T., Flouri, T., Nichols, B., Quince, C., and Mahé, F. (2016). VSEARCH: a versatile open source tool for metagenomics. *PeerJ* 4:e2584. doi: 10.7717/peerj.2584
- Rousk, J., Bååth, E., Brookes, P. C., Lauber, C. L., Lozupone, C., Caporaso, J. G., et al. (2010). Soil bacterial and fungal communities across a pH gradient in an arable soil. *ISME J.* 4, 1340–1351. doi: 10.1038/ismej.2010.58
- Santoyo, G., del Orozco-Mosqueda, M. C., and Govindappa, M. (2012). "Mechanisms of biocontrol and plant growth-promoting activity in soil bacterial species of *Bacillus* and *Pseudomonas*: a review," in *Biocontrol Science and Technology*, Vol. 22, ed. M. S. Goettel (Abingdon: Taylor & Francis Ltd), 855–872. doi: 10.1080/09583157.2012.694413.
- Schulz, S., Brankatschk, R., Dümig, A., Kögel-Knabner, I., Schlöter, M., and Zeyer, J. (2013). The role of microorganisms at different stages of ecosystem development for soil formation. *Biogeosciences* 10, 3983–3996. doi: 10.3929/ethz-b-000070776
- Segata, N., Izard, J., Waldron, L., Gevers, D., Miropolsky, L., Garrett, W. S., et al. (2011). Metagenomic biomarker discovery and explanation. *Genome Biol.* 12:R60. doi: 10.1186/gb-2011-12-6-r60
- Smith, F. W., Rae, A. L., and Hawkesford, M. J. (2000). Molecular mechanisms of phosphate and sulphate transport in plants. *Biochim. Biophys. Acta BBA Biomembr.* 1465, 236–245. doi: 10.1016/S0005-2736(00)00141-3
- Stieglmeier, M., Klingl, A., Alves, R. J. E., Rittmann, S. K. M. R., Melcher, M., Leisch, N., et al. (2014). Nitrososphaera viennensis gen. nov., sp. nov., an aerobic and mesophilic, ammonia-oxidizing archaeon from soil and a member of the archaeal phylum *Thaumarchaeota*. *Int. J. Syst. Evol. Microbiol.* 64(Pt 8), 2738–2752. doi: 10.1099/ijs.0.063172-0
- Thabet, O. B. D., Gtari, M., and Sghaier, H. (2017). Microbial diversity in phosphate rock and phosphogypsum. *Waste Biomass Valorization* 8, 2473–2483. doi: 10.1007/s12649-016-9772-1
- Thavamani, P., Samkumar, R. A., Satheesh, V., Subashchandrabose, S. R., Ramadass, K., Naidu, R., et al. (2017). Microbes from mined sites: harnessing their potential for reclamation of derelict mine sites. *Environ. Pollut.* 230, 495–505. doi: 10.1016/j.envpol.2017.06.056
- Topalovic, O., Hussain, M., and Heuer, H. (2020). Plants and associated soil microbiota cooperatively suppress plant-parasitic nematodes. *Front. Microbiol.* 11:313. doi: 10.3389/fmicb.2020.00313
- Trifi, H., Najjari, A., Achouak, W., Barakat, M., Ghedira, K., Mrad, F., et al. (2020). Metataxonomics of *Tunisian phosphogypsum* based on five bioinformatics pipelines: insights for bioremediation. *Genomics* 112, 981–989. doi: 10.1016/j.ygeno.2019.06.014
- Ullah, I., Jilani, G., Khan, K. S., Akhtar, M. S., and Rasheed, M. (2013). Phosphorous solubilization from phosphate rock by the interactive effect of *Thiobacilli* and elemental sulfur. *J. Agric. Res.* 51:03681157.
- van Bruggen, A. H. C., Goss, E. M., Havelaar, A., van Diepeningen, A. D., Finckh, M. R., and Morris, J. G. (2019). One health – cycling of diverse microbial communities as a connecting force for soil, plant, animal, human and ecosystem health. *Sci. Total Environ.* 664, 927–937. doi: 10.1016/j.scitotenv.2019.02.091
- Vurukonda, S. S. K. P., Vardharajula, S., Shrivastava, M., and SkZ, A. (2016). Enhancement of drought stress tolerance in crops by plant growth promoting rhizobacteria. *Microbiol. Res.* 184, 13–24. doi: 10.1016/j.micres.2015.12.003
- Wang, M., Tang, Y., Anderson, C. W., Jeyakumar, P., and Yang, J. (2018). Effect of simulated acid rain on fluorine mobility and the bacterial community of phosphogypsum. *Environ. Sci. Pollut. Res.* 25, 15336–15348. doi: 10.1007/s11356-018-1408-5
- Wu, Z., Yu, F., Sun, X., Wu, S., Li, X., Liu, T., et al. (2018). Long term effects of *Lespedeza bicolor* revegetation on soil bacterial communities in Dexing copper mine tailings in Jiangxi Province, China. *Appl. Soil Ecol.* 125, 192–201. doi: 10.1016/j.apsoil.2018.01.011
- Yadav, A. K., Kumar, N., Sreekrishnan, T. R., Satya, S., and Bishnoi, N. R. (2010). Removal of chromium and nickel from aqueous solution in constructed wetland: mass balance, adsorption-desorption and FTIR study. *Chem. Eng. J.* 160, 122–128. doi: 10.1016/j.cej.2010.03.019
- Ye, D., Li, T., Yu, H., Zou, L., Huang, H., Zhang, X., et al. (2020). Characteristics of bacterial community in root-associated soils of the mining ecotype of *Polygonum hydropiper*, a P-accumulating herb. *Appl. Soil Ecol.* 150:103477. doi: 10.1016/j.apsoil.2019.103477
- Zheng, B. X., Bi, Q. F., Hao, X. L., Zhou, G. W., and Yang, X. R. (2017). *Massilia phosphatilytica* sp. nov., a phosphate solubilizing bacteria isolated from a long-term fertilized soil. *Int. J. Syst. Evol. Microbiol.* 67, 2514–2519. doi: 10.1099/ijsem.0.001916
- Zouch, H., Karray, F., Armougom, F., Chifflet, S., Hirschler-Réa, A., Kharrat, H., et al. (2017). Microbial diversity in sulfate-reducing marine sediment enrichment cultures associated with anaerobic biotransformation of coastal stockpiled phosphogypsum (Sfax, Tunisia). *Front. Microbiol.* 8:1583. doi: 10.3389/fmicb.2017.01583

**Conflict of Interest:** The authors declare that the research was conducted in the absence of any commercial or financial relationships that could be construed as a potential conflict of interest.

Copyright © 2021 Mghazli, Sbabou, Hakkou, Ouhammou, El Adnani and Bruneel. This is an open-access article distributed under the terms of the Creative Commons Attribution License (CC BY). The use, distribution or reproduction in other forums is permitted, provided the original author(s) and the copyright owner(s) are credited and that the original publication in this journal is cited, in accordance with accepted academic practice. No use, distribution or reproduction is permitted which does not comply with these terms.



# Microbial Diversity and Activity During the Biodegradation in Seawater of Various Substitutes to Conventional Plastic Cotton Swab Sticks

Justine Jacquin<sup>1,2</sup>, Nolwenn Callac<sup>1,3</sup>, Jingguang Cheng<sup>1</sup>, Carolane Giraud<sup>1,3</sup>, Yonko Gorand<sup>4</sup>, Clement Denoual<sup>5</sup>, Mireille Pujo-Pay<sup>1</sup>, Pascal Conan<sup>1</sup>, Anne-Leila Meistertzheim<sup>6</sup>, Valerie Barbe<sup>7</sup>, Stéphane Bruzaud<sup>5</sup> and Jean-François Ghiglione<sup>1\*</sup>

## OPEN ACCESS

### Edited by:

Mechthild Schmitt-Jansen,  
Helmholtz Centre for Environmental  
Research (UFZ), Germany

### Reviewed by:

Gabriela Vázquez-Rodríguez,  
Autonomous University of the State  
of Hidalgo, Mexico  
Christian Lott,  
HYDRA Marine Sciences GmbH,  
Germany

### \*Correspondence:

Jean-François Ghiglione  
ghiglione@obs-banyuls.fr

### Specialty section:

This article was submitted to  
Microbiotechnology,  
a section of the journal  
Frontiers in Microbiology

**Received:** 09 September 2020

**Accepted:** 12 May 2021

**Published:** 15 July 2021

### Citation:

Jacquin J, Callac N, Cheng J,  
Giraud C, Gorand Y, Denoual C,  
Pujo-Pay M, Conan P,  
Meistertzheim A-L, Barbe V,  
Bruzaud S and Ghiglione J-F (2021)  
Microbial Diversity and Activity During  
the Biodegradation in Seawater  
of Various Substitutes to Conventional  
Plastic Cotton Swab Sticks.  
Front. Microbiol. 12:604395.  
doi: 10.3389/fmicb.2021.604395

<sup>1</sup> CNRS, UMR 7621, Laboratoire d'Océanographie Microbienne, Observatoire Océanologique de Banyuls, Sorbonne Université, Paris, France, <sup>2</sup> Innovation Plasturgie et Composites, Biopole Clermont Limagne, Saint-Beauzire, France, <sup>3</sup> CNRS, UMR 9220 ENTROPIE, Ifremer (LEAD-NC), IRD, Univ Nouvelle-Calédonie, Univ La Réunion, Nouméa, New Caledonia, <sup>4</sup> Plateforme EnRMAT, Laboratoire PROMES, Rembla de la Thermodynamique, Perpignan, France, <sup>5</sup> UMR CNRS 6027, Institut de Recherche Dupuy de Lôme (IRDL), Université de Bretagne-Sud, Lorient, France, <sup>6</sup> SAS Plastic@Sea, Observatoire Océanologique de Banyuls, Banyuls-sur-Mer, France, <sup>7</sup> Génomique Métabolique, Genoscope, Institut François Jacob, CEA, CNRS, Univ Evry, Université Paris-Saclay, Evry, France

The European Parliament recently approved a new law banning single-use plastic items for 2021 such as plastic plates, cutlery, straws, cotton swabs, and balloon sticks. Transition to a bioeconomy involves the substitution of these banned products with biodegradable materials. Several materials such as polylactic acid (PLA), polybutylene adipate terephthalate (PBAT), poly(butylene succinate) (PBS), polyhydroxybutyrate-valerate (PHBV), Bioplast, and Mater-Bi could be good candidates to substitute cotton swabs, but their biodegradability needs to be tested under marine conditions. In this study, we described the microbial life growing on these materials, and we evaluated their biodegradability in seawater, compared with controls made of non-biodegradable polypropylene (PP) or biodegradable cellulose. During the first 40 days in seawater, we detected clear changes in bacterial diversity (Illumina sequencing of 16S rRNA gene) and heterotrophic activity (incorporation of <sup>3</sup>H-leucine) that coincided with the classic succession of initial colonization, growth, and maturation phases of a biofilm. Biodegradability of the cotton swab sticks was then tested during another 94 days under strict diet conditions with the different plastics as sole carbon source. The drastic decrease of the bacterial activity on PP, PLA, and PBS suggested no bacterial attack of these materials, whereas the bacterial activity in PBAT, Bioplast, Mater-Bi, and PHBV presented similar responses to the cellulose positive control. Interestingly, the different bacterial diversity trends observed for biodegradable vs. non-biodegradable plastics allowed to describe potential new candidates involved in the degradation of these materials under marine conditions. This better understanding of the bacterial

diversity and activity dynamics during the colonization and biodegradation processes contributes to an expanding baseline to understand plastic biodegradation in marine conditions and provide a foundation for further decisions on the replacement of the banned single-used plastics.

**Keywords:** plastisphere, biofouling, plastic biodegradation, single-used plastics, microbial colonization

## INTRODUCTION

The growing worldwide use of plastics together with waste mismanagement resulted in an estimated release of more than five trillion plastic particles weighing over 250,000 tons afloat in the oceans, resulting in dramatic toxicological effects along the marine trophic chain (Eriksen et al., 2014; Wang et al., 2019). A large majority of plastic items found at sea is made of polyethylene (PE), polypropylene (PP), and polystyrene (PS), which are more likely to float, and polyvinyl chloride (PVC), nylons, and polyethylene terephthalate (PET), which are more likely to sink (Auta et al., 2017).

Government regulations have been recently established to restrict the use of single-use plastics and promote the biodegradable plastic industry. For example, since 2018, at least 127 countries have established regulations against plastic bags (UNEP, 2018). The European Parliament voted to ban many other single-use plastics for 2021, including plates, cutlery, straws, food containers, and expanded polystyrene cups as well as sticks used for cotton swabs and plastic balloons (Europarl, 2019). Biodegradable plastics have become the focus of recent researches in order to replace conventional materials made of PE, PP, PS, PVC, PET, and other high-molecular compounds. Today, commercially available biodegradable materials are of petrochemical origin, such as poly(butylene succinate) (PBS) and polybutylene adipate terephthalate (PBAT; brand name Ecoflex®), or are bio-based such as polylactic acid (PLA) and polyhydroxybutyrate-valerate (PHBV). Natural starch is also frequently offered as a solution, blended with petrochemical-based (mainly potato starch for Bioplast®) or bio-based materials (corn starch with PBAT for Mater-Bi®).

Plastic biodegradation is the microbial conversion of all its organic constituents to carbon dioxide, new microbial biomass and mineral salts under oxic conditions, or to carbon dioxide, methane, new microbial biomass, and mineral salts, under anoxic conditions (Science Advice for Policy by European Academies [SAPEA], 2020). The biodegradability of a plastic is defined according to several standards reflecting disposal condition in soil, compost, or aquatic environments. Tests are generally based on respirometry (biological oxygen demand and CO<sub>2</sub> production) attributed to the biodegradation of the plastic by microbial communities, without any other source of carbon in artificial medium, in comparison with cellulose, which serves as a reference control (standards ISO 18830:2016, ISO 19679:2016, ASTM D6691-09). Several drawbacks were pointed out by a recent paper on the ability of current standard protocols to realistically predict biodegradability in the marine environment (Harrison et al., 2018). For example, the use of preselected strains does not take into consideration the large diversity of

microorganisms colonizing plastics in natural conditions, also known as the “plastisphere” (Zettler et al., 2013) which is still poorly studied. In addition, the conventional techniques used to measure the biodegradation activity by evolution of O<sub>2</sub> or CO<sub>2</sub> generally require substantial equipment and can limit the number of experimental replicates. Other activity tests can be considered as alternative methods, such as the use of radiolabeled leucine incorporation that has been used for decades in marine microbiology (Kirchman et al., 1985) or tests based on ATP measurements (Fontanella et al., 2013). When introduced in seawater, plastics are rapidly colonized by bacteria. This process has been extensively studied, showing successive phases of biofilm formation (Dang and Lovell, 2000; Lobelle and Cunliffe, 2011; Eich et al., 2015; Erni-Cassola et al., 2019). During the first days at sea, a “conditioning film” made of inorganic and organic matter supports the initial colonization phase generally initiated by Gammaproteobacteria and Alphaproteobacteria, regardless of the material type (Oberbeckmann et al., 2015). A second phase of rapidly growing bacteria is then usually characterized by a succession of Bacteroidetes, Acidobacteria, Actinobacteria, Cyanobacteria, Firmicutes, and Planctomycetes (Salta et al., 2013). The last phase corresponds to a mature biofilm that generally appears after 15–30 days at sea and remains stable for several months, and where clear differences in bacterial abundance, diversity and activity, were found between non-biodegradable and biodegradable plastics (Eich et al., 2015; Dussud et al., 2018). Hydrocarbonoclastic bacteria (HCB) such as *Alcanivorax* sp., *Aestuariicella hydrocarbonica*, and *Marinobacter* sp. became abundant in the mature biofilm and were suggested to be potentially involved in the degradation of fossil-based plastics. However, no study has extended the experience by incubating the mature biofilm in minimum medium with the plastic as the only carbon source in order to prove its biodegradation capabilities.

Here, we used hollow cylinder sticks, such as those used for cotton swabs, made of different conventional (PP) and “biodegradable” materials as potential candidates for substitutes to conventional single-use plastics (PLA, PBS, PBAT, Mater-Bi, Bioplast, PHBV, and cellulose). We hypothesized that the properties of the distinct materials would select different marine bacterial communities with specific biodegradation capabilities. We elaborated an original two-step experimental design based on a first colonization step in natural seawater (40 days) followed by a second step of incubation in minimum medium with each plastic type as sole source of carbon and energy (94 days). Temporal dynamics of the biofilms associated with each plastic type were followed by measuring bacterial activity (<sup>3</sup>H-leucine incorporation), morphology [scanning electron microscopy (SEM)], and diversity (Illumina sequencing of 16S rRNA genes) during the successive colonization and biodegradation phases.

## MATERIALS AND METHODS

### Plastic Stick Manufacturing Process

The following list respectively, mentions the material type, its trade name, and the supplier: PP (ISPLEN PP 030 G1E, Repsol), PBAT (Ecoflex C1200, BASF), PLA (Ingeo 7001D, Natureworks), Bioplast (Bioplast 400, Biotec), PHBV (PHBV ENMAT Y1000P, TianAn Bio), Mater-Bi (Mater-Bi EF04P, Novamont), PBS (bioPBS FZ91PB, PTT MCC Biochem), and cellulose (U Bio). PHBV was preferred in this study because it is a short-chain-length polyhydroxyalkanoate (scl-PHA) that is commercially available. Extended physical and chemical characteristics of the material types are given in **Supplementary Table 1**.

In order to manufacture plastic sticks that correspond to the hollow cylinder classically used for cotton swabs, we used a machine (except for cellulose sticks) with a spinning line composed of a SCAMEX single screw extruder with a 20-mm diameter and a L/D = 20 ratio. The machine was equipped with a vertical shaping die tube, a cooling tray, a drawing bench, an online dimensional controller (tolerances  $\pm 0.01$  mm), and a winding element. In order to conform the plastic materials to the desired stick form, the extruder was equipped with a suitable tube die tailor-made by the extruder manufacturer.

Extrusion conditions were adapted according to the used plastics and to their physical and chemical characteristics (**Table 1**). Finally, sticks were cut to equivalent dimensions as commercial sticks, i.e., 72-mm length, 2.5-mm outer diameter, and 1.6-mm inner diameter. This study required 300 fragments of 5 mm for each tested material. Except for cellulose, all materials had a hole in the stick.

### Incubation Under Natural Seawater Conditions (40 Days)

Each material type was incubated in aquariums with direct circulation to the sea, as previously described (Dussud et al., 2018). Briefly, we used nine identical aquariums consisting of trays with a 1.8-L capacity (Sodispan, Madrid, Spain), in which 1.5 L of 200- $\mu$ m filtered seawater was continually renewed by direct pumping at 14-m depth in the Banyuls Bay, close to the SOLA marine observatory station (42°29'300 N–03°08'700 E, France). A flow rate of 50 ml min<sup>-1</sup> was chosen to ensure a sufficient renewal of natural bacteria (every 30 min) and a homogeneous distribution of the plastic pieces in the aquariums during the entire experiment.

Approximately 250 pieces of each material type (PP, PLA, PBS, PBAT, Bioplast, Mater-Bi, PHBV, or cellulose) in the form of sticks of 0.5-cm length were washed three times with molecular ethanol and rinsed several times with sterile milliQ water before being placed in the aquariums, with the exception of the “control aquarium,” which only contained the circulating seawater. Pieces were sampled after 7 (D7), 15 (D15), 30 (D30), and 40 days (D40). Aquariums were kept in the dark to avoid UV-driven degradation of the materials. Throughout the incubation, seawater temperature (between 12.5 and 13.5°C) and salinity (38.5) were monitored in the aquariums and were similar to the data

found at the SOLA observatory in the Banyuls Bay during this period<sup>1</sup>.

### Incubation in Minimum Medium With Plastic Sticks as Sole Carbon Source (94 Days)

After 40 days under natural seawater conditions, the remaining pieces of each of the eight material types were carefully collected with sterilized tweezers and placed in 4-ml flasks (ref. 294330, Interchim, Montluçon, France) containing 2 ml of minimum medium with no other carbon source than the materials. The composition of the minimum medium was modified from Fegatella et al. (1998): NaCl (420 mM), Na<sub>2</sub>SO<sub>4</sub> (28.8 mM), KCl (9.39 mM), NaBr (0.84 mM), H<sub>3</sub>BO<sub>3</sub> (0.485 mM), MgCl<sub>2</sub>·6H<sub>2</sub>O (0.546 mM), CaCl<sub>2</sub> (0.105 mM), NH<sub>4</sub>Cl (9.35 mM), SrCl<sub>2</sub>·6H<sub>2</sub>O (0.0638 mM), NaF (0.0714 mM), NaNO<sub>3</sub> (0.88 mM), NaH<sub>2</sub>PO<sub>4</sub>·H<sub>2</sub>O (0.036 mM), KH<sub>2</sub>PO<sub>4</sub> (0.106 mM), CuSO<sub>4</sub>·5H<sub>2</sub>O (0.04  $\mu$ M), ZnSO<sub>4</sub>·7H<sub>2</sub>O (0.08  $\mu$ M), CoCl<sub>2</sub>·6H<sub>2</sub>O (0.04  $\mu$ M), MnCl<sub>2</sub>·4H<sub>2</sub>O (0.9  $\mu$ M), Na<sub>2</sub>MoO<sub>4</sub>·2H<sub>2</sub>O (0.03  $\mu$ M), FeCl<sub>3</sub> (1.85  $\mu$ M), thiamine (0.3  $\mu$ M), biotin (2.1 nM), and vitamin B12 (0.317 nM). Pieces of each material type were sampled after 3 (D40 + 3), 7 (D40 + 7), 15 (D40 + 15), and 94 days (D40 + 94).

### Scanning Electron Microscopy

Three pieces of each of the eight material types were fixed at the beginning (D0) and at the end of the experiment (D40 + 94) with the addition of 3% (v/v) glutaraldehyde (final concentration) and stored for at least one night at 4°C. SEM was performed as previously described (Goldstein et al., 1992). Briefly, samples were washed in sodium cacodylate buffer and fixed with 1% osmium tetroxide before using successive EtOH baths (70, 95, and 100%) and liquid CO<sub>2</sub> for dehydration. About 10-nm conductive layer of Au–Pd was then applied on the surface of the samples to allow electron microscopy observation (Hitachi SEM FEG S-4500, Tokyo, Japan).

### Heterotrophic Bacterial Production

Incorporation of <sup>3</sup>H-leucine is a classical proxy of the bacterial activity in seawater (Kirchman et al., 1985), which has been recently optimized for the plastisphere by Dussud et al. (2018). Bacterial production (BP) was measured on each material type at each sampling time during the colonization and biodegradation phases. A cell detachment pretreatment was applied using three cycles of 3-min sonication bath (Deltasonic, Meaux, France) followed by 3-min vortex at maximum speed (SkyLine, Elmi Ltd., Moscow, Russia). Immediately after cell detachment, <sup>3</sup>H-leucine (specific activity 123.8 Ci mmol<sup>-1</sup>; PerkinElmer, Waltham, MA, United States) was added to all samples, which consisted of 1.5 ml of sterilized seawater containing the plastic pieces together with the detached cells. Biotic samples were treated in triplicates, and a fourth one was killed with trichloroacetic acid (TCA 50%) and served as a control of the reaction. Abiotic controls (consisting of plastic sticks of the eight material types incubated in sterile

<sup>1</sup><https://www.somlit.fr/>



**TABLE 1** | Extrusion conditions for the different plastic types.

Plastic	Temperature zone 1 °C	Temperature zone 2 °C	Temperature zone 3 °C	Temperature die °C	Screw speed tr/min	Pulling speed m/min
PP	220	220	220	220	20	3.50
PLA 7001D	170	180	190	180	25	3.90
PHA Y1000P	180	180	180	180	25	4.00
PBAT C1200	140	160	160	160	15	2.90
PBS FZ91PB	140	140	140	140	20	3.50
Mater-Bi EF04P	140	160	160	160	15	3.15
Bioplast 400	160	160	160	160	15	3.00

PP, polypropylene; PLA, polylactic acid; PHA, polyhydroxyalkanoate; PBAT, polybutylene adipate terephthalate; PBS, poly(butylene succinate).

seawater) were analyzed following the same protocol. The final leucine concentrations were 36 nmol L<sup>-1</sup> (<sup>3</sup>H-leucine at 4 nmol L<sup>-1</sup>) during the colonization phase and 150 nmol L<sup>-1</sup> after the transfer to minimum medium (<sup>3</sup>H-leucine at 1 nmol L<sup>-1</sup>). The saturation of the leucine incorporation was checked during the biodegradation phase, and a higher final leucine concentration was required in order to avoid leucine being limiting (data not shown), explaining why the final leucine concentrations differed between the colonization and degradation phases. The final <sup>3</sup>H-leucine concentration was 4.3 nmol L<sup>-1</sup> for control seawater samples. All samples were treated in triplicates and incubated in the dark at *in situ* temperature (between 12 and 15°C) for 2 h. Incubations were stopped by the addition of 50% TCA (5% final concentration), and the plastic sticks or cell pellets were washed with diluted TCA and then with cold ethanol. Radioactivity was counted after addition of liquid scintillator (Filter Count PerkinElmer) on a HIDEX 300 SL scintillation counter (LabLogic Systems, Inc., Tampa, FL, United States).

The empirical conversion factor of 1.55 ng C pmol<sup>-1</sup> of incorporated leucine was used to calculate BP (Simon and Azam, 1989). Because the exact surface of plastic sticks was difficult to measure (several layers for the cellulose, etc.), each piece was weighted with precision balance of sensitivity 0.1 mg (Precisa 125A, Swiss Quality; Precisa Gravimetrics AG, Dietikon, Switzerland), and the results were expressed in ng C·g<sup>-1</sup>·h<sup>-1</sup>.

## DNA Extraction, PCR, and Sequencing

For each material type, individual pieces were taken at all sampling times and stored at -80°C until DNA extraction. In parallel, 1 L of seawater was sampled in the control aquarium and successively filtered onto 3- and 0.2-μm pore size polycarbonate filters (47-mm diameter, Nucleopore), and filters were stored at -80°C until analysis. DNA extractions were performed on plastic sticks or filters using a classical phenol-chloroform method (Sauret et al., 2016) with slight modifications of the method for plastic samples (Debeljak et al., 2016). Briefly, the same cell detachment pretreatment was used as for BP (see above) before enzymatic and chemical cell lysis [incubation with 1 mg ml<sup>-1</sup> of lysozyme at 37°C for 45 min followed by 1 h at 50°C with 0.2 mg ml<sup>-1</sup> of proteinase K and 1% sodium dodecyl sulfate (SDS)]. DNA was quantified by spectrophotometry (Quant-iT<sup>TM</sup> PicoGreen<sup>TM</sup> dsDNA Assay Kit, Invitrogen; Thermo Fisher Scientific, Waltham, MA, United States).

PCR amplification of the V4-V5 region was performed using the primers 515-FY (5'-GTG YCA GCM GCC GCG GTA A-3') and 926-R (5'-CCG YCA ATT YMT TTR AGT TT-3') (Fuhrman et al., 1989), which are particularly well suited for marine samples (Parada et al., 2016). Sequencing was performed on Illumina MiSeq by MrDNA (Molecular Research LP, Shallowater, TX, United States) and Integrated Microbiome Resource (IMR; Dalhousie University, Halifax, NS, Canada). The sequences were analyzed using FROGS pipeline hosted in the Galaxy platform (Escudie et al., 2018), following the guidelines given in the publication. Briefly, the forward and reverse reads were assembled; and sequences were clustered using the SWARM algorithm (Mahé et al., 2014) and an aggregation distance of 3. Then, chimeras were removed using the FROGS Vsearch tool (Rognes et al., 2016). An additional filter step was used on the abundance at a 5 × 10<sup>-5</sup> threshold to select the most relevant operational taxonomic unit (OTU) sequences. The taxonomic affiliation was assigned by standard nucleotide BLAST (Camacho et al., 2009) using the SILVA 132 database 16S (Quast et al., 2013). Chloroplast, mitochondrial, and eukaryotic sequences were removed. All the 16S rRNA data are available in the National Center for Biotechnology Information (NCBI) Sequence Read Archive (SRA) repository (accession number PRJNA649857).

## Statistical Analysis

In order to allow normalization and comparisons of the data, bacterial sequences of each sample were randomly resampled in the OTU file based on the sample with the fewest sequences ( $n = 9,698$ ). These data sets were used to conduct all the analyses performed using the Rstudio software<sup>2</sup>. The α-diversity indices (Chao1, Shannon, evenness, and Simpson) and the β-diversity analysis (the Bray-Curtis similarity) were calculated with the phyloseq package (McMurdie and Holmes, 2013).

Differences between material types were tested using an ANOVA test and confirmed by a *post hoc* Tukey test. Results were considered to be significant if the *p* value was less than 0.05. Dendrogram was obtained based on the dissimilarity matrix of the Bray-Curtis and applying the Ward algorithm (Ward, 1963).

OTUs responsible for dissimilarities between pairs of clusters from the start and the end of incubation in

<sup>2</sup><https://www.r-project.org/>

minimum medium were identified using similarity percentage (SIMPER, PRIMER 6).

## RESULTS

### Scanning Electron Microscopy on the Different Plastic Types

Polypropylene, PLA, and PBS surfaces showed no visible signs of biodegradation (cracking, deformation, and holes). In addition, bacterial-cell structures on these materials were scarce and dispersed on the surface after 40 days in natural seawater followed by 94 days in minimum medium (D40 + 94). Abundant microbial colonization was observed on the surface of the other materials (PHBV, Mater-Bi, cellulose, and Bioplast), which is typical of a mature biofilm (**Figure 1**).

Three-dimensional biofilm structures were visible on the more colonized plastics, where cells colonized not only the surface layers but also the inner part of the visible cracks. A large diversity of morphological forms including spherical, rod-shaped, or spiral-shaped bacterial-like structures were observed on the surface of most of the materials. Extensive exopolysaccharide matrix was found except for PP, PLA, and PBS.

### Bacterial Production During the Successive Phases of Colonization and Transfer to Minimum Medium

During the colonization phase in natural seawater, BP was generally higher during the growth phase of the biofilm from 7 to 15 days. The highest BP values were found for PP, Bioplast, and PHBV (15.9, 12.4, and 10.5 ng C·g<sup>-1</sup>·h<sup>-1</sup>, respectively), whereas others (PLA, PBS, PBAT, and cellulose) ranged from 2.2 to 6.5 ng C·g<sup>-1</sup>·h<sup>-1</sup> during this colonization phase (**Figure 2A**). At the end of the colonization phase in natural seawater (D40), BP was even more homogeneous between the material types, ranging from 1.6 to 4.0 ng C·g<sup>-1</sup>·h<sup>-1</sup> for PP, PLA, PBS, PBAT and from 4.7 to 8.1 ng C·g<sup>-1</sup>·h<sup>-1</sup> for Mater-Bi, Bioplast, PHBV, and cellulose. Bacteria living under control seawater conditions showed stable BP during the 40 days, ranging from 12.4 to 22.3 ng C·L<sup>-1</sup>·h<sup>-1</sup> (**Supplementary Table 1**). No comparison was made between the BP values recorded between the seawater and the plastic sticks because of different measure units.

In order to anticipate the decrease of bacterial heterotrophic activity after the transfer of the plastic together with their biofilms into a minimum medium with the plastic as sole carbon source, we have changed the dilution factor of <sup>3</sup>H-leucine added to the samples at day 40 accordingly to previous results (data not shown). It did not modify the leucine uptake, but it resulted in an increase of BP values by a factor of  $5.8 \pm 2.9$  ( $n = 8$ ) for all material types. This transfer from natural seawater to minimum medium resulted in different response scenarios according to the plastic types (**Figure 2B**). A first scenario was found for PP, PLA, and PBS where the BP increased during the first week of incubation in minimum medium (with maxima of 58.8, 85.9, and 94.2 ng C·g<sup>-1</sup>·h<sup>-1</sup> at D40 + 3 or D40 + 7) and dramatically decreased thereafter (7.3, 8.7, and 11 ng C·g<sup>-1</sup>·h<sup>-1</sup> at D40 + 94).

A second scenario was observed for PBAT, Mater-Bi, Bioplast, PHBV, and cellulose, where the BP remained relatively stable after the transfer into minimum medium (41.0, 18.6, 39.8, 59.2, and 21.9 ng C·g<sup>-1</sup>·h<sup>-1</sup> at D40 + 94).

### Bacterial Community Structure, Diversity Indices, and Taxonomy During the Successive Phases of Colonization and Transfer to Minimum Medium

A total of 5,427,894 paired-end reads were acquired after sequencing all samples. After normalization based on the sample with the fewest merged sequences ( $n = 9,698$ ), 3,772,255 sequence tags were selected belonging to 978 OTUs (0.03 distance threshold). The seawater control at D40 was sequenced several times, but each sequencing failed for unknown reasons.

#### Changes in $\alpha$ -Diversity Indices

$\alpha$ -Diversity was studied using Chao1 richness, Pielou evenness, and Shannon diversity indices. Regardless of the plastic type, richness rapidly increased during the first 15 days of colonization and reached between 120 and 384 estimated OTUs after 40 days (**Supplementary Table 2**). The transfer to minimum medium did not influence richness ( $\pm 50$  estimated species) for some material types including PP, PLA, PBS, and Bioplast but resulted in a decrease for PBAT, Mater-Bi, PHBV, and cellulose when comparing D40 and D40 + 94. We observed that the Chao1 index was statistically linked to the material type after the transfer to minimum medium (ANOVA,  $p$  value = 0.0147).

The Pielou evenness index showed relatively homogeneous diversity during the colonization phase, with evenness > 0.5 for all plastics after 40 days (**Supplementary Table 2**). A slight increase was found after the transfer in minimum medium for PP, Bioplast, PHBV, and cellulose, as correlated with the Chao1 index ( $p < 0.05$ ), whereas it slightly decreased for PLA, PBS, PBAT, and Mater-Bi at the end of the incubation.

The resulting Shannon diversity was consistent with the Pielou and Chao1 indices. During the colonization phase, a decrease in the Shannon diversity index was found for the PP (2.4) due to its decrease in evenness (**Table 1**). A diversity increase was found for all the other plastics at D40 (between 2.64 and 4.40). The transfer to minimum medium resulted in an increase in diversity until the end of the experiment (between 3.67 and 3.9 at D40 + 94) for PP, PHBV, and cellulose according to the increase in evenness. Conversely, a decrease of the Shannon diversity (between 2.1 and 3.64) was caused by a decrease in richness for PBS, PBAT, and Mater-Bi or by a decrease in evenness for PLA and Bioplast.

### Microbial Communities on Plastics During the Colonization Phase in Seawater

The first colonizers growing on five of the seven plastic types immersed in seawater (PP, PLA, PBS, PBAT, and Mater-Bi) presented very similar communities (D7 and D15 of all material types grouped in Cluster 1) (ANOVA,  $p$  value = 0.221 and 0.121 for D7 and D15, respectively). Alphaproteobacteria represented 52% of the total OTU abundance in each sample, followed by Gammaproteobacteria (30%) and Bacteroidia

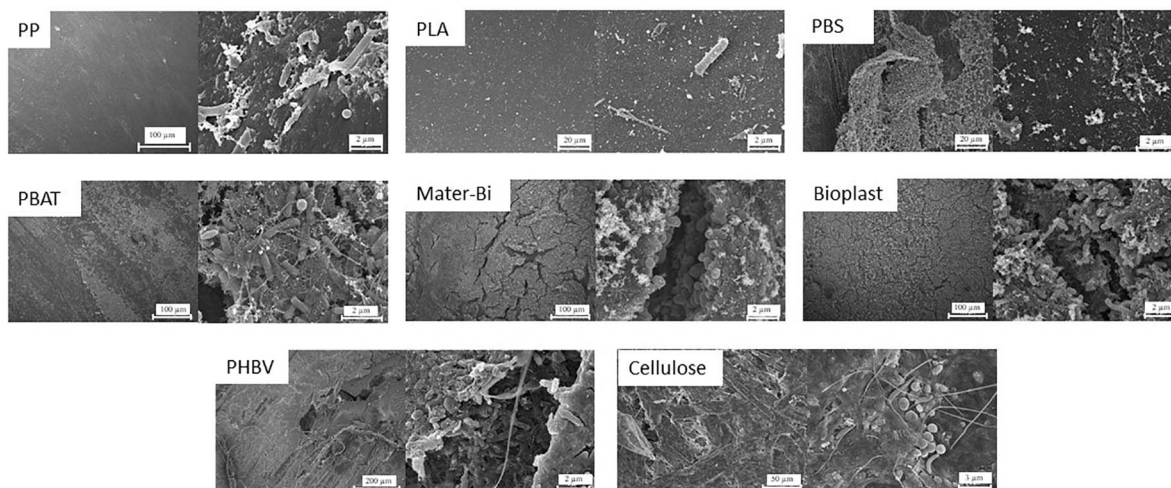


**FIGURE 1** | Scanning electron microscopy of the eight polymer types (PP, PLA, PBS, PBAT, Bioplast, Mater-Bi, PHBV, and cellulose) showing the diversity of morphologies and abundance of bacteria cell-like structures after 40 days in natural seawater followed by 94 days in minimum medium (D40 + 94). PP, polypropylene; PLA, polylactic acid; PBS, poly(butylene succinate); PBAT, polybutylene adipate terephthalate; PHBV, polyhydroxybutyrate-valerate.

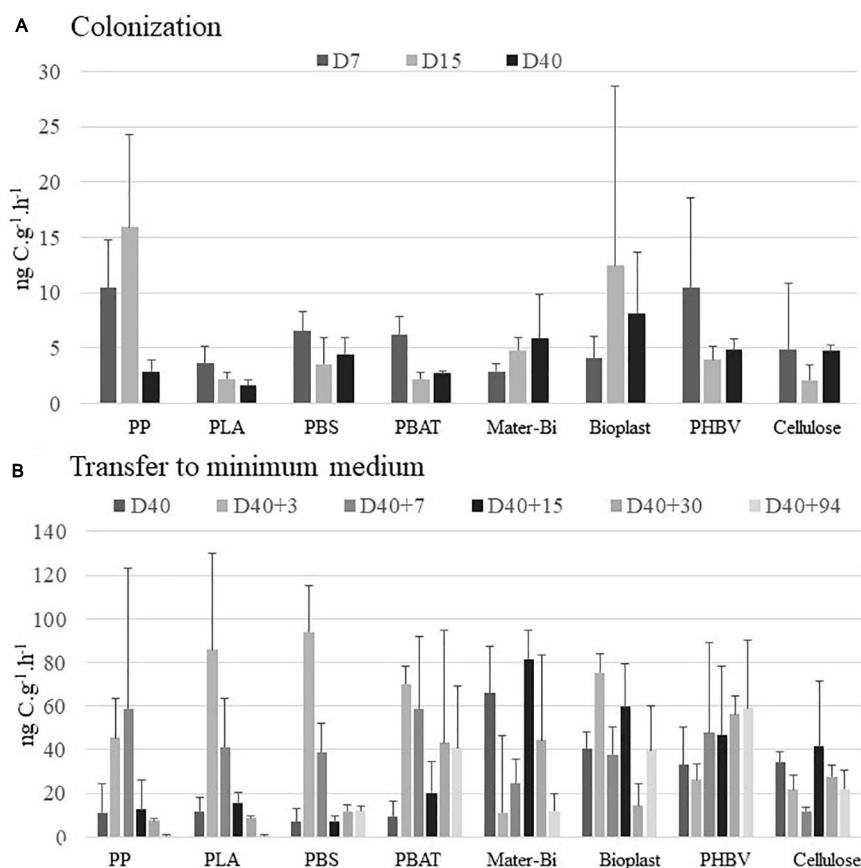


**FIGURE 2** | Bacterial production (in  $\text{ng C} \cdot \text{g}^{-1} \cdot \text{h}^{-1}$ ) **(A)** during the colonization phase in natural seawater at days 7 (D7), 15 (D15), and 40 (D40) and **(B)** after the transfer to minimum medium during 3 (D40 + 3), 7 (D40 + 7), 15 (D40 + 15), 30 (D40 + 30), and 94 days (D40 + 94). The vertical bars represent the average of the bacterial production for each material ( $n = 3$ )  $\pm$  standard deviation. Changes in BP values at D40 between panels **(A,B)** correspond to changes on dilution factor of the  $^3\text{H}$ -leucine added (see section "Materials and Methods"). BP, bacterial production.



(9%). The two most represented families were affiliated to the Alphaproteobacteria, with the Rhodobacteraceae (24%) (mainly *Sulfitobacter* sp. and *Pseudopelagicola* sp.) and the Methyloligellaceae (21%). Flavobacteriaceae (6.7%) (mainly *Croceibacter* sp. and *Aquibacter* sp.) and Nitrospiraceae (mainly *Neptunibacter* sp.) (5.5%) were also abundant during this stage. Bacteria growing on Bioplast and cellulose were grouped in a separate cluster (Cluster 3, **Figure 3**), with a lower majority of Alphaproteobacteria (32%) and higher presence of Bacteroidia (25%), together with similar abundance of Gammaproteobacteria (30%) as compared with the other plastic types (see above). Alteromonadaceae family dominated (24.5%) and was mainly represented by the *Alteromonas* sp. and *Marinobacter* sp. Flavobacteriaceae family represented 22% of the biofilm community, mainly represented by the *Wenyingshuangia* sp. Finally, like the other materials, the Rhodobacteraceae family was very abundant (21%) and was mainly represented by the genus *Sulfitobacter* sp.

Clear changes in bacterial community structures were observed after the growth phase, with clear dissimilarities between the distinct plastic types after 40 days in natural seawater (D40). PP and PLA biofilms (Cluster 2) were dominated by Alphaproteobacteria (Rhodobacteraceae) and Bacteroidia (Flavobacteriaceae). PBS and PBAT (Cluster 5) were dominated by Alphaproteobacteria (mainly Rhodobacteraceae) and Gammaproteobacteria (mainly Solimonadaceae). Bioplast and cellulose (Cluster 4) were dominated by Alphaproteobacteria (mainly Hyphomonadaceae) and Gammaproteobacteria (mainly Alteromonadaceae).

PHBV was dominated by Alphaproteobacteria (Rhodobacteraceae) followed by Gammaproteobacteria (Cellvibrionaceae) and finally Bacteroidia (Flavobacteriaceae). As for Mater-Bi, its mature biofilm was dominated by Alphaproteobacteria (Rhodobacteraceae), followed by Gammaproteobacteria (Sphingobacteriaceae) and Bacteroidia (Flavobacteriaceae).

### Biofilm Specialization After Transfer to Minimum Medium

The transfer from natural seawater to minimum medium resulted in bacterial community changes following three different scenarios according to the material types. First, the structures of the bacterial communities associated with PP, PBAT, and PBS remained stable and distinct during the 94 days of incubation. The second scenario was shared between most of the plastic types, where the initial biofilm, established during the colonization phase, remained stable for 1 week after the transfer in minimum medium (D40 + 7) and then switched to another community that remained stable until the end of the experiment (D40 + 94). This scenario was found for Bioplast, Mater-Bi, PHBV, and cellulose, even though bacterial communities growing on each material were grouped in distinct sub-clusters. A third scenario was found for PLA, which presented a chaotic dispersion of the bacterial communities among all other clusters, even if the community at the end of the experiment clustered in the Cluster 7, together with three sub-clusters composed of (i) Mater-Bi, (ii) Bioplast, and (iii) PLA, PHBV, and cellulose.

A drastic increase of Bacteroidetes and a decrease of Alpha- and Gammaproteobacteria was observed at the end of the experiment (D40 + 94) in Cluster 7. The evolution of the major OTUs found on each plastic type at the beginning (D40) and at the end (D40 + 94) of the incubation in minimum medium is described in detail in **Figure 4**.

During seawater incubation, the mature biofilm associated with the non-biodegradable PP and PLA (D40) was largely dominated by *Polycyclovorans* sp. and *Marivita* sp. (more than 62 and 49% for PP and PLA, respectively). These two OTUs became scarce at the end of the incubation in minimum medium (<2.3% at D40 + 94). Bacterial lineages present on PP after 94 days under this drastic condition were hydrocarbonoclasts *Balneola* sp., *Marinobacter* sp., *Winogradskyella* sp., and *Lewinella* sp., explaining 13.15% of the difference between D40 and D40 + 94 and representing 20% (SIMPER analysis) of the relative abundance of the biofilm during the specialization phase. The major OTU at D40 + 94 on PLA was *Planctomicrobium* sp. (56.7% of the community), which contributed to 32.31% of the difference with D40 (SIMPER analysis), where it was not detected. Other genera have emerged at D40 + 94 on this plastic such as *Arenibacter* sp., *Aureisphaera* sp., and *Marixanthomonas* sp. representing almost 11% of the relative abundance at the end of the incubation.

The mature biofilm on PBS (D40) was dominated by *Maribius* sp., *Neptuniibacter* sp., and *Bacillus* sp. representing nearly 21% of the total OTUs, while these three genera represented only 0.64% at D40 + 94. At the end of the experiment (D40 + 94), the biofilm was dominated by *Filomicrobium* sp. (31%), *Thalassobius* sp. (3%), and *Bythopirellula* sp. (2%) explaining about 23% of the disparity with the D40. These three bacterial genera were scarce until transfer into minimum medium (3%).

The dominant OTUs found in the mature biofilm (D40) on PBAT were Rhodobacteraceae at 20.37% (*Marivita* sp., *Lentibacter* sp.), Solimonadaceae at 7.1% (*Lewinella* sp.), and Methyloligellaceae at 5.6% and then switched to Saprospiraceae (42.5%) and *Filomicrobium* sp. (15.8%) at D40 + 94. These two OTUs alone explained 34.6% of the difference between the two sampling dates. As already found for PP and PLA, *Polycyclovorans* sp. was very abundant at D40 (7.1%) and was no longer detected at D40 + 94.

Incubation in minimum medium with Mater-Bi as sole carbon source resulted in the selection of *Aquimarina* sp., *Winogradskyella* sp., *Maritimibacter* sp., and *Filomicrobium* sp., which represented nearly 48% of the total OTUs at D40 + 94 but less than 2% at D40. These four genera explained 27.8% of the difference between the two sampling dates based on SIMPER analysis.

The OTUs selected at D40 + 94 for Bioplast were dominated by Microtrichaceae (12%), which belonged to the rare biosphere at D40 (<0.05%). Other genera emerged (> 9%) including *Aliiglaciecola* sp., *Filomicrobium* sp., and *Flexithrix* sp., while representing low abundance at D40 (<0.4%). On the contrary, *Alteromonas* sp. and *Oleibacter* sp. were abundant (8.8%) at D40 and became rare at D40 + 94 (<0.05%).

Selection on minimum medium with PHBV as sole carbon source showed the emergence of *Sphingorhabdus* sp., *Lewinella*



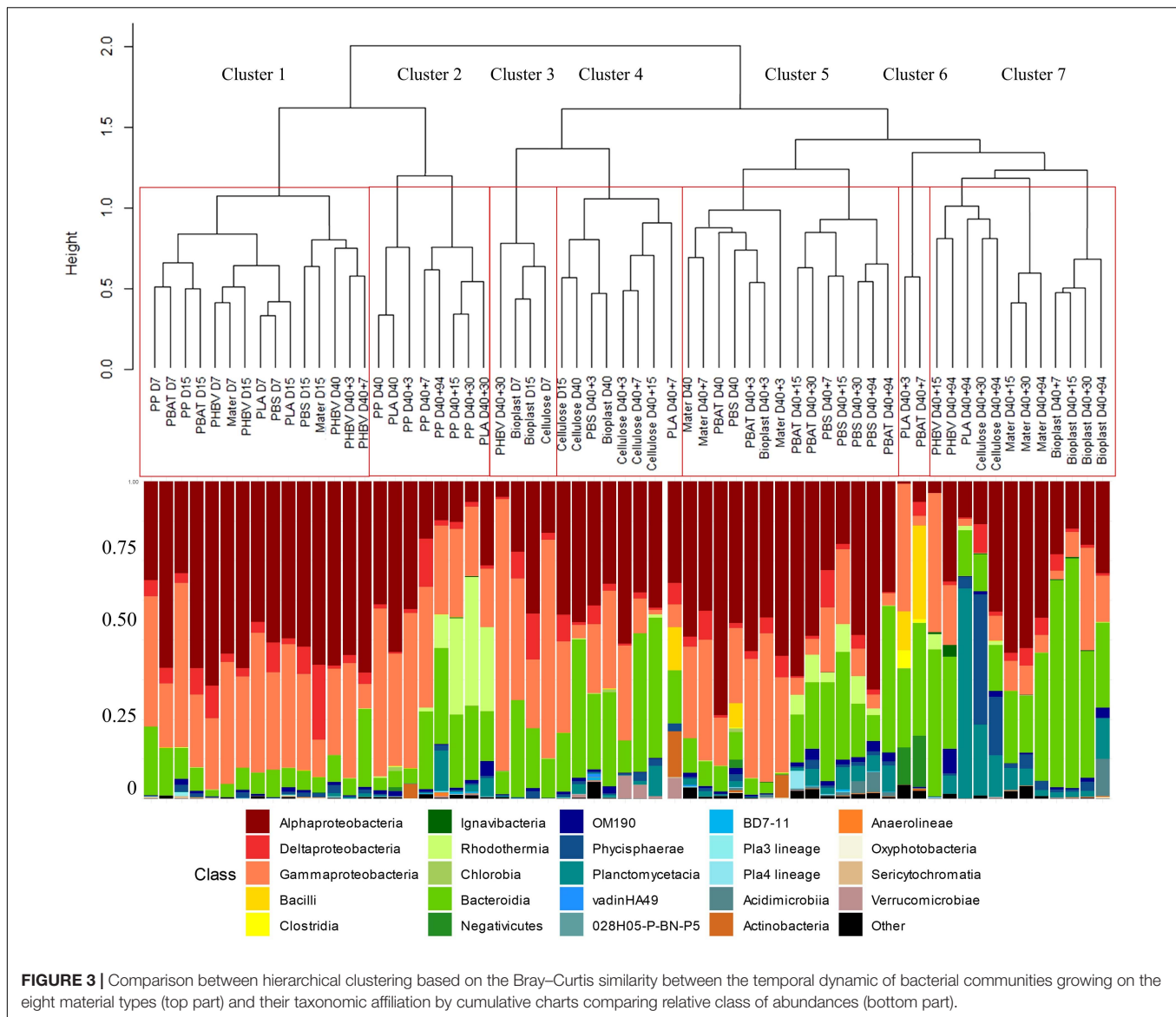


**FIGURE 3 |** Comparison between hierarchical clustering based on the Bray–Curtis similarity between the temporal dynamic of bacterial communities growing on the eight material types (top part) and their taxonomic affiliation by cumulative charts comparing relative class of abundances (bottom part).

sp., *Pseudahrensia* sp., and *Marinobacter* sp. (> 21% after D40 + 94 and <0.6% at D40), which explained 17.26% of the difference between D40 and D40 + 94 according to SIMPER analysis (Figure 4), whereas the dominant *Sedimentitalea* sp., *Thalassotalea* sp., and *Lentibacter* sp. at D40 (20% of the total OTUs) represented less than 0.1% at D40 + 94.

Cellulose selected *Parvularcula* sp., *Oleiphilus* sp., *Pirellula* sp., and *Phycisphaera* sp. at D40 + 94 (21.5% of the total OTUs at D40 + 94 compared with <1.5% at D40), which explained 16% of the difference between the two sampling dates. *Hirschia* sp. remained relatively stable between D40 (11.4%) and D40 + 94 (7.32%).

We finally focused on 35 different genera present on all the plastics and that may be considered as potential HCB. In this functional group, Gammaproteobacteria were overrepresented (40% of putative hydrocarbon degraders) followed by Bacteroidia (31%) and Alphaproteobacteria (23%). The most abundant

genera potentially involved in hydrocarbon degradation were *Neptuniibacter* sp., *Sulfitobacter* sp., *Balneola* sp., *Lentibacter* sp., and *Marinobacter* sp., which represented 52% of the total OTUs. Overall, putative HCB were abundant during the growth and maturation phases of the biofilms in seawater (between 8.4 and 38.0% of the total communities), with higher abundance generally found during the growth phase for all plastics (Table 2). Interestingly, the putative HCB decreased drastically until the end of the incubation in minimum medium with the plastics as sole carbon sources (D40 + 94). One exception was found for PP, which showed the highest percentage of putative HCB on the mature biofilm (38%), with even higher percentage found after 30 days in minimum medium (63.6%) mainly composed of *Balneola* sp., *Winogradskyella* sp., and *Marinobacter* sp. Other putative HCBs, such as *Polycylovorans* sp., *Neptuniibacter* sp., *Croceibacter* sp., and *Colweillia* sp. (Figure 4), were found in seawater during the colonization phase of most of

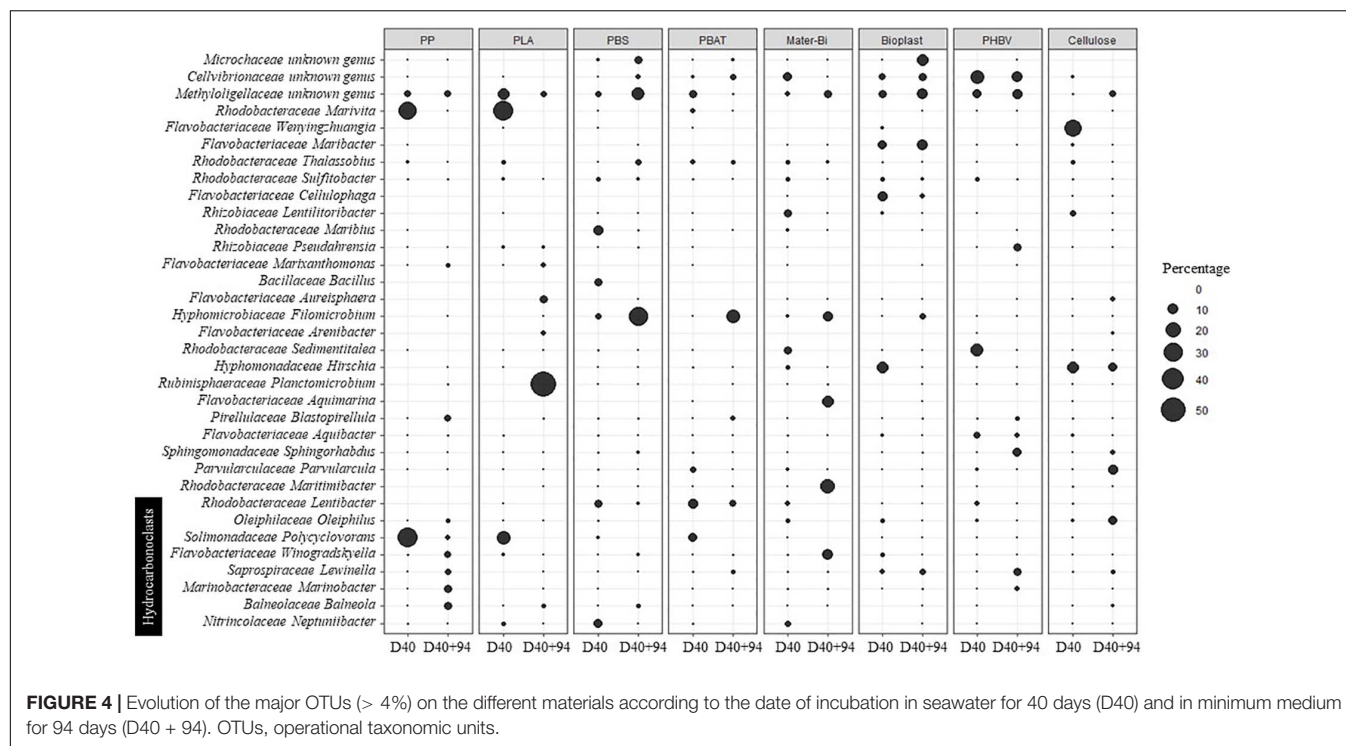


**TABLE 2 |** Percentage of OTU selected as putative HCB on each material (PP, PLA, PBS, PBAT, Mater-Bi, Bioplast, PHBV, and cellulose) according to the date of incubation in seawater during 7, 15, and 40 days (D40) followed by the transfer in minimum medium during 3 (40 + 3), 7 (40 + 7), 15 (40 + 15), 30 (40 + 30), and 94 days (40 + 94).

Days	Natural seawater			Minimum medium				
	7	15	40	40 + 3	40 + 7	40 + 15	40 + 30	40 + 94
Bioplast	21.1	21.6	12.1	55.1	7.1	9.6	5.8	6.6
Mater-Bi	23.0	14.5	13.3	37.3	19.5	6.2	10.7	13.4
PBAT	31.9	21.3	21.0	54.7	4.8	26.3	19.9	8.6
PBS	21.7	20.7	19.8	12.4	32.7	27.7	22.9	8.6
PHBV	16.0	18.5	8.4	33.4	15.8	8.3	46.1	11.1
PLA	35.1	22.3	22.7	1.4	20.1	NA	35.5	4.9
PP	32.5	26.6	38.0	21.3	37.8	60.2	63.6	26.6
Cellulose	17.4	16.3	11.2	14.1	13.9	3.3	0.9	12.3

OTU, operational taxonomic unit; HCB, hydrocarbonoclastic bacteria; PP, polypropylene; PLA, polylactic acid; PBS, poly(butylene succinate); PBAT, polybutylene adipate terephthalate; PHBV, polyhydroxybutyrate-valerate.

the materials but did not succeed in colonizing the plastics in minimum medium.

## DISCUSSION

### Formation of Mature Biofilms on all Plastic Types in Seawater Aquarium With Direct Circulation to the Sea Mimics the Natural Seawater Conditions of the North Western Mediterranean Sea

The colonization of the different material types was feasible thanks to distinct incubation in aquariums with seawater renewal

every 30 min. These aquariums presented similar hydrological conditions to those found at the SOLA observatory in the Banyuls Bay (NW Mediterranean Sea, France). During the first 40 days of incubation in seawater, temperature ( $13^{\circ}\text{C} \pm 0.5^{\circ}\text{C}$ ), chlorophyll *a*, and nutrient values (data not shown) were similar to those usually observed at the long-term SOLA observatory station (Ghiglione et al., 2005; Lambert et al., 2019). Bacterial heterotrophic activity in seawater, measured by  $^3\text{H}$ -leucine incorporation, reached  $22.3 \text{ ng C} \cdot \text{L}^{-1} \cdot \text{h}^{-1}$ , which was similar to what was generally reported *in situ* in the NW Mediterranean Sea (Pulido-Villena et al., 2012). These results showed that incubation in our aquariums with direct circulation to the sea allowed to reproduce environmental conditions, thus making extrapolation of our results to natural seawater possible.

## Growth and Maturation Phases of the Biofilms on all the Plastic Types in Seawater

In agreement with patterns observed in another study (Salta et al., 2013), we found a succession of growth and maturation phases of the biofilms for all the material types during the first 40 days of incubation in natural seawater. Each phase was linked with bacterial communities that were similar during the growth phase but became specific to the material types when the mature biofilm formed. This result is in agreement with a previous study conducted in the same region (Dussud et al., 2018).

Bacterial heterotrophic activity peaked during the growth phase of the biofilm in all plastic types (either after 7 or 15 days). These bacterial communities were very similar regardless of the plastic types, except for Bioplast and cellulose, which clustered in another group. This result was surprising considering the distinct chemical material compositions and surface properties of the plastics used in our study. It is noteworthy that bacterial communities growing on Mater-Bi (about 60% corn starch and 40% PBAT) did not cluster with cellulose and Bioplast at this stage (about 40% potato starch and 60% PLA), probably because of different surface properties of the materials that may be related to distinct polymer compositions together with the unknown effect of potentially incorporated additives (not mentioned by the manufacturer). Indeed, early stages of biofilm formation have been depicted as strongly dependent on the surface properties of plastics, including hydrophobicity, structure, and roughness (Lorite et al., 2011). This was not obvious for immersed plastics in seawater, since our results were similar with other studies that did not find distinct communities during the first weeks of biofilm formation on different plastic types (Harrison et al., 2014; De Tender et al., 2017; Dussud et al., 2018). Regardless of the plastic type, the first growth phase was mainly dominated by Proteobacteria (84% of the total abundance on all materials), followed by Bacteroidetes (12.5%). The dominance of Proteobacteria during the first stage of colonization has already been described on the plastisphere (Jacquin et al., 2019). The main classes of the Proteobacteria were Alphaproteobacteria (47.14%, mainly Methylobacteriaceae and Rhodobacteraceae) and Gammaproteobacteria (31.46%). The Methylobacteriaceae family has already been isolated on other plastic types such as polyamide, polycarbonate, or PP (Feng et al., 2020). All studied plastics were mainly colonized by members of the Rhodobacteraceae during the colonization phase and the specialization phase. This family has been depicted as a key taxonomic group in marine biofilm formation on different material types (Elifantz et al., 2013; Kviatkovski and Minz, 2015; Roager and Sonnenschein, 2019), which explained its large presence on the tested plastics. During the colonization phase, the Flavobacteriaceae family and particularly the genus *Neptuniibacter* sp., generally able to degrade hydrocarbons, was found in abundance on PLA, PBS, and Mater-Bi (Gutierrez, 2019). This result is consistent with a previous study that showed its presence only during the primary colonization phase of plastics under similar conditions (Dussud et al., 2018). In all material types, the mature biofilm that formed after 40 days of incubation in seawater showed lower values of bacterial heterotrophic activity compared with the growth phase. This is

consistent with observations made in the unique study measuring bacterial heterotrophic activities on the plastisphere (Dussud et al., 2018). It can be explained by the equilibrium reached by a biofilm at its maturity, which is related to the decrease of available labile inorganic and organic matter and also to the complex interactions (competition, commensalism, etc.) between species coexisting on plastics (Lorite et al., 2011; Henson and Phalak, 2017). Diversity in mature biofilms became specific for each plastic type, which is consistent with observations made in the natural environment (Webb et al., 2012; De Tender et al., 2017; Pinto et al., 2019).

## Convergent Signs of Biodegradation for Some Plastic Types

As recommended in several standard tests (ISO 18830:2016, ISO 19679:2016, and ASTM D6691-09), the biodegradation of the studied plastics was tested after transferring the plastic pieces into minimum medium with no other carbon or energy source (ISO 18830:2016, ISO 19679:2016). As suggested in these tests, we used cellulose as a positive control, and we considered PP as a negative control since its biodegradation was previously depicted to take years or decades in the environment (Barnes et al., 2009). Standards allow the possibility of using two types of inoculum, i.e., artificial mixing of culture of microorganisms or bacterial communities from natural seawater. These methods have been criticized since they are not able to reproduce the mature biofilms usually found on plastics in the environment (Harrison et al., 2018; Jacquin et al., 2019). In our study, we followed the development of a natural mature biofilm on eight different material types (40 days' incubation in seawater) before using that biofilm as an inoculum for further biodegradation tests.

After 94 days in minimum medium, SEM observations showed no surface modifications for PP, PLA, and PBS, whereas PBAT, Bioplast, Mater-Bi, PHBV, and cellulose exhibited observable morphological alterations, with clear evidence of swelling and erosion. Visible alterations of plastic surfaces are considered to be suitable signs of biodegradation, even if these alterations alone are not sufficient (Zettler et al., 2013). Plastics, such as PHBV, are known to undergo biofragmentation by numerous exo-enzymatic actions (amylases, proteases, and nucleases), leading to weakening of the surface of the material (Deroiné et al., 2014a, 2015). Our results are consistent with a previous study showing evidence of faster degradation of PHAs in seawater compared with other plastics such as PBS, PBAT, or PLA (Sashiwa et al., 2018). In our conditions, PHBV showed more cracks, holes, and colonization features than PBAT, Bioplast, Mater-Bi, PHBV, and cellulose (Figure 1). In parallel, SEM observations at the end of the experiment showed dispersed and isolated bacteria for PP, PLA, and PBS, whereas dense biofilms with a three-dimensional structure and substantial extracellular matrix were found for all the other plastics. PLA was previously found to degrade very slowly in seawater and remain stable at room temperature (Deroiné et al., 2014b), while PBS degradation was found to be slower when salinity increased

(Silva Dutra et al., 2019), which are also consistent results with our observations. In our conditions, the radiolabeled leucine incorporation as a proxy of bacterial biodegradation has drawn the same conclusion as the SEM analysis. Interestingly, this is the first time that this technique has been used for this purpose, whereas it has been used for decades to measure the microbial heterotrophic activity and growth in seawater (Kirchman et al., 1985).

It has been successfully used to prove the biodegradability of several other substrates, such as antifouling biocides (Maraldo and Dahllöf, 2004), hydrocarbons (Peng et al., 2020), plasticizers, and flame retardants (Vila-Costa et al., 2019), but never for plastic materials in seawater, probably because of the lack of studies in marine environments. In seawater, this technique is generally preferred to respirometry measurements ( $O_2$  consumption or  $CO_2$  production) because its sensitivity is more suitable in oligotrophic waters (Briand et al., 2004; Pulido-Villena et al., 2012). Current standards are based on respirometry analyses and generally measure  $CO_2$  by gas chromatography, total organic carbon analyzer, infrared analyzer (ISO 14855-1), or  $CO_2$  capture by soda lime (ISO 14855-2). These experimental approaches can be automated but require a significant financial investment and large laboratory spaces, which can reduce the number of experimental replicates. This has already been described as one of the limitations of the current standards on plastic biodegradation (Harrison et al., 2018). Here, we found that other activity tests based on  $^3H$ -leucine incorporation were well suited for biodegradation tests of plastic materials in seawater. Our experiments showed that bacteria living in the mature biofilm can continue to be active for several days after transfer under minimum medium with no other carbon source, as it is the case for PP, PLA, and PBS, which showed bacterial heterotrophic activities during 1 or 2 weeks before falling off. Cross-feeding of metabolites synthesized by one species to support the growth of another species to maximize utilization of available resources, together with competition to limited resources, may explain the activity observed during several days and its further decline (Pande et al., 2014; Henson and Phalak, 2017). This is an important point because such an activity could be misinterpreted as a sign of plastic biodegradation if integrative measurements were only taken at the end of the experiment. For PBAT, Bioplast, Mater-Bi, PHBV, and cellulose, the bacterial heterotrophic activity remained rather stable after 15 days in minimum medium and until the end of the experiment (94 days). Taken together with congruent results from SEM observations, we consider that the radiolabeled leucine incorporation measurement was a good proxy of their biodegradation. Our results are consistent with previous findings showing the biodegradation in soil, compost, or seawater for PBAT (Saadi et al., 2013; Weng et al., 2013; Wang et al., 2021), Mater-Bi (Kim et al., 2000), Bioplast<sup>3</sup>, PHBV (Arcos-Hernandez et al., 2015; Deroiné et al., 2015; Wang et al., 2021), and cellulose (Salehpour et al., 2018; Kliem et al., 2020; Zambrano et al., 2020). It is interesting to note that PLA, a plastic considered to be compostable and biodegradable in soil and compost

(Ren et al., 2007), did not show any sign of biodegradation under our marine experimental conditions.

## Identification of Putative Biodegraders of the Tested Materials

According to SEM and heterotrophic bacterial activity measurements, we focused on the OTUs selected at the end of the incubation in minimum medium on the plastic materials that showed clear signs of biodegradation under our experimental conditions: PBAT, Bioplast, Mater-Bi, PHBV, and cellulose. The presence of complex communities living under such strict conditions strongly suggest that they are putative biodegraders that may interact with one another in order to perform all or part of the degradation until the ultimate mineralization in  $CO_2$  (Dussud and Ghiglione, 2014). We are aware that part of the identified OTUs may not be involved in the plastic degradation but rather opportunists that may survive in the biofilm (Sauret et al., 2014). Our original procedure allowed to present here a list of putative OTUs selected from a mature biofilm grown under natural seawater conditions, which may be involved in biodegradation of the plastics.

On the PBAT, we found *Thalassobius* sp. as dominant OTUs after 94 days in minimum medium with the mature biofilm and its plastic as sole carbon source. This genus has already been suggested as potentially capable of degrading aromatic hydrocarbons in seawater (Rodrigo-Torres et al., 2017) and found in the oil polluted waters of the Gulf of Mexico (Liu et al., 2017). *Filomicrobium* sp. were also dominant at the end of the experiment and have already been observed in other marine environments (Wu et al., 2009), as well as *Prevotella* sp. and *Streptococcus* sp. known as potential pathogenic genera (Fittipaldi et al., 2012; Larsen, 2017). None of them were previously identified as potential PBAT degraders.

The bacteria growing with Mater-Bi as sole carbon source was dominated by *Filomicrobium* sp., already identified on the plastisphere of PE and PET (Muthukrishnan et al., 2018). Other groups were *Winogradskyella* sp., *Maritimibacter* sp., *Aquimarina* sp., and *Halomonas* sp., which were previously described as putative HCB (Mnif et al., 2009; Liu et al., 2017). None of them were previously identified as potential Mater-Bi (starch with PBAT) degraders.

Bacteria selected on Bioplast at the end of the experiment included *Lewinella* sp., already identified on the plastisphere of fossil-based PP, PE, and PET, as well as on biobased PHBH films (Morohoshi et al., 2018; Roager and Sonnenschein, 2019). Other potential OTUs belonging to putative HCB were *Croceitalea* sp., *Hirschia* sp., *Maribacter* sp., and *Cellulophaga* sp. None of them were previously identified as being potentially able to degrade Bioplast (starch with PLA).

Microbial communities selected after 94 days on PHBV as sole carbon source such as *Marinobacter* sp. and *Alteromonas* sp. were already known for their ability to degrade PHBV (Mergaert et al., 1995; Martinez Tobon, 2019). *Marinobacter* sp. genera contain well-known HCB capable of degrading benzene, toluene,

<sup>3</sup><https://fr.biotech.de/>



ethylbenzene, and xylene (BTEX) (Li et al., 2012), long-chain alkanes (Grimaud et al., 2012), polycyclic aromatic hydrocarbons (Gao et al., 2013; Cui et al., 2016), chlorinated solvents (Inoue et al., 2020), phenol (Zhou et al., 2020), and PHA (Kasuya et al., 2000; Martinez Tobon, 2019).

Finally, it is noteworthy that putative HCB were less abundant during the biodegradation phase (from 6 to 12% of the total OTUs) than during the colonization phase (from 8 to 35% of the total OTUs). These results were unexpected since several authors proposed that the HCB are certainly involved in plastic biodegradation since they are always found as dominant members of the microbial communities growing on fossil-based plastics recovered from the sea surface (Bryant et al., 2016; Pollet et al., 2018; Amaral-Zettler et al., 2020). Here, we showed that some HCB may actually be involved in biodegradation, but they were not a majority under our experimental conditions. HCB generally present a high ability to attach to particles and to live in a biofilm (Grimaud et al., 2012), two factors that may be more important than their ability to degrade plastics.

## Concluding Remarks

The decisions taken by the European government to reduce the use of single-use plastics and promote biodegradable materials lead to finding substitutes for conventional plastics. Here, we emphasized that materials such as PHBV, Mater-Bi, Bioplast, PBAT, and cellulose are good alternatives to banned cotton swabs generally made of non-biodegradable PP. It is noteworthy that the bio-based polymer PLA showed no signs of biodegradation under our marine conditions, whereas the fossil-based polymer PBAT showed significant evidence of biodegradation. This reinforced the distinction that has to be made between biobased and biodegradable polymers when considering alternative to conventional fossil-based plastics.

Our approach, coupling bacterial diversity and activity measurements, brought new insights on the ability of natural biofilms to biodegrade plastic materials in seawater, with this information being essential for our understanding of the microbial communities involved in the plastisphere and for future alternative biodegradation tests of plastic items in the marine environment. Our study also opens new perspectives by identifying putative bacteria potentially capable of biodegrading the tested plastic materials. These results require further studies to better understand the still largely unexplored functional processes involved in biodegradation in natural seawater.

## REFERENCES

- Amaral-Zettler, L. A., Zettler, E. R., and Mincer, T. J. (2020). Ecology of the plastisphere. *Nat. Rev. Microbiol.* 18, 139–151. doi: 10.1038/s41579-019-0308-0
- Arcos-Hernandez, M., Montano-Herrera, L., Janarthanan, O. M., Quadri, L., Anterrieu, S., Hjort, M., et al. (2015). Value-added bioplastics from services of wastewater treatment. *Water Pract. Technol.* 10:546.
- Auta, H., Emenike, C., and Fauziah, S. H. (2017). Distribution and importance of microplastics in the marine environment: a review of the sources, fate, effects, and potential solutions. *Environ. Inter.* 102, 165–176.

## DATA AVAILABILITY STATEMENT

The datasets presented in this study can be found in online repositories. The names of the repository/repositories and accession number(s) can be found in the article/ **Supplementary Material**.

## AUTHOR CONTRIBUTIONS

J-FG, JJ, and NC conceived and designed the study. NC, JJ, CG, JC, and YG carried out all the experiments and acquired the data. SB and CD provided the equipment. NC, JJ, and J-FG analyzed and interpreted the data. JJ, J-FG, NC, CG, and VB drafted the manuscript. MP-P, PC, and A-LM revised the manuscript and approved the version of the manuscript to be published. All authors contributed to the article and approved the submitted version.

## FUNDING

This project was funded by the Ministry of Ecological and Solidarity Transition of the French Republic (project BIOTIGE). This work was also supported by the European project JRA-ASSEMBLE+, the French National Research Agency (project ANR-OXOMAR), the Tara Ocean Foundation (project Microplastic 2019), and the CNRS (project PEPS'I-PHABIO).

## ACKNOWLEDGMENTS

We are grateful to Valerie Bayo and Charlene Odobel for their kind laboratory support and to Guigui PA and VF for insightful comments on the manuscript. This work is part of the PhD thesis of JJ supported by the French Ministry of Education.

## SUPPLEMENTARY MATERIAL

The Supplementary Material for this article can be found online at: <https://www.frontiersin.org/articles/10.3389/fmicb.2021.604395/full#supplementary-material>

- Barnes, D. K. A., Galgani, F., Thompson, R. C., and Barlaz, M. (2009). Accumulation and fragmentation of plastic debris in global environments. *Philos. Trans. R. Soc. B Biol. Sci.* 364, 1985–1998. doi: 10.1098/rstb.2008.0205
- Briand, E., Pringault, O., Jacquet, S., and Torreyton, J. P. (2004). The use of oxygen microprobes to measure bacterial respiration for determining bacterioplankton growth efficiency. *Limnol. Oceanogr.* 2, 406–416. doi: 10.4319/lom.2004.2.406
- Bryant, J. A., Clemente, T. M., Viviani, D. A., Fong, A. A., Thomas, K. A., Kemp, P., et al. (2016). Diversity and activity of communities inhabiting plastic debris in the North Pacific Gyre. *mSystems* 11:e00024-16.

- Camacho, C., Coulouris, G., Avagyan, V., Ma, N., Papadopoulos, J., Bealer, K., et al. (2009). BLAST+: architecture and applications. *BMC Bioinform.* 10:421. doi: 10.1186/1471-2105-10-421
- Cui, Z., Gao, W., Xu, G., Luan, X., Li, Q., Yin, X., et al. (2016). *Marinobacter aromaticivorans* sp. nov., a polycyclic aromatic hydrocarbon-degrading bacterium isolated from sea sediment. *Int. J. Syst. Evol. Microbiol.* 66, 353–359. doi: 10.1099/ijsem.0.000722
- Dang, H., and Lovell, C. R. (2000). Bacterial primary colonization and early succession on surfaces in marine waters as determined by amplified rRNA gene restriction analysis and sequence analysis of 16S rRNA genes. *Appl. Environ. Microbiol.* 66, 467–475. doi: 10.1128/aem.66.2.467-475.2000
- De Tender, C., Devriese, L. I., Haegeman, A., Maes, S., Vangeyte, J., Cattrijse, A., et al. (2017). Temporal dynamics of bacterial and fungal colonization on plastic debris in the North Sea. *Environ. Sci. Technol.* 51, 7350–7360. doi: 10.1021/acs.est.7b00697
- Debeljak, P., Pinto, M., Proietti, M., Reisser, J., Ferrari, F. F., Abbas, B., et al. (2016). Extracting DNA from ocean microplastics: a method comparison study. *Anal. Methods* 9, 1521–1523. doi: 10.1039/c6ay03119f
- Deroiné, M., César, G., Le Duigou, A., Davies, P., and Bruzaud, S. (2015). Natural degradation and biodegradation of Poly(3-Hydroxybutyrate-co-3-Hydroxyvalerate) in liquid and solid marine environments. *J. Poly. Environ.* 23, 493–505. doi: 10.1007/s10924-015-0736-5
- Deroiné, M., Le Duigou, A., Corre, Y.-M., Le Gac, P. Y., Davies, P., César, G., et al. (2014a). Accelerated ageing and lifetime prediction of poly(3-hydroxybutyrate-co-3-hydroxyvalerate) in distilled water. *Poly. Test.* 39, 70–78. doi: 10.1016/j.polymertesting.2014.07.018
- Deroiné, M., Le Duigou, A., Corre, Y.-M., Le Gac, P. Y., Davies, P., César, G., et al. (2014b). Accelerated ageing of polylactide in aqueous environments: comparative study between distilled water and seawater. *Poly. Degrad. Stabil.* 108, 319–329. doi: 10.1016/j.polymdegradstab.2014.01.020
- Dussud, C., and Ghiglione, J.-F. (2014). “Bacterial degradation of synthetic plastics,” in *Marine litter in the Mediterranean and Black Seas CIESM workshop Monographs*, ed. F. Briand (Paris: CIESM Publisher), 43–48.
- Dussud, C., Hudc, C., George, M., Fabre, P., Higgs, P., Bruzaud, S., et al. (2018). Colonization of non-biodegradable and biodegradable plastics by marine microorganisms. *Front. Microbiol.* 9:1571. doi: 10.3389/fmicb.2018.01571
- Eich, A., Mildenberger, T., Laforsch, C., and Weber, M. (2015). Biofilm and diatom succession on polyethylene (PE) and biodegradable plastic bags in two marine habitats: early signs of degradation in the pelagic and benthic zone? *PLoS One* 10:e0137201. doi: 10.1371/journal.pone.0137201
- Elifantz, H., Horn, G., Ayon, M., Cohen, Y., and Minz, D. (2013). Rhodobacteraceae are the key members of the microbial community of the initial biofilm formed in Eastern Mediterranean coastal seawater. *FEMS Microbiol. Ecol.* 85, 348–357. doi: 10.1111/1574-6941.12122
- Eriksen, M., Lebreton, L. C. M., Carson, H. S., Thiel, M., Moore, C. J., Borrorro, J. C. et al. (2014). Plastic pollution in the World's Oceans: more than 5 trillion plastic pieces weighing over 250,000 tons afloat at Sea. *PLoS One* 9:e111913. doi: 10.1371/journal.pone.0111913
- Erni-Cassola, G., Wright, R. J., Gibson, M. I., and Christie-Oleza, J. A. (2019). Early colonization of weathered polyethylene by distinct bacteria in marine coastal seawater. *Microbiol. Ecol.* 79, 517–526. doi: 10.1007/s00248-019-01424-5
- Escudé, F., Auer, L., Bernard, M., Mariadassou, M., Cauquil, L., Vidal, K., et al. (2018). FROGS: find, rapidly, OTUs with galaxy solution. *Bioinformatics* 34, 1287–1294. doi: 10.1093/bioinformatics/btx791
- Europarl (2019). *Directive (EU) 2019/904 of the European Parliament and of the Council of 5 June 2019 on the Reduction of the Impact of Certain Plastic Products on the Environment*. Available online at: <https://eur-lex.europa.eu/eli/dir/2019/904/oj>
- Fegatella, F., Lim, J., Kjelleberg, S., and Cavicchioli, R. (1998). Implications of rRNA operon copy number and ribosome content in the marine oligotrophic ultramicrobacterium *Sphingomonas* sp. strain RB2256. *Appl. Environ. Microbiol.* 64, 4433–4438. doi: 10.1128/aem.64.11.4433-4438.1998
- Feng, L., He, L., Jiang, S., Chen, J., Zhou, C., Qian, Z.-J., et al. (2020). Investigating the composition and distribution of microplastics surface biofilms in coral areas. *Chemosphere* 252:126565. doi: 10.1016/j.chemosphere.2020.126565
- Fittipaldi, N., Segura, M., Grenier, D., and Gottschalk, M. (2012). Virulence factors involved in the pathogenesis of the infection caused by the swine pathogen and zoonotic agent *Streptococcus suis*. *Fut. Microbiol.* 7, 259–279. doi: 10.2217/fmb.11.149
- Fontanella, S., Bonhomme, S., Brusson, J. M., Pitteri, S., Samuel, G., Pichon, G., et al. (2013). Comparison of biodegradability of various polypropylene films containing additives based on Mn, Mn/Fe or Co. *Polym. Degrad. Stab.* 98, 875–884. doi: 10.1016/j.polymdegradstab.2013.01.002
- Fuhrman, J. A., Sleeter, T. D., Carlson, C. A., and Proctor, L. M. (1989). Dominance of bacterial biomass in the Sargasso Sea and its ecological implications. *Mar. Ecol. Prog. Ser.* 57, 207–217. doi: 10.3354/meps057207
- Gao, W., Cui, Z., Li, Q., Xu, G., Jia, X., and Zheng, L. (2013). *Marinobacter nanhaiticus* sp. nov., polycyclic aromatic hydrocarbon-degrading bacterium isolated from the sediment of the South China Sea. *Antonie van Leeuwenhoek* 103, 485–491. doi: 10.1007/s10482-012-9830-z
- Ghiglione, J.-F., Larcher, M., and Lebaron, P. (2005). Spatial and temporal scales of variation in bacterioplankton community structure in the NW Mediterranean Sea. *Aquat. Microb. Ecol.* 40, 229–240. doi: 10.3354/ame040229
- Goldstein, J. I., Newbury, D. E., Echlin, P., Joy, D. C., Romig, A. D. Jr., Lyman, C. E., et al. (1992). “Sample preparation for biological, organic, polymeric, and hydrated materials,” in *Scanning Electron Microscopy and X-Ray Microanalysis*, (Boston, MA: Springer). doi: 10.1007/978-1-4613-0491-3\_12
- Grimaud, R., Ghiglione, J.-F., Cagnon, C., Lauga, B., Vaysse, P. J., Rodriguez-Blanco, A., et al. (2012). Genome sequence of the marine bacterium *Marinobacter hydrocarbonoclasticus* SP17, which forms biofilms on hydrophobic organic compounds. *J. Bacteriol.* 194, 3539–3540. doi: 10.1128/jb.00500-12
- Gutierrez, T. (2019). “Occurrence and roles of the obligate hydrocarbonoclastic bacteria in the ocean when there is no obvious hydrocarbon contamination,” in *Taxonomy, Genomics and Ecophysiology of Hydrocarbon-Degrading Microbes*, ed. T. J. McGenity (Cham: Springer International Publishing).
- Harrison, J. P., Boardman, C., O'Callaghan, K., Delort, A.-M., and Song, J. (2018). Biodegradability standards for carrier bags and plastic films in aquatic environments: a critical review. *R. Soc. Open Sci.* 5:171792. doi: 10.1098/rsos.171792
- Harrison, J. P., Schratzberger, M., Sapp, M., and Osborn, A. M. (2014). Rapid bacterial colonization of low-density polyethylene microplastics in coastal sediment microcosms. *BMC Microbiol.* 14:232. doi: 10.1186/s12866-014-0232-4
- Henson, M. A., and Phalak, P. (2017). Byproduct cross feeding and community stability in an in silico biofilm model of the gut microbiome. *Processes* 5:13. doi: 10.3390/pr5010013
- Inoue, Y., Fukunaga, Y., Katsumata, H., Ohji, S., Hosoyama, A., Mori, K., et al. (2020). Aerobic degradation of *cis*-dichloroethene by the marine bacterium *Marinobacter salsuginis* strain 5N-3. *J. Gen. Appl. Microbiol.* 66, 215–219. doi: 10.2323/jgam.2019.10.001
- Jacquin, J., Cheng, J., Odobel, C., Pandin, C., Conan, P., Pujo-Pay, M., et al. (2019). Microbial ecotoxicology of marine plastic debris: a review on colonization and biodegradation by the “plastisphere.” *Front. Microbiol.* 10:865. doi: 10.3389/fmicb.2019.00865
- Kasuya, K., Mitomo, H., Nakahara, M., Akiba, A., Kudo, T., Doi, Y. (2000). Identification of a marine benthic P(3HB)-degrading bacterium isolate and characterization of its P(3HB) depolymerase. *Biomacromolecules* 1, 194–201. doi: 10.1021/bm9900186
- Kliem, S., Kreutzbruck, M., and Bonten, C. (2020). Review on the biological degradation of polymers in various environments. *Materials* 13:4586.
- Kim, M.-N., Lee, A.-R., Yoon, J.-S., and Chin, I.-J. (2000). Biodegradation of poly(3-hydroxybutyrate), Sky-Green® and Mater-Bi® by fungi isolated from soils. *Eur. Polym. J.* 36, 1677–1685.
- Kirchman, D., K'nees, E., and Hodson, R. (1985). Leucine incorporation and its potential as a measure of protein synthesis by bacteria in natural aquatic systems. *Appl. Environ. Microbiol.* 49, 599–607. doi: 10.1128/aem.49.3.599-607.1985
- Kviatkovski, I., and Minz, D. (2015). A member of the Rhodobacteraceae promotes initial biofilm formation via the secretion of extracellular factor(s). *Aquat. Microb. Ecol.* 75, 155–167. doi: 10.3354/ame01754
- Lambert, S., Tragin, M., Lozano, J.-C., Ghiglione, J. F., Vaultot, D., Bouget, F. Y., et al. (2019). Rhythmicity of coastal marine picoeukaryotes, bacteria and archaea despite irregular environmental perturbations. *ISME J.* 13, 388–401.

- Larsen, J. M. (2017). The immune response to *Prevotella* bacteria in chronic inflammatory disease. *Immunology* 151, 363–374. doi: 10.1111/imm.12760
- Li, H., Zhang, Q., Wang, X.-L., Ma, X.-Y., Lin, K.-F., Liu, Y.-D., et al. (2012). Biodegradation of benzene homologues in contaminated sediment of the East China Sea. *Bioresour. Technol.* 124, 129–136. doi: 10.1016/j.biortech.2012.08.033
- Liu, J., Bacosa, H. P., and Liu, Z. (2017). Potential environmental factors affecting oil-degrading bacterial populations in deep and surface waters of the Northern Gulf of Mexico. *Front. Microbiol.* 7:2131. doi: 10.3389/fmicb.2016.02131
- Lobelle, D., and Cunliffe, M. (2011). Early microbial biofilm formation on marine plastic debris. *Mar. Pollut. Bull.* 62, 197–200. doi: 10.1016/j.marpolbul.2010.10.013
- Lorite, G. S., Rodrigues, C. M., de Souza, A. A., Kranz, C., Mizaikoff, B., Cotta, M. A. (2011). The role of conditioning film formation and surface chemical changes on *Xylella fastidiosa* adhesion and biofilm evolution. *J. Colloid Interface Sci.* 359, 289–295. doi: 10.1016/j.jcis.2011.03.066
- Mahé, F., Rognes, T., Quince, C., de Vargas, C., Dunthorn, M. (2014). Swarm: robust and fast clustering method for amplicon-based studies. *PeerJ* 2:e593. doi: 10.7717/peerj.593
- Maraldo, K., and Dahllöf, I. (2004). Indirect estimation of degradation time for zinc pyrrhione and copper pyrrhione in seawater. *Mar. Pollut. Bull.* 48, 894–901. doi: 10.1016/j.marpolbul.2003.11.013
- Martinez, T. (2019). *Biodegradation of Polyhydroxybutyrate by Bacterial Strains, Native Extracellular PHB Depolymerases, and Structural Variants*. Ph.D. thesis. Available online at: <https://era.library.ualberta.ca/items/dbb78623-781a-4f19-a957-e08222ad5f7c>
- McMurdie, P. J., and Holmes, S. (2013). phyloseq: an R package for reproducible interactive analysis and graphics of microbiome census data. *PLoS One* 8:e61217. doi: 10.1371/journal.pone.0061217
- Mergaert, J., Wouters, A., Swings, J., and Anderson, C. (1995). In situ biodegradation of poly(3-hydroxybutyrate) and poly(3-hydroxybutyrate-co-3-hydroxyvalerate) in natural waters. *Can. J. Microbiol.* 41, 154–159. doi: 10.1139/m95-182
- Mnif, S., Chamkha, M., and Sayadi, S. (2009). Isolation and characterization of *Halomonas* sp. strain C2SS100, a hydrocarbon-degrading bacterium under hypersaline conditions. *J. Appl. Microbiol.* 107, 785–794. doi: 10.1111/j.1365-2672.2009.04251.x
- Morohoshi, T., Ogata, K., Okura, T., and Sato, S. (2018). Molecular characterization of the bacterial community in biofilms for degradation of poly(3-Hydroxybutyrate-co-3-Hydroxyhexanoate) films in seawater. *Microb. Environ.* 33, 19–25. doi: 10.1264/jsme2.me17052
- Muthukrishnan, T., Al Khaburi, M., and Abed, R. M. M. (2018). Fouling microbial communities on plastics compared with wood and steel: are they substrate- or location-specific? *Microb. Ecol.* 78, 361–374. doi: 10.1007/s00248-018-1303-0
- Oberbeckmann, S., Löder, M. G. J., and Labrenz, M. (2015). Marine microplastic-associated biofilms – a review. *Environ. Chem.* 12, 551–562. doi: 10.1071/en15069
- Pande, S., Merker, H., Bohl, K., Reichelt, M., Schuster, S., De Figueiredo, L. F., et al. (2014). Fitness and stability of obligate cross-feeding interactions that emerge upon gene loss in bacteria. *ISME J.* 8, 953–962. doi: 10.1038/ismej.2013.211
- Parada, A. E., Needham, D. M., and Fuhrman, J. A. (2016). Every base matters: assessing small subunit rRNA primers for marine microbiomes with mock communities, time series and global field samples. *Environ. Microbiol.* 18, 1403–1414. doi: 10.1111/1462-2920.13023
- Peng, C., Tang, Y., Yang, H., He, Y., Liu, Y., Liu, D., et al. (2020). Time- and compound-dependent microbial community compositions and oil hydrocarbon degrading activities in seawater near the Chinese Zhoushan Archipelago. *Mar. Pollut. Bull.* 152:110907. doi: 10.1016/j.marpolbul.2020.110907
- Pinto, M., Langer, T. M., Hüffer, T., Hofmann, T., and Herndl, G. J. (2019). The composition of bacterial communities associated with plastic biofilms differs between different polymers and stages of biofilm succession. *PLoS One* 14:e0217165. doi: 10.1371/journal.pone.0217165
- Pollet, T., Berdjeb, L., Garnier, C., Durrieu, G., Le Poupon, C., Misson, B., et al. (2018). Prokaryotic community successions and interactions in marine biofilms: the key role of *Flavobacteriia*. *FEMS Microbiol. Ecol.* 94.
- Pulido-Villena, E., Ghiglione, J.-F., Ortega-Retuerta, E., Van-Wambeke, F., and Zohary, T. (2012). “Heterotrophic bacteria in the Pelagic Realm of the Mediterranean sea,” in *Life in the Mediterranean Sea: A Look at Habitat Changes*, N. Stambler (New York, NY: Nova Publishers).
- Quast, C., Pruesse, E., Yilmaz, P., Gerken, J., Schweer, T., Yarza, P., et al. (2013). The SILVA ribosomal RNA gene database project: improved data processing and web-based tools. *Nucleic Acids Res.* 41, D590–D596.
- Ren, J., Liu, Z., and Ren, T. (2007). Mechanical and thermal properties of poly(Lactic Acid)/starch/montmorillonite biodegradable blends. *Polym. Polym. Comp.* 15, 633–638. doi: 10.1177/096739110701500806
- Roager, L., and Sonnenschein, E. C. (2019). Bacterial candidates for colonization and degradation of marine plastic debris. *Environ. Sci. Technol.* 53, 11636–11643. doi: 10.1021/acs.est.9b02212
- Rodrigo-Torres, L., Pujalte, M. J., and Arahá, D. R. (2017). Draft genome sequence of *Thalassobius gelatinovorus* CECT 4357T, a roseobacter with the potential ability to degrade polycyclic aromatic hydrocarbons. *Gene Rep.* 9, 32–36. doi: 10.1016/j.genrep.2017.08.005
- Rognes, T., Flouri, T., Nichols, B., Quince, C., and Mahé, F. (2016). VSEARCH: a versatile open source tool for metagenomics. *PeerJ* 4:e2584. doi: 10.7717/peerj.2584
- Saadi, Z., Cesar, G., Bewa, H., and Benguigui, L. (2013). Fungal degradation of poly (Butylene Adipate-Co-Terephthalate) in soil and in compost. *J. Polym. Environ.* 21, 893–901.
- Salehpour, S., Jonoobi, M., Ahmadzadeh, M., Siracusa, V., Rafeian, F., and Oksman, K. (2018). Biodegradation and ecotoxicological impact of cellulose nanocomposites in municipal solid waste composting. *Int. J. Biol. Macromol.* 111, 264–270.
- Salta, M., Wharton, J. A., Blache, Y., Stokes, K. R., and Briand, J. F. (2013). Marine biofilms on artificial surfaces: structure and dynamics. *Environ. Microbiol.* 15, 2879–2893.
- Sashiwa, H., Fukuda, R., Okura, T., Sato, S., and Nakayama, A. (2018). Microbial degradation behavior in seawater of polyester blends containing poly(3-hydroxybutyrate-co-3-hydroxyhexanoate) (PHBHHx). *Mar. Drugs* 16:34. doi: 10.3390/md16010034
- Sauret, C., Séverin, T., Vétion, G., Guigue, C., Goutx, M., Pujo-Pay, M., et al. (2014). ‘Rare biosphere’ bacteria as key phenanthrene degraders in coastal seawaters. *Environ. Pollut.* 194, 246–253. doi: 10.1016/j.envpol.2014.07.024
- Sauret, C., Tedetti, M., Guigue, C., Dumas, C., Lami, R., Pujo-Pay, M., et al. (2016). Influence of PAHs among other coastal environmental variables on total and PAH-degrading bacterial communities. *Environ. Sci. Pollut. Res.* 23, 4242–4256.
- Science Advice for Policy by European Academies [SAPEA] (2020). *Biodegradability of Plastics in the Open Environment*, Vol. 10. Berlin: Science Advice for Policy by European Academies, 26356.
- Silva Dutra, L., da Souza Belan Costa, T., de Lobo, V. T. V., et al. (2019). Preparation of polymer microparticles through non-aqueous suspension polycondensations: part III—degradation of PBS microparticles in different aqueous environments. *J. Polym. Environ.* 27, 176–188. doi: 10.1007/s10924-018-1329-x
- Simon, M., and Azam, F. (1989). Protein content and protein synthesis rates of planktonic marine bacteria. *Mar. Ecol. Prog. Ser.* 51, 201–213. doi: 10.3354/meps051201
- UNEP (2018). *Legal Limits on Single-Use Plastics and Microplastics: A Global Reviews of National Laws and Regulations*. Available online at: <https://www.unep.org/resources/report/legal-limits-single-use-plastics-and-microplastics> (accessed December 6, 2018).
- Vila-Costa, M., Sebastián, M., Pizarro, M., Cerro-Gálvez, E., Lundin, D., Gasol, J. M., et al. (2019). Microbial consumption of organophosphate esters in seawater under phosphorus limited conditions. *Sci. Rep.* 9:233.
- Wang, G.-X., Huang, D., Ji, J.-H., Völker, C., and Wurm, F. R. (2021). Seawater-degradable polymers-fighting the marine plastic pollution. *Adv. Sci.* 8:2001121.
- Wang, W., Gao, H., Jin, S., Li, R., and Na, G. (2019). The ecotoxicological effects of microplastics on aquatic food web, from primary producer to human: a review. *Ecotoxicol. Environ. Saf.* 173, 110–117. doi: 10.1016/j.ecoenv.2019.01.113

- Ward, J. H. (1963). Hierarchical grouping to optimize an objective function. *J. Am. Statist. Assoc.* 58, 236–244. doi: 10.1080/01621459.1963.10500845
- Webb, H., Arnott, J., Crawford, R., and Ivanova, E. (2012). Plastic degradation and its environmental implications with special reference to poly(ethylene terephthalate). *Polymers* 5, 1–18. doi: 10.3390/polym5010001
- Weng, Y.-X., Jin, Y.-J., Meng, Q.-Y., Wang, L., Zhang, M., and Wang, Y.-Z. (2013). Biodegradation behavior of poly(butylene adipate-co-terephthalate) (PBAT), poly(lactic acid) (PLA), and their blend under soil conditions. *Polym. Test.* 32, 918–926.
- Wu, X.-L., Yu, S.-L., Gu, J., Zhao, G. F., and Chi, C. Q. (2009). *Filomicrobium insigne* sp. nov., isolated from an oil-polluted saline soil. *Int. J. Syst. Evolut. Microbiol.* 59, 300–305. doi: 10.1099/ijs.0.65758-0
- Zambrano, M. C., Pawlak, J. J., Daystar, J., Ankeny, M., Goller, C. C., Vendittia, R. A., et al. (2020). Aerobic biodegradation in freshwater and marine environments of textile microfibers generated in clothes laundering: effects of cellulose and polyester-based microfibers on the microbiome. *Mar. Pollut. Bull.* 151:1108.
- Zettler, E. R., Mincer, T. J., and Amaral-Zettler, L. A. (2013). Life in the “Plastisphere”: microbial communities on plastic marine debris. *Environ. Sci. Technol.* 47, 7137–7146. doi: 10.1021/es401288x
- Zhou, M., Dong, B., and Shao, Z. (2020). Complete genome sequence of *Marinobacter* sp. LQ44, a haloalkaliphilic phenol-degrading bacterium isolated from a deep-sea hydrothermal vent. *Mar. Genomics* 50:100697. doi: 10.1016/j.margen.2019.100697

**Conflict of Interest:** The authors declare that the research was conducted in the absence of any commercial or financial relationships that could be construed as a potential conflict of interest.

Copyright © 2021 Jacquin, Callac, Cheng, Giraud, Gorand, Denoual, Pujo-Pay, Conan, Meistertzheim, Barbe, Bruzard and Ghiglione. This is an open-access article distributed under the terms of the Creative Commons Attribution License (CC BY). The use, distribution or reproduction in other forums is permitted, provided the original author(s) and the copyright owner(s) are credited and that the original publication in this journal is cited, in accordance with accepted academic practice. No use, distribution or reproduction is permitted which does not comply with these terms.





# Bioleaching of E-Waste: Influence of Printed Circuit Boards on the Activity of Acidophilic Iron-Oxidizing Bacteria

Juan Anaya-Garzon<sup>1,2</sup>, Agathe Hubau<sup>1\*</sup>, Catherine Jouliau<sup>1</sup> and Anne-Gwénaëlle Guezennec<sup>1</sup>

<sup>1</sup> Bureau de Recherches Géologiques et Minières, Orléans, France, <sup>2</sup> Chimie ParisTech, PSL Research University, CNRS, Institut de Recherche de Chimie Paris, Paris, France

## OPEN ACCESS

### Edited by:

Mechthild Schmitt-Jansen,  
Helmholtz Centre for Environmental  
Research (UFZ), Germany

### Reviewed by:

Sabrina Hedrich,  
Freiberg University of Mining  
and Technology, Germany  
Eva Pakostova,  
Coventry University, United Kingdom

### \*Correspondence:

Agathe Hubau  
A.Hubau@brgm.fr

### Specialty section:

This article was submitted to  
Microbiotechnology,  
a section of the journal  
Frontiers in Microbiology

Received: 19 February 2021

Accepted: 12 July 2021

Published: 18 August 2021

### Citation:

Anaya-Garzon J, Hubau A,  
Jouliau C and Guezennec A-G (2021)  
Bioleaching of E-Waste: Influence of  
Printed Circuit Boards on the Activity  
of Acidophilic Iron-Oxidizing Bacteria.  
Front. Microbiol. 12:669738.  
doi: 10.3389/fmicb.2021.669738

Bioleaching is a promising strategy to recover valuable metals from spent printed circuit boards (PCBs). The performance of the process is catalyzed by microorganisms, which the toxic effect of PCBs can inhibit. This study aimed to investigate the capacity of an acidophilic iron-oxidizing culture, mainly composed of *Leptospirillum ferriphilum*, to oxidize iron in PCB-enriched environments. The culture pre-adapted to 1% (w/v) PCB content successfully thrived in leachates with the equivalent of 6% of PCBs, containing 8.5 g L<sup>-1</sup> Cu, 8 g L<sup>-1</sup> Fe, 1 g L<sup>-1</sup> Zn, 92 mg L<sup>-1</sup> Ni, 12.6 mg L<sup>-1</sup> Pb, and 4.4 mg L<sup>-1</sup> Co, among other metals. However, the inhibiting effect of PCBs limited the microbial activity by delaying the onset of the exponential iron oxidation. Successive subcultures boosted the activity of the culture by reducing this delay by up to 2.6 times under batch conditions. Subcultures also favored the rapid establishment of high microbial activity in continuous mode.

**Keywords:** iron-oxidizing bacteria, *Leptospirillum ferriphilum*, printed circuit boards, bioleaching, pre-oxidation phase, subculturing

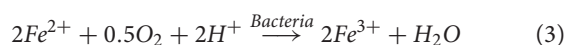
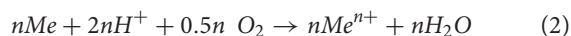
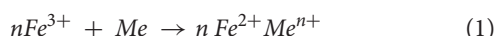
## INTRODUCTION

Printed circuit boards (PCBs) are the main processing unit for the electronic devices that have become essential to our daily lives in recent decades. Their disposal at the end of their useful life is a major challenge for the circular economy and sustainable development. Improper handling of waste PCBs is widespread, with incineration and landfilling as the easiest but polluting solutions. Waste PCBs contain heavy metals (Pb, Hg, As, Cd, Cr), polychlorinated biphenyls, polybrominated biphenyls, and epoxy resins, which are highly toxic for the environment (Kaya, 2019). Likewise, spent PCBs are a valuable source of various strategic metals, including Au, Ag, Pd, Ti, Ga, Ta, Co, Cu, Fe, Al, Zn, Sn, Pb, and Ni (Hubau et al., 2019; Kaya, 2019).

The dissolution of metals assisted by microorganisms, also known as bioleaching, is a biotechnological process that is now established worldwide. This technology is already applied at an industrial scale for the extraction of Au and Cu, and marginally for Ni, Co, and U, from primary ores (Rawlings and Johnson, 2007; Wassink and Asselin, 2019). It is now attracting considerable attention for the extraction of metals from secondary sources such as mining waste, contaminated river sludge (Zhang et al., 2018), fly ash (Xu et al., 2014), batteries (Liu et al., 2020), and spent PCBs (Bryan et al., 2015, 2020; Guezennec et al., 2015; Işildar et al., 2016; Wu et al., 2018; Hubau et al., 2020). Some of the advantages of biotechnologies compared to conventional pyrometallurgical

and hydrometallurgical recycling processes are the safety conditions for operators, operations at atmospheric pressure and room temperature, lower chemical and energy consumption, lower CO<sub>2</sub> emissions, and low initial investments (Baniyadi et al., 2019). Over the last decade, bioleaching of PCBs has been investigated at the research level in shake flasks (Adhapure et al., 2013; Arshadi and Mousavi, 2015; Bryan et al., 2015; Guezennec et al., 2015) and stirred tank reactors (STR) with capacities above 1 L (Ilyas and Lee, 2014; Guezennec et al., 2015; Mäkinen et al., 2015; Xia et al., 2017; Hubau et al., 2020).

Microorganisms employed in the bioleaching of PCBs are diverse, with both autotrophs (Xiang et al., 2010) and heterotrophs (Chi et al., 2011) and mesophilic and thermophilic (Ilyas et al., 2007) species. Chemolithotrophs acidophilic iron-oxidizing bacteria (FeOB) stand out among the group of microorganisms most frequently studied for dissolving metals (Xiang et al., 2010; Işildar et al., 2019; Hubau et al., 2020). Ferric iron and sulfuric acid act as oxidizing agents to mobilize the metals from the solid matrix (Eqs 1, 2). FeOB uses the resulting Fe(II) as a source of energy to regenerate the ferric iron in the presence of dissolved oxygen (Eq. 3), which accelerates the bioleaching process.



*Leptospirillum* can potentially thrive in bioleaching environments as they have a greater capacity for iron oxidation activity than other FeOBs (Rawlings et al., 1999; Kinnunen and Puhakka, 2004; Rawlings, 2005; Bryan et al., 2011; Guezennec et al., 2015). These acidophilic and moderately thermophilic species are highly resistant to environments containing high concentrations of Fe(III) and can survive high concentrations of other metals (Dopson and Holmes, 2014). Dopson and Holmes (2014) describe possible passive and active mechanisms these microorganisms might use to grow in the presence of a high metal content. *Leptospirillum ferriphilum* is a dominant FeOB in industrial continuous-flow biooxidation tanks for mineral extraction (Rawlings et al., 1999; Coram and Rawlings, 2002). These Gram-negative bacteria have a large number of genes related to heavy metal detoxification, oxidative stress defense, DNA repair, pH tolerance to acidic environments, and signal transduction to adapt to the external environment (Mi et al., 2011). However, one of the major challenges in PCB bioleaching remains the inhibiting effects of the waste material on the metabolism of these microorganisms (Guezennec et al., 2015; Wu et al., 2018; Arya and Kumar, 2020). PCBs can slow down/delay microbial growth and reduce microbial capacity to oxidize iron (Edward et al., 2018). Consequently, the regeneration of Fe(III) decreases along with leaching rates. It is not clear whether the toxic effect results from the metal content, the organic content of PCBs, or both (Bryan et al., 2015; Baniyadi et al., 2019). Yang et al. (2014) suggest that Pb, Ni, and plastics have

inhibiting effects on bacterial growth, but it is not evident whether there is a main limiting factor. Besides, a synergy between different metal ions can increase the level of toxicity compared to the individual effect of each metal, as described by Nurmi et al. (2009). Finally, damage to bacterial cells can also result from attrition of the bacterial membrane by solid particles (Haghshenas et al., 2009).

Different strategies have been proposed to tackle the toxicity effect of PCB bioleaching processes. The first strategy consists of separating biogenic Fe(III) production from the PCB leaching (Brandl et al., 2001; Zhu et al., 2011; Guezennec et al., 2015; Wang et al., 2018; Hubau et al., 2020), which allows microorganisms to thrive in a system without the toxic effect of PCBs. This strategy can be employed in continuous flow bioreactors to achieve high bioleaching efficiencies over short periods. Hubau et al. (2020) showed high PCB bioleaching efficiency in steady-state conditions within 48 h and 1% (w/v) PCBs. However, a long transitional regime of several months was required to achieve high and stable microbial activity.

The second strategy seeks to adapt microorganisms to the toxic waste material to improve the iron-oxidizing activity and trigger leaching efficiency (Rawlings, 2005; Haghshenas et al., 2009; Yang et al., 2009, 2014; Hubau et al., 2020). A typical method involves subculturing in a specific environment. Serial subculturing can, for instance, enhance tolerance to a high metal content and improve microbial iron oxidation activity (Bryan et al., 2011; Liu et al., 2019). The period before the microbial oxidation of iron, referred here as the pre-oxidation phase, can be used as an indicator of microbial iron oxidation activity (Das et al., 1998; Haghshenas et al., 2009). This pre-oxidation phase reflects the time required for bacteria to start actively catalyzing iron oxidation. In this sense, it is possible to estimate the evolution of bacterial tolerance to PCBs by means of serial subcultures following the pre-oxidation phase.

The main objective of this study was to investigate the capacity of FeOB cultures dominated by *L. ferriphilum* to grow and improve the iron oxidation kinetics in PCB-enriched environments. The inhibiting effects of PCBs on microorganisms were covered (i) by studying the inhibiting effect of chemically dissolved PCB metals on the microbial growth and activity of a FeOB culture in shake flasks and (ii) by investigating the microbial growth and oxidizing activity of two cultures referred to as “adapted” and “non-adapted” in a batch STR at different PCB solid loads. Strategies to tackle this inhibition were then investigated. They rely on (i) successive subcultures in batch mode and (ii) different operational modes to reach the steady state in continuous mode, as fast as possible and with high microbial activity.

## MATERIALS AND METHODS

### Bacterial Culture

This study used two FeOB cultures, referred to here as “adapted” and “non-adapted” cultures. Both come from a two-step bioprocess for PCB bioleaching, which is fully described

in previous studies (Hubau et al., 2018, 2020). The non-adapted culture, which came from a 150-mL bio-oxidation aerated column, run in continuous mode and inoculated with an acidophilic FeOB culture, showed highly efficient oxidation of Fe(II) at  $1 \text{ g L}^{-1} \text{ h}^{-1}$ , but was never in contact with PCBs. This culture was mainly made up of *L. ferriphilum* and *Sulfobacillus benefaciens*, with *L. ferriphilum* being the predominant species (Hubau et al., 2018). This ferric iron-rich lixiviant was used to feed a PCB-bioleaching STR, operated in continuous mode with 1% (w/v) PCBs for over 4 months at a hydraulic retention time (HRT) of 48 h. The adapted culture came from a leachate of the bioleaching reactor. High metal dissolution yields and rates were obtained under these conditions (Hubau et al., 2020). *L. ferriphilum* was the predominant bacterium in both cultures (Hubau et al., 2018, 2020).

The 0Cm medium used in this study is derived from 0Km with a reduced  $(\text{NH}_4)_2\text{SO}_4$  concentration (Hubau et al., 2018) and has previously enabled a robust performance of Fe(II) bio-oxidation in the aerated column and a high bioleaching yield in the STR (Hubau et al., 2020). This medium is composed of  $0.4 \text{ g L}^{-1}$   $(\text{NH}_4)_2\text{SO}_4$  (extra pure, Merck, Darmstadt, Germany),  $0.81 \text{ g L}^{-1}$   $\text{H}_3\text{PO}_4$  (analytical grade, Merck),  $0.48 \text{ g L}^{-1}$  KOH (pure pellets, Merck), and  $0.52 \text{ g L}^{-1}$   $\text{MgSO}_4 \cdot 7\text{H}_2\text{O}$  (analytical grade, Merck). The medium was supplemented with  $3 \text{ g L}^{-1}$  of Fe(II) as  $\text{FeSO}_4 \cdot 7\text{H}_2\text{O}$  (99+%, Acros Organics, Fair Lawn, NJ, United States) and was thus denoted 3Cm. The pH was adjusted to 1.2 with  $\text{H}_2\text{SO}_4$  (>95%, analytical grade, Fisher Chemical, Waltham, MA, United States).

## PCB Composition and Preparation

Samples of low-grade PCBs were collected from small appliances at the *Envie 2E Midi-Pyrenees* WEEE sorting center (France). Preparation of the PCBs and determination of the metal composition are fully described in Hubau et al. (2019). Briefly, the PCBs were shredded to reduce the particle size below  $750 \mu\text{m}$  ( $750 \mu\text{m}$  corresponding to the mesh size of the shear shredder Bohmier Maschinen GmbH) and a laboratory knife mill (Retsch, 2000). Table 1 shows the metal composition of the samples (Hubau et al., 2019).

**TABLE 1** | Element composition in % weight of low-grade PCB samples.

Element	Concentration (% weight)	Element	Concentration (% weight $\times 10^{-5}$ )
Cu	14.58	Cr	842
Fe	12.23	Co	358
Al	6.04	Ag	209
Zn	1.67	Mo	152
Sn	1.67	In	100
Pb	1.17	Au	44
Mn	0.61	Pd	25
Ni	0.34	V	22
Sb	0.20	W	15
Mg	0.14	Ga	12
		Ta	7.5
		Ge	0.75
		Pt	0.59

A solution of dissolved PCB metal ions was prepared by abiotic chemical leaching of 10% (w/v) PCBs in a stirred tank bioreactor with a working volume of 2.2 l. The setup of the STR was previously presented by Hubau et al. (2020). The chemical leaching was performed in the 0Cm culture medium with  $10 \text{ g L}^{-1}$  of Fe(III) added as  $\text{Fe}_2(\text{SO}_4)_3 \cdot x\text{H}_2\text{O}$  as a leaching agent in sulfuric acid media and adjusted to pH 1.2 with  $\text{H}_2\text{SO}_4$  (>95%, analytical grade, Fisher Chemical). An airflow rate of  $90 \text{ L h}^{-1}$  injected beneath the turbine at the bottom of the reactor via a stainless-steel pipe provided with surplus oxygen to facilitate the leaching of metals. A dual (axial/radial) impeller system in stainless steel ensured the mixing of gas, liquid, and solids with a stirring speed of 650 rpm. The temperature of the reactor was maintained at  $35^\circ\text{C}$  with a thermostatic bath (Lauda), and the pH was daily adjusted to 1.2 with  $\text{H}_2\text{SO}_4$  until the end of the experiment. Once the metal concentrations were stable (see section “Analytical Techniques”), the solution was filtered.

## Microbial Performance at Different Concentrations of PCB Leachate

The microbial growth and activity of the adapted culture were evaluated in 100-mL (working volume) shake flasks. The experiments contained 20% (v/v), 40% (v/v), 60% (v/v), or 80% (v/v) of the chemical PCB leachate (Table 2), which represented the equivalent of 2, 4, 6, and 8% of PCBs, respectively. Each flask had 10% (v/v) inoculum, the 0Cm culture medium (supplemented with a 10-fold solution of concentrated nutrients), and  $8 \text{ g L}^{-1}$  Fe(II) (adjusted with a  $10\text{-g L}^{-1}$  Fe(II) solution). All solutions were adjusted to pH 1.2 at the beginning of the experiments. The experiments were run in triplicate, with two control duplicates: 10% (v/v) inoculum without PCB leachate, and uninoculated 80% (v/v) PCB leachate. The cultures were incubated in a rotary shaker at 107 rpm and  $35^\circ\text{C}$ . The initial microbial concentration was  $10^7 \text{ cells mL}^{-1}$ . Experiments were run for 25 days, with pH, redox potential, and bacterial concentration monitored daily (See section “Analytical Techniques”). Water losses by evaporation were compensated with sterile distilled water.

## Microbial Performance During Bioleaching at Different Concentrations of Solid PCBs

The microbial growth and iron oxidation activity of the adapted and non-adapted cultures were evaluated in a 2.2-L STR with shredded solid PCBs at 1% (w/v) or 2% (w/v) in batch mode. First, bacteria were inoculated at 10% (v/v) in 3Cm medium (containing  $3 \text{ g L}^{-1}$  Fe(II) and acidified to pH 1.2) without PCBs. This step ended when the redox potential reached values above 800 mV [adjusted to be relative to a standard hydrogen electrode (SHE)], i.e., when Fe(II) was oxidized (See section “Analytical Techniques”). PCBs were subsequently added at either 1% (w/v) PCBs or 2% (w/v) PCBs. pH was daily adjusted to  $1.2 \pm 0.1$  with concentrated  $\text{H}_2\text{SO}_4$ . pH, redox potential, planktonic cell concentration, and metal concentration were monitored over time.

**TABLE 2 |** Metal concentration of the chemical PCB leachate used to test the microbial performance in shake flasks.

Element	Concentration (g L <sup>-1</sup> )	Element	Concentration (g L <sup>-1</sup> )	Element	Concentration (g L <sup>-1</sup> )
Cu	15.2	Mg	0.069	Pb	0.006
Fe	12.8	Mn	0.046	Co	0.006
Al	3.89	Sn	0.022	V	0.001
Zn	2.21	Cr	0.008	Sb	0.001
Ni	0.22				

Leaching conditions: 10% (w/v) PCBs, 10 g L<sup>-1</sup> Fe, Ag, Au, Mo, In, Pd, W, Ga, Ta, Ge, and Pt were below the detection limit (1 µg L<sup>-1</sup>).

The same reactor used for the chemical leaching of PCBs was employed for these experiments. An air flow of 60 L h<sup>-1</sup> enriched with 1% CO<sub>2</sub> was maintained, to ensure the carbon supply for microbial growth and iron oxidation activity (Guezennec et al., 2018). STR stirring speed was set at 650 rpm, and the reactor was maintained at 35°C.

## Subculturing Protocol in STR

The subcultures were studied in a two-step process, similar to the one described in the previous section, in the 2.2-L STR configuration in batch mode.

In the first experiment (S0), the batch reactor was inoculated with 10% (v/v) of the adapted culture in a 3Cm medium as first step. This step ended when the redox reached values above 800 mV vs. SHE. In the second step, 2% (w/v) PCBs were added to the reactor and the pH was daily adjusted to 1.2 with concentrated H<sub>2</sub>SO<sub>4</sub>. The test was ended when the redox again reached values above 800 mV vs. SHE. The subculture batch reactors were inoculated with 10% (v/v) from the previous test into a 3Cm medium, and the protocol as in S0 was repeated. A diagram of the subculture procedure is presented in **Figure 1**. Subcultures named S1 and S2 were successively inoculated with an interval of 1–2 days between subcultures to assure that stable conditions were reached. After the second subculture (S2), the culture was stored at room temperature in a hermetic and sterile plastic vessel for 10 days in a basement without light. Subsequently, subcultures S3, S4, and S5 were carried out as in S0. Bacterial cells at the beginning and at the end of each experiment were counted in an optimal microscope as detailed in the section “Analytical Techniques.” This quantitative method was as indicator of microbial growth. No changes were observed in the bacterial concentration after the storage period.

## Start-Up Scenarios in Continuous Mode

For these experiments, we employed a two-stage bioleaching process in continuous flow. The first stage is the aerated column with non-adapted bacteria feeding the 2.2-L STR containing the PCBs as the second stage. The aerated column contained a solid support on polypropylene for bacterial growth, while no support was included in the second stage (PCB bioleaching STR). The setup is described in detail in a previous study (Hubau et al., 2020). Three scenarios were proposed to evaluate the microbial iron oxidation activity during the start-up of the continuous process and to determine a strategy to reach the steady state as fast as possible.

In the first scenario (I), the 2.2-L STR reactor was progressively filled with the ferric iron lixiviant (generated in the aerated column), containing non-adapted bacteria and 3 g L<sup>-1</sup> of Fe(III) at redox potential above 800 mV vs. SHE. The output flow from the aerated column continuously fed the STR at 47 mL h<sup>-1</sup> with a pump to maintain an HRT of 48 h. PCBs were added once per hour at 0.45 g h<sup>-1</sup> to maintain a PCB load of 1% (w/v). Agitation started after 24 h. After 48 h, when the working volume reached 2.2 L, pumping of the effluent began.

In the second scenario (II), a test in batch mode was performed with adapted bacteria as described in the subculturing protocol. The batch had 10% (v/v) inoculum in a 3Cm medium, and the equivalent of 1% (w/v) PCBs was loaded once the redox reached over 800 mV vs. SHE. The continuous-flow bioleaching mode started at the end of this batch with the total pulp in the reactor. The aerated column effluent and PCBs fed the reactor continuously at 48 h of HRT and 1% (w/v) PCBs as in the first scenario.

In the third scenario (III), an initial bioleaching batch process was performed with 10% (v/v) of the adapted bacteria and 2% (w/v) PCBs, followed by two successive batch subcultures. Each subculture was inoculated with 50% (v/v) from the previous batch. The other 50% volume contained 3Cm. One percent (w/v) of PCBs was added after the redox rose above 800 mV vs. SHE in each subculture. After the second subculture, the continuous-flow mode started. As in scenarios I and II, the reactor worked with an HRT of 48 h and 1% (w/v) PCBs and was fed with non-adapted bacteria from the aerated column.

All the bioleaching reactors in batch and continuous-flow modes operated at 35°C, with an airflow enriched with 1% CO<sub>2</sub> of 60 L h<sup>-1</sup>, and agitation at 650 rpm. The pH was maintained lower than 1.6 to avoid Fe(III) precipitation. The start-up phase was considered finished when the redox potential maintained values above 800 mV vs. SHE in continuous mode for at least two HRT.

## Analytical Techniques

The pH values and redox potentials were monitored daily for all experiments with pH (IDS SenTix® 940) and redox (BlueLine 32-3 RX IDS) electrodes, respectively, both connected to a multiparameter portable meter (Multi 3630 IDS, WTW). Metals were analyzed with a Varian SpectraAA 300 flame atomic absorption spectroscope (FAAS). The oxidation of iron was deduced from the correlation of Yue et al. (2016) expressed in Eq. 4. This involves the redox potential ( $Eh$  in mV vs. SHE), the temperature ( $T$  in K), the number of electrons exchanged ( $n$ ), the gas constant ( $R = 8.3 \text{ J K}^{-1} \text{ mol}^{-1}$ ) and the Faraday



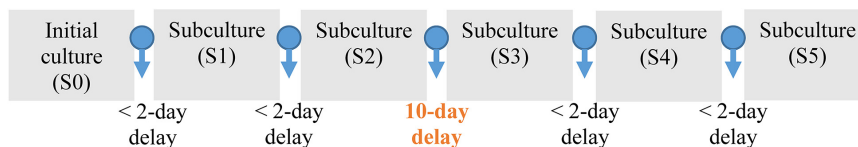


**FIGURE 1** | Scheme of the successive subculturing procedure applied on 2.2 L-STR in batch conditions. Each culture contained 3Cm medium and 2% (w/v) PCBs.

constant ( $F = 96485 \text{ C mol}^{-1}$ ), and the concentration of Fe ( $[Fe]$  in  $\text{mg L}^{-1}$ ).

$$Eh = 10 - 3x[T]^2 + 0,91T + 2,303x10^3 \frac{RT}{nF} \log \frac{[Fe(III)]}{[Fe(II)]} + 492 \quad (4)$$

To estimate the microbial growth, 20- $\mu\text{L}$  samples of the leachate were placed in a Thoma cell counting chamber and observed through an optical microscope at  $\times 400$  magnification. This technique shows the growth tendency of planktonic bacteria. The diversity of the bacterial (or prokaryotic) consortium was characterized using the capillary electrophoresis single-strand conformational polymorphism (CE-SSCP) molecular fingerprinting technique on the 16S rRNA gene encoding, using the protocol described by Hubau et al. (2018).

## RESULTS

### Microbial Performance at Different Leachate Concentrations

These experiments performed in shake flasks aimed to characterize the bacterial performance of the adapted FeOB culture in PCB environments. The PCB environment was reproduced from a concentrated PCB leachate, whose metal concentration is detailed in **Table 2**. The data show that the PCB leachate contained mainly Cu, Fe, Al, Zn, and Ni. A wide range of other metals was present in concentrations below  $100 \text{ mg L}^{-1}$ .

The effect of increased concentrations of metal-rich PCB leachates on bacterial growth and Fe(II)-oxidizing activity is presented in **Figure 2**. **Figure 2A** shows that the lag phase lasted longer at increased concentrations of PCBs, with 1 day at 20% (v/v) of PCB leachate, 2 days at 40% (v/v) of PCB leachate, and 7 days at 60% (v/v) of PCB leachate. Starting from  $10^7 \text{ cells mL}^{-1}$ , the bacterial concentration increased exponentially and reached a stationary phase at  $10^8 \text{ cells mL}^{-1}$  in conditions containing up to 60% (v/v) of PCB leachate. A similar behavior was observed in the biotic control without dissolved PCBs, which had a lag phase of 1 day. The control assay with 80% (v/v) of leachate (corresponding to 8% of PCBs) did not present a microbial growth over the 25 days of experiments, as verified through bacterial counting.

**Figure 2B** shows that the redox potential increased simultaneously with the exponential microbial growth when the solutions contained 20% (v/v) to 60% (v/v) of PCB leachate. The duration of the lag phase and the pre-oxidation phase were equal under these conditions, indicating that substrate oxidation and microbial growth were correlated. At the end of the pre-oxidation phase, the redox increased exponentially

from less than 650 mV vs. SHE to more than 900 mV vs. SHE in at most 2 days. This redox behavior can be attributed to the iron oxidation catalyzed by microorganisms and continued to a plateau, which corresponds to a complete oxidation of iron according to Eq. 4. In the biotic control without leachate, the microbial iron oxidation and the stationary microbial growth phase took 1 day longer than in the assay with 20% (v/v) of PCB. At 80% (v/v) of PCB leachate, the redox gradually increased over time, representing 37% of iron oxidized in 25 days regardless of the presence of bacteria. Therefore, no bacterial growth or iron oxidation related to the microbial iron oxidation activity were found during this period at 80% (v/v) of PCB leachate.

Despite the delay of 7 days in microbial growth and iron oxidation activity, the culture thrived in a medium with a concentration of metals six times higher than in the medium to which they were initially adapted. Based on the initial leachate concentration (**Table 2**), the solution at 60% (v/v) of PCB leachate contained  $9 \text{ g L}^{-1}$  Cu,  $2 \text{ g L}^{-1}$  Al,  $1 \text{ g L}^{-1}$  Zn,  $0.1 \text{ g L}^{-1}$  Ni,  $10 \text{ mg L}^{-1}$  Pb, and  $4 \text{ mg L}^{-1}$  Co, among other elements. According to the molecular fingerprinting test, *L. ferriphilum* is the predominant species whatever the leachate concentration, as in the test with no leachate (**Supplementary Figure 1**). This confirms the capacity of *L. ferriphilum* to grow and oxidize iron at high concentrations of mixed metals and other elements.

### Effects of Solid PCBs on Microbial Performance During Bioleaching

The purpose of these experiments was to investigate the inhibiting effect of solid PCBs on the microbial growth and pre-oxidation phase. In the experiments, metal leaching (Eqs 1, 2) and the microbial oxidation of Fe(II) to regenerate Fe(III) as a leaching agent (Eq. 3) occurred in the same reactor.

**Table 3** presents the final planktonic cell concentration and the duration of the pre-oxidation phase of cultures in the presence of 1% (w/v) PCBs and 2% (w/v) PCBs. The tendency of planktonic bacteria to grow in bioreactors with 2% (w/v) PCBs seems higher compared to reactors with 1% (w/v) PCBs. There could be an increased supply of iron for microbial growth thanks to the iron dissolution from 2% (w/v) PCBs. However, this result must be considered carefully since the addition of PCBs may interfere with the counting of bacterial cells. Besides, a considerable proportion of biomass can attach to the solids. The effects of PCB load on microbial growth were therefore difficult to measure in these conditions.

On the other hand, the increase in the PCB load prolonged the pre-oxidation phase, as in the previous experiments with the PCB leachates (**Figure 2**). The onset of microbial iron oxidation

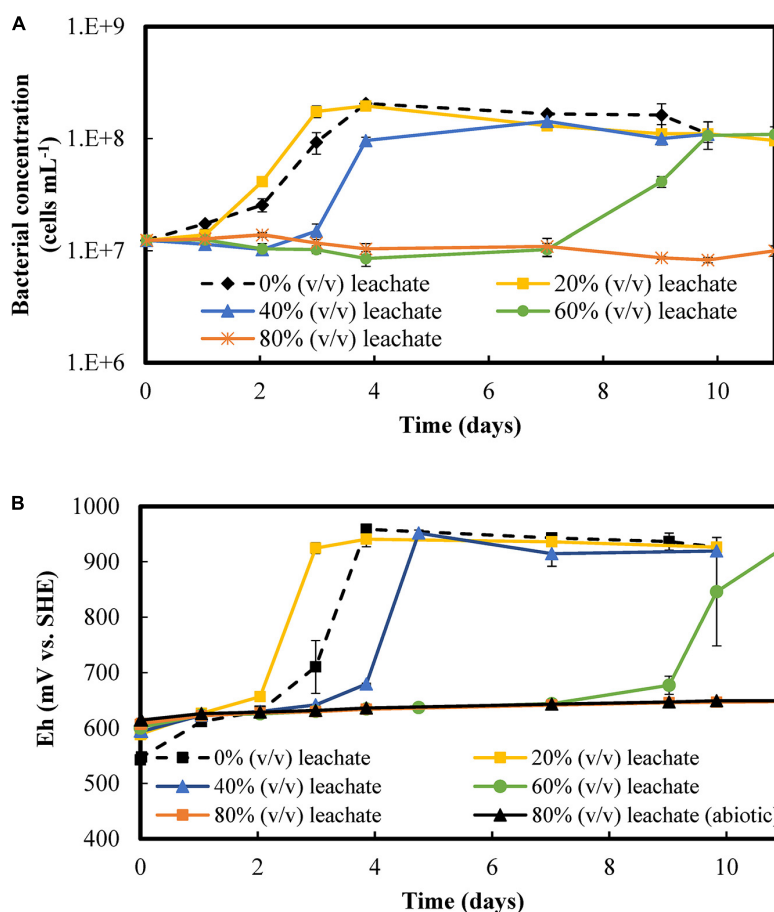


**FIGURE 2 |** Microbial activity at various concentrations of the chemical leachate produced with 10% (w/v) PCBs: **(A)** Bacterial concentration and **(B)** redox potential. The experiments were performed in shake flasks and started with  $8 \text{ g L}^{-1} \text{ Fe(II)}$  and  $10^7 \text{ cells mL}^{-1}$ . The error bars represent the range of all values obtained under fixed operating conditions. Additional information on experiments with 80% (v/v) leachate the abiotic control is available up to day 25, although no significant changes in either redox behavior or bacterial concentration were observed.

**TABLE 3 |** Final planktonic cell concentration and duration of the pre-oxidation phase in 2.2-l STR PCB bioleaching reactors in batch mode.

	Non-adapted culture		Adapted culture	
	1% (w/v) PCB	2% (w/v) PCB	1% (w/v) PCB	2% (w/v) PCB
Final planktonic cell concentration ( $\text{cells mL}^{-1}$ )	$10^7$	$6 \times 10^7$	$3 \times 10^7$	$10^8$
Pre-oxidation phase during PCB bioleaching (days)	$> 16^a$	29	11	18

<sup>a</sup>No exponential rise of the redox observed in 16 days.

The planktonic cell concentration before the addition of PCBs was  $10^7 \text{ cells mL}^{-1}$ .

took 11 days at 1% (w/v) PCBs and 18 days at 2% (w/v) PCBs with the adapted culture (**Supplementary Figure 2**). This pre-oxidation phase took consistently longer compared to the shake flask tests containing PCB leachates (**Figure 2**). Despite the different configuration, the presence of solids in the bioleaching experiments may have affected the microbial iron oxidation due to the presence of toxic solid elements such as plastics, resins, and heavy metals.

The evolution of metal concentration and dissolution yield over time is presented in **Supplementary Figure 3**. The bioleaching system took 7 days to reach a maximum dissolution

yield of 100% Cu, 70% Ni, and 100% Zn, regardless of the solid load and the microbial culture. Leachates of 1% (w/v) PCBs reached a maximum of  $2.6 \text{ g L}^{-1}$  Cu,  $30 \text{ mg L}^{-1}$  Ni, and  $303 \text{ mg L}^{-1}$  Zn, whereas leachates of 2% (w/v) PCBs contained up to  $4.2 \text{ g L}^{-1}$  Cu,  $52 \text{ mg L}^{-1}$  Ni, and  $543 \text{ mg L}^{-1}$  Zn. The leachates started with  $3 \text{ g L}^{-1}$  Fe coming from the 3Cm medium and reached up to  $3.3 \text{ g L}^{-1}$  Fe at 1% (w/v) PCBs and  $3.6 \text{ g L}^{-1}$  Fe at 2% (w/v) PCBs. The dissolution yield of Fe appears low (below 20%), but it did not consider Fe precipitation (Chen et al., 2015; Hubau et al., 2020).

## Subculturing of Bacteria From PCBs Bioleaching in Batch Conditions

The subculturing experiments in the 2.2-L STR were carried out with the adapted culture to improve the microbial capacity to oxidize iron in PCB environments by shortening the pre-oxidation phase. Each subculture initially contained  $10^7$  cells  $\text{mL}^{-1}$  and led to a final concentration of  $10^8$  cells  $\text{mL}^{-1}$  (for S0, S1, S2) and  $2 \times 10^8$  cells  $\text{mL}^{-1}$  (S3, S4, and S5). The bacterial concentration in the liquid phase increased exponentially in the first step (absence of PCBs) and continued to grow slowly afterward with no well-defined lag or exponential phases (Supplementary Figure 4).

Figure 3 shows the redox behavior of each subculture during the first stage with 3Cm medium and the second stage with the PCBs. The reference point or day 0 is considered to be the moment when 2% (w/v) PCBs were added to the system. Before that reference point, the redox increased from 600 mV vs. SHE to over 900 mV vs. SHE within 3–7 days depending on the subculture. At this point, 3 g  $\text{L}^{-1}$  of Fe were in ferric form. Drops in redox potential of around 400 mV were observed in every batch within the first hour after adding PCBs, indicating that Fe(III) was being reduced. Subsequently, a gradual increase in redox was followed by an exponential rise and a plateau phase as in the presence of PCB leachates without solids (Figure 2). All the subcultures showed an exponential rise of 250–300 mV in approximately 2 days, reaching values close to 900 mV vs. SHE. At the plateau phase, iron was considered to be completely oxidized.

After the addition of PCBs, the subcultures improved the bio-oxidation of Fe(II) by shortening the pre-oxidation phase over time. This decreased from 18 days for the first batch (S0), to 13 for the first subculture (S1), then 7 days for the second subculture (S2), as shown in Figure 3A. The pre-oxidation phase for S2 was therefore 2.6 times faster than for S0. Subsequently, the effect of storing the culture between two subcultures was tested with a 10-day pause between S2 and S3 (Figure 1). The pre-oxidation phase of S3 lasted longer (11 days), but further subcultures S4 and S5 were able to reduce this pre-oxidation phase to 10 and 7 days, respectively (Figure 3B). A similar pattern was observed in the first stage, but no pre-oxidation phase values are given since the redox was not monitored every day.

The evolution of the metal content in the leachate (Supplementary Figure 5) showed a maximum dissolution yield after 7 days as in the previous experiments, regardless of the subculture. At the end of the experiments, the leachate contained, on average, 4.5 g  $\text{L}^{-1}$  Cu, 50 mg  $\text{L}^{-1}$  Ni, and 550 mg  $\text{L}^{-1}$  Zn, among other elements.

## Start-Up Scenarios in Continuous Mode

Continuous mode enables complete dissolution of PCB metals in a short time (less than 48 h) once the bacteria adapted to the bioleaching environment (Hubau et al., 2020). However, microbial adaptation to PCBs is obtained after a long transitional regime of several months. In these experiments, the capacity of the culture to shorten the nonsteady period of a PCB bioleaching reactor in continuous mode was investigated. Three start-up

scenarios were explored to accelerate the transitional regime before the culture achieved high iron oxidation activity.

Figure 4 shows the evolution of the redox potential and bacterial concentration in the liquid phase during the start-up of the three scenarios. The first scenario (I) starts with non-adapted bacteria from the aerated column output as the only source of inoculum. In scenario II and scenario III, the adapted bacteria were first cultivated in batch mode before being used in PCBs bioleaching CSTR, without and with subcultures, respectively. These batch steps with PCBs lasted 18 days for scenario II and 14 days for scenario III (Supplementary Figure 6). Scenario I maintained a low redox and a constant planktonic bacterial concentration throughout the experiment. Besides, no growth was observed in the liquid phase. In scenario II, the redox was initially high from the previous batch and dropped during the first day as the Fe(III) was rapidly reduced. From the third day, the redox increased simultaneously with microbial growth. After 6 days, the redox reached 830 mV vs. SHE, implying complete Fe(II) oxidation, and the bacterial concentration gradually increased to reach  $2 \times 10^8$  cells  $\text{mL}^{-1}$ . Scenario III did not show any significant drop in redox over 4 days, equivalent of two HRTs. Iron was therefore maintained as Fe(III) despite the continuous addition of PCBs. At the same time, minor microbial growth was observed (the planktonic bacterial counts increased from  $4 \times 10^7$  to  $8 \times 10^7$  cells  $\text{mL}^{-1}$ ), but no clear exponential growth was detected.

## DISCUSSION

This study characterized the inhibition of microbial growth in metal-rich leachates and the iron oxidation activity of an adapted FeOB culture dominated by the iron-oxidizing species *L. ferriphilum*. The remarkable ability of *L. ferriphilum* to thrive at very low pH values and high redox potentials is well known (Rawlings et al., 1999; Hedrich et al., 2016). However, its capacity to catalyze iron oxidation can be limited by the inhibiting effect of high PCB concentrations (Arshadi and Mousavi, 2014; Wu et al., 2018). This inhibition can be due to the elevated dissolved metal concentrations, to other nonmetallic elements that may be present in PCBs, and to the solid PCB particles themselves. The FeOB culture adapted to 1% (w/v) PCBs grew and oxidized iron 1 day faster in the presence of 20% (v/v) PCB leachate (equivalent to 2% of PCBs) compared to the biotic control without PCBs. It is difficult to say whether the culture was more efficient when adapted to the leachate in this case or if the values enter in the measurement uncertainty. For media containing up to 60% (v/v) of PCB leachate, the study demonstrates a link between the concentration of the PCB leachate and the delay in bio-oxidation of Fe(II). This study also demonstrated that the addition of leachates [up to 60% (v/v)] had no impact on the final planktonic cell concentration and Fe(II) oxidation yield. In a previous study (Hubau et al., 2020), similar results were obtained with the non-adapted culture, but the bio-oxidation delay was observed at a lower metal content. An improved metal tolerance capacity of the culture adapted to elevated PCB concentrations was likely to be achieved in this study. This is consistent with the study by

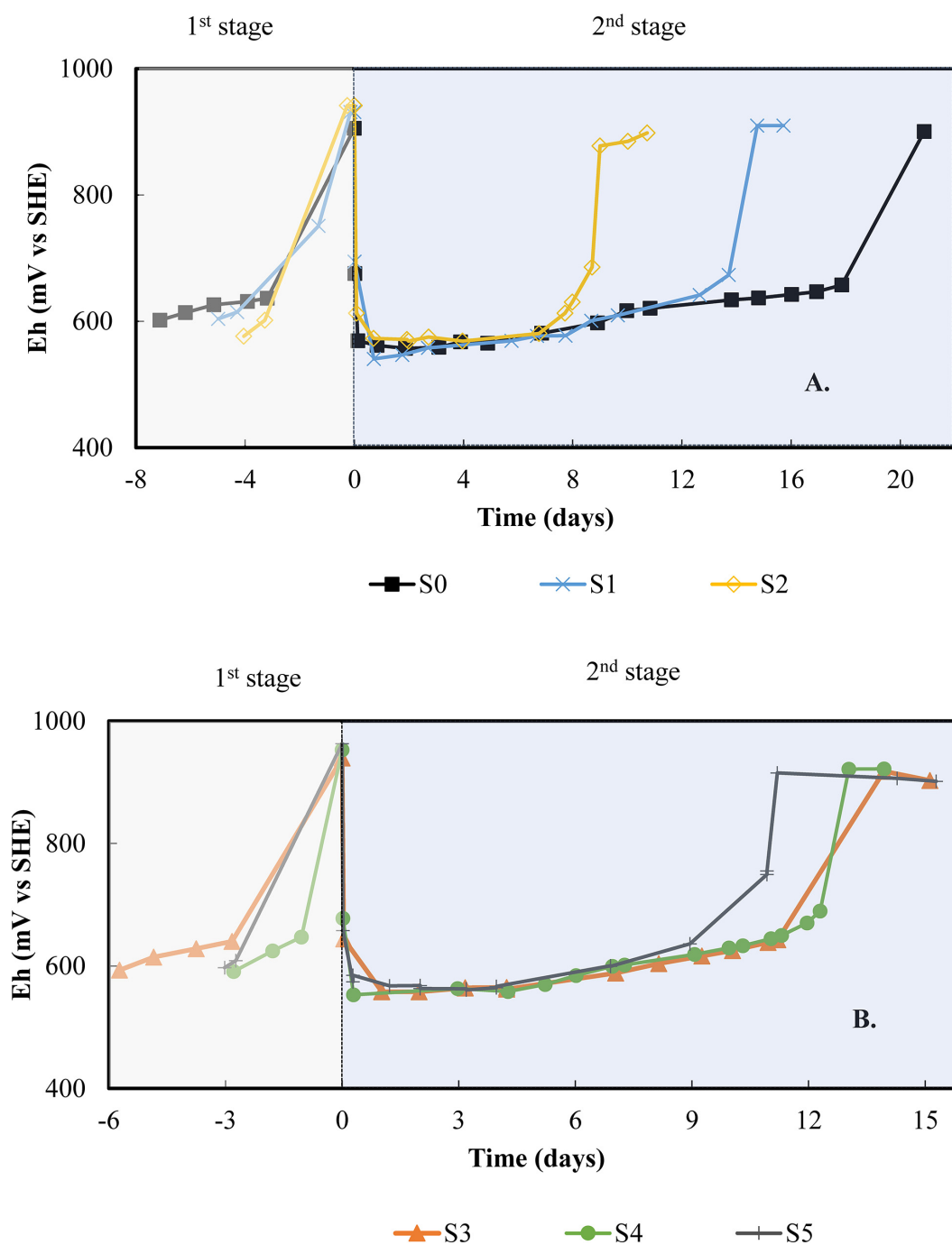


**FIGURE 3 |** Follow up of redox potential in bioleaching batch subcultures in 2.2 L-STRs: **(A)** subcultures S0, S1, and S2, **(B)** subcultures S3, S4, and S5. The first stage involves the microbial oxidation of the 3 Cm medium while the second stage starts with the addition of 2% (w/v) PCBs.

Edward et al. (2018) who reported uninhibited iron oxidation by a *L. ferriphilum*-dominated culture adapted to  $1 \text{ g L}^{-1}$  of Cu, achieving full oxidation of  $3 \text{ g L}^{-1}$  iron in 4 days in the presence of  $10 \text{ g L}^{-1}$  Cu. The combined inhibitory effects of different metals contained in PCB leachates might explain the impact on microbial activity kinetics in our FeOB culture, as has been observed by Nurmi et al. (2009). Achieving high PCB

loads is favorable for the economics of the bioleaching process. However, inhibitions of the microbial cultures have to be taken into account and only non-inhibitory pulp densities can be used.

The batch STR bioleaching experiments confirmed that elevated PCB loads extended the pre-oxidation phase. This delay was noted with both the adapted and non-adapted cultures. There was a pre-oxidation phase of 11 days at 1% (w/v) PCBs, even



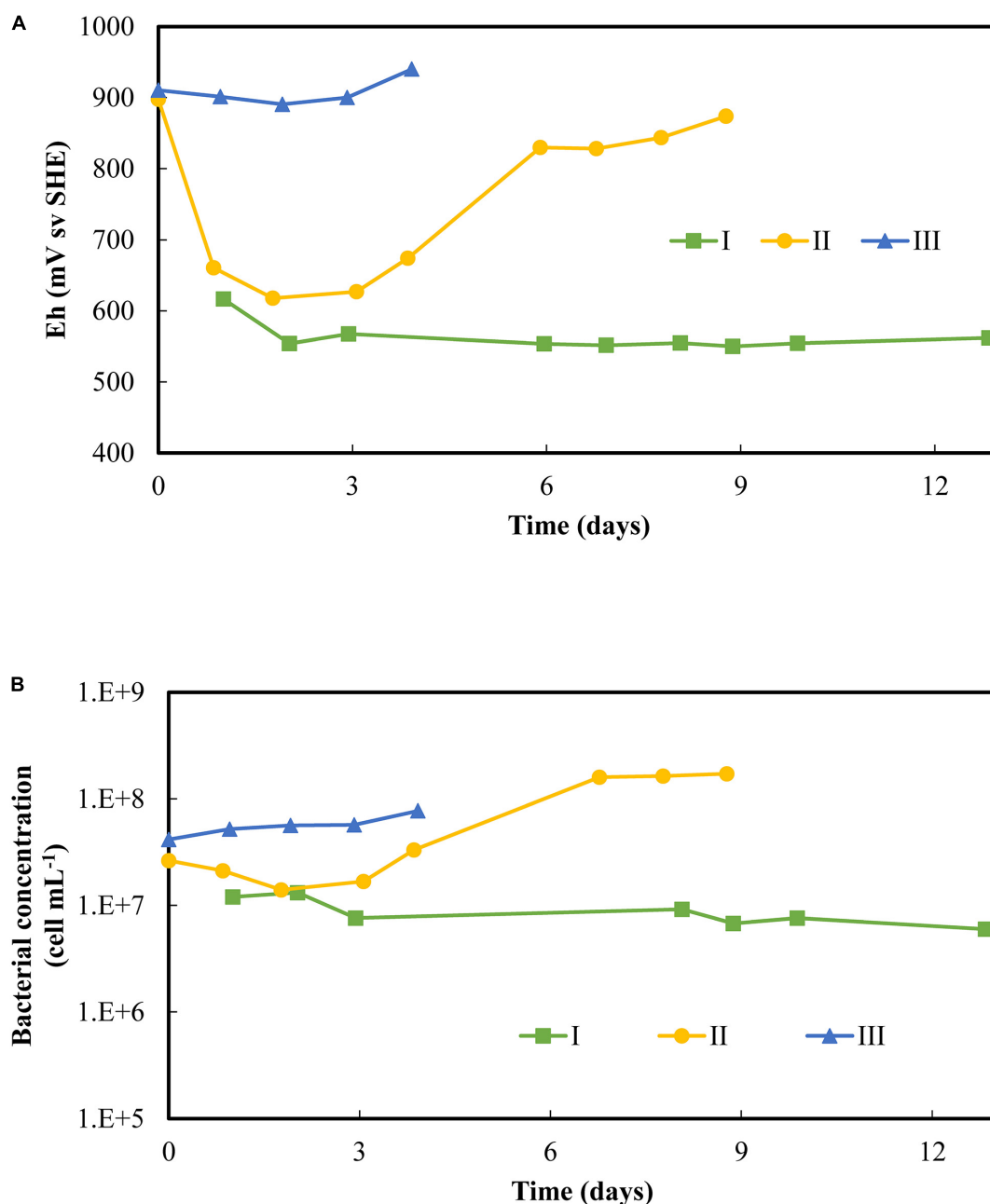


**FIGURE 4 |** Follow-up of **(A)** redox potential and **(B)** bacterial concentration overtime during the startup of continuous flow PCB bioleaching experiments in 2.2 L-STRs. Three scenarios of the startup were tested: I was only inoculated with the non-adapted culture; II performed a batch test on the adapted culture before starting the continuous flow process; III performed two successive batch subcultures on the adapted culture prior to the continuous flow process. Conditions of continuous flow bioleaching were set at 48 h of HRT and 1% (w/v) PCBs.

though the culture was adapted to that environment. The delays observed in the STRs were longer than those in shake flasks. The difference in operating conditions certainly affected the microbial activity, but the prolonged inhibiting effect in the STRs might also be related to (i) the shear stress caused by the solids and (ii) the presence of toxic elements in the solid phase.

A subculturing strategy reduced the inhibiting effect of PCBs in batch STRs. This improvement may be related to the

development of microbial resistance mechanisms allowing faster adaptation to the toxic effect of PCBs. It is also consistent with the work of Hedrich et al. (2016), in which successive subcultures improved the bioleaching rate of metals in batch bioleaching reactors. The subculturing strategy in this report achieved a maximum metal dissolution yield in 7 days despite the enhanced iron oxidation activity within subcultures. In all subcultures, the leaching agent was rapidly consumed during

the first hour. Therefore, leaching mostly occurred through the rapid reduction of Fe(III) and the slow acidic dissolution, regardless of the pre-oxidation phase (Mäkinen et al., 2015; Hubau et al., 2020). The improvement of the pre-oxidation phase was not sufficient to accelerate the dissolution of metals since, as demonstrated by Hubau et al. (2020), the regeneration of Fe(III) by bio-oxidation of Fe(II) in batch mode is longer than the time required for the chemical dissolution of metals (acidic hydrolysis). By reducing the pre-oxidation phase to less than these 7 days, dissolution of metals could be accelerated. In our study, this was not reached, and the shortest duration of the pre-oxidation phase was not determined due to the difficulty of the operational mode: the study demonstrated that the time between the end of a batch and the next subculture should be reduced to a minimum to maintain short pre-oxidation phases. The 10-day pause between subcultures adversely affected microbial iron oxidation by extending the duration of the pre-oxidation phase. At the end of one subculture, iron is completely oxidized, resulting in a lack of electron supply for bacterial metabolism. It is therefore preferable to keep the periods of time between batch subcultures short, to maintain a better supply of electrons. Long periods before subculturing have a negative effect on the attempts to shorten the pre-oxidation phase. Nevertheless, this negative effect proved to be transient, as the cultures in this study eventually regained high oxidation performance after several subcultures.

A continuous-flow bioreactor offers an interesting alternative to avoid the pauses between batch subcultures by ensuring a constant supply of iron to be oxidized, from both the medium and the PCBs themselves. It also enables the cultures to be adapted to PCBs, as well as Fe(III) to be regenerated in parallel with its consumption, thus favoring the metal dissolution by Fe(III) over the acidic hydrolysis (Hubau et al., 2020). The challenge is to reach and maintain steady-state conditions since the start-up can be a limiting issue. Thanks to the successive batch subcultures before the start-up in continuous mode, Scenario III was the most suitable strategy. It maintained high and constant microbial oxidation of iron, indicating that Fe was maintained as Fe(III) despite the continuous addition of PCBs. It was also considerably faster than in a previous study where 67 days were required to reach high redox potentials in a steady state (Hubau et al., 2020). The start-up of the process until high microbial iron oxidation activity was now almost immediate. This is a great advantage for further development of the process and its scale-up.

## CONCLUSION

This study investigated the capacity of an FeOB culture to oxidize iron in PCB environments by means of indicators such as the redox potential and microbial growth. Exponential bacterial

growth was observed and the bacteria oxidized  $8 \text{ g L}^{-1}$  of iron in the presence of a PCB leachate equivalent to 6% PCBs, which represented six times the metal content they were adapted to. However, the inhibiting effect of PCBs on microbial activity was evidenced by the delay in the bio-oxidation of Fe(II), i.e., a pre-oxidation phase. Successive subculturing shortened this delay by up to 2.5 times, reducing the inhibiting effect of PCBs in the bioleaching tests operated in batch mode. This strategy also enhanced the start-up of the continuous flow bioleaching reactor at 1% (w/v) PCBs. High microbial oxidation of iron was maintained by running several subcultures before switching to the continuous mode.

## DATA AVAILABILITY STATEMENT

The raw data supporting the conclusions of this article will be made available by the authors, without undue reservation.

## AUTHOR CONTRIBUTIONS

JA-G: conceptualization, methodology, investigation, writing—original draft, writing—review and editing, and visualization. AH: conceptualization, methodology, writing—review and editing, supervision, and project administration. CJ: conceptualization, methodology, writing—review and editing, and supervision. A-GG: conceptualization, resources, writing—review and editing, supervision, and funding acquisition. All authors contributed to the article and approved the submitted version.

## FUNDING

The *Mines Urbaines* Chair from the ParisTech foundation and the French Geological Survey (BRGM) funded this study with the support of Ecosystem.

## ACKNOWLEDGMENTS

The authors acknowledge the technical support of H. Tris in the characterization of the bacterial consortium. Funding provided by BRGM and the *Mines Urbaines* Chair are acknowledged.

## SUPPLEMENTARY MATERIAL

The Supplementary Material for this article can be found online at: <https://www.frontiersin.org/articles/10.3389/fmicb.2021.669738/full#supplementary-material>

## REFERENCES

- Adhapure, N. N., Waghmare, S. S., Hamde, V. S., and Deshmukh, A. M. (2013). Metal solubilization from powdered printed circuit boards by microbial consortium from bauxite and pyrite ores. *Appl. Biochem.* 49, 256–262. doi: 10.1134/S0003683813030034
- Arshadi, M., and Mousavi, S. M. (2014). Simultaneous recovery of Ni and Cu from computer-printed circuit boards using bioleaching: statistical

- evaluation and optimization. *Bioresour. Technol.* 174, 233–242. doi: 10.1016/j.biortech.2014.09.140
- Arshadi, M., and Mousavi, S. M. (2015). Multi-objective optimization of heavy metals bioleaching from discarded mobile phone PCBs: simultaneous Cu and Ni recovery using *Acidithiobacillus ferrooxidans*. *Sep. Purif. Technol.* 147, 210–219. doi: 10.1016/J.SEPPUR.2015.04.020
- Arya, S., and Kumar, S. (2020). Bioleaching: urban mining option to curb the menace of E-waste challenge. *Bioengineered* 11, 640–660. doi: 10.1080/21655979.2020.1775988
- Baniasadi, M., Vakili, F., Bahaloo-Horeh, N., Mousavi, S. M., and Farnaud, S. (2019). Advances in bioleaching as a sustainable method for metal recovery from E-waste: a review. *J. Ind. Eng. Chem.* 76, 75–90. doi: 10.1016/j.jiec.2019.03.047
- Brandl, H., Bosshard, R., and Wegmann, M. (2001). Computer-munching microbes: metal leaching from electronic scrap by bacteria and fungi". *Hydrometallurgy* 59, 319–326. doi: 10.1016/S0304-386X(00)00188-2
- Bryan, C. G., Joulain, C., Spolaore, P., El Achbouni, H., Challan-Belval, S., Morin, D., et al. (2011). The efficiency of indigenous and designed consortia in bioleaching stirred tank reactors. *Miner. Spec. Issue Bio Hydrometallurgy* 24, 1149–1156. doi: 10.1016/j.mineng.2011.03.014
- Bryan, C. G., Watkin, E. L., McCredon, T. J., Wong, Z. R., Harrison, S. T. L., and Kaksonen, A. H. (2015). The use of pyrite as a source of lixiviant in the bioleaching of electronic waste. *Hydrometallurgy* 152, 33–43. doi: 10.1016/j.hydromet.2014.12.004
- Bryan, C. G., Williamson, B. J., Calus-Moszkó, J., van Haute, Q., Guezennec, A. G., Gaydardzhiev, S., et al. (2020). CEReS-co-processing of coal mine & electronic wastes: novel resources for a sustainable future. *Hydrometallurgy* 197:105444. doi: 10.1016/j.hydromet.2020.105444
- Chen, S., Yang, Y., Liu, C., Dong, F., and Liu, B. (2015). Column bioleaching copper and its kinetics of waste printed circuit boards (WPCBs) by *Acidithiobacillus ferrooxidans*. *Chemosphere* 141, 162–168. doi: 10.1016/j.chemosphere.2015.06.082
- Chi, T. D., Lee, J. C., Pandey, B. D., Yoo, K., and Jeong, J. (2011). Bioleaching of gold and copper from waste mobile phone PCBs by using a cyanogenic bacterium. *Miner. Spec. Issue Bio Hydrometallurgy* 24, 1219–1222. doi: 10.1016/j.mineng.2011.05.009
- Coram, N. J., and Rawlings, D. E. (2002). Molecular relationship between two groups of the genus *Leptospirillum* and the finding that *Leptospirillum ferriphilum* Sp. Nov. Dominates South African commercial biooxidation tanks that operate at 40°C. *Appl. Environ. Microbiol.* 68, 838–845. doi: 10.1128/AEM.68.2.838-845.2002
- Das, A., Modak, J. M., and Natarajan, K. A. (1998). Surface chemical studies of *Thiobacillus ferrooxidans* with reference to copper tolerance. *Antonie van Leeuwenhoek* 73, 215–222. doi: 10.1023/A:1000858525755
- Dopson, M., and Holmes, D. S. (2014). Metal resistance in acidophilic microorganisms and its significance for biotechnologies. *Appl. Microbiol.* 98, 8133–8144. doi: 10.1007/s00253-014-5982-2
- Edward, C., Pather, T., Govender, R., Ngoma, E., Govender, E., Kotsiopoulos, A., et al. (2018). "Determination of ferrous oxidation kinetics in the presence of metals associated with printed circuit boards to determine the potential for bioleaching of E-waste," in *Proceedings of the Biohydrometallurgy '18*, Windhoek.
- Guezennec, A. G., Bru, K., Jacob, J., and d'Hugues, P. (2015). Co-processing of sulfidic mining wastes and metal-rich post-consumer wastes by biohydrometallurgy. *Biohydrometallurgy* 75, 45–53. doi: 10.1016/j.mineng.2014.12.033
- Guezennec, A. G., Joulain, C., Delort, C., Bodénan, F., Hedrich, S., and d'Hugues, P. (2018). CO<sub>2</sub> mass transfer in bioleaching reactors: CO<sub>2</sub> enrichment applied to a complex copper concentrate. *Hydrometallurgy* 180, 277–286. doi: 10.1016/j.hydromet.2018.08.006
- Haghsheenas, D. F., Keshavarz Alamdari, E., Amouei Torkmahalleh, M., Bonakdarpour, B., and Nasernejad, B. (2009). Adaptation of *Acidithiobacillus ferrooxidans* to high grade sphalerite concentrate. *Miner. Eng.* 22, 1299–1306. doi: 10.1016/j.mineng.2009.07.011
- Hedrich, S., Guézennec, A. G., Charron, M., Schippers, A., and Joulain, C. (2016). Quantitative monitoring of microbial species during bioleaching of a copper concentrate. *Front. Microbiol.* 7:2044. doi: 10.3389/fmicb.2016.02044
- Hubau, A., Chagnes, A., Minier, M., Touzé, S., Chapron, S., and Guezennec, A. G. (2019). Recycling-oriented methodology to sample and characterize the metal composition of waste printed circuit boards. *Waste Manage.* 91, 62–71. doi: 10.1016/j.wasman.2019.04.041
- Hubau, A., Minier, M., Chagnes, A., Joulain, C., Perez, C., and Guezennec, A. G. (2018). Continuous production of a biogenic ferric iron lixiviant for the bioleaching of printed circuit boards (PCBs). *Hydrometallurgy* 180, 180–191. doi: 10.1016/j.hydromet.2018.07.001
- Hubau, A., Minier, M., Chagnes, A., Joulain, C., Perez, C., Silvente, C., et al. (2020). Recovery of metals in a double-stage continuous bioreactor for acidic bioleaching of printed circuit boards (PCBs). *Sep. Purif. Technol.* 238:116481. doi: 10.1016/j.seppur.2019.116481
- Ilyas, S., Anwar, M. A., Niazi, S. B., and Ghauri, M. A. (2007). Bioleaching of metals from electronic scrap by moderately thermophilic acidophilic bacteria. *Hydrometallurgy* 88, 180–188. doi: 10.1016/j.hydromet.2007.04.007
- Ilyas, S., and Lee, J. C. (2014). Bioleaching of metals from electronic scrap in a stirred tank reactor. *Hydrometallurgy* 149, 50–62. doi: 10.1016/j.hydromet.2014.07.004
- Işıldar, A., van de Vossenberg, J., Rene, E. R., van Hullebusch, E. D., and Lens, P. N. (2016). Two-step bioleaching of copper and gold from discarded printed circuit boards (PCB). *Waste Manage.* 57, 149–157. doi: 10.1016/j.wasman.2015.11.033
- Işıldar, A., van Hullebusch, E. D., Lenz, M., Du Laing, G., Marra, A., Cesaro, A., et al. (2019). Biotechnological strategies for the recovery of valuable and critical raw materials from waste electrical and electronic equipment (WEEE)—a review. *J. Hazard. Mater.* 362, 467–481. doi: 10.1016/j.jhazmat.2018.08.050
- Kaya, M. (2019). *Electronic Waste and Printed Circuit Board Recycling Technologies. The Minerals, Metals & Materials Series*. Cham: Springer International Publishing. doi: 10.1007/978-3-030-26593-9
- Kinnunen, P., and Puhakka, J. A. (2004). High-rate ferric sulfate generation by a *Leptospirillum ferriphilum*-dominated biofilm and the role of jarosite in biomass retention in a fluidized-bed reactor. *Biotechnol. Bioeng.* 85, 697–705. doi: 10.1002/bit.20005
- Liu, R., Chen, Y., Tian, Z., Mao, Z., Cheng, H., Zhou, H., et al. (2019). Enhancing microbial community performance on acid resistance by modified adaptive laboratory evolution. *Bioresour. Technol.* 287:121416. doi: 10.1016/j.biortech.2019.121416
- Liu, X., Liu, H., Wu, W., Zhang, X., Gu, T., Zhu, M., et al. (2020). Oxidative stress induced by metal ions in bioleaching of LiCoO<sub>2</sub> by an acidophilic microbial consortium. *Front. Microbiol.* 10:3058. doi: 10.3389/fmicb.2019.03058
- Mäkinen, J., Bachér, J., Kaartinen, T., Wahlström, M., and Salminen, J. (2015). The effect of flotation and parameters for bioleaching of printed circuit boards. *Miner. Biohydrometallurgy* 75, 26–31. doi: 10.1016/j.mineng.2015.01.009
- Mi, S., Song, J., Lin, J., Che, Y., Zheng, H., and Lin, J. (2011). Complete genome of *Leptospirillum ferriphilum* ML-04 provides insight into its physiology and environmental adaptation. *J. Microbiol.* 49, 890–901. doi: 10.1007/s12275-011-1099-9
- Nurmi, P., Özkaya, B., Kaksonen, A. H., Tuovinen, O. H., and Puhakka, J. A. (2009). Inhibition kinetics of iron oxidation by *Leptospirillum ferriphilum* in the presence of ferric, nickel and zinc ions. *Hydrometallurgy* 97, 137–145. doi: 10.1016/j.hydromet.2009.02.003
- Rawlings, D. E. (2005). Characteristics and Adaptability of iron- and sulfur-oxidizing microorganisms used for the recovery of metals from minerals and their concentrates. *Microb. Cell Fact.* 4:13. doi: 10.1186/1475-2859-4-13
- Rawlings, D. E., and Johnson, B. (2007). *Biomining*. Berlin: Springer-Verlag. doi: 10.1007/978-3-540-34911-2
- Rawlings, D. E., Tributsch, H., and Hansford, G. S. (1999). Reasons why 'Leptospirillum'-like species rather than *Thiobacillus ferrooxidans* are the dominant iron-oxidizing bacteria in many commercial processes for the biooxidation of pyrite and related ores. *Microbiology* 145, 5–13. doi: 10.1099/13500872-145-1-5
- Wang, S., Chen, L., Zhou, X., Yan, W., Ding, R., Chen, B., et al. (2018). Enhanced bioleaching efficiency of copper from printed circuit boards without iron loss. *Hydrometallurgy* 180, 65–71. doi: 10.1016/j.hydromet.2018.07.010
- Wassink, B., and Asselin, E. (2019). *Copper Hydrometallurgy: Principles and Practice. 1250–3500 de Maisonneuve Blvd. West Westmount, QC: Canadian Institute of Mining, Metallurgy and Petroleum.*

- Wu, W., Liu, X., Zhang, X., Zhu, M., and Tan, W. (2018). Bioleaching of copper from waste printed circuit boards by bacteria-free cultural supernatant of iron-sulfur-oxidizing bacteria. *Bioresour. Bioprocess.* 5:10. doi: 10.1186/s40643-018-0196-6
- Xia, M. C., Wang, Y. P., Peng, T. J., Shen, L., Yu, R. L., Liu, Y. D., et al. (2017). Recycling of metals from pretreated waste printed circuit boards effectively in stirred tank reactor by a moderately thermophilic culture. *J. Biosci.* 123, 714–721. doi: 10.1016/j.jbiosc.2016.12.017
- Xiang, Y., Wu, P., Zhu, N., Zhang, T., Liu, W., Wu, J., et al. (2010). Bioleaching of copper from waste printed circuit boards by bacterial consortium enriched from acid mine drainage. *J. Hazard. Mater.* 184, 812–818. doi: 10.1016/j.jhazmat.2010.08.113
- Xu, T. J., Ramanathan, T., and Ting, Y. P. (2014). Bioleaching of incineration fly ash by *Aspergillus niger*–precipitation of metallic salt crystals and morphological alteration of the fungus. *Biotechnol. Rep.* 3, 8–14. doi: 10.1016/j.btre.2014.05.009
- Yang, T., Xu, Z., Wen, J., and Yang, L. (2009). Factors influencing bioleaching copper from waste printed circuit boards by *Acidithiobacillus ferrooxidans*. *Hydrometallurgy* 97, 29–32. doi: 10.1016/j.hydromet.2008.12.011
- Yang, Y., Chen, S., Li, S., Chen, M., Chen, H., and Liu, B. (2014). Bioleaching waste printed circuit boards by *Acidithiobacillus ferrooxidans* and its kinetics aspect. *J. Biotechnol.* 173, 24–30. doi: 10.1016/j.jbiotec.2014.01.008
- Yue, G., Guezennec, A. G., and Asselin, E. (2016). Extended validation of an expression to predict ORP and iron chemistry: application to complex solutions generated during the acidic leaching or bioleaching of printed circuit boards. *Hydrometallurgy* 164, 334–342. doi: 10.1016/j.hydromet.2016.06.027
- Zhang, Q., Yang, W., Yang, Q., Wang, T., Chen, S., Zou, M., et al. (2018). Effect of using different proportions of inoculum during bioleaching on sludge dewaterability. *Water Sci. Technol.* 2017, 802–811. doi: 10.2166/wst.2018.234
- Zhu, N., Xiang, Y., Zhang, T., Wu, P., Dang, Z., Li, P., et al. (2011). Bioleaching of metal concentrates of waste printed circuit boards by mixed culture of acidophilic bacteria. *J. Hazard. Mater.* 192, 614–619. doi: 10.1016/j.jhazmat.2011.05.062

**Conflict of Interest:** The authors declare that the research was conducted in the absence of any commercial or financial relationships that could be construed as a potential conflict of interest.

**Publisher's Note:** All claims expressed in this article are solely those of the authors and do not necessarily represent those of their affiliated organizations, or those of the publisher, the editors and the reviewers. Any product that may be evaluated in this article, or claim that may be made by its manufacturer, is not guaranteed or endorsed by the publisher.

Copyright © 2021 Anaya-Garzon, Hubau, Joulain and Guezennec. This is an open-access article distributed under the terms of the Creative Commons Attribution License (CC BY). The use, distribution or reproduction in other forums is permitted, provided the original author(s) and the copyright owner(s) are credited and that the original publication in this journal is cited, in accordance with accepted academic practice. No use, distribution or reproduction is permitted which does not comply with these terms.





# Bioaugmentation With a Consortium of Bacterial Sodium Lauryl Ether Sulfate-Degraders for Remediation of Contaminated Soils

Ludovica Rolando<sup>1</sup>, Anna Barra Caracciolo<sup>1\*</sup>, Paola Grenni<sup>1</sup>, Livia Mariani<sup>1</sup>, Jasmin Rauseo<sup>2</sup>, Francesca Spataro<sup>2</sup>, Gian Luigi Garbini<sup>1,3</sup>, Andrea Visca<sup>1</sup> and Luisa Patrolecco<sup>2</sup>

<sup>1</sup> Water Research Institute, National Research Council, Monterotondo, Italy, <sup>2</sup> Institute of Polar Sciences, National Research Council, Monterotondo, Italy, <sup>3</sup> Department of Ecological and Biological Sciences, Tuscia University, Viterbo, Italy

## OPEN ACCESS

### Edited by:

Muhammad Bilal,  
Huaiyin Institute of Technology, China

### Reviewed by:

Pankaj Bhatt,  
South China Agricultural University,  
China

Sikandar I. Mulla,  
REVA University, India

### \*Correspondence:

Anna Barra Caracciolo  
anna.barracaracciolo@irsa.cnr.it

### Specialty section:

This article was submitted to  
Microbiotechnology,  
a section of the journal  
Frontiers in Microbiology

**Received:** 12 July 2021

**Accepted:** 12 August 2021

**Published:** 22 September 2021

### Citation:

Rolando L, Barra Caracciolo A, Grenni P, Mariani L, Rauseo J, Spataro F, Garbini GL, Visca A and Patrolecco L (2021) Bioaugmentation With a Consortium of Bacterial Sodium Lauryl Ether Sulfate-Degraders for Remediation of Contaminated Soils. *Front. Microbiol.* 12:740118. doi: 10.3389/fmicb.2021.740118

The anionic surfactant sodium lauryl ether sulfate (SLES) is the main component of most commercial foaming agents (FAs) used in the excavation of highway and railway tunnels with Earth pressure balance-tunnel boring machines (EPB-TBMs). Several hundreds of millions of tons of spoil material, consisting of soil mixed with FAs, are produced worldwide, raising the issue of their handling and safe disposal. Reducing waste production and reusing by-products are the primary objectives of the “circular economy,” and in this context, the biodegradation of SLES becomes a key question in reclaiming excavated soils, especially at construction sites where SLES degradation on the spot is not possible because of lack of space for temporary spoil material storage. The aim of the present work was to apply a bacterial consortium (BC) of SLES degraders to spoil material excavated with an EPB-TBM and coming from a real construction site. For this purpose, the BC capability to accelerate SLES degradation was tested. Preliminary BC growth, degradation tests, and ecotoxicological evaluations were performed on a selected FA. Subsequently, a bioaugmentation experiment was conducted; and the microbial abundance, viability, and SLES concentrations in spoil material were evaluated over the experimental time (0.5, 3, 6, 24, 48, and 144 h). Moreover, the corresponding aqueous elutriates were extracted from all the soil samples and analyzed for SLES concentration and ecotoxicological evaluations with the bacterium *Aliivibrio fischeri*. The preliminary experiments showed the BC capability to grow under 14 different concentrations of the FA. The maximum BC growth rates and degradation efficiency (100%) were achieved with initial SLES concentrations of 125, 250, and 500 mg/L. The subsequent bioaugmentation of the spoil material with BC significantly (sixfold) improved the degradation time of SLES (DT<sub>50</sub> 1 day) compared with natural attenuation (DT<sub>50</sub> 6 days). In line with this result, neither SLES residues nor toxicity was recorded in the soil extracts showing the spoil material as a by-product promptly usable. The bioaugmentation with BC can be a very useful for cleaning spoil material produced in underground construction where its temporary storage (for SLES natural biodegradation) is not possible.

**Keywords:** anionic surfactant, foaming agents, spoil material, bioremediation, underground construction, bacterial consortium

## INTRODUCTION

The anionic surfactant sodium lauryl ether sulfate (SLES) is the main component in most foaming agents (FAs) used in the excavation of highway and railway tunnels with Earth pressure balance-tunnel boring machines (EPB-TBMs) (Barra Caracciolo et al., 2017). FAs are used to change the mechanical properties and hydraulic behavior of soil, ensuring a malleable material that can be manageably excavated and transported to temporary areas (Peila, 2014; Peila et al., 2016). Due to the numerous tunneling projects currently in progress, several hundreds of millions of tons of soil debris (spoil material) are produced worldwide annually, raising the question of how to handle and dispose of them (Rahimzadeh et al., 2018; Rolando et al., 2020). Surfactants, including SLES, can be toxic for aquatic ecosystems if present at concentrations higher than the critical micellar one (Barra Caracciolo et al., 2017; Mariani et al., 2020; Rolando et al., 2020). The presence of SLES in spoil material can influence its recycling as a by-product; in fact, if the residual concentration of SLES is high, there can be toxic effects.

Previous experiments conducted on spoil material from tunnel excavation sites demonstrated that SLES was not toxic for terrestrial organisms (e.g., *Lepidium sativum* and *Eisenia fetida*) (Galli et al., 2019). However, in some cases, it showed detrimental effects on two aquatic species (*Pseudokirchneriella subcapitata* and *Aliivibrio fischeri*) (Grenni et al., 2018; Finizio et al., 2020; Patrolecco et al., 2020; Barra Caracciolo et al., 2021). Interestingly, the bacterium *A. fischeri* was shown to be very sensitive to SLES residues. In fact, a positive correlation between SLES concentrations and a toxic effect (inhibition of bioluminescence) on the bacterium was found in a 2-year monitoring of the spoil material from a highway construction site, making it possible to establish 2 mg/L as a “threshold value” of the toxic effect in the elutriates produced from spoil material (Mariani et al., 2020).

Reducing waste production and reusing by-products are the primary objectives of the “circular economy,” and in this context, the biodegradation of SLES becomes a key question in the safe reclaiming of excavated soils. Currently, tunnel debris can be used for refilling old quarries, road constructions, and green areas and as a raw material for industrial production (Belopede and Marini, 2011).

Sodium lauryl ether sulfate has been shown to be a biodegradable compound in soils from tunnel excavation sites, but with highly variable degradation rates (Barra Caracciolo et al., 2019, 2021). In fact, concentrations of SLES in the range of 27–350 mg/kg showed variable half-lives ( $DT_{50}$ ) from 8 to 46 days (Finizio et al., 2020). These results were ascribable not only to the initial SLES concentrations but also to site-specific characteristics such as soil texture, depth, structure, mineralogy, microbial abundance, water content, and temperature, which influenced its biodegradation differently.

Although a natural attenuation (with no human intervention) of SLES is expected due to the environmental microorganisms

present in the excavated soil, degradation times cannot always meet construction site requirements. In some cases, the spoil material can be temporarily stored at the construction site for the time needed for SLES biodegradation (Barra Caracciolo et al., 2019). This practice was successfully used in a recent tunnel construction site in Italy (Mariani et al., 2020). Unfortunately, in other cases, such as tunneling for a metro inside a city, an area for spoil material temporary storage is not available. In this case, the excavated materials have to be considered waste, requiring transportation, treatment, and disposal, with a significant increase in project costs and unnecessary landfill use (Barra Caracciolo et al., 2017; Rahimzadeh et al., 2018; Patrolecco et al., 2020).

In Italy, spoil material can be classified as a by-product if the chemical thresholds for some organic and inorganic contaminants (e.g., heavy metals, hydrocarbons  $C > 12$ ) are not exceeded (Italian Decree, 2017). However, there are no SLES soil concentration limits (Annex 4 of the Italian Decree 120/2017) in EU and national legislation (Italian Decree, 2017). Consequently, the possibility that soil debris can be really considered a safe by-product is strongly related to SLES persistence and their residual concentrations, which in turn depend on abiotic and biotic site-specific conditions.

Sodium lauryl ether sulfate degradation is common in environmental bacteria able to resist the toxic effects of SLES and to degrade it (Barra Caracciolo et al., 2019). Several Gamma-Proteobacteria possess esterase enzymes that are able to break the SLES ester bond (Bornscheuer, 2002; Panda and Gowrishankar, 2005). In a recent previous work, a bacterial consortium (BC) capable of degrading completely pure SLES within 24 h was selected using enrichment cultures. The BC consisted of Gamma-Proteobacteria (99%), and the predominant (ca. 90%) genus was *Pseudomonas* (Rolando et al., 2020).

The aim of the present work was to test if adding the SLES pre-grown microbial culture (BC) to spoil material from a tunnel construction site enhanced the removal of the anionic surfactant residues, with potentially significant economic and environmental benefits.

## MATERIALS AND METHODS

### Chemicals

Methanol and chloroform of high-performance liquid chromatography (HPLC) grade, hydrochloric acid (37%), sulfuric acid (98%), and methylene blue were purchased from VWR (Radnor, PA, United States). Sodium hydrogen carbonate and anhydrous sodium carbonate were obtained from CARLO ERBA Reagents (Milan, Italy). SLES of technical grade purity was from BOC Sciences (Shirley, NY, United States). The stock solution of SLES (1,000 mg/L) was prepared in methanol and stored at  $-20^{\circ}\text{C}$ . The dilution of this stock solution was performed using ultrapure water. Ultrapure water ( $18\text{ M}\Omega \cdot \text{cm}$  quality) was obtained using a Milli-Q system Millipore (Bedford, MA, United States). Diatomaceous earth was purchased from Thermo Fisher Scientific Inc. (Waltham, MA, United States).

## Analytical Determination of Sodium Lauryl Ether Sulfate in the Foaming Agent

The SLES concentration in FA solutions, used for the preliminary BC growth and degradation test described in the *Chemicals* section, was determined by applying the methylene blue active substances (MBAS) method<sup>1</sup>. This method includes three consecutive chloroform extractions of the ionic-pair reaction between SLES and methylene blue. Subsequently, the absorbance of the SLES-MBAS complex was measured with spectrophotometry at a wavelength of 650 nm (Lambda 25UV-VIS spectrophotometer, PerkinElmer, Waltham, MA, United States). Finally, the SLES concentration was calculated using the equations obtained with the standard calibration curve (in the range from 0.05 to 4 mg/L of SLES), as previously described (Barra Caracciolo et al., 2019; Patrolecco et al., 2020). The limit of detection (LOD), calculated following the IUPAC method (IUPAC, 1999), was 0.013 mg/L.

## Preparation of Elutriates From Soil Samples

The elutriates (soil water extracts) were produced from soil samples in a 1:10 (solid/liquid) ratio, as reported in Grenni et al. (2018), following the procedure described in UNI EN 12457-4:2004 (UNI EN, 2004). This standard procedure was used to simulate possible leaching of SLES from soil to water. Briefly, an aliquot (10 g) of fresh soil sample was put into a 250-ml bottle, and the calculated amount of distilled water (taking into account the moisture of the soil sample) was added. The suspension was shaken for 24 h at 20°C in the dark and settled, and the supernatant was then centrifuged for 15 min at 9,000 rpm.

## Analytical Determination of Sodium Lauryl Ether Sulfate in Soil and Elutriates

Sodium lauryl ether sulfate was extracted from soil samples with the pressurized liquid extraction (PLE) technique (Buchi mod. E-916; Cornaredo, Milan, Italy), using methanol as the extraction solvent and following the operative conditions reported in Pescatore et al. (2020). The PLE extracts and aqueous elutriates were analyzed for SLES content using the spectrophotometric MBAS method (see section “Analytical Determination of Sodium Lauryl Ether Sulfate in the Foaming Agent”). The PLE recovery was  $96.5 \pm 1.6\%$ .

## Preliminary Bacterial Consortium Growth and Degradation Test on the Foaming Agent Selected

The previously isolated BC, capable of degrading pure SLES in 24 h and using it as the only carbon source (Rolando et al., 2020), was initially tested on a commercial FA consisting of a water solution of SLES (16%). FA was selected because it is one of the most common commercial products used in Italy and Europe for tunnel excavation with EPB-TBMs.

The capability of the BC to grow on different FA amounts was tested. For this purpose, various FA water solutions were prepared to obtain 14 SLES concentrations (0.5 mg/L, 1 mg/L, 2 mg/L, 4 mg/L, 8 mg/L, 16 mg/L, 31 mg/L, 62.5 mg/L, 125 mg/L, 250 mg/L, 500 mg/L, 1 g/L, 2 g/L, and 4 g/L). For each concentration, three replicates were considered. A control with only a mineral medium and a control with a mineral medium (MB1) and the BC were also set up. The bacterial growth was measured (every 15 min for 24 h) in terms of optical density (OD, 600<sub>nm</sub>), using a Multiskan Sky Microplate Spectrophotometer (Thermo Fisher Scientific). A 96-well plate was used to incubate the cultures at 37°C with a background shaking (180 rpm) and then read with the spectrophotometer for BC growth.

The capability of the BC to degrade the FA was then verified with the five concentrations that showed the highest growth rates (125 mg/L, 250 mg/L, 500 mg/L, 1 g/L, 2 g/L, and 4 g/L). Culture flasks (100 ml, three replicates for each condition) containing MB1 and FA solutions were incubated at 28°C in the dark and maintained on a rotary shaker at 130 rpm. A control with only MB1 and a control with MB1 and the BC were also set up. Cell growth (OD) and SLES concentration (% residual SLES concentration) were measured at 0, 6, 24, and 48 h.

## Ecotoxicological Evaluation (EC<sub>20</sub> and EC<sub>50</sub>) of the Foaming Agent

The intrinsic toxicity of the FA was evaluated using the bioluminescent bacterium *A. fischeri*, following the UNI EN ISO 11348-3:2019 protocol, reported in detail in section “*Aliivibrio fischeri* Acute Toxicity Test.” The test with *A. fischeri* was used because previous studies have demonstrated it to be very sensitive to SLES residues in spoil material (Grenni et al., 2018; Mariani et al., 2020; Patrolecco et al., 2020).

The FA toxicity was expressed as the effective concentration (EC), i.e., the concentration that causes an effect (bioluminescence inhibition in percentage) on 20% (EC<sub>20</sub>) or 50% (EC<sub>50</sub>) of the organisms tested.

A higher EC value corresponds to a lower ecotoxicological effect. The EC<sub>20</sub> and EC<sub>50</sub> were determined using the Basic Test (81.9%) performed three times. The bacterium *A. fischeri* was exposed to various FA concentrations prepared with subsequent dilutions (using distilled water) from an FA stock solution (105 mg/L). Seven diluted solutions (in the range 1.34–86.00 mg/L) of the FA were used. The EC<sub>20</sub> and EC<sub>50</sub> were statistically estimated (Microtox Omni® software V 4.2, Milan, Italy). Based on the results obtained (see sections “Preliminary Bacterial Consortium Growth and Degradation Test on the Foaming Agent Selected” and “Ecotoxicological Evaluation (EC<sub>20</sub> and EC<sub>50</sub>) of the Foaming Agent”), the commercial product FA was used for the subsequent bioaugmentation and ecotoxicological experiments, as described in the following paragraphs.

## Bioaugmentation Experiment With Spoil Material From the Construction Site

The soil samples consisted of spoil material directly obtained from the EPB-TBM operating in a railway tunnel construction

<sup>1</sup>[https://www.nemi.gov/methods/method\\_summary/7612/](https://www.nemi.gov/methods/method_summary/7612/)

in Southern Italy. The experimental set consisted of glass beakers (2,000-ml capacity) filled with about 800 g of the excavated soil. The spoil material consisted of a silty clay soil conditioned with the commercial FA containing SLES (16%). The FA treatment ratio was 1.017 L/m<sup>3</sup>, which corresponded to an expected SLES concentration of 130 mg/kg. The soil water content was 60%, corresponding to 70% of the maximum soil water-holding capacity.

The BC was seeded on the spoil material to test its capability to accelerate the FA degradation.

The overall experimental conditions were as follows (three replicates for each condition):

- Soil batches with the FA and the BC: **FA + BC soil**.
- Soil batches with only the FA: **FA soil**.
- Soil batches with only the BC: **BC soil**.
- Untreated soil batches: **Control**.

The overall experimental set was maintained at room temperature  $20 \pm 2^\circ\text{C}$  and kept open in order to simulate the temporary storage of the spoil material at the construction site. At selected times (0.5, 3, 6, 24, 48, and 144 h), three subsamples of soil from each batch were collected to analyze the microbial community [4',6-diamidino-2-phenylindole (DAPI) counts and Live/Dead] and the concentration of SLES over time. Moreover, from each soil sample, the corresponding aqueous elutriate was produced (see section "Preparation of Elutriates From Soil Samples") and analyzed for SLES concentration and ecotoxicological evaluations with the bacterium *A. fischeri*. All results refer to dry weight.

## Preparation of the Bacterial Inoculum

The BC was cultured in a mineral medium [MB1: 0.8 g/L of K<sub>2</sub>HPO<sub>4</sub>, 0.2 g/L of KH<sub>2</sub>PO<sub>4</sub>, 0.05 g/L of CaSO<sub>4</sub>·2H<sub>2</sub>O, 0.5 g/L

of MgSO<sub>4</sub>·7H<sub>2</sub>O, 0.01 g/L of FeSO<sub>4</sub>, and 1 g/L of (NH<sub>4</sub>)<sub>2</sub>SO<sub>4</sub>] with 250 mg/L of SLES and maintained at 28°C overnight. From the overnight static culture, the bacterial cells were centrifuged (9,000 rpm for 2 min) and re-suspended in distilled water and the latter plus the FA. Before the spoil material was seeded, the bacterial abundance and viability of the BC were also measured using the DAPI count and Live/Dead methods, respectively. The bacterial abundance was  $2.19 \times 10^7 \pm 1.22 \times 10^6$  cell/ml with a  $90.7 \pm 0.2\%$  of live cells.

## Total Bacterial Abundance and Cell Viability by Epifluorescence Direct Methods

A fluorescence microscope (Leica DM 4000B, Leica Microsystems GmbH, Wetzlar, Germany) was used to observe and count the total bacterial abundance and cell viability. Briefly, total bacterial abundance (No. cells/g soil) was obtained (three subsample replicates) using aliquots of samples (ranging from 0.25 to 1 ml), fixed with formaldehyde (2% final concentration), and filtered through a 25-mm black polycarbonate membrane with a porosity of 0.2 µm (Whatman) using a gentle vacuum (<0.2 bar). The filters were treated with DAPI as described in detail elsewhere (Barra Caracciolo et al., 2005a,b). The total number of bacterial cells using DAPI can detect all microbial cells in a sample regardless of their physiological status and metabolic activity.

Cell viability (% live cells/live + dead) was assessed (three subsample replicates) using aliquots of fresh samples (the same volumes used for total bacterial abundance), which were filtered through the same filters as for the DAPI counts. The filters were treated with two fluorescent dyes, SYBR Green II and propidium iodide, as described in detail elsewhere (Grenni et al., 2009). This method can detect the viability of microorganisms, because

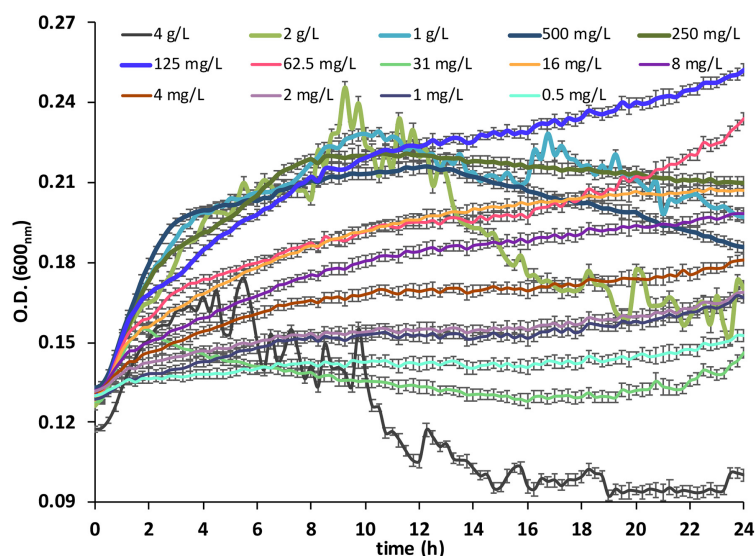


**FIGURE 1 |** Bacterial consortium growth measured as optical density (OD) at 600nm, under 14 concentrations (from 0.5 mg/L to 4 g/L) of SLES. The vertical bars represent the standard errors. SLES, sodium lauryl ether sulfate.



propidium iodide dye can only enter dead or damaged cells, and they appear red under a fluorescence microscope. Finally, the abundance of viable cells (No. viable cells/g soil) was calculated by multiplying the total bacterial abundance (obtained by DAPI counting) by cell viability.

### *Aliivibrio fischeri* Acute Toxicity Test

The acute toxicity test with *A. fischeri* was performed using a Microtox® analyzer (Model 500; Ecotox LDS, Milan, Italy) in accordance with the UNI EN ISO 11348-3: 2019 standard protocol (UNI EN, 2019). This test is based on the inhibition of the luminescence naturally emitted by the marine bacterium *A. fischeri* after its exposure to a toxic substance. Light output of the test organism, compared with a blank (toxic-free solution: distilled water containing 22% NaCl), was measured at least three times after each exposure period (5, 15, and 30 min). The difference in light output (between the sample and the blank) was ascribed to the matrix (elutriate) effect on the bacterium. The effect was calculated as a percentage of inhibition, using specific software (Microtox Omni® software V 4.2, Milan, Italy). Before the tests were carried out, the pH value of each elutriate was recorded and eventually corrected (range 6.0–8.0) using an HCl 0.1 M solution (Scheerer et al., 2006), as required by the standard procedures. The coefficient of variation (CV%: standard deviation/mean × 100) as a validity criterion (has to be <20%) was also calculated. The bacterial response (% bioluminescent inhibition) was considered toxic if it was more than 20% (Persoone et al., 2003), in accordance with the UNI EN ISO 11348-3:2019 protocol (UNI EN, 2019).

### Statistical Analysis

Any differences among data were evaluated using the Kruskal–Wallis test. The relationship between variables was calculated using a linear regression model. All statistical analyses were performed using R software version 4.1.0. Average and standard errors were estimated from three technical replicates of three biological replicates using MS Excel version 16.16.27. All figures were made using MS Excel version 16.16.27.

## RESULTS

### Preliminary Bacterial Consortium Growth and Degradation Test on the Foaming Agent Selected

A significant growth in the BC was observed with all 14 concentrations tested (Figure 1), confirming that the anionic surfactant SLES contained in the FA was a suitable carbon source.

The maximum BC growth rates are reported in Table 1. The growth rates were calculated with the following formula (Monod, 1949):

$$\mu = \frac{\log_{10} OD_x - \log_{10} OD_0}{t_x - t_0} \quad (1)$$

where OD<sub>x</sub>, optical density measured at sampling time; OD<sub>0</sub>, optical density measured at time 0; t<sub>x</sub>, sampling time; and t<sub>0</sub>, time 0.

The five SLES concentrations (125 mg/L, 250 mg/L, 500 mg/L, 1 g/L, and 2 g/L), which showed significantly ( $p < 0.01$ , Kruskal–Wallis test) higher BC growth rates, were used for the subsequent degradation experiment.

The BC was capable of growing with all five SLES concentrations tested (Figure 2A). However, a complete degradation of the anionic surfactant was observed at 48 h only with the 125, 250, and 500 mg/L concentrations (Figure 2B).

### Ecotoxicological Evaluation (EC<sub>20</sub> and EC<sub>50</sub>) of the Foaming Agent

The dose–response relationship between the FA concentration and the bioluminescence inhibition (%) after 30 min of exposure of the bacterium *A. fischeri* was determined. The EC<sub>20</sub> and EC<sub>50</sub> average values for the FA were  $3.66 \pm 0.72$  (corresponding to 0.59 mg/L of SLES) and  $10.34 \pm 1.20$  (corresponding to 1.66 mg/L of SLES) mg/L, respectively. In both cases, the CV% was less than 20%.

### Bioaugmentation Experiment

#### Total Microbial Abundance and Cell Viability in Soil

The initial microbial abundance (expressed as No. of live cells/g soil) in the spoil material used for the bioaugmentation experiment was similar in all conditions ( $1.65 \times 10^6 \pm 1.24 \times 10^5$ ). FA treatment did not have any initial detrimental effect on this microbiological parameter. An increasing trend in microbial numbers was observed between 0.5 and 48 h. A significantly ( $p < 0.01$ , Kruskal–Wallis test) higher abundance was observed in the bioaugmented soil (FA + BC soil), with a peak at 48 h (Figure 3).

#### Sodium Lauryl Ether Sulfate Concentration in Soil and Elutriates

The residual concentrations of SLES measured over the experimental time (0.5, 3, 6, 24, 48, and 144 h) in the spoil material and in the corresponding elutriates produced are shown in Figure 4 and Table 2, respectively. The initial SLES amounts in the spoil material (FA soil) and in the

**TABLE 1** | Maximum growth rates of the bacterial consortium grown under 14 different SLES concentrations.

SLES concentration (mg/L)	4,000	2,000	1,000	500	250	125	62.5	31	16	8	4	2	1	0.5
$\mu_{\max}$ (h <sup>-1</sup> )	0.037	0.047	0.043	0.044	0.043	0.043	0.037	0.035	0.037	0.023	0.018	0.014	0.013	0.010

SLES, sodium lauryl ether sulfate.

$\mu_{\max}$  = maximum growth rate during the exponential phase.

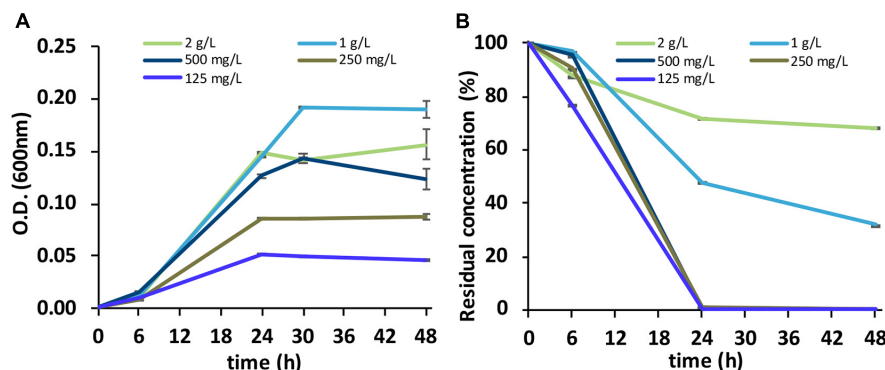


**FIGURE 2 | (A)** Growth of the BC (OD at 600<sub>nm</sub>) on the foaming agent containing SLES. **(B)** Biodegradation of SLES (residual concentration) at five concentrations (125 mg/L, 250 mg/L, 500 mg/L, 1 g/L, and 2 g/L). The vertical bars represent the standard errors. BC, bacterial consortium; SLES, sodium lauryl ether sulfate.

bioaugmented soil (FA + BC soil) were  $136 \pm 3.6$  and  $132.3 \pm 2.8$  mg/kg, respectively.

In the bioaugmented soil (FA + BC soil), 91% of SLES was degraded at 144 h. At the same sampling time, in the absence of the BC, only 54% of SLES was degraded (FA soil; **Figure 4A**).

The degradation pathways followed first-order kinetics, and the theoretical values of the disappearance time of 50% of the initial SLES concentrations ( $DT_{50}$ ) were calculated from correlations ( $r^2 = 0.93$  for FA + BC soil and 0.95 for FA soil;  $p$ -value < 0.01) between concentrations [expressed as  $\ln(C_t/C_0)$ , where  $C_t$ , SLES concentration at the sampling time and  $C_0$ , SLES concentration at day 0] versus time (**Figure 4B**).

The SLES concentration in the elutriates reflected that of the soil samples (**Table 2**). To the SLES initial concentrations in the spoil material of 136 and 132.3 mg/kg corresponded 6.0 and 5.2 mg/L of SLES in the elutriates produced from FA soil and FA + BC soil conditions, respectively.

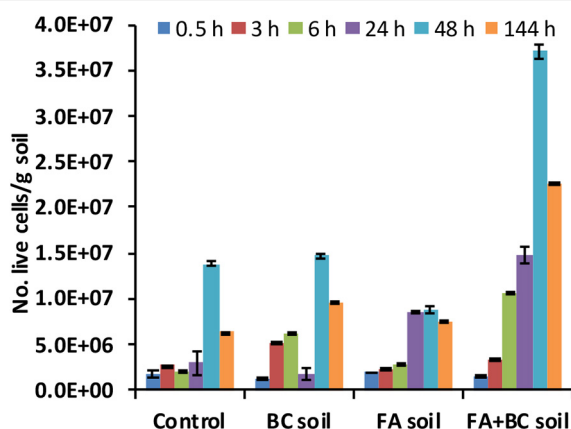


**FIGURE 3 |** Number of live cells (No. live cells/g soil) evaluated using direct fluorescence methods at different experimental times (0.5–144 h) in the various conditions. Control: untreated soil batches; BC soil: soil batches with only the bacterial consortium; FA soil: soil batches with only the foaming agent; FA + BC soil: soil batches with the foaming agent and the bacterial consortium. The vertical bars represent the standard errors.

In line with the SLES degradation observed in soil, the anionic surfactant also decreased over time in the corresponding water extract. In the bioaugmented soil, significantly lower SLES residues were detected; for example, at 24 h, a SLES concentration of 1 mg/L was found in FA + BC soil and at the same time of 5.4 mg/L in FA soil. At the end of the bioaugmentation experiment, no SLES residues were found in the FA + BC soil condition.

#### *Aliivibrio fischeri* Acute Toxicity Test

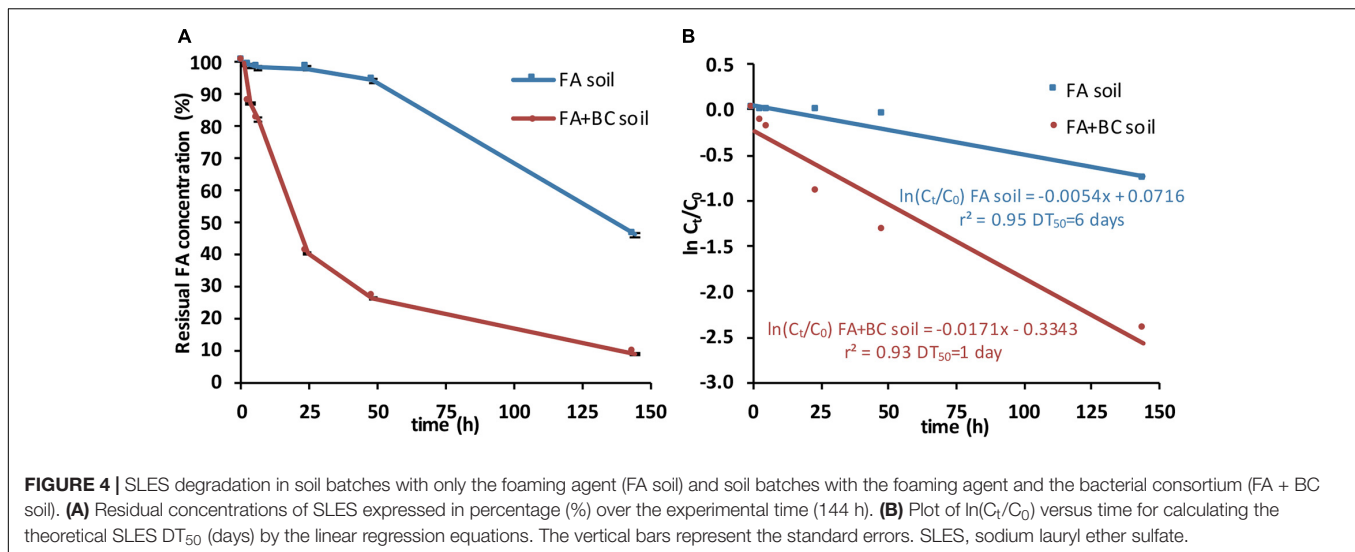
The *A. fischeri* test (**Figure 5**) was performed on water extracts (elutriates) of unconditioned (Control) and conditioned (FA soil and FA + BC soil) soils from the bioaugmentation experiment. The test was executed on samples collected at selected times (0.5, 24, 48, and 144 h).

In the Control condition (as expected), the bacterial bioluminescence was not inhibited. At the start (0.5 h) of the experiment, a toxic effect (bioluminescence inhibition >20%) was observed in elutriates of both FA and FA + BC soil; at the subsequent sampling, FA + BC soil elutriates did not show any toxicity for the *A. fischeri* bacterium. On the other hand, a toxic effect (bioluminescence inhibition >20%) was observed in FA soil until 48 h.

All validity criteria for the test were met, and all the data reported can therefore be considered valid.

## DISCUSSION

The aim of the present work was to test the capability of a previously isolated BC to enhance SLES degradation, in FA-conditioned soil collected from a tunnel construction site, in order to verify its possible use for routine bioaugmentation purposes. Bioaugmentation is a green technology used successfully for bioremediation of soil and water from several contaminants (e.g., petroleum hydrocarbons and pesticides) (Gentry et al., 2004; Abatenh et al., 2017; Arora, 2018). It consists in adding exogenous microbial populations or autochthonous ones (as in this work) with the catabolic potential to remove specific pollutants, such as pesticides



(Plangklang and Reungsang, 2011; Sun et al., 2020). One advantage of bioaugmentation is that the degradation process starts as soon as specific microbial degraders are introduced (Wu et al., 2019). The success of bioaugmentation depends on the ability of the inoculated microorganisms to continue their activity in the environment as long as necessary for contaminant removal. However, if the degradation times are relatively long (such as in the case of pesticides), competitive interactions with non-degrading microbial populations can occur, and specific environmental conditions can limit bioaugmentation efficiency during *in situ* remediation (Hibbing et al., 2010; Asok and Jisha, 2012; Stelting et al., 2014; Cavinato et al., 2017).

The fact that in our work the bacterial populations were isolated from the same soil and that SLES removal times were very low made this bioremediation strategy an example of a real nature-based solution.

Although there are several works (Cycoń et al., 2017; Nur Zaida and Piakong, 2018; Tondera et al., 2021) dealing with contaminant removal by bioaugmentation, most of them have been performed using culture media and/or in liquid media and at concentrations which do not reflect those found in real contamination scenarios (Silva et al., 2004). There are few works in which adding microbial strains to soil improved degradation of organic contaminants in field studies or directly in environmental

soil samples. Bioaugmentation can be applied using single microbial populations or a microbial consortium. For example, microbial consortia have been reported to degrade oils in polluted soil (Silva-Castro et al., 2012), in waste lubricating oil (Bhattacharya et al., 2015), in seawater (Dellagnezze et al., 2016), and in petroleum hydrocarbon in contaminated groundwater (Poi et al., 2018) and triazines in water and soil (Nasseri et al., 2014; Sagarkar et al., 2014). Triazine degradation has been performed in several bioaugmentation experiments with concentrations of these herbicides much higher than those commonly found in soil, such as in the study by Silva et al. (2004). However, in a recent work, Chen et al. (2021) showed the capability of a single bacterial population to degrade atrazine in a real contaminated soil (Chen et al., 2021).

**TABLE 2 |** SLES concentrations (mg/L) in elutriates obtained from the soil samples of the conditioned batches (FA soil and FA + BC soil) over the experimental time; SE = standard error.

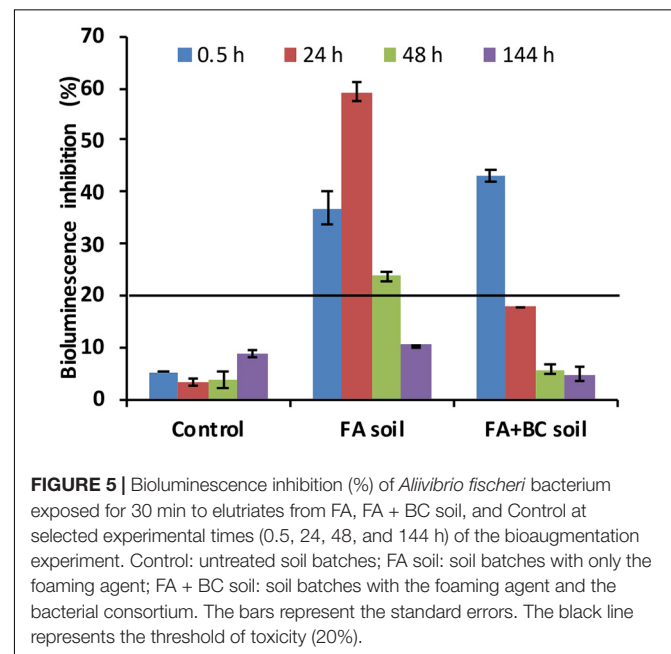
	SLES (mg/L) in elutriates			
	0.5 h	24 h	48 h	144 h
FA soil	6.0 ± 0.01	5.4 ± 0.01	2.2 ± 0.00	1.2 ± 0.00
FA + BC soil	5.2 ± 0.00	1.0 ± 0.01	0.2 ± 0.00	<LOD <sup>a</sup>

SLES, sodium lauryl ether sulfate;

FA, foaming agent;

BC, bacterial consortium.

<sup>a</sup>LOD, limit of detection.



Most works on anionic surfactants are aimed at evaluating biodegradation of sodium dodecyl sulfate, linear alkylbenzene sulfonate, and SLES in activated sludge (Hosseini et al., 2007), industrial wastewater (Karray et al., 2016; Fedeila et al., 2018), municipal wastewater (de Faria et al., 2019), and wastewater treatment plants (Paulo et al., 2017), because they are contaminants widely used in cosmetics, cleaning products, and personal care products (Barra Caracciolo et al., 2017; Hashim et al., 2018).

On the other hand, there have been no bioaugmentation experiments for remediating SLES, except for the work by Dhoubi et al. (2003). These authors found a bacterial population of Gamma-Proteobacteria (*Citrobacter braakii*) that was able to degrade high concentrations of SLES in an enrichment culture using wastewater samples from a cosmetic plant as the inoculum. This work supports our results and the role of Gamma-Proteobacteria class in removing this anionic surfactant. Interestingly, in our study, where the soil came from a real construction site and the surfactant concentrations (130 mg/kg) were those used for the excavation, the bioaugmentation of the spoil material with the BC significantly (sixfold) improved the natural degradation time of SLES. Moreover, from an applied perspective, using a microbial consortium rather than a pure culture is more advantageous because it provides the metabolic diversity and robustness needed for field applications (Tyagi et al., 2011).

Finally, the ecotoxicological results confirmed the depollution of the soil (SLES in elutriates did not exert any toxicological effect) and the high sensitivity of *A. fischeri* to SLES residues higher than 2 mg/L (before SLES degradation), in line with the findings of previous works (Mariani et al., 2020; Patrolecco et al., 2020). The use of this ecotoxicological test in supporting chemical analysis is very powerful because it is an effective tool that can evaluate an overall matrix toxicity including chemicals (e.g., possible metabolites and/or unknown elements present in soil) non-directly analyzed. Other studies used *A. fischeri* as an effective screening test for soil samples (Parvez et al., 2006; Abbas et al., 2018).

## CONCLUSION

Bioaugmentation with the BC identified at a construction site makes it possible to remove anionic surfactant residues

## REFERENCES

- Abatenh, E., Gizaw, B., Tsegaye, Z., and Wassie, M. (2017). *The Role of Microorganisms in Bioremediation-A Review*. Available online at: <https://www.peertechz.com> (accessed December 6, 2020).
- Abbas, M., Adil, M., Ehtisham-ul-Haque, S., Munir, B., Yameen, M., Ghaffar, A., et al. (2018). *Vibrio fischeri* bioluminescence inhibition assay for ecotoxicity assessment: a review. *Sci. Total Environ.* 626, 1295–1309. doi: 10.1016/j.scitotenv.2018.01.066
- Arora, N. K. (2018). Bioremediation: a green approach for restoration of polluted ecosystems. *Environ. Sustain.* 1, 305–307. doi: 10.1007/s42398-018-00036-y
- Asok, A. K., and Jisha, M. S. (2012). Biodegradation of the anionic surfactant linear alkylbenzene sulfonate (LAS) by autochthonous *Pseudomonas* sp. *Water Air Soil Pollut.* 223, 5039–5048. doi: 10.1007/s11270-012-1256-8

and clean up spoil material in a few hours, ensuring a safe by-product and saving execution time and overall costs for the tunneling industry. To our knowledge, this study is the first using a SLES-degrading BC for bioaugmentation purposes in a contaminated soil from a real environmental scenario. This remediation strategy is a promising low-cost and nature-based solution, for a prompt and safe reuse of the spoil material, avoiding its temporary storage and unnecessary waste production and transfer to landfills. This technique could be used, e.g., in the case of metro tunneling inside a city or through mountains along a sea coast, where the lack of space prevents temporary storage of the spoil material for its natural attenuation. The overall results show how a diversified approach involving chemical, microbiological, and ecotoxicological assessments of polluted soil can improve our understanding of the biodegradability of pollutants in bioremediation strategies. Further studies are in progress for finding the best practice (e.g., alginate microspheres) for seeding the BC on a large scale in construction sites.

## DATA AVAILABILITY STATEMENT

The original contributions presented in the study are included in the article/supplementary material, further inquiries can be directed to the corresponding author/s.

## AUTHOR CONTRIBUTIONS

LR, AB, PG, LM, JR, FS, GG, AV, and LP: methodology, formal analysis, and validation. LR and AB: writing, original draft preparation, and editing. AB, PG, and LP: supervision. AB: funding acquisition. All authors have read and agreed to the published version of the manuscript.

## FUNDING

This work was partially funded by Italferr Spa—Project N. 100032057.

- Barra Caracciolo, A., Ademollo, N., Cardoni, M., Di Giulio, A., Grenni, P., Pescatore, T., et al. (2019). Assessment of biodegradation of the anionic surfactant sodium lauryl ether sulphate used in two foaming agents for mechanized tunnelling excavation. *J. Hazard. Mater.* 365, 538–545. doi: 10.1016/j.jhazmat.2018.11.002
- Barra Caracciolo, A., Cardoni, M., Pescatore, T., and Patrolecco, L. (2017). Characteristics and environmental fate of the anionic surfactant sodium lauryl ether sulphate (SLES) used as the main component in foaming agents for mechanized tunnelling. *Environ. Pollut.* 226, 94–103. doi: 10.1016/j.envpol.2017.04.008
- Barra Caracciolo, A., Giuliano, G., Grenni, P., Cremisini, C., Ciccoli, R., and Ubaldi, C. (2005a). Effect of urea on degradation of terbutylazine in soil. *Environ. Toxicol. Chem.* 24, 1035–1040. doi: 10.1897/04-253R.1



- Barra Caracciolo, A., Grenni, P., Ciccoli, R., Di Landa, G., and Cremisini, C. (2005b). Simazine biodegradation in soil: Analysis of bacterial community structure by in situ hybridization. *Pest Manag. Sci.* 61, 863–869. doi: 10.1002/ps.1096
- Barra Caracciolo, A., Grenni, P., Mariani, L., Raueo, J., Di Lenola, M., Muzzini, V. G., et al. (2021). Mesocosm experiments at a tunnelling construction site for assessing re-use of spoil material as a by-product. *Water* 13:161. doi: 10.3390/w13020161
- Bellopede, R., and Marini, P. (2011). Aggregates from tunnel muck treatments. Properties and uses. *Physicochem. Probl. Miner. Process* 47, 259–266.
- Bhattacharya, M., Guchhait, S., Biswas, D., and Datta, S. (2015). Waste lubricating oil removal in a batch reactor by mixed bacterial consortium: a kinetic study. *Bioprocess Biosyst. Eng.* 38, 2095–2106. doi: 10.1007/s00449-015-1449-9
- Bornscheuer, U. T. (2002). Microbial carboxyl esterases: classification, properties and application in biocatalysis. *FEMS Microbiol. Rev.* 26, 73–81. doi: 10.1111/j.1574-6976.2002.tb00599.x
- Cavinato, C., Ugurlu, A., de Godos, I., Kendir, E., and Gonzalez-Fernandez, C. (2017). “7 - Biogas production from microalgae,” in *Woodhead Publishing Series in Energy*, eds C. Gonzalez-Fernandez and R. B. T.-M.-B. Muñoz (Sawston: Woodhead Publishing), 155–182. doi: 10.1016/B978-0-08-101023-5.00007-8
- Chen, S., Li, Y., Fan, Z., Liu, F., Liu, H., Wang, L., et al. (2021). Soil bacterial community dynamics following bioaugmentation with *Paenarthrobacter* sp. W11 in atrazine-contaminated soil. *Chemosphere* 282:130976. doi: 10.1016/j.chemosphere.2021.130976
- Cycon, M., Mroziak, A., and Piotrowska-Seget, Z. (2017). Bioaugmentation as a strategy for the remediation of pesticide-polluted soil: a review. *Chemosphere* 172, 52–71. doi: 10.1016/j.chemosphere.2016.12.129
- Dellagnenze, B. M., Vasconcellos, S. P., Angelim, A. L., Melo, V. M. M., Santisi, S., Cappello, S., et al. (2016). Bioaugmentation strategy employing a microbial consortium immobilized in chitosan beads for oil degradation in mesocosm scale. *Mar. Pollut. Bull.* 107, 107–117. doi: 10.1016/j.marpolbul.2016.04.011
- de Faria, C. V., \*Delforno, T. P., Okada, D. Y., and Varesche, M. B. A. (2019). Evaluation of anionic surfactant removal by anaerobic degradation of commercial laundry wastewater and domestic sewage. *Environ. Technol.* 40, 988–996. doi: 10.1080/09593330.2017.1414317
- Dhouib, A., Hamad, N., Hassairi, I., and Sayadi, S. (2003). Degradation of anionic surfactants by *Citrobacter braakii*. *Process Biochem.* 38, 1245–1250. doi: 10.1016/S0032-9592(02)00322-9
- Fedeila, M., Hachachi-Sadok, Z., Bautista, L. F., Simarro, R., and Nateche, F. (2018). Biodegradation of anionic surfactants by *Alcaligenes faecalis*, *Enterobacter cloacae* and *Serratia marcescens* strains isolated from industrial wastewater. *Ecotoxicol. Environ. Saf.* 163, 629–635. doi: 10.1016/j.ecoenv.2018.07.123
- Finizio, A., Patrolecco, L., Grenni, P., Galli, E., Muzzini, V. G., Raueo, J., et al. (2020). Environmental risk assessment of the anionic surfactant sodium lauryl ether sulphate in site-specific conditions arising from mechanized tunnelling. *J. Hazard. Mater.* 383:121116. doi: 10.1016/j.jhazmat.2019.121116
- Galli, E., Muzzini, V. G., Finizio, A., Fumagalli, P., Grenni, P., Barra Caracciolo, A., et al. (2019). Ecotoxicity of foaming agent conditioned soils tested on two terrestrial organisms. *Environ. Eng. Manag. J.* 18, 1703–1710. doi: 10.30638/eemj.2019.160
- Gentry, T. J., Rensing, C., and Pepper, I. L. (2004). New approaches for bioaugmentation as a remediation technology. *Crit. Rev. Environ. Sci. Technol.* 34, 447–494. doi: 10.1080/10643380490452362
- Grenni, P., Barra Caracciolo, A., Patrolecco, L., Ademollo, N., Raueo, J., Saccà, M. L., et al. (2018). A bioassay battery for the ecotoxicity assessment of soils conditioned with two different commercial foaming products. *Ecotoxicol. Environ. Saf.* 148, 1067–1077. doi: 10.1016/j.ecoenv.2017.11.071
- Grenni, P., Barra Caracciolo, A., Rodríguez-Cruz, M. S., and Sánchez-Martin, M. J. (2009). Changes in the microbial activity in a soil amended with oak and pine residues and treated with linuron herbicide. *Appl. Soil Ecol.* 41, 2–7. doi: 10.1016/j.apsoil.2008.07.006
- Hashim, N. H., Abu Bakar, A., Awang, Z., Arish, M., and Arshad, N. A. (2018). Anionic surfactants in environmental water samples: a review. *Sustain. Environ. Technol.* 1, 67–78.
- Hibbing, M. E., Fuqua, C., Parsek, M. R., and Peterson, S. B. (2010). Bacterial competition: surviving and thriving in the microbial jungle. *Nat. Rev. Microbiol.* 8, 15–25. doi: 10.1038/nrmicro2259
- Hosseini, F., Malekzadeh, F., Amirmozafari, N., and Ghaemi, N. (2007). Biodegradation of anionic surfactants by isolated bacteria from activated sludge. *Int. J. Environ. Sci. Technol.* 4, 127–132. doi: 10.1007/BF03325970
- Italian Decree (2017). D.P.R. 120/2017. Regulation on the Simplified Discipline of the Excavated Soil and Rock Management, Pursuant to Article 8 of the Decree-Law 12 September 2014, n. 133 (Decreto del Presidente della Repubblica 13 Giugno 2017, n. 120. Regolamento Recante la Disciplina Semplificata della Gestione delle terre e Rocce da Scavo, ai sensi Dell'articolo 8 del Decreto-legge 12 Settembre 2014, n. 133, Convertito, con Modificazioni, dalla legge 11 Novembre 2014, n. 164. In Italian). *Gazz. Uff. Repubb. Ital. Ser. Gen.* Vol. 183, 1–40. Available online at: <https://www.gazzettaufficiale.it/eli/gu/2017/08/07/183/sg/pdf>
- IUPAC (1999). *Harmonised Guidelines for the In-House Validation of Methods of Analysis, Technical Report*. Research Triangle Park, NC: IUPAC.
- Karray, F., Mezghani, M., Mhiri, N., Djelassi, B., and Sayadi, S. (2016). International Biodeterioration & Biodegradation Scale-down studies of membrane bioreactor degrading anionic surfactants wastewater: Isolation of new anionic-surfactant degrading bacteria. *Int. Biodeterior. Biodegradation* 114, 14–23. doi: 10.1016/j.ibiod.2016.05.020
- Mariani, L., Grenni, P., Donati, E., Raueo, J., Rolando, L., Barra Caracciolo, A., et al. (2020). Toxic response of the bacterium *Vibrio fischeri* to sodium lauryl ether sulphate residues in excavated soils. *Ecotoxicology* 29, 815–824. doi: 10.1007/s10646-020-02202-7
- Monod, J. (1949). The growth of bacterial cultures. *Annu. Rev. Microbiol.* 3, 371–394.
- Nasseri, S., Baghapour, M. A., Derakhshan, Z., and Faramarzi, M. (2014). Degradation of atrazine by microbial consortium in an anaerobic submerged biological filter. *J. Water Health* 12, 492–503. doi: 10.2166/wh.2014.162
- Nur Zaida, Z., and Piakong, M. T. (2018). “Bioaugmentation of petroleum hydrocarbon in contaminated soil: a review,” in *Microbial Action on Hydrocarbons*, eds V. Kumar, M. Kumar, and R. Prasad (Singapore: Springer Singapore), 415–439. doi: 10.1007/978-981-13-1840-5\_17
- Panda, T., and Gowrishankar, B. S. (2005). Production and applications of esterases. *Appl. Microbiol. Biotechnol.* 67, 160–169. doi: 10.1007/s00253-004-1840-y
- Parvez, S., Venkataraman, C., and Mukherji, S. (2006). A review on advantages of implementing luminescence inhibition test (*Vibrio fischeri*) for acute toxicity prediction of chemicals. *Environ. Int.* 32, 265–268. doi: 10.1016/j.envint.2005.08.022
- Patrolecco, L., Pescatore, T., Mariani, L., Rolando, L., Grenni, P., Finizio, A., et al. (2020). Environmental fate and effects of foaming agents containing sodium lauryl ether sulphate in soil debris from mechanized tunnelling. *Water* 12:2074. doi: 10.3390/w12082074
- Paulo, A. M. S., Aydin, R., Dimitrov, M. R., Vreeling, H., Cavaleiro, A. J., García-Encina, P. A., et al. (2017). Sodium lauryl ether sulfate (SLES) degradation by nitrate-reducing bacteria. *Appl. Microbiol. Biotechnol.* 101, 5163–5173. doi: 10.1007/s00253-017-8212-x
- Peila, D. (2014). Soil conditioning for EPB shield tunnelling. *KSCSE J. Civ. Eng.* 18, 831–836. doi: 10.1007/s12205-014-0023-3
- Peila, D., Picchio, A., Martinelli, D., and Negro, E. D. (2016). Laboratory tests on soil conditioning of clayey soil. *Acta Geotech.* 11, 1061–1074. doi: 10.1007/s11440-015-0406-8
- Persone, G., Marsalek, B., Blinova, I., Törökne, A., Zarina, D., Manusadzianas, L., et al. (2003). A practical and user-friendly toxicity classification system with microtests for natural waters and wastewaters. *Environ. Toxicol.* 18, 395–402. doi: 10.1002/tox.10141
- Pescatore, T., Patrolecco, L., Rolando, L., Spataro, F., Raueo, J., Grenni, P., et al. (2020). Co-presence of the anionic surfactant sodium lauryl ether sulphate and the pesticide chlorpyrifos and effects on a natural soil microbial community. *Environ. Sci. Pollut. Res.* 27, 30987–30997. doi: 10.1007/s11356-020-08840-y
- Plangklang, P., and Reungsang, A. (2011). Bioaugmentation of carbofuran residues in soil by *Burkholderia cepacia* PCL3: A small-scale field study. *Int. Biodeterior. Biodegradation* 65, 902–905. doi: 10.1016/j.ibiod.2011.02.011
- Poi, G., Shahsavari, E., Aburto-Medina, A., Mok, P. C., and Ball, A. S. (2018). Large scale treatment of total petroleum-hydrocarbon contaminated groundwater using bioaugmentation. *J. Environ. Manage.* 214, 157–163. doi: 10.1016/j.jenvman.2018.02.079
- Rahimzadeh, A., Tang, W., Sher, W., and Davis, P. (2018). “Management of excavated material in infrastructure construction-a critical review of literature,” in *International Conference on Architecture and Civil Engineering*, Sydney.

- Rolando, L., Grenni, P., Raueo, J., Pescatore, T., Patrolecco, L., Garbini, G. L., et al. (2020). Isolation and characterization in a soil conditioned with foaming agents of a bacterial consortium able to degrade sodium lauryl ether sulfate. *Front. Microbiol.* 11:1542. doi: 10.3389/fmicb.2020.01542
- Sagarkar, S., Nousiainen, A., Shaligram, S., Björklöf, K., Lindström, K., Jørgensen, K. S., et al. (2014). Soil mesocosm studies on atrazine bioremediation. *J. Environ. Manage.* 139, 208–216. doi: 10.1016/j.jenvman.2014.02.016
- Scheerer, S., Gomez, F., and Lloyd, D. (2006). Bioluminescence of *Vibrio fischeri* in continuous culture: optimal conditions for stability and intensity of photoemission. *J. Microbiol. Methods* 67, 321–329. doi: 10.1016/j.mimet.2006.04.010
- Silva, E., Fialho, A. M., Sá-Correia, I., Burns, R. G., and Shaw, L. J. (2004). Combined bioaugmentation and biostimulation to cleanup soil contaminated with high concentrations of atrazine. *Environ. Sci. Technol.* 38, 632–637. doi: 10.1021/es0300822
- Silva-Castro, G. A., Uad, I., González-López, J., Fandiño, C. G., Toledo, F. L., and Calvo, C. (2012). Application of selected microbial consortia combined with inorganic and oleophilic fertilizers to recuperate oil-polluted soil using land farming technology. *Clean Technol. Environ. Policy* 14, 719–726. doi: 10.1007/s10098-011-0439-0
- Stelting, S. A., Burns, R. G., Sunna, A., and Bunt, C. R. (2014). Survival in sterile soil and atrazine degradation of *Pseudomonas* sp. strain ADP immobilized on zeolite. *Bioremediat. J.* 18, 309–316. doi: 10.1080/10889868.2014.938723
- Sun, Y., Kumar, M., Wang, L., Gupta, J., and Tsang, D. C. W. (2020). “Biotechnology for soil decontamination: opportunity, challenges, and prospects for pesticide biodegradation,” in *Woodhead Publishing Series in Civil and Structural Engineering*, eds F. Pacheco-Torgal, V. Ivanov, and E.-E. C. Tsang (Sawston: Woodhead Publishing), 261–283. doi: 10.1016/B978-0-12-819481-2.00013-1
- Tondera, K., Chazarenc, F., Chagnon, P.-L., and Brisson, J. (2021). Bioaugmentation of treatment wetlands—a review. *Sci. Total Environ.* 775:145820. doi: 10.1016/j.scitotenv.2021.145820
- Tyagi, M., da Fonseca, M. M. R., and de Carvalho, C. C. C. R. (2011). Bioaugmentation and biostimulation strategies to improve the effectiveness of bioremediation processes. *Biodegradation* 22, 231–241. doi: 10.1007/s10532-010-9394-4
- UNI EN (2004). *UNI EN 12457-2:2004. Characterisation of Waste—Leaching-Compliance Test for Leaching of Granular Waste Materials and Sludges—Part 2: One Stage Batch Test at a Liquid to Solid Ratio of 10 l/kg for Materials with Particle Size Below 4 mm (Without or With Size Reduction)*. 30. Available online at: <http://store.uni.com/catalogo/index.php/uni-en-12457-2-2004.html>
- UNI EN (2019). *Water Quality—Determination of the Inhibitory Effect of Water Samples on the Light Emission of Vibrio fischeri (Luminescent Bacteria Test)—Part 3: Method Using Freeze-Dried Bacteria*. UNI EN ISO 11348-3:2019. Geneva: ISO.
- Wu, M., Wu, J., Zhang, X., and Ye, X. (2019). Effect of bioaugmentation and biostimulation on hydrocarbon degradation and microbial community composition in petroleum-contaminated loessal soil. *Chemosphere* 237:124456. doi: 10.1016/j.chemosphere.2019.124456

**Conflict of Interest:** The authors declare that the research was conducted in the absence of any commercial or financial relationships that could be construed as a potential conflict of interest.

**Publisher's Note:** All claims expressed in this article are solely those of the authors and do not necessarily represent those of their affiliated organizations, or those of the publisher, the editors and the reviewers. Any product that may be evaluated in this article, or claim that may be made by its manufacturer, is not guaranteed or endorsed by the publisher.

Copyright © 2021 Rolando, Barra Caracciolo, Grenni, Mariani, Raueo, Spataro, Garbini, Visca and Patrolecco. This is an open-access article distributed under the terms of the Creative Commons Attribution License (CC BY). The use, distribution or reproduction in other forums is permitted, provided the original author(s) and the copyright owner(s) are credited and that the original publication in this journal is cited, in accordance with accepted academic practice. No use, distribution or reproduction is permitted which does not comply with these terms.



# The Response of Extracellular Polymeric Substances Production by Phototrophic Biofilms to a Sequential Disturbance Strongly Depends on Environmental Conditions

Emilie Loustau<sup>1,2†</sup>, Joséphine Leflaive<sup>1\*†</sup>, Claire Boscus<sup>1</sup>, Quentin Amalric<sup>1</sup>, Jessica Ferriol<sup>1</sup>, Olga Oleinikova<sup>3</sup>, Oleg S. Pokrovsky<sup>3,4</sup>, Elisabeth Girbal-Neuhauser<sup>2</sup> and Jean-Luc Rols<sup>1</sup>

<sup>1</sup> Laboratoire Ecologie Fonctionnelle et Environnement, Université de Toulouse, CNRS, Toulouse INP, Université Toulouse 3 – Paul Sabatier (UPS), Toulouse, France, <sup>2</sup> LBAE, Université de Toulouse, Université Toulouse 3 – Paul Sabatier (UPS), Auch, France, <sup>3</sup> GET, Université de Toulouse, CNRS, IRD, Université Toulouse 3 – Paul Sabatier (UPS), Toulouse, France, <sup>4</sup> BIO-GEO-CLIM Laboratory, Tomsk State University, Tomsk, Russia

## OPEN ACCESS

### Edited by:

Carmen Palacios,  
Université de Perpignan Via Domitia,  
France

### Reviewed by:

Giulia Gionchetta,  
Swiss Federal Institute of Aquatic  
Science and Technology, Switzerland  
Ian Hawes,  
University of Waikato, New Zealand

### \*Correspondence:

Joséphine Leflaive  
josephine.leflaive@univ-tlse3.fr

†These authors share first authorship

### Specialty section:

This article was submitted to  
Microbiotechnology,  
a section of the journal  
Frontiers in Microbiology

**Received:** 15 July 2021

**Accepted:** 20 September 2021

**Published:** 11 October 2021

### Citation:

Loustau E, Leflaive J, Boscus C, Amalric Q, Ferriol J, Oleinikova O, Pokrovsky OS, Girbal-Neuhauser E and Rols J-L (2021) The Response of Extracellular Polymeric Substances Production by Phototrophic Biofilms to a Sequential Disturbance Strongly Depends on Environmental Conditions. *Front. Microbiol.* 12:742027. doi: 10.3389/fmicb.2021.742027

Phototrophic biofilms are exposed to multiple stressors that can affect them both directly and indirectly. By modifying either the composition of the community or the physiology of the microorganisms, press stressors may indirectly impact the ability of the biofilms to cope with disturbances. Extracellular polymeric substances (EPS) produced by the biofilm are known to play an important role in its resilience to various stresses. The aim of this study was to decipher to what extent slight modifications of environmental conditions could alter the resilience of phototrophic biofilm EPS to a realistic sequential disturbance (4-day copper exposure followed by a 14-day dry period). By using very simplified biofilms with a single algal strain, we focused solely on physiological effects. The biofilms, composed by the non-axenic strains of a green alga (*Uronema confervicolum*) or a diatom (*Nitzschia palea*) were grown in artificial channels in six different conditions of light intensity, temperature and phosphorous concentration. EPS quantity (total organic carbon) and quality (ratio protein/polysaccharide, PN/PS) were measured before and at the end of the disturbance, and after a 14-day rewetting period. The diatom biofilm accumulated more biomass at the highest temperature, with lower EPS content and lower PN/PS ratio while green alga biofilm accumulated more biomass at the highest light condition with lower EPS content and lower PN/PS ratio. Temperature, light intensity, and P concentration significantly modified the resistance and/or recovery of EPS quality and quantity, differently for the two biofilms. An increase in light intensity, which had effect neither on the diatom biofilm growth nor on EPS production before disturbance, increased the resistance of EPS quantity and the resilience of EPS quality. These results emphasize the importance of considering the modulation of community resilience ability by environmental conditions, which remains scarce in the literature.

**Keywords:** EPS production, phototrophic biofilm, resistance, recovery, photosynthetic efficiency

## INTRODUCTION

Understanding and predicting how communities respond and resist to disturbances in terms of composition or function are current concerns for microbial ecologists (Gonzalez et al., 2012). Ecological disturbance is defined as a causal event inducing a perturbation in a community (Rykiel, 1985). Many definitions have been proffered for the resilience of communities exposed to a disturbance. We consider here, following the recommendation by Hodgson et al. (2015), the resilience as the ability of a system to persist or maintain a function in the face of disturbance. The two measurable components of resilience are the resistance, that is the degree to which a community remains unchanged when it is subjected to a disturbance, and the recovery, that is the ability of a system to return to pre-disturbance levels (Hodgson et al., 2015; Oliver et al., 2015). Consequently, a resilient system is able to minimize the impact of the disturbance and has the ability to resume functioning under changing conditions. The resilience of microbial communities is crucial to preserve the ecological services they provide. With global change, the intensity and frequency of disturbances are likely to increase (IPCC, 2013), threatening the upholding of ecological services. By impacting the ability of microbial communities to resist to and recover after disturbances, small modifications of the environmental conditions may also represent an underestimated threat. The aim of this study was to assess in what extent the environmental conditions could influence the response of a microbial community to a complex disturbance.

Very simplified phototrophic biofilms were chosen as model of microbial community. In natural environment, biofilms are complex microbial communities composed of heterotrophic and phototrophic, eukaryotic and prokaryotic microorganisms embedded in a protective matrix of extracellular polymeric substances (EPS) (Lock, 1993). The functions fulfilled by phototrophic biofilms, such as photosynthesis, primary production, oxygen production, nutrients uptake, and contaminants removal are at the base of key ecological functions of fluvial ecosystems (Lawrence et al., 2001; Battin et al., 2003, 2016; Corcoll et al., 2012). Phototrophic biofilms are often exposed to chemical disturbances when freshwater ecosystems receive organic or inorganic pollutants (pesticides, organic solvents, heavy metals) through agriculture, domestic, and industrial uses (Segner et al., 2014). In addition to these multiple chemical stresses, the biofilms are also exposed to desiccation when the flow decreases. This stress is particularly severe in intermittent rivers which completely dry out part of the year (Datry et al., 2017). It is generally agreed that climate change will lead to more intense summer drought, higher temperatures, and more frequent episodes of intense rainfall (Acuna, 2010; Sabater et al., 2016). Hydrological and chemical stresses may affect aquatic systems either simultaneously or successively. For example, a decrease of flow before full desiccation can induce an increase in the concentration of riverine solutes (Gomez et al., 2017).

Light intensity, temperature, and nutrients are among the main environmental factors that affect the growth of phototrophic microbial communities (Lear et al., 2008;

Sabater et al., 2016; Bengtsson et al., 2018). Light is the principal energy source fueling biofilm primary production: a modification of light intensity affects biofilm growth, its physiology and the community composition (Sabater et al., 2002). Temperature increase can change algal diversity (Stevenson et al., 1996). Furthermore, temperature has a marked influence on chemical toxicity (Holmstrup et al., 2010). Lambert et al. (2016) and Pesce et al. (2018) showed that temperature can modulate phototrophic biofilm response to chronic Cu exposure: an increase in temperature reduced Cu effects on algal biomass, photosynthetic efficiency, and diatom composition. The availability and the concentration of nutrients also play an important role on changes in the structure of phototrophic biofilm communities with consequences on the sensitivity of biofilms to disturbances. For instance, as inorganic nutrient concentrations increase, the proportion of species tolerant to organic pollution increases whereas the abundance of sensitive species declines (Delgado et al., 2012). This is particularly true for phosphorus (P) which is a limiting nutrient in many aquatic ecosystems (Schindler, 1977; Schindler et al., 2008). Increasing P concentration led to a significant shift in the biofilm community composition; these changes being more pronounced in diatom- than in cyanobacteria-dominated biofilm (Leflaive et al., 2015).

One essential component of biofilms is the EPS matrix which provides a cohesion to the assemblage of organisms. EPS are produced by bacteria and microalgae through excretion, sorption, or cell lysis, and are mainly composed by polysaccharides and proteins with a certain amount of lipids, DNA and humic substances (Loustau et al., 2018). EPS create strong gradients within the biofilm by limiting access to nutrients, oxygen and light for the cells located far from the biofilm surface (Hill, 1996). Besides other functions (adhesion of microorganisms on immersed substratum, resource for the growth of heterotrophic microorganisms), the EPS matrix protects the cells from desiccation and other environmental stresses (pollutants, UV radiation, etc.), and adsorbs and accumulates organic pollutants or metal cations present in the water column (Flemming et al., 2016). EPS are certainly involved in the ability of phototrophic microorganisms to cope with disturbance and tolerate stresses, as it has been suggested for heavy metals, nanoparticles (Kroll et al., 2014), salinity (Shetty et al., 2019), or drought (Sasaki et al., 2020). Since EPS production is quantitatively and qualitatively affected by environmental conditions such as temperature and light intensity (Wolfstein and Stal, 2002; Di Pippo et al., 2012) or the presence of nanoparticles (Verneuil et al., 2015), our main hypothesis is that slight variations in environmental conditions in terms of light, temperature or nutrient concentration may impact the resilience of EPS quality and quantity to a disturbance. To test this hypothesis, we monitored the production and composition of EPS in response to a complex disturbance, in different environmental conditions of light, temperature, and nutrients. Biofilms composed by one phototrophic microorganism and the associated bacterial communities were produced in artificial streams. Such simplified biofilms were chosen in order to mainly focus on direct effects on algal physiology rather than on indirect effects through modifications of algal composition. The sequence



of disturbance was chosen to be representative of flow decrease and cessation in a river: an increase in pollutant concentration followed by desiccation. Copper, commonly found in small intermittent rivers in vineyard areas (Montuelle et al., 2010), was chosen here as a model of pollutant. Our hypotheses are that (i) the environmental conditions influence the resilience of the quality and quantity of EPS when the biofilms are exposed to a disturbance and (ii) the more an environmental parameter affects the biofilm growth, the more it affects the resilience of EPS.

## MATERIALS AND METHODS

### Pre-culture of Microorganisms

The diatom *Nitzschia palea* (Kützinger) W. Smith and the green alga *Uronema confervicolum* Lagerheim, isolated from phototrophic biofilms in the rivers Tarn and Garonne (Southwestern France), were used as the main phototrophic organisms for the two different biofilms. They were maintained in non-axenic conditions in the algae collection of the laboratory "Ecologie Fonctionnelle et Environnement" at 18°C under white light ( $30 \pm 5 \mu\text{mol photons s}^{-1} \text{m}^{-2}$ ) with light/dark periods of 16/8 h in Combo medium (Kilham et al., 1998). Individual pre-cultures were prepared for 21 days in 500-mL Erlenmeyer flasks and the biomass was homogenized using an Ultra-Turrax disperser (T25, Janke-Kunkel, 13,500 rpm, 1 min) before inoculation in the hydraulic mini-channels.

### Experimental Setup

Very simplified biofilms (one algal strain and the associated bacteria) were grown in several hydraulic mini-channels described in Loustau et al. (2019). Three modules were used, each one composed of two blocks corresponding to two separated closed circulating loops of Combo medium for the supply of four mini-channels in each block (Figure 1A). Only three mini-channels in each block were sampled for this study. Two successive experiments were performed, one for each type of biofilm cultivated on eighty supports (polyoxymethylene coupons, size 29 mm × 10 mm × 5 mm) transversally placed along each mini-channel. A flow velocity of  $0.4 \text{ m s}^{-1}$  allowing to create a homogeneous turbulent flow regime on the surface of coupons, and a circadian cycle of light/dark periods of 16/8 h were applied. A pH of  $8 \pm 0.1$  (pH meter Multi 3430 SET C) was observed during the light period. Biofilms were cultivated with a combination (Figure 1B) of two light intensities ( $70 \mu\text{mol photons s}^{-1} \text{m}^{-2}$ , *L* - high light intensity or  $30 \mu\text{mol photons s}^{-1} \text{m}^{-2}$ , *l* - low light intensity) measured with a flat quantum sensor (model LI-189, LI-COR, Inc., Lincoln, Nebraska) and two temperatures of the circulating water ( $22^\circ\text{C}$ , *T* - high temperature or  $19^\circ\text{C}$ , *t* - low temperature). Two additional conditions at high temperature and high light intensity were obtained by modifying initial P concentration compared to the initial P concentration of the culture medium ( $5.23 \text{ mg L}^{-1}$ , *P100* - 100%): a higher concentration of  $8.71 \text{ mg L}^{-1}$  (*P165* - increase of 165%) and a lower concentration of  $2.61 \text{ mg L}^{-1}$  (*P50* - decrease of 50%). For each condition, a block was inoculated

(Figure 1C). The six culture conditions were then: LTP100, LtP100, lTP100, LtP50, and lTP165.

After 14 days of biofilm growth, the physiological state of biofilm was assessed with maximum quantum yield measurements directly inside the mini-channels, and some coupons were randomly sampled for the determination of biomass and EPS (amount and composition).

After the sampling at day 14, copper ( $\text{CuSO}_4$ ) was added in the circulating nutrient medium to reach an increase of the initial Cu concentration by  $50 \mu\text{g L}^{-1}$ . Due to Cu presence in Combo culture medium ( $0.3 \mu\text{g L}^{-1}$ ), the initial Cu concentration corresponded to  $50.3 \mu\text{g L}^{-1}$ . Dissolved  $\text{Cu}^{2+}(\text{aq})$  speciation in the presence of cell exometabolites and organic ligands of the nutrient medium was assessed by using the Visual MINTEQ computer code (Gustafsson, 2011, version 3.1 for Windows, October 2014) in conjunction with a database and the NICA-Donnan humic ion binding model. Thermodynamic calculation demonstrated that  $\text{Cu}^{2+}(\text{aq})$  speciation was dominated by EDTA complexes in the form of Cu-anions, with negligible role of other organic complexes from nutrient media constituents.

At day 18, the mini-channels were quickly dried-out by removing the water in each block. The biofilms were then kept at room temperature ( $17^\circ\text{C}$ ). After 14 days of dry period (day 32), the mini-channels were re-filled with fresh culture medium with corresponding initial P concentration (*P50*, *P100*, or *P165*) for another 14-day rewetting period (until day 46).

Before the disturbance event (day 14), ten coupons were randomly selected and collected per mini-channel for the biomass characterization and fifteen for the EPS extraction, to obtain three replicates from three mini-channels per block. Biofilms were scraped from these coupons with a sterile toothbrush and suspended in 15 mL (biomass) or in 100 mL (EPS) of culture medium before analysis. At the end of the disturbance sequence (day 32), and after the rewetting period (day 46), fifteen coupons were sampled in each of the three mini-channel and biofilm was suspended in 100 mL of culture medium for EPS extraction, to obtain three replicates per block.

### Biofilm Biomass

A subsample of the biofilm suspension obtained as described above was used to assess biofilm biomass by measuring the dry weight (DW) after 72 h of drying at  $70^\circ\text{C}$  in a pre-weighed aluminum dish.

### Maximum Quantum Yield

The physiological state of phototrophic microorganisms was estimated by the maximal quantum yield of the photosystem II (PSII) (yield,  $\Phi$  PSII), corresponding to the number of open reaction centers (Rohacek and Bartak, 1999). In stressed organisms, the yield strongly decreases (Rohacek and Bartak, 1999). Though it is primarily linked to the PSII, the yield may reflect the physiological state of the organism (Parkhill et al., 2001; Laviale, 2008). The photosynthetic efficiency is specific to each algal group, precluding the comparison between the values of the different species used here. Non-invasive PhytoPAM measurements (Phytoplankton Analyzer, Heinz Walz GMBH, Effeltrich, Germany) were performed on the surface of the

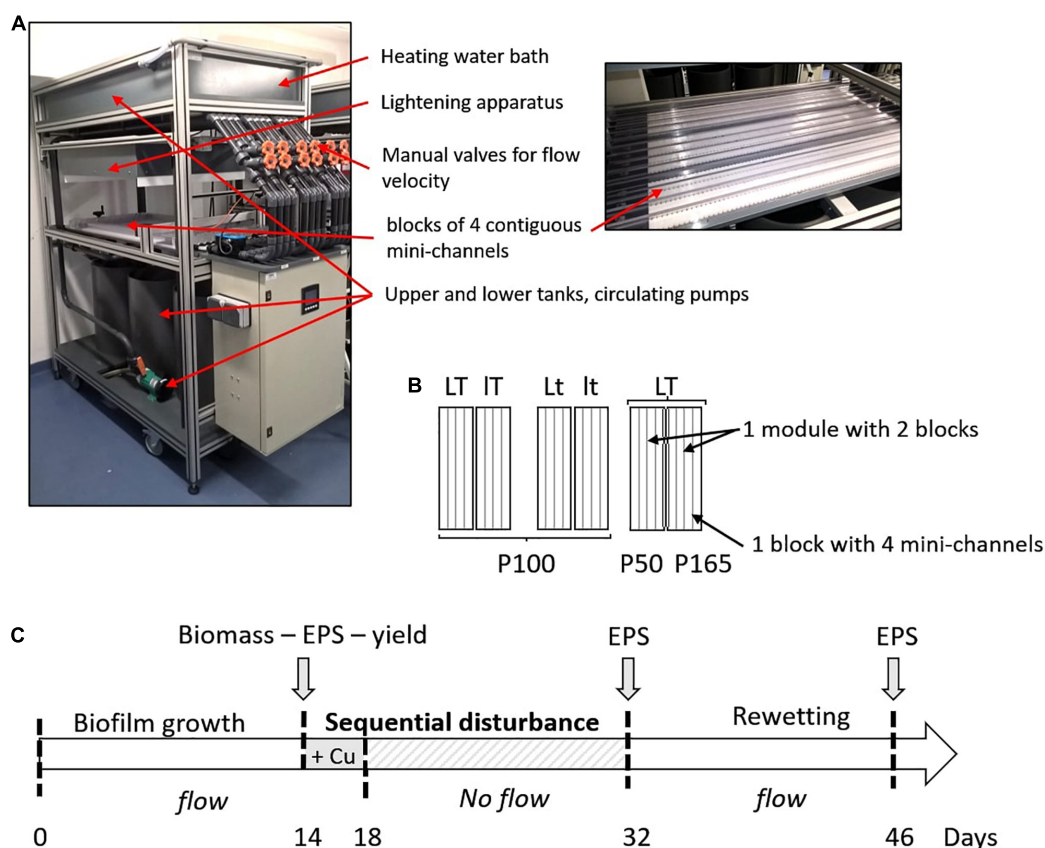


**FIGURE 1 | (A)** Photographs of one module with a detail view of the mini-channels. **(B)** Experimental design applied for the two biofilms. The experimental conditions were the same in the four mini-channels of one block. Six different conditions were tested with two levels of temperature ( $T = 22^{\circ}\text{C}$  or  $t = 19^{\circ}\text{C}$ ), light intensity ( $L = 70 \mu\text{mol s}^{-1} \text{m}^{-2}$  or  $I = 30 \mu\text{mol s}^{-1} \text{m}^{-2}$ ) and P concentration (P100 corresponds to the initial P concentration of  $5.23 \text{ mg L}^{-1}$  in the culture medium, P50 with a decrease of 50% and P165 with an increase of 165%). **(C)** Experimental setup with the step of inoculation of the mini-channels at day 0, the addition in the culture medium of Cu for a final concentration of  $50.3 \mu\text{g L}^{-1}$  at day 14, followed by a 14-day dry period, and finally a 14-day rewetting.

biofilm by measuring fluorescence response to a saturating light flash after 20 min of dark adaptation [dark-adapted state (DAS) conditions] (Baker, 2008):

$$\Phi_{\text{PSII}}(\text{DASconditions}) = 1 - (F_0/F_M); 0 < \Phi_{\text{PSII}} < 1 \quad (1)$$

$F_M$  represents the maximal fluorescence and  $F_0$  corresponds to the minimal fluorescence of the photosystem II. For each condition (in one block), thirty-two measurements were performed at day 14 (eight for each mini-channel).

## Extracellular Polymeric Substances

### Extracellular Polymeric Substances Extraction

The biofilm suspension was homogenized with an Ultra-Turrax disperser at 13,500 rpm for 1 min at room temperature. Then, a volume of the homogenized suspension corresponding to 10 mg DW was centrifuged at 4,000 g for 15 min. The pellet was washed with Phosphate Buffer Saline (PBS) solution and centrifuged again. Finally, two EPS extraction steps, following the sequential method previously developed by Loustau et al. (2018), were applied in sequence with intermediate centrifugations

(4,000 g for 15 min) to collect the supernatants containing the solubilized EPS. The first extraction step was performed with 0.22% formamide in PBS solution (stirring at 150 rpm and  $4^{\circ}\text{C}$  for 60 min) and the second one with cation exchange resin (CER, Dowex Marathon) at  $50 \text{ g g}^{-1}$  DW of biomass in PBS solution (stirring at 150 rpm and  $4^{\circ}\text{C}$  for 90 min).

The cellular integrity during the extraction steps was controlled by the measurement of chlorophyll *a* released in the supernatants, giving a cell lysis level less than 3.5% for all samples.

The total amount of EPS extracted was the sum of the EPS amounts contained in both supernatants (formamide + CER). After acidification of EPS extract with hydrochloric acid and volatilization of inorganic carbon by catalytic oxidation at  $720^{\circ}\text{C}$ , the Total Organic Carbon (TOC) was analyzed (Shimadzu TOC-L analyzer).

## Proteins and Polysaccharides Quantification

For each EPS extract, the amounts of proteins and polysaccharides were measured in analytical triplicates. Protein (PN) concentration was measured by the bicinchoninic acid (BCA) method (Smith et al., 1985). Twenty-five  $\mu\text{L}$  of EPS extract

**TABLE 1** | *P*-values for two-way and one-way ANOVAS to test the effect of environmental conditions on the biomass (DW), maximum quantum yield ( $\Phi$ PSII), EPS quantity (TOC), and EPS quality (PN/PS) of the biofilms before the disturbance.

		Temperature	Light intensity	Temp * Light	P concentration
<i>N. palea</i> biofilm	Biomass	<b>0.0256</b>	0.5431	0.6095	0.0854
	$\Phi$ PSII	<b>0.000001</b>	<b>0.0008</b>	<b>0.0461</b>	<b>0.0042</b>
	TOC	<b>0.0006</b>	0.8876	0.5189	<b>0.0004</b>
	PN/PS	0.0569	0.0777	0.0564	<b>0.0481</b>
<i>U. confervicolum</i> biofilm	Biomass	<b>0.0011</b>	<b>0.000002</b>	0.4683	<b>0.0010</b>
	$\Phi$ PSII	0.0549	0.1909	0.1909	<b>0.0496</b>
	TOC	0.1989	<b>0.0062</b>	0.0991	0.0509
	PN/PS	<b>0.0011</b>	<b>0.000002</b>	0.4683	<b>0.0047</b>

Significant *p*-values are in bold, *n* = 3.

and 200  $\mu$ L of BCA reagent (Sigma-Aldrich) were incubated in a 96-well microplate (15 min at 60°C) before measuring the optical density at 540 nm (microplate reader, Synergy Mx Biotek). Bovine serum albumin (BSA) with concentrations ranging from 0 to 800 mg L<sup>-1</sup> was used as a standard. Polysaccharide (PS) concentration was measured by the anthrone method (Dreywood, 1946). One hundred  $\mu$ L of EPS extract and 200  $\mu$ L of anthrone reagent (2% anthrone in 96% sulfuric acid) were incubated in a 96-well microplate (30 min at 60°C), cooled at room temperature for 10 min before measuring the optical density at 620 nm. Glucose with concentrations ranging from 0 to 100 mg L<sup>-1</sup> was used as a standard.

## Statistical Analyses

The pre-disturbance state was used as a reference to assess the impact of the disturbance sequence and the recovery after rewetting on EPS production (quantity and quality). The measurements realized at day 32 (D32, end of disturbance) and day 46 (D46, end of re-wetting period) were normalized by the measures realized at day 14 (D14, before disturbance), by the following expressions:

$$\text{Impact}(\%) = 100 - (100 \times V_{D32}/V_{D14}) \quad (2)$$

$$\text{Recovery}(\%) = 100 \times V_{D46}/V_{D14} \quad (3)$$

where  $V_{D14}$  represents the mean value of the parameter for the measurements performed from one block (including three mini-channels sampled) at day 14, and  $V_{D32}$  and  $V_{D46}$  represent the mean value of the same parameter for the measures performed from one mini-channel of the same block at day 32 and day 46, respectively.

Statistical analyses were performed using Statistica software (version 8). For all analyses, the normality and homoscedasticity were checked on each dataset (biofilm biomass, photosynthetic efficiency, EPS amount) with the Shapiro-Wilk test and data were transformed if needed. Two-way ANOVAs and one-way ANOVAs were used to test the effects of environmental factors (temperature and light intensity or P concentration) (i) on biofilm biomass, photosynthetic efficiency and EPS amount and composition before the disturbance or (ii) on the impact and recovery of EPS amount and composition after the disturbance

and the rewetting periods, respectively, followed by a Tukey *post hoc* test. The magnitude of the difference between pre- and post-disturbance (end of disturbance or end of rewetting period) was assessed using Hedges'g (Hedges, 1981) effect size calculated from *t*-statistics derived from student tests (Berben et al., 2012) using the R package {esc}. The magnitude of the effects of temperature, light and phosphorous concentration was measured using the partial eta-squared effect size calculated from 2-way and one-way ANOVAs with the R package {effectsize}. Data given in the text are means  $\pm$  standard error (SE). For all statistical analyses, significance was inferred at *p* < 0.05.

## RESULTS

### Combined Effects of Light Intensity, Temperature, and Phosphorus on Biofilm Physiology and Extracellular Polymeric Substances Production Before the Sequential Disturbance

The effects of light intensity, temperature, and P concentration were considered during the first 14-day period on biofilm (growth and maximum quantum yield) and EPS production (quantity as extracted TOC and quality as PN/PS ratio) (Table 1). The two biofilms showed very contrasted responses to the environmental conditions, with a higher influence of temperature on the diatom biofilm and a higher influence of light intensity and phosphorus concentration on the green alga biofilm.

The biomass production varied from  $0.21 \pm 0.03$  to  $0.51 \pm 0.06$  mg DW cm<sup>-2</sup> for *N. palea* biofilm, with a 2.4 ratio between the lowest and the highest mean values (Figure 2). The diatom growth and  $\Phi$  PSII were positively affected by the temperature. Those parameters were less impacted by the light intensity. The modification of phosphorus concentration tended to decrease both growth and  $\Phi$  PSII (Figure 2). The response of EPS production (TOC) to the environmental conditions was opposite to that of the biomass. The range of variation was narrower than for the biomass, with a 1.4 ratio between the lowest and the highest mean values. The ratio PN/PS was only significantly affected by P concentration, with the lowest value obtained at the lowest P concentration.

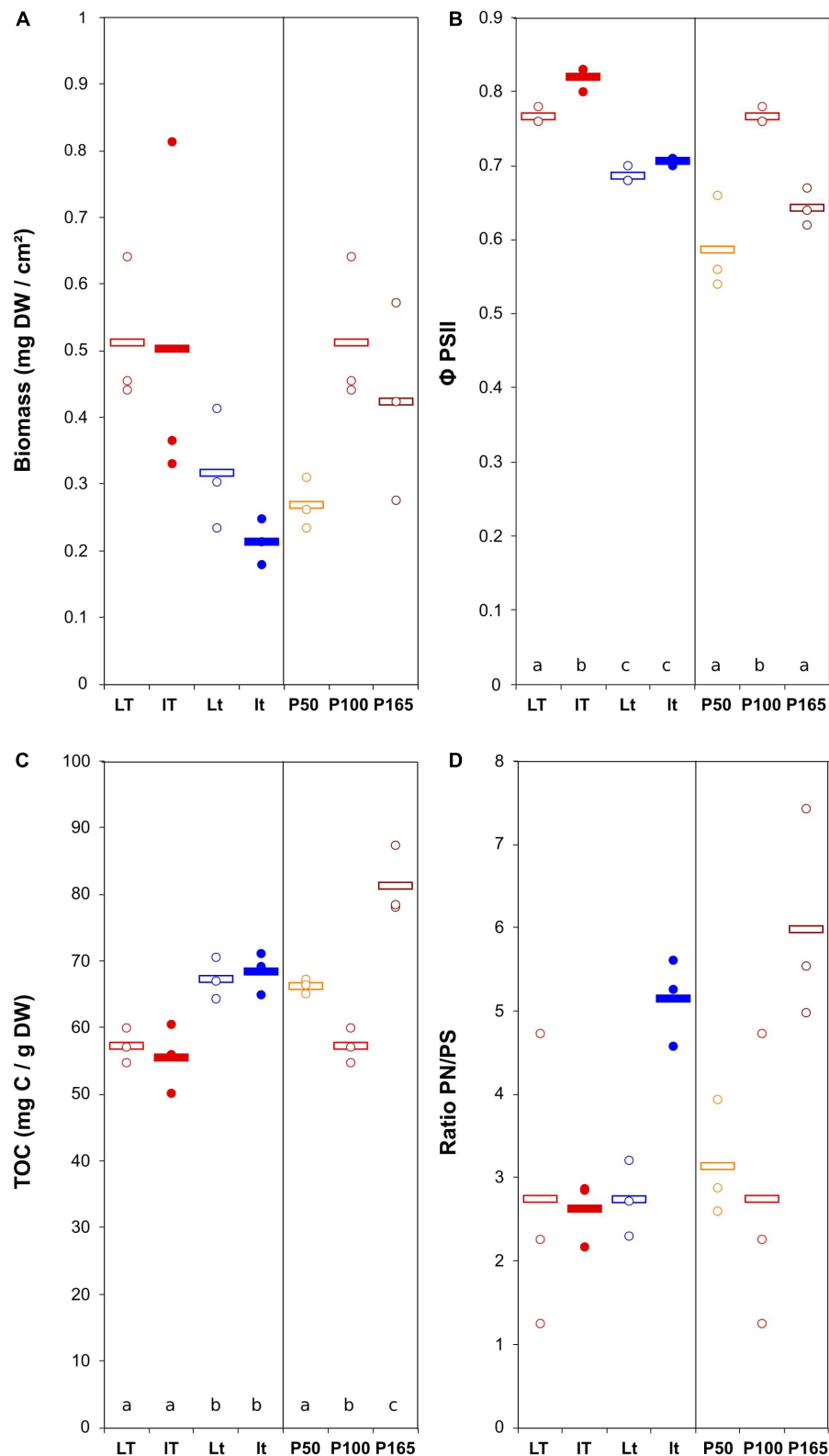


**FIGURE 2 |** Scatter plot of the biomass ( $DW$  = dry weight) (**A**), maximum quantum yield (**B**), total organic carbon (quantity of EPS) (**C**), and ratio protein/polysaccharide in the EPS (**D**) in *N. palea* biofilm before the disturbance. The letters indicate statistically homogeneous groups (Tukey *post hoc* test after ANOVA). No letters for non-significant ANOVA (the bars represent the means,  $n = 3$ ). L/l: high/low light intensity (P100), T/t: high/low temperature (P100), P50, P100, P165: 50, 100, and 165% of the standard initial phosphorous concentration, respectively, associated with L and T conditions.



The biomass production was more variable for the *U. confervicolum* biofilm, with mean values from  $0.50 \pm 0.06$  to  $2.29 \pm 0.17$  mg DW cm<sup>-2</sup> (4.6 highest/lowest ratio) (Figure 3). It was positively influenced by light intensity and negatively affected by the temperature (Table 1). The biofilm growth was also negatively impacted by P concentration. The  $\Phi$  PSII was only slightly modified by the environmental conditions. The same tendency was observed for the EPS production, with an additional negative effect of high light intensity. The PN/PS ratio in the green alga biofilm was very variable, with a 4.1 ratio between the highest and the lowest mean values. It was increased with a decrease of light intensity and temperature, and by a modification in P concentration compared to the reference condition.

To summarize these results, the increase in temperature yielded higher accumulation of diatom biofilm biomass and decreased EPS content and PN/PS ratio, while green alga biofilm accumulated more biomass at the highest light condition and exhibited lower EPS content and PN/PS ratio.

For the two biofilms, there was a significant negative correlation between biomass and EPS production ( $r = -0.49$ ,  $p = 0.025$  and  $r = -0.73$ ,  $p < 0.001$  for the diatom and green alga biofilms, respectively) (Supplementary Figure 1). For the diatom biofilm, EPS production was also negatively correlated with the maximum quantum yield ( $r = -0.70$ ,  $p < 0.001$ ). For the green alga biofilms, a positive correlation was observed ( $r = 0.63$ ,  $p = 0.002$ ), but it was driven by one treatment only. Without these points the correlation was similar to the one of the diatom biofilms ( $r = -0.47$ ,  $p = 0.05$ ).

## Impact of the Disturbance and Recovery of Extracellular Polymeric Substances Quantity and Quality

The response of the biofilms to the disturbance, in terms of EPS quantity and quality, was analyzed in two steps. First, we compared pre- and post-disturbance values to show potential resistance and recovery for each environmental condition (Figures 4, 5). The post-disturbance values were either measured at the end of the disturbance (indication of resistance) or at the end of the rewetting period (indication of recovery). Second, we assessed the effects of light, temperature and P concentration on the resistance and resilience with ANOVA and derived effect size (Figure 6 and Table 2).

The sequential disturbance had a strong impact on EPS quantity (Figure 4 and Supplementary Figures 1, 2). For the *N. palea* biofilm, it induced a decrease in EPS quantity, with the exception of the LtP100 condition (increase) and LtP100 and LTP50 conditions (no effect). For the *U. confervicolum* biofilm, the decrease in EPS quantity was observed in all conditions except the LTP50. For both biofilms, the increase in temperature increased the negative impact of the disturbance. For the *N. palea* biofilm, at the end of the rewetting period, the EPS quantity values were either identical or higher than the pre-disturbance values, while in the *U. confervicolum* biofilm they remained lower in all but one condition. For both algae, EPS quantity was less

affected by the disturbance at low phosphorus concentration than at medium and high concentrations.

The quality of EPS was very sensitive to the combined disturbance in *N. palea* biofilm but only marginally affected in *U. confervicolum* biofilm (Figure 5 and Supplementary Figures 2, 3). The disturbance induced a decrease in the PN/PS ratio in the diatom biofilm in all conditions except the LTP100 one, where no effect was observed. Contrary to the EPS quantity, no recovery was observed at the end of the rewetting period for the EPS quality.

Combined effects of temperature, light, and phosphorous concentration on the resistance and recovery were assessed with ANOVAs (Table 2) and eta-squared effect sizes (Figure 6). For the impact of disturbance on EPS quantity (Figure 6A), all the environmental factors had a significant effect for the *N. palea* biofilm. When temperature, light intensity, and P concentration increased, the impact of the disturbance increased as well. In contrast, the environmental factors had no effect on the impact of disturbance on EPS quality (Figure 6B). For *U. confervicolum* biofilm, only the phosphorous concentration modified the impact of the disturbance on both EPS quantity and quality, with opposite directions: for the quantity the impact was lower at the lowest concentration, while for EPS quantity, the impact was lower at the highest concentration.

The recovery of EPS after the rewetting period was not influenced by the same factors than the resistance to the disturbance. For the *N. palea* biofilm, P concentration modified the recovery of both EPS quantity and quality, with the lowest resilience observed for the highest concentration. The recovery of EPS quality also increased with an increase in temperature and light intensity.

## DISCUSSION

EPS are critical for the resilience of biofilms exposed to various stresses (Kroll et al., 2014; Flemming et al., 2016; Shetty et al., 2019). It is thus important that their production remains stable despite the disturbance biofilms may be exposed to. EPS production by biofilms is known to be influenced by environmental conditions (Wolfstein and Stal, 2002; Di Pippo et al., 2012). The question tackled here is in what extent variations in the environmental conditions could affect the resilience properties of EPS when biofilms are disturbed. A follow-up study would be to assess if modifications in biofilm EPS resilience can impact the functional resilience of biofilms. Our first hypothesis was confirmed, the results showing a strong influence of light, temperature, or phosphorous on the resilience of EPS quantity and quality. Contrary to our second hypothesis, the factors that influenced the most biofilm growth were not necessarily the factors influencing the EPS resilience. Moreover, factors that had no effects on biofilm growth or EPS production strongly influenced EPS resistance and recovery (e.g., light intensity for the *N. palea* biofilm).

Given that diatoms and green algae are well-known to produce high amount of EPS (de Brouwer et al., 2002; Xiao and Zheng, 2016; Bohorquez et al., 2017) and that the

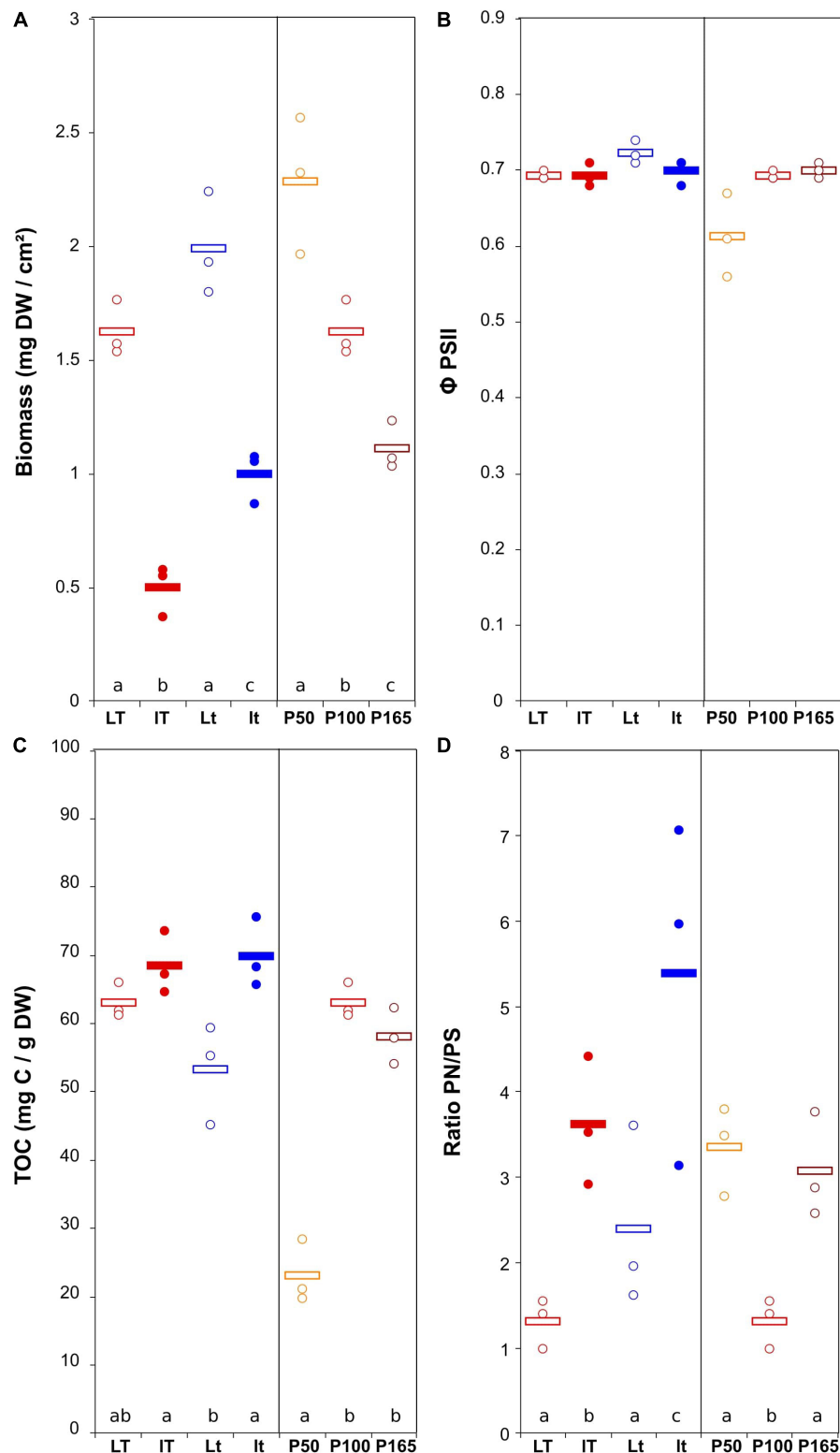
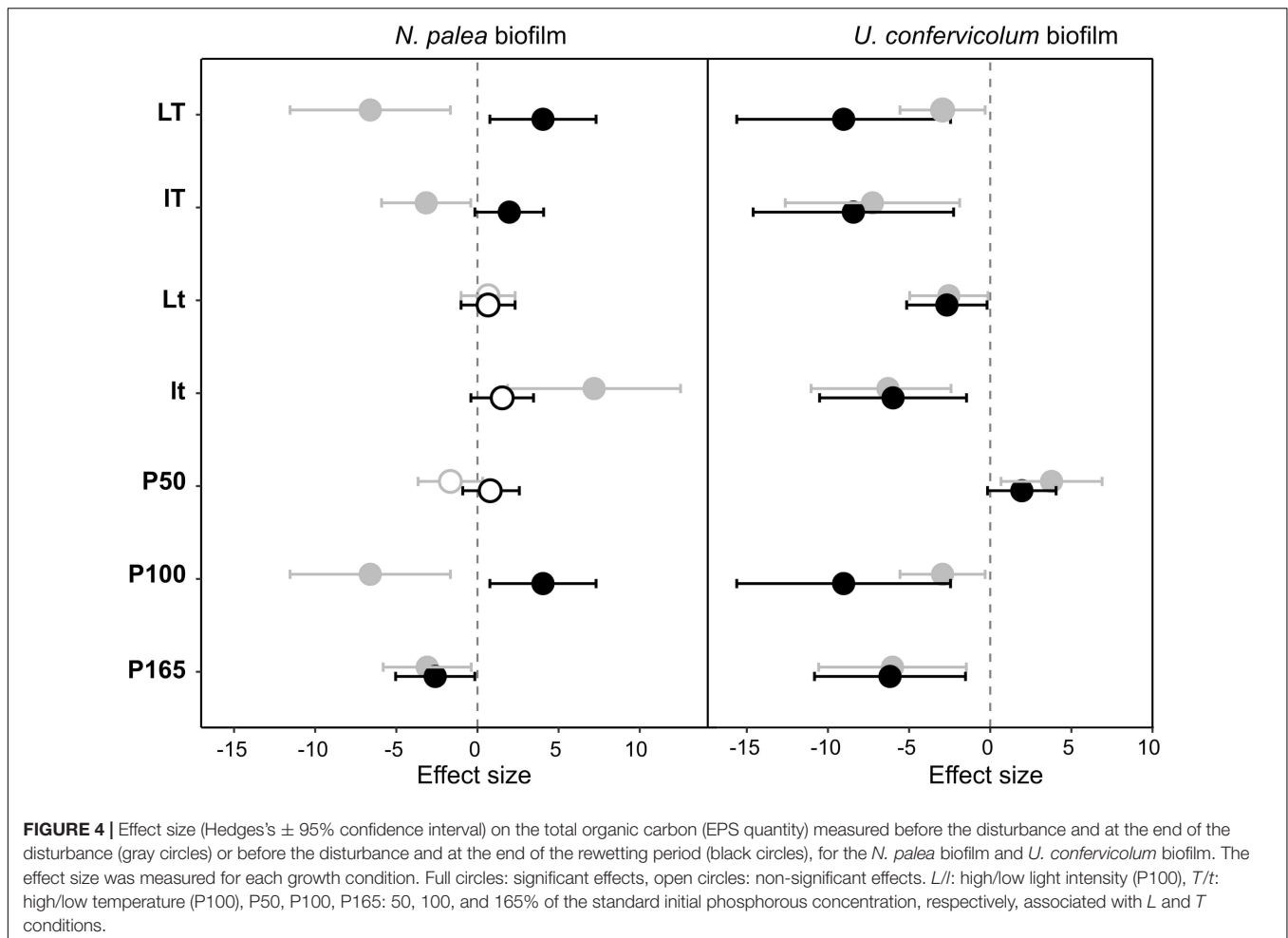


**FIGURE 3 |** Scatter plot of the biomass ( $DW$  = dry weight) (**A**), maximum quantum yield (**B**), total organic carbon (quantity of EPS) (**C**), and ratio protein/polysaccharide in the EPS (**D**) in *U. confervicolum* biofilm before the disturbance. The letters indicate statistically homogeneous groups (Tukey post hoc test after ANOVA). No letters for non-significant ANOVA (the bars represent the means,  $n = 3$ ). L/l: high/low light intensity (P100), T/t: high/low temperature (P100), P50, P100, P165: 50, 100, and 165% of the standard initial phosphorous concentration, respectively, associated with L and T conditions.



biomass of the algal cells accounted for the majority of biofilm biomass (microscopic observations), we assumed that the EPS found in the biofilms were mainly produced by algal cells. However, the analyses that were performed did not allow the distinction between algal and bacterial EPS.

### The Effects of Light Intensity, Temperature, and P Concentration on Biofilm Physiology and Extracellular Polymeric Substances Production

Despite the moderate amplitudes in the variations of the environmental conditions, strong impacts on biofilm and physiology have been observed. Although the study considered only two different simplified biofilms, it demonstrated very different patterns in the response to environmental conditions: the diatoms were more sensitive to the temperature, and the green algae were more sensitive to the light intensity. Such contrasting patterns are consistent with the conclusion of Falk et al. (1996) who stated that it is not possible to describe a general mechanism for photosynthetic adjustment to temperature that encompasses all phototrophic species because of genetic diversity and differential strategies in growth and development.

Unlike Di Pippo et al. (2012) conclusion, 30  $\mu\text{mol photons s}^{-1} \text{m}^{-2}$  in the present study provided sufficient light intensity for the development of the phototrophic biofilms. Light intensity, from 30 to 70  $\mu\text{mol photons s}^{-1} \text{m}^{-2}$ , induced no significant effect for *N. palea* biofilm growth. For the green alga biofilm, and in agreement with Ylla et al. (2009), light intensity was the limiting parameter which control the growth. *U. confervicolum* is a filamentous species and forms a thick biofilm with streamers in the water at the biofilm surface that can create a self-shading effect and the light intensity can therefore quickly become a limiting factor during biofilm development (Rao, 2010; Villanueva et al., 2011). On the contrary, the pennate diatom forms a thin biofilm and the light can be accessed by most cells. These differences in algal morphology, associated with the higher biomass reached in *U. confervicolum* biofilms, may explain the differential response to light intensity increase.

Phosphorus which is often directly involved in eutrophication processes (Smith et al., 1999), had an effect on the two phototrophic biofilms with an increase in P concentration inducing a decrease of the green alga biofilm growth and an increase in the diatom biofilm growth. These results suggest that the composition of natural phototrophic biofilms should strongly depend on the P concentration in the surface water. The

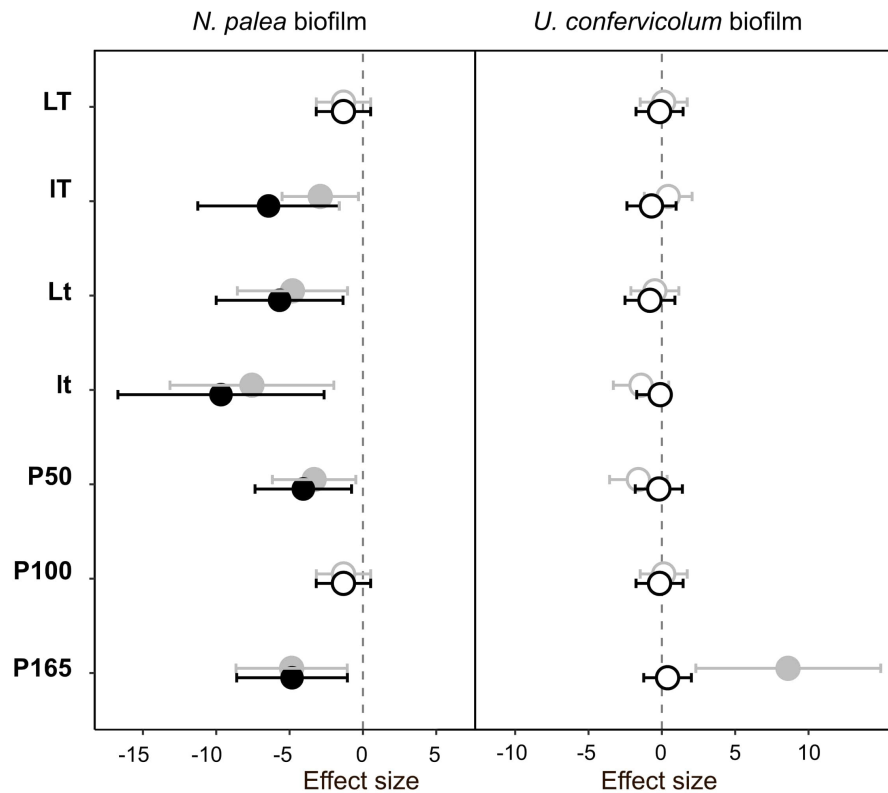


**FIGURE 5 |** Effect size (Hedges's  $\pm$  95% confidence interval) on the protein/polysaccharide ratio (EPS quality) measured before the disturbance and at the end of the disturbance (gray circles) or before the disturbance and at the end of the rewetting period (black circles), for the *N. palea* biofilm and *U. confervicolum* biofilm. The effect size was measured for each growth condition. Full circles: significant effects, open circles: non-significant effects. *L/l*: high/low light intensity (P100), *T/t*: high/low temperature (P100), P50, P100, P165: 50, 100, and 165% of the standard initial phosphorous concentration, respectively, associated with *L* and *T* conditions.

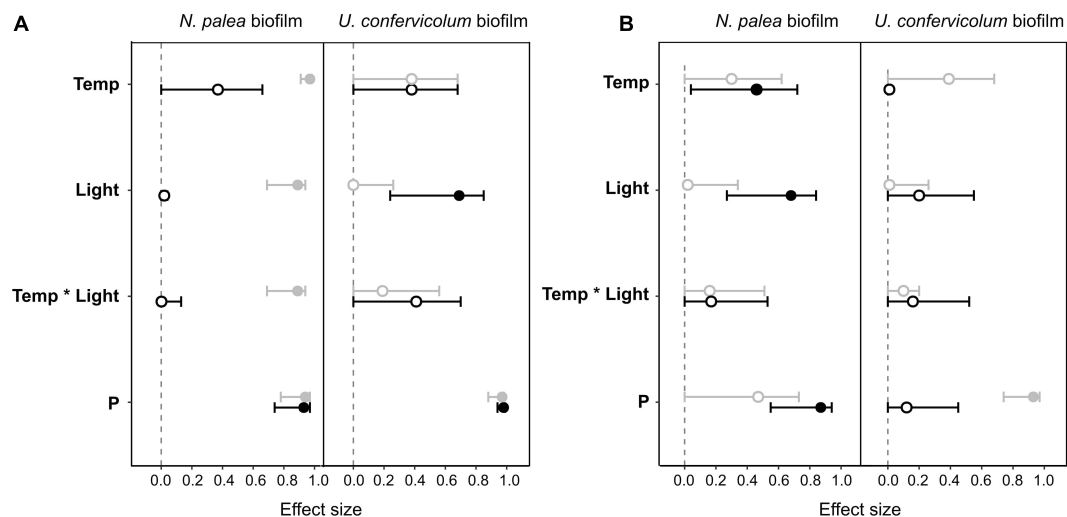


**FIGURE 6 |** Effect size (partial eta-squared  $\pm$  95% confidence interval) on the impact (gray circles) or recovery (black circles) of the total organic carbon (A) and the protein/polysaccharide ratio (B) for the *N. palea* biofilm and *U. confervicolum* biofilm for the environmental factors tested: temperature (Temp), light intensity (Light), phosphorous concentration (P). The temperature \* light intensity interaction is also given. Closed circles: significant effects, open circles: non-significant effects.



**TABLE 2** | *P*-values for two-way and one-way ANOVAS to test the effect of environmental conditions on the resistance and recovery of biofilm EPS quantity and quality.

			Temperature	Light intensity	Light * Temp	P concentration
Resistance	<i>N. palea</i> biofilm	TOC	<b>0.000001</b>	<b>0.00004</b>	<b>0.00005</b>	<b>0.0002</b>
		PN/PS	0.1018	0.6656	0.2587	0.15000
	<i>U. confervicolum</i> biofilm	TOC	0.0950	0.7290	0.2400	<b>0.00004</b>
		PN/PS	0.0525	0.7690	0.3680	<b>0.0004</b>
Recovery	<i>N. palea</i> biofilm	TOC	0.0624	0.7152	0.9074	<b>0.0004</b>
		PN/PS	<b>0.0308</b>	<b>0.0033</b>	0.2344	<b>0.002</b>
	<i>U. confervicolum</i> biofilm	TOC	0.1114	<b>0.0043</b>	0.0637	<b>0.00001</b>
		PN/PS	0.7769	0.1984	0.2503	0.67

Significant *p*-values are in bold, *n* = 3.

maximum quantum yield of the green alga biofilm was promoted by increasing P concentration in the culture medium, until it reached a plateau. In contrast, for the diatom biofilm, a decrease of the yield was observed for the highest P concentration, suggesting that a threshold was exceeded. The yield is known to be influenced by nutrient stress in algae (Parkhill et al., 2001). The P concentration used in the experiment was very high, but it was chosen according to the concentration in combo medium to keep similar growth conditions than the stock cultures. Note that the nutrient level was not adjusted during the experiments.

Concerning EPS production, weak negative correlations were observed between the maximum quantum yield and the quantity of TOC extracted. This result is rather unexpected, given that many authors have shown that EPS are released by cells concomitantly to oxygenic photosynthesis (Staats et al., 2000a) and primary production (Underwood and Paterson, 2003), assimilated to a metabolic response to stresses (Perkins et al., 2001; Orvain et al., 2003). However, there is no direct and clear link between the maximum quantum and the photosynthetic activity. The negative relationship between biofilm growth and EPS production suggests that when algal growth is limited and the photosynthesis is not, organic carbon produced through photosynthesis may be accumulated under the form of EPS, similarly to the Growth-Differentiation Balance Hypothesis for the synthesis of defense metabolites (Herms and Mattson, 1992). However, other regulation mechanisms are likely to be involved since EPS production was increased under low light intensity conditions for the green alga biofilm. Note that an increased EPS production in nutrient-limited cells has also been observed in marine diatoms (Staats et al., 2000b; Khandeparker and Bhosle, 2001).

In addition to EPS quantity, their nature was directly influenced by the environmental factors. In the two biofilms, the EPS were dominated by proteins (PN/PS ratio above 1) in all the growth conditions. EPS are often considered as essentially composed of polysaccharides, but a similar high content in proteins has been reported elsewhere, for instance for biofilms at the sediment surface, in freshwater (Gerbersdorf et al., 2009) and marine (Agogue et al., 2014) environments. The PN/PS ratio was highly variable in *U. confervicolum* biofilms. The PN/PS ratio significantly decreased (resulting from an increase of the quantity of polysaccharides) with an increase in temperature.

## The Effects of Light Intensity, Temperature, and P Concentration on Extracellular Polymeric Substances Response to the Disturbance

Although several studies considered the effects of environmental conditions on biofilm EPS quantity and quality, to our knowledge none assessed how these conditions could modulate the resistance and recovery of EPS after a disturbance. Here we showed, in agreement with our first hypothesis, that the resilience of EPS production after a complex disturbance, i.e., metal exposure followed by dry and rewetting periods, strongly depended on the environmental conditions. This dependency to the environmental conditions varied between the two simplified biofilms that were tested. Moreover, the environmental conditions impacted differently the quantitative and qualitative response of EPS to the disturbance. This opposition of the response pattern of EPS quantity and quality in the two biofilms indicates a decoupling of the regulation of those two parameters. Contrary to our second hypothesis, the environmental factors that affected the resilience of EPS production were not completely the same that affected biofilm growth, as assessed with our factorial design. Indeed, in diatom biofilms, light intensity had no effect on growth while it significantly modified the resistance of EPS quantity and the recovery of EPS quality (see Table 2). Algal species have developed various metabolic adaptations and defense systems to survive under variety of environmental stresses. A four-day metal exposure at non-toxic concentration followed a 2-week dry period was enough to cause changes in the EPS production by the two phototrophic biofilms. At the end of the disturbance, the quantity of EPS was either higher or lower than that before the disturbance, depending on growth conditions and on algal species.

The underlying idea of this experiment is that EPS resilience should contribute to biofilm functional resilience. Unfortunately, this could not directly be assessed because such experiments require the measurement of gross or net primary production. Concerning the protective role of EPS, contrasting results can be found in the literature, notably for the heavy metals. The latter can have either increasing (e.g., Miao et al., 2009) or nil effect (Mota et al., 2015) on EPS production while EPS supposedly contribute to the defense of the cells against metals. EPS are

supposed to contribute to the protection of microorganisms against disturbance through different mechanisms. For instance, drying disturbance encompasses multiple stresses such as limitation of substrate and nutrient diffusion, which can be limited by the use of extracellular polymers as a C source by the cells. Inversely, EPS produced by filamentous cells form the viscous mucilage that surrounds cells (Underwood and Paterson, 2003) and probably play an important direct role in cell protection under unfavorable conditions. Microorganisms tolerate desiccation through a set of molecular mechanisms including the production of polysaccharides that form a reservoir for water and proteins thus capable to stabilize macromolecules and membranes. Extracellular polysaccharides, probably very hydrophilic, could be very efficient to retain interstitial pore water and protect phototrophic cells against desiccation. Only for the diatom biofilm, we observed modifications of EPS composition with an increase in polysaccharides at the end of the disturbance period. However, to verify the stability of this new status, it would have been necessary to follow rewetted biofilms during a longer period. This is in agreement with Orvain et al. (2003) who suggested that polysaccharides are involved in the formation of a protective wall, supplying hydrophilic and stabilizing properties that could convey important functions to the biofilm matrix in terms of resistance to environmental stresses.

The results of this study showed a divergence in the resilience ability of two very simplified phototrophic biofilms regarding to their EPS production. It appeared that in several cases small variations in the environmental conditions had no direct effect on EPS production, while exhibited a significant effect on the resistance and recovery of EPS production after a realistic disturbance. Though the experiment was performed with very simplified biofilms, under artificial conditions, it calls a need for further investigations which are necessary to anticipate the effect of a disturbance on microbial physiology in natural biofilms. The fact that the 3-degrees temperature increase amplified the impact of the disturbance on EPS quantity suggests the existence of non-additive effects between the contamination-dry period disturbance and warming. In a context of global change, this is a preoccupying observation, which highlights the importance of considering not only the direct effects of warming and climate change on the microbial communities, but also on their indirect effects on the ability of communities to cope with additional disturbances. During the last decade, the number

of studies considering the resilience of biofilms increased, as well as the number of studies considering the responses of ecosystem components to combined stresses. However, the studies focusing on the modulation of ecosystem resilience ability by environmental conditions remain very scarce. In a context of global change, with an increasing frequency of disturbances, a considerable effort should be made in this direction.

## DATA AVAILABILITY STATEMENT

The original contributions presented in the study are included in the article/**Supplementary Material**, further inquiries can be directed to the corresponding author.

## AUTHOR CONTRIBUTIONS

EG-N, EL, JL, and J-LR designed the experiments. CB, EL, JF, J-LR, and QA contributed to the laboratory work and analyses. OO and OP realized Cu speciation calculation. EL and JL wrote the first manuscript, and then improved by the other authors.

## FUNDING

EL was supported by a Ph.D. fellowship from the French “Ministère de l’Enseignement Supérieur, de la Recherche et de l’Innovation.” This work was funded by the Idex UNITI grant of the University of Toulouse, France (No. 2016–46–CIF–D–DRDV).

## ACKNOWLEDGMENTS

We thank Didier Lambrigot for TOC measurements.

## SUPPLEMENTARY MATERIAL

The Supplementary Material for this article can be found online at: <https://www.frontiersin.org/articles/10.3389/fmicb.2021.742027/full#supplementary-material>

## REFERENCES

- Acuna, V. (2010). Flow regime alteration effects on the organic C dynamics in semiarid stream ecosystems. *Hydrobiologia* 657, 233–242. doi: 10.1007/s10750-009-0084-3
- Agogue, H., Mallet, C., Orvain, F., De Crignis, M., Mornet, F., and Dupuy, C. (2014). Bacterial dynamics in a microphytobenthic biofilm: a tidal mesocosm approach. *J. Sea Res.* 92, 36–45. doi: 10.1016/j.seares.2014.03.003
- Baker, N. R. (2008). Chlorophyll fluorescence: a probe of photosynthesis *in vivo*. *Annu. Rev. Plant Biol.* 59, 89–113. doi: 10.1146/annurev.arplant.59.032607.092759
- Battin, T. J., Besemer, K., Bengtsson, M. M., Romani, A. M., and Packmann, A. I. (2016). The ecology and biogeochemistry of stream biofilms. *Nat. Rev. Microbiol.* 14, 251–263. doi: 10.1038/nrmicro.2016.15
- Battin, T. J., Kaplan, L. A., Newbold, J. D., and Hansen, C. M. E. (2003). Contributions of microbial biofilms to ecosystem processes in stream mesocosms. *Nature* 426, 439–442. doi: 10.1038/nature02152
- Bengtsson, M. M., Wagner, K., Schwab, C., Urich, T., and Battin, T. J. (2018). Light availability impacts structure and function of phototrophic stream biofilms across domains and trophic levels. *Mol. Ecol.* 27, 2913–2925. doi: 10.1111/mec.14696
- Berben, L., Sereika, S. M., and Engberg, S. (2012). Effect size estimation: methods and examples. *Int. J. Nurs. Stud.* 49, 1039–1047. doi: 10.1016/j.ijnurstu.2012.01.015
- Bohorquez, J., McGenity, T. J., Papaspyrou, S., Garcia-Robledo, E., Corzo, A., and Underwood, G. J. C. (2017). Different types of diatom-derived extracellular polymeric substances drive changes in heterotrophic bacterial communities

- from intertidal sediments. *Front. Microbiol.* 8:245. doi: 10.3389/fmicb.2017.00245
- Corcoll, N., Bonet, B., Morin, S., Tlili, A., Leira, M., and Guasch, H. (2012). The effect of metals on photosynthesis processes and diatom metrics of biofilm from a metal-contaminated river: a translocation experiment. *Ecol. Indic.* 18, 620–631. doi: 10.1016/j.ecolind.2012.01.026
- Datry, T., Bonada, N., and Boulton, A. (2017). *Intermittent Rivers and Ephemeral Streams*. Cambridge: Academic Press.
- de Brouwer, J. F. C., Wolfstein, K., and Stal, L. J. (2002). Physical characterization and diel dynamics of different fractions of extracellular polysaccharides in an axenic culture of a benthic diatom. *Eur. J. Phycol.* 37, 37–44. doi: 10.1017/S0967026201003419
- Delgado, C., Pardo, I., and Garcia, L. (2012). Diatom communities as indicators of ecological status in Mediterranean temporary streams (Balearic Islands, Spain). *Ecol. Indic.* 15, 131–139. doi: 10.1016/j.ecolind.2011.09.037
- Di Pippo, F., Ellwood, N. T. W., Guzzon, A., Siliato, L., Micheletti, E., De Philippis, R., et al. (2012). Effect of light and temperature on biomass, photosynthesis and capsular polysaccharides in cultured phototrophic biofilms. *J. Appl. Phycol.* 24, 211–220. doi: 10.1007/s10811-011-9669-0
- Dreywood, R. (1946). Qualitative test for carbohydrate material. *Ind. Eng. Chem.* 18, 499–499. doi: 10.1021/i560156a015
- Falk, S., Maxwell, D., Laudénbach, D., and Huner, N. (1996). “Photosynthetic adjustment to temperature,” in *Photosynthesis And The Environment*, ed. N. Baker (Amsterdam: Kluwer Academic Publishers), 367–385. doi: 10.1007/0-306-48135-9\_15
- Flemming, H. C., Wingender, J., Szewzyk, U., Steinberg, P., Rice, S. A., and Kjelleberg, S. (2016). Biofilms: an emergent form of bacterial life. *Nat. Rev. Microbiol.* 14, 563–575. doi: 10.1038/nrmicro.2016.94
- Gerbersdorf, S. U., Westrich, B., and Paterson, D. M. (2009). Microbial Extracellular Polymeric Substances (EPS) in Fresh Water Sediments. *Microb. Ecol.* 58, 334–349. doi: 10.1007/s00248-009-9498-8
- Gomez, R., Arce, M. I., Baldwin, D. S., and Dahm, C. N. (2017). “Water physicochemistry in intermittent rivers and ephemeral streams,” in *Intermittent Rivers and Ephemeral Streams*, eds T. Datry, N. Bonada, and A. Boulton (Cambridge: Academic Press), 109–134. doi: 10.1016/B978-0-12-803835-2.00005-X
- Gonzalez, A., King, A., Robeson, M. S., Song, S. J., Shade, A., Metcalf, J. L., et al. (2012). Characterizing microbial communities through space and time. *Curr. Opin. Biotechnol.* 23, 431–436. doi: 10.1016/j.copbio.2011.11.017
- Gustafsson, J. (2011). *Visual MINTEQ ver. 3.0*. Available Online at: <https://vminteq.lwr.kth.se/>
- Hedges, L. V. (1981). Distribution theory for Glass’s estimator of effect size and related estimators. *J. Educ. Stat.* 6, 107–128. doi: 10.3102/10769986006002107
- Herms, D. A., and Mattson, W. J. (1992). The dilemma of plants - to grow or defend. *Q. Rev. Biol.* 67, 283–335. doi: 10.1086/417659
- Hill, W. (1996). “Effects of light,” in *Algal Ecology: Freshwater Benthic Ecosystems*, eds R. Stevenson, M. Bothwell, and R. Lowe (Cambridge: Academic Press), 121–148.
- Hodgson, D., McDonald, J. L., and Hosken, D. J. (2015). What do you mean, ‘resilient’? *Trends Ecol. Evol.* 30, 503–506. doi: 10.1016/j.tree.2015.06.010
- Holmstrup, M., Bindesbol, A. M., Oostingh, G. J., Duschl, A., Scheil, V., Kohler, H. R., et al. (2010). Interactions between effects of environmental chemicals and natural stressors: a review. *Sci. Total Environ.* 408, 3746–3762. doi: 10.1016/j.scitotenv.2009.10.067
- IPCC (2013). “Summary for policymakers in: climate Change 2013: the physical science basis,” in *Contribution of Working Group I to the Fifth Assessment Report of the Intergovernmental Panel on Climate Change*, eds T. F. Stocker, D. Qin, G. K. Plattner, M. Tignor, S. K. Allen, J. Boschung, et al. (Cambridge: Cambridge University Press), 1–30.
- Khandeparker, R. D. S., and Bhosle, N. B. (2001). Extracellular polymeric substances of the marine fouling diatom *Amphora rostrata* Wm.Sm. *Biofouling* 17, 117–127. doi: 10.1080/08927010109378471
- Kilham, S. S., Kreeger, D. A., Lynn, S. G., Goulden, C. E., and Herrera, L. (1998). COMBO: a defined freshwater culture medium for algae and zooplankton. *Hydrobiologia* 377, 147–159. doi: 10.1023/A:1003231628456
- Kroll, A., Behra, R., Kaegi, R., and Sigg, L. (2014). Extracellular Polymeric Substances (EPS) of Freshwater Biofilms Stabilize and Modify CeO<sub>2</sub> and Ag Nanoparticles. *PLoS One* 9:e110709. doi: 10.1371/journal.pone.0110709
- Lambert, A. S., Dabrin, A., Morin, S., Gahou, J., Foulquier, A., Coquery, M., et al. (2016). Temperature modulates phototrophic periphyton response to chronic copper exposure. *Environ. Pollut.* 208, 821–829. doi: 10.1016/j.envpol.2015.11.004
- Laviale, M. (2008). *Effet des Polluants sur les Communautés Périphytiques Naturelles: Apport des Mesures de Fluorescence Chlorophyllienne en Lumière Modulée (PAM)*. France: Université de Lille.
- Lawrence, J. R., Kopf, G., Headley, J. V., and Neu, T. R. (2001). Sorption and metabolism of selected herbicides in river biofilm communities. *Can. J. Microbiol.* 47, 634–641. doi: 10.1139/w01-061
- Lear, G., Anderson, M. J., Smith, J. P., Boxen, K., and Lewis, G. D. (2008). Spatial and temporal heterogeneity of the bacterial communities in stream epilithic biofilms. *FEMS Microbiol. Ecol.* 65, 463–473. doi: 10.1111/j.1574-6941.2008.00548.x
- Leflaive, J., Felten, V., Ferriol, J., Lamy, A., Ten-Hage, L., Bec, A., et al. (2015). Community structure and nutrient level control the tolerance of autotrophic biofilm to silver contamination. *Environ. Sci. Pollut. Res. Int.* 22, 13739–13752. doi: 10.1007/s11356-014-3860-1
- Lock, M. A. (1993). “Attached microbial communities in rivers,” in *Aquatic Microbiology - an Ecological Approach*, ed. T. E. Ford (Oxford: Blackwell Scientific Publications), 113–138.
- Loustau, E., Ferriol, J., Koteiche, S., Gerlin, L., Leflaive, J., Moulin, F., et al. (2019). Physiological responses of three mono-species phototrophic biofilms exposed to copper and zinc. *Environ. Sci. Pollut. Res. Int.* 26, 35107–35120. doi: 10.1007/s11356-019-06560-6
- Loustau, E., Rols, J. L., Leflaive, J., Marcato-Romain, C. E., and Girbal-Neuhausser, E. (2018). Comparison of extraction methods for the characterization of extracellular polymeric substances from aggregates of three biofilm-forming phototrophic microorganisms. *Can. J. Microbiol.* 64, 887–899. doi: 10.1139/cjm-2018-0182
- Miao, A. J., Schwehr, K. A., Xu, C., Zhang, S. J., Luo, Z. P., Quigg, A., et al. (2009). The algal toxicity of silver engineered nanoparticles and detoxification by exopolymers. *Environ. Pollut.* 157, 3034–3041. doi: 10.1016/j.envpol.2009.05.047
- Montuelle, B., Dorigo, U., Berard, A., Volat, B., Bouchez, A., Tlili, A., et al. (2010). The periphyton as a multimetric bioindicator for assessing the impact of land use on rivers: an overview of the ArdiSres-Morille experimental watershed (France). *Hydrobiologia* 657, 123–141. doi: 10.1007/s10750-010-0105-2
- Mota, R., Pereira, S. B., Meazzini, M., Fernandes, R., Santos, A., Evans, C. A., et al. (2015). Effects of heavy metals on *Cyanobacteria* sp. CCY 0110 growth, extracellular polymeric substances (EPS) production, ultrastructure and protein profiles. *J. Proteomics* 120, 75–94. doi: 10.1016/j.jprot.2015.03.004
- Oliver, T. H., Heard, M. S., Isaac, N. J. B., Roy, D. B., Procter, D., Eigenbrod, F., et al. (2015). Biodiversity and Resilience of Ecosystem Functions. *Trends Ecol. Evol.* 30, 673–684. doi: 10.1016/j.tree.2015.08.009
- Orvain, F., Galois, R., Barnard, C., Sylvestre, A., Blanchard, G., and Sauriau, P. G. (2003). Carbohydrate production in relation to microphytobenthic biofilm development: an integrated approach in a tidal mesocosm. *Microb. Ecol.* 45, 237–251. doi: 10.1007/s00248-002-2027-7
- Parkhill, J. P., Maillet, G., and Cullen, J. J. (2001). Fluorescence-based maximal quantum yield for PSII as a diagnostic of nutrient stress. *J. Phycol.* 37, 517–529. doi: 10.1046/j.1529-8817.2001.037004517.x
- Perkins, R. G., Underwood, G. J. C., Brotas, V., Snow, G. C., Jesus, B., and Ribeiro, L. (2001). Responses of microphytobenthos to light: primary production and carbohydrate allocation over an emersion period. *Mar. Ecol. Prog. Ser.* 223, 101–112. doi: 10.3354/meps223101
- Pesce, S., Lambert, A. S., Morin, S., Foulquier, A., Coquery, M., and Dabrin, A. (2018). Experimental Warming Differentially Influences the Vulnerability of Phototrophic and Heterotrophic Periphytic Communities to Copper Toxicity. *Front. Microbiol.* 9:1424. doi: 10.3389/fmicb.2018.01424
- Rao, T. S. (2010). Comparative effect of temperature on biofilm formation in natural and modified marine environment. *Aquat. Ecol.* 44, 463–478. doi: 10.1007/s10452-009-9304-1
- Rohacek, K., and Bartak, M. (1999). Technique of the modulated chlorophyll fluorescence: basic concepts, useful parameters, and some applications. *Photosynthetica* 37, 339–363. doi: 10.1023/A:1007172424619
- Rykiel, E. J. (1985). Towards a definition of ecological disturbance. *Aust. J. Ecol.* 10, 361–365. doi: 10.1111/j.1442-9993.1985.tb00897.x

- Sabater, S., Guasch, H., Romani, A., and Munoz, I. (2002). The effect of biological factors on the efficiency of river biofilms in improving water quality. *Hydrobiologia* 469, 149–156. doi: 10.1023/A:1015549404082
- Sabater, S., Timoner, X., Borrego, C., and Acuna, V. (2016). Stream biofilm responses to flow intermittency: from cells to ecosystems. *Front. Environ. Sci.* 4:14. doi: 10.3389/fenvs.2016.00014
- Sasaki, M., Takagi, A., Ota, S., Kwana, S., Sasaki, D., and Asayama, M. (2020). Coproduction of lipids and extracellular polysaccharides from the novel green alga *Parachlorella* sp. BX1.5 depending on cultivation conditions. *Biotechnol. Rep.* 25:e00392. doi: 10.1016/j.btre.2019.e00392
- Schindler, D. W. (1977). EVOLUTION OF PHOSPHORUS LIMITATION IN LAKES. *Science* 195, 260–262. doi: 10.1126/science.195.4275.260
- Schindler, D. W., Hecky, R. E., Findlay, D. L., Stainton, M. P., Parker, B. R., Paterson, M. J., et al. (2008). Eutrophication of lakes cannot be controlled by reducing nitrogen input: results of a 37-year whole-ecosystem experiment. *Proc. Natl. Acad. Sci. U. S. A.* 105, 11254–11258. doi: 10.1073/pnas.0805108105
- Segner, H., Schmitt-Jansen, M., and Sabater, S. (2014). Assessing the impact of multiple stressors on aquatic biota: the receptor's side matters. *Environ. Sci. Technol.* 48, 7690–7696. doi: 10.1021/es405082t
- Shetty, P., Gitau, M. M., and Maroti, G. (2019). Salinity stress responses and adaptation mechanisms in eukaryotic green microalgae. *Cells* 8: 1657. doi: 10.3390/cells8121657
- Smith, P. K., Krohn, R. I., Hermanson, G. T., Mallia, A. K., Gartner, F. H., Provenzano, M. D., et al. (1985). Measurement of protein using bicinchoninic acid. *Anal. Biochem.* 150, 76–85. doi: 10.1016/0003-2697(85)90442-7
- Smith, V. H., Tilman, G. D., and Nekola, J. C. (1999). Eutrophication: impacts of excess nutrient inputs on freshwater, marine, and terrestrial ecosystems. *Environ. Pollut.* 100, 179–196. doi: 10.1016/S0269-7491(99)00091-3
- Staats, N., Stal, L. J., de Winder, B., and Mur, L. R. (2000a). Oxygenic photosynthesis as driving process in exopolysaccharide production of benthic diatoms. *Mar. Ecol. Prog. Ser.* 193, 261–269. doi: 10.3354/meps193261
- Staats, N., Stal, L. J., and Mur, L. R. (2000b). Exopolysaccharide production by the epipellic diatom *Cylindrotheca closterium*: effects of nutrient conditions. *J. Exp. Mar. Biol. Ecol.* 249, 13–27. doi: 10.1016/S0022-0981(00)00166-0
- Stevenson, R., Bothwell, M., and Lowe, R. (1996). *Algal Ecology: Freshwater Benthic Ecosystems*. Cambridge: Academic Press.
- Underwood, G. J. C., and Paterson, D. M. (2003). The importance of extracellular carbohydrate production by marine epipellic diatoms. *Adv. Bot. Res.* 40, 183–240. doi: 10.1016/S0065-2296(05)40005-1
- Verneuil, L., Silvestre, J., Randrianjatovo, I., Marcato-Romain, C. E., Girbal-Neuhauser, E., Mouchet, F., et al. (2015). Double walled carbon nanotubes promote the overproduction of extracellular protein-like polymers in *Nitzschia palea*: an adhesive response for an adaptive issue. *Carbon* 88, 113–125. doi: 10.1016/j.carbon.2015.02.053
- Villanueva, V. D., Font, J., Schwartz, T., and Romani, A. M. (2011). Biofilm formation at warming temperature: acceleration of microbial colonization and microbial interactive effects. *Biofouling* 27, 59–71. doi: 10.1080/08927014.2010.538841
- Wolfstein, K., and Stal, L. J. (2002). Production of extracellular polymeric substances (EPS) by benthic diatoms: effect of irradiance and temperature. *Mar. Ecol. Prog. Ser.* 236, 13–22. doi: 10.3354/meps236013
- Xiao, R., and Zheng, Y. (2016). Overview of microalgal extracellular polymeric substances (EPS) and their applications. *Biotechnol. Adv.* 34, 1225–1244. doi: 10.1016/j.biotechadv.2016.08.004
- Ylla, I., Borrego, C., Romani, A. M., and Sabater, S. (2009). Availability of glucose and light modulates the structure and function of a microbial biofilm. *FEMS Microbiol. Ecol.* 69, 27–42. doi: 10.1111/j.1574-6941.2009.00689.x

**Conflict of Interest:** The authors declare that the research was conducted in the absence of any commercial or financial relationships that could be construed as a potential conflict of interest.

**Publisher's Note:** All claims expressed in this article are solely those of the authors and do not necessarily represent those of their affiliated organizations, or those of the publisher, the editors and the reviewers. Any product that may be evaluated in this article, or claim that may be made by its manufacturer, is not guaranteed or endorsed by the publisher.

Copyright © 2021 Loustau, Leflaive, Boscus, Amalric, Ferriol, Oleinikova, Pokrovsky, Girbal-Neuhauser and Rols. This is an open-access article distributed under the terms of the Creative Commons Attribution License (CC BY). The use, distribution or reproduction in other forums is permitted, provided the original author(s) and the copyright owner(s) are credited and that the original publication in this journal is cited, in accordance with accepted academic practice. No use, distribution or reproduction is permitted which does not comply with these terms.





# Diversity, Functions and Antibiotic Resistance of Sediment Microbial Communities From Lake Geneva Are Driven by the Spatial Distribution of Anthropogenic Contamination

Emilie Lyautey<sup>1,2</sup>, Chloé Bonnineau<sup>1</sup>, Patrick Billard<sup>3</sup>, Jean-Luc Loizeau<sup>4</sup>, Emmanuel Naffrechoux<sup>5</sup>, Ahmed Tlili<sup>6</sup>, Edward Topp<sup>7,8</sup>, Benoît J.D. Ferrari<sup>9</sup> and Stéphane Pesce<sup>1\*</sup>

## OPEN ACCESS

### Edited by:

Carmen Palacios,  
Université de Perpignan Via Domitia,  
France

### Reviewed by:

Kevin Thomas Finneran,  
Clemson University, United States  
Naresh Singhal,  
The University of Auckland,  
New Zealand

### \*Correspondence:

Stéphane Pesce  
stephane.pesce@inrae.fr

### Specialty section:

This article was submitted to  
Microbiotechnology,  
a section of the journal  
Frontiers in Microbiology

**Received:** 09 July 2021

**Accepted:** 28 September 2021

**Published:** 18 October 2021

### Citation:

Lyautey E, Bonnineau C, Billard P,  
Loizeau J-L, Naffrechoux E, Tlili A,  
Topp E, Ferrari BJD and Pesce S  
(2021) Diversity, Functions and  
Antibiotic Resistance of Sediment  
Microbial Communities From Lake  
Geneva Are Driven by the Spatial  
Distribution of Anthropogenic  
Contamination.  
Front. Microbiol. 12:738629.  
doi: 10.3389/fmicb.2021.738629

<sup>1</sup> INRAE UR RiverLy, Villeurbanne, France, <sup>2</sup> INRAE, Université Savoie Mont Blanc, CARRTEL, Thonon-les-Bains, France, <sup>3</sup> Université de Lorraine, CNRS, LIEC, Nancy, France, <sup>4</sup> Department F.A. Forel for Environmental and Aquatic Sciences, University of Geneva, Geneva, Switzerland, <sup>5</sup> EDYTEM, CNRS, Université Savoie Mont Blanc, Chambéry, France, <sup>6</sup> Eawag, Swiss Federal Institute of Aquatic Science and Technology, Dübendorf, Switzerland, <sup>7</sup> Agriculture and Agri-Food Canada, London, ON, Canada, <sup>8</sup> Department of Biology, University of Western Ontario, London, ON, Canada, <sup>9</sup> Swiss Centre for Applied Ecotoxicology (Ecotox Centre), Lausanne, Switzerland

Lake sediments are natural receptors for a wide range of anthropogenic contaminants including organic matter and toxicants such as trace metals, polycyclic aromatic hydrocarbons, polychlorinated biphenyls that accumulate over time. This contamination can impact benthic communities, including microorganisms which play a crucial role in biogeochemical cycling and food-webs. The present survey aimed at exploring whether anthropogenic contamination, at a large lake scale, can influence the diversity, structure and functions of microbial communities associated to surface sediment, as well as their genetic potential for resistance to metals and antibiotics. Changes in the characteristics of these communities were assessed in surface sediments collected in Lake Geneva from eight sampling sites in October 2017 and May 2018. These sampling sites were characterized by a large concentration range of metal and organic compound contamination. Variation between the two sampling periods were very limited for all sampling sites and measured microbial parameters. In contrast, spatial variations were observed, with two sites being distinct from each other, and from the other six sites. Benthic communities from the most contaminated sampling site (Vidy Bay, near the city of Lausanne) were characterized by the lowest bacterial and archaeal diversity, a distinct community composition, the highest abundance of antibiotic resistance genes and functional (respiration, denitrification, methanogenesis, phosphatase, and beta-glucosidase) activity levels. The second sampling site which is highly influenced by inputs from the Rhône River, exhibited low levels of diversity, a distinct community composition, high abundance of antibiotic resistance genes and the highest bacterial abundance. Overall, our results suggest that local anthropogenic contamination, including organic

matter and toxicants, is a major driver of the diversity and functioning of sediment-microbial communities in Lake Geneva. This highlights the need to consider benthic microbial communities and a suite of complementary ecotoxicological endpoints for more effective environmental risk assessments of contaminants in lake sediments.

**Keywords:** benthic communities, microbial ecotoxicology, metals, organic matter, PCB, PAH, resistance genes, urban contamination

## INTRODUCTION

The sediment compartment in lakes can act as a sink for contaminants, including not only nutrients and organic matter but also metals, persistent organic pollutants [e.g., polycyclic aromatic hydrocarbons, polychlorinated biphenyls (PAHs); polychlorinated biphenyls, polychlorinated biphenyls (PCBs)] and other substances such as pesticides or pollutants of emerging concerns (e.g., pharmaceuticals including antibiotics) (Xu et al., 2017; Codling et al., 2018; Golovko et al., 2020). Due to their hydrophobic nature, once deposited most of these contaminants associate strongly to the sediment (Sedláček et al., 2020). Therefore, the vertical depth profiles of contaminants in sediment cores generally reflect the temporal history of contamination, with increasing depth being associated with older contamination events (Lécrivain et al., 2018). On the other hand, horizontal gradients of contamination depend mainly on the distance from the contamination sources. The contamination of surface sediments (0–5 cm layer) in the littoral and pelagic zones of lakes can thus exhibit substantial spatial heterogeneity according to the distribution of point- and diffuse sources of pollution in the surrounding watershed, and contaminant fluxes carried into the lake by tributaries (Marvin et al., 2004; Lécrivain et al., 2019). Therefore, benthic communities in lake sediments can experience different exposures to contaminants including nutrients and organic matter according to their location. However, the resulting effects on these communities still under-investigated (Pesce et al., 2018) and little is known about the potential relationships between the spatial contamination heterogeneity in lake surface sediment, and the consequent spatial alterations of benthic community diversity, structure and functions (Haller et al., 2011; Sauvain et al., 2014; Jin et al., 2019).

In lake surface sediments, microorganisms are highly abundant and characterized by a large taxonomic and functional diversity, making them key players in a multitude of ecosystem processes (Schallenberg and Kalff, 1993; Pearman et al., 2020). These processes include biogeochemical cycling of nitrogen, the recycling of autochthonous and allochthonous organic matter, and the dissipation of organic contaminants (Vadeboncoeur et al., 2002; Haglund et al., 2003; Bedard, 2008; Schultz and Urban, 2008). Several laboratory studies have shown that environmental concentrations of metals (Mahamoud Ahmed et al., 2018, 2020) and organic contaminants such as pesticides (Widenfalk et al., 2004, 2008), PCBs (Diepens et al., 2015) and PAHs (Zhang et al., 2014) can affect the diversity, structure and functional potential of exposed sediment microbial communities. The structural and functional properties of microbial communities in lake sediments can vary horizontally at

a relatively limited geographical scale, according to several local environmental factors (Krzmarzick et al., 2013; Pearman et al., 2020). However, the role of anthropogenic contamination in the spatial structuration of those microbial assemblages and the resulting effects on the functional properties of lake benthic ecosystems remain largely unknown.

The contamination of Lake Geneva has been monitored with a focus on various groups of contaminants such as PAHs, PCBs, metals, pharmaceuticals, and pesticides in surface water and sediments (e.g., Poté et al., 2008; Perazzolo et al., 2010; Hoerger et al., 2014; Larras et al., 2016). For example, a large sampling survey undertaken in 2015 mapped the contamination of the surface sediments at the whole lake scale (Loizeau et al., 2017). Sediments in the Vidy Bay near the city of Lausanne were the most contaminated by metals, organic pollutants and organic matter (Loizeau et al., 2017). The high contamination of sediments in this area has been documented for decades (Grandjean et al., 1990; Poté et al., 2008; Loizeau et al., 2013; Gascon Diez et al., 2014; Masson and Tercier-Waeber, 2014). This is mainly due to historic inputs from urban sewage effluents (Gascón Díez et al., 2017), which is also reflected by the prevalence of fecal-indicator bacteria (Poté et al., 2008) and antibiotic-resistance genes (Czekalski et al., 2014). The contamination has been suggested as an important driver of microbial community structure (Haller et al., 2011). Besides this hotspot of contamination, there is relative spatial heterogeneity in the contamination at the whole Lake scale with a strong influence of the Rhone River, which is the main Lake tributary, and of the lakeshore (Loizeau et al., 2017).

In this context, we performed two sampling campaigns to investigate the spatio-temporal variations in benthic microbial communities collected in surface sediments from eight sampling sites in Lake Geneva. These sites, which are widely geographically distributed at the lake scale, cover a large range of contamination levels by metals and organic toxicants (Loizeau et al., 2017). We included one site located in the Vidy Bay and one site located near the Rhone River mouth into the lake. The objective was to assess whether spatial and/or temporal changes in the structural and functional characteristics of the studied community are driven by anthropogenic contamination. For this purpose, microbial communities in sediment samples were characterized for bacterial and archaeal population diversity, composition and structure, bacterial abundance, functional (respiration, denitrification, methanogenesis, leucine aminopeptidase, phosphatase, and beta-glucosidase) potential activities and the abundance of gene targets associated with resistance to selected metals and antibiotics. We expected the microbial community structure from these eight sites

to exhibit spatial and temporal dynamics, with functional properties linked both to community composition and to the environmental conditions prevailing in the sediment compartment on the sampling dates. Contamination levels by metals and organic toxicants were expected to select for more tolerant populations at the sampling site scale, leading to change in community structure and to increasing genetic potential of resistance, with possible impacts on ecosystem functions.

## MATERIALS AND METHODS

### Sampling Sites and Sample Collection

Lake Geneva is the largest natural lake in western Europe (580 km<sup>2</sup>, 72 km long and 14 km wide), with a maximum depth of 309 m, and a watershed surface area of 7,999 km<sup>2</sup>. The lake is located between France and Switzerland, and its major tributary and outflow is the Rhône River. The water residence time is 11.3 years (CIPEL, 2018). Lake Geneva is a deep monomictic lake with irregular complete winter overturns occurring on average every 5 years (Schwefel et al., 2016).

Sample collection was carried out on October 2017 (26th) and May 2018 (23rd, 24th, and 25th) at eight sampling sites. Sampling sites were referred as sites number 5, 6, 21, 29, 32, 36, 53, and 78 (**Figure 1**), according to the map of sampling sites of Loizeau et al. (2017). The sites were chosen to cover a large range of contamination levels by metals and organic toxicants, as reported by Loizeau et al. (2017). Sites 29, 32, 53, and 78 were sampled both years whereas sites 5, 6, 21, and 36 were only sampled in 2018 due to weather conditions in 2017. Sampling site descriptions, sampling date, geographical coordinates, and depth are provided in **Table 1**.

Surface sediment sampling was carried out using an Eckman grab sampler, and the top 15–25 cm of sediment were grabbed. Samples for subsequent analyses were collected in the Eckman grab, from the first 2-cm of sediment directly in the field, and stored for further analyses. For each site, three independent samples were collected. Each sample was sub-sampled directly on the boat, and samples were stored at 4°C during transport to the laboratory with arrival within 6 h.

### Sediment Chemical Characterization

The analyses of the physico-chemical properties of sediment from sites 29, 32, 53, and 78 were carried out on samples collected on October 2017, and from sites 5, 6, 21, and 36 on samples collected on May 2018. These analyses included concentrations of trace metals (Ti, Cr, Co, Ni, Cu, Zn, As, Mo, Ag, Cd, Sn, Pb, and Hg), 12 PCBs, 16 PAHs, and ancillary parameters [grain size distribution, organic matter (OM), carbonate and total organic carbon content (TOC), total phosphorus content (P<sub>tot</sub>)]. Ti was used as a proxy of the Rhône River influence on Lake Geneva, as suspended particle load from this river mainly originate from the erosion of Alpine rocks richer in Ti-bearing minerals than rocks from the calcareous Jura mountains drained by the others tributaries, or calcite particles directly precipitated from the water column.

Sediment grain-size distribution was determined on wet sediments using a laser diffraction analyzer (Coulter LS-100, Beckman-Coulter, United States), following the procedure described by Loizeau et al. (1994).

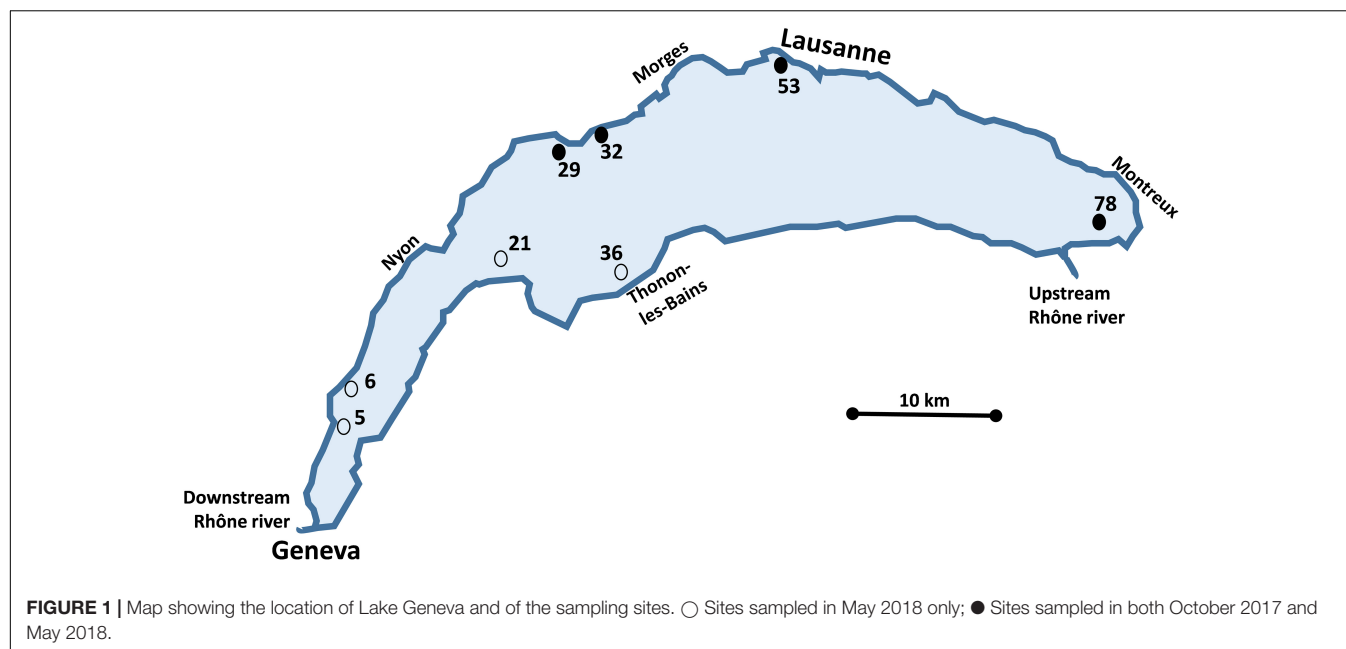
Samples were freeze-dried in a CHRIST BETA 1–8 K freeze drying unit (−54°C, 6 Pa) for a minimum of 48 h. Organic matter and calcium carbonate (CaCO<sub>3</sub>) contents in sediments were estimated by Loss on Ignition. Samples were heated to 550°C for 30 min to estimate the OM mass loss and then heated to 1000°C for another 30 min to estimate the CaCO<sub>3</sub> content (Dean, 1974). The CaCO<sub>3</sub> content was calculated by multiplying the mass loss at 1000°C by 2.2742, the molar mass ratio of calcite to carbon dioxide.

Total phosphorus (TP) was measured with a spectrophotometer (Helios Gamma UV-Vis Thermo Electroporation, Thermo scientific, United States) at 850 nm. The sediment sample preparation for TP analysis was performed as follow; 50 mg of ignited sediment (after heating at 550°C for 1 h) were diluted in 5 mL HCl 1 N and introduced in centrifuge tubes. The mixture was ultrasonicated (at ambient temperature) during 16 h and centrifuged (4000 × rpm) during 20 min. The TP concentration was determined by measuring the absorbance of the blue complex obtained after reduction of molybdophosphoric acid according to previously described method (Murphy and Riley, 1962; Harwood et al., 1969; Burrus et al., 1990).

Quadrupole based inductively coupled plasma mass spectrometry (ICPMS, model 7700 series, Agilent) was performed following sediment digestion in Teflon bombs heated to 150°C in analytical grade 2 M HNO<sub>3</sub> according to the Swiss Soil Protection Ordinance (OSol, Office Fédéral de l'environnement [OFEV], 1998). Multi-element standard solutions of different concentrations (0, 0.02, 1, 5, 20, 100, and 200 mg L<sup>−1</sup>) were used for calibration. The total variation coefficients for triplicate sample measurements were less than 10%.

Total Hg was analyzed by Cold Vapor Atomic Absorption 187 Spectrophotometry (CV-AAS) using an Advance Mercury Analyzer (Model AMA 254, Altec, Czech Republic) through dry mineralization and pre-concentration of Hg and amalgamation on a gold trap (Szakova et al., 2004). The detection limit and working range were 0.01 ng and 0.05–600 ng, respectively. The relative error was usually ±5% and always less than 10% (Roos-Barraclough et al., 2002).

Polychlorinated biphenyls and PAHs were quantified on freeze-dried sediments. PCBs and PAHs were characterized according to the method described in Mwanamoki et al. (2014). Briefly, 5 g of dry sediment were extracted with a mixture of acetone (20% of the volume) and hexane (80% of the volume) for 4 h with a Soxhlet apparatus. At this point, interfering sulfur compounds were removed by adding activated copper to the extract. The organic extract was then concentrated to 1 mL in a vacuum rotary evaporator. The extract was further subject to fractionation and clean-up over a chromatographic column containing 3 g of Silica gel. Three separated fractions were collected: first with 16 mL of hexane, then 35 mL of hexane, and finally 50 mL of hexane:dichloromethane (v/v, 1:1). The



first fraction should contain PCBs while PAHs are distributed in the three fractions. Following reduction of the volume, chemicals were measured by gas chromatography with triple mass spectrometry detection (GC–MS/MS, Thermo Scientific, TSQ Quantum XLS Ultra, Waltham, MA, United States).

## Bacterial Abundance and Functional Potential of the Microbial Community

Bacterial abundance was estimated by flow cytometry as described in Frossard et al. (2012). Briefly, 3 g of wet sediment were suspended in 10 mL of 2% formalin containing 0.1% pyrophosphate. After an ultrasonic treatment for 1 min (Branson Digital Sonifier 250, Germany) and homogenization, 1 mL subsample of each suspension was placed on top of 0.5 mL Histodenz solution (Sigma-Aldrich, Buchs, Switzerland) and centrifuged at  $17,135 \times g$  at 4°C for 90 min. The upper layer, containing bacterial cells, was recovered and stained with 0.1 mL mL<sup>-1</sup> of SYBER® Green I (Promega, Switzerland) in anhydrous dimethylsulfoxide and incubated during 15 min in the dark. A known concentration of fluorescent beads (Beckman Coulter, Switzerland) was added to the samples as a standard to determine the cell concentration. Samples were analysed with a Gallios flow cytometer (Beckman Coulter, Switzerland).

The functional potential of the microbial community was assessed through the measurement of three enzymatic activities:  $\beta$ -glucosidase,  $\beta$ -glu, EC 3.2.1.21; leucine aminopeptidase, LAP, EC 3.4.11.1; and phosphatase, Pase, EC 3.1.3.1; and three metabolic activities: aerobic respiration, denitrification and methanogenesis.

Briefly, to measure enzymatic activities, 1.2 g of wet sediment were incubated for 30 min with pre-determined optimal concentrations of the fluorogenic substrates 4-methylumbelliferyl- $\beta$ -D-glucopyranoside (MUF-Glu, CAS No. 18997-57-4) for  $\beta$ -glu, L-leucine-7-amido-4-methylcoumarin

hydrochloride (Leu-AMC, CAS No. 62480-44-8) for LAP, and 4-methylumbelliferyl phosphatase (MUF-P, CAS No. 3368-04-5) for Pase (Mahamoud Ahmed et al., 2018). After the activities were stopped with glycine buffer (0.05 M glycine, 0.2 M NH<sub>4</sub>OH, pH 10.4), the samples were centrifuged and the fluorescence in the supernatant was measured using a microplate reader (Exc: 360 nm/Em: 460 nm, Synergy HT BioTek Instruments). Results are expressed as nmol of fluorochrome (MUF or MCA) per g of sediment dw<sup>-1</sup> h<sup>-1</sup>.

Potential rates of aerobic respiration, denitrification and methanogenesis were measured with 10 g of wet sediment according to the protocols described by Foulquier et al. (2013) and slightly adapted by Mahamoud Ahmed et al. (2018). Sediment was mixed with 10 mL of distilled water under aerobic conditions (aerobic respiration), or 10 mL of a KNO<sub>3</sub> (2.16 g L<sup>-1</sup>) solution under anaerobic conditions (denitrification), or 10 mL of distilled water under anaerobic conditions (methanogenesis) in 150-mL glass flasks with rubber stoppers. Incubation flasks assigned to denitrification and methanogenesis measurements were purged three times with He to achieve anaerobiosis, and the internal pressure was then adjusted to atmospheric. For denitrification measurements, 15 mL of acetylene (C<sub>2</sub>H<sub>2</sub>, 10% v/v final volume) was added to inhibit N<sub>2</sub>O reductase. All samples were incubated at 20°C in the dark with gentle shaking. After 2 h and 5 h, headspace gasses were sampled and analyzed by gas chromatography (Agilent 490 MICRO GC). Aerobic respiration, denitrification and methanogenesis activities are expressed as ng of gaseous product (CO<sub>2</sub> or N<sub>2</sub>O or CH<sub>4</sub>, respectively) per g of sediment dw<sup>-1</sup> h<sup>-1</sup>.

## Microbial Community Structure

### DNA Extraction

Microbial sediment DNA was extracted from 0.5 g of wet sediment using a NucleoSpin Soil Kit (Macherey-Nagel EURL)



**TABLE 1 |** Presentations of the sampling site characteristics: sampling date (in bold, those when the presented physico-chemical parameters were measured), geographical coordinates, depth, and physico-chemical sediment characteristics: organic matter (OM) content ( $\pm$  SD), carbonate content ( $\pm$  SD), total organic carbon (TOC) content, total phosphorus (Ptot), and Ti concentrations, median grain size ( $\pm$  SD), and the sums of sediment concentrations of the following trace metals (Cr, Co, Ni, Cu, Zn, As, Mo, Ag, Cd, Sn, Pb, and Hg), of the seven indicator PCBs, and of PAHs.

Site	Date	Coordinates		Depth (m)	Latitude	Organic matter		Carbonate	TOC	Ptot	Median grain size		Ti	$\Sigma$ other metals		$\Sigma$ PCBI	$\Sigma$ PAH
		Longitude	Latitude			$\pm$ SD (%)	$\pm$ SD (%)				$\pm$ SD ( $\mu$ m)	(mg kg <sup>-1</sup> dw)		(mg kg <sup>-1</sup> dw)	( $\mu$ g kg <sup>-1</sup> dw)		
5	<b>May 18</b>	E6.18008	N46.26927	47		8.64 $\pm$ 0.35	48.14 $\pm$ 0.83	4.35	848.6	848.6	14.77 $\pm$ 3.26	37.3 $\pm$ 1.0	206.6	5.47	1120.8		
6	<b>May 18</b>	E6.19270	N46.29642	55		8.95 $\pm$ 0.10	44.33 $\pm$ 0.26	4.59	834.8	834.8	7.73 $\pm$ 2.73	37.6 $\pm$ 1.5	294.5	10.53	1372.4		
21	<b>May 18</b>	E6.33359	N46.37907	50		7.18 $\pm$ 0.33	42.09 $\pm$ 0.76	2.93	750.4	750.4	7.98 $\pm$ 2.79	75 $\pm$ 1.6	267.1	9.81	1139.4		
29	May 18, <b>Oct 17</b>	E6.38462	N46.45147	95		6.38 $\pm$ 0.13	31.21 $\pm$ 0.22	2.76	872.0	872.0	10.57 $\pm$ 3.01	405.5 $\pm$ 1.8	321.8	7.40	1922.2		
32	May 18, <b>Oct 17</b>	E6.42316	N46.46618	22		5.27 $\pm$ 0.21	36.61 $\pm$ 0.36	2.08	670.1	670.1	14.95 $\pm$ 3.90	177.7 $\pm$ 4.5	212.1	7.69	2262.5		
36	<b>May 18</b>	E6.45097	N. 46.37102	32		4.79 $\pm$ 0.04	48.87 $\pm$ 0.35	2.67	549.3	549.3	19.07 $\pm$ 5.31	42.5 $\pm$ 2.4	169.8	5.20	13581.1		
53	May 18, <b>Oct 17</b>	E6.58810	N46.51014	44		13.65 $\pm$ 0.09	19.70 $\pm$ 0.23	6.96	3900.0	3900.0	34.82 $\pm$ 5.00	170.7 $\pm$ 6.2	1193.4	386.55	25261.9		
78	May 18, <b>Oct 17</b>	E6.89261	N46.40998	60		2.73 $\pm$ 0.30	14.40 $\pm$ 0.32	0.68	659.4	659.4	11.12 $\pm$ 2.52	1735.6 $\pm$ 30.2	293.0	0.89	774.3		

Detailed metals, PCB and HAP concentrations are presented in **Supplementary Tables 1–3**.

following the manufacturer’s instructions with SL1 lysis buffer and additive Enhancer SX buffer. The extracted DNA was quantified fluorometrically after staining with QuantiFluor dsDNA Dye (QuantiFluor dsDNA System, Promega) using a Plate Chameleon<sup>TM</sup> fluorometer (Hidex; excitation 485 nm, emission 590 nm).

High-Throughput 16S rRNA Gene Sequencing and Bioinformatic Analysis

PCR amplification for high-throughput 16S rRNA gene amplicon sequencing was carried out with the universal primer pair 515F and 909R targeting the V4–V5 hypervariable region of the 16S rRNA gene (Wang and Qian, 2009). Indexes were integrated to both primers following the dual-indexing procedure described by Kozich et al. (2013). Triplicate PCR amplification for each sample was carried out with a total amount of ~5 ng of DNA per reaction. Amplicon products were quantified using the Picogreen assay (Life Technologies, Carlsbad, United States) and pooled equimolarly. The final pool was purified with CleanPCR beads (CleanNA). Sequencing was done by Fasteris (Geneva, Switzerland) on an Illumina HiSeq system with 2  $\times$  300 bp. The analysis yielded 3.7 Gb of sequences with an average error rate of 1.480%, and average Q30 of 85.0%. Adapters were removed using Trimmomatic (Bolger et al., 2014) and barcodes sorted using a Fasteris internal script. Sequences were then processed using the FROGS (Find Rapidly OTUs with Galaxy Solution) Galaxy-supported pipeline (Escudié et al., 2018). Paired-end reads were joined using FLASH (Magoè and Salzberg, 2011) and a quality check was performed using FastQC. Sequences with primers having no mismatch were kept. They were then filtered by size (350–500 bp) and those containing N bases were discarded. The 16S rRNA gene sequences were then denoised and clustered using the Swarm method (Mahé et al., 2015) with a three-base maximum difference, deletion of clusters with less than 0.005% abundance and cluster occurrence in a minimum of two samples of the total library. Chimeras were removed using vchime of vsearch package (Rognes et al., 2016). Affiliation was done using the Silva SSU database 123 (Quast et al., 2013) through BLAST (Altschul et al., 1990) with allowed multiple affiliation and manual curation. All analyses were done on the Galaxy instance of the INRA MIGALE bioinformatics platform<sup>1</sup>. Sequences are available at GenBank under accession number PRJNA742879.

Microbial Community Genetic Resistance Potential

Real-time PCR quantification of bacterial 16S rRNA gene abundance was carried out using the primers 968F and 1401R according to Cébron et al. (2008). For the quantification of *cusA* (encoding a copper efflux system inner membrane protein), the primer pair *cusF1* and *cusR2* (Mahamoud Ahmed et al., 2020) was used, and for the quantification of *czcA* (inner membrane protein contributing to cobalt, zinc, and cadmium efflux) the primer pair *czcF3* (5'-CCCTGGACTTCGGCATCATYGTBGAYGG-3') and *czcR1* (5'-GGCCATGGGGTGGAACATYTTNCC-3') was used. The previously described reactions and cycling conditions

<sup>1</sup><http://migale.jouy.inra.fr>

(Mahamoud Ahmed et al., 2020) were applied to both genes. To construct standard plasmids, *czcA* and *cusA* fragments were amplified from *Burkholderia* sp. S911 (accession no. KP081480) and *Cupriavidus metallidurans* CH34, respectively, and cloned into the pGEM-T vector. Gene copy numbers were established using standard curves prepared with 10-fold serial dilutions of standard plasmids. All runs were performed in an iCycler iQ system (Bio-Rad) associated with iCycler Optical System Interface software (version 2.3, Bio-Rad).

The abundance of selected antibiotic resistance gene targets (*sul1*, *strA*, *strB*, *ermB*, *ermF*, *aadA*, and *bla<sub>OXA-20</sub>*) and the class 1 integron (*intI1*) in sediment DNA was quantified by qPCR with SYBR green or Taqman probe chemistry. All procedures, primers, quality control and standards for quantification were exactly as described in Lau et al. (2020). The identities of the quantified gene targets were verified on the basis of hybridization when using TaqMan chemistry, or melting behavior when using SYBR green. Gene abundances were expressed as a ratio with the total 16S rRNA gene copies.

## Data Analyses

All statistical analyses were performed with the R free software (version 3.4.3, R Core Team, 2018). After confirming normality of the residuals (Shapiro-Wilk test; Royston, 1982) and data homoscedasticity (Fligner-Killeen test; Conover et al., 1981), significant differences between sites and dates in the enzymatic activities, metabolic potentials, bacterial abundance, OTU richness and Shannon diversity index and genetic resistance potential were sought by analysis of variance (ANOVA) and further analyzed with a *post hoc* Tukey test. Differences were considered statistically significant when the *p*-value was below 0.05.

For bacteria and archaeal diversity, Bray-Curtis similarities (BC) between samples were calculated, and distances between samples were represented using a Principal Coordinates Analysis (PCoA) with R software (Vegan package). Functional-based community parameters (enzymatic and metabolic activities, metals and antibiotic resistance genes) were analyzed using a Principal Component Analysis (PCA). The significance of the sample groupings on the ordinations was tested using Analysis Of SIMilarity (ANOSIM). The relationship between community composition and functional-based structures (based on PCoA and PCA 2-dimension projections, respectively) were evaluated using a Procrustean analysis (using R software, Vegan package). Procrustean analyses superimpose, scale and rotate one data matrix upon the other until an optimal fit is found (Jackson and Harvey, 1993; Peres-Neto and Jackson, 2001; Heino et al., 2004). Estimated residuals between original values and the derived best fit solution give the *m*<sup>2</sup> statistic, with a low *m*<sup>2</sup> statistic indicating a good level of correspondence between data matrices (Paavola et al., 2006). The PROTEST permutation procedure (999 permutations) was used to assess the statistical significance of the Procrustean fit between the two matrices (Peres-Neto and Jackson, 2001; Paavola et al., 2006). Vectors of environmental variable data were fitted onto the procrustean analysis plot using the *envfit* function of the *vegan* package. This function calculates the goodness-of-fit values (*R*<sup>2</sup>) for environmental

variables onto the procrustean analysis plot and the significance of each correlation was tested based on 999 random permutations (Oksanen et al., 2020).

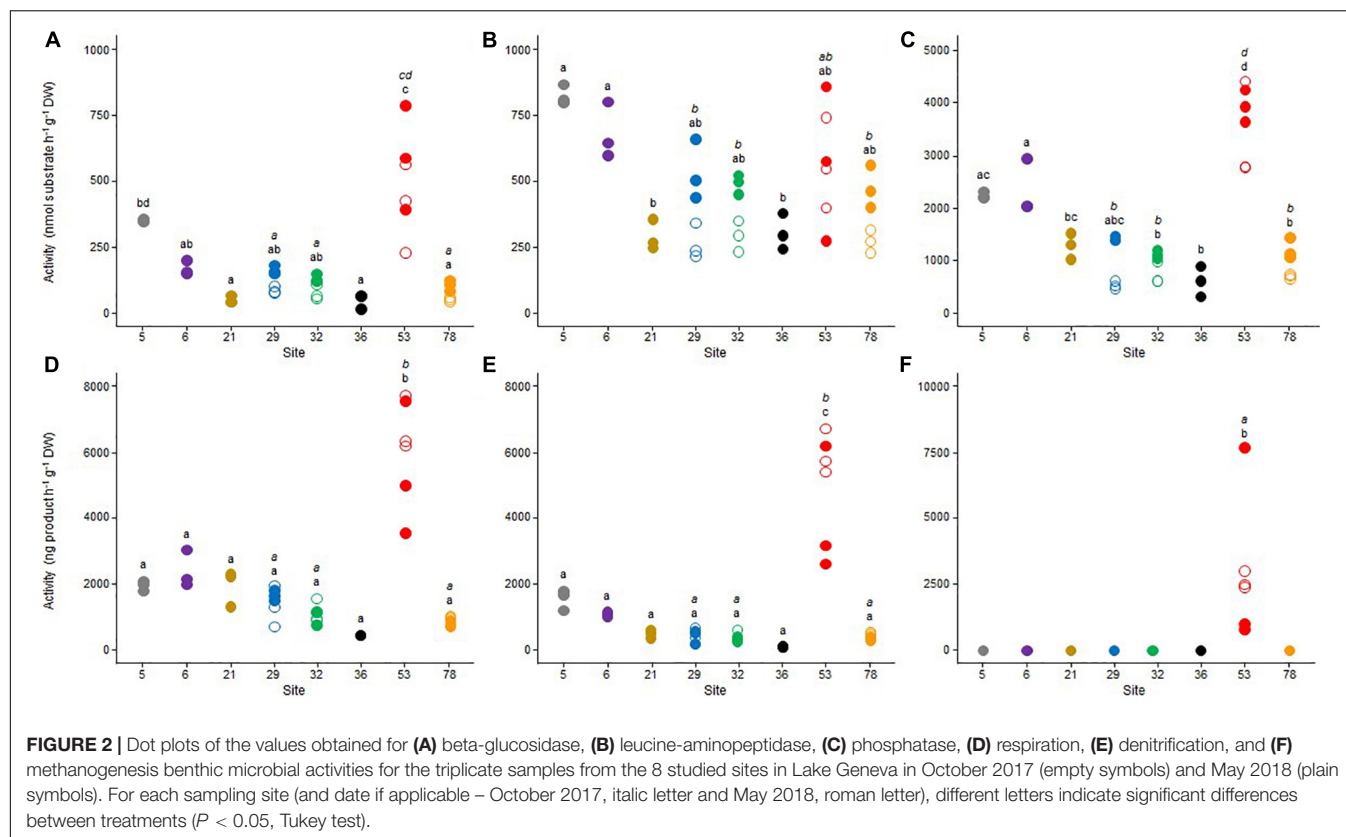
## RESULTS

### Environmental Conditions and Sediment Contamination at the Sampling Sites

The main sampling site characteristics are presented in Table 1. Surface sediments were collected at a sampling depth ranging from 22 m (site 32) to 95 m (site 29), and the median grain size varied from 8  $\mu$ m (sites 6 and 21) to 35  $\mu$ m (site 53). Sediments from the sites 53 and 78 had the highest and lowest organic matter content (13.6 and 2.7%, respectively) and total organic carbon (7.0 and 0.7%, respectively). These two sites were also characterized by lower carbonate content (about 14.4 and 19.7%, respectively) than the six other sites (i.e., 5, 6, 21, 29, 32, and 36) where it varied between 31.2% (site 29) and 48.9% (site 36). Total phosphorus concentrations were 4.5- to 7-fold higher in the site 53 (3900 mg kg<sup>-1</sup> dw) than in the seven other sites (659 to 849 mg kg<sup>-1</sup> dw). Sediments from the site 53 contained high total concentrations of metals (about 1193 mg kg<sup>-1</sup> dw) compared to the seven other ones, where it varied from 170 mg kg<sup>-1</sup> dw (site 36) to 322 mg kg<sup>-1</sup> dw (site 29). The high total concentration of metals in the site 53 was mainly due to zinc and copper (Zn and Cu, 645 and 281 mg kg<sup>-1</sup> dw, respectively; Supplementary Table 1). The sediments from site 78 contained high concentrations of titanium (Ti; 1736 mg kg<sup>-1</sup> dw) while for the other sites Ti concentrations ranged between 37 and 405 mg kg<sup>-1</sup> dw. The site 53 was also characterized by higher values for the sum of the seven indicator PCB ( $\Sigma$ 7PCBi) (387  $\mu$ g  $\Sigma$ 7PCBi kg<sup>-1</sup> dw): more than 400-fold higher than those observed in the site 78 (0.9  $\mu$ g  $\Sigma$ 7PCBi kg<sup>-1</sup> dw) and 36- to 75-fold higher than those observed in the six other sites (5.2–10.5  $\mu$ g  $\Sigma$ 7PCBi kg<sup>-1</sup> dw) (Supplementary Table 2). Sediments from sites 53 and 36 contained higher concentrations of PAH (25262  $\mu$ g kg<sup>-1</sup> dw and 13581  $\mu$ g kg<sup>-1</sup> dw, respectively) compared to the six other ones, where it varied from 774  $\mu$ g kg<sup>-1</sup> dw (site 78) to 2263  $\mu$ g kg<sup>-1</sup> dw (site 32) (Supplementary Table 3).

### Functional Potential

A set of potential microbial activities involved in the C cycle ( $\beta$ -glu, respiration, and methanogenesis), the N cycle (LAP and denitrification) and the P cycle (Pase) was measured (Figure 2). The results reflected a high spatial heterogeneity between the sampling sites. With the exception of the LAP activity (Figure 2B), sediment microbial communities from the site 53 exhibited the highest functional potential, both in October 2017 and May 2018. Methanogenesis activity (Figure 2F) was only detected in this site and  $\beta$ -glu (Figure 2A), Pase (Figure 2C), aerobic respiration (Figure 2D) and denitrification (Figure 2E) were also significantly higher than in the other sampling sites (*p* < 0.05). Significant but less marked spatial differences were also observed between the seven other sites (i.e., 5, 6, 21, 29, 32, 36, and 78) for the three enzymatic activities, which were



generally the highest in sites 5 and 6 and the lowest in sites 21 and 36 (Figures 2A–C). In contrast, no significant difference was observed between these seven sites for both aerobic respiration (Figure 2D) and denitrification (Figure 2E).

Seasonal variations between the two sampling periods were less pronounced in the four sites that have been sampled in 2017 and 2018 (i.e., 29, 32, 53, and 78). Significant differences ( $p < 0.05$ ) between October 2017 and May 2018 were only observed in site 53 for denitrification (Figure 2D) and methanogenesis (Figure 2E), with the highest values measured in October 2017.

## Microbial Community Structure

The mean bacterial abundance in the sample sediments ranged between  $0.55 \times 10^6$  to  $8.03 \times 10^6$  cells  $g^{-1}$  dw (Figure 3A). A high spatial variability was observed in October 2017, when the bacterial community from site 78 exhibited the highest abundance (about  $8.0 \times 10^6$  cells  $g^{-1}$  dw), which was about twice higher than the one measured in site 53, and threefold higher than those measured in sites 29 and 32. In these four sites, the bacterial abundance was reduced by about two- to fourfold between October 2017 and May 2018. In May 2018, abundances were more stable between the different sites, ranging from  $0.55 \times 10^6$  at site 36 to  $2.80 \times 10^6$  cells  $g^{-1}$  dw at site 78.

High-throughput amplicon sequencing of the 16S rRNA gene revealed no temporal difference in the number of OTUs affiliated to the archaea and bacteria domains (Figure 3B) and the resulting Shannon-Wiener diversity index (Figure 3C) between October

2017 and May 2018. Based on these two parameters, communities from site 53, and to a lesser extent, from site 78, exhibited the lowest diversity, whereas these two parameters were relatively similar between the six other sites. According to the sampling date and the sample replicate, the number of OTUs varied from 503 to 626 in site 53, from 947 to 1048 in site 78, and from 1067 to 1311 in the six other sites. The mean Shannon-Wiener diversity index was close to 4.0 ( $\pm 0.2$ ) in site 53, 4.9 ( $\pm 0.1$ ) in site 78, and between 5.4 and 5.8 in the six other sites.

At the Phylum (or Class for Proteobacteria) level, the microbial community was dominated by members of the Gammaproteobacteria ( $25.2 \pm 7.0\%$  of the reads), followed by members of the Bacteroidetes ( $19.4 \pm 6.9\%$ ), Deltaproteobacteria ( $13.1 \pm 5.4\%$ ), Nitrospirae ( $9.3 \pm 5.9\%$ ), and Acidobacteria ( $6.8 \pm 1.9\%$ ) (Figure 4). Community composition at site 53 was especially dominated by members of the Bacteroidetes (32%), Deltaproteobacteria (22%) and Gammaproteobacteria (20%), whereas at site 78, community composition was dominated by members of the Gammaproteobacteria (27%), Cyanobacteria (24%) and Bacteroidetes (23%). Site 5 community composition was characterized by the most important proportion of members of the Gammaproteobacteria (42%). Members of the Nitrospirae were present at low abundances at sites 53 (0.30%), 78 (4.23%) and 5 (8.05%), whereas they ranged between 11% (sites 29 and 32) and 18% (site 36). Among the less abundant groups, Actinobacteria, Chloroflexi, Nitrospirae, and other Archaea and Bacteria did not exhibit any temporal or spatial trends. For the main archaeal Phylum, Crenarchaeota peaked up to 4% at site

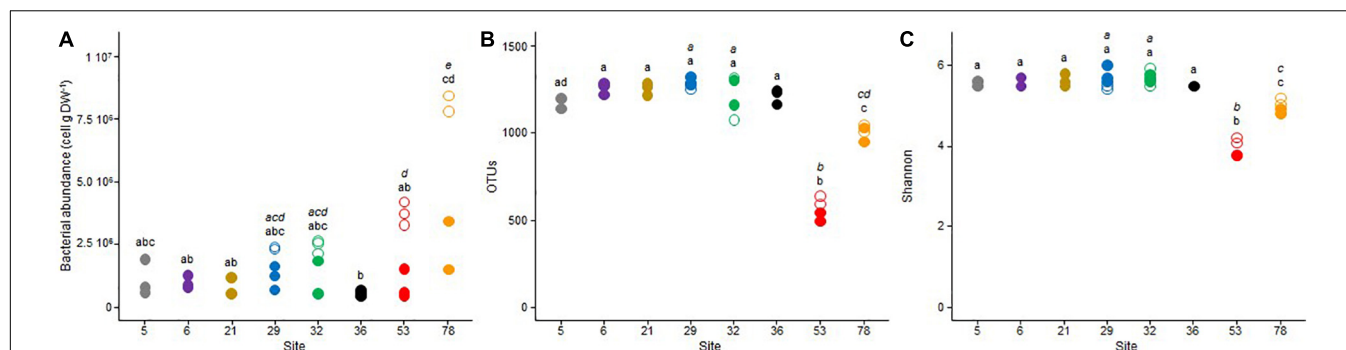


**FIGURE 3 |** Dot plots of the (A) bacterial abundance, (B) observed OTU richness, and (C) Shannon diversity index for the triplicate samples from the 8 studied sites in Lake Geneva in October 2017 (open symbols) and May 2018 (closed symbols). For each sampling site (and date if applicable – October 2017, italic letter and May 2018, roman letter), different letters indicate significant differences between treatments ( $P < 0.05$ , Tukey test).

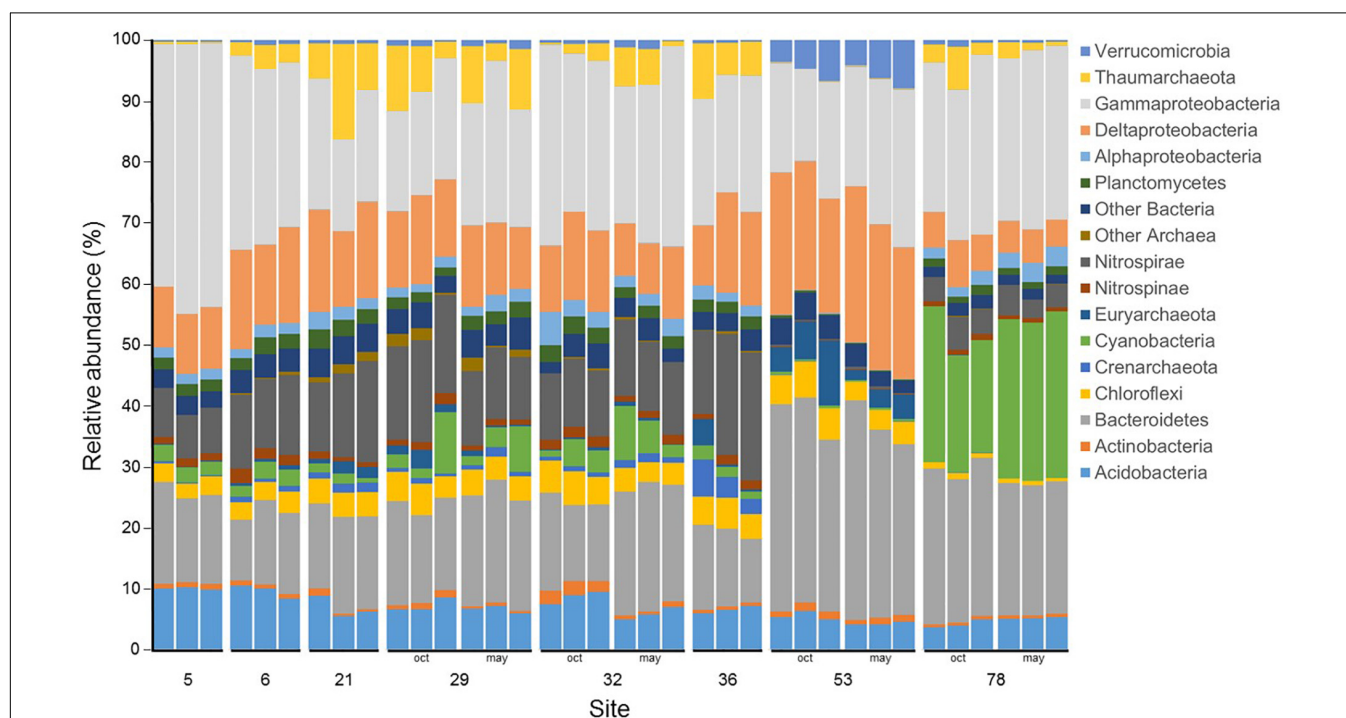


**FIGURE 4 |** Microbial community composition for the triplicate samples from the 8 studied sites in Lake Geneva in October 2017 and May 2018. The 15 more abundant phylum (or class for Proteobacteria) are represented and the remaining phylum (or class for Proteobacteria) are grouped under “Other Archaea” or “Other Bacteria”. Data is presented as relative abundance of the read counts.

36, but remained below 1.5% at other sites, Euryarchaeota were generally below 2% except at site 53 where they represented 7% of the community in October 2017 and 3% in May 2018, and Thaumarchaeota represented less than 0.5% of the community at sites 5 and 53 but between 2 and 10% elsewhere. Finally, Verrucomicrobia were below 1% in every samples but at site 53 where they accounted for 5 and 6% of the community in October 2017 and May 2018, respectively.

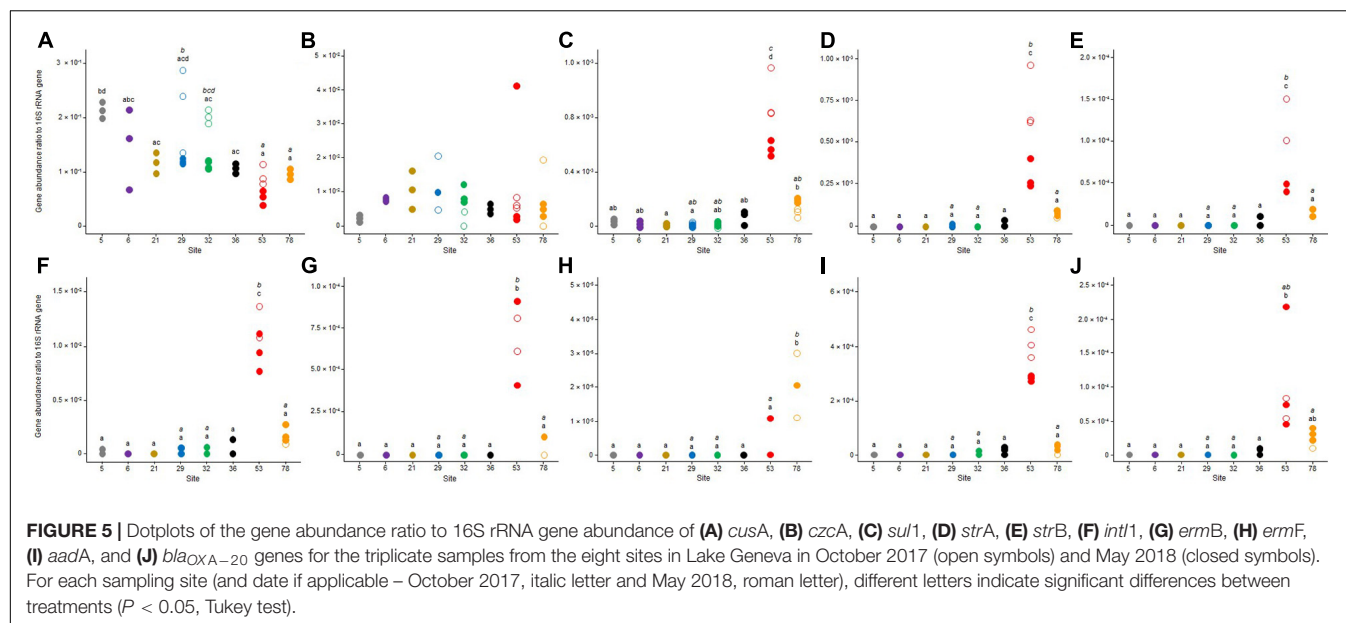
## Metal and Antibiotic Resistance Potential

Two distinct sets of quantitative PCRs were performed to, respectively, quantify two genes involved in microbial resistance

to metals (*cusA* and *czcA*, **Figures 5A,B**) and eight genes conferring antibiotic resistance (*sul1*, *strA*, *strB*, *ermB*, *ermF*, *aadA*, and *bla<sub>OXA20</sub>*), and the class 1 integron integrase *intI1* (**Figures 5C–J**).

Both metal resistance genes were detected in every site and the two sampling dates (**Figures 5A,B**). The *cusA* gene had the highest relative abundance with mean *cusA* to 16S rRNA gene relative abundances varying between about  $0.49 \times 10^{-3}$  to  $210 \times 10^{-3}$  depending on the sampling site and date (**Figure 5A**). No significant temporal variation was observed for this gene between the two sampling dates with the exception of sites 29 and 32 where mean values were about twofold higher ( $p < 0.05$ ).





in October 2017 than in May 2018. Spatial differences among the sites varied according to the sampling date. In October 2017, the relative abundance of *cusA* was significantly higher in sites 29 and 32 than in sites 53 and 78 ( $p < 0.05$ ). In May 2018, the highest relative abundance was observed in site 5 ( $204 \times 10^{-3} \pm 14 \times 10^{-3}$ ) with values significantly higher than those recorded in sites 21, 32, 36, 53, and 78 ( $p < 0.05$ ). The mean relative abundances of *czcA* to 16S rRNA varied between  $1.42 \times 10^{-3}$  and  $15.3 \times 10^{-3}$  with relatively high variations among replicates and no significant difference between sampling sites or between sampling dates (Figure 5B).

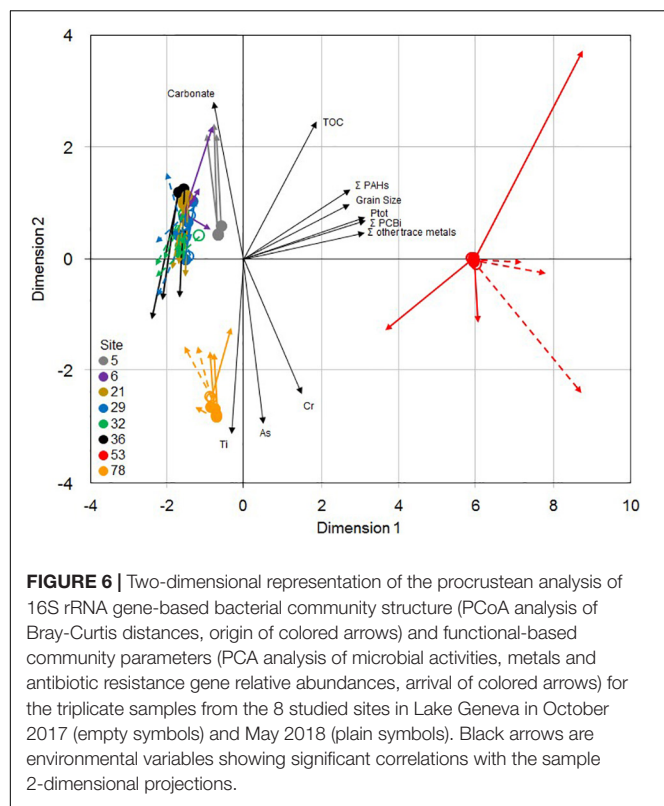
The eight genes for antibiotic resistance (Figures 5C–J) were less represented than *cusA* and *czcA*. The class 1 integron marker *int1* was detected in all samples with the highest relative abundances with mean values varying between  $98.7 \times 10^{-6}$  and  $11.2 \times 10^{-3}$  (Figure 5F). The genes *sul1*, *strA*, and *aadA* (Figures 5C,D,I) were also detected in all the samples but their highest relative abundance value was lower than  $1 \times 10^{-3}$ . The detection of *strB*, *ermB*, *ermF*, and *bla<sub>OXA-20</sub>* (Figures 5E,G,H,J) genes was variable according to sampling site, date and sample replicate, with mean relative abundances always lower than  $1 \times 10^{-4}$ . In addition to the difference among the measured genes, the results showed a high spatial heterogeneity among the sampling sites. The general tendency showed that sediment microbial communities from site 53, and to a lesser extent those from site 78, were characterized by higher relative abundances of the eight genes than the communities from the six other sites (i.e., 5, 6, 21, 29, 32, and 36). Indeed, sediment microbial communities collected in site 53 were characterized by the highest relative abundances of seven of the eight measured genes. The only exception was for the gene *ermF*, which was about threefold more represented in site 78 than in site 53 (Figure 5H). This gene was under the detection limit in the other sampling sites. At site 53, the other seven genes relative abundances were about 3- to 28-fold more abundant than in site 78 and about 30- to

2000-fold more abundant than at the 6 other sites. Moreover, no significant difference in the relative abundance of the eight genes conferring antibiotic resistance was observed in those sites (i.e., 5, 6, 21, 29, 32, and 36) (Figures 5C–J). No temporal variation was observed between the two sampling dates with the exception of site 53 where relative abundances were significantly higher in October 2017 than in May 2018 for the genes *sul1* (Figure 5C), *strA* (Figure 5D), *strB* (Figure 5E), *int1* (Figure 5F), and *aadA* (Figure 5I).

## Environmental Drivers of Microbial Structure and Functional-Based Parameters

The 2-dimensional representation of the procrustean analysis of 16S rRNA gene-based bacterial community structure (PCoA), the first 2 axes explained 74% of the variance) and functional-based community parameters (PCA, the first 2 axes explained 76% of the variance) (Figure 6) showed that sites 53 and 78 were distinct from each other, and from the six other sites (ANOSIM;  $p < 0.0001$  for PCoA, and  $p < 0.01$  for PCA), with very limited differences between the two sampling dates. Among these six sites, communities from site 5 were also slightly distinct both according to their structure and their functional parameters. The phylogenetic structure and the functional and resistance pattern of the communities displayed a highly significant level of concordance (Procrustean analysis, residual sum of squares = 0.340;  $m12 = 0.812$ ;  $p < 0.001$ ), as indicated by the relatively limited length of the colored arrows on the 2-dimension projection.

The sediment physico-chemical characteristics that were correlated with the microbial community ordinations (Figure 4 and Supplementary Table 4) were organic toxicants (PCB and PAH), phosphorus concentrations and median grain size, which were higher at site 53, some metals, which were high at sites 78



(As and Cr) and 53 (sum of Co, Ni, Cu, Zn, Mo, Ag, Cd, Sn, Pb, and Hg concentrations) and carbonate, which was lower at sites 53 and 78 (Table 1). Site 78 microbial community ordination was also significantly correlated to Ti concentration.

## DISCUSSION

This study investigated *in situ* the possible influence of the anthropogenic contamination of Lake Geneva surface sediments on benthic microbial communities by assessing spatiotemporal changes in their structure, their functional potential and their genetic potential for resistance to selected metals and antibiotics. Our results provide evidence that the multiple contaminants in sediments of Lake Geneva alter the diversity of microbial communities with consequences for the important ecological functions they provide. The magnitude of these effects depends on the types and the concentrations of contaminants in the sediments. All contaminant concentrations measured in the present study are in agreement with previous findings (Haller et al., 2011; Gascon Diez et al., 2014; Masson and Tercier-Waeber, 2014; Gascón Díez et al., 2017; Loizeau et al., 2017). In addition, our results also revealed high concentrations of PAH ( $>13.5 \mu\text{g kg}^{-1} \text{ dw}$ ) in sediments collected at site 36. Such a contamination was not reported in Loizeau et al. (2017) because organic toxicants (PAH and PCB) were not analyzed in this study site (and also not in sites 5 and 21). Our results suggest that the multi-contamination (PAH, PCB, metals, phosphorus, organic matter, and possibly microbial and genetic material) of

sediments observed in the Vidy Bay (site 53) is a strong driver of sediment microbial community structure and diversity, the latter being significantly lower than that at other sites. Some phyla were significantly less represented in the Vidy Bay, such as Planctomycetes, the *Nitrospira* genus from the phylum of Nitrospirae, whereas Euryarchaeota were mainly detected in this highly contaminated site. This archaeal phylum includes both the archaeal sulfide reducers as well as the methanogens (Chrencik and Marsh, 2012). Potential methanogenesis activity was only detected at this site, consistent with the observed abundance of methanogenic archaea, belonging to the *Methanobacterium*, *Methanolinea*, *Methanoregula*, *Methanosaeta*, *Methanosarcina* genera and to the *Methanomassiliicoccaceae* family.

In the present study, the Verrucomicrobia phylum was also more represented in the Vidy Bay than in the other sites, in contrast to previous findings (Haller et al., 2011). However, this is in line with other observations where this phylum was more abundant in very urbanized rivers than in suburban rivers (Lin et al., 2019). The urban contamination is also probably responsible for the observed higher relative abundance of members of the Bacteroidetes phylum, which includes bacteria from the human and animal gastrointestinal tract, frequently detected in wastewater, and generally considered as fecal indicators in the environment (Gomez-Donate et al., 2016; Su et al., 2017; Niestępski et al., 2020). In the Vidy Bay, fecal indicator bacteria and other activated sludge bacteria from local WWTP inputs were previously detected (Haller et al., 2009; Sauvain et al., 2014). Bacteroidetes are known to harbor a large variety of metal- or antibiotic-resistance genes that can favor their establishment and development in contaminated sediments (Chen et al., 2018; Niestępski et al., 2020). The higher abundance of gene markers associated with resistance to various classes of antibiotics (*sulI*, *strA*, *strB*, *ermB*, *ermF*, and *bla<sub>OXA-20</sub>*) and of the class 1 integron (*intI1*) detected in the Vidy Bay sediment is in accordance with the high occurrence of multiresistant bacteria and antibiotic-resistance genes previously reported at this site (Czekalski et al., 2012, 2014). Reporting in 2011 a 200-fold increase of the relative abundances of six antibiotic-resistance genes (including *sulI*) as compared to sediment sampled in the center of the lake, Czekalski et al. (2014) hypothesized that the increasing abundance of antibiotic-resistance genes was mainly due to direct inputs from wastewater effluents rather than *in situ* development of antibiotic-resistant bacteria in the lake sediment following their chronic exposure to contaminants. In the present study, given the high metal concentrations observed in the surface sediment from the Vidy Bay, the hypothesis of co-selection of antibiotic resistance by this kind of contaminant cannot be excluded (Poole, 2017; Silva et al., 2021). Although pharmaceutical residues in the collected sediments were not analyzed it is more than probable that site 53 sediment were contaminated by antibiotics (Morasch et al., 2010; Bonvin et al., 2011, 2013), potentially favoring the development of antibiotic resistance in sediment communities in response to antibiotic selection pressure (Bengtsson-Palme and Larsson, 2016). In contrast, the analysis of the metal-resistance genes *cusA* (involved in copper resistance) and *czcA* (involved in cobalt-zinc-cadmium resistance) did not show higher relative

abundances in the Vidy Bay, even if this site had the highest concentrations of Cu (about 281 mg kg<sup>-1</sup> dw), Zn (about 645 mg kg<sup>-1</sup> dw) and Cd (about 1.5 mg kg<sup>-1</sup> dw), which were 3- to 12-fold higher than the contamination with these three metals in the seven other stations. Significant increases in the relative abundance of the *cusA* and *czcA* genes in contaminated sediments compared to uncontaminated ones has been previously reported by Besaury et al. (2013) and Roosa et al. (2014). In both cases, however, the level of metal contamination was very high (total Cu > 1400 mg kg<sup>-1</sup>, Besaury et al., 2013; total Zn > 3000 mg kg<sup>-1</sup> and Cd > 35 mg kg<sup>-1</sup>, Roosa et al., 2014), as was the potential metal bioavailability. Altogether, these results question whether the qPCR quantification of these metal resistance genes is sensitive enough when contamination gradients are weak, or whether metal bioavailability in the Vidy Bay is poor and causes limited selection pressure.

More surprisingly, a notable and sometimes significant increase in the relative abundance of antibiotic-resistance genes was observed in the site 78 in comparison to the other sites other than the Vidy Bay one. This was especially the case for the *ermB* and *ermF* genes, responsible for erythromycin resistance, which were only (*ermF*) or mainly (*ermB*) detected in site 53 and 78. It cannot be excluded that the surface sediment from the site 78 has been directly contaminated by antibiotic-resistant bacteria and/or antibiotics coming from the upper section of the Rhône River, which has been shown to be an important source of contamination of Lake Geneva with pharmaceutical substances (Loizeau et al., 2013). In this site, benthic microbial richness and diversity index was impacted, being 10 to 20% lower than those observed in the other sites (excluding 53) and community composition was also affected. The relative abundance of Bacteroidetes members could also confirm inputs from sewage water located in the upper Rhône section (see related discussion above for site 53). Cyanobacteria were also significantly more represented at site 78 than the other sites, showing that this kind of microorganisms was particularly adapted to the local site characteristics. Given the water column height at this site and associated limited light penetration, it is unlikely that these microorganisms are part of a microbial mat developing at the sediment – water interface, but nutrients flowing in from the Rhône River might promote their planktonic growth following which they are deposited into sediment. Previous studies (Loizeau et al., 2012; Silva et al., 2019) found that sediment accumulation was 5- to 10-fold more rapid at this site compared to other areas of the lake.

Despite their geographical distance and their notable differences in depth and other physico-chemical characteristics, such as total organic carbon or grain size, the sediment communities collected in the less contaminated sites (i.e., 5, 6, 21, 29, and 32) and at site 36, only contaminated by high concentrations of PAH, exhibited relatively comparable structural and functional properties. All these sampling sites (as well as sites 53 and 78) had a depth below 100 m out of the 309 m of maximal depth for Lake Geneva. Extrapolation of the probe sensor data collected for the environmental survey of Lake Geneva at the deepest site indicated that water temperature at the sediment interface varied between 6 and 14°C in October

2017 and was about 6–7°C in Mai 2018, and that dissolved oxygen concentrations increased from between 6 and 8 mg L<sup>-1</sup> in October 2017 and between 9 and 12 mg L<sup>-1</sup> in May 2018 (Rimet et al., 2020), because of the first 201 m water column partial turnover on March 6, 2018 (CIPEL, 2019). Even if this data should be interpreted with care since it might not perfectly reflect the local conditions prevailing at sampling sites, whatever the measured parameter, no significant difference was observed between the sediment microbial communities collected in the shallowest (22 m; site 32) and deepest (95 m, site 29) sites. As revealed by the multivariate analysis (Figure 6), it confirms that depth, and indirectly related environmental parameters such as dissolved oxygen, light intensity, temperature, and nutrient availability (Böer et al., 2009), was not a major driver of benthic microbial community structure and functions in Lake Geneva, in contrast to other studies that linked microbial community structure changes with water depth (Edlund et al., 2006; Hewson et al., 2007; Zhang et al., 2014; Ding et al., 2015; Ruuskanen et al., 2018; Wu et al., 2019). The only observed differences between sites 5, 6, 21, 29, 32, and 36 concerned the enzymatic activities ( $\beta$ -glu, LAP, and Pase), which were higher at site 5, and to a lesser extent, at site 6. This difference could be explained, at least partly, by a higher amount of available substrates, as suggested by the higher organic matter and total organic carbon contents measured in these samples. Based on these results, it can be argued that the contamination of the sediment with high concentrations of PAH at site 36 (>13.5 mg  $\Sigma$ PAH kg<sup>-1</sup> dw) exerts no or very limited effects on the functional potential, the structure and the composition of the microbial communities, which were almost similar to those from sites characterized by 6- to 12-fold lower PAH concentrations. The limited effects of chronic PAH contamination on sediment microbial community diversity and functions has likewise been observed in coastal ecosystems (Hernandez-Raquet et al., 2006; Païssé et al., 2008; Zhang et al., 2008; Jeanbille et al., 2016), in contrast to the more important influence of other contaminants such as metals (Sun et al., 2012, 2013). The small effect of PAHs could be due to their limited toxicity (Païssé et al., 2010) and/or their limited bioavailability because of their ready sorption to sediments (Kraaij et al., 2002; Ghosh et al., 2003).

Despite the evident negative effects of the anthropogenic contamination on the diversity of sediment microbial communities of sites 53 and 78, no inhibition in their functional potential was observed. On the contrary, communities from site 53 exhibited the highest potential for most of the measured activities (i.e.,  $\beta$ -glu, Pase, aerobic respiration, denitrification and methanogenesis). It suggests that the observed shifts in their community composition reflects a long-term selection of benthic microbial species that are strongly adapted to their environment, allowing them to benefit from the regular inputs of nutrients and organic substrates that can be used as energy sources, thus making them key players in benthic biogeochemical cycles (Huang et al., 2019; Steinsberger et al., 2019). This long-term adaptation hypothesis can be supported by the very limited temporal variations that were observed in the present study between the two sampling dates. Indeed, at the four sites sampled twice (i.e., 29, 32, 53, and 78), sediment community diversity and

composition were very similar in October 2017 and May 2018, as illustrated in the multivariate analysis (Figure 6). It suggests, that, the structural characteristics of the surface sediment microbial communities of Lake Geneva are relatively stable over time, unlike the case for shallower lakes (Peng et al., 2017; Wan et al., 2017; Zhang et al., 2019).

## CONCLUSION

Using a whole lake approach, the present study highlighted that surface sediment microbial communities were impacted by anthropogenic load of contaminants including toxicants, organic matter, nutrients, and microorganisms in wastewater discharge affecting their diversity, enzymatic and metabolic functional potential as well as their genetic potential resistance to antimicrobial agents. These forcing factors appeared to yield to a more important structuration of the microbial parameters studied than the classical environmental factors generally controlling microbial diversity in lakes.

Given the ecological role of microbial communities in lake sediments, further research to better understand the consequences of anthropogenic contamination on microbial communities should focus on larger scale approaches, including more sites to cover a finer gradient of contamination in order to distinguish the relative importance of the different type of contaminants, integrating the full range of water depths from the littoral to the deeper areas, and considering a more important depth of the sediment compartment to take into account the full range of metabolic activities carried out. Together this would improve the ecotoxicological assessment of sediments in lake ecosystems to understand the consequences of multiple stress at the community level on microbial key activities and functions.

## DATA AVAILABILITY STATEMENT

The datasets presented in this study can be found in the NCBI at <https://www.ncbi.nlm.nih.gov/sra/PRJNA742879>.

## REFERENCES

- Altschul, S. F., Gish, W., Miller, W., Myers, E. W., and Lipman, D. J. (1990). Basic local alignment search tool. *J. Mol. Biol.* 215, 403–410. doi: 10.1016/S0022-2836(05)80360-2
- Bedard, D. L. (2008). A case study for microbial biodegradation: anaerobic bacterial reductive dechlorination of polychlorinated biphenyls – from sediment to defined medium. *Annu. Rev. Microbiol.* 62, 253–270. doi: 10.1146/annurev.micro.62.081307.162733
- Bengtsson-Palme, J., and Larsson, D. G. (2016). Concentrations of antibiotics predicted to select for resistant bacteria: proposed limits for environmental regulation. *Environ. Int.* 86, 140–149. doi: 10.1016/j.envint.2015.10.015
- Besaury, L., Bodilis, J., Delgas, F., Andrade, S., De la Iglesia, R., Ouddane, B., et al. (2013). Abundance and diversity of copper resistance genes *cusA* and *copA* in microbial communities in relation to the impact of copper on Chilean marine sediments. *Mar. Pollut. Bull.* 67, 16–25. doi: 10.1016/j.marpolbul.2012.12.007

## AUTHOR CONTRIBUTIONS

BF and SP conceived and designed the study. EL, J-LL, BF, and SP organized and performed the sampling. EL, CB, PB, AT, and ET were responsible for the microbial analyses. J-LL, EN, and BF were responsible for the physico-chemical analyses. EL conducted the bioinformatic and biostatistical analyses. EL and SP drafted the first version of the manuscript. All co-authors analyzed and interpreted the data, contributed to subsequent revisions to the manuscript, and approved its final submitted version.

## FUNDING

This study was partly funded by a grant of the Auvergne-Rhône-Alpes Region (CMIRA COOPERA 2016–2018 Project) and by the European Cross-Border Cooperation Program (Interreg France-Switzerland 2014–2020, SYNAQUA).

## ACKNOWLEDGMENTS

We are grateful to all the staff who have contributed to the sampling campaigns: the boat skippers, Philippe Arpagaus and Jean-Christophe Hustache, and the colleagues who collected and prepared the samples, Anaïs Charton, Christina Lüthi, Bernard Motte, Amélie Roinat, Régis Vivien, and Sandrine Vix. We thank all the persons who realized microbial and physico-chemical analyses: Anaïs Charton, Bernard Motte, Christophe Rosy, Bernadette Volat, Bettina Wagner, and Yuan-Ching Tien. We also thank OLA-IS, AnaEE-France, INRAE of Thonon-les-Bains, CIPEL for providing probe data at site SHL2.

## SUPPLEMENTARY MATERIAL

The Supplementary Material for this article can be found online at: <https://www.frontiersin.org/articles/10.3389/fmicb.2021.738629/full#supplementary-material>

- Böer, S. I., Hedtkamp, S. I. C., Van Beusekom, J. E. E., Fuhrman, J. A., Boetius, A., and Ramette, A. (2009). Time- and sediment depth-related variations in bacterial diversity and community structure in subtidal sands. *ISME J.* 3, 780–791. doi: 10.1038/ismej.2009.29
- Bolger, A. M., Lohse, M., and Usadel, B. (2014). Trimmomatic: a flexible trimmer for Illumina sequence data. *Bioinformatics* 30, 2114–2120. doi: 10.1093/bioinformatics/btu170
- Bonvin, F., Razmi, A. M., Barry, D. A., and Kohn, T. (2013). A coupled hydrodynamic-photolysis model to simulate the fate of micropollutants in Vidy Bay. *Environ. Sci. Technol.* 47, 9207–9216. doi: 10.1021/es401294c
- Bonvin, F., Rutler, R., Chèvre, N., Halder, J., and Kohn, T. (2011). Spatial and temporal presence of a wastewater-derived micropollutant plume in Lake Geneva. *Environ. Sci. Technol.* 45, 4702–4709. doi: 10.1021/es2003588
- Burrus, D., Thomas, R. L., Dominik, B., Vernet, J.-P., and Dominik, J. (1990). Characteristics of suspended sediment in the upper Rhone River, Switzerland, including the particulate forms of phosphorus. *Hydrol. Process.* 4, 85–92. doi: 10.1002/hyp.3360040108



- Cébron, A., Norini, M. P., Beguistain, T., and Leyval, C. (2008). Real-Time PCR quantification of PAH-ring hydroxylating dioxygenase (PAH-RHD $\alpha$ ) genes from Gram positive and Gram negative bacteria in soil and sediment samples. *J. Microbiol. Methods* 73, 148–159. doi: 10.1016/j.mimet.2008.01.009
- Chen, Y., Jiang, Y., Huang, H., and Mou, L. (2018). Long-term and high-concentration heavy-metal contamination strongly influences the microbiome and functional genes in Yellow River sediments. *Sci. Total Environ.* 637–638, 1400–1412. doi: 10.1016/j.scitotenv.2018.05.109
- Chrencik, B. J., and Marsh, T. L. (2012). “Contributions of methanogenic Archaeobacteria in community-driven anaerobic chromate reduction by Yellowstone National Park hot spring microorganisms,” in *Microbes in Applied Research: Current Advances and Challenges*, ed. A. Méndez-Vilas (Singapore: World Scientific), 60–64. doi: 10.1142/9789814405041\_0012
- CIPEL (2018). *Rapports sur les études et Recherches Entreprises dans le Bassin Lémanique, Campagne 2017*. Nyon: Commission Internationale Pour la Protection des Eaux du Léman, 196.
- CIPEL (2019). *Rapports sur les études et Recherches Entreprises dans le Bassin Lémanique, Campagne 2018*. Nyon: Commission internationale pour la protection des eaux du Léman, 305.
- Codling, G., Sturchio, N. C., Rockne, K. J., Li, A., Peng, H., Tse, T. J., et al. (2018). Spatial and temporal trends in poly- and per-fluorinated compounds in the Laurentian Great Lakes Erie, Ontario and St. Clair. *Environ. Pollut.* 237, 396–405. doi: 10.1016/j.envpol.2018.02.013
- Conover, W. J., Johnson, M. E., and Johnson, M. M. (1981). A comparative study of tests for homogeneity of variances, with applications to the outer continental shelf bidding data. *Am. Stat.* 35, 351–361. doi: 10.2307/1268225
- Czekalski, N., Berthold, T., Caucci, S., Egli, A., and Bürgmann, H. (2012). Increased levels of multiresistant bacteria and resistance genes after wastewater treatment and their dissemination into Lake Geneva, Switzerland. *Front. Microbiol.* 3:106. doi: 10.3389/fmicb.2012.00106
- Czekalski, N., Gascón Díez, E., and Bürgmann, H. (2014). Wastewater as a point source of antibiotic-resistance genes in the sediment of a freshwater lake. *ISME J.* 8, 1381–1390. doi: 10.1038/ismej.2014.8
- Dean, W. E. (1974). Determination of carbonate and organic matter in calcareous sediments and sedimentary rocks by loss on ignition; comparison with other methods. *J. Sediment. Res.* 44, 242–248. doi: 10.1306/74D729D2-2B21-11D7-8648000102C1865D
- Diepens, N. J., Dimitrov, M. R., Koelmans, A. A., and Smidt, H. (2015). Molecular assessment of bacterial community dynamics and functional end points during sediment bioaccumulation tests. *Environ. Sci. Technol.* 49, 13586–13595. doi: 10.1021/acs.est.5b02992
- Ding, X., Peng, X. J., Jin, B. S., Xiao, M., Chen, J. K., Li, B., et al. (2015). Spatial distribution of bacterial communities driven by multiple environmental factors in a beach wetland of the largest freshwater lake in China. *Front. Microbiol.* 6:129. doi: 10.3389/fmicb.2015.00129
- Edlund, A., Soule, T., Sjöling, S., and Jansson, J. K. (2006). Microbial community structure in polluted Baltic Sea sediments. *Environ. Microbiol.* 8, 223–232. doi: 10.1111/j.1462-2920.2005.00887.x
- Escudé, F., Auer, L., Bernard, M., Mariadassou, M., Cauquil, L., Vidal, K., et al. (2018). FROGS: find, rapidly, OTUs with Galaxy solution. *Bioinformatics* 34, 1287–1294. doi: 10.1093/bioinformatics/btx791
- Foulquier, A., Volat, B., Neyra, M., Bornette, G., and Montuelle, B. (2013). Long-term impact of hydrological regime on structure and functions of microbial communities in riverine wetland sediments. *FEMS Microbiol. Ecol.* 85, 211–226. doi: 10.1111/1574-6941.12112
- Frossard, A., Gerull, L., Mutz, M., and Gessner, M. O. (2012). Disconnect of microbial structure and function: enzyme activities and bacterial communities in nascent stream corridors. *ISME J.* 6, 680–691. doi: 10.1038/ismej.2011.134
- Gascon Díez, E., Bravo, A. G., à Porta, N., Masson, M., Graham, N. D., Stoll, S., et al. (2014). Influence of a wastewater treatment plant on mercury contamination and sediment characteristics in Vidy Bay (Lake Geneva, Switzerland). *Aquat. Sci.* 76, 21–32. doi: 10.1007/s00027-013-0325-4
- Gascón Díez, E., Corella, J. P., Adatte, T., Thevenon, F., and Loizeau, J.-L. (2017). High-resolution reconstruction of the 20th century history of trace metals, major elements, and organic matter in sediments in a contaminated area of Lake Geneva, Switzerland. *Appl. Geochem.* 78, 1–11. doi: 10.1016/j.apgeochem.2016.12.007
- Ghosh, U., Zimmerman, J. R., and Luthy, R. G. (2003). PCB and PAH speciation among particle types in contaminated harbor sediments and effects on PAH bioavailability. *Environ. Sci. Technol.* 37, 2209–2217. doi: 10.1021/es020833k
- Golovko, O., Rehrl, A. L., Köhler, S., and Ahrens, L. (2020). Organic micropollutants in water and sediment from Lake Mälaren, Sweden. *Chemosphere* 258:127293. doi: 10.1016/j.chemosphere.2020.127293
- Gomez-Donate, M., Casanovas-Massana, A., Muniesa, M., and Blanch, A. R. (2016). Development of new host-specific *Bacteroides* qPCRs for the identification of fecal contamination sources in water. *Microbiologyopen* 5, 83–94. doi: 10.1002/mbo3.313
- Grandjean, D., De Alencastro, L. F., and Tarradellas, J. (1990). Micropollutants organiques dans les effluents des stations d'épuration, les eaux du Rhône et les eaux du Léman. *Rapp. Comm. int. prot. eaux Léman contre pollut. Campagne* 1989, 199–212.
- Haglund, A. L., Lantz, P., Törnblom, E., and Tranvik, L. (2003). Depth distribution of active bacteria and bacterial activity in lake sediment. *FEMS Microbiol. Ecol.* 46, 31–38. doi: 10.1016/S0168-6496(03)00190-9
- Haller, L., Poté, J., Loizeau, J.-L., and Wildi, W. (2009). Distribution and survival of faecal indicator bacteria in the sediments of the Bay of Vidy, Lake Geneva, Switzerland. *Ecol. Indic.* 9, 540–547. doi: 10.1016/j.ecolind.2008.08.001
- Haller, L., Tonolla, M., Zopfi, J., Peduzzi, R., Wildi, W., and Poté, J. (2011). Composition of bacterial and archaeal communities in freshwater sediments with different contamination levels (Lake Geneva, Switzerland). *Water Res.* 45, 1213–1228. doi: 10.1016/j.watres.2010.11.018
- Harwood, J. E., Van Steenderen, R. A., and Kühn, A. L. (1969). A comparison of some methods for total phosphate analyses. *Water Res.* 3, 425–432. doi: 10.1016/0043-1354(69)90004-9
- Heino, J., Louhi, P., and Muotka, T. (2004). Identifying the scales of variability in stream macroinvertebrate abundance, functional composition and assemblage structure. *Freshw. Biol.* 49, 1230–1239. doi: 10.1111/j.1365-2427.2004.01259.x
- Hernandez-Raquet, G., Budzinski, H., Caumette, P., Dabert, P., Le Ménach, K., Muyzer, G., et al. (2006). Molecular diversity studies of bacterial communities of oil polluted microbial mats from the Etang de Berre (France). *FEMS Microbiol. Ecol.* 58, 550–562. doi: 10.1111/j.1574-6941.2006.00187.x
- Hewson, I., Jacobson-Meyers, M. E., and Fuhrman, J. A. (2007). Diversity and biogeography of bacterial assemblages in surface sediments across the San Pedro Basin, Southern California Borderlands. *Environ. Microbiol.* 9, 923–933. doi: 10.1111/j.1462-2920.2006.01214.x
- Hoerger, C. C., Akhtman, Y., Martelletti, L., Rutler, R., Bonvin, F., Grange, A., et al. (2014). Spatial extent and ecotoxicological risk assessment of a micropollutant-contaminated wastewater plume in Lake Geneva. *Aquat. Sci.* 76, 7–19. doi: 10.1007/s00027-013-0315-6
- Huang, C., Chen, Z., Gao, Y., Luo, Y., Huang, T., Zhu, A., et al. (2019). Enhanced mineralization of sedimentary organic carbon induced by excess carbon from phytoplankton in a eutrophic plateau lake. *J. Soils Sediments* 19, 2613–2623. doi: 10.1007/s11368-019-02261-2
- Jackson, D., and Harvey, H. (1993). Fish and benthic invertebrates: community concordance and community–environment relationships. *Can. J. Fish. Aquat. Sci.* 50, 2641–2651. doi: 10.1139/f93-287
- Jeanbille, M., Gur, J., Duran, R., Tronczynski, J., Ghiglione, J. F., Agogue, H., et al. (2016). Chronic polyaromatic hydrocarbon (PAH) contamination is a marginal driver for community diversity and prokaryotic predicted functioning in coastal sediments. *Front. Microbiol.* 7:1303. doi: 10.3389/fmicb.2016.01303
- Jin, X., Ma, Y., Kong, Z., Kou, W., and Wu, L. (2019). The variation of sediment bacterial community in response to anthropogenic disturbances of Poyang Lake, China. *Wetlands* 39, 63–73. doi: 10.1007/s13157-017-0909-1
- Kozich, J. J., Westcott, S. L., Baxter, N. T., Highlander, S. K., and Schloss, P. D. (2013). Development of a dual-index sequencing strategy and curation pipeline for analyzing amplicon sequence data on the miseq illumina sequencing platform. *Appl. Environ. Microbiol.* 79, 5112–5120. doi: 10.1128/AEM.01043-13
- Kraaij, R., Seinen, W., Tolls, J., Cornelissen, G., and Belfroid, A. C. (2002). Direct evidence of sequestration in sediments affecting the bioavailability of hydrophobic organic chemicals to benthic deposit-feeders. *Environ. Sci. Technol.* 36, 3525–3529. doi: 10.1021/es0102787
- Krzmarzick, M. J., McNamara, P. J., Crary, B. B., and Novak, P. J. (2013). Abundance and diversity of organohalide-respiring bacteria in lake sediments across a geographical sulfur gradient. *FEMS Microbiol. Ecol.* 84, 248–258. doi: 10.1111/1574-6941.12059

- Larras, F., Rimet, F., Gregorio, V., Bérard, A., Le Boulanger, C., Montuelle, B., et al. (2016). Pollution-induced community tolerance (PICT) as a tool for monitoring Lake Geneva long-term in situ ecotoxic restoration from herbicide contamination. *Environ. Sci. Pollut. Res.* 23, 4301–4311. doi: 10.1007/s11356-015-5302-0
- Lau, C. H., Tien, Y. C., Stedtfeld, R. D., and Topp, E. (2020). Impacts of multi-year field exposure of agricultural soil to macrolide antibiotics on the abundance of antibiotic resistance genes and selected mobile genetic elements. *Sci. Total Environ.* 727:138520. doi: 10.1016/j.scitotenv.2020.138520
- Lécrivain, N., Aurenche, V., Cottin, N., Frossard, V., and Clément, B. (2018). Multi-contamination (heavy metals, polychlorinated biphenyls and polycyclic aromatic hydrocarbons) of littoral sediments and the associated ecological risk assessment in a large lake in France (Lake Bourget). *Sci. Total Environ.* 619–620, 854–865. doi: 10.1016/j.scitotenv.2017.11.151
- Lécrivain, N., Frossard, V., Naffrechoux, E., and Clément, B. (2019). Looking at organic pollutants (OPs) signatures in littoral sediments to assess the influence of a local urban source at the whole lake scale. *Polycycl. Aromat. Compd.* 41, 950–962. doi: 10.1080/10406638.2019.1631195
- Lin, X., Gao, D., Lu, K., and Li, X. (2019). Bacterial community shifts driven by nitrogen pollution in river sediments of a highly urbanized city. *Int. J. Environ. Res. Public Health* 16:3794. doi: 10.3390/ijerph16203794
- Loizeau, J.-L., Arbouille, D., Santiago, S., and Vernet, J.-P. (1994). Evaluation of a wide-range laser diffraction grain-size analyzer for use with sediments. *Sedimentology* 41, 353–361. doi: 10.1111/j.1365-3091.1994.tb01410.x
- Loizeau, J.-L., Edler, P., De Alencastro, L. F., Corvi, C., and Ramseier Gentile, S. (2013). Lake Geneva pollution by micropollutants – a review of 40 years of study [La contamination du Léman par les micropolluants Revue de 40 ans d'études]. *Arch. Sci.* 66, 117–136.
- Loizeau, J.-L., Girardclos, S., and Dominik, J. (2012). Taux d'accumulation de sédiments récents et bilan de la matière particulaire dans le Léman (Suisse-France). *Arch. Sci.* 65, 81–92.
- Loizeau, J. L., Makri, S., Arpagaus, P., Ferrari, B., Casado-Martinez, C., Benejam, T., et al. (2017). Micropollutants métalliques et organiques dans les sédiments superficiel du Léman. Metallic and organic micropollutants in the surface sediments of Lake Geneva. *Rapp. Comm. Int. Prot. Eaux Léman contre Pollut. Campagne* 2016, 153–207. pdf.
- Magoë, T., and Salzberg, S. L. (2011). FLASH: fast length adjustment of short reads to improve genome assemblies. *Bioinformatics* 27, 2957–2963. doi: 10.1093/bioinformatics/btr507
- Mahamoud Ahmed, A., Lyautey, E., Bonninaeu, C., Dabrin, A., and Pesce, S. (2018). Environmental concentrations of copper, alone or in mixture with arsenic, can impact river sediment microbial community structure and functions. *Front. Microbiol.* 9:1852. doi: 10.3389/fmicb.2018.01852
- Mahamoud Ahmed, A., Tardy, V., Bonninaeu, C., Billard, P., Pesce, S., and Lyautey, E. (2020). Changes in sediment microbial diversity following chronic copper-exposure induce community copper-tolerance without increasing sensitivity to arsenic. *J. Hazard. Mater.* 391:122197. doi: 10.1016/j.jhazmat.2020.122197
- Mahé, F., Rognes, T., Quince, C., de Vargas, C., and Dunthorn, M. (2015). Swarm v2: highly scalable and high-resolution amplicon clustering. *Peer J.* 3:e1420. doi: 10.7717/peerj.1420
- Marvin, C., Painter, S., Williams, D., Richardson, V., Rossmann, R., and Van Hoof, P. (2004). Spatial and temporal trends in surface water and sediment contamination in the Laurentian Great Lakes. *Environ. Pollut.* 129, 131–144. doi: 10.1016/j.envpol.2003.09.029
- Masson, M., and Tercier-Waeber, M.-L. (2014). Trace metal speciation at the sediment-water interface of Vidy Bay: influence of contrasting sediment characteristics. *Aquat. Sci.* 76, 47–58. doi: 10.1007/s00027-013-0323-6
- Morasch, B., Bonvin, F., Reiser, H., Grandjean, D., de Alencastro, L. F., Perazzolo, C., et al. (2010). Occurrence and fate of micropollutants in the Vidy Bay of Lake Geneva, Switzerland. Part II: micropollutant removal between wastewater and raw drinking water. *Environ. Toxicol. Chem.* 29, 1658–1668. doi: 10.1002/etc.222
- Murphy, J., and Riley, J. P. (1962). A modified single solution method for the determination of phosphate in natural waters. *Anal. Chim. Acta* 27, 31–36. doi: 10.1016/S0003-2670(00)88444-5
- Mwanamoki, P., Devarajan, N., Thevenon, F., Birane, N., De Alencastro, L., Grandjean, D., et al. (2014). Trace metals and persistent organic pollutants in sediments from river-reservoir systems in Democratic Republic of Congo (DRC): spatial distribution and potential ecotoxicological effects. *Chemosphere* 111, 485–492. doi: 10.1016/j.chemosphere.2014.04.083
- Niestępski, S., Harnisz, M., Ciesielski, S., Korzeniewska, E., and Osińska, A. (2020). Environmental fate of Bacteroidetes, with particular emphasis on *Bacteroides fragilis* group bacteria and their specific antibiotic resistance genes, in activated sludge wastewater treatment plants. *J. Hazard. Mater.* 394:122544. doi: 10.1016/j.jhazmat.2020.122544
- Office Fédéral de l'environnement [OFEV] (1998). *Ordonnance du 1er Juillet 1998 sur les Atteintes Portées aux Sols (OSol)*. N° RS 814.12. Berne: OFEV.
- Oksanen, J., Blanchet, F. G., Kindt, R., Legendre, P., McGlin, D., Minchin, P. R., et al. (2020). *vegan: Community Ecology Package*. R Package Version 2.5-7. Available online at: <https://CRAN.R-project.org/package=vegan>
- Paavola, R., Muotka, T., Virtanen, R., Heino, J., Jackson, D., and Mäki-Petäys, A. (2006). Spatial scale affects community concordance among fishes, benthic macroinvertebrates, and bryophytes in streams. *Ecol. Appl.* 16, 368–379. doi: 10.1890/03-5410
- Paissé, S., Coulon, F., Goñi-Urriza, M., Peperzak, L., McGenity, T. J., and Duran, R. (2008). Structure of bacterial communities along a hydrocarbon contamination gradient in a coastal sediment. *FEMS Microbiol. Ecol.* 66, 295–305. doi: 10.1111/j.1574-6941.2008.00589.x
- Paissé, S., Goñi-Urriza, M., Coulon, F., and Duran, R. (2010). How a bacterial community originating from a contaminated coastal sediment responds to an oil input. *Microb. Ecol.* 60, 394–405. doi: 10.1007/s00248-010-9721-7
- Pearman, J. K., Biessy, L., Thomson-Laing, G., Waters, S., Vandergoes, M. J., Howarth, J. D., et al. (2020). Local factors drive bacterial and microeukaryotic community composition in lake surface sediment collected across an altitudinal gradient. *FEMS Microbiol. Ecol.* 96:fiaa070. doi: 10.1093/femsec/fiaa070
- Peng, Y., Yue, D., Xiao, L., and Qian, X. (2017). Temporal variation and co-occurrence patterns of bacterial communities in eutrophic Lake Taihu, China. *Geomicrobiol. J.* 35, 186–197. doi: 10.1080/01490451.2017.1348406
- Perazzolo, C., Morasch, B., Kohn, T., Magnet, A., Thonney, D., and Chèvre, N. (2010). Occurrence and fate of micropollutants in the Vidy Bay of Lake Geneva, Switzerland. Part I: priority list for environmental risk assessment of pharmaceuticals. *Environ. Toxicol. Chem.* 29, 1649–1657. doi: 10.1002/etc.221
- Peres-Neto, P. R., and Jackson, D. A. (2001). How well do multivariate data sets match? Evaluating the association of multivariate biological data sets: comparing the robustness of Mantel test and a Procrustean superimposition approach. *Oecologia* 129, 169–178. doi: 10.1007/s004420100720
- Pesce, S., Perceval, O., Bonninaeu, C., Casado-Martinez, C., Dabrin, A., Lyautey, E., et al. (2018). Looking at biological community level to improve ecotoxicological assessment of freshwater sediments: report on a first French-Swiss workshop. *Environ. Sci. Pollut. Res.* 25, 970–974. doi: 10.1007/s11356-017-0620-z
- Poole, K. (2017). At the nexus of antibiotics and metals: the impact of Cu and Zn on antibiotic activity and resistance. *Trends Microbiol.* 25, 820–832. doi: 10.1016/j.tim.2017.04.010
- Poté, J., Haller, L., Loizeau, J. L., Bravo, A. G., Sastre, V., and Wildi, W. (2008). Effects of a sewage treatment plant outlet pipe extension on the distribution of contaminants in the sediments of the Bay of Vidy, Lake Geneva, Switzerland. *Biores. Technol.* 99, 7122–7131. doi: 10.1016/j.biortech.2007.12.075
- Quast, C., Pruesse, E., Yilmaz, P., Gerken, J., Schweer, T., Yarza, P., et al. (2013). The SILVA ribosomal RNA gene database project: improved data processing and webbased tools. *Nucleic Acids Res.* 41, 590–596.
- R Core Team (2018). *R: A Language and Environment for Statistical Computing*. Vienna: R Foundation for Statistical Computing.
- Rimet, F., Anneville, O., Barbet, D., Chardon, C., Crépin, L., Domaizon, I., et al. (2020). The Observatory on LAKes (OLA) database: sixty years of environmental data accessible to the public: the Observatory on LAKes (OLA) database. *J. Limnol.* 79, 164–178. doi: 10.4081/jlimnol.2020.1944
- Rognes, T., Flouri, T., Nichols, B., Quince, C., and Mahé, F. (2016). VSEARCH: a versatile open source tool for metagenomics. *Peer J.* 4:e2584. doi: 10.7717/peerj.2584
- Roosa, S., Wattiez, R., Prygiel, E., Lesven, L., Billon, G., and Gillan, D. C. (2014). Bacterial metal resistance genes and metal bioavailability in contaminated sediments. *Environ. Pollut.* 189, 143–151. doi: 10.1016/j.envpol.2014.02.031
- Roos-Barraclough, F., Givélet, N., Martinez-Cortizas, A., Goodsite, M. E., Biester, H., and Shotyk, W. (2002). An analytical protocol for the determination of total

- mercury concentrations in solid peat samples. *Sci. Total Environ.* 292, 129–139. doi: 10.1016/S0048-9697(02)00035-9
- Royston, J. P. (1982). An extension of Shapiro and Wilk's W test for normality to large samples. *J. R. Stat. Soc. C Appl.* 31, 115–124. doi: 10.2307/2347973
- Ruuskanen, M. O., St Pierre, K. A., St Louis, V. L., Aris-Brosou, S., and Poulain, A. J. (2018). Physicochemical drivers of microbial community structure in sediments of Lake Hazen, Nunavut, Canada. *Front. Microbiol.* 9:1138. doi: 10.3389/fmicb.2018.01138
- Sauvain, L., Bueche, M., Junier, T., Masson, M., Wunderlin, T., Kohler-Milleret, R., et al. (2014). Bacterial communities in trace metal contaminated lake sediments are dominated by endospore-forming bacteria. *Aquat. Sci.* 76, 33–46. doi: 10.1007/s00027-013-0313-8
- Schallenberg, M., and Kalf, J. (1993). The ecology of sediment bacteria in lakes and comparisons with other aquatic ecosystems. *Ecology* 74, 919–934. doi: 10.2307/1940816
- Schultz, P., and Urban, N. R. (2008). Effects of bacterial dynamics on organic matter decomposition and nutrient release from sediments: a modeling study. *Ecol. Modell.* 210, 1–14. doi: 10.1016/j.ecolmodel.2007.06.026
- Schwefel, R., Gaudard, A., Wüest, A., and Bouffard, D. (2016). Effects of climate change on deepwater oxygen and winter mixing in a deep lake (Lake Geneva): comparing observational findings and modeling. *Water Resour. Res.* 52, 8811–8826. doi: 10.1002/2016WR019194
- Sedláček, J., Tolaszová, J., Kříženecká, S., Bábek, O., and Zimová, K. (2020). Regional contamination history revealed in coal-mining-impacted Oxbow Lake sediments. *Water Air Soil Pollut.* 231:208. doi: 10.1007/s11270-020-04583-1
- Silva, I., Tacão, M., and Henriques, I. (2021). Selection of antibiotic resistance by metals in a riverine bacterial community. *Chemosphere* 263:127936. doi: 10.1016/j.chemosphere.2020.127936
- Silva, T. A., Stutenbecker, L., Bakker, M., Costa, A., Schlunegger, F., Lane, S., et al. (2019). The sediment budget and dynamics of a delta-canyon-lobe system over the Anthropocene timescale: the Rhone River Delta, Lake Geneva (Switzerland/France). *Sedimentology* 66, 838–858. doi: 10.1111/sed.12519
- Steinsberger, T., Schmid, M., Wüest, A., Schwefel, R., Wehrli, B., and Müller, B. (2019). Organic carbon mass accumulation rate regulates the flux of reduced substances from the sediments of deep lakes. *Biogeosciences* 14, 3275–3285. doi: 10.5194/bg-14-3275-2017
- Su, J. Q., An, X. L., Li, B., Chen, Q. L., Gillings, M. R., Chen, H., et al. (2017). Metagenomics of urban sewage identifies an extensively shared antibiotic resistome in China. *Microbiome* 5:84. doi: 10.1186/s40168-017-0298-y
- Sun, M. Y., Dafforn, K. A., Brown, M. V., and Johnston, E. L. (2012). Bacterial communities are sensitive indicators of contaminant stress. *Mar. Pollut. Bull.* 64, 1029–1038. doi: 10.1016/j.marpolbul.2012.01.035
- Sun, M. Y., Dafforn, K. A., Johnston, E. L., and Brown, M. V. (2013). Core sediment bacteria drive community response to anthropogenic contamination over multiple environmental gradients. *Environ. Microbiol.* 15, 2517–2531. doi: 10.1111/1462-2920.12133
- Szakova, I., Kolišova, D., Miholova, D., and Mader, P. (2004). Single-purpose atomic absorption spectrometer AMA-254 for mercury determination and its performance in analysis of agricultural and environmental materials. *Chem. Pap.* 58, 311–315.
- Vadeboncoeur, Y., Vander Zanden, M. J., and Lodge, D. M. (2002). Putting the lake back together: reintegrating benthic pathways into lake food web models: lake ecologists tend to focus their research on pelagic energy pathways, but, from algae to fish, benthic organisms form an integral part of lake food webs. *BioScience* 52, 44–54. doi: 10.1641/0006-3568
- Wan, Y., Bai, Y., He, J., Zhang, Y., Li, R., and Ruan, X. (2017). Temporal and spatial variations of aquatic environmental characteristics and sediment bacterial community in five regions of Lake Taihu. *Aquat. Ecol.* 51, 343–358. doi: 10.1007/s10452-017-9621-8
- Wang, Y., and Qian, P. Y. (2009). Conservative fragments in bacterial 16S rRNA genes and primer design for 16S ribosomal DNA amplicons in metagenomic studies. *PLoS One* 4:e7401. doi: 10.1371/journal.pone.0007401
- Widenfalk, A., Bertilsson, S., Sundh, I., and Goedkoop, W. (2008). Effects of pesticides on community composition and activity of sediment microbes—responses at various levels of microbial community organization. *Environ. Pollut.* 152, 576–584. doi: 10.1016/j.envpol.2007.07.003
- Widenfalk, A., Svensson, J. M., and Goedkoop, W. (2004). Effects of the pesticides captan, deltamethrin, isoproturon, and pirimicarb on the microbial community of a freshwater sediment. *Environ. Toxicol. Chem.* 23, 1920–1927. doi: 10.1897/03-345
- Wu, K., Zhao, W., Wang, Q., Yang, X., Zhu, L., Shen, J., et al. (2019). The relative abundance of benthic bacterial phyla along a water-depth gradient in a plateau lake: physical, chemical, and biotic drivers. *Front. Microbiol.* 10:1521. doi: 10.3389/fmicb.2019.01521
- Xu, Y., Wu, Y., Han, J., and Li, P. (2017). The current status of heavy metal in lake sediments from China: pollution and ecological risk assessment. *Ecol. Evol.* 7, 5454–5466. doi: 10.1002/ece3.3124
- Zhang, L., Cheng, Y., Gao, G., and Jiang, J. (2019). Spatial-temporal variation of bacterial communities in sediments in Lake Chaohu, a large, shallow eutrophic lake in China. *Int. J. Environ. Res. Public Health* 16:3966. doi: 10.3390/ijerph16203966
- Zhang, W., Ki, J.-S., and Qian, P.-Y. (2008). Microbial diversity in polluted harbor sediments I: bacterial community assessment based on four clone libraries of 16S rDNA. *Estuar. Coast. Shelf Sci.* 76, 668–681. doi: 10.1016/j.ecss.2007.07.040
- Zhang, X. Z., Xie, J. J., and Sun, F. L. (2014). Effects of three polycyclic aromatic hydrocarbons on sediment bacterial community. *Curr. Microbiol.* 68, 756–762. doi: 10.1007/s00284-014-0535-6

**Conflict of Interest:** The authors declare that the research was conducted in the absence of any commercial or financial relationships that could be construed as a potential conflict of interest.

**Publisher's Note:** All claims expressed in this article are solely those of the authors and do not necessarily represent those of their affiliated organizations, or those of the publisher, the editors and the reviewers. Any product that may be evaluated in this article, or claim that may be made by its manufacturer, is not guaranteed or endorsed by the publisher.

Copyright © 2021 Lyautey, Bonninaeu, Billard, Loizeau, Naffrechoux, Tlili, Topp, Ferrari and Pesce. This is an open-access article distributed under the terms of the Creative Commons Attribution License (CC BY). The use, distribution or reproduction in other forums is permitted, provided the original author(s) and the copyright owner(s) are credited and that the original publication in this journal is cited, in accordance with accepted academic practice. No use, distribution or reproduction is permitted which does not comply with these terms.



# Driving Factors of Geosmin Appearance in a Mediterranean River Basin: The Ter River Case

Carmen Espinosa<sup>1,2</sup>, Meritxell Abril<sup>1</sup>, Èlia Bretxa<sup>2</sup>, Marta Jutglar<sup>2</sup>, Sergio Ponsá<sup>1</sup>, Núria Sellarès<sup>2</sup>, Lúdia Vendrell-Puigmitjà<sup>1</sup>, Laia Llenas<sup>1</sup>, Marc Ordeix<sup>2</sup> and Lorenzo Proia<sup>1\*</sup>

<sup>1</sup> BETA Technological Center, University of Vic – Central University of Catalonia (UVic-UCC), Vic, Spain, <sup>2</sup> CERM, Center for the Study of Mediterranean Rivers, University of Vic – Central University of Catalonia (UVic-UCC), Manlleu, Spain

## OPEN ACCESS

### Edited by:

Soizic Morin,  
INRAE Nouvelle-Aquitaine Bordeaux,  
France

### Reviewed by:

Jingrang Lu,  
Office of Research and Development,  
United States Environmental  
Protection Agency (EPA),  
United States  
Leda Giannuzzi,  
Consejo Nacional de Investigaciones  
Científicas y Técnicas (CONICET),  
Argentina

### \*Correspondence:

Lorenzo Proia  
lorenzo.proia@uvic.cat

### Specialty section:

This article was submitted to  
Microbiotechnology,  
a section of the journal  
Frontiers in Microbiology

**Received:** 15 July 2021

**Accepted:** 20 September 2021

**Published:** 01 November 2021

### Citation:

Espinosa C, Abril M, Bretxa È,  
Jutglar M, Ponsá S, Sellarès N,  
Vendrell-Puigmitjà L, Llenas L,  
Ordeix M and Proia L (2021) Driving  
Factors of Geosmin Appearance in a  
Mediterranean River Basin: The Ter  
River Case.  
Front. Microbiol. 12:741750.  
doi: 10.3389/fmicb.2021.741750

In recent decades, human activity coupled with climate change has led to a deterioration in the quality of surface freshwater. This has been related to an increase in the appearance of algal blooms, which can produce organic compounds that can be toxic or can affect the organoleptic characteristics of the water, such as its taste and odor. Among these latter compounds is geosmin, a metabolite produced by certain cyanobacteria that confers an earthy taste to water and which can be detected by humans at very low concentrations (nanogram per liter). The difficulty and cost of both monitoring the presence of this compound and its treatment is a problem for drinking water treatment companies, as the appearance of geosmin affects consumer confidence in the quality of the drinking water they supply. In this field study, the evaluation of four sampling sites with different physicochemical conditions located in the upper part of the Ter River basin, a Mediterranean river located in Catalonia (NE Spain), has been carried out, with the aim of identifying the main triggers of geosmin episodes. The results, obtained from 1 year of sampling, have made it possible to find out that: (i) land uses with a higher percentage of agricultural and industrial activity are related to high nutrient conditions in river water, (ii) these higher nutrient concentrations favor the development of benthic cyanobacteria, (iii) in late winter–early spring, when these cyanobacteria are subjected to both an imbalance of the dissolved inorganic nitrogen and soluble reactive phosphorus ratio, guided by a phosphorus concentration increase, and to cold–mild temperatures close to 10°C, they produce and release geosmin, and (iv) 1–2 weeks after cyanobacteria reach a high relative presence in the whole biofilm, an increase in geosmin concentration in water is observed, probably associated with the cyanobacteria detachment from cobbles and consequent cell lysis. These results could serve as a guide for drinking water treatment companies, indicating under what conditions they can expect the appearance of geosmin episodes and implement the appropriate treatment before it reaches consumers' tap.

**Keywords:** geosmin, field study, cyanobacteria, biofilm, global change, Mediterranean river



## INTRODUCTION

In the last decades, increasing pressures generated by human activities conjointly with global change trend led to worsened water quality in freshwater ecosystems, giving rise to several ecological issues. One of these problems, mainly caused by eutrophication and temperature rise, is the uncontrolled and unpredictable growth of algal blooms, frequently associated with organic compounds production, which can be toxic or can alter the water organoleptic characteristics, such as the taste and odor compounds (T&Os) (Clercin and Druschel, 2019). The presence of natural toxins in water often leads to bathing or consumption prohibition, whereas T&Os are a problem for drinking water treatment plants (DWTPs) due to the negative impact they have on the user's perception of the drinking water quality (Ding et al., 2014).

Regarding human activities, their huge increase in the last century significantly affected rivers' basin morphology and water quality (Rubio-Gracia et al., 2017). Particularly, basins' land uses generally shifted from forestry-dominated to agricultural, livestock, and industrial. The increase of intensive agricultural activities in the catchments has been associated with higher nutrients and pesticides concentrations in river waters, which also receive a wide range of organic and inorganic chemical stressors, such as heavy metals, from industrial and urban areas (Drury et al., 2013; Argudo et al., 2020). The effects on water quality induced by the shift of land uses are acting conjointly with the alterations associated with climate change. Climatic conditions have changed in recent decades, being observed specifically in the Mediterranean regions, a clear decrease of the average rainfall, which is becoming much more sporadic and intense, and a relevant increase of the mean air temperature (Intergovernmental Panel on Climate Change [IPCC], 2019). These consequences of climate change take a greater relevance in rivers affected by water scarcity, such as those of the Mediterranean area, where there can be prolonged periods with a very low river flow, which can lead to a higher nutrients concentration, among other parameters (e.g., salts, heavy metals, and pesticides), due to the decreased dilution capacity of the system (Karaouzas et al., 2018). These conditions can trigger the appearance of algal blooms, with a large number of cases described worldwide (Clercin and Druschel, 2019; Ho et al., 2019), and that can finally lead to the appearance of T&O compounds (Watson et al., 2016).

Among the T&O compounds produced by microorganisms, geosmin has been described as the most common in freshwater ecosystems. This metabolite is mainly produced by certain cyanobacteria and actinomycetes, being the firsts associated with geosmin episodes in freshwaters, while actinomycetes usually have a terrestrial origin (Lukassen et al., 2019). Some of the main geosmin-producing cyanobacteria identified are *Oscillatoria* sp., *Dolichospermum* sp., *Lyngbya* sp., and *Symploca* sp. (Smith et al., 2009). For a long time, due to the methodology of routine sampling, only the odorous potential of pelagic cyanobacterial taxa has been considered. However, recent studies suggested that most of the geosmin producers are benthic instead of pelagic cyanobacteria taxa (Jähnichen et al., 2011).

Most of the studies on drivers of geosmin appearance in the field have been carried out in reservoirs and lakes (Dzialowski et al., 2009; Harris et al., 2016), whereas only a few studies have investigated geosmin appearance in rivers and streams (Vilalta, 2004). Two of the main important factors associated with geosmin episodes in reservoirs have been described to be the excess of nutrient loads and alterations in its stoichiometric balance. In particular, it has been suggested that increasing nutrient concentrations and lower nitrogen to phosphorus ratio (TN:TP) can promote cyanobacteria growth and dominance in freshwater ecosystems (Olsen et al., 2016; Espinosa et al., 2021), giving rise to the appearance of geosmin episodes. Harris et al. (2016) found out that low TN:TP ratio conditions (<30:1 by mass) favor geosmin episodes in reservoirs, which could be related to an increase in cyanobacterial biovolumes at lower TN:TP ratios. In the Llobregat River (Catalonia, NE Spain), Vilalta (2004) found similar results, being geosmin concentration higher at TN:TP values close to 10:1, comparing with TN:TP = 94:1, when no geosmin was detected. From experiments carried out mainly under laboratory conditions, the appearance of geosmin has also been related to other factors such as light availability and temperature. Depending on the geosmin producers, the value of these factors differed, but in general, it has been described that low light availability together with low water temperatures favored intracellular geosmin formation (Zhang et al., 2009; Wang and Li, 2015; Alghanmi et al., 2018). Water flow also influence microbial production of geosmin, being its presence is higher under low water flow conditions (Jüttner and Watson, 2007; Espinosa et al., 2020).

As comment before, although there are studies on drivers of geosmin in reservoirs and lakes, very few have approached this topic in rivers. Geosmin occurrence can be a problem for the companies that exploit rivers to provide drinking water to the surrounding populations, as they do not know under which conditions is produced, and thus, they are unable to predict geosmin episodes. Small companies (water treated  $\approx 1,500$  L/day, drinking water users  $\approx 22,000$ ) cannot incorporate regular monitoring of geosmin concentrations in collected river waters, as analyses are complex and time-consuming, and they need specific equipment often not available in their labs. Moreover, the cost of the analytics can be high and make it difficult for the concerned companies to contract the geosmin analysis in external laboratories as a routine. The low capacity to predict geosmin presence in water leads to the reception of consumer complaints and economic losses associated with the decrease in water consumption supplied by the DWTPs. In that sense, there is a growing need to investigate and understand the drivers associated with the production of geosmin in rivers, helping DWTPs to be prepared for possible geosmin episodes and avoiding the possible costs associated with geosmin analysis *per se*.

In the Osona region (Catalonia, NE Spain), most of DWTPs collect water from the upper section of the Ter River to supply the nearby cities and villages (around 150.00 inhabitants). In recent years, they have suffered several geosmin episodes that have led to customers' complaints due to the inability to applicate the required treatment on time. This situation has generated the need for a better understanding of the environmental factors

associated with geosmin appearance. The main objective of this study was to determine the main triggers of geosmin episodes in the Ter River. To this aim, a 1-year field monitoring (2019) was carried out, analyzing a wide set of physicochemical and biological parameters at four sampling sites distributed along the upper part of the Ter River basin.

## MATERIALS AND METHODS

### Study Site

The Ter River is located in the NE of Catalonia (Spain) (Figure 1). It is characterized by Pyrenean, pre-Pyrenean, and humid continental Mediterranean climate in the upper regions of its catchment (El Ripollès and Osona) and pre-coastal Mediterranean and coastal Mediterranean climates in the lower regions (Meteocat, 2019). The Ter River is affected by environmental fluctuations typical of the Mediterranean climate, with a higher probability of precipitation during spring and autumn and dry and warm summers. In the Ter River basin (208 km-long and 3,010 km<sup>2</sup> of catchment area), several anthropogenic activities drastically affect water flow and quality. The most relevant impacts are: (i) the presence of small and frequent hydropower weirs, which significantly reduce river flow, (ii) livestock farming and intensive agriculture, leading to an increase of nutrients concentration in fields and in surface and groundwater, and (iii) a large reservoirs system, which supplies energy and raw water for drinking, agriculture, and industrial purposes to Barcelona city and Costa Brava area, which is dramatically affecting the river connectivity, and clearly dividing the catchment in two different areas: upstream and downstream reservoirs system. In this work, the upper part of the Ter River basin (upstream of the large reservoirs system) has been studied (Figure 1).

The river basin area evaluated in this study is included in the regions of El Ripollès and Osona, which cover a surface of around 2,000 km<sup>2</sup>. El Ripollès region is located at the head of the Ter River basin, starting in the Pyrenees, and it is characterized by coniferous forest, natural grasslands, broad-leaved forest, and moors and heathlands (CORINE Land Cover System, 2018). Located downstream, the Osona region is affected by strong anthropogenic pressures, being the main land uses related to non-irrigated arable fields, industrial and commercial units, and continuous and discontinuous urban fabrics (CORINE Land Cover System, 2018).

Four sampling sites (Figure 1) were chosen to perform a 1-year field study to identify the driving factors triggering geosmin episodes in the upper part of the Ter River basin. The most upstream sampling site (T1) was located 10.8 km downstream from the source of the Ter River in the Pyrenees, at Vilallonga de Ter municipality. T1 was considered as a reference sampling site, with the best water quality. The next sampling site was located along the Ter River, downstream the municipality of Ripoll (T2) (41 km downstream from the source). At this site, the Ter River has already received the input of the Freser tributary and some WWTPs effluents. The third sampling site was located at the Colonia de Borgonyà, few kilometers upstream of Torelló

municipality (T3) and 66.3 km downstream from the source. This site was selected because it is one of the collection points of the drinking water company “Aigües d'Osona S.A.,” which supplies drinking water to Torelló municipality and surroundings. The last sampling site along the Ter River (T4) was located in Gurb municipality, 100 m upstream to the collection point of “Aigües de Vic S.A.,” the drinking water company that supplies the city of Vic and surroundings, and 81.8 km downstream Ter River source.

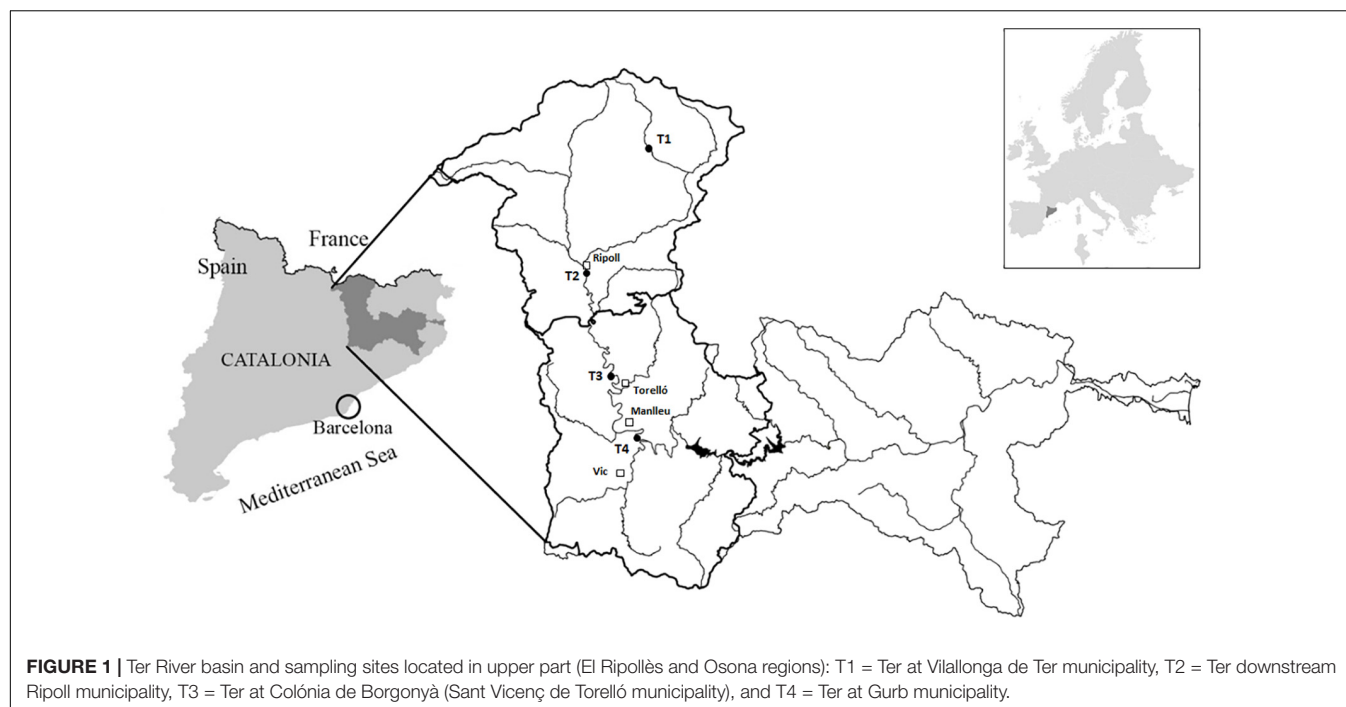
### Sampling Procedure and Physicochemical and Biological Analysis

During winter (January–March) and spring (April–June) seasons, weekly or biweekly field samplings were carried out, whereas from July to November (summer and autumn), monthly sampling campaigns were done. The higher sampling intensity during winter and spring was chosen because of the higher probability of geosmin occurrence during these seasons (Vilalta, 2004; Personal communication from drinking water companies). The nomenclature used in this study to identify the different sampling days includes the letter of the season (W = winter, Sp = spring, Su = summer, and A = autumn) followed by the number of the sampling day in this season, being, for example, W6, the name given to the sixth day of sampling in winter.

### Water Samples

The following physicochemical parameters were measured *in situ* with specific probes: temperature, dissolved oxygen concentration, and oxygen saturation (YSI professional plus, YSI Incorporated, United States), pH (XS pH7+ DHS), and electrical conductivity (XS COND 7+). Water samples were taken and filtered through 0.2-μm nylon membranes filters (Merck Millipore) before the analysis of soluble reactive phosphorus (SRP), N-NH<sub>4</sub><sup>+</sup>, N-NO<sub>2</sub><sup>-</sup>, and N-NO<sub>3</sub><sup>-</sup>. The volume filtered for SRP and N-NH<sub>4</sub><sup>+</sup> was 10 ml and for N-NO<sub>2</sub><sup>-</sup> and N-NO<sub>3</sub><sup>-</sup> was 50 ml, and the analyses were performed following the protocols established by Murphy and Riley (1962); Reardon et al. (1966), and Rand et al. (1976), respectively. The dissolved inorganic nitrogen (DIN):SRP ratio was calculated and determined as DIN divided by SRP in molar quantities. DIN concentration was determined as the sum of ammonium (N-NH<sub>4</sub><sup>+</sup>), nitrite (N-NO<sub>2</sub><sup>-</sup>), and nitrate (N-NO<sub>3</sub><sup>-</sup>) concentrations. Furthermore, 1 L of water was taken for the analysis of turbidity, suspended solids, and organic matter. Water turbidity was measured using a turbidimeter (HI 98713, HANNA Instruments). The organic matter present in water samples was estimated from the absorbance values measured at 254 nm using a spectrophotometer (NanoPhotometer<sup>TM</sup> P-360, INTEC), and the suspended solids were obtained following APHA (2005) and using a Forced air oven, MEMMERT IFE500. All samples were stored at -20°C until analysis.

A 1-L opaque glass bottle was used to collect the water sample for geosmin quantification. Bottles were stored at 4°C in dark conditions until analysis, which was performed within 48 h after collection to avoid degradation and volatilization. The protocol followed for geosmin analysis in water was described in Espinosa et al. (2021). Briefly, to analyze geosmin concentration, 50 ml of each water sample and 10 g of NaCl were added to a 100-ml



opaque reaction vial and heated at 60°C for 25 min in agitation to favor geosmin volatilization. To extract the geosmin, a 65- $\mu$ m polydimethylsiloxane/divinylbenzene fiber was used, and the separation and analysis of the extracted volatile compound were performed in a gas chromatography–mass spectrometry instrument (ISQ–TRACE GC ULTRA). The analytical detection limit was 2.5 ng/L, the analytical quantification limit was 8 ng/L, and the precision of the method was evaluated with the relative standard deviation ( $RSD \leq 20\%$ ).

### Biofilm Samples

Each sampling day, three cobbles were randomly taken from each sampling site to evaluate *in situ* the biofilm photosynthetic efficiency and the phototrophic community composition. The community photosynthetic efficiency ( $Y_{eff}$ ) and the minimum fluorescence yield ( $F_0$ ) (that can be used as an estimation of algal biomass) were measured with an amplitude modulated fluorimetry (Mini-PAM fluorometer Walz, Effeltrich, Germany), and the phototrophic community composition was evaluated with a BenthosTorch (bbe Moldaenke, Schwentineta, DK). After that, each cobble was scrapped in 60 ml of water from the same sampling site to obtain a biofilm suspension. Aliquots of this suspension were used to analyze chlorophyll-*a* (Chl-*a*), performed as described by Jeffrey and Humphrey (1975), and ash-free dry mass as described in Espinosa et al. (2020). The Margalef index was also calculated as the quotient between the carotenoid/Chl-*a* ratio, being values obtained from the spectrophotometric reading of the sample at 430 nm (carotenoids and accessory pigments concentration) and 665 nm (Chl-*a* concentration), to obtain information about the maturity of the populations (Elosegui and Sabater, 2009). These samples were stored at –20°C until analysis.

### Data Treatment

The Kolmogorov–Smirnov test was performed to verify that the variables fulfilled the conditions of normal distribution, and if they did not, they were logarithmically transformed. Physicochemical and biological data were analyzed using an analysis of variance (ANOVA) using the “aov” function (“devtools” package) in RStudio software (version 3.6.0) being the sampling site, the season, and its interaction the factors evaluated. Significant results were tested *post hoc* with a Bonferroni test. Pearson correlation coefficient tests were carried out to explore the relationship between variables. Statistical significance was set at  $p < 0.05$  for all tests performed. A redundancy discriminant analysis (RDA) was carried out to explore the potential relationship between the independent variables or potential drivers and the response variables (“vegan” and “tidyr” R packages). They were considered as potential drivers for all the water analytics except for geosmin concentration, which was considered as a response variable together with all the biofilm analytics. Forecasting models to predict the geosmin appearance according to the physicochemical data collected were generated by means of multiple regression analysis (MLR) and random forest (RF) models. The primary purpose of using a linear model was to provide a baseline against which to compare the non-linear RF model, an ensemble machine learning method that constructs a non-linear function based on an ensemble of simpler decision tree models (Kehoe et al., 2015). These models were tested for their ability to predict geosmin at different time delays, not just current conditions, to understand at what time scale geosmin can be predicted and which are the important predictors at each time lag. Models were calibrated for 11 different forecasting time lags ranging from the current level (i.e., no time lag,  $t = 0$ ) up to 10 weeks in advance—in a 1-week increment. Linear (regression)

and non-linear models (RF) were calibrated and validated (70–30%) on randomized subsets of the total dataset. The R function “lm” was used for the MLR, whereas RF models were developed with the “randomForest” package. The performance of the models was assessed by the multiple determination coefficient or  $R^2$  adjusted. The relative importance of the different predictors at different time lags was evaluated by using the “importance” function (“randomForest” package).

## RESULTS

### Geosmin Concentration

The presence and concentration of geosmin in water varied throughout the year (2019), in which the present study was carried out (Figure 2). Statistically, geosmin presence in water was significantly affected by the sampling site (ANOVA,  $F = 10.378$ ,  $p < 0.001$ ), the season ( $F = 9.007$ ,  $p < 0.001$ ), and the interaction between site and season ( $F = 2.243$ ,  $p < 0.05$ ). Sampling site T4 was statistically different from the others (Bonferroni test:  $p < 0.001$ ), being the one with the highest geosmin concentration, especially in spring ( $249 \pm 33$  ng/L) compared with the other seasons ( $p < 0.01$ ).

### Physicochemical Parameters

Some of the evaluated physicochemical variables (Table 1) significantly changed depending on the sampling site, the season, and its interaction. The lowest values reported for most of the parameters evaluated were found at sampling site T1, mainly highlighting pH, electrical conductivity, temperature, and nutrient concentrations (ANOVA,  $p < 0.05$ ). In contrast, sampling site T4 showed opposite results to T1, with very high values, especially for the nitrogen forms, whose concentration increased up to four times compared with T1, on average.

Seasonality also had an effect in some of the physicochemical parameters evaluated, being in autumn when lower pH values and dissolved oxygen were recorded, together with higher nitrites concentration (Bonferroni test,  $p < 0.01$  in all cases). Phosphate concentration and turbidity presented the highest values in spring ( $p < 0.001$ ), when, in contrast, the DIN:SRP ratio showed lower results compared with summer and autumn ( $p < 0.01$ ).

Geosmin concentration for all sampling sites and seasons was positively correlated with pH, electrical conductivity, turbidity, and phosphate concentration (Pearson's correlation,  $p < 0.01$  all cases) and negatively correlated with the DIN:SRP ratio (Pearson's correlation,  $p < 0.05$ ).

Considering that the geosmin peak was measured at T4, a specific analysis was carried on the sub-dataset regarding this sampling site. The analysis of correlations revealed that geosmin concentration was positively correlated with phosphorus concentration (Pearson's correlation:  $r = 0.789$ ,  $p < 0.01$ ) and had a negative correlation with the DIN:SRP ratio ( $r = -0.868$ ,  $p < 0.01$ ). During spring, when the highest geosmin peak was detected, the DIN:SRP ratio was significantly lower ( $47:1 \pm 16:1$ ) compared with the other seasons. On the contrary, autumn was the season showing the highest DIN:SRP

ratio ( $221:1 \pm 34:1$ ), due to the important decrease of phosphorus concentration ( $19 \pm 11 \mu\text{g P-PO}_4^{3-} \mu\text{g/L}$ ).

### Biological Parameters

Biological parameters data showed significant differences depending on the sampling site, the season, and the interaction between both factors (Table 2). Sampling site T4 showed the highest values of Chl-*a* concentration and cyanobacteria presence, being significantly different from the rest of the sampling sites (Bonferroni test,  $p < 0.01$ ). Seasonality also affected the biological parameters evaluated. Phototrophic community presented higher biomass values (estimated as microgram Chl-*a* per square centimeters) in summer ( $p < 0.01$ ), whereas the  $F_0$  value was higher in autumn ( $p < 0.05$ ), and Chl-*a* concentration and diatoms relative abundance had higher values in winter ( $p < 0.01$ ). Correlation analysis revealed that diatom abundance was negatively correlated with geosmin concentration ( $r = -0.28$ ,  $p < 0.05$ ), but no significant correlation was found between geosmin and cyanobacteria presence.

Evaluating the sampling site with the highest geosmin concentration (T4), it was found that geosmin concentration was negatively correlated with the  $F_0$  (Pearson's correlation:  $r = -0.681$ ,  $p < 0.01$ ), diatoms biomass ( $r = -0.661$ ,  $p < 0.01$ ), Margalef index ( $r = -0.643$ ,  $p < 0.01$ ), and Chl-*a* concentration ( $r = -0.533$ ;  $p < 0.05$ ).

### Geosmin Drivers

An RDA was performed with the objective to identify the relationship between the potential drivers (all the physicochemical variables except geosmin) and the response variables (all the biological variables together with geosmin) measured at the different sampling sites (Figure 3). The independent variables in the first two RDA dimensions (RDA1 and RDA2) explained 89% of the total variance in the distribution of the response parameters.

This ordination clearly separates upstream (T1 and T2) from the downstream sites (T3 and T4) along the first axis, which explains the 68.8% of variability, and is mainly driven by increasing nutrient concentrations along the Ter River gradient. The DIN:SRP relationship also influences the distribution of the sampling sites, with T1 being the site with the lowest mean values. Geosmin concentration was mainly affected by the concentration of phosphates and nitrites, the turbidity, pH, and DIN:SRP ratio values, being in agreement with the Pearson correlations found (all of them positively correlated with geosmin concentration except DIN:SRP ratio). The presence of cyanobacteria was favored by lower values of DIN:SRP, in contrast to diatoms, which presented higher values under high nitrate concentration conditions. This last situation also favored high Chl-*a* values and biofilms with higher photosynthetic efficiency (Yeff).

Considering that the highest geosmin concentrations were found at the T4 sampling site, a specific RDA was performed for this sub-dataset (Figure 4). The potential drivers for RDA1 and RDA2 explain 83.3% of the total variance in the distribution of response parameters in T4. This analysis clearly shows the effect of seasonality in the appearance of geosmin at this sampling site. In particular, the first axis, which explains the 69.71%



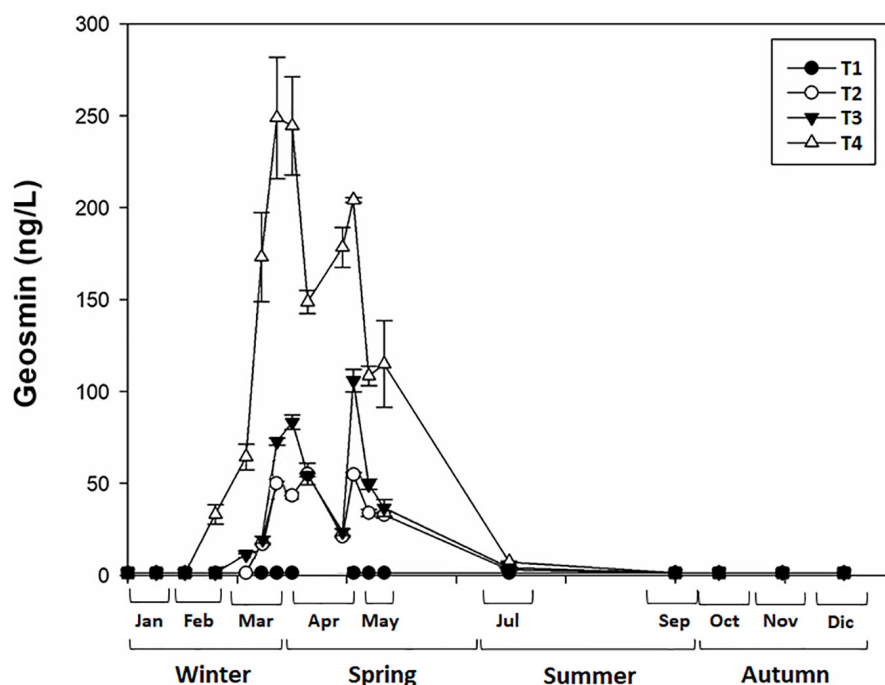


**FIGURE 2 |** Mean value and standard deviation of geosmin concentration in water for different sampling sites (T1, T2, T3, and T4) in upper part of Ter River basin (NE Catalonia, Spain) at each sampling day.

**TABLE 1 |** Mean value and standard deviation of physicochemical variables evaluated for different sampling sites (T1–T4) in upper Ter River basin (NE Catalonia, Spain) in 2019: in winter (W), spring (Sp), summer (Su), and autumn (A).

	pH	EC ( $\mu\text{S}/\text{cm}$ )	Temp. ( $^{\circ}\text{C}$ )	DO ( $\text{mg}/\text{L}$ )	Sat. (%)	N-NH <sub>4</sub> <sup>+</sup> ( $\mu\text{g}/\text{L}$ )	N-NO <sub>2</sub> <sup>-</sup> ( $\mu\text{g}/\text{L}$ )	N-NO <sub>3</sub> <sup>-</sup> ( $\text{mg}/\text{L}$ )	P-PO <sub>4</sub> <sup>3-</sup> ( $\mu\text{g}/\text{L}$ )	DIN:SRP	SS ( $\text{mg}/\text{L}$ )	Turbidity (NTU)	OM ( $A_{254\text{ nm}}$ )
T1 W	7.8 $\pm$ 0.6	153 $\pm$ 32	4.6 $\pm$ 1.3	12.1 $\pm$ 1.0	99 $\pm$ 16	55 $\pm$ 40	2 $\pm$ 1	0.37 $\pm$ 0.07	66 $\pm$ 68	27 $\pm$ 19	29 $\pm$ 19	13 $\pm$ 11	0.40 $\pm$ 0.34
Sp	7.9 $\pm$ 0.3	149 $\pm$ 37	7.4 $\pm$ 1.6	11.6 $\pm$ 1.0	105 $\pm$ 11	26 $\pm$ 13	3 $\pm$ 2	0.42 $\pm$ 0.06	96 $\pm$ 94	19 $\pm$ 14	8 $\pm$ 4	12 $\pm$ 10	0.23 $\pm$ 0.35
Su	8.1 $\pm$ 0.4	150 $\pm$ 24	12.9 $\pm$ 3.0	10.1 $\pm$ 1.0	98 $\pm$ 10	45 $\pm$ 34	9 $\pm$ 10	0.30 $\pm$ 0.20	36 $\pm$ 50	31 $\pm$ 20	6 $\pm$ 5	10 $\pm$ 7	0.30 $\pm$ 0.39
A	7.8 $\pm$ 0.4	148 $\pm$ 30	7.0 $\pm$ 2.9	11.9 $\pm$ 2.0	100 $\pm$ 18	21 $\pm$ 14	3 $\pm$ 5	0.33 $\pm$ 0.22	18 $\pm$ 10	60 $\pm$ 41	13 $\pm$ 14	10 $\pm$ 7	0.34 $\pm$ 0.44
T2 W	8.3 $\pm$ 0.4	250 $\pm$ 46	6.2 $\pm$ 2.1	12.7 $\pm$ 1.1	106 $\pm$ 10	79 $\pm$ 35	7 $\pm$ 5	0.61 $\pm$ 0.16	54 $\pm$ 40	42 $\pm$ 43	16 $\pm$ 11	23 $\pm$ 9	0.23 $\pm$ 0.26
Sp	8.3 $\pm$ 0.4	291 $\pm$ 61	9.5 $\pm$ 1.2	11.6 $\pm$ 0.7	108 $\pm$ 8	54 $\pm$ 27	9 $\pm$ 8	0.61 $\pm$ 0.14	48 $\pm$ 25	37 $\pm$ 24	23 $\pm$ 14	20 $\pm$ 8	0.13 $\pm$ 0.15
Su	8.2 $\pm$ 0.5	293 $\pm$ 67	16.0 $\pm$ 3.4	10.2 $\pm$ 1.6	104 $\pm$ 12	61 $\pm$ 33	20 $\pm$ 26	0.78 $\pm$ 0.54	29 $\pm$ 28	74 $\pm$ 44	14 $\pm$ 13	21 $\pm$ 8	0.12 $\pm$ 0.09
A	8.2 $\pm$ 0.5	324 $\pm$ 67	7.8 $\pm$ 4.4	12.8 $\pm$ 1.8	109 $\pm$ 13	45 $\pm$ 29	14 $\pm$ 16	0.48 $\pm$ 0.14	34 $\pm$ 25	69 $\pm$ 55	20 $\pm$ 17	22 $\pm$ 27	0.28 $\pm$ 0.34
T3 W	8.4 $\pm$ 0.3	343 $\pm$ 87	7.5 $\pm$ 2.4	12.9 $\pm$ 1.1	108 $\pm$ 9	80 $\pm$ 74	8 $\pm$ 5	0.75 $\pm$ 0.19	73 $\pm$ 57	50 $\pm$ 52	27 $\pm$ 16	18 $\pm$ 13	0.41 $\pm$ 0.29
Sp	8.4 $\pm$ 0.1	302 $\pm$ 85	12.0 $\pm$ 2.5	10.8 $\pm$ 1.2	103 $\pm$ 10	75 $\pm$ 70	10 $\pm$ 6	0.67 $\pm$ 0.29	73 $\pm$ 55	31 $\pm$ 18	29 $\pm$ 26	19 $\pm$ 15	0.33 $\pm$ 0.33
Su	8.5 $\pm$ 0.2	338 $\pm$ 91	17.2 $\pm$ 5.7	11.2 $\pm$ 3.1	107 $\pm$ 8	78 $\pm$ 38	19 $\pm$ 23	0.77 $\pm$ 0.50	82 $\pm$ 100	39 $\pm$ 24	19 $\pm$ 9	12 $\pm$ 5	0.35 $\pm$ 0.33
A	8.4 $\pm$ 0.2	366 $\pm$ 76	9.7 $\pm$ 5.4	12.7 $\pm$ 2.1	111 $\pm$ 12	92 $\pm$ 119	36 $\pm$ 74	0.73 $\pm$ 0.45	80 $\pm$ 113	71 $\pm$ 56	27 $\pm$ 21	12 $\pm$ 9	0.35 $\pm$ 0.35
T4 W	8.4 $\pm$ 0.3	388 $\pm$ 70	7.4 $\pm$ 2.4	12.3 $\pm$ 0.7	104 $\pm$ 8	119 $\pm$ 49	14 $\pm$ 10	1.48 $\pm$ 0.68	87 $\pm$ 87	75 $\pm$ 61	31 $\pm$ 20	21 $\pm$ 15	0.35 $\pm$ 0.20
Sp	8.3 $\pm$ 0.2	326 $\pm$ 75	13.6 $\pm$ 1.7	10.4 $\pm$ 2.0	101 $\pm$ 13	122 $\pm$ 90	19 $\pm$ 9	1.15 $\pm$ 0.42	79 $\pm$ 39	54 $\pm$ 38	34 $\pm$ 29	26 $\pm$ 21	0.35 $\pm$ 0.30
Su	8.7 $\pm$ 0.5	374 $\pm$ 66	21.2 $\pm$ 4.3	9.5 $\pm$ 1.4	106 $\pm$ 12	93 $\pm$ 33	26 $\pm$ 21	1.23 $\pm$ 0.88	102 $\pm$ 76	54 $\pm$ 53	40 $\pm$ 5	18 $\pm$ 7	0.19 $\pm$ 0.15
A	8.4 $\pm$ 0.4	405 $\pm$ 90	9.7 $\pm$ 5.4	11.9 $\pm$ 3.0	108 $\pm$ 15	75 $\pm$ 67	17 $\pm$ 9	1.60 $\pm$ 0.92	57 $\pm$ 47	150 $\pm$ 129	19 $\pm$ 20	11 $\pm$ 9	0.26 $\pm$ 0.17

OM, organic matter; SS, suspended solids.

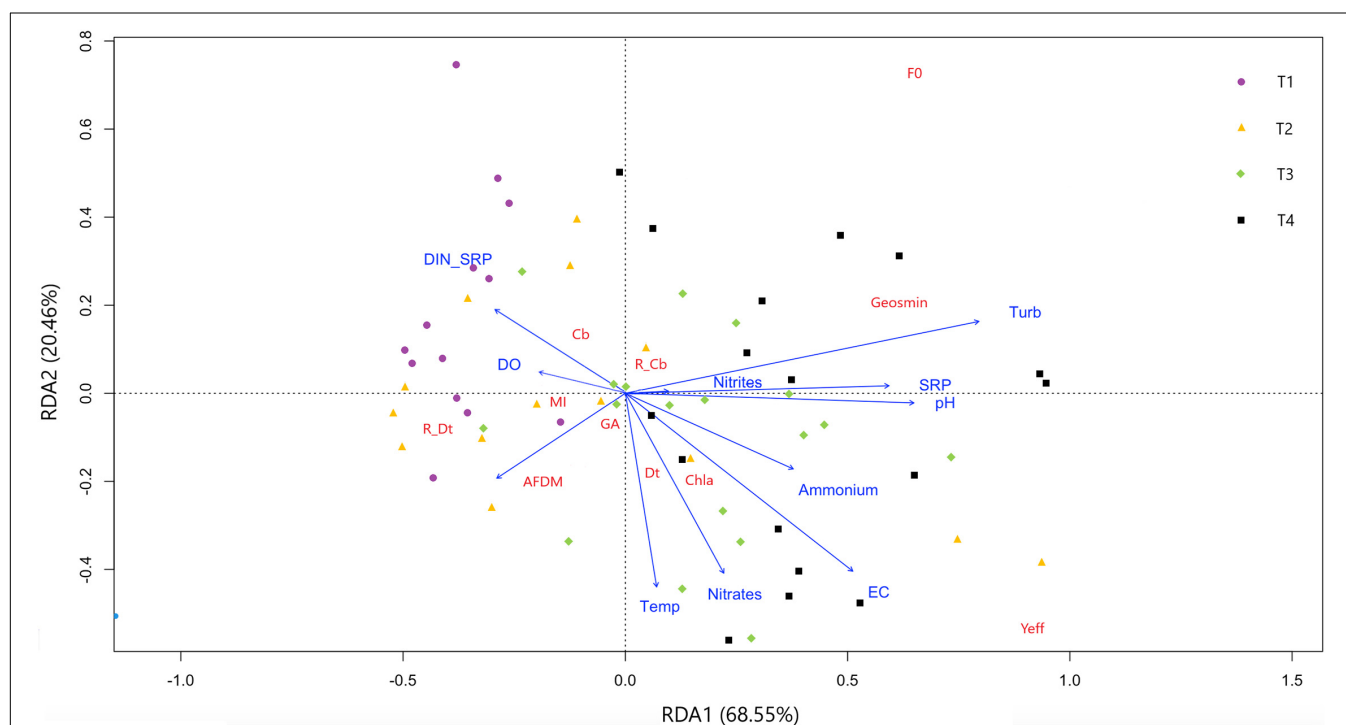
of the variability, separates winter and autumn from spring and summer samplings and is mainly driven by increasing phosphorus and nitrites concentrations and decreasing DIN:SRP values that again seem to be related to cyanobacteria abundance and geosmin concentration. More specifically, on the first sampling day of winter (W1), the tendency was to move from high DIN:SRP ratio values (187:1) toward lower values (48:1

in W6). This gradual decrease of DIN:SRP ratio was mainly guided by a relevant increase of phosphorus concentration (from  $32 \pm 3.5$  to  $70 - 100 \pm 10.4 \mu\text{g P-PO}_4^{3-}/\text{L}$ ) conjointly with a decrease in nitrate concentration (from  $2.98 \pm 0.02$  to  $1.26 \pm 0.18 \text{ mg N-NO}_3^{-}/\text{L}$ ) and coincide with the first detection (W4) and gradual increase of geosmin concentration during late winter–early spring. During this period, water temperature

**TABLE 2 |** Mean value and standard deviation of biological variables evaluated for different sampling sites (T1–T4) in upper Ter River basin (NE Catalonia, Spain) in 2019, in winter (W), spring (Sp), summer (Su), and autumn (A).

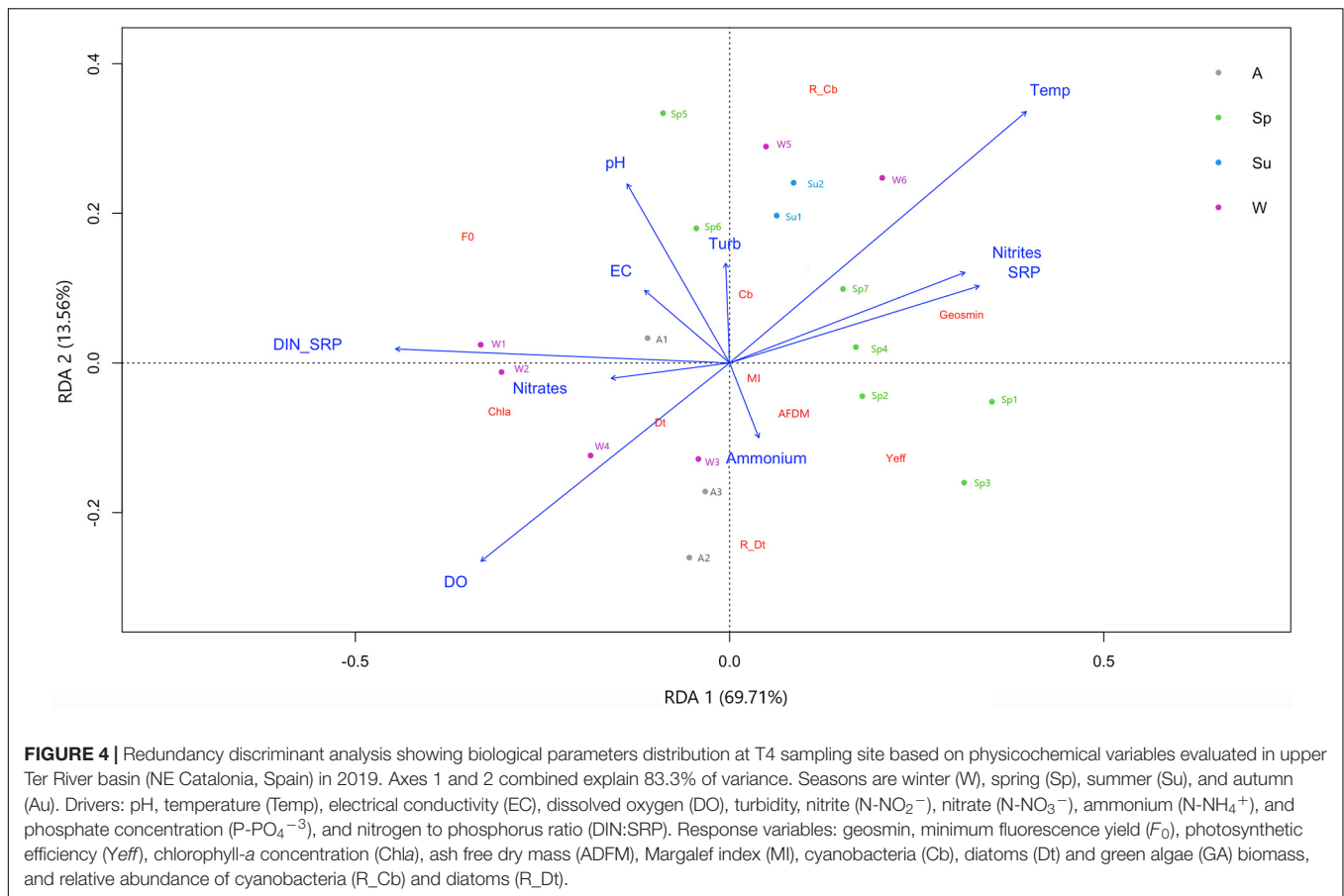
		$F_0$	$Y_{eff}$	Cyanobacteria ( $\mu\text{g}/\text{cm}^2$ )	Green algae ( $\mu\text{g}/\text{cm}^2$ )	Diatoms ( $\mu\text{g}/\text{cm}^2$ )	Cyanobacteria (%)	Green algae (%)	Diatoms (%)	Chl-a ( $\mu\text{g}/\text{cm}^2$ )	MI	AFDM ( $\text{g}/\text{m}^2$ )
T1	W	113 $\pm$ 43	322 $\pm$ 92	0.16 $\pm$ 0.08	0.02 $\pm$ 0.05	3.67 $\pm$ 2.80	7.9 $\pm$ 7.5	0.0 $\pm$ 0.0	89.9 $\pm$ 12.0	3.9 $\pm$ 3.9	2.0 $\pm$ 0.2	44 $\pm$ 59
	Sp	93 $\pm$ 54	350 $\pm$ 63	0.18 $\pm$ 0.07	0.19 $\pm$ 0.14	1.09 $\pm$ 0.33	13.3 $\pm$ 6.8	0.0 $\pm$ 0.0	73.9 $\pm$ 12.0	1.0 $\pm$ 0.8	1.9 $\pm$ 0.1	74 $\pm$ 69
	Su	89 $\pm$ 30	368 $\pm$ 132	0.91 $\pm$ 1.03	0.00 $\pm$ 0.00	0.99 $\pm$ 0.39	38.2 $\pm$ 25.7	0.0 $\pm$ 0.0	61.8 $\pm$ 25.7	0.6	2.1	46 $\pm$ 61
	A	165	277	0.54 $\pm$ 0.61	0.03 $\pm$ 0.05	1.82 $\pm$ 0.30	19.8 $\pm$ 18.8	0.0 $\pm$ 0.0	79.3 $\pm$ 20.4	3.2 $\pm$ 1.8	2.0 $\pm$ 0.2	21 $\pm$ 18
T2	W	160 $\pm$ 117	489 $\pm$ 80	0.45 $\pm$ 0.33	0.01 $\pm$ 0.03	3.21 $\pm$ 2.42	11.4 $\pm$ 5.9	0.0 $\pm$ 0.0	87.0 $\pm$ 3.3	23.9 $\pm$ 21.7	2.2 $\pm$ 0.1	299 $\pm$ 271
	Sp	127 $\pm$ 58	435 $\pm$ 145	0.49 $\pm$ 0.27	0.45 $\pm$ 0.31	1.49 $\pm$ 0.62	19.5 $\pm$ 5.9	0.0 $\pm$ 0.0	62.2 $\pm$ 8.9	2.5 $\pm$ 1.6	2.0 $\pm$ 0.2	140 $\pm$ 111
	Su	133 $\pm$ 80	452 $\pm$ 278	1.02 $\pm$ 0.35	0.00 $\pm$ 0.00	1.74 $\pm$ 0.99	39.5 $\pm$ 21.9	0.0 $\pm$ 0.0	60.5 $\pm$ 21.9	11.1	2.5	17 $\pm$ 1
	A	227	630	0.42 $\pm$ 0.36	0.00 $\pm$ 0.00	2.32 $\pm$ 1.43	14.5 $\pm$ 5.9	0.0 $\pm$ 0.0	85.5 $\pm$ 5.9	7.0 $\pm$ 8.0	2.3 $\pm$ 0.1	48 $\pm$ 41
T3	W	189 $\pm$ 64	317 $\pm$ 106	0.78 $\pm$ 0.48	0.00 $\pm$ 0.00	3.59 $\pm$ 2.32	18.8 $\pm$ 6.2	0.0 $\pm$ 0.0	81.2 $\pm$ 6.2	18.0 $\pm$ 17.3	2.4 $\pm$ 0.1	134 $\pm$ 133
	Sp	149 $\pm$ 43	355 $\pm$ 134	0.58 $\pm$ 0.26	0.03 $\pm$ 0.04	1.74 $\pm$ 0.53	24.8 $\pm$ 6.7	0.0 $\pm$ 0.0	74.0 $\pm$ 6.4	7.2 $\pm$ 3.1	2.3 $\pm$ 0.1	196 $\pm$ 208
	Su	299 $\pm$ 108	501 $\pm$ 111	1.66 $\pm$ 1.12	0.11 $\pm$ 0.16	2.38 $\pm$ 0.34	37.7 $\pm$ 15.2	0.0 $\pm$ 0.0	58.8 $\pm$ 10.3	8.1	2.3	11.2 $\pm$ 1.9
	A	335	530	1.05 $\pm$ 0.25	0.00 $\pm$ 0.00	2.98 $\pm$ 0.71	26.2 $\pm$ 4.3	0.0 $\pm$ 0.0	73.8 $\pm$ 4.3	12.3 $\pm$ 2.7	2.3 $\pm$ 0.2	81 $\pm$ 74
T4	W	219 $\pm$ 115	473 $\pm$ 106	0.91 $\pm$ 0.63	0.00 $\pm$ 0.00	4.19 $\pm$ 3.35	21.3 $\pm$ 13.7	0.0 $\pm$ 0.0	78.7 $\pm$ 13.7	31.2 $\pm$ 25.4	2.2 $\pm$ 0.2	269 $\pm$ 288
	Sp	160 $\pm$ 50	467 $\pm$ 118	0.86 $\pm$ 0.64	0.02 $\pm$ 0.05	1.80 $\pm$ 0.41	28.9 $\pm$ 11.1	0.0 $\pm$ 0.0	70.3 $\pm$ 11.6	10.3 $\pm$ 6.2	1.8 $\pm$ 0.3	140 $\pm$ 102
	Su	206 $\pm$ 0	570 $\pm$ 48	1.26 $\pm$ 0.31	0.02 $\pm$ 0.03	1.83 $\pm$ 0.02	40.2 $\pm$ 6.2	0.0 $\pm$ 0.0	59.0 $\pm$ 5.1	11.0	3.0	7
	A	318	499	0.80 $\pm$ 0.68	0.00 $\pm$ 0.00	5.10 $\pm$ 2.41	15.1 $\pm$ 14.8	0.0 $\pm$ 0.0	84.4 $\pm$ 14.8	12.9 $\pm$ 4.4	2.4 $\pm$ 0.2	48 $\pm$ 22

AFDM, ash-free dry mass; MI, Margalef index.

**FIGURE 3 |** Redundancy discriminant analysis showing response parameters distribution based on drivers evaluated in four different sampling sites in upper Ter River basin (NE Catalonia, Spain) in 2019. Axes 1 and 2 combined explain 89% of variance. Drivers: pH, temperature (Temp), electrical conductivity (EC), dissolved oxygen (DO), turbidity, nitrite ( $\text{N-NO}_2^-$ ), nitrate ( $\text{N-NO}_3^-$ ), ammonium ( $\text{N-NH}_4^+$ ), and phosphate concentration ( $\text{P-PO}_4^{3-}$ ), and nitrogen to phosphorus ratio (DIN:SRP). Response variables: geosmin, minimum fluorescence yield ( $F_0$ ), photosynthetic efficiency ( $Y_{eff}$ ), chlorophyll-a concentration (Chla), ash free dry mass (AFDM), Margalef index (MI), cyanobacteria (Cb), diatoms (Dt) and green algae (GA) biomass, and relative abundance of cyanobacteria ( $R_{Cb}$ ) and diatoms ( $R_{Dt}$ ).

increases from 4.2°C in W1 to 9.5°C in W6, keeping with average values of  $13.6 \pm 1.7^\circ\text{C}$  in spring. The same physicochemical parameters related to geosmin concentration are those that seem

to be linked to the cyanobacteria presence in the biofilm (both absolute concentration and relative abundance), with higher values at the end of winter and in summer. Conversely, the



highest concentration of Chl-*a* and diatoms occur in autumn and early winter, driven by higher values of the DIN:SRP ratio, nitrates concentration, and dissolved oxygen.

An MLR and an RF model between the physicochemical variables (drivers) and geosmin concentration was performed at different time lags (weeks) to identify which factors are the best predictors of geosmin concentration.

Both RF and MLR modeling techniques led to good model fits, but the RF was the better of the two at each time lag (based on  $R^2$  adjusted) (Table 3). At  $t = 0$  weeks (w), the  $R^2$  adj. provided by the RF is 0.70, increasing up to 0.81 at  $t = 2$ w, and decreasing below 0.5 at 8 weeks. A similar pattern is found for the MLR, but in this case, the higher predictive accuracy is 0.62 ( $t = 2$ w) and decreases below 0.5 at 6 weeks. The analysis of relative predictor importance revealed patterns associated with the time lag of

prediction (Figure 5 and Supplementary Figure 1). Before lag 4 weeks ( $t = 5 - t = 10$ w), nitrates concentration and temperature are the parameters with higher relative importance within the RF model ( $\approx 10$ –20%). From that moment on, the phosphorus concentration, the DIN:SRP ratio, and the turbidity value begin to gain relevance, being at  $t = 2$ w when the phosphorus concentration reaches its maximum (28.3%). At this time, there is also a decrease in the relative importance of nitrate concentration, which coincides with an increase in the weight of the DIN:SRP ratio within the model, which is one of the main predictors of geosmin concentration among time-lags 0–2w (22.4–15.2%). At  $t = 0$  and  $t = 1$  week, turbidity is the parameter with the higher relative importance (26.1 and 23.8%, respectively).

## DISCUSSION

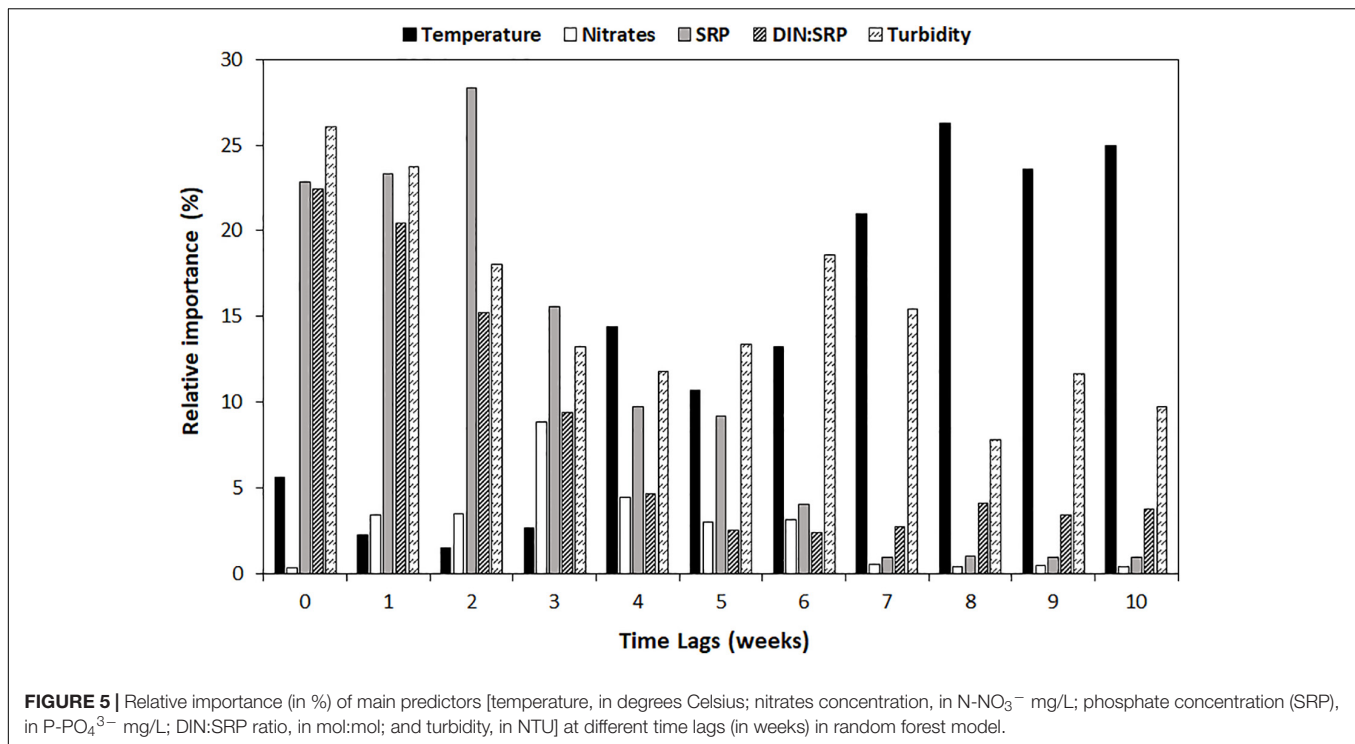
This study, carried out in the upper part of the Ter River basin, suggested the physicochemical parameters that could trigger geosmin appearance in a river where benthic cyanobacteria are the main geosmin producers.

### Geosmin Episodes in the Upper Ter River Basin

During the study, geosmin concentration varied depending on the sampling site and the season (Figure 2). Sampling sites

**TABLE 3 |** Predictive accuracy as measured by  $R^2$  adjusted for different time lags (in weeks), for multiple linear regression (MLR) and random forest (RF) models in upper Ter River basin (NE Catalonia, Spain) in 2019.

$R^2$ adj.	Time lag (weeks)										
	0	1	2	3	4	5	6	7	8	9	10
MLR	0.61	0.58	0.62	0.55	0.49	0.50	0.47	0.45	0.36	0.35	0.30
RF	0.70	0.73	0.81	0.77	0.74	0.68	0.57	0.52	0.46	0.46	0.43



differed mainly in the nutrient's concentration, being higher in T3 and T4, located downstream. The nutrient concentration pattern measured along the upper river Ter could be explained by nearby land uses, which in the Osona region (where T3 and T4 are located) are predominantly related to agriculture (35% of the total area) and urban and industrial development (CORINE Land Cover System, 2018), whereas El Ripollès region, where T1 and T2 sampling sites were located, was characterized by a high percentage of forest and pastures (between 31.2 and 42.5%). The lower levels of point and non-point pollution sources, related to dominant land-use together with the river continuum concept, could help to explain the lower nutrient concentrations found at these sampling sites (Table 1). Furthermore, forests and pastures are environments that can contribute to reducing surface erosion and soil sediment runoff, which are among the main diffuse sources of phosphorus to freshwater rivers. Ongley et al. (2010) reported that agriculture contributes >50% of the total nutrient load, and the fraction of this total load is highly dependent on the proportion of agriculture in the watershed (Shi et al., 2017). Furthermore, agricultural activities are used to have a marked seasonality, with spring being the season that, due to a greater number of rains and higher temperatures, favors better growth and development of crops. This agrees with what is observed in the agricultural activity of Osona, where most of the crops are cereals (53.7%) and forages (43.1%), whose sowing time is in late winter and spring (mainly in March) (Departament d'Agricultura, Generalitat de Catalunya). This makes agricultural land uses have a greater impact on water quality in winter and spring, when planting occurs and crops are fertilized. Moreover, in spring, a larger amount of rainfall could cause fertilizer used in the crops to overflow into the river leaches, directly or

through the contribution of groundwater, thereby leading to the deterioration of river water quality. Specifically, ammonium and phosphorus can be easily absorbed by soil particles, then being transported to streams and rivers in events of soil erosion and runoff (Withers and Jarvie, 2008). In the opposite way, nitrate is highly soluble and mobile, and when there is an excess of nitrates, it is leached to groundwater and reaches the rivers through underground flows (Grizzetti et al., 2011). The difference in the mobilization dynamic of nitrogen and phosphorus from the surface can give rise to changes in the DIN:SRP ratio.

Both the concentration of nutrients and the DIN:SRP ratio are factors related to the development of certain cyanobacteria, being described that high nutrient concentrations favor the appearance of cyanobacterial blooms (Dodds and Smith, 2016; Lee et al., 2017), in many cases related to geosmin production (Ding et al., 2014). Similar results were observed in this field study, where higher nutrient concentration may have generated favorable conditions for the cyanobacterial development within biofilm communities ( $0.91 \pm 0.58 \mu\text{g}/\text{cm}^2$  in T4 compared with  $0.33 \pm 0.44 \mu\text{g}/\text{cm}^2$  in T1, mean annual value). Some studies have described that a high nitrogen concentration is necessary for cyanobacteria blooms to occur ( $>0.8 \text{ mgTN}/\text{L}$ , Xu et al., 2015;  $\approx 0.1 \text{ mgN-NH}_4^+/\text{L}$ ,  $\approx 1.1 \text{ mgN-NO}_3^-/\text{L}$ , Espinosa et al., 2021). Perkins et al. (2019) pointed out that the ammonium concentration was key for stimulating cyanobacteria development and production of T&O compounds, specifically revealing that metabolites were associated with high ammonium relative to nitrate. In the opposite way, a study performed by Harris et al. (2016) suggested that relatively low  $\text{NO}_3:\text{NH}_3$  ratios provide conditions that favor the production of cyanobacterial metabolites. A previous study



by Jankowiak et al. (2019) described that phosphorus availability excess may stimulate cyanobacteria blooms, and some studies have pointed out that total phosphorus (TP, both organic and inorganic forms) concentration had to be between 20 and 100 µg TP/L to control the growth of cyanobacteria (Sharma et al., 2011; Li et al., 2018). Moreover, Graham et al. (2004) identified the dominance of cyanobacteria often greatest when the total nitrogen (TN):TP ratio was low (<29:1 by mass), similar to the results found by Harris et al. (2016) in a study carried out in four North American reservoirs. Vilalta et al. (2003), in a study performed in the Llobregat River (Catalonia, NE Spain), suggested that an unbalanced proportion between nitrogen and phosphorus had an effect on benthic geosmin production, being its appearance favored under low TN:TP ratios (TN:TP = 10:1). The study carried out under laboratory conditions by Espinosa et al. (2021) showed that high nutrient concentration, together with a low DIN:SRP ratio (DIN:SRP = 4:1), triggered the production and release of geosmin by the *Oscillatoria* cyanobacterium present in the biofilm. This difference in the results could be due to factors related to the study system, such as stratification, redox potential, and resuspension of nutrients in reservoirs. However, it could be pointed out that a minimum of nitrogen should be necessary to favor cyanobacteria development. Nevertheless, to trigger geosmin production, an increase in the phosphorus concentration must occur, leading to an imbalance in the DIN:SRP ratio or TN:TP ratio. A similar situation has been observed in this study, as both cyanobacteria abundance and geosmin concentration was favored by high nutrient concentrations and lower DIN:SRP ratio, led by an increase of phosphorus concentration. The effect was clearly observed at T4, the sampling site with higher nutrient concentrations, where in late winter–early spring, there was a pronounced decrease of the DIN:SRP ratio value (Figure 4), associated with an important episode of geosmin. The interaction between DIN:SRP ratio and nutrient concentration seems to be an important driver favoring the production and release of this metabolite from benthic cyanobacteria in the Ter River.

## Mismatch Between Cyanobacteria Abundance and Geosmin Concentration

Although cyanobacteria presence and geosmin production seem to be favored by the same physicochemical factors, in this field study, no significant correlation was found between both parameters. This is somehow surprising, as these microorganisms are described as the main geosmin producers in freshwater ecosystems. One reason could be that an identification of the biofilm community at the genus level was not carried out in this study, and, as previously discussed, not all cyanobacteria are geosmin producers. On the other hand, it could be explained by the relative dynamics of geosmin production and release associated with the cyanobacteria life cycle. In fact, it has been described under controlled conditions that geosmin production mainly occurs during the growth phase, and its release to water is the direct consequence of biomass decomposition and/or cell lysis (Kim et al., 2018).

Although no biofilm community identification was carried out throughout the study, biofilm samples were taken from the T4 sampling site in late March for a parallel study carried out under laboratory conditions. These samples were characterized, and the cyanobacterium *Oscillatoria* sp. was identified as the main geosmin producer (Espinosa et al., 2021). Furthermore, a visual difference detected *in situ* was the presence of floating cyanobacterial mats coming from the biofilm in winter, whereas in summer, these mats were not observed (personal observation).

Regarding the mismatch found between cyanobacteria and geosmin in late winter–early spring, it could be explained by the cyanobacterial life cycle itself. Different studies performed by Hu et al. (2001, 2003) evaluating different cyanobacterial species explained that intracellular geosmin concentration increased in proportion to biomass. In addition to intracellular accumulation, it was observed that the concentration of geosmin in water began to increase. Once these cyanobacteria reached the stationary phase, there was a rapid decrease in intracellular concentration with a corresponding rapid increase of geosmin release, indicating that cell lysis and decomposition of geosmin producers may result in large spikes of these compounds in water supplies. Similar results were observed by Cai et al. (2017); Alghanmi et al. (2018), and Espinosa et al. (2021), supporting the idea that the majority of geosmin is normally retained with cyanobacterial cells during their growth, and release to the medium occur as a consequence of lysis and cellular decomposition. Different studies have pointed out that, depending on the cyanobacterial strain, the growth phase differs. Kruskopf and Du Plessis (2006) observed that *Oscillatoria simplicissima* reached the fast growth phase after 8 days, whereas Espinosa et al. (2021) found out the maximum *Oscillatoria* sp. presence at 16 days, and Jindal et al. (2011) described that *Oscillatoria formosa* could grow exponentially for 24 days before starting the stationary phase. In this field study, the relative abundance of cyanobacteria reached its peak after 1–2 weeks of gradual increase and 1 week later started to decrease, whereas geosmin in the water started reaching its peak 1 week later. This would confirm what was observed in several studies reporting geosmin release to water as a consequence of cyanobacterial biomass decomposition and/or cell lysis.

Despite the lack of correlation between cyanobacteria abundance and the geosmin concentration, the trends that have been observed, such as the ones shown in Figure 6, can help make a hypothesis about the geosmin drivers in the upper river Ter. This figure shows a notable increase in the cyanobacteria abundance during the first months of the year, reaching almost 50% of the biofilm community at the beginning of March and decreasing strongly 15 days later, coinciding with the geosmin peak (Figure 6A). Similar behavior was observed at the end of April. Nevertheless, this trend only occurs in winter and spring. In summer, cyanobacteria presence was also high, but geosmin was not detected, indicating that the factors favoring its production are not stable throughout the year and that a set of specific conditions have to co-occur to trigger geosmin production by benthic cyanobacteria. Some of the factors that differ between these two moments were the DIN:SRP ratio and the temperature, which presented significantly lower values in

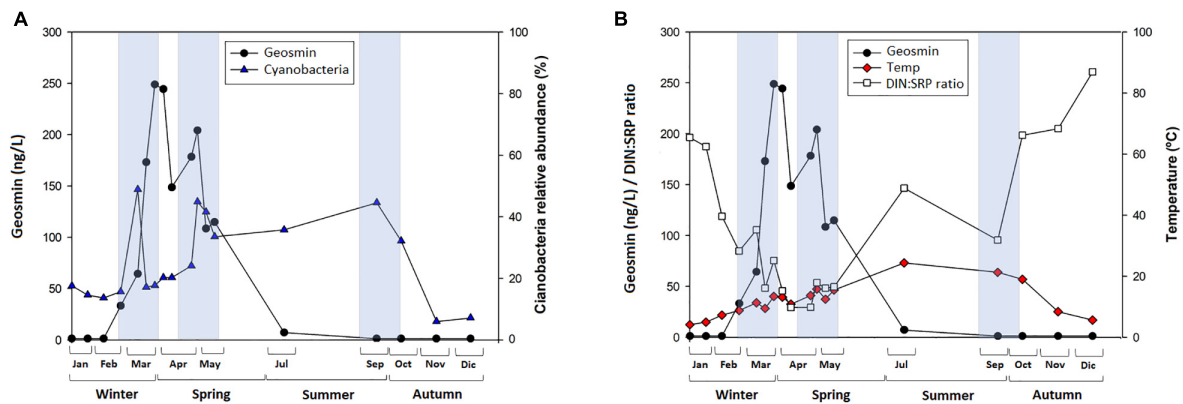


**FIGURE 6 | (A)** Mean value and standard deviation of geosmin concentration (nanogram per liter), and cyanobacteria relative abundance (%) and **(B)** mean value and standard deviation of geosmin concentration (nanogram per liter) and DIN:SRP ratio (mol/mol), water temperature (°C) in T4 sampling site for different sampling in 2019, being Jan = January, Feb = February, Mar = March, Apr = April, May = May, Jul = July, Sep = September, Oct = October, Nov = November, and Dec = December. Blue boxes indicate time when cyanobacteria relative abundance in biofilm was high.

winter–spring than in summer (**Figure 6B**). The study performed by Alghanmi et al. (2018) pointed out that many cyanobacteria grow better under 25°C conditions, but this does not imply higher geosmin production. In fact, some studies have found higher geosmin concentration and production yield at 10°C compared with higher temperatures (25 and 35°C), indicating that lower temperatures could stimulate geosmin production and favor the accumulation of geosmin in cells (Zhang et al., 2009; Wang and Li, 2015). This would agree with our study, where higher geosmin concentration was observed at lower temperatures (close to 10°C), whereas at higher temperatures (20–25°C), geosmin levels were below the detection limit (**Figure 6B**). Moreover, considering that low light conditions have been described to favor intracellular geosmin production in river biofilms (Espinosa et al., 2020), the increased light availability occurring in summer may be an additional limiting factor for microbial geosmin production in the Ter River, as higher light incidence prevents gaseous vacuoles formation and geosmin production (Li et al., 2012). In fact, different studies have shown that at temperatures ≈20–25°C, higher light intensity hinders the production of geosmin by cyanobacteria (Oh et al., 2017; Alghanmi et al., 2018).

## Change in the Relative Predictor Importance

The change in the physicochemical conditions at the different sampling sites and seasons could explain the change in the relative importance of the parameters included in the models developed at different time lags. As shown in **Figure 5**, nitrate concentration and temperature are more relevant in predicting geosmin between lags 5 and 10 (1–2 and a half months in advance), which could indicate the need for high basal nitrate conditions (Xu et al., 2015; Espinosa et al., 2021). However, for a geosmin episode to occur, it seems that a gradual increase in the phosphorus concentration, whose maximum importance as a geosmin driver within the model

is reached in lag 2-w, is needed to generate conditions that would favor the development of cyanobacteria biomass. The increase in phosphorus concentration generates an imbalance in the DIN:SRP ratio, whose values decrease as its relative importance in the model increases, up to its maximum at  $t = 0w$  (22.4%), indicating that this ratio must be kept low throughout the geosmin episode. These results agree with what was demonstrated by Espinosa et al. (2021) in a study performed under controlled conditions with biofilm communities collected from Ter River, in which cyanobacterial development (*Oscillatoria* sp.) and geosmin production were favored by higher nutrient concentration (both nitrogen and phosphorus) together with lower DIN:SRP ratio (4:1 compared with 64:1). Another parameter that has presented relatively high importance in the models is turbidity. This could have different explanations: the first one is that the lower incidence of light generated by greater turbidity promotes the development of low-light organisms, such as geosmin-producing cyanobacteria (Espinosa et al., 2020). In fact, other studies evaluating the light incidence with the Secchi Disk method have found a negative relationship between light penetration and geosmin concentration, supporting the idea that low light availability conditions may favor the development of geosmin-producing cyanobacteria (Dzialowski et al., 2009; Parr, 2014). Another explanation is that turbidity has been shown to be correlated with phosphorus concentration, mainly associated with the runoff process (Schilling et al., 2017), which has also been observed in this study. Finally, when the benthic geosmin–cyanobacteria producers are detached from the substrata, which coincide with the cells lysis and consequent geosmin release to the water column, it also releases different material, which can generate an increase in the turbidity value (i.e., solids trapped within thick biofilms in slow flow waters). This last point could explain why turbidity is the principal predictor at times 0 and 1.

The models developed with the database generated in the Ter River in 2019 have made it possible to know with a precision of 0.70–0.81 (considering 1 as the maximum possible value)

the geosmin concentration up to a month-month and a half in advance. In addition, the results generated by the models indicate that the RF algorithm offers a great option for the evaluation of long-term ecological data sets. This model has also made it possible to identify the related parameters in each lag and the necessary changes of physicochemical parameters that should occur to increase the possibility of a geosmin episode being triggered. Knowing the relative importance of geosmin drivers, as evidenced by this study, drinking water treatment companies have the possibility of advancing to geosmin episodes based on the monitoring of easier and cheaper variables. In this way, they can have enough time to implement the required treatment and prevent geosmin from reaching the consumer's tap, avoiding complaints from users by being able to offer quality drinking water continuously.

## CONCLUSION

Overall, this field study showed that factors directly and indirectly related to both global change and anthropogenic factors could be potential drivers of geosmin occurrence in Mediterranean rivers.

River stretches, which land uses of the surrounding areas favoring higher nutrient concentrations, are more susceptible to be affected by cyanobacterial blooms and geosmin episodes. For example, industrial and agricultural watersheds could lead to higher nutrient concentrations in river waters, which can favor certain cyanobacteria development (such as *Oscillatoria* sp.). Furthermore, agricultural watersheds are used to experience an increase of phosphorous concentration associated with planting and fertilization periods that may generate a DIN:SRP ratio decrease especially during late winter-early spring. This situation can favor that certain cyanobacterium would start to produce geosmin, which would be released into the water between 7 and 15 days after the cyanobacteria peak in biofilms, associated with the organism degradation or cell lysis.

These results could help to drinking water companies in the forecasting and management of geosmin episodes, being able to understand which ecological conditions are more prompt to favor

the appearance of geosmin in the water collected from surface waters and thus allowing them to implement more targeted treatment regimens before geosmin reach the consumer's tap.

## DATA AVAILABILITY STATEMENT

The raw data supporting the conclusions of this article will be made available by the authors, without undue reservation.

## AUTHOR CONTRIBUTIONS

All authors made substantial contributions to the conception or design of the work, or the acquisition, analysis, or interpretation of data for the work.

## FUNDING

We would like to acknowledge the water utilities Aigües de Vic S.A. and Aigües d'Osona S.A. (Catalonia, Spain) for their funding support in the study presented in this publication. The research leading to these results have received funding from the European Research Council under the European Union's Horizon 2020 Research and Innovation Program—H2020 INTCATCH (grant agreement n°689341). LP have received funding from the Post-doctoral Fellowships Programme Beatriu de Pinós, funded by the Secretary of Universities and Research (Government of Catalonia) and by the Horizon 2020 Programme of Research and Innovation of the European Union under the Marie Skłodowska-Curie Grant Agreement No. 801370.

## SUPPLEMENTARY MATERIAL

The Supplementary Material for this article can be found online at: <https://www.frontiersin.org/articles/10.3389/fmicb.2021.741750/full#supplementary-material>

## REFERENCES

- Alghanmi, H. A., Alkam, F. M., and Al-Tae, M. M. (2018). Effect of light and temperature on new cyanobacteria producers for geosmin and 2-methylisoborneol. *J. Appl. Phycol.* 30, 319–328. doi: 10.1007/s10811-017-1233-0
- APHA (2005). *Standard Methods for the Examination of Water and Wastewater*. 21st Edn. Washington DC: American Public Health Association/American Water Works Association/Water Environment Federation.
- Argudo, M., Gich, F., Bonet, B., Espinosa, C., Gutiérrez, M., and Guasch, H. (2020). Responses of resident (DNA) and active (RNA) microbial communities in fluvial biofilms under different polluted scenarios. *Chemosphere* 242:125108. doi: 10.1016/j.chemosphere.2019.125108
- Cai, F., Yu, G., Zhang, K., Chen, Y., Li, Q., Yang, Y., et al. (2017). Geosmin production and polyphasic characterization of *Oscillatoria limosa* Agardh ex Gomont isolated from the open canal of a large drinking water system in Tianjin City, China. *Harmful Algae* 69, 28–37. doi: 10.1016/j.hal.2017.09.006
- Clerc, N. A., and Druschel, G. K. (2019). Influence of environmental factors on the production of MIB and Geosmin metabolites by bacteria in a eutrophic reservoir. *Water Resour. Res.* 55, 5413–5430. doi: 10.1029/2018wr023651
- CORINE Land Cover System (2018). *Copernicus Global Land Service. Providing Bio-Geophysical Products of Global Land Surface*.
- Ding, Z., Peng, S., Jin, Y., Xuan, Z., Chen, X., and Yin, L. (2014). Geographical and seasonal patterns of geosmin and 2-methylisoborneol in environmental water in Jiangsu Province of China. *J. Anal. Methods Chem.* 2014:743924.
- Dodds, W. K., and Smith, V. H. (2016). Nitrogen, phosphorus, and eutrophication in streams. *Inland Waters* 6, 155–164. doi: 10.5268/iw-6.2.909
- Drury, B., Rosi-Marshall, E., and Kelly, J. J. (2013). Wastewater treatment effluent reduces the abundance and diversity of benthic bacterial communities in urban and suburban rivers. *Appl. Environ. Microbiol.* 79, 1897–1905. doi: 10.1128/aem.03527-12
- Dzialowski, A. R., Smith, V. H., Huggins, D. G., deNoyelles, F., Lim, N. C., Baker, D. S., et al. (2009). Development of predictive models for geosmin-related taste and odor in Kansas, USA, drinking water reservoirs. *Water Res.* 43, 2829–2840. doi: 10.1016/j.watres.2009.04.001
- Elosegui, A., and Sabater, S. (eds) (2009). *Conceptos y Técnicas en Ecología Fluvial*. Bilbao: Fundación BBVA.
- Espinosa, C., Abril, M., Guasch, H., Pou, N., Proia, L., Ricart, M., et al. (2020). Water flow and light availability influence on intracellular geosmin production

- in river biofilms. *Front. Microbiol.* 10:3002. doi: 10.3389/fmicb.2019.03002
- Espinosa, C., Abril, M., Ponsá, S., Ricart, M., Vendrell-Puigmitjà, L., Ordeix, M., et al. (2021). Effects of the interaction between nutrient concentration and DIN:SRP ratio on geosmin production by freshwater biofilms. *Sci. Total Environ.* 768:144473. doi: 10.1016/j.scitotenv.2020.144473
- Graham, J. L., Jones, J. R., Jones, S. B., Downing, J. A., and Clevenger, T. E. (2004). Environmental factors influencing microcystin distribution and concentration in the Midwestern United States. *Water Res.* 38, 4395–4404.
- Grizzetti, B., Bouraoui, F., Billen, G., van Grinsven, H., Cardoso, A. C., Thieu, V., et al. (2011). *Nitrogen as a Threat to European Water Quality*. Cambridge: Cambridge University Press.
- Harris, T., Smith, V., Graham, J., Van de Waal, D., Tedesco, L., and Clercin, N. (2016). Combined effects of nitrogen to phosphorus and nitrate to ammonia ratios on cyanobacterial metabolite concentrations in eutrophic Midwestern USA reservoirs. *Inland Waters* 6, 199–210. doi: 10.5268/iw-6.2.938
- Ho, J. C., Michalak, A. M., and Pahlevan, N. (2019). Widespread global increase in intense lake phytoplankton blooms since the 1980s. *Nature* 574, 667–670. doi: 10.1038/s41586-019-1648-7
- Hu, Q., Fortuna, A., Sommerfeld, M. R., and Westerhoff, P. K. (2003). “Physiological studies of MIB and geosmin-producing cyanobacteria isolated from the Phoenix drinking water supply system,” in *Poster at the CAP LTER 5th Annual Poster Symposium* (Tempe: Arizona State University), 1–4.
- Hu, Q., Sommerfeld, M., Lowry, D., Dempster, T., Westerhoff, P., Baker, L., et al. (2001). Production and release of geosmin by the cyanobacterium *Oscillatoria splendida* isolated from a Phoenix water source. *J. Phycol.* 37, 25–26.
- Intergovernmental Panel on Climate Change [IPCC] (2019). *2019 Refinement to the 2006 IPCC Guidelines for National Greenhouse Gas Inventories*. Geneva: Intergovernmental Panel on Climate Change.
- Jähnichen, S., Jäschke, K., Wieland, F., Packroff, G., and Benndorf, J. (2011). Spatio-temporal distribution of cell-bound and dissolved geosmin in Wahnbach reservoir: causes and potential odour nuisances in raw water. *Water Res.* 45, 4973–4982. doi: 10.1016/j.watres.2011.06.043
- Jankowiak, J., Hattenrath-Lehmann, T., Kramer, B. J., Ladds, M., and Gobler, C. J. (2019). Deciphering the effects of nitrogen, phosphorus, and temperature on cyanobacterial bloom intensification, diversity, and toxicity in western Lake Erie. *Limnol. Oceanogr.* 64, 1347–1370. doi: 10.1002/lno.11120
- Jeffrey, S. W., and Humphrey, G. F. (1975). New spectrophotometric equations for determining chlorophylls a, b, c1 and c2 in higher plants, algae and natural phytoplankton. *Biochem. Physiol. Plants* 167, 191–194. doi: 10.1016/s0015-3796(17)30778-3
- Jindal, N., Singh, D. P., and Khattar, J. I. S. (2011). Kinetics and physico-chemical characterization of exopolysaccharides produced by the cyanobacterium *Oscillatoria formosa*. *World J. Microbiol. Biotechnol.* 27, 2139–2146.
- Jüttner, F., and Watson, S. B. (2007). Biochemical and ecological control of geosmin and 2-methylisoborneol in source waters. *Appl. Environ. Microbiol.* 73, 4395–4406. doi: 10.1128/aem.02250-06
- Karaouzas, I., Theodoropoulos, C., Vardakas, L., Kalogianni, E., and Skoulikidis, N. (2018). A review of the effects of pollution and water scarcity on the stream biota of an intermittent Mediterranean basin. *River Res. Appl.* 34, 291–299. doi: 10.1002/rra.3254
- Kehoe, M. J., Chun, K. P., and Baulch, H. M. (2015). Who smells? Forecasting taste and odor in a drinking water reservoir. *Environ. Sci. Technol.* 49, 10984–10992. doi: 10.1021/acs.est.5b00979
- Kim, K., Park, C., Yoon, Y., and Hwang, S. J. (2018). Harmful cyanobacterial material production in the North Han river (South Korea): genetic potential and temperature-dependent properties. *Int. J. Environ. Res. Public Health* 15:444.
- Kruskopf, M., and Du Plessis, S. (2006). Growth and filament length of the bloom forming *Oscillatoria simplicissima* (Oscillatoriales, Cyanophyta) in varying N and P concentrations. *Hydrobiologia* 556, 357–362. doi: 10.1007/s10750-005-1061-0
- Lee, J., Rai, P. K., Jeon, Y. J., Kim, K. H., and Kwon, E. E. (2017). The role of algae and cyanobacteria in the production and release of odorants in water. *Environ. Pollut.* 227, 252–262. doi: 10.1016/j.envpol.2017.04.058
- Li, J., Hansson, L. A., and Persson, K. M. (2018). Nutrient control to prevent the occurrence of cyanobacterial blooms in a eutrophic lake in Southern Sweden, used for drinking water supply. *Water* 10:919.
- Li, Z., Hobson, P., An, W., Burch, M. D., House, J., and Yang, M. (2012). Earthy odor compounds production and loss in three cyanobacterial cultures. *Water Res.* 46, 5165–5173. doi: 10.1016/j.watres.2012.06.008
- Lukassen, M. B., de Jonge, N., Bjerregaard, S. M., Podduturi, R., Jørgensen, N. O., Petersen, M. A., et al. (2019). Microbial production of the off-flavor geosmin in tilapia production in Brazilian water reservoirs: importance of bacteria in the intestine and other fish-associated environments. *Front. Microbiol.* 10:2447. doi: 10.3389/fmicb.2019.02447
- Meteocat (2019). *Servei Meteorològic de Catalunya. Bolletí Climàtic Anual del 2019*. Barcelona: Generalitat de Catalunya. Departament de Territori i Sostenibilitat.
- Murphy, J., and Riley, J. P. (1962). A modified single solution method for the determination of phosphate in natural waters. *Anal. Chim. Acta* 27, 31–36. doi: 10.1016/s0003-2670(00)88444-5
- Oh, H. S., Lee, C. S., Srivastava, A., Oh, H. M., and Ahn, C. Y. (2017). Effects of environmental factors on cyanobacterial production of odorous compounds: geosmin and 2-methylisoborneol. *J. Microbiol. Biotechnol.* 27, 1316–1323. doi: 10.4014/jmb.1702.02069
- Olsen, B. K., Chislock, M. F., and Wilson, A. E. (2016). Eutrophication mediates a common off-flavor compound, 2-methylisoborneol, in a drinking water reservoir. *Water Res.* 92, 228–234. doi: 10.1016/j.watres.2016.01.058
- Ongley, E. D., Xiaolan, Z., and Tao, Y. (2010). Current status of agricultural and rural non-point source pollution assessment in China. *Environ. Pollut.* 158, 1159–1168. doi: 10.1016/j.envpol.2009.10.047
- Parr, G. (2014). *Development of Predictive Geosmin Models in Northern Colorado Lakes, Reservoirs, and Rivers 2000-2019*-CSU. Ph.D. thesis. Fort Collins, CO: Colorado State University.
- Perkins, R. G., Slavin, E. I., Andrade, T. M. C., Blenkinsopp, C., Pearson, P., Froggatt, T., et al. (2019). Managing taste and odour metabolite production in drinking water reservoirs: the importance of ammonium as a key nutrient trigger. *J. Environ. Manag.* 244, 276–284. doi: 10.1016/j.jenvman.2019.04.123
- Rand, M. C., Greenberg, A. E., and Taras, M. J. (1976). *Standard Methods for the Examination of Water and Wastewater*. Washington, DC: American Public Health Association.
- Reardon, J., Foreman, J. A., and Searcy, R. L. (1966). New reactants for the colorimetric determination of ammonia. *Clin. Chim. Acta* 14, 403–405. doi: 10.1016/0009-8981(66)90120-3
- Rubio-Gracia, F., García-Berthou, E., Zamora, L., Martí, E., Almeida, D., Espinosa, C., et al. (2017). Combined effects of hydrologic alteration and cyprinid fish in mediating biogeochemical processes in a Mediterranean stream. *Sci. Total Environ.* 601–602, 1217–1225. doi: 10.1016/j.scitotenv.2017.05.287
- Schilling, K. E., Kim, S. W., and Jones, C. S. (2017). Use of water quality surrogates to estimate total phosphorus concentrations in Iowa rivers. *J. Hydrol. Reg. Stud.* 12, 111–121. doi: 10.1016/j.ejrh.2017.04.006
- Sharma, N. K., Choudhary, K. K., Bajpai, R., and Rai, A. K. (2011). “Freshwater cyanobacterial (bluegreen algae) blooms: causes, consequences and control,” in *Impact, Monitoring and Management of Environmental Pollution*, ed. A. Al-Nemr (Hauppauge, NY: Nova Science Publishers), 73–95.
- Shi, P., Zhang, Y., Li, Z., Li, P., and Xu, G. (2017). Influence of land use and land cover patterns on seasonal water quality at multi-spatial scales. *Catena* 151, 182–190. doi: 10.1016/j.catena.2016.12.017
- Smith, V. H., DeNoyelles, F., Pan, S., Sieber-Denlinger, J., Randtke, S. J., Strasser, V. A., et al. (2009). Managing taste and odor problems in a eutrophic drinking water reservoir. *Lake Reserv. Manag.* 18, 319–323. doi: 10.1080/07438140209353938
- Vilalta, E. (2004). *Structure and Function in Fluvial Biofilms: Implications in River DOC Dynamics and Nuisance Metabolite Production*. Ph.D. thesis. Barcelona: University of Barcelona.
- Vilalta, E., Guasch, H., Muñoz, I., Navarro, E., Romaní, A. M., Valero, F., et al. (2003). Ecological factors that co-occur with geosmin production by benthic cyanobacteria. The case of the Llobregat River. *Algol. Stud.* 109, 579–592. doi: 10.1127/1864-1318/2003/0109-0579
- Wang, Z., and Li, R. (2015). Effects of light and temperature on the odor production of 2-methylisoborneol-producing *pseudanabaena* sp. and geosmin-producing *Anabaena ucrainica* (cyanobacteria). *Biochem. Syst. Ecol.* 58, 219–226. doi: 10.1016/j.bse.2014.12.013
- Watson, S. B., Monis, P., Baker, P., and Giglio, S. (2016). Biochemistry and genetics of taste- and odor-producing cyanobacteria. *Harmful Algae* 54, 112–127. doi: 10.1016/j.hal.2015.11.008



- Withers, P. J. A., and Jarvie, H. P. (2008). Delivery and cycling of phosphorus in rivers: a review. *Sci. Total Environ.* 400, 379–395.
- Xu, H., Paerl, H. W., Qin, B., Zhu, G., Hall, N. S., and Wu, Y. (2015). Determining critical nutrient thresholds needed to control harmful cyanobacterial blooms in eutrophic Lake Taihu, China. *Environ. Sci. Technol.* 49, 1051–1059. doi: 10.1021/es503744q
- Zhang, T., Li, L., Song, L., and Chen, W. (2009). Effects of temperature and light on the growth and geosmin production of *Lyngbya kuetzingii* (Cyanophyta). *J. Appl. Phycol.* 21, 279–285. doi: 10.1007/s10811-008-9363-z

**Conflict of Interest:** The authors declare that this study received funding from Aigües de Vic S.A. and Aigües d'Osona S.A. The funder was not involved in the study design, collection, analysis, interpretation of data, the writing of this article, or the decision to submit it for publication.

The handling editor SM declared a past co-authorship with several of the authors CE, MA, SP, LV-P, LL, LP.

**Publisher's Note:** All claims expressed in this article are solely those of the authors and do not necessarily represent those of their affiliated organizations, or those of the publisher, the editors and the reviewers. Any product that may be evaluated in this article, or claim that may be made by its manufacturer, is not guaranteed or endorsed by the publisher.

Copyright © 2021 Espinosa, Abril, Bretxa, Jutglar, Ponsá, Sellarès, Vendrell-Puigmitjà, Llenas, Ordeix and Proia. This is an open-access article distributed under the terms of the Creative Commons Attribution License (CC BY). The use, distribution or reproduction in other forums is permitted, provided the original author(s) and the copyright owner(s) are credited and that the original publication in this journal is cited, in accordance with accepted academic practice. No use, distribution or reproduction is permitted which does not comply with these terms.



# Microbial Transformation of Chlordecone and Two Transformation Products Formed During *in situ* Chemical Reduction

Jennifer Hellal<sup>1\*</sup>, Pierre-Loïc Saaïdi<sup>2</sup>, Sébastien Bristeau<sup>1</sup>, Marc Crampon<sup>1</sup>, Delphine Muselet<sup>2</sup>, Oriane Della-Negra<sup>2</sup>, Aourel Mauffret<sup>1</sup>, Christophe Mouvet<sup>1</sup> and Catherine Jouliau<sup>1</sup>

<sup>1</sup> BRGM, Orléans, France, <sup>2</sup> UMR 8030 Génomique Métabolique, CEA, Institut de Biologie François Jacob, Genoscope, Université d'Evry Val d'Essonne, Université Paris-Saclay, Evry, France

## OPEN ACCESS

### Edited by:

Fabrice Martin-Laurent,  
Institut National de la Recherche  
Agronomique (INRA), France

### Reviewed by:

Joaquim Vila,  
University of Barcelona, Spain  
Giovanni Pilloni,  
ExxonMobil Research  
and Engineering, United States

### \*Correspondence:

Jennifer Hellal  
j.hellal@brgm.fr

### Specialty section:

This article was submitted to  
Microbiotechnology,  
a section of the journal  
Frontiers in Microbiology

Received: 15 July 2021

Accepted: 30 September 2021

Published: 04 November 2021

### Citation:

Hellal J, Saaïdi P-L, Bristeau S,  
Crampon M, Muselet D,  
Della-Negra O, Mauffret A, Mouvet C  
and Jouliau C (2021) Microbial  
Transformation of Chlordecone  
and Two Transformation Products  
Formed During *in situ* Chemical  
Reduction.  
Front. Microbiol. 12:742039.  
doi: 10.3389/fmicb.2021.742039

Chlordecone (CLD) is a very persistent synthetic organochlorine pesticide found in the French West Indies. Recently published work has demonstrated the potential of zero-valent iron to dechlorinate CLD by *in situ* chemical reduction (ISCR) in soils under water-saturated conditions, forming mono- to penta-dechlorinated CLD transformation products. These transformation products are more mobile than CLD and less toxic; however, nothing is known about their further degradation, although increasing evidence of CLD biodegradation by bacteria is being found. The present study began with the enrichment from wastewater sludge of a CLD-transforming community which was then inoculated into fresh media in the presence of either CLD or two of the main ISCR transformation products, 10-mono-hydroCLD (-1Cl-CLD) and tri-hydroCLD (-3Cl-CLD). Carried out in triplicate batches and incubated at 38°C under anoxic conditions and in the dark, the cultures were sampled regularly during 3 months and analyzed for CLD, -1Cl-CLD, -3Cl-CLD, and possible transformation products by gas chromatography coupled to mass spectrometry. All batches showed a decrease in the amended substrates (CLD or hydroCLD). CLD degradation occurred with concomitant formation of a nine-carbon compound (pentachloroindene) and two sulfur-containing transformation products (chlordecthiol, CLD-SH; methyl chlordecysulfide, CLD-SCH<sub>3</sub>), demonstrating competing transformation pathways. In contrast, -1Cl-CLD and -3Cl-CLD only underwent a sequential reductive sulfidation/S-methylation process resulting in -1Cl-CLD-SH and -1Cl-CLD-SCH<sub>3</sub> on the one hand, and -3Cl-CLD-SH, -3Cl-CLD-SCH<sub>3</sub> on the other hand. Some sulfur-containing transformation products have been reported previously with single bacterial strains, but never in the presence of a complex microbial community. At the end of the experiment, bacterial and archaeal populations were investigated by 16S rRNA gene amplicon sequencing. The observed diversity was mostly similar in the CLD and -1Cl-CLD conditions to the inoculum with a dominant archaea genus, *Methanobacterium*, and four OTU affiliated to bacteria, identified at the family (*Spirochaetaceae*) or genus level (*Desulfovibrio*, *Aminobacterium*,

and *Soehngenia*). On the other hand, in the -3Cl-CLD condition, although the same OTU were found, *Clostridium sensu stricto* 7, *Candidatus Cloacimonas*, and *Proteiniphilum* were also present at > 2% sequences. Presence of methanogens and sulfate-reducing bacteria could contribute to sulfidation and S-methylation biotransformations. Overall, these results contribute to increasing our knowledge on the biodegradability of CLD and its transformation products, helping to progress toward effective remediation solutions.

**Keywords: chlordecone (CLD), West Indies, ISCR, bacteria, biotransformation**

## INTRODUCTION

Soils, surface water, and groundwater in Martinique and Guadeloupe (French West Indies, FWI) are contaminated with chlordecone [CLD;  $C_{10}Cl_{10}O$  or  $C_{10}Cl_{10}H_2O_2$  in hydrated form; CAS number 143-50-0; decachlorooctahydro-1,3,2-metheno-2H-cyclobuta(c,d)pentalen-2-one], a very persistent synthetic organochlorine pesticide. CLD was widely used ( $3 \text{ kg} \cdot \text{ha}^{-1}$  per year; an estimated total of 300 t) in the FWI, officially from 1972 to 1978 and from 1981 to 1993, to protect banana plantations against the banana weevil (*Cosmopolites sordidus*). CLD is a highly hydrophobic organochlorine pesticide (Kow between 4.5 and 5.4), strongly adsorbed to the soil ( $\log K_{oc} = 4.1\text{--}4.2$ ) and poorly soluble ( $2 \text{ mg} \cdot \text{l}^{-1}$  at  $25^\circ\text{C}$ ) (UNEP, 2007; U.S. Environmental Protection Agency, 2012). In Martinique, 80% of soil analyses carried out on plots that had historically been cultivated with bananas between 1970 and 1993 (18,000 ha) show CLD contamination. Its persistence in the soils of the FWI has been estimated at several decades in nitisols, centuries in ferralsols, and half a millennium in andosols. CLD builds up in food chains, and long-term chronic exposure to CLD through food and drinking water can have serious consequences on human health. Indeed, CLD is a potential carcinogen and causes liver tumors in laboratory rats and mice (Reuber, 1979). It is a reproductive and developmental toxicant, an endocrine disruptor, and a neurotoxicant depending on the exposure doses (Dallaire et al., 2012; Boucher et al., 2013; Costet et al., 2015). It is also suspected of increasing the risk of preterm birth and delaying development in young children. Epidemiological studies have made it possible to link its chronic exposure to an increase in the occurrence of prostate cancer and its recurrence (Kadhel et al., 2014; Cordier et al., 2015; Emeville et al., 2015; Multigner et al., 2016; Brureau et al., 2019). Although preventive measures such as prior authorization for cultivation, the ban on fishing, the closure of aquaculture farms, or the control of foodstuffs on display have been installed to avoid transfer to local populations, pollution of the West Indian environment remains a major problem.

Following a study conducted by the French Geological Survey (BRGM, Colombano et al., 2009), a degradation treatment based on *in situ* chemical reduction (ISCR) was identified as a promising depollution technique to treat contaminated soils on a large scale. ISCR using zero-valent iron (ZVI) or nano-ZVI is a promising depollution method used for chlorinated organic pollutants in soils or contaminated aquifers (Li et al., 2021). From 2010 to 2016, a succession of projects tested this remediation method in the laboratory and in the field (Dictor

et al., 2011; Belghit et al., 2015; Mouvet et al., 2017, 2020) and showed that ISCR leads to the formation of several dechlorination products, reducing the concentration of CLD by 70% in two of the three main types of West Indian soils (nitisols and ferralsols). This allowed plants to be cultivated with levels of contamination falling below the authorized maximum residue limit for CLD ( $20 \text{ } \mu\text{g} \cdot \text{kg}^{-1}$  wet weight) unlike untreated soils (Mouvet et al., 2017, 2020). The main degradation products formed during ISCR are hydrochlordecones that have lost one or more chlorine atoms, especially -1Cl-CLD (10-monohydrochlordecone) and -3Cl-CLD (trihydrochlordecone). Additional toxicity research has shown that these major transformation products are neither mutagenic nor genotoxic and have lower proangiogenic properties than CLD (Legeay et al., 2017). On the other hand, they are more mobile and can therefore reach groundwater more easily (Ollivier et al., 2020a,b). However, to date we do not have information on the biodegradability of these transformation products and still few elements on the biodegradation of the CLD parent molecule.

Despite the consensus at the time, which admitted that CLD was non-biodegradable (Cabidoche et al., 2009), Dolfing et al. (2012) argued that the bibliographic, thermodynamic, and experimental data suggested that the molecule is not completely refractory to a microbial attack under reducing conditions. Since then, with the progress made in analytical chemistry, several studies from independent laboratories have demonstrated a microbial degradation of CLD with opening of the bishomocubane cage and loss of a  $C_1$  fragment. In each case, CLD was incubated in laboratory conditions with either a bacterial consortia or a bacterial strain isolated from one of these consortia (i.e., *Citrobacter* sp. 86 and *Desulfovibrio* sp. 86) (Chaussonnerie et al., 2016; Chevallier et al., 2019; Lomheim et al., 2020). Recently, Della-Negra et al. (2020) have also shown that a change in incubation conditions of *Desulfovibrio* sp. 86 could also give rise to chlordecthiol, the sulfur analog of chlordecone alcohol. Taken together, these results have enabled to classify the identified transformation products resulting from CLD biotransformation into seven families. However, it should be noted that these experimental results were all obtained under artificial anaerobic conditions, which do not correspond to the real redox state of FWI soils. Additionally, several of these studies (Chevallier et al., 2019; Della-Negra et al., 2020; Lomheim et al., 2020) also highlight the presence of these seven families of transformation products in the West Indian environment, reviving the idea that the microbial biodegradation of CLD under natural conditions remains possible.

In the present study, the enrichment of a new microbial consortium from wastewater sludge capable of biotransforming 4 mg·l<sup>-1</sup> of CLD within a few weeks under reductive laboratory-controlled conditions into the same nine-carbon compound (pentachloroindene, C<sub>9</sub>Cl<sub>5</sub>H<sub>3</sub>) as previously identified in Chevallier et al. (2019) is presented. Its ability to transform either CLD, -1Cl-CLD, or -3Cl-CLD, two of the major transformation products derived from ISCR, was established, and further characterization of the transformation products formed during the incubation reveal the sulfidation and possible methylation of the three parent molecules.

## MATERIALS AND METHODS

### Chemical

CLD hydrate (98% purity) was purchased from LGC Standards (Molsheim, France). 10-Monohydrochlordecone (-1Cl-CLD) (97% purity) and trihydrochlordecone (-3Cl-CLD) (97% purity) were obtained from Alpha Chimica (Chatenay-Malabry, France). <sup>13</sup>C<sub>10</sub>-chlordecone (CLD-<sup>13</sup>C<sub>10</sub>) at 100 mg·l<sup>-1</sup> in nonane is commercialized by LGC Standards (Molsheim, France). 2,4,5,6,7-pentachloroindene C<sub>9</sub>Cl<sub>5</sub>H<sub>3</sub>, chlordecthiol, 10-monohydrochlordecthiols, and methyl chlordecysulfide were synthesized and purified according to the literature (Chevallier et al., 2019; Della-Negra et al., 2020). Chemical products used for microbiological media were purchased from VWR (France). Analytic-grade organic solvents (acetone, cyclohexane, and dichloromethane) were purchased from Fisher Scientific (Illkirch, France). The individual standards were prepared from solid standards dissolved in acetone (200 mg·l<sup>-1</sup>) and stored at -18°C.

### Consortium Enrichment

Before performing the experiment presented in this paper, enrichments were carried out using three samples: (1) sludge from a wastewater treatment plant (WWTP), collected in September 2014 from a settling tank at the Orléans-La-Source WWTP, (2) a nitisol soil in Martinique, collected in 2012, and (3) sediment from the Bourget lake, collected in 2012. The hypothesis behind using WWTP sludge and Bourget lake sediment was that bacteria found in these environments are likely to have been exposed to a large range of organic molecules, which could make them able to degrade CLD. Moreover, Orndorff and Colwell (1980) and Chaussonnerie et al. (2016) had previously isolated bacteria capable of transforming CLD from a WWTP. The hypothesis behind using soil from a contaminated field in Martinique was that bacteria exposed to CLD could be able to degrade it.

It took several years to enrich a CLD-transforming microbial community from these samples, following two steps. The first step lasted 32 months and consisted of fed batches set up in anaerobic conditions. The second step consisted of reinoculating the consortia in a liquid fresh medium. Fed batches consisted of either 150 ml of wastewater sludge and 50 ml of culture medium or 10 g of soil and 120 ml culture medium. The culture medium that was used is similar to the OECD 311

directive and composed of 2/3 Solution A (KH<sub>2</sub>PO<sub>4</sub> 0.27 g·l<sup>-1</sup>; Na<sub>2</sub>HPO<sub>4</sub>·12H<sub>2</sub>O 1.12 g·l<sup>-1</sup>; NH<sub>4</sub>Cl 0.53 g·l<sup>-1</sup>, 1 ml of an oligo-element solution: SL9—see DSMZ 1257; pH 7) and 1/3 Solution B (CaCl<sub>2</sub>·2H<sub>2</sub>O 0.075 g·l<sup>-1</sup>; MgCl<sub>2</sub>·6H<sub>2</sub>O 0.1 g·l<sup>-1</sup>). Batches were supplemented with sodium acetate and sodium lactate (8 mM each) as a carbon source and Na<sub>2</sub>S and L-cysteine (0.4 mM each) to induce reductive conditions. Abiotic controls were established in the same conditions except that batches were autoclaved (121°C, 40 min) three times at 24-h intervals followed by the addition of sodium azide (200 mg·l<sup>-1</sup>). CLD was added to all batches in order to obtain concentrations of 2 mg·l<sup>-1</sup> using a concentrated solution prepared in acetone. Finally, blank controls consisted only of culture medium supplemented with the carbon sources and reducing agents. All batches were flushed with nitrogen to eliminate O<sub>2</sub> and incubated under agitation (80 rpm) in the dark at 30°C for 20 months and then at 38°C for the following 16 months. Temperature was raised as little degradation was observed at 30°C. During the first 32 months of enrichment, the batches were sampled (15 ml) and analyzed eight times (at months 0, 2, 7, 19, 20, 25, 28, and 32) to analyze chlordecone and its known degradation products by GC-MS (see below). At four of these sampling dates, T7, T20, T25, and T28, fresh culture medium, carbon sources, and CLD were added to the batches. When this occurred, GC-MS analyses were carried out before and after the feeding. Results from these fed batches showed an accumulation of CLD transformation product 2,4,5,6,7-pentachloroindene (C<sub>9</sub>Cl<sub>5</sub>H<sub>3</sub>), especially in the batches containing WWTP sludge compared to the controls and led us to conclude that a bacterial biotransformation of CLD had occurred.

Based on these results, it was decided to pursue to the second step of the enrichments using only the WWTP batches.

The second step was carried out to further enrich a CLD-transforming microbial community. This step consisted of reinoculating WWTP fed batches in fresh culture medium (as described for step 1 and supplemented with sodium acetate and sodium lactate, 4 mM each, and the same amounts of reducers) to confirm the production of C<sub>9</sub>Cl<sub>5</sub>H<sub>3</sub>. Finally, after four reinoculations, the CLD-transforming consortium was used to inoculate the kinetic experiment presented in the present paper and described below.

### Experimental Setup for the Kinetic Experiment

The experiment was carried out in 500-ml glass Schott bottles with PTFE hermetic caps (Q-Series Cap, GL45, Omnifit®) to minimize adsorption to materials and ensure anoxic conditions. Batches consisted of 460 ml fresh culture media (as described above) inoculated with 40 ml inoculum (around 8%) and supplemented with sodium acetate and sodium lactate (8 mM each) and 0.4 mM Na<sub>2</sub>S. Controls were identical except for the inoculum. Three conditions were set up in biotic and control batches: the first received CLD (condition 1), the second 10-monohydrochlordecone (-1Cl-CLD) (condition 2), and the third trihydrochlordecone (-3Cl-CLD) (condition 3).



Initial concentrations of these substances were  $4 \text{ mg}\cdot\text{l}^{-1}$  in the batches. All conditions for controls and biotic assays were carried out in triplicates. Samples were collected for analysis of transformation products, Eh measurements, and DNA extraction at the beginning of the experiment and then after 8, 19, 29, 43, 57, and 90 days. A further sample was collected after 8 months to elucidate the fate of -1Cl-CLD and -3Cl-CLD. As this was not sufficient to conclude, fresh transfer cultures were made of conditions 2 and 3 by inoculating them into fresh media in the same conditions as the initial experiment; these transfer experiments are further referred to as condition 4 (transfer of condition 2 with -1Cl-CLD) and condition 5 (transfer of condition 3 with -3Cl-CLD).

## GC-MS Methods

### GC-MS Method 1

GC/MS/MS was achieved with a Bruker GC450 gas chromatograph, 1177 injector, automated sampler Combi Pal (CTC), and a triple-quadrupole mass spectrometer 300-MS. The instrument was equipped with a non-polar  $30 \text{ m} \times 0.25 \text{ mm} \times 0.25 \mu\text{m}$  Rtx-1 column (Restek, Lisses, France) and a split/splitless injector. One microliter was injected in splitless mode. Mass spectrometry and a GC program have been described elsewhere (Bristeau et al., 2014).

### GC-MS Method 2

A Thermo Fisher Focus GC coupled to a single-quadrupole mass spectrometer (Thermo Fisher DSQ II) was used. The instrument was equipped with a non-polar  $30 \text{ m} \times 0.25 \text{ mm} \times 0.25 \mu\text{m}$  DB-5MS column (Agilent J&W) and a split/splitless injector. Three microliters were injected in splitless mode. Ionization conditions and the GC program have been described elsewhere (Chevallier et al., 2019). Duplicate injections of all samples were performed.

## GC-MS Monitoring

### Step 1 Enrichment Batches

The 15-ml samples were extracted with dichloromethane and then analyzed by GC-MS (*GC-MS method 1*), according to the following protocol: an internal standard ( $0.3 \text{ ml}$  of  $4 \text{ mg}\cdot\text{l}^{-1}$  CLD- $^{13}\text{C}$  in acetone) was first added to the sample to correct possible biases during extraction and analysis of CLD and its transformation products. After 6 h (at room temperature), 100 ml of dichloromethane was added and the flasks were shaken for 16 h on a ping-pong shaking table at a speed of 150 rpm. The samples were then centrifuged for 10 min at 2,500 rpm if necessary (in the presence of particles). Then, 10 ml of the organic phase was evaporated and transferred to cyclohexane for a final volume of around 1 ml. The extract was stored at  $-18^\circ\text{C}$  before analysis by GC-MS. The recovery rates for this analysis protocol were estimated prior to the experiment and measured  $103 \pm 4\%$  for CLD and  $118 \pm 2\%$  for -3Cl-CLD.

Pentachloroindene was used as an identification standard. Its limited amount prevented us from developing a satisfactory quantification method. Instead, estimation of its relative

abundance was provided by calculating the relative peak area of each chlorinated species (Mouvet et al., 2017).

### Step 2 Batches and Kinetic Experiment

As there were no solid particles in the reinoculations or the batches set up to compare the transformability of CLD, -1Cl-CLD, and -3Cl-CLD, the extraction protocol was slightly modified: only 5 ml dichloromethane were added for 10 ml of culture medium. After 6 h agitation, 1.5 ml of organic phase were recovered and evaporated and the extract was retrieved in 1 ml cyclohexane. The recovery rates for this analysis protocol were estimated prior to the experiment and were  $103 \pm 5\%$  for CLD,  $74 \pm 9\%$  for -1Cl-CLD, and  $72 \pm 9\%$  for -3Cl-CLD. As previously,  $\text{C}_9\text{Cl}_5\text{H}_3$  results are shown as the area of the peaks whereas -1Cl-CLD, -3Cl-CLD, and CLD are shown in percentage of the initial amount (for examples of chromatograms, see **Supplementary Figure 1**).

## Further Characterization of Transformation Products

The initial analytical protocols allowed us to demonstrate the appearance of pentachloroindene during the biodegradation of CLD. However, it did not permit to detect any other transformation products, e.g., lower chlorinated polychloroindene or hydrochlordecone analogs (-4Cl-CLD, -5Cl-CLD) in -1Cl-CLD and -3Cl-CLD conditions. A search for other transformation products was conducted using a protocol adapted from Chevallier et al. (2019) and Della-Negra et al. (2020). Sampling for the kinetic experiment and the transfer experiment was carried out after 8 months of incubation and 90 days of incubation, respectively. Two milliliters of each biotic and abiotic experiment were collected, acidified to pH 3 with HCl, and stored at  $-18^\circ\text{C}$ . After defrosting, 750  $\mu\text{l}$  of the aqueous samples were extracted three times with 250  $\mu\text{l}$  dichloromethane. The combined organic layers were evaporated under a  $\text{N}_2$  flux, dissolved in 100  $\mu\text{l}$  chloroform, and analyzed using *GC-MS method 2*. The unambiguous presence of chlordecthiol (CLD-SH), 10-monohydrochlordecthiols (-1Cl-CLD-SH), and methyl chordecysulfide (CLD-SH $_3$ ) was demonstrated in biotic incubations (**Figure 2** and **Supplementary Figures 2, 3**). Identification was achieved using synthetic standards already available for these compounds (Della-Negra et al., 2020).

The structure of the other transformation products resulting from the biotransformation of -1Cl-CLD and -3Cl-CLD were determined from their EI-mass spectra and their GC retention times (**Supplementary Figures 3–7**).

We first focused on the two signals barely separable at retention times 18.93 min and 19.03 min present in -3Cl-CLD conditions only (**Figure 2** entries 3 and 5). They both shared the same EI mass spectrum (data not shown), thus suggesting a pair of diastereoisomers. Their two major isotopic patterns centered at  $m/z$  167 and 202 strongly resemble the predominant EI fragments at  $m/z$  201 and 236 both present in the -1Cl-CLD-SH and CLD-SH mass spectra, which were previously assigned to  $[\text{C}_5\text{Cl}_3\text{SH}_2]^+$  and  $[\text{C}_5\text{Cl}_4\text{SH}_2]^+$  (Della-Negra et al., 2020). The

observed downward shift of 34 units suggested the replacement of a Cl atom by an H atom in the studied structure. Due to the rather low intensity of the two GC-MS signals at 18.93 and 19.03 min, no expected molecular ion could be detected. Instead, the highest fragment centered at  $m/z$  371 showed an isotopic distribution compatible with the ion  $[C_{10}Cl_7H_4]^+$ . The analogous ions, namely,  $[C_{10}Cl_9H_2]^+$  and  $[C_{10}Cl_{10}H]^+$ , present in -1Cl-CLD-SH and CLD-SH mass spectra, respectively, were indeed originated from the loss of HS by the molecular ions  $[C_{10}Cl_9H_3S]^+$  and  $[C_{10}Cl_{10}H_2S]^+$  (Della-Negra et al., 2020). Lastly, the retention times 18.93 and 19.03 min were significantly higher than that of starting material -3Cl-CLD (15.84 min) as in the case of both -1Cl-CLD-SH/-1Cl-CLD (22.89–22.97 min vs. 19.12 min) and CLD-SH/CLD (24.47 min vs. 20.46 min). Based on these observations and the context of the paralleled experiments carried out with CLD, -1Cl-CLD, and -3Cl-CLD, we assigned the trihydrochlorodecithiol structure (-3Cl-CLD-SH; **Figure 2**) to these compounds.

We applied the same methodology to the two other couples of signals at retention times 24.33 min/24.45 min and 20.44 min/20.58 min formed in -1Cl-CLD and -3Cl-CLD conditions, respectively. The first two signals showed the exact same mass spectrum, again suggesting a pair of diastereoisomers. The three key isotopic patterns centered at  $m/z$  203, 213, and 250 were identical to those visible in the mass spectrum of CLD-SCH<sub>3</sub> (**Supplementary Figure 7**) and previously assigned to  $[C_5Cl_4H]^+$ ,  $[C_6Cl_3SH_4]^+$ , and  $C_6Cl_4SH_4]^+$ , respectively (Della-Negra et al., 2020). These ions strongly suggested the presence of a methylthioether moiety connected to the C5-fragment characteristic of the bishomocubane ring. An interesting difference with CLD-SCH<sub>3</sub> lies in the absence of ion  $[C_5Cl_5]^+$  that was in favor of a lower chlorinated methylchlorodecsulfide congener. Lastly, the highest isotopic pattern of the mass spectrum centered at  $m/z$  488 matched perfectly with the simulation of the molecular ion  $[C_{11}Cl_9H_5S]^+$ . We therefore ended up with the methyl monohydrochlorodecsulfide structure for these transformation products (-1Cl-CLD-SCH<sub>3</sub>; **Figure 2**). Most of the previous features remained in the mass spectrum associated with the last couple of signals at 20.44 min/20.58 min (**Supplementary Figure 4**), except that they were shifted down by 34, 68, or 102 units, depending on the fragments (**Supplementary Figure 7**). We thus concluded a common methyl trihydrochlorodecsulfide structure (-3Cl-CLD-SCH<sub>3</sub>; **Figure 2**).

## Microbial Community Monitoring

### DNA Extraction

Ten milliliters of each microcosm were sampled at each sampling time and filtered through 0.22- $\mu$ m sterile membrane filters ( $\varnothing$  2.5 cm, Millipore, Bedford, MA, United States). Membranes were stored at  $-20^\circ\text{C}$  until DNA extraction. DNA was extracted using the FastDNA® Spin Kit for Soil and the FastPrep® instrument according to the manufacturer's instructions (MP Biomedicals, Santa Ana, CA, United States), with minor modifications (30 s lysis at a speed setting of 5.0  $\text{m}\cdot\text{s}^{-1}$ , subsequent centrifugation of cell debris

for 25 min). Extracted total DNA was quantified using the QuantiFluor dsDNA Sample Kit and the Quantus fluorimeter according to the manufacturer's instructions (Promega, United States).

## Capillary Electrophoresis Single-Strand Conformation Polymorphism Fingerprinting

CE-SSCP (capillary electrophoresis single-strand conformation polymorphism) bacterial community fingerprinting was performed at each sampling date. The V3 region of the 16S rRNA gene was amplified by PCR from DNA extracts with forward primer w49 (5'-ACGGTCCAGACTCCTACGGG-3') and 5' FAM-labeled reverse primer w34 (5'-TTACCGCGGCTGCTGGCAC-3'), by 30-s hybridization at  $61^\circ\text{C}$ , and 30 s elongation at  $72^\circ\text{C}$  for 28 cycles as described previously (Delbès et al., 2001). One microliter of diluted PCR product (5- to 100-fold in nuclease-free water) was then added to a mixture of 18.6  $\mu$ l of deionized formamide and 0.4  $\mu$ l of GeneScan 600 LIZ internal DNA standard (Life Technologies, United States). To obtain single-strand DNA, samples were heat-denatured for 10 min at  $95^\circ\text{C}$  and immediately cooled on ice. CE-SSCP analyses were performed on an ABI Prism 310 genetic analyzer using a 47-cm-long capillary, a non-denaturing 5.6% CAP polymer (Life Technologies, United States), and the following electrophoresis conditions: run temperature  $32^\circ\text{C}$ , sample injection for 5 s at 15 kV, and data collection for 35 min at 12 kV. Alignment of the profiles using an internal DNA standard and assignment of peak positions were performed with Bionumerics software (Applied Maths, Sint-Martens-Latem, Belgium). Profiles are shown using the "gel view" option.

## Illumina Sequencing

At the end of the kinetic experiment (90 days of incubation), bacterial and archaeal diversity was determined by 16S rRNA gene metabarcoding. A portion of the 16S rRNA gene (V4-V5 region) was amplified using the barcoded, universal primer set (515WF/918WR) (Wang et al., 2009). PCR reactions were performed using the AccuStart II PCR ToughMix Kit, followed by cleaning (HighPrep PCR beads, MokaScience, La Madeleine Cedex, France). Pooled triplicates were submitted for sequencing on an Illumina MiSeq instrument at GeT-PlaGe (Auzerville, France). Fastq sequences were processed using FROGS (Escudé et al., 2018) based on the Galaxy analysis platform (Afgan et al., 2016). Sequences were demultiplexed and dereplicated, sequence quality was checked, oligonucleotides were removed from sequences, and sequences were filtered on additional criteria. Sequences were removed from the data set, if they exhibited ambiguous bases or did not match expectations in amplicon size. Remaining sequences were clustered into OTUs based on the iterative Swarm algorithm, then chimeras and singletons (OTUs containing only one sequence) were removed. Bacterial double affiliation was performed by blasting OTUs against the SILVA 138.1 database (Quast et al., 2013). OTUs with affiliation  $< 100\%$  at the phylum level were removed from the

data set. OTUs at lower taxonomic ranks than the phylum level were considered as “unidentified” below when the RDP bootstrap value was < 0.70. 16S rRNA gene amplicon sequencing data have been deposited in the European Nucleotide Archive (ENA) at EMBL-EBI under the study accession number PRJEB47148.

Diversity indexes (Chao1, Inverse Simpsons, and Shannon) were calculated based on the Illumina sequence data.

## RESULTS

### Evolution of Chlordecone, -1Cl- Chlordecone, -3Cl- Chlordecone, and Redox Potential

Reductive conditions were maintained during the duration of the experiment between -150 and -250 mV due to the addition of Na<sub>2</sub>S (**Supplementary Figure 8**).

In the biotic incubations, concentrations of CLD, -1Cl-CLD, and -3Cl-CLD decreased over time (**Figure 1**). Less than 10% of the initially added CLD and -1Cl-CLD were found after 90 days of incubation whereas around 30% of -3Cl-CLD persisted in the batches. In the CLD conditions, a concomitant increase of C<sub>9</sub>Cl<sub>5</sub>H<sub>3</sub> was observed through the increase in the size of the peak area (**Figure 1**). This degradation pathway with ring opening and dechlorination steps has been well documented for anaerobic microbiological degradation of CLD (Chaussonnerie et al., 2016; Chevallier et al., 2019; Della-Negra et al., 2020; Lomheim et al., 2020).

In abiotic conditions, the concentrations of CLD, -1Cl-CLD, and -3Cl-CLD decreased only slightly over time (**Figure 1**).

### Further Characterization of Transformation Products

All biotic incubations with CLD, -1Cl-CLD, and -3Cl-CLD led to a significant decrease in substrate concentration. This is most likely due to a microbiological transformation of all three compounds. In several past studies, the decrease of CLD could not be correlated with the formation of any transformation products and questions remained on its exact fate (degradation and/or sorption) (Sakakibara et al., 2011; Fernández-Bayo et al., 2013; Merlin et al., 2014; Amba Esegini et al., 2019). However, recent work by Lomheim et al. (2021) monitored the transformation of CLD into a suite of progressively more dechlorinated products, including a fully dechlorinated carboxylated indene product in anaerobic microcosms constructed with soil from Guadeloupe, suggesting that complete dechlorination of CLD is possible. For the endpoint sampling of the experiments (8 months), we therefore decided to change the extraction protocol and the analytical method used for monitoring. Acidification of the samples prior to extraction was applied as reported in Chevallier et al. (2019), and a longer gas chromatographic method was employed. GC-MS analysis revealed a series of polychlorinated compounds not only in -1Cl-CLD and -3Cl-CLD conditions but also for the CLD incubations. Comparison of the EI mass spectra and the GC retention times with the library of CLD transformation products

that we have built over the years (Chaussonnerie et al., 2016; Chevallier et al., 2019; Della-Negra et al., 2020) allowed us to unambiguously identify CLD-SH, CLD-SCH<sub>3</sub>, and -1Cl-CLD-SH (as a pair of diastereoisomers). A more detailed analysis of the mass spectra of the other unknown compounds (see section “Further Characterization of Transformation Products”) enabled us to conclude the formation of -1Cl-CLD-SCH<sub>3</sub>, -3Cl-CLD-SH, and -3Cl-CLD-SCH<sub>3</sub> (**Figure 2**, entries 2 and 3).

Additional LC-MS analysis did not allow us to detect any polychloroindene carboxylic acids (data not shown). This series of polar transformation products also named as family C have been described in other CLD microbial degradation experiments (Chevallier et al., 2019; Lomheim et al., 2020, 2021). They differ from their polychloroindene congeners due to the presence of a carboxylic acid function that makes them only detectable using LC-MS instrumentation.

The presence of small peaks of CLD-SCH<sub>3</sub> among the transformation products produced in the -1Cl-CLD and -3Cl-CLD was unexpected (**Figure 2**, entries 2 and 3). We hypothesized that this CLD-SCH<sub>3</sub> came from the initial inoculum used (8% v/v in the kinetic experiment) that probably already contained CLD-SCH<sub>3</sub> (not monitored at that time). To check this hypothesis, biotic incubations 2 and 3 were reinoculated into fresh medium (8% V/V), and after 90 days, GC-MS analysis showed only a production of -1Cl-CLD-SH and -3Cl-CLD-SH (entries 4 and 5; **Figure 2** and **Supplementary Figure 5**) and no detectable amounts of CLD-SCH<sub>3</sub>, emphasizing that its presence in incubations 2 and 3 came from the initial inoculum.

### Evolution of Bacterial Diversity Fingerprint During the Incubation

CE-SSCP profiles of bacterial diversity obtained during the incubation showed that the CLD and -1Cl-CLD conditions (except replicate 3 for -1Cl-CLD) maintained a similar diversity fingerprint over time with two to three dominant bacterial strains and showed similarities with the inoculated consortium. On the contrary, the third replicate for -1Cl-CLD differed from the inoculum, evolving more toward the profiles found in the -3Cl-CLD condition where community fingerprints differed and suggested conditions which favored the development of a larger diversity (**Supplementary Figure 9**).

At T6, after 90 days of incubation, bacterial and archaeal diversity was assessed with 16S rRNA gene metabarcoding (**Figure 3**). Results are consistent with the CE-SSCP diversity fingerprints with similar communities composed of three to four dominant bacterial OTUs in the inoculum, CLD, and -1Cl-CLD, belonging to the genera *Desulfovibrio*, *Soehngenia*, *Aminobacterium*, and to an unknown genus of *Spirochaetaceae*. Moreover, in the CLD and -1Cl-CLD [replicates (1) and (2)] and the inoculum, the main OTU that was found belongs to an archaeal genus, *Methanobacterium*, which represented up to 60% of the sequences. On the other hand, in the -3Cl-CLD condition and replicate (3) of the -1Cl-CLD condition, the relative abundance of this *Methanobacterium* is reduced and two other OTUs were present in significant relative

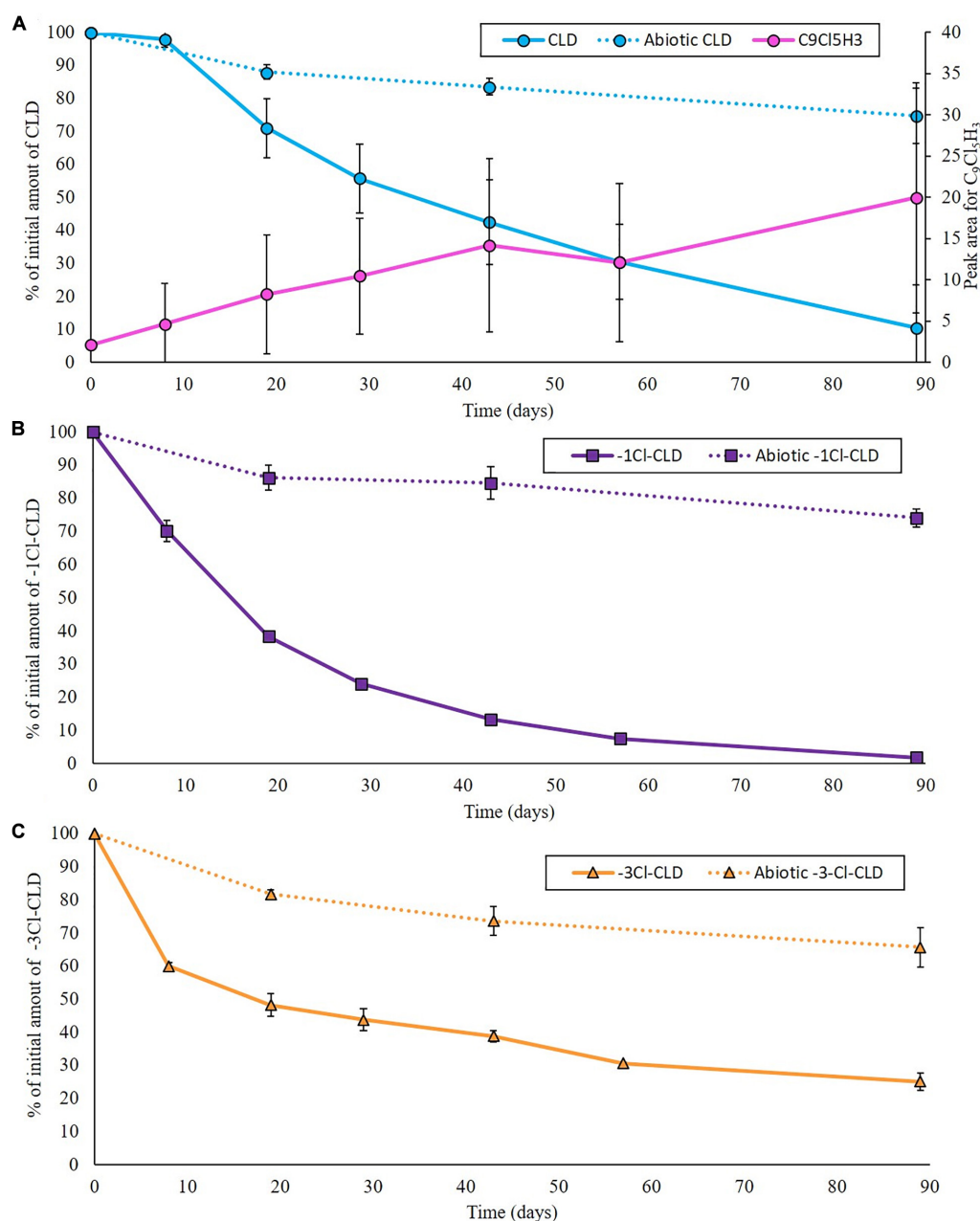


**FIGURE 1 |** Evolution of CLD (A), -1Cl-CLD (B), and -3Cl-CLD (C) over time in biotic (full lines) and abiotic (dotted lines) incubations expressed as the remaining percentage in the solution and of the peak area measured for  $C_9Cl_5H_3$ , which increased over time in the batches containing CLD. Data represent the average of three replicates, and error bars are the standard deviation.

abundances, *Candidatus Cloacimonas* and *Clostridium* as well as *Proteiniphilum*. It is possible that tolerance/resistance to CLD and -1Cl-CLD positively selected *Methanobacterium* whereas in less stressful conditions with -3Cl-CLD, other bacteria were more competitive.

An nMDS ordination (Figure 4), carried out on the OTU relative abundance data, highlights the similarities between the inoculum, CLD, and -1Cl-CLD [replicates (1) and (2)] and their difference with the -3Cl-CLD diversity. However, the ANOSIM

test carried out on these data did not have significant differences between conditions ( $p > 0.001$ ).

Finally, diversity indexes (Supplementary Figure 10) all show higher values for the -3Cl-CLD conditions, which corroborates the hypothesis that this condition was less toxic to the bacteria present in the consortium and that cells that had not grown in the inoculum, CLD, and -1Cl-CLD conditions were able to develop. Further work on the resistance/tolerance and toxicity of these compounds would be required to further understand this.



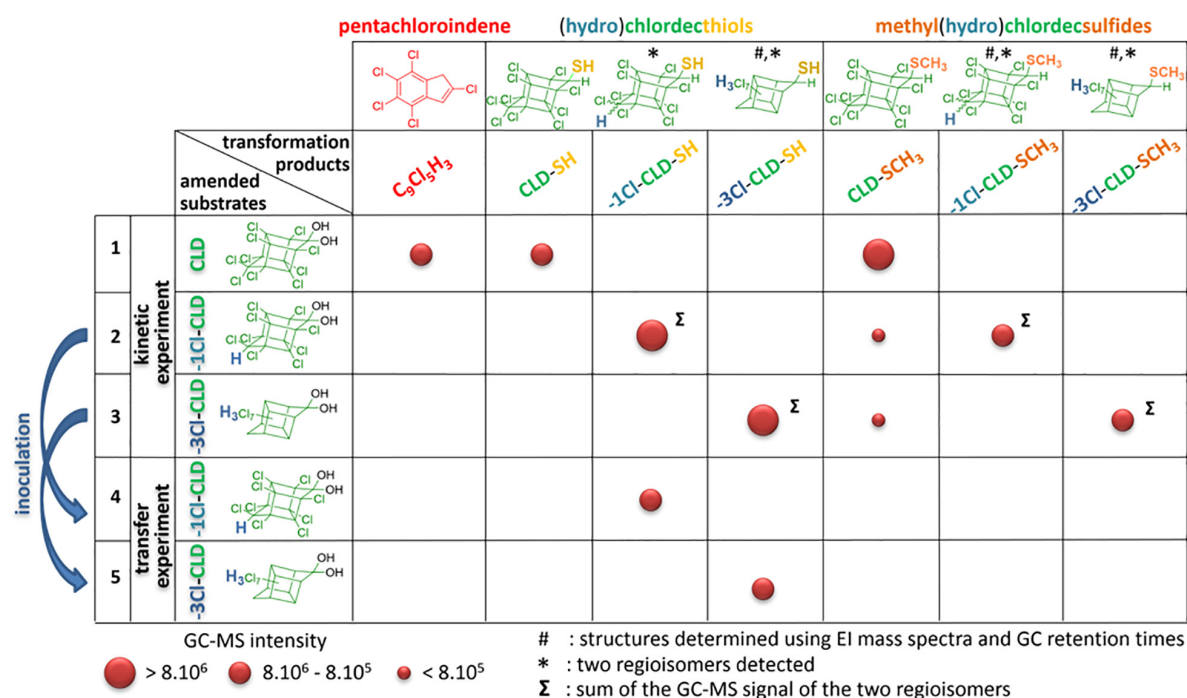


**FIGURE 2** | General overview of the transformation products resulting from CLD, -1Cl-CLD, and -3Cl-CLD incubations. Entries 1–3 correspond to the kinetic experiment conditions after 8 months while entries 4 and 5 refer to the transfer experiment (after 90 days). The size of the circles gives a qualitative overview of the intensity of the GC-MS signals observed (mean of two injections). Analyses were conducted using GC-MS method 2. Complete data are found in **Supplementary Table 1**.

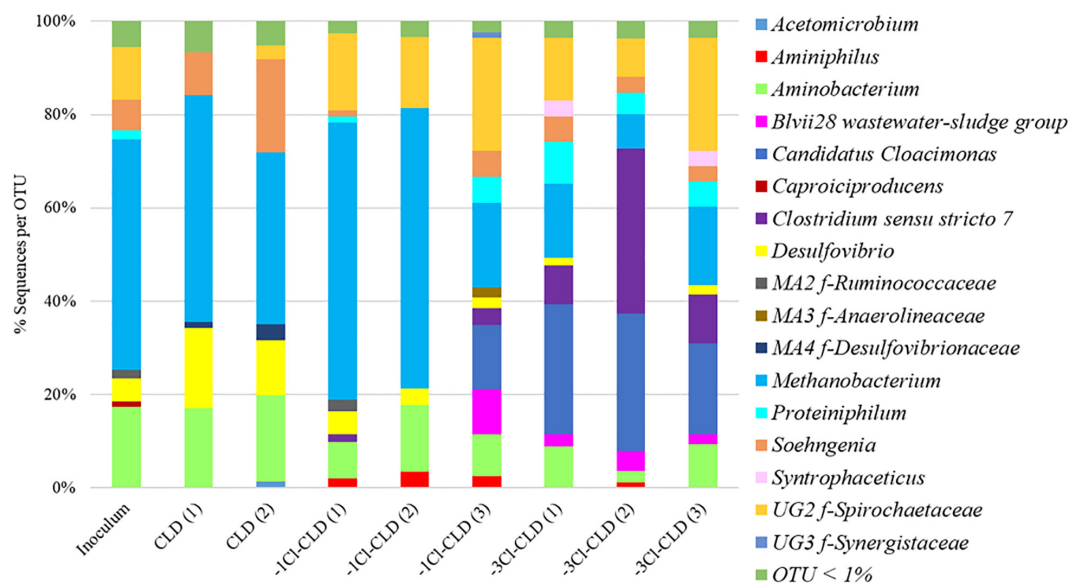


**FIGURE 3** | Histogram of the bacterial and archaeal genus represented by > 1% of the sequences and identified to the genus level. Multi-affiliated (MA) and unknown genera (UG) are given with their associated family (f).

## DISCUSSION

This work aimed to study the biodegradability potential of two major transformation products produced during

ISCR CLD remediation in soils, namely, -1Cl-CLD and -3Cl-CLD, by a microbial consortium enriched from wastewater sludge and able to transform CLD into a nine-carbon compound (pentachloroindene,  $C_9Cl_5H_3$ ) and

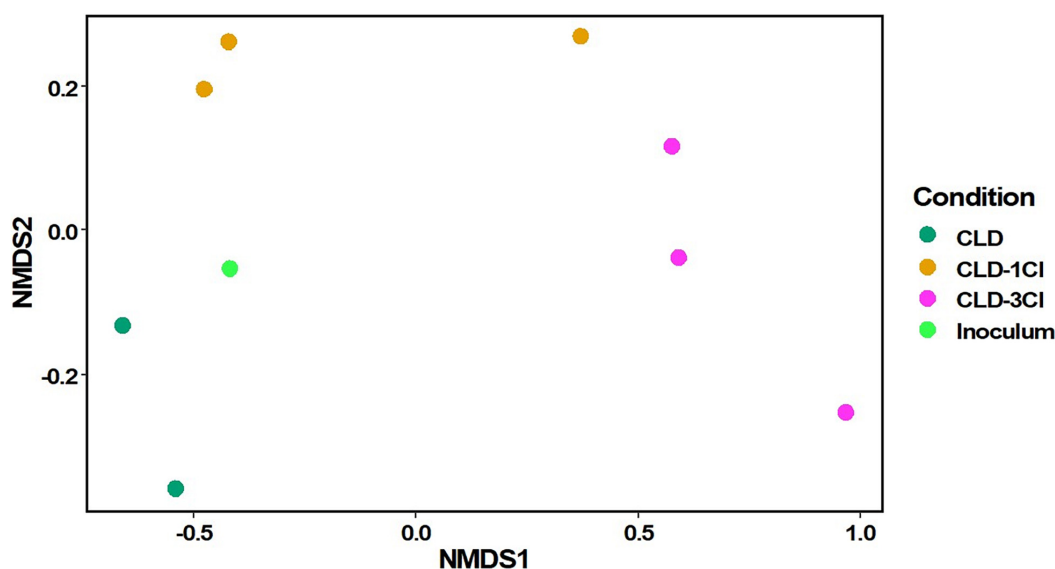


**FIGURE 4 |** nMDS ordination plot of bacterial community diversity in the different incubation conditions and the inoculum.

identify both the transformation products and the dominant genera involved.

There are only a few references of microbial transformation of CLD. Jablonski et al. (1996) is one of the earliest references with evidence of CLD biotransformation by the methanogenic archaeon *Methanosarcina thermophila* to polar and non-polar products using  $^{14}\text{C}$ -CLD. Other references testify to the formation of CLD derivatives in anaerobic or aerobic conditions (Fernández-Bayo et al., 2013; Merlin et al., 2014) but without detecting significant amounts of metabolites, as was found by Chaussonnerie et al. (2016) and Lomheim et al. (2021). During the 3-months-long incubation, CLD decreased concomitantly to the appearance of  $\text{C}_9\text{Cl}_5\text{H}_3$  (B family) as in the first enrichment steps. CLD has previously been shown to form  $\text{C}_9\text{Cl}_5\text{H}_3$  in similar conditions, in the presence of either bacterial consortia or isolated strains such as *Citrobacter* sp. 86 (Chaussonnerie et al., 2016) and *Desulfovibrio* sp. 86 (Della-Negra et al., 2020). Although the exact metabolic pathways have yet to be elucidated, recent work by Barbance et al. (2020) shows the involvement of cobalt-containing corrinoids in the microbial degradation of CLD, which could also be a possibility in the present study.

Since Chaussonnerie et al. (2016), several new families of degradation products derived from CLD have been identified by LC-HRMS (Chevallier et al., 2019; Lomheim et al., 2020, 2021). However, these families were not discovered at the end of the experiment in the present work (data not shown), suggesting either their further degradation in the incubation conditions or the inability of the enriched consortium to transform CLD to these compounds.

In the incubation conditions with either -1Cl-CLD or -3Cl-CLD, these compounds both appeared to be removed from the media. Further analysis of the transformation products did not reveal compounds from families B, C, D, and E (Chevallier et al., 2019); however, it did reveal the presence of sulfur derivatives,

namely, thiols and methylthioethers (family F, Della-Negra et al., 2020). Reinoculation experiments (Figure 2, entries 4 and 5) led to an initial formation of thiols when the incubation period was shortened compared to the kinetic experiment, indicating a probable sequence mechanism of reductive sulfidation—S-methylation (Figure 2, entries 1–3). Reinvestigation of CLD biotic incubations using a modified analytical protocol showed the same type of sulfured transformation products (CLD-SH and CLD-SCH<sub>3</sub>). This proves that the present microbial enrichment can induce both the biodegradation of CLD (formation of pentachloroindene coming from the loss of carbon, oxygen, and chlorine atoms) and the biotransformation (conversion of the gem-diol to thiols and methylthioethers) of CLD, the two pathways being in competition in the applied incubation conditions. It is worth mentioning that neither -1Cl-CLD nor -3Cl-CLD appeared to be degraded, only biotransformed. This suggests that the position of the H atom(s) of -1Cl-CLD and -3Cl-CLD may inhibit the ring opening of the bishomocubane core, common to CLD and its two lower chlorinated congeners.

On the one hand, introduction of a sulfur atom on the chlordecone scaffolding has previously been demonstrated in presence of the sulfate-reducing bacterium *Desulfovibrio* sp. 86 (Della-Negra et al., 2020). To be effective, the biotransformation required an electron acceptor containing sulfur or hydrogen sulfide and a confined atmosphere. Microbiological reductive sulfidation is not limited to chlordecone since other carbonyl derivatives have been transformed into their corresponding thiol congeners using the same conditions with *Desulfovibrio* sp. 86 (Della-Negra et al., 2021). The authors suggested that two microbiological mechanisms may occur since aldehydes were converted during the growth phase while chlordecone, 10-monohydrochlordecone, and other ketones were biotransformed during the stationary phase. The present incubation conditions

that fulfill the requirements reported by Della-Negra et al. (2021) (presence of  $H_2S$ , confined atmosphere) and the presence of OTU affiliated to the sulfate-reducing genus *Desulfovibrio* are in favor of an analogous biotransformation. As in previous studies (Della-Negra et al., 2020, 2021), no transient thioketones could be detected. These intermediate compounds are observed in the chemical version of reductive sulfidation where a two-step process (initial S/O exchange followed by a reductive step) has been proven (Ozturk et al., 2010; Della-Negra et al., 2021). Moreover, the presence of OTU affiliated to the sulfate-reducing genus *Desulfovibrio* is in favor of this hypothesis in the present study.

On the other hand, while methylated thiols (methyl chlordecysulfides) were significantly formed after a switch in the incubation condition in the work of Della-Negra et al. (2020) using *Desulfovibrio* sp. 86, the present microbial community can induce both reductive sulfidation and methylation of the intermediate thiols in a one-pot manner. The absence of methyl chlordecysulfides in the transfer experiment after 90 days (Figure 2 entries 4 and 5; Supplementary Figure 5) and the systematic presence of both thiols and their methylated analogues in the kinetic experiment (Figure 2 entries 1–3; Supplementary Figures 2–5) are indicative of a probable sequential path. Another explanation would be the modification of the consortia contents, a hypothesis that is less probable as it would occur with both -1Cl-CLD and -3Cl-CLD substrates. In fermentative conditions, *Desulfovibrio* sp. 86 was able to methylate (Della-Negra et al., 2020), but no explanation has yet been proposed for this. In the present study, it is possible that the length of the experiment (8 months) enabled these reactions, although other explanations could exist.

Indeed, the OTU with the most relative sequence abundance (around 50%) was affiliated to *Methanobacterium*, a strictly anaerobic methane-producing archaeal genus that uses  $H_2$  as an electron donor. Further work is required to evidence the role of archaea in CLD biodegradation/biotransformation, but several hypotheses can be drawn. For instance, methylated-thiol-coenzyme M methyltransferase, a key enzyme involved in the methanogenesis (Ferry and Kestead, 2007), probably produced by this archaea in the present enrichment is capable of methylating thiols via an activated methylated corrinoid. A possible cometabolic methyl transferase activity via such methyl donor could take place. *Methanobacterium* could not only be involved in the methylation of CLD-SH and congeners but also induce the ring opening of the bishomocubane ring of CLD via the corrinoids it produced. Indeed, corrinoids, such as those required in methanogenesis, play a key role in the ring opening of CLD as demonstrated by *Citrobacter* sp. 86 mutants (Barbance et al., 2020). Cofactor F430 also required in the methanogenic metabolism was found to abiotically transform CLD in the presence of a reducing reagent (Jablonski et al., 1996). The dominance of *Methanobacterium* in incubations where CLD and -1Cl-CLD and -3Cl-CLD transformation products are being degraded is stressing that methanogenic conditions are adequate for the biotransformation of such complex molecules. This statement is in line with previously reported CLD biotransformation in such conditions by the methanogenic

archaeon *Methanosarcina thermophila* (Jablonski et al., 1996). In the later study, CLD dehalogenation was suggested to occur while we rather expect sulfidation then methylation by *Methanobacterium*. Thus, our study strongly suggests that different pathways for CLD (and derivatives) transformation might exist among methanogenic genera, such as sulfidation then methylation by the genus *Methanobacterium* found in our study or dehalogenation by the genus *Methanosarcina*, as suggested by Jablonski et al. (1996). This is further supported by the absence of a source on sulfur in the incubations with *Methanosarcina*.

Based on existing literature where, either from a thermodynamic point of view (Dolfing et al., 2012) or from an experimental point of view, there are no clear reasons why bacteria should not be able to respire CLD, reductive dehalogenation stands out as the best existing option to degrade CLD. However, while the redox potential in the present experiment was mostly comprised between -150 and -250 mV, no reductive dehalogenation, i.e., the direct replacement of a chlorine by a hydrogen atom, has been observed. This differs from the recent successful microbiological transformations of CLD that consistently reported the formation of hydrochlordecones, albeit in varying proportions. Indeed, only 10-monohydrochlordecone was reported as a minor transformation product by Chaussonnerie et al. (2016), Chevallier et al. (2019), and Della-Negra et al. (2020), while Lomheim et al. (2020, 2021) demonstrated the formation of a significant amount of several hydrochlordecones. However, in these studies the redox potential was not monitored so we cannot compare our experimental conditions to theirs.

In the work of Della-Negra et al. (2020), no formation of hydrochlordecones was observed when reductive sulfidation occurred. In the case of the single bacterium *Desulfovibrio* sp. 86, the observed inhibition of reductive dechlorination and ring opening dechlorination when reductive sulfidation takes place has been investigated (Della-Negra et al., 2020) and  $H_2S$  formed by sulfate-reducing bacteria was shown to be responsible for such an inhibition. Using several biotic and abiotic additional experiments, the authors concluded that the corrinoids, known to be involved in CLD biodegradation, are probably deactivated due to the formation of a cobalt-sulfur covalent bond in the presence of  $H_2S$  that accumulates in the confined atmosphere. Of course, the composition of the microbial consortia may also play a critical role.

Microbial diversity in the present experiment was lowest in the CLD and -1Cl-CLD conditions whereas it increased compared to the inoculum in the -3Cl-CLD condition and in one of the replicates (3) of the -1Cl-CLD incubations. Where diversity was lowest, it was dominated by known gram-negative genera (*Desulfovibrio*, *Aminobacterium*, *Soehngenia*, and *Spirochaetaceae*) and the archaeal *Methanobacterium* genus. Indeed, at high exposures of CLD, gram-negative bacteria have been shown to be more resistant to CLD (Mahaffey et al., 1982). To date, only gram-negative bacteria (*Pseudomonas aeruginosa* (Orndorff and Colwell, 1980), *P. putida*, *P. maltophilia*, *P. vesicularis* (George and Claxton, 1988), *Citrobacter* sp. 86, *Citrobacter* sp. 92 (Chaussonnerie et al., 2016), and

*Desulfovibrio* sp. 86 (Della-Negra et al., 2020) as well as an archaeon (*Methanosarcina thermophila*, Jablonski et al., 1996) have been reported to partially or completely transform CLD. All microbial degradations have been performed at elevated concentrations of CLD (equal or above 10 mg·l<sup>-1</sup>) that demonstrate a strong resistance of these microorganisms, which corroborates our observations. When diversity increased in our experiments, the representation of gram-positive genera increased (*Candidatus Cloacimonas*, *Clostridium*), possibly due to the reduced toxicity of -3Cl-CLD toward these bacteria, and the relative abundance of *Methanobacterium* and *Desulfovibrio* decreased, possibly explaining the incomplete transformation of -3Cl-CLD to -3Cl-CLD-SH and -3Cl-CLD-SCH<sub>3</sub> in these incubations. Furthermore, the increase in the diversity indexes in -3Cl-CLD conditions also corroborates this hypothesis. Further work on the resistance/tolerance and toxicity of these compounds would be required to further understand this.

Identification of CLD transformation products and CLD-degrading microbial communities in soils and sediments of the French West Indies (FWI) demonstrates that natural transformation of CLD already takes place in these two types of environmental compartments (Chevallier et al., 2019; Della-Negra et al., 2020; Lomheim et al., 2020). Moreover, it has also been demonstrated that the microbial potential to further transform CLD with as many as nine chlorine atoms removed is present in these environmental compartments (Lomheim et al., 2020). However, more than 25 years after its use was forbidden, CLD pollution in the FWI is still a public health issue, implying that the mechanisms of natural CLD transformation are not particularly efficient. The present work is the fourth, after Orndorff and Colwell (1980), Chaussonnerie et al. (2016) and Lomheim et al. (2020), to report on enrichments from wastewater sludge capable of inducing CLD transformation. Anaerobic reactors of water treatment plants would thus appear as a suitable place to observe an even more effective CLD degradation. To date, only one study aimed at searching CLD transformation products in FWI raw wastewater (Devault et al., 2018). However, it failed to detect both CLD and the targeted transformation products (chlordecol and 8-monohydrochlordecone). Since sampling was carried out at the entry of the treatment plant and that chlordecol and 8-monohydrochlordecone have not been yet linked to microbial anaerobic transformation of CLD, these results should not discourage further investigation of this presumably efficient industrial degradation process.

Finally, we are aware that the experimental setup presented here is carried out in optimized laboratory conditions where Eh is maintained negative with very reducing conditions, theoretically favorable for dehalogenation. Thus, the conditions are not those found naturally in agricultural soils in the West Indies except when an ISCR treatment is applied (Mouvet et al., 2020) and the zero-valent iron combined with water saturation and soil compaction induces negative redox conditions and leads to the transformation of CLD to hydroCLDs such as the -1-Cl-CLD and -3-Cl-CLD used in this study and that would subsequently find themselves also in these conditions. In previous work, chlordecthiol (the S-containing derivative from CLD) was detected in mangrove sediments from Martinique Island

(Della-Negra et al., 2020). This environmental compartment shows favorable conditions (sulfate-reducing bacteria and anoxic conditions) for the reductive sulfidation. One can imagine that S-methylation of such thiol would occur in the presence of the numerous sulfate-reducing microorganisms. Thus, we would expect to find similar several S-containing derivatives in the FWI indies environmental provided that ISCR treatment is to be set up and dedicated analytical methods are applied (no such additional analytical procedure was used in the work published by Mouvet et al. (2020).

## DATA AVAILABILITY STATEMENT

The datasets presented in this study can be found in online repositories. The names of the repository/repositories and accession number(s) can be found below: <https://www.ebi.ac.uk/ena/browser/view/PRJEB47148>.

## AUTHOR CONTRIBUTIONS

JH, CJ, AM, and MC designed the experiment. JH, DM, OD-N, P-LS, SB, and MC carried out the experiment and the analysis (chemical and microbial). JH, CJ, SB, MC, and P-LS analyzed the data. JH and P-LS drafted the manuscript. JH, AM, and CM carried out the funding acquisition. All authors have read and agreed to the published version of the manuscript, contributed to reviewing and editing the manuscript.

## FUNDING

We gratefully acknowledge the financial support provided to the PIVOTS project by the Région Centre—Val de Loire (ARD 2020 program and CPER 2015–2020) and the French Ministry of Higher Education and Research (CPER 2015–2020 and public service subsidy to the Bureau de Recherches Géologiques et Minière). This operation was cofunded by the European Union. Europe was committed to the Centre-Val de Loire region with the European Regional Development Fund. Additional support was provided by Commissariat à l'Energie Atomique et aux Energies Alternatives (CEA), the Center National de la Recherche Scientifique (CNRS), and the University Evry Val d'Essonne (UEVE). OD-N was supported by the “IDI 2017” project funded by the IDEX Paris-Saclay, ANR-11-IDEX-0003-02.

## ACKNOWLEDGMENTS

We thank Mickaël Charron for his technical support during the experiment.

## SUPPLEMENTARY MATERIAL

The Supplementary Material for this article can be found online at: <https://www.frontiersin.org/articles/10.3389/fmicb.2021.742039/full#supplementary-material>



## REFERENCES

- Afgan, E., Baker, D., van den Beek, M., Blankenberg, D., Bouvier, D., Èech, M., et al. (2016). The Galaxy platform for accessible, reproducible and collaborative biomedical analyses: 2016 update. *Nucleic Acids Res.* 44, W3–W10. doi: 10.1093/nar/gkw343
- Amba Esegini, V., Patrice, K. G., Sylvere, N. K., and Kayem, J. (2019). Chlordecone dechlorination under aerobic conditions by *Bacillus* sp. *Int. J. Innovat. Appl. Stud.* 26, 545–555.
- Barbance, A., Della-Negra, O., Chaussonnerie, S., Delmas, V., Muselet, D., Ugarte, E., et al. (2020). Genetic analysis of *Citrobacter* sp.86 reveals involvement of corrinoids in chlordecone and lindane biotransformations. *Front. Microbiol.* 11:590061. doi: 10.3389/fmicb.2020.590061
- Belghit, H., Colas, C., Bristeau, S., Mouvet, C., and Maunit, B. (2015). Liquid chromatography–high-resolution mass spectrometry for identifying aqueous chlordecone hydrate dechlorinated transformation products formed by reaction with zero-valent iron. *Int. J. Environ. Anal. Chem.* 95, 93–105. doi: 10.1080/03067319.2014.994615
- Boucher, O., Simard, M.-N., Muckle, G., Rouget, F., Kadhel, P., Bataille, H., et al. (2013). Exposure to an organochlorine pesticide (chlordecone) and development of 18-month-old infants. *NeuroToxicology* 35, 162–168. doi: 10.1016/j.neuro.2013.01.007
- Bristeau, S., Amalric, L., and Mouvet, C. (2014). Validation of chlordecone analysis for native and remediated French West Indies soils with high organic matter content. *Anal. Bioanal. Chem.* 406, 1073–1080. doi: 10.1007/s00216-013-7160-2
- Brureau, L., Emeville, E., Helissey, C., Thome, J. P., Multigner, L., and Blanchet, P. (2019). Endocrine disrupting-chemicals and biochemical recurrence of prostate cancer after prostatectomy: a cohort study in Guadeloupe (French West Indies). *Int. J. Cancer* 146, 657–663. doi: 10.1002/ijc.32287
- Cabidoche, Y. M., Achard, R., Cattani, P., Clermont-Dauphin, C., Massat, F., and Sansoulet, J. (2009). Long-term pollution by chlordecone of tropical volcanic soils in the French West Indies: a simple leaching model accounts for current residue. *Environ. Poll.* 157, 1697–1705. doi: 10.1016/j.envpol.2008.12.015
- Chaussonnerie, S., Saaidi, P.-L., Ugarte, E., Barbance, A., Fossey, A., Barbe, V., et al. (2016). Microbial degradation of a recalcitrant pesticide: chlordecone. *Front. Microbiol.* 7:2025. doi: 10.3389/fmicb.2016.02025
- Chevallier, M. L., Della-Negra, O., Chaussonnerie, S., Barbance, A., Muselet, D., Lagarde, F., et al. (2019). Natural chlordecone degradation revealed by numerous transformation products characterized in key french West Indies environmental compartments. *Environ. Sci. Technol.* 53, 6133–6143. doi: 10.1021/acs.est.8b06305
- Colombano, S., Dumon, A., Guérin, V., and Chevrier, B. (2009). *Examen des Possibilités de Traitement de la Chlordécone Dans les sols Notamment sur les Aires D'alimentation des Captages d'eau Potable*. France: BRGM. BRGM/RP-57708-FR.
- Cordier, S., Bouquet, E., Warembourg, C., Massart, C., Rouget, F., Kadhel, P., et al. (2015). Perinatal exposure to chlordecone, thyroid hormone status and neurodevelopment in infants: the Timoun cohort study in Guadeloupe (French West Indies). *Environ. Res.* 138, 271–278. doi: 10.1016/j.envres.2015.02.021
- Costet, N., Pelé, F., Comets, E., Rouget, F., Monfort, C., Bodeau-Livinec, F., et al. (2015). Perinatal exposure to chlordecone and infant growth. *Environ. Res.* 142, 123–134. doi: 10.1016/j.envres.2015.06.023
- Dallaire, R., Muckle, G., Rouget, F., Kadhel, P., Bataille, H., Guldner, L., et al. (2012). Cognitive, visual, and motor development of 7-month-old Guadeloupean infants exposed to chlordecone. *Environ. Res.* 118, 79–85. doi: 10.1016/j.envres.2012.07.006
- Delbès, C., Leclerc, M., Zumstein, E., Godon, J. J., and Moletta, R. (2001). A molecular method to study population and activity dynamics in anaerobic digestors. *Water Sci. Technol.* 43, 51–57. doi: 10.2166/wst.2001.0013
- Della-Negra, O., Chaussonnerie, S., Fonknechten, N., Barbance, A., Muselet, D., Martin, D. E., et al. (2020). Transformation of the recalcitrant pesticide chlordecone by *Desulfovibrio* sp.86 with a switch from ring-opening dechlorination to reductive sulfidation activity. *Sci. Rep.* 10:13545. doi: 10.1038/s41598-020-70124-9
- Della-Negra, O., Le Cacher, de Bonneville, B., Chaussonnerie, S., Le Paslier, D., Frison, G., et al. (2021). Microbiological versus chemical reductive sulfidation: an experimental and theoretical study. *ACS Omega* 6, 7512–7523. doi: 10.1021/acsomega.0c06041
- Devault, D. A., Amalric, L., and Bristeau, S. (2018). Chlordecone consumption estimated by sewage epidemiology approach for health policy assessment. *Environ. Sci. Poll. Res.* 25, 29633–29642. doi: 10.1007/s11356-018-2995-x
- Dictor, M. C., Mercier, A., Lereau, L., Amalric, L., Bristeau, S., and Mouvet, C. (2011). *Décontamination de sols Pollués par la Chlordécone. Validation de Procédés de Dépollution Physico-Chimique et Biologique, Étude des Produits de Dégradation et Amélioration de la Sensibilité Analytique Pour la Chlordécone Dans les Sols*. France: BRGM. Rapport final. BRGM/RP-59481-FR, 201.
- Dolfing, J., Novak, I., Archelas, A., and Macarie, H. (2012). Gibbs free energy of formation of chlordecone and potential degradation products: implications for remediation strategies and environmental fate. *Environ. Sci. Technol.* 46, 8131–8139. doi: 10.1021/es301165p
- Emeville, E., Giusti, A., Coumoul, X., Thomé, J.-P., Blanchet, P., and Multigner, L. (2015). Associations of plasma concentrations of dichlorodiphenyldichloroethylene and polychlorinated biphenyls with prostate cancer: a case–control study in guadeloupe (French West Indies). *Environ. Health Perspect.* 123, 317–323. doi: 10.1289/ehp.1408407
- Escudie, F., Auer, L., Bernard, M., Mariadassou, M., Cauquil, L., Vidal, K., et al. (2018). FROGS: find. rapidly, OTUs with galaxy solution. *Bioinformatics* 34, 1287–1294. doi: 10.1093/bioinformatics/btx791
- Fernández-Bayo, J. D., Saison, C., Voltz, M., Disko, U., Hofmann, D., and Berns, A. E. (2013). Chlordecone fate and mineralisation in a tropical soil (andosol) microcosm under aerobic conditions. *Sci. Total Environ.* 46, 395–403. doi: 10.1016/j.scitotenv.2013.06.044
- Ferry, J. G., and Kastead, K. A. (2007). “Methanogenesis,” in *Ar-chaee: Molecular Cell Biology*, ed. R. Cavicchioli (Washington, D.C: ASM Press), 288–314. doi: 10.1128/9781555815516.ch13
- George, S. E., and Claxton, L. D. (1988). Biotransformation of chlordecone by *Pseudomonas* species. *Xenobiotica* 18, 407–416. doi: 10.3109/00498258809041677
- Jablonski, P. E., Pheasant, D. J., and Ferry, J. G. (1996). Conversion of Kepone by *Methanosarcina thermophila*. *FEMS Microbiol. Lett.* 139, 169–173. doi: 10.1111/j.1574-6968.1996.tb08198.x
- Kadhel, P., Monfort, C., Costet, N., Rouget, F., Thomé, J.-P., Multigner, L., et al. (2014). Chlordecone exposure, length of gestation, and risk of preterm birth. *Am. J. Epidemiol.* 179, 536–544. doi: 10.1093/aje/kwt313
- Legeay, S., Billat, P.-A., Clere, N., Nesslany, F., Bristeau, S., Faure, S., et al. (2017). Two dechlorinated chlordecone derivatives formed by in situ chemical reduction are devoid of genotoxicity and mutagenicity and have lower proangiogenic properties compared to the parent compound. *Environ. Sci. Poll. Res.* 25, 1–11. doi: 10.1007/s11356-017-8592-6
- Li, Y., Zhao, H.-P., and Zhu, L. (2021). Remediation of soil contaminated with organic compounds by nanoscale zero-valent iron: a review. *Sci. Total Environ.* 760:143413. doi: 10.1016/j.scitotenv.2020.143413
- Lomheim, L., Flick, R., Rambinaising, S., Gaspard, S., and Edwards, E. A. (2021). Identification of a fully dechlorinated product of chlordecone in soil microcosms and enrichment cultures. *Environ. Sci. Technol. Lett.* 8, 662–667. doi: 10.1021/acs.estlett.1c00505
- Lomheim, L., Laquitaine, L., Rambinaising, S., Flick, R., Starostine, A., Jean-Marius, C., et al. (2020). Evidence for extensive anaerobic dechlorination and transformation of the pesticide chlordecone (C10Cl10O) by indigenous microbes in microcosms from Guadeloupe soil. *PLoS One* 15:e0231219. doi: 10.1371/journal.pone.0231219
- Mahaffey, W. R., Pritchard, P. H., and Bourquin, A. W. (1982). Effects of kepone on growth and respiration of several estuarine bacteria. *Appl. Environ. Microbiol.* 43, 1419–1424. doi: 10.1128/aem.43.6.1419-1424.1982
- Merlin, C., Devers, M., Crouzet, O., Heraud, C., Steinberg, C., Mougin, C., et al. (2014). Characterization of chlordecone-tolerant fungal populations isolated from long-term polluted tropical volcanic soil in the French West Indies. *Environ. Sci. Poll. Res.* 21, 4914–4927. doi: 10.1007/s11356-013-1971-8
- Mouvet, C., Collet, B., Gaude, J.-M., Rangon, L., Bristeau, S., Senergues, M., et al. (2020). Physico-chemical and agronomic results of soil remediation by in situ chemical reduction applied to a chlordecone-contaminated nitisol at plot scale in a French Caribbean banana plantation. *Environ. Sci. Poll. Res. Int.* 27, 41063–41092. doi: 10.1007/s11356-020-07603-z

- Mouvet, C., Dictor, M.-C., Bristeau, S., Breeze, D., and Mercier, A. (2017). Remediation by chemical reduction in laboratory mesocosms of three chlordecone-contaminated tropical soils. *Environ. Sci. Poll. Res.* 24, 25500–25512. doi: 10.1007/s11356-016-7582-4
- Multigner, L., Kadhel, P., Rouget, F., Blanchet, P., and Cordier, S. (2016). Chlordecone exposure and adverse effects in French West Indies populations. *Environ. Sci. Poll. Res.* 23, 3–8. doi: 10.1007/s11356-015-4621-5
- Ollivier, P., Engevin, J., Bristeau, S., and Mouvet, C. (2020a). Laboratory study on the mobility of chlordecone and seven of its transformation products formed by chemical reduction in nitisol lysimeters of a banana plantation in Martinique (French Caribbean). *Sci. Total Environ.* 743:140757. doi: 10.1016/j.scitotenv.2020.140757
- Ollivier, P., Touzelet, S., Bristeau, S., and Mouvet, C. (2020b). Transport of chlordecone and two of its derivatives through a saturated nitisol column (Martinique, France). *Sci. Total Environ.* 704:135348. doi: 10.1016/j.scitotenv.2019.135348
- Orndorff, S. A., and Colwell, R. R. (1980). Distribution and characterization of kepone-resistant bacteria in the aquatic environment. *Appl. Environ. Microbiol.* 39, 611–622. doi: 10.1128/aem.39.3.611-622.1980
- Ozturk, T., Ertas, E., and Mert, O. (2010). A berzelius reagent, phosphorus decasulfide (P<sub>4</sub>S<sub>10</sub>), in organic syntheses. *Chem. Rev.* 110, 3419–3478. doi: 10.1021/cr900243d
- Quast, C., Pruesse, E., Yilmaz, P., Gerken, J., Schweer, T., Yarza, P., et al. (2013). The SILVA ribosomal RNA gene database project: improved data processing and web-based tools. *Nucleic Acids Res.* 41, D590–D596. doi: 10.1093/nar/gks1219
- Reuber, M. D. (1979). The carcinogenicity kepone. *J. Environ. Pathol. Toxicol.* 2, 671–686.
- Sakakibara, F., Takagi, K., Kataoka, R., Kiyota, H., Sato, Y., and Okada, S. (2011). Isolation and identification of dieldrin-degrading *Pseudonocardia* sp. strain KSF27 using a soil-charcoal perfusion method with aldrin trans-diol as a structural analog of dieldrin. *Biochem. Biophys. Res. Commun.* 411, 76–81. doi: 10.1016/j.bbrc.2011.06.096
- U.S. Environmental Protection Agency (2012). *Estimation Programs Interface Suite™ for Microsoft® Windows. v4*, 1edn Edn. Washington, DC: U.S. Environmental Protection Agency.
- UNEP (2007). *Descriptif révisé des Risques liés au Chlordécone. Rapport du Comité d'étude des Polluants Organiques Persistants sur les Travaux de sa Troisième Réunion*. Geneva: UNEP.
- Wang, Z., Tollervey, J., Briese, M., Turner, D., and Ule, J. (2009). CLIP: construction of cDNA libraries for high-throughput sequencing from RNAs cross-linked to proteins in vivo. *Methods* 48, 287–293. doi: 10.1016/j.jymeth.2009.02.021

**Conflict of Interest:** The authors declare that the research was conducted in the absence of any commercial or financial relationships that could be construed as a potential conflict of interest.

**Publisher's Note:** All claims expressed in this article are solely those of the authors and do not necessarily represent those of their affiliated organizations, or those of the publisher, the editors and the reviewers. Any product that may be evaluated in this article, or claim that may be made by its manufacturer, is not guaranteed or endorsed by the publisher.

Copyright © 2021 Hellal, Saaidi, Bristeau, Crampon, Muselet, Della-Negra, Mauffret, Mouvet and Joulain. This is an open-access article distributed under the terms of the Creative Commons Attribution License (CC BY). The use, distribution or reproduction in other forums is permitted, provided the original author(s) and the copyright owner(s) are credited and that the original publication in this journal is cited, in accordance with accepted academic practice. No use, distribution or reproduction is permitted which does not comply with these terms.



# Bacterial Abundance, Diversity and Activity During Long-Term Colonization of Non-biodegradable and Biodegradable Plastics in Seawater

Charlene Odobel<sup>1†</sup>, Claire Dussud<sup>1†</sup>, Lena Philip<sup>1,2</sup>, Gabrielle Derippe<sup>3</sup>, Marion Lauters<sup>1</sup>, Boris Eyheraguibel<sup>4</sup>, Gaëtan Burgaud<sup>5</sup>, Alexandra Ter Halle<sup>6</sup>, Anne-Leila Meistertzheim<sup>2</sup>, Stephane Bruzaud<sup>3</sup>, Valerie Barbe<sup>7</sup> and Jean-Francois Ghiglione<sup>1\*</sup>

## OPEN ACCESS

### Edited by:

Fabrice Martin-Laurent,  
Institut National de la Recherche  
Agronomique (INRA), France

### Reviewed by:

Vineet Kumar,  
Guru Ghasidas Vishwavidyalaya, India  
Prosun Tribedi,  
The Neotia University, India

### \*Correspondence:

Jean-Francois Ghiglione  
ghiglione@obs-banyuls.fr

<sup>†</sup> These authors share first authorship

### Specialty section:

This article was submitted to  
Microbiotechnology,  
a section of the journal  
Frontiers in Microbiology

Received: 01 July 2021

Accepted: 17 September 2021

Published: 18 November 2021

### Citation:

Odobel C, Dussud C, Philip L,  
Derippe G, Lauters M,  
Eyheraguibel B, Burgaud G,  
Ter Halle A, Meistertzheim A-L,  
Bruzaud S, Barbe V and Ghiglione J-F  
(2021) Bacterial Abundance, Diversity  
and Activity During Long-Term  
Colonization of Non-biodegradable  
and Biodegradable Plastics  
in Seawater.  
Front. Microbiol. 12:734782.  
doi: 10.3389/fmicb.2021.734782

<sup>1</sup> CNRS, UMR 7621, Laboratoire d'Océanographie Microbienne (LOMIC), Sorbonne Université, Observatoire Océanologique de Banyuls, Banyuls-sur-Mer, France, <sup>2</sup> SAS Plastic@Sea, Observatoire Océanologique de Banyuls, Banyuls-sur-Mer, France, <sup>3</sup> CNRS, UMR 6027, Institut de Recherche Dupuy de Lôme (IRDL), Université de Bretagne-Sud, Lorient, France, <sup>4</sup> CNRS, UMR 6296, Institut de Chimie de Clermont-Ferrand (ICCF), Université Clermont Auvergne, Clermont-Ferrand, France, <sup>5</sup> CNRS, EA 3882, Université de Brest, Laboratoire Universitaire de Biodiversité et d'Ecologie Microbienne (LUBEM), Plouzané, France, <sup>6</sup> CNRS, UMR 5623, Laboratoire des Interactions Moléculaires et Réactivité Chimique et Photochimique (IMRCP), Université de Toulouse, Toulouse, France, <sup>7</sup> CEA, CNRS, Génomique Métabolique, Genoscope, Institut François Jacob, Univ Evry, Université Paris-Saclay, Evry, France

The microorganisms living on plastics called “plastisphere” have been classically described as very abundant, highly diverse, and very specific when compared to the surrounding environments, but their potential ability to biodegrade various plastic types in natural conditions have been poorly investigated. Here, we follow the successive phases of biofilm development and maturation after long-term immersion in seawater (7 months) on conventional [fossil-based polyethylene (PE) and polystyrene (PS)] and biodegradable plastics [biobased polylactic acid (PLA) and polyhydroxybutyrate-co-hydroxyvalerate (PHBV), or fossil-based polycaprolactone (PCL)], as well as on artificially aged or non-aged PE without or with prooxidant additives [oxobiodegradable (OXO)]. First, we confirmed that the classical primo-colonization and growth phases of the biofilms that occurred during the first 10 days of immersion in seawater were more or less independent of the plastic type. After only 1 month, we found congruent signs of biodegradation for some bio-based and also fossil-based materials. A continuous growth of the biofilm during the 7 months of observation (measured by epifluorescence microscopy and flow cytometry) was found on PHBV, PCL, and artificially aged OXO, together with a continuous increase in intracellular (<sup>3</sup>H-leucine incorporation) and extracellular activities (lipase, aminopeptidase, and  $\beta$ -glucosidase) as well as subsequent changes in biofilm diversity that became specific to each polymer type (16S rRNA metabarcoding). No sign of biodegradation was visible for PE, PS, and PLA under our experimental conditions. We also provide a list of operational taxonomic units (OTUs) potentially involved in the biodegradation of these polymers under natural seawater conditions, such as *Pseudohongiella* sp. and *Marinobacter* sp. on PCL,

*Marinicella litoralis* and *Celeribacter* sp. on PHBV, or Myxococcales on artificially aged OXO. This study opens new routes for a deeper understanding of the polymers' biodegradability in seawaters, especially when considering an alternative to conventional fossil-based plastics.

**Keywords:** microbial ecotoxicology, plastisphere, biofouling, biofilm, plastic pollution

## INTRODUCTION

The marine environment has become sinks for vast quantities of anthropogenic debris, including mismanaged plastic waste, estimated to 4.8–12.7 million metric tons entering the oceans every year (Jambeck et al., 2015). Microplastics (< 5 mm) represent more than 90% of the total counts of marine plastic debris, mostly originated from larger debris fragmentation by a combination of physical, chemical, and biological processes (Eriksen et al., 2014). Microplastics are generally composed of polyethylene (PE), polypropylene (PP), and polystyrene (PS), three conventional polyolefins highly refractory to biodegradation because of their intrinsic features (Poulain et al., 2019). Issues related to marine plastic pollution are multifaceted and cross-sectoral, leading to numerous environmental, economic, and social impacts and thus calling for non-trivial legislative and non-legislative strategies, with some that have already been reported worldwide (Schnurr et al., 2018). Within the frame of transition to blue economy, a wide range of biodegradable plastics were developed as potential substitutes to conventional plastics (Science Advice for Policy by European Academies, 2020). Some are still petroleum-based, such as polycaprolactone (PCL) or oxobiodegradable plastics (OXO) made of PE with prooxidant additives stimulating abiotic oxidation processes needed for its biodegradation (Yashchuk et al., 2012; Eyheraguibel et al., 2017). Others are made from renewable resources including biological materials or agricultural resources (so called “bio-based”), such as polylactic acid (PLA) and polyhydroxybutyrate-co-hydroxyvalerate [PHBV, a commercially available polyhydroxyalkanoate (PHA)] (RameshKumar et al., 2020).

In the marine environment, the very diverse microbial communities living on any kind of plastic debris has been called “plastisphere” (Zettler et al., 2013). Microplastics offer a new habitat characterized by higher abundance and distinct communities as compared to the surrounding free-living or organic particle-attached bacteria (Dussud et al., 2018a). The colonization of new plastics released at sea until the formation of a mature biofilm has been described as a succession of several phases (Wright et al., 2020). During the first hours in marine waters, a “conditioning film” made of inorganic and organic matter supports the initial colonization phase generally initiated by Gammaproteobacteria and Alphaproteobacteria regardless of the polymer type and representing microorganisms with efficient surface adhesion (Oberbeckmann et al., 2015; Dussud et al., 2018b). A second phase consists of the biofilm growth involving a succession of rapidly growing bacteria such as Acidobacteria, Actinobacteria, Bacteroidetes, Cyanobacteria, Firmicutes, and Planctomycetes (Salta et al., 2013). The last phase that generally

appears after 15 to 30 days in seawater relates to a mature biofilm and remains stable for several months (Kirstein et al., 2018). The description of these colonization phases has been done on several conventional plastic types, including on PE-based plastic bags (Lobelle and Cunliffe, 2011; Harrison et al., 2014), polyethylene terephthalate (PET)-based plastic bottles (Oberbeckmann et al., 2014), polyvinyl chloride (PVC) (Dang et al., 2008), PS coupons (Briand et al., 2012), and in comparisons between PE, PP, PET, and polycarbonate (PC) materials (Webb et al., 2009; De Tender et al., 2017). Fewer studies have compared conventional to biodegradable plastics (including PLA, PHBV, and OXO) in terms of community composition and dynamics (Eich et al., 2015; Dussud et al., 2018a; Cheng et al., 2021), with different experimental conditions and microbial parameters that made more challenging comparison between these studies.

In this study, we describe the colonization dynamics of microplastics made of conventional (PE and PS) and biodegradable polymers (PCL, PLA, and PHBV) in seawater. We also tested the initial formulation of OXO that is recalcitrant to biodegradation and different artificially aged OXO (AA-OXO) that can be further biodegraded by oxidative mechanisms in the environment. We hypothesized that mature biofilms from biodegradable plastics differed from conventional materials, both in terms of abundance, diversity, and activities. Such differences should permit the description of potentially biodegrading plastisphere members, which may differ according to the plastic type. We present here an original and comprehensive comparison of the bacterial colonization potential on six plastic formulations incubated in seawater by coupling heterotrophic production and ectoenzyme measurements, in parallel to bacterial abundance (epifluorescence microscopy and flow cytometry) and bacterial diversity (16S rRNA metabarcoding) during a long-term colonization in seawater (7 months).

## MATERIALS AND METHODS

### Plastic Manufacturing Process

The first four polymer films were commercially available, made of low-density PE (Borealis, ref. FA6224, Austria), PS (Goodfellow, ref. 065-289-66, United States), PCL (CAPA 6800, Perstorp Company, Sweden), and PLA (Goodfellow, ref. 247-628-87, United States). The fifth film was formed from dried PHBV pellets (supplied by Tianan Biological Materials Co. Ltd., under the trade name ENMAT Y1000P, China) by using compression molded in a CarverR hydraulic press at 180°C under a pressure of 10 metric tons for 3 min. The sixth film was made of OXO with the same low-density PE as described above, but additivated with



D<sub>2</sub>W formulation based on manganese and iron and extruded at 180°C using a laboratory scale Rondol linear 18 mm blown film (provided by Symphony Environmental Ltd., United Kingdom).

We also used two artificially aged OXO (AA-OXO) made of the same OXO as described above but differing by the exposure time to UV (according to ASTM D5208: UVA 340, 0.78 W m<sup>-3</sup> nm<sup>-1</sup>) during 48 h for AA<sub>48</sub>OXO and during 144 h for AA<sub>144</sub>OXO. In both cases, UV aging was followed by a thermal aging during 96 h at 70°C (ASTM D5510) to increase the oxidation level. The same protocol was used for artificial aging of PE film by UV exposure for 144 h followed by a thermal aging during 96 h at 70°C, called AA<sub>144</sub>PE film hereafter. Artificial aging was stopped when reaching carbonyl index of 1x/100 for AA<sub>48</sub>OXO and 3x/100 for AA<sub>144</sub>OXO, where x was the film thickness. Carbonyl index values were determined as the ratio of the peak intensity at 1,715 cm<sup>-1</sup> to the peak intensity at 1,460 cm<sup>-1</sup> (Selke et al., 2015) by Fourier transform infrared spectroscopy (FTIR) analysis (Spectrum 100 equipped with an ATR attenuated total reflectance, Perkin-Elmer). The level of 1x/100 was previously demonstrated as a prerequisite for biodegradability of OXO, according to the French agreement Association Française de NORmalization (AFNOR AC t51-808, 2012). No sign of oxidation was observed for the AA<sub>144</sub>PE film by FTIR, which served as a control in our experiment.

The film's thicknesses were 200 µm for PS, PHBV, PCL, and PLA and 100 µm for PE, AA<sub>144</sub>PE, OXO, AA<sub>48</sub>OXO, and AA<sub>144</sub>OXO. Each of the nine films was cut into 100 circular pieces of 9 mm diameter with a puncher machine. Polymer pieces were sterilized with 70% ethanol and rinsed three times with sterile seawater (SSW) before incubation in natural seawater.

## Incubation Under Natural Seawater Conditions During 7 Months

Each material type was incubated in aquariums with direct circulation to the sea, as previously described (Dussud et al., 2018a). Briefly, we used 10 identical aquariums consisting of trays of 1.8 L capacity (Sodispan, Spain) continually renewed with 20 µm pre-filtered seawater (Leroy Merlin, France) by individual water delivery valves and overflow ports setting a flow rate of 0.1 L min<sup>-1</sup>. Seawater was pumped at 30 m from the coast and 4 m depth in the Banyuls bay, close to the SOLA observatory station (NW Mediterranean Sea, France). During the experiment, seawater temperature in the aquariums and in the Banyuls bay was between 12.5 and 19.5°C and salinity remained stable at 38.5. Incubations in aquariums were processed in the dark to avoid UV-related degradation of the polymers and algal development. One aquarium was used as control and contained only circulating seawater. The nine other aquariums contained the pieces of each film (PE, AA<sub>144</sub>PE, OXO, AA<sub>48</sub>OXO, AA<sub>144</sub>OXO, PS, PHBV, PCL, and PLA). Plastic pieces of each material type were sampled after 3, 10, 31, 74, 116, and 206 days, together with seawater from the control aquarium.

## Epifluorescence Microscopy

One piece of each polymer was rinsed at each sampling time with sterilized seawater and fixed for 1 h at 4°C with

1% (v/v) glutaraldehyde (final concentration) before freezing. Epifluorescence microscopy observations were done using an Olympus AX70 PROVIS after 4',6-diamidino-2-phenylindole (DAPI) staining according to Porter and Feig (1980). Pictures were taken on 10 fields of each polymer type and cell counting was done with the software Microbe Counter.

## Flow Cytometry

Three pieces of each polymer were rinsed at each sampling time with sterile seawater before cell detachment, as previously described (Dussud et al., 2018b). Briefly, cell detachment pre-treatment was performed using 1 mM pyrophosphate (30 min at room temperature in the dark) followed by a sonication step (3 × 5 s, 40 kHz, 30% amplitude, sterilized probe Branson SLPe). Cells were fixed for 1 h at 4°C with 1% (v/v) glutaraldehyde (final concentration) before freezing. In parallel, 3 × 1 ml of seawater from the control aquarium were also fixed using the same procedure. A 500 µl subsample was mixed with the nucleic acid dye SYBR Green I (final concentration 0.05% v/v, Sigma Aldrich) at room temperature for 15 min in the dark. Cell counts were performed with a FACSCanto II flow cytometer (BD Bioscience, San Jose, CA) equipped with a blue laser (488 nm, air-cooled, 20 mW solid state), as previously described (Mével et al., 2008). Cell counts were expressed as number of cells mm<sup>-2</sup> for polymers and as number of cells ml<sup>-1</sup> for seawater.

## Heterotrophic Bacterial Production

Bacterial production (BP) was measured for each polymer type and at each sampling time by <sup>3</sup>H-leucine incorporation into proteins, as previously described (Dussud et al., 2018b). Briefly, <sup>3</sup>H-leucine (specific activity 112 Ci mmol<sup>-1</sup>, Perkin Elmer) was added at 1 nM final concentration (completed with cold leucine to 150 nM) for polymer samples and 4.3 nM (completed with cold leucine to 42.8 nM) for 3 µm filtered seawater from the control aquarium. Triplicate samples were incubated in the dark at *in situ* temperature for 3 h. The polymers were rinsed with 5% TCA and 70% ethanol and then resuspended in 1.0 ml of a liquid scintillation cocktail (Ultima Gold). Radioactivity was determined in a Beckman Scintillation Counter (LS 5000CE) and data analyzed with the Microwin 2000 software. We used the empirical conversion factor of 1.55 ng C pmol<sup>-1</sup> of incorporated leucine to calculate BP (Simon and Azam, 1989). Values were given in ng C mm<sup>-2</sup> h<sup>-1</sup> for plastics and in ng C ml<sup>-1</sup> h<sup>-1</sup> for seawater.

## Extracellular Enzymatic Activities

Three extracellular enzymatic activities were analyzed for amino peptidase, β-glucosidase, and lipase. Triplicates of 1/4 of plastic piece of each material type were placed in a 96-well plate with fluorogenic model substrates that were L-leucine-7-amido-4-methyl coumarin (Leu-MCA, 10 mM final, Sigma Aldrich) for amino peptidase, 4-methylumbelliferyl-β-D-glucoside at 20 mM for β-glucosidase (MUF-β-Glc, 20 mM final, Sigma Aldrich), and 4-methylumbelliferyl-oleate for lipase (MUF-Oleate, 20 mM final, Sigma Aldrich). These saturated concentrations for amino peptidase, β-glucosidase and lipase and optimized time incubations were determined prior to the extracellular enzymatic

activity measurement (data not shown). After 4 h (for seawater) or 8 h (for plastics) of incubation, 50  $\mu$ l of a stop solution (SDS 10%) was added in all wells. Fluorescence was quantified using VICTOR3 spectrofluorometer (PerkinElmer) at a 380 nm wavelength for MCA and 364 nm for MUF substrates. A control was done in triplicate for each activity and each plastic type by adding the stop solution at the beginning of incubation. The spectrofluorometer was calibrated with MCA and MUF standard solutions diluted in sterile seawater. Values were given in  $\text{nmol mm}^{-2} \text{h}^{-1}$  for polymers and in  $\text{nmol ml}^{-1} \text{h}^{-1}$  for seawater.

## DNA Extraction, PCR Amplification, and Sequencing

Plastic pieces were sampled for all plastic types and at each sampling time with sterilized forceps and stored at  $-80^{\circ}\text{C}$  until analysis. In parallel, 1 L seawater was sampled on the same day in the control aquarium, successively filtered onto 3- $\mu\text{m}$  and 0.2- $\mu\text{m}$  pore size polycarbonate filters (47 mm diameter, Nucleopore), and filters were stored at  $-80^{\circ}\text{C}$  until analysis. DNA extraction was performed on polymers or seawater at all sampling time, using a classical phenol-chloroform method for seawater samples, modified for the plastic samples as previously described (Dussud et al., 2018b). Briefly, the modification consisted in a sonication pretreatment ( $3 \times 5$  s with 30% amplitude, sterilized probe Branson SLPe) in order to increase the detachment of biofilm forming bacteria. The molecular size and purity of the DNA extracts were analyzed by agarose gel electrophoresis (1%) and the DNA was quantified by spectrophotometry (GeneQuant II, Pharmacia Biotech). Primers for Polymerase Chain Reaction (PCR) amplification of the 16S V3–V5 region were 515F-Y and 926R, well-suited for marine samples according to Parada et al. (2016) with Illumina-specific primers and barcodes. Sequencing was performed on Illumina MiSeq by Genoscope (Evry, France). Raw FASTA files were deposited at EBI under the accession number PRJEB37662. Sequence analysis was conducted using the FROGS pipeline (Escudie et al., 2017) supported on the Galaxy instance of Toulouse Midi-Pyrenees bioinformatics platform. The pre-process tool was used to merge the paired-ends raw reads using Flash (Magoë and Salzberg, 2011) and quality filtering and primers trimming with cutadapt (Martin, 2011). Sequence clustering was performed with the Swarm algorithm (Mahé et al., 2014). Chimeras were detected with the VSEARCH algorithm, by *de novo* UCHIME method (Edgar et al., 2011; Rognes et al., 2016) and were removed. Clusters were assigned with the Silva 128 16S rRNA database (Quast et al., 2012) and clusters that did not belong to Bacteria kingdom were removed as well as chloroplast and mitochondrial sequences. The clusters that had a reads number abundance lower than 0.005% of all reads were removed, according to Bokulich et al. (2013). The number of sequences per sample was normalized by rarefaction ( $n = 17,865$ ). Finally, a table with 66 samples and 1,517 clusters was obtained.

## Statistical Analysis

For each sample, we calculated Chao1 species richness estimator, Simpson and Shannon diversity indexes, and Pielou's evenness

**TABLE 1** | OTUs richness (Observed) and diversity indexes (Chao1, Pielou, Shannon and Simpson) of free-living (F), organic particle-attached bacteria (A) and biofilms of different plastic types (PE, AA<sub>144</sub>PE, OXO, AA<sub>48</sub>OXO, AA<sub>144</sub>OXO, PS, PHBV, PCL, PLA) according to immersion time in seawater (3, 10, 31, 74, 116 and 206 days).

Sample type	Day	Observed	Chao1 $\pm$ se	Pielou	Shannon	Simpson
F	3	445	568 $\pm$ 27	0.67	4.11	0.95
	10	535	742 $\pm$ 40	0.66	4.16	0.94
	31	696	913 $\pm$ 40	0.67	4.40	0.95
	74	505	693 $\pm$ 38	0.65	4.07	0.94
	116	376	545 $\pm$ 40	0.62	3.69	0.91
	206	235	321 $\pm$ 27	0.53	2.92	0.89
A	3	810	946 $\pm$ 28	0.74	4.95	0.98
	10	905	1001 $\pm$ 21	0.80	5.47	0.98
	31	901	982 $\pm$ 19	0.86	5.86	0.99
	74	897	979 $\pm$ 19	0.80	5.46	0.99
	116	793	872 $\pm$ 19	0.81	5.40	0.99
	206	453	677 $\pm$ 51	0.68	4.13	0.96
PE	3	226	336 $\pm$ 31	0.51	2.78	0.90
	10	404	532 $\pm$ 31	0.58	3.48	0.90
	31	938	1041 $\pm$ 23	0.82	5.63	0.99
	74	738	879 $\pm$ 27	0.63	4.18	0.93
	116	412	486 $\pm$ 20	0.54	3.23	0.88
	206	777	871 $\pm$ 21	0.78	5.20	0.99
AA <sub>144</sub> PE	3	286	375 $\pm$ 25	0.56	3.16	0.91
	10	433	561 $\pm$ 32	0.66	4.01	0.95
	31	882	1000 $\pm$ 24	0.80	5.44	0.99
	74	592	681 $\pm$ 22	0.72	4.57	0.96
	116	599	654 $\pm$ 15	0.75	4.83	0.98
	206	716	854 $\pm$ 30	0.75	4.96	0.98
OXO	3	240	344 $\pm$ 30	0.54	2.96	0.89
	10	479	607 $\pm$ 28	0.71	4.40	0.98
	31	702	909 $\pm$ 37	0.64	4.22	0.96
	74	611	691 $\pm$ 21	0.72	4.64	0.97
	116	559	599 $\pm$ 12	0.77	4.88	0.98
	206	569	729 $\pm$ 32	0.57	3.60	0.91
AA <sub>48</sub> OXO	3	182	225 $\pm$ 16	0.51	2.66	0.86
	10	375	485 $\pm$ 26	0.62	3.70	0.94
	31	420	530 $\pm$ 26	0.52	3.12	0.85
	74	501	601 $\pm$ 25	0.70	4.36	0.96
	116	528	609 $\pm$ 21	0.72	4.50	0.97
	206	639	777 $\pm$ 29	0.72	4.65	0.97
AA <sub>144</sub> OXO	3	183	254 $\pm$ 26	0.50	2.61	0.82
	10	519	665 $\pm$ 30	0.59	3.70	0.94
	31	812	935 $\pm$ 25	0.74	4.94	0.97
	74	519	654 $\pm$ 31	0.71	4.42	0.96
	116	486	573 $\pm$ 22	0.68	4.23	0.95
	206	352	557 $\pm$ 51	0.61	3.56	0.93
PS	3	503	682 $\pm$ 35	0.53	3.33	0.90
	10	488	647 $\pm$ 32	0.57	3.55	0.93
	31	666	791 $\pm$ 26	0.61	3.95	0.92
	74	674	868 $\pm$ 35	0.56	3.62	0.88
	116	825	902 $\pm$ 18	0.80	5.38	0.99
	206	830	939 $\pm$ 25	0.85	5.74	0.99
PHBV	3	260	332 $\pm$ 20	0.43	2.39	0.79
	10	388	541 $\pm$ 37	0.67	3.98	0.96

(Continued)

**TABLE 1 |** (Continued)

Sample type	Day	Observed	Chao1 $\pm$ se	Pielou	Shannon	Simpson
PCL	31	317	471 $\pm$ 38	0.55	3.19	0.92
	74	609	835 $\pm$ 46	0.70	4.51	0.97
	116	535	667 $\pm$ 29	0.68	4.30	0.97
	206	343	430 $\pm$ 25	0.69	4.00	0.96
	3	478	631 $\pm$ 31	0.51	3.12	0.89
	10	271	452 $\pm$ 47	0.54	3.04	0.91
	31	738	853 $\pm$ 23	0.64	4.24	0.94
	74	357	495 $\pm$ 32	0.58	3.44	0.92
	116	370	511 $\pm$ 34	0.53	3.12	0.87
	206	158	248 $\pm$ 29	0.33	1.67	0.67
PLA	3	223	327 $\pm$ 29	0.47	2.53	0.88
	10	665	815 $\pm$ 29	0.70	4.52	0.97
	31	739	884 $\pm$ 28	0.65	4.31	0.94
	74	793	887 $\pm$ 21	0.76	5.11	0.98
	116	840	944 $\pm$ 24	0.84	5.62	0.99
	206	785	908 $\pm$ 26	0.75	5.02	0.98

using the Phyloseq package (McMurdie and Holmes, 2013) of R software suite (Table 1). The non-parametric estimator of Chao1 was calculated as follows:  $S = S_{obs} + a^2/2b * (N - 1)/N$ , where  $S_{obs}$  is the number of OTUs observed in the sample,  $N$  is the number of sequences per sample,  $a$  is the number of OTUs detected only once, and  $b$  is the number of OTUs detected only twice (Chiu et al., 2014). Simpson diversity index was computed as  $D = 1 - \sum [N_i * (N_i - 1) / (N * (N - 1))]$ , where  $N_i$  is the abundance of the  $i^{th}$  OTU in the sample (Simpson, 1949). Shannon index was calculated as  $H = -\sum [p_i * \log(p_i)]$ , where  $p_i$  is the proportion of the  $i^{th}$  OTU (Shannon and Weaver, 1949) and Pielou's evenness index was  $R = H / \log_2 S_{obs}$  (Pielou, 1966). Differences with incubation time and between biodegradable and non-biodegradable plastics in richness and diversity indexes were tested using an ANOVA test (for normally distributed data, determined by a Shapiro test) or a Kruskal–Wallis test with R software.

Unweighted-pair group method with arithmetic mean (UPGMA) dendrogram based on Bray–Curtis dissimilarities was used for visualization of beta-diversity. A series of dissimilarity profile permutation tests (SIMPROF, PRIMER 6) was performed under a simple null hypothesis of no meaningful structure within a sub-cluster. Significant branches (SIMPROF,  $p < 0.05$ , in black in Figure 4) were used to define sample clusters. One-way analysis of similarity was performed on the same distance matrix (ANOSIM, PRIMER 6) to test the significant difference and to partition the variance of the beta-diversity matrix between days of incubation and between polymer types and seawater. Similarity Percentage analysis (SIMPER) was performed to identify the contribution of each operational taxonomic unit (OTU), using PRIMER 6. A first comparison between PE and AA<sub>144</sub>PE revealed no specific species contribution of the plastisphere of one polymer to the other. The analyses then focused on the contributions of PE compared to other polymers (PHBV, PCL, OXO, AA<sub>48</sub>OXO, AA<sub>144</sub>OXO, AA<sub>144</sub>PE, PS, and PLA) at final time (D206). A threshold at 50% was applied to

identify the most relevant species. For each OTU identified, in order to improve the affiliation attributed by Silva 128 16S rRNA database, the sequence was blasted to the NCBI databases “16S ribosomal RNA from bacteria and archaea” and “nt.” In some cases and depending on the identity percentage of the matches, a new affiliation has been proposed (Table 2). The data and graphical representations were performed using R statistical software version 3.5.0 (R Core Team, 2018).

## RESULTS

### Visual Changes of the Materials

After 3 days of immersion in seawater, we observed that the translucent PHBV fragment whitened and that AA<sub>144</sub>OXO was very breakable, whereas the other plastic pieces showed no visual changes (Figure 1). The only change after 206 days in seawater was observed for PCL pieces, which showed a fivefold reduction in size compared to day 3.

### Epifluorescence Microscopy and Flow Cytometry

Epifluorescence microscopy showed the successive steps of colonization and maturation of the biofilm during 206 days in seawater (Figure 2). No or very few cells were detected on plastics after their sterilization and before their immersion in seawater. The presence of a mature biofilm together with extracellular polymeric substances was visible in all plastic types at the end of the experiment, but biofilms presented higher thickness for PCL and AA<sub>144</sub>OXO compared to the other plastics. Counting was not possible for PHBV because of autofluorescence background signal of the polymer.

It is noteworthy that no or very few cells were counted by flow cytometry after the sterilization of the plastic films and before their immersion in seawater, as found by epifluorescence microscopy. Flow cytometry confirmed the succession of phases during the colonization of the plastics (Figure 3A). The primo-colonization was characterized by a relatively high number of cell counts at day 3 (mean =  $1.6 \times 10^4$ , SD =  $1.1 \times 10^4$  cells  $\text{mm}^{-2}$ ,  $n = 9$ ) that decreased at day 10 (mean =  $4.6 \times 10^3$ , SD =  $1.1 \times 10^3$  cells  $\text{mm}^{-2}$ ,  $n = 9$ ), whatever the polymer type. Interestingly, a clear difference was found between PE and OXO (mean =  $4.7 \times 10^3$ , SD =  $5.6 \times 10^2$  cells  $\text{mm}^{-2}$ ,  $n = 9$ ) and the same polymer but artificially aged (one order of magnitude higher for AA<sub>144</sub>PE, AA<sub>48</sub>OXO, and AA<sub>144</sub>OXO).

A growing phase was found from day 10 to day 31 in all plastic films, followed by a stabilization phase of the biofilm that became mature and remains unchanged from day 31 to day 206 for PE, AA<sub>144</sub>PE, OXO, AA<sub>48</sub>OXO, PS, and PLA. Exceptions were found for PCL, PHBV, and AA<sub>144</sub>OXO that showed a continuous growth of biofilm until the end of the experiment (up to  $2.0 \times 10^4$  cells  $\text{mm}^{-2}$  after 116 days for PHBV, PCL, and AA<sub>144</sub>OXO). From 116 days in seawater, significant differences were found between cell counts on PHBV, PCL, and AA<sub>144</sub>OXO compared to other plastics ( $t$ -test,  $p$ -value  $< 0.05$ ). The cell detachment treatment was less efficient after 116 days for PHBV, PCL, and AA<sub>144</sub>OXO, since we observed much lower

**TABLE 2 |** Taxonomy, relative abundance (r.a.) and contribution (cb) details (in %) of the 41 OTUs identified by SIMPER analysis, up to 30% of cumulative dissimilarity between PE and the other 8 plastics materials (AA<sub>144</sub>PE, OXO, AA<sub>48</sub>OXO, AA<sub>144</sub>OXO, PS, PHBV, PCL, PLA) after 206 days of immersion in seawater.

OTU taxonomy	AA <sub>144</sub> PE		OXO		AA <sub>48</sub> OXO		AA <sub>144</sub> OXO		PS		PHBV		PCL		PLA	
	r.a.	cb	r.a.	cb	r.a.	cb	r.a.	cb	r.a.	cb	r.a.	cb	r.a.	cb	r.a.	cb
<i>Marinicella litoralis</i>	0	0	0	0	0	0	0	0	0.017	0	5.9	3.2	0	0	0	0
Oceanospirillales	3.0	1.6	0.17	0	0.10	0	0.034	0	0.18	0	0	0	0	0	0.37	0
Oceanospirillales	4.5	3.5	0.20	0	0.067	0	0.017	0	0.19	0	0	0	0	0	0.25	0
<i>Pseudohongiella</i> sp.	0	0	0	0	0	0	0	0	0	0	0	0	52	26	0.011	0
<i>Polycyclovorans</i> sp.	7.9	3.4	4.7	0	7.6	0	0.022	0	0.43	0	0	0	0.062	0	5.7	0
Thiopfundaceae	0.44	0	0.12	0	0.067	0	0.43	0	2.5	1.8	0.12	0	0	0	0.68	0
Chromatiaceae	0.011	0	0.0056	0	0	0	0	0	0.034	0	0	0	0.056	0	3.7	2.8
Chromatiales	1.3	0	0.13	0	0	0	0	0	0	0	0	0	0	0	0	0
<i>Spongiibacter</i> sp.	0.23	0	0.22	0	0.52	0	0.011	0	0.062	0	0	0	0.073	0	4.5	0
Cellvibrionaceae	0	0	0	0	0.090	0	12	6.8	0.0056	0	0	0	1.2	0	0.15	0
Arenicellaceae	0.011	0	0	0	0.056	0	0.63	0	0.0056	0	0	0	0	0	0.017	0
Arenicellaceae	3.9	2.6	0.85	0	1.3	0	1.3	0	1.5	0	0.045	0	0	0	0.20	0
<i>Pseudoalteromonas</i> sp.	0	0	0	0	0	0	0	0	2.5	2.2	0	0	0	0	0	0
<i>Marinobacter</i> sp.	0	0	0	0	0	0	0	0	0	0	0	0	19	9.4	0.44	0
Gammaproteobacteria	1.8	1.3	14	9.9	5.0	2.8	0.017	0	0.15	0	0	0	0	0	0.76	0
Gammaproteobacteria	0.13	0	0.050	0	0.028	0	8.0	4.5	0.77	0	2.8	0	0	0	0.34	0
Gammaproteobacteria	3.0	3.4	1.9	0	0.062	0	0.12	0	0.42	0	0	0	0	0	0.017	0
Gammaproteobacteria	0	0	0	0	0	0	0.0056	0	0	0	9.7	5.2	0.0056	0	0	0
Gammaproteobacteria	0.36	0	0.084	0	0.10	0	0.0056	0	2.3	1.8	0	0	0	0	0.24	0
Myxococcales	0	0	0	0	0.16	0	10	5.7	0.011	0	0	0	0	0	0	0
<i>Desulfovibrio</i> sp.	0	0	0	0	0	0	0	0	0	0	0	0	0	0	3.1	2.5
<i>Nitrospira</i> sp.	0.57	0	0.17	0	0.022	0	0.028	0	1.9	1.4	0	0	0	0	0.63	0
<i>Celeribacter</i> sp.	0	0	0	0	0	0	0	0	0	0	3.4	1.8	0	0	0	0
<i>Marivita</i> sp.	0	0	15	11	3.4	2.6	0.017	0	0.039	0	0	0	0	0	0.011	0
Rhodobacteraceae	0.31	0	0.050	0	0.88	0	0.0056	0	0.073	0	0	0	0	0	0.16	0
Rhodobacteraceae	0.050	0	0.045	0	0.27	0	0.039	0	0.10	0	8.9	4.8	0.38	0	1.4	0
Rhodobacteraceae	0.034	0	0.011	0	0.0056	0	0.028	0	0.11	0	4.4	2.3	0	0	0.13	0
Hyphomonadaceae	1.1	0	0.11	0	0.16	0	0	0	0.078	0	0	0	0	0	4.8	3.3
Hyphomonadaceae	0	0	0.011	0	3.2	2.4	0.0056	0	0.011	0	0.0056	0	0	0	0.0056	0
Rhodobacterales	0.017	0	20	15	6.3	4.7	0.0056	0	0.034	0	0	0	0	0	0.022	0
Rhizobiales	0	0	0	0	7.5	5.7	0	0	0	0	0	0	0	0	0.039	0
Selenomonadales	0	0	0	0	0	0	0	0	0	0	0	0	0	0	4.7	3.8
Clostridiales	0	0	0	0	0	0	0	0	0	0	0	0	0	0	4.8	3.9
Saprospirales	5.1	3.0	1.8	0	0.39	0	0.0056	0	1.1	0	0.022	0	0	0	0.20	0
Saprospirales	2.7	0	0.20	0	0.078	0	0	0	0.57	0	0	0	0	0	0.050	0
Saprospirales	1.2	0	0.49	0	0.034	0	0	0	0.16	0	0.0056	0	0	0	0.0056	0
Flavobacteriaceae	0.15	0	0.13	0	1.7	0	17	9.8	0.067	0	1.7	0	0	0	0.028	0
Flavobacteriaceae	0	0	0	0	0	0	0	0	0	0	8.2	4.4	0.0056	0	0.0056	0
Cryomorphaceae	0.19	0	0.073	0	0.050	0	0	0	0	0	0	0	0	0	4.8	3.7
Acidobacteria	3.2	0	0.82	0	0.45	0	0.045	0	0.70	0	0.11	0	0	0	0.034	0
Flavobacteriaceae	0	0	0	0	0	0	0	0	0	0	0	0	16	8.0	0.0056	0

cell counts by flow cytometry while epifluorescence microscopy confirmed the presence of abundant biofilms after 206 days. Control seawater cell counts remained stable during the entire experiment (mean =  $2.3 \pm 1.4 \times 10^5$  cells ml<sup>-1</sup>).

## Bacterial Activities

### Bacterial Heterotrophic Production

A clear distinction between biodegradable and non-biodegradable plastics was observed by cell incorporation

of radiolabeled <sup>3</sup>H-leucine (**Figure 3B**). The primo-colonizers on PE, AA<sub>144</sub>PE, OXO, PS, and PLA showed high heterotrophic activities during the first 3 days of immersion (between  $3.94 \times 10^{-2}$  ng C mm<sup>-2</sup> h<sup>-1</sup> and  $1.01 \times 10^{-1}$  ng C mm<sup>-2</sup> h<sup>-1</sup>) followed by a dramatic and continuous decrease until the end of the experiment (between  $3.87 \times 10^{-3}$  and  $1.77 \times 10^{-2}$  ng C mm<sup>-2</sup> h<sup>-1</sup> at day 206). AA<sub>48</sub>OXO exhibited the same dynamics with a slight delay in time, with high activities until day 10, followed by a sharp decrease. The three other



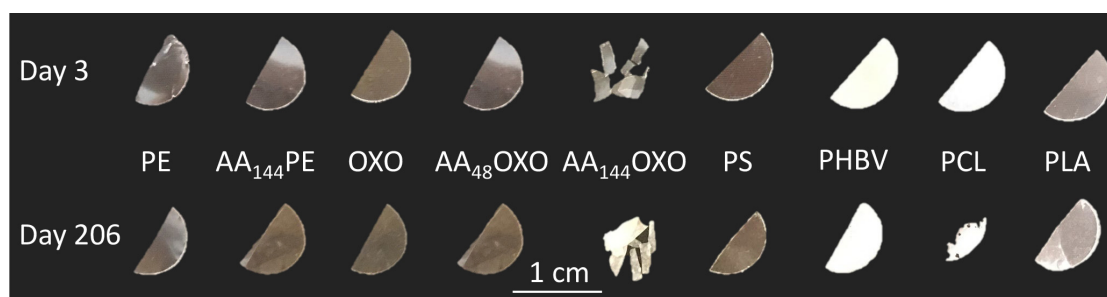


**FIGURE 1** | Plastic pieces of different composition (PE, OXO, PS, PHBV, PCL, and PLA) at the beginning (3 days) and at the end (206 days) of the experimental immersion in seawater. A pretreatment by artificial aging was applied for PE and OXO films by UV-A exposure during 48 h (AA<sub>48</sub>) or 144 h (AA<sub>144</sub>) followed by a thermal aging during 96 h at 70°C.

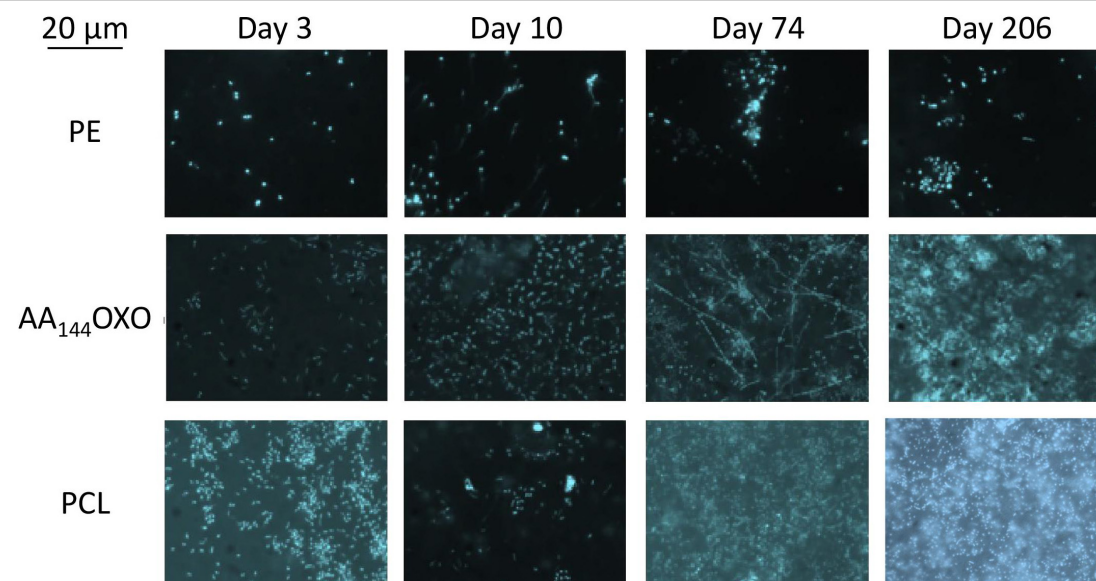


**FIGURE 2** | Epifluorescence micrographs of a selection of DAPI-stained plastics (PE, AA<sub>144</sub>OXO, and PCL) showing the formation and evolution of the biofilms of after 3, 10, 74, and 206 days of immersion in seawater. Artificial aging (AA) pretreatment applied for OXO polymers consisted in UV-A exposure during 144 h (AA<sub>144</sub>) followed by a thermal aging during 96 h at 70°C.

materials (PCL, PHBV, and AA<sub>144</sub>OXO) also presented high heterotrophic activities at the primo-colonization phase (day 3), but differed from the other plastics since their activities remained high and relatively stable until the end of the 206 days of seawater immersion. Maximum activities were found for PCL ( $2.45 \times 10^{-1} \text{ ng C mm}^{-2} \text{ h}^{-1}$ ), followed by PHBV ( $1.34 \times 10^{-1} \text{ ng C mm}^{-2} \text{ h}^{-1}$ ) and AA<sub>144</sub>OXO ( $8.69 \times 10^{-2} \text{ ng C mm}^{-2} \text{ h}^{-1}$ ). Bacterial heterotrophic production remained stable during the entire experiment in control seawater (mean =  $67.6 \pm 42.2 \text{ ng C L}^{-1} \text{ h}^{-1}$ ).

### Extracellular Enzymatic Activities

Similar trends were found when observing the extracellular aminopeptidase,  $\beta$ -glucosidase, and lipase activities (Figures 3C–E, respectively). The general trend found for bacterial heterotrophic production (see Section 3.3.1) of a high activity of the primo-colonizers (day 3;

mean =  $9.5 \times 10^{-5} \pm 3.3 \times 10^{-5} \mu\text{mol mm}^{-2} \text{ h}^{-1}$ , mean =  $7.1 \times 10^{-7} \pm 8.8 \times 10^{-7} \mu\text{mol mm}^{-2} \text{ h}^{-1}$ , and mean =  $3.8 \times 10^{-5} \pm 1.8 \times 10^{-5} \mu\text{mol mm}^{-2} \text{ h}^{-1}$  for aminopeptidase,  $\beta$ -glucosidase, and lipase, respectively) followed by a drastic decrease and further stabilization until the end of the experiment (206 days) was also found for extracellular activities. It was particularly true for lipase activities on PE, AA<sub>144</sub>PE, OXO, AA<sub>48</sub>OXO, PS, and PLA biofilms. Aminopeptidase activities (mean =  $3.75 \times 10^{-4} \pm 8.95 \times 10^{-5} \mu\text{mol mm}^{-2} \text{ h}^{-1}$  with  $n = 30$  for all plastics) and  $\beta$ -glucosidase (mean =  $1.49 \times 10^{-5} \pm 4.49 \times 10^{-6} \mu\text{mol mm}^{-2} \text{ h}^{-1}$  with  $n = 30$  for all plastics) remained low for these plastics during the entire experiment. Again, PCL, PHBV, and AA<sub>144</sub>OXO showed different trends when compared to other plastics. The highest extracellular activities were found when the biofilms became mature (after 31 days), with higher activities always found on PCL ( $3.0 \times 10^{-3} \pm 1.2 \times 10^{-3} \mu\text{mol}$

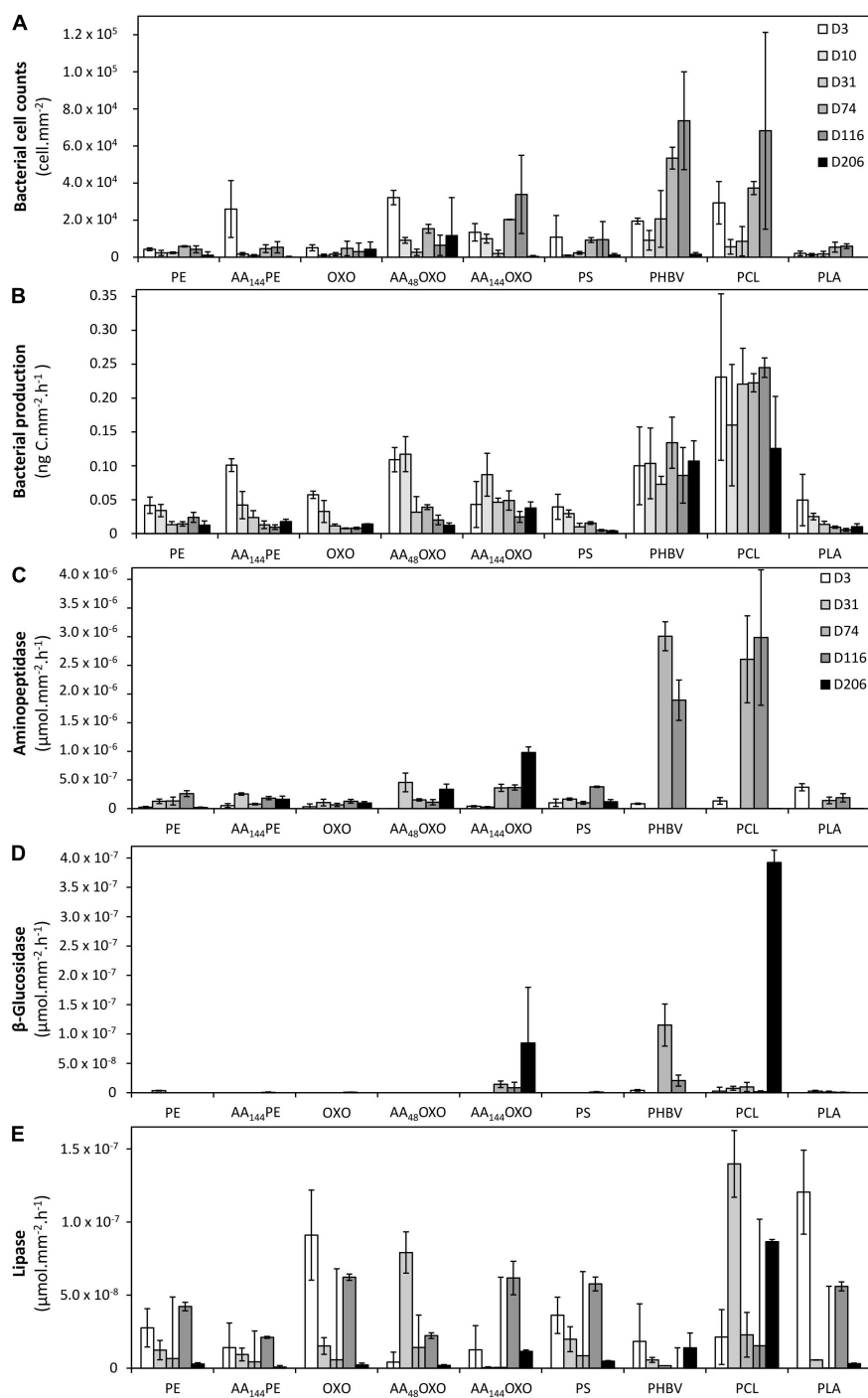


**FIGURE 3 |** Bacterial cell counts (A), bacterial heterotrophic production (B), and bacterial extracellular aminopeptidase (C),  $\beta$ -glucosidase (D), and lipase activities (E) on the different plastic types (PE, AA<sub>144</sub>PE, OXO, AA<sub>48</sub>OXO, AA<sub>144</sub>OXO, PS, PHBV, PCL, and PLA) immersed in seawater for 3, 10, 31, 74, 116, and 206 days. No data available on day 10 for extracellular activities. Error bars indicate standard deviation.

mm<sup>-2</sup> h<sup>-1</sup>,  $3.9 \times 10^{-4} \pm 2.1 \times 10^{-5}$  μmol mm<sup>-2</sup> h<sup>-1</sup>, and  $1.4 \times 10^{-4} \pm 2.3 \times 10^{-5}$  μmol mm<sup>-2</sup> h<sup>-1</sup> for aminopeptidase,  $\beta$ -glucosidase, and lipase, respectively) and PHBV ( $3.0 \times 10^{-3} \pm 2.5 \times 10^{-4}$  μmol mm<sup>-2</sup> h<sup>-1</sup>,  $1.1 \times 10^{-4} \pm 3.6 \times 10^{-5}$  μmol mm<sup>-2</sup> h<sup>-1</sup>, and

$1.8 \times 10^{-5} \pm 2.6 \times 10^{-5}$  μmol mm<sup>-2</sup> h<sup>-1</sup> for aminopeptidase,  $\beta$ -glucosidase, and lipase, respectively), followed by AA<sub>144</sub>OXO ( $9.8 \times 10^{-4} \pm 1.0 \times 10^{-4}$  μmol mm<sup>-2</sup> h<sup>-1</sup>,  $8.5 \times 10^{-5} \pm 9.5 \times 10^{-5}$  μmol mm<sup>-2</sup> h<sup>-1</sup>, and  $6.2 \times 10^{-5} \pm 1.1 \times 10^{-5}$  μmol mm<sup>-2</sup> h<sup>-1</sup> for

aminopeptidase,  $\beta$ -glucosidase, and lipase, respectively). On the other hand, extracellular enzymatic activities remained stable during the entire experiment in control seawater ( $1.1 \times 10^{-2} \pm 8.6 \times 10^{-3} \mu\text{mol L}^{-1} \text{h}^{-1}$ ,  $5.3 \times 10^{-5} \pm 1.2 \times 10^{-4} \mu\text{mol L}^{-1} \text{h}^{-1}$ , and  $1.9 \times 10^{-3} \pm 3.5 \times 10^{-3} \mu\text{mol L}^{-1} \text{h}^{-1}$  for aminopeptidase,  $\beta$ -glucosidase, and lipase, respectively).

## Dynamics of Bacterial Diversity

### Alpha- and Beta-Diversity

Illumina Miseq DNA sequencing generated 9,054,841 paired sequences for the 66 samples, failing into 1517 OTUs after randomly resampling to 17,865 sequences per sample to provide statistical robustness when comparing diversity among samples.

The evolution of the Alpha-diversity was assessed with Chao1, Pielou, Shannon, and Simpson indexes (Table 1). Whatever plastic types, all indexes increased significantly between the primo-colonization (day 3) and the maturation phase of the biofilm (day 31) (pairwise *t*-test,  $p < 0.05$ ). Chao1 species richness estimator almost doubled for all plastics between the primo-colonization and the maturation phase of the biofilm (mean = 390, SD = 135,  $n = 9$  at day 3 and mean = 846, SD = 184,  $n = 9$  at day 31) (Table 1). This index remained relatively stable until the end of the experiment for PE, AA<sub>144</sub>PE, OXO, AA<sub>48</sub>OXO, PS, and PLA biofilms, while after day 74 and up to day 206, a decrease was observed on PCL, PHBV, and AA<sub>144</sub>PE biodegradable polymers (mean = 753, SD = 147,  $n = 3$  at day 31 and mean = 411, SD = 155,  $n = 3$  at day 206). Shannon diversity index showed similar trends, with the exception of the decrease observed on the biodegradable polymers after day 74 and up to day 206, which was less on AA<sub>144</sub>PE and PHBV compared to PCL (Table 1). Bacterial diversity found in seawater on both free-living and organic particle-attached fractions was much less influenced by the temporal dynamics, where all Alpha-diversity indexes remained relatively stable during the entire course of the experiment (Shannon mean = 3.9, SD = 0.5,  $n = 6$  on free-living and mean = 5.2, SD = 0.6,  $n = 6$  on organic particle-attached fractions).

Beta-diversity analysis showed strong dissimilarity (> 90%) between the free-living bacterial communities in seawater compared to plastic samples (Figure 4). Organic particle-attached bacterial communities in seawater also formed a separated cluster, with closer similarity with plastic samples, and especially with the non-biodegradable polymers (see below). Both free-living and organic particle-attached bacterial communities remained stable during the course of the experiment, which contrasted with the succession of distinct communities found on plastics. First, bacterial communities of all plastic materials clustered together during the primo-colonization phase (day 3), with little but significant changes observed on the biofilm growing phase (ANOSIM  $R = 0.622$ ,  $p = 0.001$  between day 3 and day 10). Second, we found a clear distinction between the mature biofilms (after 31 days) found on non-biodegradable (PE, AA<sub>144</sub>PE, OXO, AA<sub>48</sub>OXO, PS, and PLA) compared to biodegradable polymers (PHBV, PCL, and AA<sub>144</sub>OXO) (ANOSIM  $R = 0.287$ ,  $p = 0.001$ ). In particular, PCL and PHBV

clusters strongly differed from the mature biofilms on other plastics, and AA<sub>144</sub>OXO formed a distinct cluster together with AA<sub>48</sub>OXO especially after 116 days of immersion in seawater.

### Taxonomic Composition

Taxonomic analyses confirmed the specificity of the plastisphere compared to seawater free-living bacteria, the latter being dominated by Alphaproteobacteria (40%, mainly SAR11 clade with 24.8%), followed by Flavobacteriia (18.5%) and Gammaproteobacteria (28%, mainly Oceanospirillaceae with 7.9%) (Figure 4). Organic particle-attached bacterial communities were also dominated by Gammaproteobacteria (34.9%, mainly *Spongiibacter* sp. 4.3%), followed by Alphaproteobacteria (16%), Flavobacteriia (15%, mainly *Luteibaculum* sp. 5.3%), and Planctomycetacia (5.6%).

Whatever the plastic type, primo-colonizers (day 3) together with bacteria of the biofilm growing phases (day 10) belonged to Alteromonadales (mean = 21% SD = 11,  $n = 18$ ), Oceanospirillales (mean = 17% SD = 14,  $n = 18$ , mainly represented by *Oleibacter* sp. and *Alcanivorax* sp.), and Cellvibrionales (mean = 10.1% SD = 9.4,  $n = 18$ , mainly represented by *Aestuariaicella* sp.). Some exceptions were found for PCL (exhibiting higher proportions of *Oleiphilus* sp.), PLA (higher proportion of *Neptuniibacter* sp.), PS, and AA<sub>144</sub>OXO (dominated by *Spongiibacter* sp.) (Figure 4).

The mature biofilms (after 31 days) differed between material types. The non-biodegradable materials (PE, AA<sub>144</sub>PE, OXO, AA<sub>48</sub>OXO, and PS) together with PLA shared high proportions of Gammaproteobacteria (mean =  $34 \pm 11\%$ ), Alphaproteobacteria (mean =  $24 \pm 16\%$ ), Sphingobacteriia (mean =  $8.8 \pm 6.2\%$ ), and Flavobacteriia (mean =  $5.0 \pm 5.6\%$ ). Gammaproteobacteria class is composed of Cellvibrionales (mean =  $13 \pm 9\%$ ), with *Spongiibacter* sp. and *Zhongshania* sp. as main representatives as well as Xanthomonadales (mean =  $5.6 \pm 5.4\%$ ) with *Polycyclovorans* sp. PE and AA<sub>144</sub>PE showed increasing proportions of Saprospiraceae (up to 23%), Planctomycetes (up to 14%, mainly OM190 clade and *Planctomyces* sp.), and Arenicellaceae (up to 7%, mainly *Arenicella* sp.) over time. The same tendency was observed for OXO and AA<sub>48</sub>OXO with Rhodobacteraceae (up to 16%) and Flavobacteriaceae (up to 5%, mainly *Gilvibacter* sp.). Interestingly, AA<sub>48</sub>OXO was distinguished by large proportions of Rhizobiales (OCS116 clade, up to 9.3%) and Hyphomonadaceae (mainly *Hirshia* sp., up to 36%). PS diversity profiles displayed higher proportions of Saprospiraceae (up to 19%, mainly *Lewinella* sp.) and Planctomycetaceae (up to 6.3%) at the end of the experiment. Likewise, PLA mature biofilm was composed of Planctomycetaceae (up to 12%, mainly *Planctomyces* sp. and *Rhodopirellula* sp.) and Flavobacteriales (up to 7%, mainly *Luteibaculum* sp.) with increasing proportions over the course of the experiment.

The diversity of mature biofilms was clearly distinct among PHBV, PCL, and AA<sub>144</sub>OXO, with higher proportions of Alphaproteobacteria (mean =  $36 \pm 24\%$ ) compared to the non-biodegradable ones, followed by Gammaproteobacteria (mean =  $29 \pm 18\%$ ) and Flavobacteriia (mean =  $11 \pm 8.1\%$ ). PHBV is composed of Flavobacteriaceae (up to 26%, mainly

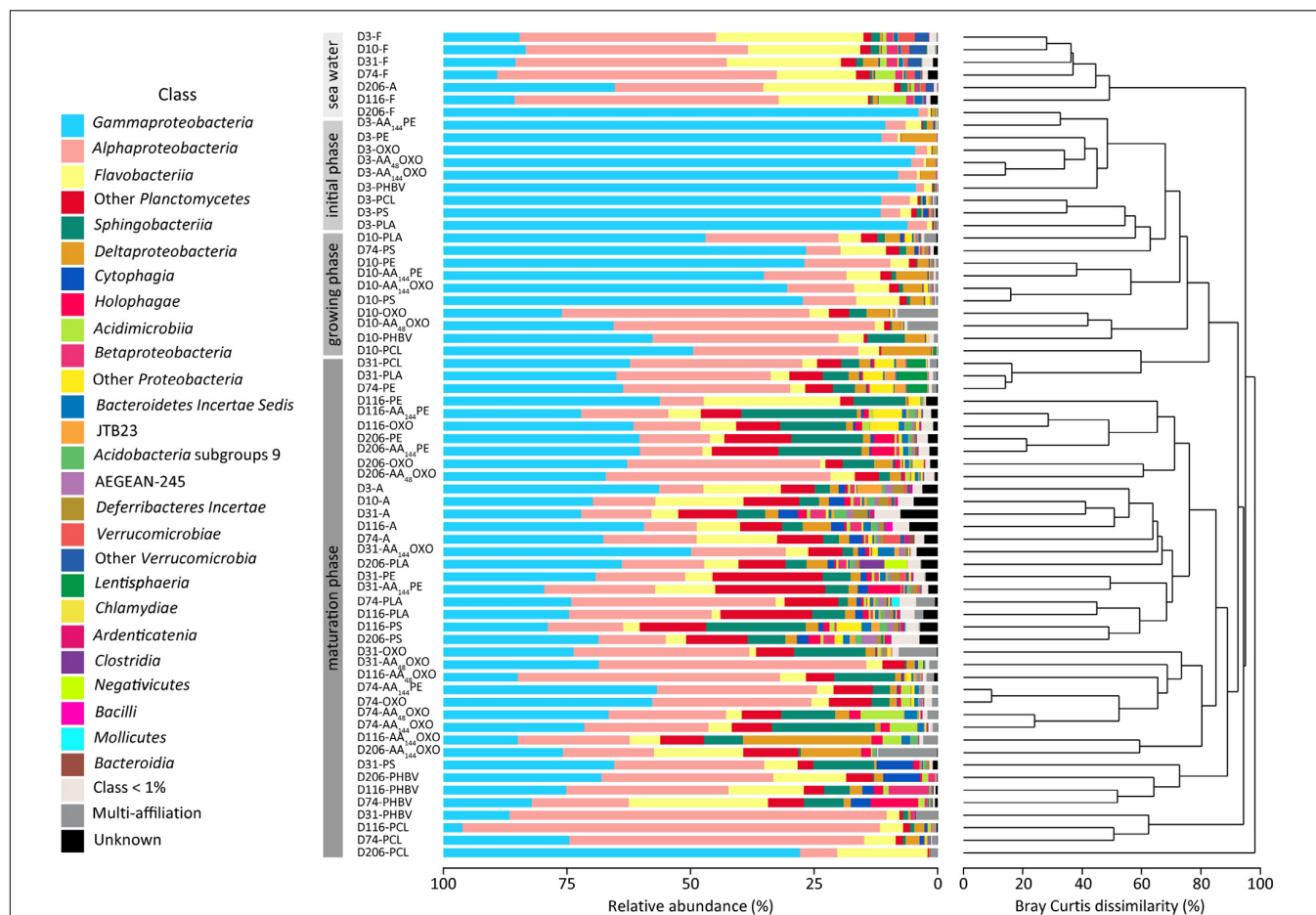


**FIGURE 4 |** Temporal variation of taxonomic abundances and community structure of free-living (F), organic particle-attached bacteria (A) and biofilms of different materials (PE, AA<sub>144</sub>PE, OXO, AA<sub>48</sub>OXO, AA<sub>144</sub>OXO, PS, PHBV, PCL, and PLA) immersed in seawater for 3, 10, 31, 74, 116, and 206 days (D), by cumulative bar charts comparing taxonomic relative abundances (left) and by UPGMA dendrogram based on Bray–Curtis dissimilarities between 16S rRNA-based sequencing profiles (right).

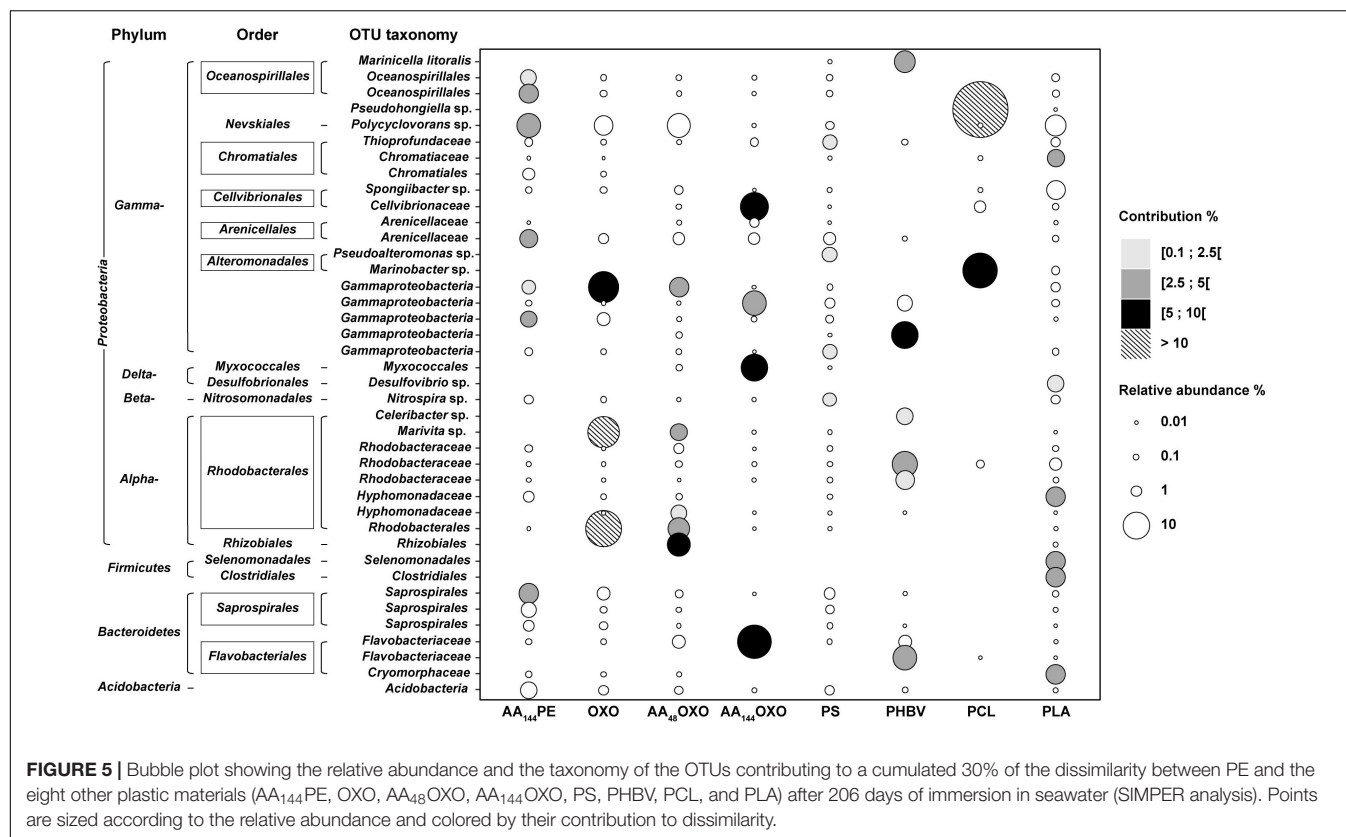
*Maritimonas* sp.), Cellvibrionaceae (up to 15%, mainly *Marinicella* sp.) and Rhizobiales (up to 12%, OCS116 clade), especially at the end of the incubation. PCL and AA<sub>144</sub>OXO shared high proportions of Cellvibrionaceae (up to 23%) and Oceanospirillaceae (up to 52%, mainly *Pseudohongiella* sp.), but also specificities among Flavobacteriaceae, mainly *Aquibacter* sp. for PCL and *Gilvibacter* sp. for AA<sub>144</sub>OXO. PCL also comprised Hyphomonadaceae (up to 40%, mainly *Hirshia* sp. and *Hyphomonas* sp.), whereas AA<sub>144</sub>OXO showed noticeable proportions of Myxococcales (up to 23%, mainly Sandaracinaceae family).

SIMPER analysis highlighted 40 dominant OTUs contributing to a cumulative 30% of the dissimilarity between PE, used as control, and the other polymers after 206 days in seawater (Figure 5). Among non-biodegradable polymers, comparison between PE and AA<sub>144</sub>PE biofilms included six specific OTUs (Oceanospirillales, *Polycyclovorans* sp., Arenicallaceae, and Saprospirales). These OTUs shared low relative abundance and contribution, indicating a rather limited effect of artificial aging on PE. Limited specificities were also found on the

other non-biodegradable materials when compared to PE control. AA<sub>48</sub>OXO biofilm exhibited five contributive OTUs, including two exclusive (affiliated to Rhizobiales and Hyphomonadaceae) and three shared with OXO (affiliated to Rhodobacterales, *Marivita* sp., and Gammaproteobacteria). PLA exhibited six specific OTUs contributing between 3.6 and 3.9% (Clostridiales, Selenomonadales, Cryomorphaceae, Hyphomodadaceae, Chromatiaceae, and *Desulfuvibrio* sp.). Note that the most abundant taxon found on PLA (*Polycyclovorans* sp., 5.7% in relative abundance) was not found as PLA-specific taxa by SIMPER analysis. PS hosted four specific OTUs (*Pseudoalteromonas*, Thioprofundaceae, Gammaproteobacteria, and *Nitrospira* sp.) but with low relative abundance (1.9 to 2.5%) and low contribution to dissimilarity with the PE control (1.4 to 2.2%).

Interestingly, the most distinct taxa were found among the biodegradable polymers (PCL, PHBV, and AA<sub>144</sub>OXO). PCL biofilm presented two highly abundant and contributive OTUs affiliated with *Pseudohongiella* sp. and *Marinobacter* sp. (52% and 19% in relative abundance, 26% and 9%





contribution, respectively). A third PCL-specific OTU affiliated with Flavobacteriaceae was identified (8% contribution and 16% relative abundance). PHBV biofilm highlighted six specific OTUs with 1.8% to 5.2% of contribution, affiliated with Cellvibrionaceae, Bacteroidetes, Rhodobacteraceae, and Flavobacteriaceae as well as *Marinicella litoralis* and *Celeribacter* sp. AA<sub>144</sub>OXO biofilm exhibited four very abundant (from 8 to 17%) and contributive (from 4.5 to 9.8%) OTUs, affiliated with Flavobacteriaceae (also present on PHBV and AA<sub>48</sub>OXO), Gammaproteobacteria, Cellvibrionaceae, and Myxococcales.

## DISCUSSION

### Successive Phases of Biofilm Formation on Plastics

Both epifluorescence microscopy and flow cytometry confirmed the succession of primo-colonization, growth, and maturation phases of the plastics biofilm, as it has been described earlier (see review by Jacquin et al., 2019). Most of the previous studies were based on experiments conducted over a several-week period, mainly on conventional polymer types generally found in the ocean (mostly PE, PET, PVC, and PS) and our study brings new data on microbial colonization of biodegradable plastics in seawater.

Our results showed a rapid bacterial colonization of more than  $5 \times 10^3$  cells mm<sup>-2</sup> on all material types, which is consistent with values found in studies focusing on

the primo-colonization of plastic biofilms (Lee et al., 2008; Oberbeckmann et al., 2015). Interestingly, we found a significant difference in cell counts on PE or OXO after only 3 days of immersion in seawater as compared to same but artificially aged polymer (one order of magnitude higher for AA<sub>144</sub>PE, AA<sub>48</sub>OXO, and AA<sub>144</sub>OXO). Such differences may be explained by the change in surface properties accompanying the artificial aging by UV and temperature (Attwood et al., 2006). Material properties (crystallinity and crystal structure, hydrophobicity, roughness, glass transition temperature, melting temperature, and modulus of elasticity) indeed play a crucial role in the selection of bacterial community in the early stage of colonization (Pompilio et al., 2008). We also observed significantly higher cell counts on PS, PHBV, and PCL as compared to PLA or PE during the primo-colonization phase, but complete characterization of surface properties was not done in this study.

The growth phase of the biofilms was characterized by cell count increase (visible by flow cytometry) together with the production of extracellular matrix (visible by epifluorescence microscopy) after 10 days of immersion in seawater. The final expansion of the biofilm to maturity was visible from day 31 to day 206 on the non-biodegradable polymers (PE, AA<sub>144</sub>PE, OXO, AA<sub>48</sub>OXO, and PS), as well as for PLA. Interestingly, the biofilm maturity was not reached for the biodegradable polymers (PCL, PHBV) and for the AA<sub>144</sub>OXO that continue to increase even after 206 days of incubation in seawater. Few other long-term studies (> 6 months) have also shown limited differences in biofilm maturation on

non-biodegradable polymers, i.e., PE, PP, PET, or polycarbonate (PC) (Webb et al., 2009; De Tender et al., 2017). Our results are consistent with another study underlining the continuous growth of PHBV biofilms in seawater (Dussud et al., 2018b), albeit limited to 45 days of immersion. Our results thus confirm this trend on PHBV but for much longer period (206 days) and extend this observation to PCL and AA<sub>144</sub>OXO. These results open new questions on the final expansion of the biofilms growing on biodegradable polymers in seawater and call for long-term incubation period in controlled conditions.

## Dynamics of Extra- and Intracellular Bacterial Activities on Plastics

This study presents pioneer results of intra- and extracellular activities of biofilms growing on various plastics. Extracellular enzymes are necessary to hydrolyze polymers and organic particles into small molecules (< 600 Da) that can cross the bacterial cell membranes *via* permeases for further intracellular degradation (Azam and Malfatti, 2007). Activities of hydrolytic enzymes such as protease, lipase, and glucosidase have already been examined for various marine particles including suspended particulate matter, marine snow, and sinking particles collected by sediment traps (Severin et al., 2016 and references cited there in), but not on plastic particles. So far, only one study evaluated the intracellular bacterial heterotrophic production on plastics (Dussud et al., 2018b). To the best of our knowledge, this is the first study to merge extra- and intracellular activities. Overall, we found that the measured extra- and intracellular activities gave the same trends, with higher activities found on biodegradable compared to non-biodegradable materials. This result underlines the complementary role of extra- and intracellular enzyme activities to decompose and transform polymers and organic molecules for further metabolization.

The primo-colonizers (day 3) were particularly active whatever the plastic types, as depicted by intracellular heterotrophic activity and also by extracellular aminopeptidase and lipase (not for b-glucosidase). Such activity peak may certainly be due to the utilization of organic matter present in the “conditioning film” that forms rapidly on hard surfaces placed in seawater (Loeb and Neihof, 1975; Dobretsov, 2010).

Thereafter, clear distinction could be made for non-biodegradable vs. biodegradable materials. Both inter- and extracellular activities decreased to remained low values from day 3 and until the end of the experiment on all the conventional materials (PE, AA<sub>144</sub>PE, OXO, and PS). Interestingly, a significant and consistent decrease was also observed on PLA, a polymer known as biodegradable under industrial composting conditions or degradable in human body (Pillai and Sharma, 2010), but not biodegradable under marine conditions (Karamanlioglu et al., 2017).

Intra- and extracellular activities (including b-glucosidase) remained stable or even increase until 206 days of immersion in seawater for the biodegradable polymers, with higher activities found for PCL and PHBV compared to AA<sub>144</sub>OXO. This appears consistent based on the intrinsic features of PCL and PHBV whose ester linkages will be degraded by hydrolytic enzymes

such as lipases. The potential activity of plastic biodegradation in seawater is determined by several standard tests based on biomass and respirometric activity measurements (mainly CO<sub>2</sub> production) under laboratory conditions during 3 months (ASTM D6691-09), 6 months (ASTM D7473-12), or 24 months (ISO 18830, ISO 19679, ASTM D7991-15). Other activity tests can be considered as alternative methods, such as tests based on ATP measurements (Fontanella et al., 2013) or bacterial heterotrophic production (Jacquin et al., 2021). We are aware that intra- and extracellular bacterial activities under natural conditions may be related to processes other than plastic biodegradation (biodegradation of organic matter and cross-feeding in the biofilm) (Pande et al., 2014), but this study provides a set of congruent results that, although not definitely compelling, gives concrete hints for effective biodegradability in seawater (Jacquin et al., 2021).

## Microbial Community Dynamics in Seawater and for Biodegradable and Non-biodegradable Plastics

Illumina MiSeq sequencing provided a set of complementary information to better understand the dynamics of bacterial abundance and activities on plastic described above, including (i) a clear distinction between communities living on plastics and the surrounding seawater, (ii) contrasted communities on biodegradable and non-biodegradable materials after 7 months of immersion in seawater, which allowed to (iii) describe new potential candidates for the biodegradation of PCL, PHBV, and artificially aged OXO in natural seawater.

First, cluster analysis showed significant distinction between bacterial communities living on plastics when compared to the free-living and organic particle-attached fractions. Such observation is now a common feature observed in the oceans worldwide (Wright et al., 2021) that reinforce the originality of the “plastisphere” compared to other microorganisms living in the surrounding seawater. In our study, we noticed that organic particle-attached communities formed a separate group that was more similar to the plastisphere compared to the free-living fraction, as already mentioned on PET drinking bottles and glass substrates in seawaters (Oberbeckmann et al., 2016). These authors suggested that the similarity between organic particle-associated and plastic biofilms may be explained by the presence of non-specific surface-colonizing microbes that represent another part of the diversity around the core plastisphere microbiome. Indeed, surface attachment capabilities of microorganisms can be triggered by organelles (e.g., flagella, pili) (Rogers et al., 2020), hydrophobicity of the outer membrane (e.g., modifications of the lipopolysaccharidic composition of some bacteria allowing better interactions with hydrophobic substances) (Krasowska and Sigler, 2014), or synthesis of surfactants (e.g., higher ability of *Lysinibacillus fusiformis* to degrade polyethylene in the presence of biosurfactants) (Mukherjee et al., 2016). We also found clear dissimilarities between the bacterial communities in the free-living fraction (dominated by Alphaproteobacteria, mainly SAR11) and the organic particle-attached fraction (dominated

by Gammaproteobacteria), which is also a common pattern in seawaters (Li et al., 2021). Both free-living and organic particle-attached communities remained relatively stable during the entire course of the experiment, with classical values found in the Mediterranean seawaters in terms of abundance, heterotrophic bacterial production, and extracellular activities (Severin et al., 2016). These results validated our capability to maintain realistic conditions for up to 206 days in an experimental setup renewed with natural seawater every 30 min.

Second, we observed a succession of communities with clear dissimilarities between biodegradable and non-biodegradable materials after 7 months of immersion in seawater. Such dissimilarities were not found during the primo-colonization (day 3) and the growth of the biofilm (day 10) that showed distinct but close communities whatever the plastic type. Primo-colonizers (day 3) together with bacteria on the growth phase of the biofilm (day 10) belonged to Gammaproteobacteria (mainly *Alteromonadaceae*, *Oceanospirillaceae*, and *Alcanivoracaceae*), which is in accordance with previous studies (Dussud et al., 2018a; Cheng et al., 2021). Under our conditions, significant dissimilarities were observed after 31 days, which corresponds to the maturity of biofilms for non-biodegradable materials on the one hand, and to the continuous growth with high extra- and intracellular activities for biodegradable materials on the other hand. After 31 to 74 days of immersion in seawater, biofilms on PCL and PHBV strongly differed from the mature biofilms of other plastics. AA<sub>144</sub>OXO also formed a distinct cluster after 116 days. This is the first time such comparison has been reported for long-term studies, as the only one study comparing bacterial abundance, activity, and diversity on biodegradable materials ended their experiment at the beginning of the biofilm maturity, i.e., after 45 days of immersion in seawater (Dussud et al., 2018a). Most of the other long-term studies over a period of more than 6 months restricted their analysis on bacterial diversity colonizing non-biodegradable polymers, such as PE, PP, PET, and PC (Webb et al., 2009; De Tender et al., 2017). We emphasized here that further studies may take into account not only the bacterial diversity living on plastics, but also the extra- and intracellular activities of the biofilm that will provide new insights into the functional role played by the plastsphere in seawaters.

Third, we describe new potential candidates for the biodegradation of PCL, PHBV, and artificially aged OXO in natural seawater, based on the congruent results of biomass increase together with high extra- and intracellular activities. We used similarity percentage analysis (SIMPER, Ghiglione et al., 2012) to identify OTUs primarily responsible for dissimilarities between pairs of PE versus PCL, PHBV, and AA-OXO after 206 days of incubation in seawater. A clear trend was observed with biodegradable polymers being dominated by a low number of highly abundant contributive OTUs when compared to non-biodegradable polymers, suggesting a specialization of the bacterial communities, providing more information to the contrasted results obtained so far, not allowing to answer whether plastics really select for specific microbial communities (Wright et al., 2020). The most important OTUs that influenced the dissimilarity between PCL and PE were *Pseudohongiella* sp. and *Marinobacter* sp. These two genera have never been listed as PCL

degraders, but the first was found highly abundant after crude oil pollution (Valencia-Agami et al., 2019; Peng et al., 2020) and the second contains well-known hydrocarbonoclastic species (Grimaud et al., 2012; Cui et al., 2016), which is consistent with the petroleum nature of the polymer. Another contributing OTU was affiliated with Flavobacteriaceae that were already shown as potential PCL degraders (Lopardo and Urakawa, 2019) or capable of using complex carbon sources (Rodriguez-Sanchez et al., 2016). We also identified putative PHBV degraders, some of them being already highlighted in similar studies, such as Bacteroidetes and others presenting the enzymatic machinery for PHA degradation, such as Celeribacters (Volova et al., 2016). We also found *Marinicella litoralis* that has never been described as a potential PHBV degrader to date (Romanenko et al., 2010; Shoji et al., 2014), as well as Rhodobacteraceae that was abundant in all material types with known ability to form biofilm on plastics and to degrade complex organic matter (Kessler et al., 2011; Flood et al., 2018). Finally, putative degraders of artificially aged OXO (AA<sub>144</sub>OXO) belonged to Gammaproteobacteria, Cellvibrionaceae, Myxococcales, and Flavobacteriaceae, which are classically observed on the plastsphere of various material types found in seawaters including PE (Zettler et al., 2013), PET (Oberbeckmann et al., 2016), and PVC (Pinto et al., 2019). Members of Myxococcales and Flavobacteriaceae presented high hydrolytic enzymes excretion and complex biopolymers degradation capacities (Shimkets et al., 2006; Amaral-Zettler et al., 2020) together with hydrocarbon degradation capabilities (Pollet et al., 2018; Gutierrez, 2019). We are aware that the description of putative OTUs involved in the biodegradation of PCL, PHBV, and AA-OXO are sometimes limited to the poor taxonomic identification based on 16S rRNA metabarcoding; however, it opens new routes for further studies to delve deeper into the understanding of the biodegradability of these materials in seawaters.

## CONCLUDING REMARKS

Through the analysis of a broad set of microbial parameters (abundance, diversity, and activities) to describe the evolution of the marine biofilms growing on six different plastic types during a long-term experiment, we demonstrated clear evidence of biodegradation on PCL, PHBV, and artificially aged OXO in seawater. Signs of biodegradation were visible after 1 month and until the end of the experiment, with significant increases of the biofilm biomass, of the intra- and extracellular activities, together with drastic changes in bacterial diversity. In contrast, we found no sign of biodegradation for PE, PS, and PLA under our experimental conditions, where the biofilms became mature after 1 month and remained relatively stable until the end of the experiment. We encourage the recording of these microbial parameters for a comprehensive connection between biofilm formation and polymer degradation when evaluating the plastic biodegradation in seawater, which is currently not taken into account in the current standards (mainly based on respirometry activities and generally performed under laboratory conditions). Our study opens also new routes for further studies

on biodegradation mechanisms, by providing a list of putative OTUs that may serve as model organisms potentially involved in the biodegradation of PCL, PHBV, and artificially aged OXO under natural seawater conditions.

Finally, it is noteworthy that the bio-based polymer PLA showed no signs of biodegradation under our experimental conditions, whereas the fossil-based polymer PCL showed significant evidence of biodegradation. This reinforced the distinction that has to be made between biobased and biodegradable polymers but also the different certification schemes for biodegradation in contrasted environments (compost, freshwater, and seawater) when considering an alternative to conventional fossil-based plastics.

## DATA AVAILABILITY STATEMENT

The datasets presented in this study can be found in online repositories. The names of the repository/repositories and accession number(s) can be found below: <https://www.ebi.ac.uk/metagenomics/>, PRJEB37662.

## AUTHOR CONTRIBUTIONS

CD, A-LM, SB, and J-FG have conceived and designed the study. CD, ML, and CO carried out all the experiments and

acquired the data. SB and BE provided the equipment. CD, CO, LP, GD, A-LM, VB, and J-FG analyzed and interpreted the data. CO, CD, VB, and J-FG drafted the manuscript. LP, GD, ML, BE, GB, AT, A-LM, and SB revised the manuscript and approved the version of the manuscript to be published. All authors contributed to the article and approved the submitted version.

## FUNDING

This work was funded by the French National Research Agency (project ANR-OXOMAR), by the Tara Ocean Foundation (project Microplastic 2019), by the European project JRA-ASSEMBLE+, and by the CNRS (project PEPSI-PHABIO).

## ACKNOWLEDGMENTS

We are grateful to Philippe Catala for his laboratory support, to Matthieu George and Pascale Fabre for insightful comments on the manuscript, to G Baby for technical support, and Guigui PA, VF, and JPJS for helpful discussion. This work is part of the Ph.D. thesis of CD supported by the French Ministry of Education.

## REFERENCES

- Amaral-Zettler, L. A., Zettler, E. R., and Mincer, T. J. (2020). Ecology of the plastisphere. *Nat. Rev. Microbiol.* 18, 139–151. doi: 10.1038/s41579-019-0308-0
- Attwood, J., Philip, M., Hulme, A., Williams, G., and Shipton, P. (2006). The effects of ageing by ultraviolet degradation of recycled polyolefin blends. *Polym. Degrad. Stab.* 91, 3407–3415. doi: 10.1016/j.polymdegradstab.2006.04.025
- Azam, F., and Malfatti, F. (2007). Microbial structuring of marine ecosystems. *Nat. Rev. Microbiol.* 5, 782–791. doi: 10.1038/nrmicro1747
- Bokulich, N. A., Subramanian, S., Faith, J. J., Gevers, D., Gordon, J. I., Knight, R., et al. (2013). Quality-filtering vastly improves diversity estimates from *Illumina* amplicon sequencing. *Nat. Methods* 10, 57–59. doi: 10.1038/nmeth.2276
- Briand, J. F., Djeridi, I., Jamet, D., Coupé, S., Bressy, C., Molmeret, M., et al. (2012). Pioneer marine biofilms on artificial surfaces including antifouling coatings immersed in two contrasting French Mediterranean coast sites. *Biofouling* 28, 453–463. doi: 10.1080/08927014.2012.688957
- Cheng, J., Jacquini, J., Conan, P., Pujo-Pay, M., Barbe, V., George, M., et al. (2021). Relative influence of plastic debris size and shape, chemical composition and phytoplankton-bacteria interactions in driving seawater plastisphere abundance, diversity and activity. *Front. Microbiol.* 11:610231. doi: 10.3389/fmicb.2020.610231
- Chiu, C.-H., Wang, Y.-T., Walther, B. A., and Chao, A. (2014). An improved nonparametric lower bound of species richness via a modified good–turing frequency formula. *Biometrics* 70, 671–682. doi: 10.1111/biom.12200
- Cui, H., Su, X., Chen, F., Wei, S., Chen, S., and Wang, J. (2016). Vertical distribution of archaeal communities in cold seep sediments from the julong methane reef area in the South China sea. *Biosci. J.* 32, 43–48.
- Dang, H., Li, T., Chen, M., and Huang, G. (2008). Cross-ocean distribution of Rhodobacterales bacteria as primary surface colonizers in temperate coastal marine waters. *Appl. Environ. Microbiol.* 74, 52–60. doi: 10.1128/aem.01400-07
- De Tender, C., Devriese, L. I., Haegeman, A., Maes, S., Vangyete, J., Cattrijsse, A., et al. (2017). Temporal dynamics of bacterial and fungal colonization on plastic debris in the North Sea. *Environ. Sci. Technol.* 51, 7350–7360. doi: 10.1021/acs.est.7b00697
- Dobretsov, S. (2010). “Marine Biofilms,” in *Biofouling*, eds S. Durr and J. Thompson (Oxford: Wiley-Blackwell), 123–136. doi: 10.1002/9781444315462.ch9
- Dussud, C., Hudec, C., George, M., Fabre, P., Higgs, P., Bruzaud, S., et al. (2018a). Colonization of non-biodegradable and biodegradable plastics by marine microorganisms. *Front. Microbiol.* 9:1571. doi: 10.3389/fmicb.2018.01571
- Dussud, C., Meistertzheim, A. L., Conan, P., Pujo-Pay, M., George, M., Fabre, P., et al. (2018b). Evidence of niche partitioning among bacteria living on plastics, organic particles and surrounding seawaters. *Environ. Pollut.* 236, 807–816. doi: 10.1016/j.envpol.2017.12.027
- Edgar, R., Haas, B., Clemente, J., Quince, C., and Knight, R. (2011). UCHIME improves sensitivity and speed of chimera detection. *Bioinformatics Oxf. Engl.* 27, 2194–2200. doi: 10.1093/bioinformatics/btr381
- Eich, A., Mildenberger, T., Laforsch, C., and Weber, M. (2015). Biofilm and diatom succession on polyethylene (PE) and biodegradable plastic bags in two marine habitats: early signs of degradation in the pelagic and benthic zone? *PLoS One* 10:e0137201. doi: 10.1371/journal.pone.0137201
- Eriksen, M., Lebreton, L. C. M., Carson, H. S., Thiel, M., Moore, C. J., Borerro, J. C., et al. (2014). Plastic pollution in the World's oceans: more than 5 trillion plastic pieces weighing over 250,000 Tons Afloat at sea. *PLoS One* 9:e111913. doi: 10.1371/journal.pone.0111913
- Escudié, F., Auer, L., Bernard, M., Mariadassou, M., Cauquil, L., Vidal, K., et al. (2017). FROGS: find, rapidly, OTUs with galaxy solution. *Bioinformatics* 34, 1287–1294. doi: 10.1093/bioinformatics/btx791
- Eyheraguibel, B., Traikia, M., Fontanella, S., Sancelme, M., Bonhomme, S., Fromageot, D., et al. (2017). Characterization of oxidized oligomers from polyethylene films by mass spectrometry and NMR spectroscopy before and after biodegradation by a *Rhodococcus rhodochrous* strain. *Chemosphere* 184, 366–374. doi: 10.1016/j.chemosphere.2017.05.137
- Flood, B. E., Leprich, D., and Bailey, J. V. (2018). Complete genome sequence of *Celeribacter baekdonensis* strain LH4, a thiosulfate-oxidizing Alphaproteobacterial isolate from gulf of Mexico continental slope sediments. *Genome Announc.* 6:e00434-18.
- Fontanella, S., Bonhomme, S., Brusson, J.-M., Pittieri, S., Samuel, G., Pichon, G., et al. (2013). Comparison of biodegradability of various polypropylene films



- containing additives based on Mn, Mn/Fe or Co. *Polym. Degrad. Stab.* 98, 875–884. doi: 10.1016/j.polydegstab.2013.01.002
- Ghiglione, J. F., Galand, P. E., Pommier, T., Pedrós-Alió, C., Maas, E. W., Bakker, K., et al. (2012). Pole-to-pole biogeography of surface and deep marine bacterial communities. *Proc. Natl. Acad. Sci. U.S.A.* 109, 17633–17638. doi: 10.1073/pnas.1208160109
- Grimaud, R., Ghiglione, J.-F., Cagnon, C., Lauga, B., Vaysse, P. J., Rodriguez-Blanco, A., et al. (2012). Genome sequence of the marine bacterium *Marinobacter hydrocarbonoclasticus* SP17, which forms biofilms on hydrophobic organic compounds. *J. Bacteriol.* 194, 3539–3540. doi: 10.1128/jb.00500-12
- Gutierrez, T. (2019). “Aerobic hydrocarbon-degrading *Gammaproteobacteria*: xanthomonadales,” in *Taxonomy, Genomics and Ecophysiology of Hydrocarbon-Degrading Microbes, Handbook of Hydrocarbon and Lipid Microbiology*, ed. T. J. McGinty (Cham: Springer International Publishing), 191–205. doi: 10.1007/978-3-030-14796-9\_4
- Harrison, J. P., Schratzberger, M., Sapp, M., and Osborn, A. M. (2014). Rapid bacterial colonization of low-density polyethylene microplastics in coastal sediment microcosms. *BMC Microbiol.* 14:232. doi: 10.1186/s12866-014-0232-4
- Jacquin, J., Callac, N., Cheng, J., Giraud, C., Gorand, Y., Denoual, C., et al. (2021). Microbial diversity and activity during the biodegradation in seawater of various substitutes to conventional plastic cotton swab sticks. *Front. Microbiol.* 12:604395. doi: 10.3389/fmicb.2021.604395
- Jacquin, J., Cheng, J., Odobel, C., Pandin, C., Conan, P., Pujo-Pay, M., et al. (2019). Microbial ecotoxicology of marine plastic debris: a review on colonization and biodegradation by the “Plastisphere”. *Front. Microbiol.* 10:865. doi: 10.3389/fmicb.2019.00865
- Jambeck, J. R., Geyer, R., Wilcox, C., Siegler, T. R., Perryman, M., Andrady, A., et al. (2015). Marine pollution. Plastic waste inputs from land into the ocean. *Science* 347, 768–771. doi: 10.1126/science.1260352
- Karamanlioglu, M., Preziosi, R., and Robson, G. D. (2017). Abiotic and biotic environmental degradation of the bioplastic polymer poly(lactic acid): a review. *Polym. Degrad. Stab.* 137, 122–130. doi: 10.1016/j.polydegstab.2017.01.009
- Kessler, J. D., Valentine, D. L., Redmond, M. C., Du, M., Chan, E. W., Mendes, S. D., et al. (2011). A persistent oxygen anomaly reveals the fate of spilled methane in the deep Gulf of Mexico. *Science* 331, 312–315. doi: 10.1126/science.1199697
- Kirstein, I. V., Wichels, A., Krohne, G., and Gerdt, G. (2018). Mature biofilm communities on synthetic polymers in seawater – Specific or general? *Mar. Environ. Res.* 142, 147–154. doi: 10.1016/j.marenvres.2018.09.028
- Krasowska, A., and Sigler, K. (2014). How microorganisms use hydrophobicity and what does this mean for human needs? *Front. Cell. Infect. Microbiol.* 4:112. doi: 10.3389/fcimb.2014.001121
- Lee, J.-W., Nam, J.-H., Kim, Y.-H., Lee, K.-H., and Lee, D.-H. (2008). Bacterial communities in the initial stage of marine biofilm formation on artificial surfaces. *J. Microbiol.* 46, 174–182. doi: 10.1007/s12275-008-0032-3
- Li, J., Gu, L., Bai, S., Wang, J., Su, L., Wei, B., et al. (2021). Characterization of particle-associated and free-living bacterial and archaeal communities along the water columns of the South China Sea. *Biogeosciences* 18, 113–133. doi: 10.5194/bg-18-113-2021
- Lobelle, D., and Cunliffe, M. (2011). Early microbial biofilm formation on marine plastic debris. *Mar. Pollut. Bull.* 62, 197–200. doi: 10.1016/j.marpolbul.2010.10.013
- Loeb, G. I., and Neihof, R. A. (1975). “Marine conditioning films,” in *Applied Chemistry at Protein Interfaces, Advances in Chemistry*, ed. R. E. Baier (Washington, DC: American Chemical Society), 319–335. doi: 10.1021/ba-1975-0145.ch016
- Lopardo, C. R., and Urakawa, H. (2019). Performance and microbial diversity of bioreactors using polycaprolactone and polyhydroxyalkanoate as carbon source and biofilm carrier in a closed recirculating aquaculture system. *Aquac. Int.* 27, 1251–1268. doi: 10.1007/s10499-019-00383-5
- Magoë, T., and Salzberg, S. L. (2011). FLASH: fast length adjustment of short reads to improve genome assemblies. *Bioinformatics* 27, 2957–2963. doi: 10.1093/bioinformatics/btr507
- Mahé, F., Rognes, T., Quince, C., de Vargas, C., and Dunthorn, M. (2014). Swarm: robust and fast clustering method for amplicon-based studies. *PeerJ PrePrints* 2:e386v1.
- Martin, M. (2011). Cutadapt removes adapter sequences from high-throughput sequencing reads. *EMBnet. J.* 17, 10–12. doi: 10.14806/ej.17.1.200
- McMurdie, P. J., and Holmes, S. (2013). phyloseq: an R package for reproducible interactive analysis and graphics of microbiome census data. *PLoS One* 8:e61217. doi: 10.1371/journal.pone.0061217
- Mével, G., Vernet, M., Goutx, M., and Ghiglione, J. F. (2008). Seasonal to hour variation scales in abundance and production of total and particle-attached bacteria in the open NW Mediterranean Sea (0–1000 m). *Biogeosciences* 5, 1573–1586. doi: 10.5194/bg-5-1573-2008
- Mukherjee, S., Chowdhuri, U. R., and Kundu, P. P. (2016). Bio-degradation of polyethylene waste by simultaneous use of two bacteria: *Bacillus licheniformis* for production of bio-surfactant and *Lysinibacillus fusiformis* for biodegradation. *RSC Adv.* 6, 2982–2992. doi: 10.1039/c5ra25128a
- Oberbeckmann, S., Löder, M. G. J., and Labrenz, M. (2015). Marine microplastic-associated biofilms – a review. *Environ. Chem.* 12, 551–562. doi: 10.1071/en15069
- Oberbeckmann, S., Loeder, M. G., Gerdt, G., and Osborn, A. M. (2014). Spatial and seasonal variation in diversity and structure of microbial biofilms on marine plastics in Northern European waters. *FEMS Microbiol. Ecol.* 90, 478–492. doi: 10.1111/1574-6941.12409
- Oberbeckmann, S., Osborn, A. M., and Duhaime, M. B. (2016). Microbes on a bottle: substrate, season and geography influence community composition of microbes colonizing marine plastic debris. *PLoS One* 11:e0159289. doi: 10.1371/journal.pone.0159289
- Pande, S., Merker, H., Bohl, K., Reichelt, M., Schuster, S., De Figueiredo, L. F., et al. (2014). Fitness and stability of obligate cross-feeding interactions that emerge upon gene loss in bacteria. *ISME J.* 8, 953–962. doi: 10.1038/ismej.2013.211
- Parada, A. E., Needham, D. M., and Fuhrman, J. A. (2016). Every base matters: assessing small subunit rRNA primers for marine microbiomes with mock communities, time series and global field samples. *Environ. Microbiol.* 18, 1403–1414. doi: 10.1111/1462-2920.13023
- Peng, C., Tang, Y., Yang, H., He, Y., Liu, Y., Liu, D., et al. (2020). Time- and compound-dependent microbial community compositions and oil hydrocarbon degrading activities in seawater near the Chinese Zhoushan Archipelago. *Mar. Pollut. Bull.* 152:110907. doi: 10.1016/j.marpolbul.2020.110907
- Pielou, E. C. (1966). The measurement of diversity in different types of biological collections. *J. Theor. Biol.* 13, 131–144. doi: 10.1016/0022-5193(66)90013-0
- Pillai, C. K. S., and Sharma, C. P. (2010). Review Paper: absorbable polymeric surgical sutures: chemistry, production, properties, biodegradability, and performance. *J. Biomater. Appl.* 25, 291–366. doi: 10.1177/0885328210384890
- Pinto, M., Langer, T. M., Hüffer, T., Hofmann, T., and Herndl, G. J. (2019). The composition of bacterial communities associated with plastic biofilms differs between different polymers and stages of biofilm succession. *PLoS One* 14:e0217165. doi: 10.1371/journal.pone.0217165
- Pollet, T., Berdjeb, L., Garnier, C., Durrieu, G., Le Poupon, C., Misson, B., et al. (2018). Prokaryotic community successions and interactions in marine biofilms: the key role of *Flavobacteriia*. *FEMS Microbiol. Ecol.* 94:fiy083.
- Pompilio, A., Piccolomini, R., Picciani, C., D’Antonio, D., Savini, V., and Di Bonaventura, G. (2008). Factors associated with adherence to and biofilm formation on polystyrene by *Stenotrophomonas maltophilia*: the role of cell surface hydrophobicity and motility. *FEMS Microbiol. Lett.* 287, 41–47. doi: 10.1111/j.1574-6968.2008.01292.x
- Porter, K. G., and Feig, Y. S. (1980). The use of DAPI for identifying and counting aquatic microflora. *Limnol. Oceanogr.* 25, 943–948. doi: 10.4319/lo.1980.25.5.0943
- Poulain, M., Mercier, M. J., Brach, L., Martignac, M., Routaboul, C., Perez, E., et al. (2019). Small microplastics as a main contributor to plastic mass balance in the north atlantic subtropical gyre. *Environ. Sci. Technol.* 53, 1157–1164. doi: 10.1021/acs.est.8b05458
- Quast, C., Priesse, E., Yilmaz, P., Gerken, J., Schweer, T., Yarza, P., et al. (2012). The SILVA ribosomal RNA gene database project: improved data processing and web-based tools. *Nucleic Acids Res.* 41, 590–596. doi: 10.1093/nar/gks1219
- R Core Team (2018). *R version 3.5.0. R Lang. Environ. Stat. Comput.* Vienna: R Foundation for Statistical Computing.
- RameshKumar, S., Shaiju, P., O’Connor, K. E., and Ramesh, B. P. (2020). Bio-based and biodegradable polymers - State-of-the-art, challenges and emerging trends. *Curr. Opin. Green Sustain. Chem.* 21, 75–81. doi: 10.1016/j.cogsc.2019.12.005

- Rodriguez-Sanchez, A., Purswani, J., Lotti, T., Maza-Marquez, P., van Loosdrecht, M. C. M., Vahala, R., et al. (2016). Distribution and microbial community structure analysis of a single-stage partial nitrification/anammox granular sludge bioreactor operating at low temperature. *Environ. Technol.* 37, 2281–2291. doi: 10.1080/09593330.2016.1147613
- Rogers, K. L., Carreres-Calabuig, J. A., Gorokhova, E., and Posth, N. R. (2020). Micro-by-micro interactions: how microorganisms influence the fate of marine microplastics. *Limnol. Oceanogr. Lett.* 5, 18–36. doi: 10.1002/lol2.10136
- Rognes, T., Flouri, T., Nichols, B., Quince, C., and Mahé, F. (2016). VSEARCH: a versatile open source tool for metagenomics. *PeerJ* 4:e2584. doi: 10.7717/peerj.2584
- Romanenko, L. A., Tanaka, N., Frolova, G. M., and Mikhailov, V. V. (2010). *Marinicella litoralis* gen. nov., sp. nov., a gammaproteobacterium isolated from coastal seawater. *Int. J. Syst. Evol. Microbiol.* 60, 1613–1619. doi: 10.1099/ijs.0.016147-0
- Salta, M., Wharton, J. A., Blache, Y., Stokes, K. R., and Briand, J.-F. (2013). Marine biofilms on artificial surfaces: structure and dynamics. *Environ. Microbiol.* 15, 2879–2893. doi: 10.1111/1462-2920.12186
- Schnurr, R. E. J., Alboiu, V., Chaudhary, M., Corbett, R. A., Quanz, M. E., Sankar, K., et al. (2018). Reducing marine pollution from single-use plastics (SUPs): a review. *Mar. Pollut. Bull.* 137, 157–171. doi: 10.1016/j.marpolbul.2018.10.001
- Science Advice for Policy by European Academies (SAPEA) (2020). *Biodegradability of Plastics in the Open Environment*. Berlin: SAPEA. doi: 10.26356/biodegradabilityplastics
- Selke, S., Auras, R., Nguyen, T. A., Castro Aguirre, E., Cheruvathur, R., and Liu, Y. (2015). Evaluation of biodegradation-promoting additives for plastics. *Environ. Sci. Technol.* 49, 3769–3777. doi: 10.1021/es504258u
- Severin, T., Sauret, C., Boutrif, M., Duhaut, T., Kessouri, F., Oriol, L., et al. (2016). Impact of an intense water column mixing (0–1500 m) on prokaryotic diversity and activities during an open-ocean convection event in the NW Mediterranean Sea. *Environ. Microbiol.* 18, 4378–4390. doi: 10.1111/1462-2920.13324
- Shannon, C. E., and Weaver, W. (1949). *The Mathematical Theory of Communication, The Mathematical Theory of Communication*. Champaign, IL: University of Illinois Press.
- Shimkets, L. J., Dworkin, M., and Reichenbach, H. (2006). “The myxobacteria,” in *The Prokaryotes: Proteobacteria: Delta, Epsilon Subclass*, Vol. 7, eds M. Dworkin, S. Falkow, E. Rosenberg, K.-H. Schleifer, and E. Stackebrandt (New York, NY: Springer), 31–115. doi: 10.1007/0-387-30747-8\_3
- Shoji, T., Sueoka, K., Satoh, H., and Mino, T. (2014). Identification of the microbial community responsible for thiocyanate and thiosulfate degradation in an activated sludge process. *Process Biochem.* 49, 1176–1181. doi: 10.1016/j.procbio.2014.03.026
- Simon, M., and Azam, F. (1989). Protein content and protein synthesis rates of planktonic marine bacteria. *Mar. Ecol. Prog. Ser.* 51, 201–213. doi: 10.3354/meps051201
- Simpson, E. H. (1949). Measurement of diversity. *Nature* 163, 688–688. doi: 10.1038/163688a0
- Valencia-Agami, S. S., Cerqueda-García, D., Putzeys, S., Uribe-Flores, M. M., García-Cruz, N. U., Pech, D., et al. (2019). Changes in the bacterioplankton community structure from southern Gulf of Mexico during a simulated crude oil spill at Mesocosm scale. *Microorganisms* 7:441. doi: 10.3390/microorganisms7100441
- Volova, T. G., Prudnikova, S. V., and Boyandin, A. N. (2016). Biodegradable poly-3-hydroxybutyrate as a fertiliser carrier. *J. Sci. Food Agric.* 96, 4183–4193. doi: 10.1002/jsfa.7621
- Webb, H. K., Crawford, R. J., Sawabe, T., and Ivanova, E. P. (2009). Poly(ethylene terephthalate) polymer surfaces as a substrate for bacterial attachment and biofilm formation. *Microbes Environ.* 24, 39–42. doi: 10.1264/jisme2.ME08538
- Wright, R. J., Erni-Cassola, G., Zadjelovic, V., Latva, M., and Christie-Oleza, J. A. (2020). Marine plastic debris: a new surface for microbial colonization. *Environ. Sci. Technol.* 54, 11657–11672. doi: 10.1021/acs.est.0c02305
- Wright, R. J., Langille, M. G. I., and Walker, T. R. (2021). Food or just a free ride? A meta-analysis reveals the global diversity of the Plastisphere. *ISME J.* 15, 789–806. doi: 10.1038/s41396-020-00814-9
- Yashchuk, O., Portillo, F. S., and Hermida, E. B. (2012). Degradation of polyethylene film samples containing oxo-degradable additives. *Procedia Materials Science* 1, 439–445. doi: 10.1016/j.mspro.2012.06.059
- Zettler, E. R., Mincer, T. J., and Amaral-Zettler, L. A. (2013). Life in the “Plastisphere”: microbial communities on plastic marine debris. *Environ. Sci. Technol.* 47, 7137–7146. doi: 10.1021/es401288x

**Conflict of Interest:** The authors declare that the research was conducted in the absence of any commercial or financial relationships that could be construed as a potential conflict of interest.

**Publisher’s Note:** All claims expressed in this article are solely those of the authors and do not necessarily represent those of their affiliated organizations, or those of the publisher, the editors and the reviewers. Any product that may be evaluated in this article, or claim that may be made by its manufacturer, is not guaranteed or endorsed by the publisher.

Copyright © 2021 Odobel, Dussud, Philip, Derippe, Lauters, Eyheraguibel, Burgaud, Ter Halle, Meistertzheim, Bruzard, Barbe and Ghiglione. This is an open-access article distributed under the terms of the Creative Commons Attribution License (CC BY). The use, distribution or reproduction in other forums is permitted, provided the original author(s) and the copyright owner(s) are credited and that the original publication in this journal is cited, in accordance with accepted academic practice. No use, distribution or reproduction is permitted which does not comply with these terms.



# Dynamics of Soil Microbial Communities During Diazepam and Oxazepam Biodegradation in Soil Flooded by Water From a WWTP

Marc Crampon<sup>1\*</sup>, Coralie Soulier<sup>1</sup>, Pauline Sidoli<sup>1</sup>, Jennifer Hellal<sup>1</sup>, Catherine Joulian<sup>1</sup>, Mickaël Charron<sup>1</sup>, Quentin Guillemoto<sup>1,2</sup>, Géraldine Picot-Colbeaux<sup>1</sup> and Marie Pettenati<sup>1</sup>

<sup>1</sup> Bureau de Recherches Géologiques et Minières, Orléans, France, <sup>2</sup> UMR 7619 METIS, Sorbonne Université, Paris, France

## OPEN ACCESS

### Edited by:

Dimitrios Georgios Karpouzas,  
University of Thessaly, Greece

### Reviewed by:

Panagiotis A. Karas,  
University of Thessaly, Greece  
Federica Spina,  
University of Turin, Italy

### \*Correspondence:

Marc Crampon  
m.crampon@brgm.fr

### Specialty section:

This article was submitted to  
Microbiotechnology,  
a section of the journal  
Frontiers in Microbiology

**Received:** 15 July 2021

**Accepted:** 20 October 2021

**Published:** 29 November 2021

### Citation:

Crampon M, Soulier C, Sidoli P,  
Hellal J, Joulian C, Charron M,  
Guillemoto Q, Picot-Colbeaux G and  
Pettenati M (2021) Dynamics of Soil  
Microbial Communities During  
Diazepam and Oxazepam  
Biodegradation in Soil Flooded by  
Water From a WWTP.  
Front. Microbiol. 12:742000.  
doi: 10.3389/fmicb.2021.742000

The demand for energy and chemicals is constantly growing, leading to an increase of the amounts of contaminants discharged to the environment. Among these, pharmaceutical molecules are frequently found in treated wastewater that is discharged into superficial waters. Indeed, wastewater treatment plants (WWTPs) are designed to remove organic pollution from urban effluents but are not specific, especially toward contaminants of emerging concern (CECs), which finally reach the natural environment. In this context, it is important to study the fate of micropollutants, especially in a soil aquifer treatment (SAT) context for water from WWTPs, and for the most persistent molecules such as benzodiazepines. In the present study, soils sampled in a reed bed frequently flooded by water from a WWTP were spiked with diazepam and oxazepam in microcosms, and their concentrations were monitored for 97 days. It appeared that the two molecules were completely degraded after 15 days of incubation. Samples were collected during the experiment in order to follow the dynamics of the microbial communities, based on 16S rRNA gene sequencing for Archaea and Bacteria, and ITS2 gene for Fungi. The evolution of diversity and of specific operating taxonomic units (OTUs) highlighted an impact of the addition of benzodiazepines, a rapid resilience of the fungal community and an evolution of the bacterial community. It appeared that OTUs from the *Brevibacillus* genus were more abundant at the beginning of the biodegradation process, for diazepam and oxazepam conditions. Additionally, Tax4Fun tool was applied to 16S rRNA gene sequencing data to infer on the evolution of specific metabolic functions during biodegradation. It finally appeared that the microbial community in soils frequently exposed to water from WWTP, potentially containing CECs such as diazepam and oxazepam, may be adapted to the degradation of persistent contaminants.

**Keywords:** benzodiazepines, soil, microbial community, biodegradation, WWTP

## INTRODUCTION

Due to the non-specificity of wastewater treatment plants (WWTPs) toward many micropollutants and in particular contaminants of emerging concern (CECs), these are frequently discharged to the environment. Several solutions exist to treat CECs, but significant knowledge gaps remain (Basheer, 2018). Recently, in order to minimize wastewater treatment costs regarding energy and

chemicals consumption, multi-barrier treatment systems that can combine engineered systems and nature-based solution (NBS), such as soil aquifer treatment (SAT) systems, were described. Hermes et al. (2019) studied the removal processes involved in a SAT context, by focusing on trace organic chemicals and their metabolites. They found that the fate of these compounds was mainly controlled by sorption onto soil constituents (especially linked to organic matter content and clays for cationic compounds), dilution, and to the nature of the compounds themselves (cationic, non-ionic, molecular weight, etc.). Biodegradation was also described as a removal process for a variety of organic contaminants, depending especially on the specificity of microorganisms present in the system (Rauch-Williams et al., 2010; Falås et al., 2016; Regnery et al., 2016), as well as the biodegradability of the considered compounds. Natural attenuation linked to microbial communities' adaptation represents a NBS for the remediation of CECs. The identification of biodegradation mechanisms could help to increase the efficiency of treatments in WWTPs and consequently limit environmental impacts. In this context, it is necessary to understand the adaptation capacity of endemic microbial communities exposed to CECs stress, and their possible role in CECs remediation in the case of soil and aquifer treatments.

Benzodiazepines are pharmaceutical CECs that are frequently found in water from WWTPs. They belong to a class of psychoactive drugs that contain a benzene and a diazepine ring in their core chemical structure. They have anticonvulsant, sedative, muscle relaxant, hypnotic, and anxiolytic properties. These molecules, especially diazepam (DZ), are described as poorly biodegradable when introduced into the environment (Redshaw et al., 2008). Some degradation pathways have been highlighted, such as demethylation, especially due to fungal enzymes (Helbling et al., 2010), but an efficient biodegradation in the environment has not yet been reported. Some researchers found that DZ was not directly degradable by bacteria, especially when other carbon sources that are more easily accessible are available, which is the case in soils (Tappin et al., 2014). They also showed that DZ degradation products from photodegradation are much more easily biodegraded by bacteria. The first stages of biodegradation could be linked to soil fungal activity, the bacteria then taking over the less complex metabolites. Oxazepam (OXA) seems to be more easily biodegradable by bacteria derived from WWTPs (Redshaw et al., 2008), but these benzodiazepines are generally described as poorly biodegradable (Tappin et al., 2014). DZ (Valium®) is certainly the best known molecule of this group and has a long-term impact because of its persistent metabolites. In humans, it is metabolized to *N*-desmethyldiazepam (also called nordazepam) ( $t_{1/2} \sim 100$  h). Nordazepam (ND, Calmday®) is then 3-hydroxylated to OXA (Serax®). The presence of the hydroxyl group allows its glucuronation and excretion in urine and explains its low half-life ( $\sim 4\text{--}15$  h) compared to DZ and ND (Kosjek et al., 2012).

Benzodiazepines are halogenated molecules, which are often considered as a factor that negatively affects biodegradation. The dehalogenation of molecules with more than two to three halogen groups is often considered possible only under anaerobic

conditions. Most of the data on the efficiency of wastewater treatments concern DZ and show that (i) less than 10% is removed during conventional biological treatment, (ii) the efficiency seems to be higher during anaerobic treatment (10–50%), and (iii) the removal rate is mainly related to sorption rather than degradation (Ternes et al., 2004; Löffler et al., 2005; Ghattas et al., 2017). Similarly, OXA is persistent in both aerobic and anaerobic treatment in the environment (Patterson et al., 2010). DZ appears to be subject to photodegradation in the environment, which may be a pathway for the removal of DZ from surface water (Boreen et al., 2003).

Although the Kow of benzodiazepines [DZ: 2.8, ND: 2.9, OXA: 2.2, Episuite (EPA)] does not appear to indicate that sorption plays a significant role in their removal (or delay), Ternes et al. (2004) classified DZ as readily adsorbable on activated carbon (99% removal on  $0.2 \text{ mg L}^{-1}$  activated carbon), and Calisto and Esteves (2009) showed that temazepam and OXA can undergo sorption on humic substances. On the other hand, sorption could limit bioaccessibility and thus decrease potential biodegradation. Löffler et al. (2005) showed that DZ was highly persistent with rapid and extensive sorption on sediments, stable in soils, groundwater, and during wastewater treatment. The same study showed that OXA is moderately persistent in the environment with a lower DT50 and a lower sorption rate on sediments than DZ. In addition, Löffler et al. (2005) did not observe any degradation of DZ to OXA in sediments, suggesting that it is difficult to compare the fate of DZ in the environment and in humans.

Consequently, the use of benzodiazepines to simultaneously study the processes of sorption and biodegradation—in order to quantitatively differentiate these two processes in the dissipation of molecules in soils—is needed to better understand its behavior in contaminated environments. Considered as persistent, resistant to biodegradation, and with supposed limited sorption ( $\text{Kow} < 3$ ), we aimed at studying the fate of DZ and OXA in soils flooded by water from WWTP with known benzodiazepine inputs. The present study focuses on biodegradation. The objectives were to assess the capacity of soil microbial communities (bacteria, archaea, and fungi), to resist and potentially degrade benzodiazepine molecules, especially DZ and OXA. A focus was made on (i) the biodegradation of mother molecules DZ and OXA in soils, and (ii) the dynamics of bacteria, archaea, and fungi communities during the degradation kinetics. The evolution of metabolic pathways was also explored, as well as links between degradation and biodiversity.

## MATERIALS AND METHODS

### Context and Soil Sampling

Soils were sampled in the reed-bed area of a SAT system implanted in the city of Agon-Coutainville (France, Normandy), located along the English Channel Coastline (**Figure 1**). The commune, with an estimated population of 2,800 residents (INSEE, 2015), is one of the oldest seaside resorts of the Manche department and harbors the largest production of shellfish in France (production and storage,  $\sim 400$  ha of shellfish parks).



The conservation of the coastal ecosystem and the associated sanitary stakes are essential for local economy and have to be fully integrated to the ongoing development of residential areas, tourism, and shellfish aquaculture (approximately 7 km of coast). Subject to a large tidal range, groundwater resources are prone to salinization in this coastal area, limiting the fresh water supply. Sustainable water management in this area must consider seasonal variations of the population (during summer vacations) and the irrigation needs of a backshore golf course. In addition, environmental regulations as well as the water framework directive must be followed (DIRECTIVE 2006/7/CE), in spite of financial constraints.

To face this demanding challenge and to preserve the estuary ecosystem from secondary treated wastewater discharged to surface water (river or sea) in Agon-Coutainville, the SAT system has been considered for more than 14 years as locally more efficient and sustainable (Picot-Colbeaux et al., 2020). The SAT consists of a fed reed-bed area of 35,000 m<sup>2</sup> with secondary treated wastewater provided by a biological WWTP. This area is divided into three parts alternatively flooded by the treated water with an average daily volume of 1,390 m<sup>3</sup> (mean 2,005–2,019) which infiltrates into a 7- to 9-m-thick sandy aquifer. Monitoring boreholes intercept sands (fine to coarse) and silty sands, which become rich in fragments of shells with depth, and then reach the altered clay from the bed rock (schist). The first meters of the aquifer always contain organic matter.

The quality of discharged treated wastewater and downstream groundwater is monitored and respects the according French regulations although many questions remain about the fate of CECs in this system. The efficiency of this combined engineered and natural system were addressed in the European AquaNES project<sup>1</sup> (Pettenati et al., 2019a,b; Picot-Colbeaux et al., 2020). Previous chemical monitoring of the study site and released water have shown non-negligible concentrations of benzodiazepines in the water at the outlet of the WWTP, especially for OXA (approximately 1,678 ng L<sup>-1</sup>), which is maybe also present as a DZ degradation by-product.

Five FR4N soil samples were taken from a 25 m<sup>2</sup> square (four points and one in the middle) from the 0–20 cm layer and were mixed and homogenized on site, representing about 25 kg of soil. Plants residues and roots were discarded. The soil sample was analyzed for main agronomic properties: granulometry, organic matter content, cation exchange capacity (CEC), N (%), C/N ratio, pH, and metal content (Aurea AgroSciences, Ardon, France), and the rest was stored at 4°C for further experiments. Sampled soil consists of a calcareous sandy soil (12.5% CaCO<sub>3</sub> content and 73.1% sand content, including 65.6% coarse sand) with an organic matter content of 4.7% and a pH<sub>KCl</sub> value of 7.5. All results for the studied parameters are listed in **Supplementary Table 3**. Metal and metalloid concentrations in the studied soil were monitored in a previous project (AquaNES H2020 project). They were found to be globally low, and these compounds do not represent a major concern on site. CECs are often detected in water samples from the site. A monitoring of the concentrations of several CECs was performed on a 3-year period on water from

the site (AquaNES project, H2020). DZ was always found below the detection limit (<20 ng L<sup>-1</sup>). OXA was detected in nearly each point, at every sampling date. OXA concentrations reached 40 ng L<sup>-1</sup> in a pond upstream of the site filled with water from the golf ponds, and 2,663 ng L<sup>-1</sup> in the WWTP outlet water.

## Experimental Setup

### Chemicals and Reagents

Diazepam and OXA standards of high purity grade (>98%) were purchased from Sigma-Aldrich (Steinheim, Germany). Diazepam D5 and oxazepam D5, used as soil extraction standards, were purchased from CIL Cluzeau (Sainte-Foy-la-Grande, France) and Sigma-Aldrich, respectively. Acetonitrile and water with UPLC/MS quality were purchased from Fisher (Illkirch, France). Methanol, phosphate buffer (KH<sub>2</sub>PO<sub>4</sub>), and formic acid were purchased from Sigma-Aldrich (Steinheim, Germany). QuEChERS commercial extraction kits (EN method) were obtained from Agilent Technologies (Santa Clara, PA, United States).

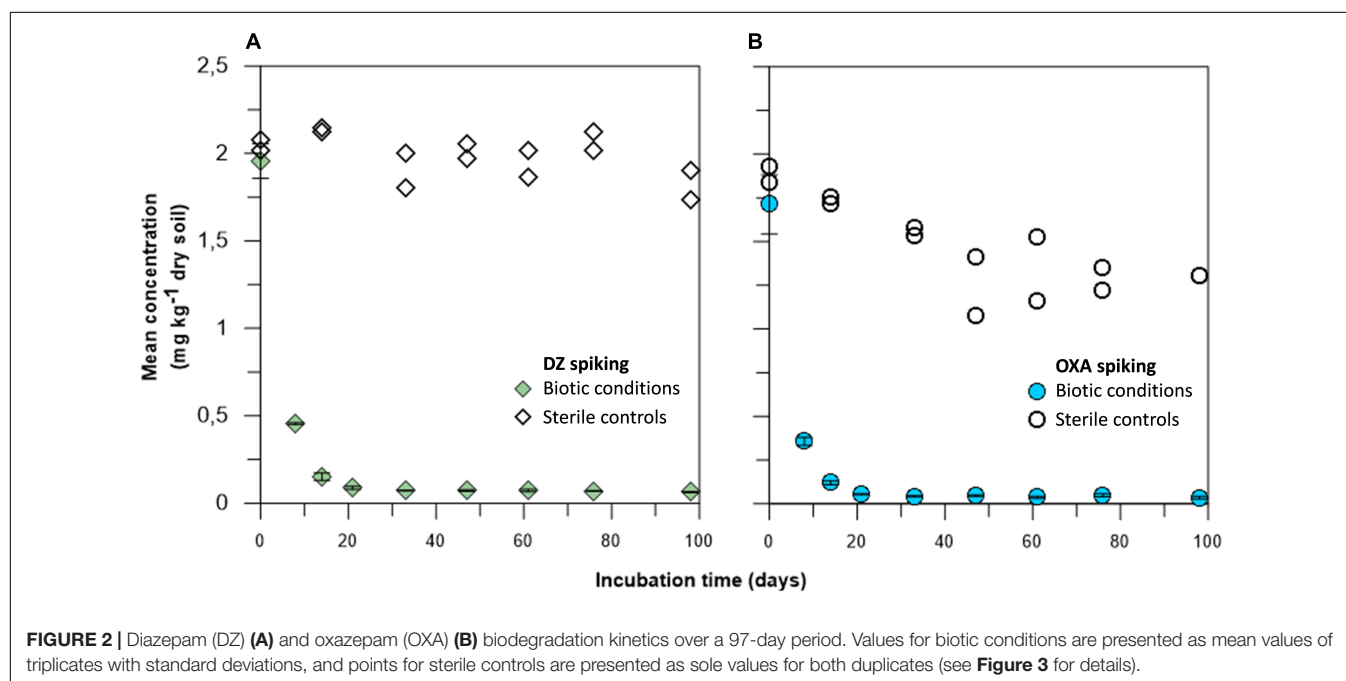
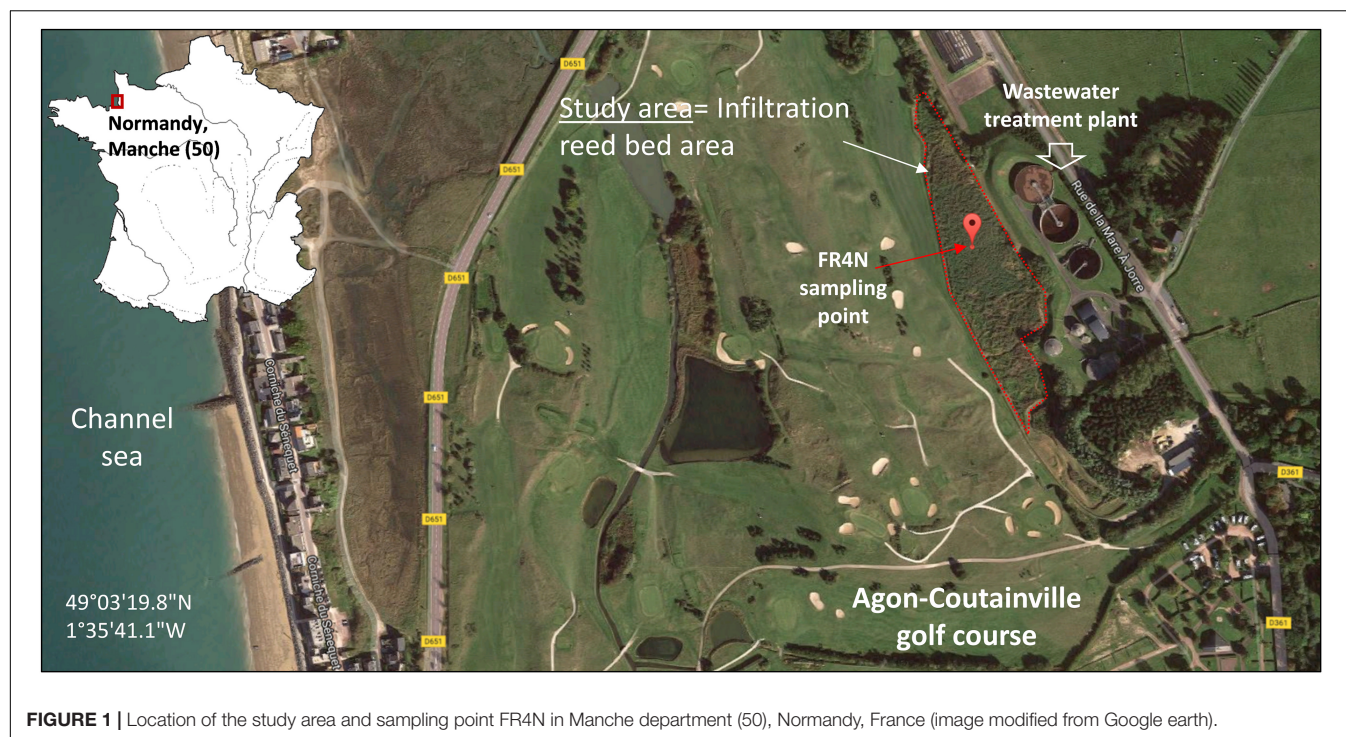
### Experimental Conditions and Soil Spiking

After sampling, the water contents and water holding capacity (WHC) were determined. Soils were sieved at 5 mm to discard all gravel or plant debris. Then, four sets of soils used for spiking the experiment (dried and crushed, one for each condition) were prepared with a final concentration of 10 mg kg<sup>-1</sup> of DZ or OXA. These were prepared using stock solutions prepared in HPLC-grade acetone. After adding the DZ or OXA, spiked soils were left for 24 h at room temperature under an extractor hood to allow the acetone to evaporate and were then homogenized by mixing. The concentrations in these spiked soils were checked and were 9.47 mg kg<sup>-1</sup> DW for OXA abiotic condition, 8.98 mg kg<sup>-1</sup> DW for OXA biotic condition, 8.42 mg kg<sup>-1</sup> DW for DZ abiotic condition, and 8.12 mg kg<sup>-1</sup> DW for DZ biotic condition.

The experiment was then set up by adding the same aliquot of these dry spiked soils to fresh soils by distributing the powder as homogeneously as possible to each of the 82 microcosms (41 DZ and 41 OXA). The initial concentration of both DZ and OXA was quantified in microcosms by using QuEChERS extraction, as described below. These concentrations were 1.96 ± 0.10 mg kg<sup>-1</sup> DW for the DZ biotic condition, 2.05 ± 0.04 mg kg<sup>-1</sup> DW for the DZ abiotic condition, 1.71 ± 0.17 mg kg<sup>-1</sup> DW for the OXA biotic condition, and 1.88 ± 0.06 mg kg<sup>-1</sup> DW for the OXA abiotic condition. It must be noted that DZ was not detected (<LQ) in the native soil, and OXA was found at a concentration of 25 µg kg<sup>-1</sup> DW soil. This native concentration was considered as negligible compared to the added OXA. To obtain a water content equal to 70% of the maximum soil WHC, deionized water was added to each microcosm and soils were homogenized again.

The experiment was conducted in triplicate for 97 days. Microcosms were sacrificed at nine sampling dates, after 0, 8, 14, 21, 33, 47, 61, 76, and 97 days of incubation. Sterile controls were performed in duplicate for seven of the sampling dates (controls at 8 and 21 days were not performed) with soils sterilized by gamma ray ionization, in the same conditions as the biotic samples. The experimental setup is presented in **Supplementary Figure 1**. Measurements of water moisture were

<sup>1</sup> www.aquan.es.eu



also performed during the course of the experiment to ensure its stability at values approximately 70% WHC.

## Chemical Analyses

### QuEChERS Extraction of Benzodiazepines

Five grams of sieved soil was weighed in a 50-ml polypropylene extraction tube and spiked with 80  $\mu$ l of a solution of isotopically labeled compounds (internal standards) and then vortexed. The

soil was then mixed with 8 ml of phosphate buffer ( $\text{KH}_2\text{PO}_4$ ) and 10 ml of acetonitrile containing 5% formic acid. The mixture was agitated with an Agitax shaking device (AgytaxLab, Madrid, Spain) for 30 s, after which QuEChERS salt was added. The tube was again agitated for 60 s and finally centrifuged (5 min, 4,000 rpm). The supernatant was entirely collected (about 10 ml per sample) and weighed. For each experimental replicate, three extractions were performed (three samples per microcosm). The

three supernatants of these three extractions were combined, yielding a total extraction volume of approximately 30 ml. This was then evaporated down to 12 ml and kept at  $-20^{\circ}\text{C}$  prior to analysis by UPLC-MS/MS.

Performance characteristics of the QuEChERS method for the selected pharmaceutical compounds were evaluated on the same soil as the one used in the microcosms. The recovery rate was calculated for each compound by spiking the soil at about  $30\text{ }\mu\text{g kg}^{-1}$  of dry soil (in triplicate) and then processing the extraction as described above. Matrix effects were studied by first extracting the sample (in triplicate, and with the procedure described above) and then spiking the total extracted sample at about  $30\text{ }\mu\text{g kg}^{-1}$  of dry soil for each compound (i.e., about  $120\text{ }\mu\text{g L}^{-1}$  in total supernatant).

### Quantification of Benzodiazepines

The analytical method was established to quantify a list of 24 pharmaceutical compounds in soil extracts. Chromatographic separation was performed with a Waters Acquity UPLC using a  $150\text{ mm} \times 2.1\text{ mm}$  UPLC-HSST3 C18  $1.8\text{ }\mu\text{m}$  column (Waters, Guyancourt, France). Ten microliters of soil extract was injected. The mobile phase was composed of solvent A (0.007% formic acid in water) and solvent B (0.007% formic acid in acetonitrile) at a constant flow of  $0.4\text{ ml/min}$ . The initial amount of B was 0% during 0.75 min and linearly increased to 100% in 15 min, followed by a 1-min isocratic mode and returned quickly to the initial conditions. These conditions were maintained for 2.5 min; the total run time was 19 min. Column and autosampler temperatures were maintained, respectively, at  $45^{\circ}\text{C}$  and  $10^{\circ}\text{C}$ . For more details, see Togola et al. (2014).

Mass spectrometry was performed on a triple quadrupole (Quattro Premier XE, Waters) in Multiple Reaction Monitoring (MRM) fitted with an electrospray ionisation (ESI) interface and controlled by MassLynx software. Mass spectrometry conditions were previously described (Togola et al., 2014). Briefly, positive and negative polarity modes were used simultaneously during the same analytical run.

The limits of quantification for DZ and OXA were evaluated at  $4\text{ }\mu\text{g kg}^{-1}$  of fresh soil. The half-life dissipation time (DT50) for DZ and OXA was calculated with a first-order kinetic model.

## Microbial Community Analyses

### Extraction and Quantification of Soil DNA

DNA extractions were performed on soils from each condition at all of the sampling times, using the FastPrep DNA Spin Kit for soils (MP Biomedicals) following the manufacturer's instructions, at a speed of  $5\text{ m s}^{-1}$  for 30 s, on 0.7–1 g of humid soil sample and eluted in  $100\text{ }\mu\text{l}$  of DES. Total extracted DNA was quantified with a Quantus Fluorometer (Promega) and stored at  $-20^{\circ}\text{C}$  prior to further analysis.

### qPCR of 16S rRNA and 18S rRNA Genes

Quantification of the bacterial 16S rRNA and fungal 18S rRNA gene copies was performed on all DNA samples by qPCR using a CFX Connect<sup>TM</sup> Real-Time PCR Detection System (Bio-Rad, France). The primers used were 341F (3'-CCTACGGGAGGCAGCAG-5') and

515R (3'-ATTACCGCGGCTGCTGGCA-5') (Lopez-Gutierrez et al., 2004) for 16S rRNA genes, and primers FF390 (5'-CGATAACGAACGAGACCT-3') and FR1 (5'-A5CCAT TCAATCGGTA5T-3') for 18S rRNA genes (Vainio and Hantula, 2000). qPCR reactions were performed in a total volume of  $20\text{ }\mu\text{l}$ , with a mix containing  $7.6\text{ }\mu\text{l}$  of sterile, nuclease- and nucleic acid-free water (MP Biomedicals, CA, United States),  $10\text{ }\mu\text{l}$  of SSO Advanced Universal SYBR Green Supermix (Bio-Rad),  $400\text{ nM}$  (16S rRNA genes) or  $500\text{ nM}$  (18S rRNA genes) of each primer,  $100\text{ ng}$  of T4 GP32 (16S rRNA genes), and  $2\text{ }\mu\text{l}$  of template DNA ( $0.1\text{--}5\text{ ng}\cdot\mu\text{l}^{-1}$ ). Sterile, nuclease- and nucleic acid-free water was used instead of DNA in negative controls. For 16S rRNA gene, PCR reactions were performed as follows: 3 min at  $95^{\circ}\text{C}$ , followed by 35 cycles: 30 s at  $95^{\circ}\text{C}/30\text{ s}$  at  $60^{\circ}\text{C}/30\text{ s}$  at  $72^{\circ}\text{C}/30\text{ s}$  at  $80^{\circ}\text{C}$ . For 18S rRNA gene, PCR reactions were performed as follows: 30 s at  $95^{\circ}\text{C}/30\text{ s}$ , 40 cycles: 15 s at  $95^{\circ}\text{C}/30\text{ s}$  at  $50^{\circ}\text{C}/30\text{ s}$  at  $72^{\circ}\text{C}/30\text{ s}$  at  $80^{\circ}\text{C}$ . At the end of the qPCR, an additional step rising from 60 to  $95^{\circ}\text{C}$  at  $0.5^{\circ}\text{C/s}$  was applied for melt curves generation.

A calibration curve was obtained from serial dilutions of a known quantity of linearized plasmids containing known copy numbers of 16S rRNA or of 18S rRNA gene. All samples, controls, and standards were analyzed in duplicate. Results were reported as number of gene copies per gram of dry soil. Generation of a specific PCR product was confirmed by melting curve analyses and agarose gel electrophoresis.

### Next-Generation Sequencing (16S rRNA Gene and ITS2)

Microbial diversity was evaluated by Illumina MiSeq sequencing of the 16S rRNA gene for bacteria and archaea and ITS2 region for fungi. Sequencing was performed on 19 samples: native soil (FR4N), and three sampling dates, in triplicates, for DZ and OXA microcosms. Chosen dates were T0, T14, and T97 for microcosms corresponding at 0, 14, and 97 days after benzodiazepines spiking, respectively. The native soil corresponded to the fresh soil that was used for microcosms, before spiking.

Amplicon libraries were constructed by INRAE Transfert (Toulouse, France). Briefly, a portion of the 16S rRNA gene (V4–V5 region) was amplified using the barcoded, universal primer set 515WF—GTGYCAGCMGCCGCGGTA/928WR—CCCGYCAATTTCMTTTRAGT (Wang and Qian, 2009). Concerning ITS2 gene for fungi, a portion of the ITS2 gene was amplified using the specific primer set w404 CTTTCCCTACACGACGCTCTTCCGATCTTGTGARTCATCG AATCTTTG/w40 GGAGTTCAGACGTGTGCTCTTCCGATCT TCCTCCGCTTATTGATATGC (Hadziavdic et al., 2014). PCR reactions were performed using the AccuStart II PCR ToughMix kit, followed by cleaning (HighPrep PCR beads, Mokasience), and pooled triplicates were submitted for sequencing on Illumina MiSeq instrument at GeT-PlaGe (Auzerville, France). Fastq files were uploaded to the Galaxy web platform (Sygenae), and the public server at usegalaxy.org was used to analyze the data, with the FROGS analysis platform (Escudié et al., 2017). For 16S rRNA gene sequences, affiliations were obtained using the Silva 138\_16S database. For ITS2, Unite\_Fungi\_8.0\_18112018 reference database was used for OTUs affiliation. The affiliation



tables and sequence counts can be found in **Supplementary Tables 1, 2**. The sizes of reads for R1 and R2 (forward and reverse) were 250 bp. For trimming, the FROGS Pre-process merging, denoising, and dereplication tool was used (Galaxy Version r3.0-3.0). Mismatch rate was set to 0.1 (maximum rate of mismatch in the overlap region of R1 and R2 in consensus sequences), and merge calculations were performed using Flash software for an expected amplicon size of 413 bp (min 340 bp and max 450 bp) for 16S rRNA genes, and 389 bp (min 267 bp and max 511 bp) for highly variable ITS2 region extracted using the FROGS ITSx tool (Galaxy Version r3.0-1.0). Then, clustering was performed using FROGS Clustering swarm amplicon sequence clustering tool (Galaxy Version r3.0-1.4) with denoising. The aggregation distance clustering was set to a maximum of 3 bp for inclusion into clusters. To remove the PCR chimera in each sample, the FROGS Remove chimera tool was used (Galaxy Version r3.0-7.0). This tool is based on the VSEARCH tool for chimera detection and removal (Rognes et al., 2016). Alpha diversity indices were calculated from the NGS data. The first index corresponds to the observed number of OTUs in data from 16S rRNA gene and ITS2 region sequencing. The Chao1 index estimates the unobserved OTUs by correcting values with OTUs that are observed only one or two times in data (correction for the rarest OTUs). The Shannon and Inverse Simpson indices give an indication of the specific richness in the samples, by linking the number of species with the specific abundance of these species in the different samples. Tax4Fun data were also generated from FROGS platform, and potential metabolic pathways were recovered by comparison of the 16S rRNA gene sequences with the KEGG database (Aßhauer et al., 2015). For the 19 samples, only 1.79–2.91% of OTUs could be mapped to KEGG organisms. All 16S rRNA gene sequences and ITS2 sequences were submitted to European Nucleotide Archive (ENA) and are available under accession numbers ERS7290419 (SAMEA9567684) to ERS7290437 (SAMEA9567702). The whole project is referenced under accession number PRJEB47338.

## Statistical Analyses

Statistical analyses were performed on XLStat software v2013.3.2 (Addinsoft, 2020). Alpha and beta diversity calculations were performed using FROGS platform. Co-occurrence networks were built using Cytoscape software v3.8.0 with CoNet add-on.

## RESULTS

### Evolution of Benzodiazepine Concentrations in Microcosms

Concentrations of DZ and OXA over time, in the different microcosms and their sterile controls, were monitored on nine sampling dates (**Figure 2**). It firstly appeared that concentrations in the sterile controls treated by gamma-ray remained high over time, especially for DZ, indicating that sterilization was effective. Consequently, the observed results in microcosms were linked to biodegradation of DZ and OXA. In the biotic soil microcosms, biodegradation or biotransformation occurred both for DZ and for OXA very quickly: DT50 for DZ, based

on a first order degradation model, was 3.9 and 3.6 days for OXA. After 20 days, barely all the spiked benzodiazepines were dissipated [ $95.5\% \pm 0.5\%$  ( $n = 3$ ) and  $96.9\% \pm 0.2\%$  ( $n = 3$ ) for DZ and OXA, respectively] (**Figure 2**), and only trace concentrations remained, whereas concentrations remained stable in sterile controls at approximately  $1.5\text{--}2\text{ mg kg}^{-1}$  DW soil. OXA concentrations tended to decrease slightly over time in sterile controls. It is not impossible that gamma-ray treatment did not destroy all microorganisms, especially sporulating microorganisms. Microorganisms in sporulated form during the sterilization could have grown later, explaining a slight biodegradation in controls especially for OXA conditions. It is also possible that abiotic degradation of OXA occurred during the experiment. Samples were stored in the dark, and benzodiazepines are resistant to photodegradation, but other abiotic reactions could have led to the observed OXA concentrations decrease in sterile controls. Results are, however, globally satisfying in sterile controls, and significantly different compared to biotic conditions. These results highlight a good removal rate of the two studied benzodiazepines in the studied soil, rather by biodegradation or biotransformation of the mother molecules.

### Bacteria and Archaea Dynamics Based on 16S rRNA Gene Abundance and Diversity

#### Initial Bacteria and Archaea Soil Diversity

Prokaryote community diversity was compared to the average diversity observed among 2,173 studied soils in France (Karimi et al., 2018). At the phylum level, differences were observed between the native FR4N soil and the mean diversity described in Karimi et al. (2018) for soils in France (**Figure 3A**). Among dominant phyla, Acidobacteria and Chloroflexi were approximately two and three times more represented, respectively, in FR4N soil compared to mean values in French soils. Although they are not highly represented, Chlamydiae, Cyanobacteria, Euryarchaeota, Spirochaetes, Nitrospirae, and Nitrospirae are, respectively, 10, 16, 422, 229, 6, and 7 times more represented in the FR4N soil compared to mean values in French soils. On the contrary, among dominant phyla, Actinobacteria, Crenarchaeota, and Firmicutes were approximately two to three times less represented in the FR4N soil compared to the mean values in French soils. Verrucomicrobia were approximately six times less represented. Among the rarest phyla, Chlorobi (0.25% in the soils of France) are absent from the studied soil. On the contrary, Calditrichaeota, Zixibacteria, Rokubacteria, Nanoarchaeaeota, Latescibacteria, and Entothaeonellaeota represented 0.25–1% of the global studied soil diversity, whereas they are not described in the main phyla found in French soils (Karimi et al., 2018).

#### Evolution of Bacterial and Archaeal Abundance

Bacterial and archaeal abundances were evaluated by quantification of the number of 16S rRNA gene copies per gram of DW soil (**Supplementary Figure 2A** for DZ conditions and **Supplementary Figure 2B** for OXA conditions). In both



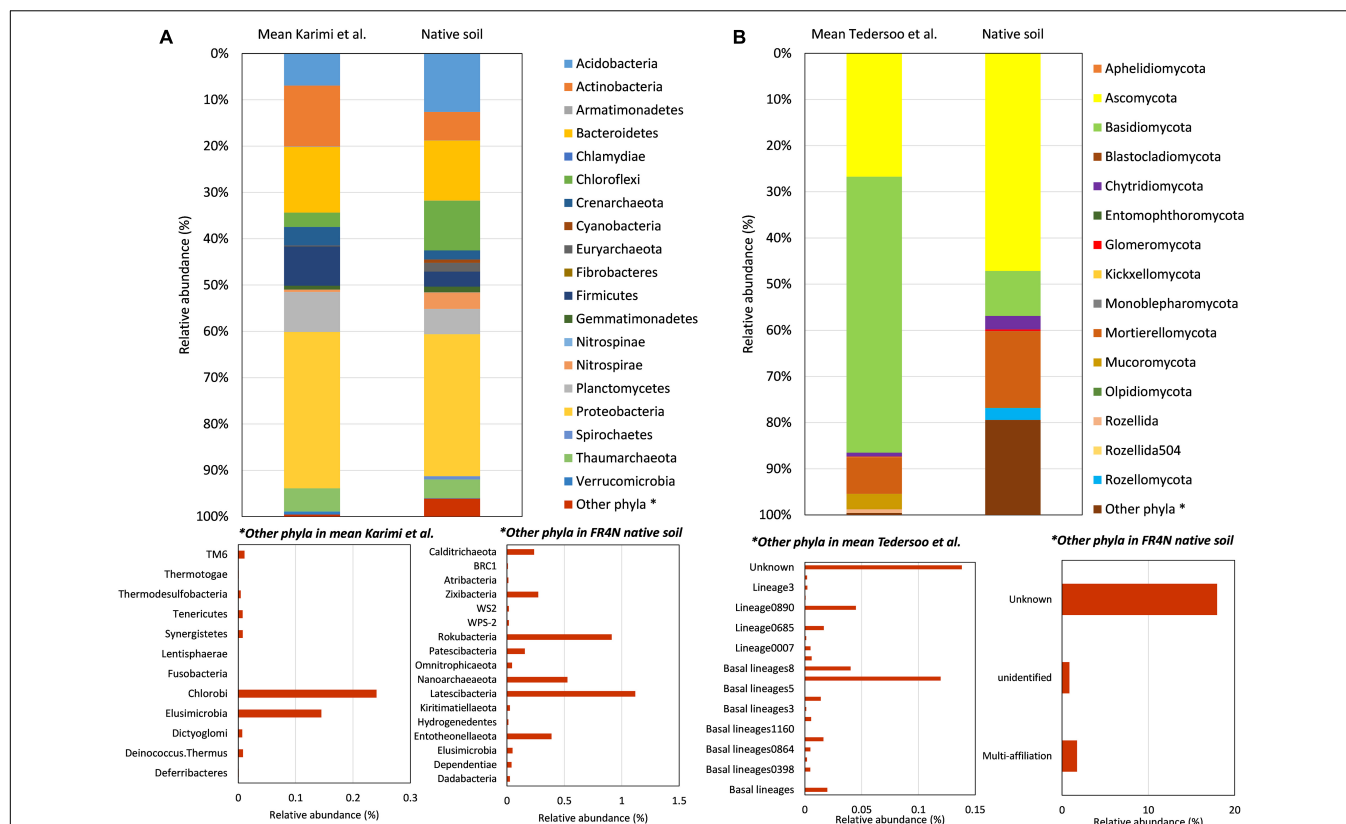


**FIGURE 3 |** Comparison of microbial diversity at the phylum level for **(A)** bacteria and archaea between FR4N soil and data from Karimi et al. (2018), and **(B)** fungal diversity between FR4N soil and data from Tedersoo et al. (2014). Data from Karimi et al. (2018) correspond to mean diversity in 2,173 soil samples from France and data from Tedersoo et al. (2014) correspond to mean values in a selection of 127 samples corresponding to representative couples of soil/climate that can be found in France (i.e., temperate coniferous forests, temperate deciduous forests, grassland, and shrubland and Mediterranean soils).

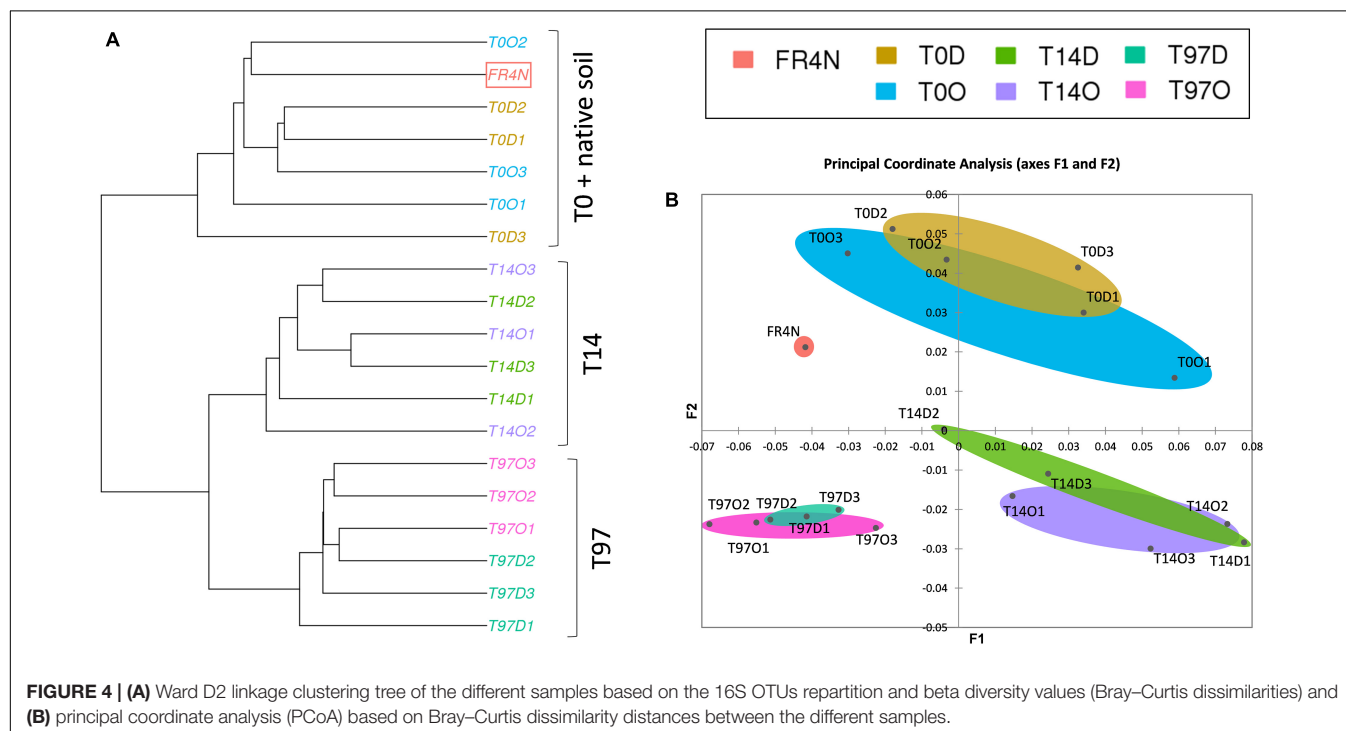


**FIGURE 4 |** **(A)** Ward D2 linkage clustering tree of the different samples based on the 16S OTUs repartition and beta diversity values (Bray–Curtis dissimilarities) and **(B)** principal coordinate analysis (PCoA) based on Bray–Curtis dissimilarity distances between the different samples.

DZ and OXA conditions, the abundance of 16S rRNA gene was significantly lower at T0, maybe due to the toxicity of added contaminants. At T8, values are intermediate, and a plateau is reached after 14 days. It appears that the period between T0 and T14 corresponds to a growth phase and that the bacterial and archaeal communities remain stable after 14 days up to the end of the monitoring at 97 days. However, they remained slightly less abundant compared to the native soil.

### Evolution of Bacterial and Archaeal Diversity

As shown by the total number of OTUs and Chao1 index, biodiversity increased after benzodiazepine addition, compared to the native soil, and did not significantly change after (Supplementary Figures 3A,B; Kruskal–Wallis test with Conover–Iman comparison,  $p < 0.05$ , Supplementary Figure 3). Results are comparable between DZ and OXA. This increase is overall low (approximately 50–100 OTUs compared to the native soil), but significant, especially looking at the “corrected” Chao1 index (Supplementary Figure 3B). The total number of OTUs is maximum at T14 (Supplementary Figure 3A), when the majority of DZ and OXA were biodegraded, and it tends to decrease at T97.

Shannon and Inverse Simpson indices (Supplementary Figures 3C,D) were lowest at T0 and highest (and significantly different, Kruskal–Wallis test with Conover–Iman comparison,  $p < 0.05$ ) at T14, for both DZ and OXA. They then tended to decrease to recover values comparable to T0 and the native soil at T97. A ward linkage-clustering tree (beta diversity; Figure 4A) highlighted three distinct groups: (i) T0 and native soil, (ii) T14, and (iii) T97. Bacterial and archaeal communities were consequently similar in native soil and at T0 (abundance was lower in T0 samples but the bacterial and archaeal diversity were similar), and they changed at T14 and T97. Biodiversity was more similar at T14 and T97 compared to T0, highlighting a change due to the addition of benzodiazepines. Small differences were observed between DZ and OXA conditions, independently from the sampling date. The PCoA analysis (Figure 4B) also revealed the three-group repartition of OTUs, for T0, T14, and T97 samples, respectively.

Evolution of the relative abundance of the 100 most abundant OTUs (sum for the 19 samples) is shown and agglomerative hierarchical clustering (AHC) of these OTUs was performed and is presented in Figure 5A. The six classes defined by the AHC are also presented in Figure 5C. Six evolution patterns could be highlighted, corresponding to the six classes defined for bacterial and archaeal OTUs. Classes a and b (yellow and brown on Figure 5C) correspond to OTUs that are much more abundant at T0 compared to the other sampling dates, in DZ and OXA conditions. They are also more abundant at T14 and T97 compared to the native soil, but to a lower extent. These classes correspond to Firmicutes, and more precisely to two different OTUs of the *Brevibacillus* genus. Class c corresponds to OTUs that are relatively more abundant at T97. This class corresponds to three archaeal OTU from the Crenarchaeota phylum and one bacterial OTU from the Firmicutes phylum (*Bacillus* genus); two of the archaeal OTUs belong to the Nitrosopumilaceae order,

and were unknown or multi-affiliated at the genus taxonomic level, and the other one belongs to the Nitrososphaeraceae order. Classes d and f correspond to the high majority of OTUs (93 OTUs over the 100 most abundant). The relative abundance of these 93 OTUs remained stable during the whole experiment. Lastly, class e corresponds to an OTU that was significantly more abundant at T14 compared to the native soil and T0, and more abundant at T97 but in a lower extent. This OTU belongs to Gammaproteobacteria, *Hydrogenophaga* genus. It appears that differences concern a low proportion of the detected OTUs and are limited to OTUs belonging to the Crenarchaeota, Firmicutes, and Gammaproteobacteria phyla.

Overall, few differences were found between DZ and OXA conditions, and the structure of the bacterial and archaeal communities was not deeply modified, indicating little effect with the addition of these contaminants.

### Fungal Biodiversity Dynamics Based on 18S rRNA Gene Abundance and ITS2 Region Sequencing

#### Initial Fungal Diversity

Contrary to prokaryotes, data for fungal diversity in French soils are not available. However, Tedersoo et al. (2014) published a worldwide repartition of soil fungal diversity. Samples corresponding to the climates/environments that can be found in France (temperate coniferous forests, temperate deciduous forests, grassland, scrubland, and Mediterranean soils, for 127 samples) were selected and compared to the fungal diversity in the FR4N soil (Figure 3B). In comparison with bacterial and archaeal diversity, larger differences were observed. Indeed, if classically Basidiomycetes are dominant in such soils, they were about six times less represented in the FR4N soil. On the contrary, Ascomycota and Mortierellomycota were two to three times more represented in the FR4N soil. Among phyla that are not highly represented, Chytridiomycota and Glomeromycota were 3.5 and 5.3 times more represented, and the Rozellomycota phylum was about 5,000 times more represented in the FR4N soil. Monoblepharomycota, Olpidiomyces, and Aphelidiomycota phyla were detected in the FR4N soil, even if they are not reported in Tedersoo et al. (2014). On the contrary, Rozellida phylum was not detected in the FR4N soil.

#### Evolution of Fungal Abundance

Fungal abundance in soils was monitored by quantifying the 18S rRNA gene. The same trend as for bacterial abundance was highlighted. Indeed, a lower fungal abundance was observed at the beginning of the experiment, and this abundance then increased up to a plateau reached after 14 days of incubation (Supplementary Figure 4). The fungal abundance remains, however, lower compared to the native soil, with approximately one log abundance difference. Differences between DZ and OXA conditions are low.

#### Evolution of Fungal Diversity

Results for fungi were different compared to bacteria and archaea ones. Indeed, for alpha diversity indices, compared to the native soil, the number of observed fungal OTUs was significantly lower

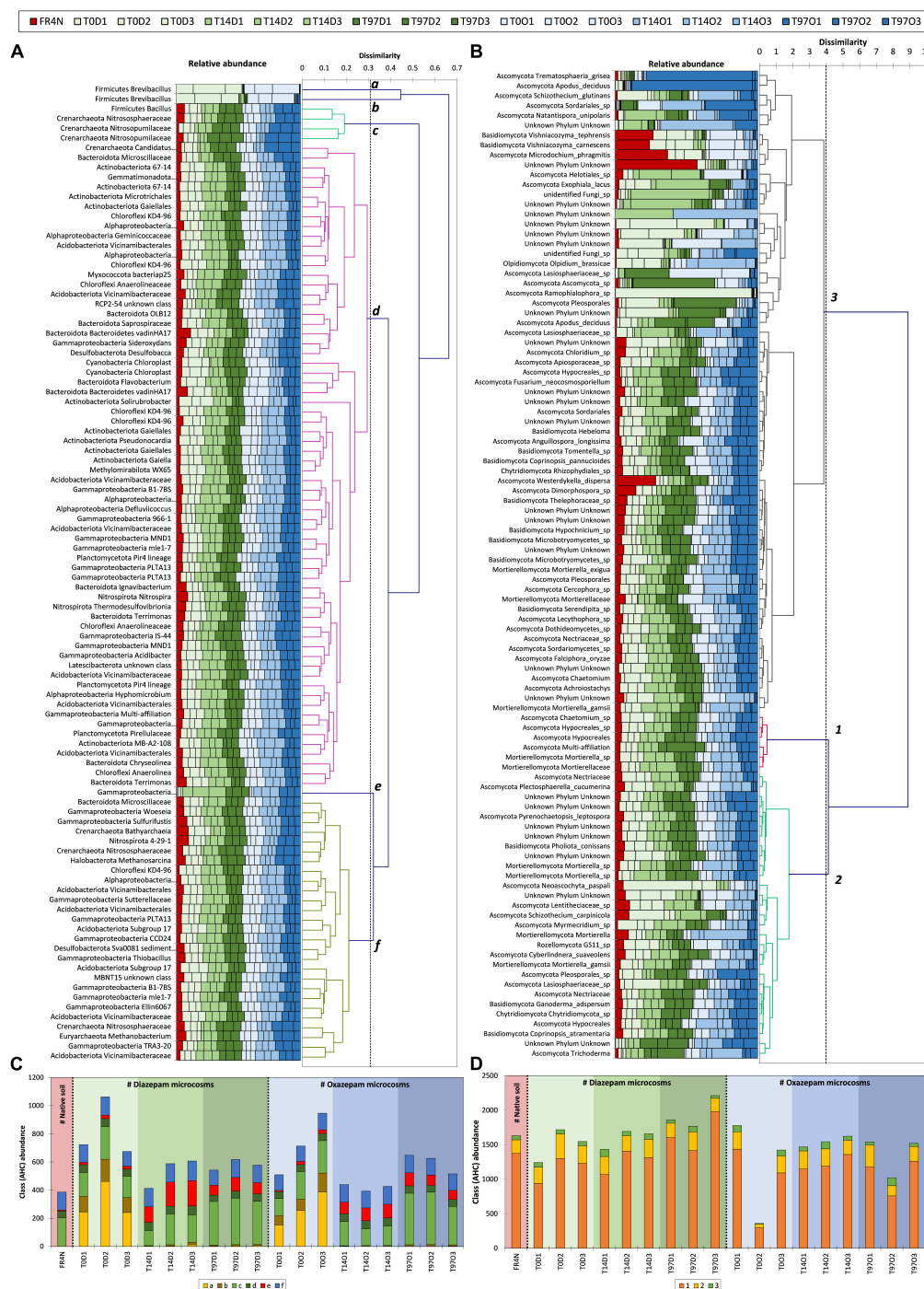
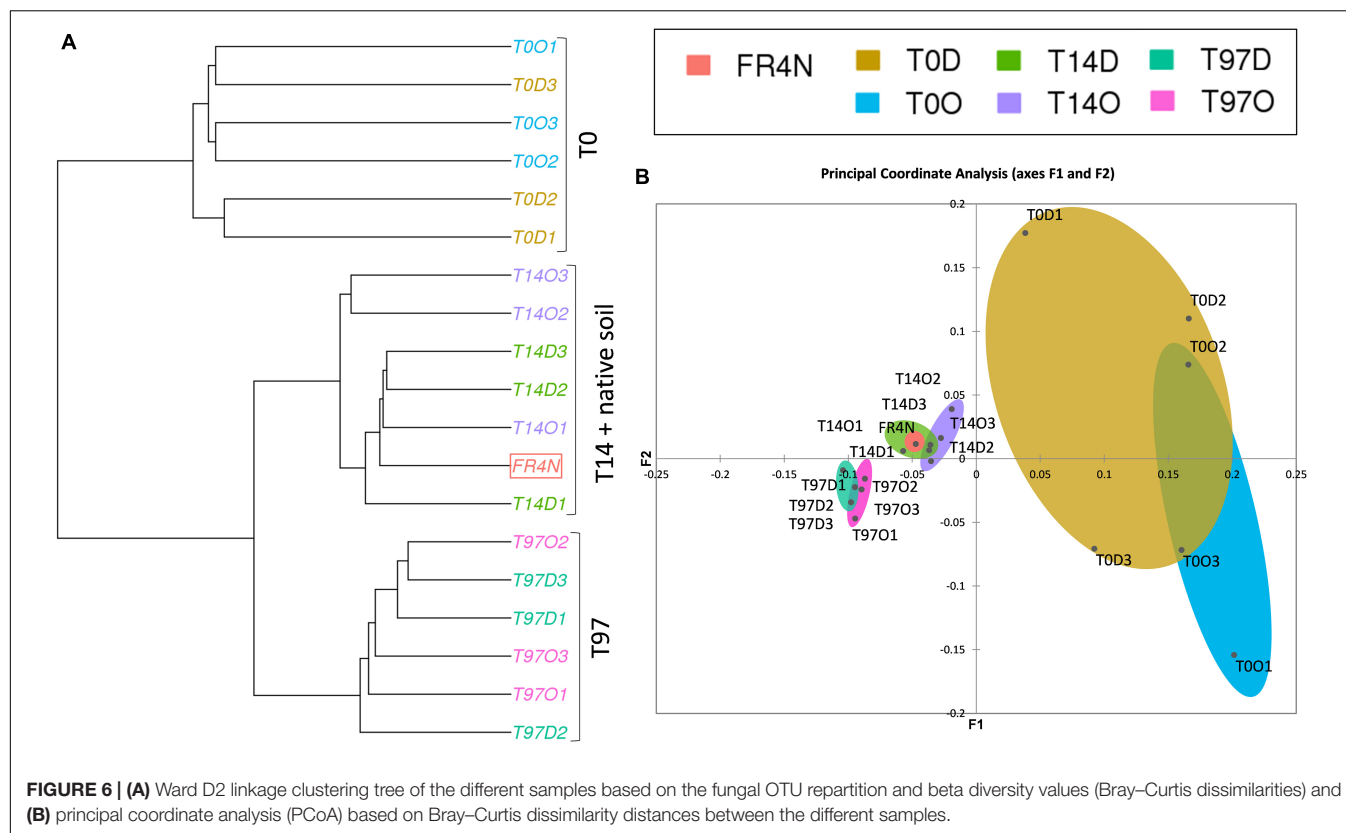


**FIGURE 5 |** Agglomerative Hierarchical Clustering evaluated from Bray–Curtis distances with proportional link as aggregation method for the 100 most abundant OTUs (sum on the 19 samples), for **(A)** bacterial and archaeal OTUs and **(B)** fungal OTUs. Panel **(C)** corresponds to the histogram presenting the repartition of the six different classes defined by AHC for bacterial and archaeal OTUs and **(D)** the three classes defined by AHC for fungal OTUs.

at T0 (**Supplementary Figures 5A,B**). The difference was less marked regarding specific richness of OTUs (**Supplementary Figures 5C,D**). Concerning the number of observed OTUs and Chao1, values were again comparable to the native soil at T14,

as they were significantly higher compared to T0 (Kruskal–Wallis test with Conover–Iman comparison,  $p < 0.05$ ). The Shannon and InvSimpson indices tended to decrease during the experiment up to T97 but no significant difference could be highlighted here. The ward linkage clustering tree of fungal OTUs



(beta diversity; **Figure 6A**) highlighted three distinct groups: (i) T0, (ii) T14 and native soil, and (iii) T97. Results thus differed from those for bacteria and archaea. Indeed, whereas T0 was similar with the native soil for bacterial and archaeal OTUs, here the native soil seems to be closer to the T14 samples. This is coherent with results from alpha diversity indices. Indeed, the impact on fungi seems to be higher right after benzodiazepines spiking. Consequently, samples from T0 are more different compared to native soil, T14 and T97. The PCoA analysis (**Figure 6B**) also revealed this “three-group” repartition. Samples from T14 and T97 were closer, and T14 was especially close to the native soil. T0 samples were the more different compared to the others, highlighting a possible higher impact of the addition of benzodiazepines for fungi.

### Identification of Fungi Taxa

Even if biodiversity indices did not show a clear response of the global fungal community to DZ and OXA spiking, some OTUs showed a specific evolution as shown by the AHC on the 100 most abundant fungal OTUs (**Figures 5B,D**). Trends are overall more difficult to observe compared to bacteria and archaea, as in some cases, there is a high variability between triplicates. Three classes could, however, be highlighted regarding their evolution during DZ and OXA biodegradation (**Figure 5D**). Classes 2 and 3 corresponded to the majority of OTUs, 29 and 65 over the 100 most abundant, respectively. These OTUs did not present a high evolution during the degradation kinetics, and values remained overall stable and comparable to the native soil. Class

1 corresponds to six OTUs, for which the observed evolution during biodegradation was different. These six OTUs belonged to two phyla, Ascomycota (four OTUs) and Mortierellomycota (two OTUs). Among Ascomycota, one OTU had multi-affiliation at a higher taxonomic level, two OTUs belonged to the Hypocreales order (unidentified at a higher taxonomic rank), and one was affiliated to the *Chaetomium* genus. Among Mortierellomycota, one OTU belonged to the *Mortierella* genus, and the other was affiliated to the Mortierellaceae family. Both of these six OTUs presented a slightly higher abundance during the biodegradation kinetics experiments and tended to be more present at T97 compared to the native soil (**Figure 5D**).

### Co-occurrence Between Most Abundant Bacterial, Archaeal, and Fungal Operating Taxonomic Units

To explore potential interactions between bacteria, archaea, and fungi, a co-occurrence network was built with the 23 most abundant bacterial OTUs and fungal OTUs and 9 most abundant OTUs for archaea (**Figure 7**). No significant mutual exclusion could be highlighted between the selected bacterial OTUs. Overall, seven significant mutual exclusions were highlighted, one between bacteria and archaea, three between bacteria and fungi, and three between archaea and fungi. Mutual exclusions were observed (i) between the Sutterellaceae and Nitrosopumilaceae families and (ii) an OTU affiliated



to the Pleosporale order; (iii) between the Chloroplast order and Mortierellaceae family; (iv) between *Mortierella* genus (close from *Mortierella gamsii*) and Thaumarchaeota archaeon MY2; (v) between *Methanosarcina* genus and (vi) one OTU from the Nitrososphaeraceae family; and (vii) between the *Hydrogenophaga* genus and an OTU from the GS11 fungal order (**Figure 7**). Co-occurrences were more abundant compared to mutual exclusions, but within kingdoms only. Indeed, no significant co-occurrences were highlighted between taxa of bacteria/archaea/fungi. High co-occurrence of the 23 most abundant bacterial OTUs was observed, not for every OTU but for the majority of them. For archaea, co-occurrence was especially observed between Nitrososphaeraceae family and *Methanosarcina* genus, and between one OTU from the Nitrosopumilaceae family and another one close to Thaumarchaeota archaeon MY2. Concerning fungi, no co-occurrence between the 23 selected OTUs could be highlighted.

## Exploration of the Evolution of Metabolic Pathways Using Tax4Fun

Only approximately 2% of bacterial and archaeal OTUs could be mapped to KEGG pathways; fungi were not considered in this approach. Nevertheless, a total of 3,554 metabolic pathways were detected in the data from the OTUs affiliation. These were compared between samples from microcosms during benzodiazepine biodegradation and the native soils. Among the 3,554 pathways, some were enhanced compared to the native soils (the majority), and some declined. Indeed, among the 3,554 characterized pathways, between 44.9 and 49.4% were enhanced by at least 10% compared to the native soil, 9.7–21.1% by 50%, 3.3–8.6% by 100%, 0.1–1.4% by 500%, and 0.06% to 0.6% by 1,000% (20 pathways). The latter were five transferases, five Oxidoreductases, seven hydrolases, one lyase, and three proteins linked to ADP/ATP metabolism (**Supplementary Table 1**). Most of them were linked to redox reactions and to ADP-ATP cycles, highlighting an increase in microbial global activity. A few more functions were highlighted in DZ conditions compared to OXA, but overall results are close between the two molecules, suggesting that the processes involved in their biodegradation may be similar.

## DISCUSSION

The objectives of this study were to assess the capacity of soil microbial communities (bacteria, archaea, and fungi) from a study site periodically flooded by water from a WWTP, to resist and potentially degrade benzodiazepine molecules, especially DZ and OXA when introduced into the soil. The study was based on a soil sampled in a soil aquifer treatment (SAT) context, where water previously treated in a WWTP are injected in the SAT area. The aim was to focus on two recalcitrant CECs, DZ, and OXA, and simulate an

input in the studied soil to study their behavior, including microbial biodegradation.

## Soil Biodiversity in a Soil Aquifer Treatment Context at Agon-Coutainville

It was previously shown that biodiversity in river could be affected by WWTP effluents (Drury et al., 2013; Blunt et al., 2018). Our study highlights that it may also be the case for soils in a SAT context. At the prokaryotic phylum level, several differences were found between the study soil and the mean diversity of French soils as described by Karimi et al. (2018) (**Figure 3A**). Among dominant phyla, Acidobacteria and Chloroflexi were approximately two and three times more represented, respectively, in our soil. Acidobacteria and Chloroflexi phyla contain diverse metabolic profiles, including strong links with carbon cycle. Acidobacteria are very commonly found in different environments including soils (de Chaves et al., 2019). Genomic and physiological characteristics of Acidobacteria were recently reviewed (Kielak et al., 2016). They concluded that many gaps still exist to fully understand the functional role of Acidobacteria in the soil C degradation process. However, it was also shown that both microbial C degradation processes and acidobacterial communities can be affected by soil management (de Chaves et al., 2019), suggesting a potential impact of soil use and characteristics on the abundance of Acidobacteria. The phylum Chloroflexi is composed of diverse groups of organisms that include anoxygenic photoautotrophs, aerobic chemoheterotrophs, thermophilic organisms, and anaerobic organisms that obtain energy through reductive dehalogenation of organic chlorinated compounds (Gupta, 2013). Other phyla such as Chlamydiae, Cyanobacteria, Euryarchaeota, Spirochaetes, Nitrospinae, and Nitrospirae were found to be overrepresented compared to mean values in French soils. Actinobacteria, Crenarchaeota, and Firmicutes were approximately two to three times less represented, and Verrucomicrobia were approximately six times less represented. The identity of the rarest phyla (such as Calditerrichaeota, Rokubacteria, Nanoarchaeota, Latescibacteria, Chlorobi, and Elusimicrobia) was also found to be different. The repeated inputs of organic substances from WWTP in the studied soil could explain their higher abundance compared to “classical” abundances in soil. Differences could also come from the microbial inputs from the WWTP biological treatment. Indeed, Drury et al. (2013) showed that the input of WWTP effluent modified the nature of bacterial communities in water and sediments (Drury et al., 2013), especially due to the input of contaminants from WWTP.

Concerning fungi in the studied soil (**Figure 3B**), Basidiomycetes were found to be about six times less represented, whereas Ascomycota and Mortierellomycota were two to three times more represented. Basidiomycetes are generally described as the principal fungal phylum in soils in terms of abundance (Tedersoo et al., 2014). In our case, Ascomycota were the dominant phyla. Fungi are heterotrophic organisms; they need organic carbon from external sources to live. With soil pH and plant cover (Wubet et al., 2012), total organic carbon (TOC)

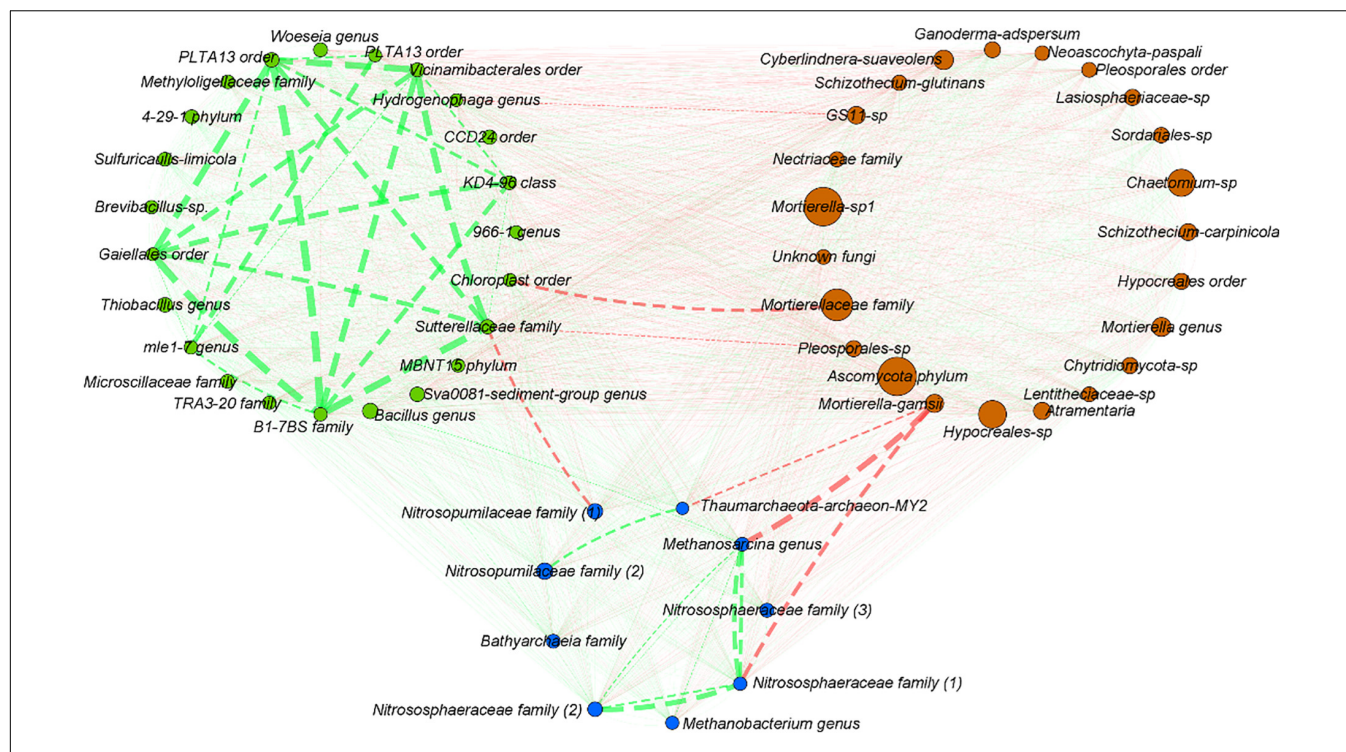


**FIGURE 7 |** Co-occurrence network between the 23 most abundant bacterial OTUs, the 9 most abundant archaeal OTUs, and the 23 most abundant fungal OTUs. Network was built using Pearson, Spearman, and Bray–Curtis analyses, both for significance thresholds  $<0.05$ . Co-occurrences (co-presence marked in green, mutual exclusion marked in red) are highlighted if significant for at least two of the three previously cited methods. The line width is proportional to the weight of the correlation, ranged from  $-0.828$  to  $-0.710$  for mutual exclusion (red) and from  $0.881$  to  $0.981$  for co-presence (green). The number of OTUs represented was chosen arbitrarily after many assays to make the network more readable as possible.

content is generally described as the main parameter controlling the abundance and diversity of soil fungal communities (Tederloo et al., 2014; Liu et al., 2015, 2018a,b). The specificity of the studied soil, with high organic matter, and contaminants, contains all the ingredients for fungal development. Liu et al. (2015) showed that the relative abundance of Basidiomycota was negatively correlated ( $r = -0.600$ ) to the soil carbon content in a selection of 25 soil samples (Liu et al., 2015). For Ascomycota, a high carbon content was more positively correlated to Ascomycota abundance. Our soil contains 4.7% of organic matter, corresponding to  $47 \text{ g kg}^{-1} \text{ dw soil}$ , which is a quite high OM content. This is possibly the reason why Basidiomycota were found to be less abundant, and Ascomycota more abundant compared to classical values. Moreover, it was shown that Ascomycota were the main representatives of the fungal community in a soil contaminated by PAHs and trace metals (Bourceret et al., 2016). The input of (organic) contaminants from WWTP effluents could then also explain the dominance of Ascomycota. Among phyla that are not highly represented classically, significant differences could also be highlighted. Rozellomycota were about 5,000 times more represented in our soil compared to mean values from Tederloo et al. (2014). Rozellomycota constitutes the basal lineage of the kingdom of fungi. They predominately feed by osmotrophic nutrition (Tederloo et al., 2018), meaning that they feed on dissolved substances. The high inputs of dissolved substance

from WWTP could explain why Rozellomycota are 5,000 times more represented compared to classical soils. They could also take part in the degradation of organic micropollutants. Presently, little is known about Rozellomycota, but our results suggest that they may be used as a bioindicator to characterize an environment impacted by WWTP effluents or sewage sludges.

## Biodegradation/Biotransformation of Diazepam and Oxazepam

In our study, sorbed DZ and OXA were extracted during the QueChers procedure; biodissipation as well as extraction procedure could be attested thanks to comparison with sterile gamma-ray ionized controls, where concentrations remained stable during the experiment. It is thus possible to affirm that a biological process occurred, explaining the observed dissipation of DZ and OXA in the microcosms. Our dissipation kinetics results are highly more rapid compared to most of the results previously described. Indeed, in the studied soil, DT50 was 3.9 and 3.6 days for DZ and OXA, respectively, and after 97 days (and even almost after 20 days),  $95.51\% \pm 0.49\%$  and  $96.87\% \pm 0.22\%$  of the spiked DZ and OXA, respectively, were dissipated due to biological activity of fungi, bacteria, and/or archaea.

The biodegradability of DZ and OXA is often described as very limited in the environment as well as in lab-scale biological experiments (Ternes et al., 2004; Redshaw et al.,

2008; Suarez et al., 2010; Klaminder et al., 2015; Greskowiak et al., 2017; Min et al., 2018). They were also shown to be resistant to biological treatments in WWTPs (Falås et al., 2016), explaining their inputs in the studied soil. Indeed, most of the data on the efficiency of WWTP treatments concerns DZ and shows that (i) less than 10% is removed during conventional biological treatment, (ii) the efficiency seems to be higher during anaerobic treatment (10–50%), and (iii) the removal rate is mainly related to sorption rather than degradation (Ghattas et al., 2017). Similarly, OXA is described as persistent in both aerobic and anaerobic treatments (Patterson et al., 2010; Kosjek et al., 2012). Some degradation pathways were, however, highlighted, such as demethylation (Helbling et al., 2010), but an efficient biodegradation in the environment has not yet been reported. Different values available in the literature for DZ and OXA biodegradation are listed in **Table 1**. Some researchers found that DZ was not directly degradable by bacteria, especially when other carbon sources more easily accessible are available, which is the case in soils (Tappin et al., 2014). A mixed microbial culture from activated sludge treatment has also been shown to demethylate DZ to form 7-chloro-5-phenyl-3H-1,4-benzodiazepin-2-one (Helbling et al., 2010). The same culture also formed a mono-hydroxylated DZ derivative, but the exact position of the hydroxyl group was not further specified. Redshaw et al. (2008) investigated the susceptibility to microbial degradation of a selection of CECs, including DZ and OXA, in short-term (60 days) bacterial liquid cultures derived from sewage sludge amended soil. They highlighted that DZ was not degraded or transformed after 60 days, but up to 40% OXA was removed in liquid cultures (**Table 1**). Kosjek et al. (2012) compared the reports of PBT profiler<sup>2</sup> (21.10.2011) with the results of their WWTP pilot, consisting of a succession of 4-L units in open circuit under oxic and then anoxic conditions. According to pbtprofiler.net, DZ and OXA are not persistent in water (DT50 < 60 days). These molecules are moderately persistent in soils (DT50 = 60–180 days) and very persistent in sediments (DT50 > 180 days). Based on their experience in anoxic bioreactors or oxic–anoxic cascades, the removal of DZ (100 µg L<sup>-1</sup> continuous feed) was less than 32%. Similarly, the OXA abatement in oxic conditions was less than 24%. On the other hand, removal in anoxic conditions reached 67% after 1 year of feeding the bioreactor, and the authors suggest an effect of biomass adaptation over time to be confirmed by biomass analyses (quantity and diversity). In our soil, a continuous exposure to CECs, including benzodiazepines, by periodic flooding by WWTP water, could have led to a strong adaptation of the soil microbial community. Löffler et al. (2005) showed that DZ was highly persistent with rapid and extensive sorption on sediments, stable in soils, groundwater, and during wastewater treatment. The same study showed that OXA is moderately persistent in the environment with a DT50 and a lower sorption rate on sediments than DZ. In addition, Löffler et al. (2005) did not observe any degradation of DZ to OXA in sediments. Carballa et al. (2006) showed a removal of 38% ± 21% to 60% ± 18% of DZ (depending on temperature) in anaerobic

bioreactors simulating a WWTP treatment. An adaptation of the bacterial community in sludge was highlighted, and better yields were obtained with water thermal pretreatment. Suarez et al. (2010) investigated the degradation of CECs in lab-scale experiments using activated sludge reactors under aerobic and anoxic conditions (Suarez et al., 2010). They highlighted that DZ and trimethoprim were highly resistant to biological transformation, and that the degradation rate for studied CECs was highly dependent on the specific microbial species.

Other studies showed that fungi, especially *via* laccases enzymes, are able to degrade and/or transform benzodiazepines. Ostadhadi-Dehkordi et al. (2012) showed a DZ and OXA removal after 48 h of 18.6 and 18.7%, respectively, in lab-scale experiment using purified fungal laccase from Ascomycete *Paraconiothyrium*. They showed that adding enzyme mediators increased the yields up to 61.4 and 71.2% for DZ and OXA, respectively. However, this study was performed in water samples, in controlled conditions, and with a purified laccase (Ostadhadi-Dehkordi et al., 2012). Ambrus et al. (1975) showed that the fungus *Aspergillus niger* J/8 N was able to demethylate DZ to form 7-chloro-5-phenyl-3H-1,4-benzodiazepin-2-one. This study is the first to describe the ability of fungi to biotransform DZ. Rodarte-Morales et al. (2011) studied the potential ability of three white rot fungi strains to degrade pharmaceutical and personal care products (PPCPs) including DZ: an anamorph species of *Bjerkandera* sp. R1, *Bjerkandera adusta*, and *Phanerochaete chrysosporium*. They showed that most of the studied PPCPs were completely degraded except fluoxetine and DZ. DZ recoveries were between 23 and 57% at the end of the experiment, where, for example, carbamazepine was completely degraded.

Overall, DZ and OXA seem to be highly recalcitrant to microbial degradation, but, even if research in this way is still needed, some bacteria or fungi, *via* several degradation pathways, are able to biotransform and/or biodissipate and/or completely biodegrade these compounds. The monitoring of the biodiversity evolution during the biodegradation can then help to find candidates able to perform DZ and OXA biodegradation.

## Bacterial and Archaeal Candidates for Biodegradation of Diazepam and Oxazepam

As shown in **Figure 8A**, the main bacteria showing a specific behavior during DZ and OXA biodegradation are two OTUs from the *Brevibacillus* genus and one from the *Hydrogenophaga* genus. *Brevibacillus* has been proposed as a biological tool by Panda et al. (2014) especially for biotechnological applications due, for example, to their ability to biodegrade low-density polyethylene, to act as a candidate bio-control agent, and as a tool for structural and functional biology (Panda et al., 2014). *Brevibacillus parabrevis* has been shown to degrade low-density polyethylene (LDPE), a recalcitrant thermoplastic made from petroleum, by forming a biofilm on LDPE surface, or with granular LDPE as sole carbon source and without nitrogen (Pramila et al., 2012). Also, *Brevibacillus brevis* has been described as able to biodegrade triphenyltin (TPT), a highly toxic endocrine disruptor used as ingredient for antifouling products and

<sup>2</sup>pbtprofiler.net



**TABLE 1** | Generally described DZ and OXA biodegradation in environmental samples, cultures from environmental sample, or experimental biodegradation studies.

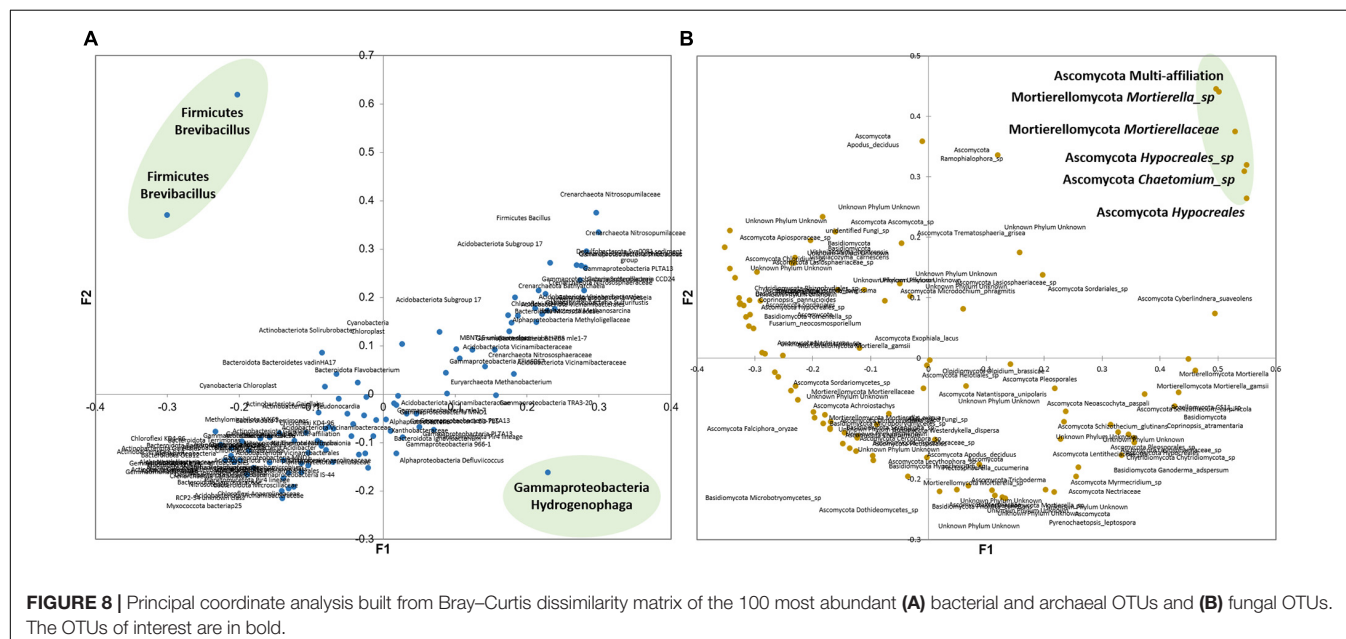
	DT50 (days)	Removal (%) (after X days)	Matrix	Concentrations	Comments	References
Diazepam	311 ± 25 (water: 34 ± 5)	–	Sediment/water	500 ng/g	Batches OECD 308 (mineralization: <2%, sorption: 60%)	Löffler et al., 2005
	38	–	Water		PBT profiler; <60 days : not persistent	Kosjek et al., 2012
	75	–	Soil		PBT profiler: >60 days: moderately persistent	Kosjek et al., 2012
	340	–	Sediment		PBT profiler: >180 days: very persistent	Kosjek et al., 2012
	–	–	River sediment		Batches (Kd = 1.9–24.8 L/Kg, log Koc = 2.4–2.8)	Stein et al., 2008
	280	–	Freshwater		Drinking water intake (Lake Mead)	Blunt et al., 2018
	280	–	Freshwater		Colorado river	Blunt et al., 2018
	–	0% (60 days)	Bacterial liquid culture from sewage sludge amended soil		Aerobic bioreactor	Redshaw et al., 2008
	–	18.6% (2 days)	Lab-scale experiment using purified fungal laccase from Ascomycete <i>Paraconiothyrium</i>		In water samples, in controlled conditions, and with a purified laccase, Without enzyme mediators	Ostadhadi-Dehkordi et al., 2012
	–	61.4% (2 days)	Lab-scale experiment using purified fungal laccase from Ascomycete <i>Paraconiothyrium</i>		In water samples, in controlled conditions, and with a purified laccase, With enzyme mediators	Ostadhadi-Dehkordi et al., 2012
	–	38 ± 21%–60 ± 18% (20 days)	Anaerobic digesters simulating WWTP treatment		Mesophilic at 37°C and pre-treatment thermophilic at 55°C, better results with thermal pre-treatment	Carballa et al., 2006
	–	17 ± 11% (440 days)	Aerobic bioreactor fed with WWTP influent		Experiments performed under nitrifying and denitrifying conditions	Suarez et al., 2010
	–	16 ± 17% (440 days)	Anoxic bioreactor fed with WWTP influent		Experiments performed under nitrifying and denitrifying conditions	Suarez et al., 2010
	3.9	95.51 ± 0.49% (97 days)	Soil	1 mg/kg	Soil in a SAT context, infiltration reed bed area, periodically flooded by WWTP effluent	This study
Oxazepam	54 ± 3 (water: 34 ± 5)	–	Sediment/water	100 ng/g	Batches OECD 308	Löffler et al., 2005
					(mineralization: nd, sorption: 19–29%)	
	38	–	Water		PBT profiler: <60 days: not persistent	Kosjek et al., 2012
	75	–	Soil		PBT profiler: >60 days: moderately persistent	Kosjek et al., 2012
	340	–	Sediment		PBT profiler: >180 days: very persistent	Kosjek et al., 2012
	–	–	River sediment		Batches (Kd = 2.0–23.50 L/Kg, log Koc = 2.4–2.7)	Stein et al., 2008
	–	40% (60 days)	Bacterial liquid culture from sewage sludge amended soil		Aerobic bioreactor	Redshaw et al., 2008
	–	18.7% (2 days)	Lab-scale experiment using purified fungal laccase from Ascomycete <i>Paraconiothyrium</i>		In water samples, in controlled conditions, and with a purified laccase, without enzyme mediators	Ostadhadi-Dehkordi et al., 2012
	–	71.2% (2 days)	Lab-scale experiment using purified fungal laccase from Ascomycete <i>Paraconiothyrium</i>		In water samples, in controlled conditions, and with a purified laccase, with enzyme mediators	Ostadhadi-Dehkordi et al., 2012
	3.6	96.87 ± 0.22% (97 days)	Soil	1 mg/kg	Soil in a SAT context, infiltration reed bed area, periodically flooded by WWTP effluent	This study



**TABLE 2** | Percentage of metabolic pathways (KEGG) increased or decreased compared to the native soil, at T0, T14, and T97.

		Percentage among the 3,554 metabolic pathways					
		T0D	T14D	T97D	T0O	T14O	T97O
Metabolic pathways increased compared to the native soil	>+10%	44.88	45.61	46.65	47.89	48.51	49.41
	>+50%	17.14	21.05	9.74	20.26	19.75	13.28
	>+100%	6.56	3.55	3.29	8.58	3.32	4.00
	>+500%	1.44	0.11	0.11	1.35	0.11	0.11
	>+1,000%	0.56	0.11	0.06	0.34	0.06	0.06
Metabolic pathways decreased compared to the native soil	<-10%	37.14	36.07	16.04	30.78	30.84	17.75
	<-50%	3.15	2.08	0.39	2.59	2.00	0.20
	<-100%	0.00	0.00	0.00	0.00	0.00	0.00

For increased functions, results are presented for functions increased by 10, 50, 100, 500, and 1,000%; for decreased functions, results are presented for functions decreased by 10, 50, and 100%.



fungicides (Ye et al., 2013). Yang and Lee (2007) highlighted the ability of *Brevibacillus* sp. strain P-6 to degrade phenol. The strain was isolated from an acclimated mixed culture, and cultivated with phenols. They found that *Brevibacillus* sp. strain P-6 was able to completely remove phenol within 93 h of incubation, at concentrations lower than 200 mg L<sup>-1</sup> (Yang and Lee, 2007). Overall, *Brevibacillus* genus has often been described as able to biodegrade organic contaminants, including contaminants with an aromatic ring, which could explain why it was highly more abundant in our soil after DZ and OXA introduction. This suggests that *Brevibacillus* strains were involved in the first biodegradation steps. This higher abundance of *Brevibacillus* is connected to the higher abundance of specific metabolic pathways (increased by more than 1,000% compared to native soil, **Supplementary Table 4**) highlighted with tax4fun tool. Some pathways involving Oxidoreductase, hydrolase, and lyase enzymes are acting on ester bonds, methane metabolism, or biosynthesis of secondary metabolites. These pathways were probably involved in the observed biotransformation of DZ and

OXA, even if the high range of possible reactions involving these enzymes does not help to clearly identify the pathways.

*Hydrogenophaga* genus has often been described as able to biodegrade aromatic compounds such as polycyclic aromatic hydrocarbons (PAHs). A species from *Hydrogenophaga* genus was found to be relatively more abundant especially at T14 when most of DZ and OXA were degraded. Xin et al. (2010) showed that *Hydrogenophaga palleronii* LHJ38 grew on naphthalene as sole carbon and energy source, in minimal medium with 2 g L<sup>-1</sup> naphthalene, highlighting its naphthalene biodegradation capacity (Xin et al., 2010). Yan et al. (2017) identified a PAHs-degrading strain, *Hydrogenophaga* sp. PYR1, isolated from PAH-contaminated river sediments. *Hydrogenophaga* sp. PYR1 was able to degrade high-molecular-weight polycyclic aromatic hydrocarbons (pyrene and Benzo[a]pyrene) under both aerobic and anaerobic conditions (Benzo[a]pyrene was degraded only under anaerobic conditions). These PAHs, being recalcitrant to microbial biodegradation, especially Benzo[a]pyrene, suggest that *Hydrogenophaga* may representa

good candidate for bioremediation approaches (Yan et al., 2017). Yang et al. (2016) showed that *Hydrogenophaga atypical* QY7-2 efficiently degraded 3-Methyldiphenylether (MDE), an important alkyl-substituted diphenyl ether compound that is widely used as an intermediate in the synthesis of pyrethroid insecticides. The strain was isolated from activated sludge and was able to grow with MDE as sole carbon source, and to perform MDE complete mineralization, suggesting the ability to degrade aromatic rings (Yang et al., 2016). Gan et al. (2011) studied a co-culture consisting of *Hydrogenophaga* sp. PBC and *Ralstonia* sp. PBA, isolated from textile WWTP. The culture could tolerate and utilize 4-aminobenzenesulfonate (4-ABS) as sole carbon, nitrogen, and sulfur source under aerobic condition (Gan et al., 2011). *Hydrogenophaga* sp. H7 was also shown to simultaneously degrade 3-hydroxybenzoate (3-HBA) or 4-HBA (3-/4-HBA) during culture (Fan et al., 2019). Their results suggest that *Hydrogenophaga* sp. H7 is an ideal candidate for degradation of aromatic compounds. Regarding archaea, mainly Nitrosopumilaceae and Nitrososphaeraceae families presented specific evolutions, but in a lower extent compared to previously described bacteria, with a slightly higher abundance at T97. Both Nitrosopumilaceae and Nitrososphaeraceae belong to the Thaumarchaeota phylum, which is an important ammonia oxidizer group in different environments including soils, in aerobic conditions, and was the first archaeal phylum identified as involved in nitrification (Brochier-Armanet et al., 2012). Thaumarchaeota and especially Nitrosopumilaceae and Nitrososphaeraceae families are consequently chemolithoautotrophic organisms, able to grow *via* aerobic ammonia oxidation and CO<sub>2</sub> fixation, with some organic material needed to support growth. The water from WWTP containing ammonia (approximately 0.2 mg/L), with regular inputs, could explain the presence of these taxa. The higher abundance observed at the end of our experiment could be linked to previous biodegradation of contaminants, leading to CO<sub>2</sub> releases. All conditions could then have been reached during the experiment for the archaeal taxa growth. Thaumarchaeota may not have been specifically involved in DZ and OXA biodegradation, but their abundance could be part of the result of the biodegradation.

Regarding tax4Fun results, the highest impact is observed at T0, partly due to the *Brevibacillus* abundance at T0. These results concern only highly increased functions, but many others could have been necessary for benzodiazepine biodegradation. The tax4fun results may give perspectives for further studies, but it is not possible here to state on the different steps and enzymes involved in benzodiazepines biodegradation, as there are many, and it is not an obligation to observe an increase higher than 1,000% to explain a degradation pathway. For example, all function from group 3.5 (Acting on carbon-nitrogen bonds, other than peptide bonds), detected 131 times, increased between 15.7 and 28.3% compared to the native soil, with maximum at T14 after most of benzodiazepines were degraded. Such enzymes were probably necessary to perform benzodiazepine degradation, but

their relative abundance did not increase significantly compared to the native soil. Functions increased by >1,000% were consequently probably involved in a high range of reactions and are not highly specific to benzodiazepine biodegradation (list of these functions in **Supplementary Table 4**). Most of these functions were detected mainly at T0. At T97, only two functions remain higher than 1,000% compared to the native soil, phenylalanine ammonia-lyase (EC:4.3.1.24) and NAD(P)H-quinone oxidoreductase subunit 6 (EC:1.6.5.3), suggesting that once biodegradation is completed, the soil returns to its original functions. If tax4fun provides a means to further exploit 16S rRNA genes dataset and draw hypotheses on the functional capabilities of microbial communities, results should be taken with caution as they remain only predictive and depend on functional information available from public genome databases.

Other functions decreased compared to the native soil (**Table 2**), but to a lower extent. Indeed, no function decreased lower than 100% compared to the native soil, and only 0.2–3.2% were decreased up to 50% compared to the native soil. This highlights that soil functions were conserved after benzodiazepines addition.

## Fungal Candidates for Biodegradation of Diazepam and Oxazepam

Fungi are heterotrophic organisms. It is consequently harder to clearly link biodegradation of specific organic compounds to their abundance, especially when other carbon sources are available, which is the case in soils. It is, however, assumed that the abundance and growth of some specific OTUs in both microcosms ( $n = 3$ ) suggest that these OTUs resisted DZ and OXA presence, and that they could have been involved in their biodegradation as their abundance increased over time. Six OTUs belonging to two phyla presented this evolution. Four OTUs belonged to Ascomycota and two OTUs belonged to Mortierellomycota (**Figure 8B**). Many *Mortierella* spp. are chitinolytic, and some species were described as able to degrade cellulose from plants to get sugar for their growth, *via* the xylanase enzymatic reaction. Ascomycota, as well as other fungi, require organic compounds as energy sources. This phylum has a wide range of metabolic capabilities and is also able to degrade biopolymers from plants such as lignin and cellulose (Boddy and Hiscox, 2017). It is admitted that fungi able to degrade complex biopolymers such as lignin or cellulose are also able to degrade recalcitrant organic compounds, such as polychlorobiphenyls (PCB), chlordecone, or polycyclic aromatic hydrocarbons (Cvancarova et al., 2012; Mao and Guan, 2016; Kadri et al., 2017). Consequently, the higher abundance of some OTUs belonging to Mortierellomycota and Ascomycota phyla after 97 days in our experiments could be linked to the biodegradation of the studied compounds.

Our results suggest that some specific OTUs evolved differently compared to others and were sometimes highly more abundant compared to the initial native soil. For

bacteria and archaea, the shift in the community seemed to remain even after contaminant degradation, whereas for fungi, the structure of the community recovered values comparable to the native soil. A direct identification of degraders, bacteria, archaea, or fungi, is not possible in this kind of experiment, but it is interesting to observe the evolution and possible implications of specific OTUs, at the community level, as occurring in the environment. The biodegradation of the targeted compounds DZ and OXA when introduced onto soil was highly more rapid compared to the literature. This result suggests that the soil microbial community is well adapted to these CECs, due to regular inputs from WWTP, and that in that case, biodegradation can occur rapidly, with DT50 of less than 4 days in our study. The study site infiltration zone, being close from the sea and with low depth groundwater, is reassuring about the fate of DZ and OXA and the possible contamination of the sea. Moreover, the potential degradation/transformation by-products were not yet studied, and further studies will explore these aspects, to ensure that no more toxic and/or recalcitrant compounds are released by these biological reactions in soil.

## CONCLUSION

Biodegradation or biotransformation of DZ and OXA faster than previously described was observed in a soil receiving water from a WWTP, with a DT50 of less than 4 days. The analysis of the abundance, diversity, identity, and potential metabolisms of the soil bacterial, archaeal, and fungal communities has provided information on the identity of the microorganisms that potentially participated in benzodiazepines dissipation. The *Brevibacillus* and *Hydrogenophaga* bacterial genera especially presented specific evolution, with higher abundances right after DZ and OXA addition for *Brevibacillus*, and right after most DZ and OXA were degraded for *Hydrogenophaga*. These genera are known to degrade persistent organic contaminants, and seem to be good candidates to perform assays on benzodiazepine biodegradation. Future research on the metabolic capacities of *Brevibacillus* and *Hydrogenophaga* genera, as pure cultures or rather in bacterial, archaeal, and fungal communities in soil to promote cometabolism processes, could be explored. Moreover, the implication of the fungal Ascomycota, Mortierellomycota, or Rozellomycota phyla, which were found to be more abundant in the initial soil, on xenobiotics, and especially CEC biodegradation or biotransformation, could be explored. The abundance of Rozellomycota could represent a good bioindicator of a contamination by WWTP effluent rich in dissolved organic contaminants. A screening of this fungal OTU could be interesting in diverse contexts, especially in (ground)water impacted by WWTP effluents or sewage sludge spreading.

Even if disappearance of mother molecules DZ and OXA was clearly highlighted in the biotic soil microcosms in our study, it is so far not possible to clearly affirm if this was due to

biodegradation (up to biodegradation by-products or to complete mineralization) or biotransformation of mother compounds. Performing a complete non-target screening of the different extracted samples, with the aim to identify the degradation compounds produced during the experiment and to confirm biodegradation or biotransformation pathways, is consequently planned.

## DATA AVAILABILITY STATEMENT

All sequences were submitted to European Nucleotide Archive (ENA) database. 16S rRNA gene sequences and ITS2 sequences are available for the 19 samples under accession numbers ERS7290419 (SAMEA9567684) to ERS7290437 (SAMEA9567702). The whole project is referenced under accession number PRJEB47338.

## AUTHOR CONTRIBUTIONS

MaC contributed to the experimental design, carried out experimental work, data analysis, and drafted the manuscript. CS, PS, JH, and CJ contributed to the experimental design, data analysis, and drafting and revising of the manuscript. GP-C, QG, and MP allowed access and provided information on the Agon-Coutainville site, and revised the manuscript. MiC carried out a part of the lab experiments in the study. All authors contributed to the article and approved the submitted version.

## FUNDING

We thank European Commission for financial support through the H2020 AquaNES EU project under agreement number no. 689450. The authors also gratefully acknowledge the financial support provided to the PIVOTS project by the Centre – Val de Loire Region (ARD 2020 program and CPER 2015-2020) and the French Ministry of Higher Education and Research (CPER 2015-2020 and public service subsidy to BRGM). Support from the European Union via the European Regional Development Fund is also acknowledged. Finally, the authors wish to thank BRGM for the financial support on the internal TOFIDEM project and funds received for open access publication.

## ACKNOWLEDGMENTS

We wish to thank SIGENAE Group and UMR-1280 PhAN Inra-Université de Nantes for their work on FROGS platform.

## SUPPLEMENTARY MATERIAL

The Supplementary Material for this article can be found online at: <https://www.frontiersin.org/articles/10.3389/fmicb.2021.742000/full#supplementary-material>

## REFERENCES

- Ambrus, G., Albrecht, K., and Horváth, G. (1975). Microbiological degradation of diazepam. *Acta Microbiol. Acad. Sci. Hung.* 22, 145–152.
- Alfhauer, K. P., Wemheuer, B., Daniel, R., and Meinicke, P. (2015). Tax4Fun: predicting functional profiles from metagenomic 16S rRNA data. *Bioinformatics* 31, 2882–2884. doi: 10.1093/bioinformatics/btv287
- Basheer, A. A. (2018). Chemical chiral pollution: impact on the society and science and need of the regulations in the 21st century. *Chirality* 30, 402–406. doi: 10.1002/chir.22808
- Blunt, S. M., Sackett, J. D., Rosen, M. R., Benotti, M. J., Trenholm, R. A., Vanderford, B. J., et al. (2018). Association between degradation of pharmaceuticals and endocrine-disrupting compounds and microbial communities along a treated wastewater effluent gradient in Lake Mead. *Sci. Total Environ.* 622–623, 1640–1648. doi: 10.1016/j.scitotenv.2017.10.052
- Boddy, L., and Hiscox, J. (2017). “Fungal ecology: principles and mechanisms of colonization and competition by saprotrophic fungi,” in *The Fungal Kingdom*, eds J. Heitman, B. Howlett, P. Crous, E. Stukenbrock, T. James, and N. A. R. Gow (Washington, DC: ASM Press), 293–308. doi: 10.1128/microbiolspec.FUNK-0019-2016
- Boreen, A. L., Arnold, W. A., and McNeill, K. (2003). Photodegradation of pharmaceuticals in the aquatic environment: a review. *Aquat. Sci.* 65, 320–341. doi: 10.1007/s00027-003-0672-7
- Bourceret, A., Cébron, A., Tisserant, E., Poupin, P., Bauda, P., Beguiristain, T., et al. (2016). The bacterial and fungal diversity of an aged PAH- and heavy metal-contaminated soil is affected by plant cover and edaphic parameters. *Microb. Ecol.* 71, 711–724. doi: 10.1007/s00248-015-0682-8
- Brochier-Armanet, C., Gribaldo, S., and Forterre, P. (2012). Spotlight on the Thaumarchaeota. *ISME J.* 6, 227–230. doi: 10.1038/ismej.2011.145
- Calisto, V., and Esteves, V. I. (2009). Psychiatric pharmaceuticals in the environment. *Chemosphere* 77, 1257–1274. doi: 10.1016/j.chemosphere.2009.09.021
- Carballa, M., Omil, F., Alder, A. C., and Lema, J. M. (2006). Comparison between the conventional anaerobic digestion of sewage sludge and its combination with a chemical or thermal pre-treatment concerning the removal of pharmaceuticals and personal care products. *Water Sci. Technol.* 53, 109–117. doi: 10.2166/wst.2006.241
- Cvancarova, M., Kresinova, Z., Filipova, A., Covino, S., and Cajthaml, T. (2012). Biodegradation of PCBs by ligninolytic fungi and characterization of the degradation products. *Chemosphere* 88, 1317–1323. doi: 10.1016/j.chemosphere.2012.03.107
- de Chaves, M. G., Silva, G. G. Z., Rossetto, R., Edwards, R. A., Tsai, S. M., and Navarrete, A. A. (2019). Acidobacteria subgroups and their metabolic potential for carbon degradation in sugarcane soil amended with vinasse and nitrogen fertilizers. *Front. Microbiol.* 10:1680. doi: 10.3389/fmicb.2019.01680
- Drury, B., Rosi-Marshall, E., and Kelly, J. J. (2013). Wastewater treatment effluent reduces the abundance and diversity of benthic bacterial communities in urban and suburban rivers. *Appl. Environ. Microbiol.* 79, 1897–1905. doi: 10.1128/aem.03527-12
- Escudé, F., Auer, L., Bernard, M., Mariadassou, M., Cauquil, L., Vidal, K., et al. (2017). FROGS: find, rapidly, OTUs with galaxy solution. *Bioinformatics* 34, 1287–1294. doi: 10.1093/bioinformatics/btx791
- Falás, P., Wick, A., Castronovo, S., Habermacher, J., Ternes, T. A., and Joss, A. (2016). Tracing the limits of organic micropollutant removal in biological wastewater treatment. *Water Res.* 95, 240–249. doi: 10.1016/j.watres.2016.03.009
- Fan, X., Nie, L., Shi, K., Wang, Q., Xia, X., and Wang, G. (2019). Simultaneous 3-/4-hydroxybenzoates biodegradation and arsenite oxidation by *Hydrogenophaga* sp. H7. *Front. Microbiol.* 10:1346. doi: 10.3389/fmicb.2019.01346
- Gan, H. M., Shahir, S., Ibrahim, Z., and Yahya, A. (2011). Biodegradation of 4-aminobenzenesulfonate by *Ralstonia* sp. PBA and *Hydrogenophaga* sp. PBC isolated from textile wastewater treatment plant. *Chemosphere* 82, 507–513. doi: 10.1016/j.chemosphere.2010.10.094
- Ghattas, A.-K., Fischer, F., Wick, A., and Ternes, T. A. (2017). Anaerobic biodegradation of (emerging) organic contaminants in the aquatic environment. *Water Res.* 116, 268–295. doi: 10.1016/j.watres.2017.02.001
- Greskowiak, J., Hamann, E., Burke, V., and Massmann, G. (2017). The uncertainty of biodegradation rate constants of emerging organic compounds in soil and groundwater – A compilation of literature values for 82 substances. *Water Res.* 126, 122–133. doi: 10.1016/j.watres.2017.09.017
- Gupta, R. S. (2013). “Chapter two - molecular markers for photosynthetic bacteria and insights into the origin and spread of photosynthesis,” in *Advances in Botanical Research*, ed. J. T. Beatty (Cambridge, MA: Academic Press), 37–66.
- Hadziavdic, K., Lekang, K., Lanzen, A., Jonassen, I., Thompson, E. M., and Troedsson, C. (2014). Characterization of the 18S rRNA gene for designing universal eukaryote specific primers. *PLoS One* 9:e87624. doi: 10.1371/journal.pone.0087624
- Helbling, D. E., Hollender, J., Kohler, H. P., Singer, H., and Fenner, K. (2010). High-throughput identification of microbial transformation products of organic micropollutants. *Environ. Sci. Technol.* 44, 6621–6627. doi: 10.1021/es100970m
- Hermes, N., Jewell, K. S., Schulz, M., Müller, J., Hübner, U., Wick, A., et al. (2019). Elucidation of removal processes in sequential biofiltration (SBF) and soil aquifer treatment (SAT) by analysis of a broad range of trace organic chemicals (TOCs) and their transformation products (TPs). *Water Res.* 163:114857. doi: 10.1016/j.watres.2019.114857
- Kadri, T., Rouissi, T., Brar, S. K., Cledon, M., Sarma, S., and Verma, M. (2017). Biodegradation of polycyclic aromatic hydrocarbons (PAHs) by fungal enzymes: a review. *J. Environ. Sci.* 51, 52–74. doi: 10.1016/j.jes.2016.08.023
- Karimi, B., Terrat, S., Dequiedt, S., Saby, N. P., Horrigue, W., Lelièvre, M., et al. (2018). Biogeography of soil bacteria and archaea across France. *Sci. Adv.* 4:eat1808. doi: 10.1126/sciadv.aat1808
- Kielak, A. M., Barreto, C. C., Kowalchuk, G. A., van Veen, J. A., and Kuramae, E. E. (2016). The ecology of Acidobacteria: moving beyond genes and genomes. *Front. Microbiol.* 7:744. doi: 10.3389/fmicb.2016.00744
- Klaminder, J., Brodin, T., Sundelin, A., Anderson, N. J., Fahlman, J., Jonsson, M., et al. (2015). Long-term persistence of an anxiolytic drug (Oxazepam) in a large freshwater lake. *Environ. Sci. Technol.* 49, 10406–10412. doi: 10.1021/acs.est.5b01968
- Kosjek, T., Perko, S., Zupanc, M., Zanoški Hren, M., Landeka Dragičević, T., Žigon, D., et al. (2012). Environmental occurrence, fate and transformation of benzodiazepines in water treatment. *Water Res.* 46, 355–368. doi: 10.1016/j.watres.2011.10.056
- Liu, J., Chen, X., Shu, H.-Y., Lin, X.-R., Zhou, Q.-X., Bramryd, T., et al. (2018a). Microbial community structure and function in sediments from e-waste contaminated rivers at Guiyu area of China. *Environ. Pollut.* 235, 171–179. doi: 10.1016/j.envpol.2017.12.008
- Liu, J., Ngoc Ha, V., Shen, Z., Dang, P., Zhu, H., Zhao, F., et al. (2018b). Response of the rhizosphere microbial community to fine root and soil parameters following *Robinia pseudoacacia* L. afforestation. *Appl. Soil Ecol.* 132, 11–19. doi: 10.1016/j.apsoil.2018.08.004
- Liu, J., Sui, Y., Yu, Z., Shi, Y., Chu, H., Jin, J., et al. (2015). Soil carbon content drives the biogeographical distribution of fungal communities in the black soil zone of northeast China. *Soil Biol. Biochem.* 83, 29–39. doi: 10.1016/j.soilbio.2015.01.009
- Löffler, D., Römbke, J., Meller, M., and Ternes, T. A. (2005). Environmental fate of pharmaceuticals in water/sediment systems. *Environ. Sci. Technol.* 39, 5209–5218. doi: 10.1021/es0484146
- Lopez-Gutierrez, J. C., Henry, S., Hallet, S., Martin-Laurent, F., Catroux, G., and Philippot, L. (2004). Quantification of a novel group of nitrate-reducing bacteria in the environment by real-time PCR. *J. Microbiol. Methods* 57, 399–407. doi: 10.1016/j.mimet.2004.02.009
- Mao, J., and Guan, W. (2016). Fungal degradation of polycyclic aromatic hydrocarbons (PAHs) by *Scopulariopsis brevicaulis* and its application in bioremediation of PAH-contaminated soil. *Acta Agric. Scand. Section B Soil Plant Sci.* 66, 399–405. doi: 10.1080/09064710.2015.1137629
- Min, X., Li, W., Wei, Z., Spinney, R., Dionysiou, D. D., Seo, Y., et al. (2018). Sorption and biodegradation of pharmaceuticals in aerobic activated sludge system: a combined experimental and theoretical mechanistic study. *Chem. Eng. J.* 342, 211–219. doi: 10.1016/j.cej.2018.01.012
- Ostadhadi-Dehkordi, S., Tabatabaei-Sameni, M., Forootanfar, H., Kolahdouz, S., Ghazi-Khansari, M., and Faramarzi, M. A. (2012). Degradation of some benzodiazepines by a laccase-mediated system in aqueous solution. *Bioresour. Technol.* 125, 344–347. doi: 10.1016/j.biortech.2012.09.039
- Panda, A. K., Bisht, S. S., DeMondal, S., Kumar, N. S., Gurusubramanian, G., and Panigrahi, A. K. (2014). *Brevibacillus* as a biological tool: a short review. *Antonie Van Leeuwenhoek* 105, 623–639. doi: 10.1007/s10482-013-0099-7



- Patterson, B. M., Shackleton, M., Furness, A. J., Pearce, J., Descourvieres, C., Linde, K. L., et al. (2010). Fate of nine recycled water trace organic contaminants and metal(loid)s during managed aquifer recharge into an anaerobic aquifer: column studies. *Water Res.* 44, 1471–1481. doi: 10.1016/j.watres.2009.10.044
- Pettenati, M., Picot-Colbeaux, G., Mathurin, F., Soulier, C., Togola, A., Devau, N., et al. (2019a). *Novel Monitoring-Modelling Systems to Manage Qualitative and Quantitative Status of Coastal Aquifers. Deliverable H2020-WATER No. D2.3.1, AquaNES Project (Demonstrating Synergies in Combined Natural and Engineered Processes for Water Treatment Systems).*
- Pettenati, M., Picot-Colbeaux, G., Thomas, L., Aurouet, A., Neyens, D., Appels, J., et al. (2019b). *Combined Natural and Engineered Systems (cNES) for Managed Aquifer Recharge (MAR) & Soil Aquifer Treatment (SAT) System With Water Storage and Quality Improvement, "in: ISMAR 10 Madrid, May 2019).*
- Picot-Colbeaux, G. P. M., Mathurin, F., Nakache, F., Guillemoto, Q., Baisset, M., Devau, N., et al. (2020). "Sustainable coastal MAR-SAT system in agencoutainville (Normandy), France. Case study 16 in," in *Exemplary Case Studies of Sustainable and Economic Managed Aquifer Recharge*, (Paris: UNESCO Publication).
- Pramila, R., Padmavathy, K., Ramesh, K. V., and Mahalakshmi, K. (2012). *Brevibacillus parabrevis, Acinetobacter baumannii and Pseudomonas citronellolis*-Potential candidates for biodegradation of low density polyethylene (LDPE). *Afr. J. Bacteriol. Res.* 4, 9–14.
- Rauch-Williams, T., Hoppe-Jones, C., and Drewes, J. E. (2010). The role of organic matter in the removal of emerging trace organic chemicals during managed aquifer recharge. *Water Res.* 44, 449–460. doi: 10.1016/j.watres.2009.08.027
- Redshaw, C. H., Cooke, M. P., Talbot, H. M., McGrath, S., and Rowland, S. J. (2008). Low biodegradability of fluoxetine HCl, diazepam and their human metabolites in sewage sludge-amended soil. *J. Soils Sediments* 8:217. doi: 10.1007/s11368-008-0024-2
- Regnery, J., Wing, A. D., Kautz, J., and Drewes, J. E. (2016). Introducing sequential managed aquifer recharge technology (SMART) – From laboratory to full-scale application. *Chemosphere* 154, 8–16. doi: 10.1016/j.chemosphere.2016.03.097
- Rodarte-Morales, A. I., Feijoo, G., Moreira, M. T., and Lema, J. M. (2011). Degradation of selected pharmaceutical and personal care products (PPCPs) by white-rot fungi. *World J. Microbiol. Biotechnol.* 27, 1839–1846. doi: 10.1007/s11274-010-0642-x
- Rognes, T., Flouri, T., Nichols, B., Quince, C., and Mahé, F. (2016). VSEARCH: a versatile open source tool for metagenomics. *PeerJ* 4:e2584. doi: 10.7717/peerj.2584
- Stein, K., Ramil, M., Fink, G., Sander, M., and Ternes, T. A. (2008). Analysis and sorption of psychoactive drugs onto sediment. *Environ. Sci. Technol.* 42, 6415–6423. doi: 10.1021/es702959a
- Suarez, S., Lema, J. M., and Omil, F. (2010). Removal of pharmaceutical and personal care products (PPCPs) under nitrifying and denitrifying conditions. *Water Res.* 44, 3214–3224. doi: 10.1016/j.watres.2010.02.040
- Tappin, A. D., Loughnane, J. P., McCarthy, A. J., and Fitzsimons, M. F. (2014). Bacterio-plankton transformation of diazepam and 2-amino-5-chlorobenzophenone in river waters. *Environ. Sci. Process. Impacts* 16, 2227–2236. doi: 10.1039/C4EM00306C
- Tedersoo, L., Bahram, M., Pölme, S., Kõljalg, U., Yorou, N. S., Wijesundera, R., et al. (2014). Global diversity and geography of soil fungi. *Science* 346:1256688. doi: 10.1126/science.1256688
- Tedersoo, L., Sánchez-Ramírez, S., Kõljalg, U., Bahram, M., Döring, M., Schigel, D., et al. (2018). High-level classification of the Fungi and a tool for evolutionary ecological analyses. *Fungal Divers.* 90, 135–159. doi: 10.1007/s13225-018-0401-0
- Ternes, T., Janew-Habibvi, M. L., Knacker, T., Kreuzinger, N., and Siegrist, H. (2004). *Assessment of Technologies for the Removal of Pharmaceuticals and Personal Care Products in Sewage and Drinking Water Facilities to Improve the Indirect Potable Water Reuse. Detailed Report of the POSEIDON Project.* Available online at: [https://iwr.tuwien.ac.at/fileadmin/mediapoolwasserguete/Projekte/ARCEM/200605\\_Final-Report-POSEIDON.pdf](https://iwr.tuwien.ac.at/fileadmin/mediapoolwasserguete/Projekte/ARCEM/200605_Final-Report-POSEIDON.pdf)
- Togola, A., Baran, N., and Coureau, C. (2014). Advantages of online SPE coupled with UPLC/MS/MS for determining the fate of pesticides and pharmaceutical compounds. *Anal. Bioanal. Chem.* 406, 1181–1191. doi: 10.1007/s00216-013-7248-8
- Vainio, E. J., and Hantula, J. (2000). Direct analysis of wood-inhabiting fungi using denaturing gradient gel electrophoresis of amplified ribosomal DNA. *Mycol. Res.* 104, 927–936. doi: 10.1017/s0953756200002471
- Wang, Y., and Qian, P.-Y. (2009). Conservative fragments in bacterial 16S rRNA genes and primer design for 16S ribosomal DNA amplicons in metagenomic studies. *PLoS One* 4:e7401. doi: 10.1371/journal.pone.0007401
- Wubet, T., Christ, S., Schöning, I., Boch, S., Gawlich, M., Schnabel, B., et al. (2012). Differences in soil fungal communities between european beech (*Fagus sylvatica* L.) dominated forests are related to soil and understory vegetation. *PLoS One* 7:e47500. doi: 10.1371/journal.pone.0047500
- Xin, J. Y., Wang, Y., Zhang, Y. X., and Xia, C. G. (2010). Paraffin oil-enhanced biodegradation of naphthalene by *Hydrogenophaga palleronii* LHJ38. *Adv. Mater. Res.* 113–116, 243–249. doi: 10.4028/www.scientific.net/amr.113-116.243
- Yan, Z., Zhang, Y., Wu, H., Yang, M., Zhang, H., Hao, Z., et al. (2017). Isolation and characterization of a bacterial strain *Hydrogenophaga* sp. PYR1 for anaerobic pyrene and benzo[a]pyrene biodegradation. *RSC Adv.* 7, 46690–46698. doi: 10.1039/C7RA09274A
- Yang, C.-F., and Lee, C.-M. (2007). Enrichment, isolation, and characterization of phenol-degrading *Pseudomonas resinovorans* strain P-1 and *Brevibacillus* sp. strain P-6. *Int. Biodeterior. Biodegradation* 59, 206–210. doi: 10.1016/j.ibiod.2006.09.010
- Yang, Q., Cai, S., Dong, S., Chen, L., Chen, J., and Cai, T. (2016). Biodegradation of 3-methyldiphenylether (MDE) by *Hydrogenophaga* atypical strain QY7-2 and cloning of the methy-oxidation gene mdeABCD. *Sci. Rep.* 6:39270. doi: 10.1038/srep39270
- Ye, J., Yin, H., Peng, H., Bai, J., Xie, D., and Wang, L. (2013). Biosorption and biodegradation of triphenyltin by *Brevibacillus brevis*. *Bioresour. Technol.* 129, 236–241. doi: 10.1016/j.biortech.2012.11.076

**Conflict of Interest:** The authors declare that the research was conducted in the absence of any commercial or financial relationships that could be construed as a potential conflict of interest.

**Publisher's Note:** All claims expressed in this article are solely those of the authors and do not necessarily represent those of their affiliated organizations, or those of the publisher, the editors and the reviewers. Any product that may be evaluated in this article, or claim that may be made by its manufacturer, is not guaranteed or endorsed by the publisher.

Copyright © 2021 Crampon, Soulier, Sidoli, Hellal, Joulain, Charron, Guillemoto, Picot-Colbeaux and Pettenati. This is an open-access article distributed under the terms of the Creative Commons Attribution License (CC BY). The use, distribution or reproduction in other forums is permitted, provided the original author(s) and the copyright owner(s) are credited and that the original publication in this journal is cited, in accordance with accepted academic practice. No use, distribution or reproduction is permitted which does not comply with these terms.



# Resistance and Resilience of Soil Nitrogen Cycling to Drought and Heat Stress in Rehabilitated Urban Soils

Mehdi Fikri<sup>1,2</sup>, Catherine Joulain<sup>1</sup>, Mikael Motelica-Heino<sup>2</sup>, Marie-Paule Norini<sup>1</sup> and Jennifer Hellal<sup>1\*</sup>

<sup>1</sup> BRGM, DEPA/GME, Orléans, France, <sup>2</sup> ISTO, UMR 7327, CNRS-Université d'Orléans-Brgm, Orléans, France

## OPEN ACCESS

### Edited by:

Dimitrios Georgios Karpouzas,  
University of Thessaly, Greece

### Reviewed by:

Katharina Kujala,  
University of Oulu, Finland  
Myrto Tsiknia,  
Agricultural University of Athens,  
Greece

### \*Correspondence:

Jennifer Hellal  
j.hellal@brgm.fr

### Specialty section:

This article was submitted to  
Microbiotechnology,  
a section of the journal  
Frontiers in Microbiology

**Received:** 18 June 2021

**Accepted:** 12 November 2021

**Published:** 22 December 2021

### Citation:

Fikri M, Joulain C,  
Motelica-Heino M, Norini M-P and  
Hellal J (2021) Resistance  
and Resilience of Soil Nitrogen  
Cycling to Drought and Heat Stress  
in Rehabilitated Urban Soils.  
Front. Microbiol. 12:727468.  
doi: 10.3389/fmicb.2021.727468

In the context of climate change and biodiversity loss, rehabilitation of degraded urban soils is a means of limiting artificialization of terrestrial ecosystems and preventing further degradation of soils. Ecological rehabilitation approaches are available to reinitiate soil functions and enhance plant development. However, little is known about the long-term stability of rehabilitated soils in terms of soil functions when further natural or anthropogenic perturbations occur. Based on rehabilitated urban soils, the present study sought to evaluate the resistance and resilience of soil functions linked to carbon cycling and phosphate dynamics in addition to nitrogen cycling and related microbial communities after a heat and drought stress. A laboratory experiment was conducted in microcosms under controlled temperature conditions, with four contrasted soils collected from a rehabilitated urban brownfield; an initial, non-rehabilitated soil (IS), a technosol with a high organic matter level (HO), and two technosols with less organic matter (LO1 and LO2), together with their respective controls (no stress). Changes in potential denitrification (PDR), nitrification (PNR) rates, and their interactive relationships with soil microbial activities and soil physicochemical properties were determined following a combined heat (40°C) and drought stress period of 21 days. Measurements were carried out immediately after the stress (resistance), and then also 5, 30, and 92 days after soil rewetting at 60% water holding capacity (resilience). Microbial activities involved in soil functions such as carbon cycling and phosphate dynamics proved to be of low resistance in all soils except for IS; however, they were resilient and recovered rapidly after rewetting. On the other hand, the microbial activities and gene abundances that were measured in relation to nitrogen cycling processes showed that for denitrification, activities were more rapidly resilient than gene abundances whereas for nitrification the activities and gene abundances were resilient in the same way. Results suggest that, unless the soils contain high amounts of organic matter, microbial communities in imported soils can be more vulnerable to environmental pressures such as drought and heat than communities already present. This should be considered when rehabilitating degraded soils.

**Keywords:** soil functions, resistance, resilience, N-cycling, bacteria, denitrification, nitrification, rehabilitation

## INTRODUCTION

Anthropized soils have increased significantly in France since the first industrial revolution in the eighteenth century and the increasing urban sprawl. This has led to soil artificialization, which is defined as the process by which soils change use from an agricultural or natural state to a constructed building or a parking lot, for example (Pascual Aguilar et al., 2011), leading to the degradation of its ecological functions. Soil artificialization has occurred especially at the cost of agricultural lands [87% of artificialized soils in France between 2006 and 2015 used to be agricultural lands (CGDD, 2015)]. Additionally, brownfields with degraded soils can cover vast surfaces in urban and peri-urban areas. These are usually characterized by a low to moderate chemical contamination and limited fertility preventing their reuse without a prior rehabilitation process (Vincent et al., 2018). In light of the rising challenge to limit urban expansion at the expense of agricultural and natural terrestrial ecosystems, urban planning needs to take into consideration the requalification of brownfields and promote their productive potential. Moreover, the reuse of abandoned urban spaces and soil rehabilitation are key factors for protecting vital ecosystem services (Vincent et al., 2018).

Many studies have taken an interest in the rehabilitation of agricultural soils (De Noni and Viennot, 1993; Song et al., 2017; Nesper et al., 2019; Norton and Ouyang, 2019). However, to our knowledge, few studies have investigated soil ecological functions in rehabilitated urban soils. Lorenz and Lal (2009) reported that there are both similarities and differences concerning carbon (C) and nitrogen (N) biogeochemical cycling between urban and natural soils. These authors stated that the main differences reside in modifications of pH, compaction, moisture, and organic matter content in urban soils due to human activities, which influence critical soil biogeochemical processes like nitrification and denitrification. In addition, microbial communities in urban soils are substantially affected by human activities through the disturbance of biotic and abiotic soil properties (Li et al., 2018). Urbanization also affects nutrient cycling and their distribution, leading to increased N and P contents in soils (Sardans et al., 2006; Hobbie et al., 2017) as well as the accumulation of nutrients (Noe and Hupp, 2005). Moreover, urban environments may also suffer heat island effects, thus increasing soil temperature (Oke, 1989) which can significantly affect microbial activity (Carreiro et al., 2009) and affect major biogeochemical (C, N, and P) cycles in soils (Bapiri et al., 2010; Gleeson et al., 2010; Kaurin et al., 2018). Microorganisms are the main drivers for N-cycling due to their various adaptive strategies and their capacity to use various energy sources (Philippot et al., 2013). Nitrogen is an essential element for biota growth in soil (Jackson et al., 2008). N-cycling in terrestrial ecosystems is a complex process because N exists under gaseous, dissolved, and particulate forms. Nevertheless, in soils, N pathways are regulated by five interlinked microbial processes: fixation ( $\text{N}_2 \rightarrow \text{NH}_4^+$ ), mineralization ( $\text{N}_{\text{org}} \rightarrow \text{NH}_4^+$ ), nitrate ammonification ( $\text{NO}_3^- \rightarrow \text{NH}_4^+$ ), nitrification ( $\text{NH}_4^+ \rightarrow \text{NO}_3^-$ ), and denitrification ( $\text{NO}_3^- \rightarrow \text{N}_2$ ) (Hallin et al., 2009). Previous studies reported that soil's physicochemical properties and abundances of related microbial genes are key

factors in determining soil nitrification and denitrification (Jia and Conrad, 2009; Li et al., 2009; Hynes and Germida, 2012; Zhang et al., 2017; Zhang and Ji, 2018).

The increase in drought frequency and duration, which are typically combined with heat waves and interspersed rewetting, is raising questions concerning the capacity of microorganisms to adapt to such events in Mediterranean regions for example (Gibelin and Déqué, 2003; Guillot et al., 2019). Moreover, especially for agricultural soils, soil microbial communities can be resistant and even resilient to drought, as they are adapted to seasonal climatic extremes (Griffiths and Philippot, 2013; Kaurin et al., 2018). Therefore, in the context of soil rehabilitation it is essential to understand the response of N-cycling functions to drought periods, and the eventual impact on related microbial communities' structure.

This article addresses knowledge gaps concerning rehabilitated urban soils in terms of the stability (resistance and resilience) of key microbial functions to heat and drought stress. The study investigates the effects of such a stress on global microbial activity and N-cycling functions (denitrification and nitrification) in rehabilitated urban soils. In addition, the effect of stress on specific microbial activities (basal respiration, phosphatase and  $\beta$ -glucosidase activities, and molecular microbial biomass) was also investigated. We hypothesized that soil's N-cycling functions and microbial activities would be more resistant and resilient to heat (40°C) and drought stress in a soil with a high organic matter level. Finally, through this evaluation of the stability of several key soil microbial processes, this study also aims to compare three rehabilitation itineraries, two with low organic matter technosols with different plantations (LO1 and LO2) and an imported technosol with a high organic matter contents (HO), with the initial soil (IS) to give a first account of the best choice of rehabilitation.

## MATERIALS AND METHODS

### Site Description and Soil Sampling

The experimental site of Pierre Bénite is located in Lyon metropolis in France. It has a semi-continental climate with an average annual temperature of 12°C and average annual rainfall of 1,015 mm. Summers are typically hot, and temperatures can reach 40°C. This site located along the Rhône riverbank was initially filled with alluvial sand and gravel then used for several industrial activities. A part of the brownfield was rehabilitated in 2016 during the REBU project (REBU, 2016), with the objective of developing vegetation cover and soil biota by restoring major biogeochemical cycles in soils (C, N, and P) and evaluating the best cost-effective approach. Several experimental modalities were set up using different imported or on-site materials and then received a mixture of PGPR (plant growth-promoting rhizobacteria) involved in nitrogen fixation and mycorrhiza combined with a seed composition adapted to the pedo-climatic conditions and containing a mixture rich in *Fabaceae* and *Poaceae*, as well as other species found on site. Selection of seed compositions and microbial inoculations

were provided and carried out by Valorhiz (Montferrier-sur-Lez, France).<sup>1</sup> In April 2019, 3 years after their rehabilitation, four of these modalities were chosen for the present experiment: the initial, non-rehabilitated soil consisting of a sandy material (IS modality); two modalities that had received the same imported low organic matter content technosol but with two different seed mixtures (LO1 and LO2 modalities, young plants and an accompanying seed composition and a “convalescent” seed composition, respectively); and an imported technosol rich in organic matter (HO) that received the same seed composition as LO1.

Surface soils (0–20 cm) were sampled nine times from each plot following an “M” pattern with an auger and put in sterile sampling bags (Whirl-Pak®). Composite samples were sieved at 4 mm in the laboratory and stored at 20°C for a few days until the experiment.

Soil textures were determined using a LaMotte 1067 soil texture kit (LaMotte Co., Chestertown, MD, United States), following the manufacturer’s protocol. IS is a loamy sand soil (80.7% sand, 16.2% silt, and 3.1% clay). LO1 (40% sand, 45.1% silt, and 14.7% clay) and LO2 (41.3% sand, 43.6% silt, and 15.1% clay) are loamy soils, and HO is a sandy loam soil (53.7% sand, 31.7% silt, and 14.8% clay).

## Experimental Setup

Microcosms consisted of 200 ml polystyrene pots filled with 100 g of equivalent dry soil and humidified to 60% water holding capacity (WHC), prepared in triplicates with soils from the four plots (IS, LO1, LO2, and HO, respectively). Half of the microcosms were controls, and the other half was used for stressing conditions. Before starting the experiment, all microcosms were pre-incubated for 2 weeks prior to the stress period to stabilize the microbial communities.

Then, several steps were carried out as described in **Figure 1**.

**Step 1:** a heat (40°C) and drought stress period was applied to soils during 21 days; T0 corresponds to the end of this period for stressed soils and controls.

**Step 2:** the stressed soils were re-humidified to 60% WHC, and another sampling took place 5 days later (T5).

**Step 3:** Two more sampling operations were performed 30 days (T30), and 92 days after the stress ended (T92).

Controls and stressed soils from step 2 onward were incubated in a phytotron (plant growth chamber, Memmert HPP750 IPP PLUS, Büchenbach, Germany) at 20°C in the dark with 60% air–water saturation. Soil moisture was maintained at 60% WHC by weighing the soils once a week and, if necessary, adjusting the water contents with Mont Roucoux mineral water ( $\text{Ca}^{2+}$  2.9 mg·l<sup>-1</sup>;  $\text{Mg}^{2+}$  0.5 mg·l<sup>-1</sup>;  $\text{Na}^{+}$  3 mg·l<sup>-1</sup>;  $\text{NO}_3^{-}$  2 mg·l<sup>-1</sup>;  $\text{SO}_4^{2-}$  3 mg·l<sup>-1</sup>) of which the composition is comparable to rainwater. Basal respiration and phosphatase and  $\beta$ -glucosidase activities were measured at every sampling point, as described below. N-cycling functions were assessed by measuring potential denitrification rates (PDR) and potential nitrification rates (PNR), while N-cycling microbial communities were characterized by measuring gene abundances.

Soil samples for enzyme activities and microbial DNA extractions were frozen at –80 and –20°C, respectively. For N transformation rates, soil samples were dried at 60°C and kept in sealed containers for total N and total C measurements.

## Physicochemical Parameters

Soil pH<sub>water</sub> was measured following the norm NF ISO 10390 (ISO, N. 10390, 2005). Total C, total H, and total N concentrations were measured in soil samples (5 mg of dry soil, ground and sieved at 160  $\mu\text{m}$  to which ~2 mg of vanadium pentoxide was added to accelerate the reaction) using an elemental Flash pyrolysis (Flash 2000, Thermo Fisher Scientific, Waltham, MA, United States). Total organic C was measured using the Rock-Eval pyrolysis technique (Rock-Eval 6 Turbo, Vinci Technologies, Nanterre, France).

## Soil Microbial Community Characterization

### Microbial Basal Respiration

Microbial basal respiration was measured for all samples at every sampling time using the soil respiration system (MicroResp<sup>TM</sup> James Hutton Ltd., Aberdeen, United Kingdom, according to Campbell et al., 2003), following the manufacturer’s protocol.<sup>2</sup> MicroResp<sup>TM</sup> is a colorimetric method based on CO<sub>2</sub> release detection in a 96-well plate by a gel containing a colored indicator (cresol red) that changes color from purple to yellow when in contact with CO<sub>2</sub>. The CO<sub>2</sub> emission by soil microorganisms was estimated before and after a 6 h incubation period at 25°C. The colorimetric assessment was performed at  $\lambda = 570$  nm by an Omega SPECTROstar (BMG Labtech, Ortenberg, Germany) microplate spectrophotometer.

### Enzymatic Activities

The activities of two microbial enzymes involved in C and P cycles were measured at each sampling time:  $\beta$ -glucosidase ( $\beta$ -Glu) which acts on the osidic bonds of glucose and degrades cellulose, and phosphatase (Phos) which degrades phosphatase esters and is responsible for catalyzing the phosphoester bond resulting in the liberation of phosphate. Measurements were carried out according to the norm (ISO, N. 20130, 2018), which uses a colorimetric method to detect the intensity of enzyme activities during an incubation period in microplates. Different substrates were used for the measurements of enzyme activities: 4-nitrophenyl  $\beta$ -D-glucopyranoside (CAS no. 2492-87-7) for  $\beta$ -Glu quantification and 4-nitrophenylphosphate disodium salt hexahydrate (CAS no. 333338-18-4) for Phos quantification. Enzyme activity is measured by detecting the formation of para-nitrophenol (PNP) which was read at  $\lambda = 405$  nm using an Omega SPECTROstar (BMG Labtech) microplate spectrophotometer. Results were expressed in mU·g<sup>-1</sup><sub>dry soil</sub> (namely, nmol·min<sup>-1</sup>·g<sup>-1</sup><sub>dry soil</sub>).

### Soil DNA Extraction and Quantitative Real-Time PCR

Soil DNA extractions were carried out at each sampling time on subsamples of between 0.4 and 0.8 g dry soil with the FastDNA®

<sup>1</sup> www.valorhiz.fr

<sup>2</sup> https://www.microresp.com/



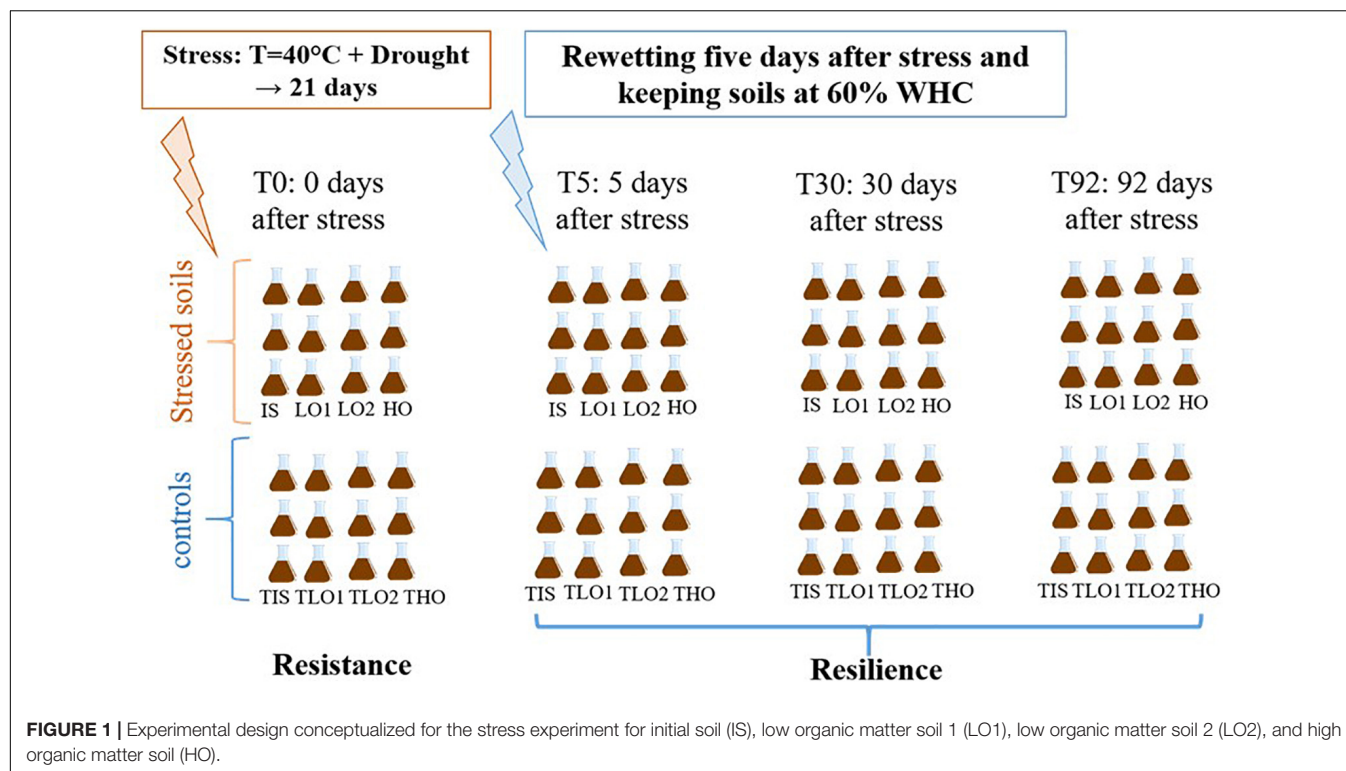


**TABLE 1 |** Primers used for the determination of functional genes related to N-cycling in soils.

Genes	Primers	Target	Base sequences	References
<i>narG</i>	<i>narG</i> -F	Nitrate reductase	TCGCCSATYCCGGCSATGTC	Bru et al., 2007
	<i>narG</i> -R		GAGTTGTACCACTCRGCSGAYTCSG	
<i>nosZ</i>	<i>nosZ</i> -2F	Nitrous oxide reductase	CGCRACGGCAASAAGGTSMSST	Henry et al., 2006
	<i>nosZ</i> -2R		CAKRTGCAKSGCCTGGAGAA	
<i>amoA</i>	<i>amoA</i> -1F	Bacterial ammonia mono-oxygenase	GGGGTTTCTACTGGTGGT	Rotthauwe et al., 1997
	<i>amoA</i> -2R		CCCCTCKGSAAGCCTTCTTC	

Spin Kit for soil and the FastPrep-24™ instrument following the manufacturer's (MP Biomedicals, Santa Ana, CA, United States) protocol and the following specific conditions: samples were homogenized for 30 s at a speed setting of 5.0 m·s<sup>-1</sup>, then centrifuged for 20 min at 14,000 rpm. DNA was quantified using the Quantus™ fluorometer (Promega, Charbonnières-les-Bains, France) with the Promega QuantiFluor® dsDNA System, following the manufacturer's recommendation.

Quantitative real-time PCR (qPCR) was used to measure bacterial abundance in soils by quantifying 16S rRNA gene copies. All samples were run in duplicates in a CFX96 Optical Real-Time detection System (Bio-Rad Laboratories, Inc., Hercules, CA, United States) in a 20 µl final volume containing 10 µl of SsoAdvanced Supermix (Bio-Rad), 0.16 µl of forward primer 341F (5'-CCTACGGGAGGCAGCAG-3') (50 µM), 0.16 µl reserve primer 515R (5'-ATTACCGCGGCTGCTGGCA-3') (50 µM), 0.2 µl T4 GP 32 (500 ng·µl<sup>-1</sup>; MP Biomedicals), 2 µl DNA at 1 ng·µl<sup>-1</sup>, and ultrapure water. Thermocycling conditions were as follows: 3 min at 95°C; 35 cycles of 30 s at 95°C, 30 s at 60°C, 30 s at 72°C, and 30 s at 80°C. N-cycling's

functional gene abundances were also measured using qPCR in a CFX96 system, in a 20-µl final volume with 10 µl of SsoAdvanced Supermix (Bio-Rad), 0.2 µl of each primer (50 µM) (Table 1), 0.2 µl T4 GP32 (500 ng·µl<sup>-1</sup>) (only for the *narG* gene), and 2 µl of DNA at 1 ng·µl<sup>-1</sup>, completed with ultrapure water. Thermal cycling conditions were as follows: for the *nosZ* gene: 2 min at 95°C; 40 cycles of 15 s at 95°C, 15 s at 62°C, 30 s at 72°C, and 30 s at 80°C; for the *narG* gene: 3 min at 95°C; 6 cycles consisting of 30 s at 95°C and 30 s at 63°C with a touchdown at -1°C by cycle and 30 s at 72°C; and 34 cycles consisting of 30 s at 95°C, 30 s at 58°C, 30 s at 72°C, and 30 s at 80°C; and for the *amoA* gene: 5 min at 95°C; 40 cycles consisting of 15 s at 95°C, 30 s at 55°C, and 30 s at 72°C, and 30 s at 80°C. At the end of each qPCR, a melting curve analysis was generated by applying a final step of 0.5°C temperature increment every 10 s, from 65 to 95°C.

For each gene, calibration curves were obtained using serial dilutions of a known quantity of linearized plasmids containing known copy numbers of the gene. Blank controls without DNA with ultrapure water were carried out in every

qPCR analysis. The amplification efficiencies of target genes ranged between 87.3 and 96.3%, with  $R^2$  values between 0.99 and 1.

### Determination of Soil N Transformation Rates

PDR were determined by the acetylene block technique of Petersen et al. (2012) and later used by Zhang et al. (2018). The method consists of measuring  $N_2O$  emissions by gas chromatography (TRACE<sup>TM</sup> 13,000) after adding acetylene to block its transformation to  $N_2$  in anaerobic conditions at the end of a 24 h incubation period.

PNR were determined by placing soils (5 g equivalent dry soil) into 70 ml containers. Soils were further treated with 100 mgN·kg<sup>-1</sup> (dry weight) (NH<sub>4</sub>)<sub>2</sub>SO<sub>4</sub>. Samples were adjusted to 60% WHC using deionized water and were incubated at 20°C for 7 days. At the end of the incubation period, samples were extracted with a 2 M KCl solution (5:1 solution of soil ratio). Extracts were shaken vertically at 200 rpm for 1 h, then later filtered with 0.2 µm acetate cellulose ClearLine<sup>®</sup> filters. Extracts were analyzed for N-NH<sub>4</sub>, N-NO<sub>2</sub>, and N-NO<sub>3</sub> concentrations using colorimetric techniques, Thermo Fisher Gallery<sup>TM</sup> for ammonium (references 984362 and 984363) and nitrite (reference 984371), and a Merck kit adapted for high salinity because of the extractant used (KCl) (Reference 1.14942.0001). Results were expressed in mgN·day<sup>-1</sup>·kg<sup>-1</sup><sub>drysoil</sub> between day 0 and day 7.

### Statistical Analysis

Kruskal–Wallis multiple comparison tests were conducted to compare mean values at the 5% level using R software R-3.6.1 (R Core Team, 2018), agricolae package. Differences were considered significant for  $p$ -values <0.05. Data of all soils at all measurement periods were analyzed by principal component analysis also using R software, FactoMineR and factoextra packages.

## RESULTS

### Initial Soil Physicochemical Properties

All soil pH ranged between 7.6 and 9.1, and IS had the highest pH value, followed by HO, LO2, and LO1 (Table 2). HO and IS had the highest total C contents followed by LO1 and then LO2. HO's TOC content was significantly higher (~7-fold) than all other soils, followed by LO1, then LO2 and finally IS. Total N contents

ranged between 0.5 and 1.6 g·kg<sup>-1</sup><sub>drysoil</sub> for all soils, and LO1 and HO had the highest values, followed by LO2, then IS. HO's C/N was significantly higher (~3-fold) than all other soils, followed by LO2 and LO1, then IS. HO's H content was significantly higher (~2-fold) than all other soils, followed by LO1, then LO2 and finally IS. HO and LO2 N-NH<sub>4</sub> contents were significantly higher (~5-fold the minimal value) than LO1 and IS. N-NO<sub>3</sub> contents ranged between 6.9 mgN·kg<sup>-1</sup> and 17.7 (mgN·kg<sup>-1</sup>); LO1 had the highest value, followed by HO, LO2, and IS.

### Characterization of Soil Microbial Communities and Activities

#### Changes in Total Microbial Biomass and Enzymatic Activities

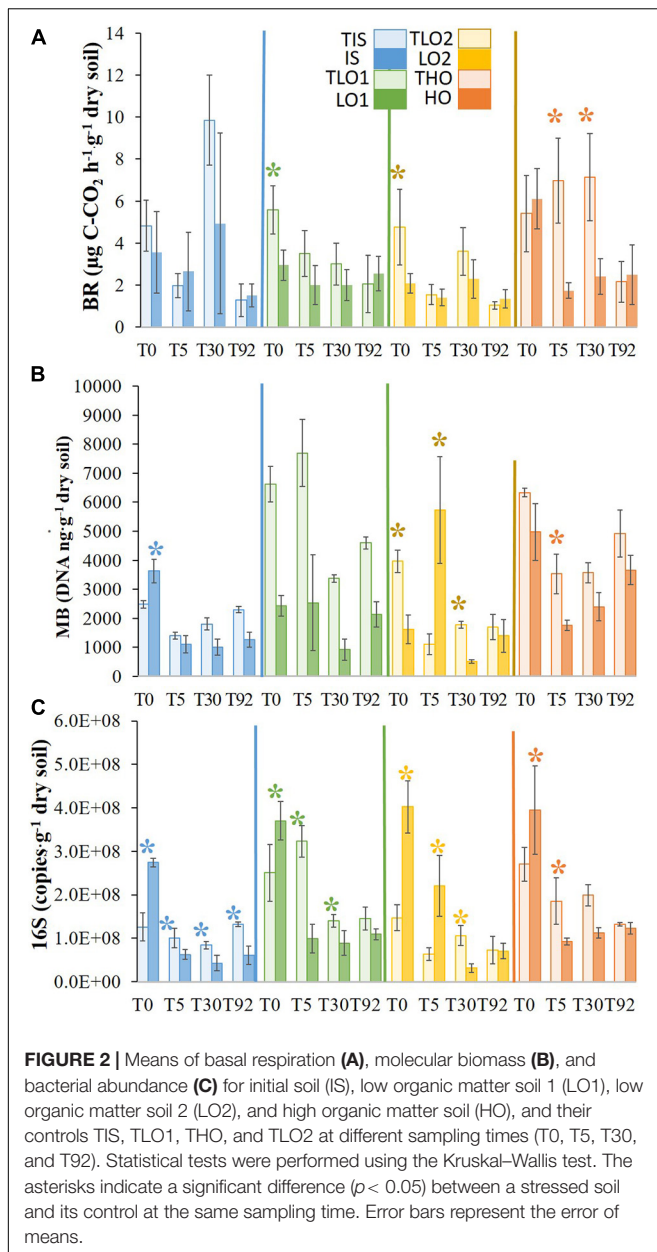
Basal respiration (BR) was measured at all sampling times to assess the level of microbial activity in the microcosms (Figure 2A). Just after the stress at T0, BRs of LO1 and LO2 were significantly lower than those of controls TLO1 and TLO2 (~2- and 2.5-fold, respectively). In contrast, BRs in soils HO and IS (6.1 and 3.6 µgC-CO<sub>2</sub>·h<sup>-1</sup>·g<sup>-1</sup><sub>drysoil</sub>, respectively) were not affected by the stress as no significant differences were found compared to BRs of controls THO (5.4 and 4.8 µgC-CO<sub>2</sub>·h<sup>-1</sup>·g<sup>-1</sup><sub>drysoil</sub>, respectively). After rewetting at T5, only the BR of soil HO was found to be significantly lower than that of control THO (~4-fold), while no significant differences were found for all the other soils. At T30, HO's BR was the only measurement that was significantly lower than its control THO (~3-fold). No significant differences were found between treatments and controls at T92. However, we observed that overall BR declined between T0 and T92 for all unstressed soils.

The heat and drought stress significantly decreased the molecular biomass (MB) of LO1 and LO2 soils compared to controls at T0 (~3- and 2.5-fold, respectively) (Figure 2B). In contrast, MB in HO was not significantly affected, and MB in IS increased significantly (~1.5-fold) compared to controls at T0. Five days after rewetting, MB in LO2 had increased significantly (~5-fold) compared to control. In contrast, IS, LO1, and HO's MB were significantly lower (~1.3-, 3-, and 3-fold) than controls at T5. MBs in LO1 and LO2 were significantly lower than those of controls (~4- and 3.5-fold) at T30; in contrast, no significant differences were found between HO and its control. Finally, at T92, no significant differences were found between stressed soils and controls. The stresses also significantly increased bacterial abundance (16S rRNA gene copies) in soils compared to controls

**TABLE 2 |** Physicochemical properties of soils at T0.

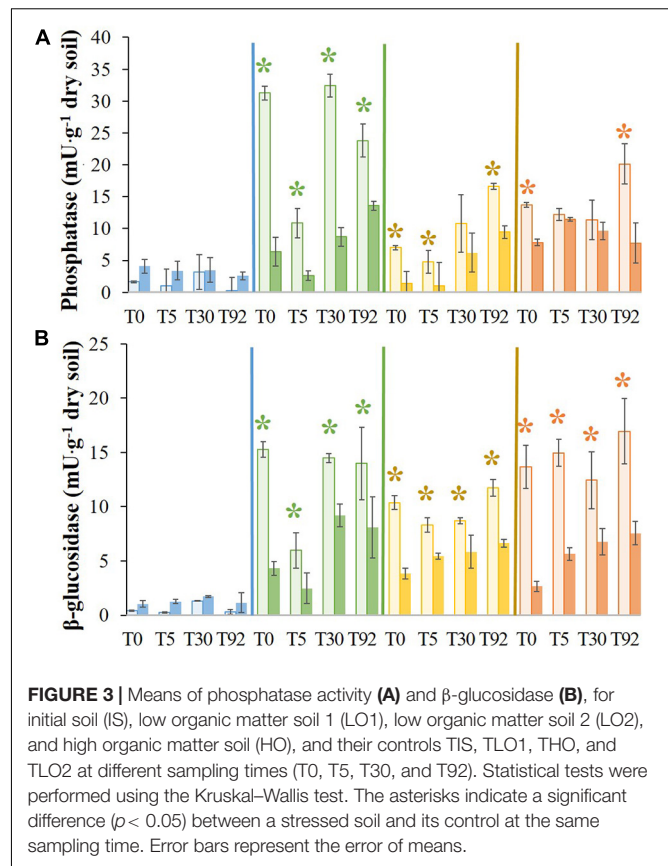
Samples	pH	Total C (g·kg <sup>-1</sup> )	TOC (g·kg <sup>-1</sup> )	Total N (g·kg <sup>-1</sup> )	C/N	Total H (g·kg <sup>-1</sup> )	N-NH <sub>4</sub> (mgN-NH <sub>4</sub> ·kg <sup>-1</sup> )	N-NO <sub>3</sub> (mgN-NO <sub>3</sub> ·kg <sup>-1</sup> )
IS	9.1±0.0a	3±0.0a	3.7±0.5d	0.6±0.0c	6.3±0.1ab	1.8±0.1d	5±0.8b	6.9±0.1b
LO1	7.6±0.1d	1.1±0.0b	8.4±0.1b	1.6±0.1a	5.2±0.3b	3.5±0.1b	5.4±0.9b	17.7±0.1a
LO2	7.8±0.0c	0.95±0.3c	7.7±0.2c	1.3±0.2b	5.7±0.7b	3±0.3c	29±5a	10.4±0.3ab
HO	8±0.0b	3±0.3a	25±3a	1.5±0.2a	16.1±1.7a	3.9±0.2a	25±3.5a	14±0.2a

Sample names refer as follows: initial soil (IS), low organic matter (LO1), low organic matter 2 (LO2), high organic matter (HO). Mean values and error of means are indicated; C, N, and H measurements were carried out for six replicates while other parameters are in triplicates. Significant differences found using the Kruskal–Wallis test are indicated with different letters.



at T0 (**Figure 2C**). However, 5 days (T5) after rewetting the soils, bacterial abundance decreased significantly for the IS, LO1, and HO soils ( $\sim 4$ -fold) compared to controls and LO2 was less affected ( $\sim 2$ -fold decrease). At T30, 16S rRNA gene abundance was still significantly lower in stressed soils than in the controls, except for HO. At the final sampling time T92, 16S rRNA gene abundance was approximately the same as controls in all soils except for IS where it was still significantly lower. Finally, results showed that 16S rRNA gene abundance had a tendency to decrease with the incubation time, as abundances were significantly lower at T92 compared to T0 for all soils.

After the stress at T0, phosphatase activities in LO1, HO, and LO2 decreased significantly ( $\sim 5$ -,  $\sim 2$ -, and  $\sim 5$ -fold, respectively) compared to the controls TLO1, THO, and TLO2 (**Figure 3A**).



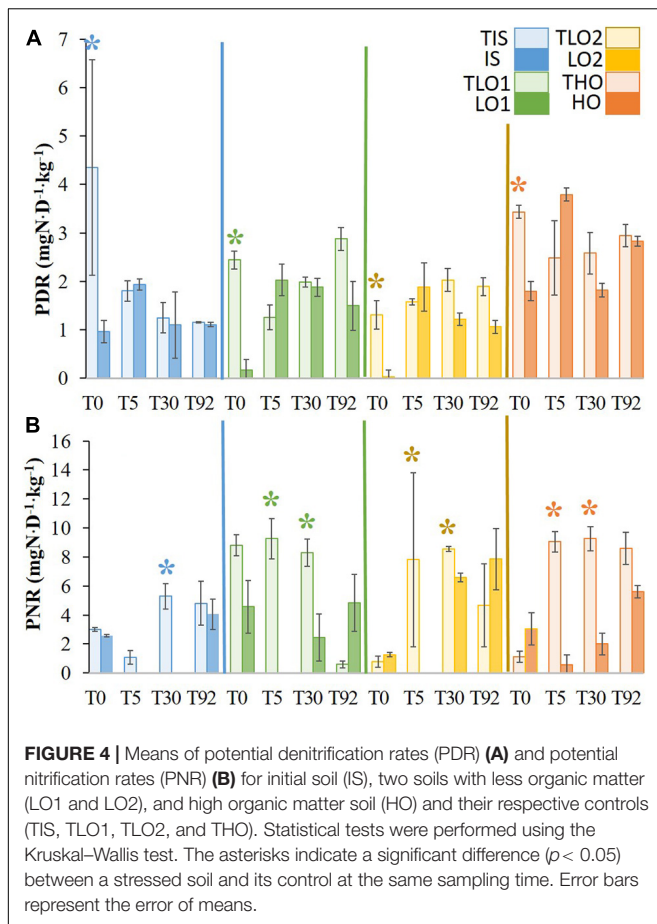
On the contrary, activity increased significantly ( $\sim 2.5$ -fold) compared to its control TIS. At T5, 5 days after rewetting the stressed soils, phosphatase activities in LO1 and LO2 remained significantly lower ( $\sim 4$ - and  $\sim 5$ -fold, respectively) than controls TLO1 and TLO2. On the contrary, no significant differences were found between IS and HO and their controls TIS and THO at T5. Furthermore, only one significant difference was found at T30 which was LO1 being lower than TLO1 ( $\sim 4$ -fold). In all stressed soils at T92, phosphatase activities were significantly lower than in controls at T92 except for IS. IS showed the lowest activity compared to other soils.

Results presented in **Figure 3B** show that at T0,  $\beta$ -glucosidase activities in LO1, LO2, and HO were significantly lower ( $\sim 3.5$ -,  $\sim 3$ -, and  $\sim 5$ -fold, respectively) than the controls TLO1, TLO2, and THO. Then, the  $\beta$ -glucosidase activity in these soils remained significantly lower than in controls all along the experiment at T5 ( $\sim 2.4$ -,  $1.5$ -, and  $2.6$ -fold, respectively), T30 ( $\sim 6$ -,  $1.5$ -, and  $2$ -fold, respectively), and T92 ( $1.1$ -,  $1.7$ -, and  $2.2$ -fold, respectively). In contrast, no significant differences were found for IS between controls and treatments after stress, although its activity was the lowest compared to other soils.

### Changes in Denitrification and Nitrification Functions

After the stress, PDR decreased significantly in all soils compared to the respective controls (**Figure 4A**). Five days after the stress and rewetting (T5), all previously affected soils recovered PDR at the same order of magnitude as their respective controls.



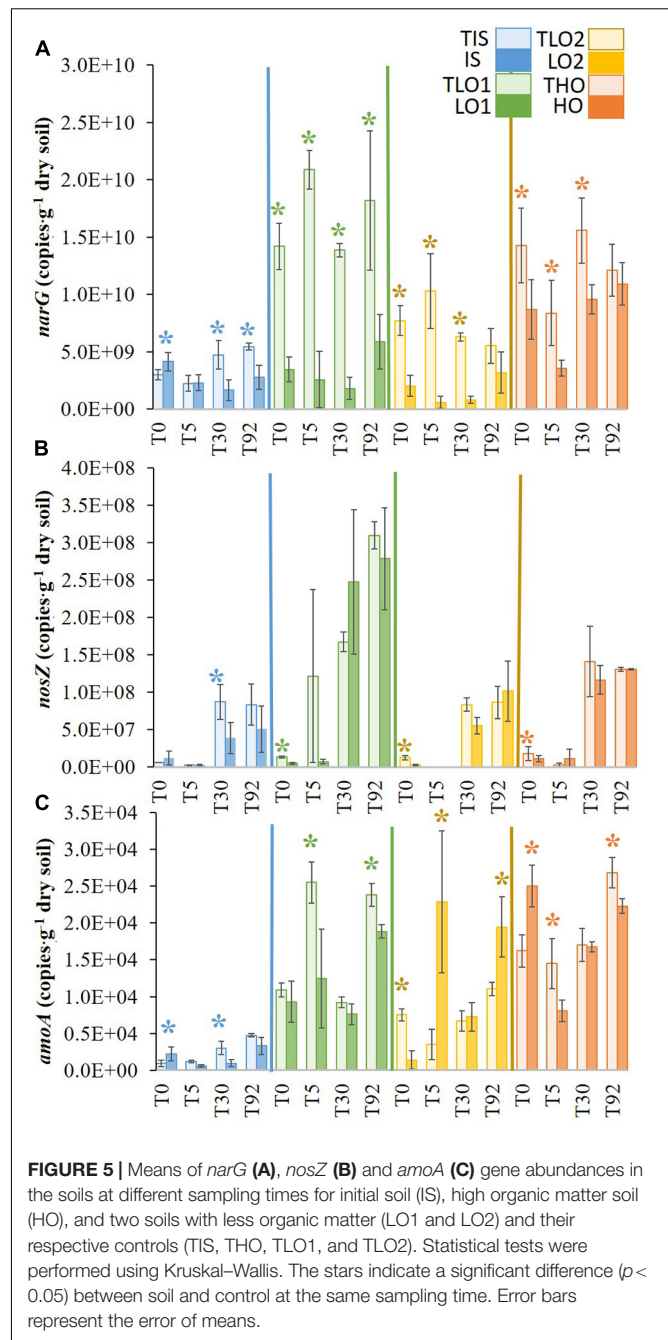


Furthermore, no significant differences in PDR were found between soils and controls at T30 and T92 either.

At T0 just after the stress, no significant differences in PNR were found between treatments and controls (Figure 4B). After rewetting (T5), PNR decreased significantly for all stressed soils compared to controls except for IS. PNR were significantly lower in stressed soils, compared to controls at T30 for all soils. At T92, no significant differences in PNR were found between stressed soils and controls.

### Changes in Denitrifying and Nitrifying Microbial Communities

At T0, the stress significantly decreased the *narG* gene copy abundances in LO1, LO2, and HO soils (~4-, 7-, and 1.6-fold, respectively) compared to controls TLO1, TLO2, and THO (Figure 5A). In contrast, the stress significantly increased the abundance of *narG* gene copies in IS at T0 (~1.3-fold) compared to control TIS. Five days after rewetting at T5, *narG* gene abundances for all soils were significantly lower than controls except for IS. Thirty days after the stress period (T30), *narG* gene abundances were significantly lower than controls in all soils. At the final sampling time T92, *narG* gene copy numbers in IS and LO1 were significantly lower (~2- and 3-fold, respectively) than controls TIS and TLO1. In contrast, no



significant differences were found between HO, LO2, and their controls THO and TLO2 at T92.

Although *nosZ* gene copy abundances were low in all soils at T0, significant differences were found between the stressed soils and their controls for LO1, HO, and LO2 (~2.6-, 1.6-, and 4.6-fold, respectively) compared to controls TLO1, THO, and TLO2 (Figure 5B). Five days after rewetting (T5), no significant differences were found between soils and controls. Thirty days after the stress (T30), *nosZ* gene abundance in IS was significantly lower (~2-fold) than the control TIS, whereas no significant differences were found between all other soils and controls at



T30. At the final sampling time T92, no significant differences were found between treatments and controls for all soils. The results showed that *nosZ* gene abundances were significantly higher at T30 and T92 compared to T0 and T5 and that the number of *nosZ* gene copies increased significantly after T5 for all soils and controls.

After the stress period at T0, both IS and HO had significantly higher (~2- and 1.5-fold, respectively) *amoA* gene abundances than controls TIS and THO. No significant difference was found between TLO1 and LO1, while LO2 was significantly lower (~2-fold) than TLO1 (**Figure 5C**). Five days after rewetting (T5), *amoA* gene abundances were significantly higher compared to controls for LO2 (~6-fold) whereas they were lower for LO1 and HO (~2- and 1.8-fold, respectively) and not significantly different for IS. Thirty days after the stress (T30), *amoA* gene abundances were significantly lower (~3-fold) than controls in IS, whereas no significant differences were observed for the other soils. At the final sampling date (T92), *amoA* gene abundances were significantly higher than controls for LO2 (~2-fold) whereas they were comparable to controls for LO1, HO and IS.

## Principal Component Analysis of Biological Parameters

PCA was carried out on the following parameters: PDR, PNR, phosphatase activity (Phos),  $\beta$ -glucosidase activity ( $\beta$ -Glu), BR, BM, and *nosZ*, *narG*, *amoA*, and 16S rRNA gene abundances for all soils at all sampling times. Results indicated that PC1 and PC2 accounted for 43.8% of the total variance (**Figure 6**). THO and TLO2 soils were positioned on the right side of PC1, mainly explained by *narG* gene abundances, Phos and PNR. The PCA also showed that the positions of soils and controls at T0 tended to be in the lower part of the plot along the second axis, whereas soils and controls from other sampling times (T5, T30, and T92) were positioned higher up along the second axis, which is mainly driven by 16S rRNA gene abundances, MB and  $\beta$ -Glu (**Figure 6**). No clear correlations between PNR, PDR, and corresponding *amoA* gene abundances and *nosZ* and *narG* gene abundances could be distinguished from the PCA. Furthermore, linear regressions (data not shown) did not demonstrate any significant correlations either between PDRs and functional gene abundances (*narG* and *nosZ*), or between PNR and *amoA* gene abundances.

## DISCUSSION

### Heat and Drought Stress Affected Carbon Mineralization and Nutrient Dynamics on the Short Term

#### Carbon Mineralization and Phosphate Dynamics Were Not Resistant to Stress

The microbial process of carbon mineralization, which contributes to the ecological function of organic matter stock and dynamics, was evaluated by measuring microbial MB, bacterial abundance, soil respiration, and  $\beta$ -glucosidase activity and

generally decreased following heat and drought stress. Microbial biomass was measured using MB, the quantity of DNA extracted from soil which is an indicator of the biological state of an environment (Dequiedt et al., 2011; Bouchez et al., 2016) and was durably impacted by stress in the present study. BR was the most affected in LO1 and LO2 after the stress period (T0). Previous work made similar observations where heat and drought stress drastically affected BR in French agricultural soils (Bérard et al., 2012), in tropical soils, and in Australian agricultural soils (Liang et al., 2014; Yu et al., 2014, respectively). The reasons behind this decrease may be a physiological effect on microorganisms, as drought can cause cell desiccation and lysis (Göransson et al., 2013), or the thermal denaturation of microbial enzymes (Bérard et al., 2011). However, bacterial abundance appeared to increase in all soils directly after stress (T0) which was in contradiction with the other results.  $\beta$ -Glucosidase is an enzyme responsible for the breakdown of several forms of carbohydrates, especially cellulose, which make its role fundamental for nutrient availability and cycling (Singhania et al., 2013). Compared to their respective controls,  $\beta$ -glucosidase activity ( $\beta$ -glu) decreased significantly after the stress (T0) in all soils except IS, indicating a low resistance of this enzymatic activity to heat and drought stress. Our results are comparable to other authors who have also reported a decrease in soil  $\beta$ -glu due to drought stress in Mediterranean grasslands and subtropical Acrisol (Sardans and Peñuelas, 2005; Liang et al., 2014, respectively), grass plantations (Sanaullah et al., 2011), and Mediterranean semiarid soils (Hueso et al., 2011). Heat and drought stress can induce a critical situation for soil microbial communities causing cell death, and thus an alteration of enzymatic activities involved in C-cycling (Lamersdorf et al., 1998).

Phosphatase activity is involved in the transformation of phosphorous compounds (Amador et al., 1997), and its activity is essential in P-cycling. Its activity contributes to the process of phosphate cycling and the ecological function of nutrient availability to plants and soil organisms. Phosphatase activities were significantly lower in all soils at T0 in the stressed soils compared to the controls except in IS, showing a low resistance of the activity to drought and heat stress. These findings are in accordance with studies showing that experimental drought stress reduced alkaline phosphatase activity in *Quercus ilex* Mediterranean forest soils (Sardans et al., 2008) and in Mediterranean terrestrial ecosystems (Sardans and Peñuelas, 2005).

Thus, heat and drought stress impacted microbial functions involved in carbon mineralization and phosphate dynamics in rehabilitated urban soils, demonstrating the vulnerability of these soils.

### Carbon Mineralization and Phosphate Dynamics' Resilience to Stress

The following sampling times, T5, T30, and T92 after soil rewetting, enabled to monitor the bacterial communities' resilience to the heat and drought stress for the different ecological functions. Overall, except for MB in LO1, carbon mineralization was resilient for MB, BR, and bacterial abundance after 92 days, as was found by Bérard et al. (2012), in which BR

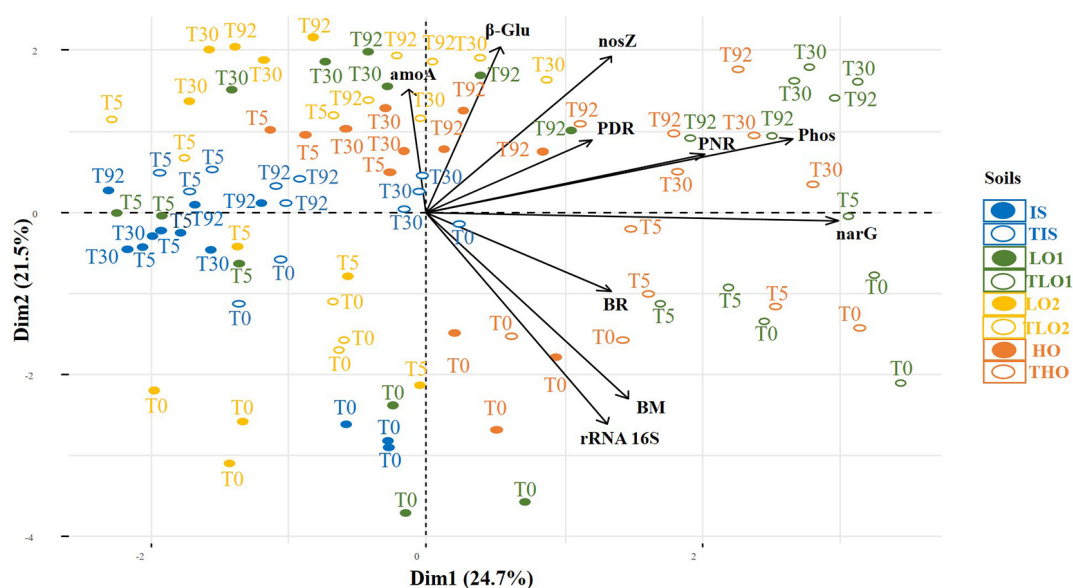


**FIGURE 6 |** Principal component analysis (PCA) of soil initial soil (IS), two soils with less organic matter (LO1 and LO2), and high organic matter soil (HO), and their respective controls (TIS, THO, TLO1, and TLO2), at different sampling times (T0, T5, T30, and T92). The data analyzed are PNR (potential nitrification rates), PDR (potential denitrification rates), BR (basal respiration), phosphatase and  $\beta$ -glucosidase activities, MB (molecular biomass), phosphatase and *nosZ*, *narG*, and *amoA* gene abundances.

recovered after 96 days. Microorganisms have evolved defense mechanisms allowing them to recover after perturbation. Some heat-tolerant bacteria like *Actinobacteria* can survive desiccation stress by increasing synthesized ribosomes to grow quickly once conditions become favorable (Barnard et al., 2013). This could have been the case for our soils as microorganisms could have adopted this preparation strategy, accelerated their cell division, and increased their biomass after re-humidification. The *Firmicutes* phylum also includes bacteria with heat and drought tolerance mechanisms (De Vos et al., 2009). Additionally, if bacteria from phyla such as *Firmicutes* and *Actinobacteria* were favored during the stress period, this may explain the increase in the copy numbers of the gene coding for 16S rRNA as both these phyla have been shown to possess multiple copies of this gene in their genome (Sun et al., 2013; Větrovský and Baldrian, 2013).

However, the heat and drought stress irreversibly altered  $\beta$ -glu and phosphatase activities. Previous studies have reported that drought can strongly limit enzymatic activities (Henry, 2013; Siebielec et al., 2020). In a previous study involving a heat stress (50°C),  $\beta$ -glu activity decreased by twofold in French agricultural soils (Riah-Anglet et al., 2015), which is somewhat comparable with HO where the activity decreased by 1.7-fold. Drought also reduced phosphatase activity in forest soils in Spain (Sardans and Peñuelas, 2010). This could be explained by the fact that heat stress can cause a decrease in enzyme synthesis and secretion (Allison, 2005). Our results showed that with the exception of IS, none of the soil  $\beta$ -glu and phosphatase activities had recovered after 92 days. Siebielec et al. (2020) found more contrasting results as phosphatase activity had a full recovery in loamy agricultural soils after a 1-month drought period.

Although microbial functions involved in carbon cycling and phosphate dynamics were poorly resistant to the drought and temperature stress, they appeared to recover rapidly as discussed. However, future work could question how many stress events such soils could support before irreversibly affecting these functions, in turn altering nutrient availability and disrupting the cycling of essential elements.

### Organic Matter Contents in the Rehabilitated Soils and Acclimation in Existing Soils Could Explain the Resilience of Carbon Mineralization

IS was the initial, un-rehabilitated soil and did not undergo any modifications during the initial REBU project. Therefore, although overall biomass and activities were lower in this soil compared to the others, its intrinsic microbial communities could be more adapted to drought and heat conditions by regularly undergoing seasonal changes. Similar findings were reported in a study where heat and drought stress (21-day period) had less impact on the BR of soils that were pre-exposed to stress, compared to those which were not pre-exposed in French agricultural soils (Bérard et al., 2012). Furthermore, it has already been evidenced that for soil microbial communities, a preselection by drying and rewetting reduces the impact of additional drought stress (Fierer et al., 2003; Williams, 2007; Bouskil et al., 2013; Zeglin et al., 2013; Wang et al., 2014; Bérard et al., 2015). This is probably because drought causes changes in the ecophysiology of microbial communities, and a pre-exposure to stress favored a fraction of microbial communities best adapted to heat and drought conditions (Anderson and Domsch, 1985, 1993).

Soil HO showed the highest total organic carbon content (Table 2). On the contrary to LO1 and LO2, HO's BR was not affected by heat and drought stress. This might be explained by its higher content of available C making microbial communities more resistant to stress (Sanaullah et al., 2011; Canarini et al., 2017). It is known that organic C is an important driver of BR in soils (Romero-Freire et al., 2016), and drought affects soil processes indirectly by altering the substrate's availability to microorganisms (Schimel, 2018). This can be explained by the decline of diffusion rates when drought increases, as microorganisms become resource deprived which limits their capacity of using acclimation methods that require carbon and energy (Schimel et al., 2007). This suggestion is further supported by the fact that HO's MB was resistant to drought, in contrast to LO1 and LO2, which declined. This can be explained by microorganisms resorting to dormancy to avoid stress, therefore reducing growth efficiency and allocating more resources to survival instead of reproduction (Schimel et al., 2007). Higher organic matter content in soil can improve water retention, therefore mitigating water availability for microorganisms. In a study conducted in US maize fields, results showed that higher organic matter content in soils was associated with higher crop yields. Analyses indicated that this positive association of soil organic matter and yields is partially explained by positive effects of soil OM on available water capacity (Kane et al., 2021). This is crucial for microbial survival as water loss can cause a loss of cell turgor (Harris, 2015), which can be catastrophic for microorganisms and result in interferences with physiological functions, reduce metabolic processes, and eventually lead to cell death (Schimel, 2018).

In turn, low organic matter contents could affect other soil microbial processes such as phosphatase activity and nutrient availability (Bonmati et al., 1991; Olander and Vitousek, 2000), which could explain the overall low values of phosphatase activity in IS, correlating with the low N and TOC values, whereas HO's phosphatase activity was resilient. IS also had the lowest  $\beta$ -glu activity compared to other soils, which might be due to less available organic substrates for  $\beta$ -glu such as cellulose (Hueso et al., 2011). This finding is in accordance with other studies where the increase in organic carbon enhanced soil  $\beta$ -glu activity (Eivazi and Tabatabai, 1990; Piotrowska and Koper, 2010).

## Nitrogen Cycling Processes

### Denitrification and Nitrification Were Affected Differently by Drought and Heat Stress

#### Denitrification Activities Were More Rapidly Resilient Than Gene Abundance

The effects of drought and heat stress on the nitrogen cycle were evaluated by determining both the nitrification and denitrification potentials in soils and the abundances of functional genes involved in soil N-cycling. All stressed soils showed low resistance for PDRs to drought and heat stress. Many studies have shown that drought decreases the denitrification process in different terrestrial ecosystems like tropical forests (Almaraz et al., 2019), grasslands (Hartmann et al., 2013; Keil

et al., 2015), and agricultural fields (Homyak et al., 2017). However, even though they were impacted by the stress, PDR in all soils recovered quickly after rewetting and were resilient in the short, mid, and long terms (T5, T30, and T92). Denitrifying enzymes originate from an enzyme pool known to be tolerant of extended drought periods, which would explain the rapid recovery of the denitrification process after rewetting (Peterjohn, 1991). A recent experiment on a managed grassland, conducted by Harris et al. (2021), also monitored an increase in  $N_2O$  fluxes that the authors attributed to denitrification when rewetting the soils after a drought period. Davidson (1992) reported that denitrification could be resilient in response to drought stress as it can be activated within minutes to hours after soil rewetting and the flush of available C and N caused by the rewetting of stressed soils can lead to the resuscitation of dormant denitrifiers (Six et al., 2002). Another sign that the denitrifying bacterial communities were affected by stress was the decrease at T0 of the abundances of *narG* and *nosZ* genes in LO1, HO, and LO2. Unlike PDR, the abundances of genes involved in denitrification were not resilient at T5 and T30 following rewetting. Consequently, during extreme dry conditions, we might expect a decrease in denitrification and denitrifying bacterial populations as shown by Bremner and Blackmer (1978) and later by Butterbach-Bahl and Dannenmann (2011). However, in the present study we chose to monitor *narG* and *nosZ* gene copy numbers as indicators of the impact of the heat and drought stress on denitrification, although other genes are also key functional markers of denitrification; in particular, *nirK* and *nirS* genes play an important role in an intermediary step of denitrification, the production of NO which is rapidly further reduced to  $N_2O$ . These two genes are in the genome of nitrite-reducing denitrifiers, which consists of a highly phylogenetically diverse functional guild (Wei et al., 2015; Bonilla-Rosso et al., 2016). Thus, the resilience of PDR in our experiment could be attributed to nitrite-reducing activity, implying that it was the final denitrification step and reduction of  $N_2O$  to  $N_2$  that was highly impacted by the stress. Further work would enable to specifically distinguish impacts of heat and drought stress on the different steps of the denitrification process.

#### Nitrification Activities Were Resistant, as Were Gene Abundances

PNR showed no significant differences between stressed soils and controls for all soils at T0, suggesting that the nitrifying communities in all soils were resistant to stress. Hartmann et al. (2013) reported similar findings in grassland soils where PNR were not affected by drought in experimental plots where precipitations were blocked for 41 days. Furthermore, nitrification potentials were reported to be higher in dry and hot summer seasons compared to wet seasons in grasslands in California United States (Parker and Schimel, 2011). Drought actually increased the abundance of *amoA* genes in IS soil, which is in accordance with Bremner and Blackmer (1978) and Kaurin et al. (2018), who reported that during extreme conditions an increase in nitrifiers and nitrification is expected. Davidson (1992) also reported drought-resistant nitrifying microbial communities that are adapted to survive long dry



summer seasons in grasslands. However, PNR in LO1 and HO decreased significantly 5 days after rewetting (T5), which is in accordance with results reported by Tan et al. (2018) showing that nitrification rates decreased significantly with soil moisture increase, contrarily to denitrification that increases with moisture. However, overall *amoA* gene abundances in soils were lower than abundances reported by other studies in German arable soil and in rice paddy fields (Radl et al., 2015; Zhang et al., 2018, respectively). This may be due to the domination of nitrifying archaeal over bacterial groups especially under drought conditions in arable soils (Radl et al., 2015) and in urban soils (Wang et al., 2017). In contrast, our results were somewhat comparable to mountain abandoned meadow soils (Fuchslueger, 2014). Overall the N-cycling function seemed less affected by stress than the C-cycling and the phosphate dynamics-function as PDR was resilient and PNR was resistant.

### No Significant Correlations Were Found Between Soil N-Cycling Processes and Functional Genes Abundances

In the present study, we found no significant correlations between *narG* and *nosZ* functional genes abundances and corresponding N-cycling functions (data not shown). Although some studies have found that denitrifier and nitrifier community compositions are important factors in the regulation of denitrification and nitrification processes (Petersen et al., 2012; Zhang et al., 2017, 2018; Zhang and Ji, 2018), others did not suggest any relationship between the two (Hallin et al., 2009; Attard et al., 2011; Graham et al., 2014). One likely reason for these differences is that many microorganisms carry denitrification genes at any given moment but only a subset of the total community is active and carries out denitrification. Another reason for the lack of a relationship in the present work could be the interference of other parameters such as abiotic characteristics, environmental conditions, or the lack of data to show a clear trend. In a study conducted by Graham et al. (2016), the authors suggested that N-cycling processes are more driven by the edaphic characteristics of soils than by the abundances of functional genes in tropical rainforest soil samples using only edaphic factors. In addition, models containing only edaphic factors data explained N-cycling variation more than models using both gene abundance data. Rocca et al. (2015) published a review where they conducted a meta-analysis of the relationships between gene abundances and corresponding process rates linked to the C- or N-cycling. Authors reported that within the 59 chosen studies, there was a significant but weak positive relationship between gene abundance and the corresponding process ( $r = 0.3$ ,  $p < 0.0001$ ,  $n = 189$ ) using the Pearson product-moment test. They analyzed studies exclusively using gene abundances measured by qPCR and including the bacterial *amoA* gene in relation to nitrification, and *narG* and *nosZ* genes to denitrification. Thus, the non-significant correlations found in our study might also be due to dataset dimensions. Again, further analysis of other functional genes encoding different steps of nitrogen cycling, such as *nirK* and *nirS* as mentioned previously, could bring more insight on the links between activity measurements and potentials.

## CONCLUSION—THE PROS AND CONS OF SOIL REHABILITATION ON CARBON MINERALIZATION AND NITROGEN CYCLING

Heat and drought stress affected both carbon mineralization and phosphate dynamics by altering soil respiration and microbial enzymatic activities, in some cases causing irreversible shifts in the activity's state. This is probably due to stress causing cell desiccation, lysis, and thermal denaturation of enzymes. Soil respiration showed resilience after 96 days, possibly due to desiccation-resistant bacteria such as *Actinobacteria* or *Firmicutes*. Furthermore, the non-rehabilitated soil IS showed resistance of microbial activity involved in nutrient cycling functions, suggesting a previous adaptation of its microbial communities to drought and heat stress as the soil was not rehabilitated. Thus, it can be suggested that an initial soil could be more resistant and resilient in terms of soil functioning as its microbial communities may have acquired a greater flexibility to environmental conditions. However, this soil is characterized with a low level of activity compared to other soils, which highlights the importance of organic matter contents in stimulating microbial activities. Furthermore, microbial activities involved in carbon cycling and nutrient availability in HO were more resilient to stress than LO1 and LO2, highlighting this rehabilitation trajectory as the most optimal on the short term. Our findings highlight the importance of organic matter content and pre-exposition to stress in determining the performance of soil carbon cycling and phosphate dynamics in rehabilitated urban soils.

Microbial activities and genetic potentials regarding processes involved in nitrogen cycling were more resilient. Denitrification processes were sensitive to heat and drought as they decreased significantly in all soils following the stress. However, they recovered quickly due to the resilience of denitrification enzymes and their tolerance to drought. Furthermore, denitrifying bacterial communities were also affected by stress as *narG* and *nosZ* gene abundances decreased significantly but did not recover after rewetting, suggesting that rewetting soils either boosts denitrifying communities' activity, not abundance, or boosts nitrite-reducing denitrifiers increasing  $N_2O$  production but not  $N_2$ . Further measurements of *nirK* and *nirS* gene abundance, which encode nitrite reduction, are required to elucidate this. In contrast, PNR were not affected by stress, and nitrifying bacterial communities showed resistance to stress as *amoA* gene abundances were not affected. Moreover, no correlations were found between functional gene abundances and corresponding denitrification and nitrification rates, which is probably due to the interference of other environmental parameters or simply because of our dataset dimensions.

In conclusion, although the poor initial state of the existing soil IS was confirmed by the low activities we measured, it was resistant and resilient to the heat and drought stress, probably due to its pre-exposure to these stress *in situ*. Among the



rehabilitation solutions tested in the present study, i.e., either an organic-matter-rich technosol (HO) or a less rich organic-matter technosol (LO1 and LO2), although the LO soils were the cheaper option, they suffered more from the heat and drought stress, suggesting that even though the initial cost was more important for HO, it may be the better solution on the long run. Also, considering the LO1 and LO2 soils, it appeared that globally in the control soils during the experiment, LO1 activities and gene abundances were overall higher than in LO2 control soils. Future work is required to understand the impact of the types of plants seeded on site on these differences. Finally, an in-between solution may be to amend the IS with organic matter or adapted seeds and microbial inoculation as the bacterial communities in this soil are already resistant and resilient to temperature and drought stress.

## DATA AVAILABILITY STATEMENT

The raw data supporting the conclusions of this article will be made available by the authors, without undue reservation.

## REFERENCES

- Allison, S. D. (2005). Cheaters, diffusion and nutrients constrain decomposition by microbial enzymes in spatially structured environments. *Ecol. Lett.* 8, 626–635. doi: 10.1111/j.1461-0248.2005.00756.x
- Almaraz, M., Groffman, P. M., and Porder, S. (2019). Effects of changes in nitrogen availability on nitrogen gas emissions in a tropical forest during a drought. *J. Geophys. Res. Biogeosci.* 124, 2917–2926. doi: 10.1029/2018JG004851
- Amador, J., Glucksman, A., Lyons, J., and Görres, J. (1997). Spatial distribution of soil phosphatase activity within a riparian forest. *Soil Sci.* 162, 808–825. doi: 10.1097/00010694-199711000-00005
- Anderson, T., and Domsch, K. H. (1985). Determination of ecophysiological maintenance carbon requirements of soil microorganisms in a dormant state. *Biol. Fertil. Soils* 1, 81–89. doi: 10.1007/BF00255134
- Anderson, T. H., and Domsch, K. H. (1993). The metabolic quotient for CO<sub>2</sub> (qCO<sub>2</sub>) as a specific activity parameter to assess the effects of environmental conditions, such as pH, on the microbial biomass of forest soils. *Soil Biol. Biochem.* 25, 393–395. doi: 10.1016/0038-0717(93)90140-7
- Attard, E., Recous, S., Chabbi, A., Berranger, C., Guillaumaud, N., Labreuche, J., et al. (2011). Soil environmental conditions rather than denitrifier abundance and diversity drive potential denitrification after changes in land uses. *Glob. Chang. Biol. Bioenergy* 17, 1975–1989. doi: 10.1111/j.1365-2486.2010.02340.x
- Bapiri, A., Bååth, E., and Rousk, J. (2010). Drying–rewetting cycles affect fungal and bacterial growth differently in an arable soil. *Microb. Ecol.* 60, 419–428. doi: 10.1007/s00248-010-9723-5
- Barnard, R. L., Osborne, C. A., and Firestone, M. K. (2013). Responses of soil bacterial and fungal communities to extreme desiccation and rewetting. *ISME J.* 7, 2229–2241. doi: 10.1038/ismej.2013.104
- Bérard, A., Ben Sassi, M., Kaisermann, A., and Renault, P. (2015). Soil microbial community responses to heat wave components: drought and high temperature. *Clim. Res.* 66, 243–264. doi: 10.3354/cr01343
- Bérard, A., Boucher, T., Sévenier, G., Pablo, A. L., and Gros, R. (2011). Resilience of soil microbial communities impacted by severe drought and high temperature in the context of Mediterranean heat waves. *Eur. J. Soil Sci.* 47, 333–342. doi: 10.1016/j.ejsobi.2011.08.004
- Bérard, A., Bouchet, T., Sévenier, G., Pablo, A. L., and Gros, R. (2012). Severe drought-induced community tolerance to heat wave. An experimental study on soil microbial processes. *J. Soils Sediments* 12, 513–518. doi: 10.1007/s11368-012-0469-1
- Bonilla-Rosso, G., Wittorf, L., Jones, C. M., and Hallin, S. (2016). Design and evaluation of primers targeting genes encoding NO-forming nitrite reductases:

## AUTHOR CONTRIBUTIONS

MF, CJ, MM-H, M-PN, and JH: conceptualization, methodology, validation, writing—review and editing, and supervision. MF and M-PN: experiment, sampling, microbiological analysis, and investigation. MF: writing original draft preparation and data curation. CJ, MM-H, and JH: project administration and funding acquisition. All authors have read and agreed to the published version of the manuscript.

## FUNDING

The research was supported by a Ph.D. grant accorded to MF and co-financed by the ADEME and the BRGM.

## SUPPLEMENTARY MATERIAL

The Supplementary Material for this article can be found online at: <https://www.frontiersin.org/articles/10.3389/fmicb.2021.727468/full#supplementary-material>

- implications for ecological inference of denitrifying communities. *Sci. Rep.* 6:39208. doi: 10.1038/srep39208
- Bonmati, M., Ceccanti, B., and Nanniperi, P. (1991). Spatial variability of phosphatase, urease, protease, organic carbon and total nitrogen in soil. *Soil Biol. Biochem.* 23, 391–396. doi: 10.1016/0038-0717(91)90196-Q
- Bouchez, T., Blieux, A. L., Dequiedt, S., Domaizon, I., Dufresne, A., Ferreira, S., et al. (2016). Molecular microbiology methods for environmental diagnosis. *Environ. Chem. Lett.* 14, 423–441.
- Bouskil, N., Lim, H. C., Borglin, S., Salve, R., Wood, T. E., Silver, W. L., et al. (2013). Pre-exposure to drought increases the resistance of tropical forest soil bacterial communities to extended drought. *ISME J.* 7, 384–394. doi: 10.1038/ismej.2012.113
- Bremner, J. M., and Blackmer, A. M. (1978). Nitrous oxide: emission from soils during nitrification of fertilizer nitrogen. *Science* 199, 295–296. doi: 10.1126/science.199.4326.295
- Bru, D., Sarr, A., and Philippot, L. (2007). Relative abundances of proteobacterial membrane-bound and periplasmic nitrate reductases in selected environments. *Appl. Environ. Microbiol.* 73, 5971–5974. doi: 10.1128/aem.00643-07
- Butterbach-Bahl, K. B., and Dannenmann, M. (2011). Denitrification and associated soil N<sub>2</sub>O emissions due to agricultural activities in a changing climate. *Curr Opin Environ Sustain* 3, 389–395. doi: 10.1016/j.cosust.2011.08.004
- Campbell, C., Chapman, S., and Davidson, M. (2003). A rapid microtiter plate method to measure dioxide evolved from carbon substrate amendments so as to determine the physiological profiles of soil microbial communities by using whole soil. *Appl. Environ. Microbiol.* 69, 3593–3599. doi: 10.1128/AEM.69.6.3593-3599.2003
- Canarini, A., Kier, L. P., and Dijkstra, F. A. (2017). ‘Soil carbon loss regulated by drought intensity and available substrate: a meta-analysis’. *Soil Biol. Biochem.* 112, 90–99. doi: 10.1016/j.soilbio.2017.04.020
- Carreiro, M. M., Pouyat, R., Tripler, C., and Zhu, W. X. (2009). *Carbon and Nitrogen Cycling in Soils of Remnant Forests Along Urban–Rural Gradients: Case Studies in the New York Metropolitan Area and Louisville, Kentucky, in Ecology of Cities and Towns: A Comparative Approach*. Cambridge: Cambridge University Press, 308–328. doi: 10.1017/CBO9780511609763.020
- CGDD (2015). Le point sur l’occupation des Sols en France, l’occupation des sols en France?: Progression plus Modérée de l’artificialisation Entre 2006 et 2012., (2019). Available online at: <https://www.actu-environnement.com/media/pdf/news-26026-soes-artificialisation-sols.pdf> (accessed April, 2019).

- Davidson, E. A. (1992). Sources of Nitric Oxide and Nitrous Oxide following Wetting of Dry Soil. *Soil Sci. Soc. Am. J.* 56, 95–102. doi: 10.2136/sssaj1992.03615995005600010015x
- De Noni, G., and Viennot, M. (1993). Mutations recentes de l'agriculture equatorienne et consequences sur la durabilite des agrosystemes andins. *Pédol* 28, 277–288.
- Dequiedt, S., Saby, N. P. A., Lelievre, M., Jolivet, C., Thioulouse, J., Toutain, B., et al. (2011). Biogeographical patterns of soil molecular microbial biomass as influenced by soil characteristics and management. *Glob. Ecol. Biogeogr.* 20, 641–652. doi: 10.1111/j.1466-8238.2010.00628.x
- De Vos, P., Garrity, G. M., Jones, D., Krieg, N. R., Ludwig, W., Rainey, F. A., et al. (2009). "The Firmicutes," in *Bergey's Manual of Systematic Bacteriology*, eds P. De Vos, G. M. Garrity, D. Jones, N. R. Krieg, W. Ludwig, F. A. Rainey, et al. (New York, NY: Springer).
- Fierer, N., Schimel, J. P., and Holden, P. A. (2003). Influence of drying – rewetting frequency on soil bacterial community structure. *Microb. Ecol.* 45, 63–71. doi: 10.1007/s00248-002-1007-2
- Fuchslueger, L. (2014). Effects of drought on nitrogen turnover and abundances of ammonia-oxidizers in mountain grassland. *Biogeosci. Discuss.* 11, 9183–9214. doi: 10.5194/bgd-11-9183-2014
- Gibelin, A. L., and Déqué, M. (2003). Anthropogenic climate change over the Mediterranean region simulated by a global variable resolution model. *Clim. Dyn.* 20, 327–339. doi: 10.1007/s00382-002-0277-1
- Gleeson, D. B., Müller, C., Banerjee, S., Ma, W., Siciliano, S. D., and Murphy, D. V. (2010). Response of ammonia oxidizing archaea and bacteria to changing water filled pore space. *Soil Biol. Biochem.* 42, 1888–1891. doi: 10.1016/j.soilbio.2010.06.020
- Göransson, H., Godbold, D. L., Jones, D. L., and Rousk, J. (2013). Bacterial growth and respiration responses upon rewetting dry forest soils: impact of drought-legacy. *Soil Biol. Biochem.* 57, 477–486. doi: 10.1016/j.soilbio.2012.08.031
- Graham, E. B., Knelman, J. E., Schindlbacher, A., Siciliano, S., Breulmann, M., Yannarell, A., et al. (2016). Microbes as engines of ecosystem function: when does community structure enhance predictions of ecosystem processes? *Front. Microbiol.* 7:214. doi: 10.3389/fmicb.2016.00214
- Graham, E. B., Wieder, W. R., Leff, J. W., Weintraub, S. R., Townsend, A. R., Cleveland, C. C., et al. (2014). Do we need to understand microbial communities to predict ecosystem function? A comparison of statistical models of nitrogen cycling processes. *Soil Biol. Biochem.* 68, 279–282. doi: 10.1016/j.soilbio.2013.08.023
- Griffiths, B. S., and Philippot, L. (2013). Insights into the resistance and resilience of the soil microbial community. *FEMS Microbiol. Rev.* 37, 112–129. doi: 10.1111/j.1574-6976.2012.00343.x
- Guillot, E., Hinsinger, P., Dufour, L., Roy, J., and Bertrand, I. (2019). With or without trees: resistance and resilience of soil microbial communities to drought and heat stress in a Mediterranean agroforestry system. *Soil Biol. Biochem.* 129, 122–135. doi: 10.1016/j.soilbio.2018.11.011
- Hallin, S., Jones, C. M., Schloter, M., and Philippot, L. (2009). Relationship between n-cycling communities and ecosystem functioning in a 50-year-old fertilization experiment. *ISME J.* 3, 597–605. doi: 10.1038/ismej.2008.128
- Harris, E., Diaz-Pines, E., Stoll, E., Schloter, M., Schulz, S., Duffner, C., et al. (2021). Denitrifying pathways dominate nitrous oxide emissions from managed grassland during drought and rewetting. *Sci. Adv.* 7:eabb7118. doi: 10.1126/sciadv.abb7118
- Harris, R. F. (2015). Effect of water potential on microbial growth and activity. *Water Potential Relat. Soil Microbiol.* 9, 23–95. doi: 10.2136/SSASPECPUB9.C2
- Hartmann, A. A., Barnard, R. L., Marhan, S., and Niklaus, P. A. (2013). Effects of drought and N-fertilization on N cycling in two grassland soils. *Oecologia* 171, 705–717. doi: 10.1007/s00442-012-2578-3
- Henry, H. A. L. (2013). Reprint of "Soil extracellular enzyme dynamics in a changing climate". *Soil Biol. Biochem.* 56, 53–59. doi: 10.1016/j.soilbio.2012.10.022
- Henry, S., Bru, D., Stres, S., Hallet, S., and Philippot, L. (2006). Quantitative detection of the *nosZ* gene, encoding nitrous oxide reductase, and comparison of the abundances of 16S rRNA, *narG*, *nirK*, and *nosZ* genes in soils. *Appl. Environ. Microbiol.* 72, 5181–5189. doi: 10.1128/AEM.00231-06
- Hobbie, S. E., Finlay, J. C., Janke, B. D., Nidzgorski, D. A., Millet, D. B., and Baker, L. A. (2017). Correction: contrasting nitrogen and phosphorus budgets in urban watersheds and implications for managing urban water pollution. *Proc. Natl. Acad. Sci. U.S.A.* 114, E4116. doi: 10.1073/pnas.1706049114
- Homyak, P. M., Allison, S. D., Huxman, T. E., Goulden, M. L., and Treseder, K. K. (2017). Effects of drought manipulation on soil nitrogen cycling: a meta-analysis. *J. Geophys. Res. Biogeosci.* 122, 3260–3272. doi: 10.1002/2017JG004146
- Hueso, S., Hernández, T., and García, C. (2011). Resistance and resilience of the soil microbial biomass to severe drought in semiarid soils: the importance of organic amendments. *Appl. Soil Ecol.* 50, 27–36. doi: 10.1016/j.apsoil.2011.07.014
- Hynes, H. M., and Germida, J. J. (2012). Relationship between ammonia oxidizing bacteria and bioavailable nitrogen in harvested forest soils of central Alberta. *Soil Biol. Biochem.* 46, 18–25. doi: 10.1016/j.soilbio.2011.10.018
- Jackson, E. L., Burger, C., and Cavnarno, T. R. (2008). Roots, nitrogen transformations, and ecosystem services. *Annu. Rev. Plant Biol.* 59, 341–363. doi: 10.1146/annurev.arplant.59.032607.092932
- Jia, Z., and Conrad, R. (2009). Bacteria rather than Archaea dominate microbial ammonia oxidation in an agricultural soil. *Environ. Microbiol.* 11, 1658–1671. doi: 10.1111/j.1462-2920.2009.01891.x
- Kane, D. A., Bradford, M. A., Fuller, E., Oldfield, E. E., and Wood, S. (2021). Soil organic matter protects US maize yields and lowers crop insurance payouts under drought. *Environ. Res. Lett.* 16:044018. doi: 10.1088/1748-9326/abe492
- Kaurin, A., Mihelič, R., Kastelec, D., Grčman, H., Bru, D., and Philipot, L. (2018). Resilience of bacteria, archaea, fungi and N-cycling microbial guilds under plough and conservation tillage, to agricultural drought. *Soil Biol. Biochem.* 120, 233–245. doi: 10.1016/j.soilbio.2018.02.007
- Keil, D., Niklaus, P. A., Von Riedmatten, L., Boeddinghaus, R. S., Dormann, C., and Scherer-Lorenzen, M. (2015). Effects of warming and drought on potential N<sub>2</sub>O emissions and denitrifying bacteria abundance in grasslands with different land-use. *FEMS Microbiol. Ecol.* 91, 1–9. doi: 10.1093/femsec/fiv066
- Lamersdorf, N. P., Beier, K. B., Black, K., Bredemeier, M., Cummins, T., Farrell, E. P., et al. (1998). Effect of drought experiments using roof installations on acidification/nitrification of soils. *For. Ecol. Manag.* 101, 95–109. doi: 10.1016/S0378-1127(97)00128-X
- Li, G., Sun, X. G., Ren, Y., Luo, X. S., and Zhu, Y. G. (2018). Urban soil and human health: a review. *Eur. J. Soil Sci.* 69, 196–215. doi: 10.1111/ejss.12518
- Li, X., Zhu, Y. G., Cavnarno, T. R., Chen, M., Sun, J., Chen, X., et al. (2009). Do ammonia-oxidizing archaea respond to soil Cu contamination similarly as ammonia-oxidizing bacteria? *Plant Soil.* 324, 209–217. doi: 10.1007/s11104-009-9947-7
- Liang, C., Zhu, X., Fu, S., Méndez, A., Gasco, G., and Ferreira, J. P. (2014). Biochar alters the resistance and resilience to drought in a tropical soil. *Environ. Res. Lett.* 9:064013. doi: 10.1088/1748-9326/9/6/064013
- Lorenz, K., and Lal, R. (2009). Biogeochemical C and N cycles in urban soils. *Environ. Int.* 35, 1–8. doi: 10.1016/j.envint.2008.05.006
- Nesper, M., Kueffer, C., Krishnan, S., Kushalappa, C. G., and Ghazoul, J. (2019). Simplification of shade tree diversity reduces nutrient cycling resilience in coffee agroforestry. *J. Appl. Ecol.* 56, 119–131. doi: 10.1111/1365-2664.13176
- Noe, G. B., and Hupp, C. R. (2005). Carbon, nitrogen, and phosphorus accumulation in floodplains of Atlantic Coastal Plain rivers, USA. *Ecol. Appl.* 15, 1178–1190. doi: 10.1890/04-1677
- Norton, J., and Ouyang, Y. (2019). Controls and adaptive management of nitrification in agricultural soils. *Front. Microbiol.* 10:1931. doi: 10.3389/fmicb.2019.01931
- Oke, T. R. (1989). Micromet urban forest. *R. Soc. Open Sci.* 324, 335–349. doi: 10.1098/rstb.1989.0051
- Olander, L. P., and Vitousek, P. M. (2000). Regulation of soil phosphatase and chitinase activity by N and P availability. *Biogeochemistry* 49, 175–190. doi: 10.1023/A:1006316117817
- Parker, S. S., and Schimel, J. P. (2011). Soil nitrogen availability and transformations differ between the summer and the growing season in a California grassland. *Appl. Soil Ecol.* 48, 185–192. doi: 10.1016/j.apsoil.2011.03.007
- Pascual Aguilar, J. A., Sanz García, J., de Bustamante Gutierrez, I., and Kallache, M. (2011). "Using environmental metrics to describe the spatial and temporal evolution of landscape structure and soil hydrology and fertility," in *Proceedings of the Spatial2: Spatial Data Methods for Environmental and Ecological processes*. (Foggia), 1–5.
- Peterjohn, W. T. (1991). Denitrification: enzyme content and activity in desert soils. *Soil Biol. Biochem.* 23, 845–855. doi: 10.1016/0038-0717(91)90096-3
- Petersen, D. G., Blazewicz, S., Firestone, M., Herman, D. J., Turetsky, M., and Waldrop, M. (2012). Abundance of microbial genes associated with

- nitrogen cycling as indices of biogeochemical process rates across a vegetation gradient in Alaska. *Environ. Microbiol.* 14, 993–1008. doi: 10.1111/j.1462-2920.2011.02679.x
- Philippot, L., Spor, A., Hénault, C., Bru, D., Bizouard, F., Jones, C. M., et al. (2013). Loss in microbial diversity affects nitrogen cycling in soil. *ISME J.* 7, 1609–1619. doi: 10.1038/ismej.2013.34
- Piotrowska, A., and Koper, J. (2010). Soil  $\beta$ -glucosidase activity under winter wheat cultivated in crop rotation systems depleting and enriching the soil in organic matter. *J. Elem.* 15, 593–600. doi: 10.5601/jelem.2010.15.3.593-600
- R Core Team (2018). *R: A Language and Environment for Statistical Computing*. Vienna: R Foundation for Statistical Computing. Available online at: <https://www.R-project.org/>
- Radl, V., Kindler, R., Welzl, G., Albert, A., Wilke, B. M., Amelung, W., et al. (2015). Drying and rewetting events change the response pattern of nitrifiers but not of denitrifiers to the application of manure containing antibiotic in soil. *Appl. Soil Ecol.* 95, 99–106. doi: 10.1016/j.apsoil.2015.06.016
- REBU (2016). Available online at: <moz-extension://d71dad57-548d-4ff9-b868-35ab0f8e7a51/enhanced-reader.html?openApp&pdf=https%3A%2F%2Fwww.ademe.fr%2Fsites%2Fdefault%2Ffiles%2Fassets%2Fdocuments%2Ffiche-laureat-rebu-valorhiz.pdf> (Accessed January 18, 2021).
- Riah-Anglet, W., Trinsoutrot-Gattina, I., Martin-Laurent, F., Laroche-Ajzenberga, E., Norinia, M.-P., Latour, X., et al. (2015). Soil microbial community structure and function relationships: a heat stress experiment. *Appl. Soil Ecol.* 86, 121–130. doi: 10.1016/j.apsoil.2014.10.001
- Rocca, J. D., Hall, E. K., Lennon, J. T., Evans, S. E., Waldrop, M. P., Cotner, J. B., et al. (2015). Relationships between protein-encoding gene abundance and corresponding process are commonly assumed yet rarely observed. *J. ISME* 9, 1693–1699.
- Romero-Freire, A., Sierra Aragon, M., Martínez Garzón, F. J., and Martín Peinado, F. J. M. (2016). Is soil basal respiration a good indicator of soil pollution? *Geoderma* 263, 132–139. doi: 10.1016/j.geoderma.2015.09.006
- Rothauwe, J. H., Witzel, K. P., and Liesack, W. (1997). The ammonia monooxygenase structural gene amoA as a functional marker: molecular fine-scale analysis of natural ammonia-oxidizing populations. *Appl. Environ. Microbiol.* 63, 4704–4712. doi: 10.1128/aem.63.12.4704-4712.1997
- Sanaullah, M., Blagodatskaya, E., Chabbi, A., Rumpel, C., and Kuzyakov, Y. (2011). Drought effects on microbial biomass and enzyme activities in the rhizosphere of grasses depend on plant community composition. *Appl. Soil Ecol.* 48, 38–44. doi: 10.1016/j.apsoil.2011.02.004
- Sardans, J., and Peñuelas, J. (2005). Drought decreases soil enzyme activity in a Mediterranean *Quercus ilex* L. forest. *Soil Biol. Biochem.* 37, 455–461. doi: 10.1016/j.soilbio.2004.08.004
- Sardans, J., and Peñuelas, J. (2010). Soil enzyme activity in a mediterranean forest after six years of drought. *Soil Sci. Soc. Am. J.* 74, 838–851. doi: 10.2136/sssaj2009.0225
- Sardans, J., Peñuelas, J., and Estiarte, M. (2006). Warming and drought alter soil phosphatase activity and soil P availability in a Mediterranean shrubland. *Plant Soil* 289, 227–238. doi: 10.1007/s11104-006-9131-2
- Sardans, J., Peñuelas, J., and Ogaya, R. (2008). Experimental drought reduced acid and alkaline phosphatase activity and increased organic extractable P in soil in a *Quercus ilex* Mediterranean forest. *Eur. J. Soil Biol.* 44, 509–520. doi: 10.1016/j.ejsobi.2008.09.011
- Schimel, J., Balser, T. C., and Wallenstein, M. (2007). Microbial stress response physiology and its implications for ecosystem function. *Ecology* 88, 1386–1394. doi: 10.1890/06-0219
- Schimel, J. P. (2018). Life in dry soils: effects of drought on soil microbial communities and processes. *Annu. Rev. Ecol. Evol. Syst.* 49, 409–432. doi: 10.1146/annurev-ecolsys-110617-062614
- Siebielec, S., Siebielec, G., Klimkowicz-Pawlas, A., Gałazka, A., Grządziel, J., and Stuczyński, T. (2020). Impact of water stress on microbial community and activity in sandy and loamy soils. *Agronomy* 10:1429. doi: 10.3390/agronomy10091429
- Singhania, R. R., Patel, A. K., Sukumaran, R. K., Larroche, C., and Pandey, A. (2013). Role and significance of beta-glucosidases in the hydrolysis of cellulose for bioethanol production. *Bioresour. Technol.* 127, 500–507. doi: 10.1016/j.biortech.2012.09.012
- Six, J., Conant, R. T., Paul, E. A., and Paustian, K. (2002). Stabilization mechanisms of soil organic matter: implications for C-saturation of soils. *Plant Soil* 241, 155–176. doi: 10.1023/A:1016125726789
- Song, A., Fan, F., Yin, C., Wen, S., Zhang, Y., Fan, X., et al. (2017). The effects of silicon fertilizer on denitrification potential and associated genes abundance in paddy soil. *Biol. Fertil. Soils* 53, 627–638. doi: 10.1007/s00374-017-1206-0
- Sun, D.-L., Jiang, X., Wu, Q. L., and Zhou, N.-Y. (2013). Intragenomic heterogeneity of 16S rRNA genes causes overestimation of prokaryotic diversity. *Appl. Environ. Microbiol.* 79, 5962–5969. doi: 10.1128/AEM.01282-13
- Eivazi, F., and Tabatabai, M. A. (1990). Factors affecting glucosidase and galactosidase activities in soils. *Soil Biol. Biochem.* 22, 891–897. doi: 10.1016/0038-0717(90)90126-K
- Tan, X., Shao, D., and Gu, W. (2018). Effects of temperature and soil moisture on gross nitrification and denitrification rates of a Chinese lowland paddy field soil. *Paddy Water Environ.* 16, 687–698. doi: 10.1007/s10333-018-0660-0
- Větrovský, T., and Baldrian, P. (2013). The variability of the 16S rRNA gene in bacterial genomes and its consequences for bacterial community analyses. *PLoS One* 8:e57923. doi: 10.1371/journal.pone.0057923
- Vincent, Q., Auclerc, A., Beguiristain, T., and Leyval, C. (2018). Assessment of derelict soil quality: abiotic, biotic and functional approaches. *Sci. Total Environ.* 613, 990–1002. doi: 10.1016/j.scitotenv.2017.09.118
- Wang, H., Marshall, C. W., Cheng, M., Xu, H., Li, H., Yang, X., et al. (2017). Changes in land use driven by urbanization impact nitrogen cycling and the microbial community composition in soils. *Sci. Rep.* 7:44049. doi: 10.1038/srep44049
- Wang, H., Yang, J. P., Yang, S. H., Yang, Z. C., and Lv, Y. M. (2014). Effect of a 10°C-elevated temperature under different water contents on the microbial community in a tea orchard soil. *Eur. J. Soil Sci.* 62, 113–120. doi: 10.1016/j.ejsobi.2014.03.005
- Wei, W., Isobe, K., Nishizawa, T., Zhu, L., Shiratori, Y., Ohte, N., et al. (2015). Higher diversity and abundance of denitrifying microorganisms in environments than considered previously. *ISME J.* 9, 1954–1965. doi: 10.1038/ismej.2015.9
- Williams, M. A. (2007). Response of microbial communities to water stress in irrigated and drought-prone tallgrass prairie soils. *Soil Biol. Biochem.* 39, 2750–2757. doi: 10.1016/j.soilbio.2007.05.025
- Yu, Z., Wang, G., and Marschner, P. (2014). Drying and rewetting - Effect of frequency of cycles and length of moist period on soil respiration and microbial biomass. *Eur. J. Soil Biol.* 62, 132–137. doi: 10.1016/j.ejsobi.2014.03.007
- Zeglin, L. H., Bottomley, P. J., Jumpponen, A., Rice, C. W., Arango, M., Lindsley, A., et al. (2013). Altered precipitation regime affects the function and composition of soil microbial communities on multiple time scales. *Ecology* 94, 2334–2345. doi: 10.1890/12-2018.1
- Zhang, Y., and Ji, G. (2018). Quantitative responses of potential nitrification and denitrification rates to the size of microbial communities in rice paddy soils. *Chemosphere* 211, 970–977. doi: 10.1016/j.chemosphere.2018.08.047
- Zhang, M., Bai, S. H., Tang, L., Zhang, Y., Teng, Y., and Xu, Z. (2017). Linking potential nitrification rates, nitrogen cycling genes and soil properties after remediating the agricultural soil contaminated with heavy metal and fungicide. *Chemosphere* 184, 892–899. doi: 10.1016/j.chemosphere.2017.06.081
- Zhang, M., Wang, W., Wang, D., Heenan, M., and Xu, Z. (2018). Short-term responses of soil nitrogen mineralization, nitrification and denitrification to prescribed burning in a suburban forest ecosystem of subtropical Australia. *Sci. Total Environ.* 642, 879–886. doi: 10.1016/j.scitotenv.2018.06.144

**Conflict of Interest:** The authors declare that the research was conducted in the absence of any commercial or financial relationships that could be construed as a potential conflict of interest.

**Publisher's Note:** All claims expressed in this article are solely those of the authors and do not necessarily represent those of their affiliated organizations, or those of the publisher, the editors and the reviewers. Any product that may be evaluated in this article, or claim that may be made by its manufacturer, is not guaranteed or endorsed by the publisher.

Copyright © 2021 Fikri, Joulain, Motelica-Heino, Norini and Hellal. This is an open-access article distributed under the terms of the Creative Commons Attribution License (CC BY). The use, distribution or reproduction in other forums is permitted, provided the original author(s) and the copyright owner(s) are credited and that the original publication in this journal is cited, in accordance with accepted academic practice. No use, distribution or reproduction is permitted which does not comply with these terms.

# Advantages of publishing in Frontiers



## OPEN ACCESS

Articles are free to read  
for greatest visibility  
and readership



## FAST PUBLICATION

Around 90 days  
from submission  
to decision



## HIGH QUALITY PEER-REVIEW

Rigorous, collaborative,  
and constructive  
peer-review



## TRANSPARENT PEER-REVIEW

Editors and reviewers  
acknowledged by name  
on published articles

## Frontiers

Avenue du Tribunal-Fédéral 34  
1005 Lausanne | Switzerland

Visit us: [www.frontiersin.org](http://www.frontiersin.org)

Contact us: [frontiersin.org/about/contact](http://frontiersin.org/about/contact)



## REPRODUCIBILITY OF RESEARCH

Support open data  
and methods to enhance  
research reproducibility



## DIGITAL PUBLISHING

Articles designed  
for optimal readership  
across devices



## FOLLOW US

@frontiersin



## IMPACT METRICS

Advanced article metrics  
track visibility across  
digital media



## EXTENSIVE PROMOTION

Marketing  
and promotion  
of impactful research



## LOOP RESEARCH NETWORK

Our network  
increases your  
article's readership